

# PHONONS AND ELECTRON CORRELATIONS IN HIGH-TEMPERATURE AND OTHER NOVEL SUPERCONDUCTORS

GUEST EDITORS: ALEXANDRE SASHA ALEXANDROV, CARLO DI CASTRO,  
IGOR MAZIN, AND DRAGAN MIHAILOVIC





---

**Phonons and Electron Correlations in  
High-Temperature and Other Novel  
Superconductors**

Advances in Condensed Matter Physics

---

**Phonons and Electron Correlations in  
High-Temperature and Other Novel  
Superconductors**

Guest Editors: Alexandre Sasha Alexandrov,  
Carlo Di Castro, Igor Mazin, and Dragan Mihailovic



---

Copyright © 2010 Hindawi Publishing Corporation. All rights reserved.

This is a special issue published in volume 2010 of “Advances in Condensed Matter Physics.” All articles are open access articles distributed under the Creative Commons Attribution License, which permits unrestricted use, distribution, and reproduction in any medium, provided the original work is properly cited.

## Editorial Board

Alexandre Sasha Alexandrov, UK  
Dario Alfè, UK  
Bohdan Andraka, USA  
Daniel Arovas, USA  
A. Bansil, USA  
Ward Beyermann, USA  
Mark Bowick, USA  
Gang Cao, USA  
Ashok Chatterjee, India  
Ruplal N. P. Choudhary, India  
Kim Chow, Canada  
Oleg Derzhko, Ukraine  
Thomas Peter Devereaux, USA  
Dorothy Duffy, UK  
Gayanath Fernando, USA  
Jörg Fink, Germany  
Yuri Galperin, Norway  
Russell Giannetta, USA  
Gabriele F. Giuliani, USA

James L. Gole, USA  
P. Guptasarma, USA  
M. Zahid Hasan, USA  
Yurij Holovatch, Ukraine  
David Huber, USA  
Nigel E. Hussey, UK  
Philippe Jacquod, USA  
Jan Alexander Jung, Canada  
Dilip Kanhere, India  
Feo V. Kusmartsev, UK  
Robert Leisure, USA  
Heiner Linke, USA  
Rosa Lukaszew, USA  
Dmitrii Maslov, USA  
Yashowanta N. Mohapatra, India  
Abhijit Mookerjee, India  
Victor Moshchalkov, Belgium  
Charles Myles, USA  
Donald Naugle, USA

Vladimir A. Osipov, Russia  
Rolfe Petschek, USA  
Joseph Poon, USA  
Ruslan Prozorov, USA  
Leonid Pryadko, USA  
Charles Rosenblatt, USA  
Romano Rupp, Austria  
Alfonso San-Miguel, France  
Mohindar S. Seehra, USA  
Sergei Sergeenkov, Russia  
Ivan Smalyukh, USA  
Daniel L. Stein, USA  
Michael C. Tringides, USA  
Sergio E. Ulloa, USA  
Attila Virosztek, Hungary  
Nigel Wilding, UK  
Gary Wysin, USA  
Gergely Zimanyi, USA

# Contents

**Phonons and Electron Correlations in High-Temperature and Other Novel Superconductors,**

Alexandre Sasha Alexandrov, Carlo Di Castro, Igor Mazin, and DraganMihailovic

Volume 2010, Article ID 206012, 2 pages

**Electronic and Lattice Dynamical Properties of the Iron-Based Superconductors LiFeAs and NaFeAs,**

R. A. Jishi and H. M. Alyahyaei

Volume 2010, Article ID 804343, 6 pages

**Polaron Mass and Electron-Phonon Correlations in the Holstein Model,** Marco Zoli

Volume 2010, Article ID 815917, 15 pages

**Manifestations of the Electron-Phonon Coupling in the Spectroscopy of High-Temperature Superconductors,** A. S. Mishchenko

Volume 2010, Article ID 306106, 27 pages

**Local Electron-Lattice Interactions in High-Temperature Cuprate Superconductors,** Hugo Keller and Annette Bussmann-Holder

Volume 2010, Article ID 393526, 17 pages

**Hard-Wired Dopant Networks and the Prediction of High Transition Temperatures in Ceramic Superconductors,** J. C. Phillips

Volume 2010, Article ID 250891, 13 pages

**Supercell Band Calculations and Correlation for High- $T_C$  Copper Oxide Superconductors,** T. Jarlborg

Volume 2010, Article ID 912067, 7 pages

**The Phenomenology of Iron Pnictides Superconductors Explained in the Framework of s-Wave Three-Band Eliashberg Theory,** G. A. Ummarino

Volume 2010, Article ID 167985, 6 pages

**Competition of Superconductivity and Charge Density Waves in Cuprates: Recent Evidence and Interpretation,** A. M. Gabovich, A. I. Voitenko, T. Ekino, Mai Suan Li, H. Szymczak, and M. Pękała

Volume 2010, Article ID 681070, 40 pages

**Phonons in  $A_3C_60$  Lattice and Structural Dynamics,** Sven Larsson

Volume 2010, Article ID 627452, 6 pages

**Antiadiabatic Theory of Superconducting State Transition: Phonons and Strong Electron Correlations—The Old Physics and New Aspects,** Pavol Baňacký

Volume 2010, Article ID 752943, 36 pages

**Lattice Instability in High Temperature Superconducting Cuprates and FeAs Systems: Polarons Probed by EXAFS,** H. Oyanagi and C. J. Zhang

Volume 2010, Article ID 484578, 10 pages

**Misfit Strain in Superlattices Controlling the Electron-Lattice Interaction via Microstrain in Active Layers**, Nicola Poccia, Alessandro Ricci, and Antonio Bianconi  
Volume 2010, Article ID 261849, 7 pages

**Giant Electron-Phonon Anomaly in Doped  $\text{La}_2\text{CuO}_4$  and Other Cuprates**, D. Reznik  
Volume 2010, Article ID 523549, 24 pages

**Electron-Phonon Interaction in the High- $T_C$  Cuprates in the Framework of the Van Hove Scenario**, Jacqueline Bouvier and Julien Bok  
Volume 2010, Article ID 472636, 9 pages

**Spin-Lattice Coupling and Superconductivity in Fe Pnictides**, T. Egami, B. V. Fine, D. Parshall, A. Subedi, and D. J. Singh  
Volume 2010, Article ID 164916, 7 pages

**Existence of an Intermediate Metallic Phase at the SDW-CDW Crossover Region in the One-Dimensional Holstein-Hubbard Model at Half-Filling**, Ashok Chatterjee  
Volume 2010, Article ID 350787, 14 pages

**Real-Time Observation of Cuprates Structural Dynamics by Ultrafast Electron Crystallography**, F. Carbone, N. Gedik, J. Lorenzana, and A. H. Zewail  
Volume 2010, Article ID 958618, 27 pages

**Material and Doping Dependence of the Nodal and Antinodal Dispersion Renormalizations in Single- and Multilayer Cuprates**, S. Johnston, W. S. Lee, Y. Chen, E. A. Nowadnick, B. Moritz, Z.-X. Shen, and T. P. Devereaux  
Volume 2010, Article ID 968304, 13 pages

**Through a Lattice Darkly: Shedding Light on Electron-Phonon Coupling in the High  $T_c$  Cuprates**, D. R. Garcia and A. Lanzara  
Volume 2010, Article ID 807412, 23 pages

**Bosonic Spectral Function and the Electron-Phonon Interaction in HTSC Cuprates**, E. G. Maksimov, M. L. Kulić, and O. V. Dolgov  
Volume 2010, Article ID 423725, 64 pages

**Electron-Phonon Interaction in Strongly Correlated Systems**, M. Capone, C. Castellani, and M. Grilli  
Volume 2010, Article ID 920860, 18 pages

## Editorial

# Phonons and Electron Correlations in High-Temperature and Other Novel Superconductors

**Alexandre Sasha Alexandrov,<sup>1</sup> Carlo Di Castro,<sup>2</sup> Igor Mazin,<sup>3</sup> and Dragan Mihailovic<sup>4</sup>**

<sup>1</sup>Department of Physics, Loughborough University, Loughborough LE11 3TU, UK

<sup>2</sup>Dipartimento di Fisica, Università degli Studi di Roma "La Sapienza", Piazzale Aldo Moro 5, 00185 Roma, Italy

<sup>3</sup>U.S. Naval Research Laboratory, code 6390, 4555 Overlook Avenue SW, Washington, DC 20375, USA

<sup>4</sup>Department of Complex Matter, Jozef Stefan Institute, Ljubljana 1001, Slovenia

Correspondence should be addressed to Alexandre Sasha Alexandrov, a.s.alexandrov@lboro.ac.uk

Received 7 June 2010; Accepted 7 June 2010

Copyright © 2010 Alexandre Sasha Alexandrov et al. This is an open access article distributed under the Creative Commons Attribution License, which permits unrestricted use, distribution, and reproduction in any medium, provided the original work is properly cited.

Since the discovery of high-temperature superconductivity in 1986 by George Bednorz and Alex Müller, there has been a huge theoretical effort to understand the mechanism behind it. A lanthanum copper oxide, doped with barium, was the first compound displaying this phenomenon, and now many more high-temperature superconductors based on copper and oxygen have been discovered. These make up the cuprate family of superconductors. More recently fullerenes, MgB<sub>2</sub>, and in particular iron-based superconductors with high-transition temperatures have been discovered. Cuprates are different from conventional metallic superconductors in that they originate from the charge-doping of parent Mott insulators. The superconductivity arises in weakly coupled doped layers held together by ionic bonding. As well as their high-T<sub>c</sub>, they display many unique properties. For instance, they exhibit two different energy scales: a "superconducting" gap (SG) that develops below the superconducting critical temperature which can be seen by extrinsic and intrinsic tunnelling experiments, as well as by high-resolution angle-resolved photoemission experiments; and another gap-like feature, the so-called "pseudogap" (PG), that exists in the superconducting state and well above T<sub>c</sub>, in the underdoped region with doping smaller than the optimal value at which the maximum T<sub>c</sub> occurs. The PG phenomenon was first observed through spin response in underdoped YBa<sub>2</sub>Cu<sub>3</sub>O<sub>7- $\delta$</sub> . Many experiments have since detected this PG, including extrinsic and intrinsic tunnelling; photoemission, pump-probe spectroscopies, calorimetric, and many others. Initially this gap was interpreted as manifestation of preformed electron pairs existing above T<sub>c</sub> called small

bipolarons, bound together by a strong electron-phonon interaction (EPI). Since then many theoretical explanations have been proposed for the origin of the PG which can roughly be divided into two groups. The first of these groups argues that the PG originates from some competing order, either static or fluctuating, possibly also giving rise to inhomogeneous states. The second group interprets the pseudogap as a precursor of superconductivity and suggests the existence above T<sub>c</sub> of preformed pairs with no coherence. Despite intensive research, a microscopic theory capable of describing unusual ARPES and tunnelling data has remained elusive and so the relationship between the SG and PG has remained a debated issue. A detailed and consistent interpretation of the SG, PG, and many other unusual properties could shed light on the key effective interactions in cuprate superconductors. In this regard, the interplay of EPI with correlations could be relevant.

The recently discovered Fe-based high-temperature superconductors (pnictides) also represent a challenging case for the theory of superconductivity. They appear to be rather different from cuprates in terms of their electronic structure; magnetic order, correlation effects, superconducting symmetry; their parent state is metallic rather than insulating. So far, the most popular suggestion for the pairing mechanism has been one that assigns the role of an intermediate boson to spin fluctuations with wave vectors close to  $Q = (\pi, \pi)$  (in the Brillouin zone). There are two ways to generate such spin fluctuations: one assumes superexchange between the second neighbours in the Fe lattice and the other exploits the fact that the noninteracting spin susceptibility calculated

using the electron band structure has a peak, or rather a broad maximum close to  $(\pi, \pi)$ . A strong argument in favour of the latter scenario is the case of FeSe, where a sister magnetic compound FeTe shows an antiferromagnetic order at a different wave vector  $(\pi, 0)$  both in the experiment and in the calculations, but the calculated spin susceptibility still peaks at  $Q = (\pi, \pi)$  and the experiment also observes spin fluctuations with the same wave vector. On the other hand, the interplay between spin fluctuations, correlations, and EPI remains a challenging open problem, taking into account controversial isotope effects, structural instabilities, low carrier densities; and some other peculiarities of pnictides.

The absence of consensus on the physics of cuprate superconductors and the recent discovery of iron-based compounds with high-transition temperatures has reemphasized the fundamental importance of understanding the origin of high-temperature superconductivity. Some first principle calculations based on density functional theory (DFT) often predict a rather weak electron-phonon interaction insufficient to explain high transition temperatures. A number of researchers have the opinion that correlations select momentum and frequency windows where EPI is more efficient. Others maintain that the repulsive electron-electron interaction in novel superconductors provides pairing and thus offers high transition temperatures without phonons. On the other hand, some recent studies using numerical techniques cast doubt that simple repulsive models can account for high-temperature superconductivity. Besides, there is substantial experimental evidence that EPI is an important player and needs to be included in a successful theory of high- $T_c$  superconductivity. This was the motivation for the Editors to provide an international forum that would address the intriguing issue of the interplay between strong electronic correlations and sizeable electron-phonon coupling.

This special issue includes both original results and summarizing overviews. The Editors hope that this publication will stimulate the continuing efforts to understand high-temperature and other unconventional superconductors.

*Alexandre Sasha Alexandrov*  
*Carlo Di Castro*  
*Igor Mazin*  
*Dragan Mihailovic*

## Research Article

# Electronic and Lattice Dynamical Properties of the Iron-Based Superconductors LiFeAs and NaFeAs

R. A. Jishi and H. M. Alyahyaei

Department of Physics, California State University, Los Angeles, CA 90032, USA

Correspondence should be addressed to R. A. Jishi, raljishi@exchange.calstatela.edu

Received 3 March 2009; Accepted 17 June 2009

Academic Editor: Igor Mazin

Copyright © 2010 R. A. Jishi and H. M. Alyahyaei. This is an open access article distributed under the Creative Commons Attribution License, which permits unrestricted use, distribution, and reproduction in any medium, provided the original work is properly cited.

The electronic structure and lattice vibrational frequencies of the newly discovered superconductors, LiFeAs and NaFeAs, are calculated within density functional theory. We show that, in the vicinity of the Fermi energy, the density of states is dominated by contributions from Fe 3d states. We also calculate the electron-phonon coupling strength and show that it is too weak to account for the observed values of the superconducting transition temperatures. This seems to indicate that the iron-based superconductors are not of the conventional type.

## 1. Introduction

A new class of layered, high- $T_c$  superconductors has been recently discovered. Kamihara et al. [1] reported a superconducting transition temperature  $T_c = 26$  K in fluorine-doped LaFeAsO. Shortly afterwards, it was found that under pressure  $T_c$  increased to 43 K [2]. Replacement of lanthanum with other rare earth metals gave a series of superconducting compounds  $\text{ReFeAsO}_{1-x}\text{F}_x$ , where Re = Ce, Pr, Nd, Sm, or Gd, with transition temperatures close to or exceeding 50 K [3–8]. Oxygen deficient samples were also synthesized and found to superconduct at 55 K [9–11]. Hole doping, through the partial substitution of La with Sr, or Gd with Th, was also found to yield superconducting compounds [12, 13]. Using-high pressure techniques, it was possible to increase the concentration of the F-dopant [14] and to synthesize superconducting compounds where La is replaced by the late rare earth elements Tb and Dy [15, 16]. The parent compound  $\text{ReFeAsO}$  is a layered compound consisting of a stack of alternating ReO and FeAs layers. Each ReO layer consists of an O-sheet surrounded by two Re sheets. Similarly, each FeAs layer consists of an Fe-sheet surrounded by two As sheets such that each Fe atom is tetrahedrally coordinated to four As atoms. Neutron diffraction measurements [17–20] establish that the Fe magnetic moments adopt a collinear antiferromagnetic (*c*-AFM) order whereby ferromagnetic

chains are coupled antiferromagnetically along the direction orthogonal to the chains.

Superconductivity was also discovered in a second class of compounds containing FeAs layers, namely,  $\text{AFe}_2\text{As}_2$ , where A is an alkaline earth metal. Hole doping, by partial replacement of A with alkali metals, results in superconducting compounds with  $T_c$  reaching 38 K in  $\text{BaFe}_2\text{As}_2$  and  $\text{SrFe}_2\text{As}_2$  [21–25]. Partial substitution of Fe with Co was also shown to give a superconducting compound with  $T_c = 22$  K [26]. Similarly to the first class, in the parent compounds the Fe magnetic moments in this second class have a collinear AFM order with a spin-stripes pattern [27–29]. In both classes, the Fe magnetic moments in the parent compounds exhibit magnetic order, at low temperature, which disappears upon doping, making way for the emergence of superconductivity. This leads to the reasonable belief that strong electronic correlations are important in these systems, and that superconductivity in these compounds is somehow connected to magnetic fluctuations [30–42]. Indeed, the electron-phonon coupling in  $\text{LaOFeAs}$  was estimated to be too small [43] to give rise to superconductivity within the conventional BCS formulation. [44]

Recently, a third class of iron-based superconductors was discovered. LiFeAs and NaFeAs were found to superconduct below 18 K and 9 K, respectively, [45–48]. It turns out that in these two compounds no magnetic order is detected at

all temperatures. In some sense, these two compounds are important with regards to understanding the mechanism of superconductivity in iron-based superconductors. The absence of spin density wave (SDW) transition, on the one hand, and the relatively low  $T_c$  in comparison with the first two classes of iron-based superconductors, on the other hand, make these two compounds possible candidates for being conventional BCS superconductors.

Band structure calculations, using local density approximation (LDA) within density functional theory (DFT), were recently reported for LiFeAs [49, 50]. It was found that LiFeAs is semimetallic, and that the density of states (DOSs) near the Fermi level is dominated by the Fe 3d states. Thus, the electronic structure of stoichiometric LiFeAs is similar to that of the parent compounds of the first class, with a hole cylinder at the Brillouin zone (BZ) center, electron cylinders at the BZ corners, and an electronic DOS that decreases strongly with increasing energy in the vicinity of the Fermi energy.

In this work we report DFT calculations of the electronic and lattice properties of LiFeAs and NaFeAs. In particular, we calculate the electron-phonon coupling strength and show that it is too weak to account for the superconducting transition temperatures observed in these compounds. Our calculations, together with previous calculations [44] of the electron-phonon coupling strength in LaOFeAs, seem to indicate that iron-based superconductors are not of the conventional type.

## 2. Method

The electronic structure calculations are carried out using the all-electron full-potential linear augmented plane wave (FP-LAPW) method as implemented in WIEN2K code [51]. The exchange-correlation potential was calculated using the generalized gradient approximation (GGA) as proposed by Pedrew, Burke, and Ernzerhof (PBE) [52]. The radii of the muffin-tin spheres for the various atoms were chosen so that the neighboring spheres almost touch each other. We set the parameter  $R_{MT}K_{max} = 7$ , where  $R_{MT}$  is the smallest muffin-tin radius, and  $K_{max}$  is a cutoff wave vector. The valence wave functions inside the muffin-tin spheres are expanded in terms of spherical harmonics up to  $l_{max} = 10$ , and in terms of plane waves with a wave vector cutoff  $K_{max}$  in the interstitial region. The charge density is Fourier expanded up to  $G_{max} = 13a_0^{-1}$ , where  $a_0$  is the Bohr radius. Convergence of the self-consistent field calculations is attained with a total energy convergence tolerance of 0.01 mRy.

The calculation of the frequencies of the vibrational modes and the electron-phonon coupling parameter was performed using ultrasoft pseudopotentials and an expansion of the wave function of the valence electrons in terms of plane waves, with an energy cutoff of 30 Rydbergs [53]. The charge density is Fourier expanded with an energy cutoff of 400 Rydbergs. The dynamical matrices and the electron-phonon coupling parameter are calculated using DFT in the linear response approximation. In calculating the phonon frequencies, the electronic integration is carried out using a uniform mesh of  $N_k = 4 \times 4 \times 4$   $k$ -points in the Brillouin

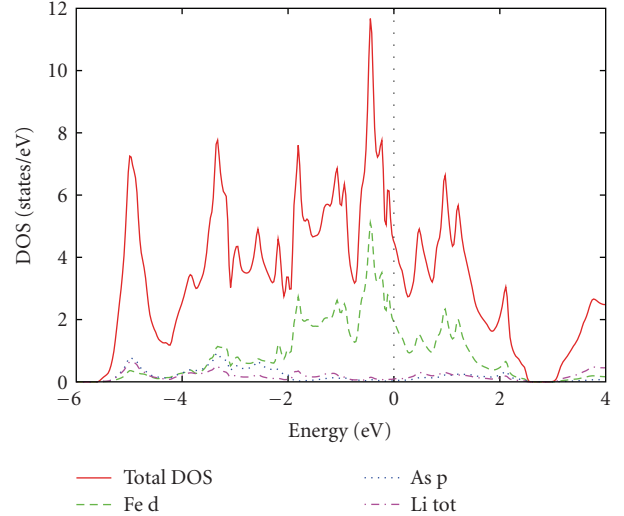


FIGURE 1: Density of states (DOSs) in LiFeAs. Both the total and atomic DOSs are shown. The Fermi energy is the zero energy. Near the Fermi energy, the DOS is dominated by the Fe 3d states.

zone. On the other hand, the electronic density of states, used in computing the electron-phonon coupling parameter  $\lambda$ , is calculated using a finer mesh of  $16 \times 16 \times 16$   $k$ -points. The value of  $\lambda$  is obtained by averaging over a uniform mesh of  $N_q = 4 \times 4 \times 4$  phonon momentum  $q$ -points. The phonon dispersion curves are obtained by Fourier interpolation of the dynamical matrices computed on the  $N_q$  points mesh.

In the electronic and lattice calculations, the experimental values of the low-temperature lattice constants and atomic positions [45–48] are used. For both compounds, the crystal is tetragonal with space group  $P4/nmm$ . In LiFeAs, the lattice constants are  $a = 3.76982 \text{ \AA}$ ,  $c = 6.30693 \text{ \AA}$ , whereas in NaFeAs,  $a = 3.94729 \text{ \AA}$ , and  $c = 6.99112 \text{ \AA}$ .

## 3. Results and Discussion

Our results for the electronic structure calculations for LiFeAs and NaFeAs are summarized in Figures 1 and 2, respectively, where the electronic density of states (DOSs) is displayed. For LiFeAs, our calculated DOS is similar to that reported earlier [49, 50]. In both LiFeAs and NaFeAs, the DOS plots show some generic features that are common to the parent compounds of the iron-based superconductors: a DOS that is dominated by the Fe 3d states in the vicinity of the Fermi energy, with only a small contribution from the As and alkali metal states and that is strongly decreasing with energy near the Fermi energy.

It should be noted that in a unit cell of LiFeAs, for example, there are two Li, two Fe, and two As atoms. Thus to get the total atomic DOS, the values of the atomic DOS shown in 1 should be multiplied by 2. The total DOS is the sum of the total atomic DOS and the DOS in the interstitial region.

Since the DOS at the Fermi energy,  $N(E_F)$ , is  $\sim 4$  states/eV in both LiFeAs and NaFeAs, which is not very small, and because of the relatively lower  $T_c$  compared with the

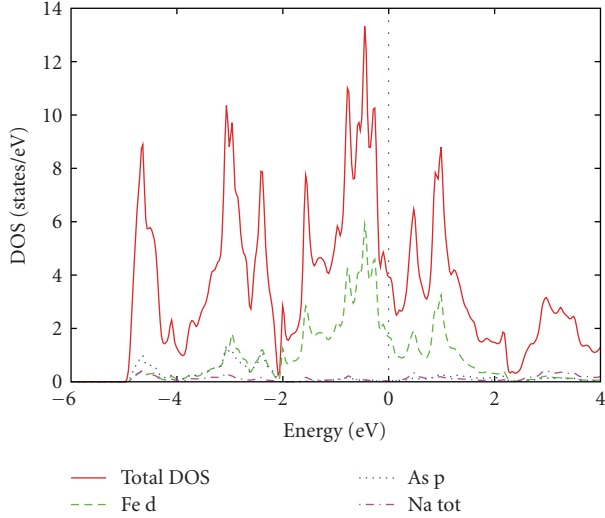


FIGURE 2: Density of states (DOSs) in NaFeAs. Both the total and atomic DOSs are shown. The Fermi energy is the zero energy. Near the Fermi energy, the DOS is dominated by the Fe 3d states.

other iron-based superconductors, one may wonder whether electron-phonon coupling may lie behind the mechanism for superconductivity in LiFeAs and NaFeAs. This notion may be given more credence by the observation that a sodium atom is about three times more massive than a lithium atom, so that if the attractive electron-electron interaction is mediated by the alkali-metal atomic vibrations, then this difference in the mass could explain the difference in the values of  $T_c$  between the two compounds via the well-known isotope effect.

To test this idea, we carried out a calculation of the phonon dispersion curves and the electron-phonon coupling strength in these compounds. Since the crystallographic point group in LiFeAs and NaFeAs is  $D_{4h}$ , the vibrational modes at  $\Gamma$ , the BZ center, are decomposed according to the following irreducible representations:

$$\Gamma_{\text{phonon}} = 2A_{1g} + B_{1g} + 3E_g + 3A_{2u} + 3E_u. \quad (1)$$

The acoustic modes, with vanishing frequency at  $\Gamma$ , the BZ center, transform according to the  $A_{2u}$  and  $E_u$  irreducible representations. Excluding the acoustic modes, we are left with 15 modes with nonzero frequencies; among these, the symmetric ones are Raman-active, while the antisymmetric modes are infrared-active. The calculated frequencies of the Raman- and infrared-active modes at the  $\Gamma$  point of the BZ are given in Table 1. The phonon dispersion curves in LiFeAs, plotted along high symmetry directions in the BZ, are shown in Figure 3, and the corresponding curves in NaFeAs are given in Figure 4. Our results for the phonon frequencies at the BZ center may be checked by Raman scattering and infrared absorption experiments, while the phonon dispersion curves may be checked by neutron scattering measurements.

We calculated the electron-phonon coupling parameter  $\lambda$  and found it to be 0.29 and 0.27 for LiFeAs and NaFeAs, respectively. For conventional superconductors,

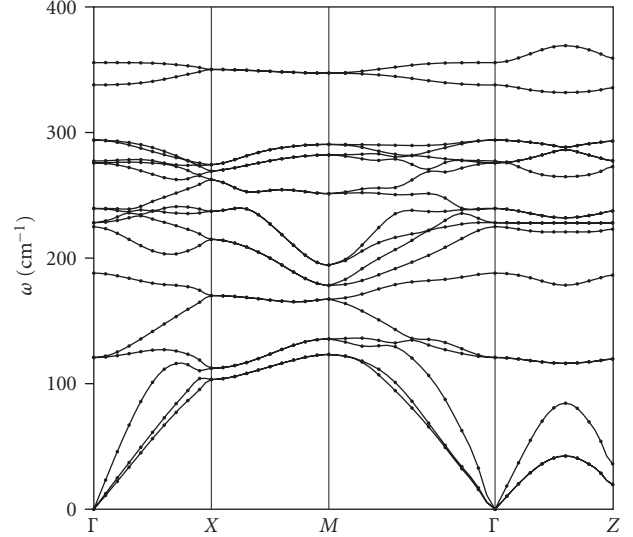


FIGURE 3: Phonon dispersion curves in LiFeAs, plotted along high symmetry directions of the Brillouin zone.

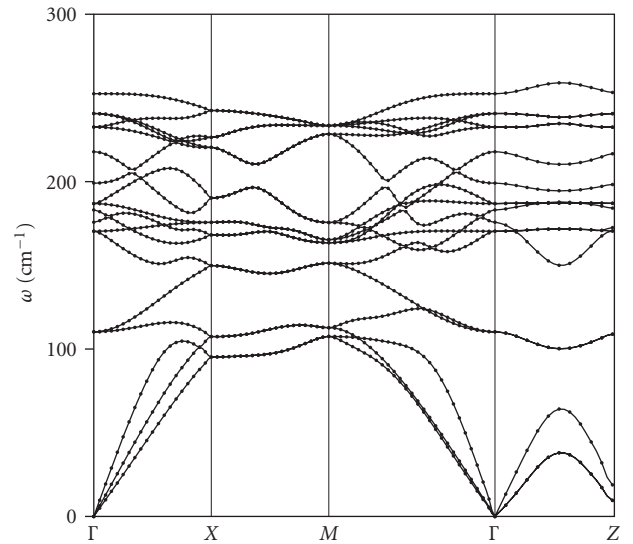


FIGURE 4: Phonon dispersion curves in NaFeAs, plotted along high symmetry directions of the Brillouin zone.

where the attractive electron-electron interaction is mediated by phonons, the transition temperature is given by the Allen and Dynes [54] modified McMillan's formula [55]

$$T_c = \frac{\omega_{\log}}{1.2} \exp\left[\frac{-1.04(1 + \lambda)}{\lambda - \mu^*(1 + 0.62\lambda)}\right], \quad (2)$$

where  $\omega_{\log}$  is the logarithmic average phonon frequency, expressed in degrees Kelvin, and  $\mu^*$  is the Coulomb pseudopotential parameter, usually taken to be  $\sim 0.13$ . Since  $\omega_{\log}$  in LiFeAs and NaFeAs is of the order of 100 K, the resulting value of  $T_c$  is much less than 1 K. We conclude that the electron-phonon coupling is too weak to account for superconductivity in this class of iron-based superconductors.

TABLE 1: The calculated frequencies, in  $\text{cm}^{-1}$ , of the Raman- and infrared-(IR-) active modes in LiFeAs and NaFeAs. The modes are classified by the irreducible representations (irreps) according to which they transform.

		$\omega(\text{irrep})/\text{cm}^{-1}$					
LiFeAs	Ramman	121 ( $E_g$ )	188 ( $A_{1g}$ )	225 ( $B_{1g}$ )	240 ( $E_g$ )	294 ( $E_g$ )	356 ( $A_{1g}$ )
	IR	228 ( $E_u$ )	276 ( $E_u$ )	277 ( $A_{2u}$ )	338 ( $A_{2u}$ )		
NaFeAs	Ramman	110 ( $E_g$ )	176 ( $A_{1g}$ )	187 ( $E_g$ )	199 ( $A_{1g}$ )	218 ( $B_{1g}$ )	241 ( $E_g$ )
	IR	170 ( $E_u$ )	183 ( $A_u$ )	233 ( $E_u$ )	253 ( $A_{2u}$ )		

There are some puzzling questions that beset this third class of iron-based superconductors. In the parent compounds of the first two classes of iron-based superconductors, magnetic order is established at low temperatures, where the Fe magnetic moments adopt a collinear antiferromagnetic (c-AFM) order with a stripe-like pattern; this is unequivocally confirmed by both neutron diffraction measurements [17–20] and DFT calculations [31–39]. In the first class, it is only upon electron doping through the replacement of a small percentage of oxygen atoms with fluorine atoms, or the removal of a small percentage of oxygen atoms, that the magnetic order is suppressed and superconductivity emerges. In the second class of iron-based superconductors, magnetic order is suppressed by hole doping through the replacement of some alkaline earth atoms with alkali atoms. To better understand the situation in the third class of iron-based superconductors, we carried out spin-polarized DFT calculations on stoichiometric LiFeAs and NaFeAs, in addition to the calculations reported above for the nonmagnetic phases of these compounds. We considered, within GGA, various spin arrangements on the Fe sites. Similarly to the case of the first two classes, we find that the c-AFM phase, with a spin-stripes pattern, is indeed the lowest energy phase. Within GGA, the energy of the c-AFM phase in LiFeAs is lower than the AFM phase by 0.081 eV per Fe atom (eV/Fe), lower than the ferromagnetic (FM) phase by 0.085 eV/Fe, and lower than the nonmagnetic phase by 0.123 eV/Fe. For NaFeAs, the energy of the c-AFM phase is lower than the AFM phase by 0.048 eV/Fe, lower than the FM phase by 0.205 eV/Fe, and lower than the nonmagnetic phase by 0.182 eV/Fe. The calculated magnetic moment on an Fe site is  $2.18 \mu_B$  in the case of NaFeAs, and  $1.76 \mu_B$  in the case of LiFeAs, where  $\mu_B$  is the Bohr magneton. Thus, according to our DFT calculations, stoichiometric LiFeAs and NaFeAs should be similar to the parent compounds of the first two classes, and they should not superconduct; instead, at low temperature, the stoichiometric compounds should display magnetic order. Deviations from stoichiometry, on the other hand, may suppress the magnetic order, making way for superconductivity, just like doping does in the first two classes of iron-based compounds. In the case of LiFeAs, it is indeed the case that the synthesized superconducting compounds were not stoichiometric, the chemical formula being  $\text{Li}_{1-x}\text{FeAs}$  [47]. The situation is less clear in the case of NaFeAs [48], but we believe, on the basis of our spin-polarized calculations and the absence of any detectable magnetic order at low temperatures, that the synthesized NaFeAs samples may also be nonstoichiometric.

We should note, however, that our results on the magnetic structure of the third class of compounds are only tentative. One problem is that the calculated magnetic moment per Fe site is too large in comparison with the experimental value in LaFeAsO, where the Fe moments also adopt c-AFM order, albeit with a magnetic moment of only  $0.36 \mu_B$  [17]. It has been shown by various groups [56–58] that even though the Fe moments adopt the stripe-AFM order in the undoped LaFeAsO compound, yet the stabilization energy and the value of the Fe magnetic moment are sensitive to the type of exchange-correlation functional employed in the calculation, and to the position of the As atom. At this point, all we can say is that DFT calculations within GGA using PBE exchange correlation potential suggest that stoichiometric LiFeAs and NaFeAs compounds will display magnetic order at low temperatures.

## 4. Conclusions

In conclusion, we have presented the results of electronic structure calculations on LiFeAs and NaFeAs, members of a new class of superconducting compounds. In similarity to other iron-based superconductors, the density of states in the vicinity of the Fermi energy is found to be dominated by contributions from the Fe 3d states. We have also calculated the Raman and infrared phonon frequencies at the Brillouin zone center, as well the phonon dispersion curves along high symmetry directions in the Brillouin zone. We have evaluated the electron-phonon coupling parameter in LiFeAs and NaFeAs and found its value to be too small to account for the observed superconducting transition temperatures in these compounds. Our results, taken together with previous estimates of the electron-phonon coupling strength in LaFeAsO, seem to suggest clearly that iron-based superconductors are not of the conventional type, where the attractive electron-electron interaction is mediated by phonons.

## References

- [1] Y. Kamihara, T. Watanabe, M. Hirano, and H. Hosono, “Iron-based layered superconductor  $\text{La}[\text{O}_{1-x}\text{F}_x]\text{FeAs}$  ( $x = 0.05\text{--}0.12$ ) with  $T_c = 26$  K,” *Journal of the American Chemical Society*, vol. 130, no. 11, pp. 3296–3297, 2008.
- [2] H. Takahashi, K. Igawa, K. Arii, Y. Kamihara, M. Hirano, and H. Hosono, “Superconductivity at 43 K in an iron-based layered compound  $\text{LaO}_{1-x}\text{F}_x\text{FeAs}$ ,” *Nature*, vol. 453, no. 7193, pp. 376–378, 2008.

- [3] G. F. Chen, Z. Li, D. Wu, et al., "Superconductivity at 41 K and its competition with spin-density-wave instability in layered  $\text{CeO}_{1-x}\text{F}_x\text{FeAs}$ ," *Physical Review Letters*, vol. 100, no. 24, Article ID 247002, 2008.
- [4] Z.-A. Ren, J. Yang, W. Lu, et al., "Superconductivity at 52 K in iron based F doped layered quaternary compound  $\text{Pr}[\text{O}_{1-x}\text{F}_x]\text{FeAs}$ ," *Materials Research Innovations*, vol. 12, no. 3, pp. 105–106, 2008.
- [5] Z.-A. Ren, J. Yang, W. Lu, et al., "Superconductivity in the iron-based F-doped layered quaternary compound  $\text{Nd}[\text{O}_{1-x}\text{F}_x]\text{FeAs}$ ," *Europhysics Letters*, vol. 82, no. 5, Article ID 57002, 2008.
- [6] X. H. Chen, T. Wu, G. Wu, R. H. Liu, H. Chen, and D. F. Fang, "Superconductivity at 43 K in  $\text{SmFeAsO}_{1-x}\text{F}_x$ ," *Nature*, vol. 453, no. 7196, pp. 761–762, 2008.
- [7] Z.-A. Ren, W. Lu, J. Yang, et al., "Superconductivity at 55 K in iron-based F-doped layered quaternary compound  $\text{Sm}[\text{O}_{1-x}\text{F}_x]\text{FeAs}$ ," *Chinese Physics Letters*, vol. 25, no. 6, pp. 2215–2216, 2008.
- [8] P. Cheng, L. Fang, H. Yang, et al., "Superconductivity at 36 K in gadolinium-arsenide oxides  $\text{GdO}_{1-x}\text{F}_x\text{FeAs}$ ," *Science in China, Series G*, vol. 51, no. 6, pp. 719–722, 2008.
- [9] J. Yang, Z.-C. Li, W. Lu, et al., "Superconductivity at 53.5 K in  $\text{GdFeAsO}_{1-\delta}$ ," *Superconductor Science and Technology*, vol. 21, no. 8, Article ID 082001, 2008.
- [10] G. Wu, Y. J. Yan, T. Wu, et al., "Superconductivity induced by oxygen deficiency in  $\text{La}_{0.85}\text{Sr}_{0.15}\text{FeAsO}_{1-\delta}$ ," *Physical Review B*, vol. 78, no. 9, Article ID 092503, 2008.
- [11] Z.-A. Ren, G.-C. Che, X.-L. Dong, et al., "Superconductivity and phase diagram in iron-based arsenic-oxides  $\text{ReFeAsO}_{1-\delta}$  ( $\text{Re} = \text{rare-earth metal}$ ) without fluorine doping," *Europhysics Letters*, vol. 83, no. 1, Article ID 17002, 2008.
- [12] H.-H. Wen, G. Mu, L. Fang, H. Yang, and X. Zhu, "Superconductivity at 25 K in hole-doped  $(\text{La}_{1-x}\text{Sr}_x)\text{OFeAs}$ ," *Europhysics Letters*, vol. 82, no. 1, Article ID 17009, 2008.
- [13] C. Wang, L. Li, S. Chi, et al., "Thorium-doping-induced superconductivity up to 56 K in  $\text{Gd}_{1-x}\text{Th}_x\text{FeAsO}$ ," *Europhysics Letters*, vol. 83, no. 6, Article ID 67006, 2008.
- [14] W. Lu, X.-L. Shen, J. Yang, et al., "Superconductivity at 41.0 K in the F-doped  $\text{LaFeAsO}_{1-x}\text{F}_x$ ," *Solid State Communications*, vol. 148, no. 3-4, pp. 168–170, 2008.
- [15] J.-W. G. Bos, G. B. S. Penny, J. A. Rodgers, D. A. Sokolov, A. D. Huxley, and J. P. Attfield, "High pressure synthesis of late rare earth  $\text{RFeAs}(\text{O},\text{F})$  superconductors;  $\text{R} = \text{Tb}$  and  $\text{Dy}$ ," *Chemical Communications*, no. 31, pp. 3634–3635, 2008.
- [16] L.-J. Li, Y.-K. Li, Z.-A. Ren, et al., "Superconductivity above 50 K in  $\text{Tb}_{1-x}\text{Th}_x\text{FeAsO}$ ," *Physical Review B*, vol. 78, no. 13, Article ID 132506, 2008.
- [17] C. de la Cruz, Q. Huang, J. W. Lynn, et al., "Magnetic order close to superconductivity in the iron-based layered  $\text{LaO}_{1-x}\text{F}_x\text{FeAs}$  systems," *Nature*, vol. 453, no. 7197, pp. 899–902, 2008.
- [18] J. Zhao, Q. Huang, C. de la Cruz, et al., "Structural and magnetic phase diagram of  $\text{CeFeAsO}_{1-x}\text{F}_x$  and its relation to high-temperature superconductivity," *Nature Materials*, vol. 7, no. 12, pp. 953–959, 2008.
- [19] J. Zhao, Q. Huang, C. de la Cruz, et al., "Lattice and magnetic structures of  $\text{PrFeAsO}$ ,  $\text{PrFeAsO}_{0.85}\text{F}_{0.15}$ , and  $\text{PrFeAsO}_{0.85}$ ," *Physical Review B*, vol. 78, no. 13, Article ID 132504, 2008.
- [20] Y. Qiu, W. Bao, Q. Huang, et al., "Crystal structure and antiferromagnetic order in  $\text{NdFeAsO}_{1-x}\text{F}_x$  ( $x = 0.0$  and  $0.2$ ) superconducting compounds from neutron diffraction measurements," *Physical Review Letters*, vol. 101, no. 25, Article ID 257002, 2008.
- [21] M. Rotter, M. Tegel, and D. Johrendt, "Superconductivity at 38 K in the iron arsenide  $(\text{Ba}_{1-x}\text{K}_x)\text{Fe}_2\text{As}_2$ ," *Physical Review Letters*, vol. 101, no. 10, Article ID 107006, 2008.
- [22] G.-F. Chen, Z. Li, G. Li, et al., "Superconductivity in hole-doped  $(\text{Sr}_{1-x}\text{K}_x)\text{Fe}_2\text{As}_2$ ," *Chinese Physics Letters*, vol. 25, no. 9, pp. 3403–3405, 2008.
- [23] K. Sasmal, B. Lv, B. Lorenz, et al., "Superconducting fe-based compounds  $(\text{A}_{1-x}\text{Sr}_x)\text{Fe}_2\text{As}_2$  with  $\text{A} = \text{K}$  and  $\text{Cs}$  with transition temperatures up to 37 K," *Physical Review Letters*, vol. 101, no. 10, Article ID 107007, 2008.
- [24] G. Wu, R. H. Liu, Y. J. Yan, et al., "Transport properties and superconductivity in  $\text{Ba}_{1-x}\text{M}_x\text{Fe}_2\text{As}_2$  ( $\text{M} = \text{La}$  and  $\text{K}$ ) with double FeAs layers," *Europhysics Letters*, vol. 84, no. 2, Article ID 27010, 2008.
- [25] N. Ni, S. L. Bud'ko, A. Kreyssig, et al., "Anisotropic thermodynamic and transport properties of single-crystalline  $\text{Ba}_{1-x}\text{K}_x\text{Fe}_2\text{As}_2$  ( $x = 0$  and  $0.45$ )," *Physical Review B*, vol. 78, no. 1, Article ID 014507, 2008.
- [26] A. S. Sefat, R. Jin, M. A. McGuire, B. C. Sales, D. J. Singh, and D. Mandrus, "Superconductivity at 22 K in co-doped  $\text{BaFe}_2\text{As}_2$  crystals," *Physical Review Letters*, vol. 101, no. 11, Article ID 117004, 2008.
- [27] Q. Huang, Y. Qiu, W. Bao, et al., "Neutron-diffraction measurements of magnetic order and a structural transition in the parent  $\text{BaFe}_2\text{As}_2$  compound of FeAs-based high-temperature superconductors," *Physical Review Letters*, vol. 101, no. 25, Article ID 257003, 2008.
- [28] K. Kitagawa, N. Katayama, K. Ohgushi, M. Yoshida, and M. Takigawa, "Commensurate itinerant antiferromagnetism in  $\text{BaFe}_2\text{As}_2$ :  $^{75}\text{As}$ -NMR studies on a self-flux grown single crystal," *Journal of the Physical Society of Japan*, vol. 77, no. 11, Article ID 114709, 2008.
- [29] Y. Su, P. Link, A. Schneidewind, et al., "Antiferromagnetic ordering and structural phase transition in  $\text{Ba}_2\text{Fe}_2\text{As}_2$  with Sn incorporated from the growth flux," *Physical Review B*, vol. 79, no. 6, Article ID 064504, 2009.
- [30] D. J. Singh and M.-H. Du, "Density functional study of  $\text{LaFeAsO}_{1-x}\text{F}_x$ : a low carrier density superconductor near itinerant magnetism," *Physical Review Letters*, vol. 100, no. 23, Article ID 237003, 2008.
- [31] K. Haule, J. H. Shim, and G. Kotliar, "Correlated electronic structure of  $\text{LaO}_{1-x}\text{F}_x\text{FeAs}$ ," *Physical Review Letters*, vol. 100, no. 22, Article ID 226402, 2008.
- [32] J. Dong, H. J. Zhang, G. Xu, et al., "Competing orders and spin-density-wave instability in  $\text{La}(\text{O}_{1-x}\text{F}_x)\text{FeAs}$ ," *Europhysics Letters*, vol. 83, no. 2, Article ID 27006, 2008.
- [33] F. Ma and Z.-Y. Lu, "Iron-based layered compound  $\text{LaFeAsO}$  is an antiferromagnetic semimetal," *Physical Review B*, vol. 78, no. 3, Article ID 033111, 2008.
- [34] C. Cao, P. J. Hirschfeld, and H.-P. Cheng, "Proximity of antiferromagnetism and superconductivity in  $\text{LaFeAsO}_{1-x}\text{F}_x$ : effective Hamiltonian from ab initio studies," *Physical Review B*, vol. 77, no. 22, Article ID 220506, 2008.
- [35] T. Yildirim, "Origin of the 150-K anomaly in  $\text{LaFeAsO}$ : competing antiferromagnetic interactions, frustration, and a structural phase transition," *Physical Review Letters*, vol. 101, no. 5, Article ID 057010, 2008.
- [36] Z. -Y. Weng, "Hidden SDW order and effective low-energy theory for FeAs superconductors," *Physica E: Low-dimensional Systems and Nanostructures*, vol. 41, no. 7, pp. 1281–1284, 2009.
- [37] F. Ma, Z.-Y. Lu, and T. Xiang, "Arsenic-bridged antiferromagnetic superexchange interactions in  $\text{LaFeAsO}$ ," *Physical Review B*, vol. 78, no. 22, Article ID 224517, 2008.

- [38] Z. P. Yin, S. Lebegue, M. J. Han, B. P. Neal, S. Y. Savrasov, and W. E. Pickett, "Electron-hole symmetry and magnetic coupling in antiferromagnetic LaFeAsO," *Physical Review Letters*, vol. 101, no. 4, Article ID 047001, 2008.
- [39] S. Ishibashi, K. Terakura, and H. Hosono, "A possible ground state and its electronic structure of a mother material (LaOFeAs) of new superconductors," *Journal of the Physical Society of Japan*, vol. 77, no. 5, Article ID 053709, 2008.
- [40] Q. Si and E. Abrahams, "Strong correlations and magnetic frustration in the high T<sub>c</sub> iron pnictides," *Physical Review Letters*, vol. 101, no. 7, Article ID 076401, 2008.
- [41] C. Fang, H. Yao, W.-F. Tsai, J. Hu, and S. A. Kivelson, "Theory of electron nematic order in LaFeAsO," *Physical Review B*, vol. 77, no. 22, Article ID 224509, 2008.
- [42] C. Xu, M. Müller, and S. Sachdev, "Ising and spin orders in the iron-based superconductors," *Physical Review B*, vol. 78, no. 2, Article ID 020501, 2008.
- [43] L. Boeri, O. V. Dolgov, and A. A. Golubov, "Is LaFeAsO<sub>1-x</sub>F<sub>x</sub> an electron-phonon superconductor?" *Physical Review Letters*, vol. 101, no. 2, Article ID 026403, 2008.
- [44] J. Bardeen, L. N. Cooper, and J. R. Schrieffer, "Theory of superconductivity," *Physical Review*, vol. 108, no. 5, pp. 1175–1204, 1957.
- [45] M. J. Pitcher, D. R. Parker, P. Adamson, et al., "Structure and superconductivity of LiFeAs," *Chemical Communications*, no. 45, pp. 5918–5920, 2008.
- [46] J. H. Tapp, Z. Tang, B. Lv, et al., "LiFeAs: an intrinsic FeAs-based superconductor with T<sub>c</sub> = 18 K," *Physical Review B*, vol. 78, no. 6, Article ID 060505, 2008.
- [47] X. C. Wang, Q. Q. Liu, Y. X. Lv, et al., "The superconductivity at 18 K in LiFeAs system," *Solid State Communications*, vol. 148, no. 11-12, pp. 538–540, 2008.
- [48] D. R. Parker, M. J. Pitcher, P. J. Baker, et al., "Structure, antiferromagnetism and superconductivity of the layered iron arsenide NaFeAs," *Chemical Communications Articles*, pp. 2189–2191, 2009.
- [49] I. A. Nekrasov, Z. V. Pchelkina, and M. V. Sadovskii, "Electronic structure of new LiFeAs high-T<sub>c</sub> superconductor," *JETP Letters*, vol. 88, no. 8, pp. 543–545, 2008.
- [50] D. J. Singh, "Electronic structure and doping in BaFe<sub>2</sub>As<sub>2</sub> and LiFeAs: density functional calculations," *Physical Review B*, vol. 78, no. 9, Article ID 094511, 2008.
- [51] P. Blaha, K. Schwarz, G. K. H. Madsen, D. Kvasnicka, and J. Luitz, *WIEN2K, An Augmented Plane Wave + Local Orbitals Program for Calculating Crystal Properties*, Technische Universität, Wien, Austria, 2001.
- [52] J. P. Perdew, K. Burke, and M. Ernzerhof, "Generalized gradient approximation made simple," *Physical Review Letters*, vol. 77, no. 18, pp. 3865–3868, 1996.
- [53] P. Giannozzi, et al., <http://www.quantum-espresso.org>.
- [54] P. B. Allen and R. C. Dynes, "Transition temperature of strongly-coupled superconductors reanalyzed," *Physical Review B*, vol. 12, no. 3, pp. 905–922, 1975.
- [55] W. L. McMillan, "Transition temperature of strongly-coupled superconductors," *Physical Review*, vol. 167, no. 2, pp. 331–344, 1968.
- [56] I. I. Mazin, M. D. Johannes, L. Boeri, K. Koepernik, and D. J. Singh, "Problems with reconciling density functional theory calculations with experiment in ferropnictides," *Physical Review B*, vol. 78, no. 8, Article ID 085104, 2008.
- [57] A. N. Yaresko, G.-Q. Liu, V. N. Antonov, and O. K. Andersen, "Interplay between magnetic properties and Fermi surface nesting in iron pnictides," *Physical Review B*, vol. 79, no. 14, Article ID 144421, 2009.
- [58] S. Sharma, J. K. Dewhurst, S. Shallcross, et al., "Magnetic properties of LaO<sub>1-x</sub>F<sub>x</sub>FeAs," <http://arxiv.org/abs/0810.4278>.

## Review Article

# Polaron Mass and Electron-Phonon Correlations in the Holstein Model

**Marco Zoli**

*Dipartimento di Fisica, Università di Camerino, 62032 Camerino, Italy*

Correspondence should be addressed to Marco Zoli, zoli.marco@libero.it

Received 25 May 2009; Accepted 26 July 2009

Academic Editor: Sasha Alexandrov

Copyright © 2010 Marco Zoli. This is an open access article distributed under the Creative Commons Attribution License, which permits unrestricted use, distribution, and reproduction in any medium, provided the original work is properly cited.

The Holstein Molecular Crystal Model is investigated by a strong coupling perturbative method which, unlike the standard Lang-Firsov approach, accounts for retardation effects due to the spreading of the polaron size. The effective mass is calculated to the second perturbative order in any lattice dimensionality for a broad range of (anti)adiabatic regimes and electron-phonon couplings. The crossover from a large to a small polaron state is found in all dimensionalities for adiabatic and intermediate adiabatic regimes. The phonon dispersion largely smoothes such crossover which is signalled by polaron mass enhancement and on-site localization of the correlation function. The notion of self-trapping together with the conditions for the existence of light polarons, mainly in two- and three-dimensions, is discussed. By the imaginary time path integral formalism I show how nonlocal electron-phonon correlations, due to dispersive phonons, renormalize downwards the  $e$ - $ph$  coupling justifying the possibility for light and essentially small 2D Holstein polarons.

## 1. Introduction

The interest for phonons and lattice distortions in High-Temperature Superconductors (HTSc) is today more than alive [1, 2]. While the microscopic origin of the pairing mechanism in cuprate HTSc has not yet been unravelled, evidence has been provided [3–8] that electron-lattice interactions and local lattice fluctuations are correlated with the onset of the superconducting transition [9–11]. Recent investigations [12] would suggest a similar role for the lattice also in the newly discovered layered pnictide-oxide quaternary superconducting compounds [13–15]. In fact, the discovery of HTSc in copper oxides [16] was motivated by the knowledge that the Jahn-Teller effect [17–19] is strong in  $\text{Cu}^{2+}$ . In nonlinear molecules a lattice distortion lifts the degeneracy of the electronic states and lowers the overall ground state energy: the energy gain is the Jahn-Teller stabilization energy which can be measured optically. As vibrational and electronic energies are of the same order, the nuclear motion cannot be separated from the electrons and the combined electron-lattice object becomes a mobile Jahn-Teller polaron [20] which can be described

in terms of the nonlinear Holstein Hamiltonian [21]. Over the last twenty years, the focus on the HTSc has largely contributed to trigger the study of the polaron properties [22–25]. Earlier and more generally, polarons had become a significant branch in condensed matter physics [26–29] as Landau introduced the concept of an electron which can be trapped by digging its own hole in an ionic crystal [30]. A strong coupling of the electron to its own lattice deformation implies violation of the Migdal theorem [31] and polaron collapse of the electron band [32] with the appearance of time retarded interactions in the system. A great advance in the field came after Feynman used the path integrals [33] to calculate energy and effective mass of the Fröhlich polaron [34, 35] by a variational method [36]. In the statistical path integral, the quantum mechanical electron motion is represented by a real space path  $\mathbf{x}(\tau)$  being function of an imaginary time  $\tau$  whose range has an upper bound given by the inverse temperature. As a key feature of the Feynman treatment, the phonon degrees of freedom can be integrated out exactly (being the action quadratic and linear in the oscillator coordinates) but leave a substantial trace as a time retarded potential naturally emerges in the

exact integral action. *The electron, at any imaginary time, interacts with its position at a past time.* This self interaction mirrors the fact that the lattice needs some time to readjust to the deformation induced by the electron motion and follow it. For decades, the Fröhlich polaron problem has been extensively treated by path integral techniques [37–39] which, remarkably, can be applied for any value of the coupling constant [40]. A review work on the Fröhlich polaron is in [41].

With regard to small polarons, path integral investigations started with the groundbreaking numerical work by De Raedt and Legendijk [42–44] who derived fundamental properties for the Holstein polaron. While a sizable electron-phonon coupling is a requisite for polaron formation [45–47], also the dimensionality and degree of adiabaticity of the physical system could essentially determine the stability and behavior of the polaron states [48–62]. When the characteristic phonon energy is smaller than the electronic energy the system is set in the adiabatic regime. In materials such as the HTSc, colossal magnetoresistance oxides [63–65], organic molecular crystals [66], DNA molecules [67, 68] and finite quantum structures [69, 70], intermediate adiabatic polarons are relevant as carriers are strongly coupled to high energy optical phonons. For the HTSc systems, a path integral description had been proposed for polaron scattering by anharmonic potentials, due to lattice structure instabilities, as a possible mechanism for the nonmetallic behavior of the  $c$ -axis resistivity [71, 72].

It has been questioned whether small (bi)polarons could indeed account for high  $T_c$  due to their large effective mass [73] but, later on, it was recognized that dispersive phonons renormalize the effective coupling in the Holstein model yielding much lighter masses [74]. Also long range Fröhlich  $e$ - $ph$  interactions provide a pairing mechanism and bipolaron mass consistent with high  $T_c$  [75–78] while accounting, among others, for angle-resolved photoemission spectroscopy data in cuprates HTSc [79, 80].

In view of the relevance of the polaron mass issue, I review in this article some work [81] on the Holstein polaron *with dispersive phonons* which examines the notion of self-trapping and estimates some polaron properties in the parameter space versus lattice dimensionality. The latter is introduced in the formalism by modelling the phonon spectrum through a force constant approach which weighs the first neighbors intermolecular shell. This is done in the spirit of the work by Holstein [82] on the small polaron motion for a one-dimensional narrow band system. Calculating the polaron hopping between localized states due to multiphonon scattering processes in perturbation theory, Holstein first pointed out that the phonon dispersion was in fact *a vital ingredient of the theory* whereas a dispersionless spectrum would yield a meaningless divergent hopping probability. Time dependent perturbative theory, the hopping integral being the perturbation, applies as long as the *interaction time* is shorter than the polaron lifetime on a state. Computing the time integral for the hopping probability, I had earlier shown [53] that such interaction time is shorter in higher dimensionality thus making the time dependent perturbative method more appropriate

in the latter conditions. For a given dimensionality, the interaction time is also reduced by increasing the strength of the intermolecular forces hence, the phonon dispersion. Consistently also the crossover temperature between band-like motion (at low  $T$ ) and hopping motion (at high  $T$ ) [83] shifts upwards, along the  $T$  axis, in higher dimensional systems with larger coordination numbers. Hopping polaron motion is the relevant transport mechanism in several systems including DNA chains [84, 85].

It is worth emphasizing that our previous investigations on the Holstein polaron and the present paper assume dimensional effects as driven by the lattice while the electron transfer integral is a scalar quantity. In a different picture, first proposed by Emin [86] for quasi 1D solids in the adiabatic limit and recently generalized by variational exact diagonalization techniques [87], the electron transfer integral is instead a vector whose components are switched on in order to treat anisotropic polaron properties. The system dimensionality is then increased by tuning the electronic subsystem parameters, the 3D case corresponding to an isotropic hopping integral, whereas the phonon spectrum is dispersionless. While the method to introduce the system dimensionality in [87] differs from ours, some trends regarding the polaron mass in 1D and 3D are apparently at variance with ours as it will be pointed out in the following discussion.

Being central to polaron studies, the effective mass behavior ultimately reflects the abovementioned property of the polaron problem: when the electron moves through the lattice, it induces and drags a lattice deformation which however does not follow instantaneously, the retardation causing a spread in the size of the quasiparticle. The electron-phonon correlation function provides a measure of the deformation around the instantaneous position of the electron and may be used to quantify the polaron size. Several refined theoretical tools, including quantum Monte Carlo calculations [42], density matrix renormalization group [88], variational methods [89, 90] and exact diagonalization techniques [91, 92] have been applied to the Holstein Hamiltonian to compute such polaron characteristics covering various regimes of electron-phonon coupling and adiabatic ratio. While a qualitative and often quantitative [88, 89] agreement among several numerical methods has emerged especially with regard to ground state polaron properties, we feel that analytical investigations may provide a useful insight also in the specific regime of intermediate adiabaticity and  $e$ - $ph$  coupling for which the leading orders of perturbation theory traditionally fail in the weak coupling [93] or become less accurate in the strong coupling [94, 95].

Extremely interesting is that range of  $e$ - $ph$  couplings which are sufficiently strong to allow for polaron formation but not too strong to prevent the polaron from moving through the lattice. When the relevant energy scales for electrons and phonons are not well separated, such range of couplings produces a composite particle which is not trapped by its lattice deformation. It is this intermediate regime which forms the focus of the present work.

The retardation effect and its consequences are here treated by means of a variational analytical method based

on the Modified Lang Firsov (MLF) transformation [96] which considerably improves the standard Lang Firsov (LF) [97] approach on which strong coupling perturbation theory (SCPT) is based. Section 2 provides the generalities of the MLF method applied to the dispersive Holstein Hamiltonian. In Section 3, the polaron mass is calculated in the (anti)adiabatic regimes covering a broad range of cases in parameter space. The spreading of the adiabatic polaron size over a few lattice sites is shown in Section 4 through computation of the electron-phonon correlations. In Section 5, I give further physical motivations for the existence of light Holstein polarons: using a path-integral method, I show how the electron-phonon coupling is renormalized downwards in momentum space by nonlocal correlations arising from the dispersive nature of the phonon spectrum. Some final remarks are in Section 6.

## 2. Modified Lang-Firsov Method

The Holstein diatomic molecular model was originally cast [21] in the form of a discrete nonlinear Schrödinger equation for electrons whose probability amplitude at a molecular site depends on the interatomic vibration coordinates [98]. The nonlinearities are tuned by the electron-phonon coupling  $g$ , whose strength drives the crossover between a *large* and a *small* polaron for a given value of the adiabatic parameter. The polaron radius is measured with respect to the lattice constant [99, 100]. When the size of the lattice distortion is of the same order of (or less than) the lattice constant the polaron has a small radius and the discreteness of the lattice must be taken into account.

In second quantization the dimension dependent Holstein Hamiltonian with dispersive harmonic optical phonons reads

$$H = -t \sum_{\langle ij \rangle} c_i^\dagger c_j + g \sum_i n_i (b_i^\dagger + b_i) + \sum_{\mathbf{q}} \omega_{\mathbf{q}} b_{\mathbf{q}}^\dagger b_{\mathbf{q}}, \quad (1)$$

where  $t$  is the hopping integral and the first sum is over  $z$  nearest neighbors.  $c_i^\dagger$  and  $c_i$  are the real space electron creation and annihilation operators at the  $i$ -site,  $n_i (= c_i^\dagger c_i)$  is the number operator,  $b_i^\dagger$  and  $b_i$  are the phonons creation and annihilation operators.  $b_{\mathbf{q}}^\dagger$  is the Fourier transform of  $b_i^\dagger$  and  $\omega_{\mathbf{q}}$  is the frequency of the phonon with vector momentum  $\mathbf{q}$ . Unlike the Su-Schrieffer-Heeger Hamiltonian [101, 102] a paradigmatic model in polymer physics, in (1) the electron hopping does not depend on the relative displacement between adjacent molecular sites hence, the phonon created by  $b_i^\dagger$  is locally coupled to the electronic density.

The LF transformation uses a phonon basis of fixed displacements (at the electron residing site) which diagonalizes the Hamiltonian in (1) in absence of hopping. The hopping term is then treated as a perturbation [74, 94]. However the standard LF approach does not account for the retardation between the electron and the lattice deformations which induces a spread in the size of the polaron. Precisely this effect becomes important for the intermediate  $e$ - $ph$  coupling values which may be appropriate for some HTSc.

The idea underlying the MLF transformation [103] is that to consider the displacements of the oscillators *at different sites* around an electron in order to describe the retardation effect. For the present case of dispersive phonon the MLF transformation, applied to the Hamiltonian in (1), reads

$$\begin{aligned} \tilde{H} &= e^S H e^{-S}, \\ S &= \sum_{\mathbf{q}} \lambda_{\mathbf{q}} n_{\mathbf{q}} (b_{-\mathbf{q}}^\dagger - b_{\mathbf{q}}), \\ n_{\mathbf{q}} &= \frac{1}{\sqrt{N}} \sum_i n_i e^{-i\mathbf{q} \cdot \mathbf{R}_i} = \frac{1}{\sqrt{N}} \sum_{\mathbf{k}} c_{\mathbf{k}+\mathbf{q}}^\dagger c_{\mathbf{k}}, \end{aligned} \quad (2)$$

where  $\mathbf{R}_i$  are the lattice vectors, and  $\lambda_{\mathbf{q}}$  are the variational parameters which represent the shifts of the equilibrium positions of the oscillators (quantized ion vibrations) with momentum  $\mathbf{q}$ . The conventional Lang-Firsov transformation is recovered by setting  $\lambda_{\mathbf{q}} = g/\omega_{\mathbf{q}}$ .

Explicitly, the MLF transformed Holstein Hamiltonian in (2) is

$$\begin{aligned} \tilde{H} &= -\epsilon_p \sum_i n_i - t_p \sum_{ij} c_i^\dagger c_j \\ &\times \exp \left[ \frac{1}{\sqrt{N}} \sum_{\mathbf{q}} \lambda_{\mathbf{q}} b_{\mathbf{q}}^\dagger (e^{i\mathbf{q} \cdot \mathbf{R}_i} - e^{i\mathbf{q} \cdot \mathbf{R}_j}) \right] \\ &\times \exp \left[ -\frac{1}{\sqrt{N}} \sum_{\mathbf{q}} \lambda_{\mathbf{q}} b_{\mathbf{q}} (e^{-i\mathbf{q} \cdot \mathbf{R}_i} - e^{-i\mathbf{q} \cdot \mathbf{R}_j}) \right] \\ &+ \sum_{\mathbf{q}} \omega_{\mathbf{q}} b_{\mathbf{q}}^\dagger b_{\mathbf{q}} + \sum_{\mathbf{q}} (g - \lambda_{\mathbf{q}} \omega_{\mathbf{q}}) n_{\mathbf{q}} (b_{-\mathbf{q}}^\dagger + b_{\mathbf{q}}), \end{aligned} \quad (3)$$

where the polaron self-energy  $\epsilon_p$  is

$$\epsilon_p = \frac{1}{N} \sum_{\mathbf{q}} (2g - \lambda_{\mathbf{q}} \omega_{\mathbf{q}}) \lambda_{\mathbf{q}}, \quad (4)$$

and the polaronic hopping is

$$\begin{aligned} t_p &= t \exp \left[ -\frac{1}{N} \sum_{\mathbf{q}} \lambda_{\mathbf{q}}^2 \left( 1 - \frac{\gamma_{\mathbf{q}}}{z} \right) \right], \\ \gamma_{\mathbf{q}} &= 2 \sum_{i=x,y,z} \cos q_i. \end{aligned} \quad (5)$$

The coordination number  $z$  is twice the system dimensionality.

Looking at (3), it is clear that the unperturbed Hamiltonian  $H_0$  can be taken as

$$H_0 = -\epsilon_p \sum_i n_i + \sum_{\mathbf{q}} \omega_{\mathbf{q}} b_{\mathbf{q}}^\dagger b_{\mathbf{q}}, \quad (6)$$

while the remaining part of the Hamiltonian ( $\tilde{H} - H_0$ ) in the MLF basis is considered as the perturbation part.

The energy eigenstates of  $H_0$  are given by

$$|\phi_i, \{n_{\mathbf{q}}\}\rangle = c_i^\dagger |0\rangle_e |n_{\mathbf{q}_1}, n_{\mathbf{q}_2}, n_{\mathbf{q}_3}, \dots\rangle_{ph}, \quad (7)$$

where  $i$  is the electron site, and  $n_{\mathbf{q}_1}$ ,  $n_{\mathbf{q}_2}$ , and  $n_{\mathbf{q}_3}$  are the phonon occupation numbers in the phonon momentum states  $\mathbf{q}_1$ ,  $\mathbf{q}_2$ , and  $\mathbf{q}_3$ , respectively. The lowest energy eigenstate of the unperturbed Hamiltonian has no phonon excitations, that is,  $n_{\mathbf{q}} = 0$  for all  $\mathbf{q}$ . The ground state has an energy  $E_0^0 = -\epsilon_p$  and is  $N$ -fold degenerate, where  $N$  is the number of sites in the system. The perturbation lifts the degeneracy, and to first order in  $t$  the ground state energy of the 3D-polaron with momentum  $\mathbf{k}$  is given by

$$E_0(\mathbf{k}) = -\epsilon_p - t_p \gamma_{\mathbf{k}}. \quad (8)$$

The second-order correction to the ground-state energy of the polaron with momentum  $\mathbf{k}$  is given by

$$E_0^{(2)}(\mathbf{k}) = \sum_{\mathbf{k}'} \sum_{\{n_{\mathbf{q}}\}} \frac{1}{\sum_{\mathbf{q}} n_{\mathbf{q}} \omega_{\mathbf{q}}} \times \left| \langle \{n_{\mathbf{q}}\}, \mathbf{k}' \mid \tilde{H} - H_0 \mid \mathbf{k}, \{0\} \rangle \right|^2, \quad (9)$$

where, in principle, intermediate states having all possible phonon numbers contribute to (9).

By minimizing the zone center ground state energy, the variational parameters  $\lambda_{\mathbf{q}}$  are obtained as

$$\lambda_{\mathbf{q}} = \frac{g}{\omega_{\mathbf{q}} + z t_p (1 - \gamma_{\mathbf{q}}/z)}, \quad (10)$$

and, by (10), the one phonon matrix element between the ground state  $|\mathbf{k} = \mathbf{0}, \{n_{\mathbf{q}} = 0\}\rangle$  and the first excited state  $\langle 1_{\mathbf{q}}, \mathbf{k}' \mid$  vanishes. Then, the one phonon excitation process yields no contribution to (9). By (10) one gets the  $\lambda_{\mathbf{q}}$ 's for the 1D, 2D, and 3D systems and, via (5), the narrowing of the polaron band [104].

### 3. Polaron Mass

Given the formal background, the polaron mass is calculated both for the Lang-Firsov and for the Modified Lang-Firsov method to the second order in SCPT. Generally the second order correction (i) makes a relevant contribution to the ground state energy, (ii) does not affect the bandwidth, (iii) introduces the mass dependence on the adiabatic parameter which would be absent in the first order. Altogether the polaron landscape introduced by the second order SCPT is much more articulated than the simple picture suggested by the first order of SCPT which nonetheless retains its validity towards the antiadiabatic limit. In first order SCPT, ground state energy, bandwidth, and effective mass appear as equivalent, interchangeable properties to describe the polaron state while band narrowing and abrupt mass enhancement are *coincident* signatures of small polaron formation in parameter space. However, there is no compelling physical reason for such coincidence to occur as the bandwidth is in fact a zone edge quantity whereas the effective mass is a zone center quantity. Thus, by decoupling onset of the band narrowing and self trapping of the polaron mass, the second

order of SPCT provides the framework for a richer polaron structure in momentum space.

As emphasized in Section 1, dispersive phonons have a relevant role in the Holstein model: a dispersionless spectrum would in fact predict *larger polaron bandwidths in lower dimensionality* and yield a *divergent site jump probability* for the small polaron in time dependent perturbation theory [82, 105]. Here, a lattice model is assumed in which first neighbors molecular sites interact through a force constants pair potential. Then, the optical phonon spectrum is given in 1D, 2D (square lattice), and 3D (simple cubic lattice), respectively, by

$$\omega_{1D}^2(\mathbf{q}) = \frac{\alpha + \gamma}{M} + \frac{1}{M} \sqrt{\alpha^2 + 2\alpha\gamma \cos q + \gamma^2},$$

$$\omega_{2D}^2(\mathbf{q}) = \frac{\alpha + 2\gamma}{M} + \frac{1}{M} \sqrt{\alpha^2 + 2\alpha\gamma g(\mathbf{q}) + \gamma^2(2 + h(\mathbf{q}))},$$

$$\omega_{3D}^2(\mathbf{q}) = \frac{\alpha + 3\gamma}{M} + \frac{1}{M} \sqrt{\alpha^2 + 2\alpha\gamma j(\mathbf{q}) + \gamma^2(3 + l(\mathbf{q}))},$$

$$g(\mathbf{q}) = \cos q_x + \cos q_y,$$

$$h(\mathbf{q}) = 2 \cos(q_x - q_y),$$

$$j(\mathbf{q}) = \cos q_x + \cos q_y + \cos q_z,$$

$$l(\mathbf{q}) = 2 \cos(q_x - q_y) + 2 \cos(q_x - q_z) + 2 \cos(q_y - q_z), \quad (11)$$

where  $\alpha$  is the intramolecular force constant and  $\gamma$  is the intermolecular first neighbors force constant.  $M$  is the reduced molecular mass. Thus, the intra- and intermolecular energies are  $\omega_0 = \sqrt{2\alpha/M}$  and  $\omega_1 = \sqrt{\gamma/M}$ , respectively. Some care should be taken in setting the phonon energies as the second order perturbative term grows faster than the first order by increasing  $\omega_1$  [74]. Hence too large dispersions may cause a breakdown of the SCPT. In terms of  $\omega_0$ , the dimensionless parameter  $zt/\omega_0$  defines the adiabatic ( $zt/\omega_0 > 1$ ) and the antiadiabatic ( $zt/\omega_0 < 1$ ) regime. Some other choices are found in literature with  $t/\omega_0 > 1$  or  $t/\omega_0 > 1/4$  defining the adiabatic regime. As shown below, such discrepancies may lead to significantly different interpretations of the polaron behavior in parameter space mainly for higher dimensions.

Hereafter I take  $\omega_0 = 100$  meV and tune  $t$  to select a set of  $zt/\omega_0$  which sample both antiadiabatic and adiabatic regime without reaching the adiabatic limit. The dynamics of the lattice is in fact central to our investigation. A *moderate to strong* range of  $e$ - $ph$  couplings is assumed ( $g/\omega_0 \gtrsim 1$ ) so that the general conditions for polaron formation are fulfilled throughout the range of adiabatic ratios [22, 95].

Figure 1 plots the ratio of the one-dimensional polaron mass to the bare band mass, against the  $e$ - $ph$  coupling, calculated both in the Lang-Firsov scheme and in the Modified Lang-Firsov expression. The intermediate regime  $2t = \omega_0$  is assumed in Figure 1(a). While at very strong couplings the MLF plots converge towards the LF predictions, a remarkably different behavior between the LF and the MLF mass shows up for moderate  $g$ . The LF method overestimates the polaron

mass for  $g \in [\sim 1 - 2]$ , and mostly, it does not capture the rapid mass increase found instead in the MLF description. Note that, around the crossover, the MLF polaron mass is of order ten times the bare band mass choosing  $\omega_1 = 60$  meV. Large intermolecular energies enhance the phonon spectrum thus reducing the effective masses in both methods. In the MLF method, large  $\omega_1$  tend also to smooth the mass behavior in the crossover region.

Figure 1(b) presents the case of an adiabatic regime: the discrepancies between LF and MLF plots are relevant for a broad range of  $e$ - $ph$  couplings. The latter is more extended for larger intermolecular energies as also seen in Figure 1(a). Mass renormalization is poor in the MLF curves up to the crossover which is clearly signalled by a sudden *although continuous* mass enhancement whose abruptness is significantly smoothed for the largest values of intermolecular energies.

Figure 1(c) shows a fully antiadiabatic case in which the LF and MLF plots practically overlap throughout the whole range of couplings. This confirms that the LF method is appropriate in the antiadiabatic limit which is essentially free from retardation effects. Unlike the previous cases the MLF plots are always smooth versus  $g$  indicating that no *self-trapping* event occurs in the antiadiabatic regime. Here the polaron does not trap as it is always small for the whole range of couplings.

It should be reminded that the concept of *self-trapping* traditionally indicates an abrupt transition between an infinite size state at weak  $e$ - $ph$  couplings and a finite (small) size polaron at strong  $e$ - $ph$  couplings. In one-dimension, according to the traditional adiabatic polaron theory [106–108], the polaron solution is always the ground state of the system and no self-trapping occurs. Instead, in higher dimensionality a minimum coupling strength is required to form finite size polarons, hence self-trapped polarons can exist at couplings larger than that minimum.

However, these conclusions have been critically reexamined in the recent polaron literature and the same notion of *polaron size* has been questioned due to the complexity of the polaron quasiparticle itself [109, 110]. Certainly, as a shrinking of the polaron size yields a weight increase, the polaron mass appears as the most reliable indicator of the self-trapping transition. The latter, as the results in Figure 1 suggest, is rather a crossover essentially dependent on the degree of adiabaticity of the system and crucially shaped by the internal structure of the phonon cloud which I have modelled by tuning the intermolecular forces. In this view, self trapping events can be found also in the parameter space of 1D systems. This amounts to say that also finite size polarons can self-trap if a sudden, although continuous, change in their effective mass occurs for some values of the  $e$ - $ph$  couplings in some portions of the intermediate/adiabatic regime. The continuity of such event follows from the fact that the ground state energy is analytic function of  $g$  for optical phonon dispersions [111]; hence the possibility of phase transitions is ruled out in the Holstein model. At finite temperature phase transitions cannot occur as the free energy is smooth for any phonon dispersion [112–114].

As fluctuations in the lattice displacements around the electron site are included in the MLF variational wavefunction, the calculated polaron mass should not display discontinuities by varying the Hamiltonian parameters through the crossover [115]. Mathematically the crossover points are selected through the simultaneous occurrence of a maximum in the first logarithmic derivative and a zero in the second logarithmic derivative of the MLF polaron mass with respect to the coupling parameter. Such inflection points, corresponding to the points of the most rapid increase for  $m^*$ , are marked in Figure 2 on the plots of the mass ratios computed for a broad range of (anti)adiabatic parameters both in one, two, and three dimensions.

In 1D, see Figure 2(a), the crossover occurs for  $g$  values between  $\sim 1.8$  and  $2.3$  and the corresponding self-trapped polaron masses are of order  $\sim 5$ – $50$  times the bare band mass thus suggesting that relatively light small polarons can exist in 1D molecular solids with high phonon spectrum. The onset of the self-trapping line is set at the intermediate value  $2t = \omega_0$  and the self-trapped mass values grow versus  $g$  by increasing the degree of adiabaticity. There is no self-trapping in the fully antiadiabatic regime as the electron and the dragged phonon cloud form a compact unit also at moderate  $e$ - $ph$  couplings. Then, the mass increase is always smooth in the antiadiabatic regime.

Some significant results are found in 2D as shown in Figure 2(b): (i) for a given  $g$  and adiabaticity ratio, the 2D mass is lighter than the 1D mass and the 2D LF limit is attained at a value which is roughly one order of magnitude smaller than in 1D; (ii) the crossover region is shifted upwards along the  $g$  axis with the self trapping events taking place in the range,  $g \sim 2.2$ – $2.6$ ; the masses are of order  $\sim 5$ – $10$  times the bare band mass; (iii) the line of self-trapping events changes considerably with respect to the 1D plot; the marked curve is parabolic in 2D with an extended descending branch starting at the intermediate value  $4t/\omega_0 = 1$ ; (iv) in the deep adiabatic regime, the lattice dimensionality smoothens the mass increase versus  $g$ .

This effect is even more evident in 3D, see Figure 2(c), as there are no signs of abrupt mass increase even for the largest values of the adiabatic parameter. At the crossover, 3D masses are of order  $\sim 5$ – $10$  times the bare band mass with the self trapping points lying in the range,  $g \sim 2.5$ – $2.9$ . At very large couplings the mass ratio becomes independent of  $t$  and converges towards the LF value. In this region (and for the choice  $\omega_1 = 60$  meV) the 3D Lang-Firsov mass is one order of magnitude smaller than the 2D mass. As the coordination number grows versus dimensionality, large intermolecular forces are more effective in hardening the 3D phonon spectrum thus leading to lighter 3D polaron masses than 2D ones.

The self trapping transition appears in Figure 2 as smoother in higher dimensions thus contradicting the trend found by previous investigations, markedly by exact diagonalization techniques [60, 87] and variational calculations [116]. Two reasons may be invoked to resolve the discrepancy, the first being more physical and the second more technical. (1) From (11), it can be easily seen that  $\omega_d^2[\mathbf{q} = (0, 0, 0)] - \omega_d^2[\mathbf{q} = (\pi, \pi, \pi)] = 2d\omega_1^2$ . Then, for

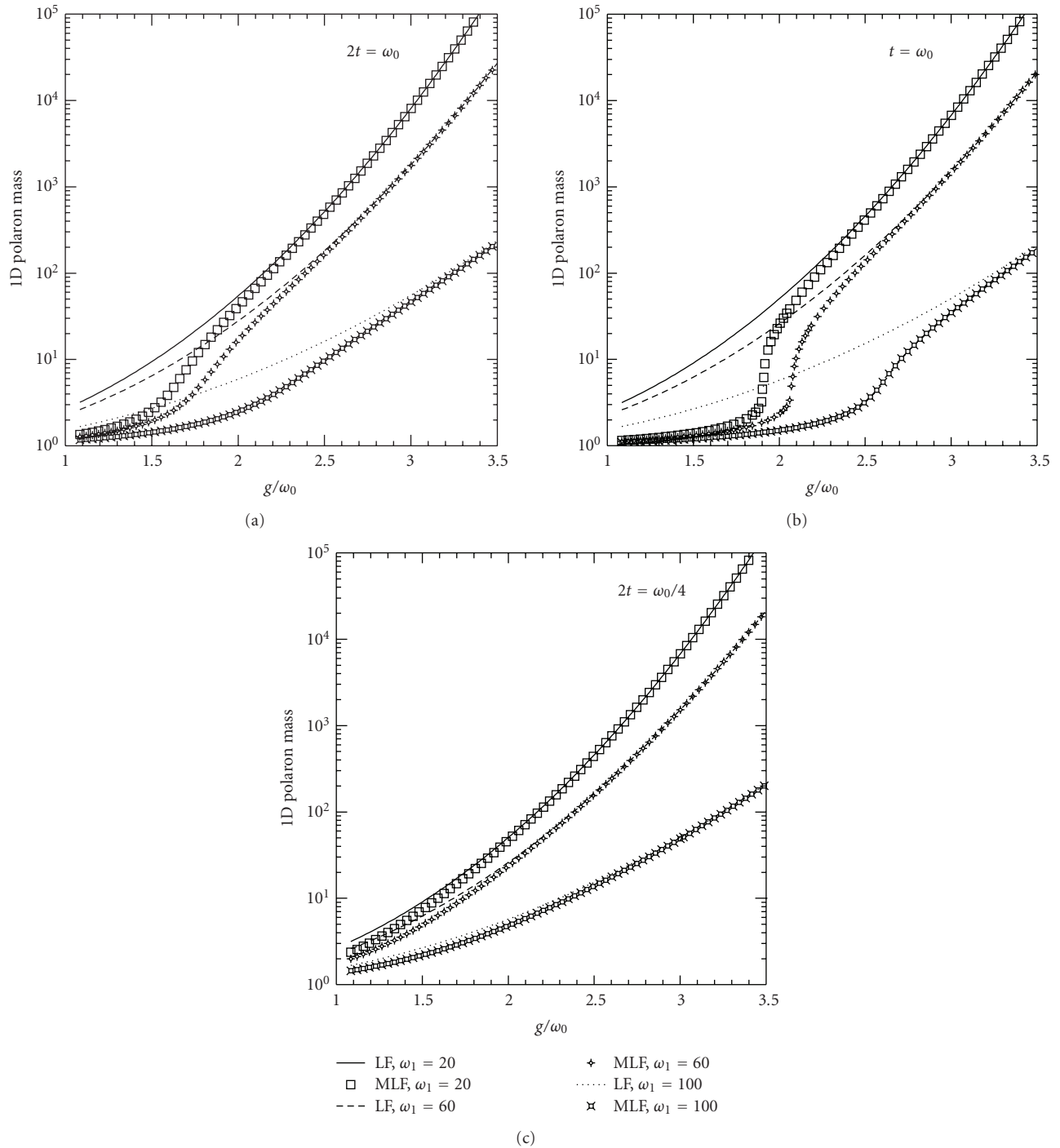


FIGURE 1: Ratio of the one-dimensional polaron mass to the bare band mass versus  $e$ - $ph$  coupling according to the Lang-Firsov and the Modified Lang-Firsov methods. The adiabatic parameter is set at (a) the intermediate value,  $2t/\omega_0 = 1$ ; (b) a fully adiabatic regime,  $2t/\omega_0 = 2$ ; and (c) an antiadiabatic regime,  $2t/\omega_0 = 0.25$ .  $\omega_0 = 100$  meV and  $\omega_1$  (in units meV) are the *intramolecular* and *intermolecular* energies of the diatomic molecular chain, respectively.

a given  $\omega_1$ , the phonon band is more dispersive in higher dimensionality  $d$ . Hence increasing the system dimension corresponds to attribute larger weight to the intermolecular forces which ultimately smoothen the crossover as made evident in Figure 1. (2) The works in [60, 87, 116] take  $t/\omega_0$

as adiabatic ratio in any dimension whereas our calculation spans the same range of  $zt/\omega_0$  values in any dimension. Thus, for instance, the fully adiabatic  $zt/\omega_0 = 3$  plots in Figure 2 would correspond to an antiadiabatic case in 3D ( $t/\omega_0 = 1/2$ ) and a slightly adiabatic case in 1D ( $t/\omega_0 = 3/2$ ) following the

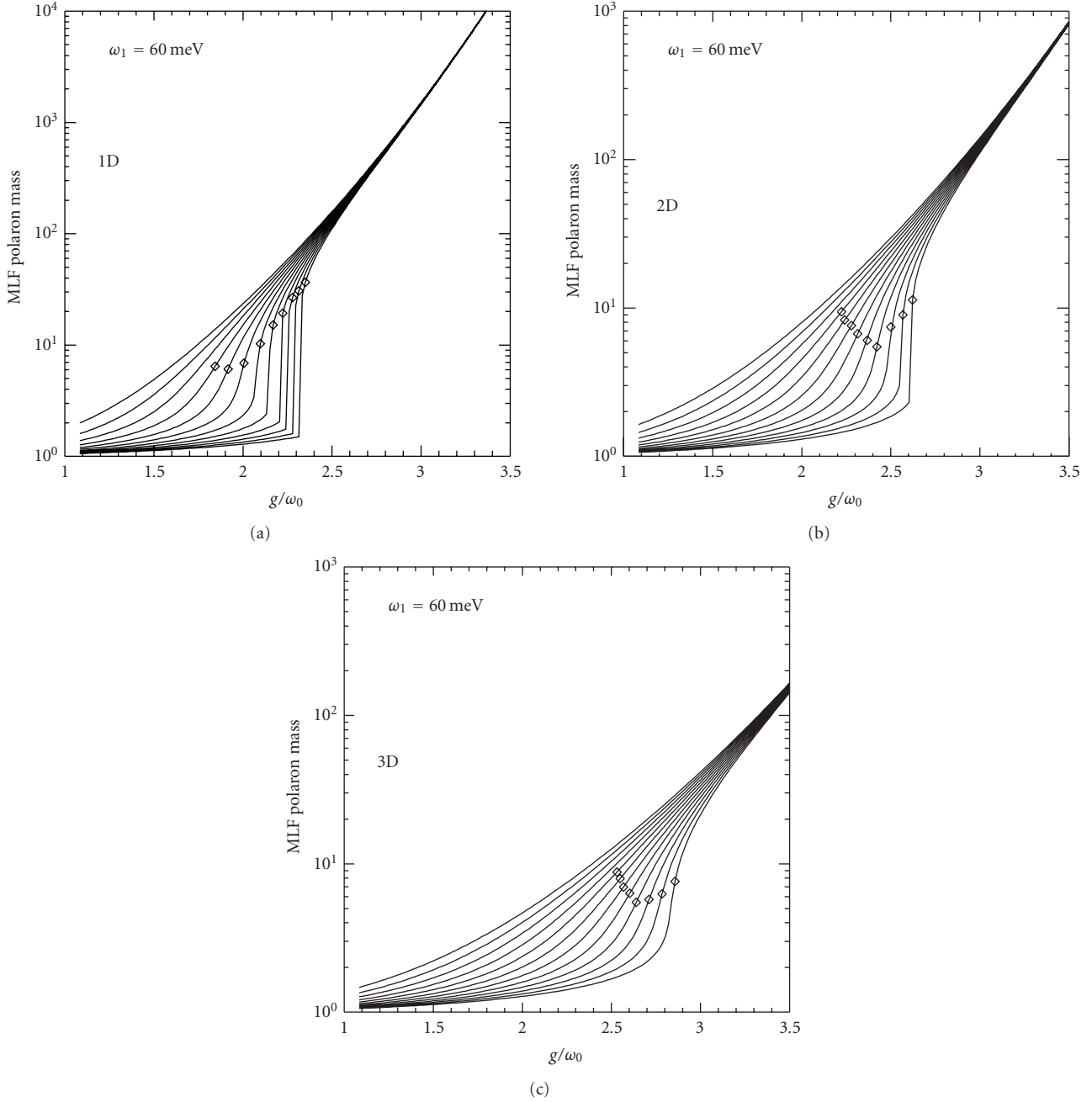


FIGURE 2: Ratio of the Modified Lang-Firsov polaron mass to the bare band mass versus  $e$ - $ph$  coupling in (a) 1D, (b) 2D, and (c) 3D. A set of twelve  $zt/\omega_0$  values ranging from the antiadiabatic to the adiabatic regime is considered. From left to right:  $zt/\omega_0 = 0.25, 0.5, 0.75, 1.0, 1.25, 1.5, 1.75, 2.0, 2.25, 2.5, 2.75, 3.0$ .  $\omega_0 = 100$  meV. The diamonds mark the occurrence of the self-trapping event.

definition in [60, 87, 116]. Consistently, the 3D *antiadiabatic* polaron mass is smoother than the 1D *adiabatic* polaron mass. Vice versa, assuming the same ratio, that is,  $t/\omega_0 = 1/2$ , one should compare the rightmost plot in Figure 2(c) with the fourth from left in Figure 2(a): the latter is smoother than the former as the 1D case is now antiadiabatic while the 3D case is fully adiabatic.

Nonetheless, the findings displayed in Figure 2 agree with density matrix renormalization group [88], variational Hilbert space [60] methods and weak coupling perturbation

theory [57] in predicting a lighter mass in higher dimensionality.

#### 4. Electron-Phonon Correlations

Within the MLF formalism one may also compute the electron-phonon correlation functions in the polaron ground state. This offers a measure of the polaron size as electron and phonons displacements can be taken at different neighbors sites. The on-site  $\chi_0$ , the first neighbor site  $\chi_1$

and the second neighbor site  $\chi_2$  correlation functions are plotted in Figure 3 against the  $e$ - $ph$  coupling both in 1D and 2D. For  $g \sim 1$ , there is some residual quasiparticle weight (not appreciable on this scale) associated with  $\chi_3$  and  $\chi_4$  which however tend to vanish by increasing the coupling. An adiabatic regime is assumed to point out the self-trapping event which occurs when  $\chi_0 \sim 1$  and  $\chi_n \sim 0$  for  $n \geq 1$ . This happens for  $g \sim 2$  in 1D and  $g \sim 2.5$  in 2D for the lowest case of  $\omega_1$  here considered. By studying the correlation functions for two values of  $\omega_1$  it is seen how the intermolecular forces smooth the crossover and extend the polaron size over a larger range of  $g$ . The case  $\omega_1 = 60$  meV, which allows a comparison with Figure 2, is intermediate between the two plots presented in Figure 3. In such case the self trapping appears at  $g \sim 2.3$  in 1D in fair agreement with the corresponding inflection point in the 1D effective mass (see fifth curve from right in Figure 2(a)). In 2D the polaron size shrinks at slightly larger  $g$  than in 1D and the on-site localization occurs at  $g$  somewhat larger than the mass inflection point.

Altogether the diamond marked loci displayed in Figure 2 indicate that strong mass renormalization is accompanied by on-site (or two sites) polaron localization thus identifying the self trapping line with the formation of small polarons. Before the crossover takes place, for instance, at  $1 \leq g \leq 2$  in Figure 3(a), the 1D polaron spreads over a few (two to four) lattice sites. This is the also the range of couplings in which the polaron band shows the largest deviations [91] from the cosine-like band of standard LF perturbation theory [94] due to the importance of longer (than nearest neighbors) hopping processes. The notion of *intermediate polaron* seems to us as the most appropriate for such mobile and relatively light objects.

## 5. Path Integral Method

The results obtained so far can be put on sound physical bases by applying the space-time path integral method to the dispersive Holstein Hamiltonian. The method permits to incorporate the effect of the electron-phonon correlations in a momentum dependent effective  $e$ - $ph$  coupling.

The phonons operators in (1) can be generally written in terms of the isotropic displacement field  $u_n$  as

$$b_i^\dagger + b_i = \frac{1}{N} \sum_{\mathbf{q}} \sqrt{2M\omega(\mathbf{q})} \sum_n \exp(i\mathbf{q} \cdot (\mathbf{R}_i - \mathbf{R}_n)) u_n. \quad (12)$$

Then, the  $e$ - $ph$  term in (1) transforms as follows:

$$H^{e-ph} = \frac{g}{N} \sum_{\mathbf{q}} \sqrt{2M\omega(\mathbf{q})} \sum_{i,n} c_i^\dagger c_i u_n \exp(i\mathbf{q} \cdot (\mathbf{R}_i - \mathbf{R}_n)). \quad (13)$$

The sum over  $n$  spans all  $n$ th neighbors of the  $\mathbf{R}_i$  lattice site in any dimensionality. It is clear that the phonon dispersion introduces  $e$ - $ph$  real space correlations which would be absent in a dispersionless model. Note that (13) contains the same physics as the  $e$ - $ph$  term in (1). Fourier transforming the atomic displacement field and taking the

lattice constant  $|\mathbf{a}| = 1$ , from (13), I get for a linear chain and a square lattice, respectively:

$$\begin{aligned} H_d^{e-ph} &= \frac{g}{N^{3/2}} \sum_i c_i^\dagger c_i \sum_{\mathbf{q}, \mathbf{q}'} \sqrt{2M\omega(\mathbf{q})} \exp(i\mathbf{q}' \cdot \mathbf{R}_i) \\ &\quad \times u_{\mathbf{q}'} S_d(\mathbf{q}' - \mathbf{q}), \\ S_{1D}(q' - q) &\equiv 1 + 2 \sum_{n=1}^{n^*} \cos(n(q' - q)), \\ S_{2D}(\mathbf{q}' - \mathbf{q}) &\equiv 1 + 2 \sum_{n=1}^{n^*} \left[ \cos(n\Delta q_x) + \cos(n\Delta q_y) \right] \\ &\quad + 2 \sum_{m,n=1}^{n^*} \left[ \cos(m\Delta q_x + n\Delta q_y) \right. \\ &\quad \left. + \cos(m\Delta q_x - n\Delta q_y) \right], \\ \Delta q_x &\equiv q'_x - q_x, \\ \Delta q_y &\equiv q'_y - q_y. \end{aligned} \quad (14)$$

While, in principle, the sum over  $n$  should cover all the  $N$  sites in the lattice, the cutoff  $n^*$  permits to monitor the behavior of the coupling term as a function of the range of the  $e$ - $ph$  correlations. In particular, in 1D the integer  $n$  numbers of the neighbors shells up to  $n^*$  while in the square lattice, the  $n^* = 1$  term includes the second neighbors shell, the sum up to  $n^* = 2$  includes the fifth neighbors shells,  $n^* = 3$  covers the ninth shell, and so on. Switching off the interatomic forces,  $\omega(\mathbf{q}) = \omega_0$ , one would recover from (14) a local  $e$ - $ph$  coupling model with  $S_d \equiv 1$ . As no approximation has been done at this stage (14) is general.

*5.1. Semiclassical Holstein Model.* I apply to the Holstein Hamiltonian space-time mapping techniques [117–119] to write the general path integral for an electron particle in a bath of dispersive phonons. The method has been used to treat also  $e$ - $ph$  polymer models [120, 121] in which the electron hopping causes a *shift* in the atomic displacements and, as a consequence, the vertex function depends on both the electronic and the phononic wave vector. Such *shift* is however absent in the Holstein model as (1) makes clear [122, 123].

I introduce  $\mathbf{x}(\tau)$  and  $\mathbf{y}(\tau')$  as the electron coordinates at the  $i$  and  $j$  lattice sites, respectively, and the electronic Hamiltonian (first term in (1)) transforms into

$$H^e(\tau, \tau') = -t \left( c^\dagger(\mathbf{x}(\tau)) c(\mathbf{y}(\tau')) + c^\dagger(\mathbf{y}(\tau')) c(\mathbf{x}(\tau)) \right), \quad (15)$$

where  $\tau$  and  $\tau'$  are continuous variables ( $\in [0, \beta]$ ) in the Matsubara Green's functions formalism with  $\beta$  being the inverse temperature hence the electron hops are not constrained to first neighbors sites. After setting  $\tau' = 0$ ,  $\mathbf{y}(0) \equiv 0$ , the electron operators are thermally averaged over the ground state of the Hamiltonian. As a result, the average

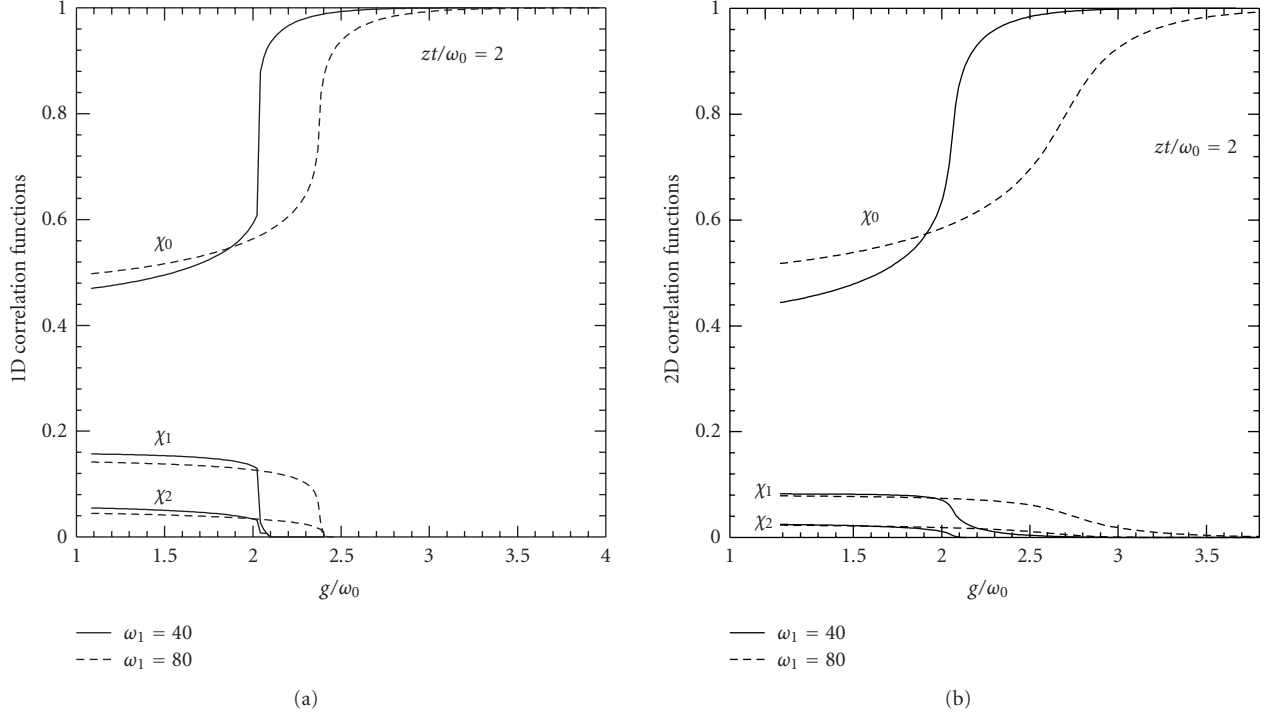


FIGURE 3: Electron-phonon correlation functions: on-site  $\chi_0$ , first neighbor site  $\chi_1$  and second neighbor site  $\chi_2$  versus  $e$ - $ph$  coupling in (a) 1D and (b) 2D. An adiabatic regime is considered and two values of intermolecular energy are assumed.

energy per lattice site,  $h^e(\tau) \equiv \langle H^e(\tau) \rangle / N$ , associated to electron hopping reads (in  $d$  dimensions):

$$h^e(\tau) = -t(G[-\mathbf{x}(\tau), -\tau] + G[\mathbf{x}(\tau), \tau]),$$

$$G[\mathbf{x}(\tau), \tau] = \frac{1}{\beta} \int \frac{d\mathbf{k}}{\pi^d} \exp[i\mathbf{k} \cdot \mathbf{x}(\tau)] \sum_n \frac{\exp(-i\hbar\nu_n\tau)}{i\hbar\nu_n - \epsilon_{\mathbf{k}}}, \quad (16)$$

where  $\nu_n$  are the fermionic Matsubara frequencies and  $\epsilon_{\mathbf{k}}$  is the electron dispersion relation.

Consider now the  $e$ - $ph$  term. The spatial  $e$ - $ph$  correlations contained in (14) are mapped onto the time axis introducing the  $\tau$  dependence in the displacement field:  $u_{\mathbf{q}} \rightarrow u_{\mathbf{q}}(\tau)$ . Assuming periodic atomic particle paths:  $u_{\mathbf{q}}(\tau + \beta) = u_{\mathbf{q}}(\tau)$ , the displacement is expanded in  $N_F$  Fourier components:

$$u_{\mathbf{q}}(\tau) = u_o + \sum_{n=1}^{N_F} 2 \left( (\Re u_n)_{\mathbf{q}} \cos(\omega_n \tau) - (\Im u_n)_{\mathbf{q}} \sin(\omega_n \tau) \right) \quad (17)$$

with  $\omega_n = 2n\pi/\beta$ . I take a semiclassical version of the Holstein Hamiltonian [124], assuming that the phonon coordinates in (14) as classical variables interacting with quantum mechanical fermion operators. Such approximation may affect the thermodynamics of the system as the quantum lattice fluctuations in fact play a role mainly for intermediate values of the  $e$ - $ph$  coupling [89, 125].

Averaging (14) on the electronic ground state, the  $e$ - $ph$  energy per lattice site is defined as

$$\frac{\langle H_d^{e-ph} \rangle}{N} = \sum_{\mathbf{q}} \langle H_d^{e-ph} \rangle_{\mathbf{q}},$$

$$\langle H_d^{e-ph} \rangle_{\mathbf{q}} = \frac{g}{N^{3/2}} \sqrt{2M\omega(\mathbf{q})} \sum_{\mathbf{q}'} \rho_{\mathbf{q}'} u_{\mathbf{q}'} S_d(\mathbf{q}' - \mathbf{q}), \quad (18)$$

$$\rho_{\mathbf{q}'} = \frac{1}{N} \sum_i \langle c_i^\dagger c_i \rangle \exp(i\mathbf{q}' \cdot \mathbf{R}_i).$$

Then, on the base of (17) and (18), I identify the perturbing source current [126] for the Holstein model with the  $\tau$  dependent averaged  $e$ - $ph$  Hamiltonian term:

$$j(\tau) = \sum_{\mathbf{q}} j_{\mathbf{q}}(\tau), \quad (19)$$

$$j_{\mathbf{q}}(\tau) \equiv \langle H_d^{e-ph} \rangle_{\mathbf{q}}.$$

Note that the Holstein source current does not depend on the electron path coordinates. The time dependence is incorporated only in the atomic displacements. This property will allow us to disentangle phonon and electron degrees of freedom in the path integral and in the total partition function.

After these premises, one can proceed to write the general path integral for an Holstein electron in a bath of dispersive phonons. Assuming a mixed representation, the electron

paths are taken in real space while the phonon paths are in momentum space. Thus, the electron path integral reads

$$\begin{aligned} & \langle \mathbf{x}(\beta) | \mathbf{x}(0) \rangle \\ &= \prod_{\mathbf{q}} \langle \mathbf{x}(\beta) | \mathbf{x}(0) \rangle_{\mathbf{q}}, \\ & \langle \mathbf{x}(\beta) | \mathbf{x}(0) \rangle_{\mathbf{q}} \\ &= \int Du_{\mathbf{q}}(\tau) \exp \left[ - \int_0^\beta d\tau \frac{M}{2} \left( \dot{u}_{\mathbf{q}}^2(\tau) + \omega^2(\mathbf{q}) u_{\mathbf{q}}^2(\tau) \right) \right] \\ & \quad \times \int D\mathbf{x}(\tau) \exp \left[ - \int_0^\beta d\tau \left( \frac{m}{2} \dot{\mathbf{x}}^2(\tau) + h^e(\tau) - j_{\mathbf{q}}(\tau) \right) \right], \end{aligned} \quad (20)$$

where  $m$  is the electron mass. The perturbing current in (20) is integrated over  $\tau$  using (17) and (19). The result is

$$\begin{aligned} & \int_0^\beta d\tau j_{\mathbf{q}}(\tau) = \beta u_{\mathbf{q}} g_d(\mathbf{q}), \\ & g_d(\mathbf{q}) = \frac{g}{N^2} \sqrt{2M\omega(\mathbf{q})} \sum_{\mathbf{q}'} \rho_{\mathbf{q}'} S_d(\mathbf{q}' - \mathbf{q}), \end{aligned} \quad (21)$$

where  $g_d(\mathbf{q})$  is thus a time averaged  $e$ - $ph$  potential.

The total partition function can be derived from (20) by imposing the closure condition both on the phonons (see (17)) and on the electron paths,  $\mathbf{x}(\beta) = \mathbf{x}(0)$ . Using (21), I obtain

$$\begin{aligned} Z_T &= \prod_{\mathbf{q}} \oint Du_{\mathbf{q}} \exp \left[ \beta u_{\mathbf{q}} g_d(\mathbf{q}) - \int_0^\beta d\tau \frac{M}{2} \left( \dot{u}_{\mathbf{q}}^2(\tau) + \omega_{\mathbf{q}}^2 u_{\mathbf{q}}^2(\tau) \right) \right] \\ & \quad \times \oint D\mathbf{x} \exp \left[ - \int_0^\beta d\tau \left( \frac{m}{2} \dot{\mathbf{x}}^2(\tau) + h^e(\tau) \right) \right], \end{aligned} \quad (22)$$

where  $\oint Du_{\mathbf{q}}$  and  $\oint D\mathbf{x}$  are the measures of integration which normalize the kinetic terms in the phonon field and electron actions, respectively [126].

The phonon degrees of freedom in (22) can be integrated out analytically yielding:

$$\begin{aligned} Z_T &= \prod_{\mathbf{q}} P(\mathbf{q}) \times \oint D\mathbf{x}(\tau) \\ & \quad \times \exp \left[ - \int_0^\beta d\tau \left( \frac{m}{2} \dot{\mathbf{x}}^2(\tau) + h^e(\tau) \right) \right], \\ P(\mathbf{q}) &= \frac{1}{\beta \omega(\mathbf{q})} \exp \left[ \frac{(g_d(\mathbf{q}) \lambda_M)^2}{2\pi \omega(\mathbf{q})^2} \right] \\ & \quad \times \prod_{n=1}^{N_F} \frac{(2n\pi)^2}{(2n\pi)^2 + (\beta \omega(\mathbf{q}))^2} \end{aligned} \quad (23)$$

being  $\lambda_M = \sqrt{\pi \hbar^2 \beta / M}$ .

Equation (23) is the final analytical result from which the thermodynamics of the model can be computed [123].

The exponential function in  $P(\mathbf{q})$  embodies the effect of the non local correlations due to the dispersive nature of the phonon spectrum. Phonon and electron contributions to the partition function are decoupled although the effective potential  $g_d(\mathbf{q})$  carries a dependence on the electron density profile in momentum space through the function  $\rho_{\mathbf{q}}$ .

**5.2. Electron-Phonon Coupling.** The time (temperature) averaged  $e$ - $ph$  potential in (21) is computed in the case of a linear chain and of a square lattice. As an example, I take the electron density profile as  $\rho_q = \rho_o \cos(q)$  in 1D and  $\rho_{\mathbf{q}} = \rho_o \cos(q_x) \cos(q_y)$  for the 2D system. Since the momentum integration runs over  $q_i \in [0, \pi/2]$ ,  $\rho_o$  represents in both cases the total electron density. More structured density functions containing longer range oscillations are not expected to change the trend of the results hereafter presented. Low-energy phonon spectra parameters are here assumed,  $\omega_0 = 20$  meV and  $\omega_1 = 10$  meV. Setting  $g = 3$ , I take a strong Holstein coupling although the general trend of the results holds for any value of  $g$ .

In Figure 4(a),  $g_{1D}(q)/\rho_o$  is plotted for three choices of the cutoff  $n^*$  to emphasize how the potential depends on the  $e$ - $ph$  interaction range. The constant value of the potential obtained for  $\omega_1 = 0$  is also reported on. For short correlations ( $n^* = 4$ ) there is a range of wave vectors in which the effective coupling becomes even larger than in the dispersionless case: this is due to the fact that the approximation related to a short cutoff is not sufficiently accurate. In fact, extending the range of the  $e$ - $ph$  correlations, the effective potential is progressively and substantially reduced for all momenta with respect to the dispersionless Holstein model. Numerical convergence for  $g_{1D}(q)$  is found at the value  $n^* = 24$  which corresponds to 48 lattice sites along the chain. Then, the 1D coupling renormalization is  $q$ -dependent and generally larger for  $q \sim \pi/2$  where the phonon dispersion generates stronger  $e$ - $ph$  correlations. Exact diagonalization techniques [91] had found that multiphonon states with longer range hopping processes substantially soften the polaron band narrowing with respect to the predictions of standard SCPT with the largest deviations occurring at the polaron momentum  $\sim \pi/2$ . In fact strong, nonlocal  $e$ - $ph$  correlations should favour hopping on further than neighbors sites occupied by phonons belonging to the lattice deformation.

The projections of the two-dimensional  $e$ - $ph$  potential along the  $y$  component of the wave vector is shown in Figure 4(b) for three values of the cutoff. For  $n^* = 1$  the correlation range is extended to the second neighbor shell thus including 8 lattice sites. For  $n^* = 2$  and  $n^* = 3$  the normalization is over 24 and 48 lattice sites, respectively. Then, the three values of  $n^*$  in 2D span as many lattice sites as the three values of  $n^*$  in 1D, respectively. I have made this choice to normalize consistently the potential for the linear chain and the square lattice. There is a strong renormalization for the 2D effective potential with respect to the dispersionless case for any value of the wave vector. Remarkably, the reduction is already evident for  $n^* = 1$ . By extending the correlation range this tendency becomes more pronounced for  $q_y$  close to the center and to the edge of

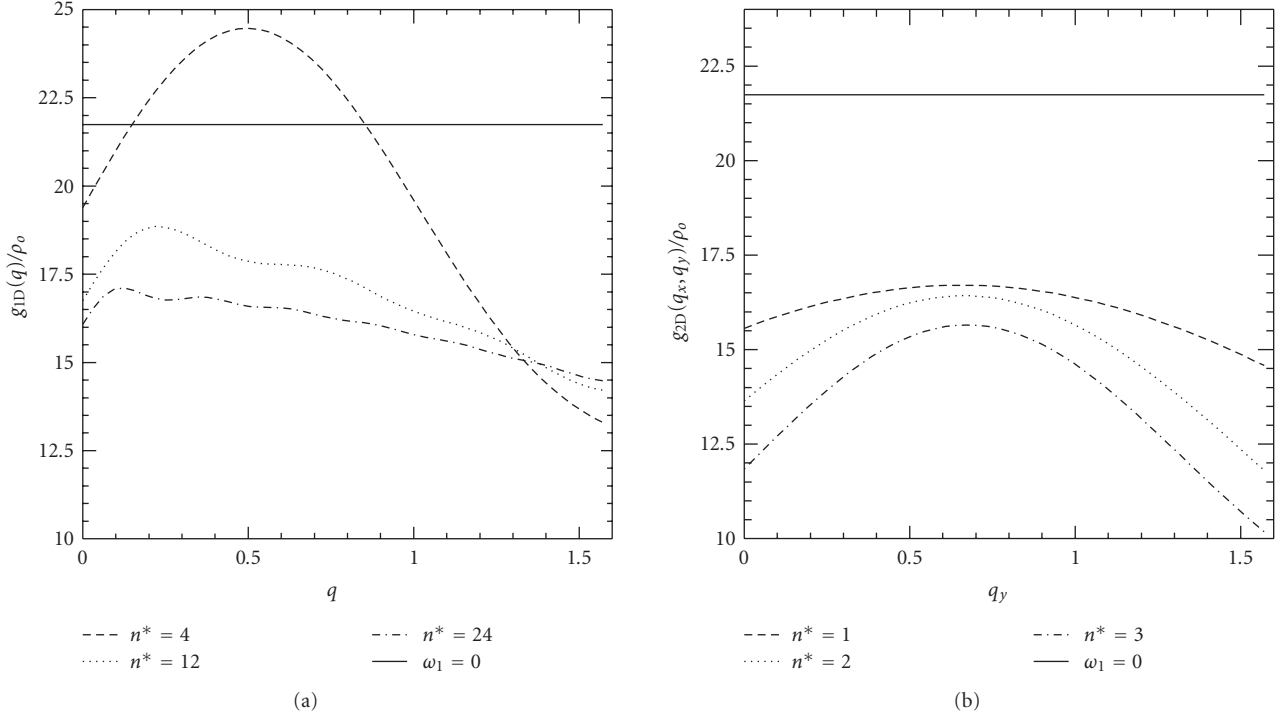


FIGURE 4: (a) Time averaged  $e$ - $ph$  coupling (in units  $\text{meV}\text{\AA}^{-1}$  versus wave vector for a linear chain.  $n^*$  represents the cutoff on the  $e$ - $ph$  correlations.  $\rho_0$  is the electron density.  $\omega_0 = 20$  meV and  $\omega_1 = 10$  meV.  $g = 3$ . The dispersionless  $e$ - $ph$  coupling is obtained for  $\omega_1 = 0$ . (b) Time averaged  $e$ - $ph$  coupling in two dimensions versus the  $y$  component of the momentum. The cases  $n^* = 1$ ,  $n^* = 2$ , and  $n^* = 3$  imply that the correlation range includes the second, the fifth and the ninth neighbors shell, respectively. The input parameters are as in (a).

the reduced Brillouin zone. An analogous behavior is found by projecting the 2D potential along the  $q_x$  axis. The 2D potential stabilizes by including the 9th neighbor shell ( $n^* = 3$ ) in the correlation range.

Then, an increased range for the  $e$ - $ph$  correlations leads to a very strong reduction of the effective coupling, an effect which is qualitatively analogous to that one would get by hardening the phonon spectrum. This is the physical reason underlying the fact that the Holstein polaron mass can be light.

## 6. Conclusions

According to the traditional notion of small polaron, the strong electron coupling to the lattice deformation implies a polaron collapse of the electron bandwidth ( $zt$ ) and remarkable mass renormalization. Thus, bipolaronic theories have been thought of being inconsistent with superconductivity at high  $T_c$  as the latter is inversely proportional to the bipolaron effective mass. Motivated by these issues, I have investigated the conditions for the existence of light polarons in the Holstein model and examined the concept of self-trapping versus dimensionality for a broad range of (anti)adiabatic regimes. The self trapping events correspond to the points of the most rapid increase for the polaron effective mass versus the  $e$ - $ph$  coupling. A modified version of the Lang-Firsov transformation accounts for the spreading of the polaron size due to retardation effects which are relevant

mainly for moderate  $e$ - $ph$  couplings. Assuming large optical phonon frequencies ( $\omega_0$ ), it is found that polaron masses display an abrupt although continuous increase driven by the  $e$ - $ph$  coupling in any dimension, included the 1D case. Such self trapping events occur in the adiabatic and intermediate ( $zt/\omega_0 \sim 1$ ) regimes provided that the  $e$ - $ph$  coupling is very strong ( $g/\omega_0 \geq 2$ ). The second-order of strong coupling perturbation theory permits to decouple two fundamental properties of the polaron landscape, namely, band narrowing and effective mass enhancement. I have considered a range of  $e$ - $ph$  couplings ( $g/\omega_0 \geq 1$ ) in which the conditions for polaron formation are fulfilled. For a given value of the adiabatic ratio, the onset of the band narrowing anticipates, along the  $g$  axis, the crossover to the heavy polaron state which pins the quasiparticle essentially on one lattice site. In such buffer zone, between band narrowing onset and self trapping, the charge carriers can be appropriately defined as *intermediate polarons*.

In all dimensions, there is room for non trapped intermediate polarons in the region of the moderate couplings. Such polarons spreads over a few lattice sites and their real space extension grows with dimensionality. Thus, analytical methods can suitably describe some polaron properties also in that interesting intermediate window of  $e$ - $ph$  couplings (i.e.,  $1 \leq g/\omega_0 \leq 2$  for the 1D system) in which adiabatic polarons are not large but not yet on-site localized. In the square lattice, at the onset of the self trapping state, the *polaron over bare electron* mass ratios are  $\sim 5$ – $10$  and even smaller for lower couplings.

The physical origins for the possibility of light polarons have been analysed treating the dispersive Holstein Hamiltonian model by the imaginary time path integral method. The perturbing source current is the time averaged  $e$ - $ph$  Hamiltonian term. The partition function of the model has been derived integrating out the phonon degrees of freedom in semiclassical approximation. Focusing on the role of the intermolecular forces, I have quantitatively determined the effects of the dispersive spectrum on the time-averaged  $e$ - $ph$  coupling which incorporates the nonlocality effects. It is found that, in the square lattice, the  $e$ - $ph$  coupling is strongly renormalized downwards and this phenomenon is already pronounced by the (minimal) inclusion of the second neighbors intermolecular shell. This may explain why 2D Holstein polarons can be light while the real space range of the  $e$ - $ph$  correlations is relatively short.

## Acknowledgment

Joyous and fruitful collaboration with Professor A. N. Das is acknowledged.

## References

- [1] C. Gadermaier, A. S. Alexandrov, V. V. Kabanov, et al., "Electron-phonon coupling in cuprate high-temperature superconductors determined from exact electron relaxation rates," <http://arxiv.org/abs/0902.1636>.
- [2] J. Mustre de León, J. Miranda Mena, and A. R. Bishop, "Microstrain and polaronic correlation in a model system," *Journal of Physics: Conference Series*, vol. 108, no. 1, Article ID 012020, 2008.
- [3] H. Oyanagi and A. Bianconi, Eds., *Physics in Local Lattice Distortions*, American Institute of Physics, New York, NY, USA, 2001.
- [4] A. Bianconi, N. L. Saini, A. Lanzara, et al., "Determination of the local lattice distortions in the  $\text{CuO}_2$  plane of  $\text{La}_{1.85}\text{Sr}_{0.15}\text{CuO}_4$ ," *Physical Review Letters*, vol. 76, no. 18, pp. 3412–3415, 1996.
- [5] A. Lanzara, P. V. Bogdanov, X. J. Zhou, et al., "Evidence for ubiquitous strong electron-phonon coupling in high-temperature superconductors," *Nature*, vol. 412, no. 6846, pp. 510–514, 2001.
- [6] J. Mustre de Leon, M. Acosta-Alejandro, S. D. Conradson, and A. R. Bishop, "Local structure fluctuations as a signature of an inhomogeneous ground state in high- $T_c$  superconductors," *Journal of Synchrotron Radiation*, vol. 12, no. 2, pp. 193–196, 2005.
- [7] J. Lee, K. Fujita, K. McElroy, et al., "Interplay of electron-lattice interactions and superconductivity in  $\text{Bi}_2\text{Sr}_2\text{CaCu}_2\text{O}_{8+\delta}$ ," *Nature*, vol. 442, no. 7102, pp. 546–550, 2006.
- [8] H. Oyanagi, A. Tsukada, M. Naito, and N. L. Saini, "Local structure of superconducting  $(\text{La}, \text{Sr})_2\text{CuO}_4$  under strain: microscopic mechanism of strain-induced  $T_c$  variation," *Physical Review B*, vol. 75, no. 2, Article ID 024511, 2007.
- [9] Y. Bar-Yam, T. Egami, J. Mustre de Leon, and A. R. Bishop, Eds., *Lattice Effects in High  $T_c$  Superconductors*, World Scientific, Singapore, 1992.
- [10] A. S. Alexandrov and N. F. Mott, "Bipolarons," *Reports on Progress in Physics*, vol. 57, no. 12, pp. 1197–1288, 1994.
- [11] V. Z. Kresin and S. A. Wolf, "Colloquium: electron-lattice interaction and its impact on high  $T_c$  superconductivity," *Reviews of Modern Physics*, vol. 81, no. 2, pp. 481–501, 2009.
- [12] C. J. Zhang, H. Oyanagi, Z. H. Sun, Y. Kamihara, and H. Hosono, "Low-temperature lattice structure anomaly in the  $\text{LaFeAsO}_{0.93}\text{F}_{0.07}$  superconductor by x-ray absorption spectroscopy: evidence for a strong electron-phonon interaction," *Physical Review B*, vol. 78, no. 21, Article ID 214513, 2008.
- [13] H. Takahashi, K. Igawa, K. Arii, Y. Kamihara, M. Hirano, and H. Hosono, "Superconductivity at 43 K in an iron-based layered compound  $\text{LaO}_{1-x}\text{F}_x\text{FeAs}$ ," *Nature*, vol. 453, no. 7193, pp. 376–378, 2008.
- [14] X. H. Chen, T. Wu, G. Wu, R. H. Liu, H. Chen, and D. F. Fang, "Superconductivity at 43 K in  $\text{SmFeAsO}_{1-x}\text{F}_x$ ," *Nature*, vol. 453, no. 7196, pp. 761–762, 2008.
- [15] A. Bussmann-Holder, A. Simon, H. Keller, and A. R. Bishop, "Superconductivity in Fe and As based compounds: a bridge between  $\text{MgB}_2$  and cuprates," <http://arxiv.org/abs/0906.2286>.
- [16] J. G. Bednorz and K. A. Müller, "Possible high  $T_c$  superconductivity in the Ba-La-Cu-O system," *Zeitschrift für Physik B: Condensed Matter*, vol. 64, no. 2, pp. 189–193, 1986.
- [17] H. A. Jahn and E. Teller, "Stability of polyatomic molecules in degenerate electronic states. I. Orbital degeneracy," *Proceedings of the Royal Society A*, vol. 161, no. 905, pp. 220–235, 1937.
- [18] R. Englman, *The Jahn-Teller Effect in Molecules and Crystals*, Wiley Interscience, New York, NY, USA, 1972.
- [19] T. Mertelj, V. V. Kabanov, and D. Mihailovic, "Charged particles on a two-dimensional lattice subject to anisotropic Jahn-teller interactions," *Physical Review Letters*, vol. 94, no. 14, Article ID 147003, 4 pages, 2005.
- [20] K. H. Höck, H. Nickisch, and H. Thomas, "Jahn-Teller effect in itinerant electron systems: The Jahn-Teller polaron," *Helvetica Physica Acta*, vol. 56, p. 237, 1983.
- [21] T. Holstein, "Studies of polaron motion—part I: the molecular-crystal model," *Annals of Physics*, vol. 8, no. 3, pp. 325–342, 1959.
- [22] A. S. Alexandrov and A. B. Krebs, "Polarons in high temperature superconductors," *Uspekhi Fizicheskikh Nauk*, vol. 163, p. 1, 1992, English translation in *Soviet Physics Uspekhi*, vol. 35, p. 345, 1992.
- [23] A. S. Alexandrov, "Bipolaron anisotropic flat bands, Hall mobility edge, and metal-semiconductor duality of overdoped high- $T_c$  oxides," *Physical Review B*, vol. 53, no. 5, pp. 2863–2869, 1996.
- [24] J. T. Devreese, *Polarons in Encyclopedia of Applied Physics*, vol. 14, VCH, New York, NY, USA, 1996.
- [25] A. S. Alexandrov, Ed., *Polarons in Advanced Materials*, vol. 103 of *Springer Series in Materials Science*, Canopus, Bristol, UK, 2007.
- [26] S. I. Pekar, "Local quantum states of an electron in an ideal ionic crystal," *Journal of Physics USSR*, vol. 10, p. 341, 1946.
- [27] L. D. Landau and S. I. Pekar, "Effective mass of a polaron," *Zhurnal Eksperimental'noi i Teoreticheskoi Fiziki*, vol. 18, p. 419, 1948.
- [28] E. I. Rashba, "The theory of strong interactions of electron excitations with the lattice vibrations in molecular solids," *Optika i Spektroskopiya*, vol. 2, p. 75, 1957.
- [29] G. L. Sewell, "Electrons in polar crystal," *Philosophical Magazine*, vol. 3, p. 1361, 1958.
- [30] L. D. Landau, "Electron motion in crystal lattices," *Physikalische Zeitschrift der Sowjetunion*, vol. 3, p. 664, 1933.

- [31] A. B. Migdal, "Interaction between electrons and the lattice vibrations in a normal metal," *Journal of Experimental and Theoretical Physics*, vol. 34, p. 1438, 1958, English translation in *Soviet Physics. JETP*, vol. 34, p. 996, 1958.
- [32] A. S. Alexandrov and E. A. Mazur, "Electron-phonon system with strong coupling and violation of the Migdal-Eliashberg theory," *Zhurnal Eksperimental'noi i Teoreticheskoi Fiziki*, vol. 96, p. 1773, 1989, English translation in *Soviet Physics. JETP*, vol. 69, p. 1001, 1989.
- [33] R. P. Feynman, "Space-time approach to non-relativistic quantum mechanics," *Reviews of Modern Physics*, vol. 20, no. 2, pp. 367–387, 1948.
- [34] H. Fröhlich, H. Pelzer, and S. Zienau, "Properties of slow electrons in polar materials," *Philosophical Magazine*, vol. 41, p. 221, 1950.
- [35] H. Fröhlich, "Interaction of electrons with lattice vibrations," *Proceedings of the Royal Society of London A*, vol. 215, p. 291, 1952.
- [36] R. P. Feynman, "Slow electrons in a polar crystal," *Physical Review*, vol. 97, no. 3, pp. 660–665, 1955.
- [37] J. T. Devreese, "Feynman's 1955 Polaron Paper: a landmark in the Application of Path Integrals," in *Proceedings of the 6th International Conference on: Path Integrals from peV to TeV—50 Years after Feynman's Paper*, p. 22, World Scientific Publishing, 1999.
- [38] G. Ganbold and G. V. Efimov, "Fröhlich-Feynman polaron in d dimensions," in *Proceedings of the 6th International Conference on: Path Integrals from peV to TeV—50 Years after Feynman's Paper*, p. 387, World Scientific Publishing, 1999.
- [39] J. T. Devreese, "Optical properties of few and many Fröhlich polarons from 3D to 0D," in *Polarons in Advanced Materials*, vol. 103 of *Springer Series in Materials Science*, pp. 3–62, Canopus and Springer, Bath, UK, 2007.
- [40] J. Tempere, W. Casteels, M. K. Oberthaler, E. Timmermans, and J. T. Devreese, "Feynman path-integral treatment of the BEC-impurity polaron," <http://arxiv.org/abs/0906.4455>.
- [41] J. T. Devreese and A. S. Alexandrov, "Fröhlich polaron and bipolaron: recent developments," *Reports on Progress in Physics*, vol. 72, no. 6, Article ID 066501, 2009.
- [42] H. De Raedt and A. Lagendijk, "Critical quantum fluctuations and localization of the small polaron," *Physical Review Letters*, vol. 49, no. 20, pp. 1522–1525, 1982.
- [43] H. De Raedt and A. Lagendijk, "Numerical calculation of path integrals: the small-polaron model," *Physical Review B*, vol. 27, no. 10, pp. 6097–6109, 1983.
- [44] H. De Raedt and A. Lagendijk, "Numerical study of Holstein's molecular-crystal model: adiabatic limit and influence of phonon dispersion," *Physical Review B*, vol. 30, no. 4, pp. 1671–1678, 1984.
- [45] D. M. Eagles, "Theory of transitions from large to nearly-small polarons, with application to Zr-doped superconducting SrTiO<sub>3</sub>," *Physical Review*, vol. 181, no. 3, pp. 1278–1290, 1969.
- [46] J. Ranninger and U. Thibblin, "Two-site polaron problem: electronic and vibrational properties," *Physical Review B*, vol. 45, no. 14, pp. 7730–7738, 1992.
- [47] A. S. Alexandrov, V. V. Kabanov, and D. K. Ray, "From electron to small polaron: an exact cluster solution," *Physical Review B*, vol. 49, no. 14, pp. 9915–9923, 1994.
- [48] Y. Toyozawa, "Self-trapping of an electron by the acoustical mode of lattice vibration. Part I," *Progress of Theoretical Physics*, vol. 26, p. 29, 1961.
- [49] G. Kopidakis, C. M. Soukoulis, and E. N. Economou, "Electron-phonon interaction, localization, and polaron formation in one-dimensional systems," *Physical Review B*, vol. 51, no. 21, pp. 15038–15052, 1995.
- [50] H. Fehske, H. Röder, G. Wellein, and A. Mitrriotis, "Hole-polaron formation in the two-dimensional Holstein t-J model: a variational Lanczos study," *Physical Review B*, vol. 51, no. 23, pp. 16582–16593, 1995.
- [51] J. M. Robin, "Spectral properties of the small polaron," *Physical Review B*, vol. 56, no. 21, pp. 13634–13637, 1997.
- [52] D. W. Brown, K. Lindenberg, and Y. Zhao, "Variational energy band theory for polarons: mapping polaron structure with the global-local method," *Journal of Chemical Physics*, vol. 107, no. 8, pp. 3179–3195, 1997.
- [53] M. Zoli, "Two- and three-dimensional polaronic motion: beyond the Holstein model," *Physical Review B*, vol. 57, no. 17, pp. 10555–10559, 1998.
- [54] M. Capone, S. Ciuchi, and C. Grimaldi, "The small-polaron crossover: comparison between exact results and vertex correction approximation," *Europhysics Letters*, vol. 42, no. 5, pp. 523–528, 1998.
- [55] Y. Zolotaryuk, P. L. Christiansen, and J. J. Rasmussen, "Polaron dynamics in a two-dimensional anharmonic Holstein model," *Physical Review B*, vol. 58, no. 21, pp. 14305–14319, 1998.
- [56] A. H. Romero, D. W. Brown, and K. Lindenberg, "Polaron effective mass, band distortion, and self-trapping in the Holstein molecular-crystal model," *Physical Review B*, vol. 59, no. 21, pp. 13728–13740, 1999.
- [57] A. H. Romero, D. W. Brown, and K. Lindenberg, "Effects of dimensionality and anisotropy on the Holstein polaron," *Physical Review B*, vol. 60, no. 20, pp. 14080–14091, 1999.
- [58] A. S. Mishchenko, N. Nagaosa, N. V. Prokof'ev, A. Sakamoto, and B. V. Svistunov, "Self-trapping of polarons in the Rashba-Pekar model," *Physical Review B*, vol. 66, no. 2, Article ID 020301, 4 pages, 2002.
- [59] O. S. Barišić, "Variational study of the Holstein polaron," *Physical Review B*, vol. 65, no. 14, Article ID 144301, 10 pages, 2002.
- [60] L.-C. Ku, S. A. Trugman, and J. Bonča, "Dimensionality effects on the Holstein polaron," *Physical Review B*, vol. 65, no. 17, Article ID 174306, 10 pages, 2002.
- [61] H. Zheng and M. Avignon, "Intermediate region between large and small polarons in many-electron systems," *Physical Review B*, vol. 68, no. 2, Article ID 024301, 12 pages, 2003.
- [62] S. Ciuchi, F. de Pasquale, S. Fratini, and D. Feinberg, "Dynamical mean-field theory of the small polaron," *Physical Review B*, vol. 56, no. 8, pp. 4494–4512, 1997.
- [63] R. von Helmolt, J. Wecker, B. Holzapfel, L. Schultz, and K. Samwer, "Giant negative magnetoresistance in perovskite-like La<sub>2/3</sub>Ba<sub>1/3</sub>MnO<sub>x</sub> ferromagnetic films," *Physical Review Letters*, vol. 71, no. 14, pp. 2331–2333, 1993.
- [64] S. Jin, T. H. Tiefel, M. McCormack, R. A. Fastnacht, R. Ramesh, and L. H. Chen, "Thousandfold change in resistivity in magnetoresistive La-Ca-Mn-O films," *Science*, vol. 264, no. 5157, pp. 413–415, 1994.
- [65] G. Zhao, "Polarons in colossal magnetoresistive and high-temperature superconducting materials," in *Polarons in Advanced Materials*, A. S. Alexandrov, Ed., vol. 103 of *Springer Series in Materials Science*, pp. 569–598, Canopus, Bristol, UK, 2007.
- [66] K. Hannelwald, V. M. Stojanović, J. M. T. Schellekens, P. A. Bobbert, G. Kresse, and J. Hafner, "Theory of polaron bandwidth narrowing in organic molecular crystals," *Physical Review B*, vol. 69, no. 7, Article ID 075211, 7 pages, 2004.

- [67] J. A. Berashevich, V. Apalkov, and T. Chakraborty, "Polaron tunneling dynamics of a linear polymer of nucleotides," *Journal of Physics: Condensed Matter*, vol. 20, no. 7, Article ID 075104, 2008.
- [68] J. H. Ojeda, R. P. A. Lima, F. Domínguez-Adame, and P. A. Orellana, "Trapping and motion of polarons in weakly disordered DNA molecules," *Journal of Physics: Condensed Matter*, vol. 21, no. 28, Article ID 285105, 2009.
- [69] A. Zazunov and T. Martin, "Transport through a molecular quantum dot in the polaron crossover regime," *Physical Review B*, vol. 76, no. 3, Article ID 033417, 2007.
- [70] H. Fehske, G. Wellein, J. Loos, and A. R. Bishop, "Localized polarons and doorway vibrons in finite quantum structures," *Physical Review B*, vol. 77, no. 8, Article ID 085117, 2008.
- [71] M. Zoli, "c-axis resistivity in high-Tc superconductors," *Physical Review B*, vol. 56, no. 1, pp. 111–114, 1997.
- [72] M. Zoli, "Path-integral approach to resistivity anomalies in anharmonic systems," *Physical Review B*, vol. 63, no. 17, pp. 1743011–1743015, 2001.
- [73] B. K. Chakraverty, J. Ranninger, and D. Feinberg, "Experimental and theoretical constraints of bipolaronic superconductivity in high Tc materials: an impossibility," *Physical Review Letters*, vol. 81, no. 2, pp. 433–436, 1998.
- [74] M. Zoli, "Lattice-dynamics effects on small-polaron properties," *Physical Review B*, vol. 61, no. 21, pp. 14523–14530, 2000.
- [75] A. S. Alexandrov and P. E. Kornilovitch, "Mobile small polaron," *Physical Review Letters*, vol. 82, no. 4, pp. 807–810, 1999.
- [76] A. S. Alexandrov, "Polaron dynamics and bipolaron condensation in cuprates," *Physical Review B*, vol. 61, no. 18, pp. 12315–12327, 2000.
- [77] J. P. Hague, P. E. Kornilovitch, J. H. Samson, and A. S. Alexandrov, "Superlight small bipolarons in the presence of a strong coulomb repulsion," *Physical Review Letters*, vol. 98, no. 3, Article ID 037002, 2007.
- [78] A. S. Alexandrov, "Superconducting polarons and bipolarons," in *Polarons in Advanced Materials*, A. S. Alexandrov, Ed., vol. 103 of *Springer Series in Materials Science*, pp. 257–310, Canopus, Bristol, UK, 2007.
- [79] A. S. Alexandrov and J. Ranninger, "Polaronic effects in the photoemission spectra of strongly coupled electron-phonon systems," *Physical Review B*, vol. 45, no. 22, pp. 13109–13112, 1992.
- [80] A. S. Alexandrov and C. J. Dent, "Angle-resolved photoemission in doped charge-transfer Mott insulators," *Physical Review B*, vol. 60, no. 22, pp. 15414–15422, 1999.
- [81] M. Zoli and A. N. Das, "Polaron crossover in molecular solids," *Journal of Physics: Condensed Matter*, vol. 16, no. 21, pp. 3597–3607, 2004.
- [82] T. Holstein, "Studies of polaron motion—part II: the "small" polaron," *Annals of Physics*, vol. 8, no. 3, pp. 343–389, 1959.
- [83] A. A. Gogolin, "Mobility of a small polaron at low temperatures," *Physica Status Solidi (b)*, vol. 103, no. 1, pp. 397–409, 1981.
- [84] K.-H. Yoo, D. H. Ha, J.-O. Lee, et al., "Electrical conduction through poly(dA)-poly(dT) and poly(dG)-poly(dC) DNA molecules," *Physical Review Letters*, vol. 87, no. 19, Article ID 198102, 4 pages, 2001.
- [85] B. B. Schmidt, M. H. Hettler, and G. Schön, "Nonequilibrium polaron hopping transport through DNA," *Physical Review B*, vol. 77, no. 16, Article ID 165337, 2008.
- [86] D. Emin, "Self-trapping in quasi-one-dimensional solids," *Physical Review B*, vol. 33, no. 6, pp. 3973–3975, 1986.
- [87] A. Alvermann, H. Fehske, and S. A. Trugman, "Solution of the Holstein polaron anisotropy problem," *Physical Review B*, vol. 78, no. 16, Article ID 165106, 2008.
- [88] E. Jeckelmann and S. R. White, "Density-matrix renormalization-group study of the polaron problem in the Holstein model," *Physical Review B*, vol. 57, no. 11, pp. 6376–6385, 1998.
- [89] J. Bonča, S. A. Trugman, and I. Batistić, "Holstein polaron," *Physical Review B*, vol. 60, no. 3, pp. 1633–1642, 1999.
- [90] D. W. Brown, K. Lindenberg, and Y. Zhao, "Variational energy band theory for polarons: mapping polaron structure with the global-local method," *Journal of Chemical Physics*, vol. 107, no. 8, pp. 3179–3195, 1997.
- [91] G. Wellein and H. Fehske, "Polaron band formation in the Holstein model," *Physical Review B*, vol. 56, no. 8, pp. 4513–4517, 1997.
- [92] G. Wellein and H. Fehske, "Self-trapping problem of electrons or excitons in one dimension," *Physical Review B*, vol. 58, no. 10, pp. 6208–6218, 1998.
- [93] F. Marsiglio, "Pairing in the Holstein model in the dilute limit," *Physica C*, vol. 244, no. 1-2, pp. 21–34, 1995.
- [94] W. Stephan, "Single-polaron band structure of the Holstein model," *Physical Review B*, vol. 54, no. 13, pp. 8981–8984, 1996.
- [95] M. Capone, W. Stephan, and M. Grilli, "Small-polaron formation and optical absorption in Su-Schrieffer-Heeger and Holstein models," *Physical Review B*, vol. 56, no. 8, pp. 4484–4493, 1997.
- [96] J. Chatterjee and A. N. Das, "Comparison of perturbative expansions using different phonon bases for the two-site Holstein model," *Physical Review B*, vol. 61, no. 7, pp. 4592–4602, 2000.
- [97] I. J. Lang and Y. A. Firsov, "Kinetic theory of semiconductors with low mobility," *Journal of Experimental and Theoretical Physics: Soviet Physics*, vol. 16, p. 1301, 1963.
- [98] V. M. Kenkre, H.-L. Wu, and I. Howard, "Effects of interaction-potential nonlinearities and restoring-force anharmonicities in the discrete nonlinear Schrödinger equation," *Physical Review B*, vol. 51, no. 22, pp. 15841–15846, 1995.
- [99] D. Emin, "On the existence of free and self-trapped carriers in insulators: an abrupt temperature-dependent conductivity transition," *Advances in Physics*, vol. 22, no. 1, pp. 57–116, 1973.
- [100] A. H. Romero, D. W. Brown, and K. Lindenberg, "Exact weak-coupling radius of the Holstein polaron in one, two, and three dimensions," *Physics Letters A*, vol. 254, no. 5, pp. 287–291, 1999.
- [101] M. Zoli, "Mass renormalization in the Su-Schrieffer-Heeger model," *Physical Review B*, vol. 66, no. 1, Article ID 012303, 4 pages, 2002.
- [102] M. Zoli, "Path integral methods in the Su-Schrieffer-Heeger polaron problem," in *Polarons in Advanced Materials*, A. S. Alexandrov, Ed., vol. 103 of *Springer Series in Materials Science*, pp. 231–256, Canopus, Bristol, UK, 2007.
- [103] A. N. Das and P. Choudhury, "Stability and nature of polarons in a two-site two-electron model," *Physical Review B*, vol. 49, no. 18, pp. 13219–13222, 1994.
- [104] P. Choudhury and A. N. Das, "Small-to-large polaron crossover in one dimension using variational phonon-averaging techniques," *International Journal of Modern Physics B*, vol. 15, no. 13, pp. 1923–1937, 2001.

- [105] J. Yamashita and T. Kurosawa, "On electronic current in NiO," *Journal of Physics and Chemistry of Solids*, vol. 5, no. 1-2, pp. 34–43, 1958.
- [106] D. Emin and T. Holstein, "Adiabatic theory of an electron in a deformable continuum," *Physical Review Letters*, vol. 36, no. 6, pp. 323–326, 1976.
- [107] V. V. Kabanov and O. Y. Mashtakov, "Electron localization with and without barrier formation," *Physical Review B*, vol. 47, no. 10, pp. 6060–6064, 1993.
- [108] G. Kalosakas, S. Aubry, and G. P. Tsironis, "Polaron solutions and normal-mode analysis in the semiclassical Holstein model," *Physical Review B*, vol. 58, no. 6, pp. 3094–3104, 1998.
- [109] D. W. Brown and Z. Ivić, "Unification of polaron and soliton theories of exciton transport," *Physical Review B*, vol. 40, no. 14, pp. 9876–9887, 1989.
- [110] A. H. Romero, D. W. Brown, and K. Lindenberg, "Electron-phonon correlations, polaron size, and the nature of the self-trapping transition," *Physics Letters A*, vol. 266, no. 4–6, pp. 414–420, 2000.
- [111] H. Löwen, "Absence of phase transitions in Holstein systems," *Physical Review B*, vol. 37, no. 15, pp. 8661–8667, 1988.
- [112] B. Gerlach and H. Löwen, "Proof of the nonexistence of (formal) phase transitions in polaron systems. I," *Physical Review B*, vol. 35, no. 9, pp. 4291–4296, 1987.
- [113] B. Gerlach and H. Löwen, "Proof of the nonexistence of (formal) phase transitions in polaron systems. II," *Physical Review B*, vol. 35, no. 9, pp. 4297–4303, 1987.
- [114] B. Gerlach and H. Löwen, "Analytical properties of polaron systems or: do polaronic phase transitions exist or not?" *Reviews of Modern Physics*, vol. 63, no. 1, pp. 63–90, 1991.
- [115] H. B. Shore and L. M. Sander, "Ground state of the exciton-phonon system," *Physical Review B*, vol. 7, no. 10, pp. 4537–4546, 1973.
- [116] P. Hamm and G. P. Tsironis, "Barrier crossing to the small Holstein polaron regime," *Physical Review B*, vol. 78, no. 9, Article ID 092301, 2008.
- [117] D. R. Hamann, "Path integral theory of magnetic alloys," *Physical Review B*, vol. 2, no. 5, pp. 1373–1392, 1970.
- [118] C. C. Yu and P. W. Anderson, "Local-phonon model of strong electron-phonon interactions in A15 compounds and other strong-coupling superconductors," *Physical Review B*, vol. 29, no. 11, pp. 6165–6186, 1984.
- [119] M. Zoli, "Phonon thermodynamics versus electron-phonon models," *Physical Review B*, vol. 70, no. 18, Article ID 184301, 6 pages, 2004.
- [120] M. Zoli, "Path integral description of a semiclassical Su-Schrieffer-Heeger model," *Physical Review B*, vol. 67, no. 19, Article ID 195102, 2003.
- [121] M. Zoli, "Path integral of the two-dimensional Su-Schrieffer-Heeger model," *Physical Review B*, vol. 71, no. 20, Article ID 205111, 5 pages, 2005.
- [122] M. Zoli, "Path integral of the Holstein model with a 4 on-site potential," *Physical Review B*, vol. 72, no. 21, Article ID 214302, 7 pages, 2005.
- [123] M. Zoli, "Nonlocal electron-phonon correlations in a dispersive Holstein model," *Physical Review B*, vol. 71, no. 18, Article ID 184308, 2005.
- [124] N. K. Voulgarakis and G. P. Tsironis, "Stationary and dynamical properties of polarons in the anharmonic Holstein model," *Physical Review B*, vol. 63, no. 1, Article ID 014302, 2001.
- [125] A. La Magna and R. Pucci, "Variational study of the discrete Holstein model," *Physical Review B*, vol. 53, no. 13, pp. 8449–8456, 1996.
- [126] H. Kleinert, *Path Integrals in Quantum Mechanics, Statistics, and Polymer Physics*, World Scientific, Singapore, 1995.

## Review Article

# Manifestations of the Electron-Phonon Coupling in the Spectroscopy of High-Temperature Superconductors

A. S. Mishchenko<sup>1,2</sup>

<sup>1</sup> *Cross-Correlated Materials Research Group (CMRG), ASI, RIKEN, Wako 351-0198, Japan*

<sup>2</sup> *Russian Research Centre, Kurchatov Institute, Moscow 123182, Russia*

Correspondence should be addressed to A. S. Mishchenko, mishchenko@riken.jp

Received 28 June 2009; Accepted 28 July 2009

Academic Editor: Sasha Alexandrov

Copyright © 2010 A. S. Mishchenko. This is an open access article distributed under the Creative Commons Attribution License, which permits unrestricted use, distribution, and reproduction in any medium, provided the original work is properly cited.

A review of experimental and theoretical results on the spectroscopy of high-temperature superconductors is presented. The models where hole doped into antiferromagnet interacts both with magnetic subsystem and with phonons are considered. Theoretical results of these models for phonon spectra, angle resolved photoemission spectra, and optical conductivity are presented. Comparison with experimental data gives evidence for the strong electron-phonon coupling in the undoped and weakly doped high-temperature superconductors. The strength of electron-phonon coupling decreases with doping though at the optimal doping the compounds are still in the intermediate coupling regime.

## 1. Introduction

The role of the electron-phonon interaction (EPI) in the high-temperature superconductors is debated for many years. Firm opinions range from the complete negation of its role [1] up to the statement that the polaron binding energy is larger than the characteristic magnetic energy by an order of magnitude and, hence, the magnetic subsystem is not important [2, 3]. Of course there is an opinion that both magnetic and lattice subsystems are important [4].

Up to the very recent times it seemed that the spectral properties of cuprates can be explained considering only magnetic subsystem. The dispersion of the peak in the Angle Resolved Photoemission (ARPES) spectra was well reproduced by  $tt't''$ -J model [5] which is the model with a hole moving on the antiferromagnetic background [6–8]. Also, t-J model predicted a peak in the Optical Conductivity (OC) [9–22], situated roughly at the same energy as the Mid Infrared (MIR) band observed in experiments [23–28]. However, improvement of the experimental technique and advances in theoretical methods make them capable of seeing fine details of spectra which occurred to be quite different in experiment and theory. In experiment, the resolution of ARPES technique reached few meV [5] and the ellipsometry

technique [29, 30] gave possibility to measure OC without Kramers-Kronig relation which introduce uncertainty into the experimental data. In theory, recently developed Diagrammatic Monte Carlo (DMC) method [31–56] became capable of avoiding serious approximations in a significant set of models describing strongly correlated systems.

One of the main and most evident contradiction between theory and experiment was the linewidth of the ARPES peak in undoped cuprates. Although the dispersion of the peak is well reproduced by  $tt't''$ -J model, its width is very broad in experiment [57] and very narrow in theory [37]. Naively, contribution of EPI cannot explain the large width since the coupling to phonons, in addition to broadening, must also change the dispersion of the particle which, in turn, is already well described by the pure  $tt't''$ -J model. However, as was shown in [42, 58], in the strong coupling regime of EPI the situation is exactly the same as in experiment. The polaron quasiparticle has very small weight and cannot be seen in experiment while shake-off Franck-Condon peak completely reproduces the dispersion of the pure magnetic model without EPI. Naturally, in such case the chemical potential must be pinned not to the observed broad shake-off peak but to the real invisible quasiparticle. Such decoupling of the chemical potential from the broad peak was observed

in experiment [59] a few months after prediction had been made in [42].

Further theoretical and experimental studies brought more evidences of the importance of EPI in cuprates. One of the evidences is the two-peak structure of the MIR part of OC in the underdoped compounds which is easily reproduced by taking the EPI into account [51]. Another confirmation is the anomalous temperature dependence of the width of the ARPES peak which can be explained only by the interplay of magnetic and lattice system [50, 60]. Various estimates for the EPI strength [50, 61–63] give the value  $\lambda \approx 1$  for undoped compounds. The strength of EPI decreases with increase of the concentration of holes reaching the intermediate coupling regime at optimal doping [51, 64].

In Section 2 we introduce the models describing the physics of the interplay between magnetic and lattice degrees of freedom in cuprates. Then, we discuss different aspects of manifestation of the EPI in the phonon spectra, ARPES, and OC in Section 3. The influence of strong electronic correlations on the EPI is discussed in Section 4 and the final conclusions are presented in Section 5.

## 2. Models

The prototypical model for high-temperature superconductors is the three band model [65]. This model contains one  $3d x^2 - y^2$  orbital of Cu and two oxygen  $p$  orbitals in the  $\text{CuO}_2$  plain. The Hamiltonian

$$\begin{aligned} \hat{H}_{3B} = & \varepsilon_O \sum_{i\delta\sigma} a_{i\delta\sigma}^\dagger a_{i\delta\sigma} + \varepsilon_d \sum_{i\sigma} c_{i\sigma}^\dagger c_{i\sigma} \\ & + U \sum_i n_{i\uparrow} n_{i\downarrow} + t_{pd} \sum_{i\delta\sigma} P_\delta (c_{i\sigma}^\dagger a_{i\delta\sigma} + \text{h.c.}) \end{aligned} \quad (1)$$

includes term with Coulomb repulsion  $U$  on Cu ion and term describing hopping between Cu and O with amplitude  $t_{pd}$ . The vector  $\delta$  defines oxygen position in the unit cell and runs over  $(a/2, 0)$  and  $(0, a/2)$  in the second term and over  $(\pm a/2, 0)$  and  $(0, \pm a/2)$  in the last term.  $P_\delta = -P_{-\delta}$  is even operator. Operator  $a_{i\delta\sigma}^\dagger$  ( $c_{i\sigma}^\dagger$ ) is the creation operator of electron with spin  $\sigma$  on the oxygen (cooper) ion. Energy  $\varepsilon_d$  ( $\varepsilon_O$ ) corresponds to Cu (O) orbital.

The t-J model is derived from the three-band model. The site  $i$  in the t-J model corresponds to the position of cooper ion. In the undoped system all Cu ions have configuration  $d^9$  and each site is occupied by one hole. Doped holes go mostly to the O sites and form with hole the Zhang-Rice singlet [66]. This singlet is an empty state in the t-J model described by the following Hamiltonian:

$$\hat{H}_{t-J} = -t \sum_{\langle ij \rangle \sigma} (\tilde{c}_{i\sigma}^\dagger \tilde{c}_{j\sigma} + \text{h.c.}) + J \sum_{\langle ij \rangle} (\mathbf{S}_i \mathbf{S}_j + \frac{n_i n_j}{4}). \quad (2)$$

Here  $\tilde{c}_{j\sigma}$  is projected (to avoid double occupancy) fermionic annihilation operator,  $n_i < 2$  is the number operator,  $\mathbf{S}_i$  is spin 1/2 operator,  $J$  is the exchange integral, and  $\langle ij \rangle$  is restricted to near neighbors in two-dimensional lattice.

Expressing spin operators in terms of spin waves and making Fourier and Bogoliubov transformations one can

derive the t-J Hamiltonian in the spin wave approximation [22, 67–71]. Adding hoppings to the second  $t'$  and third  $t''$  near neighbors  $t'$  and  $t''$  [6–8, 72–76] one arrives to the Hamiltonian of the  $tt't''$ -J model (3) in the spin wave approximation. A hole ( $h_{\mathbf{k}}$  is its annihilation operator) with dispersion  $\varepsilon(\mathbf{k}) = 4t' \cos(k_x) \cos(k_y) + 2t'' [\cos(2k_x) + \cos(2k_y)]$  moves in the field of magnons ( $\alpha_{\mathbf{k}}$  is annihilation operator of the magnon):

$$\hat{H}_{t-J}^0 = \sum_{\mathbf{k}} \varepsilon(\mathbf{k}) h_{\mathbf{k}}^\dagger h_{\mathbf{k}} + \sum_{\mathbf{k}} \omega_{\mathbf{k}} \alpha_{\mathbf{k}}^\dagger \alpha_{\mathbf{k}}. \quad (3)$$

The dispersion of magnons is  $\omega_{\mathbf{k}} = 2J\sqrt{1 - \gamma_{\mathbf{k}}^2}$ , where  $\gamma_{\mathbf{k}} = (\cos k_x + \cos k_y)/2$ . The hole is scattered by magnons

$$\hat{H}_{t-J}^{\text{h-m}} = N^{-1/2} \sum_{\mathbf{k}, \mathbf{q}} M_{\mathbf{k}, \mathbf{q}} [h_{\mathbf{k}}^\dagger h_{\mathbf{k}-\mathbf{q}} \alpha_{\mathbf{q}} + \text{h.c.}] \quad (4)$$

with the scattering vertex  $M_{\mathbf{k}, \mathbf{q}}$ . Amplitudes  $t$ ,  $t'$ , and  $t''$  describe hoppings to the nearest, next nearest, and next next nearest neighbors. The simplest t-J model corresponds to the case when  $t'$  and  $t''$  are set to zero. For hole (electron) doping the signs of the hopping amplitudes are  $t > 0$ ,  $t' < 0$ , and  $t'' > 0$  ( $t < 0$ ,  $t' > 0$ ,  $t'' < 0$ ) [76–79]. Note that t-J model can be also derived from the Hubbard model [80, 81]

$$H_H = -t \sum_{\langle ij \rangle \sigma} (\tilde{c}_{i\sigma}^\dagger \tilde{c}_{j\sigma} + \text{h.c.}) + U \sum_i n_{i\uparrow} n_{i\downarrow} \quad (5)$$

with large  $U \rightarrow \infty$ .

In the generalized  $tt't''$ -J-Holstein ( $tt't''$ -J-H) model the short range EPI with dispersionless phonons with frequency  $\Omega_0$ ,

$$\hat{H}^{\text{ph}} = \Omega_0 \sum_{\mathbf{k}} b_{\mathbf{k}}^\dagger b_{\mathbf{k}}, \quad (6)$$

is described by Holstein Hamiltonian:

$$\hat{H}^{\text{e-ph}} = N^{-1/2} \sum_{\mathbf{k}, \mathbf{q}} \frac{\sigma}{\sqrt{2M\Omega_0}} [h_{\mathbf{k}}^\dagger h_{\mathbf{k}-\mathbf{q}} b_{\mathbf{q}} + \text{h.c.}]. \quad (7)$$

Here  $\sigma$  is the coupling constant which is determined by the strength of coupling of the hole to the lattice displacement and which does not depend on the mass of isotope. The expression in front of square bracket is the standard Holstein coupling constant  $\gamma = \sigma/\sqrt{2M\Omega_0}$ . Another frequently used coupling constant is  $g = \gamma/\Omega_0$ . The most frequently used measure for the strength of the EPI is the dimensionless coupling constant  $\lambda = \gamma^2/4t\Omega_0$ .

The reason for the strong EPI in the system described by the t-J model is the large energy involved into formation of the Zhang-Rice singlet. This energy of several eVs in the rigid lattice is trivial constant. However, when the lattice is deformed by phonons, change of the amplitudes  $t_{pd}$  leads to the strong EPI [61, 82–93]. Estimate for EPI obtained from the three-band model is  $\lambda \approx 1$  [62].

Another source of EPI is the Fröhlich interaction with the phonons polarized along  $c$  axis which broaden and soften with increase of doping [94, 95]. These phonons

recently attracted interest [96] driven by new ARPES data on  $\text{Bi}_2\text{Sr}_2\text{CuO}_6$  [97]. However, importance of such phonons was noted long ago [98].

Large EPI in cuprates arises due to strong electronic correlations [61, 89] because calculations by Local Density Approximation (LDA) method give the coupling constants which are smaller by an order of magnitude [99]. However, these results are doubtful since the phonon linewidth, obtained by LDA [100], is considerably smaller than the linewidth seen in experiment [101]. The authors of [102] claim that the kink cannot be driven by EPI because effect of EPI on ARPES spectra is negligible. However, as it was shown in [103], calculations by the method used in [102] do not reproduce the linewidth of phonons seen in experiment [104–108]. Hence, conclusions of [102] about kinks are at least doubtful.

### 3. Spectroscopy

There is no adopted agreement whether kinks in ARPES dispersion are driven by interaction with phonons or magnetic resonance mode. However, recent experiments on the isotope effect of the ARPES spectra give confidence that the kinks are due to interaction with phonons. Another evidence for the phonon origin of the kinks follows from the ARPES spectra measurements in the electron doped compounds where kinks and magnetic resonance mode are located on absolutely different energies. The results concerning kinks are presented in Section 3.1.

The most obvious and undebatable evidence for EPI can be found in phonon spectra where EPI is manifested in the softening and broadening of particular phonons. Experimental and theoretical results on the phonon anomalies are reviewed in Section 3.2.

Theoretically, ARPES signal measured in the undoped compounds corresponds to the Lehmann Function (LF) of a hole in the  $t't''$ -J model. The LF of this model [6, 37, 72] has a narrow  $\delta$ -functional peak at low-energies and high-energy incoherent continuum. Dispersion of the low-energy peak is in perfect agreement with the experimental momentum dependence. However, even the narrowest width of the experimental peak in the nodal point  $(\pi/2, \pi/2)$  is larger than the dispersion bandwidth [57, 59]. This is the main contradiction of the experiment with the  $t't''$ -J model because the theoretical width of the peak in the nodal point is zero [37]. The interpretation of the linewidth in terms of EPI [109] was suggested long ago but confronted with the fact that EPI must not only broaden the line but considerably change the dispersion. Solution to the problem of the large linewidth of ARPES line is presented in Section 3.3. For  $\lambda > 0.4$  in the t-J-H model the agreement with experiment is perfect. At strong EPI the quasiparticle loses its weight, becomes dispersionless, and cannot be seen in ARPES spectra. The whole weight of the quasiparticle is transformed into the broad Franck-Condon shake-off peak whose dispersion inherits the dispersion of the pure t-J model.

The estimate of  $\lambda$  was done by several methods. The most detailed and convincing estimates were done in [62]

where  $\lambda$  was determined from the calculation of the change of Zhang-Rice singlet energy with lattice deformation, from the linewidth of the peak, and the distance of the Franck-Condon peak from the chemical potential. All these methods give  $\lambda \sim 1$  which is enough to bring the system into the strong coupling regime. These and other methods to determine  $\lambda$  are described in the Section 3.4.

One of the most important experiments to reveal the role of EPI is the isotope effect on the ARPES spectra. Experimentally, the isotope effect on the ARPES of doped compounds was measured many times [110–113] but the most reliable result is obtained in [113]. Keeping in mind how many contradictions were overcome to measure the isotope effect on the doped compounds it is clear why the isotope effect on the undoped compounds, where preparation of specimens is more difficult, was not measured up to now. However, there is a theoretical prediction for the undoped case [46] which is presented in Section 3.5.

It was noted long ago [60] that the net influence of the polaronic effect is unable to explain anomalous temperature dependence of the ARPES spectra. Also, the pure t-J model is unable to explain the experimental data too [114]. However, the joint influence of the magnetic and lattice degrees of freedom, as it is shown in Section 3.6, perfectly explains the anomalous temperature dependence.

One more proof of the interplay of magnetic and lattice effects can be got from the study of the OC of the weakly doped compounds. Two-peak structure of the MIR OC was tacitly resolved in many measurements [23, 27, 115–120]. Recent measurement by ellipsometry resolved the two-peak structure clearly [51]. Section 3.7 reviews results of the calculation of the OC in the framework of the t-J-H model [51] where theoretical OC shows two-peak structure due to interplay of magnetic and lattice degrees of freedom. Dependence of the OC on doping gives possibility to estimate dependence of the coupling constant  $\lambda$  on doping. It is shown that with  $\lambda \sim 1$  in the weakly doped systems the effective EPI decreases with doping coming to the moderate coupling regime  $\lambda \sim 0.5$  at the optimal doping.

There are many evidences that the local EPI of the Holstein model cannot explain many features of the high-temperature superconductors. First, it is well known that the very nature of coupling to the Zhang-Rice singlet and Fröhlich coupling to the  $c$ -axis phonons leads to nonlocal coupling vertexes. Second, the local coupling to phonons leads to huge masses of the holes which are not observed in experiment. One can continue with the fact that the local EPI leads to the contradicting to experiment stability of the antiferromagnetism in doped systems though above motivation is enough to look at the models where EPI is not local. Results concerning nonlocal EPI are presented in Section 3.8.

**3.1. Kinks.** The nature of the kinks is debated since its' discovery. Reasonable explanation of kinks is a battlefield between groups explaining its nature by the interaction with phonons and others prescribing the anomaly to the interaction with the magnetic resonance mode. Typical kinks in ARPES spectra are shown in Figure 1. Early studies [64,

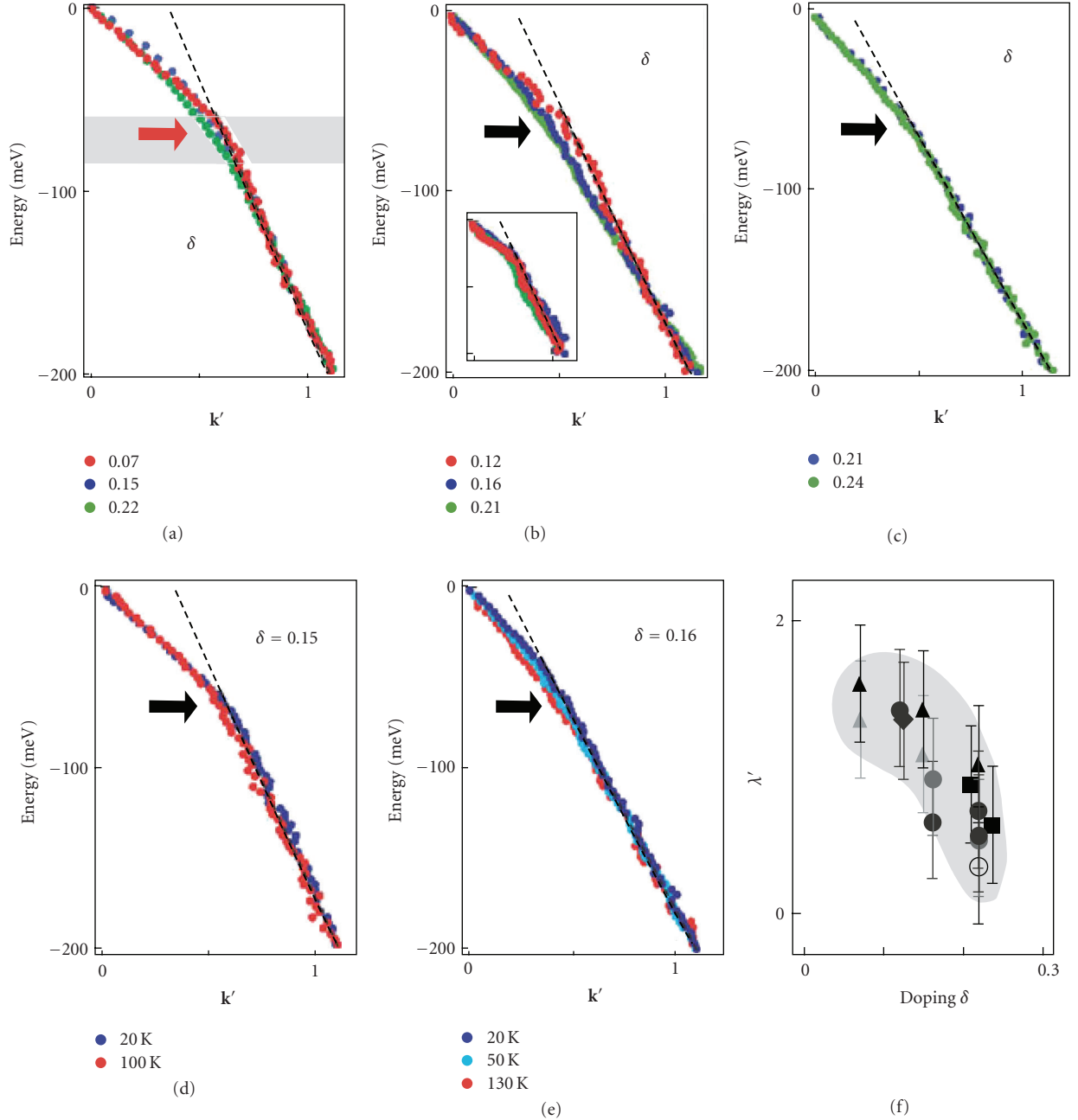


FIGURE 1: Quasiparticle dispersion in the direction  $(0,0) - (\pi,\pi)$  in the compounds  $\text{La}_{2-x}\text{Sr}_x\text{CuO}_4$  (LSCO),  $\text{Bi}_2\text{Sr}_2\text{CuO}_6$  (Bi2201), and  $\text{Bi}_2\text{Sr}_2\text{CaCu}_2\text{O}_8$  (Bi2212) at different temperatures and dopings. Panel (f) shows the value  $1 + \lambda'$ , evaluated by the change of the dispersion angle in the weak coupling theory for noninteracting electrons in metal, after Lanzara et al. [64].

121–127] indicated that the anomaly is located on the energy 70 meV. Later, refined analysis showed [97, 128] that there are structures with smaller energy. Kinks are observed not only along the nodal direction  $(0,0) - (\pi,\pi)$  but also in other directions [125–127, 129, 130].

Kinks were explained by interaction with phonons [90, 91, 131, 132] and by interaction with magnetic resonance mode [129, 133–139] which is observed in the magnetic neutron scattering on the cuprates [140–143]. Actually, it is very difficult to discern theoretically whether kink is

governed by magnetic or lattice subsystem. Detailed study [144] has led to conclusion that it is difficult to state which modes give the origin to the kink.

However, the nature of the kink can be revealed by experiments. There are two unambiguous evidences of the phononic nature of the kink. The first proof is obtained in [145]. As it is noted in [145] the optical phonons have energies 40 meV and 70 meV [146, 147] while the energy of the magnetic resonance mode in the hole doped compounds is 40 meV [140, 148]. Therefore, it was very

difficult to distinguish between phononic and magnetic scenarios because of the similar energy scales of magnetic and phononic excitations. However, recently found magnetic resonance mode in the electron doped compounds [149, 150] is on the energy of 10 meV and does not correspond to the energy of the kink whose energy is the same as it was in the hole doped compounds.

Another unambiguous evidence of the phononic nature of the kink follows from the isotope effect on the kink [113]. The change of the ARPES spectra occurs only in the close vicinity of the kink and the characteristic energy of the shift is  $3.4 \pm 0.5$  meV. Theoretical estimate for the isotopic shift of the breathing mode at the energy 70 meV is 3.9 meV. This value is in the excellent agreement with the measured isotopic shift.

**3.2. Phonons.** EPI decreases the frequencies of phonons and leads to decay of the phonons when the line observed in the inelastic neutrons scattering broadens. To determine which of the phonons are anomalous one makes an attempt to fit the experimental phonon branches by some standard, say, shell model. The phonons laying considerably lower than those predicted by the shell model are considered to be anomalous. From this point of view the breathing and half-breathing phonons are anomalous in doped systems [94, 101, 108, 147, 151–156].

Another characteristic feature of the anomalous phonon is the short lifetime manifested in the broad peak with large linewidth which sometimes reaches 5 meV [101] which is an order of magnitude larger than those of another lines whose linewidth is limited by experimental resolution. For example, breathing and half-breathing phonons connected strongly to Zhang-Rice singlet have large linewidth whereas the quadrupole ones which are not coupled to the singlet are narrow [108]. The phonon  $O_{\bar{z}}$  associated with the movement of the oxygen perpendicular to the  $\text{CuO}_2$  plain has large width of 16 meV [94, 95]. One more anomalous phonon is  $B_{1g}$  one changing its width with temperature [146, 157–159]. There is one more phonon anomaly with wave vector  $\mathbf{q} = (0.25, 0, 0)$  which was believed to be associated with stripe-like inhomogeneities of charge distribution [104] at the doping level  $x \approx 1/8$ . However, the same anomaly is observed at  $x \approx 0.08$  [160]. Moreover, it was noticed that the energy and momentum of the kink in ARPES match the corresponding parameters of the phonons [161].

In one of the first theoretical papers considering lattice vibrations in cuprates the phonon softening was found by exact diagonalization technique in the model where effective Hamiltonian was obtained from the three-band model [162]. Softening of the breathing  $\mathbf{q} = (\pi, \pi)$  and half-breathing  $\mathbf{q} = (\pi, 0)$  phonons was calculated in [83, 84, 87, 92]. The calculation predicted dependence of the softening on the doping concentration which was later confirmed experimentally [95]. Also, theoretical data on the phonon broadening [84] showed, in agreement with experiment, that the peak width is maximal at  $\mathbf{q} = (\pi, 0)$  and much smaller at  $\mathbf{q} = (\pi, \pi)$ .

The authors of the paper [88] studied the dependence of the EPI matrix element on the wave vectors of the electron

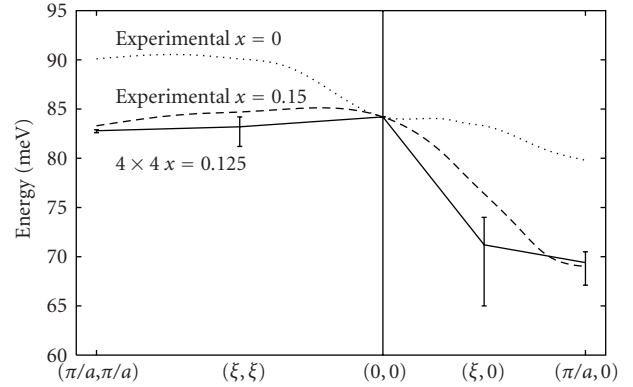


FIGURE 2: Phonon dispersion in the  $(1, 0)$  and  $(1, 1)$  directions. Experimental results are shown by dotted lines for  $x = 0$  and  $x = 0.15$ . Theoretical results (full curve) are shown for  $x = 0.125$ . The bars in theoretical results show the spread due to different boundary conditions, after Rösch and Gunnarsson [61].

and phonon and concluded that the interaction is strongly anisotropic. The authors found that the maximum of the broadening of the longitudinal optical phonons is associated with effective coupling of the  $d$ -symmetry pairing. Papers [163, 164] considered the charge response of the high-temperature superconductors arising from the ionic nature of the compounds. These papers predicted strong softening of the phonons with displacement along  $c$ -axis prior to experiment.

Using the first principle calculations and three-band model the paper [61] introduces the t-J-H model with derived from the first principles parameters. The exact diagonalization used to obtain the phonon spectral function gives the phonon dispersion which is in a good agreement with experimental data (see Figure 2) at the doping concentration  $x \approx 0.125$ .

**3.3. Ghost Particles in the ARPES.** The spectral function of the t-J-H model (3)–(7) was previously calculated by exact diagonalization (ED) of small clusters [165] and in the Non-Crossing Approximation (NCA) where all crossings of propagators are neglected [166, 167]. However, small size of the clusters in ED gives essentially discrete spectrum and prevent from studying of the lineshape [165, 168]. On the other hand the NCA is valid, strictly speaking, only for the weak coupling to phonons [42]. The NCA is good for magnons since the spin 1/2 cannot be flipped more than one time and, hence, the multiple accumulation of the bosons on one site is impossible. However, there is an accumulation of multiple bosons in the EPI channel and, hence, one has to avoid NCA for correct treatment of the EPI.

The implementation of the DMC method in [42] takes into account the mutual crossing of the phonon propagators but neglects both crossing of the phonon and magnon lines and mutual crossing of magnon lines. The NCA in the pure t-J model, as it was shown by comparison of the NCA results with the ED data [67, 68, 71, 169, 170], is good for  $J/t \leq 0.4$ . Similar conclusion is drawn for the t-J-H model [171]. Also, recent calculations of the spectral function of the t-J-H

model [172] by variational method [173, 174], which does not use NCA, confirmed the approximation made in [42].

Figures 3(a)–3(e) show the low-energy part of the spectral function in the ground state at  $\mathbf{k} = (\pi/2, \pi/2)$  in the regime of weak, intermediate and strong EPI.  $\lambda$ -dependence of the energies of the peaks (see Figure 3(f)),  $Z^{\mathbf{k}=(\pi/2, \pi/2)}$ -factor of the lowest peak (see Figure 3(g)), and average number of phonons in the phonon cloud (see Figure 3(h)) is typical for the self-trapping phenomenon [40, 175, 176].

Momentum dependence of the spectral function is shown in Figures 4(a)–4(d). Energy of the lowest peak with small spectral weight (shown by vertical arrows in Figures 4(a)–4(d)) does not demonstrate any visible momentum dependence. To the contrary, dispersion of the broad peak is perfectly reproduced by the relation (see Figure 4(e))

$$\varepsilon_{\mathbf{k}} = \varepsilon_{\min} + \frac{W_{J/t}}{5} \times \left\{ [\cos k_x + \cos k_y]^2 + \frac{[\cos(k_x + k_y) + \cos(k_x - k_y)]^2}{4} \right\}, \quad (8)$$

which perfectly describes the dispersion of the pure t-J model in the wide range of parameters  $0.1 < J/t < 0.9$  [71]. Note that such behavior of the broad Franck-Condon shake-off peak is robust for the whole strong coupling regime of the EPI.

At low temperature the spectral function in the adiabatic approximation is the sum of transitions between the lower  $E_{\text{low}}(Q)$  and the upper  $E_{\text{up}}(Q)$  sheet of the adiabatic potential. The transitions are weighted by the wave function of the lower sheet  $|\psi_{\text{low}}(Q)|^2$  [58]. If EPI is absent both in the initial  $E_{\text{low}}(Q) = Q^2/2$  and final  $E_{\text{up}}(Q) = \mathcal{D} + Q^2/2$  states of transition, the spectral peak has maximum at the energy  $\mathcal{D}$ . However, if the EPI  $\Delta E_{\text{up}}(Q) = -\lambda Q$  is present only in the final state  $\Delta E_{\text{up}}(Q) = -\lambda Q$ , the upper sheet of the adiabatic potential  $E_{\text{up}}(Q) = \mathcal{D} - \lambda^2/2 + (Q - \lambda)^2$  has the same energy at  $Q = 0$ . Hence, since the maximum of the probability in the initial state  $|\psi_{\text{low}}(Q)|^2$  is at  $Q = 0$ , the energy of the peak of the spectral function of the transition is still at the same energy  $\mathcal{D}$  (see Figure 4(f)). Note that the situation described above is the same as in the ARPES experiment in undoped cuprates. There is no EPI in the half-filled system (initial state) but there is EPI in the system with hole (final state).

The lowest dispersionless peak with small weight is too small to be easily observed in experiment. To the contrary one can easily observe wide Franck-Condon shake-off peak which mimics the dispersion of the pure t-J model. This theoretical picture suggests that the chemical potential of the weakly doped cuprates should not be associated with the broad peak but must be pinned by invisible real quasiparticle. The above conclusion was lately confirmed in experiment [59] (see Figure 5). Chemical potential is pinned to the peak B while the energy of the broad peak A is far from the peak B.

**3.4. The Values of  $\lambda$ .** One of the most detailed study of the strength of the EPI was undertaken by several methods in

[62]. For the explanation of the large linewidth of the ARPES spectra in the undoped  $\text{La}_2\text{CuO}_4$  the authors of [62] use the Hamiltonian obtained from the reduction of the three-band model. The parameters of the model were such that they give correct description of the phonon spectra in the realistic model of the  $\text{La}_2\text{CuO}_4$  with 21 phonon branches [61]. The EPI in the realistic model with 21 phonon branches reads

$$H_{\text{ep}} = \frac{1}{\sqrt{N}} \sum_{\mathbf{q}\nu i} g_{\mathbf{q}\nu} (1 - n_i) \sqrt{2\omega_{\mathbf{q}\nu}} Q_{\mathbf{q}\nu} e^{i\mathbf{q}\mathbf{R}_i}. \quad (9)$$

This Hamiltonian describes the interaction with the empty places forming singlet in the t-J model. Interaction is linear with respect to the lattice coordinates  $Q_{\mathbf{q}\nu}$  and coupling constants  $g_{\mathbf{q}\nu}$ . The phonon mode of frequency  $\omega_{\mathbf{q}\nu}$  is defined by its wave vector  $\mathbf{q}$  and phonon branch index  $\nu$ .  $n_i$  is the electron filling of the site  $\mathbf{R}_i$  and the total number of sites is  $N$ .

Effective EPI constant is defined in [62] as

$$\lambda \equiv \frac{1}{N} \sum_{\mathbf{q}\nu} \frac{|g_{\mathbf{q}\nu}|^2}{4t\omega_{\mathbf{q}\nu}}. \quad (10)$$

The value of  $\lambda$  at  $t = 0.4$  eV is estimated as  $\lambda = 1.2$ . Authors of [62] calculated the differential spectral distribution of the effective EPI

$$\gamma(\omega) = \frac{1}{N} \sum_{\mathbf{q}\nu} \frac{|g_{\mathbf{q}\nu}|^2}{\omega_{\mathbf{q}\nu}} \delta(\omega - \omega_{\mathbf{q}\nu}). \quad (11)$$

The spectral distribution (11) is compared with the fine structure of renormalization of the dispersion in the vicinity of kink measured in [128]. Good agreement of these two data encourages to believe into the phononic nature of the kinks and ensures that the estimate for the effective  $\lambda$  is correct.

To estimate the value of effective EPI from the difference of the energy of the real quasiparticle and Franck-Condon peak authors of [62] introduced the scaling  $g_{\mathbf{q}\nu} \rightarrow \Lambda g_{\mathbf{q}\nu}$  of the coupling constant in the (10). The theoretical binding energy for  $\Lambda = 1$  is 1.2 eV which is considerably larger than the experimental value 0.5 eV. The binding energy is proportional to  $\Lambda^2$  and even small overestimate of the coupling constants, originating from the underestimate of the screening in the shell model, can lead to strong overestimate of the binding energy. Reasonable values of the binding energy and linewidth can be obtained for  $\Lambda = 0.8$  which corresponds to  $\lambda = 0.75$ . Thus, one can conclude that EPI in the undoped cuprates ranges like  $0.75 < \lambda < 1.2$ . These values are larger than  $\lambda_c = 0.6$  [46] which is required for transition of the  $t't''$ -J-H model into the strong coupling regime.

Another source of the information about the strength of the EPI is the temperature dependence of the ARPES spectra. Comparison of the experimentally measured temperature dependence [177] and that calculated from the t-J-H model [50] gives the estimate  $0.5 < \lambda < 1.0$ . Comparison of the experimental and theoretical data for high-energy part of the ARPES spectra gives the same values. The

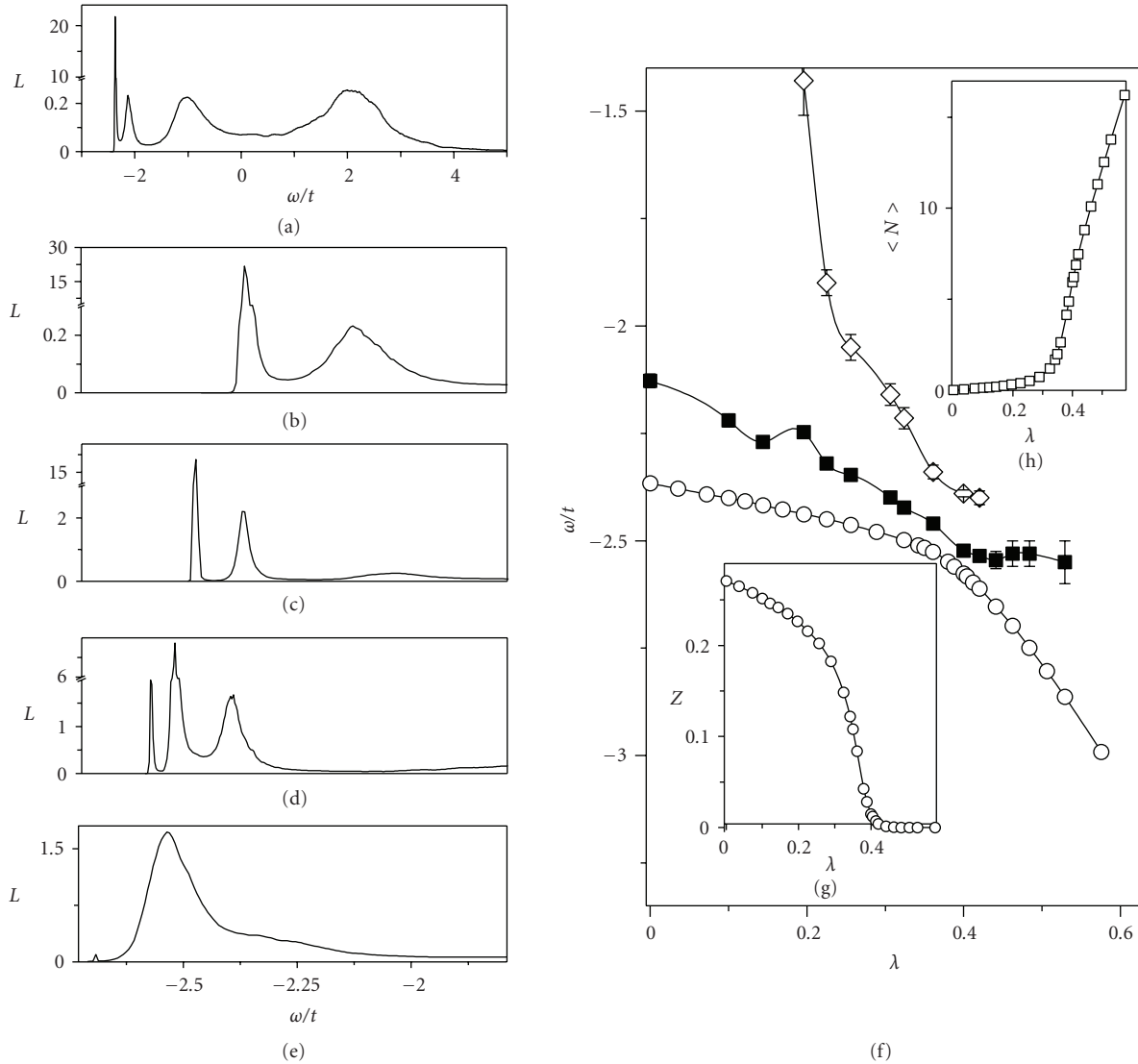


FIGURE 3: (a) Lehmann spectral function  $L$  of the ground state at  $\mathbf{k} = (\pi/2, \pi, 2)$  for  $J/t = 0.3$  and  $\lambda = 0$ . Low-energy spectral function  $L$  in the ground state  $\mathbf{k} = (\pi/2, \pi, 2)$  at  $J/t = 0.3$ : (b)  $\lambda = 0$ ; (c)  $\lambda = 0.3$ ; (d)  $\lambda = 0.4$ ; (e)  $\lambda = 0.46$ .  $\lambda$ -dependence at  $J/t = 0.3$ : (f) energies of the lowest resonances; (g)  $Z$ -factor of the lowest resonance; (h) average number of phonons.

waterfalls, observed in the range 1 to 2 meV [178–182], were reproduced by artificial broadening of the string resonances of the t-J model [183, 184]. Consecutive search for the physical mechanism for the artificial broadening led to conclusion that the broadening caused solely by nonzero temperature is not enough to explain the linewidth and has to take into account rather considerable EPI [63] with  $\lambda = 0.65$ .

Another method to get the value of  $\lambda$  is to compare the theoretical growth of the linewidth when the energy of quasi-particle exceeds the frequency of the dispersionless phonon with that measured above the kink energy. Such analysis for experimentally measured ARPES spectra in the electron doped compounds  $\text{Sm}_{2-x}\text{Ce}_x\text{CuO}_4$  ( $x = 0.1, 0.15, 0.18$ ),  $\text{Nd}_{2-x}\text{Ce}_x\text{CuO}_4$  ( $x = 0.15$ ), and  $\text{Eu}_{2-x}\text{Ce}_x\text{CuO}_4$  [145] gives the estimate  $\lambda = 0.8$ .

Recently developed method of time resolved electron diffraction is capable of studying the time evolution of the excited states [185]. Comparison of the experimental data with the results obtained in the framework of the theory of relaxation in metals [186] led to conclusion that anisotropic  $\lambda$  is in the range  $0.08 < \lambda < 0.55$ . And last, comparison of the isotope shift of the OC of the undoped compounds [187] with theoretical results [188] gave the estimate  $\lambda \geq 1$  [189].

**3.5. Isotope Effect in ARPES.** Experimentally, isotope effect (IE) was studied only for highly doped compounds and the main emphasis was made on studies of the kinks. The ARPES spectra data were measured in compounds where oxygen was represented by  $^{16}\text{O}$  and  $^{18}\text{O}$  isotopes. The first results for IE on the kinks in ARPES spectra [110, 190] received a lot of skepticism caused by the structure of the isotope shift.

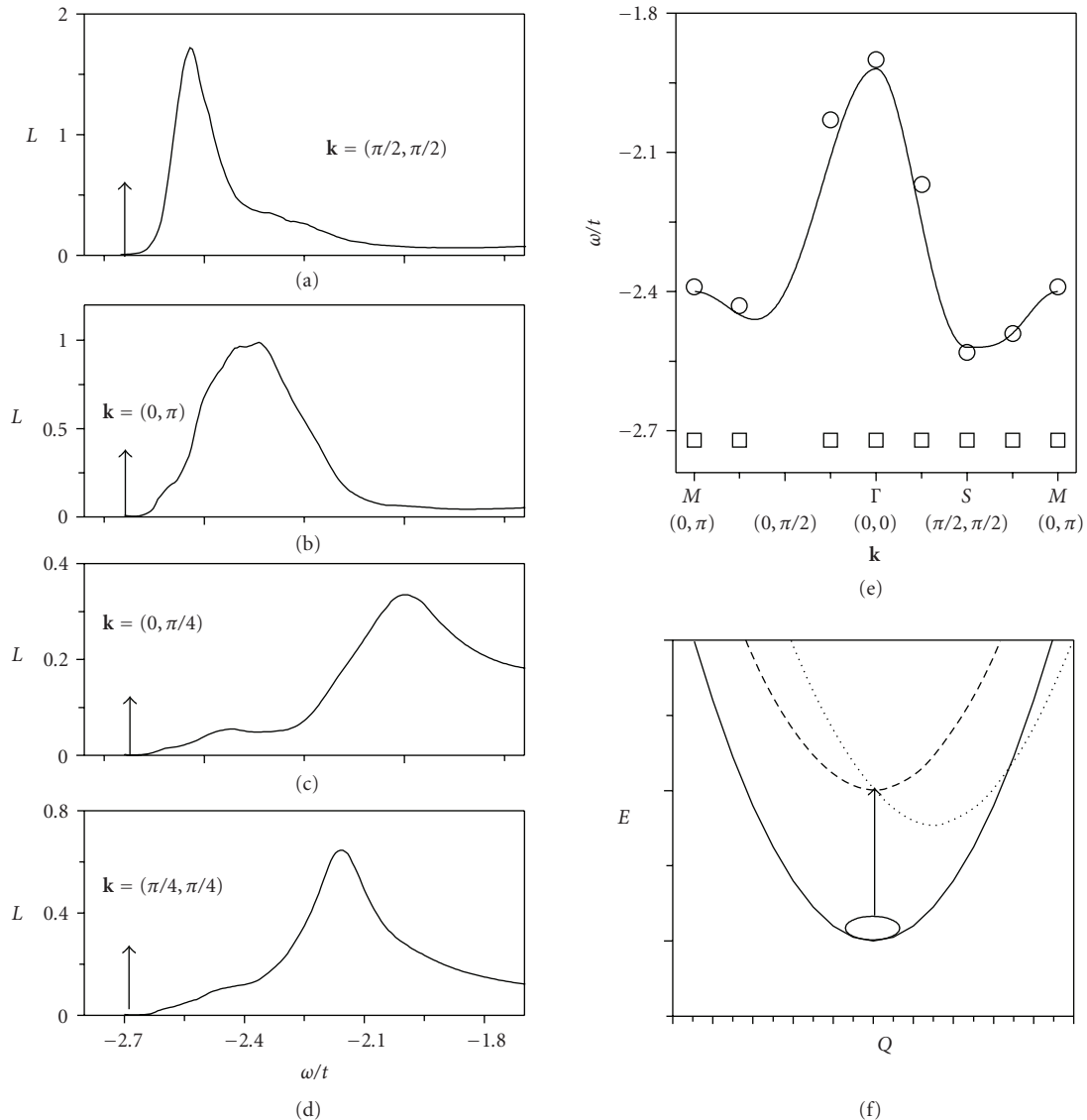


FIGURE 4: Low-energy part of the spectral function of the hole at  $J/t = 0.3$  and  $\lambda = 0.46$  (a)–(d). The vertical arrows in (a)–(d) denote the position of the quasiparticle invisible in the scale of the figure because of low weight. (e) Dispersion of resonances at  $J/t = 0.3$ : broad resonance (circles) and the quasiparticle with small weight (squares) at  $\lambda = 0.46$ . The solid line is the dispersion of the hole (8) in the pure t-J model at  $J/t = 0.3$  ( $W_{J/t=0.3} = 0.6$ ) and  $\varepsilon_{\min} = -2.52$ . Panel (f) shows the potential of ground state  $Q^2/2$  (solid line), potential of the excited state without the lattice relaxation (dashed line), and potential of the excited state after the lattice relaxation  $D + (Q - \lambda)^2/2 - \lambda^2/2$  (dotted line).

The shift was observed in the high-energy region beyond the phonon energy.

Further experiments were in contradiction with the results obtained in [110, 190]. Measurements [111] did not observe the IE at large energies. It was also noted that even tiny sample misalignment of 0.1 degree can lead to considerable shifts at large energies. Also, measurements presented in [111] noted the general shift of the spectral features by 3 meV which is consistent with results of tunneling experiments [191, 192].

The most detailed and precise analysis of the IE on ARPES spectra was presented in [113]. IE on ARPES was observed only in the vicinity of the kink and the shift of

spectral feature around  $3.4 \pm 0.5$  meV (see Figure 6) was found. Extremely high precision of the measurement done in [113] arises from the novel method of low-energy ARPES with resolution much higher [193] than that typical for conventional ARPES technique. Calculations show that the breathing mode at the energy 70 meV has to be shifted by the IE by 3.9 meV which is in perfect agreement with experimental data.

There are a lot of studies of the IE on the polaronic systems. Holstein model was studied in [194–197] by the path integral Monte Carlo method [198] and Dynamical Mean Field Theory (DMFT) method [199]. The change of the effective mass by the isotope substitution is the largest

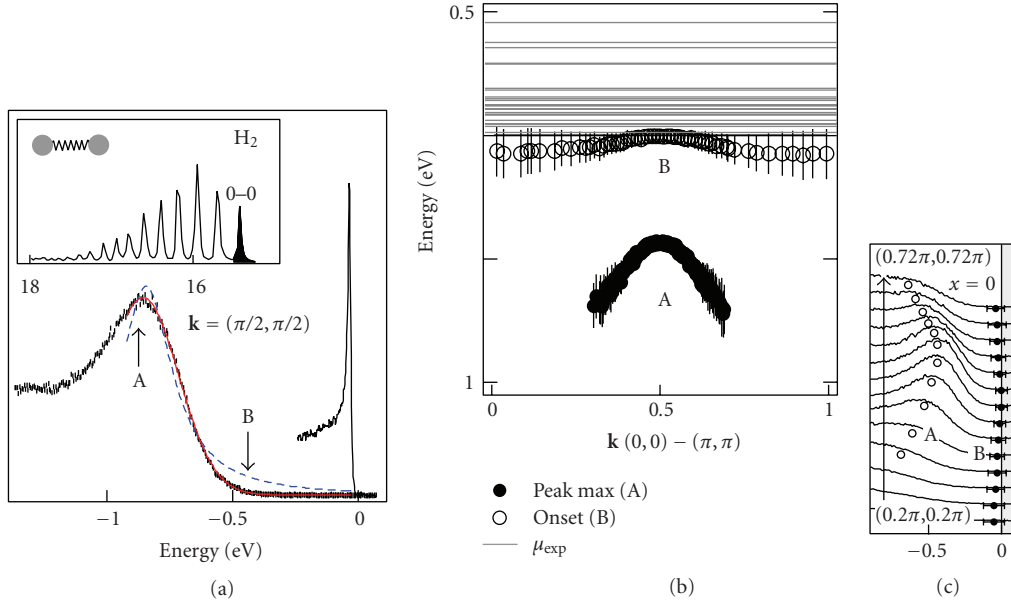


FIGURE 5: (a) ARPES spectrum of the undoped  $\text{Ca}_2\text{CuO}_2\text{Cl}_2$  in the nodal point  $\mathbf{k} = (\pi/2, \pi/2)$  fitted by Lorentzian (dashed line) and Gaussian (thick solid line). The notations A and B define the maximum of the peak and the point where spectral density arises, respectively. Narrow peak in the vicinity of zero energy is the ARPES spectrum of  $\text{SrRuO}_4$ . (b) Dispersion of A and B. The positions of the chemical potentials for different samples are shown by the horizontal lines. (c) Experimental ARPES spectra in the vicinity of the nodal point, after Shen et al. [59].

in the intermediate coupling regime. The IE in the Holstein-Hubbard systems was studied in [200–202].

The IE on the ARPES spectra for three-band model was studied in [132]. The interplay of EPI and electronic correlation is neglected in this paper but, however, the usage of the realistic model leads to many new and interesting conclusions. In agreement with experiment [113] the maximal IE is observed in the vicinity of the phonon frequency. It was also concluded that the kink cannot be caused by the electronic subsystem alone.

Nowadays it is important to attempt experiments to study IE on the ARPES spectra of undoped compounds. In addition to the high-temperature superconductors, there are other systems where broadening of the ARPES peak by EPI can be considered as a possible scenario. The list of such systems includes diatomic molecules [203], manganites with colossal magnetoresistance [204], quasi-one-dimensional Peierls conductors [205, 206], and Verwey magnetites [207].

Theoretical study of the IE on ARPES spectra of undoped system, specific for high-temperature superconductors because of choice of the  $t't''$ -J-H model, was done in [46]. Dimensionless coupling constant  $\lambda = \gamma^2/4t\Omega$  does not depend on the isotope mass in case when the relation between phonon frequency and mass  $\Omega \sim 1/\sqrt{M}$  holds. The isotopic factor is defined as  $\kappa_{\text{iso}} = \Omega/\Omega_0 = \sqrt{M_0/M}$ . Parameters for  $t't''$ -J-H model were chosen to reproduce the experimental ARPES spectra dispersion [6]:  $J/t = 0.4$ ,  $t'/t = -0.34$ , and  $t''/t = 0.23$ . Phonon frequency [5] is  $\Omega_0/t = 0.2$  and the isotopic factor for change from  $^{16}\text{O}$  to  $^{18}\text{O}$  is  $\kappa_{\text{iso}} = \sqrt{16/18}$ .

To avoid errors the ARPES spectra in [46] were calculated for nonsubstituted compound ( $\kappa_{\text{nor}} = 1$ ), actual isotope

substituted compound ( $\kappa_{\text{iso}} = \sqrt{16/18}$ ), and imaginary anti-isotope substituted compound ( $\kappa_{\text{ant}} = \sqrt{18/16}$ ). Monotonic dependence of the spectral function and other parameters on  $\kappa$  ensures in the absence of instability. The errorbar of a number  $\mathcal{A}$  can be evaluated using values  $\mathcal{A}_{\text{iso}} - \mathcal{A}_{\text{nor}}$ ,  $\mathcal{A}_{\text{nor}} - \mathcal{A}_{\text{ant}}$ , and  $(\mathcal{A}_{\text{iso}} - \mathcal{A}_{\text{ant}})/2$ .

Figure 7 shows the IE on the low-energy part of ARPES spectra for different EPI couplings in the nodal and antinodal points. All spectral features are shifted to larger energies for larger mass ( $\kappa < 1$ ). The shift of the broad Franck-Condon peak is considerably larger than the shift of the narrow peak corresponding to the real quasiparticle. Moreover, for larger values of  $\lambda$  the shift of quasiparticle energy goes to zero and the only influence of the IE is the decrease of the spectral weight  $Z$  with the increase of the isotope mass. To the contrary, shift of the Franck-Condon peak is not suppressed by the increase of EPI. In all cases, except the spectral function in the nodal point at  $\lambda = 0.62$  (see Figures 7(a) and 7(b)) where weight  $Z$  of the quasiparticle is still large, there is general feature of the IE on the broad Franck-Condon peak. The height of this peak increases with increase of the isotope mass. Taking into account the sum rule  $\int_{-\infty}^{+\infty} L_{\mathbf{k}}(\omega) = 1$ , very small weight  $Z$  of the quasiparticle peak, and the complete absence of IE on the high energy spectrum [46] one can conclude that the Franck-Condon peak decreases its width with the increase of the isotope mass.

The spectral function of the independent oscillator model is the Poisson distribution [208]:

$$L(\omega) = \exp\left[-\frac{\xi_0}{\kappa}\right] \sum_{l=0}^{\infty} \frac{[\xi_0/\kappa]^l}{l!} \mathcal{G}_{\kappa,l}(\omega). \quad (12)$$

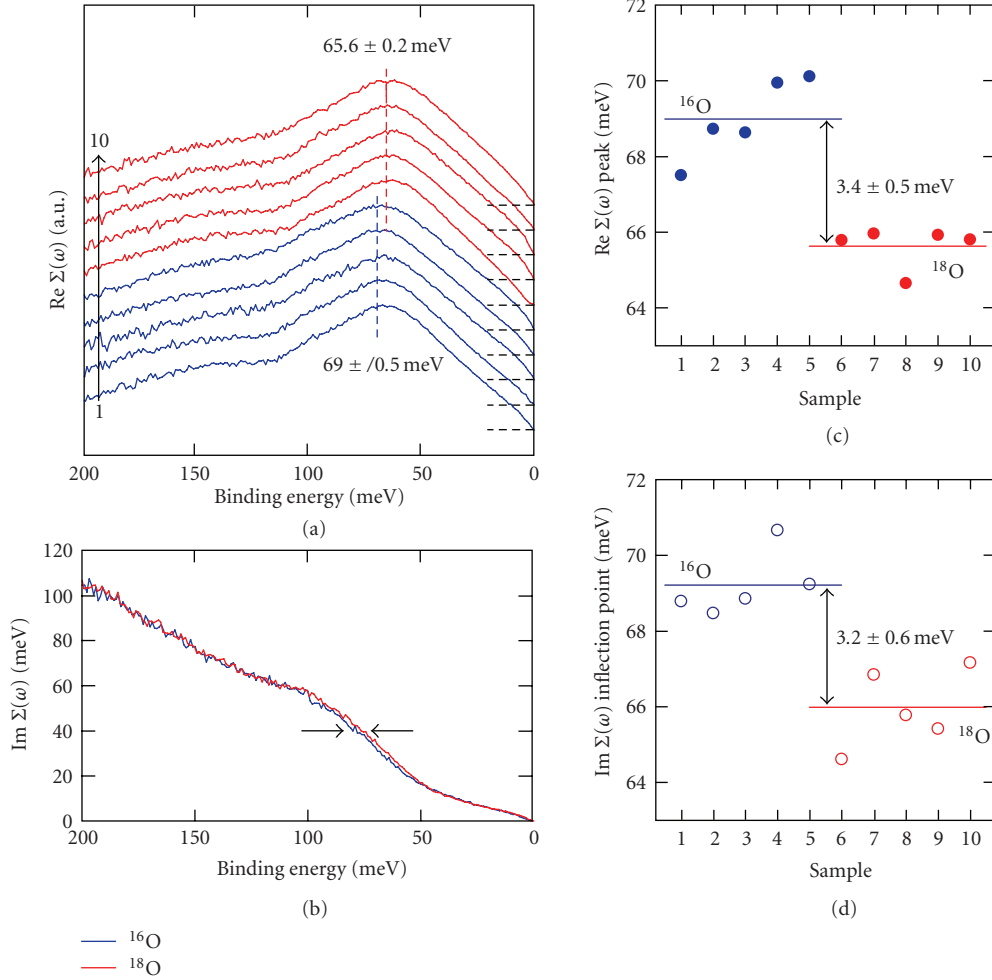


FIGURE 6: (a) Real part of the self-energy  $\text{Re}\Sigma(\omega)$  from five samples both for  $^{16}\text{O}$  (lower curves) and  $^{18}\text{O}$  (upper curves). All  $\text{Re}\Sigma(\omega)$  are deduced by subtracting a bare band dispersion from the experimental one. (b) Imaginary part of the self-energy  $\text{Im}\Sigma(\omega)$  determined from the full width of the momentum distribution curves. (c), (d) Obtained kink energy as a function of sample numbers both for  $^{16}\text{O}$  (to the left) and  $^{18}\text{O}$  (to the right) from  $\text{Re}\Sigma(\omega)$  and  $\text{Im}\Sigma(\omega)$ , after Iwasawa et al. [113].

Here  $\xi_0 = \gamma_0^2/\Omega_0^2 = 4t\lambda/\Omega_0$  is dimensionless coupling constant for initial system, and  $\mathcal{G}_{\kappa,l}(\omega) = \delta[\omega + 4t\lambda - \Omega_0\kappa l]$  is a  $\delta$ -function. For strong EPI limit the exactly solvable independent oscillator model is very helpful to describe the IE on ARPES spectra because the most of properties of the numeric solution are very close to the properties of the spectrum described (12).

**3.6. Temperature Dependence of ARPES.** The unique feature of the undoped and underdoped compounds with high-temperature superconductivity is the strong interplay of the lattice and magnetic degrees of freedom. One of the most vivid consequence of this interplay is the anomalous temperature dependence of the ARPES spectra. Really, it was realized long ago that the very scale of the experimental temperature dependence is considerably larger than that predicted by the conventional polaron theory [60]. The magnetic subsystem alone is also a wrong candidate [114] to describe the experimental anomaly since the typical

energy scale of the magnon energy is  $\sim 2J \approx 0.2$  eV which is even larger than the typical phonon energies  $\sim \Omega_0 \approx 0.04$  eV. Recent studies revealed one more puzzling feature questioning the polaronic scenario in general. The temperature dependence of the width of the broad Franck-Condon peak is linear in the range  $200 \text{ K} < T < 400 \text{ K}$  [177] and extrapolates to zero at zero temperature.

Previously, the ARPES spectra of the t-J-H model were studied by exact diagonalization method [165, 209, 210], in the noncrossing approximation [166, 167], and by DMC method [42, 46]. All these calculations were done for the case of zero temperature. All the above methods have their own difficulties preventing their reliable and fast generalization to finite temperatures.

A novel method capable of obtaining reliable data on the ARPES spectra of the t-J-H model at finite temperature was developed in [50, 211]. The main difficulty for studying of the t-J-H model lies in the profound difference between interactions of a hole with phonons and magnons. The

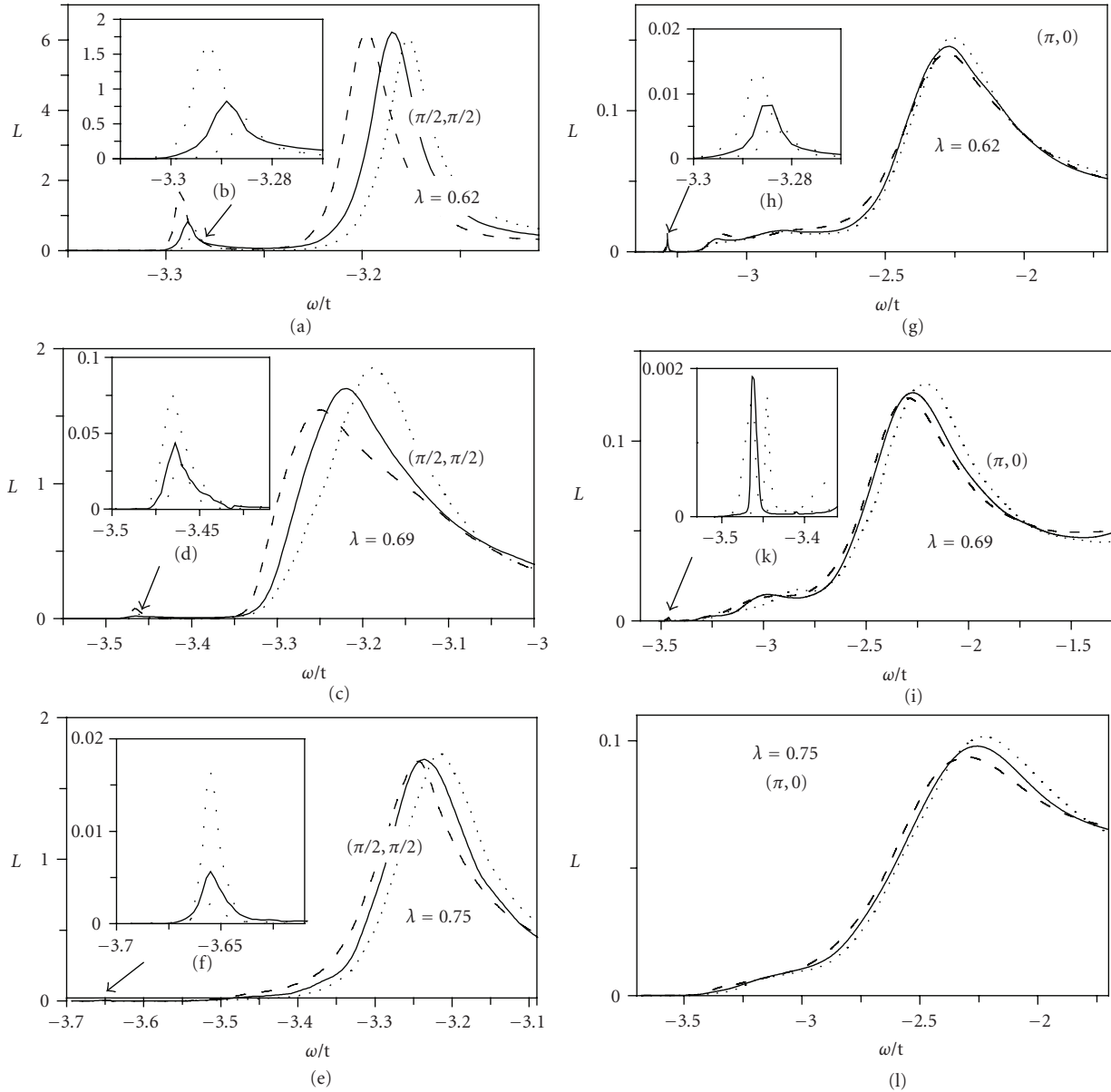


FIGURE 7: Low-energy part of the spectral function. Spectra of normal, isotope substituted, and “anti-isotope” substituted compounds are drawn by solid, dotted, and dashed lines, respectively. (a), (c), (e) and (g), (i), (l) correspond to nodal  $(\pi/2, \pi/2)$  and antinodal  $(\pi, 0)$  points. Insets (b), (d), (f), (h), and (k) show the peak corresponding to real quasiparticle.

Hybrid Dynamical Momentum Average (HDMA) method, developed in [50], just using difference of two interactions treating them with different techniques. The HDMA method unites advantages of classical Momentum Average (MA) method [212–221], which keeps information on the dispersion of the bare quasiparticle, and self-consistent Dynamical Mean Field Theory approximation (DMFT) [222–232], which is capable of treating strong but local interactions nonperturbatively.

Although the energy scales of bosons and phonons are basically the same, the nature of interactions of the hole with magnons and phonons is considerably different. The interaction with magnons is essentially momentum

dependent and always weak. Really, spin 1/2 cannot be flipped more than once limiting, thus, the maximal number of magnons on one site to one [233]. Hence, for small enough values of  $J/t$  [68, 171] NCA is a good approximation. To the contrary, interaction with phonons is local and can be very strong. Thus, one cannot use NCA for phonons since it fails already for intermediate couplings [42]. Hence, one is to treat magnons by a weak coupling method which is able to handle the momentum dependence carefully and sum the phonon variables by a local nonperturbative method.

Nonperturbative approaches which neglect the momentum dependence of self energy on momentum are MA

and DMFT methods. In both cases, the hole self-energy is expressed in terms of continuous fraction:

$$\Sigma_{\text{h-ph}}[\alpha(\omega)] = \frac{\gamma^2 \alpha(\omega - \Omega_0)}{1 - \frac{2\gamma^2 \alpha(\omega - \omega_0) \alpha(\omega - 2\Omega_0)}{1 - \frac{3\gamma^2 \alpha(\omega - 2\Omega_0) \alpha(\omega - 3\Omega_0)}{1 - \dots}}} \quad (13)$$

Then, DMFT and MA differ in the definition of the function  $\alpha(\omega)$  which is determined from the self-consistent procedure in DMFT and obtained from the momentum average of the Green function in MA. Suggested in [50] approach introduces the self-energy as a sum of contribution from magnetic and phononic subsystems:

$$\Sigma_{\text{tJH}}(\mathbf{k}, \omega) = \Sigma_{\text{h-mag}}^{\text{SCBA}}(\mathbf{k}, \omega) + \Sigma_{\text{h-ph}}[\alpha_{\text{tJH}}(\omega)]. \quad (14)$$

Weak and anisotropic interaction with magnons is treated in NCA:

$$\Sigma_{\text{h-mag}}^{\text{SCBA}}(\mathbf{k}, \omega) = \sum_{\mathbf{q}} \frac{M_{\mathbf{k},\mathbf{q}}^2}{\omega - \omega_{\mathbf{q}} - \Sigma_{\text{tJH}}(\mathbf{k} - \mathbf{q}, \omega - \omega_{\mathbf{q}}) + i\varepsilon}, \quad (15)$$

while the function  $\alpha(\omega)$  for the phonon part of the hole self-energy

$$\alpha_{\text{tJH}}(\omega) = \frac{1}{N} \sum_{\mathbf{k}} \frac{1}{\omega - \Sigma_{\text{h-mag}}^{\text{SCBA}}(\mathbf{k}, \omega) + i\varepsilon} \quad (16)$$

is expressed in terms of momentum-averaged bare Green function whose momentum dependence is determined by magnetic self-energy (16) obtained in NCA. Usage of MA instead of DMFT in (16) is crucial since the DMFT even does not distinguish even between t-J<sub>z</sub> and t-J model [223]. To the contrary, results obtained from (13)–(16), as it is shown by comparison with DMC data [42], correctly reproduce not only the ground state properties but the spectral function too.

The advantage of the suggested in [50] approach is that it is easily generalized to finite temperatures. Transforming magnetic self-energy  $\Sigma_{\text{h-mag}}^{\text{SCBA}}(\mathbf{k}, \omega)$  [208, 234] to the Matsubara form, one gets

$$\Sigma_{\text{h-mag}}^{\text{SCBA}}(\mathbf{k}, \omega) = \sum_{\mathbf{q}} \frac{M_{\mathbf{k},\mathbf{q}}^2 (1 + n_b(\omega_{\mathbf{q}}))}{\omega - \omega_{\mathbf{q}} - \Sigma_{\text{tJH}}(\mathbf{k} - \mathbf{q}, \omega - \omega_{\mathbf{q}}) + i\varepsilon} + \sum_{\mathbf{q}} \frac{M_{\mathbf{k}+\mathbf{q},\mathbf{q}}^2 (n_b(\omega_{\mathbf{q}}))}{\omega + \omega_{\mathbf{q}} - \Sigma_{\text{tJH}}(\mathbf{k} + \mathbf{q}, \omega + \omega_{\mathbf{q}}) + i\varepsilon}, \quad (17)$$

where  $n_b(\omega)$  is the Bose distribution. To generalize the phonon self-energy (13) to finite temperatures one uses the momentum-independent relation [225, 226]

$$\Sigma_{\text{h-ph}}[\alpha(\omega)] = \alpha^{-1}(\omega) - \sum_{n=0}^{\infty} \frac{(1-x)x^n}{\alpha^{-1}(\omega) - A_n(\omega) - B_n(\omega)}. \quad (18)$$

Here  $x = \exp(-\beta\Omega_0)$ , and  $A_n(\omega)$  and  $B_n(\omega)$  are known functions depending on the coupling constant and frequency [50]. Also, (14), (16), (17), and (18) are solved self-consistently. The spectral functions obtained from these equations obey three first sum rules for any coupling constants and temperatures [212, 220]. Hence, the peak position and its width should be reliable.

Temperature dependence of the spectral function in the ground state  $k = (\pi/2, \pi/2)$  for different  $\lambda$ s is shown in Figure 8. The general trends are in agreement with experiments [60, 109, 177, 235]. Distance of the Franck-Condon peak from the chemical potential and its width increases with the increase of temperature. Note that peak width is a constant up to the temperature  $T \approx \Omega_0/2 \approx 200$  K and then show a linear temperature dependence (see Figure 8). This linear dependence, if no data for low temperatures, can be indeed extrapolated to wrong low temperature values. However, in accordance with recent experiments [60, 236], the linewidth saturates at temperatures  $T \leq \Omega_0/2$  to a constant value. Note that the slope of the temperature dependence for  $T > \Omega_0/2$  does not depend on  $\lambda$  whereas the saturation values of the linewidth for  $T < \Omega_0/2$  are very sensitive to the strength of EPI.

Hence, temperature dependence of the Franck-Condon peaks in the low-energy (0.3–0.6 eV) part of the ARPES spectra manifests strong EPI. The evidence of the strong EPI was recently found in the high-energy ARPES too. It follows from the temperature dependence of high-energy “waterfall” features in ARPES [63]. The “waterfalls” at the energies 1–2 eV are the parts of the ARPES spectra where dispersion is parallel to the energy axis in the energy-momentum reference frame [178–182]. At first, the structure of “waterfalls” was reproduced by artificial broadening of the spectra of the t-J model [183, 184]. Then, an attempt to explain the artificial broadening by finite temperature and EPI was made in [63]. The method of self-consistent treatment of Dyson equation [68, 69, 237] was generalized to finite temperature and EPI is added. It is concluded [63] that the finite temperature alone is not enough to explain the effect and strong EPI is compulsory to explain the data.

Another explanation of the “waterfalls” was suggested in [238] where spectral density at large energies is attributed to contribution of localized states.

**3.7. Multippeak Structure of the Optical Conductivity Mediated by EPI.** The optical conductivity (OC) of the weakly doped cuprates has the following characteristic features [23, 24, 70]. The high-energy part of OC in undoped systems has the peak at  $\omega \cong 1.5$  eV which corresponds to charge transition between p-orbitals of O and d-orbitals of Cu. Low-energy part of OC, caused by movement of holes, arises with doping. The Drude contribution at the lowest energy in proportional to the holes concentration  $x$  and the relaxation rate of the Drude theory is proportional to temperature. Puzzling part of the OC is the mid infrared (MIR) peak with doping-dependent frequency around  $\omega_{\text{MIR}} \cong 0.5$  eV whose interpretation is still far from adopted [25]. Theoretically the OC of t-J model was studied in the low density limit and a peak at  $2J \approx 0.28$  eV was found [9–22] (for typical  $t = 0.4$  eV

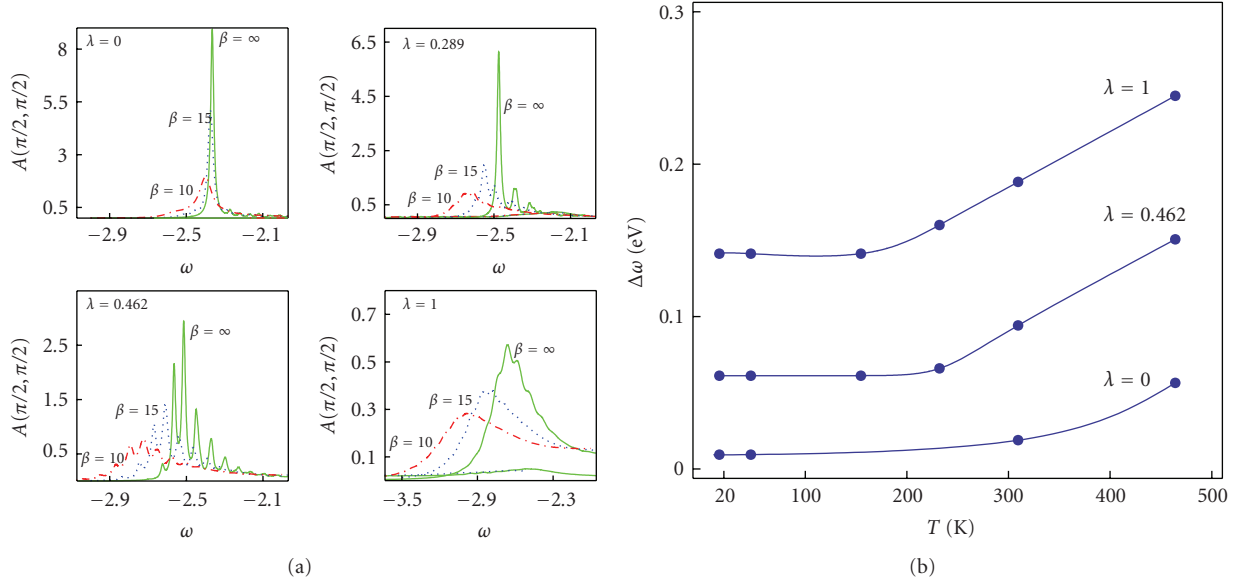


FIGURE 8: (a) Spectral functions for different  $\lambda$  and temperatures  $\beta = t/T$ . (b) Peak width  $\Delta\omega$  as a function of temperature  $T$  for the t-J model ( $\lambda = 0$ ) and t-J-H model in the strong coupling EPI limit ( $\lambda = 0.462$  and  $\lambda = 1$ ). Temperature is in Kelvins under assumption that  $t = 0.4$  eV.

and  $J = 0.35t$ ). The above energy is almost two times smaller than the low-doping experimental value 0.5 eV. Hence, to shift theoretical peak of the t-J model to higher energies, one can try to add EPI and consider t-J-H model.

However, OC of the t-J-H model was studied by ED [165], using NCA both for phonons and magnons [167], and by DMFT method which is exact in the infinite dimension limit [224]. NCA is not valid for strong EPI and small systems in ED method give too discrete spectrum. Beside, it is not known whether infinite dimension is a good approximation for the two-dimensional (2D) system. To circumvent the above difficulties, the OC was calculated in [51] by DMC method for 2D infinite system and without NCA in the phonon channel. Theoretical data were compared with experimental ones obtained by ellipsometry, Figure 9 shows OC (a) in Holstein model, (b) t-J model and (c) t-J-H model. Experimental result is in Figure 9(d). No model, except the t-J-H one, reproduces even the gross features of the experiment. The most striking feature is the two-peak structure of MIR band. There is an MIR peak at  $\omega_{\text{MIR}} = 4600 \text{ cm}^{-1}$  and a low-energy peak at  $\omega = 1000 \text{ cm}^{-1}$  which is situated just above the phonon lines at around  $800 \text{ cm}^{-1}$ . Note that in the t-J model, the MIR peak is at  $\omega_{t\text{-J}} \cong 2J \cong 2000 \text{ cm}^{-1}$ . However, EPI of t-J-H model shifts the peak to its experimentally observed frequencies.

It is shown in [51] that the lower peak of OC originates from the phonon-mediated scattering of the hole between the states located in the coherent t-J band and the threshold of the optical absorption corresponds to the phonon energy. The higher energy peak is a magnetic satellite of the lower peak. Note that its energy is higher in comparison with system where EPI is set to zero. Assuming strong coupling regime, when one can take advantage of the Franck-Condon scheme [48], one can explain this shift to higher energies as

follows. The fluctuations of the energies on different sites of the lattice are around the Franck-Condon relaxation energy. On the other hand, these fluctuations are frozen during the characteristic time of optical transition. Hence, the energy of transition of the hole from the ground to excited state is the sum of the Franck-Condon energy and that of excited magnon.

Figure 10 shows how OC changes with increase of  $\lambda$ . OC at weak coupling shows low-energy peak which intensity starts just above the phonon energy and there is apparent two-peak structure of the absorption. Actually, the two-peak structure was observed in experiment even in early measurements [23, 27, 115–120]. Especially apparent two-peak structure is seen in OC measured by ellipsometry in the weakly doped  $\text{Eu}_{1-x}\text{Ca}_x\text{Ba}_2\text{Cu}_3\text{O}_6$  (see Figure 9(d)). The low-energy peak is close to the phonon energy up to  $\lambda \approx 0.4$  when the system comes into the strong coupling regime [42] and for  $\lambda > 0.4$  all peaks quickly enhance their energies (see Figure 11(a)). To reveal the nature of the low-energy peak the OC of the effective Holstein model was studied. In this model, the hopping integral was chosen  $\tilde{t} = 0.4t$  to reproduce the enhancement of the mass in the t-J model. Besides, the crossover to the strong coupling regime occurs in the effective model at  $\lambda \approx 0.4$ . The OC of such model well reproduces the low-energy part of the t-J-H model (see Figure 11(b)).

Doping dependence of the kink angles in ARPES [64] suggests that the EPI strength decreases with doping and, hence, experimentally observed softening of the MIR energy with doping [25, 26, 28] is because of decrease of EPI. Theoretically, the decrease of the effective EPI with doping was found for a gas of Fröhlich polarons [239–242]. Comparison of the experimental position of the MIR peak with the results of the t-J-H model gives the estimate [51] for change of the

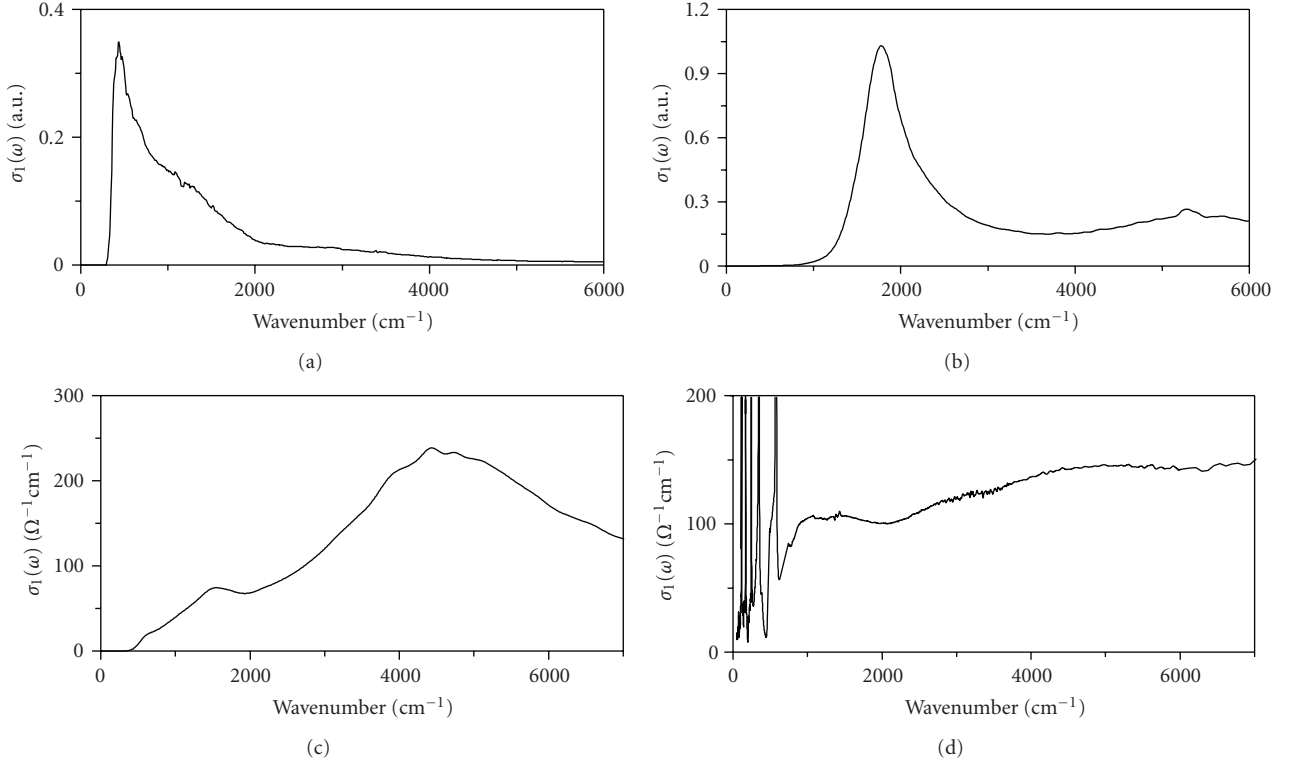


FIGURE 9: Typical OC of different models in two-dimensions and experimental data in weakly doped system: (a) Holstein model at  $\lambda = 0.44$ ; (b) t-J model at  $J = 0.3$ ; (c) t-J-H at  $J = 0.3$  and  $\lambda = 0.39$ ; (d) in-plane OC of doped by  $x = 1.5\%$  holes  $\text{Eu}_{1-x}\text{Ca}_x\text{Ba}_2\text{Cu}_3\text{O}_6$  at  $T = 10$  K. Theoretical energy scale assumes  $t = 0.3$  eV ( $1 \text{ eV} = 8065.5 \text{ cm}^{-1}$ ). The absolute values of the theoretical  $\sigma_1$  estimated assuming that hopping distance in plane is  $a = 3.86 \text{ \AA}$  and the bulk concentration of holes is  $n_h = 1.72 \times 10^{-23} \text{ cm}^{-3}$ .

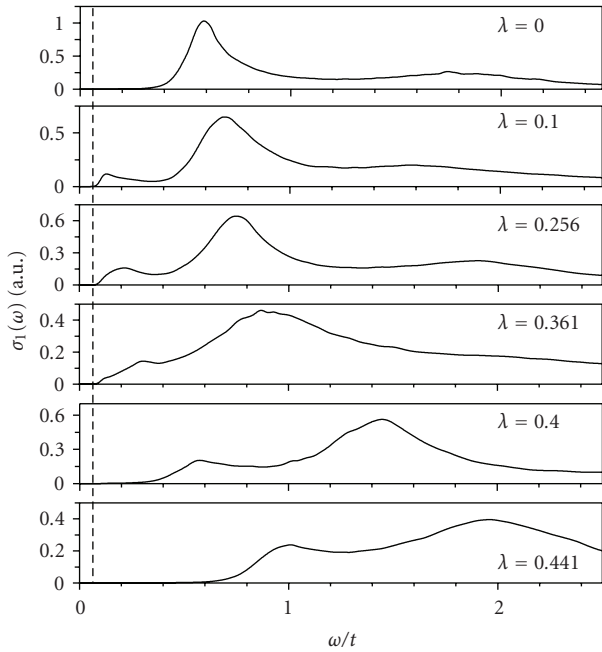


FIGURE 10: Optical conductivity of a one hole in the t-J-H model calculated by DMC method at  $J/t = 0.3$  for different  $\lambda$ . Vertical line at  $\omega/t = 0.1$  shows phonon energy.

effective EPI with doping (Figures 11(c) and 11(d)). The figures show the ratio of the coupling constant at the given doping to that at zero doping. However, since zero doping is characterized by the coupling constant  $\lambda(x = 0) \approx 1$  (see Section 3.4), one can think of the data in Figures 11(c) and 11(d) as showing the absolute value of  $\lambda(x)$ . Note very similar behavior of  $\lambda(x)$  for different compounds. It is clear that the compounds become superconducting when the system is not already in the strong coupling regime of the EPI. However, the value of the EPI strength  $\lambda \approx 0.5$  is still considerable.

Alternative explanation of the doping dependence of the MIR energy by the doping dependence of the exchange integral  $J(x)$  was suggested in [224, 243]. One cannot distinguish between  $J(x)$ - and  $\lambda(x)$ -scenario just looking on OC. However,  $\lambda(x)$ -scenario easily explains experimentally observed strong dependence of the kink angle on concentration [64, 97, 121, 128]. To the contrary,  $J(x)$ -approach [224, 243] does not give an explanation. Experimental data in electron doped  $\text{Nd}_{2-x}\text{Ce}_x\text{CuO}_4$  were interpreted as indicating that  $\lambda$  does not show doping dependence [145]. However, the range where  $\lambda$  is determined in [145] is too narrow to reach the final conclusion.

The polaronic scenario was used to interpret OC in cuprates many times [115, 242, 245–249]. However, all these cited papers discussed the one-peak structure and did not describe the complex two-peak structure of the

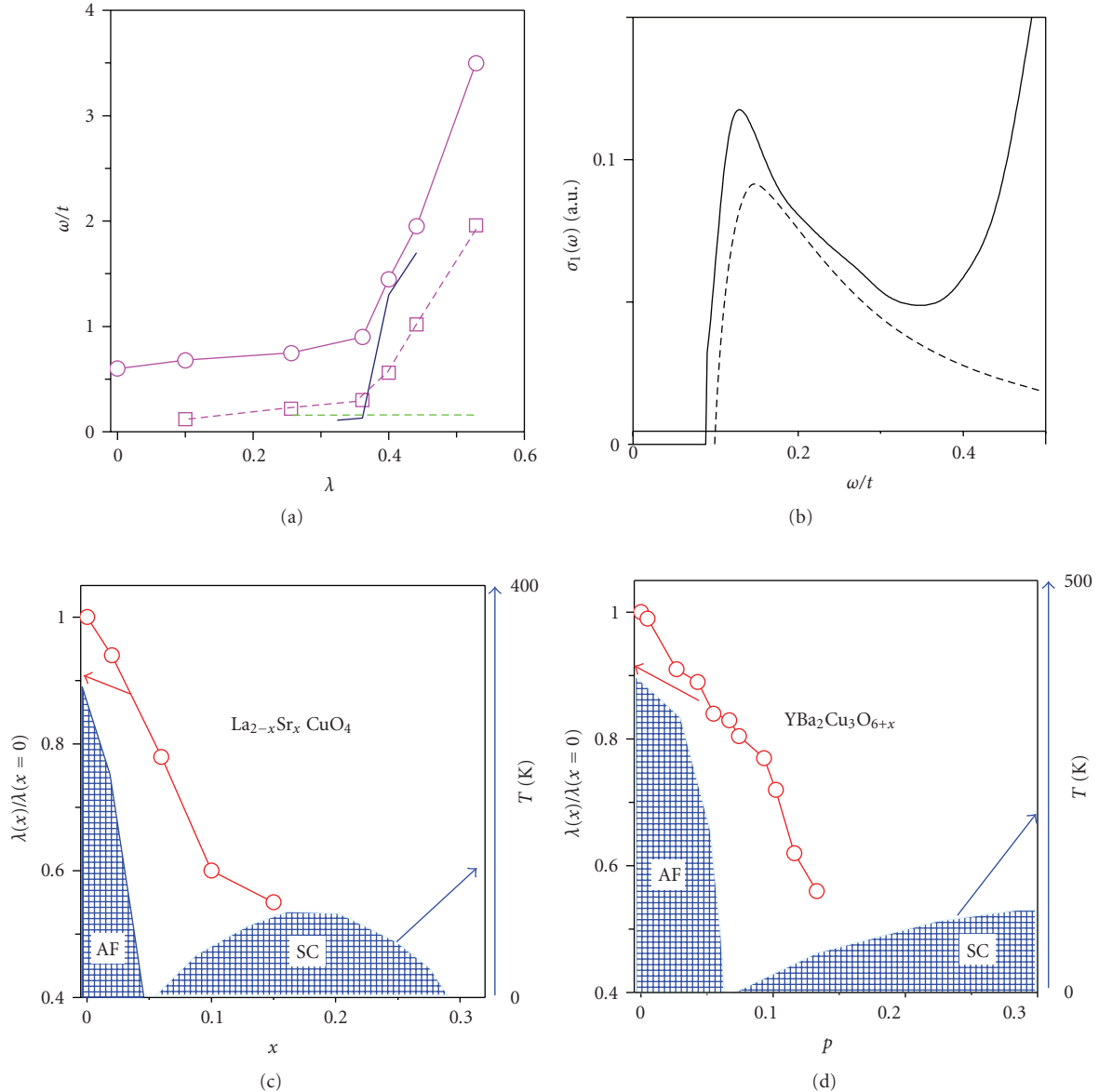


FIGURE 11: (a) Energies of the dominant MIR peak (solid line with circles) and low-energy peak (dashed line with squares) of the t-J-H model versus  $\lambda$ . Energies of the dominant peaks of the Holstein model for  $t = 1$  (dashed line) and for  $\tilde{t} = 0.4$  (solid line). (b) OC of the t-J-H model (solid line) and effective Holstein model with  $\tilde{t} = 0.4$  (dashed line). Both OC are for  $\lambda = 0.1$ . (c) and (d) Ratio of the effective coupling constants on doping  $x$  (or real concentration  $p$  of the hole in plain for YBCO [244]) and that at almost zero doping. Effective  $\lambda(x)$  is determined by the fit of the MIR position at given doping.

experimental spectra. One of exceptions where two-peak structure is discussed is [250]. It is pointed out that the two-peak structure of OC occurs at some coupling constants in the Fröhlich model [41, 48]. There is also some range of coupling constants where two-peak structure of OC is seen in the Holstein model [251]. However, one needs fine tuning of the EPI strength to get the two-peak OC in the Fröhlich or Holstein model. To the contrary, the two-peak structure is the robust property of the experimental data and the OC of the t-J-H model. The authors of [250] used similar approaches [252, 253] to calculate the OC and ARPES

spectra and found clear relation between the position of the peaks in ARPES and OC spectra.

Another interpretation of the low-energy peak of OC is given in [254], where the peak is considered to be of the purely magnetic origin. It seems that in the framework of the interpretation given in [254] the low-energy peak is connected with local magnetic excitations. Therefore, the nature of the low-energy peak is still under debate theoretically although experimentally it is a vivid feature of the OC of many cuprates with different doping levels [23, 27, 115–120].

3.8. *Nonlocal EPI.* The simplest model (3)–(7) does not reproduce all peculiarities of cuprates. The reason is that actually EPI vertex depends on momenta of both hole and phonon [61, 82, 85–90, 92, 93]. As a result, some properties of the t-J-H model do not match experimental data. For example, effective mass of a hole in the strong coupling regime is very large which is in contradiction with rather moderate masses of carriers observed in experiment [25]. Even more profound disagreement with experiment was found in [210]. It was shown there that in the strong coupling regime of the t-J-H model the mobile hole is transformed into the localized one with four broken bonds around it. In such case, the percolation model predicts that the antiferromagnetic model survives up to hole concentration  $x = 0.5$  which is in severe disagreement with experiment where antiferromagnetic phase is limited by the doping concentrations  $x \leq 0.02$ – $0.04$ . Similar trend was noted in [255] where it was demonstrated that EPI helps to survival of the antiferromagnetism since EPI suppresses the motion of the holes which is necessary to suppress antiferromagnetism.

The minimal Hamiltonian of the t-t'-t''-J model with nonlocal EPI consists of the sum of the Hamiltonian of the t-t'-t''-J model, phonon Hamiltonian with phonon frequency  $\omega_0$ , and the Hamiltonian of nonlocal EPI

$$H_{\text{h-ph}} = \omega_0 \sum_l g(l) \sum_{i \in A} f_i^\dagger f_i (c_{i+l}^\dagger + c_{i+l}) + \omega_0 \sum_l g(l) \sum_{i \in B} h_i^\dagger h_i (c_{i+l}^\dagger + c_{i+l}), \quad (19)$$

which is defined in terms of local coupling constant  $g(0) = g$  and nonlocal coupling to the displacements of near neighbors  $g(\vec{\delta}) = g_1$ . However,  $f$  and  $h$  denote annihilation operators of two sublattices of the two-dimensional antiferromagnetic lattice.

The problem of nonlocal EPI in t-t'-t''-J model was solved in [49] with a novel approach. In that approach, starting from the state of a hole in an antiferromagnet, one defines the states of the basis  $|h\rangle_j |[\prod_i |\mu_i\rangle] | \vec{q}_1, \dots, \vec{q}_l, l \rangle$ . Here  $|h\rangle_j$  is a hole at site  $j$  and  $i$  runs through the whole lattice. The set of states  $| \vec{q}_1, \dots, \vec{q}_l, l \rangle$  is limited by magnons which component of the  $l$ th order is enough to reproduce the results of NCA [256]. As it is shown in [49],  $l = 4$  is enough for  $J/t \geq 0.3$  since diagonalization of this  $l \leq 4$  basis in the retraceable path approximation [257] gives results reproducing those of the NCA.

However, the hardest problem for the numeric solution comes from the phonon basis. Exponential growth of the phonon basis with coupling previously limited the system sizes to 10 sites [165]. The problem is circumvented by usage of the coherent states (CS) [258, 259] which are the canonical transformations of the phonon basis:

$$|h, i\rangle = e^{gh(b_i - b_i^\dagger)} |0\rangle_i^{(ph)} = e^{-g^2 h^2 / 2} \sum_{n=0}^{\infty} \frac{(-gh)^n}{\sqrt{n!}} |n\rangle_i \quad (20)$$

with free parameter  $h$ . Such approach can treat  $8 \times 8$  lattices which are the largest systems ever treated for t-J and related

models which include coupling to phonons. CS with  $h = 0$  is the bare state and for  $h = 1$  it is the exact solution to the independent oscillators model with local EPI coupling  $g$ . A comparison with DMC data showed [49] that four CSs are enough for reliable treatment of t-t'-t''-J model in all coupling regimes.

The t-t'-t''-J-H model was compared in [49] with the model where interaction with the displacements on near neighbors  $g_1 = g/2$  (see (19)) was added. Figure 12 shows dependence on  $\lambda/\lambda_c$  of the ground state spectral weight  $Z$ , spin deviation SD, and magnon-mediated kinetic energy  $K_t$ . Spin deviation  $SD = (S_{\text{AFM}} - \langle S_{\text{NN}} \rangle) / S_{\text{AFM}}$  is a measure of how the spin  $S_{\text{NN}}$  on the neighboring to the hole site deviates from the value of spin  $S_{\text{AFM}}$  in the ideal antiferromagnet. The decrease of  $Z$  is a measure of suppression of coherent motion of the hole whereas the absolute values of  $K_t$  and SD are the measures of intensity of the near neighbor hoppings. Decrease of  $K_t$  and SD indicates suppression by EPI of the movement of a hole on near neighbors.

Nonlocality of the EPI is manifested in the following features. Coherent motion is suppressed stronger at  $\lambda < \lambda_c$  and weaker at  $\lambda > \lambda_c$  (see Figure 12(a)). Also, intensity of the near neighbors hoppings is considerably weaker suppressed by nonlocal EPI than by the local one. The last statement is easy to illustrate in the strong coupling regime where one can think in terms of the adiabatic potential. The adiabatic potential in the strong coupling regime is a  $\delta$ -function giving no possibility of a motion of the hole over the near neighbors. To the contrary, for long-range EPI, the adiabatic potential is not steep and, thus, the motion of the hole over the near neighbors is not suppressed even in the strong coupling limit. Such mobility over the near neighbor gives possibility to destroy the antiferromagnetic state even in the strong coupling regime. Besides, the polaron with nonlocal EPI is lighter in the strong coupling regime. For example, for  $\lambda = 1.1\lambda_c$  the diagonal  $m_d$  ( $k_x = k_y$ ) and transverse  $m_t$  ( $k_x = -k_y$ ) masses for the local EPI are  $m_d = 200$  and  $m_t = 88$  whereas for nonlocal EPI the masses  $m_d = 20$  and  $m_t = 10$  are considerably lighter. Lighter mass for nonlocal EPI [98, 195, 260–265] or dispersive phonons [266–269] was observed in many models.

Common influence of long-range EPI and on site repulsion binds polarons into mobile inter-site bipolarons [270, 271]. For peculiar lattice structures such polarons can be very light [272].

Manifestation of the nonlocality of the EPI can be seen in the OC [4, 273]. For example, the peak in the OC of the Holstein model in the strong coupling regime is seen on the energy  $2\epsilon_p$ , where  $\epsilon_p$  is the polaron binding energy. On the other hand, the peak of OC in the models with long-range EPI is on the considerably smaller energies [273]. It can be explained by the fact that OC is defined in terms of the current-current correlation function. The current operator in the polaronic models with near neighbor hopping corresponds to the transition of a quasiparticle to the neighboring site. The shifted electron in the Holstein model loses the energy  $\epsilon_p$  and leaves the excited phonons with the same energy on the initial site. For the long-range EPI the phonons are excited on the polaron site and on the

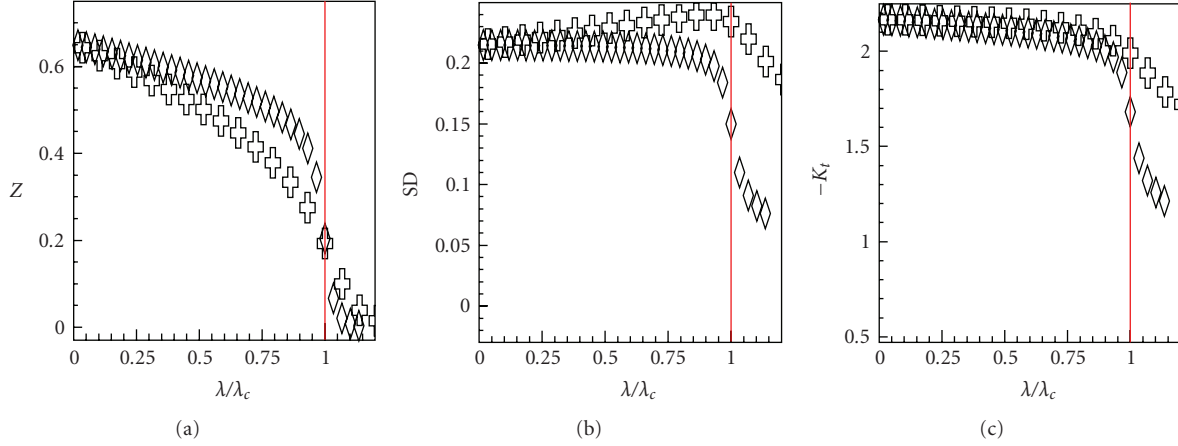


FIGURE 12: (a) Spectral weight, (b) spin deviation (b), and (c) average kinetic energy of mediated by magnons near neighbor transitions for  $g_1 = 0$  (diamonds) and  $g_1 = 0.5g$  (crosses). Other parameters are  $J/t = 0.4$ ,  $\omega_0/t = 0.2$ ,  $t' = -0.5t$ ,  $t'' = 0.4t$ , and  $N = 4 \times 4 = 16$ . Critical  $\lambda_c$  is set at such coupling where the spectral weight of the ground state reaches 0.3 of the unrenormalized by EPI weight.

neighboring sites which leads to considerably weaker lattice relaxation during transition to the neighboring site. Hence, the energy of the peak in OC for nonlocal EPI is smaller.

The peculiarities of the influence of nonlocal EPI is determined not only by the range but also by its fine structure. Comparison of buckling and breathing phonons is made in [274]. In the Hamiltonian:

$$H_{\text{Br-Bu}} = \gamma \sum_{\mathbf{i}, \delta} (b_{\mathbf{i}, \delta} + b_{\mathbf{i}, \delta}^\dagger) (n_{\mathbf{i}} \pm n_{\mathbf{i}+\delta}), \quad (21)$$

where  $\mathbf{i}$  is position of cooper and  $\delta = x, y$  is the link direction. Plus (minus) corresponds to buckling (breathing) mode. It is shown [274] that the breathing mode suppresses the kinetic energy considerably stronger than it is done by buckling mode. Breathing phonon decreases the energy of one site and increases it on the neighboring one. To the contrary, the buckling mode changes the energy of the neighboring sites in the same direction and, hence, does not suppress the kinetic energy effectively. Studies of influence of the EPI structure on the properties of polarons can be found in [98, 194, 195, 262, 275].

#### 4. Electronic Correlations and EPI

Manifestations of the EPI in the properties of particles and phonons are profoundly different although the first naive but correct impressions is that both elementary excitations become softer and broader. Let a hole (phonon) in a system without EPI has dispersion  $\varepsilon(\mathbf{k}) = \varepsilon(\mathbf{k})$  ( $\varepsilon(\mathbf{k}) = \omega(\mathbf{k})$ ). In such system, experimentally observed response in ARPES (neutron scattering) is expressed in terms of spectral function  $S(\mathbf{k}, \omega)$  having the form of a delta function  $S(\mathbf{k}, \omega) = \delta(\omega - \varepsilon(\mathbf{k}))$ . EPI leads to additional self-energy part of the Green function of a hole (phonon)  $\Theta(\mathbf{k}, \omega) = \Sigma(\mathbf{k}, \omega)$

( $\Theta(\mathbf{k}, \omega) = \Pi(\mathbf{k}, \omega)$ ). With this self-energy, the spectral function, measured in experiment, reads

$$S(\mathbf{k}, \omega) = \frac{1}{\pi} \frac{|\text{Im}\Theta(\mathbf{k}, \omega)|}{[\omega - \varepsilon(\mathbf{k}) - \text{Re}\Theta(\mathbf{k}, \omega)]^2 + [|\text{Im}\Theta(\mathbf{k}, \omega)|]^2}. \quad (22)$$

Imaginary part  $|\text{Im}\Theta(\mathbf{k}, \omega)|$  determines the EPI-driven broadening.

There is a sum rule for phonon self-energy in the  $t$ - $J$  model (in the  $U \rightarrow \infty$  limit of Hubbard model) when charge fluctuations in the half-filled system are completely suppressed [83, 276]:

$$\frac{1}{\pi N} \sum_{\mathbf{k}} \int_{-\infty}^{\infty} |\text{Im}\Pi(\mathbf{k}, \omega)| d\omega \approx \gamma^2 [2\delta(1 - \delta)]. \quad (23)$$

Here  $N$  is number of sites and  $\delta$  is concentration of holes which is zero in half-filled system. Naturally, with no empty spaces in half-filled system there is no charge fluctuations at all and the phonons are left untouched. Increase of  $\delta$  adds empty states and the charge fluctuations renormalize and broaden phonons. To the contrary, one does not need doping to see the manifestations of EPI in ARPES spectra. For  $\delta = 0$  the sum rule for the hole self-energy reads [276]

$$\frac{1}{\pi} \int_{-\infty}^0 \text{Im}\Sigma(\mathbf{k}, \omega - i0^+) d\omega = \gamma^2. \quad (24)$$

Thus, half-filled system does not suppresses EPI in the ARPES channel. The reason is that ARPES creates its own hole even in the half filled system. This hole is a charge whose fluctuations are not suppressed (see also [277]).

In general,  $U$  suppresses EPI. Also, DMFT calculations show [278–280] that EPI in paramagnetic system is severely depressed by correlations. Antiferromagnetic state considerably enhances the role of EPI in comparison with paramagnetic system [281]. Doping suppresses the EPI contribution to the electronic properties. To the contrary,

contribution of EPI into the phonon properties increases with doping (cf. (23)).

In any case, for small filling of the t-J model, one can conclude that in comparison with the Holstein model with small filling the influence of the EPI is larger for the t-J model. This result was verified by a number of calculations [42, 165, 282–284]. Comparing critical coupling of the t-J-H (3)–(7) model  $\lambda_{t-J}^c \approx 0.4$  [42] with the critical coupling of the Holstein model with the same hopping  $t\lambda_H^c \approx 1$ , one concludes that the interaction of the hole with magnons makes the transition into the strong coupling regime faster.

For a hole in the bottom of the band the ratio of effective  $\lambda$  for the t-J model and  $\lambda_0$  for the Holstein model with bare mass  $m_0 = 1/(2t)$  depends on numerous factors [4, 166, 171]:

$$\frac{\lambda}{\lambda_0} \approx 4Z_0^2 \frac{\sqrt{m_{\parallel} m_{\perp}}}{m_0}. \quad (25)$$

The decreasing factor  $Z_0 < 1$  arises because of the shift of the spectral density to higher frequencies. On the other hand, larger effective masses of the t-J model  $m_{\parallel} > m_0$  and  $m_{\perp} > m_0$  enhance the influence of EPI. The factor 4 arising because of 4-fold degeneracy of the ground state on the wave vectors  $(\pm\pi/2, \pm\pi/2)$  becomes sometimes decisive. At  $J/t = 0.2$ , one has  $Z_0^2 = 0.05$  and  $\sqrt{m_{\parallel} m_{\perp}} = 10m_0$ . In this case there is doubling of the EPI, partly due to the factor 4. For large  $J/t = 2$ , the enhancement of EPI  $\lambda/\lambda_0 \approx 16$  can be very large. One can conclude that the change of the role of EPI usually has no universal trends and very often determined by fine features of the model, dimensionality, filling, and so forth. For example, the role of EPI is suppressed by Coulomb repulsion in the ground state of one-dimensional Mott insulator [285] whereas its role in formation of the exciton spectrum is enhanced by the same Coulomb repulsion [286].

One of the factors influencing the role of EPI in cuprates is typical for cuprates inhomogeneity [287–290]. Moderate and even weak EPI can lead to dramatic changes of the properties of inhomogeneous electronic gas [291]. Interfaces and surfaces are another inhomogeneities enhancing the role of EPI [292]. Similar conclusions can be drawn from many numeric calculations [53, 293–298].

Current review is restricted to theoretical approaches considering strong correlations. The significant number of important results of band structure calculations, the incomplete list is [299–310], revealing large  $\lambda \geq 1$  value of EPI, are not discussed here because of space limitation.

## 5. Conclusions

This review presents a lot of evidences for the important role of the EPI in formation of the spectral properties of underdoped cuprates. Theoretical efforts to reveal the fingerprints of the EPI in spectral response went through the sequence of models with increasing complexity. The simplest models with short range EPI in the ideal lattice at zero temperature were the systems to start with. Then, the progress went through generalizations to finite temperatures, to nonlocal EPI, and to systems with imperfections.

The ultimate goal of theory is to describe the realistic situation in cuprates. Such goal requires further development of the numeric approaches since the realistic description of cuprates requires methods which are capable of describing an infinite systems with imperfections at finite temperature.

## Acknowledgments

This review is supported by RFBR 07-02-0067a. The author acknowledges stimulating discussions with N. Nagaosa, N. V. Prokof'ev, B. V. Svistunov, Yu. Kagan, A. S. Alexandrov, G. De Filippis, V. Cataudella, A. Sakamoto, Z.-X. Shen, T. P. Devereaux, C. Bernhard, J. Zaanen, G. Sawatzky, K. M. Shen, J. Bonča, E. Cappelluti, S. Ciuchi, M. Berciu, T. Egami, J. T. Devreese, T. Tohyama, O. Gunnarsson, G. Sangiovanni, and C. Kim.

## References

- [1] P. W. Anderson, *The Theory of Superconductivity in the High- $T_c$  Cuprates*, Princeton University Press, Princeton, NJ, USA, 1997.
- [2] A. S. Alexandrov, "Bose-Einstein condensation of strongly correlated electrons and phonons in cuprate superconductors," *Journal of Physics: Condensed Matter*, vol. 19, no. 12, Article ID 125216, 2007.
- [3] A. S. Alexandrov, "Bipolaron anisotropic flat bands, Hall mobility edge, and metal-semiconductor duality of over-doped high- $T_c$  oxides," *Physical Review B*, vol. 53, no. 5, pp. 2863–2869, 1996.
- [4] O. Gunnarsson and O. Rösch, "Interplay between electron-phonon and Coulomb interactions in cuprates," *Journal of Physics: Condensed Matter*, vol. 20, no. 4, Article ID 043201, 2008.
- [5] A. Damascelli, Z. Hussain, and Z.-X. Shen, "Angle-resolved photoemission studies of the cuprate superconductors," *Reviews of Modern Physics*, vol. 75, no. 2, pp. 473–541, 2003.
- [6] T. Xiang and J. M. Wheatley, "Quasiparticle energy dispersion in doped two-dimensional quantum antiferromagnets," *Physical Review B*, vol. 54, no. 18, pp. R12653–R12656, 1996.
- [7] V. I. Belinicher, A. L. Chernyshev, and V. A. Shubin, "Generalized  $t$ - $t'$ -J model: parameters and single-particle spectrum for electrons and holes in copper oxides," *Physical Review B*, vol. 53, no. 1, pp. 335–342, 1996.
- [8] V. I. Belinicher, A. L. Chernyshev, and V. A. Shubin, "Single-hole dispersion relation for the real  $\text{CuO}_2$  plane," *Physical Review B*, vol. 54, no. 21, pp. 14914–14917, 1996.
- [9] T. M. Rice and F. C. Zhang, "Frequency-dependent conductivity from carriers in Mott insulators," *Physical Review B*, vol. 39, no. 1, pp. 815–818, 1989.
- [10] W. Stephan and P. Horsch, "Optical properties of one- and two-dimensional Hubbard and  $t$ -J models," *Physical Review B*, vol. 42, no. 13, pp. 8736–8739, 1990.
- [11] D. Poilblanc and E. Dagotto, "Optical mass in the  $t$ -J model," *Physical Review B*, vol. 44, no. 1, pp. 466–469, 1991.
- [12] D. Poilblanc, "Twisted boundary conditions in cluster calculations of the optical conductivity in two-dimensional lattice models," *Physical Review B*, vol. 44, no. 17, pp. 9562–9581, 1991.
- [13] E. Dagotto, A. Moreo, F. Ortolani, D. Poilblanc, and J. Riera, "Static and dynamical properties of doped Hubbard clusters," *Physical Review B*, vol. 45, no. 18, pp. 10741–10760, 1992.

- [14] J.-I. Igarashi and P. Fulde, “Drude weight and optical conductivity of doped antiferromagnets,” *Physical Review B*, vol. 48, no. 17, pp. 12713–12722, 1993.
- [15] J. Jaklič and P. Prelovšek, “Finite-temperature conductivity in the planar  $t$ - $J$  model,” *Physical Review B*, vol. 50, no. 10, pp. 7129–7132, 1994.
- [16] G. Jackeli and N. M. Plakida, “Charge dynamics and optical conductivity of the  $t$ - $J$  model,” *Physical Review B*, vol. 60, no. 8, pp. 5266–5275, 1999.
- [17] M. Moraghebi, S. Yunoki, and A. Moreo, “Optical conductivity and resistivity of a hole-doped spin-fermion model for cuprates,” *Physical Review B*, vol. 66, no. 21, Article ID 214522, 5 pages, 2002.
- [18] A. M. Tikofsky, R. B. Laughlin, and Z. Zou, “Computation of the optical conductivity of the  $t$ - $J$  model using anyon techniques,” *Physical Review Letters*, vol. 69, no. 25, pp. 3670–3673, 1992.
- [19] N. M. Plakida, “Optical conductivity in the  $t$ - $J$  model,” *Zeitschrift für Physik B*, vol. 103, no. 3-4, pp. 383–390, 1997.
- [20] R. Eder, P. Wróbel, and Y. Ohta, “Optical conductivity of strongly correlated electron systems,” *Physical Review B*, vol. 54, no. 16, pp. R11034–R11037, 1996.
- [21] B. Kyung and S. I. Mukhin, “Dynamics of a small density of holes in a two-dimensional quantum antiferromagnet,” *Physical Review B*, vol. 55, no. 6, pp. 3886–3893, 1997.
- [22] E. Dagotto, “Correlated electrons in high-temperature superconductors,” *Reviews of Modern Physics*, vol. 66, no. 3, pp. 763–840, 1994.
- [23] N. D. Basov and T. Timusk, “Electrodynamics of high- $T_C$  superconductors,” *Reviews of Modern Physics*, vol. 77, no. 2, pp. 721–729, 2005.
- [24] M. A. Kastner, R. J. Birgeneau, G. Shirane, and Y. Endoh, “Magnetic, transport, and optical properties of monolayer copper oxides,” *Reviews of Modern Physics*, vol. 70, no. 3, pp. 897–928, 1998.
- [25] Y. S. Lee, K. Segawa, Z. Q. Li, et al., “Electrodynamics of the nodal metal state in weakly doped high- $T_C$  cuprates,” *Physical Review B*, vol. 72, no. 5, Article ID 054529, 2005.
- [26] S. L. Cooper, D. Reznik, A. Kotz, et al., “Optical studies of the  $a$ -,  $b$ -, and  $c$ -axis charge dynamics in  $\text{YBa}_2\text{Cu}_3\text{O}_{6+x}$ ,” *Physical Review B*, vol. 47, no. 13, pp. 8233–8248, 1993.
- [27] G. A. Thomas, D. H. Rapkine, S. L. Cooper, et al., “Optical excitations of a few charges in cuprates,” *Physical Review B*, vol. 45, no. 5, pp. 2474–2479, 1992.
- [28] S. Uchida, T. Ido, H. Takagi, T. Arima, Y. Tokura, and S. Tajima, “Optical spectra of  $\text{La}_{2-x}\text{Sr}_x\text{CuO}_4$ : effect of carrier doping on the electronic structure of the  $\text{CuO}_2$  plane,” *Physical Review B*, vol. 43, no. 10, pp. 7942–7954, 1991.
- [29] R. M. A. Azzam and N. M. Bashara, *Ellipsometry and Polarized Light*, North Holland, New York, NY, USA, 1996.
- [30] D. U. Fluckiger, “Analytic methods in the determination of optical properties by spectral ellipsometry,” *Journal of the Optical Society of America A*, vol. 15, no. 8, pp. 2228–2232, 1998.
- [31] N. V. Prokof’ev, B. V. Svistunov, and I. S. Tupitsyn, “Exact, complete, and universal continuous-time worldline Monte-Carlo approach to the statistics of discrete quantum systems,” *Zhurnal Eksperimental’noj i Teoreticheskoy Fiziki*, vol. 114, no. 2, pp. 570–590, 1998.
- [32] N. V. Prokof’ev, B. V. Svistunov, and I. S. Tupitsyn, “Exact, complete, and universal continuous-time worldline Monte Carlo approach to the statistics of discrete quantum systems,” *Journal of Experimental and Theoretical Physics*, vol. 87, no. 2, pp. 310–321, 1998.
- [33] N. V. Prokof’ev and B. V. Svistunov, “Polaron problem by diagrammatic quantum Monte Carlo,” *Physical Review Letters*, vol. 81, no. 12, pp. 2514–2517, 1998.
- [34] A. S. Mishchenko, N. V. Prokof’ev, A. Sakamoto, and B. V. Svistunov, “Diagrammatic quantum Monte Carlo study of the Fröhlich polaron,” *Physical Review B*, vol. 62, no. 10, pp. 6317–6336, 2000.
- [35] A. S. Mishchenko and N. Nagaosa, “Quasidegenerate self-trapping in one-dimensional charge transfer exciton,” *Physical Review Letters*, vol. 86, no. 20, pp. 4624–4627, 2001.
- [36] A. S. Mishchenko, N. V. Prokof’ev, B. V. Svistunov, and A. Sakamoto, “Comprehensive study of Fröhlich polaron,” *International Journal of Modern Physics B*, vol. 15, no. 28–30, pp. 3940–3943, 2001.
- [37] A. S. Mishchenko, N. V. Prokof’ev, and B. V. Svistunov, “Single-hole spectral function and spin-charge separation in the  $t$ - $J$  model,” *Physical Review B*, vol. 64, no. 3, Article ID 033101, 4 pages, 2001.
- [38] E. A. Burovski, A. S. Mishchenko, N. V. Prokof’ev, and B. V. Svistunov, “Diagrammatic quantum Monte Carlo for two-body problems: applied to excitons,” *Physical Review Letters*, vol. 87, no. 18, Article ID 186402, 4 pages, 2001.
- [39] A. S. Mishchenko, N. Nagaosa, N. V. Prokof’ev, B. V. Svistunov, and E. A. Burovski, “Properties of exciton and exciton-polaron: exact numeric solution,” *Nonlinear Optics*, vol. 29, p. 257, 2002.
- [40] A. S. Mishchenko, N. Nagaosa, N. V. Prokof’ev, A. Sakamoto, and B. V. Svistunov, “Self-trapping of polarons in the Rashba-Pekar model,” *Physical Review B*, vol. 66, no. 2, Article ID 020301, 4 pages, 2002.
- [41] A. S. Mishchenko, N. Nagaosa, N. V. Prokof’ev, A. Sakamoto, and B. V. Svistunov, “Optical conductivity of the Fröhlich polaron,” *Physical Review Letters*, vol. 91, no. 23, Article ID 236401, 4 pages, 2003.
- [42] A. S. Mishchenko and N. Nagaosa, “Electron-phonon coupling and a polaron in the  $t$ - $J$  model: from the weak to the strong coupling regime,” *Physical Review Letters*, vol. 93, no. 3, Article ID 036402, 2004.
- [43] A. S. Mishchenko, “Diagrammatic Monte Carlo method as applied to the polaron problems,” *Uspekhi Fizicheskikh Nauk*, vol. 175, no. 9, p. 925, 2005.
- [44] A. S. Mishchenko, “Diagrammatic Monte Carlo method as applied to the polaron problems,” *Physica-Uspekhi*, vol. 48, no. 9, pp. 887–902, 2005.
- [45] A. S. Mishchenko and N. Nagaosa, “Theory of excitation spectra of electron-phonon coupled systems,” *Journal of the Physical Society of Japan*, vol. 75, no. 1, Article ID 011003, 2006.
- [46] A. S. Mishchenko and N. Nagaosa, “Numerical study of the isotope effect in underdoped high-temperature superconductors: calculation of the angle-resolved photoemission spectra,” *Physical Review B*, vol. 73, no. 9, Article ID 092502, 4 pages, 2006.
- [47] A. S. Mishchenko and N. Nagaosa, “ARPES spectra of polaron in the  $t$ - $J$  model,” *Journal of Physics and Chemistry of Solids*, vol. 67, no. 1–3, pp. 259–261, 2006.
- [48] G. De Filippis, V. Cataudella, A. S. Mishchenko, C. A. Perroni, and J. T. Devreese, “Validity of the Franck-Condon principle in the optical spectroscopy: optical conductivity of the Fröhlich polaron,” *Physical Review Letters*, vol. 96, no. 13, Article ID 136405, 4 pages, 2006.

- [49] G. De Filippis, V. Cataudella, A. S. Mishchenko, and N. Nagaosa, "Nonlocal composite spin-lattice polarons in high temperature superconductors," *Physical Review Letters*, vol. 99, no. 14, Article ID 146405, 2007.
- [50] V. Cataudella, G. De Filippis, A. S. Mishchenko, and N. Nagaosa, "Temperature dependence of the angle resolved photoemission spectra in the undoped cuprates: self-consistent approach to the  $t$ - $J$  holstein model," *Physical Review Letters*, vol. 99, no. 22, Article ID 226402, 2007.
- [51] A. S. Mishchenko, N. Nagaosa, Z.-X. Shen, et al., "Charge dynamics of doped holes in high  $T_c$  cuprate superconductors: a clue from optical conductivity," *Physical Review Letters*, vol. 100, no. 16, Article ID 166401, 2008.
- [52] E. Burovski, H. Fehske, and A. S. Mishchenko, "Exact treatment of exciton-polaron formation by diagrammatic Monte Carlo simulations," *Physical Review Letters*, vol. 101, no. 11, Article ID 116403, 2008.
- [53] A. S. Mishchenko, N. Nagaosa, A. Alvermann, et al., "Localization-delocalization transition of a polaron near an impurity," *Physical Review B*, vol. 79, no. 18, Article ID 180301, 2009.
- [54] A. S. Mishchenko, "Polarons by exact Diagrammatic Monte Carlo and Stochastic optimization method," in *Materials and Systems with Reduced Dimensionalities*, G. Iadonisi, G. De Filippis, and J. Ranninger, Eds., p. 177, IOS Press, Amsterdam, The Netherlands, 2006.
- [55] A. S. Mishchenko and N. Nagaosa, "Spectroscopic properties of polarons in strongly correlated systems by exact diagrammatic Monte Carlo method," in *Polarons in Complex Matter*, A. S. Alexandrov, Ed., Springer Series in Material Science, pp. 503–544, Springer, New York, NY, USA, 2007.
- [56] A. S. Mishchenko, "Diagrammatic Monte Carlo and stochastic optimization methods for complex composite objects in macroscopic baths," in *Computational Many-Particle Physics*, H. Fehske, R. Schneider, and A. Weisse, Eds., vol. 739 of *Lecture Notes in Physics*, pp. 367–395, Springer, New York, NY, USA, 2008.
- [57] B. O. Wells, Z.-X. Shen, A. Matsuura, et al., " $E$  versus  $k$  relations and many body effects in the model insulating copper oxide  $\text{Sr}_2\text{CuO}_2\text{Cl}_2$ ," *Physical Review Letters*, vol. 74, no. 6, pp. 964–967, 1995.
- [58] O. Rösch and O. Gunnarsson, "Dispersion of incoherent spectral features in systems with strong electron-phonon coupling," *European Physical Journal B*, vol. 43, no. 1, pp. 11–18, 2005.
- [59] K. M. Shen, F. Ronning, D. E. Lu, et al., "Missing quasiparticles and the chemical potential puzzle in the doping evolution of the cuprate superconductors," *Physical Review Letters*, vol. 93, no. 26, Article ID 267002, 2004.
- [60] C. Kim, F. Ronning, A. Damascelli, et al., "Anomalous temperature dependence in the photoemission spectral function of cuprates," *Physical Review B*, vol. 65, no. 17, Article ID 174516, 7 pages, 2002.
- [61] O. Rösch and O. Gunnarsson, "Electron-phonon interaction in the  $t$ - $J$  model," *Physical Review Letters*, vol. 92, no. 14, Article ID 146403, 2004.
- [62] O. Rösch, O. Gunnarsson, X. J. Zhou, et al., "Polaronic behavior of undoped high- $T_c$  cuprate superconductors from angle-resolved photoemission spectra," *Physical Review Letters*, vol. 95, no. 22, Article ID 227002, 4 pages, 2005.
- [63] S. Kar and E. Manousakis, "Finite-temperature spectral function of a hole in a quantum antiferromagnet and the role of phonons," *Physical Review B*, vol. 78, no. 6, Article ID 064508, 2008.
- [64] A. Lanzara, P. V. Bogdanov, X. J. Zhou, et al., "Evidence for ubiquitous strong electron-phonon coupling in high-temperature superconductors," *Nature*, vol. 412, no. 6846, pp. 510–514, 2001.
- [65] V. J. Emery, "Theory of high- $T_c$  superconductivity in oxides," *Physical Review Letters*, vol. 58, no. 26, pp. 2794–2797, 1987.
- [66] F. C. Zhang and T. M. Rice, "Effective Hamiltonian for the superconducting Cu oxides," *Physical Review B*, vol. 37, no. 7, pp. 3759–3761, 1988.
- [67] C. L. Kane, P. A. Lee, and N. Read, "Motion of a single hole in a quantum antiferromagnet," *Physical Review B*, vol. 39, no. 10, pp. 6880–6897, 1989.
- [68] Z. Liu and E. Manousakis, "Dynamical properties of a hole in a Heisenberg antiferromagnet," *Physical Review B*, vol. 45, no. 5, pp. 2425–2437, 1992.
- [69] Z. Liu and E. Manousakis, "Spectral function of a hole in the  $t$ - $J$  model," *Physical Review B*, vol. 44, no. 5, pp. 2414–2417, 1991.
- [70] E. Manousakis, "The spin-Heisenberg antiferromagnet on a square lattice and its application to the cuprous oxides," *Reviews of Modern Physics*, vol. 63, no. 1, pp. 1–62, 1991.
- [71] F. Marsiglio, A. E. Ruckenstein, S. Schmitt-Rink, and C. M. Varma, "Spectral function of a single hole in a two-dimensional quantum antiferromagnet," *Physical Review B*, vol. 43, no. 13, Article ID 10882, 1991.
- [72] B. Kyung and R. A. Ferrell, "Quasiparticle dispersion of the insulating copper oxide  $\text{Sr}_2\text{CuO}_2\text{Cl}_2$  by employing vertical and horizontal double hoppings," *Physical Review B*, vol. 54, no. 14, pp. 10125–10130, 1996.
- [73] T. K. Lee and C. T. Shih, "Dispersion of a single hole in the  $t$ - $J$  model," *Physical Review B*, vol. 55, no. 9, pp. 5983–5987, 1997.
- [74] T. Tohyama and S. Maekawa, "Role of next-nearest-neighbor hopping in the  $t$ - $t'$ - $J$  model," *Physical Review B*, vol. 49, no. 5, pp. 3596–3599, 1994.
- [75] T. K. Lee, C.-M. Ho, and N. Nagaosa, "Theory for slightly doped antiferromagnetic Mott insulators," *Physical Review Letters*, vol. 90, no. 6, Article ID 067001, 4 pages, 2003.
- [76] T. Tohyama, "Asymmetry of the electronic states in hole- and electron-doped cuprates: exact diagonalization study of the  $t$ - $t'$ - $J$  model," *Physical Review B*, vol. 70, no. 17, Article ID 174517, 12 pages, 2004.
- [77] T. Tohyama and S. Maekawa, "Electronic states in the antiferromagnetic phase of electron-doped high- $T_c$  cuprates," *Physical Review B*, vol. 64, no. 21, Article ID 212505, 4 pages, 2001.
- [78] T. Tohyama and S. Maekawa, "Doping dependence of chemical potential and entropy in hole- and electron-doped high- $T_c$  cuprates," *Physical Review B*, vol. 67, no. 9, Article ID 092509, 3 pages, 2003.
- [79] C. Kim, P. J. White, Z.-X. Shen, et al., "Systematics of the photoemission spectral function of cuprates: insulators and hole- and electron-doped superconductors," *Physical Review Letters*, vol. 80, no. 19, pp. 4245–4248, 1998.
- [80] Yu. A. Izyumov, "The  $t$ - $J$  model for strongly correlated electrons and high- $T_c$  superconductors," *Uspekhi Fizicheskikh Nauk*, vol. 167, no. 5, pp. 496–497, 1997.
- [81] Yu. A. Izyumov, "Strongly correlated electrons: the  $t$ - $J$  model," *Physica-Uspekhi*, vol. 40, no. 5, pp. 445–476, 1997.
- [82] T. P. Devereaux, A. Virosztek, and A. Zawadowski, "Charge-transfer fluctuation, d-wave superconductivity, and the  $B_{1g}$  Raman phonon in cuprates," *Physical Review B*, vol. 51, no. 1, pp. 505–514, 1995.

- [83] G. Khaliullin and P. Horsch, "Theory of the density fluctuation spectrum of strongly correlated electrons," *Physical Review B*, vol. 54, no. 14, pp. R9600–R9603, 1996.
- [84] G. Khaliullin and P. Horsch, "Density fluctuations and phonon renormalization in the  $t$ - $J$  model," *Physica C*, vol. 282–287, part 3, pp. 1751–1752, 1997.
- [85] M. Opel, R. Hackl, T. P. Devereaux, et al., "Physical origin of the buckling in  $\text{CuO}_2$ : electron-phonon coupling and Raman spectra," *Physical Review B*, vol. 60, no. 13, pp. 9836–9844, 1999.
- [86] T. P. Devereaux, A. Virosztek, and A. Zawadowski, "Neutron scattering and the  $B_{1g}$  phonon in the cuprates," *Physical Review B*, vol. 59, no. 22, pp. 14618–14623, 1999.
- [87] P. Horsch, G. Khaliullin, and V. Oudovenko, "Density response of the  $t$ - $J$  model and renormalization of breathing and half-breathing phonon modes: a slave-fermion calculation," *Physica C*, vol. 341–348, part 1, pp. 117–120, 2000.
- [88] S. Ishihara and N. Nagaosa, "Interplay of electron-phonon interaction and electron correlation in high-temperature superconductivity," *Physical Review B*, vol. 69, no. 14, Article ID 144520, 13 pages, 2004.
- [89] O. Rösch and O. Gunnarsson, "Electron-phonon interaction in the three-band model," *Physical Review B*, vol. 70, no. 22, Article ID 224518, 7 pages, 2004.
- [90] T. P. Devereaux, T. Cuk, Z.-X. Shen, and N. Nagaosa, "Anisotropic electron-phonon interaction in the cuprates," *Physical Review Letters*, vol. 93, no. 11, Article ID 117004, 4 pages, 2004.
- [91] T. Cuk, F. Baumberger, D. H. Lu, et al., "Coupling of the  $B_{1g}$  Phonon to the antinodal electronic states of  $\text{Bi}_2\text{Sr}_2\text{Ca}_{0.92}\text{Y}_{0.08}\text{Cu}_2\text{O}_{8+\delta}$ ," *Physical Review Letters*, vol. 93, no. 11, Article ID 117003, 4 pages, 2004.
- [92] P. Horsch and G. Khaliullin, "Doping dependence of density response and bond-stretching phonons in cuprates," *Physica B*, vol. 359–361, pp. 620–622, 2005.
- [93] N. Bulut and D. J. Scalapino, " $d_{x^2-y^2}$  symmetry and the pairing mechanism," *Physical Review B*, vol. 54, no. 21, pp. 14971–14973, 1996.
- [94] L. Pintschovius and W. Reichardt, "Neutron scattering in layered copper-oxide superconductors," in *Physics and Chemistry of Materials with Low-Dimensional Structures, Vol. 20*, A. Furrer, Ed., p. 165, Kluwer Academic Publishers, Dordrecht, The Netherlands, 1998.
- [95] L. Pintschovius, "Electron-phonon coupling effects explored by inelastic neutron scattering," *Physica Status Solidi B*, vol. 242, no. 1, pp. 30–50, 2005.
- [96] W. Meevasana, T. P. Devereaux, N. Nagaosa, Z.-X. Shen, and J. Zaanen, "Calculation of overdamped  $c$ -axis charge dynamics and the coupling to polar phonons in cuprate superconductors," *Physical Review B*, vol. 74, no. 17, Article ID 174524, 6 pages, 2006.
- [97] W. Meevasana, N. J. C. Ingle, D. H. Lu, et al., "Doping dependence of the coupling of electrons to bosonic modes in the single-layer high-temperature  $\text{Bi}_2\text{Sr}_2\text{CuO}_6$  superconductor," *Physical Review Letters*, vol. 96, no. 15, Article ID 157003, 4 pages, 2006.
- [98] A. S. Alexandrov and P. E. Kornilovitch, "Mobile small polaron," *Physical Review Letters*, vol. 82, no. 4, pp. 807–810, 1999.
- [99] W. E. Pickett, "Electronic structure of the high-temperature oxide superconductors," *Review of Modern Physics*, vol. 61, pp. 433–512, 1989.
- [100] K.-P. Bohnen, R. Heid, and M. Krauss, "Phonon dispersion and electron-phonon interaction for  $\text{YBa}_2\text{Cu}_3\text{O}_7$  from first-principles calculations," *Europhysics Letters*, vol. 64, no. 1, pp. 104–110, 2003.
- [101] L. Pintschovius and M. Braden, "Anomalous dispersion of LO phonons in  $\text{La}_{1.85}\text{Sr}_{0.15}\text{CuO}_4$ ," *Physical Review B*, vol. 60, no. 22, pp. R15039–R15042, 1999.
- [102] F. Giustino, M. L. Cohen, and S. G. Louie, "Small phonon contribution to the photoemission kink in the copper oxide superconductors," *Nature*, vol. 452, no. 7190, pp. 975–978, 2008.
- [103] D. Reznik, G. Sangiovanni, O. Gunnarsson, and T. P. Devereaux, "Photoemission kinks and phonons in cuprates," *Nature*, vol. 455, no. 7213, pp. E6–E7, 2008.
- [104] D. Reznik, L. Pintschovius, M. Ito, et al., "Electron-phonon coupling reflecting dynamic charge inhomogeneity in copper oxide superconductors," *Nature*, vol. 440, no. 7088, pp. 1170–1173, 2006.
- [105] D. Reznik, L. Pintschovius, M. Fujita, K. Yamada, G. D. Gu, and J. M. Tranquada, "Electron-phonon anomaly related to charge stripes: static stripe phase versus optimally doped superconducting  $\text{La}_{1.85}\text{Sr}_{0.15}\text{CuO}_4$ ," *Journal of Low Temperature Physics*, vol. 147, no. 3-4, pp. 353–364, 2007.
- [106] L. Pintschovius, D. Reznik, W. Reichardt, et al., "Oxygen phonon branches in  $\text{YBa}_2\text{Cu}_3\text{O}_7$ ," *Physical Review B*, vol. 69, no. 21, Article ID 214506, 11 pages, 2004.
- [107] H. Uchiyama, A. Q. R. Baron, S. Tsutsui, et al., "Softening of Cu-O bond stretching phonons in tetragonal  $\text{HgBa}_2\text{CuO}_{4+\delta}$ ," *Physical Review Letters*, vol. 92, no. 19, Article ID 197005, 4 pages, 2004.
- [108] L. Pintschovius, D. Reznik, and K. Yamada, "Oxygen phonon branches in overdoped  $\text{La}_{1.7}\text{Sr}_{0.3}\text{Cu}_3\text{O}_4$ ," *Physical Review B*, vol. 74, no. 17, Article ID 174514, 5 pages, 2006.
- [109] J. J. M. Poethuizen, R. Eder, N. T. Hien, M. Matoba, A. A. Menovsky, and G. A. Sawatzky, "Single hole dynamics in the  $\text{CuO}_2$  plane at half filling," *Physical Review Letters*, vol. 78, no. 4, pp. 717–720, 1997.
- [110] G.-H. Gweon, T. Sasagawa, S. Y. Zhou, et al., "An unusual isotope effect in a high-transition-temperature superconductor," *Nature*, vol. 430, no. 6996, pp. 187–190, 2004.
- [111] J. F. Douglas, H. Iwasawa, Z. Sun, et al., "Superconductors: unusual oxygen isotope effects in cuprates?" *Nature*, vol. 446, no. 7133, p. E5, 2007.
- [112] H. Iwasawa, Y. Aiura, T. Saitoh, et al., "A re-examination of the oxygen isotope effect in ARPES spectra of  $\text{Bi}2212$ ," *Physica C*, vol. 463–465, pp. 52–55, 2007.
- [113] H. Iwasawa, J. F. Douglas, K. Sato, et al., "Isotopic fingerprint of electron-phonon coupling in high- $T_c$  cuprates," *Physical Review Letters*, vol. 101, no. 15, Article ID 157005, 2008.
- [114] J. Van den Brink and O. P. Sushkov, "Single-hole Green's functions in insulating copper oxides at nonzero temperature," *Physical Review B*, vol. 57, no. 6, pp. 3518–3524, 1998.
- [115] S. Lupi, P. Maselli, M. Capizzi, P. Calvani, P. Giura, and P. Roy, "Evolution of a polaron band through the phase diagram of  $\text{Nd}_{2-x}\text{Ce}_x\text{CuO}_{4-y}$ ," *Physical Review Letters*, vol. 83, no. 23, pp. 4852–4855, 1999.
- [116] S. Lupi, P. Calvani, M. Capizzi, P. Maselli, W. Sadowski, and E. Walker, "Infrared optical conductivity of the Nd-Ce-Cu-O system," *Physical Review B*, vol. 45, no. 21, pp. 12470–12477, 1992.
- [117] S. Lupi, M. Capizzi, P. Calvani, et al., "Fano effect in the  $a$ - $b$  plane of  $\text{Nd}_{1.96}\text{Ce}_{0.04}\text{CuO}_{4+y}$ : evidence of phonon interaction with a polaronic background," *Physical Review B*, vol. 57, no. 2, pp. 1248–1252, 1998.

- [118] M. A. Quijada, D. B. Tanner, R. J. Kelley, M. Onellion, H. Berger, and G. Margaritondo, "Anisotropy in the ab-plane optical properties of  $\text{Bi}_2\text{Sr}_2\text{CaCu}_2\text{O}_8$  single-domain crystals," *Physical Review B*, vol. 60, no. 21, pp. 14917–14934, 1999.
- [119] Y. Onose, Y. Taguchi, K. Ishizaka, and Y. Tokura, "Doping dependence of pseudogap and related charge dynamics in  $\text{Nd}_{2-x}\text{Ce}_x\text{CuO}_4$ ," *Physical Review Letters*, vol. 87, no. 21, Article ID 217001, 4 pages, 2001.
- [120] N. L. Wang, P. Zheng, T. Feng, et al., "Infrared properties of  $\text{La}_{2-x}(\text{Ca}, \text{Sr})_x\text{CaCu}_2\text{O}_{6+\delta}$  single crystals," *Physical Review B*, vol. 67, no. 13, Article ID 134526, 5 pages, 2003.
- [121] P. D. Johnson, T. Valla, A. V. Fedorov, et al., "Doping and temperature dependence of the mass enhancement observed in the cuprate  $\text{Bi}_2\text{Sr}_2\text{CaCu}_2\text{O}_{8+\delta}$ ," *Physical Review Letters*, vol. 87, no. 17, Article ID 86394, 1770074 pages, 2001.
- [122] T. Valla, A. V. Fedorov, P. D. Johnson, et al., "Evidence for quantum critical behavior in the optimally doped cuprate  $\text{Bi}_2\text{Sr}_2\text{CaCu}_2\text{O}_{8+\delta}$ ," *Science*, vol. 285, no. 5436, pp. 2110–2113, 1999.
- [123] A. Kaminski, J. Mesot, H. Fretwell, et al., "Quasiparticles in the superconducting state of  $\text{Bi}_2\text{Sr}_2\text{CaCu}_2\text{O}_{8+\delta}$ ," *Physical Review Letters*, vol. 84, no. 8, pp. 1788–1791, 2000.
- [124] P. V. Bogdanov, A. Lanzara, S. A. Kellar, et al., "Evidence for an energy scale for quasiparticle dispersion in  $\text{Bi}_2\text{Sr}_2\text{CaCu}_2\text{O}_8$ ," *Physical Review Letters*, vol. 85, no. 12, pp. 2581–2584, 2000.
- [125] A. Kaminski, M. Randeria, J. C. Campuzano, et al., "Renormalization of spectral line shape and dispersion below  $T_c$  in  $\text{Bi}_2\text{Sr}_2\text{CaCu}_2\text{O}_{8+\delta}$ ," *Physical Review Letters*, vol. 86, no. 6, pp. 1070–1073, 2001.
- [126] A. D. Gromko, A. V. Fedorov, Y.-D. Chuang, et al., "Mass-renormalized electronic excitations at  $(\pi, 0)$  in the superconducting state of  $\text{Bi}_2\text{Sr}_2\text{CaCu}_2\text{O}_{8+\delta}$ ," *Physical Review B*, vol. 68, no. 17, Article ID 174520, 2003.
- [127] T. Sato, H. Matsui, T. Takahashi, et al., "Observation of band renormalization effects in hole-doped high- $T_c$  superconductors," *Physical Review Letters*, vol. 91, no. 15, Article ID 157003, 2003.
- [128] X. J. Zhou, J. Shi, T. Yoshida, et al., "Multiple bosonic mode coupling in the electron self-energy of  $(\text{La}_{2-x}\text{Sr}_x)\text{CuO}_4$ ," *Physical Review Letters*, vol. 95, no. 11, Article ID 117001, 4 pages, 2005.
- [129] M. R. Norman, H. Ding, J. C. Campuzano, et al., "Unusual dispersion and line shape of the superconducting state spectra of  $\text{Bi}_2\text{Sr}_2\text{CaCu}_2\text{O}_{8+\delta}$ ," *Physical Review Letters*, vol. 79, no. 18, pp. 3506–3509, 1997.
- [130] T. K. Kim, A. A. Kordyuk, S. V. Borisenko, et al., "Doping dependence of the mass enhancement in  $(\text{Pb}, \text{Bi})_2\text{Sr}_2\text{CaCu}_2\text{O}_8$  at the antinodal point in the superconducting and normal states," *Physical Review Letters*, vol. 91, no. 16, Article ID 167002, 4 pages, 2003.
- [131] R. Zeyher and A. Greco, "Low-energy renormalization of the electron dispersion of high- $T_c$  superconductors," *Physical Review B*, vol. 64, no. 14, Article ID 140510, 4 pages, 2001.
- [132] S. Koikegami and Y. Aiura, "Kink structure in the electronic dispersion of high- $T_c$  superconductors from the electron-phonon interaction," *Physical Review B*, vol. 77, no. 18, Article ID 184519, 2008.
- [133] M. R. Norman and H. Ding, "Collective modes and the superconducting-state spectral function of  $\text{Bi}_2\text{Sr}_2\text{CaCu}_2\text{O}_8$ ," *Physical Review B*, vol. 57, no. 18, pp. R11089–R11092, 1998.
- [134] M. Eschrig and M. R. Norman, "Neutron resonance: modeling photoemission and tunneling data in the superconducting state of  $\text{Bi}_2\text{Sr}_2\text{CaCu}_2\text{O}_{8+\delta}$ ," *Physical Review Letters*, vol. 85, no. 15, pp. 3261–3264, 2000.
- [135] D. Manske, I. Eremin, and K. H. Bennemann, "Analysis of the elementary excitations in high- $T_c$  cuprates: explanation of the new energy scale observed by angle-resolved photoemission spectroscopy," *Physical Review Letters*, vol. 87, no. 17, Article ID 177005, 4 pages, 2001.
- [136] M. Eschrig and M. R. Norman, "Dispersion anomalies in bilayer cuprates and the odd symmetry of the magnetic resonance," *Physical Review Letters*, vol. 89, no. 27, Article ID 277005, 4 pages, 2002.
- [137] D. Manske, I. Eremin, and K. H. Bennemann, "Renormalization of the elementary excitations in hole- and electron-doped cuprates due to spin fluctuations," *Physical Review B*, vol. 67, no. 13, Article ID 134520, 12 pages, 2003.
- [138] A. V. Chubukov and M. R. Norman, "Dispersion anomalies in cuprate superconductors," *Physical Review B*, vol. 70, no. 17, Article ID 174505, 12 pages, 2004.
- [139] D. Manske, *Theory of Unconventional Superconductors: Cooper Pairing Mediated by Spin Excitations*, vol. 202 of *Springer Tracts in Modern Physics*, Springer, Heidelberg, Germany, 2004.
- [140] H. F. Fong, P. Bourges, Y. Sidis, et al., "Neutron scattering from magnetic excitations in  $\text{Bi}_2\text{Sr}_2\text{CaCu}_2\text{O}_{8+\delta}$ ," *Nature*, vol. 398, no. 6728, pp. 588–591, 1999.
- [141] H. A. Mook, M. Yethiraj, G. Aeppli, T. E. Mason, and T. Armstrong, "Polarized neutron determination of the magnetic excitations in  $\text{YBa}_2\text{Cu}_3\text{O}_7$ ," *Physical Review Letters*, vol. 70, no. 22, pp. 3490–3493, 1993.
- [142] H. F. Fong, B. Keimer, P. W. Anderson, D. Reznik, F. Doğan, and I. A. Aksay, "Phonon and magnetic neutron scattering at 41 meV in  $\text{YBa}_2\text{Cu}_3\text{O}_7$ ," *Physical Review Letters*, vol. 75, no. 2, pp. 316–319, 1995.
- [143] B. Vignolle, S. M. Hayden, D. F. McMorrow, et al., "Two energy scales in the spin excitations of the high-temperature superconductor  $\text{La}_{2-x}\text{Sr}_x\text{CuO}_4$ ," *Nature Physics*, vol. 3, no. 3, pp. 163–167, 2007.
- [144] A. W. Sandvik, D. J. Scalapino, and N. E. Bickers, "Effect of an electron-phonon interaction on the one-electron spectral weight of a  $d$ -wave superconductor," *Physical Review B*, vol. 69, no. 9, Article ID 094523, 11 pages, 2004.
- [145] S. R. Park, D. J. Song, C. S. Leem, et al., "Angle-resolved photoemission spectroscopy of electron-doped cuprate superconductors: isotropic electron-phonon coupling," *Physical Review Letters*, vol. 101, no. 11, Article ID 117006, 4 pages, 2008.
- [146] D. Reznik, B. Keimer, F. Dogan, and I. A. Aksay, "q dependence of self-energy effects of the plane oxygen vibration in  $\text{YBa}_2\text{Cu}_3\text{O}_7$ ," *Physical Review Letters*, vol. 75, no. 12, pp. 2396–2399, 1995.
- [147] R. J. McQueeney, Y. Petrov, T. Egami, M. Yethiraj, G. Shirane, and Y. Endoh, "Anomalous dispersion of LO phonons in  $\text{La}_{1.85}\text{Sr}_{0.15}\text{CuO}_4$  at low temperatures," *Physical Review Letters*, vol. 82, no. 3, pp. 628–631, 1999.
- [148] P. Dai, H. A. Mook, S. M. Hayden, et al., "The magnetic excitation spectrum and thermodynamics of high- $T_c$  superconductors," *Science*, vol. 284, no. 5418, pp. 1344–1347, 1999.
- [149] S. D. Wilson, P. Dai, S. Li, S. Chi, H. J. Kang, and J. W. Lynn, "Resonance in the electron-doped high-transition-temperature superconductor  $\text{PrLaCe}_{0.12}\text{CuO}_{4-\delta}$ ," *Nature*, vol. 442, no. 7098, pp. 59–62, 2006.
- [150] J. Zhao, P. Dai, S. Li, P. G. Freeman, Y. Onose, and Y. Tokura, "Neutron-spin resonance in the optimally electron-doped

- superconductor  $\text{Nd}_{1.85}\text{Ce}_{0.15}\text{CuO}_{4-\delta}$ ,” *Physical Review Letters*, vol. 99, no. 1, Article ID 017001, 4 pages, 2007.
- [151] L. Pintschovius, N. Pyka, W. Reichardt, et al., “Lattice dynamical studies of HTSC materials,” *Physica C*, vol. 185–189, pp. 156–161, 1991.
- [152] L. Pintschovius and M. Braden, “Phonon anomalies in  $\text{La}_2\text{CuO}_{4-\delta}$ ,” *Journal of Low Temperature Physics*, vol. 105, no. 3-4, pp. 813–818, 1996.
- [153] W. Reichardt, “Cu-O bond-stretching vibrations in  $\text{YBa}_2\text{Cu}_3\text{O}_7$  studied by inelastic neutron scattering,” *Journal of Low Temperature Physics*, vol. 105, no. 3-4, pp. 807–812, 1996.
- [154] R. J. McQueeney, J. L. Sarrao, P. G. Pagliuso, P. W. Stephens, and R. Osborn, “Mixed lattice and electronic states in high-temperature superconductors,” *Physical Review Letters*, vol. 87, no. 7, Article ID 077001, 4 pages, 2001.
- [155] L. Pintschovius, W. Reichardt, M. Kläser, T. Wolf, and H. V. Löhneysen, “Pronounced in-plane anisotropy of phonon anomalies in  $\text{YBa}_2\text{Cu}_3\text{O}_{6.6}$ ,” *Physical Review Letters*, vol. 89, no. 3, Article ID 037001, 4 pages, 2002.
- [156] J.-H. Chung, T. Egami, R. J. McQueeney, et al., “In-plane anisotropy and temperature dependence of oxygen phonon modes in  $\text{YBa}_2\text{Cu}_3\text{O}_{6.95}$ ,” *Physical Review B*, vol. 67, no. 1, Article ID 014517, 9 pages, 2003.
- [157] N. Pyka, W. Reichardt, L. Pintschovius, G. Engel, J. Rossat-Mignod, and J. Y. Henry, “Superconductivity-induced phonon softening in  $\text{YBa}_2\text{Cu}_3\text{O}_7$  observed by inelastic neutron scattering,” *Physical Review Letters*, vol. 70, no. 10, pp. 1457–1460, 1993.
- [158] S. L. Cooper, M. V. Klein, B. G. Pazol, J. P. Rice, and D. M. Ginsberg, “Raman scattering from superconducting gap excitations in single-crystal  $\text{YBa}_2\text{Cu}_3\text{O}_{7-\delta}$ ,” *Physical Review B*, vol. 37, no. 10, pp. 5920–5923, 1988.
- [159] C. Thomsen, M. Cardona, B. Gegenheimer, R. Liu, and A. Simon, “Untwinned single crystals of  $\text{YBa}_2\text{Cu}_3\text{O}_7$ —: an optical investigation of the a-b anisotropy,” *Physical Review B*, vol. 37, no. 16, pp. 9860–9863, 1988.
- [160] J. Graf, M. D’Astuto, P. Giura, et al., “In-plane copper-oxygen bond-stretching mode anomaly in underdoped  $\text{La}_{2-x}\text{Sr}_x\text{CuO}_{4+\delta}$  measured with high-resolution inelastic X-ray scattering,” *Physical Review B*, vol. 76, no. 17, Article ID 172507, 2007.
- [161] J. Graf, M. D’Astuto, C. Jozwiak, et al., “Bond stretching phonon softening and kinks in the angle-resolved photoemission spectra of optimally doped  $\text{Bi}_2\text{Sr}_{1.6}\text{La}_{0.4}\text{Cu}_2\text{O}_{6+\delta}$  superconductors,” *Physical Review Letters*, vol. 100, no. 22, Article ID 227002, 2008.
- [162] K. J. von Szczepanski and K. W. Becker, “Coupling of electrons and phonons in a doped antiferromagnet,” *Zeitschrift für Physik B*, vol. 89, no. 3, pp. 327–334, 1992.
- [163] C. Falter and M. Klenner, “Nonadiabatic and nonlocal electron-phonon interaction and phonon-plasmon mixing in the high-temperature superconductors,” *Physical Review B*, vol. 50, no. 13, pp. 9426–9433, 1994.
- [164] C. Falter, M. Klenner, and G. A. Hoffmann, “Phonon renormalization and c-axis phonon-plasmon mixing in  $\text{La}_2\text{CuO}_4$ ,” *Physical Review B*, vol. 52, no. 5, pp. 3702–3710, 1995.
- [165] B. Bäuml, G. Wellein, and H. Fehske, “Optical absorption and single-particle excitations in the two-dimensional Holstein  $t$ - $J$  model,” *Physical Review B*, vol. 58, no. 7, pp. 3663–3676, 1998.
- [166] A. Ramak, P. Horsch, and P. Fulde, “Effective mass of quasi-particles in a  $t$ - $J$  model with electron-phonon interactions,” *Physical Review B*, vol. 46, no. 21, pp. 14305–14308, 1992.
- [167] B. Kyung, S. I. Mukhin, V. N. Kostur, and R. A. Ferrell, “Spectral properties of the  $t$ - $J$  model in the presence of hole-phonon interaction,” *Physical Review B*, vol. 54, no. 18, pp. 13167–13174, 1996.
- [168] H. Röder, H. Fehske, and R. N. Silver, “The ordering of polarons in the Holstein  $t$ - $J$  model: an application to  $\text{La}_{2-x}\text{Sr}_x\text{NiO}_{4+y}$ ,” *Europhysics Letters*, vol. 28, no. 4, pp. 257–262, 1994.
- [169] S. Schmitt-Rink, C. M. Varma, and A. E. Ruckenstein, “Spectral function of holes in a quantum antiferromagnet,” *Physical Review Letters*, vol. 60, no. 26, pp. 2793–2796, 1988.
- [170] G. Martinez and P. Horsch, “Spin polarons in the  $t$ - $J$  model,” *Physical Review B*, vol. 44, no. 1, pp. 317–331, 1991.
- [171] O. Gunnarsson and O. Rösch, “Electron-phonon coupling in the self-consistent Born approximation of the  $t$ - $J$  model,” *Physical Review B*, vol. 73, no. 17, Article ID 174521, 2006.
- [172] J. Bonča, S. Maekawa, T. Tohyama, and P. Prelovšek, “Spectral properties of a hole coupled to optical phonons in the generalized  $t$ - $J$  model,” *Physical Review B*, vol. 77, no. 5, Article ID 054519, 2008.
- [173] J. Bonča, S. A. Trugman, and I. Batistić, “Holstein polaron,” *Physical Review B*, vol. 60, no. 3, pp. 1633–1642, 1999.
- [174] J. Bonča, S. Maekawa, and T. Tohyama, “Numerical approach to the low-doping regime of the  $t$ - $J$  model,” *Physical Review B*, vol. 76, no. 3, Article ID 035121, 6 pages, 2007.
- [175] E. I. Rashba, “Self-trapping of excitons,” in *Modern Problems in Condensed Matter Sciences*, V. M. Agranovich and A. A. Maradudin, Eds., vol. 2, p. 543, North Holland, Amsterdam, The Netherlands, 1982.
- [176] A. S. Ioselevich and E. I. Rashba, “Theory of nonradiative trapping in crystals,” in *Modern Problems in Condensed Matter Sciences*, vol. 34, p. 347, North Holland, Amsterdam, The Netherlands, 1992.
- [177] K. M. Shen, F. Ronning, W. Meevasana, et al., “Angle-resolved photoemission studies of lattice polaron formation in the cuprate  $\text{Ca}_2\text{CuO}_2\text{Cl}_2$ ,” *Physical Review B*, vol. 75, no. 7, Article ID 075115, 2007.
- [178] F. Ronning, K. M. Shen, N. P. Armitage, et al., “Anomalous high-energy dispersion in angle-resolved photoemission spectra from the insulating cuprate  $\text{Ca}_2\text{CuO}_2\text{Cl}_2$ ,” *Physical Review B*, vol. 71, no. 9, Article ID 094518, 5 pages, 2005.
- [179] J. Graf, G.-H. Gweon, K. McElroy, et al., “Universal high energy anomaly in the angle-resolved photoemission spectra of high temperature superconductors: possible evidence of spinon and holon branches,” *Physical Review Letters*, vol. 98, no. 6, Article ID 067004, 2007.
- [180] B. P. Xie, K. Yang, D. W. Shen, et al., “High-energy scale revival and giant kink in the dispersion of a cuprate superconductor,” *Physical Review Letters*, vol. 98, no. 14, Article ID 147001, 2007.
- [181] T. Valla, T. E. Kidd, W.-G. Yin, et al., “High-energy kink observed in the electron dispersion of high-temperature cuprate superconductors,” *Physical Review Letters*, vol. 98, no. 16, Article ID 167003, 2007.
- [182] W. Meevasana, X. J. Zhou, S. Sahrakorpi, et al., “Hierarchy of multiple many-body interaction scales in high-temperature superconductors,” *Physical Review B*, vol. 75, no. 17, Article ID 174506, 2007.
- [183] E. Manousakis, “String excitations of a hole in a quantum antiferromagnet and photoelectron spectroscopy,” *Physical Review B*, vol. 75, no. 3, Article ID 035106, 2007.

- [184] E. Manousakis, “Possible observation of “string excitations” of a hole in a quantum antiferromagnet,” *Physics Letters A*, vol. 362, no. 1, pp. 86–89, 2007.
- [185] F. Carbone, D.-S. Yang, E. Giannini, and A. H. Zewail, “Direct role of structural dynamics in electron-lattice coupling of superconducting cuprates,” *Proceedings of the National Academy of Sciences of the United States of America*, vol. 105, no. 51, pp. 20161–20166, 2008.
- [186] P. B. Allen, “Theory of thermal relaxation of electrons in metals,” *Physical Review Letters*, vol. 59, no. 13, pp. 1460–1463, 1987.
- [187] M. Grüninger, D. van der Marel, A. Damascelli, A. Erb, T. Nunner, and T. Kopp, “Midinfrared absorption in  $\text{YBa}_2\text{Cu}_3\text{O}_6$ : evidence for a failure of spin-wave theory for spin 1/2 in two dimensions,” *Physical Review B*, vol. 62, no. 18, pp. 12422–12426, 2000.
- [188] I. Eremin, O. Kamaev, and M. V. Eremin, “Possible isotope effect on the resonance peak formation in high- $T_c$  cuprates,” *Physical Review B*, vol. 69, no. 9, Article ID 094517, 5 pages, 2004.
- [189] G.-M. Zhao, “Evidence for very strong electron-phonon coupling in  $\text{YBa}_2\text{Cu}_3\text{O}_6$ ,” *Physical Review B*, vol. 75, no. 10, Article ID 104511, 2007.
- [190] G.-H. Gweon, S. Y. Zhou, M. C. Watson, T. Sasagawa, H. Takagi, and A. Lanzara, “Strong and complex electron-lattice correlation in optimally doped  $\text{Bi}_2\text{Sr}_2\text{CaCu}_2\text{O}_{8+\delta}$ ,” *Physical Review Letters*, vol. 97, no. 22, Article ID 227001, 2006.
- [191] J. Lee, K. Fujita, K. McElroy, et al., “Interplay of electron-lattice interactions and superconductivity in  $\text{Bi}_2\text{Sr}_2\text{CaCu}_2\text{O}_{8+\delta}$ ,” *Nature*, vol. 442, no. 7102, pp. 546–550, 2006.
- [192] A. De Lozanne, “Superconductivity: hot vibes,” *Nature*, vol. 442, no. 7102, pp. 522–523, 2006.
- [193] J. D. Koralek, J. F. Douglas, N. C. Plumb, et al., “Laser based angle-resolved photoemission, the sudden approximation, and quasiparticle-like spectral peaks in  $\text{Bi}_2\text{Sr}_2\text{CaCu}_2\text{O}_{8+\delta}$ ,” *Physical Review Letters*, vol. 96, no. 1, Article ID 017005, 2006.
- [194] J. P. Hague, P. E. Kornilovitch, A. S. Alexandrov, and J. H. Samson, “Effects of lattice geometry and interaction range on polaron dynamics,” *Physical Review B*, vol. 73, no. 5, Article ID 054303, 14 pages, 2006.
- [195] P. E. Spencer, J. H. Samson, P. E. Kornilovitch, and A. S. Alexandrov, “Effect of electron-phonon interaction range on lattice polaron dynamics: a continuous-time quantum Monte Carlo study,” *Physical Review B*, vol. 71, no. 18, Article ID 184310, 2005.
- [196] P. E. Kornilovitch and A. S. Alexandrov, “Isotope effect on the electron band structure of doped insulators,” *Physical Review B*, vol. 70, no. 22, Article ID 224511, 2004.
- [197] P. E. Kornilovitch, “Giant enhancement of anisotropy by electron-phonon interaction,” *Physical Review B*, vol. 59, no. 21, pp. 13531–13534, 1999.
- [198] P. E. Kornilovitch, “Continuous-time quantum Monte Carlo algorithm for the lattice polaron,” *Physical Review Letters*, vol. 81, no. 24, pp. 5382–5385, 1998.
- [199] P. Paci, M. Capone, E. Cappelluti, S. Ciuchi, C. Grimaldi, and L. Pietronero, “Polaronic and nonadiabatic phase diagram from anomalous isotope effects,” *Physical Review Letters*, vol. 94, no. 3, Article ID 036406, 4 pages, 2005.
- [200] S. Andergassen, S. Caprara, C. Di Castro, and M. Grilli, “Anomalous isotopic effect near the charge-ordering quantum criticality,” *Physical Review Letters*, vol. 87, no. 5, Article ID 056401, 4 pages, 2001.
- [201] S. Fratini and S. Ciuchi, “Spectral properties and isotope effect in strongly interacting systems: Mott-Hubbard insulator versus polaronic semiconductor,” *Physical Review B*, vol. 72, no. 23, Article ID 235107, 9 pages, 2005.
- [202] P. Paci, M. Capone, E. Cappelluti, S. Ciuchi, and C. Grimaldi, “Isotope effects in the Hubbard-Holstein model within dynamical mean-field theory,” *Physical Review B*, vol. 74, no. 20, Article ID 205108, 2006.
- [203] G. A. Sawatzky, “Testing Fermi-liquid models,” *Nature*, vol. 342, no. 6249, pp. 480–481, 1989.
- [204] D. S. Dessau, T. Saitoh, C.-H. Park, et al., “k-dependent electronic structure, a large “ghost” fermi surface, and a pseudogap in a layered magnetoresistive oxide,” *Physical Review Letters*, vol. 81, no. 1, pp. 192–195, 1998.
- [205] L. Perfetti, H. Berger, A. Reggiani, et al., “Spectroscopic indications of polaronic carriers in the quasi-one-dimensional conductor  $(\text{TaSe}_4)_2\text{I}$ ,” *Physical Review Letters*, vol. 87, no. 21, Article ID 216404, 2001.
- [206] L. Perfetti, S. Mitrovic, G. Margaritondo, et al., “Mobile small polarons and the Peierls transition in the quasi-one-dimensional conductor  $\text{K}_{0.3}\text{MoO}_3$ ,” *Physical Review B*, vol. 66, no. 7, Article ID 075107, 8 pages, 2002.
- [207] D. Schrupp, M. Sing, M. Tsunekawa, et al., “High-energy photoemission on  $\text{Fe}_3\text{O}_4$ : small polaron physics and the Verwey transition,” *Europhysics Letters*, vol. 70, no. 6, pp. 789–795, 2005.
- [208] G. D. Mahan, *Many Particle Physics*, Plenum Press, New York, NY, USA, 2000.
- [209] H. Röder, H. Fehske, and H. Büttner, “Exact diagonalization study of the two-dimensional  $t$ - $J$  model with adiabatic Holstein phonons: single-hole case,” *Physical Review B*, vol. 47, no. 19, pp. 12420–12425, 1993.
- [210] P. Prelovšek, R. Zeyher, and P. Horsch, “Self-localization of composite spin-lattice polarons,” *Physical Review Letters*, vol. 96, no. 8, Article ID 086402, 4 pages, 2006.
- [211] V. Cataudella, G. De Filippis, A. S. Mishchenko, and N. Nagaosa, “Evidences of the charge-lattice interaction in undoped cuprates,” *Journal of Superconductivity and Novel Magnetism*, vol. 22, no. 1, pp. 17–20, 2009.
- [212] M. Berciu, “Green’s function of a dressed particle,” *Physical Review Letters*, vol. 97, no. 3, Article ID 036402, 2006.
- [213] G. L. Goodvin, M. Berciu, and G. A. Sawatzky, “Green’s function of the Holstein polaron,” *Physical Review B*, vol. 74, no. 24, Article ID 245104, 2006.
- [214] M. Berciu, “Berciu Replies—comment on “Green’s function of a dressed particle,”” *Physical Review Letters*, vol. 98, no. 20, Article ID 209702, 1 pages, 2007.
- [215] M. Berciu and G. L. Goodvin, “Systematic improvement of the momentum average approximation for the Green’s function of a Holstein polaron,” *Physical Review B*, vol. 76, no. 16, Article ID 165109, 2007.
- [216] L. Covaci and M. Berciu, “Holstein polaron: the effect of coupling to multiple-phonon modes,” *Europhysics Letters*, vol. 80, no. 6, Article ID 67001, 2007.
- [217] L. Covaci and M. Berciu, “Survival of the dirac points in rippled graphene,” *Physical Review Letters*, vol. 100, no. 25, Article ID 256405, 2008.
- [218] G. L. Goodvin and M. Berciu, “Momentum average approximation for models with electron-phonon coupling dependent on the phonon momentum,” *Physical Review B*, vol. 78, no. 23, Article ID 235120, 2008.
- [219] L. Covaci and M. Berciu, “Polaron formation in the presence of Rashba spin-orbit coupling: implications for spintronics,”

- Physical Review Letters*, vol. 102, no. 18, Article ID 186403, 2009.
- [220] O. S. Barišić, “Comment: Green’s function of a dressed particle,” *Physical Review Letters*, vol. 98, no. 20, Article ID 209701, 2007.
- [221] O. S. Barišić, “Diagrammatic content of the dynamical mean-field theory for the Holstein polaron problem in finite dimensions,” *Physical Review B*, vol. 76, no. 19, Article ID 193106, 2007.
- [222] J. K. Freericks, M. Jarrell, and D. J. Scalapino, “Holstein model in infinite dimensions,” *Physical Review B*, vol. 48, no. 9, pp. 6302–6314, 1993.
- [223] E. Cappelluti and S. Ciuchi, “Magnetic and lattice polaron in the Holstein  $t$ - $J$  model,” *Physical Review B*, vol. 66, no. 16, Article ID 165102, 12 pages, 2002.
- [224] E. Cappelluti, S. Ciuchi, and S. Fratini, “Polaronic features in the optical properties of the Holstein  $t$ - $J$  model,” *Physical Review B*, vol. 76, no. 12, Article ID 125111, 2007.
- [225] M. Cini and A. D. Andrea, “Exactly solved electron-boson models in condensed matter and molecular physics by a generalised recursion method,” *Journal of Physics C*, vol. 21, pp. 193–235, 1988.
- [226] S. Ciuchi, et al., “Dynamical mean-field theory of the small polaron,” *Physical Review B*, vol. 56, p. 4494, 1997.
- [227] A. J. Millis, R. Mueller, and B. I. Shraiman, “Fermi-liquid-to-polaron crossover. I. General results,” *Physical Review B*, vol. 54, no. 8, pp. 5389–5404, 1996.
- [228] P. Benedetti and R. Zeyher, “Holstein model in infinite dimensions at half-filling,” *Physical Review B*, vol. 58, no. 21, pp. 14320–14334, 1998.
- [229] D. Meyer, A. C. Hewson, and R. Bulla, “Gap formation and soft phonon mode in the Holstein model,” *Physical Review Letters*, vol. 89, no. 19, Article ID 196401, 4 pages, 2002.
- [230] J. E. Han, O. Gunnarsson, and V. H. Crespi, “Strong superconductivity with local Jahn-Teller phonons in  $C_{60}$  solids,” *Physical Review Letters*, vol. 90, no. 16, Article ID 167006, 4 pages, 2003.
- [231] M. Capone and S. Ciuchi, “Polaron crossover and bipolaronic metal-insulator transition in the half-filled Holstein model,” *Physical Review Letters*, vol. 91, no. 18, Article ID 186405, 4 pages, 2003.
- [232] M. Capone, P. Carta, and S. Ciuchi, “Dynamical mean field theory of polarons and bipolarons in the half-filled Holstein model,” *Physical Review B*, vol. 74, no. 4, Article ID 045106, 2006.
- [233] H. Barentzen, “Intermediate-coupling theory of the spin polaron in the  $t$ - $J$  model,” *Physical Review B*, vol. 53, no. 9, pp. 5598–5608, 1996.
- [234] S. Yunoki, A. Macridin, and G. Sawatzky, private communication.
- [235] J. J. M. Pothuizen, Ph.D. thesis, Groningen, The Netherlands, 1998.
- [236] C. Kim, private communication.
- [237] Z. Liu and E. Manousakis, “Loop-expansion study of the single-hole spectral function in the  $t$ - $J$  model,” *Physical Review B*, vol. 51, no. 5, pp. 3156–3162, 1995.
- [238] A. S. Alexandrov and K. Reynolds, “Angle-resolved photoemission spectroscopy of band tails in lightly doped cuprates,” *Physical Review B*, vol. 76, no. 13, Article ID 132506, 4 pages, 2007.
- [239] G. De Filippis, V. Cataudella, and G. Iadonisi, “Normal state properties of an interacting large polaron gas,” *European Physical Journal B*, vol. 8, no. 3, pp. 339–351, 1999.
- [240] J. Lorenzana, “Instability due to long-range Coulomb interaction in a liquid of Feynman polarons,” *Europhysics Letters*, vol. 53, no. 4, pp. 532–538, 2001.
- [241] J. Tempere and J. T. Devreese, “Sum rule for the optical absorption of an interacting many-polaron gas,” *European Physical Journal B*, vol. 20, no. 1, pp. 27–33, 2001.
- [242] J. Tempere and J. T. Devreese, “Optical absorption of an interacting many-polaron gas,” *Physical Review B*, vol. 64, no. 10, Article ID 104504, 10 pages, 2001.
- [243] E. Cappelluti, S. Ciuchi, and S. Fratini, “Polaronic signatures in the optical properties of the electron-doped cuprate superconductor  $Nd_{2-x}Ce_xCuO_4$ ,” *Physical Review B*, vol. 79, no. 1, Article ID 012502, 4 pages, 2009.
- [244] R. Liang, D. A. Bonn, and W. N. Hardy, “Evaluation of  $CuO_2$  plane hole doping in  $YBa_2Cu_3O_{6+x}$  single crystals,” *Physical Review B*, vol. 73, no. 18, Article ID 180505(R), 4 pages, 2006.
- [245] D. Mihailović, C. M. Foster, K. Voss, and A. J. Heeger, “Application of the polaron-transport theory to  $\sigma(\omega)$  in  $Tl_2Ba_2Ca_{1-x}Gd_xCu_2O_8$ ,  $YBa_2Cu_3O_{7-\delta}$ , and  $La_{2-x}Sr_xCuO_4$ ,” *Physical Review B*, vol. 42, no. 13, pp. 7989–7993, 1990.
- [246] X.-X. Bi and P. C. Eklund, “Polaron contribution to the infrared optical response of  $La_{2-x}Sr_xCuO_{4+\delta}$  and  $La_{2-x}Sr_xNiO_{4+\delta}$ ,” *Physical Review Letters*, vol. 70, no. 17, pp. 2625–2628, 1993.
- [247] A. S. Alexandrov and N. Mott, *Polarons and Bipolarons*, World Scientific, Singapore, 1995.
- [248] J. T. Devreese and J. Tempere, “Large-polaron effects in the infrared spectrum of high- $T_c$  cuprate superconductors,” *Solid State Communications*, vol. 106, no. 5, pp. 309–313, 1998.
- [249] J. T. Devreese, “Fröhlich polarons from 0D to 3D: concepts and recent developments,” *Journal of Physics: Condensed Matter*, vol. 19, no. 25, Article ID 255201, 23 pages, 2007.
- [250] A. E. Myasnikova and E. N. Myasnikov, “Correlation of optical conductivity and angle-resolved photoemission spectra of strong-coupling large polarons and its display in cuprates,” *Physical Review B*, vol. 77, no. 16, Article ID 165136, 11 pages, 2008.
- [251] A. S. Mishchenko, unpublished.
- [252] E. N. Myasnikov, A. E. Myasnikova, and Z. P. Mastropas, “Multiphonon generation during photodissociation of slow Landau-Pekar polarons,” *Zhurnal Éksperimental’noi i Teoreticheskoi Fiziki*, vol. 129, no. 3, pp. 548–565, 2006.
- [253] E. N. Myasnikov, A. E. Myasnikova, and Z. P. Mastropas, “Multiphonon generation during photodissociation of slow Landau-Pekar polarons,” *Journal of Experimental and Theoretical Physics*, vol. 102, no. 3, pp. 480–496, 2006.
- [254] L. Vidmar, J. Bonča, and S. Maekawa, “Optical conductivity in the  $t$ - $J$  Holstein model,” *Physical Review B*, vol. 79, no. 12, Article ID 125120, 6 pages, 2009.
- [255] A. Macridin, B. Moritz, M. Jarrell, and T. Maier, “Synergistic polaron formation in the Hubbard-Holstein model at small doping,” *Physical Review Letters*, vol. 97, no. 5, Article ID 056402, 4 pages, 2006.
- [256] A. Ramšak and P. Horsch, “Spin polarons in the  $t$ - $J$  model: shape and backflow,” *Physical Review B*, vol. 48, no. 14, pp. 10559–10562, 1993.
- [257] W. F. Brinkman and T. M. Rice, “Single-particle excitations in magnetic insulators,” *Physical Review B*, vol. 2, no. 5, pp. 1324–1338, 1970.
- [258] V. Cataudella, G. De Filippis, F. Martone, and C. A. Perroni, “Variational approach to the optimized phonon technique for electron-phonon problems,” *Physical Review B*, vol. 70, no. 19, Article ID 193105, 4 pages, 2004.

- [259] G. De Filippis, V. Cataudella, V. M. Ramaglia, and C. A. Perroni, "Static and dynamic polaron features in a coherent-state basis," *Physical Review B*, vol. 72, no. 1, Article ID 014307, 7 pages, 2005.
- [260] A. Fujimori, A. E. Bocquet, K. Morikawa, et al., "Electronic structure and electron-phonon interaction in transition metal oxides with  $d_0$  configuration and lightly doped compounds," *Journal of Physics and Chemistry of Solids*, vol. 57, no. 10, pp. 1379–1384, 1996.
- [261] C. A. Perroni, V. Cataudella, and G. De Filippis, "Polaron features for long-range electron-phonon interaction," *Journal of Physics: Condensed Matter*, vol. 16, no. 9, pp. 1593–1601, 2004.
- [262] M. Berciu and G. A. Sawatzky, "Light polarons and bipolarons for a highly inhomogeneous electron-boson coupling," *Europhysics Letters*, vol. 81, no. 5, Article ID 57008, 6 pages, 2008.
- [263] J. Bonča and S. A. Trugman, "Bipolarons in the extended Holstein Hubbard model," *Physical Review B*, vol. 64, no. 9, Article ID 094507, 4 pages, 2001.
- [264] A. S. Alexandrov and B. Ya. Yavidov, "Small adiabatic polaron with a long-range electron-phonon interaction," *Physical Review B*, vol. 69, no. 7, Article ID 073101, 4 pages, 2004.
- [265] J. T. Devreese and A. S. Alexandrov, "Fröhlich polaron and bipolaron: recent developments," *Reports on Progress in Physics*, vol. 72, no. 6, Article ID 066501, 52 pages, 2009.
- [266] M. Zoli, "Two- and three-dimensional polaronic motion: beyond the Holstein model," *Physical Review B*, vol. 57, no. 17, pp. 10555–10559, 1998.
- [267] M. Zoli, "Lattice-dynamics effects on small-polaron properties," *Physical Review B*, vol. 61, no. 21, pp. 14523–14530, 2000.
- [268] M. Zoli and A. N. Das, "Polaron crossover in molecular solids," *Journal of Physics: Condensed Matter*, vol. 16, no. 21, pp. 3597–3607, 2004.
- [269] A. S. Alexandrov, *Theory of Superconductivity: From Weak to Strong Coupling*, Institute of Physics Publishing, Bristol, UK.
- [270] A. S. Alexandrov, "Bipolaron anisotropic flat bands, Hall mobility edge, and metal-semiconductor duality of overdoped high- $T_c$  oxides," *Physical Review B*, vol. 53, no. 5, pp. 2863–2869, 1996.
- [271] A. S. Alexandrov and P. E. Kornilovitch, "The Fröhlich-Coulomb model of high-temperature superconductivity and charge segregation in the cuprates," *Journal of Physics: Condensed Matter*, vol. 14, no. 21, pp. 5337–5348, 2002.
- [272] J. P. Hague, P. E. Kornilovitch, J. H. Samson, and A. S. Alexandrov, "Superlight small bipolarons in the presence of a strong coulomb repulsion," *Physical Review Letters*, vol. 98, no. 3, Article ID 037002, 4 pages, 2007.
- [273] H. Fehske, J. Loos, and G. Wellein, "Lattice polaron formation: effects of unscreened electron-phonon interaction," *Physical Review B*, vol. 61, no. 12, pp. 8016–8025, 2000.
- [274] T. Sakai, D. Poilblanc, and D. J. Scalapino, "Hole pairing and phonon dynamics in generalized two-dimensional  $t$ - $J$  Holstein models," *Physical Review B*, vol. 55, no. 13, pp. 8445–8451, 1997.
- [275] C. Slezak, A. Macridin, G. A. Sawatzky, M. Jarrell, and T. A. Maier, "Spectral properties of Holstein and breathing polarons," *Physical Review B*, vol. 73, no. 20, Article ID 205122, 10 pages, 2006.
- [276] O. Rösch and O. Gunnarsson, "Apparent electron-phonon interaction in strongly correlated systems," *Physical Review Letters*, vol. 93, no. 23, Article ID 237001, 4 pages, 2004.
- [277] O. Rösch, G. Sangiovanni, and O. Gunnarsson, "Sum rules and vertex corrections for electron-phonon interactions," *Physical Review B*, vol. 75, no. 3, Article ID 035119, 9 pages, 2007.
- [278] M. Capone, G. Sangiovanni, C. Castellani, C. Di Castro, and M. Grilli, "Phase separation close to the density-driven mott transition in the Hubbard-Holstein model," *Physical Review Letters*, vol. 92, no. 10, Article ID 106401, 4 pages, 2004.
- [279] G. Sangiovanni, M. Capone, C. Castellani, and M. Grilli, "Electron-phonon interaction close to a mott transition," *Physical Review Letters*, vol. 94, no. 2, Article ID 026401, 4 pages, 2005.
- [280] G. Sangiovanni, M. Capone, and C. Castellani, "Relevance of phonon dynamics in strongly correlated systems coupled to phonons: dynamical mean-field theory analysis," *Physical Review B*, vol. 73, no. 16, Article ID 165123, 9 pages, 2006.
- [281] G. Sangiovanni, O. Gunnarsson, E. Koch, C. Castellani, and M. Capone, "Electron-phonon interaction and antiferromagnetic correlations," *Physical Review Letters*, vol. 97, no. 4, Article ID 046404, 4 pages, 2006.
- [282] J. Zhong and H.-B. Schüttler, "Polaronic anharmonicity in the Holstein-Hubbard model," *Physical Review Letters*, vol. 69, no. 10, pp. 1600–1603, 1992.
- [283] H. Fehske, H. Röder, G. Wellein, and A. Mitrriotis, "Hole-polaron formation in the two-dimensional Holstein  $t$ - $J$  model: a variational Lanczos study," *Physical Review B*, vol. 51, no. 23, pp. 16582–16593, 1995.
- [284] G. Wellein, H. Röder, and H. Fehske, "Polarons and bipolarons in strongly interacting electron-phonon systems," *Physical Review B*, vol. 53, no. 15, pp. 9666–9675, 1996.
- [285] H. Matsueda, T. Tohyama, and S. Maekawa, "Electron-phonon coupling and spin-charge separation in one-dimensional Mott insulators," *Physical Review B*, vol. 74, no. 24, Article ID 241103, 4 pages, 2006.
- [286] H. Matsueda, A. Ando, T. Tohyama, and S. Maekawa, "Enhancement of phonon effects in photoexcited states of one-dimensional Mott insulators," *Physical Review B*, vol. 77, no. 19, Article ID 193112, 4 pages, 2008.
- [287] T. Hanaguri, C. Lupien, Y. Kohsaka, et al., "A 'checkerboard' electronic crystal state in lightly hole-doped  $\text{Ca}_{2-x}\text{Na}_x\text{CuO}_2\text{Cl}_2$ ," *Nature*, vol. 430, no. 7003, pp. 1001–1005, 2004.
- [288] Y. Kohsaka, C. Taylor, K. Fujita, et al., "An intrinsic bond-centered electronic glass with unidirectional domains in underdoped cuprates," *Science*, vol. 315, no. 5817, pp. 1380–1385, 2007.
- [289] S. H. Pan, J. P. O'Neal, R. L. Badzey, et al., "Microscopic electronic inhomogeneity in the high- $T_c$  superconductor  $\text{Bi}_2\text{Sr}_2\text{CaCu}_2\text{O}_{8+x}$ ," *Nature*, vol. 413, no. 6853, pp. 282–285, 2001.
- [290] P. M. Singer, A. W. Hunt, and T. Imai, " $^{63}\text{Cu}$  NQR evidence for spatial variation of hole concentration in  $\text{La}_{2-x}\text{Sr}_x\text{CuO}_4$ ," *Physical Review Letters*, vol. 88, no. 4, Article ID 047602, 4 pages, 2002.
- [291] N. Pavlenko and T. Kopp, "Electron-phonon coupling in a two-dimensional inhomogeneous electron gas: consequences for surface spectral properties," *Journal of Physics: Condensed Matter*, vol. 20, no. 39, Article ID 395203, 7 pages, 2008.
- [292] N. Pavlenko and T. Kopp, "Interface controlled electronic charge inhomogeneities in correlated heterostructures," *Physical Review Letters*, vol. 97, no. 18, Article ID 187001, 4 pages, 2006.

- [293] J. P. Hague, P. E. Kornilovitch, and A. S. Alexandrov, "Trapping of lattice polarons by impurities," *Physical Review B*, vol. 78, no. 9, Article ID 092302, 4 pages, 2008.
- [294] S. M. Girvin and M. Jonson, "Dynamical electron-phonon interaction and conductivity in strongly disordered metal alloys," *Physical Review B*, vol. 22, no. 8, pp. 3583–3597, 1980.
- [295] F. X. Bronold and H. Fehske, "Anderson localization of polaron states," *Physical Review B*, vol. 66, no. 7, Article ID 073102, 4 pages, 2002.
- [296] F. X. Bronold, A. Alvermann, and H. Fehske, "Anderson localization in strongly coupled disordered electron-phonon systems," *Philosophical Magazine*, vol. 84, no. 7, pp. 673–704, 2004.
- [297] A. Alvermann and H. Fehske, "Chebyshev approach to quantum systems coupled to a bath," *Physical Review B*, vol. 77, no. 4, Article ID 045125, 17 pages, 2008.
- [298] M. Berciu, A. S. Mishchenko, and N. Nagaosa, "Holstein polaron in the presence of disorder," <http://arxiv.org/abs/0906.1233>.
- [299] I. I. Mazin, E. G. Maksimov, S. N. Rashkeev, S. Y. Savrasov, and Y. A. Uspenskii, "Optical properties of metal oxides of the  $\text{La}_2\text{CuO}_4$  type," *Pisma Zh. Eksp. Teor. Fiz.*, vol. 47, p. 94, 1987, English translation in *Soviet Physics-JETP Letters*, vol. 47, p. 113, 1988.
- [300] E. G. Maksimov, S. N. Rashkeev, S. Yu. Savrasov, and Yu. A. Uspenskii, "Microscopic studies of the optical spectra of  $\text{YBa}_2\text{Cu}_3\text{O}_7$ ," *Physical Review Letters*, vol. 63, no. 17, pp. 1880–1883, 1989.
- [301] S. N. Rashkeev, et al., "Electronic structure and optical properties of  $\text{YBa}_2\text{Cu}_3\text{O}_7$ ," *Zhurnal Éksperimental'noi i Teoreticheskoi Fiziki*, vol. 97, p. 1688, 1990, translated in *Soviet Physics. JETP*, vol. 70, p. 952, 1990.
- [302] S. V. Shulga, O. V. Dolgov, and E. G. Maksimov, "Electronic states and optical spectra of HTSC with electron-phonon coupling," *Physica C*, vol. 178, no. 4–6, pp. 266–274, 1991.
- [303] E. G. Maksimov, H. J. Kaufmann, E. K. H. Salje, Y. De Wilde, N. Bontemps, and J. P. Contour, "Comparative analysis of the optical spectra of  $\text{YBa}_2\text{Cu}_3\text{O}_7$ ," *Solid State Communications*, vol. 112, no. 8, pp. 449–454, 1999.
- [304] T. Jarlborg, "Weak screening of high frequency phonons and superconductivity in  $\text{YBa}_2\text{Cu}_3\text{O}_7$ ," *Solid State Communications*, vol. 71, no. 8, pp. 669–671, 1989.
- [305] R. E. Cohen, W. E. Pickett, and H. Krakauer, "Theoretical determination of strong electron-phonon coupling in  $\text{YBa}_2\text{Cu}_3\text{O}_7$ ," *Physical Review Letters*, vol. 64, no. 21, pp. 2575–2578, 1990.
- [306] R. Zeyher, "Importance of long-range electron-phonon coupling in high- $T_c$  superconductors," *Zeitschrift für Physik B*, vol. 80, no. 2, pp. 187–192, 1990.
- [307] H. Krakauer, W. E. Pickett, and R. E. Cohen, "Large calculated electron-phonon interactions in  $\text{La}_{2-x}\text{M}_x\text{CuO}_4$ ," *Physical Review B*, vol. 47, no. 2, pp. 1002–1015, 1993.
- [308] E. G. Maksimov, "High-temperature superconductivity: the current state," *Physics-Uspokhi*, vol. 43, no. 10, pp. 965–990, 2000, Russian translation in *Uspokhi Fizicheskikh Nauk*, vol. 170, p. 1033, 2000.
- [309] O. V. Dolgov and S. V. Shulga, "Analysis of intermediate boson spectra from FIR data for HTSC and heavy fermion systems," *Journal of Superconductivity*, vol. 8, no. 5, pp. 611–612, 1995.
- [310] J. P. Carbotte, E. Schachinger, and D. N. Basov, "Coupling strength of charge carriers to spin fluctuations in high-temperature superconductors," *Nature*, vol. 401, no. 6751, pp. 354–356, 1999.

## Review Article

# Local Electron-Lattice Interactions in High-Temperature Cuprate Superconductors

Hugo Keller<sup>1</sup> and Annette Bussmann-Holder<sup>2</sup>

<sup>1</sup>Physik-Institut Universität Zürich, Winterthurerstraße 190, 8057 Zürich, Switzerland

<sup>2</sup>Max-Planck-Institut für Festkörperforschung, Heisenbergstraße 1, 70569 Stuttgart, Germany

Correspondence should be addressed to Annette Bussmann-Holder, a.bussmann-holder@fkf.mpg.de

Received 26 June 2009; Accepted 29 July 2009

Academic Editor: Sasha Alexandrov

Copyright © 2010 H. Keller and A. Bussmann-Holder. This is an open access article distributed under the Creative Commons Attribution License, which permits unrestricted use, distribution, and reproduction in any medium, provided the original work is properly cited.

Recent experimental observations of unconventional isotope effects, multiband superconductivity, and unusual local lattice responses are reviewed and shown to be naturally explained within a two-component scenario where local polaronic effects are important. It is concluded that purely electronic mechanisms of high-temperature superconductivity are incomplete and unable to capture the essential physics of cuprates and other layered superconductors.

## 1. Introduction

The discovery of high-temperature superconductivity (HTSC) in cuprates [1] was motivated by the knowledge that copper is one of the strongest Jahn-Teller ions in the periodic system [2]. The basic ingredient of the Jahn-Teller effect is the lifting of the electronic band degeneracy due to a lattice distortion. This has been shown to give rise to Jahn-Teller polaron formation [3] where electronic and lattice degrees of freedom are undistinguishable and form a new quasiparticle sharing the same wave function. Thus lattice and electronic responses are coupled and give rise to multiple novel effects which are absent in a conventional Fermi liquid and an electron-phonon coupled superconductor.

However, soon after the discovery of HTSC, novel mechanisms have been suggested as origin of the pairing glue which neglect completely any lattice responses. These ideas have mainly been invoked in view of the facts that (i) at optimum doping, that is, at the maximum value of the superconducting transition temperature  $T_c$ , the isotope effect on  $T_c$  is negligibly small [4]; (ii) the superconducting transition temperatures above liquid nitrogen are beyond the BCS scheme; (iii) the antiferromagnetic (AFM) properties of the undoped insulating parent compounds are a consequence of a strong onsite Coulomb repulsion; (iv) a  $d$ -wave superconducting order parameter seems to be realized.

These facts have been taken as evidence that  $t$ - $J$  physics or a two-dimensional Hubbard model is sufficient to capture the essential ingredients of the physics of cuprate high-temperature superconductors (HTSs).

That these ideas are insufficient in explaining the phenomenon of HTSC in cuprates has been demonstrated by the observation of strong lattice responses at the onset of the pseudogap phase as well as at  $T_c$  [5–12]. Phonon anomalies and anomalous local lattice responses have been reported for both regimes [13–15]. Unexplained within the above mentioned electronic models are all isotope effects observed in the cuprates. These range from a doping dependent isotope effect on  $T_c$  [4, 16], the superconducting energy gap [17], the penetration depth [16], the Néel temperature  $T_N$  [18], the spin glass phase temperature  $T_g$  [18], and the pseudogap onset temperature  $T^*$  [19]. This implies that over the whole and very complex phase diagram of cuprates isotope effects are observed which will be discussed in more detail below. Even though these findings do not necessarily support a lattice mediated pairing mechanism, they are evidence that lattice effects play an essential role and cannot be neglected in any models for HTSC.

Another support for the importance of the lattice to HTSC stems from the fact that superconductivity is only observed upon doping the stoichiometric parent compounds which leads to an energy imbalance in all important physical

properties: the extra charge introduced by doping leads to a charge mismatch which has to be compensated; the size difference of the doped ions creates local strain fields surrounding the dopant; the antiferromagnetism is rapidly destroyed; in spite of the large onsite Coulomb repulsion the system adopts metallic properties.

The failure of purely electronic models to describe the physics of cuprate HTSs is also demonstrated by the observation that superconductivity is not based on a purely  $d$ -wave order parameter, but that at least two components are involved here. This has been postulated early on [20, 21] and shown unambiguously recently [22–25]. Details are elucidated below.

The local lattice response to superconductivity as well as to the pseudogap phase has been shown to be quite unusual since the mean square Cu-O displacement exhibits novel features at each of these phases [7, 8, 26–28]. The normally expected Debye-Waller behavior appears as a background here, and divergences in it at  $T^*$  and  $T_c$  are overlaid on it. These features are rather uncommon in solid state physics and certainly beyond any purely electronic model. They are not observed in a specific cuprate family only, but in all investigated compounds from which it can be concluded that they are intrinsic and generic.

As has been demonstrated early, cuprates are highly inhomogeneous with multiple components which interact with each other but are governed by different—even though coexisting—ground states [20–25, 29–33]. The energy imbalance introduced by dopants has been explained in terms of polaron formation [34] where a transition from a polaron liquid to a polaron glass has been suggested to be realized [35, 36]. Another approach where lattice effects are of vital importance is based on bipolaron formation where preformed pairs Bose condense at  $T_c$  [37]. Rather related is the idea that superconducting islands form above  $T_c$  which form percolating path ways and gain coherence at  $T_c$  [38–40]. The two-component scenario is also an important ingredient in a two-story house model where anti-Jahn-Teller physics attains importance [41]. Another approach is based on the idea that a crossover from a Bose Einstein to BCS scenario takes place [29, 30]. Not all of the above ideas are able to explain the unconventional isotope effects, but especially models including polaron/bipolaron formation [42] show that these are realized in agreement with experimental observations [37, 43–46]. The suggestion of multiband superconductivity in complex materials has been made soon after the BCS theory [47–50], and it has been reinvented for cuprate HTSs after their discovery [51–54]. Thus it seems that many experiments and also many theoretical approaches clearly abandon the plain vanilla idea and support each other in a very consistent way.

In the following first experimental results are presented. In the beginning isotope experiments are described, then data presented which strongly support multiband superconductivity in cuprate HTSs, followed by the description of experiments on local lattice responses. Next, a multiband model with polaronic coupling is introduced which consistently describes the experimental data. Finally, conclusions are made.

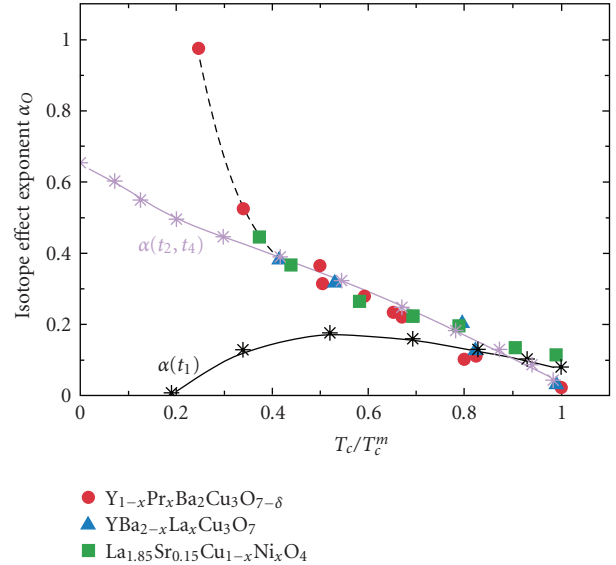


FIGURE 1: Oxygen isotope ( $^{16}\text{O}/^{18}\text{O}$ ) effect (OIE) exponent  $\alpha_O$  versus  $t_c = T_c/T_c^m$  for various families of cuprate HTSs ( $T_c^m$  denotes the maximum  $T_c$  for a particular family). Red circles:  $\text{Y}_{1-x}\text{Pr}_x\text{Ba}_2\text{Cu}_3\text{O}_{7-\delta}$ ; blue triangles:  $\text{YBa}_{2-x}\text{La}_x\text{Cu}_3\text{O}_7$ ; green squares:  $\text{La}_{1.85}\text{Sr}_{0.15}\text{Cu}_{1-x}\text{Ni}_x\text{O}_4$ . The references to the experimental data are given in [16]. The black dashed line is a guide to the eye. The black stars and solid line refer to the calculated  $\alpha_O$  when only the nearest neighbour hopping integral  $t_1$  is renormalized, whereas the purple stars and solid line refer to the renormalization of  $t_2, t_4$  [43–46].

## 2. Experimental Results

**2.1. Isotope Effects.** The oxygen-isotope ( $^{16}\text{O}/^{18}\text{O}$ ) effect (OIE) on the transition temperature  $T_c$  in HTSs was investigated already shortly after the discovery of HTSC [4]. The OIE on  $T_c$  is defined by the OIE exponent  $\alpha_O = -d \ln T_c / d \ln M_O$ , where  $M_O$  denotes the oxygen ion mass ( $^{16}\text{O}$  or  $^{18}\text{O}$ ). Numerous experiments revealed that for all cuprate HTS families the OIE exponent  $\alpha_O$  shows a generic trend: in the underdoped regime  $\alpha_O$  is large (even exceeding the BCS value of  $\alpha_O = 0.5$ ) and becomes small close to optimal doping [4, 16, 56, 57]. An example of this generic behavior of  $\alpha_O$  as a function of  $T_c/T_c^m$  for various families of cuprate HTSs is displayed in Figure 1 ( $T_c^m$  denotes the maximum  $T_c$  for a particular HTS family).

The almost vanishing OIE at optimum doping is contrasted to the strongly enhanced one in the underdoped limit close to the antiferromagnetic (AFM) phase boundary. Here, the OIE well exceeds the BCS limit and exhibits unusually large values. This is striking since the proximity to the AFM regime would suggest that spin fluctuations gain importance and dominate over any lattice effects. This observation clearly marks the breakdown of purely electronic models.

The early suggestion that the apex oxygen ions contribute in a special way to superconductivity stems from the fact that strongly anharmonic dynamics are involved in out of plane oxygen ion vibrations [58–62]. These polar almost instable modes carry huge dipole moments and cause the

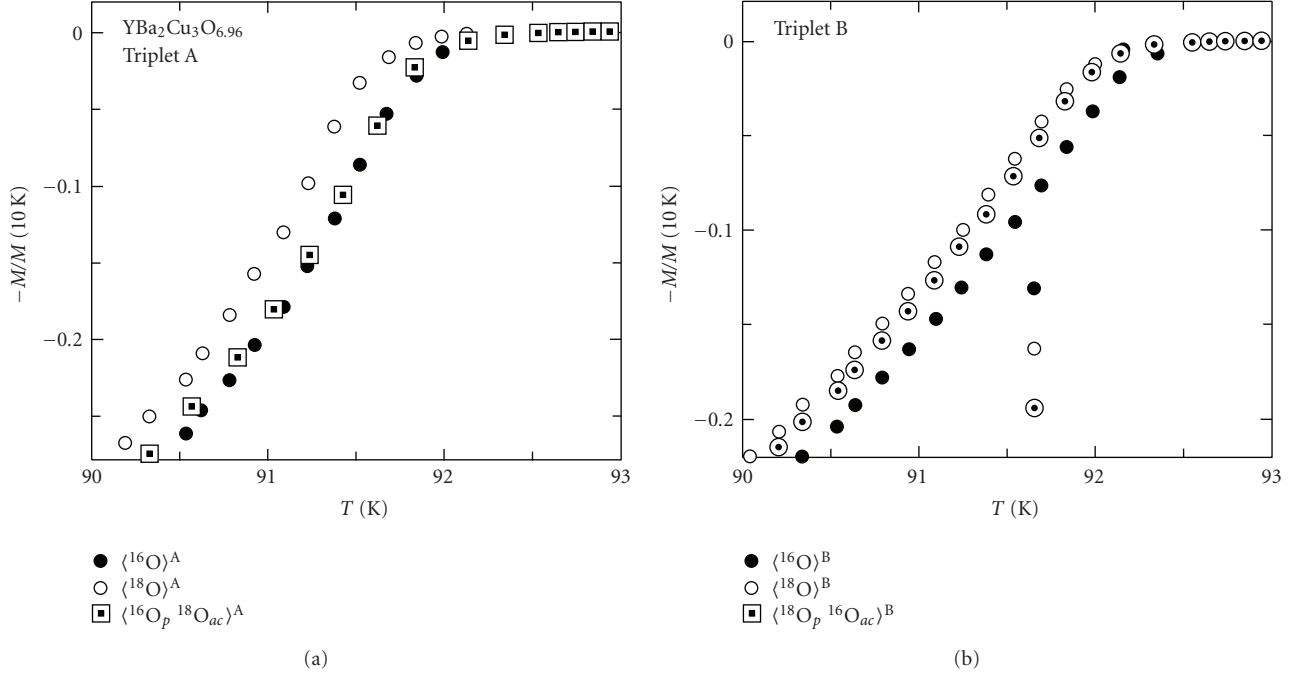


FIGURE 2: Magnetization curves near  $T_c$ , showing the SOIE in optimally doped  $\text{YBa}_2\text{Cu}_3\text{O}_{7-\delta}$  for  $x = 6.957(2)$  (triplet A) and  $x = 6.963(3)$  (triplet B). Here  $p$ ,  $a$ , and  $c$  denote the different oxygen ion sites in  $\text{YBa}_2\text{Cu}_3\text{O}_{7-\delta}$  ( $p$ : planar oxygen ion sites;  $a$ : apical oxygen ion sites;  $c$ : chain oxygen ion sites). For example,  $\langle^{18}\text{O}_p \text{ }^{16}\text{O}_{ac}\rangle^B$  denotes a sample from batch B with  $^{18}\text{O}$  in  $\text{CuO}_2$  planes and  $^{16}\text{O}$  in the apical and chain sites. It is evident that the planar oxygen atoms mainly contribute to the total OIE on  $T_c$ , after [55].

high dielectric constants observed in cuprate HTSs [63]. In order to test these ideas, site selective oxygen-isotope effect (SOIE) experiments are the only tool to differentiate between the role played by the in-plane and the out of plane oxygen ions. SOIE experiments are extremely difficult, and so far could only be realized for the  $\text{Y}_{1-x}\text{Pr}_x\text{Ba}_2\text{Cu}_3\text{O}_{7-\delta}$  system, since for this system the oxygen ion site occupation can be controlled thermally [55, 64–66]. Careful back exchange experiments were performed to ensure that the doping level for both isotopes remains identical. In addition, Raman experiments were undertaken to clearly differentiate from the eigenmodes where oxygen isotope replacements were made. As an example, Figure 2 shows the magnetization curves near  $T_c$  of the SOIE study of optimally doped  $\text{YBa}_2\text{Cu}_3\text{O}_{7-\delta}$  by Zech et al. [55]. It is evident that the planar oxygen ions mainly contribute to the total OIE on  $T_c$ . Moreover, detailed SOIE investigations of  $\text{Y}_{1-x}\text{Pr}_x\text{Ba}_2\text{Cu}_3\text{O}_{7-\delta}$  clearly revealed that the planar oxygen atoms mainly contribute (almost 100%) to the total OIE on  $T_c$  at all doping levels, whereas the chain and apical oxygen ions contribute only negligibly to it (see Figure 3) [55, 64–66]. This finding could point to a dominant role played by the in-plane oxygen ions, but this is, however, misleading since the density of states of the in-plane oxygen ions is much larger than the one of the out-of-plane oxygen ions and thus it cannot be concluded that these ions are irrelevant to superconductivity, which will be detailed below [67].

An OIE on the in-plane magnetic penetration depth  $\lambda_{ab}$  should be absent within the BCS theory since electronic

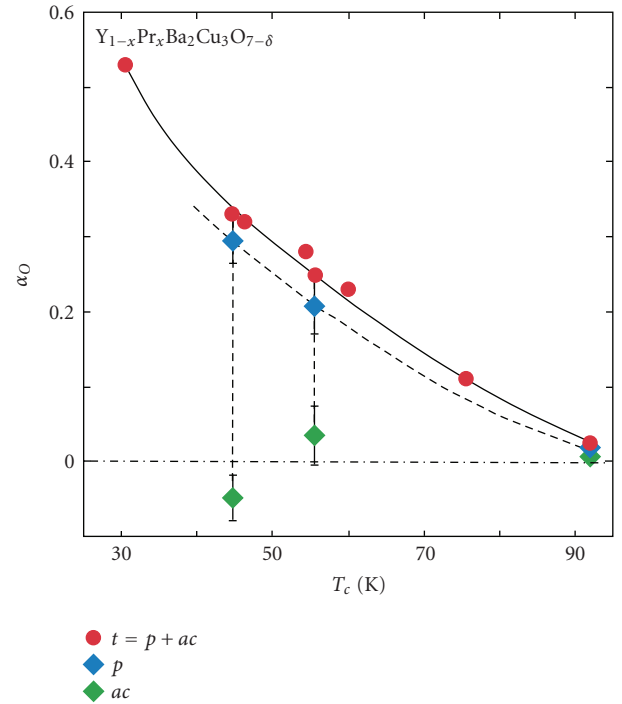


FIGURE 3: Total ( $t$ ) and partial ( $p$ ,  $ac$ ) OIE exponent  $\alpha_O$  as a function of  $T_c$  for  $\text{Y}_{1-x}\text{Pr}_x\text{Ba}_2\text{Cu}_3\text{O}_{7-\delta}$  ( $t$ : all oxygen ion sites;  $p$ : planar oxygen ion sites;  $ac$ : apex and chain oxygen ion sites). Solid and dashed lines are guides to the eye, after [16].

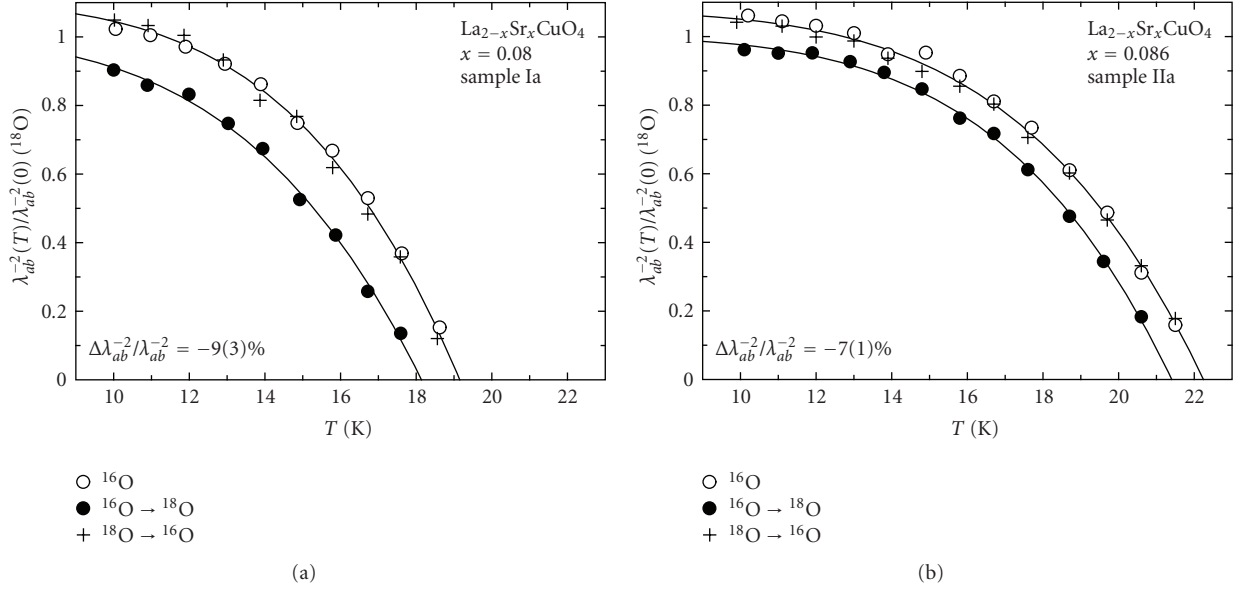


FIGURE 4: Normalized superfluid density (in-plane penetration depth)  $\lambda_{ab}^{-2}(T)/\lambda_{ab}^{-2}(0)$  for the  $^{16}\text{O}$ - and  $^{18}\text{O}$ -substituted microcrystals of  $\text{La}_{2-x}\text{Sr}_x\text{CuO}_4$  ((a):  $x = 0.080$ , (b):  $x = 0.086$ ). The reproducibility of the oxygen exchange was checked by the back exchange (crosses), after [68].

and phononic degrees of freedom are treated as independent (adiabatic approximation). In the opposite limit, however, an isotope effect on  $\lambda_{ab}$  is possible, which corresponds to strong coupling as is given in polaronic models. This implies that the effective carrier mass  $m^*$  can no longer be decoupled from the ionic mass  $M$ , giving rise to an isotope effect on the magnetic penetration depth which is not expected for conventional phonon-mediated superconductors. Indeed, a substantial OIE on the zero-temperature in-plane magnetic penetration depth  $\lambda_{ab}(0)$  was observed in several families of HTSs at different doping levels using various experimental techniques [16, 56, 57, 68, 70–72]. As an example, Hofer et al. [68] investigated the OIE on  $T_c$  and  $\lambda_{ab}(0)$  in microcrystals of underdoped  $\text{La}_{2-x}\text{Sr}_x\text{CuO}_4$  with a mass of only  $\approx 100 \mu\text{g}$  using a highly sensitive magnetic torque device to measure the magnetization of these tiny crystals. Figure 4 shows the temperature dependence of  $\lambda_{ab}^{-2}(T)/\lambda_{ab}^{-2}(0)$  extracted from the magnetic torque data for two oxygen-isotope exchanged microcrystals of  $\text{La}_{2-x}\text{Sr}_x\text{CuO}_4$ .

The doping dependent OIE on  $\lambda_{ab}(0)$  is appreciable as can be seen in Figure 4. Since it is observed in various different cuprates, it must be concluded that it is generic to HTSs. It is interesting to note that the OIE on  $\lambda_{ab}(0)$  found for different families of cuprates exhibits almost the same generic trend with doping as the one on  $T_c$  (see Figure 5). At low doping a linear correlation between both OIE's is observed:  $\Delta\lambda_{ab}(0)/\lambda_{ab}(0) \approx |\Delta T_c/T_c|$ . However, near optimal doping, a deviation from this linear behaviour occurs, and  $\Delta\lambda_{ab}(0)/\lambda_{ab}(0) \approx 10 |\Delta T_c/T_c|$ . The linear correlation at low doping is well explained by the polaronic model [43–46] described below. However, this model cannot account for the deviations near optimum doping. This is due to the fact that the polaronic coupling was assumed to be doping

independent which is an oversimplification. At optimum doping the polaronic coupling should be smaller than in the underdoped regime which still would yield an isotope effect on the penetration depth but a vanishing one on  $T_c$ .

The OIE's discussed so far already provide clear evidence that purely electronic models cannot describe the complex physics of HTSs. Another doping dependent OIE on the average zero-temperature superconducting gap  $\bar{\Delta}_0$  further supports this conclusion.

In conventional superconductors the isotope effect on the superconducting energy gap  $\Delta_0$  is simply determined by the isotope effect on  $T_c$  through the relation  $2\Delta_0/k_B T_c \approx 3.52$ . However, in cuprate HTSs this relation is not necessarily fulfilled, because  $T_c$  depends strongly on doping. In addition, as discussed below, cuprate HTSs have a complex superconducting order parameter, namely, an admixture of  $s + d$ -wave symmetry. A systematic study of the OIE on the average gap  $\bar{\Delta}_0 = (1/2)\sqrt{\bar{\Delta}_s^2 + \bar{\Delta}_d^2}$  ( $\bar{\Delta}_s \equiv s$ -wave gap,  $\bar{\Delta}_d \equiv d$ -wave gap) in  $\text{Y}_{1-x}\text{Pr}_x\text{Ba}_2\text{Cu}_3\text{O}_{7-\delta}$  for various doping levels  $x$  was carried out by means of SQUID magnetization experiments [17]. Note that the above defined average gap equally weighs the  $s$ - and  $d$ -wave contributions. In reality the gaps could contribute with different weights to the average one depending on the doping level. However, this would introduce an additional parameter which is not accessible experimentally. For this reason we have assumed the simplest possible form of the average gap as given above. The values of  $\bar{\Delta}_0$  extracted from the temperature dependence of the superfluid density were found to be proportional to  $T_c$  with  $2\bar{\Delta}_0/k_B T_c \approx 5.34$  as predicted prior to the experiment by the polaron model [43–46] described here. It is substantially larger than the BCS value of 3.52. As shown in Figure 6, the OIE on  $\bar{\Delta}_0$  scales linearly with the one on  $T_c$ , exhibiting a

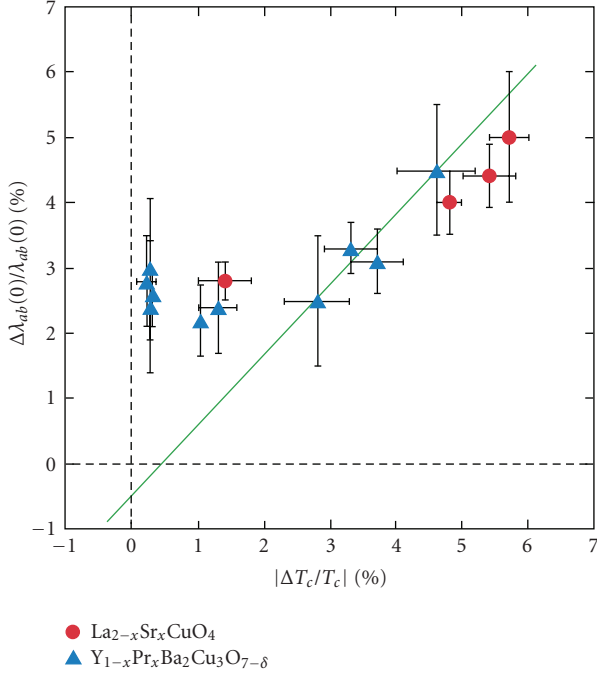


FIGURE 5: Plot of the OIE shift  $\Delta\lambda_{ab}(0)/\lambda_{ab}(0)$  versus the OIE shift  $|\Delta T_c/T_c|$  for  $\text{La}_{2-x}\text{Sr}_x\text{CuO}_4$  and  $\text{Pr}_x\text{Y}_{1-x}\text{Ba}_2\text{Cu}_3\text{O}_{7-\delta}$  using different experimental techniques and types of samples. The data are summarized in [16, Table 1]. The solid line corresponds to model calculations of the OIE on  $\Delta\lambda_{ab}(0)/\lambda_{ab}(0)$  obtained from the theoretical results for the average gap [43–46, 69], after [43–46].

sign reversal of the OIE's on  $\bar{\Delta}_0$  and  $T_c$  near optimal doping as predicted in [43–46] and discussed below.

Cuprate HTSs exhibit a rich phase diagram as a function of doping (see Figure 7). The undoped parent compounds show long range 3D antiferromagnetic (AFM) order. When holes are doped into the  $\text{CuO}_2$  planes, the AFM order is rapidly destroyed and only short-range AFM correlations survive even in the superconducting (SC) region of the phase diagram giving rise to a spin-glass (SG) state. Consequently, the SC and the SG phases coexist within a small doping range. With increasing doping, the SG phase disappears and a pure SC phase with increasing superconducting transition temperature  $T_c$  emerges. Four different phases can thus be distinguished: the AFM phase, the SG phase, the SG + SC phase, and the SC phase. The relation and interplay of these phases is still a controversial and open issue, since key experiments that may clarify this fundamental questions are still missing. Therefore, it is very interesting to investigate the OIE's on the corresponding transition temperatures between the various phases.

Several years ago the Zurich group observed a huge OIE on the spin-glass freezing temperature  $T_g$  in  $\text{La}_{2-x}\text{Sr}_x\text{Cu}_{1-z}\text{Mn}_z\text{O}_4$  ( $x = 0.03$  and  $0.05$ ;  $z = 0.02$ ) by means of muon-spin rotation ( $\mu\text{SR}$ ) [73]. This is a clear signature that the spin dynamics in cuprates are ultimately correlated with the lattice. Recently, the same group performed a detailed OIE study of the various phases (SC, SG + SC, SG, AFM) in the prototype cuprate system

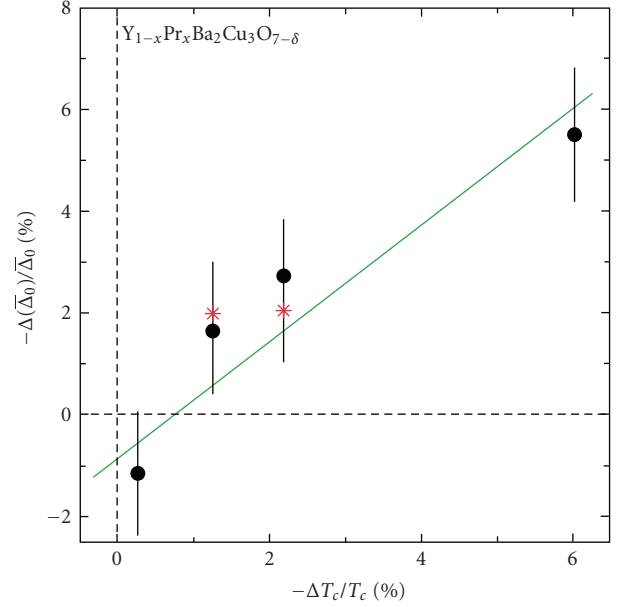


FIGURE 6: Comparison of the OIE shift of the average superconducting gap  $\bar{\Delta}_0$  to the one on the transition temperature  $T_c$  for  $\text{Y}_{1-x}\text{Pr}_x\text{Ba}_2\text{Cu}_3\text{O}_{7-\delta}$  ( $x = 0.0, 0.2, 0.3, 0.45$ ). Circles refer to the experimental data. The stars represent back exchange data. The solid green line is discussed, after [17].

$\text{Y}_{1-x}\text{Pr}_x\text{Ba}_2\text{Cu}_3\text{O}_{7-\delta}$  by means of  $\mu\text{SR}$  and magnetization experiments [18]. These techniques have the advantage of being direct, bulk sensitive, unambiguous, and able to measure  $T_c$  as well as  $T_g$  in the region where both coexist. The results of this OIE study are displayed in Figure 7. All transition temperatures  $T_c$ ,  $T_g$ , and  $T_N$  exhibit an OIE which is the strongest, where the respective phase (SC, SG, and AFM) terminates. It is interesting to note that the OIE on  $T_g$  and  $T_N$  are *sign reversed* as compared to the one on  $T_c$ . In the coexistence region of the SG and SC phase (SG + SC) a small OIE on  $T_c$  corresponds to a large negative OIE on  $T_g$  and vice versa. This observation suggests that in this regime phase separation sets in where the superfluid density coexists with a nonsuperfluid density related to the SG state. Since the OIE on  $T_c$  can be accounted for by polaron formation [43–46], the one on  $T_g$  is very likely driven by the same physics. By relating  $T_N$  to the metal insulator transition, a reduction in kinetic energy caused by polaron formation explains this unconventional OIE as well [18, 43–46].

In addition to the OIE's observed on all the phase lines in the generic phase diagram of cuprate HTSs (see Figure 7(a)), a huge OIE was also detected on the pseudogap temperature  $T^*$ , providing further evidence that lattice effects are relevant here as well. In particular, XANES experiments in  $\text{La}_{2-x}\text{Sr}_x\text{CuO}_4$  [74] as well as inelastic neutron scattering studies of  $\text{HoBa}_2\text{Cu}_4\text{O}_8$  and  $\text{La}_{1.81}\text{Sr}_{0.18}\text{Ho}_{0.04}\text{CuO}_4$  [19] yielded a large and *sign reversed* OIE on  $T^*$ . As an example, the results for  $\text{HoBa}_2\text{Cu}_4\text{O}_8$  are shown in Figure 8. It is interesting to note that neutron scattering experiments revealed an even larger  $^{63}\text{Cu}/^{65}\text{Cu}$  isotope effect on  $T^*$  which is not present in  $\text{La}_{1.81}\text{Sr}_{0.18}\text{Ho}_{0.04}\text{CuO}_4$  [19]. This finding

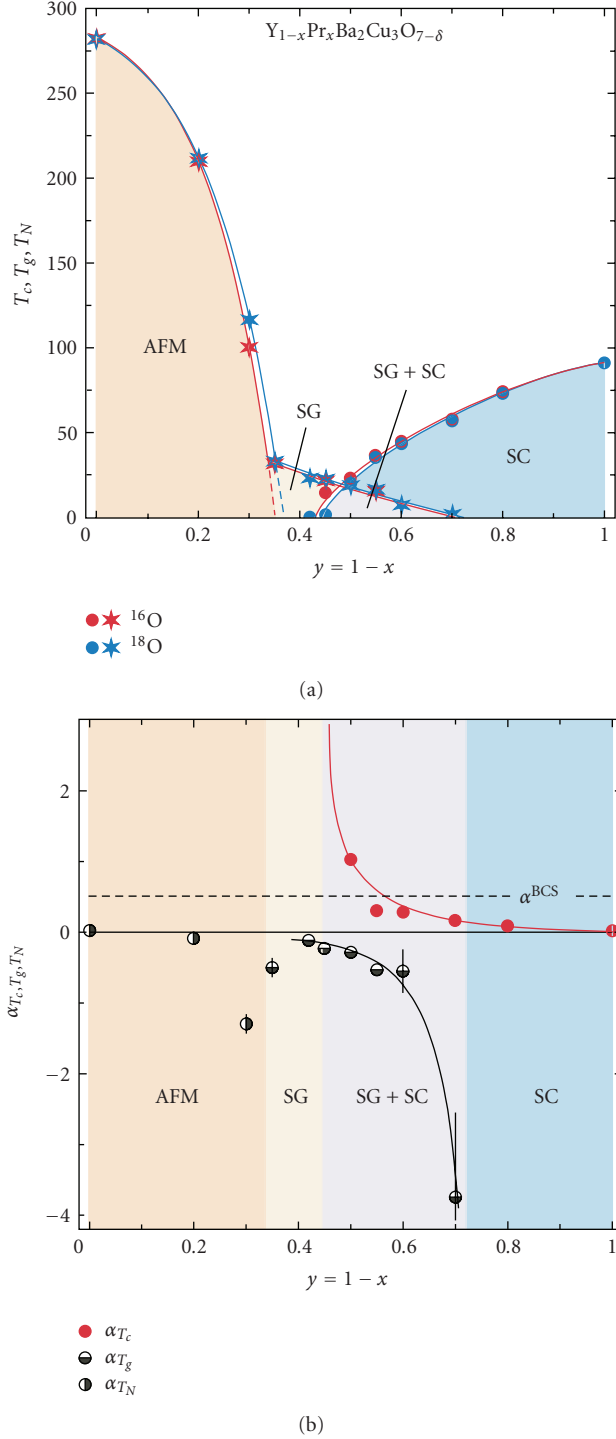


FIGURE 7: (a) Dependence of the superconducting transition ( $T_c$ ), the spin-glass ordering ( $T_g$ ), and the antiferromagnetic ordering ( $T_N$ ) temperatures for  $^{16}O/^{18}O$ -substituted  $Y_{1-x}Pr_xBa_2Cu_3O_{7-\delta}$  on the Pr content  $y = 1 - x$ . The solid lines are guides to the eye. The areas denoted by “AFM”, “SG”, and “SC” represent the antiferromagnetic, the spin-glass, and the superconducting regions, respectively, and “SG + SC” corresponds to the region where spin-glass magnetism coexists with superconductivity. (b) OIE exponents  $\alpha_O$  of  $T_c$ ,  $T_g$ , and  $T_N$  for  $^{16}O/^{18}O$ -substituted  $Y_{1-x}Pr_xBa_2Cu_3O_7$  as a function of the Pr content  $y = 1 - x$ . The dashed line corresponds to the BCS value  $\alpha_O^{BCS} = 0.5$ . The solid lines are guides to the eye, after [18].

supports the idea that an umbrella-type mode is involved in the formation of the pseudogap state in  $HoBa_2Cu_4O_8$ . Since  $La_{1.81}Sr_{0.18}Ho_{0.04}CuO_4$  has no apical oxygen, this mode is absent in this compound. These huge isotope effects have been interpreted in terms of dynamical charge ordering [43–46]. The two-component picture discussed in this paper implies that also ordering in the spin system (charge poor region) sets in around  $T^*$  as observed in  $YBa_2Cu_4O_8$  by means of NQR [75]. This is consistent with the almost vanishing OIE on  $T^*$  (comparable to the OIE on  $T_c$ ) detected by NQR which is mainly sensitive to the spin system [75].

**2.2. Mixed Order Parameter Symmetries.** From, for example, phase sensitive experiments [76] it has been concluded that the order parameter in cuprate HTSs has pure  $d$ -wave symmetry, which is possible only if the  $CuO_2$  planes have strictly cubic symmetry. However, either static or dynamic distortions of the  $CuO_2$  planes are present which destroy the cubic symmetry and are mostly ignored theoretically. Early on it has been emphasized that cuprate HTSs must have a multicomponent order parameter, since many experiments are incompatible with a single  $d$ -wave scenario [20, 21]. This implies that coexisting superconducting gaps with different pairing symmetries must be present, namely,  $s$ -wave and  $d$ -wave. This suggestion has been supported by a number of experiments using various experimental techniques, including nuclear magnetic resonance (NMR) [77, 78], Raman scattering [79, 80], phase-sensitive experiments [81], and neutron crystal-field spectroscopy [82], to give only a few examples. In addition,  $c$ -axis tunneling data provide evidence that the gap along the  $c$ -axis is dominantly of  $s$ -wave symmetry [83, 84]. Soon after the BCS theory coupled gaps have been postulated to be realized in complex materials where various electronic bands lie in the vicinity of the Fermi surface [47–50]. The experimental verification of these ideas was, however, made much later in Nb doped  $SrTiO_3$  [85] and long been believed to be an unusual exception. After the discovery of two-gap superconductivity in  $MgB_2$  [86] a vast amount of compounds have been shown to exhibit this phenomenon. Especially, in the newly discovered FeAs superconductors with rather high  $T_c$ 's unique features for the existence of two gaps have been seen [87]. Since  $c$ -axis experiments are rare for cuprates and most tunneling data are in the  $ab$ -plane, different tools have to be used to demonstrate the existence of  $s + d$ -wave superconductivity in cuprates. In order to probe the existence of coupled order parameters *bulk sensitive* experiments on single crystals are required. Muon-spin rotation ( $\mu$ SR) has demonstrated to be a unique tool to investigate the temperature dependence of the superfluid density in the *bulk* of a superconductor, from which, in turn, the superconducting gaps can be derived. A clear indication for the existence of two gaps is the appearance of an inflection point in the superfluid density at low temperatures. Such an anomaly was detected in  $MgB_2$  and shown to stem from the coexistence of a large and a small gap [86]. In cuprate HTSs a similar anomaly was observed in the in-plane superfluid density in single-crystal  $La_2Sr_{2-x}CuO_4$  determined by means of

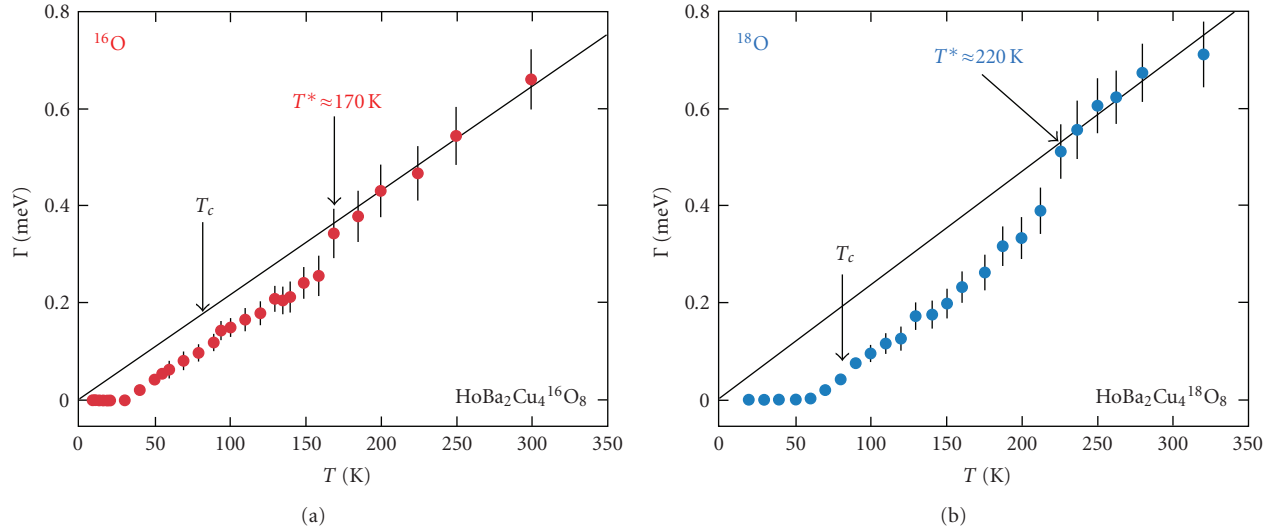


FIGURE 8: Temperature dependence of the intrinsic line width  $\Gamma$  (HWHM) corresponding to the  $\Gamma_3 \rightarrow \Gamma_4$  ground-state crystal field transition in oxygen-isotope exchanged  $\text{HoBa}_2\text{Cu}_4\text{O}_8$  as determined from inelastic neutron scattering experiments. The solid lines correspond to the line width in the normal state calculated by the Korringa law, after [19].

$\mu\text{SR}$  experiments and analyzed in terms of coupled  $s + d$  wave order parameters (Figure 9) [22–25]. In order to show that this feature is not material dependent but intrinsic to cuprates similar experiments were performed for single crystals of  $\text{YBa}_2\text{Cu}_3\text{O}_{7-\delta}$  and  $\text{YBa}_2\text{Cu}_4\text{O}_8$  where it was possible to determine the temperature dependence of the superfluid density along all three crystallographic axis  $a$ ,  $b$ , and  $c$  [22–25]. The results are shown in Figure 10, from which it can be seen that in both compounds an inflection point appears along the  $a$ - and  $b$ -axis, which is absent along the  $c$ -axis. The analysis of these data yields  $s + d$  wave order parameters in the  $ab$ -planes, whereas along the  $c$ -axis predominantly an  $s$ -wave component exists.

The observation of a pronounced inflection point in the in-plane superfluid density at low temperatures in all three systems (Figures 9 and 10) is a signature of the coexistence of a small and a large gap. From the magnetic field dependence of the superfluid density it is concluded [22–25] that in the  $\text{CuO}_2$  planes a small  $s$ -wave gap coexists with a dominant  $d$ -wave gap. As shown in Figure 10, the temperature dependence of the superfluid density along the  $c$ -axis differs considerably from those in the  $b$ -planes. The absence of an inflection point and the saturation at low temperatures (compare  $\sigma_a$  and  $\sigma_b$  with  $\sigma_c$  in Figure 10) are characteristic for a pure  $s$ -wave gap. From a theoretical point of view, a mixed order parameter scenario [43–46] requires that also a small  $d$ -wave admixture should be present. However, the  $d$ -wave component appears to be too small to be observed experimentally [22–25].

In conclusion, the unique behaviour of the temperature dependence of the superfluid density observed in all three cuprate systems strongly suggests that the order parameter is more complex than expected for a single  $d$ -wave order parameter, and that this complex order parameter is an intrinsic and generic feature of all cuprate HTSs. In

particular, the finding that the gap along the  $c$ -axis has a predominant  $s$ -wave character demonstrates the importance of the coupling between the  $\text{CuO}_2$ -planes, and that 2D physics concentrating on the  $\text{CuO}_2$  planes only is rather insufficient and incomplete. It is important to mention that the coexistence of an  $s$ - and  $d$ -wave gap not only is a consequence of the static or dynamic degree of orthorhombicity but also results from the fact that two components dominate the physics of HTSs. These experimental facts are completely neglected in many theoretical models.

**2.3. Local Lattice Responses.** About 10 years after the discovery of HTSC a number of local probes have been used to study the in-plane and out-of-plane Cu-O distances in order to gain information about the local structure in cuprates [5–8, 10–13, 26–28]. Here, especially, the extended X-ray absorption fine structure (EXAFS) technique has proven to be a useful tool. The early experiments [5–8] reported not only two distinctly different Cu-O bond lengths in the Cu-apical-oxygen distance but also anomalies in these as a function of temperature. While far above  $T_c$  the first anomaly was observed and related to  $T^*$ , the second developed in the SC phase. Besides of the  $c$ -axis-related anomalies, also the in-plane Cu-O bond length was shown to be characterized by similar anomalies and two length scales [7, 8]. The interpretation of the data was made in terms of stripe like modulations of the local structure setting in at  $T^*$ , where undistorted and distorted areas coexist. More recently, high-resolution EXAFS studies have concentrated on the in-plane Cu-O distance and investigated this in the presence of different dopants [26–28]. In the latter studies an anomalous upturn in the mean square in-plane Cu-O distance has been reported with two clear anomalies appearing at  $T^*$  and below  $T_c$ . Typical results are shown in Figure 11 and in comparison to the theoretical results as inset to Figure 16. Note that

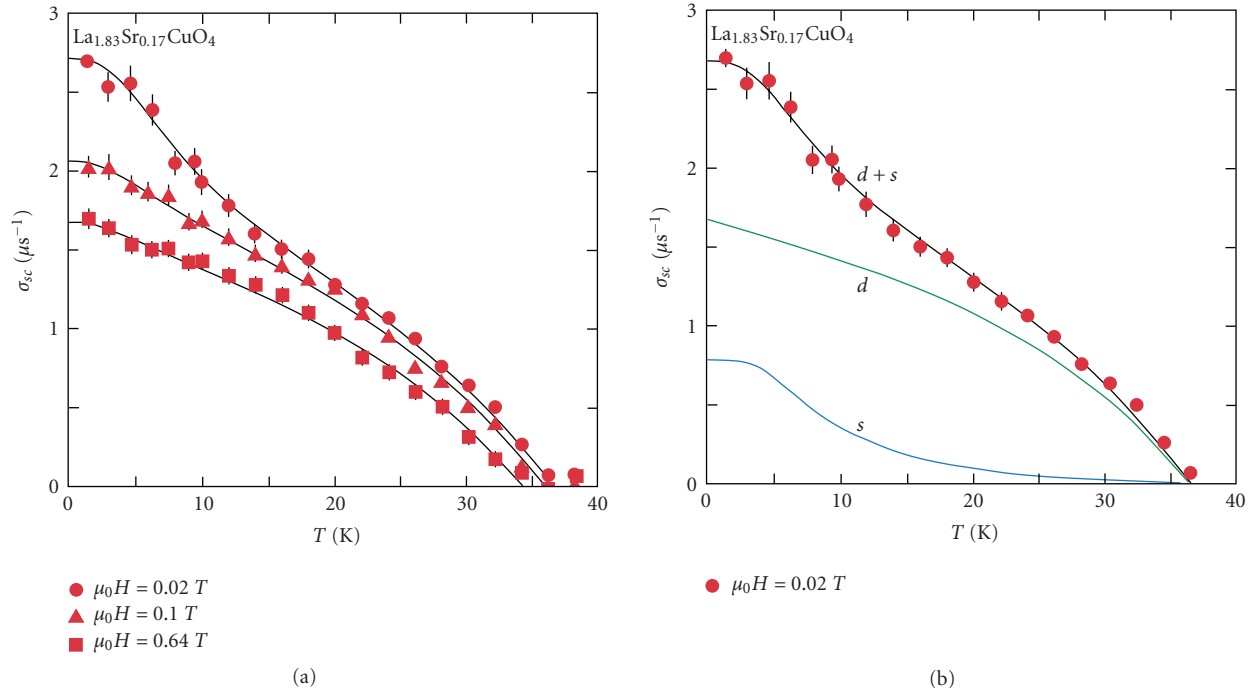


FIGURE 9: Temperature dependence of the  $\mu$ SR relaxation rate  $\sigma_{sc} \propto \lambda_{ab}^{-2}$  of single crystals of  $\text{La}_{1.83}\text{Sr}_{0.17}\text{CuO}_4$  measured at magnetic field strengths of 0.02, 0.1, and 0.64 T. Lines in panels (a) and (b) represent calculations using a two-gap model [22–25]. The green and blue lines in panel (b) show the individual contributions from the  $d$ - and  $s$ -wave gap, after [22–25].

such anomalies are rather untypical in conventional solids and even absent in highly anharmonic compounds with strong soft mode behaviour. Since the experiments test ionic displacements which correlate with  $T^*$  and  $T_c$ , an explanation of these is beyond any purely electronic model. In addition, the appearance of these anomalies along the  $c$ -axis points to pronounced  $c$ -axis involvement, as has been stressed from the penetration depth data.

### 3. Theoretical Modeling

The theoretical understanding of the pairing mechanism in cuprate HTSs remains controversial where basically two distinctly different approaches have been pursued in the last years: one is based on a purely electronic mechanism where the large onsite Coulomb repulsion  $U$  at the Cu site is assumed to play a major role. This approach can either be cast into a 2D Hubbard model or in extreme cases, when  $U$  is much larger than the hopping integral, or be modeled by the so-called  $t$ - $J$  Hamiltonian. Obviously, all lattice effects are ignored whereby isotope effects, as observed experimentally and being described above, are regarded as unimportant. Nevertheless, an explanation for these is offered by postulating that the hopping integrals depend on the oxygen isotope mass. This implies that the unique energy scale as given by  $J = 4t^2/U$  becomes isotope dependent. Since  $J$  in this approach dominates the AFM regime as well as the SC region, both corresponding transition temperatures, namely,  $T_N$ ,  $T_c$ , should have equal

isotope dependencies. This is in contrast to the above described isotope experiments where  $T_N$  and  $T_c$  have *opposite signs* of the OIE. Also, the many correlations between lattice anomalies and superconductivity are missing in these scenarios. 2D Hubbard and  $t$ - $J$  models are based on a single  $d$ -wave order parameter and do not admit for the complex order parameters as observed experimentally. In this respect both approaches rely on a homogeneous picture in contrast to the observed inhomogeneity of HTSC. A rather dramatic failure of these purely electronic approaches is the inability to account for the  $c$ -axis  $s$ -wave gap. The third dimension is almost completely ignored and important contributions from the out-of-plane structural elements missing. As such, the completely decoupled  $\text{CuO}_2$  planes alone should be superconducting, which is again in contrast to experiments.

An alternative approach to HTSC is based on electron-lattice interactions, where conventional BCS theory and polaron and bipolaron formation are considered [29–46]. The problem with the standard electron-phonon-coupled superconductivity lies in the fact that the high values of  $T_c$  require large coupling constants, which, in turn, may easily lead to lattice instabilities. Also, as already mentioned above, an isotope effect on the penetration depth is absent, and a doping dependent OIE on  $T_c$  is not present. As such, polaronic or bipolaronic scenarios are more likely to be realized in HTSs. This is also favored by the energy mismatch introduced upon doping. The extra charge which enters the stoichiometric antiferromagnetic matrix requires strong screening through the lattice, which undergoes anomalous local distortions around these charges which have been

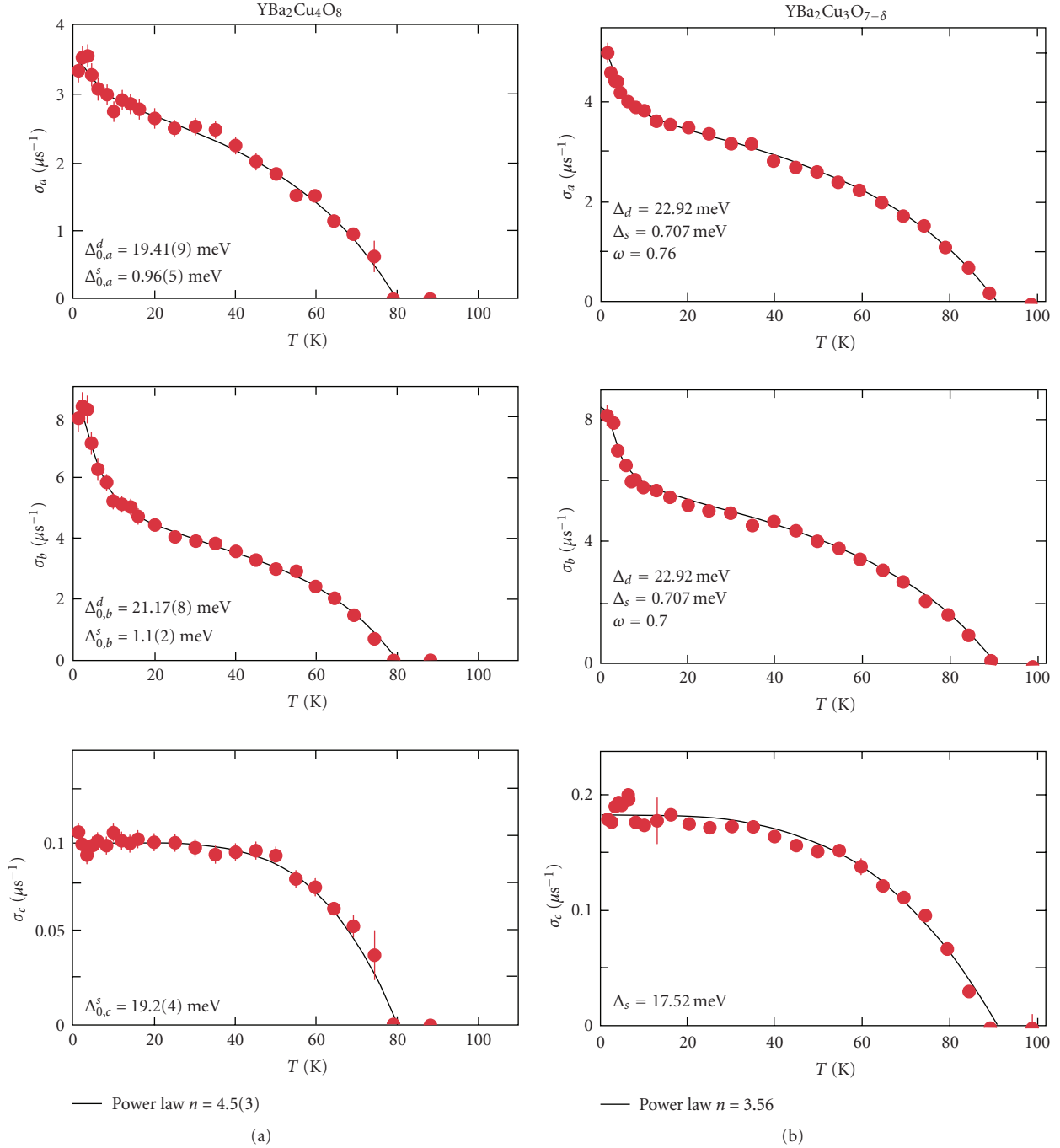


FIGURE 10: (a) Temperature dependences of the  $\mu$ SR relaxation rate  $\sigma_a \propto \lambda_a^{-2}$ ,  $\sigma_b \propto \lambda_b^{-2}$ , and  $\sigma_c \propto \lambda_c^{-2}$  of single crystals of  $\text{YBa}_2\text{Cu}_4\text{O}_8$  measured along the three principal crystallographic axes  $a$ ,  $b$ ,  $c$ . (b) Temperature dependence of the  $\mu$ SR relaxation rate  $\sigma_a \propto \lambda_a^{-2}$ ,  $\sigma_b \propto \lambda_b^{-2}$ , and  $\sigma_c \propto \lambda_c^{-2}$  of single crystals of  $\text{YBa}_2\text{Cu}_3\text{O}_{7-\delta}$  measured along the three principal crystallographic axes  $a$ ,  $b$ ,  $c$ . The lines in (a) and (b) are results from model calculations as discussed in [22–25], after [22–25].

addressed above [5–13, 26–28]. This strong interaction between dopant and the lattice leads to local polaron formation. While at high temperatures these polarons are randomly distributed over the lattice, the large strain fields, which accompany them, require a self-organization into dynamical patterns like, for example, stripes [43–46]. This patterning takes place at the onset temperature  $T^*$  of the

pseudogap phase and leads to the coexistence of metallic distorted regions with “pseudo” antiferromagnetic insulating regimes [43–46]. Both regions are not independent of each other but interact dynamically through the lattice and local charge transfer. In the superconducting phase the polarons persist and contribute to superconductivity through pair formation and interband interactions [43–46, 88].

Besides of the electronic response to doping and local lattice effects, also the lattice experiences important renormalizations since electronic and lattice degrees of freedom are undistinguishable. This shows up in local mode softening due to the electronic cloud trapped by the lattice and influences—in turn—the relative mean square Cu-O lattice displacement [88]. An unusual upturn at the point where the polarons gain coherence appears and another anomaly upon the onset of superconductivity takes place. This second anomaly depends, however, on the pairing symmetry and is most pronounced for the case of an  $s$ -wave order parameter.

The above described scenario is modeled by the following (simplified) Hamiltonian [43–46, 89, 90]:

$$H = H_d + H_c + H_{cd} + H_L + H_{L-d} + H_{L-c}, \quad (1)$$

where  $H_d, H_c$  refer to the purely electronic energies of the AFM matrix and the doped holes, and  $H_{cd}$  is the interaction between both and resembles a hybridization term. The last three terms are the pure lattice part, the electron-lattice interactions with the AFM holes, and the doped holes, respectively. The terms in (1) are explicitly given by [43–46, 88–90]

$$\begin{aligned} H_d &= \sum_{i,\sigma} \varepsilon_d d_{i,\sigma}^\dagger d_{i,\sigma} + \sum_{i,j,\sigma,\sigma'} t_{ij} (d_{i,\sigma}^\dagger d_{j,\sigma'} + c.c.) \\ &\quad + U \sum_i n_{d,i} n_{d,i}, \\ H_c &= \sum_{i,\sigma} \varepsilon_c c_{i,\sigma}^\dagger c_{i,\sigma} + \sum_{i,j,\sigma,\sigma'} t_{ij} (c_{i,\sigma}^\dagger c_{j,\sigma'} + h.c.), \\ H_{cd} &= \sum_{i,j,\sigma,\sigma'} t_{cd} (c_{i,\sigma}^\dagger d_{j,\sigma'} + c.c.), \\ H_L &= \sum_i \frac{p_i^2}{2M_i} + \frac{1}{2} M \omega^2 Q_i^2, \\ H_{L-d} &= \sum_{i,j,\sigma,\sigma'} [g n_{d,i} Q_i + \tilde{g} (c_{i,\sigma}^\dagger d_{j,\sigma'} + d_{i,\sigma}^\dagger c_{j,\sigma'}) Q_j], \\ H_{L-c} &= \sum_{i,j,\sigma,\sigma'} [g n_{c,i} Q_i + \tilde{g} (c_{i,\sigma}^\dagger d_{j,\sigma'} + d_{i,\sigma}^\dagger c_{j,\sigma'}) Q_j]. \end{aligned} \quad (2)$$

The electronic states within the antiferromagnetic background are denoted by creation and annihilation operators  $d^\dagger, d$ , with density  $n_d = d^\dagger d$ , those within the lattice distorted areas are labelled  $c^\dagger, c$ , and  $n_c = c^\dagger c$ .  $\varepsilon$  are the site  $i$  dependent energies,  $t$  are the hopping integrals, and  $U$  is the onsite Coulomb repulsion within the AFM matrix. In the hole rich areas  $U$  becomes meaningless since it is strongly reduced by the electron-lattice coupling and might even become attractive there. The coupling between the lattice and the electronic subsystems consists of a diagonal coupling proportional to  $g$  and an off-diagonal coupling proportional to  $\tilde{g}$  which enables charge transfer processes between the two regimes. Principally, the couplings between the  $c$  and  $d$  regimes are not identical, but for simplicity they are assumed to be the same here. For simplicity the lattice Hamiltonian is taken to be harmonic with  $p$  and  $Q$  being site  $i$  dependent

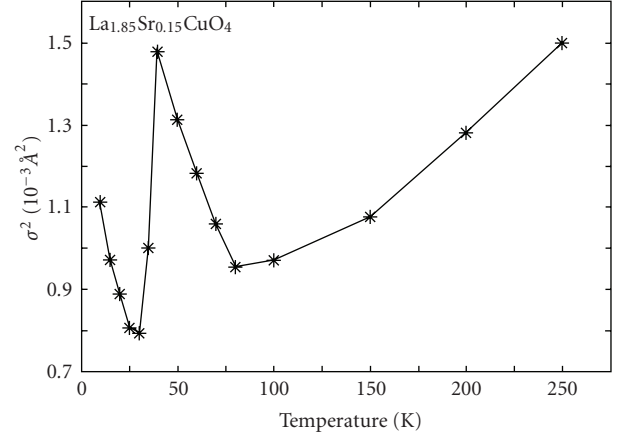


FIGURE 11: The mean square in-plane Cu-O bond distance of  $\text{La}_{1.85}\text{Sr}_{0.15}\text{CuO}_4$  as a function of temperature. After [26–28].

momentum and conjugate displacement coordinates with frequency  $\omega$  and  $M$  the ionic mass.

In order to decouple lattice and electronic degrees of freedom a Lang-Firsov canonical transformation [91] is performed which corresponds to  $\tilde{H} = e^{-S} H e^S$ . This induces an exponential band narrowing in the electronic energies together with a level shift proportional to  $\Delta^* = (1/2N) \sum_q (g_q^2 / \hbar \omega_q)$  and a rigid oscillator shift in the lattice degrees of freedom as follows:

$$\begin{aligned} \tilde{c}_i &= c_i \exp \left( \sum_q g_q [b_q^+ - b_q] \right), \\ \tilde{c}_i^\dagger &= c_i^\dagger \exp \left( - \sum_q g_q [b_q^+ - b_q] \right), \\ \tilde{d}_i &= d_i \exp \left( \sum_q g_q [b_q^+ - b_q] \right), \\ \tilde{d}_i^\dagger &= d_i^\dagger \exp \left( - \sum_q g_q [b_q^+ - b_q] \right), \\ \tilde{b}_q &= b_q + \sum_q g_q n_i, \quad \tilde{b}_q^+ = b_q^+ + \sum_q g_q n_i. \end{aligned} \quad (3)$$

As is obvious from (2), a coupled feedback from the lattice to the electronic degrees of freedom and vice versa results. We first concentrate on the renormalizations of the electronic subsystem and then discuss those experienced by the lattice.

The electronic kinetic energy renormalization is given by  $t_i \rightarrow \tilde{t}_i = t_i \exp[-g^2 \coth(\hbar \omega / 2kT)]$ , whereas the site dependent energies transform to  $\varepsilon \rightarrow \tilde{\varepsilon} - \Delta^*$ ,  $\Delta^* = (1/2N) \sum_q (g_q^2 / \hbar \omega_q)$ , and  $U$  has to be replaced by  $\tilde{U} = U - (g_q^2 / \hbar \omega_q)$ . The lattice-induced hybridization terms experience an important renormalization since density-density interactions are a consequence which facilitate multiband superconductivity and lead to strong enhancements of  $T_c$  [92, 93].

The electronic part of the transformed Hamiltonian can be cast into an effective BCS scheme which is, however, extended to account for multiband superconductivity. The resulting Hamiltonian reads [43–46, 92, 93]

$$\begin{aligned}
H &= H_0 + H_1 + H_2 + H_{12}, \\
H_0 &= \sum_{k_1\sigma} \xi_{k_1} c_{k_1\sigma}^\dagger c_{k_1\sigma} + \sum_{k_2\sigma} \xi_{k_2} d_{k_2\sigma}^\dagger d_{k_2\sigma}, \\
H_1 &= - \sum_{k_1 k_1' q} V_1(k_1, k_1') c_{k_1+q/2}^\dagger c_{-k_1+q/2}^\dagger c_{-k_1'+q/2} c_{k_1'+q/2}, \\
H_2 &= - \sum_{k_2 k_2' q} V_2(k_2, k_2') d_{k_2+q/2}^\dagger d_{-k_2+q/2}^\dagger d_{-k_2'+q/2} d_{k_2'+q/2}, \\
H_{12} &= - \sum_{k_1 k_2 q} V_{12}(k_1, k_2) \\
&\quad \times \left\{ c_{k_1+q/2}^\dagger c_{-k_1+q/2}^\dagger d_{-k_2+q/2}^\dagger d_{k_2+q/2} + h.c. \right\}, \tag{4}
\end{aligned}$$

where  $H_0$  is the kinetic energy of band  $c, d$  with  $\xi_{k_i} = \tilde{\epsilon}_i - \epsilon_{k_i} - \mu$ ,  $i = c, d$ ,  $\mu$  is the chemical potential which controls the band filling, and the band dispersion is given by the simplified scheme as suggested by LDA calculations [94]:

$$\begin{aligned}
\epsilon_{c,d}(k) &= -2t_1 (\cos k_x a + \cos k_y b) + 4t_2 \cos k_x a \cos k_y b \\
&\quad + 2t_3 (\cos 2k_x a + \cos 2k_y b) \\
&\quad \mp \frac{t_4 (\cos k_x a - \cos k_y b)^2}{4} - \mu \tag{5}
\end{aligned}$$

with  $t_1, t_2$ , and  $t_3$  being nearest, next, and third nearest neighbour hopping integrals, whereas  $t_4$  is the interplanar hopping term which becomes relevant in multilayer systems. Principally, all hopping integrals should be affected by the polaronic effects. It turns out, however, that a renormalization of the 3rd nearest neighbour hopping term has no influence on any of the below investigated physical properties. The terms  $H_1, H_2, H_{12}$  provide the pairing potentials in the  $c$  and  $d$  bands and the pairwise exchange between both bands. The pairing interactions can be represented in factorized form in order to account for anisotropic pairings like, for example, extended  $s$ -wave or  $d$ -wave pairing. Guided by the experimental data which have been presented above (see Figures 9 and 10), it is assumed that in the  $c$ -channel  $s$ -wave pairing is realized whereas in the  $d$ -channel a  $d$ -wave order parameter exists. From (4) coupled gap equations can be derived which are given by [92, 93]

$$\begin{aligned}
\langle c_{k_1\uparrow}^\dagger c_{-k_1\downarrow}^\dagger \rangle &= \frac{\bar{\Delta}_{k_1}}{2E_{k_1}} \tanh \frac{\beta E_{k_1}}{2} = \bar{\Delta}_{k_1} \Phi_{k_1}, \\
\langle d_{k_2\uparrow}^\dagger d_{-k_2\downarrow}^\dagger \rangle &= \frac{\bar{\Delta}_{k_2}}{2E_{k_2}} \tanh \frac{\beta E_{k_2}}{2} = \bar{\Delta}_{k_2} \Phi_{k_2},
\end{aligned}$$

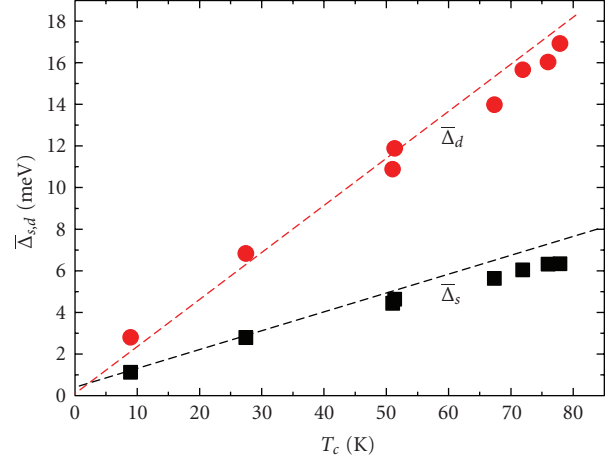


FIGURE 12: Dependence of the  $s$ -wave gap  $\bar{\Delta}_s$  (black squares) and the  $d$ -wave gap  $\bar{\Delta}_d$  (red circles) on the corresponding  $T_c$ . The dashed lines are a guide to the eye.

$$\begin{aligned}
\bar{\Delta}_{k_1} &= \sum_{k_1'} V_1(k_1, k_1') \bar{\Delta}_{k_1'} \Phi_{k_1} + \sum_{k_2} V_{1,2}(k_1, k_2) \bar{\Delta}_{k_2} \Phi_{k_2}, \\
\bar{\Delta}_{k_2} &= \sum_{k_2'} V_2(k_2, k_2') \bar{\Delta}_{k_2'} \Phi_{k_2} + \sum_{k_1} V_{2,1}(k_2, k_1) \bar{\Delta}_{k_1} \Phi_{k_1}. \tag{6}
\end{aligned}$$

These have to be solved simultaneously and selfconsistently for each temperature  $T$ , and  $T_c$  is defined by the condition  $\bar{\Delta}_{k_i} = 0$ . The dependencies of these gaps on  $T_c$  are shown in Figure 12. While the  $s$ -wave gap to  $T_c$  ratio is distinctly smaller than the BCS value ( $2\bar{\Delta}_s/kT_c = 3.33$ ), the one of the  $d$ -wave gap ( $2\bar{\Delta}_d/kT_c = 9.68$ ) is substantially enhanced. The average gap to  $T_c$  value ( $2\bar{\Delta}/kT_c = 5.34$ ) remains enhanced as compared to the BCS prediction and agrees with experimentally observed one (see Section 2.1).

Isotope effects on the gaps are possible through the dependence of the band energies on the polaronic coupling which carries a mass dependence. These have been calculated as a function of the chemical potential and are shown in Figure 13. The isotope effects on both gaps are of the same order of magnitude and are doping dependent. In the underdoped regime the OIE is substantially larger than around optimum doping where it almost vanishes (see Figure 6, where the full green line stems from model calculations). Most importantly, however, the model predicts a sign reversal of it in the overdoped regime as is seen experimentally and shown in Figure 6 [17].

A doping dependent OIE on  $T_c$  stems also from the polaronic renormalization of the single particle energies. Here, however, not all considered hopping integrals contribute equally, but it is found that the nearest neighbour hopping integral  $t_1$  leads to a sign reversal of the OIE at small dopings and thus can be discarded to contribute to the OIE (see black solid line and symbols in Figure 1). This wrong trend for the isotope effect stemming from the renormalization of  $t_1$  arises from the related density of states which increases with

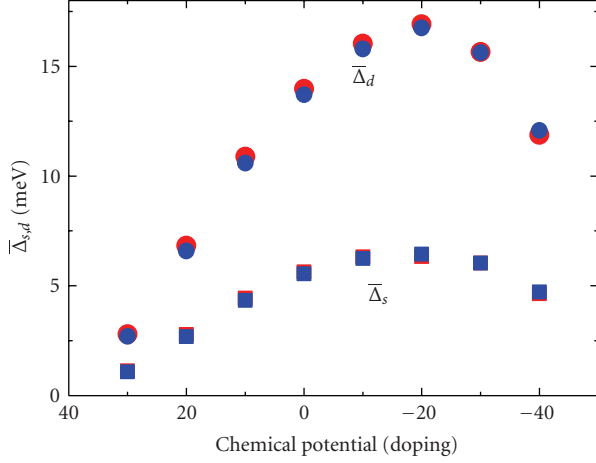


FIGURE 13: Dependence of the  $s$ -wave gap  $\bar{\Delta}_s$  (squares) and  $d$ -wave gap  $\bar{\Delta}_d$  (circles) on the chemical potential. The red symbols are for  $^{16}\text{O}$ , the blue ones for  $^{18}\text{O}$ .

increasing oxygen ion mass. The correct trend for the OIE is obtained from the renormalization of the second,  $t_2$ , and interplanar hopping integrals,  $t_4$  (see purple solid line and symbols in Figure 1). This admits to draw conclusions about the relevant lattice mode which causes the OIE, namely, the  $Q_2$ -type Jahn-Teller mode with important contributions from a  $c$ -axis mode [43–46, 88].

The experimentally observed SOIE (Figures 2 and 3) has theoretically been attributed to the density of states at the Fermi energy  $E_F$  of the related oxygen ions [67]. Since the apical and chain oxygen ions have a small density of states at  $E_F$  as compared to the in-plane oxygen ions, the large difference in both causes also the difference in their contribution to the total OIE.

From (4)–(6) the superfluid stiffness is calculated within linear response theory [95] through the relation between current and the induced transverse gauge field:

$$\rho_s^i = \frac{1}{2V} \times \sum_k \left\{ \left( \frac{\partial \xi_{k_i}}{\partial k_i} \right)^2 \frac{\partial f(E_{k_i})}{\partial E_{k_i}} + \frac{1}{2} \frac{\partial^2 \xi_{k_i}}{\partial k_i^2} \left[ 1 - \frac{\xi_{k_i}}{E_{k_i}} \tanh \frac{E_{k_i}}{2kT} \right] \right\}, \quad (7)$$

where  $E(k) = \sqrt{\xi_k^2 + \bar{\Delta}_0^2}$ . The superfluid stiffness is characterized by two components related to the coupled gaps and has an additional in-plane anisotropy caused by orthorhombicity. Since the two gaps considered above have largely different values (Figures 12 and 13), the superfluid stiffness exhibits an inflection point at low temperatures as is seen experimentally (see Figures 9 and 10). A typical example is shown in Figure 14 which closely resembles the results shown in Figures 9 and 10.

Obviously, also an oxygen isotope dependence on the in-plane penetration depth results from (7). This is in quantitative agreement with the experimental data shown

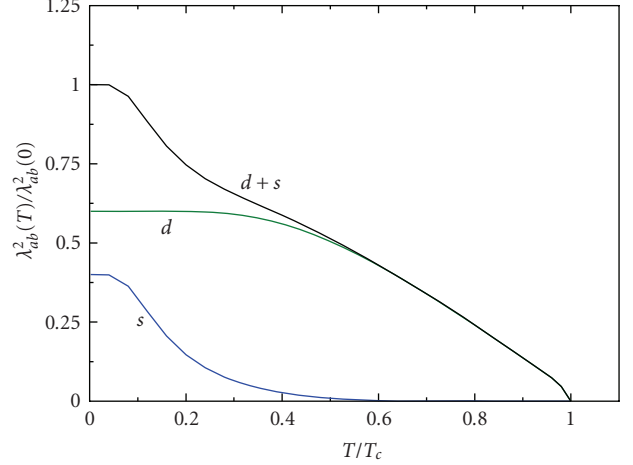


FIGURE 14: The individual components of  $\lambda_{ab}^2(T)/\lambda_{ab}^2(0)$  as a function of the normalized temperature  $T/T_c$  (blue:  $s$ -wave; green:  $d$ -wave) to the total (black line) normalized in-plane penetration depth.

in Figure 4, as long as the underdoped regime is concerned. The correlation between the OIE on  $\lambda_{ab}$  and the one on  $T_c$  (see Figure 5, solid green line) is, however, only obeyed for small and intermediate doping levels while for optimal doping deviations between experiment and theory are seen. These are—most likely—attributable to the theoretical simplification of using a doping independent polaronic coupling constant  $g$  (see (2)).

Finally, the lattice response to polaron formation is addressed. The lattice harmonic oscillators experience a rigid shift proportional to  $\sum_q g_{q,j}^2 n_i$ . By staying at a mean field level and neglecting cross terms, the renormalized phonon frequency is approximated by [88]

$$\tilde{\omega}_{q,j}^2 = \omega_{q,j}^{(0)2} - \frac{g_{q,j}^2}{N(E_F)} \sum_k \frac{1}{\varepsilon(k)} \tanh \frac{\varepsilon(k)}{k_B T}, \quad (8)$$

where  $N(E_F)$  is the density of states at the Fermi level,  $\varepsilon(k)$  is given by (5), and  $\omega_{q,j}^{(0)}$  is the bare branch  $j$  and momentum  $q$  dependent lattice mode frequency. For temperatures  $T < T_c$   $\varepsilon(k)$  in (8) has to be replaced by  $E(k) = \sqrt{\varepsilon(k)^2 + \bar{\Delta}_0(k)^2}$  with  $\bar{\Delta}_0(k)$  being the average superconducting energy gap. Its momentum dependence is taken as a parameter: we consider possible  $s$ ,  $d$ , and  $s+d$  wave symmetries here. From (8), *finite momentum* mode softening can set in if the normal mode unrenormalized frequency  $\omega_{q,j}^{(0)}$  is reduced by the electronic energy, corresponding to  $\tilde{\omega}_{q,j}^2 \rightarrow 0$ . Obviously, this situation is controlled by the dependence on the coupling strength  $g_{q,j}$  (8) which we use as a variable to calculate the mode freezing temperature where  $\tilde{\omega}_{q,j}^2 = 0$ . Since the electronic energies due to their coupling to the lattice degrees of freedom and the unrenormalized mode energies are both isotope dependent, the freezing temperature is isotope dependent as well. This dependence is huge, sign reversed, and of the same order of magnitude as the experimentally observed OIE on  $T^*$  (see Figure 8) [19, 74]. In the present approach the freezing

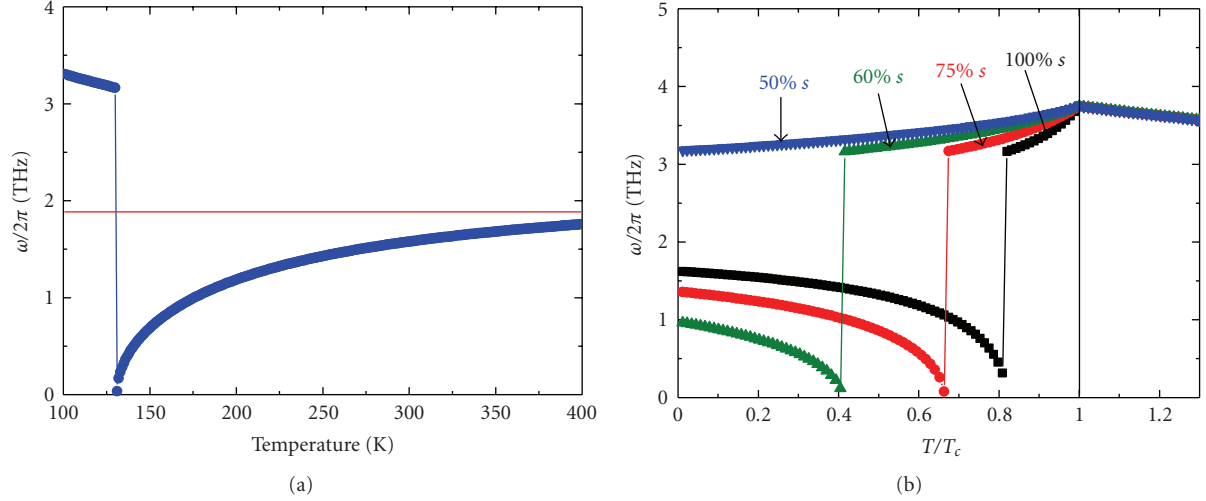


FIGURE 15: (a) Temperature dependence of the polaronic mode for  $T > T_c$ . The dashed line indicates the unrenormalized local mode frequency and the deviation from it signals the onset of the polaron formation temperature. (b) Dependence of the polaronic mode on the reduced temperature  $T/T_c$ . The colour code refers to the  $s + d$  wave admixture as indicated in the graph.

temperature, which we identify with  $T^*$ , signals the onset of a dynamically modulated, patterned structure (of *local* coherent polarons), where the superstructure modulation is defined by the  $q$ -value, where  $\tilde{\omega}_{q,j}^2 = 0$  and  $T^*$  is defined through the implicit relation

$$\omega_{q,j}^{(o)2} = \frac{g_{q,j}^2}{N(E_F)} \sum_k \frac{1}{\varepsilon(k)} \tanh \frac{\varepsilon(k)}{k_B T^*}. \quad (9)$$

The complete softening of the renormalized local mode frequency, which signals the onset of polaron coherence, is shown in Figure 15(a) as a function of temperature for  $T > T_c$ . Above  $T^*$ , typical *local* mode softening is observed beginning approximately 220 K above  $T^*$  as is evident from the deviations of the unrenormalized mode frequency indicated by the dashed line in Figure 15(a). This high-temperature scale signals the onset of polaron formation with random distribution on the lattice. At  $T^*$  the polarons become *locally* coherent and spatially patterned. Below  $T^*$  the dynamics are fast but still preserve their spatial self-organization. In this regime almost no temperature dependence in the polaronic mode is present. For temperatures  $T < T^*$  the opening of the superconducting gap influences these local dynamics massively, since now *global* coherence sets in. This is especially dramatic if the superconducting order parameter has an  $s$ -wave component.

In Figure 15(b) this temperature regime is shown with varying amounts of  $s$ -wave admixture to a  $d$ -wave order parameter. For a pure  $s$ -wave order parameter a substantial softening of the polaronic mode is observed in the immediate vicinity of  $T_c$ . With increasing  $d$ -wave contribution the softening shifts to lower temperatures and is already lost for 50%  $d + 50\%$   $s$  wave composition: only a small cusp at  $T_c$  indicates the onset of superconductivity.

An important consequence of the above local mode softening is related to the mean square Cu-O displacement

$\sigma^2(T)$  involved in the polaron formation. Here actually two copper-oxygen displacements are relevant for most HTS materials, one within the  $ab$ -planes, and the other one referring to the Cu-apical oxygen displacement [10–12]. Mostly, however, only the former is accessible to experiments, since this is substantially shorter than the latter one. Using the fluctuation/dissipation theorem we find  $\sigma^2(T) = \hbar / (M \tilde{\omega}_{q,j}) \coth(\hbar \tilde{\omega}_{q,j} / 2k_B T)$ . The calculated temperature dependence of  $\sigma^2(T)$  is shown in Figure 16. Above  $T^*$   $\sigma^2(T)$  obeys the Debye-Waller temperature dependence, however, enhanced at the onset temperature of polaron formation. At  $T^*$  a divergence in  $\sigma^2(T)$  appears caused by the freezing of the polaronic mode. Such a behaviour has been observed experimentally in various cuprate HTSs, and a typical experimental result is shown in Figure 11 and in the inset to Figure 16 [5, 7, 8, 10–12, 26–28]. The previously used assignment of  $T^*$  is different from our definition, since in [5, 7, 8, 10–12, 26–28]  $T^*$  has been related to the onset of deviations from the Debye Waller behaviour; that is,  $T^*$ , in those references, is higher than the actual polaron freezing temperature.

With decreasing coupling strength  $g$ , not only does  $T^*$  decrease but also the peak width and height diminish, becoming unobservable for small coupling. For temperatures below and slightly above  $T_c$  the temperature dependence of  $\sigma^2(T)$  is strongly affected by the superconducting gap symmetry, as anticipated from the  $T$ -dependence of the polaronic mode. With increasing admixture of a  $d$ -wave component to the primarily  $s$ -wave gap symmetry, the peak in  $\sigma^2(T)$  shifts to lower temperatures and is completely suppressed if the  $d$ -wave component achieves 50% or more. However, a similar suppression of this divergence is found if the renormalization of the hopping elements occurs for the second and interplanar hopping integrals only. In this case the coupling strength is the relevant parameter: the smaller it is, the more the peak is suppressed. The complete

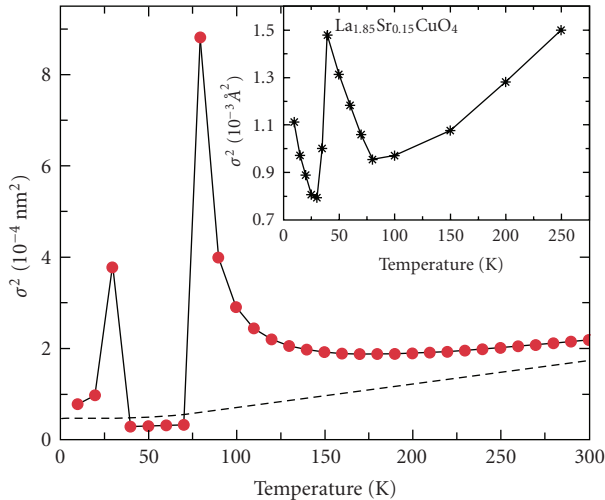


FIGURE 16: Calculated temperature dependence of the mean square Cu-O displacement  $\sigma^2(T)$ .  $T^*$  is defined as the temperature where the first divergence in  $\sigma^2(T)$  appears (in this example at  $T = 100$  K). The lower temperature divergence occurs at or below  $T_c$  depending on the pairing symmetry as explained in the text. The inset shows the experimental results obtained in [26–28].

suppression that takes place for a 50%  $s$ -wave +50%  $d$ -wave order parameter does not occur, but a substantial shift to temperatures well below  $T_c$  occurs. *This means that whenever a peak in  $\sigma^2(T)$  is observed for temperatures  $T \leq T_c$ , the superconducting order parameter cannot be purely  $d$ -wave but must have an additional isotropic  $s$ -wave admixture.* This conclusion is strongly supported by the above described  $\mu$ SR experiments (see Figures 9 and 10).

#### 4. Conclusions

Various unconventional isotope effects observed in cuprate HTSs have been reviewed, and it has been shown that besides of these effects all phases appearing in the complex hole doping dependent phase diagram show isotope dependencies. In addition, compelling experimental evidence has been given that the order parameter in these systems is not a single  $d$ -wave one but consists of coexisting  $s$ - and  $d$ -wave contributions which change in composition with the crystallographic directions. In the  $\text{CuO}_2$  planes a well visible  $s + d$  wave order parameter is realized whereas along the  $c$ -axis the  $d$ -wave part is almost missing and the experimental features are compatible with an  $s$ -wave order parameter. This finding implies that concentrating on the planes only is rather insufficient and incomplete.

The experimental results have been modelled within a two-component scenario where the doped holes lead to polaron formation and constitute a subsystem in the pseudo-AFM matrix. Both components are not phase separated but interact dynamically with each other thereby leading to multiband superconductivity. The observed isotope effects are a natural consequence of polaron formation and convincing agreement with experimental data is achieved.

The local lattice response observed experimentally has been shown to originate from the polaronic feedback effect on the lattice degrees of freedom which results in local mode softening and divergences in the Cu-O mean square displacement. Especially at  $T^*$  the polarons gain coherence and persist in the superconducting phase. Within this scenario the pseudogap phase is a precursor phase to superconductivity which supports it but does not yet reflect the symmetries of the superconducting order parameters. The symmetry of the superconducting order parameter has been shown to influence in a crucial way this displacement, since an  $s$ -wave order parameter causes another divergence in this displacement whereas a  $d$ -wave order parameter has almost no effect on it. The experimental data suggest that coupled order parameters are realized.

All experiments described in this review cannot be understood within purely electronic models. In addition, in those the important contributions from the  $c$ -axis are missing. The data and their theoretical interpretation are in line with the original idea of Jahn-Teller polarons as novel glue for electron pairing, which was the initiating motivation for the discovery of HTSC in cuprates [1, 42].

#### Acknowledgments

It is a pleasure to acknowledge illuminating discussions with K. A. Müller, H. Oyanagi, A. Simon, R. Khasanov, and A. R. Bishop. Financial support is acknowledged from the Swiss National Science Foundation, the K. Alex Müller Foundation, and the European Program CoMePhS.

#### References

- [1] J. G. Bednorz and K. A. Müller, “Possible high  $T_c$  superconductivity in the Ba-La-Cu-O system,” *Zeitschrift für Physik B*, vol. 64, no. 2, pp. 189–193, 1986.
- [2] K. A. Müller, in *Magnetic Resonance and Relaxation*, R. Blinc, Ed., pp. 192–208, North-Holland, Amsterdam, The Netherlands, 1966.
- [3] K.-H. Höck, H. Nickisch, and H. Thomas, “Jahn-Teller effect in itinerant electron systems: the Jahn-Teller polaron,” *Helvetica Physica Acta*, vol. 56, pp. 237–243, 1983.
- [4] J. P. Franck, in *Physical Properties in High Temperature Superconductors IV*, D. M. Ginsberg, Ed., pp. 189–293, World Scientific, Singapore, 1994.
- [5] A. Bianconi and N. L. Saini, “Nanoscale lattice fluctuations in cuprates and manganites,” in *Superconductivity in Complex Systems*, K. A. Müller and A. Bussmann-Holder, Eds., vol. 114 of *Structure and Bonding*, pp. 287–330, Springer, Berlin, Germany, 2005.
- [6] S. J. L. Billinge, G. H. Kwei, and H. Takagi, “Local octahedral tilts in  $\text{La}_{2-x}\text{Ba}_x\text{CuO}_4$ : evidence for a new structural length scale,” *Physical Review Letters*, vol. 72, no. 14, pp. 2282–2285, 1994.
- [7] A. Bianconi, N. L. Saini, A. Lanzara, et al., “Determination of the local lattice distortions in the  $\text{CuO}_2$  plane of  $\text{La}_{1.85}\text{Sr}_{0.15}\text{CuO}_4$ ,” *Physical Review Letters*, vol. 76, no. 18, pp. 3412–3415, 1996.
- [8] N. L. Saini, A. Lanzara, H. Oyanagi, et al., “Local lattice instability and stripes in the  $\text{CuO}_2$  plane of the  $\text{La}_{1.85}\text{Sr}_{0.15}\text{CuO}_4$

- system by polarized XANES and EXAFS,” *Physical Review B*, vol. 55, no. 18, pp. 12759–12769, 1997.
- [9] R. P. Sharma, S. B. Ogale, Z. H. Zhang, et al., “Phase transitions in the incoherent lattice fluctuations in  $\text{YBa}_2\text{Cu}_3\text{O}_{7-\delta}$ ,” *Nature*, vol. 404, no. 6779, pp. 736–740, 2000.
- [10] J. Mustre de Leon, S. D. Conradson, I. Batistić, and A. R. Bishop, “Evidence for an axial oxygen-centered lattice fluctuation associated with the superconducting transition in  $\text{YBa}_2\text{Cu}_3\text{O}_7$ ,” *Physical Review Letters*, vol. 65, no. 13, pp. 1675–1678, 1990.
- [11] A. R. Bishop, D. Mihailovic, and J. Mustre de Leon, “Signatures of mesoscopic Jahn-Teller polaron inhomogeneities in high-temperature superconductors,” *Journal of Physics: Condensed Matter*, vol. 15, no. 9, pp. L169–L175, 2003.
- [12] J. Mustre de Leon, M. Acosta-Alejandro, S. D. Conradson, and A. R. Bishop, “Change of the in-plane Cu-O bond distribution in  $\text{La}_2\text{CuO}_{4.1}$  across  $T_c$ ,” *Journal of Physics and Chemistry of Solids*, vol. 69, no. 9, pp. 2288–2291, 2008.
- [13] T. Egami, “Electron-phonon coupling in high- $T_c$  superconductors,” in *Superconductivity in Complex Systems*, K. A. Müller and A. Bussmann-Holder, Eds., vol. 114 of *Structure and Bonding*, p. 267, Springer, Berlin, Germany, 2005.
- [14] H. Uchiyama, A. Q. R. Baron, S. Tsutsui, et al., “Softening of Cu-O bond stretching phonons in tetragonal  $\text{HgBa}_2\text{CuO}_{4+\delta}$ ,” *Physical Review Letters*, vol. 92, no. 19, Article ID 197005, 4 pages, 2004.
- [15] T. Fukuda, J. Mizuki, K. Ikeuchi, K. Yamada, A. Q.R. Baron, and S. Tsutsui, “Doping dependence of softening in the bond-stretching phonon mode of  $\text{La}_{2-x}\text{Sr}_x\text{CuO}_4$  ( $0 \leq x \leq 0.29$ ),” *Physical Review B*, vol. 71, no. 6, Article ID 060501, 4 pages, 2005.
- [16] H. Keller, “Unconventional isotope effects in cuprate superconductors,” in *Superconductivity in Complex Systems*, K. A. Müller and A. Bussmann-Holder, Eds., vol. 114 of *Structure and Bonding*, p. 143, Springer, Berlin, Germany, 2005.
- [17] R. Khasanov, S. Strässle, K. Conder, E. Pomjakushina, A. Bussmann-Holder, and H. Keller, “Universal correlations of isotope effects in  $\text{Y}_{1-x}\text{Pr}_x\text{Ba}_2\text{Cu}_3\text{O}_{7-\delta}$ ,” *Physical Review B*, vol. 77, no. 10, Article ID 104530, 5 pages, 2008.
- [18] R. Khasanov, A. Shengelaya, D. di Castro, et al., “Oxygen isotope effects on the superconducting transition and magnetic states within the phase diagram of  $\text{Y}_{1-x}\text{Pr}_x\text{Ba}_2\text{Cu}_3\text{O}_{7-\delta}$ ,” *Physical Review Letters*, vol. 101, no. 7, Article ID 077001, 4 pages, 2008.
- [19] A. Furrer, “Neutron scattering investigations of charge inhomogeneities,” in *Superconductivity in Complex Systems*, K. A. Müller and A. Bussmann-Holder, Eds., vol. 114 of *Structure and Bonding*, p. 171, Springer, Berlin, Germany, 2005.
- [20] K. A. Müller, “Possible coexistence of s- and d-wave condensates in copper oxide superconductors,” *Nature*, vol. 377, no. 6545, pp. 133–135, 1995.
- [21] K. A. Müller and H. Keller, in *High  $T_c$  Superconductivity: 10 years after the Discovery*, p. 7, Kluwer Academic Publishers, Dordrecht, The Netherlands, 1997.
- [22] R. Khasanov, A. Shengelaya, A. Maisuradze, et al., “Experimental evidence for two gaps in the high-temperature  $\text{La}_{1.83}\text{Sr}_{0.17}\text{CuO}_4$  superconductor,” *Physical Review Letters*, vol. 98, no. 5, Article ID 057007, 4 pages, 2007.
- [23] R. Khasanov, S. Strässle, D. Di Castro, et al., “Multiple gap symmetries for the order parameter of cuprate superconductors from penetration depth measurements,” *Physical Review Letters*, vol. 99, no. 23, Article ID 237601, 4 pages, 2008.
- [24] R. Khasanov, A. Shengelaya, J. Karpinski, et al., “s-wave symmetry along the c-axis and s+d in-plane superconductivity in bulk  $\text{YBa}_2\text{Cu}_4\text{O}_8$ ,” *Journal of Superconductivity and Novel Magnetism*, vol. 21, no. 2, pp. 81–85, 2008.
- [25] A. Bussmann-Holder, R. Khasanov, A. Shengelaya, et al., “Mixed order parameter symmetries in cuprate superconductors,” *Europhysics Letters*, vol. 77, no. 2, Article ID 27002, 4 pages, 2007.
- [26] H. Oyanagi, A. Tsukuda, M. Naito, and N. L. Saini, “Local structure of superconducting  $(\text{La,Sr})_2\text{CuO}_4$  under strain: microscopic mechanism of strain-induced  $T_c$  variation,” *Physical Review B*, vol. 75, no. 2, Article ID 024511, 6 pages, 2007.
- [27] H. Oyanagi, C. Zhang, A. Tsukada, and M. Naito, “Lattice instability in high temperature superconducting cuprates probed by X-ray absorption spectroscopy,” *Journal of Physics: Conference Series*, vol. 108, Article ID 012038, 12 pages, 2008.
- [28] C. J. Zhang and H. Oyanagi, “Local lattice instability and superconductivity in  $\text{La}_{1.85}\text{Sr}_{0.15}\text{Cu}_{1-x}\text{M}_x\text{O}_4$  ( $M = \text{MN, Ni, and Co}$ ),” *Physical Review B*, vol. 79, no. 6, Article ID 064521, 8 pages, 2009.
- [29] S. Robaskiewicz, R. Micnas, and J. Ranninger, “Superconductivity in the generalized periodic Anderson model with strong local attraction,” *Physical Review B*, vol. 36, no. 1, pp. 180–201, 1987.
- [30] B. K. Chakraverty, “Superconductive solutions for a two-band Hamiltonian,” *Physical Review B*, vol. 48, no. 6, pp. 4047–4053, 1993.
- [31] L. P. Gor’kov and A. V. Sokol, *JETP Letters*, vol. 46, p. 420, 1987.
- [32] W. A. Little and M. J. Holcomb, “Analysis of the pairing interaction in the cuprates,” *Journal of Superconductivity*, vol. 13, no. 5, pp. 695–698, 2000.
- [33] C. F. Richardson and N. W. Ashcroft, “Effective electron-electron interactions and the theory of superconductivity,” *Physical Review B*, vol. 55, no. 22, pp. 15130–15145, 1997.
- [34] J. E. Hirsch, “Polaronic superconductivity in the absence of electron-hole symmetry,” *Physical Review B*, vol. 47, no. 9, pp. 5351–5358, 1993.
- [35] J. B. Goodenough and J.-S. Zhou, “Correlation bag and high- $T_c$  superconductivity,” *Physical Review B*, vol. 42, no. 7, pp. 4276–4287, 1990.
- [36] J. B. Goodenough, J.-S. Zhou, and J. Chan, “Copper oxide superconductors: a distinguishable thermodynamic state,” *Physical Review B*, vol. 47, no. 9, pp. 5257–5286, 1993.
- [37] A. S. Alexandrov, “Superconducting polarons and bipolarons,” in *Polarons in Advanced Materials*, A. S. Alexandrov, Ed., Materials Science, p. 257, Springer, Dordrecht, The Netherlands, 2007.
- [38] Yu. N. Ovchinnikov, S. A. Wolf, and V. Z. Kresin, “Inhomogeneity of the superconducting state and consequent diamagnetism above  $T_c$ : application to the cuprates,” *Physical Review B*, vol. 60, no. 6, pp. 4329–4333, 1999.
- [39] Yu. N. Ovchinnikov, S. A. Wolf, and V. Z. Kresin, “Intrinsic inhomogeneities in superconductors and the pseudogap phenomenon,” *Physical Review B*, vol. 63, no. 6, Article ID 064524, 6 pages, 2001.
- [40] Yu. N. Ovchinnikov and V. Z. Kresin, “Inhomogeneous superconductor in an ac field: application to the pseudogap region,” *Physical Review B*, vol. 65, no. 21, Article ID 214507, 8 pages, 2002.
- [41] H. Kamimura, S. Matsuno, Y. Suwa, and H. Ushio, “Occurrence of d-wave pairing in the phonon-mediated mechanism of high temperature superconductivity in cuprates,” *Physical Review Letters*, vol. 77, no. 4, pp. 723–726, 1996.

- [42] K. A. Müller, "On the superconductivity in hole doped cuprates," *Journal of Physics: Condensed Matter*, vol. 19, no. 25, Article ID 251002, 13 pages, 2007.
- [43] A. Bussmann-Holder and H. Keller, "Polaron formation as origin of unconventional isotope effects in cuprate superconductors," *European Physical Journal B*, vol. 44, pp. 487–490, 2005.
- [44] A. Bussmann-Holder, H. Keller, and K. A. Müller, "Evidences for poaron formation in cuprates," in *Superconductivity in Complex Systems*, K. A. Müller and A. Bussmann-Holder, Eds., vol. 114 of *Structure and Bonding*, p. 367, Springer, Dordrecht, The Netherlands, 2005.
- [45] A. Bussmann-Holder and H. Keller, "Polaron effects in high- $T_c$  cuprate superconductors," in *Polarons in Advanced Materials*, A. S. Alexandrov, Ed., Materials Science, p. 599, Springer, Dordrecht, The Netherlands, 2007.
- [46] H. Keller, A. Bussmann-Holder, and K. A. Müller, "Jahn-Teller physics and high- $T_c$  superconductivity," *Materials Today*, vol. 11, pp. 38–46, 2008.
- [47] H. Suhl, B. T. Matthias, and L. Walker, "Bardeen-cooperschrieffer theory of superconductivity in the case of overlapping bands," *Physical Review Letters*, vol. 3, no. 12, pp. 552–554, 1959.
- [48] V. Moskalenko, "Superconductivity of metals taking into account overlapping of the energy bands," *Fiz. Metal. Metalov.*, vol. 8, p. 503, 1959.
- [49] B. Geilikman, R. Zaishev, and V. Z. Kresin, *Fiz. Tverd. Tela.*, vol. 9, p. 693, 1967.
- [50] B. Geilikman, R. Zaishev, and V. Z. Kresin, *Soviet Physics-Solid State*, vol. 9, p. 542, 1966.
- [51] V. Z. Kresin and S. Wolf, "Multigap structure in the cuprates," *Physica C*, vol. 169, no. 5-6, pp. 476–484, 1990.
- [52] V. Z. Kresin and S. A. Wolf, "Major normal and superconducting parameters of high- $T_c$  oxides," *Physical Review B*, vol. 41, no. 7, pp. 4278–4285, 1990.
- [53] V. Z. Kresin and S. A. Wolf, "Induced superconducting state and two-gap structure: application to cuprate superconductors and conventional multilayers," *Physical Review B*, vol. 46, no. 10, pp. 6458–6471, 1992.
- [54] V. Z. Kresin, S. Wolf, and G. Deutscher, "The effect of phonon-mediated charge transfer and internal proximity effect on the properties of multigap cuprate superconductors," *Physica C*, vol. 191, no. 1-2, pp. 9–14, 1992.
- [55] D. Zech, H. Keller, K. Conder, et al., "Site-selective oxygen isotope effect in optimally doped  $\text{YBa}_2\text{Cu}_3\text{O}_{6+x}$ ," *Nature*, vol. 371, no. 6499, pp. 681–683, 1994.
- [56] G.-M. Zhao, K. Conder, H. Keller, and K. A. Müller, "Oxygen isotope effects in  $\text{La}_{2-x}\text{Sr}_x\text{CuO}_4$ : evidence for polaronic charge carriers and their condensation," *Journal of Physics: Condensed Matter*, vol. 10, no. 40, pp. 9055–9066, 1998.
- [57] G. M. Zhao, H. Keller, and K. Conder, "Unconventional isotope effects in the high-temperature cuprate superconductors," *Journal of Physics: Condensed Matter*, vol. 13, no. 29, pp. R569–R587, 2001.
- [58] K. A. Müller, "On the oxygen isotope effect and apex anharmonicity in high  $T_c$  cuprates," *Zeitschrift für Physik B*, vol. 80, p. 193, 1990.
- [59] A. Bussmann-Holder and A. R. Bishop, "Anharmonicity in the  $c$  direction of high- $T_c$  oxides," *Physical Review B*, vol. 51, no. 10, pp. 6640–6644, 1995.
- [60] A. Bussmann-Holder and A. R. Bishop, "Anharmonic electron and phonon effects in the  $c$ -axis infrared conductivity of high- $T_c$  oxides," *Physical Review B*, vol. 51, no. 5, pp. 3246–3249, 1995.
- [61] A. Bussmann-Holder and A. R. Bishop, "Anharmonicity-induced multiphonon processes in high-temperature superconductors," *Physical Review B*, vol. 44, no. 6, pp. 2853–2856, 1991.
- [62] A. Bussmann-Holder, A. R. Bishop, and I. Batistić, "Unconventional electron-phonon interactions in high-temperature superconductors," *Physical Review B*, vol. 43, no. 16, pp. 13728–13731, 1991.
- [63] D. Mihailović, I. Poberaj, and A. Mertelj, "Characterization of the pyroelectric effect in  $\text{YBa}_2\text{Cu}_3\text{O}_{7-\delta}$ ," *Physical Review B*, vol. 48, no. 22, pp. 16634–16640, 1993.
- [64] M. Cardona, R. Liu, C. Thomsen, et al., "Effect of isotopic substitution of oxygen on  $T_c$  and the phonon frequencies of high  $T_c$  superconductors," *Solid State Communications*, vol. 67, no. 8, pp. 789–793, 1988.
- [65] G.-M. Zhao, J. W. Ager III, and D. E. Morris, "Site dependence of large oxygen isotope effect in  $\text{Y}_{0.7}\text{Pr}_{0.3}\text{Ba}_2\text{Cu}_3\text{O}_{6.97}$ ," *Physical Review B*, vol. 54, no. 21, pp. 14982–14985, 1996.
- [66] R. Khasanov, A. Shengelaya, E. Morenzoni, et al., "Site-selective oxygen isotope effect on the magnetic-field penetration depth in underdoped  $\text{Y}_{0.6}\text{Pr}_{0.4}\text{Ba}_2\text{Cu}_3\text{O}_{7-\delta}$ ," *Physical Review B*, vol. 68, no. 22, Article ID 220506, 4 pages, 2003.
- [67] A. Bussmann-Holder, A. R. Bishop, L. Genzel, and A. Simon, "Doping dependence of  $T_c$  and its related isotope effect in high-temperature superconductors," *Physical Review B*, vol. 55, no. 17, pp. 11751–11755, 1997.
- [68] J. Hofer, K. Conder, T. Sasagawa, et al., "Oxygen-isotope effect on the in-plane penetration depth in underdoped  $\text{La}_{2-x}\text{Sr}_x\text{CuO}_4$  single crystals," *Physical Review Letters*, vol. 84, no. 18, pp. 4192–4195, 2000.
- [69] A. Bussmann-Holder, H. Keller, A. R. Bishop, A. Simon, R. Micnas, and K. A. Müller, "Unconventional isotope effects as evidence for polaron formation in cuprates," *Europhysics Letters*, vol. 72, no. 3, pp. 423–429, 2005.
- [70] G.-M. Zhao and D. E. Morris, "Observation of a possible oxygen isotope effect on the effective mass of carriers in  $\text{YBa}_2\text{Cu}_3\text{O}_{6.94}$ ," *Physical Review B*, vol. 51, no. 22, pp. 16487–16490, 1995.
- [71] G.-M. Zhao, M. B. Hunt, H. Keller, and K. A. Müller, "Evidence for polaronic supercarriers in the copper oxide superconductors  $\text{La}_{2-x}\text{Sr}_x\text{CuO}_4$ ," *Nature*, vol. 385, no. 6613, pp. 236–238, 1997.
- [72] R. Khasanov, D. G. Eshchenko, H. Luethkens, et al., "Direct observation of the oxygen isotope effect on the in-plane magnetic field penetration depth in optimally doped  $\text{YBa}_2\text{Cu}_3\text{O}_{7-\delta}$ ," *Physical Review Letters*, vol. 92, no. 5, Article ID 057602, 4 pages, 2004.
- [73] A. Shengelaya, G.-M. Zhao, C. M. Aegerter, K. Conder, I. M. Savic, and H. Keller, "Giant oxygen isotope effect on the spin glass transition in  $\text{La}_{2-x}\text{Sr}_x\text{Cu}_{1-z}\text{Mn}_z\text{O}_4$  as revealed by muon spin rotation," *Physical Review Letters*, vol. 83, no. 24, pp. 5142–5145, 1999.
- [74] A. Lanzara, G. M. Zhao, N. L. Saini, et al., "Oxygen-isotope shift of the charge-stripe ordering temperature in  $\text{La}_{2-x}\text{Sr}_x\text{CuO}_4$  from X-ray absorption spectroscopy," *Journal of Physics: Condensed Matter*, vol. 11, pp. L541–L546, 1999.
- [75] F. Raffa, T. Ohno, M. Mali, et al., "Isotope dependence of the spin gap in  $\text{YBa}_2\text{Cu}_4\text{O}_8$  as determined by Cu NQR relaxation," *Physical Review Letters*, vol. 81, no. 26, pp. 5912–5915, 1998.
- [76] C. C. Tsuei and J. R. Kirtley, "Pairing symmetry in cuprate superconductors," *Reviews of Modern Physics*, vol. 72, no. 4, pp. 969–1016, 2000.
- [77] J. A. Martindale, P. C. Hammel, W. L. Hults, and J. L. Smith, "Temperature dependence of the anisotropy of the planar

- oxygen nuclear spin-lattice relaxation rate in  $\text{YBa}_2\text{Cu}_3\text{O}_y$ ,” *Physical Review B*, vol. 57, no. 18, pp. 11769–11774, 1998.
- [78] J. Haase and C. P. Slichter, “Charge density variations or stripes in  $\text{YBa}_2\text{Cu}_3\text{O}_{6+y}$ ,” *Journal of Superconductivity*, vol. 1, no. 3, pp. 473–475, 2003.
- [79] B. Friedl, C. Thomsen, and M. Cardona, “Determination of the superconducting gap in  $\text{RBa}_2\text{Cu}_3\text{O}_{7-\delta}$ ,” *Physical Review Letters*, vol. 65, no. 7, pp. 915–918, 1990.
- [80] T. Masui, M. Limonov, H. Uchiyama, S. Lee, and S. Tajima, “Raman study of carrier-overdoping effects on the gap in high- $T_c$  superconducting cuprates,” *Physical Review B*, vol. 68, no. 6, Article ID 060506, 4 pages, 2003.
- [81] J. R. Kirtley, C. C. Tsuei, A. Ariando, C. J. M. Verwijs, S. Harkema, and H. Hilgenkamp, “Angle-resolved phase-sensitive determination of the in-plane gap symmetry in  $\text{YBa}_2\text{Cu}_3\text{O}_{7-\delta}$ ,” *Nature Physics*, vol. 2, no. 3, pp. 190–194, 2006.
- [82] A. Furrer, “Admixture of an s-wave component to the d-wave gap symmetry in high-temperature superconductors,” *Journal of Superconductivity and Novel Magnetism*, vol. 21, no. 1, pp. 1–5, 2008.
- [83] A. G. Sun, D. A. Gajewski, M. B. Maple, and R. C. Dynes, “Observation of Josephson pair tunneling between a high- $T_c$  cuprate ( $\text{YBa}_2\text{Cu}_3\text{O}_{7-\delta}$ ) and a conventional superconductor (Pb),” *Physical Review Letters*, vol. 72, no. 14, pp. 2267–2270, 1994.
- [84] Q. Li, Y. N. Tsay, M. Suenaga, R. A. Klemm, G. D. Gu, and N. Koshizuka, “ $\text{Bi}_2\text{Sr}_2\text{CaCu}_2\text{O}_{8+\delta}$  bicrystal c-axis twist Josephson junctions: a new phase-sensitive test of order parameter symmetry,” *Physical Review Letters*, vol. 83, no. 20, pp. 4160–4163, 1999.
- [85] G. Binnig, A. Baratoff, H. E. Hoenig, and J. G. Bednorz, “Two-band superconductivity in Nb-Doped  $\text{SrTiO}_3$ ,” *Physical Review Letters*, vol. 45, no. 16, pp. 1352–1355, 1980.
- [86] F. Giubileo, D. Roditchev, W. Sacks, et al., “Two-gap state density in  $\text{MgB}_2$ : a true bulk property or a proximity effect?” *Physical Review Letters*, vol. 87, no. 17, Article ID 177008, 4 pages, 2001.
- [87] R. Khasanov, D. V. Evtushinsky, A. Amato, et al., “Two-gap superconductivity in  $\text{Ba}_{1-x}\text{K}_x\text{Fe}_2\text{As}_2$ : a complementary study of the magnetic penetration depth by muon-spin rotation and angle-resolved photoemission,” *Physical Review Letters*, vol. 102, no. 18, Article ID 187005, 4 pages, 2009.
- [88] A. Bussmann-Holder, H. Keller, A. R. Bishop, A. Simon, and K. A. Müller, “Polaron coherence as origin of the pseudogap phase in high temperature superconducting cuprates,” *Journal of Superconductivity and Novel Magnetism*, vol. 21, no. 6, pp. 353–357, 2008.
- [89] A. Bussmann-Holder and H. Keller, “Evidence for polaron formation in high-temperature superconducting cuprates: experiment and theory,” *Journal of Superconductivity and Novel Magnetism*, vol. 22, no. 2, pp. 123–129, 2009.
- [90] A. Bussmann-Holder and H. Keller, “Unconventional isotope effects, multi-component superconductivity and polaron formation in high temperature cuprate superconductors,” *Journal of Physics: Conference Series*, vol. 108, Article ID 012019, 16 pages, 2008.
- [91] S. G. Lang and Yu. A. Firsov, “Kinetic theory of semiconductors with low mobility,” *Soviet Physics-JETP*, vol. 16, p. 1302, 1963.
- [92] A. Bussmann-Holder, R. Micnas, and A. R. Bishop, “Enhancements of the superconducting transition temperature within the two-band model,” *European Physical Journal B*, vol. 37, no. 3, pp. 345–348, 2003.
- [93] R. Micnas, S. Robaskiewicz, and A. Bussmann-Holder, “Two-component scenario for non-conventional (exotic) superconductors,” in *Superconductivity in Complex Systems*, K. A. Müller and A. Bussmann-Holder, Eds., vol. 114 of *Structure and Bonding*, p. 13, Springer, Dordrecht, The Netherlands, 2005.
- [94] E. Pavarini, I. Dasgupta, T. Saha-Dasgupta, O. Jepsen, and O. K. Anderson, “Band-structure trend in hole-doped cuprates and correlation with  $T_c$ ,” *Physical Review Letters*, vol. 87, no. 4, Article ID 047003, 4 pages, 2001.
- [95] R. Micnas and B. Tobijaszewska, “Superfluid properties of the extended Hubbard model with intersite electron pairing,” *Journal of Physics: Condensed Matter*, vol. 14, no. 41, pp. 9631–9649, 2002.

## Review Article

# Hard-Wired Dopant Networks and the Prediction of High Transition Temperatures in Ceramic Superconductors

**J. C. Phillips**

*Department of Physics and Astronomy, Rutgers University, Piscataway, NJ 08854-8019, USA*

Correspondence should be addressed to J. C. Phillips, [jcphillips8@comcast.net](mailto:jcphillips8@comcast.net)

Received 22 May 2009; Accepted 17 August 2009

Academic Editor: Sasha Alexandrov

Copyright © 2010 J. C. Phillips. This is an open access article distributed under the Creative Commons Attribution License, which permits unrestricted use, distribution, and reproduction in any medium, provided the original work is properly cited.

I review the multiple successes of the discrete hard-wired dopant network model ZZIP, and comment on the equally numerous failures of continuum models, in describing and predicting the properties of ceramic superconductors. The prediction of transition temperatures can be regarded in several ways, either as an exacting test of theory, or as a tool for identifying theoretical rules for defining new homology models. Popular “first principle” methods for predicting transition temperatures in conventional crystalline superconductors have failed for cuprate HTSC, as have parameterized models based on  $\text{CuO}_2$  planes (with or without apical oxygen). Following a path suggested by Bayesian probability, it was found that the glassy, self-organized dopant network percolative model is so successful that it defines a new homology class appropriate to ceramic superconductors. The reasons for this success in an exponentially complex (non-polynomial complete, NPC) problem are discussed, and a critical comparison is made with previous polynomial (PC) theories. The predictions are successful for the superfamily of all ceramics, including new non-cuprates based on FeAs in place of  $\text{CuO}_2$ .

## 1. Introduction

The prediction of transition temperatures  $T_c$  is rightly considered to be one of the most difficult problems in theoretical physics. Here one should distinguish between a true (or bare) prediction (the value of  $T_c$  is not known when the prediction is made), and a postdated calculation carried out according to certain rules after  $T_c$  has been measured experimentally. If the rules (sometimes called “first principles”) have been established for similar materials, and they are faithfully applied to the new case, then the validity of the rules can be tested by the success of the prediction. If the number of example materials where the rules have been applied previously is large compared to the number of adjustable parameters, then the prediction can be said to be based on homology, namely, the supposed microscopic similarity of the phase transition of the new material to those previously studied.

Perhaps the best-known example of a “bare” prediction of a transition temperature was [1] for superfluidity of  $^3\text{He}$ . The predicted value of  $T_c$  was 100 mK, whereas the measured value [2] of  $T_c$  was 3.6 mK, so the predicted

value was too large by a factor of  $\sim 30$ . The most successful predated prediction of  $T_c$  for superconductors based on homology was for the high-pressure phase of Si [3], where the experimental maximum  $T_c$  is 8.2 K, and estimation of  $T_c$  using the most popular rules gave  $T_c = 5$  K. A number of postdated predictions of superconductive  $T_c$  have been made based on homology models and “first principles” rules. The rules depend mainly on the Fermi-surface average of the electron-phonon coupling constant  $\lambda$  and the phonon frequency squared ( $\lambda\langle\omega^2\rangle$ ). The most popular of these have been the prediction of  $T_c$  in  $\text{MgB}_2$  based on homologies with simple metals such as Al, where the predicted and experimental values are both about 40 K [4]. Equally impressive has been the prediction of  $T_c$  in 5% B-doped CVD diamond, where the predicted and experimental values are  $T_c = 22$  K and  $T_c = 11$  K, respectively [5]. The agreement here between theory and experiment is better than it appears to be, as some of the B may have formed electrically inactive dimers. This example illustrates the strengths and limitations of homology arguments based on first principles, as the material properties of B-doped CVD

## Continuum versus network phase diagrams

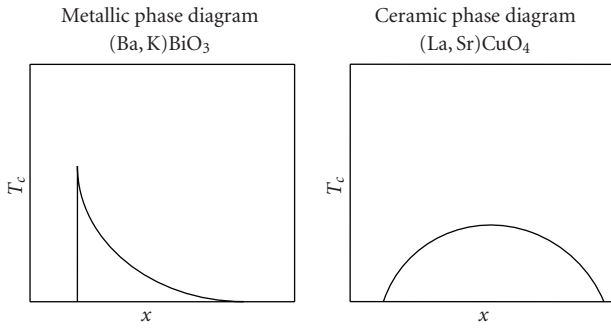


FIGURE 1: There are large qualitative differences between the phase diagrams of layered ceramic cuprates, such as  $\text{La}_{2-x}\text{Sr}_x\text{CuO}_4$ , and cubic  $\text{Ba}_{1-x}\text{K}_x\text{BiO}_3$ . The former requires a percolative model, but the superconductive properties of the latter can be explained using a traditional BCS continuum model.

diamond are a far cry from those of single-crystal Al or  $\text{MgB}_2$ .

The success of crystalline models for electron-phonon interactions in  $\text{MgB}_2$ , and their failure in ceramic superconductors, is sometimes cited as “proof” that ceramic HTSC is not caused by electron-phonon interactions. This argument completely ignores the fact that doping is required to render ceramic materials metallic and superconductive, whereas substitutional doping of  $\text{MgB}_2$  drastically depresses  $T_c$ . From these contrary chemical doping trends it is already obvious that something drastically different from crystalline superconductivity must be happening to cause ceramic HTSC. These drastic differences are likely to be caused by the strong disorder introduced by the dopants. Perhaps the most dramatic differences are apparent in the phase diagrams of  $T_c(x)$  in  $\text{Ba}_{1-x}\text{K}_x\text{BiO}_3$  compared to  $\text{La}_{2-x}\text{Sr}_x\text{CuO}_4$ , as shown in Figure 1. As both compounds are oxides, one might have expected to see similar phase diagrams, but clearly the standard parabolic  $T_c(x)$  of the cuprates is not seen in the triangular  $T_c(x)$  of  $\text{Ba}_{1-x}\text{K}_x\text{BiO}_3$ . The latter is well understood: as  $x$  decreases, the dopant free charge density decreases, and with it the screening of electron-phonon interactions, so  $T_c(x)$  increases right up to the metal-insulator transition. Our main task for the ceramic superconductors is now to explain the parabolic dependence of  $T_c(x)$  (which is not difficult in a glassy network model), and to predict  $T_c^{\max}(x)$  at optimal doping (much harder).

Other examples of  $T_c$  predictions are the proton order-disorder transition in high-pressure ice, where the predicted and experimental values are 98 K and 72 K, respectively (KOH doping) [6], and strained thin-film ferroelectrics, where large shifts in the Curie temperature  $T_c$  are predicted, and there is a good agreement between theory and experiment after correcting the domain effects [7]. In magnetic materials, the values of  $T_c$  calculated by self-consistent fields with frozen magnons are in generally good agreement with experiment within about 20%, even for complex ternary alloys with mixed ferro- and antiferromagnetic interactions [8]. All of these successful calculations have occurred in well-ordered crystals; methods based on ideal lattice models

thus may not be equally successful for strongly disordered materials like ceramic superconductors.

## 2. Exotic Superexchange and Traditional Electron-Phonon Interactions

Much of the theoretical literature over the last two decades has been devoted to discussing nonphonon models of HTSC. Did Bednorz and Mueller suppose, when they discovered HTSC in the cuprates, that they were also opening what would turn out to be a Pandora’s box for theorists? Certainly, by looking for superconductivity in a family of materials known not for metallic, but for antiferromagnetic properties, they were already behaving as contrarians, who worked evenings on this project, as they felt that this research direction would not meet with the approval of their immediate superiors. Had they consulted me, I would have asked them why they expected to find superconductivity in these pseudoperovskites. Their explanation that the strongest electron-phonon interactions are found in the best ferroelectrics (like  $\text{BaTiO}_3$ , which has the closely related perovskite structure) would not have satisfied me. The perovskites exhibit many displacive distortions, and a would be metal should be rendered insulating by Jahn-Teller distortions.

In fact, my general argument was correct for almost all such materials, almost all, but with a few crucial exceptions(!) As I later learned, the crystal chemist who discovered  $\text{La}_2\text{CuO}_4$  had made a prescient remark (references for this and many other older papers can be found in my book [9]). He noted that  $\text{La}_2\text{CuO}_4$  was the only cuprate known at that time with an undistorted tetragonal structure. In all other cuprates the lattice planes had buckled due to strong Jahn-Teller distortions, and these same distortions would suppress metallic conductivity and of course superconductivity. No one could blame theory (or me) for not predicting the rigidity of  $\text{CuO}_2$  planes, and I was off the hook for the moment, but there were much bigger challenges yet to come.

These new challenges emerged in a way that took me even more by surprise than the Bednorz-Mueller discovery. It had been known for decades that superconductivity and magnetism are incompatible, because electron-spin scattering breaks Cooper pairs. There are elaborate many-body ways of deriving this result (based on four-particle scattering diagrams called plaquettes), but the simplest way is to invoke Helmholtz’ theorem, which states that any vector field can be decomposed into complementary parts: solenoidal (magnetic) and irrotational (extensive, in other words, superconductive). This is, in fact, a “poor man’s” way of deriving the Meissner effect.

Soon phase diagrams appeared that showed that as the doping level increased, magnetism faded and superconductivity appeared, just as one would have expected. However, even before phase diagrams became available, theorists had jumped in with explanations, and the first explanation was not the most natural one, but the most surprising one, even more surprising than the discovery itself. Anderson proposed that HTSC was caused not by phonons, but by superexchange between spins(!), a subject that he had discussed in 1950

for insulators. It seems that he had long hoped to find superexchange in metals, and it appeared to him that HTSC were just what he had been looking for. He termed his new mechanism “RVB” and it soon became by far his most cited paper (~5000 citations so far). Anderson is still advocating RVB [10] and that HTSC was caused not by phonons, but by superexchange between spins(!), and he has persuaded many distinguished theorists to join him [11]. His example has stimulated many frivolous theories.

Of course, not everyone was in love with superexchange. Sir Neville Mott had always championed a common-sense approach (today known more popularly by the computer scientists’ acronym KISS), and initially he suggested that HTSC could be caused by a mixture of electron and spin interactions. However, he soon abandoned spin altogether, and turned to “bipolarons” by which he meant Cooper pairs formed by very strong and very localized electron-phonon interactions [12, 13]. However, while there is no doubt that very localized electron-phonon interactions exist at dopants (such as interstitial O) in these materials, it is not easy, especially with such large unit cells and so many normal modes, to distinguish experimentally such dopant interactions from host Jahn-Teller distortions. Indeed, even in the old intermetallic “high temperature” superconductors, with  $T_c \sim 20 + K$ , it was often Jahn-Teller distortions (or other lattice instabilities) that had ultimately limited  $T_c$  [9], while magnetic interactions, even with small amounts of magnetic impurities, quickly destroyed superconductivity. T. D. Lee also suggested that HTSC might be more like Bose-Einstein condensation, and there are still papers on HTSC using the B-E approach. In my opinion, this approach is insufficiently material-specific, and does not identify the key aspects (like the rigidity of  $\text{CuO}_2$  planes) that make the cuprates special.

From the point of view of materials science, what was special about the cuprates was (and still is) that they are at the cutting edge (sometimes called the bleeding edge) of new materials: not only are they complex chemically, but also oxides per se previously enjoyed a very poor reputation among crystallographers: the samples were often oxygen-deficient, and the sample quality was often so poor that X-ray structural determinations did not meet the standards required for publication in archival diffraction journals. It seemed to me [14] that these problems suggested that these strongly disordered materials should be regarded as mechanically marginally stable (MMS). MMS is apparently unapproachable theoretically; the reason is that too little is known about interatomic forces, and with many atoms/(unit cell), even small errors in these will cause the dynamical matrix to produce negative values of  $\omega_\alpha^2(q)$  for some  $q$  and some mode  $\alpha$ . The current state of the art (2009) is that MMS in ferroelastic and ferroelectric  $\text{BaTiO}_3$  (but not  $\text{La}_2\text{CuO}_4$ ) has been solved by brute-force first-principles pseudopotential calculations. However, even the host compound  $\text{La}_2\text{CuO}_4$  is a very long way from  $\text{La}_{2-x}\text{Sr}_x\text{CuO}_4$  (large lattice distortions near dopants are always ignored, as they are a large problem for brute-force approaches, but as we will see, there are other ways to deal with them).

When  $T_c$  is calculated for HTSC using crystalline continuum metallic ( $\lambda\langle\omega^2\rangle$  or Eliashberg) rules, not only are the predicted values too low but also the chemical trends are wrong (with some fudging of the adjustable Coulomb repulsion parameter  $\mu^*$ ,  $T_c$  in  $\text{La}_{2-x}\text{Sr}_x\text{CuO}_4$  may be brought close to experiment ( $x_c = 0.15$ ,  $T_c = 38$  K), but the same value of  $\mu^*$  in  $\text{YBa}_2\text{Cu}_3\text{O}_{7-x}$  gives  $T_c < 1$  K, a failure compared to experiment ( $x_c = 0.1$ ,  $T_c = 90$  K) [15]. The feature that distinguishes ceramic HTSC from metals is their strong disorder, as reflected in complex patterns of nanodomains on a length scale  $\sim 3$  nm [16, 17]. In the presence of strong disorder, superconductivity may become molecular in character [12, 13], in which case  $T_c$  could be as high as 380 K [18]. Unfortunately, this upper bound is too weak, and is unlikely to be reached, because in the presence of strong electron-phonon interactions the metallic band at  $E_F$  will be split by a Jahn-Teller effect (e.g., monovalent dopants could form electrically inactive dimers); worse still, the entire compound may not be dopable, or may phase-separate.

### 3. Chemical Factors: Size, Apical Oxygens, Electronegativity, and Valence

A different and more global approach to the exponential complexity associated with strong disorder relies on traditional analysis of chemical factors (valid in crystals, molecules, and glasses) [19] to analyze trends in  $T_c$ . Some have argued that cuprate superconductivity must be localized in the  $\text{CuO}_2$  planes [20], but if this were the case, the maximum  $T_c$ 's in each material family,  $T_c^{\text{max}}$ , would be nearly constant, much like the planar lattice constant. This is far from being the case. As one can easily see from structural systematics [19], the central problem in ceramic superconductors lies in making a ceramic conducting by heavy doping. Light doping (as in semiconductors) is not enough because as the ceramic dielectric constant is small, the dopant orbitals are also small, and these will not overlap unless the dopant level is high. Maximum doping levels in rigid semiconductors are typically  $< 1\%$ , so something special is required to support the high doping levels found in ceramic superconductors and still avoid phase separation.

In cuprates, the special factor is the exceptional rigidity of  $\text{CuO}_2$  planes (see Section 2), which allows the intervening insulating layers to be soft and flexible. Because core repulsive potentials are “hard” it is then relatively easy to dope the soft insulating layers. Note that normally one thinks of metals as soft, and ionic insulators as hard. The cuprates and a few other layered ceramics reverse the normal ordering, and this is what makes it possible for them to be HTSC. There are no mysterious superexchange interactions between spins; most of the antiferromagnetic regions have disappeared by the time the doping is large enough for the materials to be metallic. The pseudogaps are still present, and they play a necessary role, but whether or not they are caused by magnetic interactions (unlikely) or charge density waves (or Jahn-Teller distortions) (probably) is incidental. The highest  $T_c$ , reached at optimal doping in a given alloy will depend on the dopant configuration relative to the regions occupied

by the pseudogaps. That, in turn, will depend on the relative sizes of the ions, a packing (actually, a dynamical packing) question that is well beyond the reach of present and probably any future theory. As we will see in the following section, with a sufficiently large data base this difficulty can be handled by advanced statistical methods.

Kamimura recognized that the  $\text{CuO}_2$  planes alone could not explain HTSC, no matter how exotic the interactions within them, and he suggested that apical oxygens could play an important role [21]; several succeeding “apical oxygen” papers also proved quite popular [22, 23]. There have always been strong indications that apical oxygens are coupled to interlayer dopants (especially interstitial oxygen, which is close to apical oxygens and can form dynamical vibrational bands with them) based on chemical trends between apical oxygen bond lengths, ordering and  $T_c$  [24], and we will see further evidence of such correlations later. However, specific apical oxygen models always introduced atomic orbitals and their overlaps, which generates many parameters to fit one observable, a situation that always leads to “excellent” agreement between “predicted” and experimental values. In fact, the most popular model [23] is based on the difference between the Madelung potentials at the planar and apical oxygen sites, calculated with an artistic point ion model where most of the many charges in the unit cell are freely “assigned” (e.g., although O is usually  $2-$ , in some cases it is “assigned” a charge of  $1+$ , and many liberties are taken with “assigned” cationic charges). A parameterized discussion of correlations between apical oxygen bond lengths  $d_a$  and  $T_c$  [25] gave plausible trends, but it covered only a few cases with no predictions of  $T_c$ , showing the limitations of  $d_a$  as a configuration coordinate. More generally, one should not use extensively parameterized atomic models ( $\text{CuO}_2$  planes + apical oxygens) to discuss differences between pseudogapped regions and superconductive regions, as this difference is almost surely due to different dopant distributions [26].

When one considers seven different structural factors, including apical oxygen bond lengths, and correlates them with  $T_c$ , one finds that the obvious ionic variable, the average over *all* host atoms of the difference between cation and anion electronegativities ( $\langle\Delta X\rangle$ ), gives the best fit to  $T_c$  [27]. (This is the ionic analogue of the covalent molecular model [14].) Bearing in mind that different dynamical packings can be used to maximize  $T_c$ , we can now test the validity of  $\langle\Delta X\rangle$  as a coupling parameter by plotting  $T_c^{\max}(\langle\Delta X\rangle)$ . The results are quite disappointing, as they yield a scatter-shot plot [28], which means that the traditional chemical approach is too simple to explain HTSC (the reason is that to produce a strong electron-phonon interaction, we need a soft lattice, and soft lattices will be found near a covalent-ionic-metallic triple point, which will not depend on  $\langle\Delta X\rangle$  alone). It is just at this point, when nothing seems to work, that we can find the answer, using only the elements discussed so far.

#### 4. Successful Prediction of $T_c^{\max}$

We begin by realizing that volume factors although they are not known in detail, can be included implicitly in the

analysis by focusing initially not on  $T_c(Y)$ , but rather on the largest transition temperatures  $T_c^{\max}(Y)$ , where  $Y$  is any other chemical factor. In other words, if the volume factor has already been optimized, then the material in question will have  $T_c = T_c^{\max}(Y)$ . For those familiar with Bayesian probability, this approach is readily recognized: Bayesian probability interprets the concept of probability as a contingent “measure of a state of knowledge” and not as a frequency in orthodox statistics (further details can be found from your browser). Bayesian methods can be extremely effective, but the Bayesian filter requires a large data base. In what follows, the basic Bayesian conclusions are tested by employing the full ceramic HTSC data base, which has now grown quite large, including ceramics based on metallic layers other than  $\text{CuO}_2$  planes and apical ions other than oxygen.

At this point there are only two chemical configuration coordinates remaining: electron/atom ( $e/a$ ) ratio (which determines the Fermi line of a two-dimensional metal), and valence, which apparently is relevant for perovskites and pseudoperovskites, where the average coordination number is far lower than in metals. In a continuum model the  $e/a$  ratio would be the relevant one, while in a valence bond network model valence is the key coordinate; this coordinate can compete with structural coordination numbers [14]. The latter are much the same for most cuprates, and are unlikely candidates for  $Y$ . Moreover, decades of research on a parallel problem, network glasses, have shown (particularly when comparing silicate and chalcogenide alloy glasses) that the MMS of such densely packed glasses (which permits them to avoid crystallization) depends primarily on the number of Pauling resonating valence bonds  $R$  (e.g., in  $\text{NaCl}$  there is one Pauling resonating valence bond/ion, although the coordination numbers are six) [29]. The value of  $R$  for Cu in the cuprates is 2. There are similarly obvious rules for  $R$  for other elements (including those with mixed valence, Tl,  $+1$ ,  $+3$ , and Bi,  $+3$ ,  $+5$ ) [30], and of course,  $R(\text{O}) = 2$ , while  $e/a(\text{O}) = 6$ . The conclusion (also taking into account many results for network glasses) is that while  $R$  is a good coordinate for ionic and covalent molecules, it is a very accurate configuration coordinate for strongly disordered networks, even in the presence of lone pair interactions [28]. The valence bonds that one is counting determine the MMS of the network, while the dopants provide the metallic carriers. Of course, in metallic superconductors,  $e/a$  is the relevant chemical factor, so by replacing  $e/a$  with  $R$ , we have not only identified the central difference between metallic and ceramic superconductivity, but we have done so quantitatively.

#### 5. MMS and Coarse Graining

The question remains of how valence or  $R$  is to be averaged over the many atoms in the unit cell: should the rigid metallic planes be weighted more heavily, or the soft layers between them, where the dopants are. Again decades of research on network glasses have shown that the best weighting is the simplest, that is, equal weighting ( $\langle R \rangle$ ) for all atoms

provides the best description of glass-forming ability and the glass transition, because the overall network is mechanically marginally stable (MMS). As discussed earlier, shell-model calculations [31] of phonon spectra in HTSC are generally unable to predict very soft modes, especially those associated with dopants. Quite revealing is the fact that the fitted effective charges for “soft layer” rare earth cations in shell models of LSCO and YBCO phonon spectra derived from neutron scattering were inexplicably *negative* [32]. Neutron scattering has successfully identified Jahn-Teller distortions associated with high-frequency optical modes, and these set the overall scale [30] for  $T_c^{\max}$ , but it is unable to resolve very soft modes [33].

Although MMS is concealed from experiment and theory in HTSC, the simple and universal assumption of equal weighting of all atoms is fully effective. In retrospect, it is easy to see why equal weighting works so well. HTSC exhibits nanodomains spanning  $\sim 10$  unit cells [16, 17], so the soft modes implied by MMS are spread not only over a single unit cell, but in fact over many unit cells (coarse graining), all of which are sufficiently disordered by dopants and pseudogap instabilities that equal weighting within a unit cell becomes almost as accurate as in fully homogeneous network glasses.

Guided by these considerations, which are general, specific, simple, and free of adjustable parameters, we plotted  $T_c^{\max}(\langle R \rangle)$ , with the results shown in Figure 3. It is important to understand how the predictive dotted line was drawn. First, note that all the HTSC with  $R \geq 2$  are well known, and in fact were discovered chronologically with decreasing  $\langle R \rangle$ , starting with  $\text{Ba}_{1-x}\text{K}_x\text{BiO}_3$  (a cubic perovskite, with a phase diagram quite different from the cuprates, and only hints of an emerging nanodomain structure [30], but it still fits nicely on the smooth dotted line). Secondly, if one knows only the ascending curve for  $\langle R \rangle \geq 2$ , one might reasonably extrapolate it to very large  $T_c^{\max}(\langle R \rangle)$  for  $\langle R \rangle < 2$ . When the predictive dotted line was drawn initially, only one point was known for  $\langle R \rangle < 2$  that for the oxyhalide  $\text{NCCOC}(\text{Na}_x\text{Ca}_{2-x-y}\text{CuO}_2\text{Cl}_2)$  with Na (not O!) dopants, an apical Cl (not O!) and  $T_c \sim 40$  K. There is no phenomenological reason to suppose that this value of  $T_c$  represents a realization of  $T_c^{\max}$ , that is, that  $T_c \sim 40$  K =  $T_c^{\max}$ . Nevertheless, one can note that  $T_c(\text{NCCOC})$  is approximately the mirror image of  $T_c(\text{LSCO})$  about  $\langle R \rangle = 2$ , so on the basis of percolative symmetry it seemed natural to draw the predictive line as shown. Later,  $\text{Ba}_2\text{Ca}_2\text{Cu}_3\text{O}_6\text{F}_2$  (apical F) was reported to have  $T_c = 55$  K, which is comfortably below  $T_c^{\max} = 78$  K on the predicted line, so this point was added to the published Figure [30] as its first “predictive” success, assuming that this value still did not represent a realization of  $T_c^{\max}$ . Finally postdated improved sample preparation [34] gave  $T_c(\text{BCCOF}) = 76$  K, reducing the discrepancy between the predicted value of  $T_c^{\max}$  and experimental value of  $T_c$  for BCCOF from 23 K to 2 K. This is a very convincing second (and predated) predictive theoretical success, especially considering that neither NCCOC nor BCCOF contain apical O, which means that the homology is unexpectedly general. Of course, further large increases in  $T_c(\text{NCCOC}$  or  $\text{BCCOF})$  by 20 K would be sufficient to falsify the theory, although even then

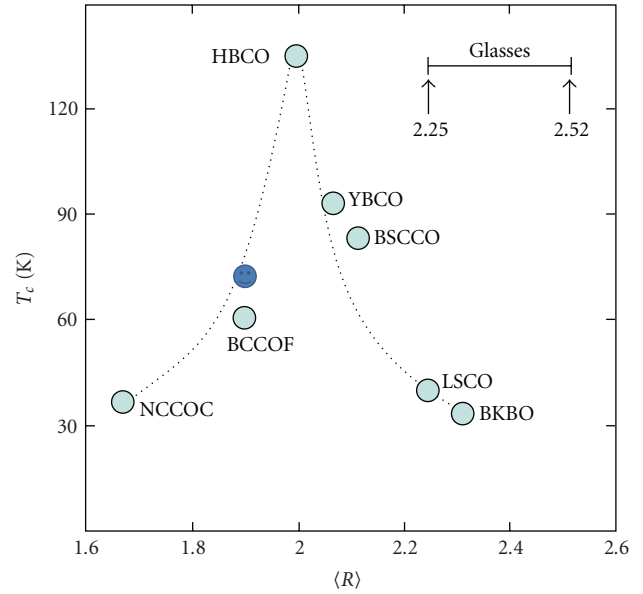


FIGURE 2: The master function for HTSC,  $T_c^{\max}(\langle R \rangle)$ , provides a least upper bound for bulk layered superconductors, and is believed to be accurate to 10 K. This function is based on the zigzag percolative model for self-organized HTSC dopant networks [28, 30]. The original figure [30] has been modified to include the most recent data [34] on BCCOF; the acronyms are as in [30]. Covalent network glasses [20] are centered on  $\langle R \rangle = 2.4$ , but the stabilizing effect of the rigid  $\text{CuO}_2$  planes shifts the cuprate center to  $\langle R \rangle = 2$ .

it would be better than the only available alternatives which predict  $T_c^{\max}$  higher by as much as 200 K.

The analysis given here is based on minimal logical and statistical considerations, but the results were actually derived from a physical model that the author first proposed 20 years ago [35]. The zigzag self-organized percolative model (ZZIP) has many attractive features: for instance, the energy scale for  $T_c^{\max}$ , which is merely set empirically in Figure 3, is apparently set for  $\langle R \rangle \geq 2$  by the Jahn-Teller shift in the (100) LO phonon energy (there are no oxyhalide data for  $\langle R \rangle < 2$ ), as shown by Figure 3(b) in [30], which suggests a close dopant-mediated relation between the soft acoustic and optic modes. Substantial evidence shows that percolative filaments are formed at high temperatures and account for many features of transport up to at least 300 K [30]. At present there exists no alternative model that can predict  $T_c^{\max}$  in HTSC.

## 6. Cuprate-Like Superconductivity

There are several new marginally stable families of layered crystals that exhibit many similarities to the cuprates: there are many atoms per unit cell, with displacive lattice instabilities, vicinal antiferromagnetic phases, and so forth, including ionic  $\text{Li}_x\text{ZrNCl}$  [36] and the rapidly growing covalent superfamily based on FeAs, such as  $\text{LaFeAsO}_{1-x}\text{F}_x$  [37]. Are these similarities accidental, or can the percolative cuprate

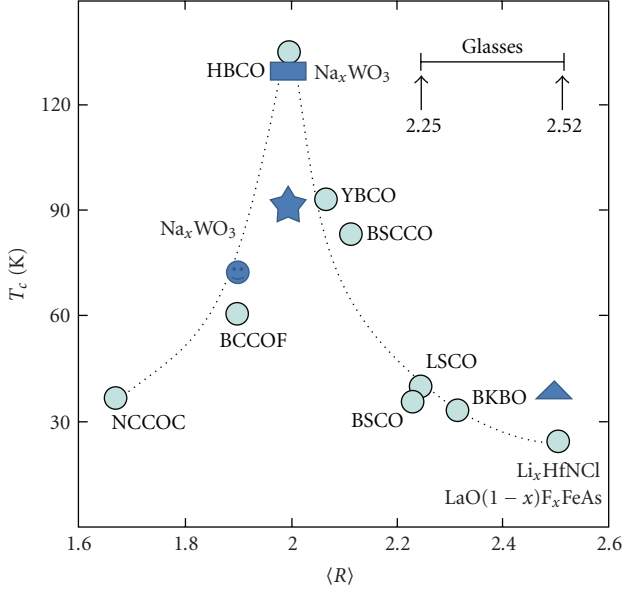


FIGURE 3: As in Figure 2, but now the noncuprate data have been added, so the Figure has become rather “busy.”

ionic superfamily model explain HTSC in these noncuprate-layered materials *with no additional assumptions*? In fact, the percolative model *easily* explains the similarities, by bringing these new materials into the general framework of self-organized networks. This has already been done for ionic  $\text{Li}_x(\text{Zr,Hf})\text{NCl}$  ( $T_c \sim 15\text{K}–25\text{K}$ ) [38], so now a similar discussion is given here for the covalent  $\text{LaFeAsO}_{1-x}\text{F}_x$  superfamily ( $T_c \sim 26\text{K}–43\text{K}$ ) [37], which is much larger and the subject of hundreds of recent studies.

Because these materials are mechanically only marginally stable, they are strongly disordered when doped, and are generally far from optimized with respect to HTSC. Marginal lattice stability determines the overall scale for  $T_c$ , as the phonon energy shift measured by neutron scattering associated with Jahn-Teller doubling of the unit cell of LO phonons correlates linearly with  $T_c^{\text{max}}$  in the cuprates [30]; of course, spin and antiferromagnetic exchange show no such scaling, and are irrelevant. The least upper bound for  $T_c$ , called  $T_c^{\text{max}}$ , has a strongly percolative character, as it peaks exponentially at  $\langle R \rangle = 2$ , where  $\langle R \rangle$  is the average valence number of all the atoms [28, 30].

The master function  $T_c^{\text{max}}(\langle R \rangle)$  is shown in Figure 2 for the cuprates; the peak at  $\langle R \rangle = 2$  has a cut-off exponential character. The point for ionic  $\text{Li}_x\text{HfNCl}$  was discussed previously [38], and we now discuss the points for the  $\text{LaFeAsO}_{1-x}\text{F}_x$  family ( $T_c \sim 26\text{K}–43\text{K}$ ). Here  $R(\text{Fe}) = 2$ , just as for Cu, because Fe is in a  $2+$  valence state [39, 40] in a virtual crystal model. This band model also shows the beginnings of self-organization, in that the average height  $h$  of As is found to shift with  $x$  [41]; had the calculation been carried out with a large supercell centered on an F dopant?,  $h(\text{As})$  would have varied with distance from F. This virtual crystal relaxation effect alone shows that  $N(E_F)$  varies slowly and smoothly with doping (which means that

the apparent Fermi planar line becomes very broad near a critical point), and hence effective medium models cannot explain HTSC. However, from this one should not conclude that electron-phonon interactions do not cause HTSC, as these interactions (not superexchange!) do set the overall energy scale [30] through Jahn-Teller distortions on and near percolative paths, and these distortions are especially large near dopants.

When one calculates  $\langle R \rangle$  for undoped  $\text{LaFeAsO}$ , one obtains  $\langle R \rangle = 2.5$ , which places  $\text{LaFeAsO}_{1-x}\text{F}_x$  ( $T_c = 26\text{K}$ ) very close to  $\text{Li}_x\text{ZrNCl}$  on the master curve of Figure 2, so that the theory appears to succeed effortlessly. However,  $T_c$  is maximized at  $43\text{K}$  for pressures near  $4\text{GPa}$  [42], an increase of  $60\%$ , which is much more than is seen in cuprates, and exceeds the upper bound of the master curve. Does this falsify the theory? No, because the equilibrium cuprate master function  $T_c^{\text{max}}(\langle R \rangle)$  remains valid for the  $\text{Li}_x\text{ZrNCl}$  and  $\text{LaFeAsO}_{1-x}\text{F}_x$  families, but the pressure dependence in the latter family is larger than in the cuprates, as Fe-As bonding is more covalent than largely ionic Cu–O bonding [42], due to the larger Pauling electronegativity  $X$  differences ( $X(\text{Fe}) = 1.8$ ,  $X(\text{As}) = 2.0$ ,  $X(\text{Cu}) = 1.9$ ,  $X(\text{O}) = 3.5$ ) in the cuprates. Covalent bonding also seems to limit the range of  $\langle R \rangle$  for which stable crystals can form; thus the smallest value of  $\langle R \rangle$  for the FeAs family seems to be near  $2.3$  in  $(\text{Ba}_{0.55}\text{K}_{0.45})\text{Fe}_2\text{As}_2$  [43].

It is striking that this covalent FeAs stability range of  $2.3 < \langle R \rangle < 2.5$  is very similar to the range  $2.25 < \langle R \rangle < 2.52$  for stress-free covalent glasses previously shown [28, 30] in Figure 2. (Again this is a rather remarkably successful predated prediction.) Thus the covalent instabilities of the host lattice, especially the reduced rigidity of the FeAs plane relative to the  $\text{CuO}_2$  plane, are the factor that shifts the value of  $\langle R \rangle$  at which  $T_c^{\text{max}}$  peaks from  $\langle R \rangle_{\text{max}} = 2.0$  in the ionic cuprates to  $\langle R \rangle_{\text{max}} = 2.5$  in the  $\text{LaFeAsO}_{1-x}\text{F}_x$  family. In both cases,

$$\langle R \rangle_{\text{max}} = R(\text{metallic plane}), \quad (1)$$

so that the average connectivity of the undoped insulating plane is matched to that of the metallic plane. Apparently this hidden topological layer symmetry (1) determines the maximum electron-phonon interactions in marginally stable layered pseudoperovskites.

## 7. Surfaces and Interfaces

The percolative master function  $T_c^{\text{max}}(\langle R \rangle)$  is determined from bulk data on layered crystals, so one can ask whether or not this function can explain trends in  $T_c^{\text{max}}$  at surfaces and layer interfaces. Determining  $\langle R \rangle$  at surfaces and interfaces is much more difficult than in the bulk, where it is natural to average  $R$  over all atoms, as the self-organized structure is marginally stable overall, and soft modes that are critically bound to percolative superconductive paths should have long wave lengths, as  $T_c^{\text{max}}$  is still small compared to the melting temperature. However, in layered thin crystalline films with epitaxial interfaces or in clusters at doped free surfaces, similar percolative behavior is expected. This turns out to be

the case for the  $\text{La}_2\text{CuO}_4\text{-La}_{2-x}\text{Sr}_x\text{CuO}_4$  ( $x = 0.45$ ) interface, where  $T_c \sim 50$  K, after enhancement by exposure to ozone from  $\sim 30$  K [44]. The giant ozone enhancement is readily explained by the addition of oxygen dopants, absorbed by  $\text{La}_2\text{CuO}_4$  to give  $\text{La}_2\text{CuO}_{4+\delta}$  with  $\delta \sim 0.15$ . However, the maximum  $T_c$  obtainable in this way is  $\sim 30$  K for both layers separately, apparently producing a mystery.

Let us look at this mystery with the master curve:  $\langle R \rangle = 16/7$  in LCO = 2.28,  $= (16 - x)/7$  in  $\text{La}_{(2-x)}\text{Sr}_x\text{CuO}_4$ , so with  $x$  (or  $\delta$ ) = 0.15,  $\langle R \rangle = 2.26$ , and with  $x = 0.45$ ,  $\langle R \rangle = 2.22$ . This would give a decrease in  $\langle R \rangle$  between  $x = 0.15$  and  $x = 0.45$  of 0.04, and so we get something like  $T_c = 35 \text{ K} + (0.04/0.28) (150 - 35) \text{ K} = 50 \text{ K}$ . Of course, this is just a plausible guess at the interfacial structure, but the master function has given the trend correctly, not only qualitatively but also semiquantitatively (something no other theory has been able to do: virtual crystal theories predict  $T_c < 1$  K, from which it has often been erroneously concluded that electron-phonon interactions do not cause HTSC!).

Now we turn to a much more difficult problem, for which the data base is small, but still robust: a surface monolayer of  $\text{A}_x\text{WO}_3$ , where  $A$  is an alkali metal (Na [45] or Cs[46]). While bulk  $\text{Na}_x\text{WO}_3$  exhibits superconductivity only near 1 K, here for Na superconductivity appears around 100 K; for Cs there are two phase transitions, a bulk one with lower  $T_c$  at higher doping, and a re-entrant percolative one with higher  $T_c$  at lower doping. Moreover, Na- and Li- (but not K-) doped surfaces of nanoclusters of  $\text{WO}_3$  embedded in a variety of nanoporous hosts (carbon inverse opal, carbon nanotube paper, or platinum sponge) show diamagnetic anomalies with an onset  $T$  of 130 K [47]. Note that  $\text{WO}_3$  (with its simpler unit cell, subject only to Jahn-Teller distortions) itself is nonmagnetic, as is another HTSC(BKBO, (Ba,K)BiO<sub>3</sub>).

These data can be combined with the master function  $T_c^{\max}(\langle R \rangle)$  to construct a model of percolative self-organization at surfaces. In bulk  $\text{WO}_3$  the valence of  $W$  is 6, and  $\langle R \rangle = 3.0$ , far to the right on the master function  $T_c^{\max}(\langle R \rangle)$ , where  $T_c^{\max}(3) < 5$  K. Near the surface the valence of  $W$  could be 2 (just as with Cu in the cuprates, and Fe in the FeAs compounds). To explain  $T_c \sim 130$  K, one must assume  $\langle R \rangle = 2$ . A percolative  $\text{W}_s\text{O}$  surface chain then has  $\langle R \rangle = 2$ . These surface chains are entropically broken into stress-relieving fragments. Intercalated Li or Na ions connect the chain fragments, thereby increasing their conductivity and their screening of internal ionic fields, just as in the bulk percolative model. The embedded clusters are not connected, so the result is “localized nonpercolative superconductivity” still with  $\langle R \rangle = 2$  [48]. In the free surface case [45, 46], thermal fluctuations disrupt superconductivity above 100 K. Both of these  $\langle R \rangle = 2$  points are shown in Figure 2. Considering the rapid progress in nanoscience, it may be possible to obtain similar pairs of percolative and cluster points for other HTSC.

Finally, self-organized percolation enables us to understand how cointercalation of organic molecules  $M$  with Li in ionic  $\text{Li}_x\text{M}_y\text{HfNCl}$  can uniformly enhance  $T_c(x)$  by up to 30%, over a wide range  $0.15 \leq x \leq 0.50$ , even though the average interlayer spacing  $d$  varies by as much as 30% [49]. The intercalated organic molecules reduce the dielectric

screening of Li-centered electron-phonon interactions by other Li ions. Note that the nominal concentration  $x$  of the Li ions may refer only to patches that strongly diffract; the superconductive paths may pass through patches with a concentration  $x_0$  different from  $x$ , explaining why  $T_c$  is apparently constant over a wide range of  $x$ . Only a few percolative paths are required to exclude Abrikosov vortices and produce HTSC; this is why  $T_c$  often increases when the average density of states  $N(E_F)$  decreases (e.g., in the cuprates compared to the covalent FeAs family, or the ionic  $\text{Li}_x\text{M}_y\text{HfNCl}$  family [38]). This is yet another example of the paradoxes generated by attempting to understand a self-organized percolative phase in terms of continuum concepts such as Bloch-wave Fermi surfaces, modulation doping, or plasmon waves. Note that these points have often been made in earlier papers on the topological percolative model, long before any of these new materials were discovered.

## 8. Mapping ZZI Percolative Paths

For most of the last two decades experiment has provided largely circumstantial support for the zigzag interlayer percolative (ZZIP) network model shown in Figure 4, but recently more direct evidence has appeared. The model has two key elements: the dopants, often interstitial oxygen, whose positions are not easily determined, and the zigzag network paths themselves. The zigzag network paths are associated with strong electron-phonon interactions, which are especially strong for interlayer displacements. This has enabled the zig and the zag of the paths to be identified by a spectacular combination of time-resolved electron diffraction [50], for the  $c$ -axis zag component of the paths, and anisotropically strong kinks in quasiparticle dispersion observed by angle-resolved photoemission [51], for the ab planar zig component of the paths. The data show that the  $c$ -axis Cu-O zag component has faster dynamics when the femtosecond pulse probe is polarized along the planar Cu-O zig component, to which it can be coupled through planar Cu-O bond buckling. It is difficult to understand these correlations unless the  $c$ -axis zag component is actually topologically connected to the planar zig component. One might argue that such a connection occurs only at low temperatures, and would be ineffective at the high excitation energies of the electron diffraction experiment, but this is not correct. High-temperature transport data show that the self-organization (hard wiring) of the ZZIP network begins already at annealing temperatures [30]; the results are fully consistent with the zigzag network model discussed in dozens of papers over the last 20 years. There remains one puzzling aspect: anisotropy is observed in both Bi2212 and Bi2223 by ARPES, but only in the former by electron diffraction. The extra layer in the latter would not appear to erase the planar anisotropy, but it is possible that Bi2223 has a high density of stacking faults. Depending on the geometry of the percolative paths, such faults could erase the observed anisotropy by scattering percolative carriers.

While we are on the subject of percolation versus continuum models, it is important to realize that while the presence of self-organized percolative paths introduces

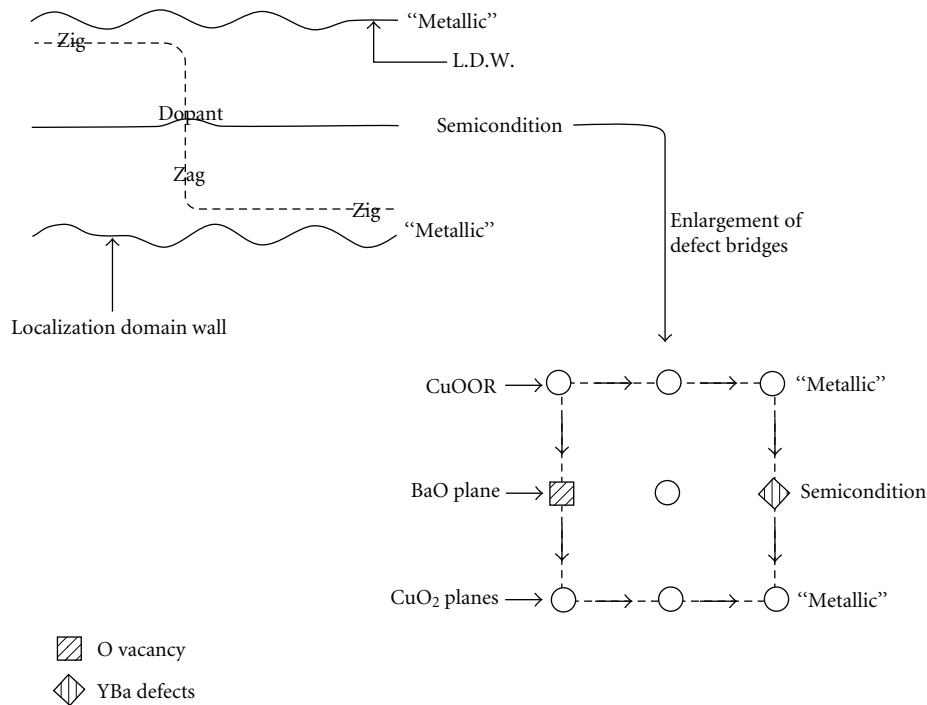


FIGURE 4: The original ZZIP model, reprinted from [35]. Parts of the original ZZIP path are now labeled “zig” or “zag.” In 1989 it was not clear what the interlayer dopants were and they were simply called defects, but it is now clear that they are usually interstitial oxygen atoms, except in  $\text{La}_{2-x}\text{Sr}_x\text{CuO}_4$ , where they are the substitutional Sr ions.

exponential complexity into the Bohmian wave-packet basis states [52] used to form Cooper pairs, it in no way alters the nature of the attractive electron-phonon interactions responsible for forming the pairs. These two points have often been confused, and the failure of continuum plane wave basis states to describe cuprate HTSC has often been used to argue that electron-phonon interactions do not cause HTSC [11]. Because the fraction of carriers involved in percolative paths is small, many negative indications of strong electron-phonon coupling have been found; for example, bulk phonon softening is so small as to be unobservable by neutron scattering at high energies [33]. Therefore it is gratifying that quasiparticle tunneling across a break junction *perpendicular* to the superconducting copper oxide planes showed 11 phonon features that match precisely with Raman spectra [53], decisively showing that HTSC is indeed caused by electron-phonon interactions along the  $c$ -axis, as previously argued from dynamical relaxation experiments [54]. Also the long-expected isotope effect at the phonon kink has been observed by ARPES [55]. The fact that *all* the  $c$ -axis phonon bands appear in the break junction experiment, and not just those associated with the O buckling mode in the  $\text{CuO}_2$  plane [51], strongly supports the present model of zigzag percolative paths in a marginally stable all-atom network. Finally, it is worth stressing that the phonon features that correlate by far the best with  $T_c$  are exactly those of the atoms in the soft insulating layer [56, Figures 11 and 12], as assumed in the zigzag model, and not the atoms in the rigid  $\text{CuO}_2$  layer, as is often wrongly assumed [51].

There is one interesting aspect of the original 1989 ZZIP model that was confirmed experimentally by anomalous X-ray diffraction [57], but the significance of the data was not realized because they were not connected to the theoretical model. Namely, in the model the metallic layer nanodomains are staggered, as this facilitates the construction of filamentary paths that pass through dopants in the nonmetallic layers. The data showed that “in each  $\text{CuO}_2$  bilayer the flat stripes in a first layer are close to the bent stripes in the second layer” from which it was concluded that such a staggered structure “suppresses the electronic coupling between the two adjacent planes”. In the ZZIP model just the opposite is true: the nanodomains are staggered in order to increase the electronic coupling between the two adjacent planes, and this is part of the self-organization of the “hard-wired” filamentary network that is formed at high temperatures (above 300 K), as shown by many normal-state transport anomalies, notably the linearity in  $T$  of the planar resistivity [7], compared to the  $T^2$  dependence characteristic of a Fermi liquid. Of course, in a one-dimensional filament, intrafilamentary scattering always gives such a linear dependence.

A few comments are in order regarding the parabolic form of  $T_c(x)$ . This starts for small  $x$  when the percolation threshold  $x_1$  is reached, and it ends for large  $x = x_2$  when all the isolated percolative paths have lost their separate identities and become metallic bundles. At and above  $x = x_2$  continuum theory becomes valid, and it immediately shows that  $T_c(x)$  for  $x \geq x_2$  is either very small or zero. The reason for this is simple: the charge density is so low that Coulomb

repulsive interactions outweigh attractive electron-phonon interactions, just as they do in metals like Na and Cu itself.

## 9. Single-Layer Cuprates: Mechanically Marginally Unstable (MMU)

The importance of self-organized percolative paths is nicely brought out by the single-layer compound  $\text{HgBa}_2\text{CuO}_{4+\delta}$  [58], which has  $\langle R \rangle = 2$ . This compound has the largest  $T_c = 95$  K of any single-layer cuprate, but it does not appear in our figures because it is isovalent to  $\text{HBCO}(\text{HgBa}_2\text{Ca}_2\text{Cu}_3\text{O}_8)$ , which also has  $\langle R \rangle = 2$  and  $T_c = T_c^{\max} = 135$  K. There are several interesting aspects to  $\text{HgBa}_2\text{CuO}_{4+\delta}$ : the Cu–O bond lengths (including the apical O) are expanded by the Ba ions (which act as spacers), and the soft Hg layer is strongly disordered (as expected in the zigzag model). If superconductivity were confined to the  $\text{CuO}_2$  layer [21] and the apical O [22, 23], this expansion should have greatly depressed  $T_c$  (because of strengthened Coulomb or ionic interactions), but the contrary occurred. In the 1989 zigzag model [35] the  $\text{CuO}_2$  layer functions as an electrical connector, while the strong e-p interactions occur in the soft, strongly disordered Hg layer, so the relatively large  $T_c = 95$  K is a natural feature of the model. The coupling of HTSC to lattice disorder (not order!) is directly and elegantly shown in [59]. Superconductive formation and overlap of zigzag percolative filamentary arrays can increase lattice disorder. When the  $\text{CuO}_2$  layers were under compressive strain (so that the critical axial zag paths were under tensile strain, and thus more flexible), this is what was observed as  $T$  decreased well below  $T_c$ , where the superconductive energy is largest. Very similar effects appear in the FeAs family as well [59]; a more extensive percolative discussion will be given elsewhere.

None of the single-layer cuprates produces a  $T_c^{\max}(\langle R \rangle)$  for any  $\langle R \rangle$ . However, the single-layer cuprates form an interesting homology family in their own right; in contrast to Section 5, they can be described as mechanically marginally unstable (MMU). Theorists have long known that individual planes readily buckle. When this happens in the cuprates, the pseudogap charge density wave regions expand, the metallic regions contract, and  $n_s$  (the density of superconductive carriers) rapidly drops, and with it  $T_c$  [30]. Thus another factor comes into play, to stabilize the overall MMU network, and retain larger metallic regions. This factor is the purely ionic static Madelung potential (the rigid ion model omits polarization or screening energies, which are important dynamically, but less important statically) [60]. Within the restricted context of single-layer cuprates only, it appears that it is this factor that dominates  $T_c$ . Note, however, that the single-layer cuprate family never contributes to  $T_c^{\max}$ , and therefore this family should be regarded as nonoptimally packed ceramic superconductors (and, therefore, more in need of stabilization). Moreover, the stabilizing space-filling (buttressing) effect of the large Ba ions in  $\text{HgBa}_2\text{CuO}_{4+\delta}$  is not accounted for by the Madelung potential, and here  $T_c$  lies well above the Madelung trend line for the other single-layer cuprates [60]. This is further evidence that the single-layer

MMU cuprates form a different homology family from the multilayer MMS family.

Among the (relatively) low  $T_c$  ceramic superconductors,  $\text{Bi}_2\text{Sr}_{2-x}\text{La}_x\text{CuO}_{6+\delta}$  has attracted much interest because here it appears that the pseudogap and superconductive gap are best separated [61, 62] relative to other micaceous multilayer cuprates. The reason for this is clear: not only is this material MMU, but also the stabilizing ionic factors are weak, reducing the density of superconductive filaments and filament-filament interactions, and producing a more homogeneous superconductive gap that is well separated from a much larger pseudogap.

What else can we learn from the single-layer cuprate MMU family?  $(\text{La}, \text{Sr})_2\text{CuO}_4$  is a member of this family, and it also falls on the master function  $T_c^{\max}(\langle R \rangle)$  of MMS superconductors, and so is also an optimally packed ceramic zigzag percolative superconductor. Which factor (MMS or MMU) is more important at the  $\text{La}_2\text{CuO}_4\text{--La}_{2-x}\text{Sr}_x\text{CuO}_4$  ( $x = 0.45$ ) interface? In the MMU case, we know that the Madelung potential that stabilizes  $\text{CuO}_2$  planes decreases as  $x$  increases, in accordance with the fact that  $T_c(\text{La}_{2-x}\text{Sr}_x\text{CuO}_4) = 0$  ( $x = 0.45$ ). However, the Madelung potential at the  $\text{La}_2\text{CuO}_4\text{--La}_{2-x}\text{Sr}_x\text{CuO}_4$  ( $x = 0.45$ ) interface can be estimated to be that of  $\text{La}_{2-x}\text{Sr}_x\text{CuO}_4$  ( $x = 0.22$ ), so that  $T_c$  should have decreased from 38 K at  $x = 0.15$  to  $\sim 30$  K. In fact,  $T_c$  increased from 30 K to 50 K, which is what the master function  $T_c^{\max}(\langle R \rangle)$  of MMS superconductors predicts (Section 7). At optimized interfaces, percolative effects dominate, which is what happened with  $\text{A}_x\text{WO}_3$  surface layers (Section 7).

## 10. Conclusions

The present review shows that the original ZZIP model [35, Figure 4] continues to provide an excellent universal guide to the phenomenology of ceramic superconductors. Initially, it explained the large qualitative differences between HTSC in cubic and layered ceramics (Figure 1). It is the only theoretical model so far that has been able predictively to predict  $T_c(\text{BCCOF}) \sim 75$  K, but it also quantitatively predicts superconductive  $T_c$ , even for noncuprate HTSC, starting only from the cuprates, which no other theoretical model has done. The self-organized marginally stable percolative model unexpectedly transcends conventional chemistry (the materials covered include cuprates, tungstates, zirconates, ferrics, arsenides, bismates, oxides, halides, Li-, Na-, Cs-, O-, F-, Cl-doped, and the structures include bulk, interface, and nanocluster surfaces); so far as I know, there is no other example in solid phase transitions where theory of any kind (continuum or otherwise) can predict transition temperatures with such universal success. The results make an overwhelming case for a new homology class of glassy network doped superconductors, separate and distinct from continuum metallic superconductors.

As noted previously [30], the theory predicts  $T_c^{\max}$  with an accuracy of 10 K, compared to a melting point of order  $10^3$  K, which is an accuracy of 1%. However, this success contains a subtle aspect, which is that because HTSC is concerned with marginally stable lattices, it is important

to build this theoretical mechanism into the analysis from the outset (Section 4). This has been done by mapping  $T_c^{\max}(Y)$ , and examining different choices of  $Y$ : only  $Y = R$  gives the apparently exponentially resonant peak that is strongly suggestive of percolation.

The theoretical debates stimulated by HTSC have lasted for more than 20 years, and have often severely tried the patience of the physics community. Were they worth it? I believe they were and still are. The basic issue was, and still is, whether it is legitimate to treat a discrete, exponentially complex problem involving strongly disordered, self-organized materials, at the cutting edge of materials science, with the same simplistic continuum methods (including polynomial Hamiltonian algebra and/or Landau order parameters) that students have learned work so well for toy models and some simple crystalline solids. The experimental evidence strongly suggests that this discrete, exponentially complex problem can be solved by focusing on its essential topological features, derived from the network structures of ceramic HTSC [29].

Global topology is still something of an oddity among mathematical disciplines (it is very young, dating from  $\sim 1877$ ). It is standard among computer scientists, but it is unfamiliar to most chemists and physicists. It is ideally suited to treat complexity problems, including many far afield from science, such as economics [63, 64] and difficult problems in biology, such as the network of protein-protein interactions [65]; for pioneering research in NPC computer algorithms addressing exponential complexity  $R. M. Karp$  was awarded the 2008 Kyoto Prize. It also transcends the otherwise theoretically insuperable barriers of exponentially complex (NPC, nonpolynomial complete), aperiodic self-organization commonly encountered not only in HTSC but also in protein science [66, 67]. From sandpiles to proteins, it appears that the best documented examples of self-organized criticality (SOC) are found in network glasses [29] and HTSC [68].

*Postscript.* The (by now very old) debate over whether HTSC is caused by conventional electron-phonon interactions, or by exotic electron-spin interactions, continues even for the cuprates [69] although it would appear from Raman scattering experiments to have been settled conclusively in favor of phonons [53, 56, 70]. In particular, infrared optical spectra [69] contain a mixture of overlapping superconductive and pseudogap (or Jahn-Teller) features that are not easily separated, even in optimally doped samples. As the infrared spectra are dominated by electric dipole transitions, it is difficult to believe that any of the “coincidences” between isolated neutron magnetic resonances and fictive single optical resonances used to fit [69] these entangled gap spectra are significant, especially as results internally consistent with gap phase diagrams measured by other methods do not appear to have been obtained for underdoped and optimally doped phases. Simpler and better polaronic fits show no correlations between midinfrared peak positions and  $T_c$  [71].

These infrared data merely reinforce the large qualitative difference between layered ceramics and cubic  $Ba_{1-x}K_xBiO_3$  shown also in the phase diagrams of Figure 1; the latter has a normal BCS-type infrared spectrum with  $E_g/k T_c = 3.2(3)$

[72]. There have been many studies of the metal-insulator transition at  $x = 0.3$  in  $Ba_{1-x}K_xBiO_3$  and these have been interpreted in terms of bipolaron formation [73]. However, a more appealing interpretation of the  $Ba_{1-x}K_xBiO_3$  metal-insulator transition would be the onset of percolative metallic patches, as the “bipolaronic” infrared dopant peak appears to merge with the CDW band edge at  $x = 0.3$ , where  $T_c$  is largest. In other words, the two lattice deformations merge to form nonfilamentary continuum superconductive metallic regions in a first order metal-insulator transition.

Application of “first principle” continuum theories to the FeAs family has uniformly led to the conclusion that electron-phonon interactions cannot cause HTSC in this family [39–41, 74, 75]; similar conclusions were reached earlier for the cuprates [15]. The correct conclusion is that continuum (ideal lattice) approximations are invalid because of strong disorder and nanoscale phase separation [76–78], as well as the much more subtle exponentially complex consequences of zigzag self-organized percolation, ZZIP (Section 8). The combination of electron-phonon interactions and ionicity readily explains [79] how superconductivity in the covalent (noncentral interatomic forces) FeAs family can be much more isotropic than in the cuprates [80], yet still retain a lowered dimensionality. Strong disorder explains “hump-dip” pseudogap tunneling features in terms of charge density waves [81].

Probably the most accurate ceramic HTSC phase diagrams are those obtained by studying the planar resistivity  $\square_{ab}(T)$ , which is most linear in  $T$  at and near optimal doping [30, 82]. The dopant network-forming interactions, although individually weak, are cumulatively very strong because the dielectric energy gained by screening internal electric fields increases as the network conductivity increases due to dopant self-organization. The maximization of the  $T$ -linearity of  $\square_{ab}(T)$  near optimal doping [30, 82] was the first normal-state transport anomaly to be discovered, but in the intervening 20 years theory has been unable to derive this maximization, and it seems unlikely that this extremal will ever be derived using conventional polynomial methods (e.g., Landau Fermi liquid theory predicts a  $T^2$  dependence). This situation is typical of exponentially complex problems which are characteristic of networks, but it can be repaired by carefully designed experiments.

In ceramic HTSC self-organization effects manifest themselves by a sharpening of properties characteristic of networks. An obvious and trivial example of such sharpening is the narrowing of the superconductive transition itself, which can be promoted by annealing; this is a small effect for traditional metallic superconductors, but a large effect in ceramic HTSC. If the maximization of the  $T$ -linearity of  $\square_{ab}(T)$  near optimal doping is indeed caused by network self-organization, then that should be manifested by an increase in  $T$ -linearity upon annealing. Studies of redistribution of oxygen at a fixed oxygen content in the chain layers of slightly underdoped YBCO with a nonlinear  $\square_{ab}(T)$  showed [83] that annealing for 2–8 hours at 400–420 K does lead to an increase of  $T_c$  by about 1 K and a reduction of the nonlinear component in  $\square_{ab}(T)$  by  $\sim 10$ –15% just above  $T_c$ .

The classic work of [82] has recently been extended to high magnetic fields well above  $T_c$ , with spectacular results [84]. It is found that the  $\square_{ab}(T)$  regime which is most linear in  $T$  occurs in  $\text{La}_{2-x}\text{Sr}_x\text{CuO}_4$  at  $x = x_c = 0.185(5)$ , and that this linear regime extends at fixed  $x$  vertically all the way from  $T = 0$  right up to the highest  $T$  studied (200 K). This result is inexplicable if one thinks of  $(x, T) = (x_c, 0)$  as a “quantum critical point,” but it is perfectly understandable in the context of a hard-wired ZZIP network, formed at the annealing temperature [30]. In fact, one can go further: the vertical linear  $T$  regime is shaped like an hour glass, wide at  $T = 0$  and  $T = 200$  K, and narrow at  $T \sim 100$  K. This narrowing is due to the formation of pseudogap islands, which requires a reformation of the nanodomain network at low  $T$ , into a doubly percolative network, with two kinds of dopants [30].

Naturally, percolative conductive paths are phase-sensitive, and when this aspect is combined with the effects of long-range conductive screening of internal electric fields, it is easier to understand why descriptions of disorder using functions dependent on amplitudes alone (such as the participation ratio) are insufficient to describe filamentary self-organization [85]. Finally, it is worth mentioning that the philosophy employed here in the search for a satisfactory percolative solution to this exponentially complex glassy network problem [29] can be justified (after the fact of its success) not only heuristically but also by formal Boolean algebra [86]. This algebra shows that the determining factor in fixing the properties of exponentially complex systems is their topology, not their geometry [87, 88]. Of course, topology is a characteristic feature of networks, especially in strongly disordered layered structures, that is absent from continuum (ideal lattice) models.

## Acknowledgment

I am grateful to Professor T. H. Geballe for stimulating my interest in MMU ceramic cuprate superconductors.

## References

- [1] K. A. Brueckner, T. Soda, P. W. Anderson, and P. Morel, “Level structure of nuclear matter and liquid  $\text{He}^3$ ,” *Physical Review*, vol. 118, no. 5, pp. 1442–1446, 1960.
- [2] R. C. Richardson, “The Pomeranchuk effect,” *Reviews of Modern Physics*, vol. 69, no. 3, pp. 683–690, 1997.
- [3] K. J. Chang, M. M. Dacorogna, M. L. Cohen, J. M. Mignot, G. Chouteau, and G. Martinez, “Superconductivity in high-pressure metallic phases of Si,” *Physical Review Letters*, vol. 54, no. 21, pp. 2375–2378, 1985.
- [4] A. Y. Liu, I. I. Mazin, and J. Kortus, “Beyond Eliashberg superconductivity in  $\text{MgB}_2$ : anharmonicity, two-phonon scattering, and multiple gaps,” *Physical Review Letters*, vol. 87, no. 8, Article ID 087005, 4 pages, 2001.
- [5] J. E. Moussa and M. L. Cohen, “Constraints on  $T_c$  for superconductivity in heavily boron-doped diamond,” *Physical Review B*, vol. 77, no. 6, Article ID 064518, 2008.
- [6] C. Knight, S. J. Singer, J.-L. Kuo, T. K. Hirsch, L. Ojamäe, and M. L. Klein, “Hydrogen bond topology and the ice VII/VIII and Ih/XI proton ordering phase transitions,” *Physical Review E*, vol. 73, no. 5, Article ID 056113, 2006.
- [7] D. G. Schlom, L.-Q. Chen, C.-B. Eom, K. M. Rabe, S. K. Streiffer, and J.-M. Triscone, “Strain tuning of ferroelectric thin films,” *Annual Review of Materials Research*, vol. 37, pp. 589–626, 2007.
- [8] E. Şaşoğlu, L. M. Sandratskii, P. Bruno, and I. Galanakis, “Exchange interactions and temperature dependence of magnetization in half-metallic Heusler alloys,” *Physical Review B*, vol. 72, Article ID 184415, 11 pages, 2005.
- [9] J. C. Phillips, *Physics of High- $T_c$  Superconductors*, Academic Press, Boston, Mass, USA, 1989.
- [10] P. W. Anderson, “The resonating valence bond state in  $\text{La}_2\text{CuO}_4$  and superconductivity,” *Science*, vol. 235, no. 4793, pp. 1196–1198, 1987.
- [11] P. W. Anderson, P. A. Lee, M. Randeria, T. M. Rice, N. Trivedi, and F. C. Zhang, “The physics behind high-temperature superconducting cuprates: the ‘plain vanilla’ version of RVB,” *Journal of Physics: Condensed Matter*, vol. 16, no. 24, pp. R755–R769, 2004.
- [12] A. Alexandrov and J. Ranninger, “Bipolaronic superconductivity,” *Physical Review B*, vol. 24, no. 3, pp. 1164–1169, 1981.
- [13] A. S. Alexandrov and N. F. Mott, “Bipolarons,” *Reports on Progress in Physics*, vol. 57, no. 12, pp. 1197–1288, 1994.
- [14] J. C. Phillips, “Giant defect-enhanced electron-phonon interactions in ternary copper oxide superconductors,” *Physical Review Letters*, vol. 59, no. 16, pp. 1856–1859, 1987.
- [15] F. Giustino, M. L. Cohen, and S. G. Louie, “Small phonon contribution to the photoemission kink in the copper oxide superconductors,” *Nature*, vol. 452, no. 7190, pp. 975–978, 2008.
- [16] J. C. Phillips and J. Jung, “Nanodomain structure and function of high-temperature superconductors,” *Philosophical Magazine B*, vol. 81, no. 8, pp. 745–756, 2001.
- [17] K. McElroy, J. Lee, J. A. Slezak, et al., “Atomic-scale sources and mechanism of nanoscale electronic disorder in  $\text{Bi}_2\text{Sr}_2\text{CaCu}_2\text{O}_{8+\delta}$ ,” *Science*, vol. 309, no. 5737, pp. 1048–1052, 2005.
- [18] J. E. Moussa and M. L. Cohen, “Using molecular fragments to estimate electron-phonon coupling and possible superconductivity in covalent materials,” *Physical Review B*, vol. 78, no. 6, Article ID 064502, 2008.
- [19] K. M. Rabe, J. C. Phillips, P. Villars, and I. D. Brown, “Global multinary structural chemistry of stable quasicrystals, high- $T_c$  ferroelectrics, and high- $T_c$  superconductors,” *Physical Review B*, vol. 45, no. 14, pp. 7650–7676, 1992.
- [20] A. J. Leggett, “What do we know about high  $T_c$ ?” *Nature Physics*, vol. 2, no. 3, pp. 134–136, 2006.
- [21] H. Kamimura and M. Eto, “ $^1\text{A}_{1g}$  to  $^3\text{B}_{1g}$  conversion at the onset of superconductivity in  $\text{La}_{2-x}\text{Sr}_x\text{CuO}_4$  due to the apical oxygen effect,” *Journal of the Physical Society of Japan*, vol. 59, no. 9, pp. 3053–3056, 1990.
- [22] C. D. Castro, L. F. Feiner, and M. Grilli, “Symmetry of hole states in superconducting oxides: correlation with  $T_c$ ,” *Physical Review Letters*, vol. 66, no. 24, pp. 3209–3212, 1991.
- [23] Y. Ohta, T. Tohyama, and S. Maekawa, “Apex oxygen and critical temperature in copper oxide superconductors: universal correlation with the stability of local singlets,” *Physical Review B*, vol. 43, no. 4, pp. 2968–2982, 1991.
- [24] J. C. Phillips, “Coherent resonant pinning, oxygen ordering, and high-temperature superconductivity in the multilayer cuprates,” *Physical Review Letters*, vol. 72, no. 24, pp. 3863–3866, 1994.

- [25] H. Oesterreicher, "Plane isolation model for superconducting  $T_c$  prediction using an 'parent-calibration' obtained for  $\text{YBa}_2\text{CuCu}_2\text{O}_y$  and applied to other model systems," *Solid State Communications*, vol. 142, no. 10, pp. 583–586, 2007.
- [26] M. Mori, G. Khaliullin, T. Tohyama, and S. Maekawa, "Origin of the spatial variation of the pairing gap in Bi-based high temperature cuprate superconductors," *Physical Review Letters*, vol. 101, no. 24, Article ID 247003, 2008.
- [27] X. Wang, H. Song, G. Qiu, and D. Wang, "Empirical criteria of superconductivity for some oxides," *Journal of Materials Science and Technology*, vol. 16, no. 3, pp. 327–331, 2000.
- [28] J. C. Phillips, "Is there a lowest upper bound for superconductive transition temperatures?" *Chemical Physics Letters*, vol. 451, no. 1–3, pp. 98–101, 2008.
- [29] P. Boolchand, G. Lucovsky, J. C. Phillips, and M. F. Thorpe, "Self-organization and the physics of glassy networks," *Philosophical Magazine*, vol. 85, no. 32, pp. 3823–3838, 2005.
- [30] J. C. Phillips, "Self-organized networks and lattice effects in high-temperature superconductors," *Physical Review B*, vol. 75, no. 21, Article ID 214503, 2007.
- [31] H. Uchiyama, A. Q. R. Baron, S. Tsutsui, et al., "Softening of Cu-O bond stretching phonons in tetragonal  $\text{HgBa}_2\text{CuO}_{4+\delta}$ ," *Physical Review Letters*, vol. 92, no. 19, Article ID 197005, 4 pages, 2004.
- [32] S. L. Chaplot, W. Reichardt, L. Pintschovius, and N. Pyka, "Common interatomic potential model for the lattice dynamics of several cuprates," *Physical Review B*, vol. 52, no. 10, pp. 7230–7242, 1995.
- [33] A. D. Christianson, M. D. Lumsden, O. Delaire, et al., "Phonon density of states of  $\text{LaFeAsO}_{1-x}\text{F}_x$ ," *Physical Review Letters*, vol. 101, no. 15, Article ID 157004, 2008.
- [34] S. Shimizu, H. Mukuda, Y. Kitaoka, et al., "Self-doped superconductivity in tri-layered  $\text{Ba}_2\text{Ca}_2\text{Cu}_3\text{O}_6\text{F}_2$ : a  $^{63}\text{Cu}$ -NMR study," *Physica B*, vol. 403, no. 5–9, pp. 1041–1043, 2008.
- [35] J. C. Phillips, "Direct evidence for the quantum interlayer defect-assisted percolation model of cuprate high- $T_c$  superconductivity," *Physical Review B*, vol. 39, no. 10, pp. 7356–7358, 1989.
- [36] S. Yamanaka, K.-I. Hotehama, and H. Kawaji, "Superconductivity at 25.5 K in electron-doped layered hafnium nitride," *Nature*, vol. 392, no. 6676, pp. 580–582, 1998.
- [37] Y. Kamihara, T. Watanabe, M. Hirano, and H. Hosono, "Iron-based layered superconductor  $\text{La}[\text{O}_{1-x}\text{F}_x]\text{FeAs}$  ( $x = 0.05 - 0.12$ ) with  $T_c = 26$  K," *Journal of the American Chemical Society*, vol. 130, no. 11, pp. 3296–3297, 2008.
- [38] J. C. Phillips, "Nanostructural model of metal-insulator transition in layered  $\text{Li}_x\text{ZrNCl}$  superconductors," *Physical Review B*, vol. 77, no. 10, Article ID 104534, 2008.
- [39] D. J. Singh and M.-H. Du, "Density functional study of  $\text{LaFeAsO}_{1-x}\text{F}_x$ : a low carrier density superconductor near itinerant magnetism," *Physical Review Letters*, vol. 100, no. 23, Article ID 237003, 2008.
- [40] G. Saffarini, J. M. Saiter, and J. Matthiesen, "Thermal stability and percolation threshold of Ge-Se-Fe glasses," *Materials Letters*, vol. 61, no. 2, pp. 432–436, 2007.
- [41] D. J. Singh, "Electronic structure and doping in  $\text{BaFe}_2\text{As}_2$  and  $\text{LiFeAs}$ : density functional calculations," *Physical Review B*, vol. 78, no. 9, Article ID 094511, 2008.
- [42] H. Takahashi, K. Igawa, K. Arii, Y. Kamihara, M. Hirano, and H. Hosono, "Superconductivity at 43 K in an iron-based layered compound  $\text{LaO}_{1-x}\text{F}_x\text{FeAs}$ ," *Nature*, vol. 453, no. 7193, pp. 376–378, 2008.
- [43] M. S. Torikachvili, S. L. Bud'ko, N. Ni, and P. C. Canfield, "Effect of pressure on the structural phase transition and superconductivity in  $(\text{Ba}_{1-x}\text{K}_x)\text{Fe}_2\text{As}_2$  ( $x = 0$  and 0.45) and  $\text{SrFe}_2\text{As}_2$  single crystals," *Physical Review B*, vol. 78, no. 10, Article ID 104527, 6 pages, 2008.
- [44] A. Gozar, G. Logvenov, L. F. Kourkoutis, et al., "High-temperature interface superconductivity between metallic and insulating copper oxides," *Nature*, vol. 455, no. 7214, pp. 782–785, 2008.
- [45] S. Reich and Y. Tsabba, "Possible nucleation of a 2D superconducting phase on  $\text{WO}_3$  single crystals surface doped with  $\text{Na}^+$ ," *European Physical Journal B*, vol. 9, no. 1, pp. 1–4, 1999.
- [46] G. Leitus, H. Cohen, and S. Reich, "Interplay of Cs concentration, dimensionality and superconductivity in  $\text{Cs}_x\text{WO}_3$ ," *Physica C*, vol. 371, no. 4, pp. 321–329, 2002.
- [47] A. E. Aliev, "High- $T_c$  superconductivity in nanostructured  $\text{Na}_x\text{WO}_{3-y}$ : sol-gel route," *Superconductor Science and Technology*, vol. 21, no. 11, Article ID 115022, 9 pages, 2008.
- [48] Y. Kopelevich, R. R. da Silva, A. Rougier, and I. A. Luk'yanchuk, "Charge ordering in amorphous  $\text{WO}_x$  films," *Physica Letters*, vol. 368, no. 5, pp. 419–422, 2007.
- [49] T. Takano, T. Kishiume, Y. Taguchi, and Y. Iwasa, "Interlayer-spacing dependence of  $T_c$  in  $\text{Li}_x\text{M}_y\text{HfNCl}$  ( $M$ : molecule) superconductors," *Physical Review Letters*, vol. 100, no. 24, Article ID 247005, 4 pages, 2008.
- [50] F. Carbone, D.-S. Yang, E. Giannini, and A. H. Zewail, "Direct role of structural dynamics in electron-lattice coupling of superconducting cuprates," *Proceedings of the National Academy of Sciences of the United States of America*, vol. 105, no. 51, pp. 20161–20166, 2008.
- [51] T. P. Devereaux, T. Cuk, Z.-X. Shen, and N. Nagaosa, "Anisotropic electron-phonon interaction in the cuprates," *Physical Review Letters*, vol. 93, no. 11, Article ID 117004, 4 pages, 2004.
- [52] V. A. Rassolov and S. Garashchuk, "Computational complexity in quantum chemistry," *Chemical Physics Letters*, vol. 464, no. 4–6, pp. 262–264, 2008.
- [53] H. Shim, P. Chaudhari, G. Logvenov, and I. Bozovic, "Electron-phonon interactions in superconducting  $\text{La}_{1.84}\text{Sr}_{0.16}\text{CuO}_4$  films," *Physical Review Letters*, vol. 101, no. 24, Article ID 247004, 4 pages, 2008.
- [54] J. C. Phillips, "Electron-phonon interactions cause high-temperature superconductivity," *Philosophical Magazine B*, vol. 82, no. 8, pp. 931–942, 2002.
- [55] H. Iwasawa, J. F. Douglas, K. Sato, et al., "Isotopic fingerprint of electron-phonon coupling in high- $T_c$  cuprates," *Physical Review Letters*, vol. 101, no. 15, Article ID 157005, 2008.
- [56] D. Lampakis, E. Liarokapis, and C. Panagopoulos, "Micro-Raman evidence for topological charge order across the superconducting dome of  $\text{La}_{2-x}\text{Sr}_x\text{CuO}_4$ ," *Physical Review B*, vol. 73, no. 17, Article ID 174518, 2006.
- [57] A. Bianconi, M. Luscignoli, N. L. Saini, P. Bordet, Å. Kvik, and P. G. Radaelli, "Stripe structure of the  $\text{CuO}_2$  plane in  $\text{Bi}_2\text{Sr}_2\text{CaCu}_2\text{O}_{8+y}$  by anomalous X-ray diffraction," *Physical Review B*, vol. 54, no. 6, pp. 4310–4314, 1996.
- [58] N. Barišić, Y. Li, X. Zhao, et al., "Demonstrating the model nature of the high-temperature superconductor  $\text{HgBa}_2\text{CuO}_{4+\delta}$ ," *Physical Review B*, vol. 78, no. 5, Article ID 054518, 2008.
- [59] C. J. Zhang and H. Oyanagi, "Local lattice instability and superconductivity in  $\text{La}_{1.85}\text{Sr}_{0.15}\text{Cu}_{1-x}\text{M}_x\text{O}_4$  ( $M=\text{Mn}, \text{Ni}, \text{and Co}$ )," *Physical Review B*, vol. 79, no. 6, Article ID 064521, 8 pages, 2009.

- [60] F. Illas, D. Muñoz, C. de Graaf, and I. de P. R. Moreira, “Unexpected role of Madelung potential in monoplanar high- $T_c$  cuprate superconductors,” *Chemical Physics Letters*, vol. 379, no. 3-4, pp. 291–296, 2003.
- [61] M. C. Boyer, W. D. Wise, K. Chatterjee, et al., “Imaging the two gaps of the high-temperature superconductor  $\text{Bi}_2\text{Sr}_2\text{CuO}_{6+x}$ ,” *Nature Physics*, vol. 3, no. 11, pp. 802–806, 2007.
- [62] J.-H. Ma, Z.-H. Pan, F. C. Niestemski, et al., “Coexistence of competing orders with two energy gaps in real and momentum space in the high temperature superconductor  $\text{Bi}_2\text{Sr}_{2-x}\text{La}_x\text{CuO}_{6+\delta}$ ,” *Physical Review Letters*, vol. 101, no. 20, Article ID 207002, 2008.
- [63] G. Leibon, S. Pauls, D. Rockmore, and R. Savell, “Topological structures in the equities market network,” *Proceedings of the National Academy of Sciences of the United States of America*, vol. 105, no. 52, pp. 20589–20594, 2008.
- [64] S. Saavedra, F. Reed-Tsochas, and B. Uzzi, “Asymmetric disassembly and robustness in declining networks,” *Proceedings of the National Academy of Sciences of the United States of America*, vol. 105, no. 43, pp. 16466–16471, 2008.
- [65] K. Venkatesan, J.-F. Rual, A. Vazquez, et al., “An empirical framework for binary interactome mapping,” *Nature Methods*, vol. 6, no. 1, pp. 83–90, 2009.
- [66] M. A. Moret and G. F. Zebende, “Amino acid hydrophobicity and accessible surface area,” *Physical Review E*, vol. 75, no. 1, Article ID 011920, 2007.
- [67] A. E. Kister and J. C. Phillips, “A stringent test for hydrophobicity scales: two proteins with 88% sequence identity but different structure and function,” *Proceedings of the National Academy of Sciences of the United States of America*, vol. 105, no. 27, pp. 9233–9237, 2008.
- [68] J. C. Phillips, “Quantum percolation in cuprate high-temperature superconductors,” *Proceedings of the National Academy of Sciences of the United States of America*, vol. 105, no. 29, pp. 9917–9919, 2008.
- [69] J. Yang, J. Hwang, E. Schachinger, et al., “Exchange boson dynamics in cuprates: optical conductivity of  $\text{HgBa}_2\text{CuO}_{4+\delta}$ ,” *Physical Review Letters*, vol. 102, no. 2, Article ID 027003, 2009.
- [70] W. Guyard, A. Sacuto, M. Cazayous, et al., “Temperature dependence of the gap size near the brillouin-zone nodes of  $\text{HgBa}_2\text{CuO}_{4+\delta}$  superconductors,” *Physical Review Letters*, vol. 101, no. 9, Article ID 097003, 2008.
- [71] S. Cojocaru, R. Citro, and M. Marinaro, “Incoherent midinfrared charge excitation and the high-energy anomaly in the photoemission spectra of cuprates,” *Physical Review B*, vol. 75, no. 22, Article ID 220502, 2007.
- [72] C. U. Jung, J. H. Kong, B. H. Park, T. W. Noh, and E. J. Choi, “Far-infrared transmission studies on a superconducting  $\text{BaPb}_{1-x}\text{Bi}_x\text{O}_3$  thin film: effects of a carrier scattering rate,” *Physical Review B*, vol. 59, no. 13, pp. 8869–8874, 1999.
- [73] T. Nishio, J. Ahmad, and H. Uwe, “Spectroscopic observation of bipolaronic point defects in  $\text{Ba}_{1-x}\text{K}_x\text{BiO}_3$ ,” *Physical Review Letters*, vol. 95, no. 17, Article ID 176403, 4 pages, 2005.
- [74] K. Haule, J. H. Shim, and G. Kotliar, “Correlated electronic structure of  $\text{LaO}_{1-x}\text{F}_x\text{FeAs}$ ,” *Physical Review Letters*, vol. 100, no. 22, Article ID 226402, 2008.
- [75] T. Yildirim, “Strong coupling of the Fe-Spin state and the As-As hybridization in Iron-Pnictide superconductors from first-principle calculations,” *Physical Review Letters*, vol. 102, no. 3, Article ID 037003, 2009.
- [76] I. Nowik and I. Felner, “Mössbauer spectroscopy determination of iron foreign phases in the superconducting systems;  $\text{RAsFeO}_{1-x}$ ,  $\text{RAsFeO}_{1-x}\text{F}_x$ , and  $\text{Sr}_{1-x}\text{K}_x\text{Fe}_2\text{As}_2$ ,” *Journal of Superconductivity and Novel Magnetism*, vol. 21, no. 5, pp. 297–300, 2008.
- [77] A. S. Alexandrov, “Phase separation of electrons strongly coupled with phonons in cuprates and manganites,” *Journal of Superconductivity and Novel Magnetism*, vol. 22, no. 2, pp. 95–101, 2009.
- [78] A. V. Boris, N. N. Kovaleva, S. S. A. Seo, et al., “Signatures of electronic correlations in optical properties of  $\text{LaFeAsO}_{1-x}\text{F}_x$ ,” *Physical Review Letters*, vol. 102, no. 2, Article ID 027001, 2009.
- [79] A. S. Alexandrov, “Unconventional pairing symmetry of layered superconductors caused by acoustic phonons,” *Physical Review B*, vol. 77, no. 9, Article ID 094502, 2008.
- [80] H. Q. Yuan, J. Singleton, F. F. Balakirev, et al., “Nearly isotropic superconductivity in  $(\text{Ba,K})\text{Fe}_2\text{As}_2$ ,” *Nature*, vol. 457, no. 7229, pp. 565–568, 2009.
- [81] T. Ekino, A. M. Gabovich, M. S. Li, M. Pekała, H. Szymczak, and A. I. Voitenko, “Temperature-dependent pseudogap-like features in tunnel spectra of high- $T_c$  cuprates as a manifestation of charge-density waves,” *Journal of Physics: Condensed Matter*, vol. 20, no. 42, Article ID 425218, 2008.
- [82] Y. Ando, S. Komiyama, K. Segawa, S. Ono, and Y. Kurita, “Electronic phase diagram of high- $T_c$  cuprate superconductors from a mapping of the In-plane resistivity curvature,” *Physical Review Letters*, vol. 93, no. 26, Article ID 267001, 2004.
- [83] J. Jung and M. M. Abdelhadi, “Electrical transport and oxygen disorder in YBCO,” *International Journal of Modern Physics B*, vol. 17, no. 18–20, pp. 3465–3469, 2003.
- [84] R. A. Cooper, Y. Wang, B. Vignolle, et al., “Anomalous criticality in the electrical resistivity of  $\text{La}_{2-x}\text{Sr}_x\text{CuO}_4$ ,” *Science*, vol. 323, no. 5914, pp. 603–607, 2009.
- [85] M. F. Islam and H. Nakanishi, “The effect of local phases of wave function on transmission of a quantum particle through two dimensional clusters,” *European Physical Journal B*, vol. 65, no. 4, pp. 555–564, 2008.
- [86] S. Cocco and R. Monasson, “Exponentially hard problems are sometimes polynomial, a large deviation analysis of search algorithms for the random satisfiability problem, and its application to stop-and-restart resolutions,” *Physical Review E*, vol. 66, no. 3, Article ID 037101, 4 pages, 2002.
- [87] B. Luque, O. Miramontes, and L. Lacasa, “Number theoretic example of scale-free topology inducing self-organized criticality,” *Physical Review Letters*, vol. 101, no. 15, Article ID 158702, 2008.
- [88] T. Rohlfs, “Self-organization of heterogeneous topology and symmetry breaking in networks with adaptive thresholds and rewiring,” *Europhysics Letters*, vol. 84, no. 1, Article ID 10004, 2008.

## Research Article

# Supercell Band Calculations and Correlation for High- $T_C$ Copper Oxide Superconductors

**T. Jarlborg**

*DPMC, University of Geneva, 24 Quai Ernest-Ansermet, 1211 Geneva 4, Switzerland*

Correspondence should be addressed to T. Jarlborg, thomas.jarlborg@unige.ch

Received 24 June 2009; Accepted 12 August 2009

Academic Editor: Igor Mazin

Copyright © 2010 T. Jarlborg. This is an open access article distributed under the Creative Commons Attribution License, which permits unrestricted use, distribution, and reproduction in any medium, provided the original work is properly cited.

First principle band calculations based on local versions of density functional theory (DFT), together with results from nearly free-electron models, can describe many typical but unusual properties of the high- $T_C$  copper oxides. The methods and a few of the most important results are reviewed. Some additional calculations are presented, and the problems with the commonly used approximate versions of DFT for oxides are discussed with a few ideas for corrections. It is concluded that rather modest corrections to the approximate DFT, without particular assumptions about strong correlation, can push the ground state towards antiferro magnetic (AFM) order. Spin fluctuations interacting with phonons are crucial for the mechanism of superconductivity in this scenario.

## 1. Introduction

It is often assumed that strong correlation is important for an understanding of the high- $T_C$  problem [1–3]. The failure of the local approximations to the exchange-correlation functional, such as the local (spin) density approximation, LDA, or LSDA [4–7], to produce the antiferro magnetic (AFM) insulating state of many undoped transition metal oxides is generally quoted as the essential reason for discarding DFT calculations for high- $T_C$  copper oxides [3]. DFT is essentially exact, but the approximations to make it practical for use in real applications seem inappropriate for oxides. However, despite this problem, there are several LDA results that fit to the observed high- $T_C$  properties, provided that doping and supercells are considered in order to account for imperfect lattice conditions such as stripes, phonons, or spin waves [8–10]. Here is presented a short review of those DFT results together with a discussion of the correlation problem and an attempt to include further corrections to LSDA. Estimations of couplings  $\lambda$  caused by spin-phonon coupling (SPC) and pure spin fluctuations are also made.

## 2. Nearly Free-Electron Model

The spin polarized potential from an AFM order (like that of undoped  $\text{La}_2\text{CuO}_4$ ) can be generated from  $V_{\text{AFM}}(\mathbf{x}) =$

$V_0 \exp(-i\vec{Q} \cdot \vec{x})$ , where  $\vec{Q} = \pi/a_0$  is at the Brillouin Zone (BZ) boundary, so that there is one Cu site with spin up and one with spin down within a distance  $a_0$  ( $a_0$  is the lattice constant). The potential of the other spin has a phase shift of  $\pi$ . The band dispersion from a 1-dimensional (1D) nearly free-electron model (NFE) is obtained from a  $2 \times 2$  eigenvalue problem, and it has a gap of  $2V_0$  at the zone boundary. Suppose now that an additional potential modulation  $V_q(\mathbf{x}) = V_q \exp(i\vec{q} \cdot \vec{x})$  exists, and that  $|\vec{q}| \ll |\vec{Q}|$ , so that its periodicity or “wavelength” is much larger than  $2a_0$ . The product of these two modulations can be written  $V(\mathbf{x}) = V_q \exp(-i(\vec{Q} - \vec{q}) \cdot \vec{x})$ , where the two amplitudes are combined into one coefficient,  $V_q$ . Figure 1 shows the real space configurations along the 100-direction. This potential describes AFM modulations in stripes, with magnetic nodes (Cu with zero moment) separated by  $a_0 Q/q$ . The values of  $V_q$  for phonons or spin waves of different lengths are not known from the NFE model, but some values will be fed in from the ab initio Linear Muffin-Tin Orbital (LMTO, [11, 12]) calculations, as will be described here in after. The LMTO calculations are slow for large supercells. The cells need to be large to cover the periodicity of realistic phonon and/or spin-waves, and so far it has been possible to extend the cells in one direction only, usually the CuO bond direction. In contrast, the NFE model is very simple

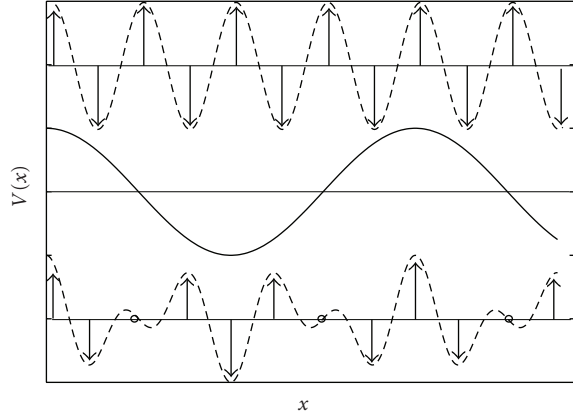


FIGURE 1: A picture of how stripe-like configurations are made up from the product of two plane wave potentials. The arrows in the upper row show the AFM moments on Cu sites given by the envelope function  $\text{Re}(\exp(-i\vec{Q} \cdot \vec{x}))$  (broken line), and the unit cell contains 2 Cu sites along  $\vec{x}$ . The second row shows the modulation  $\text{Re}(\exp(i\vec{q} \cdot \vec{x}))$  (here  $q = Q/4$ ) and the last row is the product  $\text{Re}(\exp(-i(\vec{Q} - \vec{q}) \cdot \vec{x}))$  with the new spin configurations on the Cu. The striped unit cell contains 8 Cu sites.

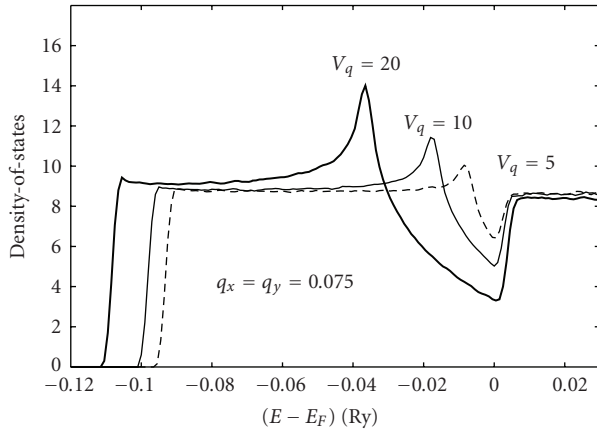


FIGURE 2: Examples of the DOS from the 2D NFE model for 3 different strengths of  $V_q$  (in mRy) for  $\vec{q} = (0.075, 0.075)$ .

and it can easily be extended to two dimensions (2D). The band dispersion for  $k$ -points  $(k_x, k_y)$  is now obtained from the eigenvalues of a  $3 \times 3$  matrix [13]. Not only stripe order but also “checkerboard” configuration can be modeled.

Examples of the density-of-states (DOSs) for 3 different  $V_q$ 's are shown in Figure 2. The potential modulations are parallel to the CuO bond directions along  $\vec{x}$  and  $\vec{y}$ , and so the gaps appear on the  $(k_x, 0)$  and  $(0, k_y)$  lines, as shown in Figure 3. However, almost no effect from  $V_q$  appears on the band dispersion in the diagonal direction (along  $(k, k)$ ). Therefore, the Fermi surface (FS) is not affected along the diagonal, but fluctuations, described through amplitude variations of  $V_q$  for different positions and different time, will make the FS smeared in the two bond directions. An example of this is shown in Figure 4.

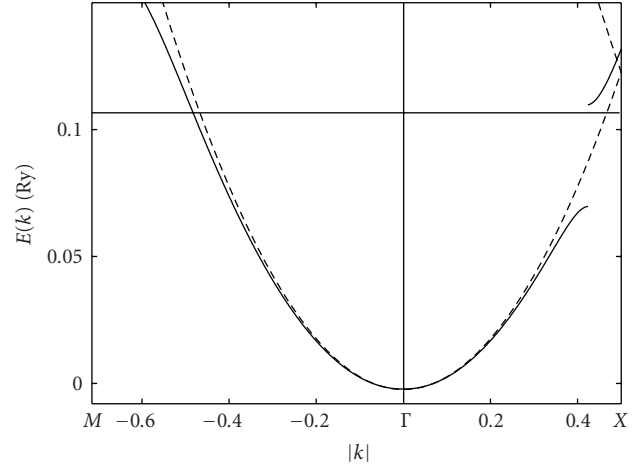


FIGURE 3: An example of the 2D NFE bands along  $(k, 0)$  and  $(k, k)$  for  $q_x = q_y = 0.075$  and  $V_q = 20$  mRy (full line). The FE band without potential perturbations ( $V_q = 0$ ) is shown by the broken line. The thin horizontal line is at the DOS minimum, which is situated at 0.15 holes/cell.

### 3. Ab Initio 1D-LMTO

By 1D (1-dimensional) LMTO we mean ab initio LMTO calculations for long (and narrow) supercells most often oriented along the CuO bond direction [14, 15]. These calculations are based on the local version of DFT, the local (spin) density approximation, LDA, or LSDA [4, 5]. Cells with phonon distortions and/or spin waves within lengths of 4, 8, and 12 lattice constants are typically considered in these calculations. The wavelengths of spin waves are twice as long as those of phonons. Hole doping,  $h$ , in  $\text{La}_{(2-h)}\text{Ba}_h\text{CuO}_4$  (LBCO) is generally modeled by the virtual crystal approximation (VCA) where the nuclear and electronic La-charges (57.0) are reduced to  $(57-h/2)$  to account for a perfectly delocalized doping ( $h$  in holes per Cu). But some calculations with real La/Ba substitutions show that improved superconducting properties can be expected from periodic doping distributions [16]. The maximal phonon distortion,  $u_i$ , for different sites,  $i$ , and AFM magnetic moments on Cu,  $m$ , depend on temperature,  $T$ , force constants, and spin stiffness. Appropriate values of  $u_i(T)$  and  $m(T)$  at  $T \approx 100$  K are deduced from experiments and calculations [17–22].

A striking result of these calculations (also made for  $\text{HgBa}_2\text{CuO}_4$ ) is that a gap (or a pseudogap) will open up in the DOS, very similar to what is found in the NFE models. The gap will appear near to  $E_F$  for the undoped material if the wavelengths ( $\Lambda$ ) are long, while for short phonons or spin waves the gap moves to lower energy [8]. In summary,  $\Lambda = 1/h$ , where  $\Lambda$  is in units of  $a_0$  and  $h$  is the number of holes per Cu.

A second important result is that the spin waves will be stronger, and the pseudogaps will be deeper, if the waves coexist with phonon distortions of the correct wave length and phase [14]. Interactions between phonons and spin waves have also been suggested in order to explain neutron

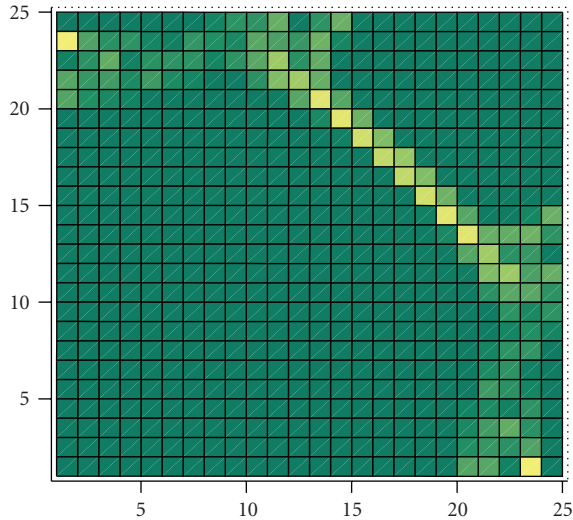


FIGURE 4: An example of the Fermi surface in the 2D NFE model with fluctuations of  $V_q$ . The FS is well defined in the diagonal direction, while the fluctuations makes it diffuse in the  $x$  and  $y$ -directions.

scattering [23, 24]. Phonons like the “half-breathing” O-mode and modes with  $z$ -displacements of La and apical oxygen are most effective in this process of SPC. This mechanism offers direct explanations of phonon softening,  $q$ -dependent spin excitations, and various isotope effects [10, 15].

The rather few LMTO results permit to establish only a few values of  $V_q$  for different  $q$ 's,  $i$  of the phonons and spin waves. A general trend of larger  $V_q$  for long wave lengths seems clear, both for phonons and for spin waves. A procedure based on the partial character of the states above and below the gap in the NFE model confirms this trend for spin waves, and it permits to fill in some of the  $q$ -dependent points not calculated by LMTO. In all this gives some confidence in the  $q$ ,  $i$ -variations of  $V_q$ . However, one can expect more vivid variations of the spin part near  $q \rightarrow 0$ , because LDA underestimates the transition towards AFM.

When these  $V_q$ -values are fed into the 2D NFE model, it gives an approximately linear variation of  $q$  as function of  $h$ , up to a saturation near  $q \sim 0.125$  for  $h$  larger than  $\sim 0.13$  [13]. Hence, the linear dependence for low  $h$  is in qualitative agreement with the result from 1D-LMTO, but the pace is different. This is probably because the gap opens *both* along  $x$  and  $y$  in the 2D NFE model, which makes the progression of the gap a bit slower than in 1D. The saturation is because the  $V_q$ 's decrease for increasing  $q$  and it becomes impossible to open a gap at the low energy where  $E_F$  should be for large  $h$ . However, if  $q_x$  and  $q_y$  are assumed to be different in the 2D NFE model, it is possible to follow one gap towards lower energy. A second weaker gap moves to higher energy.

#### 4. Superconductivity

The emerging picture from these band results is that moderately strong spin fluctuations, which exist for many

combinations of  $\vec{q}$  and  $\omega$ , will be enhanced through SPC to some particular phonon distortions. The selection depends on the atomic character of the phonon mode as well as on doping and wave length (i.e., on  $\vec{q}$ ). The latter is because the pseudogap appears at  $E_F$  so that a maximum amount of kinetic energy can be gained from the SPC mode. This is for low  $T$  when the states below the gap is of one spin and well separated from the (unoccupied) state of the other spin above the gap. But for increasing  $T$  there will be mixed occupations of the states around  $E_F$  through the Fermi-Dirac function (and through thermal disorder), which will decrease the spin density. This will decrease the spin polarization of the potential, which in turn will decrease the spin density even more, and at some temperature  $T^*$  the support of the pseudogap from the spin wave will collapse [10]. The fact that  $V_q$  is the largest at low doping favors larger  $T^*$  when  $h \rightarrow 0$ . A high DOS at  $E_F$  is important for a high superconducting  $T_C$  and therefore is the pseudogap in competition with superconductivity in underdoped cuprates [13].

It was suggested that nonadiabatic electron-phonon coupling could be enhanced in the cuprates, because of the low Fermi velocity in the  $z$ -direction [25, 26]. This velocity is comparable to the vibrational velocity and the electronic screening appeared to be insufficient. However, the screening can be made by other electrons moving within the planes. Moreover, phonon frequencies calculated within LDA without assumptions of incomplete screening, agree satisfactory with experimental frequencies [19–21]. Instead, excitations of virtual phonons coupled to spin waves can be important for the mechanism of superconductivity, but SPC makes the separation between pure electron-phonon coupling,  $\lambda_{ep}$ , and  $\lambda$  caused by spin fluctuations,  $\lambda_{sf}$ , less clear.

The important observation is that atomic phonon distortions will trigger enhancement of spin waves. If so, the possibility for larger  $\lambda_{ep}$  is open, because instead for the common approach to ignore spin effects in electron-phonon coupling, there are larger matrix elements when the spin polarized part of the potential is involved. This is readily imagined for a system which is nonmagnetic when phonon distortions are absent, but magnetic when the distortions are present. An estimation of pure  $\lambda_{ep}$  and the coupling parameter for SPC,  $\lambda_{SPC}$ , in LBCO has been presented earlier [23]. With a total  $N(E_F) \approx 0.9$  (eV · cell · spin) $^{-1}$ , and distortion amplitudes and potential shifts as in [13] this leads to  $\lambda'_s$  of the order 0.36 and 0.6 for pure phonons and SPC, respectively [23]. These values appear sufficiently large for a large  $T_C$  in simple BCS-type formulations, but the precise relation for  $T_C$  depends also on other parameters [27].

The third mechanism is that spin fluctuations work without coupling to phonon excitations. Still, phonon distortions might be present and will in that case be important for enhancements of rapid (high energy) spin fluctuations. For instance, it was found that the local exchange enhancement (for AFM) on Cu sites is the largest when the surrounding atoms (La or oxygen) have been pushed away from the Cu, and this leads to SPC between phonons and spin waves with equal  $\vec{q}$  and  $\omega$  [13]. But strong high- $\omega$  spin excitations should also be possible on rows of Cu with

TABLE 1: Total energy ( $\Delta E$ , mRy per Cu), matrix element for spin fluctuations ( $\Delta V$  in mRy),  $\lambda_{sf}$ , and local Stoner enhancement,  $S$ , calculated for lattices of LBCO with two phonon distortions and without distortions.

Phonon	$\Delta E$	$\Delta V$	$\lambda_{sf}$	$S$
No phonon	12.7	9	0.03	1.6
Plane-O	8.2	12.5	0.12	2.6
La	7.4	12.0	0.11	2.4

enhanced exchange, perpendicular to the phonon. Ab initio calculations are not easy for such configurations because of the large size of the required unit cells, but one can use some of the existing results for first estimations of  $\lambda_{sf}$  for rapid spin fluctuation (so rapid that the phonon distortions appear to be static compared to the spin fluctuation). The enhancements depend on the different types of distortions as was discussed above. In this case we calculate  $\lambda_{sf} = N \langle dV/dm \rangle^2 / (d^2E/dm^2)$ , where  $V$  is the potential,  $E$  is the total energy of the spin wave, and  $m$  is the magnetic moment (per Cu) [28, 29]. The difference in free energy between nonpolarized and an induced (by magnetic field) AFM wave can be written  $E_m = E_0 + \kappa m^2$ , so that  $d^2E/dm^2 = 2\kappa$ , which permits to calculate  $\lambda_{sf} = N \cdot (\Delta V)^2 / \kappa$  for “harmonic” spin fluctuations. With parameters from the band results this makes  $\lambda_{sf}$  equal to 0.03 when no lattice distortions are present, and 0.12 and 0.11 when the lattice contain distortions; see Table 1.

The frequency has not been calculated explicitly, but a shortcut via exchange enhancements can be used for a simple estimation, as for FM fluctuations [28–30]. Thus,  $\omega_{sf} \approx 1/(4NS)$ , where  $S = \Delta V/\Delta H$  is the local Stoner enhancement (on Cu) and  $\Delta H$  is the external field (5 mRy in these calculations). This makes  $\omega_{sf}$  100–200 meV depending on the type of lattice distortion. Figure 5 shows the combined results for direct  $\lambda_{SPC}$  and indirect  $\lambda_{sf}$  as function of frequency. The general shape is similar as the electron-boson coupling function that has been extracted from recent optical spectra on Hg- and Bi-based copper oxides [31].

The amplitudes of  $\lambda_{SPC}$  and  $\lambda_{sf}$  increase further if both of the latter distortions (plane oxygen *and* La) are considered in the calculation. The matrix element increases to about 14.5 mRy. Despite this relative increase, it is seen that pure spin fluctuations give not as large  $\lambda$ 's as for SPC. This is especially clear when all lattice modes are considered. However, these pure spin fluctuations can be important for superconductivity, since they appear at large  $\omega$ . In contrast, SPC is essentially limited to below the highest phonon frequency, that is, to 50–70 meV. The relatively small absolute values of  $\lambda_{sf}$  are partly caused by the use of LDA. Improved DF schemes, which could predict an AFM insulating state for the undoped systems, would lead to larger exchange enhancements, larger  $\lambda_{sf}$ , and lower  $\omega_{sf}$  in doped systems.

## 5. Correlation and Corrections to LDA

The question is whether the real electron-electron correlation in the oxides is much larger than what is included

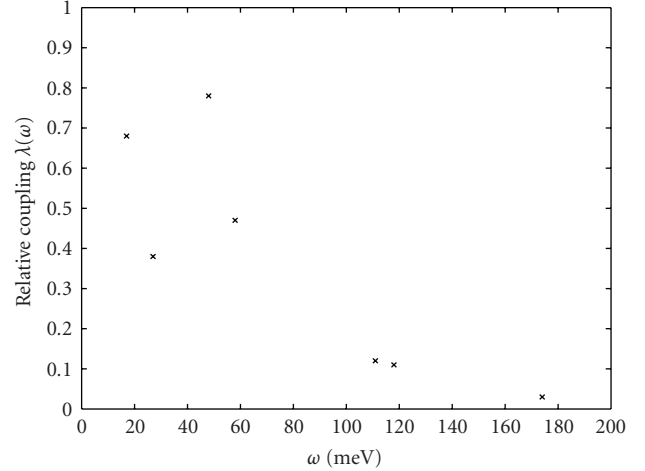


FIGURE 5: The relative strength of  $\lambda_{SPC}$  (the first 4 points) and  $\lambda_{sf}$  (the 3 points at the highest energies). The latter will move towards lower energy if the exchange enhancement increases, while the points for SPC are fixed near the phonon energies; see the text.

in LDA. The latter includes exchange and correlation (XC) for an electron gas of varying density with the electron gas radius  $r_s = 0.62\rho^{-1/3}$  as parameter. The density  $\rho$  contains one electron within  $r_s$ . The largest values of  $r_s$  ( $\approx 2$  a.u.) are found in the low-density valence-electron region between the atoms, but they are still smaller than any typical atomic radius,  $R_A$  in transition metals, their oxides, and these cuprates. This gives a major argument against using a strong on-site correlation parameter to an atom, because the effect of an additional electron will readily be screened out and is not noticed beyond  $r_s$ . In low-density materials, however, such as the alkali metals,  $r_s \approx R_A$  and on-site correlation could be advocated. But LDA seems to describe alkali metals well, which provides an additional argument in favor of local approximations of DFT.

The fact is that LSDA does not produce an AFM insulating ground state of several oxides, and so the problem is real and it may be related to the spin-polarized part of the potential. Small errors with important consequences of this type are known for LSDA. A well-known example is for Fe, where LSDA predicts nonmagnetic (NM) face-centered cubic (fcc) lattice as the ground state, whereas the generalized gradient approximation (GGA, [6]) correctly finds the ferro magnetic (FM) body-centered cubic (bcc) ground state [32–34]. The difference between LDA and GGA is not large concerning the bands, magnetic moments, and other properties. The band properties of bcc Fe are quite good in calculations using both these DFT functionals. But the order of the total energies for FM-bcc and NM-fcc is reversed in the two cases.

An additional indication that the AFM insulating state of the cuprates is not far away in LSDA is the fact that the AFM moment depends on the number of  $k$ -points. A sufficient number of  $k$ -points is required for convergence, but early works noticed that the AFM ground state became stable if a coarse  $k$ -point mesh was used [35–37]. A similar

conclusion for the appearance of weak ferromagnetism in highly doped LBCO can be understood from DOS effects and the Stoner criterion [38]. Thus, as for Fe, a small detail can have large consequences. It might be that the total energy difference between two very different ground states (fcc nonmagnetic and bcc-magnetic for Fe, and NM metallic and AFM insulating for cuprates) are very close, so that small errors in the computational details lead to the “wrong” ground state.

Another indication of a nearby AFM state is that LMTO calculations with off-center linearization energies can stabilize AFM in  $\text{HgBa}_2\text{CuO}_4$  in calculations with sufficient number of  $k$ -points. The normal procedure in LMTO is to chose linearization energies at the center of the occupied subbands, but if they are chosen at the bottom of the bands, it leads to a slight localization of the states. An AFM order needs less hybridization energy and AFM can be stabilized [39]. This is rather ad hoc, since LMTO should not be made in such a way. A theoretical justification is need for a better DFT scheme.

A first workable nonlocal density functional is the GGA (generalized gradient correction [6]), where the gradient, or the first derivative of the charge density,  $d\rho(r)/dr$ , brings out corrections to the LSDA. The gradients are mainly radial in atoms and solids because of the steep drop in charge density for increasing  $r$  close to an atom. Only valence electrons have large amplitudes in the interstitial region between the atoms, where the gradients are moderate. However, higher gradients such as the second derivative of the density can be large in the interstitial, a feature not captured by the GGA. Nevertheless, by using GGA in the LMTO calculations for LBCO there is some improvement, since the required critical magnetic field for having a gap is reduced by about 25 percent compared to LSDA.

Densities with quadratic dependence as function of  $r$  around a fixed point at  $r = 0$  are used in a 2-particle model for calculations of correlation including corrections due to the second derivatives. A noninteracting density with quadratic gradients has the form

$$\rho(r) = \rho_0 + \frac{d^2\rho}{dr^2} \frac{r^2}{2}. \quad (1)$$

The Schrödinger equation is solved for a density of electrons surrounding a fixed electron at  $r = 0$ , where it is taken into account that the effective mass is  $1/2$  [40, 41]. The interacting potential can be written as

$$V(r) = \frac{e^2}{r} + \frac{\ell(\ell+1)}{r^2} + \mu_{xc}(r) + V_{\text{ext}}(r). \quad (2)$$

The exchange correlation within the surrounding electron cloud is taken into account through LDA ( $\mu_{xc}$ ), and the external potential  $V_{\text{ext}}$  can include relative kinetic energy variations. The two last terms in  $V(r)$  are not very important for the results for gradient variations. The strongest term is the unscreened Coulomb repulsion that diverges at  $r = 0$ . The second term, the centrifugal term, is included only for exchange (with  $\ell = 1$ , higher  $\ell$  will have higher energy), when the Pauli principle requires that the density for equal spin must be zero at  $r = 0$  [41].

The solution  $\Psi(E, r)$  of the Schrödinger equation for this potential is used to calculate the XC energy as the difference in Coulomb energy between interacting and noninteracting densities;  $\mu = \int (\Psi(E, r)^2 - \rho(r))/r d^3r$ . The energy  $E$  is determined from a required boundary condition of  $\Psi(E, r_s)$ . The variation of the correlation potential on the second gradient is quite easy to understand. If the gradient is positive, so that there is a tendency for a “hole” at  $r = 0$ , it will be less effective for the Coulomb repulsion to make the correlation hole deeper at this point. Therefore,  $\mu_c$  will decrease for positive density gradients near the interstitial region. The gradient can change closer to the high-density regions near the nuclei and make the correlation larger than for a constant density, but correlation becomes negligible in comparison to exchange when the density is high. The C-correction is parametrized through the electron gas parameter  $r_s$  and  $Q = \rho(r_s)/\rho(0)$ , so that  $C = 1 - 5\sqrt{Q}/4 + \sqrt{r_s} * Q/2$  for  $Q > 1$  and as the inverse of this parametrization if  $Q < 1$ . The expression is only applied for  $Q$  between  $-0.25$  and  $0.8$ , and  $C - 1$  is used as a scaling factor of the correlation part from LDA. This correction makes the potential a little more repulsive in the interstitial region. The Cu-d states become more localized, which can promote AFM order; see Table 2.

One fundamental theorem of DFT is that of “v-representability”, that essentially says that there is a one-to-one correspondence between the density  $\rho(r)$  and potential  $V(r)$  [4]. The only possibility is that two equivalent charge densities can give an uninteresting shift in the potential, which can be absorbed by the shift of the energy spectrum. Imagine now that an external potential is applied to an electron gas of varying density  $\rho(r)$ . The free electron wave functions will oscillate more if more kinetic energy is given to the electron gas, or less if kinetic energy is subtracted, even if  $\rho$  remains constant. The exchange part of the potential (X) will be modified because of the ability of the wave function to readjust itself around a second electron of the same spin (to create an exchange “hole”), as can be imagined from Slater exchange [7] or the two-particle model [41]. A similar change occurs for correlation (C), which is caused by the immediate Coulomb repulsion between all electron pairs. If  $\rho$  is constant in space, there is only an uninteresting potential shift, but for varying charge densities there can be more subtle effects. The LDA is derived from the principle of density variations at the Fermi energy, and the relation between  $E_F$  (which is a measure of the kinetic energy) and density is given by

$$E_F^{(1)}(r) = (3\pi^2\rho(r))^{2/3}. \quad (3)$$

This relation can be compared to  $E_F^{(2)}(r) = E_F - V(r)$  within real atoms, where  $E_F$  is from the band calculation with potential  $V(r)$ . Except for  $r$  very close to the nuclei there is not too large difference between  $E_F^{(1)}(r)$  and  $E_F^{(2)}(r)$ . In some regions the two values can be quite different. If so, it implies that the density is not in equilibrium with the kinetic energy as was used in the derivation of the LDA potential. Oxygen sites in oxides are often negatively charged, which suggests that the kinetic energy should be smaller than what comes out from (1). These effects are moderated by the fact that the

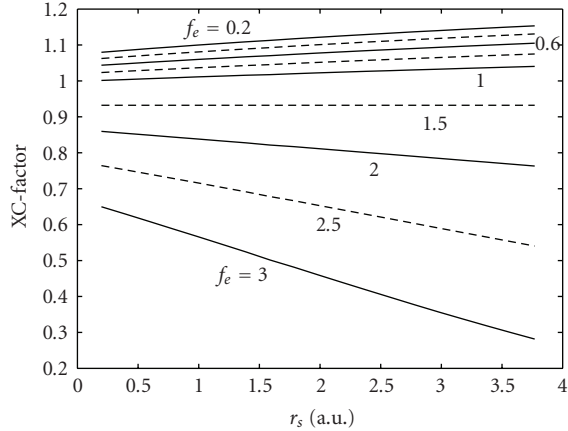


FIGURE 6: The calculated values of the scaling function  $X$  as function of  $r_s$  and  $f_e$  (see text).

TABLE 2: The required applied magnetic fields (in mRy on Cu) in order to obtain a zero gap in LMTO calculations which include the different corrections to the potential; see the text.

LSDA	GGA	GGA+C	GGA+X	GGA+C+X
8.8	6.6	5.5	5.0	4.0

charge transfer is a result of an attractive potential. It turns out that positive and negative deviations from (1) exist in shells within all atoms.

Thus, band calculations with correction for the kinetic energy will be attempted where the local exchange potential is written as

$$\mu_x(f_e, r_s) = X(f_e, r_s)\mu_{KS}(r_s), \quad (4)$$

where  $X(f_e, r_s)$  is a scaling function of the normal Kohn-Sham potential  $\mu_{KS}$ , and  $f_e = E_F^{(1)}(r_s)/E_F^{(2)}(r_s)$ .

A derivation of the scaling function  $X(f_e, r_s)$  can be done directly from the Slater functions by use of energy shifts in the arguments of the plane waves [7]. However, negative shifts leading to localized waves have to be avoided, and the resulting  $X$ -function seems too sensitive to small variations of  $f_e$ . As an alternative we determine the scaling function from a two-particle model as in [40, 41], with a renormalization to make  $X(1, r_s) = 1$ . The result is displayed in Figure 6 for the appropriate range of  $r_s$  and  $f_e$ . The real value of  $f_e$  for  $r \leq 0.05 R_{RWS}$  increases and can be larger than 50 near the nuclei. This is extreme and  $f_e$  is here cut-off at 3.

In preliminary calculations for undoped LBCO we do a rescaling of the exchange due to kinetic energy and of correlation due to second gradients. The comparison is made with standard LSDA for an AFM unit cell where a staggered magnetic field is applied to the Cu sites, and it is found that a field of  $\pm 8.8$  mRy is the limit for having a zero gap ( $E_g \sim 0.25$  mRy). The magnetic moment is then  $\pm 0.18 \mu_B$  per Cu. The amplitude of the required magnetic field to obtain a zero gap is reduced when the calculations include the correction factors; see Table 2. The absolute values can depend on details of the band calculations [39], but the trend

towards a stability of an AFM state is clear. Corrections of this type will be interesting for seeing enhanced spin fluctuations for long wave length spin waves in doped cuprates. Further enhancements of  $\lambda_{sf}$  can also be expected [13]. Potential corrections must ultimately be tested for other types of materials in order to verify that some properties will not deteriorate. Here for the cuprates the corrections permit to proceed in the modeling of more properties from the band results.

## 6. Conclusion

Results of band calculations for supercells with frozen phonons and spin waves suggest that a Fermi-liquid state can cause pseudogaps and dynamic stripes. Together with an NFE model it is possible to describe the doping dependence of many normal state properties of the cuprates. The coupling between phonon distortions and spin fluctuations seems to be crucial for the mechanism of superconductivity, so that the spin-polarized part of  $\lambda$  is most enhanced by simultaneous excitations of phonons and spin waves. Two different mechanisms for superconductivity mediated by spin fluctuations are possible. The largest coupling parameter is when a phonon is excited together with the spin fluctuation. Lower couplings,  $\lambda_{sf}$  at larger energies, are independent of the phonon excitation, but these spin fluctuations can nevertheless profit from possible phonon distortions of the lattice. Still, absolute numbers are too small when using LDA, as is also concluded from the absence of AFM stability in LDA calculations for undoped systems. However, it is argued that corrections due to higher-order density gradients and kinetic energy are able to bring the band calculations closer to AFM. This is shown in calculations for undoped LBCO by yet very approximate corrections due to nonlocality and kinetic energy. Refinements of such corrections will be of interest for application to supercells, including doping, phonon distortions, and spin waves, since it can be expected that realistic  $\lambda'_s$  will be obtained.

## References

- [1] J. Orenstein and A. J. Millis, "Advances in the physics of high-temperature superconductivity," *Science*, vol. 288, no. 5465, pp. 468–474, 2000.
- [2] M. T. Czyżyk and G. A. Sawatzky, "Local-density functional and on-site correlations: the electronic structure of  $\text{La}_2\text{CuO}_4$  and  $\text{LaCuO}_3$ ," *Physical Review B*, vol. 49, no. 20, pp. 14211–14228, 1994.
- [3] A. Damascelli, Z.-X. Shen, and Z. Hussain, "Angle-resolved photoemission studies of the cuprate superconductors," *Reviews of Modern Physics*, vol. 75, no. 2, pp. 473–541, 2003.
- [4] W. Kohn and L. J. Sham, "Self-consistent equations including exchange and correlation effects," *Physical Review*, vol. 140, no. 4A, pp. A1133–A1138, 1965.
- [5] O. Gunnarsson and B. I. Lundqvist, "Exchange and correlation in atoms, molecules, and solids by the spin-density-functional formalism," *Physical Review B*, vol. 13, no. 10, pp. 4274–4298, 1976.
- [6] J. P. Perdew and W. Yue, "Accurate and simple density functional for the electronic exchange energy: generalized

- gradient approximation,” *Physical Review B*, vol. 33, no. 12, pp. 8800–8802, 1986.
- [7] J. C. Slater, “A simplification of the Hartree-Fock method,” *Physical Review*, vol. 81, no. 3, pp. 385–390, 1951.
- [8] T. Jarlborg, “Spin waves and large electron-phonon coupling near the metal-insulator transition in hole-doped high- $T_c$  oxides,” *Physical Review B*, vol. 64, no. 6, Article ID 060507, 4 pages, 2001.
- [9] T. Jarlborg, “Spin-phonon interaction and band effects in the high- $T_c$  superconductor  $\text{HgBa}_2\text{CuO}_4$ ,” *Physical Review B*, vol. 68, no. 17, Article ID 172501, 4 pages, 2003.
- [10] T. Jarlborg, “Effects of spin-phonon interaction within the  $\text{CuO}$  plane of high- $T_c$  superconductors,” *Physica C*, vol. 454, no. 1-2, pp. 5–14, 2007.
- [11] O. K. Andersen, “Linear methods in band theory,” *Physical Review B*, vol. 12, no. 8, pp. 3060–3083, 1975.
- [12] T. Jarlborg and G. Arbmán, “The electronic structure of some A15 compounds by semiself-consistent band calculations,” *Journal of Physics F*, vol. 7, no. 9, pp. 1635–1649, 1977.
- [13] T. Jarlborg, “Properties of high- $T_c$  copper oxides from the nearly-free-electron model,” *Physical Review B*, vol. 76, no. 14, Article ID 140504, 4 pages, 2007.
- [14] T. Jarlborg, “Spin-phonon interaction in doped high- $T_c$  superconductors from density functional calculations,” *Physics Letters A*, vol. 295, no. 2-3, pp. 154–159, 2002.
- [15] T. Jarlborg, “Properties of high- $T_c$  copper oxides from band models of spin-phonon coupling,” *Journal of Superconductivity and Novel Magnetism*, vol. 22, no. 3, pp. 247–250, 2009.
- [16] T. Jarlborg, “Mechanisms for higher  $T_c$  in copper oxide superconductors: ideas from band calculations,” *Applied Physics Letters*, vol. 94, no. 21, Article ID 212503, 2009.
- [17] J. Humlíček, A. P. Litvinchuk, W. Kress, et al., “Lattice vibrations of  $\text{Y}_{1-x}\text{Pr}_x\text{Ba}_2\text{Cu}_3\text{O}_7$ : theory and experiment,” *Physica C*, vol. 206, no. 3-4, pp. 345–359, 1993.
- [18] C. Thomsen and M. Cardona, “Raman scattering in high- $T_c$  superconductors,” in *Physical Properties of High-Temperature Superconductors*, D. M. Ginsberg, Ed., vol. 409, World Scientific, Singapore, 1989.
- [19] H. Chen and J. Callaway, “Phonons and superconductivity in  $\text{Nd}_{2-x}\text{Ce}_x\text{CuO}_4$ ,” *Physical Review B*, vol. 46, no. 21, pp. 14321–14324, 1992.
- [20] R. E. Cohen, W. E. Pickett, and H. Krakauer, “Theoretical determination of strong electron-phonon coupling in  $\text{YBa}_2\text{Cu}_3\text{O}_7$ ,” *Physical Review Letters*, vol. 64, no. 21, pp. 2575–2578, 1990.
- [21] O. K. Andersen, A. I. Liechtenstein, O. Rodriguez, et al., “Electrons, phonons, and their interaction in  $\text{YBa}_2\text{Cu}_3\text{O}_7$ ,” *Physica C*, vol. 185–189, pp. 147–155, 1991.
- [22] T. Jarlborg and G. Santi, “Role of thermal disorder on the electronic structure in high- $T_c$  compounds,” *Physica C*, vol. 329, no. 4, pp. 243–257, 2000.
- [23] T. Jarlborg, “Spin-phonon coupling and  $q$ -dependence of spin excitations and high- $T_c$  superconductivity from band models,” *Physical Review B*, vol. 79, no. 9, Article ID 094530, 7 pages, 2009.
- [24] P. Piekarczyk and T. Egami, “Dynamic charge transfer and spin-phonon interaction in high- $T_c$  superconductors,” *Physical Review B*, vol. 72, no. 5, Article ID 054530, 9 pages, 2005.
- [25] T. Jarlborg, “Weak screening of high frequency phonons and superconductivity in  $\text{YBa}_2\text{Cu}_3\text{O}_7$ ,” *Solid State Communications*, vol. 71, no. 8, pp. 669–671, 1989.
- [26] T. Jarlborg, “Restricted screening and non-adiabatic electron-phonon coupling in high- $T_c$  oxides,” *Physics Letters A*, vol. 164, no. 3-4, pp. 345–348, 1992.
- [27] A. Abanov, A. V. Chubukov, and M. R. Norman, “Gap anisotropy and universal pairing scale in a spin-fluctuation model of cuprate superconductors,” *Physical Review B*, vol. 78, Article ID 220507, 4 pages, 2008.
- [28] T. Jarlborg, “Spin fluctuations, electron-phonon coupling and superconductivity in near-magnetic elementary metals—Fe, Co, Ni and Pd,” *Physica C*, vol. 385, no. 4, pp. 513–524, 2003.
- [29] T. Jarlborg, “Ferromagnetic and antiferromagnetic spin fluctuations and superconductivity in the hcp-phase of Fe,” *Physics Letters A*, vol. 300, no. 4-5, pp. 518–523, 2002.
- [30] I. I. Mazin and D. J. Singh, “Ferromagnetic spin fluctuation induced superconductivity in  $\text{Sr}_2\text{RuO}_4$ ,” *Physical Review Letters*, vol. 79, no. 4, pp. 733–736, 1997.
- [31] E. van Heumen, E. Muhlethaler, A. B. Kuzmenko, et al., “Optical determination of the relation between the electron-boson coupling function and the critical temperature in high- $T_c$  cuprates,” *Physical Review B*, vol. 79, no. 18, Article ID 184512, 7 pages, 2009.
- [32] J. Kübler, “Magnetic-moments of ferromagnetic and antiferromagnetic bcc and fcc iron,” *Physics Letters A*, vol. 81, p. 81, 1981.
- [33] C. S. Wang, B. M. Klein, and H. Krakauer, “Theory of magnetic and structural ordering in iron,” *Physical Review Letters*, vol. 54, no. 16, pp. 1852–1855, 1985.
- [34] B. Barbiellini, E. G. Moroni, and T. Jarlborg, “Effects of gradient corrections on electronic structure in metals,” *Journal of Physics: Condensed Matter*, vol. 2, no. 37, pp. 7597–7611, 1990.
- [35] T. C. Leung, X. W. Wang, and B. N. Harmon, “Band theoretical study of magnetism in  $\text{Sc}_2\text{CuO}_4$ ,” *Physical Review B*, vol. 37, pp. 384–388, 1988.
- [36] G. Y. Guo, W. M. Temmermann, and G. M. Stocks, “On the metal-semiconductor transition and antiferromagnetism in  $\text{La}_2\text{CuO}_4$ ,” *Journal of Physics C*, vol. 21, p. L103, 1988.
- [37] W. E. Pickett, “Electronic structure of the high-temperature oxide superconductors,” *Reviews of Modern Physics*, vol. 61, no. 2, pp. 433–512, 1989.
- [38] B. Barbiellini and T. Jarlborg, “Importance of local band effects for ferromagnetism in hole-doped  $\text{La}_2\text{CuO}_4$  cuprate superconductors,” *Physical Review Letters*, vol. 101, no. 15, Article ID 157002, 2008.
- [39] T. Jarlborg, “Anti-ferromagnetism, spin-phonon interaction and the local-density approximation in high- $T_c$  superconductors,” *Journal of Physics: Condensed Matter*, vol. 16, no. 13, pp. L173–L178, 2004.
- [40] B. Barbiellini and T. Jarlborg, “A simple approach towards non-local potentials: theory and applications,” *Journal of Physics: Condensed Matter*, vol. 1, no. 45, pp. 8865–8876, 1989.
- [41] T. Jarlborg, “Pair correlation functions for exchange and correlation in uniform spin densities,” *Physics Letters A*, vol. 260, no. 5, pp. 395–399, 1999.

## Research Article

# The Phenomenology of Iron Pnictides Superconductors Explained in the Framework of *s*-Wave Three-Band Eliashberg Theory

**G. A. Ummarino**

*Dipartimento di Fisica and CNISM, Politecnico di Torino, Corso Duca degli Abruzzi 24, 10129 Torino, Italy*

Correspondence should be addressed to G. A. Ummarino, giovanni.ummarino@infm.polito.it

Received 25 May 2009; Revised 10 August 2009; Accepted 3 September 2009

Academic Editor: Igor Mazin

Copyright © 2010 G. A. Ummarino. This is an open access article distributed under the Creative Commons Attribution License, which permits unrestricted use, distribution, and reproduction in any medium, provided the original work is properly cited.

The *s*-wave three-band Eliashberg theory can simultaneously reproduce the experimental critical temperatures and the gap values of the superconducting materials  $\text{LaFeAsO}_{0.9}\text{F}_{0.1}$ ,  $\text{Ba}_{0.6}\text{K}_{0.4}\text{Fe}_2\text{As}_2$  and  $\text{SmFeAsO}_{0.8}\text{F}_{0.2}$  as exponent of the more important families of iron pnictides. In this model the dominant role is played by interband interactions and the order parameter undergoes a sign reversal between hole and electron bands (*s* $\pm$ -wave symmetry). The values of all the gaps (with the exact experimental critical temperature) can be obtained by using high values of the electron-boson coupling constants and small typical boson energies (in agreement with experiments).

The discovery of Fe-based pnictide superconductors [1–3] has aroused great interest in the scientific community. For the first time noncuprate superconductor shows high critical temperature. In these systems, as in cuprates, the superconductivity occurs upon charge doping of a magnetic parent compound above a certain critical value. The more relevant difference is that in cuprates the parent compound is a Mott insulator with localized charge carriers and a strong Coulomb repulsion between electrons, while in the pnictides it is a bad metal and shows a tetragonal to orthorhombic structural transition below  $\approx 140$  K, followed by the onset of an antiferromagnetic spin-density-wave ordering [4]. Charge doping gives rise to superconductivity and, at the same time, inhibits the occurrence of both the static magnetic order and the structural transition. The Fermi surface consists of two or three hole-like sheets around the  $\Gamma$  point in the first Brillouin zone and two electron-like sheets around *M* point. Up to now, the most intensively studied systems are the 1111 compounds,  $\text{ReFeAsO}_{1-x}\text{F}_x$  (Re = La, Sm, Nd, Pr, etc.) and the 122 ones, hole- or electron-doped  $\text{AFe}_2\text{As}_2$  (A = Ba, Sr, Ca).

At present it is not completely clear what is the microscopic pairing mechanism responsible for superconductivity.

The conventional phonon-mediated coupling mechanism is too weak and cannot explain the observed high  $T_c$  within the standard Migdal-Eliashberg theory [5, 6]. The calculated  $T_c$  increases only marginally with the inclusion of multiband effects and remains far from experimental values. On the other hand, the magnetic nature of the parent compound seems to favor a coupling mechanism based on nesting-related antiferromagnetic spin fluctuations [7]. In this case an interband sign reversal of the order parameter between different sheets of the Fermi surface (*s* $\pm$  symmetry) is predicted. The number, amplitude, and symmetry of the superconducting energy gaps are indeed fundamental physical quantities that any microscopic model of superconductivity has to account for. Experiments with powerful techniques such as ARPES, point-contact spectroscopy, and STM, have been carried out to study the superconducting gaps in pnictides (for a review see [8]). Although the results are sometimes in disagreement with each other, a multigap scenario is emerging with evidence for rather high gap ratios,  $\Delta_1/\Delta_2 \approx 2\text{--}3$  [8]. A two-band BCS model cannot account either for the amplitude of the experimental gaps or for their ratio. Three-band BCS models have been investigated [9–11] which can reproduce the experimental gap ratio but not

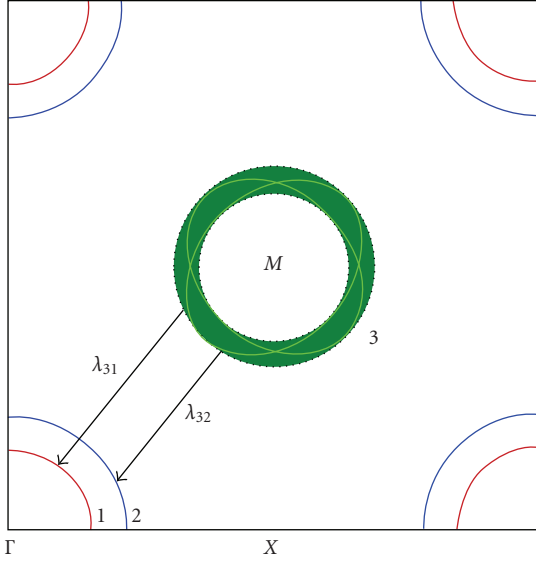


FIGURE 1: Schematic drawing of the multiband model used in this work. The two hole bands (1 and 2) are centered around the  $\Gamma$  point, while the equivalent electron band (3) around the  $M$  point of the reduced Brillouin zone.

the exact experimental gap values when the experimental  $T_c$  is exactly reproduced. In this regard, a reliable study has to be carried out within the framework of the Eliashberg theory for strong coupling superconductors [12–18], due to the possible high values of the coupling constants necessary to explain the experimental data.

By using this strong-coupling approach, I show here that the superconducting iron pnictides represent a case of dominant negative interband-channel superconductivity ( $s\pm$ -wave symmetry) with high values of the electron-boson coupling constants and small typical boson energies. Furthermore I prove that a small contribution of intraband coupling does not significantly affect the obtained results and that the contribution of the Coulomb pseudopotential is negligible.

The electronic structure of pnictides can be approximately reproduced by using a three-band model (Figure 1) with two hole bands (1 and 2) and one equivalent electron band (3) [9]. The  $s$ -wave order parameters of the hole bands  $\Delta_1$  and  $\Delta_2$  have opposite sign with respect to that of the electron  $\Delta_3$  [7]. In such systems intraband coupling could be provided by phonons while interband coupling by antiferromagnetic spin fluctuations which in a one-band system are always pair breaking but here, in a multiband system, the interband terms can contribute to increase the critical temperature. In the multiband Eliashberg equations the spin fluctuations term in the intraband channel has positive sign for the renormalization functions  $Z_i$  and negative sign for the superconducting order parameters  $\Delta_i$  thus leading to a strong reduction of  $T_c$ . However, if we consider negative interband contributions in the  $\Delta_i$  equations, the final result can be an increase of the critical temperature [19].

The generalization of the Eliashberg theory [12–18] for multiband systems has already been used with success to

study the  $\text{MgB}_2$  superconductor [20–23]. To obtain the gaps and the critical temperature within the  $s$ -wave, three-band Eliashberg equations, one has to solve six coupled equations for the gaps  $\Delta_i(i\omega_n)$  and the renormalization functions  $Z_i(i\omega_n)$ , where  $i$  is a band index that ranges between 1 and 3 (see Figure 1) and  $\omega_n$  are the Matsubara frequencies. For completeness we included in the equations the nonmagnetic and magnetic impurity scattering rates in the Born approximation,  $\Gamma_{ij}^N$  and  $\Gamma_{ij}^M$ . In the imaginary-axis formulation [24] the equations are

$$\begin{aligned} \omega_n Z_i(i\omega_n) &= \omega_n + \sum_j \left( \Gamma_{ij}^N + \Gamma_{ij}^M \right) N_j^Z(i\omega_n) \\ &+ \pi T \sum_{m,j} \Lambda_{ij}^Z(i\omega_n, i\omega_m) N_j^Z(i\omega_m), \end{aligned} \quad (1)$$

$$\begin{aligned} Z_i(i\omega_n) \Delta_i(i\omega_n) &= \sum_j \left( \Gamma_{ij}^N - \Gamma_{ij}^M \right) N_j^\Delta(i\omega_n) \\ &+ \pi T \sum_{m,j} \left[ \Lambda_{ij}^\Delta(i\omega_n, i\omega_m) - \mu_{ij}^*(\omega_c) \right] \\ &\times \theta(\omega_c - |\omega_m|) N_j^\Delta(i\omega_m), \end{aligned} \quad (2)$$

where  $\Lambda_{ij}^Z(i\omega_n, i\omega_m) = \Lambda_{ij}^{\text{ph}}(i\omega_n, i\omega_m) + \Lambda_{ij}^{\text{sp}}(i\omega_n, i\omega_m)$ ,  $\Lambda_{ij}^\Delta(i\omega_n, i\omega_m) = \Lambda_{ij}^{\text{ph}\Delta}(i\omega_n, i\omega_m) - \Lambda_{ij}^{\text{sp}\Delta}(i\omega_n, i\omega_m)$ .  $\theta$  is the Heaviside function and  $\omega_c$  is a cut-off energy. In particular,  $\Lambda_{ij}^{\text{ph,sp}}(i\omega_n, i\omega_m) = 2 \int_0^{+\infty} d\Omega \Omega \alpha_{ij}^2 F^{\text{ph,sp}}(\Omega) / [(\omega_n - \omega_m)^2 + \Omega^2]$ , where ph means “phonon” and sp “spin fluctuations.” Finally,  $N_j^\Delta(i\omega_m) = \Delta_j(i\omega_m) / \sqrt{\omega_m^2 + \Delta_j^2(i\omega_m)}$  and  $N_j^Z(i\omega_m) = \omega_m / \sqrt{\omega_m^2 + \Delta_j^2(i\omega_m)}$ .

In the real axis formulation the multiband  $s$ -wave Eliashberg equations [25, 26] are

$$\begin{aligned} \omega Z_i(\omega) &= \omega + \sum_j \left( \Gamma_{ij}^N + \Gamma_{ij}^M \right) N_j^Z(\omega) \\ &+ \sum_j \int_{-\infty}^{+\infty} d\omega' \Lambda_{ij}^Z(\omega, \omega') \text{Real} \left[ N_j^Z(\omega') \right] \text{OOC} \end{aligned} \quad (3)$$

$$\begin{aligned} Z_i(\omega) \Delta_i(\omega) &= \sum_j \left( \Gamma_{ij}^N - \Gamma_{ij}^M \right) N_j^\Delta(\omega) \\ &+ \sum_j \int_{-\infty}^{+\infty} d\omega' \left[ \Lambda_{ij}^\Delta(\omega, \omega') - \mu_{ij}^*(\omega_c) \theta(\omega_c - |\omega'|) \right] \\ &\times \text{Real} \left[ N_j^\Delta(\omega') \right], \end{aligned} \quad (4)$$

where now  $\Lambda_{ij}^Z(\omega, \omega') = \Lambda_{ij}^{\text{ph}}(\omega, \omega') + \Lambda_{ij}^{\text{sp}}(\omega, \omega')$ ,  $\Lambda_{ij}^\Delta(\omega, \omega') = \Lambda_{ij}^{\text{ph}\Delta}(\omega, \omega') - \Lambda_{ij}^{\text{sp}\Delta}(\omega, \omega')$ . In particular,  $\Lambda_{ij}^{\text{ph,sp}\Delta}(\omega, \omega') = \int_0^{+\infty} d\Omega (\alpha_{ij}^2 F^{\text{ph,sp}}(\Omega) / 2) [(\tanh(\omega'/2T) + \coth(\Omega/2T)) / (\omega' + \Omega - \omega - i\delta) - (\tanh(\omega'/2T) - \coth(\Omega/2T)) / (\omega' - \Omega - \omega - i\delta)]$ ,

and  $N_j^A(\omega) = \Delta_j(\omega)/\sqrt{\omega^2 - \Delta_j^2(\omega)}$  and  $N_j^Z(\omega) = \omega/\sqrt{\omega^2 - \Delta_j^2(\omega)}$ .

In principle the solution of the three-band Eliashberg equations shown in (1) (or (2)) requires a huge number of input parameters: (i) nine electron-phonon spectral functions,  $\alpha_{ij}^2 F^{\text{ph}}(\Omega)$ ; (ii) nine electron-SF spectral functions,  $\alpha_{ij}^2 F^{\text{sp}}(\Omega)$ ; (iii) nine elements of the Coulomb pseudopotential matrix,  $\mu_{ij}^*(\omega_c)$ ; (iv) nine nonmagnetic  $\Gamma_{ij}^N$  and nine paramagnetic  $\Gamma_{ij}^M$  impurity scattering rates.

It is obvious that a practical solution of these equations requires a drastic reduction in the number of free parameters of the model. According to the work of Mazin et al. [7] I know that (i)  $\lambda_{ii}^{\text{ph}} \gg \lambda_{ij}^{\text{ph}} \approx 0$ , that is, phonons mainly provide intraband coupling but the total electron-phonon coupling constant  $\sum_i \lambda_{ii}^{\text{ph}}$  should be very small [5, 6], (ii)  $\lambda_{ij}^{\text{sp}} \gg \lambda_{ii}^{\text{sp}} \approx 0$ , that is, SF mainly provide interband coupling. I include these features in the simplest three-band model by posing  $\lambda_{ii}^{\text{ph}} = \lambda_{ij}^{\text{ph}} = 0$ ,  $\lambda_{ii}^{\text{sp}} = 0$ , and  $\mu_{ii}^*(\omega_c) = \mu_{ij}^*(\omega_c) = 0$ . Here, of course, it is  $\lambda_{ij}^{\text{ph,sp}} = 2 \int_0^{\omega_c} d\Omega (\alpha_{ij}^2 F^{\text{ph,sp}}(\Omega)/\Omega)$ . Moreover, I set  $\Gamma_{ij}^N = \Gamma_{ij}^M = 0$  in (1)-(2) and (3)-(4).

Within these approximations, the electron-boson coupling-constant matrix  $\lambda_{ij} = \lambda_{ij}^{\text{sp}}$  becomes [9]

$$\begin{pmatrix} 0 & 0 & \lambda_{13} = \lambda_{31}\nu_1 \\ 0 & 0 & \lambda_{23} = \lambda_{32}\nu_2 \\ \lambda_{31} & \lambda_{32} & 0 \end{pmatrix}, \quad (5)$$

where  $\nu_1 = N_1(0)/N_3(0)$ ,  $\nu_2 = N_2(0)/N_3(0)$ , and  $N_i(0)$  is the normal density of states at the Fermi level for the  $i$ -band ( $i = 1, 2, 3$  according to Figure 1).

I initially solved the Eliashberg equations on the imaginary axis to calculate the critical temperature and, by means of the technique of the Padè approximants [27, 28], to obtain the low-temperature value of the gaps because in presence of a strong coupling interaction or of impurities, the value of  $\Delta_i(i\omega_n=0)$  obtained by solving the imaginary-axis Eliashberg equations can be very different from the value of  $\Delta_i$  obtained from the real-axis Eliashberg equations [29]. I also solved the three-band Eliashberg equations in the real-axis formulation.

I reproduced the critical temperature and the gap values in three representative cases: (i) the compound  $\text{LaFeAsO}_{0.9}\text{F}_{0.1}$  with  $T_c = 27$  K where point-contact spectroscopy measurements gave  $\Delta_1(0) \approx 3.8$  meV and  $\Delta_2(0) \approx 8.0$  meV [30]; (ii) the compound  $\text{Ba}_{0.6}\text{K}_{0.4}\text{Fe}_2\text{As}_2$  with  $T_c = 37$  K where ARPES measurements gave  $\Delta_1(0) \approx 12.1$  meV,  $\Delta_2(0) \approx 5.5$  meV, and  $\Delta_3(0) \approx 12.8$  meV [31]; (iii) the compound  $\text{SmFeAsO}_{0.8}\text{F}_{0.2}$  with  $T_c = 52$  K where, according to point-contact spectroscopy measurements,  $\Delta_1(0) \approx 17.0$  meV and  $\Delta_2(0) \approx 5.7$  meV [32, 33].

Inelastic neutron-scattering experiments suggest that the typical boson energy possibly responsible for superconductivity ranges roughly between 10 and 30 meV [34, 35]. In the numerical simulations I used spectral functions with Lorentzian shape, that is,  $\alpha_{ij}^2 F(\Omega) = C_{ij}[L(\Omega + \Omega_{ij}, Y_{ij}) - L(\Omega - \Omega_{ij}, Y_{ij})]$ , where  $L(\Omega \pm \Omega_{ij}, Y_{ij}) = [(\Omega \pm \Omega_{ij})^2 + (Y_{ij})^2]^{-1}$ ,  $C_{ij}$  are the normalization constants necessary to

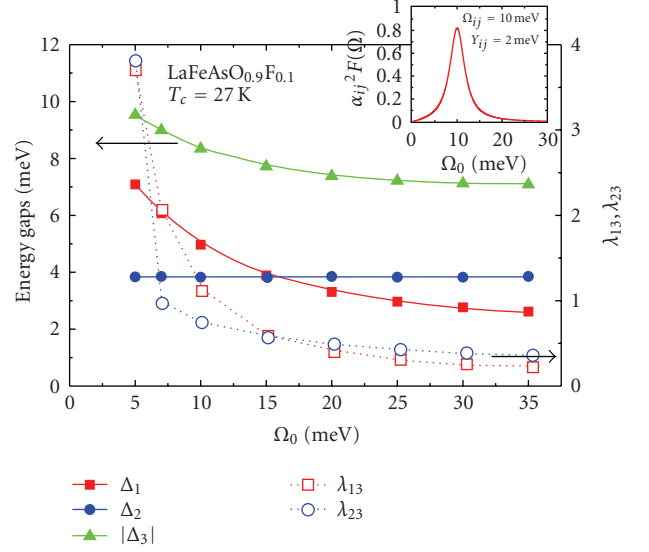


FIGURE 2: Full symbols, left axis: calculated gap values at  $T = 2$  K for  $\text{LaFeAsO}_{0.9}\text{F}_{0.1}$  as a function of typical boson energy  $\Omega_0$ . Open symbols, right axis: electron-boson coupling constants,  $\lambda_{13}$  and  $\lambda_{23}$ , as a function of  $\Omega_0$ . The inset shows the spectral function used in this model in the case  $\Omega_{ij} = 10$  meV.

obtain the proper values of  $\lambda_{ij}$  while  $\Omega_{ij}$  and  $Y_{ij}$  are the peak energies and half-widths, respectively. In all the calculations I always set  $\Omega_{ij} = \Omega_0$ , with  $\Omega_0$  ranging between 5 and 35 meV and  $Y_{ij} = 2$  meV. The cut-off energy is  $\omega_c = 12 \cdot \Omega_0$  and the maximum quasiparticle energy is  $\omega_{\text{max}} = 16 \cdot \Omega_0$ .

In the  $T_c = 27$  K case I know that  $\nu_1 = 0.03$  and  $\nu_2 = 1$  [36] while in the  $T_c = 37$  K case  $\nu_1 = 1$  and  $\nu_2 = 2$  [9] and in the  $T_c = 52$  K case I have  $\nu_1 = 0.4$  and  $\nu_2 = 0.5$  [37]. Once the energy of the boson peak  $\Omega_0$  is set, only two free parameters are left in the model:  $\lambda_{31}$  and  $\lambda_{32}$ .

By properly selecting the values of these parameters it is relatively easy to obtain the experimental values of the critical temperature and of the small gap, which is well known. It is more difficult to reproduce the values of the large gaps of bands 1 and 3 since, due to the high  $2\Delta_{1,3}/k_B T_c$  ratio (of the order of 8-9), high values of the coupling constants and small boson energies are required. Figures 2, 3, and 4 show the values of the calculated gaps (full symbols, left axis) as a function of the boson peak energy,  $\Omega_0$ . The corresponding values of  $\lambda_{13}$  and  $\lambda_{12}$ , chosen in order to reproduce the values of  $T_c$  and of the small gap,  $\Delta_2$ , are also shown in the figure (open symbols, right axis). In all materials examined, only when  $\Omega_0 \leq 10$  meV the values of the large gap correspond to the experimental data. Indeed, when  $\Omega_0$  increases, the values of  $\Delta_1$  and  $\Delta_3$  strongly decrease. As a consequence, a rather small energy of the boson peak together with a very strong coupling (particularly in the 3-1 channel) is needed in order to obtain the experimental  $T_c$  and the correct gap values. In this regard, it is worth noticing that the absolute values of the large gaps *cannot* be reproduced in a interband-only, two-band Eliashberg model [38], as well as within a three-band BCS model. In the latter case it is only possible to obtain a ratio of the gaps close to the experimental one [10, 11].

TABLE 1: The effect of the intraband terms and Coulomb interaction on the gap values.

Pure interband	$\lambda_{ii} = 0.$	$\mu_{ij}^* = 0$	$\Omega_0 = 10 \text{ meV}$
Free parameters	$\lambda_{31} = 4.267$	$\lambda_{32} = 1.138$	—
Results	$\Delta_1 = 10.29 \text{ meV}$	$\Delta_2 = 5.56 \text{ meV}$	$ \Delta_3  = 10.22 \text{ meV}$
Intraband	$\lambda_{ii} = 0.4$	$\mu_{ij}^* = 0$	$\Omega_0 = 10 \text{ meV}$
Free parameters	$\lambda_{31} = 3.866$	$\lambda_{32} = 0.471$	—
Results	$\Delta_1 = 10.30 \text{ meV}$	$\Delta_2 = 5.62 \text{ meV}$	$ \Delta_3  = 10.24 \text{ meV}$
Intraband and Coulomb	$\lambda_{ii} = 0.4$	$\mu_{ij}^* = 0.1$	$\Omega_0 = 10 \text{ meV}$
Free parameters	$\lambda_{31} = 2.730$	$\lambda_{32} = 0.758$	—
Results	$\Delta_1 = 7.49 \text{ meV}$	$\Delta_2 = 5.72 \text{ meV}$	$ \Delta_3  = 7.98 \text{ meV}$

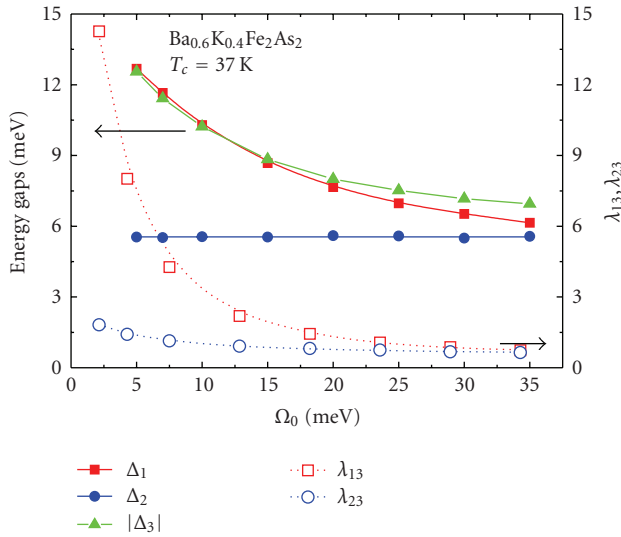


FIGURE 3: Full symbols, left axis: calculated gap values at  $T = 2 \text{ K}$  for  $\text{Ba}_{0.6}\text{K}_{0.4}\text{Fe}_2\text{As}_2$  as a function of typical boson energy  $\Omega_0$ . Open symbols, right axis: electron-boson coupling constants,  $\lambda_{13}$  and  $\lambda_{23}$ , as a function of  $\Omega_0$ .

I also tested the effect into the model of a small intraband coupling (possibly of phonon origin). In the case of  $\text{Ba}_{0.6}\text{K}_{0.4}\text{Fe}_2\text{As}_2$  ( $T_c = 37 \text{ K}$ ) I fixed  $\Omega_0 = 10 \text{ meV}$  and  $\lambda_{ii} = 0.4$  since I know indeed that this coupling cannot be very high [5, 6]. Then I determined the free parameters  $\lambda_{31}$  and  $\lambda_{32}$  in order to obtain  $T_c = 37 \text{ K}$ . It might be thought that this term can sensibly contribute to increase the gap values but, as can be seen in Table 1, this is not the case as the gap values only show a slight increase.

The effect of Coulomb interaction was also investigated for the case shown in Table 1 where a weak intraband coupling is included. I chose  $\mu_{ij}^* = \mu_{ii}^* = 0.1$  and, as expected, I found that the intraband Coulomb pseudopotential has a negligible effect while the interband one [19] strongly contributes to raise  $T_c$  and reduces in a considerable way [24] the value of  $\lambda_{31}$ . In this case, as shown in Table 1, it is only possible to obtain the correct value of the small gap because the electron-boson coupling is now too small and it is impossible to reproduce the value of the big gap. As a

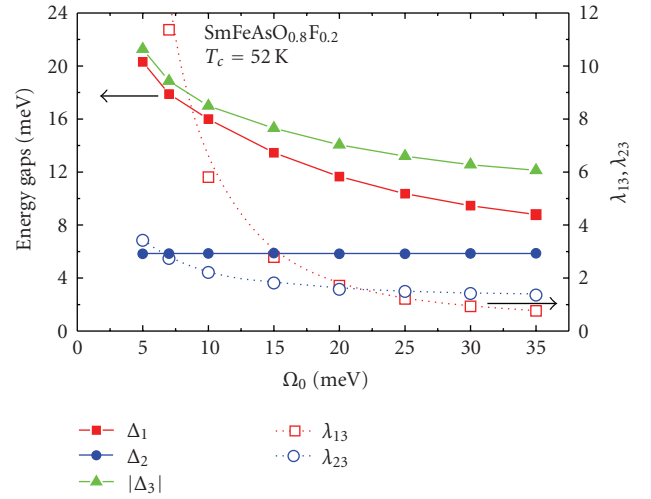


FIGURE 4: Full symbols, left axis: calculated gap values at  $T = 2 \text{ K}$  for  $\text{SmFeAsO}_{0.8}\text{F}_{0.2}$  as a function of the typical boson energy  $\Omega_0$ . Open symbols, right axis: electron-boson coupling constants,  $\lambda_{13}$  and  $\lambda_{23}$ , as a function of  $\Omega_0$ .

consequence, this result seems to exclude a strong interband Coulomb interaction in these compounds.

I also calculated the superconductive density of states in all three cases. The parameters used for the  $T_c = 27.00 \pm 0.01 \text{ K}$  case are  $\Omega_0 = 10 \text{ meV}$ ,  $\lambda_{13} = 1.115$ , and  $\lambda_{32} = 0.743$ , for the  $T_c = 37.00 \pm 0.01 \text{ K}$  case  $\Omega_0 = 10 \text{ meV}$ ,  $\lambda_{13} = 4.267$ , and  $\lambda_{23} = 1.138$  and for  $T_c = 52.00 \pm 0.01 \text{ K}$  case  $\Omega_0 = 10 \text{ meV}$ ,  $\lambda_{13} = 5.808$ , and  $\lambda_{23} = 2.208$ .

The value of coupling constant  $\lambda_{31}$  is in the range 1–6 and this fact, at a first glance, may seem very unusual but these systems have some peculiarities in common with the heavy fermions superconductors. For example, in the compound  $\text{LaFeAsO}_{0.9}\text{F}_{0.1}$ , the normal state at  $T_c$  is asymmetric and pseudogapped, with two broad maxima that are progressively smoothed out on increasing the temperature [30]. This shape is very similar to that observed by point contact spectroscopy in materials with long-range spin-density-wave order, like  $\text{URu}_2\text{Si}_2$  [39, 40]. The calculated superconductive normalized conductances are shown in Figure 5; the presence

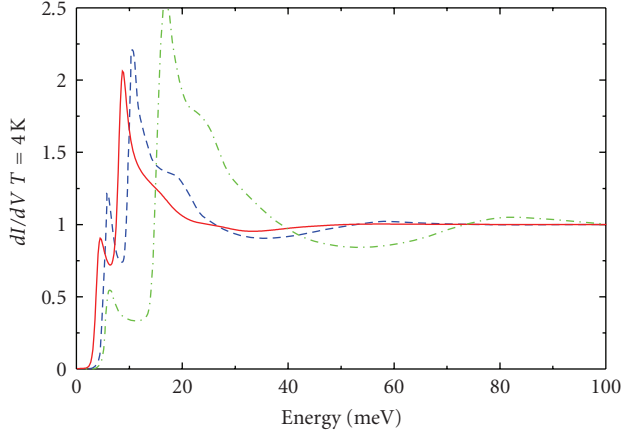


FIGURE 5: Calculated energy dependence of the superconductive normalized tunneling conductance at  $T = 4$  K for  $\text{LaFeAsO}_{0.9}\text{F}_{0.1}$  ( $T_c = 27$  K, red solid line),  $\text{Ba}_{0.6}\text{K}_{0.4}\text{Fe}_2\text{As}_2$  ( $T_c = 37$  K, dash blue line), and for  $\text{SmFeAsO}_{0.8}\text{F}_{0.2}$  ( $T_c = 52$  K, green dash-dot line).

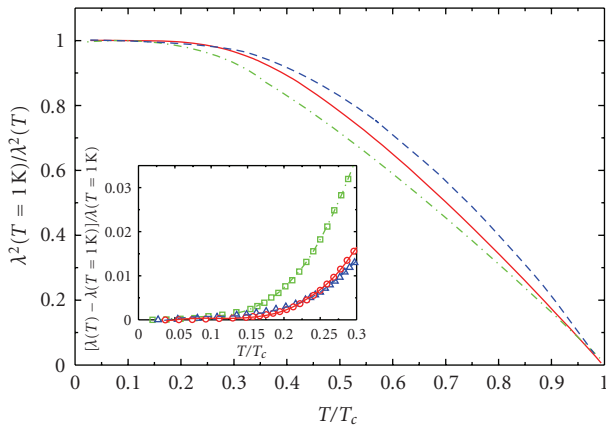


FIGURE 6: Calculated temperature dependence of the penetration depth ( $[\lambda(T)/\lambda(T = 1\text{K})]^2$ ) for  $\text{LaFeAsO}_{0.9}\text{F}_{0.1}$  ( $T_c = 27$  K, red solid line),  $\text{Ba}_{0.6}\text{K}_{0.4}\text{Fe}_2\text{As}_2$  ( $T_c = 37$  K, dash blue line), and for  $\text{SmFeAsO}_{0.8}\text{F}_{0.2}$  ( $T_c = 52$  K, green dash-dot line). The inset shows the behaviour of  $[\lambda(T) - \lambda(T = 1\text{K})]/\lambda(T = 1\text{K})$  obtained by solution of Eliashberg equations: red circles for  $\text{LaFeAsO}_{0.9}\text{F}_{0.1}$ , dark blue triangle for  $\text{Ba}_{0.6}\text{K}_{0.4}\text{Fe}_2\text{As}_2$ , green squares for  $\text{SmFeAsO}_{0.8}\text{F}_{0.2}$ . The lines are the third-order polynomial fits.

of a hump at  $\Omega \approx \Omega_0 + \Delta_1$  is a typical strong coupling effect [41]. This feature, of course, is more evident when  $\lambda_{13}$  is bigger. By cause of thermal broadening it is impossible to separate the peaks of the gaps  $\Delta_1$  and  $\Delta_3$ .

The penetration depth as a function of temperature has been calculated in the three cases and is reported in Figure 6. It is in qualitative agree with the experimental data [42]. The inset shows the behaviour of  $[\lambda(T) - \lambda(T = 1\text{K})]/\lambda(T = 1\text{K})$  at low temperature. Although at sufficiently low temperature an exponential fit may be certainly possible the inset shows that, on a larger  $T$  range (up to  $T/T_c \sim 0.3$ ) these curves can be best fitted by a third-order polynomial as experimentally observed [42].

In conclusion, I have shown that the newly discovered iron pnictides very likely represent a case of dominant negative interband-channel pairing superconductivity where an electron-boson coupling, such as the electron-spin fluctuations one, can become a fundamental ingredient to increase  $T_c$  in a multiband strong-coupling picture. In particular, the present results prove that a simple three-band model in strong-coupling regime can reproduce in a quantitative way the experimental  $T_c$  and the energy gaps of the pnictide superconductors with only two free parameters,  $\lambda_{31}$  and  $\lambda_{32}$ , provided that the typical energies of the spectral functions are of the order of 10 meV and the coupling constants are very high ( $1 < \lambda_{31} < 6$ ).

## Acknowledgments

The author thanks I. I. Mazin for useful discussions, Mauro Tortello and Dario Daghero for manuscript revision.

## References

- [1] Y. Kamihara, T. Watanabe, M. Hirano, and H. Hosono, “Iron-based layered superconductor  $\text{La}[\text{O}_{1-x}\text{F}_x]\text{FeAs}$  ( $x = 0.05 - 0.12$ ) with  $T_c = 26\text{K}$ ,” *Journal of the American Chemical Society*, vol. 130, no. 11, pp. 3296–3297, 2008.
- [2] Z.-A. Ren, W. Lu, J. Yang, et al., “Superconductivity at 55 K in iron-based F-doped layered quaternary compound  $\text{Sm}[\text{O}_{1-x}\text{F}_x]\text{FeAs}$ ,” *Chinese Physics Letters*, vol. 25, no. 6, pp. 2215–2216, 2008.
- [3] M. Rotter, M. Tegel, and D. Johrendt, “Superconductivity at 38 K in the iron arsenide  $(\text{Ba}_{1-x}\text{K}_x)\text{Fe}_2\text{As}_2$ ,” *Physical Review Letters*, vol. 101, no. 10, Article ID 107006, 2008.
- [4] C. de La Cruz, Q. Huang, J. W. Lynn, et al., “Magnetic order close to superconductivity in the iron-based layered  $\text{LaO}_{1-x}\text{F}_x\text{FeAs}$  systems,” *Nature*, vol. 453, no. 7197, pp. 899–902, 2008.
- [5] L. Boeri, O. V. Dolgov, and A. A. Golubov, “Is  $\text{LaFeAsO}_{1-x}\text{F}_x$  an electron-phonon superconductor?” *Physical Review Letters*, vol. 101, no. 2, Article ID 026403, 4 pages, 2008.
- [6] L. Boeri, O. V. Dolgov, and A. A. Golubov, “Electron-phonon properties of pnictide superconductors,” *Physica C*, vol. 469, no. 9–12, pp. 628–634, 2009.
- [7] I. I. Mazin, D. J. Singh, M. D. Johannes, and M. H. Du, “Unconventional superconductivity with a sign reversal in the order parameter of  $\text{LaFeAsO}_{1-x}\text{F}_x$ ,” *Physical Review Letters*, vol. 101, no. 5, Article ID 057003, 2008.
- [8] *Physica C* 469, 2009, Special Issue on Pnictides.
- [9] I. I. Mazin and J. Schmalian, “Pairing symmetry and pairing state in ferropnictides: theoretical overview,” *Physica C*, vol. 469, no. 9–12, pp. 614–627, 2009.
- [10] L. Benfatto, M. Capone, S. Caprara, C. Castellani, and C. di Castro, “Multiple gaps and superfluid density from interband pairing in a four-band model of the iron oxypnictides,” *Physical Review B*, vol. 78, no. 14, Article ID 140502, 4 pages, 2008.
- [11] E. Z. Kuchinskii and M. V. Sadovskii, “Multiple bands: a key to high-temperature superconductivity in iron arsenides?” *Journal of Experimental and Theoretical Physics Letters*, vol. 11, no. 3, pp. 156–160, 2009.
- [12] G. M. Eliashberg, “Interactions between electrons and lattice vibrations in a superconductor,” *Soviet Physycs. JETP Letters*, vol. 11, no. 3, pp. 696–702, 1960.

- [13] D. J. Scalapino, "The Electron-phonon interaction and strong-coupling superconductors," in *Superconductivity*, R. D. Parks, Ed., p. 449, Marcel Dekker, New York, NY, USA, 1969.
- [14] J. P. Carbotte, "Properties of boson-exchange superconductors," *Reviews of Modern Physics*, vol. 62, no. 4, pp. 1027–1157, 1990.
- [15] P. B. Allen and B. Mitrovich, "Theory of superconducting  $T_c$ ," in *Solid State Physics*, H. Ehrenreich, F. Seitz, and D. Turnbull, Eds., vol. 37, Academic Press, New York, NY, USA, 1982.
- [16] F. Marsiglio and J. P. Carbotte, "Electron-phonon superconductivity," in *The Physics of Conventional and Unconventional Superconductors*, K. H. Bennemann and J. B. Ketterson, Eds., p. 233, Springer, New York, NY, USA, 2003.
- [17] F. Marsiglio, "Eliashberg theory of the critical temperature and isotope effect. Dependence on bandwidth, band-filling, and direct Coulomb repulsion," *Journal of Low Temperature Physics*, vol. 87, no. 5-6, pp. 659–682, 1992.
- [18] C. R. Leavens and E. Talbot, "Effect of thermal phonons on the superconducting transition temperature," *Physical Review B*, vol. 28, no. 3, pp. 1304–1313, 1983.
- [19] G. A. Ummarino, "Effects of magnetic impurities on two-band superconductor," *Journal of Superconductivity and Novel Magnetism*, vol. 20, no. 7-8, pp. 639–642, 2007.
- [20] S. V. Shulga, S.-L. Drechsler, G. Fuchs, et al., "Upper critical field peculiarities of superconducting  $YnI_2B_2C$  and  $LuNi_2B_2C$ ," *Physical Review Letters*, vol. 80, no. 8, pp. 1730–1733, 1998.
- [21] S. D. Adrian, S. A. Wolf, O. V. Dolgov, S. Shulga, and V. Z. Kresin, "Density of states and the energy gap in superconducting cuprates," *Physical Review B*, vol. 56, no. 13, pp. 7878–7881, 1997.
- [22] G. A. Ummarino, R. S. Gonnelli, S. Massidda, and A. Bianconi, "Two-band Eliashberg equations and the experimental  $T_c$  of the diboride  $Mg_{1-x}Al_xB_2$ ," *Physica C*, vol. 407, no. 3-4, pp. 121–127, 2004.
- [23] E. J. Nicol and J. P. Carbotte, "Properties of the superconducting state in a two-band model," *Physical Review B*, vol. 71, no. 5, Article ID 054501, 18 pages, 2005.
- [24] G. A. Ummarino, "Iron-based layered compounds: the effect of negative interband coupling," *Journal of Superconductivity and Novel Magnetism*, vol. 22, no. 6, pp. 603–607, 2009.
- [25] O. V. Dolgov, R. K. Kremer, J. Kortus, A. A. Golubov, and S. V. Shulga, "Thermodynamics of two-band superconductors: the case of  $MgB_2$ ," *Physical Review B*, vol. 72, no. 2, Article ID 024504, 2005.
- [26] D. Parker, O. V. Dolgov, M. M. Korshunov, A. A. Golubov, and I. I. Mazin, "Extended  $s_{\pm}$  scenario for the nuclear spin-lattice relaxation rate in superconducting pnictides," *Physical Review B*, vol. 78, no. 13, Article ID 134524, 5 pages, 2008.
- [27] H. J. Vidberg and J. W. Serene, "Solving the Eliashberg equations by means of N-point Padé approximants," *Journal of Low Temperature Physics*, vol. 29, no. 3-4, pp. 179–192, 1977.
- [28] C. R. Leavens and D. S. Ritchie, "Extension of the N-point Padé approximants solution of the Eliashberg equations to  $T \sim T_C$ ," *Solid State Communications*, vol. 53, no. 2, pp. 137–142, 1985.
- [29] G. A. Ummarino and R. S. Gonnelli, "Real-axis direct solution of the d-wave Eliashberg equations and the tunneling density of states in optimally doped  $Bi_2Sr_2CaCu_2O_{8+x}$ ," *Physica C*, vol. 328, no. 3, pp. 189–194, 1999.
- [30] R. S. Gonnelli, D. Daghero, M. Tortello, et al., "Coexistence of two order parameters and a pseudogaplike feature in the iron-based superconductor  $LaFeAsO_{1-x}F_x$ ," *Physical Review B*, vol. 79, no. 18, Article ID 184526, 11 pages, 2009.
- [31] H. Ding, P. Richard, K. Nakayama, et al., "Observation of Fermi-surface-dependent nodeless superconducting gaps in  $Ba_{0.6}K_{0.4}Fe_2As_2$ ," *Europhysics Letters*, vol. 83, no. 4, Article ID 47001, 2008.
- [32] D. Daghero, M. Tortello, R. S. Gonnelli, V. A. Stepanov, N. D. Zhigadlo, and J. Karpinski, "Evidence for two-gap nodeless superconductivity in  $SmFeAsO_{1-x}F_x$  from point-contact Andreev-reflection spectroscopy," *Physical Review B*, vol. 80, no. 6, 2009.
- [33] D. Daghero, M. Tortello, R. S. Gonnelli, et al., "Point-contact Andreev-reflection spectroscopy in  $ReFeAsO_{1-x}F_x$  (Re = La, Sm): possible evidence for two nodeless gaps," *Physica C*, vol. 469, no. 9–12, pp. 512–520, 2009.
- [34] A. D. Christianson, E. A. Goremychkin, R. Osborn, et al., "Unconventional superconductivity in  $Ba_{0.6}K_{0.4}Fe_2As_2$  from inelastic neutron scattering," *Nature*, vol. 456, no. 7224, pp. 930–932, 2008.
- [35] R. Osborn, S. Rosenkranz, E. A. Goremychkin, and A. D. Christianson, "Inelastic neutron scattering studies of the spin and lattice dynamics in iron arsenide compounds," *Physica C*, vol. 469, no. 9–12, pp. 498–506, 2009.
- [36] M. V. Sadovskii, "High-temperature superconductivity in iron-based layered iron compounds," *Physics-Uspekhi*, vol. 51, no. 12, pp. 1201–1227, 2008.
- [37] I. I. Mazin, private communication.
- [38] O. V. Dolgov, I. I. Mazin, D. Parker, and A. A. Golubov, "Interband superconductivity: contrasts between Bardeen-Cooper-Schrieffer and Eliashberg theories," *Physical Review B*, vol. 79, no. 6, Article ID 060502, 2009.
- [39] K. Hasselbach, J. R. Kirtley, and P. Lejay, "Point-contact spectroscopy of superconducting  $URu_2Si_2$ ," *Physical Review B*, vol. 46, no. 9, pp. 5826–5829, 1992.
- [40] R. Escudero, F. Morales, and P. Lejay, "Temperature dependence of the antiferromagnetic state in  $URu_2Si_2$  by point-contact spectroscopy," *Physical Review B*, vol. 49, no. 21, pp. 15271–15275, 1994.
- [41] G. A. Ummarino, R. S. Gonnelli, and D. Daghero, "Tunneling conductance of SIN junctions with different gap symmetries and non-magnetic impurities by direct solution of real-axis Eliashberg equations," *Physica C*, vol. 377, no. 3, pp. 292–303, 2002.
- [42] R. Prozorov, M. A. Tanatar, R. T. Gordon, et al., "Anisotropic London penetration depth and superfluid density in single crystals of iron-based pnictide superconductors," *Physica C*, vol. 469, no. 9–12, pp. 582–589, 2009.

## Review Article

# Competition of Superconductivity and Charge Density Waves in Cuprates: Recent Evidence and Interpretation

A. M. Gabovich,<sup>1</sup> A. I. Voitenko,<sup>1</sup> T. Ekino,<sup>2</sup> Mai Suan Li,<sup>3</sup> H. Szymczak,<sup>3</sup> and M. Pękała<sup>4</sup>

<sup>1</sup>*Institute of Physics, National Academy of Sciences of Ukraine, 46 Nauka Avenue, Kyiv 03680, Ukraine*

<sup>2</sup>*Graduate School of Integrated Arts and Sciences, Hiroshima University, Higashi-Hiroshima 739-8521, Japan*

<sup>3</sup>*Institute of Physics, Al. Lotników 32/46, 02-668 Warsaw, Poland*

<sup>4</sup>*Department of Chemistry, University of Warsaw, Al. Żwirki i Wigury 101, 02-089 Warsaw, Poland*

Correspondence should be addressed to A. M. Gabovich, alexander.gabovich@gmail.com

Received 2 June 2009; Accepted 1 September 2009

Academic Editor: Sasha Alexandrov

Copyright © 2010 A. M. Gabovich et al. This is an open access article distributed under the Creative Commons Attribution License, which permits unrestricted use, distribution, and reproduction in any medium, provided the original work is properly cited.

Explicit and implicit experimental evidence for charge density wave (CDW) presence in high- $T_c$  superconducting oxides is analyzed. The theory of CDW superconductors is presented. It is shown that the observed pseudogaps and dip-hump structures in tunnel and photoemission spectra are manifestations of the same CDW gapping of the quasiparticle density of states. Huge pseudogaps are transformed into modest dip-hump structures at low temperatures,  $T$ , when the electron spectrum superconducting gapping dominates. Heat capacity jumps at the superconducting critical temperature and the paramagnetic limit are calculated for CDW superconductors. For a certain range of parameters, the CDW state in a  $d$ -wave superconductor becomes reentrant with  $T$ , the main control quantity being a portion of dielectrically gapped Fermi surface. It is shown that in the weak-coupling approximation, the ratio between the superconducting gap at zero temperature  $\Delta(T = 0)$  and  $T_c$  has the Bardeen-Cooper-Schrieffer value for  $s$ -wave Cooper pairing and exceeds the corresponding value for  $d$ -wave pairing of CDW superconductors. Thus, large experimentally found values  $2\Delta(T = 0)/T_c \approx 5 \div 8$  are easily reproduced with reasonable input parameter values of the model. The conclusion is made that CDWs play a significant role in cuprate superconductivity.

## 1. Introduction

Ever since the earliest manifestations of high- $T_c$  superconductivity were found in 1986 [1], the whole theoretical power [2–22] has been applied to explain and describe various normal and superconducting properties of various oxide families with critical temperatures,  $T_c$ , ranging up to 138 K to date [23–27]. Unfortunately, even conceptual understanding of the mechanisms and character of superconductivity in cuprates is still lacking. Strictly speaking, there is a number of competing paradigms, every of them pretending to be “the theory of superconductivity” (see, e.g., [2]) but not recognized as such by other respected experts in the field.

After the discovery of high- $T_c$  oxides, experimentalists found several other superconducting families with  $T_c$  higher than 23.2 K reached by the precuprate record-holder,  $\text{Nb}_3\text{Ge}$  [28, 29]. For instance, one may refer to fullerides [30, 31],

doped bismuthates [32–34], hafnium nitrides [35, 36], and magnesium diborides [37–40]. One should also mention more controversial cases of superconducting oxides  $\text{H}_x\text{WO}_3$  with  $T_c \approx 120$  K [41] and  $\text{Sr}_{0.9}\text{La}_{0.1}\text{PbO}_{3-\delta}$  with  $T_c \approx 65$  K [42]. Finally, an unexpected and counter-intuitive discovery of the iron-based oxypnictide [43, 44] or oxygen-free pnictide [45] layered superconductors with  $T_c$  over 50 K has been made recently (see also reviews [46–49]).

Presumably, the latter materials with FeAs layers have been overlooked as possible candidates for high- $T_c$  superconductors, since Fe ions in solids usually possess magnetic moments, which promote magnetic ordering, the latter being detrimental to superconductivity, especially the spin-singlet one [50–55]. Strictly speaking, such an omission is of no surprise because superconductivity in oxides is rather gentle, sensible to impurities, including the excess or deficiency of oxygen [56] in these nonstoichiometric [57, 58]

compounds. Recent discovery [59] of previously unnoticed high- $T_c$  superconductivity in parent compounds  $T'-R_2\text{CuO}_4$  ( $R = \text{Pr, Nd, Sm, Eu, Gd}$ ) is very symptomatic in this regard, since an accurate removal of apical oxygen from thin films raised  $T_c$  from exact zero (those compositions were earlier considered by theoreticians as typical correlated Mott-Hubbard insulators) to 32.5 K for  $\text{Nd}_2\text{CuO}_4$ . As for the ferroarsenide family, one of its members,  $\text{EuFe}_2(\text{As}_{0.7}\text{P}_{0.3})_2$ , reveals a true superconducting transition at 26 K, followed by the ferromagnetic ordering of  $\text{Eu}^{2+}$  magnetic moments below 20 K, coexisting with superconductivity [60], which is quite unusual in view of the antagonism indicated above between two kinds of cooperative phenomena.

What is more, none of the mentioned superconductors except  $\text{Ba}_{1-x}\text{K}_x\text{BiO}_3$  [33] were discovered due to theoretical predictions. Hence, one may consider the theoretical discovery of  $\text{Ba}_{1-x}\text{K}_x\text{BiO}_3$  as an accidental case, since, according to the well-known chemist Cava: “one of the joys of solid state chemistry is its unpredictability” [61]. The same opinion was expressed by the other successive chemist Hosono: “understanding the mechanism with respect to predicting the critical temperature of a material is far from complete at the present stage even for brilliant physicists. Such a situation provides a large opportunity including a good luck for material scientists who continue the exploration for a new material, not limited to superconductors, and a new functionality based on their own view points” [48]. That is why Pickett recently made a sad remark that “the next breakthrough in superconductivity will not be the result of surveying the history of past breakthroughs” [62]. It means that *microscopic* theories of superconductivity are incapable of describing specific materials precisely, although *together* they give an adequate overall picture. In this connection, the failure of the most sophisticated approaches to make *any* prediction of true or, at least “bare”  $T_c$ , (provided that the corresponding  $T_c$ -value is not known *a priori*) despite hundreds of existing superconductors with varying fascinating properties, forced Phillips [63] to reject all apparently *first-principle* continuum theories in favor of his own percolative filamentary theory of superconductivity [64–67] (see also the random attractive Hubbard model studies of superconductivity [68, 69] and the analysis of competition between superconductivity and charge density waves studied in the framework of similar scenarios [70–72]). We totally agree with such considerations in the sense of the important role of disorder in superconductors with high  $T_c$  on the verge of crystal lattice instability [73–83]. Nevertheless, it is questionable whether a simple one-parameter “master function” of [63, 67] would be able to make *quantitative* and practically precise predictions of  $T_c$ . As for the qualitative correctness of the dependence  $T_c$  versus weighted number  $\langle R \rangle$  of Pauling resonating valence bonds [63, 67, 84], it can be considered at least as a useful guideline in the superconductivity ocean. The phenomenological character of the master function (chemical trend diagram)  $T_c(\langle R \rangle)$  is an advantage rather than a shortcoming of this approach, as often happens in the physics of superconductors (see, e.g., more or less successful criteria of superconductivity with different extent of phenomenology [85–98]).

On the other hand, attempts to build sophisticated microscopic theories of the boson-mediated Bardeen-Cooper-Schrieffer (BCS) attraction, treating the Coulomb repulsion as a single Coulomb pseudopotential constant  $\mu^*$ , are incapable of predicting actual critical superconducting properties [63, 91, 99–101]. The same can be said [67] about Hubbard-Hamiltonian models with extremely strong repulsive Coulomb energy parameter  $U$ , which is formally based on the opposite ideology (see, e.g., [102, 103]). As an example of the theories described above, one can indicate work [104], where the strong-coupling Eliashberg equations for the electron-phonon mechanism of superconductivity [105, 106] were solved numerically taking into account even vertex corrections and treating the dispersive Coulomb interaction not on equal footing, but as a simple constant  $\mu^*$ . In this connection, it seems that the prediction of [104] that the maximal  $T_c$  for new iron-based superconductors is close to 90 K is unjustified. Of course, the same is true for other studies of such a kind.

It is remarkable that, for hole- and electron-doped cuprates, there is still no clarity concerning the specific mechanisms of superconductivity [17, 107–115] and the order parameter symmetry [109, 116–130], contrary to the “official” viewpoint [131–133]) and even the very character of the phenomenon (in particular, there have been furious debates concerning the Cooper pairing versus boson condensation dilemma in cuprates [8, 134, 135]). The same seems to be true for other old and new “exotic” superconductors [46, 107, 108, 136–153], their exoticism being in essence a degree of our ignorance.

It would be of benefit to consider all indicated problems in detail for all classes of superconductors and show possible solutions. Unfortunately, it cannot be done even in the scope of huge treatises (see, e.g., [154–157]). The objective of this review is much more modest. Specifically, it deals mostly with high- $T_c$  cuprate materials, other superconductors being mentioned only for comparison. Moreover, in the present state of affairs, it would be too presumptuous to pretend to cover all aspects of the oxide superconductivity. Hence, we will restrict ourselves to the analysis of lattice instabilities and concomitant charge density waves (CDWs) in high- $T_c$  oxides. Their interplay with superconductivity is one of the fascinating and fundamentally important phenomena observed in cuprates and discussed by us earlier [158–160]. Nevertheless, in this rapidly developing branch of the solid state physics, many new theories and experimental data on various CDW superconductors appeared during last years. They are waiting for both unbiased and thorough analysis. This article discusses this new information, referring the reader to our previous reviews for more general and established issues, as well as some cumbersome technical details.

The outline of this review is as follows. In Section 2, for the sake of completeness, we briefly consider possible mechanisms of superconductivity in cuprates, the problem of the relationship between BCS pairing and Bose-Einstein condensation (BEC), and the multigapness of the superconducting order parameter. Section 3 is devoted to the experimental evidence for CDWs, the so-called

pseudogaps, dip-hump structures, and manifestations of intrinsic inhomogeneity in cuprate materials. The original theory of CDW superconductors and the interpretation of CDW-related phenomena in high- $T_c$  oxides are presented in Section 4. At the end of Section 4, some recent data on coexistence between superconductivity and spin density waves (SDWs)—a close analogue of CDWs—are covered. This topic became hot once more after the discovery of ferro-pnictides [43–48, 161]. Short conclusions are made in Section 5.

## 2. Considerations on Peculiarities and Mechanisms of Superconductivity in Oxides

When  $\text{BaPb}_{1-x}\text{Bi}_x\text{O}_{3-\delta}$  (BPB) was shown [162] to be a superconductor with a huge (at that time!)  $T_c \approx 13$  K for  $x \approx 0.25$ , a rather low concomitant concentration of current carriers  $n \approx 1.5 \div 4.5 \times 10^{21} \text{ cm}^{-3}$ , and poor electric conductivity [56] (the phase diagram of BPB is extremely complex, with a number of partial metal-insulator structural transitions [56, 163–167]), it looked like an exception. Now, it is fully recognized that oxides with highest  $T_c$  are bad metals from the viewpoint of normal state conductivity [168]. In particular, the mean free path of current carriers is of the order of the crystal lattice constant, so that the Ioffe-Regel criterion of the metal-insulator transition [169] is violated. Moreover, there exists an oxide superconductor  $\text{SrTiO}_{3-\delta}$  with a tiny maximal  $T_c \approx 0.5$  K, attained by doping, but an extremely small  $n < 10^{20} \text{ cm}^{-3}$  [170]. Note that the undoped semiconducting  $\text{SrTiO}_{3-\delta}$  is so close to the metal-insulator border that it may be transformed into a metal by the electrostatic-field effect [171] (this technique has been successfully applied to other oxides [172]). Moreover, a two-dimensional metallic layer has been discovered [173] at the interface between two insulating oxides  $\text{LaAlO}_{3-\delta}$  and  $\text{SrTiO}_{3-\delta}$ , which was later found to be superconducting with  $T_c \approx 0.2$  K [174, 175]. The appearance of superconductivity at nonmetallic charge carrier densities in oxides of different classes comprises a hint that it is not wise to treat various oxide families separately (see, e.g., [176]), all of them having similar perovskite-like ion structures [23, 25, 26, 177–181] and similar normal and superconducting properties [27], whatever the values of their critical parameters are. As for the apparent dispersion of the latter among superconducting oxides, it mostly reflects their conventional exponential dependences on atomic and itinerant-electron characteristics [9, 10].

The junior member of the superconducting oxide family,  $\text{SrTiO}_{3-\delta}$ , demonstrates (although not in a spectacular manner) several important peculiarities, which are often considered as properties intrinsic primarily to high- $T_c$  cuprates. Indeed, in addition to the low  $n$ , this polar, almost ferroelectric [182, 183], material was shown to reveal polaron conductivity [184] and is suspected to possess bipolaron superconductivity [185–187], first suggested by Vinetskii almost 50 years ago [188]. It means that  $\text{SrTiO}_{3-\delta}$  might be not a Bardeen-Cooper-Schrieffer (BCS) superconductor [189] with a large coherence length  $\xi_0 \gg a_0$ , where  $a_0$

is the crystal lattice constant, but most likely an example of a material with  $\xi_0 \approx a_0$ , so that a Bose-condensation of local electron pairs would occur at  $T_c$ , according to the Schafroth-Butler-Blatt scenario [190] or its later extensions [8, 134, 135, 191–199].

The concept of bipolarons (local charge carrier pairs) has been later applied to BPB [200–203],  $\text{Ba}_{1-x}\text{K}_x\text{BiO}_{3-\delta}$  (BKB,  $T_c \leq 30$  K [204, 205]) [203, 206, 207] and cuprates [195, 199, 208–211]. It was explicitly shown for BPB and BKB by X-ray absorption spectroscopy [203] that bipolaronic states and CDWs coexist and compete, which might lead, in particular, to the observed nonmonotonic dependence  $T_c(x)$  [212]. At the same time, Hall measurements demonstrate that the more appropriate characteristics  $T_c(n)$  is monotonic [56, 213, 214], so that the expected suppression of  $T_c$  at high  $n$  as a consequence of screening of the electron-phonon matrix elements [99, 215, 216] is not achieved here as opposed to the curve  $T_c(n)$  [170] in reduced samples of  $\text{SrTiO}_{3-\delta}$ . As for cuprates, the bipolaron superconductivity mechanism, as well as any other BEC scheme, in its pure state would require an existence of the preformed electron (hole) pairs (bipolarons), which might be the case [177, 217], and a prior destruction of the Fermi surface (FS), the condition contradicting observations (see, e.g., [218]). Therefore, boson-fermion models for charge carriers in superconductors was introduced [134, 219–225] and, later on, severely criticized [226, 227]. In any case, the available objections concern the bipolaronic mechanism of superconductivity itself, the occurrence of polaronic effect in oxides with high dielectric permittivities raising no doubt [115, 177, 199, 228–232].

It is remarkable that the boson-fermion approach mentioned above is not a unique tool for describing superconductivity in complex systems. A necessary “degree of freedom” connected to another group of charge carriers has been introduced, for example, as the so-called ( $-U$ )-centers [233–235], earlier suggested by Anderson [236] as a phenomenological reincarnation of bipolarons in amorphous materials [188]. Independently, narrow-band nondegenerate charge carriers submerged into the sea of itinerant electrons were proposed for cuprates as another, not fully hybridized kind of the “second heavy component” [237, 238]. For completeness, we should also mention a quite different model involving a second heavy charge carrier subsystem ( $d$ -electrons in transition metals [239] or heavy holes in degenerate semiconductors [240]), necessary to convert high-frequency Langmuir plasmons intrinsic to the itinerant electron component into the ion-acoustic collective excitation branch, in order that a high- $T_c$  superconductivity would appear. Those hopes, however, lack support from any evidence in natural or artificial systems (see the analysis of plasmon mechanisms [206, 241–247], the optimism of some authors seems to us and others [248] a little bit exaggerated). As can be readily seen from the References given above, all nonconventional approaches, rejecting or generalizing the BCS scheme and going back to the explanations of a relatively weak superconductivity in degenerate semiconductors [138, 191, 215, 249–252], have been applied to every family of superconducting oxides, including cuprates.

Strontium titanate became a testing ground [253] of one further attractive idea (based on the same concept of several interacting charge carrier components) of two-gap or multigap superconductivity, with the interband interplay being crucial to the substantial increase of  $T_c$  and other critical parameters. The corresponding models came into being in connection with the transition  $s$ - $d$  metals [254, 255]. They were subsequently applied to analyze superconductivity in multivalley semiconductors [256, 257], high- $T_c$  oxides [231, 258–266],  $\text{MgB}_2$  [40, 267–269],  $\text{ZrB}_{12}$  [270],  $\text{V}_3\text{Si}$  [271],  $\text{Mg}_{10}\text{Ir}_{19}\text{B}_{16}$  [272],  $\text{YNi}_2\text{B}_2\text{C}$  [273],  $\text{NbSe}_2$  [274, 275],  $\text{R}_2\text{Fe}_3\text{Si}_5$  ( $R = \text{Lu, Sc}$ ) [276],  $\text{Sc}_5\text{Ir}_4\text{Si}_{10}$  [277],  $\text{Na}_{0.35}\text{CoO}_2 \cdot 1.3\text{H}_2\text{O}$  [278] as well as pnictides  $\text{LaFeAsO}_{1-x}\text{F}_x$  [279],  $\text{LaFeAsO}_{0.9}\text{F}_{0.1}$  [280],  $\text{SmFeAsO}_{0.9}\text{F}_{0.1}$  [281], and  $\text{Ba}_{0.55}\text{K}_{0.45}\text{Fe}_2\text{As}_2$  [282],  $\text{Ba}_{1-x}\text{K}_x\text{Fe}_2\text{As}_2$  with  $T_c \approx 32\text{ K}$  [283]. We did not explicitly include into the list such modifications of magnesium diboride as  $\text{Mg}_{1-x}\text{Al}_x\text{B}_2$  or  $\text{Mg}(\text{B}_{1-x}\text{C}_x)_2$ , and so forth.

Since, instead of one, two or more well-separated superconducting energy gaps, a continuous, sometimes wide, gap distribution is often observed (see results for  $\text{Nb}_3\text{Sn}$  in [284] and  $\text{MgB}_2$  in [285–289]), the original picture of the gap multiplicity in the momentum,  $\mathbf{k}$ , space loses its beauty, whereas the competing scenario [76, 290] of the spatial ( $\mathbf{r}$ -space) extrinsic or intrinsic gap spread becomes more adequate and predictive [77–79]. For the case of cuprates, it has been recently shown experimentally that the spread is really spatial, but corresponds to the pseudogap (CDW gap) rather than its superconducting counterpart, the latter most probably being a single one [291] (see also the discussion in [83] and below).

In accordance with what was already mentioned, the application of very different, sometimes conflicting, models to oxide families, including cuprates, means an absence of a deep insight into the nature of their superconducting and normal state properties. We are not going to analyze here the successes and failures of the *microscopic* approaches to high- $T_c$  superconductivity in detail; instead we want to emphasize that even the boson-mediators (we accept the applicability of the Cooper-pairing concept to oxides on the basis of crucial flux-quantization experiments [292, 293]) are not known for sure. Indeed, at the early stages of the high- $T_c$  studies, magnons were considered as glue, coupling electrons or holes. The very temperature-composition (doping) phase diagrams supported this idea, since undoped and slightly doped oxides were found antiferromagnetic [26, 103, 294–304]. However, a plethora of theories suggesting virtual spin fluctuations as the origin of superconductivity in high- $T_c$  oxides and leading to the  $d_{x^2-y^2}$  symmetry of the superconducting order parameter have been developed [6, 11, 15, 103, 302, 305–310].

Fortunately for the scholars, it became clear that reality is richer for oxides than was expected, so that (i) the order parameter may include a substantial  $s$ -wave admixture [109, 116–129]; and (ii) phonons still exist in perovskite crystal lattices, inevitably affecting or, may be, even determining the pairing process [4, 10, 112, 115, 311], not to talk about polaron and bipolaron effects discussed above. It should be noted that there are reasonable scenarios of

$d$ -wave order parameter symmetry in the framework of the electron-phonon interaction alone [208, 312–316] (a similar conclusion was made for the case of plasmon mechanism [317]).

At the same time, if one adopts a substantial (crucial?) role of spin-fluctuation mechanism in superconductivity, the ubiquitous phonons can (i) be neutral to the dominant  $d$ -wave pairing; (ii) act synergetically with spin fluctuations; (iii) or reduce  $T_c$ , as it would have been for switched-off phonons. The existing theories support all three variants, although some authors cautiously avoid any direct conclusions [103]. For instance, Kulić demonstrated the destructive interference between both mechanisms of superconductivity [4]. Phononic reduction of the magnetically induced  $T_c$  was claimed in [308, 318], whereas anisotropic phonons seem to enhance  $T_c$ , thus obtained [319]. Finally, according to [228, 320, 321], spins and phonons act constructively in cuprates. Once again, the microscopic approach was incapable of unambiguously predicting a result for the extremely complex system.

One should bear in mind that the problem is much wider than the interplay between spin excitations and phonons. Namely, it is more correct to consider the interplay between Coulomb inter-electron and electron-lattice interactions [232, 322]. Of course, the latter is also Coulombic in nature, phonons being simply an ion sound, that is, ion Langmuir plasma oscillations [323] screened in this case by degenerate light electrons [324] (thus, acoustic phonons constitute a similar phenomenon as the acoustic plasmons in the electron system [239, 240] with an accuracy to frequencies). One of the main difficulties is how to separate the metal constituents in order that some contributions would not be counted twice [322, 325–333]. Since it is possible to do rigorously only in primitive plasma-like models [91, 92, 99, 251, 322], the problem has not been solved. Therefore, empirical considerations remain the main source of future success for experimentalists, as it happened, for example, in the case of  $\text{MgB}_2$  [37].

### 3. CDWs and CDW-Related Phenomena in Cuprates

The reasoning presented in Section 2 demonstrates that for the objects concerned, it is insufficient to rely only on microscopic theories, so that phenomenological approaches should deserve respect and attention. In actual truth, they might not be less helpful in understanding the normal and superconducting properties of cuprates, being generalizations of a great body of experimental evidence collected during last decades. In this section, we are going to show that two very important features are common to all high- $T_c$  families. Specifically, these are the intrinsic inhomogeneity of nonstoichiometric superconducting ceramic and single crystalline samples [334–343] and the persistence of CDWs [340, 344, 345] and other phenomena, which we also consider as CDW manifestations (dip-hump structures, DHS [339, 346–348], and pseudogaps below and above  $T_c$  [349–358] in tunneling spectra and angle-resolved photoemission spectra, ARPES).

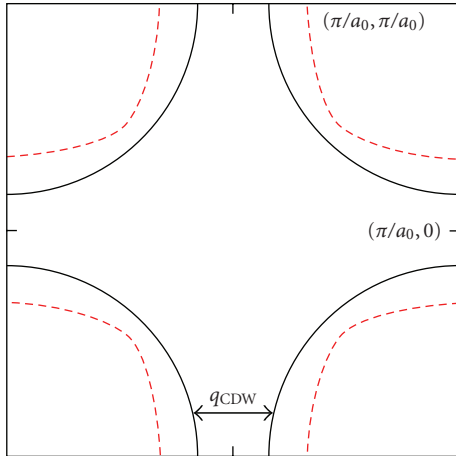


FIGURE 1: (Color online) Fermi surface nesting; and tight-binding-calculated Fermi surface (solid black curve) of optimally doped  $\text{Bi}_2\text{Sr}_2\text{CuO}_{6+\delta}$  based on ARPES data [373]. The nesting wave vector (black arrow) in the antinodal flat band region has length  $2\pi/6.2a_0$ . Underdoped  $\text{Bi}_2\text{Sr}_2\text{CuO}_{6+\delta}$  Fermi surfaces (shown schematically as red dashed lines) show a reduced volume and longer nesting wave vector, consistent with a CDW origin of the doping-dependent checkerboard pattern reported here (Taken from [344]).

CDWs were seen directly as periodic incommensurate structures in superconducting  $\text{Bi}_2\text{Sr}_2\text{CaCu}_2\text{O}_{8+\delta}$  (BSCCO) using various experimental methods [12, 334, 359–370]. Photoemission studies reveal the  $4a_0 \times 4a_0$  charge-ordered “checkerboard” state in  $\text{Ca}_{2-x}\text{Na}_x\text{CuO}_2\text{Cl}_2$  [371], and tunnel measurements visualized the same kind of ordering in BSCCO [370]. Scanning tunnel microscopy (STM) measurements found CDWs in  $\text{Bi}_2\text{Sr}_{1.4}\text{La}_{0.6}\text{CuO}_{6+\delta}$  ( $T_c^{\text{max}} \approx 29\text{ K}$ ) with an incommensurate period and CDW wave vectors  $\mathbf{Q}$  depending on oxygen doping degree [340]. The same method revealed nondispersive (energy-independent) checkerboard CDWs in  $\text{Bi}_{2-y}\text{Pb}_y\text{Sr}_{2-z}\text{La}_z\text{CuO}_{6+x}$  ( $T_c \approx 35\text{ K}$  for the optimally doped composition) [344]. In this case,  $\mathbf{Q}$  substantially depends on doping, rising from  $\pi a_0^{-1}/6.2$  in an optimally doped sample to  $\pi a_0^{-1}/4.5$  for an underdoped sample with  $T_c \approx 25\text{ K}$ . It is easily explained by the authors taking into account the shrinkage of the hole FS with decreasing hole number, so that the vector  $\mathbf{Q}$  that links the flat nested FS sections grows, whereas the CDW period decreases (see Figure 1). One should note that, in the presence of impurities (e.g., an inevitably non-homogeneous distribution of oxygen atoms), the attribution of the observed charge order (if any) to unidirectional or checkerboard type might be ambiguous [372].

A similar coexistence of CDWs and superconductivity was observed in a good many different kinds of materials with a reduced dimensionality of their electron system, so that the corresponding FS includes nested (congruent) sections [158–160]. For completeness, we will add some new cases discovered after our previous reviews were published. First of all, the analogy between CDWs in cuprates and layered dichalcogenides was proved by ARPES [352, 374–376]. It should be noted that CDW competition with

superconductivity in cuprates was supposed as early as in 1987 on the basis of heat capacity and optical studies [377], whereas the similarity between high- $T_c$  oxides and dichalcogenides was first noticed by Klemm [378, 379]. Additionally, a new dichalcogenide system  $\text{Cu}_x\text{TiSe}_2$  was found with coexisting superconductivity and CDWs (at  $0.04 < x < 0.06$ ) [380, 381]. The coexistence between two phenomena was observed in the organic material  $\alpha\text{-(BEDT-TTF)}_2\text{KHg(SCN)}_4$ , but superconductivity was attributed to boundaries between CDW domains, where the CDW order parameter is suppressed [382]. High-pressure studies of another organic conductor  $(\text{Per})_2[\text{Au}(\text{mnt})_2]$  revealed an appearance of superconductivity after the CDW suppression [383]. Still, it remained unclear, whether some remnants of CDWs survived in the superconducting region of the phase diagram. Application of high pressure also suppressed CDWs in the compound  $\text{TbTe}_3$  at about  $P = 2.3\text{ GPa}$ , inducing superconductivity with  $T_c \approx 1.2\text{ K}$ , enhanced to  $4\text{ K}$  at  $P = 12.4\text{ GPa}$  [384], the behavior demonstrating the competition of Cooper and electron-hole pairings for the FS [385, 386]. The same experiments in this quasi-two-dimensional material revealed two kinds of CDW anomalies merging at  $P = 2.3\text{ GPa}$ , as well as antiferromagnetism, which makes this object especially promising. Finally, CDWs were found in another superconducting oxide  $\text{Na}_{0.3}\text{CoO}_2 \cdot 1.3\text{ H}_2\text{O}$  by specific heat investigations [387–389], showing two-energy-gap superconductivity for as-prepared samples and non-superconducting CDW dielectrized state after ageing of the order of days. The sample ageing is a situation widely met for superconductors [390, 391], whereas the dielectrization of as-synthesized superconducting ceramic samples accompanied by a transformation of bulk superconductivity into a percolating one with the CDW background was observed for BPB long ago [56, 392]. Nevertheless, such a scenario was not proved directly at that time, while the bulk heat capacity peak in  $\text{Na}_{0.3}\text{CoO}_2 \cdot 1.3\text{ H}_2\text{O}$  [387–389] unequivocally shows the emergence of CDWs instead of superconductivity.

We emphasize that CDWs compete with superconductivity, whenever they meet on the same FS. This is the experimental fact, which agrees qualitatively with a number of theories [385, 386, 393–397].

Returning to cuprates, we want to emphasize that the existence of pseudogaps above and below  $T_c$  is one of their most important features. Pseudogap manifestations are diverse, but their common origin consists in the (actually, observed) depletion of the electron densities of states (DOS). It is natural that tunnel and ARPES experiments, which are very sensitive to DOS variations, made the largest contribution to the cuprate pseudogap data base (see references in our works [81–83, 158–160]). Recent results show that the concept of two gaps (the superconducting gap and the pseudogap, the latter considered here as a CDW gap) [82, 352, 353, 357, 377, 398–404] begins to dominate in the literature over the one-gap concept [211, 355, 405–416], according to which the pseudogap phenomenon is most frequently treated as a precursor of superconductivity (for instance, a gas of bipolarons that Bose-condenses below  $T_c$  [413] or a  $d$ -wave superconducting-like state without a long-range phase rigidity [416]). The main arguments,

which make the one-gap viewpoint less probable, is the coexistence of both gaps below  $T_c$  [349, 417], their different position in the momentum space of the two-dimensional Brillouin zone [351, 353, 356, 418, 419], and their different behaviors in the external magnetic fields  $H$  [420], for various dopings [417], and under the effects of disordering [419].

Nevertheless, some puzzles still remain unresolved in the pseudogap physics. For instance, Kordyuk et al. [352] found that the pseudogap in  $\text{Bi}(\text{Pb})_2\text{Sr}_2\text{Ca}(\text{Tb})\text{Cu}_2\text{O}_{8+\delta}$  revealed by ARPES is nonmonotonic in  $T$ . Such a behavior, as they indicated, might be related to the existence of commensurate and incommensurate CDW gaps, in a close analogy with the case of dichalcogenides [421]. Another photoemission study of  $\text{La}_{1.875}\text{Ba}_{0.125}\text{CuO}_4$  has shown [354] that there seems to be two different pseudogaps: a  $d$ -wave-like pseudogap—a precursor to superconductivity—near the node of the truly superconducting gap and a pseudogap in the antinodal momentum region—it became more or less familiar to the community during last years [350, 351, 353, 356, 403, 418, 419] and is identified by us as the CDW gap.

Despite existing ambiguities, the most probable scenario of the competition between CDW gaps (pseudogaps) and superconducting gaps in high- $T_c$  oxides, in particular, in BSCCO, includes the former emerging at antinodal (nested) sections of the FS and the latter dominating over the nodal sections (see Figure 2, reproduced from [403], where BSCCO was investigated, and results for  $(\text{Bi,Pb})_2(\text{Sr,L a})_2\text{CuO}_{6+\delta}$  presented in [356]). Since CDW gaps are much larger than their superconducting counterparts, the simultaneous existence of the superconducting gaps in the antinodal region might be overlooked in the experiments. This picture means that the theoretical model of the partial dielectric gapping (of CDW origin or caused by a related phenomenon—spin density waves, SDWs) belonging to Bilbro and McMillan [385] (see also [56, 158–160, 386, 397, 422–428]) is adequate for cuprates. On the other hand, the coexistence of CDW and superconducting gaps, each of them spanning the whole FS [429–432], can happen only for extremely narrow parameter ranges [433]. Moreover, as is clearly seen from data presented in Figure 2 [403] and a lot of other measurements for different classes of superconductors, complete dielectric gapping has not been realized. The reason is obvious: nested FS sections cannot spread over the whole FS, since the actual crystal lattice is always three-dimensional and three-dimensionality effects lead to the inevitable FS warping detrimental to nesting conditions formulated below.

It is interesting that pseudogaps were also observed in oxypnictides  $\text{LaFeAsO}_{1-x}\text{F}_x$  and  $\text{LaFePO}_{1-x}\text{F}_x$  by ARPES [434] and  $\text{SmFeAsO}_{0.8}\text{F}_{0.2}$  by femtosecond spectroscopy [435], where SDWs might play the same role as CDWs do in cuprates. At the same time, in iron arsenide  $\text{Ba}_{1-x}\text{K}_x\text{Fe}_2\text{As}_2$ , photoemission studies detected a peculiar electronic ordering with a  $(\pi/a_0, \pi/a_0)$  wave vector [436], a true nature of which is still not known, but which might be related either to the magnetic reconstruction of the electron subsystem (SDWs) and/or to structural transitions (when CDWs accompanied by periodic crystal lattice distortions emerge in the itinerant electron liquid near the structural transition

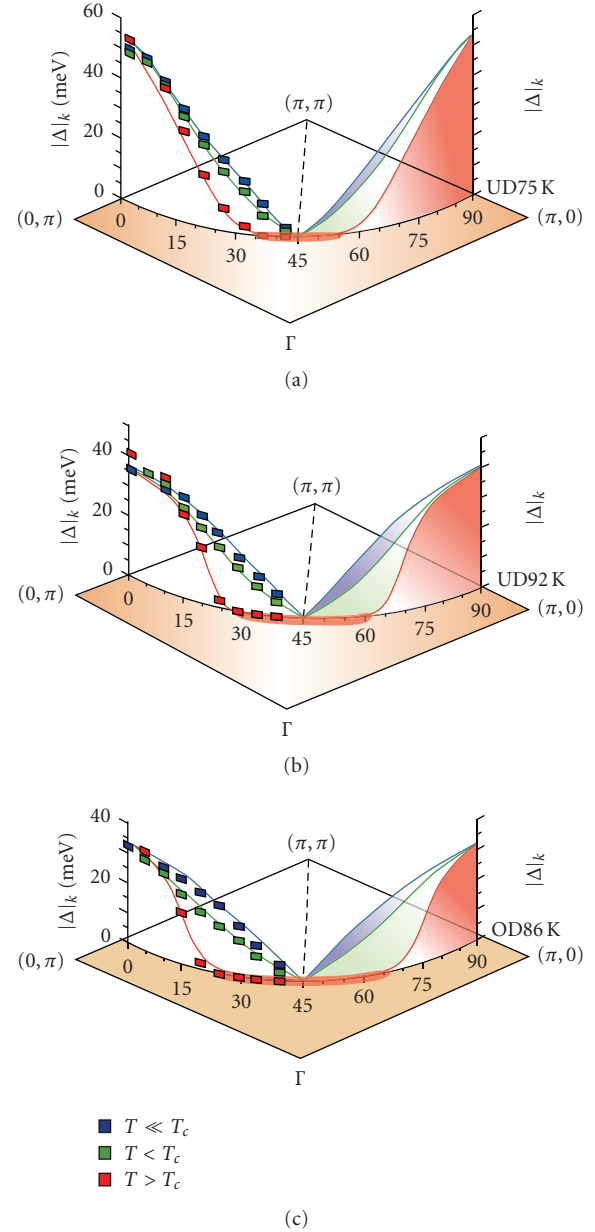


FIGURE 2: (Color online) Schematic illustrations of the gap function evolution for three different doping levels of  $\text{Bi}_2\text{Sr}_2\text{CaCu}_2\text{O}_{8+\delta}$ . (a) Underdoped sample with  $T_c = 75$  K. (b) Underdoped sample with  $T_c = 92$  K. (c) Overdoped sample with  $T_c = 86$  K. At 10 K above  $T_c$  there exists a gapless Fermi arc region near the node; a pseudogap has already fully developed near the antinodal region (red curves). With increasing doping, this gapless Fermi arc elongates (thick red curve on the Fermi surface), as the pseudogap effect weakens. At  $T < T_c$  a  $d$ -wave like superconducting gap begins to open near the nodal region (green curves); however, the gap profile in the antinodal region deviates from the simple  $d_{x^2-y^2}$  form. At a temperature well below  $T_c$  ( $T \ll T_c$ ), the superconducting gap with the simple  $d_{x^2-y^2}$  form eventually extends across entire Fermi surface (blue curves) in (b) and (c) but not in (a). (Taken from [403].)

temperature  $T_d$  [437, 438]). The interplay between structural and magnetic instabilities is important for pnictides [161],

since, for example, structural and SDW anomalies appear jointly at 140 K in  $\text{BaFe}_2\text{As}_2$  [439]. It is not inconceivable that pnictides may be a playground for density waves as well as high- $T_c$  oxides, with a rich variety of attendant manifestations.

The DHS is another visiting card of cuprates, being a peculiarity in tunnel and photoemission spectra at low  $T \ll T_c$  and energies much higher than those of coherent superconducting peaks [81–83, 160, 339, 347, 348, 440, 441]. It is remarkable that in the S-I-N tunnel junctions, where S, I, and N stand for a high- $T_c$  superconductor, an insulator, and a normal metal, respectively, a DHS might appear for either one bias voltage  $V$  polarity only [347] or both [442, 443], depending on the specific sample. In S-I-N junctions, current-voltage-characteristics (CVCs) with two symmetrically located DHSs (one per branch) are also observed, but with amplitudes that can differ drastically [442, 443]. In S-I-S symmetric junctions, DHS structures are observable (or not) in CVC branches of both polarities simultaneously [347], which seems quite natural. It is very important that although the CVC for every in the series of S-I-N junctions with BSCCO as a superconducting electrodes was nonsymmetric, especially due to the presence of the DHS, the CVC obtained by averaging over an ensemble of such junctions turned out almost symmetric, or at least its nonsymmetry turned out much lower than the nonsymmetry of every CVC taken into consideration [443].

There is quite a number of interpretations concerning this phenomenon [347, 444–450]. We have discussed most of them in detail in our previous publications, whereas our theory and necessary reference to other models will be presented below.

STM mapping of high- $T_c$  oxide samples revealed substantial inhomogeneities of energy gap spatial distribution [334, 336, 338, 339, 341–343, 363, 370, 441, 451–459]. The same conclusion was made from the interlayer tunneling spectroscopy [460, 461], more conventional S-I-N tunnel (point-contact) studies [440, 442], optical femtosecond relaxation spectroscopy [337], and inelastic neutron scattering measurements [335]. It is quite natural that some inhomogeneity should exist, since the oxygen content is always nonstoichiometric in those compounds [304]. Indeed, correlations were found between oxygen dopant atom positions and the nanoscale electronic disorder probed by STM [336]. The problem has been recently investigated theoretically making allowance for electrostatic modulations of various system parameters by impurity atoms [462].

Nevertheless, the gap distributions occurred to be anomalously large, with sometimes conspicuous two-peak structures in BSCCO [451, 457, 463],  $\text{Bi}_2\text{Sr}_{1.6}\text{Gd}_{0.4}\text{CuO}_{6+\delta}$  [338],  $(\text{Cu,C})\text{Ba}_2\text{Ca}_3\text{Cu}_4\text{O}_{12+\delta}$  [440], and  $\text{TlBa}_2\text{Ca}_2\text{Cu}_2\text{O}_{10-\delta}$  [442]. Nanoscale electronic nonhomogeneity on the crystal surface was shown to substantially affect the CDW-like DOS modulation observed by STM in  $\text{Bi}_2\text{Sr}_{1.4}\text{La}_{0.6}\text{CuO}_{6+\delta}$  [340].

Large gap scatterings obviously do not correlate with sharp transitions into the superconducting state at any doping of well prepared samples (implying Cooper-pairing

homogeneity), which was demonstrated, for example, by specific heat studies [464]. To solve the problem, one should bear in mind that the gaps measured by STM technique are of two kinds (in our opinion, superconducting gaps and pseudogaps—CDW gaps), which cannot be easily distinguished experimentally [81–83, 160, 337]. The guess was proved in [291], where contributions of both gaps in the STM spectra of  $(\text{Bi}_{0.62}\text{Pb}_{0.38})_2\text{Sr}_2\text{CuO}_{6+x}$  were separated by an ingenious trick. Namely, the authors normalized the measured local conductances by removing the larger-gap inhomogeneous background. Then, it became clear that the superconducting gap is more or less homogeneous over the sample's surface, whereas the larger gap (the pseudogap, i.e., the CDW gap) is essentially inhomogeneous.

The intimate origin of the pseudogap variations is currently not understood. At the same time, the inhomogeneity of electron characteristics is also inherent to the related solid solutions BPB, which was demonstrated by spatially resolved electron energy loss spectroscopy [465]. It is reasonable to suggest that this inhomogeneity both in BPB and high- $T_c$  oxides is strengthened near free surfaces in agreement with Josephson current measurements across BPB bicrystal tunnel boundaries [466].

Still, there is an interesting phenomenon, which might explain trends for electric properties in cuprates to be inhomogeneous. We mean a spontaneous phase separation, suggested long ago for antiferromagnets [467–470] and the electron gas in paramagnets [471–474]. This idea was later transformed into stripe activity in cuprate and manganite physics, where alternating conducting and magnetic regions constituted separated “phases” [12, 302, 475–480]. Recently, a lot of evidence for local lattice distortions, Jahn-Teller polaron occurrence, and other percolation and filamentary structure formation appeared [177, 217, 228, 481–485], supporting new sophisticated theoretical efforts in the science of phase separation [84, 230, 379, 486–493], mostly but not necessarily dealing with high- $T_c$  oxides. The electronic inhomogeneity in cuprates, as discussed above, belongs to the same category of phenomena. Whatever its origin, intrinsic inhomogeneity of cuprates and other oxides seems to be an important feature that needs explanation in order to understand superconductivity (much more homogeneous) itself. Note that electronic phase separation into magnetic and nonmagnetic domains was also found in the iron pnictide superconductor  $\text{Ba}_{1-x}\text{K}_x\text{Fe}_2\text{As}_2$  [494], whereas disorder-induced inhomogeneities of superconducting properties was observed in TiN films [495].

Another high- $T_c$  oxide,  $\text{YBa}_2\text{Cu}_3\text{O}_{6+x}$ , containing CuO chains in addition to  $\text{CuO}_2$  planes, was known for a long time as a material exhibiting one-dimensional CDWs [496]. However, the authors of more recent tunnel measurements [497] concluded that the would-be CDW manifestations might have a different nature, since the observed one-dimensional modulation wavelengths have rather a strong dispersion. Nevertheless, it seems that in view of the large CDW amplitude scatter in BSCCO discovered later, this conclusion is premature, with local variations of the FS shape being a possible origin of CDW wave vector modifications.

As one sees from the evidence discussed above, CDW modulations are observed in cuprates both directly (as patterns of localized energy-independent electron states in the conventional  $\mathbf{r}$ -space) and indirectly (as concomitant gapping phenomena). The pseudogap energy  $E_{\text{PG}} > \Delta_{\text{SC}}$  constitutes an appropriate scale for CDW gapping. Here,  $\Delta_{\text{SC}}$  is the superconducting gap. On the other hand, at low energies  $E < \Delta_{\text{SC}}$ , single-particle tunneling spectroscopy probes mixed electron-hole  $d$ -wave Bogoliubov quasiparticles [498], which are delocalized excitations. In this case, it is natural to describe the tunnel conductance in the momentum,  $\mathbf{k}$ -space. The interference between Bogoliubov quasiparticles is especially strong for certain wave vectors  $\mathbf{q}_i$  ( $i = 1, \dots, 16$ ) connecting extreme points on the constant energy contours [499–502]. The interference  $\mathbf{k}$ -space patterns involve those wave vectors [343, 416, 499, 503–505], this picture being distinct from and complementary to the partially disordered CDW unidirectional or checkerboard structures [344, 359, 365, 371, 458, 506–508].

It is remarkable that interference  $\mathbf{r}$ -space patterns on cuprate surfaces, the latter being in the superconducting state, are not detected, contrary to the clear-cut STM observations of electron de Broglie standing waves, induced by point defects or step edges, revealed in conductance maps on the normal metal surfaces [509, 510]. The latter waves are in effect Friedel oscillations [511] formed by two-dimensional normal electron density crests and troughs with the wave length  $\pi/k_F$ ,  $\mathbf{k}_F$  being the Fermi wave vector. On the other hand, spatial oscillating structures of local DOS in the  $d$ -wave superconducting state are determined by other representative vectors  $\mathbf{q}_i$ , so that the characteristic oscillations can be denominated as Friedel-like ones at most [502, 512]. Nevertheless, the attenuation of both kinds of spatial oscillations due to superconducting modifications of the screening medium should be more or less similar. Namely, in the isotropic superconducting state, the electron gas polarization operator loses its original singularity at  $k = 2k_F$  for gapped FS sections [513]. As a consequence, Friedel oscillations gain an extra factor  $\exp(-2r/\pi\xi_0)$  [514, 515], where  $\xi_0$  is the BCS coherence length [498]. For  $d$ -wave superconductors, the attenuation will be weaker and will totally disappear in the order-parameter node directions. However, those distinctions are not crucial, since the nodes have a zero measure. The modification of screening by formation of Bogoliubov quasiparticles in  $d$ -wave high- $T_c$  oxides explains the absence of conspicuous spatial structures in STM maps, which correspond to the wave vectors  $\mathbf{q}_i$  mentioned above.

We consider the observed CDWs in oxides as a consequence of electron-hole (dielectric) pairing on the nested sections of corresponding FSs [158–160, 516]. Such a viewpoint is also clearly supported by the experiments in layered dichalcogenides [374–376], the materials analogous to cuprates in the sense of superconductivity appearance against the dielectric (CDW) partial gapping background [378, 379]. At the same time, other sources of CDW instabilities are also possible [517, 518]. As for the microscopic mechanism causing CDW formation, it might be an electron-phonon (Peierls insulator) [519, 520] or a Coulomb

one (excitonic insulator) [431, 521, 522], or their specific combination. Excitonic instability may also lead to the SDW state [522, 523], also competing with superconductivity for the FS [160, 524–529]. It should be noted that researchers asserted that they found plenty of Peierls insulators or partially gapped Peierls metals [158–160, 530–532]. At the same time, the excitonic phase, being mathematically identical in the mean-field limit [533] and physically similar [534] to the Peierls insulator, was not identified unequivocally. One can only mention that some materials claimed to be excitonic insulators, namely, a layered transition-metal dichalcogenide 1T-TiSe<sub>2</sub> with a commensurate CDW [535, 536], alloys TmSe<sub>0.45</sub>Te<sub>0.55</sub> [537], Sm<sub>1-x</sub>La<sub>x</sub>S [538], and Ta<sub>2</sub>NiSe<sub>5</sub> with a *direct band gap* at the Brillouin zone  $\Gamma$  point in the parent high- $T$  state [539]. Therefore it is reasonable that precisely in the later case, the low- $T$  excitonic state is not accompanied by CDWs.

It is necessary to indicate that in many cases, the claimed “charge stripe order” and the more unpretentious “charge order” are an euphemism describing the old good CDWs: “Stripes is a term that is used to describe unidirectional density-wave states, which can involve unidirectional charge modulations (charge stripes) or coexisting charge and spin-density order spin stripes” [12]. We do not think it makes sense to use the term “stripes” in the cases of pure CDW or spin-density-wave (SDW) ordered states. At the same time, this term should be reserved for different possible more general kinds of microseparation [12, 477, 479, 540–542], having nothing or little to do with periodic lattice distortions, FS nesting, or Van Hove singularities. The need to avoid misnomers and duplications while naming concepts is quite general in science, as was explicitly stressed by John Archibald Wheeler, who himself coined many terms in physics (“black hole” included) [543].

In this connection, it seems that some experimentalists unnecessarily vaguely attribute the spatially periodical charge structure in the low-temperature tetragonal phase of La<sub>1.875</sub>Ba<sub>0.125</sub>CuO<sub>4</sub>, revealed by X-ray scattering [544], to the hypothetical nematic structure or the checkerboard Wigner crystal. Indeed, quite similar spatial charge structures found in La<sub>1.875</sub>Ba<sub>0.125-x</sub>Sr<sub>x</sub>CuO<sub>4</sub> by neutron scattering [545] were correctly and without reservation identified as CDW-related ones, whereas a checkerboard structure (if any) can be considered as a superposition of two mutually perpendicular CDWs. The same can be written about the “stripe” terminology used in [546], where X-ray scattering revealed a periodical charge structure in the low-temperature tetragonal phase of another cuprate La<sub>1.8-x</sub>Eu<sub>0.2</sub>Sr<sub>x</sub>CuO<sub>4</sub>.

One should mention two other possible collective states competing with Cooper pairing. Namely, these are states with microscopic orbital and spin currents that circulate in the ground state of excitonic insulator (there can be four types of the latter [522]). The concept of the state with current circulation, preserving initial crystal lattice translational symmetry, was invoked to explain cuprate properties [547]. Another order parameter, hidden from clear-cut identification by its supposed extreme sensitivity to sample imperfection, is the so-called  $d$ -density wave-order parameter [548, 549]. It is nothing but a CDW order parameter times the same

form-factor  $f(k) = \cos(k_x) - \cos(k_y)$ , the product being similar to that for  $d_{x^2-y^2}$ -superconductors. Here,  $k_x$  and  $k_y$  are the wave-vector components in the  $\text{CuO}_2$  plane. To some extent, the dielectric order parameter of the Bilbro-McMillan model [159, 160, 385] and its generalizations—they are presented below—contains the same physical idea as in the  $d$ -density-wave model: nonuniformity of the CDW gap function in the momentum space.

Although the destructive CDW action on superconductivity of many good materials is beyond question [56, 160, 380, 384, 545, 550, 551], it *does not mean* that maximal  $T_c$  are limited by *this factor only*. For instance,  $T_c$  falls rapidly with the hole concentration  $p$  in overdoping regions of  $T_c - p$  phase diagrams for different Pb-substituted  $\text{Bi}_2\text{Sr}_2\text{CuO}_{6+\delta}$  compounds, even in the case when the critical doping value  $p_{\text{cr}}$  corresponding to  $T_d \rightarrow 0$  lies outside the superconducting dome [552]. A Cu-doped superconducting chalcogenide  $\text{Cu}_x\text{TiSe}_2$  constitutes another example confirming the same trend [380]. Namely, CDW manifestations die out for  $x \gtrsim 0.06$ , whereas  $T_c$  starts to decrease for  $x > x_{\text{optimal}} = 0.08$ . As has been already mentioned, overdoping can reduce  $T_c$  simply owing to screening of matrix elements for electron-phonon interaction [99, 215, 216].

#### 4. Theory of CDW Superconductors and Its Application to Cuprates

The majority of our results presented below were obtained for  $s$ -wave superconductors with CDWs. It is a case, directly applicable to many materials (e.g., dichalcogenides, trichalcogenides, tungsten brozes, etc.). On the other hand, as was indicated above, the exact symmetry of the superconducting order parameter in cuprates is not known, although the  $d$ -wave variant is considered by most researchers in the field as the ultimate truth. Notwithstanding any future solution of the problem, our theory of CDW-related peculiarities in quasiparticle tunnel CVCs can be applied to cuprates, since we are not interested in small energies  $eV < \Delta$ , where the behavior of a reconstructed DOS substantially depends on whether it is the  $s$ - or  $d$ -wave order parameter [553–555]. Here,  $e > 0$  is the elementary charge, and  $\Delta$  is the amplitude of the superconducting order parameter. As for the thermodynamics of CDW superconductors, we present both  $s$ - and  $d$ -cases, each of them having their own specific features.

**4.1. Thermodynamics of  $s$ -Wave CDW Superconductors.** The Dyson-Gorkov equations for the normal ( $\mathcal{G}_{ij}$ ) and anomalous ( $\mathcal{F}_{ij}$ ) temperature Green's functions in the case of coupled superconducting  $\Delta_{ij}^{\alpha\gamma}$  and dielectric (CDW)  $\Sigma_{ij}^{\alpha\gamma}$  matrix order parameters are the starting point of calculations and can be found elsewhere [160, 386, 397, 426, 427]. Greek superscripts correspond to electron spin projections, and italic subscripts describe the natural split of the FS into degenerate (nested,  $d$ ) and non-degenerate (non-nested,  $n$ ) sections. For the quasiparticles on the nested sections, the standard condition leading to the CDW gapping holds:

$$\xi_1(\mathbf{p}) = -\xi_2(\mathbf{p} + \mathbf{Q}), \quad (1)$$

where  $\mathbf{p}$  is the quasimomentum,  $\mathbf{Q}$  is the CDW vector (see the discussion above), Planck's constant  $\hbar = 1$ . This equation binds the electron and hole bands  $\xi_{1,2}(\mathbf{p})$  for the excitonic insulator [431, 522] and different parts of the one-dimensional self-congruent band in the Peierls insulator case [516]. At the same time, the rest of the FS remains undistorted below  $T_d$  and is described by the electron spectrum branch  $\xi_3(\mathbf{p})$ . Such an approach was suggested long ago by Bilbro and McMillan [385]. We adopt the strong-mixing approximation for states from different FS sections. This means an appearance of a single superconducting order parameter for  $d$  and  $nd$  FS sections. The spin-singlet structure ( $s$ -wave superconductivity and CDWs) of the matrix normal ( $\Sigma_{ij}^{\alpha\gamma} = \Sigma\delta_{\alpha\beta}$ ) and anomalous ( $\Delta_{ij}^{\alpha\gamma} = I_{\alpha\beta}$ ) self-energy parts (where  $(I_{\alpha\beta})^2 = -\delta_{\alpha\beta}$ ) in the weak-coupling limit is suggested. Here,  $\delta_{\alpha\beta}$  is the Kronecker delta. The self-consistency equations for the order parameters obtained in accordance with the fundamentals can be expressed in the following form [386]:

$$\begin{aligned} 1 &= V_{\text{BCS}}N(0)[\mu I(D) + (1 - \mu)I(\Delta)], \\ 1 &= V_{\text{CDW}}N(0)\mu I(D), \end{aligned} \quad (2)$$

where

$$I(x) = \int_0^\Omega \frac{d\xi}{\sqrt{\xi^2 + x^2}} \tanh \frac{\sqrt{\xi^2 + x^2}}{2T}. \quad (3)$$

Here, the Boltzmann constant  $k_B = 1$ ,  $V_{\text{BCS}}$  and  $V_{\text{CDW}}$  are contact four-fermion interactions responsible for superconductivity and CDW gapping, respectively. The gap

$$D(T) = [\Delta^2(T) + \Sigma^2(T)]^{1/2} \quad (4)$$

is a combined gap appearing on the nested FS sections, whereas the order parameter  $\Delta$  defines the resulting observed gap on the rest of the FS (compared with the situation in cuprates [344, 350, 356, 403]). The parameter  $\mu$  characterizes the degree of the FS dielectrization (hereafter, we use this nonconventional term instead of “gapping” in some places to avoid confusion with the superconducting gapping), so that  $N_d(0) = \mu N(0)$  and  $N_{nd}(0) = (1 - \mu)N(0)$  are the electron DOSs per spin on the FS for the nested and nonnested sections, respectively. The upper limit in (3) is the relevant cut-off frequency, which is assumed to be equal for both interactions. If the cut-offs BCS and CDW are considered different, the arising correction,  $\log(\Omega_{\text{CDW}}/\Omega_{\text{BCS}})$ , is logarithmically small [385] and does not change qualitatively the subsequent results. Only in the case of almost complete electron spectrum dielectric gapping ( $\mu \rightarrow 1$ ) does the difference between BCS and CDW become important for the phase coexistence problem [433]. This situation is, however, of no relevance for substances with detectable superconductivity, since  $T_c$  tends to zero for  $\mu \rightarrow 1$ . In this subsection, we confine ourselves to the case  $\text{Re}\Sigma > 0$ ,  $\text{Im}\Sigma = 0$ , since the phase  $\varphi$  of the complex order parameter  $\Sigma \equiv |\Sigma|e^{i\varphi}$  does not affect the thermodynamic properties, whereas tunnel currents *do depend* on  $\varphi$  [160, 556, 557], which will be demonstrated explicitly below.

Introducing the bare order parameters  $\Delta_0 = 2\Omega \exp[-1/V_{\text{BCS}}N(0)]$  and  $\Sigma_0 = 2\Omega \exp[-1/V_{\text{CDW}}N_d(0)]$ , we can rewrite the system of (2) in an equivalent form, convenient for numerical calculations:

$$\begin{aligned} I_M[\Delta, T, \Delta(0)] &= 0, \\ I_M(D, T, \Sigma_0) &= 0, \end{aligned} \quad (5)$$

where

$$I_M(G, T, G_0) = \int_0^\infty \left( \frac{1}{\sqrt{\xi^2 + G^2}} \tanh \frac{\sqrt{\xi^2 + G^2}}{2T} - \frac{1}{\sqrt{\xi^2 + G_0^2}} \right) d\xi \quad (6)$$

is the standard Mühlischlegel integral [558], the root of which  $G = s\text{Mü}(G_0, T)$  is the well-known gap dependence for the  $s$ -wave BCS superconductor [9],  $G_0 = G(T=0)$ , and [385]

$$\Delta(0) = (\Delta_0 \Sigma_0^{-\mu})^{1/(1-\mu)}. \quad (7)$$

However, (5) mean that both gaps  $\Delta(T)$  and  $D(T)$  have the BCS form  $G = s\text{Mü}(G_0, T)$  [386], namely: (i)  $\Delta(T) = s\text{Mü}[\Delta(0), T]$ , that is, the actual value of the superconducting gap of the CDW superconductor at  $T=0$  is  $\Delta(0)$  rather than  $\Delta_0$ , and the actual superconducting critical temperature is  $T_c = \gamma\Delta(0)/\pi$ ; (ii) at the same time,  $D(T) = s\text{Mü}(\Sigma_0, T)$ , which determines  $T_d = \gamma\Sigma_0/\pi$ . Here,  $\gamma = 1.7810\dots$  is the Euler constant.

From (4), we obtain that, at  $T=0$ ,

$$\Sigma_0^2 = \Delta^2(0) + \Sigma^2(0). \quad (8)$$

Replacing  $\Delta(0)$  by its value (7), we arrive at the conclusion that in the model of  $s$ -wave superconductor with partial CDW gapping, two order parameters coexist only if  $\Delta_0 < \Sigma_0$ . Then, according to (7),  $\Delta(0) < \Delta_0$ ; that is, the formation of the CDW, if it happens, always inhibits superconductivity, in agreement with the totality of experiments [160, 375, 380, 382, 551]. Also, vice versa, according to (4), for  $T < T_c$ ,  $\Sigma(T) < s\text{Mü}(\Sigma_0, T)$ ; that is, superconductivity suppresses dielectrization.

In Figure 3, the dependences  $\Delta(T)$  and  $\Sigma(T)$  are shown for various parameters of the partially dielectrized CDW  $s$ -wave superconductor. It can be easily inferred from the data shown in both panels that, in agreement with the foregoing,  $\Delta(T)/\Delta(0)$  curves coincide with the Mühlischlegel one for any values of the dimensionless parameters  $\mu$  and  $\sigma_0 \equiv \Sigma_0/\Delta_0$ . The novel feature, which has been overlooked in other investigations, is the possibility of such a strong suppression of  $\Sigma$  for low enough  $T$  that it becomes *smaller* than  $\Delta$ , although  $T_d$  is larger than  $T_c$  (see Figure 3(b)). This intriguing situation can be realized for the parameter  $\sigma_0$  close to unity. One should note that the actual gaps  $\Delta$  and  $D$  (the former coincides with the superconducting order parameter) are monotonic functions of  $T$ . However the dielectric order parameter is not.

The magnitudes of  $T_c$  and  $\Delta(0)$  strongly depend on  $\mu$  and  $\sigma_0$ , although the simple BCS-like scaling between them

survives, that is, for CDW  $s$ -wave superconductors  $\Delta(0)/T_c = \pi/\gamma \approx 1.76$ . Although for, say,  $\Sigma_0 \geq 1.5\Delta_0$  and reasonable  $\mu = 0.5$  [386], the demand of self-consistency between  $\Sigma(T)$  and  $\Delta(T)$  becomes less important quantitatively. It justifies our previous approach with  $T$ -independent  $\Sigma$  [427] and the estimation of combined gap as  $(\Delta_{\text{BCS}}^2(T) + \Delta_{\text{PG}}^2)^{1/2}$  with  $T$ -independent  $\Delta_{\text{PG}}$  made on the basis of interlayer tunneling measurements in BSCCO mesas [559]; self-consistency leads to new qualitative effects and cannot be avoided. As for the magnitude of the very  $\Delta_{\text{PG}}$ , inferred from tunneling measurements, it was found in [559] to be substantially smaller than that of  $\Delta_{\text{BCS}}(T \rightarrow 0)$ , whereas the opposite case turned out to be true both for BSCCO [349, 399, 560, 561],  $\text{Bi}_{2-x}\text{Pb}_x\text{Sr}_2\text{CaCu}_2\text{O}_{8+\delta}$  [460], and  $(\text{Bi,Pb})_2\text{Sr}_2\text{Ca}_2\text{Cu}_3\text{O}_{10+\delta}$  [562]. Other tunnel measurement for BSCCO [417] revealed  $\Delta_{\text{PG}} > \Delta_{\text{BCS}}(T \rightarrow 0)$  for underdoped samples and  $\Delta_{\text{PG}} < \Delta_{\text{BCS}}(T \rightarrow 0)$  for overdoped ones. A marked sensitivity of  $\Delta_{\text{PG}}$  to doping together with strong inhomogeneity, discovered in Bi-based ceramics [334–336, 338, 343, 359, 440, 441, 456–458, 563, 564] and  $\text{Ca}_{2-x}\text{Na}_x\text{CuO}_2\text{Cl}_2$  [565], may be responsible for the indicated discrepancies.

Since the BCS character of the gap dependences for the CDW  $s$ -wave superconductor is preserved, the  $T$ -dependence of the heat capacity  $C$  for the doubly gapped electron liquid (i.e., below the actual  $T_c$ ) equals to the superposition of two BCS-like functions:

$$C(T) = \frac{2\pi^2 N(0)}{3} \left[ (1-\mu) T_c c_{\text{BCS}} \left( \frac{T}{T_c} \right) + \mu T_d c_{\text{BCS}} \left( \frac{T}{T_d} \right) \right], \quad (9)$$

where

$$c_{\text{BCS}} \left( t = \frac{T}{T_c^{\text{BCS}}} \right) = \frac{C_{\text{BCS}}(T)}{C_{\text{BCS}}(T = T_c^{\text{BCS}} + 0)}. \quad (10)$$

It should be noted that the normalized discontinuity  $\Delta C/C_n(T_c)$  at the superconducting phase transition may also serve as indirect evidence for the CDW gap on the FS, because in this case it is *not at all* a trivial BCS jump:

$$\frac{\Delta C_{\text{BCS}}}{\gamma_S T_c} = \frac{12}{7\zeta(3)} \approx 1.43. \quad (11)$$

Here,  $C_n(T) = \gamma_S T \equiv (2\pi^2 N(0)/3)T$  is the normal electron-gas heat capacity, whereas  $\gamma_S$  is the Sommerfeld constant. CDW-driven deviations from the BCS behavior was recognized long ago [425, 566]. However, only the self-consistent approach [386] allows us to give a quantitative answer at any value of the parameters appropriate to the partially CDW-gapped superconductor. It can be seen from Figure 4(a), where the conventionally normalized superconducting phase transition anomaly is shown as a function of  $\mu$ . The discontinuity is always smaller than the BCS value (11), in agreement with previous qualitative considerations [425, 566]. At the same time, the BCS ratio is restored not only for  $\mu = 0$ , that is, in the absence of the dielectrization, but also for  $\mu \rightarrow 1$ . In the former case, it is clear, because we are dealing with a conventional BCS superconductor. On the other hand, for large enough  $\mu$ , CDW gapping

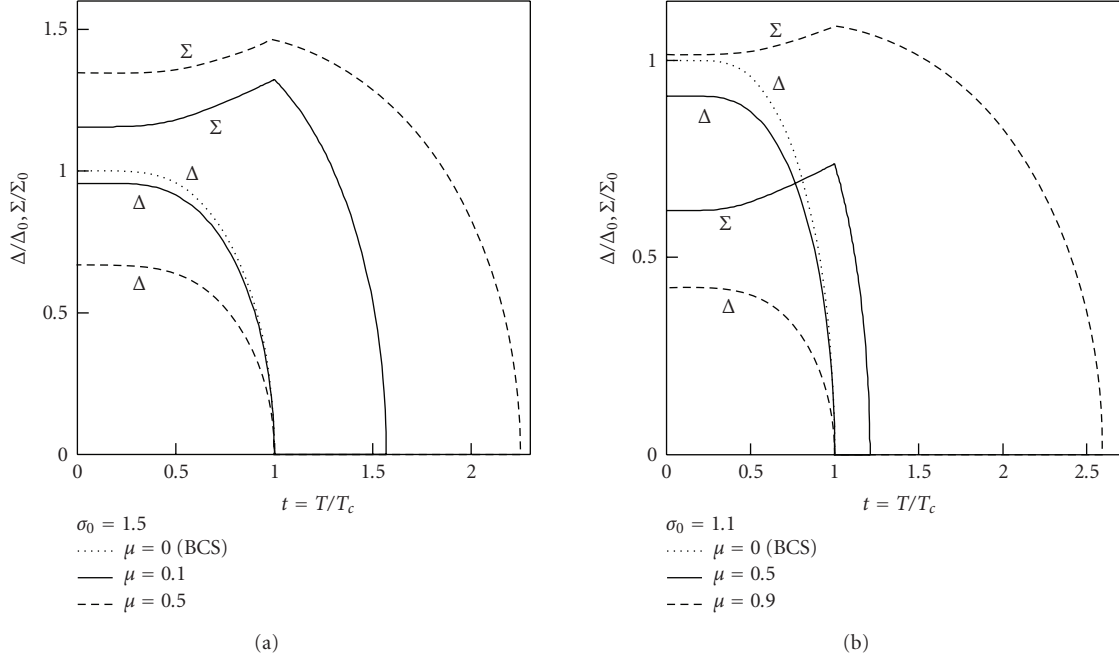


FIGURE 3: Temperature dependences of the superconducting ( $\Delta$ ) and dielectric ( $\Sigma$ ) order parameters for different values of the dimensionless parameters  $\mu$  (the portion of the nested Fermi surface sections, where the charge-density-wave, CDW, gap develops) and  $\sigma_0$  (see explanations in the text). (Taken from [386].)

almost completely destroys superconductivity, so  $T_c \ll T_d$ . Therefore, in the relevant superconducting  $T$  range, the contribution to  $C(T)$  from the  $d$  FS sections, governed by the gap  $D \approx \Sigma$ , becomes exponentially small. Another term, determined by the  $n$  FS section, ensures the BCS limiting value of the normalized discontinuity.

The dependences of  $\Delta C/C_n$  on  $\sigma_0$  for various values of  $t$  are depicted in Figure 4(b). One sees that the effect is large for  $\sigma_0$  close to unity, whereas the difference between 1.43 and  $\Delta C/C_n$  goes to zero as  $\sigma_0^{-2}$ , verifying the asymptotical result [425]. It should be noted that the heat capacity calculation scheme adopted for  $s$ -wave CDW superconductors can be applied also to other types of order parameter symmetry.

Experimental data on heat capacity, which could confirm the expressed ideas, are scarce. For  $\text{Nb}_3\text{Sn}$ , it was recently shown by specific heat measurements using the thermal relaxation technique that  $T_c \approx 17 \div 18$  K is reduced when the critical temperature of the martensitic transition  $T_d \approx 42 \div 53$  K grows [567]. Unfortunately, a large difference between  $T_c$  and  $T_d$  made the effects predicted by us quite small here, which is probably the reason why they have not been observed in these studies.

As for cuprates, reference should be made to  $\text{La}_{2-x}\text{Ba}_x\text{CuO}_{4-y}$  [568],  $\text{La}_{2-x}\text{Sr}_x\text{CuO}_{4-y}$  [569], and  $\text{YBa}_2\text{Cu}_3\text{O}_{7-y}$  [570], where underdoping led to a reduction of  $\Delta C/C_n$ . The same is true for measurements of the heat capacity in  $\text{Bi}_2\text{Sr}_{2-x}\text{La}_x\text{CuO}_{6+\delta}$  single crystals [571], which demonstrated that the ratio  $\Delta C/C_n$  for a strongly underdoped sample turned out to be about 0.25, that is, much below BCS values  $12/7\zeta(3) \approx 1.43$  and  $8/7\zeta(3) \approx 0.95$  [572] for  $s$ -wave and  $d$ -wave superconductivity, respectively.

There is also an opposite evidence for the relationship  $\Delta C/C_n > 1.43$ , for example, in the electron-doped high- $T_c$  oxide  $\text{Pr}_{1.85}\text{Ce}_{0.15}\text{CuO}_{4-\delta}$  [573]. More details, as well as information on other CDW superconductors, can be found in [386]. In any case, despite the well-known challenging controversy for BPB [392, 574–576], the problem was not studied enough for any superconducting oxide family, probably due to experimental difficulties.

**4.2. Enhancement of the Paramagnetic Limit in  $s$ -Wave CDW Superconductors.** Upper critical magnetic fields  $H_{c2}$  [577–579] (along with critical currents [132, 579, 580]) belong to main characteristics of superconductors crucial for their applications. In particular, knowing the upper limits on upper critical fields is necessary to produce superconducting materials for high-performance magnets, not to talk about scientific curiosity.

One of such limiting factors is the paramagnetic destruction of spin-singlet superconductivity, which was discovered long ago theoretically by Clogston [581] and Chandrasekhar [582]. In the framework of the BCS theory, they obtained a limit

$$H_p^{\text{BCS}} = \frac{\Delta_{\text{BCS}}(T=0)}{\mu_B^* \sqrt{2}} \quad (12)$$

from above on  $H_{c2}$  at zero temperature,  $T$ . Here,  $\Delta_{\text{BCS}}(T)$  is the energy gap in the quasiparticle spectrum of BCS  $s$ -wave superconductor, and  $\mu_B^*$  is the effective Bohr magneton, which may not coincide with its bare value  $\mu_B = e\hbar/2mc$ , where  $\hbar$  is Planck's constant, equal to unity in the whole

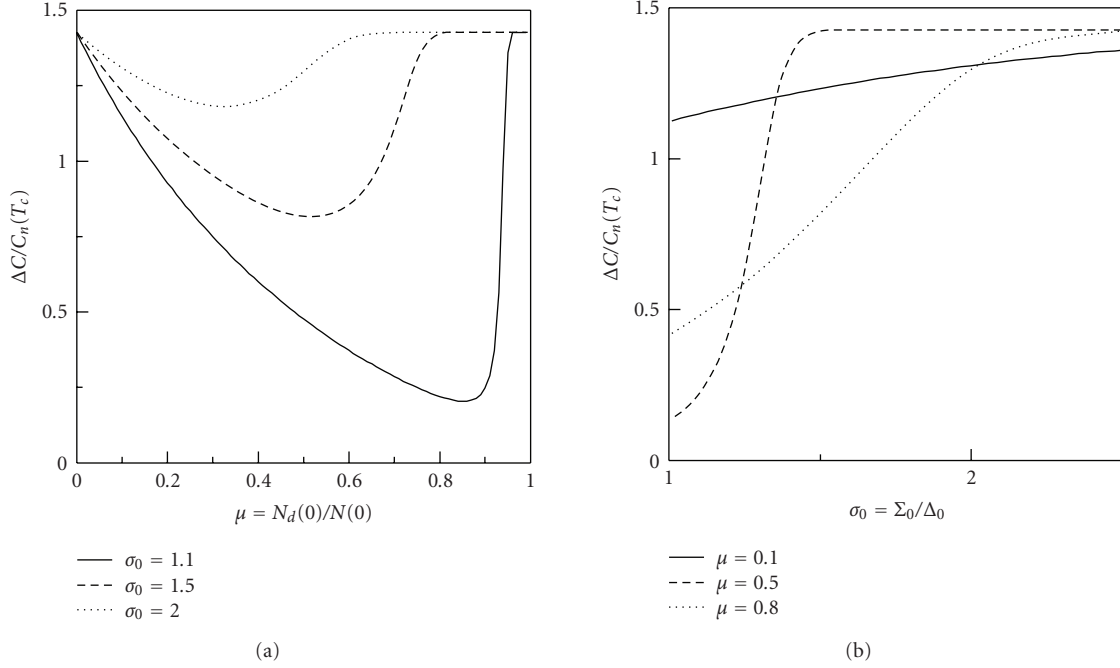


FIGURE 4: Dependences of the normalized heat capacity discontinuity  $\Delta C$  at  $T_c$  on  $\mu$  (a) and  $\sigma_0$  (b). (Taken from [386].)

article but shown here explicitly for clarity,  $m$  is the electron mass, and  $c$  is the velocity of light.

Limit (12) may be overcome at a high concentration of strong spin-orbit scatterers, when the spins of the electrons, constituting the Cooper pairs, are flipped [583]. Then, the actual  $H_{c2}(T = 0)$  starts to exceed [584] the classical bound. Such an enhancement of  $H_{c2}$  has been observed, for example, in Al films coated with Pt monolayers [585]. The Pt atoms served there as strong spin-orbit scatterers due to their large nuclear charge  $Z$ . One should indicate a possibility of exceeding value (12), if the energy,  $E$ , dependence of the normal state density of states is significant, which is the case in the neighborhood of the van Hove singularity [518]. Then, the BCS approximation of  $N(E) \simeq N(0)$  is no longer valid, so that the actual  $H_p$  may become larger than limit (12) [586].

We have found another reason, why the Clogston-Chandrasekhar value can be exceeded. Namely, it is the appearance of a partial CDW-driven dielectric gap on the  $d$  sections of the FS [427, 587–589]. The expected increase of the calculated limiting paramagnetic field  $H_p$  for CDW superconductors, as compared to  $H_p^{\text{BCS}}$ , is intimately associated with paramagnetic properties of the normal CDW state, which are very similar to those for BCS  $s$ -wave superconductors [382, 590–592].

It should be emphasized that the very self-consistency of the two-gap solution [386] made the treatment of the paramagnetic limit problem [589] transparent and less involved than previous approximations [427, 587, 588].

To calculate the paramagnetic limit, we considered the relevant free energies  $F$  per unit volume for all possible ground state phases in an external magnetic field  $H$ . The parent nonreconstructed phase (actually existing only above  $T_d!$ ), with both superconducting and CDW pairings switched

off and in the absence of  $H$ , served as a reference point. At  $T < T_d$ , we deal with relatively small differences  $\delta F$  reckoned from this hypothetical “doubly-normal” state [498]. In our case, in the Clogston-Chandrasekhar spirit [581, 582], there are two energy differences to be compared [589], specifically, that of a paramagnetic phase in the magnetic field [593] (diamagnetic effects are not taken into account when one is interested in the paramagnetic limit *per se*)

$$\delta F_p = -N(0)(\mu_B^* H)^2 \quad (13)$$

and that of a CDW-superconducting phase

$$\delta F_s = -N_n(0) \frac{\Delta^2(0)}{2} - N_d(0) \frac{D^2(0)}{2}. \quad (14)$$

Here,  $\Delta(0)$  is determined by (7), whereas  $D(0)$ , as stems from (8), is equal to  $\Sigma_0 = \pi T_d/\gamma$ . A simple algebra leads to the analytical equation for the increase of the paramagnetic limit over the Clogston-Chandrasekhar value (12):

$$\left( \frac{H_p}{H_p^{\text{BCS}}} \right)^2 = 1 + \mu \left[ \left( \frac{\Sigma_0}{\Delta_0} \right)^{2/(1-\mu)} - 1 \right]. \quad (15)$$

This relationship is expressed in terms of genuine (bare) system parameters  $\mu$ ,  $\Sigma_0$ , and  $\Delta_0$ . However, experimentalists are interested in the dependence of  $H_p/H_p^{\text{BCS}}$  on actual measurable quantities. The transformation of (15) can be easily made, and one arrives at the final formula

$$\begin{aligned} \left( \frac{H_p}{H_p^{\text{BCS}}} \right)^2 &= 1 + \mu \left[ \left( \frac{\Sigma(0)}{\Delta(0)} \right)^2 - 1 \right] \\ &= 1 + \mu \left[ \left( \frac{T_d}{T_c} \right)^2 - 1 \right]. \end{aligned} \quad (16)$$

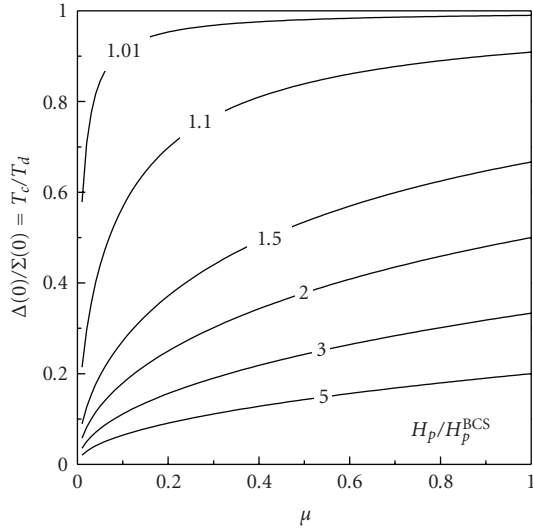


FIGURE 5: Contour plot of the ratio  $H_p/H_p^{\text{BCS}}$  on the plane  $(T_c/T_d, \mu)$ . Here  $H_p$  is the paramagnetic limit for CDW superconductors and  $H_p^{\text{BCS}}$  is that for BCS spin-singlet superconductors,  $T_c$  and  $T_d$  are the observed critical temperatures of the superconducting and CDW transitions, respectively. (Taken from [589].)

To calculate the expected paramagnetic limit, one needs to know  $\mu$ , which was estimated, for example, as 0.2 for NbSe<sub>3</sub> [594] or 0.15 for La<sub>2-x</sub>Sr<sub>x</sub>CuO<sub>4</sub> [595].

The contour curves in the parameter space obtained from (16) are displayed in Figure 5. One can readily see that for typical  $T_c/T_d \approx 0.05\text{--}0.2$  (some A15 compounds are rare exceptions [160]) and moderate values of  $\mu \approx 0.3\text{--}0.5$ , the augmentation of the paramagnetic limit becomes very large. There is a number of CDW superconductors [589], where the increase of the paramagnetic limit was detected, in accordance with the results presented here. Unfortunately, not so much can be said about high- $T_c$  oxides. It seems that extremely high values of  $H_{c2}$  observed in these materials are the reason of the unjustified neglect to the problem.

**4.3. Dip-Hump Structures and Pseudogaps in Tunnel Current-Voltage Characteristics for Junctions Involving CDW Superconductors.** In Section 3, a lot of evidence was presented concerning dip-hump structures (DHSs) and pseudogaps in high- $T_c$  oxides [81–83, 160, 559]. Broadly speaking, pseudogaps and DHSs have much in common. In particular, they can coexist with superconducting coherent peaks, their appearance in current-voltage characteristics (CVCs) is to some extent random, and their shapes are sample-dependent. Therefore, a suggestion inevitably arises that those two phenomena might be governed by the same mechanism. Our main assumption is that both pseudogaps and dip-hump structures are driven by CDW instabilities discussed above and that their varying appearances are coupled with the intrinsic, randomly inhomogeneous electronic structure of cuprates. In the strict sense, according to the adopted scenario, both DHSs and pseudogaps are the manifestations of the *same* dielectric DOS depletion,

the former being a result of superimposed CDW- and superconductivity-induced CVC features below  $T_c$ . To justify our approach, it is crucial that direct spatial correlations between irregular patterns of CDW three-dimensional supermodulations [365] and topographic maps of the superconducting gap amplitudes on the BSCCO surface were displayed by tunneling spectroscopy [458].

A detailed description of our approaches to the problems of tunneling through junctions with CDW isotropic superconductors as electrodes, and the emergence of DHSs in the CVCs of high- $T_c$  oxides can be found elsewhere [81–83, 160, 386, 596]. Here, we will present only a summary of our new results, briefly touching only those issues that are necessary for the rest of the paper to be self-contained.

We should emphasize different roles of the order parameter phases in determining quasiparticle tunnel currents. Concerning the superconducting order parameter, its phase may be arbitrary unless we are interested in the Josephson current across the junction. On the other hand, the CDW phase  $\varphi$  governs quasiparticle CVCs of junctions with CDW superconductors as electrodes [556, 557]. The value of  $\varphi$  can be pinned by various mechanisms in both excitonic and Peierls insulators, so that  $\varphi$  acquires the values either 0 or  $\pi$  in the first case [522] or is arbitrary in the unpinned state of the Peierls insulator [516]. At the same time, in the case of an inhomogeneous CDW superconductor, which will be discussed below, a situation can be realized, where  $\varphi$  values are not correlated over the junction area. Then, the contributions of elementary tunnel currents may compensate one another to some extent, and this configuration can be phenomenologically described by introducing a certain effective phase  $\varphi_{\text{eff}}$  of the CDW order parameter. If the spread of the phase  $\varphi$  is random, the most probable value for  $\varphi_{\text{eff}}$  is  $\pi/2$ , and the CVC for a nonsymmetric junction involving CDW superconductor becomes symmetric.

Most often, CVCs for cuprate-I-N (i.e., S-I-N) junctions reveal a DHS only at  $V = V_S - V_N < 0$  [597–599], so that the occupied electron states below the Fermi level are probed for CDW superconductors. In our approach, it corresponds to the phase  $\varphi$  close to  $\pi$ . This preference may be associated with some unidentified features of the CDW behavior near the sample surface.

On the other hand, there are S-I-N junctions, where DHS structures are similar for both  $V$  polarities [347, 442, 443, 600]. As for those pseudogap features, which were unequivocally observed mostly at high  $T$ , no preferable  $V$ -sign of their manifestations was found. We note that the symmetry of the tunnel conductance  $G(V) = dJ/dV$ , where  $J$  is the tunnel current through the junction, might be due either to the microscopic advantage of the CDW state with  $\varphi = \pi/2$  or to the superposition of different current paths in every measurement covering a spot with a linear size of a CDW coherence length at least. Both possibilities should be kept in mind. The variety of  $G(V)$  patterns in the S-I-N set-up for the same material and with identical doping is very remarkable, showing that the tunnel current is rather sensitive to the CDW phase  $\varphi$ . Nevertheless, the very appearance of the superconducting domain structure for cuprates with local domain-dependent gaps and critical

temperatures [601] seems quite plausible for materials with small coherence lengths. Essentially the same approach has been proposed earlier to explain superconducting properties of magnesium diboride [78].

On the basis of information presented above and using the self-consistent solutions for  $\Delta(T)$  and  $\Sigma(T)$ , we managed to describe the observed rich variety of  $G(V)$  patterns by calculating quasiparticle tunnel CVCs  $J(V)$  for two typical experimental set-ups. Namely, we considered S-I-N and S-I-S junctions, where “S” here means a CDW superconductor. A unique tunnel resistance in the normal state  $R$  enters into all equations, since we assume the incoherent tunneling to occur, in accordance with the previous analysis for BSCCO [122, 602]. The used Green’s function method followed the classical approach of Larkin and Ovchinnikov [603]. We skip all (quite interesting) technical details, since they can be found elsewhere [81–83, 160, 386, 596].

The obtained equations for  $J(V)$  form the basis for calculations both  $J(V)$  and  $G(V)$  (sub-, superscripts  $ns$  and  $s$  denote S-I-N and S-I-S junctions, resp.). They must be supplemented with a proper account of the nonhomogeneous background, since, as was several times stressed above, STM maps of the cuprate crystal surfaces consist of random nano-scale patches with different gap depths and widths, as well as coherent edge sharpnesses. In this connection, our theory assumes the combination CDW + inhomogeneity to be responsible for the appearance of the DHSs. Our main conclusion is that it is the dispersion of the parameter  $\Sigma_0$ —and, as a result, the  $D$ -peak smearing (the  $\Delta$ -peak also becomes smeared but to a much lesser extent)—that is the most important to reproduce experimental pictures. The value of the FS gapping degree  $\mu$  is mainly responsible for the amplitude of the DHSs. At the same time, neither the scattering of the parameter  $\mu$  nor that of the superconducting order parameter  $\Delta_0$  can result in the emergence of smooth DHSs, so that sharp CDW features remain unaltered. Therefore, for our purpose, it was sufficient to average only over  $\Sigma_0$  rather than simultaneously over all parameters of CDW superconductors, although the variation of any individual parameter made the resulting theoretical CVCs more similar to experimental ones.

Although it is a well-recognized matter of fact that CDW-driven  $D$ -singularities in  $G(V)$  scatter more strongly for a nonhomogeneous medium than main coherent superconducting peaks at  $eV = \pm\Delta$  (S-I-N junctions) or  $\pm 2\Delta$  (S-I-S junctions), this phenomenon has not yet been explained. It seems that the sensitivity of the Peierls [604, 605] or excitonic-insulator [431, 606] order parameters to the Coulomb potential of the impurities, for example, oxygen ions, might be the reason of such a dispersion. On the other hand,  $s$ -wave superconductivity is robust against impurity influence (Anderson theorem [607–609]). As for anisotropic superconductivity with  $d$ -wave or other kinds of symmetry, they are suppressed by nonmagnetic impurity scattering [3, 554, 610, 611] due to scattering-induced order parameter isotropization. Their survival in disordered cuprate samples, especially in the context of the severe damage inflicted by impurities on the pseudogap, testifies that the Cooper-pair order parameter includes a substantial isotropic component.

The parameter  $\Sigma_0$  was assumed to be distributed within the interval  $[\Sigma_0 - \delta\Sigma_0, \Sigma_0 + \delta\Sigma_0]$ . The normalized weight function  $W(x)$  was considered as a bell-shaped fourth-order polynomial within this interval and equal to zero beyond it (see the discussions in [81]). In any case, the specific form of  $W(x)$  is not crucial for the final results and conclusions.

Our approach is in essence the BCS-like one. It means, in particular, that we do not take a possible quasiparticle “dressing” by impurity scattering and the electron-boson interaction, as well as the feedback influence of the superconducting gapping, into account [612, 613]. Those effects, important *per se*, cannot qualitatively change the random two-gap character of superconductivity in cuprates.

As was already mentioned, we have assumed so far that both  $\Delta$  and  $\Sigma$  are  $s$ -wave-order parameters. Nevertheless, our approach to CVC calculations is qualitatively applicable to superconductors with the  $d$ -wave symmetry, if not to consider the intragap voltage range  $|eV| < \Delta$ .

The results of calculations presented below show that the same CDW + inhomogeneity combination can explain DHSs at low  $T$  as well as the pseudogap phenomena at high  $T$ , when the DHS is smoothed out. Thus, theoretical  $T$ -dependences of tunnel CVCs mimic the details of the DHS transformation into the pseudogap DOS depletion for nonsymmetric and symmetric junctions, involving cuprate electrodes. We consider the CDW-driven phenomena, DHS included, as the tip of an iceberg, a huge underwater part of which is hidden by strong superconducting manifestations, less influenced by randomness than their CDW counterpart. To uncover this part, one should raise  $T$ , which is usually done with no reference to the DHS, the latter being substantially smeared by the Fermi-distribution thermal factor. It is this DOS depletion phenomenon that is connected to the pseudogapping phenomena [14, 18, 334, 348, 399, 441].

The results of calculations of  $G^{ns}(V)$  in the case when parameter  $\Sigma_0$  is assumed to scatter are shown in Figure 6 for  $\varphi = \pi$ . The value  $\varphi = \pi$  was selected, because this case corresponds to the availability of the DHS in the negative-voltage branch of the nonsymmetric CVC, and such an arrangement is observed in the majority of experimental data. In accordance with our basic equations, all the four existing CVC peculiarities at  $eV = \pm\Delta$  and  $\pm D$  become smeared, although to various extent: the large singularities at  $eV = \pm\Delta$  almost preserve their shape, the large singularity at  $eV = -D$  transforms into a DHS, and the small one at  $eV = D$  disappears on the scale selected. The one-polarity dip-hump peculiarity in experimental CVCs for BSCCO [597] is reproduced excellently. Owing to relationship (7), the actual parameter  $\Delta$  also disperses, but, due to the small value of  $\mu$ , this fluctuation becomes too small to be observed in the plot. Thus, the calculated CVCs of Figure 6 demonstrate all principal features intrinsic to the tunnel conductivity of S-I-N junctions at low  $T$ , involving CDW superconductors, specifically, asymmetry with respect to the  $V$  sign is associated with the phase  $\varphi \neq \pi/2$  of the CDW-order parameter, the emerging CDW induces singularities at  $eV = \pm D$ , whereas the intrinsic CDW inhomogeneity transforms the major one into a DHS, totally suppressing the minor.

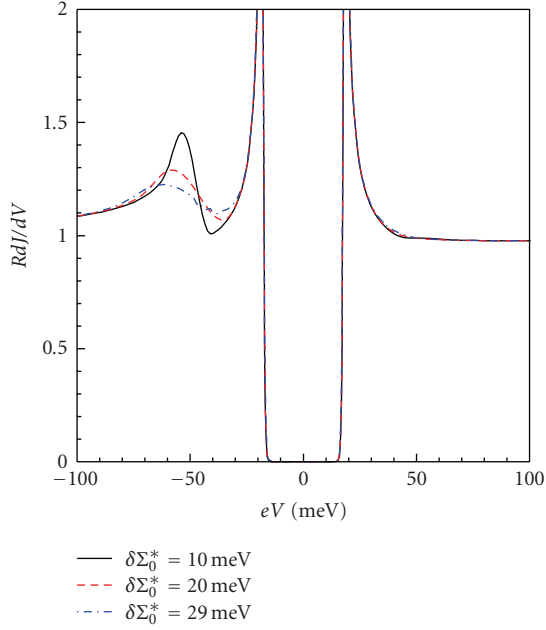


FIGURE 6: (Color online) Bias voltage,  $V$ , dependences of the dimensionless differential conductance  $RG(V) = RdJ/dV$  for the tunnel junction between an inhomogeneous CDW superconductor and a normal metal, expressed in energy units. Here,  $J$  is the quasiparticle tunnel current,  $R$  is the resistance of the junction in the normal state, and  $e > 0$  is the elementary charge. The bare parameters of the CDW superconductor are  $\Delta_0^* = 20$  meV,  $\Sigma_0^* = 50$  meV, and  $\mu = 0.1$ ; the temperature  $T = 4.2$  K. Various dispersions  $\delta\Sigma_0^*$  centered around the mean value  $\Sigma_0^* = 50$  meV. (Taken from [81].)

An example of the transformation, with  $T$ , of the DHS-decorated tunnel spectra into the typical pseudogap-like ones is shown in Figure 7 for S-I-N junctions with  $\varphi = \pi$  (panel (a)) and  $\pi/2$  (panel (b)). The CDW-superconductor parameters are  $\Delta_0 = 20$  meV,  $\Sigma_0 = 50$  meV,  $\mu = 0.1$ , and  $\delta\Sigma_0 = 20$  meV; the temperature  $T = 4.2$  K. For this parameter set, the “actual” superconducting critical temperatures  $T_c$  of random domains lie within the interval of 114–126 K, and  $T_d$  is in the range of 197–461 K. From Figure 7(a), the transformation of the DHS-including pattern of the CVCs calculated for  $T \ll T_c$  into the pseudogap-like ones in the vicinity of  $T_c$  or above it becomes clear. The asymmetric curves displayed in (a) are similar to the measured STM  $G^{ns}(V)$  dependences for overdoped and underdoped BSCCO compositions [441]. The overall asymmetric slope of the experimental curves, which is independent of gaps and  $T$ , constitutes the main distinction between them and our theoretical results. It might be connected to the surface charge carrier depletion induced by CDWs and mentioned above. Another interesting feature of our results is a modification and a shift of the  $\Delta$ -peak. Although  $\Delta$  diminishes as  $T$  grows, the  $\Delta$ -peak moves toward higher bias voltages; such a behavior of the  $\Delta$ -peak is to be undoubtedly associated with its closeness to the  $\Sigma$ -governed DHS. In experiments, a confusion of identifying this  $\Delta$ -driven singularity with a pseudogap feature may arise,

since the observed transformation of  $\Delta$ -features into  $D$ -ones looks very smooth [348].

It is notable that in the case of asymmetric  $G^{ns}(V)$ , the low- $T$  asymmetry preserves well into the normal state, although the DHS as such totally disappears. The extent of the sample randomness substantially governs CVC patterns. Therefore, pseudogap features might be less or more pronounced for the same materials and doping levels. At the same time, for the reasonable spread of the problem parameters, the superconducting coherent peaks always survive the averaging (below  $T_c$ , of course), in accordance with experiment. Our results also demonstrate that the dependences  $\Delta(T)$  taken from the tunnel data may be somewhat distorted in comparison to the true ones due to the unavoidable  $\Delta$  versus  $\Sigma$  interplay. One should stress that in our model, “hump” positions, which are determined mainly by  $\Sigma$  rather than by  $\Delta$ , anticorrelate with true superconducting gap values  $\Delta$  inferred from the coherent peaks of  $G(V)$ . It is exactly what was found for nonhomogeneous BSCCO samples [614].

Similar CDW-related features should be observed in the CVCs measured for symmetric S-I-S junctions. The  $G^s(V)$  dependences for this case with the same sets of parameters as in Figure 7 are shown in Figure 8. In analogy with symmetric junctions between BCS superconductors, one would expect an appearance of singularities at  $eV = \pm 2\Delta$ ,  $\pm(D + \Delta)$ , and  $\pm 2D$ . Such, indeed, is the case. However, the magnitudes of the features are quite different (the details of the analysis can be found in [81, 83]). As readily seen, the transformation of the symmetric DHS pattern into the pseudogap-like picture is similar to that for the nonsymmetric junction. This simplicity is caused by a smallness of the parameter  $\mu = 0.1$ , so that the features at  $eV = \pm 2D$ , which are proportional to  $\mu^2$ , are inconspicuous on the chosen scale. At the same time, the singularities at  $eV = \pm(D + \Delta)$  are of the *square-root type*. Note that for *arbitrary*  $\Sigma$ - and  $\Delta$ -magnitudes, those energies do not coincide with the values  $\pm(\Sigma + \Delta)$  (in more frequently used notation,  $\pm(\Delta_{PG} + \Delta_{SG})$ ), which can be sometimes met in literature [615]. The later relation becomes valid only for  $\Sigma \gg \Delta$ .

The appearance of the  $T$ -driven zero-bias peaks is a salient feature of certain CVCs displayed in Figure 8. As is well known [603], this peak is caused by tunneling of thermally excited quasiparticles between empty states with an enhanced DOS located above and below equal superconducting gaps in symmetric S-I-S junctions. Such a feature was found, for example, in  $G^s(V)$  measured for grain-boundary symmetric tunnel junctions in epitaxial films of the  $s$ -wave oxide CDWS  $Ba_{1-x}K_xBiO_3$  [616]. One should be careful not to confuse this peak with the dc Josephson peak restricted to  $V = 0$ , which is often seen for symmetric high- $T_c$  junctions [399]. The distinction consists in the growth of the quasiparticle zero-bias maximum with increasing  $T$  up to a certain temperature, followed by its drastic reduction. On the other hand, the Josephson peak decreases monotonously as  $T \rightarrow T_c$ .

The profile and the behavior of the zero-bias peak at nonzero  $T$  can be explained in our case by the fact that, in effect, owing to the nonhomogeneity of electrodes,

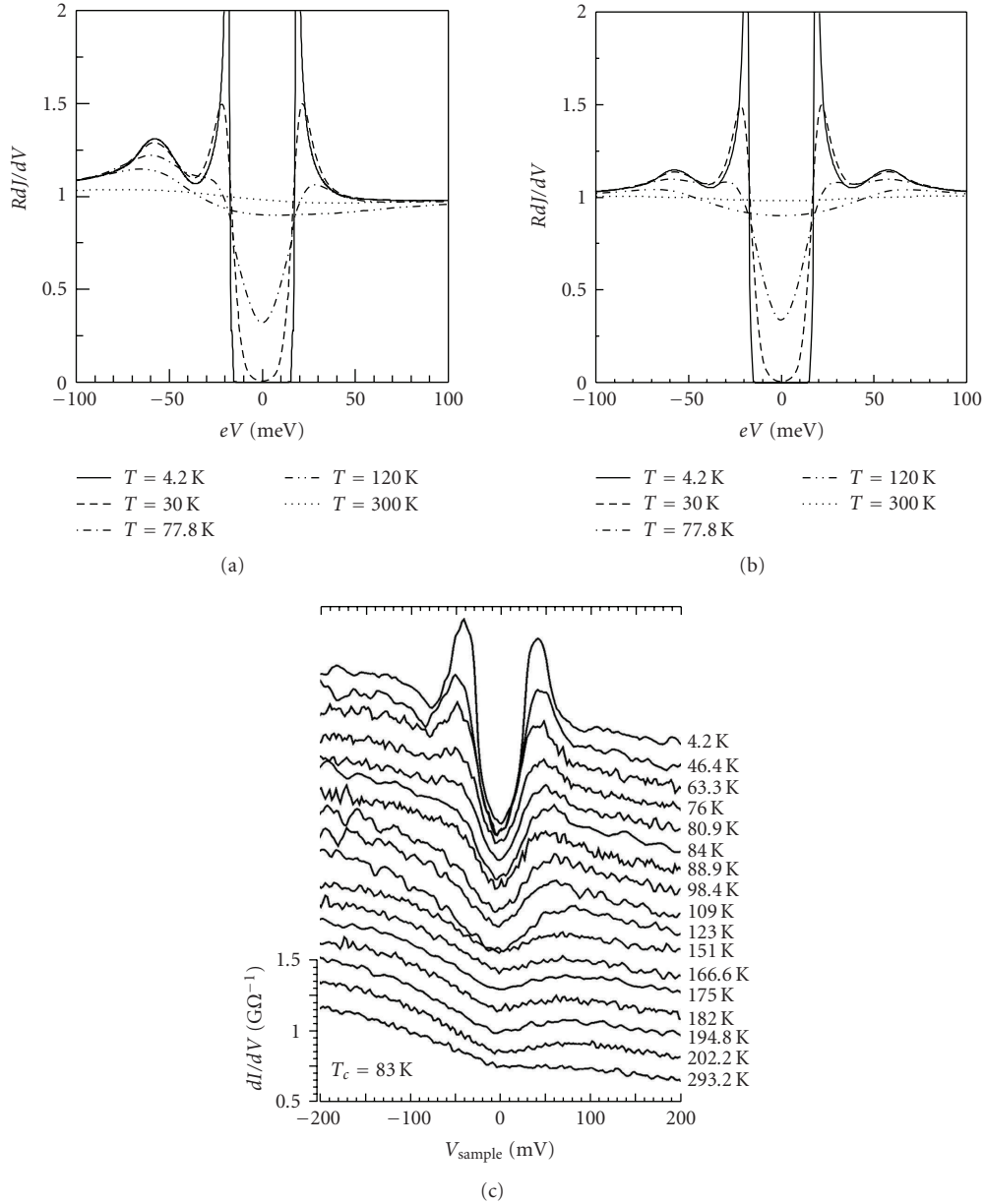


FIGURE 7:  $G(V)$  dependences for the tunnel junction between an inhomogeneous CDWS and a normal metal for various temperatures  $T$ . The CDW order parameter phase  $\varphi = \pi$  (a) and  $\pi/2$  (b), and the spread of the CDW order parameter-amplitude  $\delta\Sigma_0^* = 20$  meV. All other parameters are indicated in the text. (c) STM spectra for underdoped BSCCO-Ir junctions registered at various temperatures. (Reprinted from [598], taken from [83].)

the junction is a combination of a large number of *symmetric* and *nonsymmetric* junctions with varying gap parameters. The former compose a mutual contribution to the current in the vicinity of the  $V = 0$  point, and the width of this contribution along the  $V$ -axis is governed by temperature alone. On the other hand, every junction from the latter group gives rise to an elementary current peak in the CVC at a voltage equal to the relevant gap difference. All such elementary contributions form something like a hump around the zero-bias point, and the width of this hump along the  $V$ -axis is governed by the sum of actual—dependent on

the zero- $T$  values and on the temperature itself—gap spreads in both electrodes. It is clear that the  $T$ -behavior of the current contribution of either group is rather complicated, to say nothing of their combination.

From our CVCs calculated for both nonsymmetric (Figures 6 and 7) and symmetric (Figure 8) junctions, it comes about that the “dip” is simply a depression between the hump, which is mainly of the CDW origin, and the superconducting coherent peak. Therefore, as has been noted in [617], the dip has no separate physical meaning. It disappears as  $T$  increases, because the coherent peak forming

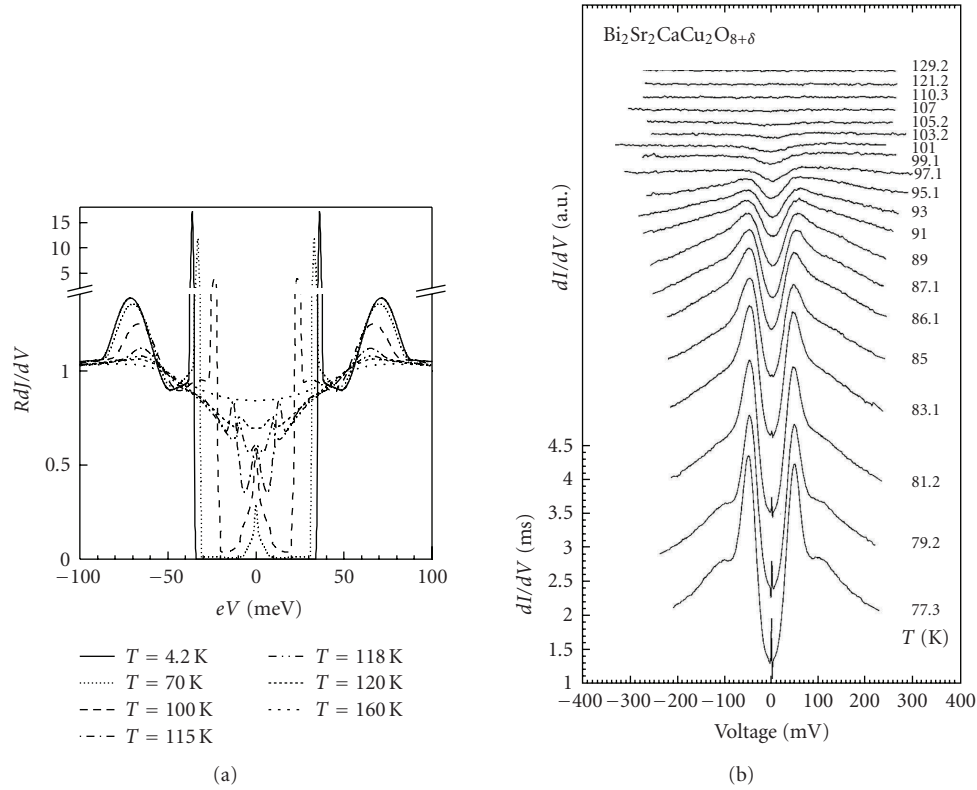


FIGURE 8: (a) The same as in Figure 7(a), but for a symmetric junction between similar CDW superconductors. (b) Temperature variations of experimental differential current-voltage characteristics (CVCs) for a  $\text{Bi}_2\text{Sr}_2\text{CaCu}_2\text{O}_{8+\delta}$  break junction. (Reprinted from [399], taken from [83].)

the other shoulder of the dip fades down, so that the former dip, by expanding to the  $V = 0$  point, becomes an integral constituent of the shallow pseudogap minimum.

Therefore, it became clear that the CDW manifestations against the nonhomogeneous background can explain both *subtle* DHS structures in the tunnel spectra for high- $T_c$  oxides and *large* pseudogap features observed both below and above  $T_c$ . The DHS is gradually transformed into the pseudogap-like DOS, lowering as  $T$  grows. Hence, both phenomena are closely interrelated, being in essence the manifestations of the same CDW-governed feature smeared by inhomogeneity of CDW superconductors. Therefore, the DHS and pseudogap features should not be treated separately. The dependences of the calculated CVCs on the CDW phase  $\varphi$  fairly well describe the variety of asymmetry manifestations in the measured tunnel spectra for BSCCO and related compounds.

**4.4. Coexistence of CDWs and  $d$ -Wave Superconductivity.** We recognize that some of our results, which were obtained assuming that the superconducting order parameter coexisting with CDWs is isotropic, might be applicable to cuprates with certain reservations, since a large body of evidence in favor of  $d_{x^2-y^2}$  symmetry in high- $T_c$  oxides [131, 132, 305, 306, 618, 619] is available, although there are experimentally-based objections [109, 116–129]. In any case, it seems

instructive to extend the partial dielectrization approach to  $d$ -wave Cooper pairing. For simplicity, we argue in terms of two-dimensional first Brillouin zone and Fermi surface, neglecting  $c$ -axis quasiparticle dispersion, which should be taken into account, in principle [620]. Since the dielectric,  $\Sigma$ , and superconducting,  $d$ -wave  $\Delta$ , order parameters have different momentum dependences, their joint presence in the electron spectrum is no longer reduced to a combined gap (4), as it was for isotropic superconductivity.

In the  $d$ -wave case, superconductivity is described by a weak-coupling model with a Hamiltonian given, for example, in [553, 621]. In accordance with photoemission [371, 622–624] and STM [359, 368, 370, 506, 507, 512, 625] data (see Figure 1), the mean-field CDW Hamiltonian is restricted to momenta near flat-band regions, antinodal from the viewpoint of the four-lobe  $d$ -wave gap-function  $\Delta(T) \cos 2\theta$  [306]. In those regions, the nesting conditions (1) between pairs of mutually coupled quasiparticle branches are fulfilled. For instance, static CDW wave vectors  $\mathbf{Q} = (\pm 2\pi/4.2a_0, 0)$  and  $(0, \pm 2\pi/4.2a_0)$ —with an accuracy of 15%—in  $\text{Bi}_2\text{Sr}_2\text{CaCu}_2\text{O}_{8+\delta}$  are revealed in STM studies [359]. Thus, we characterize a CDW checkerboard state (symmetric with respect to  $\pi/2$ -rotations) by four sectors in the momentum space centered with the lobes and with an opening  $2\alpha$  each ( $\alpha < \pi/4$ ). It should be noted that vectors  $\mathbf{Q}$  depend on doping, which was explicitly shown

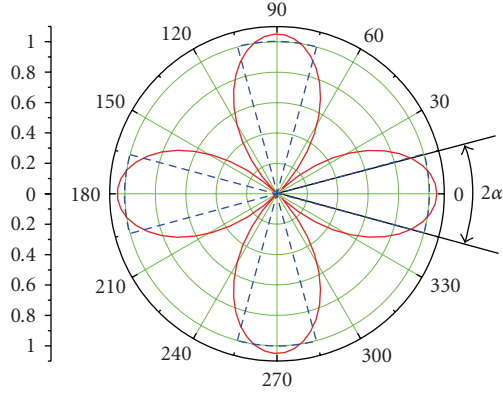


FIGURE 9: (Color online) Order-parameter maps for a conventional  $d$ -wave superconductor ( $\Delta$ , solid curve) and a partially gapped CDW metal ( $\Sigma$ , dashed curve).

for  $\text{Bi}_2\text{Sr}_2\text{CuO}_{6+\delta}$  [343]. The dielectric (CDW-induced) order parameter is  $\Sigma(T)$  inside the  $2\alpha$ -cones, being angle-independent here, and zero outside (see Figure 9).

The plausibility of this scenario is supported—at least partially—by recent STM studies of intrinsically inhomogeneous BSCCO samples [626]. Specifically, the authors analyzed the composition, temperature, and angular dependences of the gaps on various FS sections and showed that nodal superconducting gaps for overdoped specimens exhibit more or less conventional  $d$ -wave behavior, whereas in underdoped samples nodal (superconducting) and antinodal gaps (CDW gaps, as is assumed here) superimpose on one another in tunnel spectra. It is important that for underdoped compositions antinodal gaps do not change drastically with  $T$ , when crossing  $T_c$ . The conclusion made in [626] that the entire FS contributes to bulk superconductivity in overdoped samples corresponds—if proved to be correct—to the actual shrinkage of nested FS sections, that is, to  $\mu \rightarrow 0$ .

We obtained a new set of Dyson-Gor'kov equations for normal and superconducting Green's functions for the system with electron-hole of whatever nature and  $d$ -wave Cooper pairings, which were solved in the same straightforward manner as in the  $s$ -wave case [160, 386] (see above). We arrived at the system of two coupled equations for  $\Delta(T)$  and  $\Sigma(T)$ :

$$\int_0^{\mu\pi/4} I_M(\sqrt{\Sigma^2 + \Delta^2 \cos^2 2\theta}, T, \Sigma_0) d\theta = 0, \quad (17)$$

$$\int_0^{\mu\pi/4} I_M(\sqrt{\Sigma^2 + \Delta^2 \cos^2 2\theta}, T, \Delta_0) \cos^2 2\theta d\theta + \int_{\mu\pi/4}^{\pi/4} I_M(\Delta \cos 2\theta, T, \Delta_0) \cos^2 2\theta d\theta = 0, \quad (18)$$

where  $\mu = 4\alpha/\pi$  is the dielectrically gapped portion of the FS for the specific model of partial gapping, shown in Figure 9, and  $I_M(\Delta \cos 2\theta, T, \Delta_0)$  is the Mühschlegel integral (6). The analysis of the generic  $T$ - $\delta$  phase diagram for cuprates shows that both  $\Sigma_0$  and  $\mu$  reduce with doping, whereas the hole-like FS pockets centered at the  $(\pi/a_0, \pi/a_0)$  point of the Brillouin zone shrink for every specific high- $T_c$  oxide (see, e.g., [343]).

On the other hand, in the absence of CDW gapping, (18) becomes a  $d$ -wave gap equation:

$$\int_0^{\pi/4} I_M(\Delta \cos 2\theta, T, \Delta_0) \cos^2 2\theta d\theta = 0, \quad (19)$$

the solution of which  $\Delta = d\text{Mü}(\Delta_0, T)$  is known [553, 621]. In particular, the critical temperature is  $T_{c0} = (2\Omega\gamma/\pi) \exp[-1/V_{\text{BCS}}N(0)]$ , as in the  $s$ -wave case. From (19), it follows that in agreement with [553],  $(\Delta_0/T_{c0})_d = (2/\sqrt{e})(\pi/\gamma)$ , revealing a modified “ $d$ -wave” BCS-ratio different from the  $s$ -pairing value

$$\left(\frac{\Delta_0}{T_{c0}}\right)_s = \frac{\pi}{\gamma} \approx 0.824 \left(\frac{\Delta_0}{T_{c0}}\right)_d. \quad (20)$$

Here,  $e$  is the base of natural logarithm. It is evident that our model takes into account many-body correlations both explicitly (the emergence of two pairings) and implicitly (via the renormalization of the parameters  $\Sigma_0$  and  $\mu$ ). Weak-coupling values of the ratio  $\Delta_0/T_{c0}$  for other anisotropic order parameter symmetries do not differ much from the value of  $(\Delta_0/T_{c0})_d$  [627, 628].

Due to the different order parameter symmetry, readily seen from (17) and (18), the situation is mathematically more involved than for isotropic CDW superconductors, where a simple relationship (4) takes place. This was not recognized in a recent work [629], where the opposite wrong statement was made. *Prima facie* subtle mathematical differences between descriptions of  $s$ -wave and  $d$ -wave CDW superconductors lead to conspicuous physical consequences. Indeed, the numerical dependences  $\Delta(T)$  and  $\Sigma(T)$  found from (17) and (18) and shown in Figure 10 differ *qualitatively* from their counterparts  $\Delta_s(T)$  and  $\Sigma_s(T)$  in a certain range of model parameters. (In this subsection, we do not introduce a natural subscript “ $d$ ” for brevity.) Figure 10 (a) demonstrates that a reduction of the bare parameter  $\Sigma_0$ , keeping  $\Delta_0$  and  $\mu$  constant, resulting in the transformation of  $\Sigma(T)$  with a cusp at  $T = T_c$  and a concave region at  $T < T_c$  (the behavior appropriate for CDW  $s$ -superconductors in the whole allowable parameter range, as is demonstrated in Figure 3) into curves describing a *novel* peculiar reentrant CDW state. It is remarkable that the reentrance found by us is appropriate to an extremely simple basic model with two competing order parameters. At the same time, the CDW structures in real systems may be much more complicated with nonmonotonic  $T$ -dependencies even in the absence of superconductivity [352].

Let us formulate conditions necessary to observe this crossover. First, (20) means that  $\Delta(T)/\Delta_0$  for conventional  $d$ -superconductors is steeper than  $(\Delta(T)/\Delta_0)_s$ . In our case, it means that  $\Delta(T)/\Delta_0$ , when the CDW disappears, is steeper than  $\Sigma(T)/\Sigma_0$  in the absence of superconductivity, which is described by (6). Hence, for the CDW phase to exist (the upper critical temperature  $T_{\text{CDW}}^u > 0$ ), it should be  $T_{\text{CDW}}^u = (\gamma/\pi)\Sigma_0 > T_{c0} = (\sqrt{e}\gamma/2\pi)\Delta_0$ . As a consequence, the first constraint on the model parameters should be fulfilled:  $\Sigma_0 > (\sqrt{e}/2)\Delta_0 \approx 0.824\Delta_0$ . The constraint stems from the competition between emerging  $\Delta$  and  $\Sigma$  on the  $d$  FS section only. The actual coexistence between superconductivity and

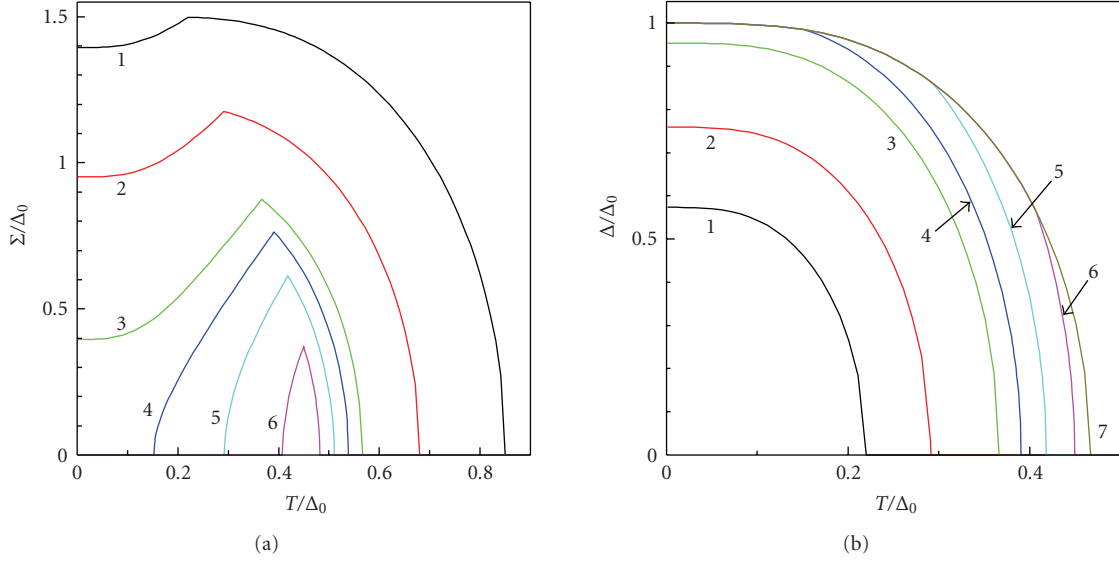


FIGURE 10: (Color online) Temperature,  $T$ , dependences of the normalized (a) CDW  $\Sigma$  and (b) superconducting  $\Delta$  gap functions.  $\Delta_0$  equal to  $\Delta(T = 0)$  when CDWs are absent is 1. The values of  $\Sigma_0/\Delta_0$  equal to  $\Sigma(T = 0)/\Delta_0$  in the absence of superconductivity are 1.5 (1), 1.2 (2), 1 (3), 0.95 (4), 0.9 (5), 0.85 (6), and 0.8 (7);  $\mu = 0.3$ .

CDWs was not involved in these reasonings, so the inequality does not include the control parameter  $\mu$ . Therefore,  $T_{\text{CDW}}^u$  thus defined coincides with  $T_{\text{CDW}0}$ .

Second, below the lower critical temperature of the CDW reentrance region,  $T_{\text{CDW}}^l$ , if any, (18) defines  $\Delta(T) = d\text{M}\ddot{u}(\Delta_0, T)$ , and we should use (17) with  $T = T_{\text{CDW}}^l$  and  $\Delta(T_{\text{CDW}}^l) = d\text{M}\ddot{u}(\Delta_0, T_{\text{CDW}}^l)$  to determine  $T_{\text{CDW}}^l(\Delta_0, \Sigma_0, \mu)$  numerically. The crossover value of  $\Sigma_0^{\text{cr}}$ , when  $T_{\text{CDW}}^l = 0$ , corresponds to the separatrix on the order parameter- $T$  plane, dividing possible  $\Sigma(T)$ -curves (see Figure 10(a)) into two types: reentrant and nonreentrant. However, (17) brings about  $\Sigma_0^{\text{cr}} = \Delta_0 \exp[(4/\mu\pi) \int_0^{\mu\pi/4} \ln(\cos 2\theta) d\theta]$ . To observe the reentrant behavior, the second constraint should be  $\Sigma < \Sigma_0^{\text{cr}}$ . For the curves in Figure 10,  $\mu = 0.3$  was chosen, so that we obtain the reentrance range  $0.824\Delta_0 < \Sigma_0 < 0.963\Delta_0$ , which agrees with numerical solutions of the full self-consistent equation set. We emphasize that CDWs survives the competition with  $d$ -wave superconductivity even at  $\Sigma_0/\Delta_0 < 1$ , which is not the case for stronger isotropic Cooper pairing (see the discussions above).

In Figure 10(b), the concomitant  $\Delta(T)$  dependences are depicted. One sees how  $d$ -wave superconductivity, suppressed at large  $\Sigma_0$ , recovers in the reentrance parameter region. Therefore, two regimes of CDW manifestation can be observed in superconductors. In both cases, the CDW is seen as a pseudogap above  $T_c$  [81, 83] in photoemission and tunnel experiments. However, the corresponding DHS at low  $T$  may either be observed or not, depending on whether the reentrance occurs. This might be an additional test for an anisotropic (not necessarily  $d_{x^2-y^2}$ -wave) Cooper pairing to dominate in cuprates.

To control the change-over between different regimes in cuprates, one can use either hydrostatic pressure or doping. In both cases,  $\mu$  is the main varying parameter. In Figure 11,

the curves  $\Sigma(T)$  and  $\Delta(T)$  are shown for  $\Sigma_0/\Delta_0 = 0.9$  and various  $\mu$ . It is readily seen how drastic is the low- $T$  depression of  $\Sigma$  by superconductivity, when the dielectrically gapped FS sectors are small enough. Doping  $\text{Bi}_2\text{Sr}_2\text{CaCu}_2\text{O}_{8+\delta}$  [403] and  $(\text{Bi,Pb})_2(\text{Sr,L a})_2\text{CuO}_{6+\delta}$  [356] with oxygen was shown to sharply shrink the parameter  $\mu$ . Note that the  $\Delta(T)$  dependences are distorted by CDWs, and they do *not* coincide with the scaled “parent” curve— $d\text{M}\ddot{u}(T)$ , in this case—in contrast to what should be observed for CDW  $s$ -superconductors (Figure 3). Therefore, various observed forms of  $\Delta(T)$  *per se* cannot unambiguously testify to the superconducting pairing symmetry. Moreover, cuprate superconductivity might be, for example, a mixture of  $s$ - and  $d$ -wave contributions [130, 630].

It is evident that different strengths of CDW-imposed suppression of the superconducting energy gap in the electron spectrum  $\Delta$  and the critical temperature  $T_c$  must change the ratio  $\Delta(0)/T_c$ —the benchmark of *weak-coupling* superconductivity (see (20)). If one recalls that, as was shown above, this ratio in CDW  $s$ -superconductors remains the same as in conventional  $s$ -ones, the situation becomes very intriguing. In Figure 12(a), the dependences of  $2\Delta(0)/T_c$  and  $T_c/\Delta_0$  ratios on  $\Sigma_0/\Delta_0$  are displayed. One sees that  $2\Delta(0)/T_c$  sharply increases with  $\Sigma_0/\Delta_0$  for  $\Sigma_0/\Delta_0 \leq 1$  and swiftly saturates for larger  $\Sigma_0/\Delta_0$ , whereas  $T_c/\Delta_0$  decreases almost evenly. The saturation value proves to be 5.2 for  $\mu = 0.3$ . We stress that such large enhancement of  $2\Delta(0)/T_c$  agrees well with experimental data [441, 478, 631, 632] for cuprates and *cannot* be achieved taking into account strong-coupling electron-boson interaction effects for reasonable relationships between  $T_c$  and effective boson frequencies  $\omega_E$  [633, 634] (one can hardly accept, e.g., the value  $T_c/\omega_E \approx 0.3$  [634] as practically meaningful). Furthermore, the destruction of the alternating-sign superconducting order

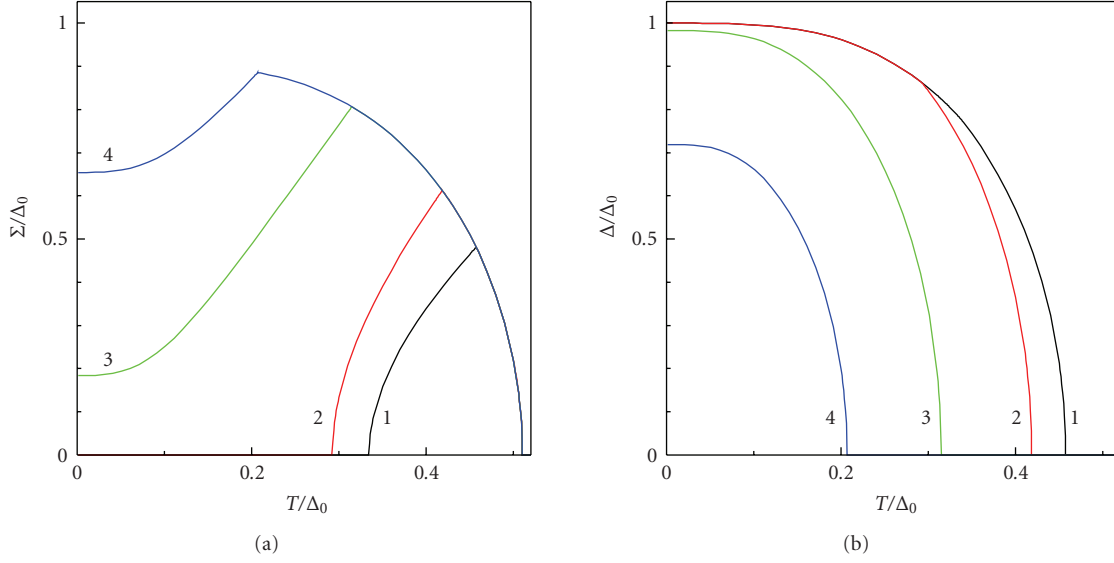


FIGURE 11: (Color online) The same as in Figure 10 but for  $\Sigma_0/\Delta_0 = 0.9$  and  $\mu = 0.1$  (1), 0.3 (2), 0.5 (3), 0.6 (4).

parameter by impurity scattering approximated by collective boson modes also could not explain [635] high values of  $2\Delta(0)/T_c$ , for example, inherent to underdoped BSCCO [347, 597]. Therefore, our weak-coupling model is *sufficient* to explain—*on its own*—the large magnitude of  $2\Delta(0)/T_c$  in cuprates, possible strong-coupling effects resulting in at most minor corrections.

Another possible alternative reason of high  $2\Delta(0)/T_c$  ratios might be a singular energy dependence of the normal-state electron DOS near the FS, for instance, near the Van Hove anomalies in low-dimensional electron subsystems [518]. It turned out, however, that, at least in the weak-coupling (BCS) approximation for *s*-wave Cooper pairing, the ratio  $2\Delta(0)/T_c$  is not noticeably altered [636, 637]. Moreover, calculations in the framework of the strong-coupling Eliashberg theory [10] showed that the van Hove singularity influence on  $T_c$  is even smaller than in the BCS limit [638]. Furthermore, weak-coupling calculations for orthorhombically distorted hole-doped cuprate superconductors (without CDWs) demonstrated that  $2\Delta(0)/T_c$  can be estimated as an intermediate between *s*-wave and *d*-wave limits [639], being smaller than needed to explain the experiment. It means that our approach remains so far the only one capable of explaining high  $2\Delta(0)/T_c \approx 5 \div 8$  (and even larger values [632]) for cuprates. We emphasize that it is very important to reconcile theoretical values for  $2\Delta(0)/T_c$  as well as  $\Delta C/\gamma_S T_c$  with experimental ones. Otherwise, the microscopic theory becomes “too” phenomenological with  $\Delta/T_c$  as an *additional free parameter* of the system [640].

It is instructive from the methodological point of view to mention a previous unsuccessful attempt to explain the increase of  $2\Delta(0)/T_c$  by a pseudogap influence [641]. The authors of this reference assumed the *identical d*-wave symmetry for both the superconducting,  $\Delta(T)$ , and

temperature-independent pseudogap,  $E_{PG}$ , order parameters. Additionally, dielectric gapping was supposed to be effectively complete rather than partial, the latter being intrinsic to our model and follows from the experiments for cuprates. These circumstances excluded self-consistency from the approach and led to superfluous restrictions imposed on  $E_{PG}$ , namely,  $E_{PG} \lesssim 0.53\Delta_0(T=0)$ , where  $\Delta_0(T=0)$  is the parent superconducting order parameter amplitude. At the same time, it is well known that for existing CDW superconductors the strength of CDW instability is at least not weaker than that of its Cooper-pairing counterpart [160]. We should emphasize once more that the *main peculiarity* of our model, dictated by the observations, which led to the adequate description of thermodynamic properties for *d*-wave superconductors with CDWs, is the distinction between relevant order parameter symmetries.

The  $\mu$ -dependences of  $2\Delta(0)/T_c$  and  $T_c/\Delta_0$  are shown in Figure 12(b). They illustrate that  $2\Delta(0)/T_c$  can reach rather large values, if the dielectric gapping sector is wide enough. This growth is however limited by a drastic drop of  $T_c$  leading to a quick disappearance of superconductivity. We think that it is exactly the case of underdoped cuprates, when a decrease of  $T_c$  is accompanied by a conspicuous widening of the superconducting gap. For instance, such a scenario was clearly observed in break-junction experiments for  $\text{Bi}_2\text{Sr}_2\text{CaCu}_2\text{O}_{8+\delta}$  samples with a large doping range [642].

As was pointed out in [478], various photoemission and tunneling measurements for different cuprate families show a typical average value  $2\Delta(0)/T_c \approx 5.5$ . From Figure 12(b), we see that this ratio corresponds to  $\mu \approx 0.35$  at  $\Sigma_0/\Delta_0 = 1$ . The other curve readily gives  $T_c/\Delta_0 \approx 0.35$ . Since  $\Delta_0/T_{c0} \approx 2.14$  for a *d*-wave superconductor (see above), we obtain  $T_c/T_{c0} \approx 0.75$ , being quite a reasonable estimation of  $T_c$ -reduction by CDWs.

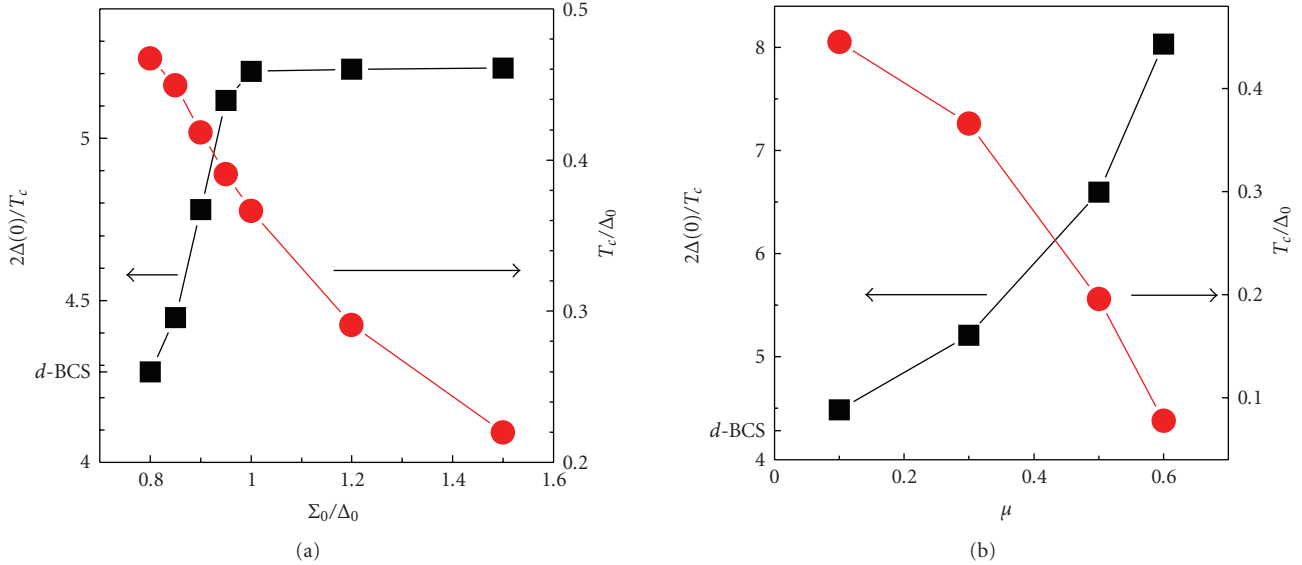


FIGURE 12: (Color online) Dependences of  $2\Delta(0)/T_c$  (squares) and  $T_c/\Delta_0$  (circles) on  $\Sigma_0/\Delta_0$  (panel (a),  $\mu = 0.3$ ) and  $\mu$  (panel (b),  $\Delta_0/\Sigma_0 = 1$ ).  $T_c$  is the superconducting critical temperature,  $d$ -BCS  $\approx 4.28$  is a value for a conventional superconductor with  $d$ -wave symmetry of the order parameter.

**4.5. SDWs and Superconductivity.** There are plenty of materials, where SDWs compete with superconductivity, although a simultaneous existence of the order parameters cannot be always proved [160, 643, 644]. For completeness, we give here certain short comments on the latest developments in this direction.

During the last years, an interest arose to the phase with the hidden order parameter in  $\text{URu}_2\text{Si}_2$ , emerging at about 17.5 K and being some kind of SDWs, coexisting with superconductivity at  $T < 1.5$  K [153, 645–647]. It should be noted that the partial gapping idea applied to SDW materials [397, 422–424, 566, 648–650] was invoked to explain ordering in this compound at the times of the discovery [651].

More attention was paid to Cr and its alloys, where CDWs and SDWs are linked and coexist [652, 653]. It might be interesting to observe mutual influence of CDWs and SDWs on superconductivity [654–657].

The problem of an interplay between SDWs and superconductivity received strong impetus recently, especially because of the fundamental discovery of magnetic element-based high- $T_c$  pnictide superconductors [49, 654–657]. Theoretical efforts were also continued (see, e.g., [658–662]). It is worthwhile noting that, for certain doping ranges, superconducting cuprates also demonstrate [663] the coexistence of Cooper pairing with SDWs rather than CDWs, the latter being appropriate for the majority of high- $T_c$  oxide compositions (see above and [160]).

Although the coexistence of superconductivity with SDWs or more exotic orbital antiferromagnetic and spin current ordering [522, 548, 664] is left beyond the scope of this review, the relevant physics is not less fascinating than that of their CDW-involving analogues.

## 5. Conclusions

The presented material testifies that CDWs play the important role in high- $T_c$  oxides and govern some of the properties that usually have been considered as solely determined by superconductivity *per se*. Sometimes CDWs manifest themselves explicitly (observed checkerboard or unidirectional structures, DHSs, pseudogaps) but, in the majority of phenomena, they “only”—but often drastically—change the magnitude of certain effects in the superconducting state (the heat capacity anomaly, the paramagnetic limit, the  $T$ -dependence of  $H_{c2}$ , the  $\Delta(0)/T_c$  ratio). Cuprates are not unique as materials with coexisting CDWs and superconductivity, but the scale of the interplay is very large here due to the strength of the Cooper pairing in those compounds.

## Acknowledgments

The authors are grateful to Antonio Bianconi, Sergei Borisenko, Ilya Eremin, Peter Fulde, Stefan Kirchner, Alexander Kordyuk, Dirk Manske, and Kurt Scharnberg for useful discussions. A. M. Gabovich and A. I. Voitenko are also grateful to Kasa im. Józefa Mianowskiego, Polski Koncern Naftowy ORLEN, and Fundacja Zygmunta Zaleskiego as well as to project no. 23 of the 2009–2011 Scientific Cooperation Agreement between Poland and Ukraine for the financial support of their visits to Warsaw. A. M. Gabovich highly appreciates the 2008 and 2009 Visitors Programs of the Max Planck Institute for the Physics of Complex Systems (Dresden, Germany). T. Ekino was partly supported by a Grant-in-Aid for Scientific Research (nos. 19540370, 19105006, 19014016) of Japan Society of Promotion of Science. M. S. Li

was supported by the Ministry of Science and Informatics in Poland (grant no. 202-204-234).

## References

- [1] J. G. Bednorz and K. A. Müller, "Possible high  $T_c$  superconductivity in the Ba-La-Cu-O system," *Zeitschrift für Physik B*, vol. 64, no. 2, pp. 189–193, 1986.
- [2] P. W. Anderson, *The Theory of Superconductivity in the High- $T_c$  Cuprates*, Princeton University Press, Princeton, NJ, USA, 1997.
- [3] V. P. Mineev and K. V. Samokhin, *Introduction to Unconventional Superconductivity*, Gordon and Breach Science, Amsterdam, The Netherlands, 1999.
- [4] M. L. Kulić, "Interplay of electron-phonon interaction and strong correlations: the possible way to high-temperature superconductivity," *Physics Reports*, vol. 338, no. 1-2, pp. 1–264, 2000.
- [5] S. L. Drechsler, H. Rosner, J. Málek, and H. Eschrig, "Electronic and magnetic properties of cuprate chains and related materials. From bandstructure to aspects of many-body physics in real materials," in *High- $T_c$  Superconductors and Related Materials. Material Science, Fundamental Properties, and Some Future Electronic Applications*, S. L. Drechsler and T. Mishonov, Eds., p. 81, Kluwer Academic Publishers, Dordrecht, The Netherlands, 2001.
- [6] N. M. Plakida, *Spectroscopy of High- $T_c$  Superconductors: A Theoretical View*, Taylor and Francis, New York, NY, USA, 2003.
- [7] Y. Yanase, T. Jujo, T. Nomura, H. Ikeda, T. Hotta, and K. Yamada, "Theory of superconductivity in strongly correlated electron systems," *Physics Reports*, vol. 387, no. 1–4, pp. 1–149, 2003.
- [8] A. S. Alexandrov, *Theory of Superconductivity: From Weak to Strong Coupling*, IOP, Philadelphia, Pa, USA, 2003.
- [9] L. Pitaevskii, "Theoretical foundation: phenomenology and microscopic theory," in *The Physics of Superconductors. Vol. 1: Conventional and High- $T_c$  Superconductors*, K. H. Bennemann and J. B. Ketterson, Eds., p. 23, Springer, Berlin, Germany, 2003.
- [10] J. P. Carbotte and F. Marsiglio, "Electron-phonon superconductivity," in *The Physics of Superconductors. Vol. 1: Conventional and High- $T_c$  Superconductors*, K. H. Bennemann and J. B. Ketterson, Eds., p. 233, Springer, Berlin, Germany, 2003.
- [11] A. V. Chubukov, D. Pines, and J. Schmalian, "A spin fluctuation model for  $d$ -wave superconductivity," in *The Physics of Superconductors. Vol. 1: Conventional and High- $T_c$  Superconductors*, K. H. Bennemann and J. B. Ketterson, Eds., p. 495, Springer, Berlin, Germany, 2003.
- [12] S. A. Kivelson, I. P. Bindloss, E. Fradkin, et al., "How to detect fluctuating stripes in the high-temperature superconductors," *Reviews of Modern Physics*, vol. 75, no. 4, pp. 1201–1241, 2003.
- [13] D. Manske, *Theory of Unconventional Superconductors. Cooper-Pairing Mediated by Spin Excitations*, Springer, New York, NY, USA, 2004.
- [14] E. W. Carlson, V. J. Emery, S. A. Kivelson, and D. Orgad, "Concepts in high temperature superconductivity," in *The Physics of Superconductors. Vol. 2: Conventional and High- $T_c$  Superconductors*, K. H. Bennemann and J. B. Ketterson, Eds., p. 275, Springer, Berlin, Germany, 2004.
- [15] D. Manske, I. Eremin, and K. H. Bennemann, "Electronic theory for superconductivity in high- $T_c$  cuprates and  $\text{Sr}_2\text{RuO}_4$ ," in *The Physics of Superconductors. Vol. 2: Conventional and High- $T_c$  Superconductors*, K. H. Bennemann and J. B. Ketterson, Eds., p. 731, Springer, Berlin, Germany, 2004.
- [16] A. J. Leggett, "Superfluid  $^3\text{He}$  and the cuprate superconductors," in *The Physics of Superconductors. Vol. 2: Conventional and High- $T_c$  Superconductors*, K. H. Bennemann and J. B. Ketterson, Eds., p. 1087, Springer, Berlin, Germany, 2004.
- [17] M. L. Kulić, "Electron-phonon interaction and strong correlations in high-temperature superconductors: One can not avoid the unavoidable," in *Lectures on the Physics of Highly Correlated Electron Systems VIII: Eighth Training Course*, A. Avella and F. Mancini, Eds., p. 75, American Institute of Physics, Melville, NY, USA, 2004.
- [18] M. Eschrig, "The effect of collective spin-1 excitations on electronic spectra in high- $T_c$  superconductors," *Advances in Physics*, vol. 55, no. 1-2, pp. 47–183, 2006.
- [19] A. V. Balatsky, I. Vekhter, and J.-X. Zhu, "Impurity-induced states in conventional and unconventional superconductors," *Reviews of Modern Physics*, vol. 78, no. 2, pp. 373–433, 2006.
- [20] A.-M. S. Tremblay, B. Kyung, and D. Sénéchal, "Pseudogap and high-temperature superconductivity from weak to strong coupling. Towards quantitative theory," *Fizika Nizkikh Temperatur*, vol. 32, no. 4-5, pp. 561–595, 2006.
- [21] B. Edegger, V. N. Muthukumar, and C. Gros, "Gutzwiller-RVB theory of high-temperature superconductivity: results from renormalized mean-field theory and variational Monte Carlo calculations," *Advances in Physics*, vol. 56, no. 6, pp. 927–1033, 2007.
- [22] V. Barzykin and D. Pines, "Universal behaviour and the two-component character of magnetically underdoped cuprate superconductors," *Advances in Physics*, vol. 58, no. 1, pp. 1–65, 2009.
- [23] J. Hauck and K. Mika, "Classification of superconducting oxide structures," *Superconductor Science and Technology*, vol. 8, no. 5, pp. 374–381, 1995.
- [24] Z. Fisk and J. L. Sarrao, "The new generation high-temperature superconductors," *Annual Review of Materials Science*, vol. 27, no. 1, pp. 35–67, 1997.
- [25] J. Hauck and K. Mika, "Structure families of superconducting oxides and interstitial alloys," *Superconductor Science and Technology*, vol. 11, no. 7, pp. 614–630, 1998.
- [26] R. J. Cava, "Oxide superconductors," *Journal of the American Ceramic Society*, vol. 83, no. 1, pp. 5–28, 2000.
- [27] H. R. Ott, "High- $T_c$  superconductivity," in *The Physics of Superconductors. Vol. 1: Conventional and High- $T_c$  Superconductors*, K. H. Bennemann and J. B. Ketterson, Eds., p. 385, Springer, Berlin, Germany, 2003.
- [28] J. R. Gavaler, M. A. Janocko, and C. K. Jones, "Preparation and properties of high- $T_c$  Nb-Ge films," *Journal of Applied Physics*, vol. 45, no. 7, pp. 3009–3013, 1974.
- [29] L. R. Testardi, "Structural instability and superconductivity in A-15 compounds," *Reviews of Modern Physics*, vol. 47, no. 3, pp. 637–648, 1975.
- [30] K. Holczer and R. L. Whetten, "Superconducting and normal state properties of the  $\text{A}_3\text{C}_{60}$  compounds," *Carbon*, vol. 30, no. 8, pp. 1261–1276, 1992.
- [31] O. Gunnarsson, "Superconductivity in fullerenes," *Reviews of Modern Physics*, vol. 69, no. 2, pp. 575–606, 1997.
- [32] R. J. Cava, B. Batlogg, J. J. Krajewski, et al., "Superconductivity near 30 K without copper: the  $\text{Ba}_{0.6}\text{K}_{0.4}\text{BiO}_3$  perovskite," *Nature*, vol. 332, no. 6167, pp. 814–816, 1988.
- [33] L. F. Mattheiss, E. M. Gyorgy, and D. W. Johnson Jr., "Superconductivity above 20 K in the Ba-K-Bi-O system," *Physical Review B*, vol. 37, no. 7, pp. 3745–3746, 1988.

- [34] G.-M. Zhao, "Muon spin relaxation and magnetic measurements on  $\text{Ba}_{0.63}\text{K}_{0.37}\text{BiO}_3$ : evidence for polaronic strong-coupling phonon-mediated pairing," *Physical Review B*, vol. 76, no. 2, Article ID 020501, 4 pages, 2007.
- [35] S. Yamanaka, K. Hotehama, and H. Kawaji, "Superconductivity at 25.5 K in electron-doped layered hafnium nitride," *Nature*, vol. 392, no. 6676, pp. 580–582, 1998.
- [36] S. Yamanaka, "High- $T_c$  superconductivity in electron-doped layer structured nitrides," *Annual Review of Materials Science*, vol. 30, pp. 53–82, 2000.
- [37] J. Nagamatsu, N. Nakagawa, T. Muranaka, Y. Zenitani, and J. Akimitsu, "Superconductivity at 39 K in magnesium diboride," *Nature*, vol. 410, no. 6824, pp. 63–64, 2001.
- [38] J. Akimitsu and T. Muranaka, "Superconductivity in  $\text{MgB}_2$ ," *Physica C*, vol. 388–389, pp. 98–102, 2003.
- [39] V. A. Drozd, A. M. Gabovich, P. Gierłowski, M. Pękała, and H. Szymczak, "Transport properties of bulk and thin-film  $\text{MgB}_2$  superconductors: effects of preparation conditions," *Physica C*, vol. 402, no. 4, pp. 325–334, 2004.
- [40] X. X. Xi, "Two-band superconductor magnesium diboride," *Reports on Progress in Physics*, vol. 71, no. 11, Article ID 116501, 26 pages, 2008.
- [41] S. Reich, G. Leitus, R. Popovitz-Biro, A. Goldbourt, and S. Vega, "A possible 2D  $\text{H}_x\text{WO}_3$  superconductor with a  $T_c$  of 120 K," *Journal of Superconductivity and Novel Magnetism*, vol. 22, no. 4, pp. 343–346, 2009.
- [42] A. M. Gabovich, V. A. Drozd, M. Pękała, T. Ekino, and R. Ribeiro, "Competition between superconductivity and charge carrier localization in plumbates," in *Superconductivity Research Advances*, J. E. Nolan, Ed., p. 149, Nova Science, New York, NY, USA, 2007.
- [43] H. Takahashi, K. Igawa, K. Arii, Y. Kamihara, M. Hirano, and H. Hosono, "Superconductivity at 43 K in an iron-based layered compound  $\text{LaO}_{1-x}\text{F}_x\text{FeAs}$ ," *Nature*, vol. 453, no. 7193, pp. 376–378, 2008.
- [44] H. Hosono, "Layered iron pnictide superconductors: discovery and current status," *Journal of the Physical Society of Japan*, vol. 77, pp. 1–8, 2008.
- [45] M. Rotter, M. Tegel, and D. Johrendt, "Superconductivity at 38 K in the iron arsenide  $(\text{Ba}_{1-x}\text{K}_x)\text{Fe}_2\text{As}_2$ ," *Physical Review Letters*, vol. 101, no. 10, Article ID 107006, 4 pages, 2008.
- [46] A. L. Ivanovskii, "New high-temperature superconductors based on rare earth and transition metal oxyarsenides and related phases: synthesis, properties and simulation," *Uspekhi Fizicheskikh Nauk*, vol. 178, p. 1273, 2008.
- [47] T. C. Ozawa and S. M. Kauzlarich, "Chemistry of layered d-metal pnictide oxides and their potential as candidates for new superconductors," *Science and Technology of Advanced Materials*, vol. 9, no. 3, Article ID 033003, 11 pages, 2008.
- [48] H. Hosono, "Two classes of superconductors discovered in our material research: iron-based high temperature superconductor and electride superconductor," *Physica C*, vol. 469, no. 9–12, pp. 314–325, 2009.
- [49] C. Day, "Iron-based superconductors," *Physics Today*, vol. 62, no. 8, pp. 36–40, 2009.
- [50] V. L. Ginzburg, "About ferromagnetic superconductors," *Zhurnal Eksperimental'noi i Teoreticheskoi Fiziki*, vol. 31, p. 202, 1956.
- [51] M. B. Maple and Ø. Fischer, Eds., *Superconductivity in Ternary Compounds II, Superconductivity and Magnetism*, vol. 34 of *Topics in Current Physics*, Springer, Berlin, Germany, 1982.
- [52] L. N. Bulaevskii, A. I. Buzdin, M. L. Kulić, and S. V. Panjukov, "Coexistence of superconductivity and magnetism theoretical predictions and experimental results," *Advances in Physics*, vol. 34, no. 2, pp. 175–261, 1985.
- [53] L. N. Bulaevskii, "Magnetic superconductors," in *Superconductivity, Superdiamagnetism, Superfluidity*, V. L. Ginzburg, Ed., p. 69, Mir, Moscow, Russia, 1987.
- [54] Yu. A. Izyumov, M. I. Katsnelson, and Yu. N. Skryabin, *Itinerant Electron Magnetism*, Fiziko-Matematicheskaya Literatura, Moscow, Russia, 1994.
- [55] A. I. Buzdin, "Proximity effects in superconductor-ferromagnet heterostructures," *Reviews of Modern Physics*, vol. 77, no. 3, pp. 935–976, 2005.
- [56] A. M. Gabovich and D. P. Moiseev, "Metalloxyde superconductor  $\text{BaPb}_{1-x}\text{Bi}_x\text{O}_3$ : unusual properties and new applications," *Uspekhi Fizicheskikh Nauk*, vol. 150, p. 599, 1986.
- [57] R. Collongues, *La Non-Stoichiometrie*, Masson, Paris, France, 1971.
- [58] A. M. Stoneham and L. W. Smith, "Defect phenomena in superconducting oxides and analogous ceramic oxides," *Journal of Physics: Condensed Matter*, vol. 3, no. 3, pp. 225–278, 1991.
- [59] O. Matsumoto, A. Utsuki, A. Tsukada, H. Yamamoto, T. Manabe, and M. Naito, "Synthesis and properties of superconducting  $T\text{-R}_2\text{CuO}_4$  ( $R = \text{Pr, Nd, Sm, Eu, Gd}$ )," *Physical Review B*, vol. 79, no. 10, Article ID 100508, 4 pages, 2009.
- [60] Z. Ren, Q. Tao, S. Jiang, et al., "Superconductivity induced by phosphorus doping and its coexistence with ferromagnetism in  $\text{EuFe}_2(\text{As}_{0.7}\text{P}_{0.3})_2$ ," *Physical Review Letters*, vol. 102, no. 13, Article ID 137002, 4 pages, 2009.
- [61] R. J. Cava, "Contemporary superconducting materials," *Chemical Communications*, no. 43, pp. 5373–5377, 2005.
- [62] W. E. Pickett, "The next breakthrough in phonon-mediated superconductivity," *Physica C*, vol. 468, no. 2, pp. 126–135, 2008.
- [63] J. C. Phillips, "Hard-wired dopant networks and the prediction of high transition temperatures in ceramic superconductors," *Advances in Condensed Matter Physics*, vol. 2010, Article ID 250891, 13 pages, 2010.
- [64] J. C. Phillips, "Zigzag filamentary theory of longitudinal optical phonons in high-temperature superconductors," *Philosophical Magazine B*, vol. 81, no. 1, pp. 35–53, 2001.
- [65] J. C. Phillips and J. Jung, "Nanodomain structure and function of high-temperature superconductors," *Philosophical Magazine B*, vol. 81, no. 8, pp. 745–756, 2001.
- [66] J. C. Phillips, "Percolative model of nanoscale phase separation in high-temperature superconductors," *Philosophical Magazine B*, vol. 82, no. 7, pp. 783–790, 2002.
- [67] J. C. Phillips, "Self-organized networks and lattice effects in high-temperature superconductors," *Physical Review B*, vol. 75, no. 21, Article ID 214503, 23 pages, 2007.
- [68] G. Litak, A. M. Martin, B. Györfy, J. F. Annett, and K. I. Wysokiński, "Van Hove singularity and  $d$ -wave pairing in disordered superconductors," *Physica C*, vol. 309, no. 3–4, pp. 257–262, 1998.
- [69] G. Litak and B. Györfy, "Random negative-U hubbard model," *Physical Review B*, vol. 62, no. 10, pp. 6629–6637, 2000.
- [70] G. Litak, B. Györfy, and K. I. Wysokiński, "Charge and order parameter fluctuations in disordered superconductors," *Physica C*, vol. 308, no. 1–2, pp. 132–146, 1998.
- [71] G. Litak, "Charge and phase fluctuations in attractive Hubbard model," *Physica C*, vol. 387, no. 1–2, pp. 86–88, 2003.

- [72] G. Litak, "Charge order versus superconductivity in inhomogeneous systems," *Journal of Superconductivity and Novel Magnetism*, vol. 22, no. 3, pp. 265–267, 2009.
- [73] A. M. Gabovich and A. I. Voitenko, "Temperature-dependent inelastic electron scattering and superconducting state properties," *Physics Letters A*, vol. 190, no. 2, pp. 191–195, 1994.
- [74] A. M. Gabovich and A. I. Voitenko, "Influence of inelastic quasiparticle scattering on thermodynamic and transport properties of high- $T_c$  oxides," *Physica C*, vol. 258, no. 3–4, pp. 236–252, 1996.
- [75] A. M. Gabovich, "Power-law low-temperature asymptotics for spatially nonhomogeneous  $s$ -wave superconductors," *Fizika Nizkikh Temperatur*, vol. 25, no. 7, pp. 677–684, 1999.
- [76] A. M. Gabovich and A. I. Voitenko, "Influence of order-parameter nonhomogeneities on low-temperature properties of superconductors," *Physical Review B*, vol. 60, no. 10, pp. 7465–7472, 1999.
- [77] A. M. Gabovich, A. I. Voitenko, M. S. Li, and H. Szymczak, "Heat capacity of mesoscopically disordered superconductors: implications for  $\text{MgB}_2$ ," *Fizika Nizkikh Temperatur*, vol. 28, no. 11, pp. 1126–1137, 2002.
- [78] A. M. Gabovich, M. S. Li, M. Pękała, H. Szymczak, and A. I. Voitenko, "Heat capacity of mesoscopically disordered superconductors with emphasis on  $\text{MgB}_2$ ," *Journal of Physics: Condensed Matter*, vol. 14, no. 41, pp. 9621–9629, 2002.
- [79] A. M. Gabovich, M. S. Li, M. Pękała, H. Szymczak, and A. I. Voitenko, "Heat capacity of mesoscopically inhomogeneous superconductors: theory and applications to  $\text{MgB}_2$ ," *Physica C*, vol. 405, no. 3–4, pp. 187–211, 2004.
- [80] T. Ekino, A. M. Gabovich, M. S. Li, et al., "Spatially heterogeneous character of superconductivity in  $\text{MgB}_2$  as revealed by local probe and bulk measurements," *Physica C*, vol. 426–431, no. 1, pp. 230–233, 2005.
- [81] A. M. Gabovich and A. I. Voitenko, "Charge-density-wave origin of the dip-hump structure in tunnel spectra of the BSCCO superconductor," *Physical Review B*, vol. 75, no. 6, Article ID 064516, 13 pages, 2007.
- [82] T. Ekino, A. M. Gabovich, M. S. Li, M. Pękała, H. Szymczak, and A. I. Voitenko, "Analysis of the pseudogap-related structure in tunneling spectra of superconducting  $\text{Bi}_2\text{Sr}_2\text{CaCu}_2\text{O}_{8+\delta}$  revealed by the break-junction technique," *Physical Review B*, vol. 76, no. 18, Article ID 180503, 4 pages, 2007.
- [83] T. Ekino, A. M. Gabovich, M. S. Li, M. Pękała, H. Szymczak, and A. I. Voitenko, "Temperature-dependent pseudogap-like features in tunnel spectra of high- $T_c$  cuprates as a manifestation of charge-density waves," *Journal of Physics: Condensed Matter*, vol. 20, no. 42, Article ID 425218, 15 pages, 2008.
- [84] J. C. Phillips, "Is there a lowest upper bound for superconductive transition temperatures?" *Journal of Physics: Conference Series*, vol. 108, no. 1, Article ID 012033, 6 pages, 2008.
- [85] B. T. Matthias, "Anticorrelations in superconductivity," *Physica*, vol. 55, pp. 69–72, 1971.
- [86] F. E. Wang and M. A. Mitchell, "A new correlation: superconducting critical temperature vs number of naturally occurring isotopes among superconducting elements," *Solid State Communications*, vol. 15, no. 5, pp. 867–869, 1974.
- [87] D. M. Gualtieri, "The correlation between the superconducting critical temperature and the number of stable isotopes among superconducting elements," *Solid State Communications*, vol. 16, no. 7, pp. 917–918, 1975.
- [88] I. O. Kulik, "Superconductivity and macroscopic stability criteria for electron-phonon systems," *Zhurnal Eksperimental'noj i Teoreticheskoi Fiziki*, vol. 66, p. 2224, 1974.
- [89] I. O. Kulik, "Spin fluctuations and superconductivity," *Fizika Nizkikh Temperatur*, vol. 2, p. 486, 1976.
- [90] A. M. Gabovich, "On the criterion of superconductivity of metals," *Ukrainskii Fizychnyi Zhurnal*, vol. 22, p. 2072, 1977.
- [91] A. M. Gabovich and D. P. Moiseev, "Superconductivity of metals with the allowance for ion core repulsion," *Fizika Nizkikh Temperatur*, vol. 4, p. 1115, 1978.
- [92] A. M. Gabovich and D. P. Moiseev, "Isotope effect in jellium and Brout models," *Fizika Tverdogo Tela*, vol. 23, p. 1511, 1981.
- [93] I. M. Chapnik, "On the possible relation between the absence of superconductivity in Au and Pd-Ag alloys and the negative sign of the Hall coefficient," *Journal of Physics F*, vol. 13, no. 5, pp. 975–978, 1983.
- [94] I. M. Chapnik, "Regularities in the occurrence of superconductivity," *Journal of Physics F*, vol. 14, no. 8, pp. 1919–1921, 1984.
- [95] J. E. Hirsch, "Correlations between normal-state properties and superconductivity," *Physical Review B*, vol. 55, no. 14, pp. 9007–9024, 1997.
- [96] C. Buzea and K. Robbie, "Assembling the puzzle of superconducting elements: a review," *Superconductor Science and Technology*, vol. 18, no. 1, pp. R1–R8, 2005.
- [97] F. Huber, H. P. Roeser, and M. von Schoenermark, "A correlation between  $T_c$  of Fe-based HT superconductors and the crystal super lattice constants of the doping element positions," *Journal of the Physical Society of Japan*, vol. 77, pp. 142–144, 2008.
- [98] B. J. Taylor and M. B. Maple, "Formula for the critical temperature of superconductors based on the electronic density of states and the effective mass," *Physical Review Letters*, vol. 102, no. 13, Article ID 137003, 4 pages, 2009.
- [99] A. M. Gabovich, "About superconductivity of polar semiconductors," *Fizika Tverdogo Tela*, vol. 22, no. 11, pp. 3231–3235, 1980.
- [100] R. Baquero, "What determines the magnitude of  $T_c$  in HTSC?" in *Frontiers in Contemporary Physics—EAV08*, L. M. M. Zetina, G. T. Vega, M. G. Rocla, L. F. R. Oclioa, and R. L. Fernández, Eds., p. 218, American Institute of Physics, Melville, NY, USA, 2008.
- [101] X. Blase, E. Bustarret, C. Chapelier, T. Klein, and C. Marceat, "Superconducting group-IV semiconductors," *Nature Materials*, vol. 8, no. 5, pp. 375–382, 2009.
- [102] B. E. C. Koltenbah and R. Joynt, "Material-specific gap function in the  $t$ - $J$  model of high-temperature superconductors," *Reports on Progress in Physics*, vol. 60, no. 1, pp. 23–56, 1997.
- [103] M. Ogata and H. Fukuyama, "The  $t$ - $J$  model for the oxide high- $T_c$  superconductors," *Reports on Progress in Physics*, vol. 71, no. 3, Article ID 036501, 45 pages, 2008.
- [104] W. Fan, "Predictions of highest transition-temperature for electron-phonon superconductors," *Physica C*, vol. 469, no. 4, pp. 177–181, 2009.
- [105] G. M. Eliashberg, "Interaction of electrons with lattice vibrations in a superconductor," *Zhurnal Eksperimental'noi i Teoreticheskoi Fiziki*, vol. 38, p. 966, 1960.
- [106] G. M. Eliashberg, "Temperature Green's functions of electrons in a superconductor," *Zhurnal Eksperimental'noi i Teoreticheskoi Fiziki*, vol. 39, p. 1437, 1960.
- [107] B. Brandow, "Characteristic features of the exotic superconductors," *Physics Reports*, vol. 296, no. 1, pp. 1–63, 1998.

- [108] B. Brandow, "Explanation of the exotic superconductors by a valence-fluctuation pairing mechanism," *Philosophical Magazine B*, vol. 80, no. 6, pp. 1229–1297, 2000.
- [109] G.-M. Zhao, "Experimental constraints on the physics of cuprates," *Philosophical Magazine B*, vol. 81, no. 10, pp. 1335–1388, 2001.
- [110] G.-M. Zhao, "Pairing interactions and pairing mechanism in high-temperature copper oxide superconductors," *Physical Review B*, vol. 71, no. 10, Article ID 104517, 9 pages, 2005.
- [111] A. S. Alexandrov, "High temperature superconductivity due to a long-range electron-phonon interaction, application to isotope effects, thermomagnetic transport and nanoscale heterogeneity in cuprates," *Journal of Superconductivity*, vol. 18, no. 5–6, pp. 603–612, 2005.
- [112] W. E. Pickett, "Design for a room-temperature superconductor," *Journal of Superconductivity and Novel Magnetism*, vol. 19, no. 3–5, pp. 291–297, 2006.
- [113] A. M. Kadin, "Coherent lattice vibrations in superconductors," *Physica C*, vol. 468, no. 4, pp. 255–259, 2008.
- [114] J. Tahir-Kheli and W. A. Goddard III, "The Chiral Plaquette Polaron Paradigm (CPPP) for high temperature cuprate superconductors," *Chemical Physics Letters*, vol. 472, no. 4–6, pp. 153–165, 2009.
- [115] V. Z. Kresin and S. A. Wolf, "Colloquium: electron-lattice interaction and its impact on high  $T_c$  superconductivity," *Reviews of Modern Physics*, vol. 81, no. 2, pp. 481–501, 2009.
- [116] C. Panagopoulos and T. Xiang, "Relationship between the superconducting energy gap and the critical temperature in high- $T_c$  superconductors," *Physical Review Letters*, vol. 81, no. 11, pp. 2336–2339, 1998.
- [117] R. A. Klemm and K. Scharnberg, "Theory of bicrystal  $c$ -axis twist Josephson junctions," *International Journal of Modern Physics B*, vol. 15, no. 24–25, pp. 3164–3189, 2001.
- [118] G.-M. Zhao, "Identification of the bulk pairing symmetry in high-temperature superconductors: evidence for an extended  $s$  wave with eight line nodes," *Physical Review B*, vol. 64, no. 2, Article ID 024503, 10 pages, 2001.
- [119] B. H. Brandow, "Arguments and evidence for a node-containing anisotropic  $s$ -wave gap form in the cuprate superconductors," *Physical Review B*, vol. 65, no. 5, Article ID 054503, 5 pages, 2002.
- [120] B. H. Brandow, "Strongly anisotropic  $s$ -wave gaps in exotic superconductors," *Philosophical Magazine*, vol. 83, no. 21, pp. 2487–2519, 2003.
- [121] G.-M. Zhao, "The magnetic resonance in high-temperature superconductors: evidence for an extended  $s$ -wave pairing symmetry," *Philosophical Magazine B*, vol. 84, no. 36, pp. 3869–3882, 2004.
- [122] R. A. Klemm, "The phase-sensitive  $c$ -axis twist experiments on  $\text{Bi}_2\text{Sr}_2\text{CaCu}_2\text{O}_{8+\delta}$  and their implications," *Philosophical Magazine*, vol. 85, no. 8, pp. 801–853, 2005.
- [123] T. H. Geballe, "The never-ending search for high-temperature superconductivity," *Journal of Superconductivity and Novel Magnetism*, vol. 19, no. 3–5, pp. 261–276, 2006.
- [124] R. Baquero, "Superconductivity today: a brief panorama," in *Advanced Summer School in Physics 2005*, O. Rosas-Ortiz, M. Carbajal, and O. Miranda, Eds., p. 301, American Institute of Physics, Melville, NY, USA, 2006.
- [125] R. Khasanov, S. Strässle, D. Di Castro, et al., "Multiple gap symmetries for the order parameter of cuprate superconductors from penetration depth measurements," *Physical Review Letters*, vol. 99, no. 23, Article ID 237601, 4 pages, 2007.
- [126] T. Das, R. S. Markiewicz, and A. Bansil, "Nodeless  $d$ -wave superconducting pairing due to residual antiferromagnetism in underdoped  $\text{Pr}_{2-x}\text{Ce}_x\text{CuO}_{4-\delta}$ ," *Physical Review Letters*, vol. 98, no. 19, Article ID 197004, 4 pages, 2007.
- [127] G.-M. Zhao, "Precise determination of the superconducting gap along the diagonal direction of  $\text{Bi}_2\text{Sr}_2\text{CaCu}_2\text{O}_{8+y}$ : evidence for an extended  $s$ -wave gap symmetry," *Physical Review B*, vol. 75, no. 14, Article ID 140510, 4 pages, 2007.
- [128] R. Khasanov, A. Shengelaya, A. Maisuradze, et al., "Nodeless superconductivity in the infinite-layer electron-doped cuprate superconductor  $\text{Sr}_{0.9}\text{La}_{0.1}\text{CuO}_2$ ," *Physical Review B*, vol. 77, no. 18, Article ID 184512, 6 pages, 2008.
- [129] R. Prozorov, "Superfluid density in a superconductor with an extended  $d$ -wave gap," *Superconductor Science and Technology*, vol. 21, no. 8, Article ID 082003, 3 pages, 2008.
- [130] M. Bakr, A. P. Schnyder, L. Klam, et al., "Electronic and phononic Raman scattering in detwinned  $\text{YBa}_2\text{Cu}_3\text{O}_{6.95}$  and  $\text{Y}_{0.85}\text{Ca}_{0.15}\text{Ba}_2\text{Cu}_3\text{O}_{6.95}$ :  $s$ -wave admixture to the  $d_{x^2-y^2}$ -wave order parameter," *Physical Review B*, vol. 80, no. 6, Article ID 064505, 11 pages, 2009.
- [131] C. C. Tsuei and J. R. Kirtley, "Pairing symmetry in cuprate superconductors," *Reviews of Modern Physics*, vol. 72, no. 4, pp. 969–1016, 2000.
- [132] H. Hilgenkamp and J. Mannhart, "Grain boundaries in high- $T_c$  superconductors," *Reviews of Modern Physics*, vol. 74, no. 2, pp. 485–549, 2002.
- [133] C. C. Tsuei and J. R. Kirtley, "Pairing symmetry in cuprate superconductors: phase-sensitive tests," in *The Physics of Superconductors. Vol. 1: Conventional and High- $T_c$  Superconductors*, K. H. Bennemann and J. B. Ketterson, Eds., p. 647, Springer, Berlin, Germany, 2003.
- [134] R. Micnas, J. Ranninger, and S. Robaszkiewicz, "Superconductivity in narrow-band systems with local nonretarded attractive interactions," *Reviews of Modern Physics*, vol. 62, no. 1, pp. 113–171, 1990.
- [135] A. S. Alexandrov, "Polaronic and bipolaronic high- $T_c$  superconductivity," in *Models and Phenomenology for Conventional and High-Temperature Superconductivity*, G. Iadonisi, J. R. Schrieffer, and M. L. Chiofalo, Eds., p. 309, IOS Press, Amsterdam, The Netherlands, 1998.
- [136] T. Skośkiewicz, A. W. Szafranski, W. Bujnowski, and B. Baranowski, "Isotope effect in the superconducting palladium-hydrogen-deuterium system," *Journal of Physics C*, vol. 7, no. 15, pp. 2670–2676, 1974.
- [137] B. Stritzker, "Ion implantation and superconductivity," *Journal of Nuclear Materials*, vol. 72, no. 1–2, pp. 256–262, 1978.
- [138] T. Matsubara and A. Kotani, Eds., *Superconductivity in Magnetic and Exotic Materials*, Springer, Berlin, Germany, 1984.
- [139] A. Taraphder, R. Pandit, H. R. Krishnamurthy, and T. V. Ramakrishnan, "The exotic barium bismuthates," *International Journal of Modern Physics B*, vol. 10, no. 8, pp. 863–955, 1996.
- [140] A. M. Gabovich, "Possibility of cold fusion in palladium deuterides: screening effects and connection to superconducting properties," *Philosophical Magazine B*, vol. 76, no. 1, pp. 107–118, 1997.
- [141] N. D. Mathur, F. M. Grosche, S. R. Julian, et al., "Magnetically mediated superconductivity in heavy fermion compounds," *Nature*, vol. 394, no. 6688, pp. 39–43, 1998.
- [142] E. Bauer, G. Hilscher, H. Michor, et al., "Heavy fermion superconductivity and magnetic order in noncentrosymmetric  $\text{CePt}_3\text{Si}$ ," *Physical Review Letters*, vol. 92, no. 2, Article ID 027003, 4 pages, 2004.

- [143] S. G. Ovchinnikov, "Exotic superconductivity and magnetism in ruthenates," *Uspekhi Fizicheskikh Nauk*, vol. 173, no. 1, pp. 27–51, 2003.
- [144] A. P. Mackenzie and Y. Maeno, "The superconductivity of  $\text{Sr}_2\text{RuO}_4$  and the physics of spin-triplet pairing," *Reviews of Modern Physics*, vol. 75, no. 2, pp. 657–712, 2003.
- [145] P. S. Riseborough, G. M. Schmiedeschoff, and J. L. Smith, "Heavy fermion superconductivity," in *The Physics of Superconductors. Vol. 2: Conventional and High- $T_c$  Superconductors*, K. H. Bennemann and J. B. Ketterson, Eds., p. 889, Springer, Berlin, Germany, 2004.
- [146] P. Thalmeier, G. Zwignagl, O. Stockert, G. Sparn, and F. Steglich, "Superconductivity in heavy Fermion compounds," in *Frontiers in Superconducting Materials*, A. V. Narlikar, Ed., p. 109, Springer, Berlin, Germany, 2005.
- [147] D. A. Bonn, "Are high-temperature superconductors exotic?" *Nature Physics*, vol. 2, no. 3, pp. 159–166, 2006.
- [148] S. Fujimoto, "Electron correlation and pairing states in superconductors without inversion symmetry," *Journal of the Physical Society of Japan*, vol. 76, no. 5, Article ID 051008, 14 pages, 2007.
- [149] Y. Kitaoka, H. Mukuda, M. Yashima, and A. Harada, "Unconventional pairing states in heavy-fermion superconductors studied by the NQR/NMR experiments," *Journal of the Physical Society of Japan*, vol. 76, no. 5, Article ID 051001, 15 pages, 2007.
- [150] T. Sakakibara, A. Yamada, J. Custers, et al., "Nodal structures of heavy fermion superconductors probed by the specific-heat measurements in magnetic fields," *Journal of the Physical Society of Japan*, vol. 76, no. 5, Article ID 051004, 11 pages, 2007.
- [151] J. L. Sarrao and J. D. Thompson, "Superconductivity in cerium- and plutonium-based '115' materials," *Journal of the Physical Society of Japan*, vol. 76, no. 5, Article ID 051013, 9 pages, 2007.
- [152] Y. Haga, H. Sakai, and S. Kambe, "Recent advances in the 5f-relevant electronic states and unconventional superconductivity of actinide compounds," *Journal of the Physical Society of Japan*, vol. 76, no. 5, Article ID 051012, 21 pages, 2007.
- [153] Y. Kasahara, T. Iwasawa, H. Shishido, et al., "Gap structure and exotic superconducting state of  $\text{URu}_2\text{Si}_2$ ," *Journal of Physics: Conference Series*, vol. 150, Article ID 052098, 4 pages, 2009.
- [154] R. D. Parks, Ed., *Superconductivity*, vol. 1, Marcel Dekker, New York, NY, USA, 1969.
- [155] R. D. Parks, Ed., *Superconductivity*, vol. 2, Marcel Dekker, New York, NY, USA, 1969.
- [156] K. H. Bennemann and J. B. Ketterson, Eds., *The Physics of Superconductors. Vol. 1: Conventional and High- $T_c$  Superconductors*, Springer, Berlin, Germany, 2003.
- [157] K. H. Bennemann and J. B. Ketterson, Eds., *The Physics of Superconductors. Vol. 2: Conventional and High- $T_c$  Superconductors*, Springer, Berlin, Germany, 2004.
- [158] A. M. Gabovich and A. I. Voitenko, "Superconductors with charge- and spin-density waves: theory and experiment," *Fizika Nizkikh Temperatur*, vol. 26, no. 5, pp. 419–452, 2000.
- [159] A. M. Gabovich, A. I. Voitenko, J. F. Annett, and M. Ausloos, "Charge- and spin-density-wave superconductors," *Superconductor Science and Technology*, vol. 14, no. 4, pp. R1–R27, 2001.
- [160] A. M. Gabovich, A. I. Voitenko, and M. Ausloos, "Charge- and spin-density waves in existing superconductors: competition between Cooper pairing and Peierls or excitonic instabilities," *Physics Reports*, vol. 367, no. 6, pp. 583–709, 2002.
- [161] I. I. Mazin and J. Schmalian, "Pairing symmetry and pairing state in ferropnictides: theoretical overview," *Physica C*, vol. 469, no. 9–12, pp. 614–627, 2009.
- [162] A. W. Sleight, J. L. Gillson, and P. E. Bierstedt, "High-temperature superconductivity in the  $\text{BaPb}_{1-x}\text{Bi}_x\text{O}_3$  systems," *Solid State Communications*, vol. 17, no. 1, pp. 27–28, 1975.
- [163] S. Tajima, S. Uchida, A. Masaki, et al., "Electronic states of  $\text{BaPb}_{1-x}\text{Bi}_x\text{O}_3$  in the semiconducting phase investigated by optical measurements," *Physical Review B*, vol. 35, no. 2, pp. 696–703, 1987.
- [164] S. Tajima, H. Ishii, I. Rittaporn, et al., "Vacuum-ultraviolet spectra and band structure of  $\text{BaPb}_{1-x}\text{Bi}_x\text{O}_3$ ," *Physical Review B*, vol. 38, no. 2, pp. 1143–1147, 1988.
- [165] D. T. Marx, P. G. Radaelli, J. D. Jorgensen, et al., "Metastable behavior of the superconducting phase in the  $\text{BaBi}_{1-x}\text{Pb}_x\text{O}_3$  system," *Physical Review B*, vol. 46, no. 2, pp. 1144–1156, 1992.
- [166] M. Yasukawa and N. Murayama, "A phase transition with an abrupt electrical resistivity change around 800 K in  $\text{BaBi}_{0.5}\text{Pb}_{0.5}\text{O}_3$ ," *Physica C*, vol. 297, no. 3-4, pp. 326–332, 1998.
- [167] A. Yamamoto, T. Furumochi, and S. Tajima, "Metal-insulator transition and superconductivity in Sr- and La-substituted  $\text{BaPb}_{1-x}\text{Bi}_x\text{O}_3$ ," *Physica C*, vol. 328, no. 1, pp. 118–124, 1999.
- [168] V. J. Emery and S. A. Kivelson, "Superconductivity in bad metals," *Physical Review Letters*, vol. 74, no. 16, pp. 3253–3256, 1995.
- [169] N. F. Mott and E. A. Davis, *Electron Processes in Non-Crystalline Materials*, Clarendon Press, Oxford, UK, 1979.
- [170] J. F. Schooley, W. R. Hosler, E. Ambler, J. H. Becker, M. L. Cohen, and C. S. Koonce, "Dependence of the superconducting transition temperature on carrier concentration in semiconducting  $\text{SrTiO}_3$ ," *Physical Review Letters*, vol. 14, no. 9, pp. 305–307, 1965.
- [171] K. Shibuya, T. Ohnishi, T. Sato, and M. Lippmaa, "Metal-insulator transition in  $\text{SrTiO}_3$  induced by field effect," *Journal of Applied Physics*, vol. 102, no. 8, Article ID 083713, 2007.
- [172] C. H. Ahn, A. Bhattacharya, M. Di Ventura, et al., "Electrostatic modification of novel materials," *Reviews of Modern Physics*, vol. 78, no. 4, pp. 1185–1212, 2006.
- [173] A. Ohtomo and H. Y. Hwang, "A high-mobility electron gas at the  $\text{LaAlO}_3/\text{SrTiO}_3$  heterointerface," *Nature*, vol. 427, no. 6973, pp. 423–426, 2004.
- [174] N. Reyren, S. Thiel, A. D. Caviglia, et al., "Superconducting interfaces between insulating oxides," *Science*, vol. 317, no. 5842, pp. 1196–1199, 2007.
- [175] S. Gariglio, N. Reyren, A. D. Caviglia, and J.-M. Triscone, "Superconductivity at the  $\text{LaAlO}_3/\text{SrTiO}_3$  interface," *Journal of Physics: Condensed Matter*, vol. 21, no. 16, Article ID 164213, 2009.
- [176] L. J. de Jongh, "A comparative study of (BI)polaronic (super)conductivity in high- and low- $T_c$  superconducting oxides," *Physica C*, vol. 152, no. 2, pp. 171–216, 1988.
- [177] T. Egami and S. J. L. Billinge, "Lattice effects in high temperature superconductors," *Progress in Materials Science*, vol. 38, no. 1, pp. 359–424, 1994.
- [178] K. S. Aleksandrov and B. V. Beznosikov, "Hierarchy of perovskite-like crystals: a review," *Fizika Tverdogo Tela*, vol. 39, p. 785, 1997.
- [179] K. S. Aleksandrov and J. Bartolomé, "Structural distortions in families of perovskite-like crystals," *Phase Transitions*, vol. 74, no. 3, pp. 255–335, 2001.

- [180] M. Karppinen and H. Yamauchi, "Control of the charge inhomogeneity and high- $T_c$  superconducting properties in homologous series of multi-layered copper oxides," *Materials Science and Engineering R*, vol. 26, no. 3, pp. 51–96, 1999.
- [181] T. Yamauchi, M. Isobe, and Y. Ueda, "Charge order and superconductivity in vanadium oxides," *Solid State Sciences*, vol. 7, no. 7, pp. 874–881, 2005.
- [182] A. S. Barker Jr. and M. Tinkham, "Far-infrared ferroelectric vibration mode in  $\text{SrTiO}_3$ ," *Physical Review*, vol. 125, no. 5, pp. 1527–1530, 1962.
- [183] M. E. Lines and A. M. Glass, *Principles and Application of Ferroelectrics and Related Materials*, Clarendon Press, Oxford, UK, 1977.
- [184] C. Z. Bi, J. Y. Ma, J. Yan, et al., "Electron-phonon coupling in Nb-doped  $\text{SrTiO}_3$  single crystal," *Journal of Physics: Condensed Matter*, vol. 18, no. 8, pp. 2553–2561, 2006.
- [185] D. M. Eagles, "Superconductivity at very low carrier concentrations and indications of a charged bose gas in  $\text{SrTi}_{0.97}\text{Zr}_{0.03}\text{O}_3$ ," *Solid State Communications*, vol. 60, no. 6, pp. 521–524, 1986.
- [186] M. Jourdan, N. Blümer, and H. Adrian, "Superconductivity of  $\text{SrTiO}_{3-\delta}$ ," *European Physical Journal B*, vol. 33, no. 1, pp. 25–30, 2003.
- [187] M. Jourdan and H. Adrian, "Possibility of unconventional superconductivity of  $\text{SrTiO}_{3-\delta}$ ," *Physica C*, vol. 388–389, pp. 509–510, 2003.
- [188] V. L. Vinetskii, "Bipolar states of current carriers in ionic crystals," *Zhurnal Eksperimental'noi i Teoreticheskoi Fiziki*, vol. 40, p. 1459, 1961.
- [189] J. Bardeen, L. N. Cooper, and J. R. Schrieffer, "Theory of superconductivity," *Physical Review*, vol. 108, no. 5, pp. 1175–1204, 1957.
- [190] M. R. Schafroth, S. T. Butler, and J. M. Blatt, "Quasichemical equilibrium approach to superconductivity," *Helvetica Physica Acta*, vol. 30, p. 93, 1957.
- [191] D. M. Eagles, "Possible pairing without superconductivity at low carrier concentrations in bulk and thin-film superconducting semiconductors," *Physical Review*, vol. 186, no. 2, pp. 456–463, 1969.
- [192] A. S. Alexandrov and J. Ranninger, "Theory of bipolarons and bipolaronic bands," *Physical Review B*, vol. 23, no. 4, pp. 1796–1801, 1981.
- [193] A. S. Alexandrov and J. Ranninger, "Bipolaronic superconductivity," *Physical Review B*, vol. 24, no. 3, pp. 1164–1169, 1981.
- [194] A. S. Alexandrov, J. Ranninger, and S. Robaszkiewicz, "Bipolaronic superconductivity: thermodynamics, magnetic properties, and possibility of existence in real substances," *Physical Review B*, vol. 33, no. 7, pp. 4526–4542, 1986.
- [195] D. Emin and M. S. Hillery, "Formation of a large singlet bipolaron: application to high-temperature bipolaronic superconductivity," *Physical Review B*, vol. 39, no. 10, pp. 6575–6593, 1989.
- [196] R. Friedberg, T. D. Lee, and H. C. Ren, "A correction to Schafroth's superconductivity solution of an ideal charged boson system," *Annals of Physics*, vol. 208, no. 1, pp. 149–215, 1991.
- [197] A. S. Alexandrov and N. F. Mott, "Bipolarons," *Reports on Progress in Physics*, vol. 57, no. 12, pp. 1197–1288, 1994.
- [198] R. Friedberg and T. D. Lee, "Comments on the superconductivity solution of an ideal charged boson system," *Journal of Superconductivity and Novel Magnetism*, vol. 19, no. 3–5, pp. 277–282, 2006.
- [199] J. T. Devreese and A. S. Alexandrov, "Fröhlich polaron and bipolaron: recent developments," *Reports on Progress in Physics*, vol. 72, no. 6, Article ID 066501, 2009.
- [200] T. M. Rice and L. Sneddon, "Real-space and  $k$ -space electron pairing in  $\text{BaPb}_{1-x}\text{Bi}_x\text{O}_3$ ," *Physical Review Letters*, vol. 47, no. 9, pp. 689–692, 1981.
- [201] I. B. Bischofs, V. N. Kostur, and P. B. Allen, "Polaron and bipolaron defects in a charge density wave: a model for lightly doped  $\text{BaBiO}_3$ ," *Physical Review B*, vol. 65, no. 11, Article ID 115112, 7 pages, 2002.
- [202] I. B. Bischofs, P. B. Allen, V. N. Kostur, and R. Bhargava, "Topological doping of a three-dimensional Peierls system: predicted structure of doped  $\text{BaBiO}_3$ ," *Physical Review B*, vol. 66, no. 17, Article ID 174108, 5 pages, 2002.
- [203] M. Merz, N. Nücker, S. Schuppler, et al., "X-ray absorption of  $\text{Ba}_{1-x}\text{K}_x\text{BiO}_3$  and  $\text{BaPb}_{1-y}\text{Bi}_y\text{O}_3$ : competition between bipolaronic and charge-density wave states," *Europhysics Letters*, vol. 72, no. 2, pp. 275–281, 2005.
- [204] D. G. Hinks, B. Dabrowski, J. D. Jorgensen, et al., "Synthesis, structure and superconductivity in the  $\text{Ba}_{1-x}\text{K}_x\text{BiO}_{3-y}$  system," *Nature*, vol. 333, no. 6176, pp. 836–838, 1988.
- [205] A. I. Golovashkin, L. N. Zherikhina, G. V. Kuleshova, A. M. Tskhovrebov, and M. L. Norton, "Self-consistent spatially inhomogeneous state in HTSC  $\text{Ba}_{1-x}\text{K}_x\text{BiO}_3$  single crystals," *Pis'ma v Zhurnal Eksperimental'noi i Teoreticheskoi Fiziki*, vol. 129, p. 684, 2006.
- [206] G. Iadonisi, M. Chiofalo, V. Cataudella, and D. Ninno, "Phonon-plasmon cooperative effects in the dilute large-bipolaron gas: a possible mechanism for high- $T_c$  superconductivity," *Physical Review B*, vol. 48, no. 17, pp. 12966–12978, 1993.
- [207] T. Nishio, J. Ahmad, and H. Uwe, "Spectroscopic observation of bipolaronic point defects in  $\text{Ba}_{1-x}\text{K}_x\text{BiO}_3$ ," *Physical Review Letters*, vol. 95, no. 17, Article ID 176403, 4 pages, 2005.
- [208] A. S. Alexandrov, " $d$ -wave Bose-Einstein condensate and tunnelling in superconducting cuprates," *Physica C*, vol. 305, no. 1–2, pp. 46–56, 1998.
- [209] A. S. Alexandrov and V. V. Kabanov, "Parameter-free expression for superconducting  $T_c$  in cuprates," *Physical Review B*, vol. 59, no. 21, pp. 13628–13631, 1999.
- [210] A. S. Alexandrov, "Polaron dynamics and bipolaron condensation in cuprates," *Physical Review B*, vol. 61, no. 18, pp. 12315–12327, 2000.
- [211] Q. Chen, J. Stajic, S. Tan, and K. Levin, "BCS-BEC crossover: from high temperature superconductors to ultracold superfluids," *Physics Reports*, vol. 412, no. 1, pp. 1–88, 2005.
- [212] L. S. Marchenko, D. P. Moiseev, E. A. Muzalevskii, and S. K. Uvarova, "Superconductivity in the solid-solutions  $\text{BaPb}_{1-x}\text{Bi}_x\text{O}_3$ ," *Inorganic Materials*, vol. 15, p. 1492, 1979.
- [213] T. D. Thanh, A. Koma, and S. Tanaka, "Superconductivity in the  $\text{BaPb}_{1-x}\text{Bi}_x\text{O}_3$  system," *Applied Physics*, vol. 22, no. 2, pp. 205–212, 1980.
- [214] D. P. Moiseev, S. K. Uvarova, and M. B. Fenik, "Hall voltage and conductivity in the superconducting oxide system  $\text{BaPbO}_3\text{--BaBiO}_3$ ," *Fizika Tverdogo Tela*, vol. 23, p. 2347, 1981.
- [215] M. L. Cohen, "Superconductivity in low-carrier-density systems: degenerate semiconductors," in *Superconductivity*, R. D. Parks, Ed., vol. 1, p. 615, Marcel Dekker, New York, NY, USA, 1969.
- [216] Y. Takada, "Theory of superconductivity in polar semiconductors and its application to  $n$ -type semiconducting  $\text{SrTiO}_3$ ," *Journal of the Physical Society of Japan*, vol. 49, no. 4, pp. 1267–1275, 1980.

- [217] T. Egami, "Nano-scale complexities in the superconducting cuprates," *Journal of Physics and Chemistry of Solids*, vol. 69, no. 9, pp. 2191–2194, 2008.
- [218] L. Pietronero and E. Cappelluti, "Superconductivity, nonadiabaticity and strong correlation in the light of recent experiments," *Journal of Physics: Conference Series*, vol. 108, no. 1, Article ID 012025, 2008.
- [219] R. Friedberg and T. D. Lee, "Gap energy and long-range order in the boson-fermion model of superconductivity," *Physical Review B*, vol. 40, no. 10, pp. 6745–6762, 1989.
- [220] J. Ranninger and J. M. Robin, "The boson-fermion model of high- $T_c$  superconductivity. Doping dependence," *Physica C*, vol. 253, no. 3-4, pp. 279–291, 1995.
- [221] J. Ranninger and J. M. Robin, "Manifestations of the pseudogap in the boson-fermion model for Bose-Einstein-condensation-driven superconductivity," *Physical Review B*, vol. 53, no. 18, pp. R11961–R11963, 1996.
- [222] E. Altman and A. Auerbach, "Plaquette boson-fermion model of cuprates," *Physical Review B*, vol. 65, no. 10, Article ID 104508, 15 pages, 2002.
- [223] T. Domański and K. I. Wysokiński, "Effect of disorder on superconductivity in the boson-fermion model," *Physical Review B*, vol. 66, no. 6, Article ID 064517, 6 pages, 2002.
- [224] R. Micnas, S. Robaszkiewicz, and A. Bussmann-Holder, "Anisotropic superconductivity in systems with coexisting electrons and local pairs," *Physical Review B*, vol. 66, no. 10, Article ID 104516, 9 pages, 2002.
- [225] R. Micnas, "Superfluid transition temperature of the boson-fermion model on a lattice," *Physical Review B*, vol. 76, no. 18, Article ID 184507, 5 pages, 2007.
- [226] A. S. Alexandrov, "Boson-fermion model beyond the mean-field approximation," *Journal of Physics: Condensed Matter*, vol. 8, no. 37, pp. 6923–6932, 1996.
- [227] A. S. Alexandrov, "Self-energy catastrophe of the boson-fermion model of high-temperature superconductors," *Physica C*, vol. 316, no. 3, pp. 239–242, 1999.
- [228] T. Egami, "Electron-phonon coupling in high- $T_c$  superconductors," in *Superconductivity in Complex Systems*, K. A. Müller and A. Bussmann-Holder, Eds., vol. 114 of *Structure and Bonding*, p. 267, Springer, Berlin, Germany, 2005.
- [229] M. Fratini, N. Poccia, and A. Bianconi, "The Feshbach resonance and nanoscale phase separation in a polaron liquid near the quantum critical point for a polaron Wigner crystal," *Journal of Physics: Conference Series*, vol. 108, no. 1, Article ID 012036, 2008.
- [230] A. R. Bishop, "HTC oxides: a collusion of spin, charge and lattice," *Journal of Physics: Conference Series*, vol. 108, no. 1, Article ID 012027, 2008.
- [231] A. Bussmann-Holder and H. Keller, "Unconventional isotope effects, multi-component superconductivity and polaron formation in high temperature cuprate superconductors," *Journal of Physics: Conference Series*, vol. 108, no. 1, Article ID 012019, 2008.
- [232] O. Gunnarsson and O. Rösch, "Interplay between electron-phonon and Coulomb interactions in cuprates," *Journal of Physics: Condensed Matter*, vol. 20, no. 4, Article ID 043201, 2008.
- [233] C. S. Ting, D. N. Talwar, and K. L. Ngai, "Possible mechanism of superconductivity in metal-semiconductor eutectic alloys," *Physical Review Letters*, vol. 45, no. 14, pp. 1213–1216, 1980.
- [234] Y. Bar-Yam, "Two-component superconductivity. I. Introduction and phenomenology," *Physical Review B*, vol. 43, no. 1, pp. 359–377, 1991.
- [235] Y. Bar-Yam, "Two-component superconductivity. II. Copper oxide high- $T_c$  superconductors," *Physical Review B*, vol. 43, no. 4, pp. 2601–2614, 1991.
- [236] P. W. Anderson, "Model for the electronic structure of amorphous semiconductors," *Physical Review Letters*, vol. 34, no. 15, pp. 953–955, 1975.
- [237] G. A. Levin and K. F. Quader, "Tunneling asymmetry in high- $T_c$  cuprates: possible evidence for a submerged band with nondegenerate fermions," *Physical Review B*, vol. 48, no. 21, pp. 16184–16187, 1993.
- [238] K. F. Quader and G. A. Levin, "Origin and consequences of the 'gap' in the cuprate normal state," *Philosophical Magazine B*, vol. 74, no. 5, pp. 611–632, 1996.
- [239] H. Fröhlich, "Superconductivity in metals with incomplete inner shells," *Journal of Physics C*, vol. 1, no. 2, pp. 544–548, 1968.
- [240] E. A. Pashitskii, "Plasmon mechanism of superconductivity in degenerate semiconductors and semimetals. I," *Pis'ma v Zhurnal Eksperimental'noi i Teoreticheskoi Fiziki*, vol. 55, p. 2387, 1968.
- [241] J. Ruvalds, "Are there acoustic plasmons?" *Advances in Physics*, vol. 30, no. 5, pp. 677–695, 1981.
- [242] Y. Takada, "Plasmon mechanism of superconductivity in the multivalley electron gas," *Journal of the Physical Society of Japan*, vol. 61, pp. 238–253, 1992.
- [243] R. Blank and H. Haug, "Theory of plasmon-assisted electron pairing in semiconductors," *Physica Status Solidi B*, vol. 188, no. 1, pp. 105–123, 1995.
- [244] E. A. Pashitskii, "Low frequency charge density excitations and high- $T_c$  superconductivity in cuprate metal-oxide compounds. 1. The HTSC problem prior to a discovery of the high- $T_c$  superconductors: Predictions and premises," *Fizika Nizkikh Temperatur*, vol. 21, p. 995, 1995.
- [245] E. A. Pashitskii, "Low frequency charge density excitations and high- $T_c$  superconductivity in cuprate metal-oxide compounds. 2. The HTSC problem after discovery of high-temperature superconductors: Achievements and outlooks," *Fizika Nizkikh Temperatur*, vol. 21, p. 1091, 1995.
- [246] A. Bill, H. Morawitz, and V. Z. Kresin, "Electronic collective modes and superconductivity in layered conductors," *Physical Review B*, vol. 68, no. 14, Article ID 144519, 12 pages, 2003.
- [247] E. A. Pashitskii and V. I. Pentegov, "On the plasmon mechanism of high- $T_c$  superconductivity in layered crystals and two-dimensional systems," *Fizika Nizkikh Temperatur*, vol. 34, no. 2, pp. 148–160, 2008.
- [248] V. P. Antropov, O. Gunnarsson, and A. I. Liechtenstein, "Phonons, electron-phonon, and electron-plasmon coupling in  $C_{60}$  compounds," *Physical Review B*, vol. 48, no. 10, pp. 7651–7664, 1993.
- [249] J. K. Hulm, M. Ashkin, D. W. Deis, and C. K. Jones, in *Progress in Low Temperature Physics*, vol. 6, p. 205, North-Holland, Amsterdam, The Netherlands, 1970.
- [250] V. L. Ginzburg and D. A. Kirzhnits, Eds., *Problem of High-Temperature Superconductivity*, Nauka, Moscow, Russia, 1977.
- [251] V. L. Ginzburg and D. A. Kirzhnits, Eds., *High Temperature Superconductivity*, Consultants Bureau, New York, NY, USA, 1982.
- [252] S. A. Némov and Yu. I. Ravich, "Thallium dopant in lead chalcogenides: investigation methods and peculiarities," *Uspekhi Fizicheskikh Nauk*, vol. 168, p. 817, 1998.

- [253] G. Binnig, A. Baratoff, H. E. Hoenig, and J. G. Bednorz, "Two-band superconductivity in Nb-doped SrTiO<sub>3</sub>," *Physical Review Letters*, vol. 45, no. 16, pp. 1352–1355, 1980.
- [254] V. A. Moskalenko, "Superconductivity of metals taking into account the overlap of the energy bands," *Fizika Metallov i Metallovedenie*, vol. 8, p. 503, 1959.
- [255] H. Suhl, B. T. Matthias, and L. R. Walker, "Bardeen-Cooper-Schrieffer theory of superconductivity in the case of overlapping bands," *Physical Review Letters*, vol. 3, no. 12, pp. 552–554, 1959.
- [256] A. M. Gabovich and E. A. Pashitskii, "Superconductivity of many-valley semiconductors," *Ukrainskii Fizychnyi Zhurnal*, vol. 20, p. 1814, 1975.
- [257] A. L. Kasatkin and E. A. Pashitskii, "Josephson effect in two-band superconductors," *Ukrainskii Fizychnyi Zhurnal*, vol. 21, p. 578, 1976.
- [258] L. N. Bulaevskii and M. V. Zyskin, "Energy gap in layered superconductors," *Physical Review B*, vol. 42, no. 16, pp. 10230–10240, 1990.
- [259] V. Z. Kresin and S. A. Wolf, "Induced superconducting state and two-gap structure: application to cuprate superconductors and conventional multilayers," *Physical Review B*, vol. 46, no. 10, pp. 6458–6471, 1992.
- [260] S. H. Liu and R. A. Klemm, "Energy gap structure and tunneling characteristics of layered superconductors," *Physica C*, vol. 216, no. 3–4, pp. 293–304, 1993.
- [261] N. Klein, N. Tellmann, H. Schulz, K. Urban, S. A. Wolf, and V. Z. Kresin, "Evidence of two-gap s-wave superconductivity in YBa<sub>2</sub>Cu<sub>3</sub>O<sub>7-x</sub> from microwave surface impedance measurements," *Physical Review Letters*, vol. 71, no. 20, pp. 3355–3358, 1993.
- [262] A. Bussmann-Holder, L. Genzel, A. Simon, and A. R. Bishop, "Gap distribution and multigap-coupling in high T<sub>c</sub>'s," *Zeitschrift für Physik B*, vol. 92, no. 2, pp. 149–154, 1993.
- [263] N. Kristoffel, P. Konsin, and T. Örd, "Two-band model for high-temperature superconductivity," *La Rivista Del Nuovo Cimento*, vol. 17, no. 9, pp. 1–41, 1994.
- [264] P. Konsin and B. Sorkin, "Time-dependent Ginzburg-Landau equations for a two-band superconductor and the relaxation times of the order parameters in Y<sub>1-x</sub>Ca<sub>x</sub>Ba<sub>2</sub>Cu<sub>3</sub>O<sub>7-δ</sub>," *Physica Status Solidi B*, vol. 244, no. 9, pp. 3254–3259, 2007.
- [265] A. Bussmann-Holder, R. Khasanov, A. Shengelaya, et al., "Mixed order parameter symmetries in cuprate superconductors," *Europhysics Letters*, vol. 77, no. 2, Article ID 27002, 4 pages, 2007.
- [266] O. V. Dolgov, I. I. Mazin, D. Parker, and A. A. Golubov, "Interband superconductivity: contrasts between Bardeen-Cooper-Schrieffer and Eliashberg theories," *Physical Review B*, vol. 79, no. 6, Article ID 060502, 4 pages, 2009.
- [267] A. Y. Liu, I. I. Mazin, and J. Kortus, "Beyond Eliashberg superconductivity in MgB<sub>2</sub>: anharmonicity, two-phonon scattering, and multiple gaps," *Physical Review Letters*, vol. 87, no. 8, Article ID 087005, 4 pages, 2001.
- [268] I. I. Mazin and V. P. Antropov, "Electronic structure, electron-phonon coupling, and multiband effects in MgB<sub>2</sub>," *Physica C*, vol. 385, no. 1–2, pp. 49–65, 2003.
- [269] X. X. Xi, "MgB<sub>2</sub> thin films," *Superconductor Science and Technology*, vol. 22, no. 4, Article ID 043001, 15 pages, 2009.
- [270] V. A. Gasparov, N. S. Sidorov, and I. I. Zver'Kova, "Two-gap superconductivity in ZrB<sub>12</sub>: temperature dependence of critical magnetic fields in single crystals," *Physical Review B*, vol. 73, no. 9, Article ID 094510, 11 pages, 2006.
- [271] Yu. A. Nefyodov, A. M. Shuvaev, and M. R. Trunin, "Microwave response of V<sub>3</sub>Si single crystals: evidence for two-gap superconductivity," *Europhysics Letters*, vol. 72, no. 4, pp. 638–644, 2005.
- [272] I. Bonalde, R. L. Ribeiro, W. Brämer-Escamilla, G. Mu, and H. H. Wen, "Possible two-gap behavior in noncentrosymmetric superconductor Mg<sub>10</sub>Ir<sub>19</sub>B<sub>16</sub>: a penetration depth study," *Physical Review B*, vol. 79, no. 5, Article ID 052506, 4 pages, 2009.
- [273] C. L. Huang, J.-Y. Lin, C. P. Sun, et al., "Comparative analysis of specific heat of YNi<sub>2</sub>B<sub>2</sub>C using nodal and two-gap models," *Physical Review B*, vol. 73, no. 1, Article ID 012502, 4 pages, 2006.
- [274] C. L. Huang, J.-Y. Lin, Y. T. Chang, et al., "Experimental evidence for a two-gap structure of superconducting NbSe<sub>2</sub>: a specific-heat study in external magnetic fields," *Physical Review B*, vol. 76, no. 21, Article ID 212504, 4 pages, 2007.
- [275] M. D. Hossain, Z. Salman, D. Wang, et al., "Low-field cross spin relaxation of <sup>8</sup>Li in superconducting NbSe<sub>2</sub>," *Physical Review B*, vol. 79, no. 14, Article ID 144518, 6 pages, 2009.
- [276] T. Tamegai, Y. Nakajima, T. Nakagawa, G. J. Li, and H. Harima, "Two-gap superconductivity in R<sub>2</sub>Fe<sub>3</sub>Si<sub>5</sub> (R = Lu and Sc)," *Journal of Physics: Conference Series*, vol. 150, Article ID 052264, 4 pages, 2009.
- [277] Y. Nakajima, G. J. Li, and T. Tamegai, "Low-temperature specific-heat study of Sc<sub>5</sub>Ir<sub>4</sub>Si<sub>10</sub>," *Journal of Physics: Conference Series*, vol. 150, Article ID 052180, 4 pages, 2009.
- [278] N. E. Phillips, N. Oeschler, R. A. Fisher, J. E. Gordon, M.-L. Foo, and R. J. Cava, "Specific-heat of Na<sub>0.35</sub>CoO<sub>2</sub>.1.3H<sub>2</sub>O: effects of sample age and pair breaking on two-gap superconductivity," *Physica C*, vol. 460–462, part 1, pp. 473–474, 2007.
- [279] R. S. Gonnelli, M. Tortello, D. Daghero, G. A. Ummarino, V. A. Stepanov, and J. S. Kim, "Two-gap superconductivity in the Fe-1111 superconductor LaFeAsO<sub>1-x</sub>F<sub>x</sub>: a point-contact Andreev-reflection study," *Central European Journal of Physics*, vol. 7, no. 2, pp. 251–256, 2009.
- [280] P. Samuely, P. Szabó, Z. Pribulov, M. E. Tillman, S. L. Bud'ko, and P. C. Canfield, "Possible two-gap superconductivity in NdFeAsO<sub>0.9</sub>F<sub>0.1</sub> probed by point-contact Andreev-reflection spectroscopy," *Superconductor Science and Technology*, vol. 22, no. 1, Article ID 014003, 6 pages, 2009.
- [281] Y.-L. Wang, L. Shan, L. Fang, P. Cheng, C. Ren, and H.-H. Wen, "Multiple gaps in SmFeAsO<sub>0.9</sub>F<sub>0.1</sub> revealed by point-contact spectroscopy," *Superconductor Science and Technology*, vol. 22, no. 1, Article ID 015018, 6 pages, 2009.
- [282] P. Szabó, Z. Pribulová, G. Pristáš, S. L. Bud'ko, P. C. Canfield, and P. Samuely, "Evidence for two-gap superconductivity in Ba<sub>0.55</sub>K<sub>0.45</sub>Fe<sub>2</sub>As<sub>2</sub> from directional point-contact Andreev-reflection spectroscopy," *Physical Review B*, vol. 79, no. 1, Article ID 012503, 4 pages, 2009.
- [283] R. Khasanov, D. V. Evtushinsky, A. Amato, et al., "Two-gap superconductivity in Ba<sub>1-x</sub>K<sub>x</sub>Fe<sub>2</sub>As<sub>2</sub>: a complementary study of the magnetic penetration depth by muon-spin rotation and angle-resolved photoemission," *Physical Review Letters*, vol. 102, no. 18, Article ID 187005, 4 pages, 2009.
- [284] A. I. Golovashkin and A. N. Lykov, "Gap peculiarities of the current-voltage characteristics of superconducting contacts with direct conductivity," *Trudy Fiz. Inst. Akad. Nauk SSSR*, vol. 190, p. 144, 1988.
- [285] A. Sharoni, I. Felner, and O. Millo, "Tunneling spectroscopy and magnetization measurements of the superconducting properties of MgB<sub>2</sub>," *Physical Review B*, vol. 63, no. 22, Article ID 220508, 4 pages, 2001.

- [286] T. Takasaki, T. Ekino, T. Muranaka, H. Fujii, and J. Akimitsu, "Superconducting gap in polycrystalline MgB<sub>2</sub> studied by electron tunneling," *Physica C*, vol. 378–381, part 1, pp. 229–233, 2002.
- [287] Yu. G. Naidyuk, I. K. Yanson, L. V. Tyutrina, et al., "Superconducting energy gap distribution in c-axis oriented MgB<sub>2</sub> thin film from point contact study," *JETP Letters*, vol. 75, no. 5, pp. 238–241, 2002.
- [288] H. Schmidt, J. F. Zasadzinski, K. E. Gray, and D. G. Hinks, "Break-junction tunneling on MgB<sub>2</sub>," *Physica C*, vol. 385, no. 1-2, pp. 221–232, 2003.
- [289] T. Ekino, T. Takasaki, T. Muranaka, J. Akimitsu, and H. Fujii, "Tunneling spectroscopy of the superconducting gap in MgB<sub>2</sub>," *Physical Review B*, vol. 67, no. 9, Article ID 094504, 2003.
- [290] B. Barbiellini, O. Fischer, M. Peter, Ch. Renner, and M. Weger, "Gap distribution of the tunneling spectra in Bi<sub>2</sub>Sr<sub>2</sub>CaCu<sub>2</sub>O<sub>x</sub> and some other superconductors," *Physica C*, vol. 220, no. 1-2, pp. 55–60, 1994.
- [291] M. C. Boyer, W. D. Wise, K. Chatterjee, et al., "Imaging the two gaps of the high-temperature superconductor Bi<sub>2</sub>Sr<sub>2</sub>CuO<sub>6+x</sub>," *Nature Physics*, vol. 3, no. 11, pp. 802–806, 2007.
- [292] C. E. Gough, M. S. Colclough, E. M. Forgan, et al., "Flux quantization in a high- $T_c$  superconductor," *Nature*, vol. 326, no. 6116, p. 855, 1987.
- [293] M. N. Keene, T. J. Jackson, and C. E. Gough, "Demonstration of the phase coherence of the superconducting wavefunctions between conventional and high- $T_c$  superconductors," *Nature*, vol. 340, no. 6230, pp. 210–211, 1989.
- [294] E. Dagotto, "Correlated electrons in high-temperature superconductors," *Reviews of Modern Physics*, vol. 66, no. 3, pp. 763–840, 1994.
- [295] A. P. Kampf, "Magnetic correlations in high temperature superconductivity," *Physics Reports*, vol. 249, no. 4-5, pp. 219–351, 1994.
- [296] W. Brenig, "Aspects of electron correlations in the cuprate superconductors," *Physics Reports*, vol. 251, no. 3-4, pp. 153–266, 1995.
- [297] M. Imada, A. Fujimori, and Y. Tokura, "Metal-insulator transitions," *Reviews of Modern Physics*, vol. 70, no. 4, pp. 1039–1263, 1998.
- [298] S. Sachdev, "Colloquium: order and quantum phase transitions in the cuprate superconductors," *Reviews of Modern Physics*, vol. 75, no. 3, pp. 913–932, 2003.
- [299] E. Demler, W. Hanke, and S.-C. Zhang, "SO(5) theory of antiferromagnetism and superconductivity," *Reviews of Modern Physics*, vol. 76, no. 3, pp. 909–974, 2004.
- [300] T. Schneider, in *The Physics of Superconductors. Vol. I: Conventional and High- $T_c$  Superconductors*, K. H. Bennemann and J. B. Ketterson, Eds., p. 111, Springer, Berlin, Germany, 2004.
- [301] T. Schneider and H. Keller, "Implications evinced by the phase diagram, anisotropy, magnetic penetration depths, isotope effects and conductivities of cuprate superconductors," *New Journal of Physics*, vol. 6, Article ID 144, 18 pages, 2004.
- [302] P. A. Lee, N. Nagaosa, and X.-G. Wen, "Doping a Mott insulator: physics of high-temperature superconductivity," *Reviews of Modern Physics*, vol. 78, no. 1, Article ID 17, 69 pages, 2006.
- [303] K. M. Shen and J. C. S. Davis, "Cuprate high- $T_c$  superconductors," *Materials Today*, vol. 11, no. 9, pp. 14–21, 2008.
- [304] H. Alloul, J. Bobroff, M. Gabay, and P. J. Hirschfeld, "Defects in correlated metals and superconductors," *Reviews of Modern Physics*, vol. 81, no. 1, Article ID 45, 64 pages, 2009.
- [305] D. J. Scalapino, "The case for  $d_{x^2-y^2}$  pairing in the cuprate superconductors," *Physics Reports*, vol. 250, no. 6, pp. 329–365, 1995.
- [306] J. F. Annett, N. D. Goldenfeld, and A. J. Leggett, "Experimental constraints on the pairing state of the cuprate superconductors: an emerging consensus," in *Physical Properties of High Temperature Superconductors V*, D. M. Ginsberg, Ed., p. 375, World Scientific, River Ridge, NJ, USA, 1996.
- [307] D. Pines, "Understanding high temperature superconductors: progress and prospects," *Physica C*, vol. 282–287, part 1, pp. 273–278, 1997.
- [308] T. S. Nunner, J. Schmalian, and K. H. Bennemann, "Influence of electron-phonon interaction on spin-fluctuation-induced superconductivity," *Physical Review B*, vol. 59, no. 13, pp. 8859–8868, 1999.
- [309] D. Manske, I. Eremin, and K. H. Bennemann, "Theory for electron-doped cuprate superconductors:  $d$ -wave symmetry order parameter," *Physical Review B*, vol. 62, no. 21, pp. 13922–13925, 2000.
- [310] T. Dahm, V. Hinkov, S. V. Borisenko, et al., "Strength of the spin-fluctuation-mediated pairing interaction in a high-temperature superconductor," *Nature Physics*, vol. 5, no. 3, pp. 217–221, 2009.
- [311] M. L. Cohen, "Electron-phonon-induced superconductivity," *Journal of Superconductivity and Novel Magnetism*, vol. 19, no. 3–5, pp. 283–290, 2006.
- [312] G. Varelogiannis, "Phonon-mediated unconventional superconductivity in strongly correlated systems," *Physical Review B*, vol. 57, no. 21, pp. 13743–13764, 1998.
- [313] G. Varelogiannis, "Small- $q$  electron-phonon interaction and the phase diagram of the cuprates," *Physica C*, vol. 460–462, part 2, pp. 1125–1126, 2007.
- [314] A. S. Alexandrov, " $d$ -wave checkerboard bose condensate of mobile bipolarons," *International Journal of Modern Physics B*, vol. 21, no. 13-14, pp. 2301–2312, 2007.
- [315] H. Kamimura and H. Ushio, "On the interplay of Jahn-Teller physics and Mott physics in cuprates," *Journal of Physics: Conference Series*, vol. 108, no. 1, Article ID 012030, 2008.
- [316] A. S. Alexandrov, "Unconventional pairs glued by conventional phonons in cuprate superconductors," *Journal of Superconductivity and Novel Magnetism*, vol. 22, no. 2, pp. 103–107, 2009.
- [317] E. A. Pashitskii and V. I. Pentegov, "The role of the charge density fluctuations and many-body Coulomb correlations in the mechanism of high-temperature superconductivity in cuprate metal-oxides," *Fizika Nizkikh Temperatur*, vol. 27, no. 2, pp. 140–152, 2001.
- [318] H.-B. Schüttler and C.-H. Pao, "Isotope effect in  $d$ -wave superconductors," *Physical Review Letters*, vol. 75, no. 24, pp. 4504–4507, 1995.
- [319] Yu. Bang, "Effects of phonon interaction on pairing in high- $T_c$  superconductors," *Physical Review B*, vol. 78, no. 7, Article ID 075116, 2008.
- [320] A. I. Lichtenstein and M. L. Kulić, "Electron-boson interaction can help  $d$  wave pairing self-consistent approach," *Physica C*, vol. 245, no. 1-2, pp. 186–192, 1995.
- [321] T. Egami, P. Piekarczyk, and J.-H. Chung, "Role of phonons in the mechanism of high-temperature superconductivity," *Physica C*, vol. 408–410, no. 1–4, pp. 292–295, 2004.

- [322] E. G. Maksimov, "Electron-phonon interaction and superconductivity," *Trudy Fiz. Inst. Akad. Nauk SSSR*, vol. 86, p. 101, 1975.
- [323] L. Tonks and I. Langmuir, "Oscillations in ionized gases," *Physical Review*, vol. 33, no. 2, pp. 195–210, 1929.
- [324] D. Bohm and T. Staver, "Application of collective treatment of electron and ion vibrations to theories of conductivity and superconductivity," *Physical Review*, vol. 84, no. 4, pp. 836–837, 1951.
- [325] V. P. Silin and A. A. Rukhadze, *Electromagnetic Properties of Plasma and Plasma-Like Media*, Gosatomizdat, Moscow, Russia, 1961.
- [326] E. G. Brovman and Yu. M. Kagan, "Phonons in non-transition metals," *Uspekhi Fizicheskikh Nauk*, vol. 112, p. 369, 1974.
- [327] B. T. Geilikman, "Adiabatic perturbation theory for metals and the problem of the lattice stability," *Uspekhi Fizicheskikh Nauk*, vol. 115, p. 403, 1975.
- [328] M. A. Eggington and A. J. Leggett, "Is ODLRO a necessary condition for superfluidity?" *Collective Phenomena*, vol. 2, p. 81, 1975.
- [329] B. T. Geilikman, *Studies in Low Temperature Physics*, Atomizdat, Moscow, Russia, 1979.
- [330] V. M. Kontorovich, "Dynamical equations of the elasticity theory in metals," *Uspekhi Fizicheskikh Nauk*, vol. 142, p. 265, 1984.
- [331] S. Yu. Savrasov and E. G. Maksimov, "Ab initio calculations of the lattice dynamics of crystals," *Uspekhi Fizicheskikh Nauk*, vol. 165, p. 773, 1995.
- [332] E. G. Maksimov, D. Yu. Savrasov, and S. Yu. Savrasov, "Electron-phonon interaction and physical properties of metals," *Uspekhi Fizicheskikh Nauk*, vol. 167, p. 353, 1997.
- [333] E. G. Maksimov and A. E. Karakozov, "On nonadiabatic effects in phonon spectra of metals," *Uspekhi Fizicheskikh Nauk*, vol. 178, p. 561, 2008.
- [334] J. Lee, K. Fujita, K. McElroy, et al., "Interplay of electron-lattice interactions and superconductivity in  $\text{Bi}_2\text{Sr}_2\text{CaCu}_2\text{O}_{8+\delta}$ ," *Nature*, vol. 442, no. 7102, pp. 546–550, 2006.
- [335] D. Reznik, L. Pintschovius, M. Ito, et al., "Electron-phonon coupling reflecting dynamic charge inhomogeneity in copper oxide superconductors," *Nature*, vol. 440, no. 7088, pp. 1170–1173, 2006.
- [336] K. McElroy, J. Lee, J. A. Slezak, et al., "Atomic-scale sources and mechanism of nanoscale electronic disorder in  $\text{Bi}_2\text{Sr}_2\text{CaCu}_2\text{O}_{8+\delta}$ ," *Science*, vol. 309, no. 5737, pp. 1048–1052, 2005.
- [337] D. Mihailovic and V. V. Kabanov, "Dynamic inhomogeneity, pairing and superconductivity in cuprates," in *Superconductivity in Complex Systems*, K. A. Muller and A. Bussmann-Holder, Eds., vol. 114 of *Structure and Bonding*, p. 331, Springer, Berlin, Germany, 2005.
- [338] A. Sugimoto, S. Kashiwaya, H. Eisaki, et al., "Enhancement of electronic inhomogeneities due to out-of-plane disorder in  $\text{Bi}_2\text{Sr}_2\text{CuO}_{6+\delta}$  superconductors observed by scanning tunneling spectroscopy," *Physical Review B*, vol. 74, no. 9, Article ID 094503, 2006.
- [339] A. Yazdani, "Visualizing pair formation on the atomic scale and the search for the mechanism of superconductivity in high- $T_c$  cuprates," *Journal of Physics: Condensed Matter*, vol. 21, no. 16, Article ID 164214, 2009.
- [340] T. Kato, T. Machida, Y. Kamijo, R. Miyashita, and H. Sakata, "Spatial correlation between the LDOS modulation and electronic inhomogeneity in  $\text{Bi}_2\text{Sr}_{2-x}\text{La}_x\text{CuO}_{6+\delta}$ ," *Journal of Physics: Conference Series*, vol. 150, Article ID 052101, 4 pages, 2009.
- [341] K. Kudo, T. Nishizaki, N. Okumura, and N. Kobayashi, "Electronic inhomogeneity in Pb-substituted  $\text{Bi}_2\text{Sr}_2\text{CuO}_{6+\delta}$  studied by STM/STS measurements," *Journal of Physics: Conference Series*, vol. 150, Article ID 052133, 4 pages, 2009.
- [342] M. Suzuki, T. Hamatani, Y. Yamada, K. Anagawa, and T. Watanabe, "Significantly doping-dependent Josephson critical current—inhomogeneity in real space or heterogeneity in k-space," *Journal of Physics: Conference Series*, vol. 150, Article ID 052252, 4 pages, 2009.
- [343] W. D. Wise, K. Chatterjee, M. C. Boyer, et al., "Imaging nanoscale Fermi-surface variations in an inhomogeneous superconductor," *Nature Physics*, vol. 5, no. 3, pp. 213–216, 2009.
- [344] W. D. Wise, M. C. Boyer, K. Chatterjee, et al., "Charge-density-wave origin of cuprate checkerboard visualized by scanning tunnelling microscopy," *Nature Physics*, vol. 4, no. 9, pp. 696–699, 2008.
- [345] X. M. Li, F. H. Li, H. Q. Luo, L. Fang, and H.-H. Wen, "Transmission electron microscopy study of one-dimensional incommensurate structural modulation in superconducting oxides  $\text{Bi}_{2+x}\text{Sr}_{2-x}\text{CuO}_{6+\delta}$  ( $0.10 \leq x \leq 0.40$ )," *Superconductor Science and Technology*, vol. 22, no. 6, Article ID 065003, 2009.
- [346] A. Mourachkine, *High-Temperature Superconductivity in Cuprates*, Kluwer Academic Publishers, Dordrecht, The Netherlands, 2002.
- [347] J. F. Zasadzinski, "Tunneling spectroscopy of conventional and unconventional superconductors," in *The Physics of Superconductors. Vol. 1: Conventional and High- $T_c$  Superconductors*, K. H. Bennemann and J. B. Ketterson, Eds., p. 591, Springer, Berlin, Germany, 2003.
- [348] Ø. Fischer, M. Kugler, I. Maggio-Aprile, C. Berthod, and C. Renner, "Scanning tunneling spectroscopy of high-temperature superconductors," *Reviews of Modern Physics*, vol. 79, no. 1, pp. 353–419, 2007.
- [349] V. M. Krasnov, A. Yurgens, D. Winkler, P. Delsing, and T. Claeson, "Evidence for coexistence of the superconducting gap and the pseudogap in Bi-2212 from intrinsic tunneling spectroscopy," *Physical Review Letters*, vol. 84, no. 25, pp. 5860–5863, 2000.
- [350] M. Oda, Y. H. Liu, T. Kurosawa, K. Takeyama, N. Momono, and M. Ido, "On the relations among the pseudogap, electronic charge order and Fermi-arc superconductivity in  $\text{Bi}_2\text{Sr}_2\text{CaCu}_2\text{O}_{8+\delta}$ ," *Journal of Physics: Conference Series*, vol. 108, Article ID 012008, 6 pages, 2008.
- [351] K. Tanaka, W. S. Lee, Z. Hussain, and Z. X. Shen, "Direct evidence of two gaps in underdoped Bi2212," *Journal of Physics: Conference Series*, vol. 108, no. 1, Article ID 012014, 2008.
- [352] A. A. Kordyuk, S. V. Borisenko, V. B. Zabolotnyy, et al., "Nonmonotonic pseudogap in high- $T_c$  cuprates," *Physical Review B*, vol. 79, no. 2, Article ID 020504, 2009.
- [353] W. S. Lee, I. M. Vishik, D. H. Lu, and Z.-X. Shen, "A brief update of angle-resolved photoemission spectroscopy on a correlated electron system," *Journal of Physics: Condensed Matter*, vol. 21, no. 16, Article ID 164217, 2009.
- [354] R.-H. He, K. Tanaka, S.-K. Mo, et al., "Energy gaps in the failed high- $T_c$  superconductor  $\text{La}_{1.875}\text{Ba}_{0.125}\text{CuO}_4$ ," *Nature Physics*, vol. 5, no. 2, pp. 119–123, 2009.
- [355] J. Meng, W. Zhang, G. Liu, et al., "Monotonic d-wave superconducting gap of the optimally doped  $\text{Bi}_2\text{Sr}_{1.6}\text{La}_{0.4}\text{CuO}_6$  superconductor by laser-based angle-resolved photoemission

- spectroscopy,” *Physical Review B*, vol. 79, no. 2, Article ID 024514, 2009.
- [356] T. Kondo, R. Khasanov, T. Takeuchi, J. Schmalian, and A. Kaminski, “Competition between the pseudogap and superconductivity in the high- $T_c$  copper oxides,” *Nature*, vol. 457, no. 7227, pp. 296–300, 2009.
- [357] M. L. Teague, A. D. Beyer, M. S. Grinolds, S. I. Lee, and N.-C. Yeh, “Observation of vortices and hidden pseudogap from scanning tunneling spectroscopic studies of the electron-doped cuprate superconductor  $\text{Sr}_{0.9}\text{La}_{0.1}\text{CuO}_2$ ,” *Europhysics Letters*, vol. 85, no. 1, Article ID 17004, 2009.
- [358] A. Sugimoto, K. Shohara, T. Ekino, et al., “Scanning tunneling microscopy/spectroscopy on multi-layered cuprate superconductor  $\text{Ba}_2\text{Ca}_5\text{Cu}_6\text{O}_{12}(\text{O}_{1-x}\text{F}_x)_2$ ,” *Physica C*, vol. 469, no. 15–20, pp. 1020–1023, 2009.
- [359] K. Mcelroy, D.-H. Lee, J. E. Hoffman, et al., “Coincidence of checkerboard charge order and antinodal state decoherence in strongly underdoped superconducting  $\text{Bi}_2\text{Sr}_2\text{CaCu}_2\text{O}_{8+\delta}$ ,” *Physical Review Letters*, vol. 94, no. 19, Article ID 197005, 2005.
- [360] J. P. Castellan, B. D. Gaulin, H. A. Dabkowska, et al., “Two- and three-dimensional incommensurate modulation in optimally-doped  $\text{Bi}_2\text{Sr}_2\text{CaCu}_2\text{O}_{8+\delta}$ ,” *Physical Review B*, vol. 73, no. 17, Article ID 174505, 2006.
- [361] J. Etrillard, P. Bourges, and C. T. Lin, “Incommensurate composite structure of the superconductor  $\text{Bi}_2\text{Sr}_2\text{CaCu}_2\text{O}_{8+\delta}$ ,” *Physical Review B*, vol. 62, no. 1, pp. 150–153, 2000.
- [362] G. Kinoda, T. Hasegawa, S. Nakao, et al., “Electronic structures of two-phase microstructures  $\alpha$  and  $\beta$  in heavily Pb-doped  $\text{Bi}_2\text{Sr}_2\text{CaCu}_2\text{O}_y$  single crystals investigated by scanning tunneling microscopy/spectroscopy,” *Applied Physics Letters*, vol. 83, no. 6, pp. 1178–1180, 2003.
- [363] A. Sugimoto, S. Kashiwaya, H. Eisaki, et al., “Correlation between modulation structure and electronic inhomogeneity on Pb-doped Bi-2212 single crystals,” *Physica C*, vol. 426–431, part 1, pp. 390–395, 2005.
- [364] M. Vershinin, S. Misra, S. Ono, Y. Abe, Y. Ando, and A. Yazdani, “Local ordering in the pseudogap state of the high- $T_c$  superconductor  $\text{Bi}_2\text{Sr}_2\text{CaCu}_2\text{O}_{8+\delta}$ ,” *Science*, vol. 303, no. 5666, pp. 1995–1998, 2004.
- [365] A. Bianconi, M. Lusignoli, N. L. Saini, P. Bordet, A. Kvik, and P. G. Radaelli, “Stripe structure of the  $\text{CuO}_2$  plane in  $\text{Bi}_2\text{Sr}_2\text{CaCu}_2\text{O}_{8+y}$  by anomalous X-ray diffraction,” *Physical Review B*, vol. 54, no. 6, pp. 4310–4314, 1996.
- [366] E. V. L. de Mello and E. S. Caixeiro, “The theory of local superconductivity and phase separation applied to cuprates,” *Journal of Superconductivity*, vol. 18, no. 5-6, pp. 53–57, 2005.
- [367] V. Z. Kresin, Yu. N. Ovchinnikov, and S. A. Wolf, “Inhomogeneous superconductivity and the “pseudogap” state of novel superconductors,” *Physics Reports*, vol. 431, no. 5, pp. 231–259, 2006.
- [368] J. E. Hoffman, E. W. Hudson, K. M. Lang, et al., “A four unit cell periodic pattern of quasi-particle states surrounding vortex cores in  $\text{Bi}_2\text{Sr}_2\text{CaCu}_2\text{O}_{8+\delta}$ ,” *Science*, vol. 295, no. 5554, pp. 466–469, 2002.
- [369] N. Momono, A. Hashimoto, Y. Kobatake, S. Nakamura, M. Oda, and M. Ido, “STM/STS study on local electronic states of underdoped  $\text{Bi}_2\text{Sr}_2\text{CaCu}_2\text{O}_{8+\delta}$ ,” *International Journal of Modern Physics B*, vol. 19, no. 1–3, pp. 231–234, 2005.
- [370] A. Hashimoto, N. Momono, M. Oda, and M. Ido, “Scanning tunneling microscopy and spectroscopy study of  $4a \times 4a$  electronic charge order and the inhomogeneous pairing gap in superconducting  $\text{Bi}_2\text{Sr}_2\text{CaCu}_2\text{O}_{8+\delta}$ ,” *Physical Review B*, vol. 74, no. 6, Article ID 064508, 2006.
- [371] K. M. Shen, F. Ronning, D. H. Lu, et al., “Nodal quasiparticles and antinodal charge ordering in  $\text{Ca}_{2-x}\text{Na}_x\text{CuO}_2\text{Cl}_2$ ,” *Science*, vol. 307, no. 5711, pp. 901–904, 2005.
- [372] J. A. Robertson, S. A. Kivelson, E. Fradkin, A. C. Fang, and A. Kapitulnik, “Distinguishing patterns of charge order: stripes or checkerboards,” *Physical Review B*, vol. 74, no. 13, Article ID 134507, 2006.
- [373] W. Meevasana, N. J. C. Ingle, D. H. Lu, et al., “Doping dependence of the coupling of electrons to bosonic modes in the single-layer high-temperature  $\text{Bi}_2\text{Sr}_2\text{CaCu}_2\text{O}_6$  superconductor,” *Physical Review Letters*, vol. 96, no. 15, Article ID 157003, 2006.
- [374] D. S. Inosov, V. B. Zabolotnyy, D. V. Evtushinsky, et al., “Fermi surface nesting in several transition metal dichalcogenides,” *New Journal of Physics*, vol. 10, Article ID 125027, 2008.
- [375] S. V. Borisenko, A. A. Kordyuk, V. B. Zabolotnyy, et al., “Two energy gaps and fermi-surface “arcs” in  $\text{NbSe}_2$ ,” *Physical Review Letters*, vol. 102, no. 16, Article ID 166402, 2009.
- [376] D. S. Inosov, D. V. Evtushinsky, V. B. Zabolotnyy, et al., “Temperature-dependent Fermi surface of  $2H\text{-TaSe}_2$  driven by competing density wave order fluctuations,” *Physical Review B*, vol. 79, no. 12, Article ID 125112, 2009.
- [377] A. M. Gabovich, V. A. Medvedev, D. P. Moiseev, et al., “Superconductivity and thermal anomalies in the properties of the crystal lattice of the metal oxide  $\text{La}_{1.8}\text{Ba}_{0.2}\text{CuO}_4$ ,” *Fizika Nizkikh Temperatur*, vol. 13, no. 8, pp. 844–847, 1987.
- [378] R. A. Klemm, “Striking similarities between the pseudogap phenomena in cuprates and in layered organic and dichalcogenide superconductors,” *Physica C*, vol. 341–348, pp. 839–842, 2000.
- [379] R. A. Klemm, “Origin of the pseudogap in high temperature superconductors,” in *Nonequilibrium Physics at Short Time Scales: Formation of Correlations*, K. Morawetz, Ed., p. 381, Springer, Berlin, Germany, 2004.
- [380] E. Morosan, H. W. Zandbergen, B. S. Dennis, et al., “Superconductivity in  $\text{Cu}_x\text{TiSe}_2$ ,” *Nature Physics*, vol. 2, no. 8, pp. 544–550, 2006.
- [381] S. L. Bud’ko, P. C. Canfield, E. Morosan, R. J. Cava, and G. M. Schmiedeshoff, “Thermal expansion and effect of pressure on superconductivity in  $\text{Cu}_x\text{TiSe}_2$ ,” *Journal of Physics: Condensed Matter*, vol. 19, Article ID 176230, 8 pages, 2005.
- [382] M. V. Kartsovnik, D. Andres, W. Biberacher, P. D. Grigoriev, E. A. Schuberth, and H. Müller, “New electronic phase transitions in  $\alpha\text{-(BEDT-TTF)}_2\text{KHg(SCN)}_4$ ,” *Journal de Physique IV*, vol. 114, pp. 191–197, 2004.
- [383] D. Graf, J. S. Brooks, M. Almeida, et al., “Evolution of superconductivity from a charge-density-wave ground state in pressurized  $(\text{Per})_2[\text{Au}(\text{mnt})_2]$ ,” *Europhysics Letters*, vol. 85, no. 2, Article ID 27009, 2009.
- [384] J. J. Hamlin, D. A. Zocco, T. A. Sayles, M. B. Maple, J.-H. Chu, and I. R. Fisher, “Pressure-induced superconducting phase in the charge-density-wave compound terbium tritelluride,” *Physical Review Letters*, vol. 102, no. 17, Article ID 177002, 2009.
- [385] G. Bilbro and W. L. McMillan, “Theoretical model of superconductivity and the martensitic transformation in A15 compounds,” *Physical Review B*, vol. 14, no. 5, pp. 1887–1892, 1976.
- [386] A. M. Gabovich, M. S. Li, H. Szymczak, and A. I. Voitenko, “Thermodynamics of superconductors with charge-density waves,” *Journal of Physics: Condensed Matter*, vol. 15, no. 17, pp. 2745–2753, 2003.

- [387] N. Oeschler, R. A. Fisher, N. E. Phillips, J. E. Gordon, M.-L. Foo, and R. J. Cava, "Specific heat of  $\text{Na}_{0.3}\text{CoO}_2 \cdot 1.3\text{H}_2\text{O}$ : two energy gaps, nonmagnetic pair breaking, strong fluctuations in the superconducting state, and effects of sample age," *Physical Review B*, vol. 78, no. 5, Article ID 054528, 2008.
- [388] H. Fu, N. Oeschler, R. A. Fisher, et al., "Competition between superconductivity and charge-density wave order in  $\text{Na}_{0.3}\text{CoO}_2 \cdot 1.3\text{H}_2\text{O}$ ," *Journal of Superconductivity and Novel Magnetism*, vol. 22, no. 3, pp. 295–298, 2009.
- [389] N. E. Phillips, R. A. Fisher, H. Fu, et al., "Superconductivity and charge-density-wave order in  $\text{Na}_{0.3}\text{CoO}_2 \cdot 1.3\text{H}_2\text{O}$ ," *Journal of Physics: Conference Series*, vol. 150, Article ID 052210, 2009.
- [390] M. S. Li, "Paramagnetic Meissner effect and related dynamical phenomena," *Physics Reports*, vol. 376, no. 3, pp. 133–223, 2003.
- [391] G. K. Perkins, Y. Bugoslavsky, A. D. Caplin, et al., "Effects of proton irradiation and ageing on the superconducting properties of single crystalline and polycrystalline  $\text{MgB}_2$ ," *Superconductor Science and Technology*, vol. 17, no. 1, pp. 232–235, 2004.
- [392] A. M. Gabovich, D. P. Moiseev, L. V. Prokopovich, S. K. Uvarova, and V. E. Yachmenev, "Experimental proof of bulk superconductivity in perovskite system  $\text{BaPb}_{1-x}\text{Bi}_x\text{O}_3$ ," *Zhurnal Éksperimental'noi i Teoreticheskoi Fiziki*, vol. 86, p. 1727, 1984.
- [393] I. R. Gomersall and B. L. Gyorffy, "On the connection between high superconducting transition temperature,  $T_c$ , and lattice instability in transition metal compounds:  $\text{NbN}$ ," *Journal of Physics F*, vol. 3, pp. L138–L144, 1973.
- [394] J. C. Phillips, "Lattice instabilities and high-temperature superconductivity," *Physical Review Letters*, vol. 26, no. 10, pp. 543–546, 1971.
- [395] I. Nakayama, "Structural transformation and superconductivity in A-15 compounds," *Journal of the Physical Society of Japan*, vol. 43, p. 1533, 1977.
- [396] A. M. Gabovich, D. P. Moiseev, and A. S. Shpigel, "The nature of superconductivity for solid solutions  $\text{BaPb}_{1-x}\text{Bi}_x\text{O}_3$  with a perovskite structure. Role of the electron spectrum dielectrization," *Zhurnal Éksperimental'noi i Teoreticheskoi Fiziki*, vol. 83, p. 1383, 1982.
- [397] A. M. Gabovich and A. S. Shpigel, "Thermodynamics of superconductors with charge and spin-density waves," *Journal of Physics F*, vol. 14, no. 12, pp. 3031–3039, 1984.
- [398] A. M. Gabovich, "Partial dielectrization model for oxide superconductivity," in *High- $T_c$  Superconductivity, Experiment and Theory*, A. S. Davydov and V. M. Loktev, Eds., pp. 161–169, Springer, Berlin, Germany, 1992.
- [399] T. Ekino, Y. Sezaki, and H. Fujii, "Features of the energy gap above  $T_c$  in  $\text{Bi}_2\text{Sr}_2\text{CaCu}_2\text{O}_{8+\delta}$  as seen by break-junction tunneling," *Physical Review B*, vol. 60, no. 9, pp. 6916–6922, 1999.
- [400] J. Demsar, R. Hudej, J. Karpinski, V. V. Kabanov, and D. Mihailovic, "Quasiparticle dynamics and gap structure in  $\text{HgBa}_2\text{Ca}_2\text{Cu}_3\text{O}_{8+\delta}$  investigated with femtosecond spectroscopy," *Physical Review B*, vol. 63, no. 5, Article ID 054519, 7 pages, 2001.
- [401] M. Le Tacon, A. Sacuto, A. Georges, et al., "Two energy scales and two distinct quasiparticle dynamics in the superconducting state of underdoped cuprates," *Nature Physics*, vol. 2, no. 8, pp. 537–543, 2006.
- [402] K. Tanaka, W. S. Lee, D. H. Lu, et al., "Distinct fermi-momentum-dependent energy gaps in deeply underdoped  $\text{Bi2212}$ ," *Science*, vol. 314, no. 5807, pp. 1910–1913, 2006.
- [403] W. S. Lee, I. M. Vishik, K. Tanaka, et al., "Abrupt onset of a second energy gap at the superconducting transition of underdoped  $\text{Bi2212}$ ," *Nature*, vol. 450, no. 7166, pp. 81–84, 2007.
- [404] T. Das, R. S. Markiewicz, and A. Bansil, "Competing order scenario of two-gap behavior in hole-doped cuprates," *Physical Review B*, vol. 77, no. 13, Article ID 134516, 2008.
- [405] V. J. Emery and S. A. Kivelson, "Importance of phase fluctuations in superconductors with small superfluid density," *Nature*, vol. 374, no. 6521, pp. 434–437, 1995.
- [406] M. R. Norman, D. Pines, and C. Kallin, "The pseudogap: friend or foe of high  $T_c$ ?" *Advances in Physics*, vol. 54, no. 8, pp. 715–733, 2005.
- [407] T. Valla, A. V. Fedorov, J. Lee, J. C. Davis, and G. D. Gu, "The ground state of the pseudogap in cuprate superconductors," *Science*, vol. 314, no. 5807, pp. 1914–1916, 2006.
- [408] A. Kanigel, U. Chatterjee, M. Randeria, et al., "Protected nodes and the collapse of fermi arcs in high- $T_c$  cuprate superconductors," *Physical Review Letters*, vol. 99, no. 15, Article ID 157001, 2007.
- [409] A. Kanigel, U. Chatterjee, M. Randeria, et al., "Evidence for pairing above the transition temperature of cuprate superconductors from the electronic dispersion in the pseudogap phase," *Physical Review Letters*, vol. 101, no. 13, Article ID 137002, 2008.
- [410] H.-B. Yang, J. D. Rameau, P. D. Johnson, T. Valla, A. Tsvetik, and G. D. Gu, "Emergence of preformed cooper pairs from the doped Mott insulating state in  $\text{Bi}_2\text{Sr}_2\text{CaCu}_2\text{O}_{8+\delta}$ ," *Nature*, vol. 456, no. 7218, pp. 77–80, 2008.
- [411] M. Shi, J. Chang, S. Pailhès, et al., "Coherent  $d$ -Wave superconducting gap in underdoped  $\text{La}_{2-x}\text{Sr}_x\text{CuO}_4$  by angle-resolved photoemission spectroscopy," *Physical Review Letters*, vol. 101, no. 4, Article ID 047002, 2008.
- [412] S. Hüfner and F. Müller, "Temperature dependence of the gaps of high-temperature superconductors in the Fermi-arc region," *Physical Review B*, vol. 78, no. 1, Article ID 014521, 2008.
- [413] S. Hüfner, M. A. Hossain, A. Damascelli, and G. A. Sawatzky, "Two gaps make a high-temperature superconductor?" *Reports on Progress in Physics*, vol. 71, no. 6, Article ID 062501, 2008.
- [414] K. Nakayama, T. Sato, Y. Sekiba, et al., "Evolution of a pairing-induced pseudogap from the superconducting gap of  $(\text{Bi,Pb})_2\text{Sr}_2\text{CuO}_6$ ," *Physical Review Letters*, vol. 102, no. 22, Article ID 227006, 2009.
- [415] C.-C. Chien, Y. He, Q. Chen, and K. Levin, "Two-energy-gap preformed-pair scenario for cuprate superconductors: implications for angle-resolved photoemission spectroscopy," *Physical Review B*, vol. 79, no. 21, Article ID 214527, 2009.
- [416] J. Lee, K. Fujita, A. R. Schmidt, et al., "Spectroscopic fingerprint of phase-incoherent superconductivity in the underdoped  $\text{Bi}_2\text{Sr}_2\text{CaCu}_2\text{O}_{8+\delta}$ ," *Science*, vol. 325, no. 5944, pp. 1099–1103, 2009.
- [417] V. M. Krasnov, "Interlayer tunneling spectroscopy of  $\text{Bi}_2\text{Sr}_2\text{CaCu}_2\text{O}_{8+\delta}$ : a look from inside on the doping phase diagram of high- $T_c$  superconductors," *Physical Review B*, vol. 65, no. 14, Article ID 140504, 4 pages, 2002.
- [418] E. E. M. Chia, J.-X. Zhu, D. Talbayev, et al., "Observation of competing order in a high- $T_c$  superconductor using femtosecond optical pulses," *Physical Review Letters*, vol. 99, no. 14, Article ID 147008, 2007.
- [419] M. Hashimoto, T. Yoshida, A. Fujimori, et al., "Effects of out-of-plane disorder on the nodal quasiparticle and superconducting gap in single-layer  $\text{Bi}_2\text{Sr}_{1.6}\text{L}_{0.4}\text{CuO}_{6+\delta}$

- ( $L = \text{La, Nd, Gd}$ ),” *Physical Review B*, vol. 79, no. 14, Article ID 144517, 2009.
- [420] V. M. Krasnov, A. E. Kovalev, A. Yurgens, and D. Winkler, “Magnetic field dependence of the superconducting gap and the pseudogap in  $\text{Bi2212}$  and  $\text{HgBr}_2\text{-Bi2212}$ , studied by intrinsic tunneling spectroscopy,” *Physical Review Letters*, vol. 86, no. 12, pp. 2657–2660, 2001.
- [421] D. E. Moncton, J. D. Axe, and F. J. DiSalvo, “Neutron scattering study of the charge-density wave transitions in  $2\text{H-TaSe}_2$  and  $2\text{H-NbSe}_2$ ,” *Physical Review B*, vol. 16, no. 2, pp. 801–819, 1977.
- [422] K. Machida, “Spin density wave and superconductivity in highly anisotropic materials,” *Journal of the Physical Society of Japan*, vol. 50, pp. 2195–2202, 1981.
- [423] K. Machida and T. Matsubara, “Spin density wave and superconductivity in highly anisotropic materials. II. Detailed study of phase transitions,” *Journal of the Physical Society of Japan*, vol. 50, p. 3231, 1981.
- [424] K. Machida, “Spin density wave and superconductivity in highly anisotropic materials. III. Energy gap structure and non-magnetic impurity effects,” *Journal of the Physical Society of Japan*, vol. 51, p. 1420, 1982.
- [425] A. M. Gabovich, D. P. Moiseev, and A. S. Shpigel, “Thermodynamic properties of superconducting ceramics  $\text{BaPb}_{1-x}\text{Bi}_x\text{O}_3$ ,” *Journal of Physics C*, vol. 15, no. 18, pp. L569–L572, 1982.
- [426] A. M. Gabovich and A. S. Shpigel, “Influence of impurity scattering on the critical temperature of superconductors with a partial gap in the electron spectrum,” *Journal of Low Temperature Physics*, vol. 51, no. 5–6, pp. 581–599, 1983.
- [427] A. M. Gabovich, A. S. Gerber, and A. S. Shpigel, “Thermodynamics of superconductors with charge- and spin-density waves,” *Physica Status Solidi B*, vol. 141, no. 2, pp. 575–587, 1987.
- [428] A. M. Gabovich and A. S. Shpigel, “Upper critical magnetic field of superconductors with a dielectric gap on the Fermi-surface sections,” *Physical Review B*, vol. 38, no. 1, pp. 297–306, 1988.
- [429] K. Levin, D. L. Mills, and S. L. Cunningham, “Incompatibility of BCS pairing and the Peierls distortion in one-dimensional systems. I. Mean-field theory,” *Physical Review B*, vol. 10, no. 9, pp. 3821–3831, 1974.
- [430] K. Levin, S. L. Cunningham, and D. L. Mills, “Incompatibility of BCS pairing and the Peierls distortion in one-dimensional systems. II. Fluctuation effects,” *Physical Review B*, vol. 10, no. 9, pp. 3832–3843, 1974.
- [431] Yu. V. Kopayev, “About the interplay theory between electron and structural transformations and superconductivity,” *Trudy Fiz. Inst. Akad. Nauk SSSR*, vol. 86, p. 3, 1975.
- [432] C. A. Balseiro and L. M. Falicov, “Superconductivity and charge-density waves,” *Physical Review B*, vol. 20, no. 11, pp. 4457–4464, 1979.
- [433] A. M. Gabovich and E. A. Pashitskii, “About the existence of mixed phase superconductor-excitonic-insulator in intrinsic semimetals,” *Fizika Tverdogo Tela*, vol. 17, p. 1584, 1975.
- [434] Y. Ishida, T. Shimojima, K. Ishizaka, et al., “Temperature-dependent pseudogap in the oxypnictides  $\text{LaFeAsO}_{1-x}\text{F}_x$  and  $\text{LaFePO}_{1-x}\text{F}_x$  seen via angle-integrated photoemission,” *Physical Review B*, vol. 79, no. 6, Article ID 060503, 2009.
- [435] T. Mertelj, V. V. Kabanov, C. Gadermaier, et al., “Distinct pseudogap and quasiparticle relaxation dynamics in the superconducting state of nearly optimally doped  $\text{SmFeAsO}_{0.8}\text{F}_{0.2}$  single crystals,” *Physical Review Letters*, vol. 102, no. 11, Article ID 117002, 2009.
- [436] V. B. Zabolotnyy, D. S. Inosov, D. V. Evtushinsky, et al., “ $(\pi, \pi)$  electronic order in iron arsenide superconductors,” *Nature*, vol. 457, no. 7229, pp. 569–572, 2009.
- [437] R. H. Friend and D. Jérôme, “Periodic lattice distortions and charge density waves in one- and two-dimensional metals,” *Journal of Physics C*, vol. 12, no. 8, pp. 1441–1477, 1979.
- [438] P. B. Littlewood and V. Heine, “The effect of electron-electron interactions on the Peierls transition in metals with strong nesting of Fermi surfaces,” *Journal of Physics C*, vol. 14, no. 21, pp. 2943–2949, 1981.
- [439] M. Rotter, M. Tegel, D. Johrendt, I. Schellenberg, W. Hermes, and R. Pöttgen, “Spin-density-wave anomaly at 140 K in the ternary iron arsenide  $\text{BaFe}_2\text{As}_2$ ,” *Physical Review B*, vol. 78, no. 2, Article ID 020503, 2008.
- [440] N. Miyakawa, K. Tokiwa, S. Mikusu, et al., “Tunneling studies of multilayered superconducting cuprate  $\text{Ba}_2\text{Ca}_3\text{Cu}_4\text{O}_{12+\delta}$ ,” *International Journal of Modern Physics B*, vol. 17, no. 18–20, pp. 3612–3616, 2003.
- [441] K. K. Gomes, A. N. Pasupathy, A. Pushp, S. Ono, Y. Ando, and A. Yazdani, “Visualizing pair formation on the atomic scale in the high- $T_c$  superconductor  $\text{Bi}_2\text{Sr}_2\text{CaCu}_2\text{O}_{8+\delta}$ ,” *Nature*, vol. 447, no. 7144, pp. 569–572, 2007.
- [442] N. Miyakawa, K. Tokiwa, S. Mikusu, et al., “Tunneling spectroscopy of trilayer high- $T_c$  cuprate,  $\text{TlBa}_2\text{Ca}_2\text{Cu}_2\text{O}_{10+\delta}$ ,” *International Journal of Modern Physics B*, vol. 19, no. 1–3, pp. 225–229, 2005.
- [443] Y. DeWilde, N. Miyakawa, P. Guptasarma, et al., “Unusual strong-coupling effects in the tunneling spectroscopy of optimally doped and overdoped  $\text{Bi}_2\text{Sr}_2\text{CaCu}_2\text{O}_{8+\delta}$ ,” *Physical Review Letters*, vol. 80, no. 1, pp. 153–156, 1998.
- [444] M. Eschrig and M. R. Norman, “Neutron resonance: modeling photoemission and tunneling data in the superconducting state of  $\text{Bi}_2\text{Sr}_2\text{CaCu}_2\text{O}_{8+\delta}$ ,” *Physical Review Letters*, vol. 85, no. 15, pp. 3261–3264, 2000.
- [445] J.-X. Zhu, J. Sun, Q. Si, and A. V. Balatsky, “Effects of a collective spin resonance mode on the scanning tunneling microscopy spectra of  $d$ -wave superconductors,” *Physical Review Letters*, vol. 92, no. 1, Article ID 017002, 4 pages, 2004.
- [446] J. F. Zasadzinski, L. Ozyuzer, L. Coffey, K. E. Gray, D. G. Hinks, and C. Kendziora, “Persistence of strong electron coupling to a narrow boson spectrum in overdoped  $\text{Bi}_2\text{Sr}_2\text{CaCu}_2\text{O}_{8+\delta}$  tunneling data,” *Physical Review Letters*, vol. 96, no. 1, Article ID 017004, 2006.
- [447] J.-X. Zhu, A. V. Balatsky, T. P. Devereaux, et al., “Fourier-transformed local density of states and tunneling into a  $d$ -wave superconductor with bosonic modes,” *Physical Review B*, vol. 73, no. 1, Article ID 014511, 9 pages, 2006.
- [448] P. W. Anderson and N. P. Ong, “Theory of asymmetric tunneling in the cuprate superconductors,” *Journal of Physics and Chemistry of Solids*, vol. 67, no. 1–3, pp. 1–5, 2006.
- [449] G. L. de Castro, C. Berthod, A. Piriou, E. Giannini, and Ø. Fischer, “Preeminent role of the van Hove singularity in the strong-coupling analysis of scanning tunneling spectroscopy for two-dimensional cuprate superconductors,” *Physical Review Letters*, vol. 101, no. 26, Article ID 267004, 2008.
- [450] J. Nieminen, H. Lin, R. S. Markiewicz, and A. Bansil, “Origin of the electron-hole asymmetry in the scanning tunneling spectrum of the high-temperature  $\text{Bi}_2\text{Sr}_2\text{CaCu}_2\text{O}_{8+\delta}$  superconductor,” *Physical Review Letters*, vol. 102, no. 3, Article ID 037001, 2009.
- [451] J.-X. Liu, J.-C. Wan, A. M. Goldman, Y. C. Chang, and P. Z. Jiang, “Features of the density of states of high- $T_c$  superconductors probed by vacuum tunneling,” *Physical Review Letters*, vol. 67, no. 16, pp. 2195–2198, 1991.

- [452] T. Cren, D. Roditchev, W. Sacks, and J. Klein, "Nanometer scale mapping of the density of states in an inhomogeneous superconductor," *Europhysics Letters*, vol. 54, no. 1, pp. 84–90, 2001.
- [453] S. H. Pan, J. P. O'Neal, R. L. Badzey, et al., "Microscopic electronic inhomogeneity in the high- $T_c$  superconductor  $\text{Bi}_2\text{Sr}_2\text{CaCu}_2\text{O}_{8+x}$ ," *Nature*, vol. 413, no. 6853, pp. 282–285, 2001.
- [454] K. M. Lang, V. Madhavan, J. E. Hoffman, et al., "Imaging the granular structure of high- $T_c$  superconductivity in underdoped  $\text{Bi}_2\text{Sr}_2\text{CaCu}_2\text{O}_{8+\delta}$ ," *Nature*, vol. 415, no. 6870, pp. 412–416, 2002.
- [455] G. Kinoda, S. Nakao, T. Motohashi, et al., "Inhomogeneous electronic structures in heavily Pb-doped  $\text{Bi}_2\text{Sr}_2\text{CaCu}_2\text{O}_y$  single crystals probed by low temperature STM/STS," *Physica C*, vol. 388–389, pp. 273–274, 2003.
- [456] H. Mashima, N. Fukuo, Y. Matsumoto, et al., "Electronic inhomogeneity of heavily overdoped  $\text{Bi}_{2-x}\text{Pb}_x\text{Sr}_2\text{CuO}_y$  studied by low-temperature scanning tunneling microscopy/spectroscopy," *Physical Review B*, vol. 73, no. 6, Article ID 060502, 4 pages, 2006.
- [457] A. C. Fang, L. Capriotti, D. J. Scalapino, et al., "Gap-inhomogeneity-induced electronic states in superconducting  $\text{Bi}_2\text{Sr}_2\text{CaCu}_2\text{O}_{8+\delta}$ ," *Physical Review Letters*, vol. 96, no. 1, Article ID 017007, 2006.
- [458] J. A. Slezak, J. Lee, M. Wang, et al., "Imaging the impact on cuprate superconductivity of varying the interatomic distances within individual crystal unit cells," *Proceedings of the National Academy of Sciences of the United States of America*, vol. 105, no. 9, pp. 3203–3208, 2008.
- [459] K. Fujita, J. Lee, M. Wang, et al., "Imaging the effect of electron lattice interactions on high- $T_c$  superconductivity in  $\text{Bi}_2\text{Sr}_2\text{CaCu}_2\text{O}_{8+\delta}$ ," *Journal of Physics: Conference Series*, vol. 108, no. 1, Article ID 012028, 2008.
- [460] K. Anagawa, T. Watanabe, and M. Suzuki, "Superconducting gap and pseudogap for overdoped  $\text{Bi}_{2-x}\text{Pb}_x\text{Sr}_2\text{CaCu}_2\text{O}_{8+\delta}$  using 60 ns time-scale short-pulse interlayer tunneling spectroscopy," *Physical Review B*, vol. 73, no. 18, Article ID 184512, 2006.
- [461] Y. Yamada and M. Suzuki, "Interlayer tunneling spectroscopy for deeply underdoped  $\text{Bi}_2\text{Sr}_2\text{CaCu}_2\text{O}_{8+\delta}$ : spectroscopic evidence for inhomogeneous superconductivity," *Physical Review B*, vol. 74, Article ID 054508, 2006.
- [462] S. Johnston, F. Vernay, and T. P. Devereaux, "Impact of an oxygen dopant in  $\text{Bi}_2\text{Sr}_2\text{CaCu}_2\text{O}_{8+\delta}$ ," *Europhysics Letters*, vol. 86, p. 37007, 2009.
- [463] J.-H. Ma, Z.-H. Pan, F. C. Niestemski, et al., "Coexistence of competing orders with two energy gaps in real and momentum space in the high temperature superconductor  $\text{Bi}_2\text{Sr}_{2-x}\text{La}_x\text{CuO}_{6+\delta}$ ," *Physical Review Letters*, vol. 101, no. 20, Article ID 207002, 2008.
- [464] J. L. Tallon and J. W. Loram, "Comment on "thermodynamic transitions in inhomogeneous  $d$ -wave superconductors"" *Physical Review B*, vol. 79, no. 9, Article ID 096501, 2009.
- [465] A. Gutiérrez-Sosa, U. Bangert, and W. R. Flavell, "Investigations of chemical and electronic inhomogeneities in  $\text{BaPb}_{1-x}\text{Bi}_x\text{O}_3$  via highly spatially resolved electron energy loss spectroscopy," *Journal of Applied Physics*, vol. 94, no. 10, pp. 6639–6643, 2003.
- [466] I. Roshchin, V. Stepankin, and A. Kuznetsov, "Reentrant superconducting transport behavior of single grain boundary Josephson junction in  $\text{BaPb}_{1-x}\text{Bi}_x\text{O}_3$  bicrystals," *Journal of Low Temperature Physics*, vol. 100, no. 3–4, pp. 229–240, 1995.
- [467] E. L. Nagaev, "Ground state and anomalous magnetic moment of conduction electrons in an antiferromagnetic semiconductor," *Pis'ma Zhurnal Eksperimental'noi i Teoreticheskoi Fiziki*, vol. 6, p. 484, 1967.
- [468] E. L. Nagaev, "Ferromagnetic domains in a semiconducting antiferromagnet," *Zhurnal Eksperimental'noi i Teoreticheskoi Fiziki*, vol. 54, p. 228, 1968.
- [469] E. L. Nagaev, *Physics of Magnetic Semiconductors*, Nauka, Moscow, Russia, 1979.
- [470] E. L. Nagaev, "Phase separation in high-temperature superconductors and related magnetic systems," *Uspekhi Fizicheskikh Nauk*, vol. 165, p. 529, 1995.
- [471] M. A. Krivoglaz, "Electron states near the phase transition point and in disordered systems," *Fizika Tverdogo Tela*, vol. 11, p. 2230, 1969.
- [472] M. A. Krivoglaz, "Fluctuonic states of electrons," *Uspekhi Fizicheskikh Nauk*, vol. 111, p. 617, 1973.
- [473] M. A. Krivoglaz and A. I. Karasevskii, "Condensation in in the system of polarons or fluctuations with the formation of the nonhomogeneous state and peculiarities of conductance," *Pis'ma Zhurnal Eksperimental'noi i Teoreticheskoi Fiziki*, vol. 19, p. 454, 1974.
- [474] M. A. Krivoglaz, *Diffuse Scattering of X-Rays and Neutrons by Fluctuations*, Springer, Berlin, Germany, 1996.
- [475] J. M. Tranquada, B. J. Sternlieb, J. D. Axe, Y. Nakamura, and S. Uchida, "Evidence for stripe correlations of spins and holes in copper oxide superconductors," *Nature*, vol. 375, no. 6532, pp. 561–563, 1995.
- [476] J. M. Tranquada, "Phase separation, charge segregation and superconductivity in layered cuprates," in *Neutron Scattering in Layered Copper-Oxide Superconductors*, A. Furrer, Ed., pp. 225–260, Kluwer Academic Publishers, Dordrecht, The Netherlands, 1998.
- [477] M. B. Salamon and M. Jaime, "The physics of manganites: structure and transport," *Reviews of Modern Physics*, vol. 73, no. 3, pp. 583–628, 2001.
- [478] A. Damascelli, Z. Hussain, and Z.-X. Shen, "Angle-resolved photoemission studies of the cuprate superconductors," *Reviews of Modern Physics*, vol. 75, no. 2, pp. 473–541, 2003.
- [479] T. Yanagisawa, "Lattice distortions and stripes in the underdoped region of high- $T_c$  cuprates," *Journal of Physics A*, vol. 36, no. 35, pp. 9337–9349, 2003.
- [480] J. M. Tranquada, H. Woo, T. G. Perring, et al., "Quantum magnetic excitations from stripes in copper oxide superconductors," *Nature*, vol. 429, no. 6991, pp. 534–538, 2004.
- [481] O. N. Bakharev, I. M. Abu-Shiekh, H. B. Brom, A. A. Nugroho, I. P. McCulloch, and J. Zaanen, "NMR evidence for a two-step phase separation in  $\text{Nd}_{1.85}\text{Ce}_{0.15}\text{CuO}_{4-\delta}$ ," *Physical Review Letters*, vol. 93, no. 3, Article ID 037002, 1 pages, 2004.
- [482] C. J. Zhang and H. Oyanagi, "Effects of local lattice disorder on the superconductivity studied by XAFS," *Journal of Physics: Conference Series*, vol. 108, no. 1, Article ID 012048, 2008.
- [483] H. Oyanagi, C. Zhang, A. Tsukada, and M. Naito, "Lattice instability in high temperature superconducting cuprates probed by X-ray absorption spectroscopy," *Journal of Physics: Conference Series*, vol. 108, no. 1, Article ID 012038, 2008.
- [484] Y. Koike, T. Adachi, Y. Tanabe, K. Omori, T. Noji, and H. Sato, "Inhomogeneous superconductivity in both underdoped and overdoped regimes of high- $T_c$  cuprates," *Journal of Physics: Conference Series*, vol. 108, no. 1, Article ID 012003, 2008.
- [485] H. Keller, A. Bussmann-Holder, and K. A. Müller, "Jahn-Teller physics and high- $T_c$  superconductivity," *Materials Today*, vol. 11, no. 9, pp. 38–46, 2008.

- [486] J. C. Phillips, A. Saxena, and A. R. Bishop, "Pseudogaps, dopants, and strong disorder in cuprate high-temperature superconductors," *Reports on Progress in Physics*, vol. 66, no. 12, pp. 2111–2182, 2003.
- [487] R. A. Klemm, "The pseudogap and the superconducting order parameter in inhomogeneous  $\text{Bi}_2\text{Sr}_2\text{CaCu}_2\text{O}_{8+\delta}$ ," *Journal of Superconductivity and Novel Magnetism*, vol. 17, no. 1, pp. 69–74, 2004.
- [488] J. C. Phillips, "Quantum percolation in cuprate high-temperature superconductors," *Proceedings of the National Academy of Sciences of the United States of America*, vol. 105, no. 29, pp. 9917–9919, 2008.
- [489] F. V. Kusmartsev and M. Saarela, "What is the most important for a nanoscale structure formations in HTSC? Spin, phonon or third way in Coulomb interaction and correlations?" *Journal of Physics: Conference Series*, vol. 108, no. 1, Article ID 012029, 2008.
- [490] F. V. Kusmartsev and M. Saarela, "Two-component physics of cuprates and superconductor-insulator transitions," *Superconductor Science and Technology*, vol. 22, no. 1, Article ID 014008, 2009.
- [491] B. Fine and T. Egami, "Intermediate spin-charge order in the cuprates," *Journal of Physics: Conference Series*, vol. 108, no. 1, Article ID 012005, 2008.
- [492] M. Müller and B. I. Shklovskii, "Compensation-driven superconductor-insulator transition," *Physical Review B*, vol. 79, no. 13, Article ID 134504, 2009.
- [493] A. S. Alexandrov, "Phase separation of electrons strongly coupled with phonons in cuprates and manganites," *Journal of Superconductivity and Novel Magnetism*, vol. 22, no. 2, pp. 95–101, 2009.
- [494] J. T. Park, D. S. Inosov, Ch. Niedermayer, et al., "Electronic phase separation in the slightly underdoped iron pnictide superconductor  $\text{Ba}_{1-x}\text{K}_x\text{Fe}_2\text{As}_2$ ," *Physical Review Letters*, vol. 102, no. 11, Article ID 117006, 2009.
- [495] B. Sacépé, C. Chapelier, T. I. Baturina, V. M. Vinokur, M. R. Baklanov, and M. Sanquer, "Disorder-induced inhomogeneities of the superconducting state close to the superconductor-insulator transition," *Physical Review Letters*, vol. 101, no. 15, Article ID 157006, 2008.
- [496] H. L. Edwards, A. L. Barr, J. T. Markert, and A. L. De Lozanne, "Modulations in the  $\text{CuO}$  chain layer of  $\text{YBa}_2\text{Cu}_3\text{O}_{7-\delta}$ : charge density waves?" *Physical Review Letters*, vol. 73, no. 8, pp. 1154–1157, 1994.
- [497] D. J. Derro, E. W. Hudson, K. M. Lang, et al., "Nanoscale one-dimensional scattering resonances in the  $\text{CuO}$  chains of  $\text{YBa}_2\text{Cu}_3\text{O}_{6+x}$ ," *Physical Review Letters*, vol. 88, no. 9, Article ID 097002, 4 pages, 2002.
- [498] A. A. Abrikosov, *Fundamentals of the Theory of Metals*, North-Holland, Amsterdam, The Netherlands, 1987.
- [499] K. McElroy, R. W. Simmonds, J. E. Hoffman, et al., "Relating atomic-scale electronic phenomena to wave-like quasiparticle states in superconducting  $\text{Bi}_2\text{Sr}_2\text{CaCu}_2\text{O}_{8+\delta}$ ," *Nature*, vol. 422, no. 6932, pp. 592–596, 2003.
- [500] T. Pereg-Barnea and M. Franz, "Theory of quasiparticle interference patterns in the pseudogap phase of the cuprate superconductors," *Physical Review B*, vol. 68, no. 18, Article ID 180506, 4 pages, 2003.
- [501] T. Pereg-Barnea and M. Franz, "Quasiparticle interference patterns as a test for the nature of the pseudogap phase in the cuprate superconductors," *International Journal of Modern Physics B*, vol. 19, no. 4, pp. 731–761, 2005.
- [502] T. S. Nunner, W. Chen, B. M. Andersen, A. Melikyan, and P. J. Hirschfeld, "Fourier transform spectroscopy of  $d$ -wave quasiparticles in the presence of atomic scale pairing disorder," *Physical Review B*, vol. 73, no. 10, Article ID 104511, 7 pages, 2006.
- [503] T. Hanaguri, Y. Kohsaka, J. C. Davis, et al., "Quasiparticle interference and superconducting gap in  $\text{Ca}_{2-x}\text{Na}_x\text{CuO}_2\text{Cl}_2$ ," *Nature Physics*, vol. 3, no. 12, pp. 865–871, 2007.
- [504] Y. Kohsaka, C. Taylor, P. Wahl, et al., "How Cooper pairs vanish approaching the Mott insulator in  $\text{Bi}_2\text{Sr}_2\text{CaCu}_2\text{O}_{8+\delta}$ ," *Nature*, vol. 454, no. 7208, pp. 1072–1078, 2008.
- [505] T. Hanaguri, Y. Kohsaka, M. Ono, et al., "Coherence factors in a high- $T_c$  cuprate probed by quasi-particle scattering off vortices," *Science*, vol. 323, no. 5916, pp. 923–926, 2009.
- [506] C. Howald, H. Eisaki, N. Kaneko, M. Greven, and A. Kapitulnik, "Periodic density-of-states modulations in superconducting  $\text{Bi}_2\text{Sr}_2\text{CaCu}_2\text{O}_{8+\delta}$ ," *Physical Review B*, vol. 67, no. 1, Article ID 014533, 10 pages, 2003.
- [507] T. Hanaguri, C. Lupien, Y. Kohsaka, et al., "A 'checkerboard' electronic crystal state in lightly hole-doped  $\text{Ca}_{2-x}\text{Na}_x\text{CuO}_2\text{Cl}_2$ ," *Nature*, vol. 430, no. 7003, pp. 1001–1005, 2004.
- [508] Y. Kohsaka, C. Taylor, K. Fujita, et al., "An intrinsic bond-centered electronic glass with unidirectional domains in underdoped cuprates," *Science*, vol. 315, no. 5817, pp. 1380–1385, 2007.
- [509] M. F. Crommie, C. P. Lutz, and D. M. Eigler, "Imaging standing waves in a two-dimensional electron gas," *Nature*, vol. 363, no. 6429, pp. 524–527, 1993.
- [510] G. A. Fiete and E. J. Heller, "Colloquium: theory of quantum corrals and quantum mirages," *Reviews of Modern Physics*, vol. 75, no. 3, pp. 933–948, 2003.
- [511] J. Friedel, "Metallic alloys," *Il Nuovo Cimento*, vol. 7, supplement 2, pp. 287–311, 1958.
- [512] J. E. Hoffman, K. McElroy, D.-H. Lee, et al., "Imaging quasiparticle interference in  $\text{Bi}_2\text{Sr}_2\text{CaCu}_2\text{O}_{8+\delta}$ ," *Science*, vol. 297, no. 5584, pp. 1148–1151, 2002.
- [513] A. M. Gabovich and E. A. Pashitskii, "Polarization operator of the superconducting electron gas. Kohn anomalies and charge screening in superconductors," *Ukrainskii Fizychnyi Zhurnal*, vol. 18, p. 549, 1973.
- [514] J. P. Hurault, "Note sur les polarisations de spin et de charge autour d'une impurete dans un supraconducteur," *Journal de Physique*, vol. 26, p. 252, 1965.
- [515] A. M. Gabovich, L. G. Il'chenko, and E. A. Pashitskii, *Fizika Tverdogo Tela*, vol. 21, p. 2191, 1979.
- [516] G. Grüner, *Density Waves in Solids*, Addison-Wesley, Reading, Mass, USA, 1994.
- [517] T. M. Rice and G. K. Scott, "New mechanism for a charge-density-wave instability," *Physical Review Letters*, vol. 35, no. 2, pp. 120–123, 1975.
- [518] R. S. Markiewicz, "A survey of the Van Hove scenario for high- $T_c$  superconductivity with special emphasis on pseudogaps and striped phases," *Journal of Physics and Chemistry of Solids*, vol. 58, no. 8, pp. 1179–1310, 1997.
- [519] R. Peierls, "Zur Theorie der elektrischen und thermischen Leitfähigkeit von Metallen," *Annals of Physics*, vol. 4, p. 121, 1930.
- [520] R. E. Peierls, *Quantum Theory of Solids*, Clarendon Press, Oxford, UK, 1955.
- [521] L. V. Keldysh and Yu. V. Kopayev, *Fizika Tverdogo Tela*, vol. 6, p. 2791, 1964.

- [522] B. I. Halperin and T. M. Rice, "The excitonic state at the semiconductor-semimetal transition," in *Solid State Physics*, vol. 21, p. 115, Academic Press, New York, NY, USA, 1968.
- [523] A. N. Kozlov and L. A. Maksimov, "On the metal-insulator phase transition. Divalent crystal," *Zhurnal Eksperimental'noi i Teoreticheskoi Fiziki*, vol. 48, p. 1184, 1965.
- [524] T. Ishiguro and K. Yamaji, *Organic Superconductors*, Springer, Berlin, Germany, 1990.
- [525] C. Schlenker, J. Dumas, M. Greenblatt, and S. van Smaalen, Eds., *Physics and Chemistry of Low-Dimensional Inorganic Conductors*, Plenum Press, New York, NY, USA, 1996.
- [526] B. Kyung, "Mean-field study of the interplay between antiferromagnetism and  $d$ -wave superconductivity," *Physical Review B*, vol. 62, no. 13, pp. 9083–9088, 2000.
- [527] H. Wilhelm, D. Jaccard, R. Duprat, et al., "The case for universality of the phase diagram of the Fabre and Bechgaard salts," *European Physical Journal B*, vol. 21, no. 2, pp. 175–183, 2001.
- [528] C. Colin, C. R. Pasquier, and K. Bechgaard, "Multi-phase coexistence in the organic conductor (TMTSF)<sub>2</sub>ReO<sub>4</sub>," *Journal de Physique*, vol. 131, pp. 313–314, 2005.
- [529] A. Aperis, G. Varelogiannis, P. B. Littlewood, and B. D. Simons, "Coexistence of spin density wave,  $d$ -wave singlet and staggered  $\pi$ -triplet superconductivity," *Journal of Physics: Condensed Matter*, vol. 20, Article ID 434235, 5 pages, 2008.
- [530] J. T. Devreese, R. P. Evrard, and V. E. van Doren, Eds., *Highly Conducting One-Dimensional Solids*, Plenum Press, New York, NY, USA, 1979.
- [531] P. Monceau, Ed., *Electronic Properties of Inorganic Quasi-One-Dimensional Compounds—Part II: Experimental*, D. Reidel, Dordrecht, The Netherlands, 1985.
- [532] S. Roth and D. Carroll, *One-Dimensional Metals*, Wiley-VCH, Weinheim, Germany, 2004.
- [533] M. J. Rice and Yu. N. Gartstein, "The excitonic ground state of the half-filled Peierls insulator," *Journal of Physics: Condensed Matter*, vol. 17, no. 29, pp. 4615–4620, 2005.
- [534] W. Kohn and D. Sherrington, "Two kinds of bosons and bose condensates," *Reviews of Modern Physics*, vol. 42, no. 1, pp. 1–11, 1970.
- [535] H. Cercellier, C. Monney, F. Clerc, et al., "Evidence for an excitonic insulator phase in  $1T$ -TiSe<sub>2</sub>," *Physical Review Letters*, vol. 99, no. 14, Article ID 146403, 4 pages, 2007.
- [536] C. Monney, H. Cercellier, F. Clerc, et al., "Spontaneous exciton condensation in  $1T$ -TiSe<sub>2</sub>: BCS-like approach," *Physical Review B*, vol. 79, no. 4, Article ID 045116, 11 pages, 2009.
- [537] B. Bucher, P. Steiner, and P. Wachter, "Excitonic insulator phase in TmSe<sub>0.45</sub>Te<sub>0.55</sub>," *Physical Review Letters*, vol. 67, no. 19, pp. 2717–2720, 1991.
- [538] P. Wachter, A. Jung, and P. Steiner, "Pressure-driven metal-insulator transition in La-doped SmS: excitonic condensation," *Physical Review B*, vol. 51, no. 8, pp. 5542–5545, 1995.
- [539] Y. Wakisaka, T. Suda, K. Takubo, et al., "Excitonic insulator state in Ta<sub>2</sub>NiSe<sub>5</sub> probed by photoemission spectroscopy," *Physical Review Letters*, vol. 103, no. 2, Article ID 026402, 4 pages, 2009.
- [540] J. Zaanen, "Superconductivity: quantum stripe search," *Nature*, vol. 440, no. 7088, pp. 1118–1119, 2006.
- [541] P. Wróbel, "Checkerboard or stripes: hard-core bosons on the checkerboard lattice as a model of charge ordering in planar cuprates," *Physical Review B*, vol. 74, no. 1, Article ID 014507, 8 pages, 2006.
- [542] V. Cvetkovic, Z. Nussinov, S. Mukhin, and J. Zaanen, "Observing the fluctuating stripes in high- $T_c$  superconductors," *Europhysics Letters*, vol. 81, no. 2, Article ID 27001, 6 pages, 2008.
- [543] C. W. Misner, K. S. Thorne, and W. H. Zurek, "John Wheeler, relativity, and quantum information," *Physics Today*, vol. 62, no. 4, pp. 40–46, 2009.
- [544] P. Abbamonte, A. Rusydi, S. Smadici, G. D. Gu, G. A. Sawatzky, and D. L. Feng, "Spatially modulated 'Mottness' in La<sub>2-x</sub>Ba<sub>x</sub>CuO<sub>4</sub>," *Nature Physics*, vol. 1, pp. 155–158, 2005.
- [545] M. Fujita, H. Goka, K. Yamada, and M. Matsuda, "Competition between charge- and spin-density-wave order and superconductivity in La<sub>1.875</sub>Ba<sub>0.125-x</sub>Sr<sub>x</sub>CuO<sub>4</sub>," *Physical Review Letters*, vol. 88, no. 16, Article ID 167008, 4 pages, 2002.
- [546] J. Fink, E. Schierle, E. Weschke, et al., "Charge ordering in La<sub>1.8-x</sub>Eu<sub>0.2</sub>Sr<sub>x</sub>CuO<sub>4</sub> studied by resonant soft X-ray diffraction," *Physical Review B*, vol. 79, no. 10, Article ID 100502, 4 pages, 2009.
- [547] C. M. Varma, "Non-Fermi-liquid states and pairing instability of a general model of copper oxide metals," *Physical Review B*, vol. 55, no. 21, pp. 14554–14580, 1997.
- [548] H. J. Schulz, "Fermi-surface instabilities of a generalized two-dimensional Hubbard model," *Physical Review B*, vol. 39, no. 4, pp. 2940–2943, 1989.
- [549] S. Chakravarty, R. B. Laughlin, D. K. Morr, and C. Nayak, "Hidden order in the cuprates," *Physical Review B*, vol. 63, no. 9, Article ID 094503, 10 pages, 2001.
- [550] D. Jérôme, C. Berthier, P. Molinié, and J. Rouxel, "Layer compounds. Charge density waves in transition metal compounds. Electronic properties of transition metal dichalcogenides: connection between structural instabilities and superconductivity," *Journal de Physique*, vol. 37, pp. C4–C125, 1976.
- [551] O. Degtyareva, M. V. Magnitskaya, J. Kohanoff, et al., "Competition of charge-density waves and superconductivity in sulfur," *Physical Review Letters*, vol. 99, Article ID 155505, 4 pages, 2007.
- [552] K. Kudo, N. Okumura, Y. Miyoshi, T. Nishizaki, T. Sasaki, and N. Kobayashi, "Narrow carrier concentration range of superconductivity and critical point of pseudogap formation temperature in Pb-substituted Bi<sub>2</sub>Sr<sub>2</sub>CuO<sub>6+δ</sub>," *Journal of the Physical Society of Japan*, vol. 78, no. 8, Article ID 084722, 5 pages, 2009.
- [553] H. Won and K. Maki, " $d$ -wave superconductor as a model of high- $T_c$  superconductors," *Physical Review B*, vol. 49, no. 2, pp. 1397–1402, 1994.
- [554] H. Won, K. Maki, and E. Puchkaryov, in *High- $T_c$  Superconductors and Related Materials: Material Science, Fundamental Properties, and Some Future Electronic Applications*, S. L. Drechsler and T. Mishonov, Eds., p. 375, Kluwer Academic, Dordrecht, The Netherlands, 2001.
- [555] H. Won, S. Haas, D. Parker, S. Telang, A. Ványolos, and K. Maki, in *Lectures on the Physics of Highly Correlated Electron Systems IX: Ninth Training Course*, A. Avella and F. Mancini, Eds., p. 3, American Institute of Physics, Melville, NY, USA, 2005.
- [556] A. M. Gabovich and A. I. Voitenko, "Josephson tunnelling involving superconductors with charge-density waves," *Journal of Physics: Condensed Matter*, vol. 9, no. 19, pp. 3901–3920, 1997.
- [557] A. M. Gabovich and A. I. Voitenko, "Asymmetrical tunneling between similar metallic junctions with charge-density or spin-density waves: the case of broken symmetry," *Physical Review B*, vol. 56, no. 13, pp. 7785–7788, 1997.

- [558] B. Mühlischlegel, “Die thermodynamischen Funktionen des Supraleiters,” *Zeitschrift für Physik A*, vol. 155, no. 3, pp. 313–327, 1959.
- [559] V. M. Krasnov, “Temperature dependence of the bulk energy gap in underdoped  $\text{Bi}_2\text{Sr}_2\text{CaCu}_2\text{O}_{8+\delta}$ : evidence for the mean-field superconducting transition,” *Physical Review B*, vol. 79, no. 21, Article ID 214510, 17 pages, 2009.
- [560] M. Suzuki and T. Watanabe, “Discriminating the superconducting gap from the pseudogap in  $\text{Bi}_2\text{Sr}_2\text{CaCu}_2\text{O}_{8+\delta}$  by interlayer tunneling spectroscopy,” *Physical Review Letters*, vol. 85, no. 22, pp. 4787–4790, 2000.
- [561] T. Ekino, S. Hashimoto, T. Takasaki, and H. Fujii, “Tunneling spectroscopy of the normal-state gap in  $(\text{Bi, Pb})_2\text{Sr}_2\text{Ca}_2\text{Cu}_3\text{O}_{10+\delta}$ ,” *Physical Review B*, vol. 64, no. 9, Article ID 092510, 4 pages, 2001.
- [562] T. Ekino, Y. Sezaki, S. Hashimoto, and H. Fujii, “Observation of the energy gap above  $(\text{Bi, Pb})_2\text{Sr}_2\text{Ca}_2\text{Cu}_3\text{O}_{10+\delta}$  using break-junction tunneling,” *Journal of Low Temperature Physics*, vol. 117, no. 3-4, pp. 359–363, 1999.
- [563] A. Sugimoto, T. Ekino, and H. Eisaki, “Nanoscale modulation of local barrier height on Bi-based cuprate superconductors observed by scanning tunneling microscopy/spectroscopy,” *Journal of the Physical Society of Japan*, vol. 77, no. 4, Article ID 043705, 4 pages, 2008.
- [564] J. W. Alldredge, J. Lee, K. McElroy, et al., “Evolution of the electronic excitation spectrum with strongly diminishing hole density in superconducting  $\text{Bi}_2\text{Sr}_2\text{CaCu}_2\text{O}_{8+\delta}$ ,” *Nature Physics*, vol. 4, no. 4, pp. 319–326, 2008.
- [565] Y. Kohsaka, K. Iwaya, S. Satow, M. Azuma, M. Takano, and H. Takagi, “Imaging nanoscale electronic inhomogeneity in the lightly doped mott insulator  $\text{Ca}_{2-x}\text{Na}_x\text{CuO}_2\text{Cl}_2$ ,” *Physical Review Letters*, vol. 93, no. 9, Article ID 097004, 4 pages, 2004.
- [566] A. M. Gabovich and A. S. Shpigel, *Fizika Tverdogo Tela*, vol. 26, p. 1569, 1984.
- [567] R. Escudero, F. Morales, and S. Bernès, “Specific heat studies of pure  $\text{Nb}_3\text{Sn}$  single crystals at low temperature,” *Journal of Physics: Condensed Matter*, vol. 21, no. 32, Article ID 325701, 7 pages, 2009.
- [568] N. E. Phillips, R. A. Fisher, and J. E. Gordon, in *Progress in Low Temperature Physics*, vol. 13, p. 267, Elsevier, Amsterdam, The Netherlands, 1992.
- [569] J. W. Loram, K. A. Mirza, W. Y. Liang, and J. Osborne, “A systematic study of the specific heat anomaly in  $\text{La}_{2-x}\text{Sr}_x\text{CuO}_4$ ,” *Physica C*, vol. 162–164, part 1, pp. 498–499, 1989.
- [570] J. L. Tallon and J. W. Loram, “Doping dependence of  $T^*$ —what is the real high- $T_c$  phase diagram?” *Physica C*, vol. 349, no. 1-2, pp. 53–68, 2001.
- [571] H.-H. Wen, G. Mu, H. Luo, et al., “Specific-heat measurement of a residual superconducting state in the normal state of underdoped  $\text{Bi}_2\text{Sr}_{2-x}\text{La}_x\text{CuO}_{6+\delta}$  cuprate superconductors,” *Physical Review Letters*, vol. 103, no. 6, Article ID 067002, 4 pages, 2009.
- [572] B. Krunavakarn, S. Kaskamalas, and S. Yoksan, “Thermodynamic properties of a BCS superconductor,” *Physica C*, vol. 338, no. 4, pp. 305–315, 2000.
- [573] H. Balci and R. L. Greene, “Thermodynamic properties of  $\text{Pr}_{1.85}\text{Ce}_{0.15}\text{CuO}_{4-\delta}$ ,” *Physical Review B*, vol. 70, no. 14, Article ID 140508, 4 pages, 2004.
- [574] C. E. Methfessel, A. R. Stewart, B. T. Matthias, and C. K. N. Patel, “Why is there no bulk specific heat anomaly at the superconducting transition temperature of  $\text{BaPb}_{1-x}\text{Bi}_x\text{O}_3$ ?” *Proceedings of the National Academy of Sciences of the United States of America*, vol. 77, no. 11, pp. 6307–6308, 1980.
- [575] S. Tanaka, K. Kitazawa, and T. Tani, *Annual Report of the Engineering Research Institute, Faculty of Engineering, University of Tokyo*, vol. 41, p. 131, 1982.
- [576] M. Sato, H. Fujishita, and S. Hoshino, “Specific heat anomaly of  $\text{BaPb}_{1-x}\text{Bi}_x\text{O}_3$  at the superconducting transition,” *Journal of Physics C*, vol. 16, no. 13, pp. L417–L421, 1983.
- [577] B. B. Schwartz and S. Foner, “Large-scale applications of superconductivity,” *Physics Today*, vol. 30, p. 34, 1977.
- [578] D. Larbalestier, G. Fisk, B. Montgomery, and D. Hawksworth, “High-field superconductivity,” *Physics Today*, vol. 39, no. 3, pp. 24–35, 1986.
- [579] D. Larbalestier, A. Gurevich, D. M. Feldmann, and A. Polyanskii, “High- $T_c$  superconducting materials for electric power applications,” *Nature*, vol. 414, no. 6861, pp. 368–377, 2001.
- [580] S. Kang, A. Goyal, J. Li, et al., “High-performance high- $T_c$  superconducting wires,” *Science*, vol. 311, no. 5769, pp. 1911–1914, 2006.
- [581] A. M. Clogston, “Upper limit for the critical field in hard superconductors,” *Physical Review Letters*, vol. 9, no. 6, pp. 266–267, 1962.
- [582] B. S. Chandrasekhar, “A note on the maximum critical field of high-field superconductors,” *Applied Physics Letters*, vol. 1, no. 1, pp. 7–8, 1962.
- [583] P. Fulde, “High field superconductivity in thin films,” *Advances in Physics*, vol. 22, no. 6, pp. 667–719, 1973.
- [584] R. C. Bruno and B. B. Schwartz, “Magnetic field splitting of the density of states of thin superconductors,” *Physical Review B*, vol. 8, no. 7, pp. 3161–3178, 1973.
- [585] P. M. Tedrow and R. Meservey, “Experimental test of the theory of high-field superconductivity,” *Physical Review Letters*, vol. 43, no. 5, pp. 384–387, 1979.
- [586] R. G. Dias and J. A. Silva, “Huge metastability in high- $T_c$  superconductors induced by parallel magnetic field,” *Physical Review B*, vol. 67, no. 9, Article ID 092511, 4 pages, 2003.
- [587] A. M. Gabovich, E. A. Pashitskii, and A. S. Shpigel, “Exceeding of paramagnetic limit in superconductors with dielectric gap on the Fermi surface,” *Zhurnal Eksperimental’noi i Teoreticheskoi Fiziki*, vol. 28, p. 302, 1978.
- [588] A. M. Gabovich, E. A. Pashitskii, and A. S. Shpigel, “Paramagnetic limit of superconductors with a dielectric gap on the Fermi surface,” *Zhurnal Eksperimental’noi i Teoreticheskoi Fiziki*, vol. 77, p. 1157, 1979.
- [589] A. Gabovich, A. I. Voitenko, and T. Ekino, “Enhanced paramagnetic limit of the upper critical magnetic field for superconductors with charge-density waves,” *Journal of Physics: Condensed Matter*, vol. 16, no. 21, pp. 3681–3690, 2004.
- [590] R. H. McKenzie, “Is the ground state of  $\alpha$ -(BEDT-TTF) $_2\text{MHg}(\text{SCN})_4$  [M = K, Rb, Tl] a charge-density wave or a spin-density wave?” <http://arxiv.org/abs/cond-mat/9706235>.
- [591] N. Harrison, “Destabilization of a charge-density wave by an oscillatory chemical potential,” *Physical Review Letters*, vol. 83, no. 7, pp. 1395–1398, 1999.
- [592] J. S. Qualls, L. Balicas, J. S. Brooks, N. Harrison, L. K. Montgomery, and M. Tokumoto, “Competition between Pauli and orbital effects in a charge-density-wave system,” *Physical Review B*, vol. 62, no. 15, pp. 10008–10012, 2000.
- [593] L. D. Landau and E. M. Lifshits, *Electrodynamics of Continuous Media*, Pergamon, New York, NY, USA, 1984.
- [594] N. P. Ong and P. Monceau, “Anomalous transport properties of a linear-chain metal:  $\text{NbSe}_3$ ,” *Physical Review B*, vol. 16, no. 8, pp. 3443–3455, 1977.

- [595] S. Sugai, Y. Takayanagi, and N. Hayamizu, "Phason and amplitudon in the charge-density-wave phase of one-dimensional charge stripes in  $\text{La}_{2-x}\text{Sr}_x\text{CuO}_4$ ," *Physical Review Letters*, vol. 96, no. 13, Article ID 137003, 4 pages, 2006.
- [596] A. M. Gabovich and A. I. Voitenko, "Nonstationary Josephson effect for superconductors with charge-density waves," *Physical Review B*, vol. 55, no. 2, pp. 1081–1099, 1997.
- [597] N. Miyakawa, J. F. Zasadzinski, L. Ozyuzer, et al., "Predominantly superconducting origin of large energy gaps in underdoped  $\text{Bi}_2\text{Sr}_2\text{CaCu}_2\text{O}_{8+\delta}$  from tunneling spectroscopy," *Physical Review Letters*, vol. 83, no. 5, pp. 1018–1021, 1999.
- [598] Ch. Renner, B. Revaz, J.-Y. Genoud, K. Kadowakj, and Ø. Fischer, "Pseudogap precursor of the superconducting gap in under- and overdoped  $\text{Bi}_2\text{Sr}_2\text{CaCu}_2\text{O}_{8+\delta}$ ," *Physical Review Letters*, vol. 80, no. 1, pp. 149–152, 1998.
- [599] A. K. Gupta and K.-W. Ng, "ab-plane tunneling spectroscopy of underdoped  $\text{Bi}_2\text{Sr}_2\text{CaCu}_2\text{O}_y$ ," *Physical Review B*, vol. 58, no. 14, pp. R8901–R8904, 1998.
- [600] J. F. Zasadzinski, L. Ozyuzer, N. Miyakawa, K. E. Gray, D. G. Hinks, and C. Kendziora, "Correlation of tunneling spectra in  $\text{Bi}_2\text{Sr}_2\text{CaCu}_2\text{O}_{8+\delta}$  with the resonance spin excitation," *Physical Review Letters*, vol. 87, no. 6, Article ID 067005, 4 pages, 2001.
- [601] D. N. Dias, E. S. Caixeiro, and E. V. L. de Mello, "Magnetic properties of cuprate superconductors based on a phase separation theory," *Physica C*, vol. 468, no. 6, pp. 480–486, 2008.
- [602] A. Bille, R. A. Klemm, and K. Scharnberg, "Models of c-axis twist Josephson tunneling," *Physical Review B*, vol. 64, no. 17, Article ID 174507, 23 pages, 2001.
- [603] A. I. Larkin and Yu. N. Ovchinnikov, "Tunnel effect between superconductors in an alternating field," *Zhurnal Eksperimental'noi i Teoreticheskoi Fiziki*, vol. 51, p. 1535, 1966.
- [604] W. A. Roshen, "Thermodynamic properties of charge-density waves," *Physical Review B*, vol. 31, no. 11, pp. 7296–7305, 1985.
- [605] I. Báldea, "Reentrant charge-density wave in the one-dimensional system with impurities—a self-consistent approach," *Physica Scripta*, vol. 42, no. 6, pp. 749–760, 1990.
- [606] J. Zittartz, "Theory of the excitonic insulator in the presence of normal impurities," *Physical Review*, vol. 164, no. 2, pp. 575–582, 1967.
- [607] A. A. Abrikosov and L. P. Gor'kov, "On the theory of superconducting alloys. 1. Electrodynamics of alloys at the absolute zero," *Zhurnal Eksperimental'noi i Teoreticheskoi Fiziki*, vol. 35, p. 1558, 1958.
- [608] A. A. Abrikosov and L. P. Gor'kov, "Superconducting alloys at temperatures above the absolute zero," *Zhurnal Eksperimental'noi i Teoreticheskoi Fiziki*, vol. 36, p. 319, 1959.
- [609] P. W. Anderson, "Theory of dirty superconductors," *Journal of Physics and Chemistry of Solids*, vol. 11, no. 1-2, pp. 26–30, 1959.
- [610] H. Kim, G. Preosti, and P. Muzikar, "Penetration depth and impurity scattering in unconventional superconductors:  $T = 0$  results," *Physical Review B*, vol. 49, no. 5, pp. 3544–3547, 1994.
- [611] Y. Sun and K. Maki, "Impurity effects in d-wave superconductors," *Physical Review B*, vol. 51, no. 9, pp. 6059–6063, 1995.
- [612] D. Manske, I. Eremin, and K. H. Bennemann, "Analysis of the elementary excitations in high- $T_c$  cuprates: explanation of the new energy scale observed by angle-resolved photoemission spectroscopy," *Physical Review Letters*, vol. 87, no. 17, Article ID 177005, 4 pages, 2001.
- [613] D. S. Inosov, S. V. Borisenko, I. Eremin, et al., "Relation between the one-particle spectral function and dynamic spin susceptibility of superconducting  $\text{Bi}_2\text{Sr}_2\text{CaCu}_2\text{O}_{8-\delta}$ ," *Physical Review B*, vol. 75, no. 17, Article ID 172505, 4 pages, 2007.
- [614] A. N. Pasupathy, A. Pushp, K. K. Gomes, et al., "Electronic origin of the inhomogeneous pairing interaction in the high- $T_c$  superconductor  $\text{Bi}_2\text{Sr}_2\text{CaCu}_2\text{O}_{8+\delta}$ ," *Science*, vol. 320, no. 5873, pp. 196–201, 2008.
- [615] M.-H. Bae, J.-H. Park, J.-H. Choi, H.-J. Lee, and K.-S. Park, "Pseudogap behavior revealed in interlayer tunneling in overdoped  $\text{Bi}_2\text{Sr}_2\text{CaCu}_2\text{O}_{8+x}$ ," *Physical Review B*, vol. 77, no. 9, Article ID 094519, 8 pages, 2008.
- [616] A. Kussmaul, E. S. Hellman, E. H. Hartford Jr., and P. M. Tedrow, "Superconductor-insulator-superconductor tunneling in  $\text{Ba}_{1-x}\text{K}_x\text{BiO}_3$  grain boundaries," *Applied Physics Letters*, vol. 63, no. 20, pp. 2824–2826, 1993.
- [617] A. Mourachkine, "Origin of dips in tunneling dI/dV characteristics of cuprates," *Physica C*, vol. 460–462, pp. 956–957, 2007.
- [618] D. J. van Harlingen, "Phase-sensitive tests of the symmetry of the pairing state in the high-temperature superconductors—evidence for  $d_{x^2-y^2}$  symmetry," *Reviews of Modern Physics*, vol. 67, no. 2, pp. 515–535, 1995.
- [619] J. Mannhart and P. Chaudhari, "High- $T_c$  bicrystal grain boundaries," *Physics Today*, vol. 54, no. 11, pp. 48–53, 2001.
- [620] N. E. Hussey, M. Abdel-Jawad, A. Carrington, A. P. Mackenzie, and L. Balicas, "A coherent three-dimensional Fermi surface in a high-transition-temperature superconductor," *Nature*, vol. 425, no. 6960, pp. 814–817, 2003.
- [621] K. Yang and S. L. Sondhi, "Response of a  $d_{x^2-y^2}$  superconductor to a Zeeman magnetic field," *Physical Review B*, vol. 57, no. 14, pp. 8566–8570, 1998.
- [622] A. Kanigel, M. R. Norman, M. Randeria, et al., "Evolution of the pseudogap from Fermi arcs to the nodal liquid," *Nature Physics*, vol. 2, no. 7, pp. 447–451, 2006.
- [623] M. Hashimoto, T. Yoshida, K. Tanaka, et al., "Distinct doping dependences of the pseudogap and superconducting gap of  $\text{La}_{2-x}\text{Sr}_x\text{CuO}_4$  cuprate superconductors," *Physical Review B*, vol. 75, no. 14, Article ID 140503, 4 pages, 2007.
- [624] K. McElroy, "Death of a Fermi surface," *Nature Physics*, vol. 2, no. 7, pp. 441–442, 2006.
- [625] Y. H. Liu, K. Takeyama, T. Kurosawa, N. Momono, M. Oda, and M. Ido, " $4a \times 4a$  electronic charge order enhanced in the inhomogeneous pseudogap state of  $\text{Bi}_2\text{Sr}_2\text{CaCu}_2\text{O}_{8+\delta}$ ," *Physical Review B*, vol. 75, no. 21, Article ID 212507, 4 pages, 2007.
- [626] A. Pushp, C. V. Parker, A. N. Pasupathy, et al., "Extending universal nodal excitations optimizes superconductivity in  $\text{Bi}_2\text{Sr}_2\text{CaCu}_2\text{O}_{8+\delta}$ ," *Science*, vol. 324, no. 5935, pp. 1689–1693, 2009.
- [627] D. Einzel, "Universal parameters in the response of unconventional superconductors," *Journal of Low Temperature Physics*, vol. 126, no. 3-4, pp. 867–880, 2002.
- [628] D. Einzel, "Analytic two-fluid description of unconventional superconductivity," *Journal of Low Temperature Physics*, vol. 131, no. 1-2, pp. 1–24, 2003.
- [629] B.-L. Yu, J. C. F. Wang, A. D. Beyer, et al., "Possible competing order-induced Fermi arcs in cuprate superconductors," *Solid State Communications*, vol. 149, no. 7-8, pp. 261–265, 2009.
- [630] A. Furrer, "Admixture of an s-wave component to the d-wave gap symmetry in high-temperature superconductors," *Journal of Superconductivity and Novel Magnetism*, vol. 21, no. 1, pp. 1–5, 2008.

- [631] T. Hasegawa, H. Ikuta, and K. Kitazawa, "Tunneling spectroscopy of oxide superconductors," in *Physical Properties of High Temperature Superconductors III*, D. M. Ginsberg, Ed., p. 525, World Scientific, Singapore, 1992.
- [632] M. Oda, N. Momono, and M. Ido, "What is the energy scale in determining the  $T_c$  of cuprate superconductivity?" *Superconductor Science and Technology*, vol. 13, no. 11, pp. R139–R146, 2000.
- [633] B. T. Geilikman, V. Z. Kresin, and N. F. Masharov, "Transition temperature and energy gap for superconductors with strong coupling," *Journal of Low Temperature Physics*, vol. 18, no. 3–4, pp. 241–271, 1975.
- [634] J. P. Carbotte and C. Jiang, "Strong-coupling effects in  $d$ -wave superconductors," *Physical Review B*, vol. 48, no. 6, pp. 4231–4234, 1993.
- [635] R. Combescot and X. Leyronas, "A simple theory for high  $\Delta/T_c$  ratio in  $d$ -wave superconductors," *European Physical Journal B*, vol. 23, no. 2, pp. 159–163, 2001.
- [636] D. C. Mattis and M. Molina, "Ratio  $2\Delta_0/kT_c$  in superconductivity," *Physical Review B*, vol. 44, no. 22, pp. 12565–12566, 1991.
- [637] P. Udamsamuthirun, S. Ratanaburi, N. Saentalard, and S. Yoksan, "The ratio  $2\Delta_0/T_c$  in BCS superconductivity," *Journal of Superconductivity*, vol. 9, no. 6, pp. 603–604, 1996.
- [638] R. J. Radtke, K. Levin, H.-B. Schüttler, and M. R. Norman, "Role of Van Hove singularities and momentum-space structure in high-temperature superconductivity," *Physical Review B*, vol. 48, no. 21, pp. 15957–15965, 1993.
- [639] D. Einzel and I. Schürer, "Weak coupling theory of clean ( $d + s$ )-wave superconductors," *Journal of Low Temperature Physics*, vol. 117, no. 1–2, pp. 15–52, 1999.
- [640] H. Padamsee, J. E. Neighbor, and C. A. Shiffman, "Quasiparticle phenomenology for thermodynamics of strong-coupling superconductors," *Journal of Low Temperature Physics*, vol. 12, no. 3–4, pp. 387–411, 1973.
- [641] I. Tifrea, I. Grosu, and M. Crisan, "Pseudogap influence on the  $2\Delta_0/T_c$  ratio in  $d$ -wave superconductors," *Physica C*, vol. 371, no. 2, pp. 104–110, 2002.
- [642] N. Miyakawa, P. Guptasarma, J. F. Zasadzinski, D. G. Hinks, and K. E. Gray, "Strong dependence of the superconducting gap on oxygen doping from tunneling measurements on  $\text{Bi}_2\text{Sr}_2\text{CaCu}_2\text{O}_{8-\delta}$ ," *Physical Review Letters*, vol. 80, no. 1, pp. 157–160, 1998.
- [643] C. Pasquier, P. Auban-Senzier, T. Vuletic, S. Tomic, M. Heritier, and D. Jérôme, "Coexistence of superconductivity and spin density wave orderings in Bechgaard and Fabre salts," *Journal de Physique*, vol. 12, no. 9, pp. 197–200, 2002.
- [644] D. Jérôme, "The development of organic conductors: organic superconductors," *Solid State Sciences*, vol. 10, no. 12, pp. 1692–1700, 2008.
- [645] J. R. Jeffries, N. P. Butch, B. T. Yukich, and M. B. Maple, "Competing ordered phases in  $\text{URu}_2\text{Si}_2$ : hydrostatic pressure and rhenium substitution," *Physical Review Letters*, vol. 99, no. 21, Article ID 217207, 4 pages, 2007.
- [646] J. A. Janik, H. D. Zhou, Y.-J. Jo, et al., "Itinerant spin excitations near the hidden order transition in  $\text{URu}_2\text{Si}_2$ ," *Journal of Physics: Condensed Matter*, vol. 21, no. 19, Article ID 192202, 4 pages, 2009.
- [647] S. Elgazzar, J. Ruzs, M. Amft, P. M. Oppeneer, and J. A. Mydosh, "Hidden order in  $\text{URu}_2\text{Si}_2$  originates from Fermi surface gapping induced by dynamic symmetrybreaking," *Nature Materials*, vol. 8, no. 4, pp. 337–341, 2009.
- [648] G. C. Psaltakis and E. W. Fenton, "Superconductivity and spin-density waves: organic superconductors," *Journal of Physics C*, vol. 16, no. 20, pp. 3913–3932, 1983.
- [649] E. W. Fenton, "Cooper pairing in the presence of inhomogeneous magnetism," *Progress of Theoretical Physics*, no. 80, pp. 94–102, 1984.
- [650] A. M. Gabovich and A. I. Voitenko, "Non-stationary Josephson tunneling involving superconductors with spin-density waves," *Physica C*, vol. 329, no. 3, pp. 198–230, 2000.
- [651] T. T. M. Palstra, A. A. Menovsky, J. V. D. Berg, et al., "Superconducting and magnetic transitions in the heavy-fermion system  $\text{URu}_2\text{Si}_2$ ," *Physical Review Letters*, vol. 55, no. 24, pp. 2727–2730, 1985.
- [652] A. J. A. de Oliveira and P. C. de Camargo, "Spin-density waves and charge-density waves in Cr alloys," in *Handbook of Advanced Magnetic Materials Bolume IV: Advanced Magnetic Materials: Properties and Applications*, Y. Liu, D. J. Sellmyer, and D. Shindo, Eds., p. 159, Springer, Heidelberg, Germany, 2006.
- [653] R. Jaramillo, Y. Feng, J. C. Lang, et al., "Breakdown of the Bardeen-Cooper-Schrieffer ground state at a quantum phase transition," *Nature*, vol. 459, no. 7245, pp. 405–409, 2009.
- [654] H. Chen, Y. Ren, Y. Qiu, et al., "Coexistence of the spin-density wave and superconductivity in  $\text{Ba}_{1-x}\text{K}_x\text{Fe}_2\text{As}_2$ ," *Europhysics Letters*, vol. 85, no. 1, Article ID 17006, 5 pages, 2009.
- [655] K. Terashima, Y. Sekiba, J. H. Bowen, et al., "Fermi surface nesting induced strong pairing in iron-based superconductors," *Proceedings of the National Academy of Sciences of the United States of America*, vol. 106, no. 18, pp. 7330–7333, 2009.
- [656] P. M. R. Brydon and C. Timm, "Theory of the excitonic spin-density-wave state in iron pnictides," *Physical Review B*, vol. 79, no. 18, Article ID 180504, 4 pages, 2009.
- [657] S. A. J. Kimber, A. Kreyssig, Y.-Z. Zhang, et al., "Similarities between structural distortions underpressure and chemical doping in superconducting  $\text{BaFe}_2\text{As}_2$ ," *Nature Materials*, vol. 8, no. 6, pp. 471–475, 2009.
- [658] M. M. Korshunov and I. Eremin, "Theory of magnetic excitations in iron-based layered superconductors," *Physical Review B*, vol. 78, no. 14, Article ID 140509, 4 pages, 2008.
- [659] I. Dimov, P. Goswami, X. Jia, and S. Chakravarty, "Competing order, Fermi surface reconstruction, and quantum oscillations in underdoped high-temperature superconductors," *Physical Review B*, vol. 78, no. 13, Article ID 134529, 14 pages, 2008.
- [660] B. Pradhan and G. C. Rout, "Antiferromagnetic and superconducting gaps of some superconductors," *Physica C*, vol. 468, no. 1, pp. 72–80, 2008.
- [661] A. D. Beyer, C.-T. Chen, M. S. Grinolds, M. L. Teague, and N.-C. Yeh, "Competing orders and the doping and momentum dependent quasiparticle excitations in cuprate superconductors," *Physica C*, vol. 468, no. 6, pp. 471–479, 2008.
- [662] A. B. Vorontsov, M. G. Vavilov, and A. V. Chubukov, "Interplay between magnetism and superconductivity in the iron pnictides," *Physical Review B*, vol. 79, no. 6, Article ID 060508, 4 pages, 2009.
- [663] A. N. Lavrov, L. P. Kozeeva, M. R. Trunin, and V. N. Zverev, "Competition and coexistence of antiferromagnetism and superconductivity in  $\text{RBa}_2\text{Cu}_3\text{O}_{6+x}$  ( $R = \text{Lu}, \text{Y}$ ) single crystals," *Physical Review B*, vol. 79, no. 21, Article ID 214523, 6 pages, 2009.
- [664] A. A. Gorbatsevich and Yu. V. Kopae, "Magnetic state with orbital toroidal ordering and superdiamagnetism," in *Superconductivity, Superdiamagnetism, Superfluidity*, V. L. Ginzburg, Ed., pp. 175–241, Mir, Moscow, Russia, 1987.

## Research Article

# Phonons in $A_3C_{60}$ Lattice and Structural Dynamics

**Sven Larsson**

*Department of Chemistry, Chalmers University of Technology, 412 96 Göteborg, Sweden*

Correspondence should be addressed to Sven Larsson, slarsson@chalmers.se

Received 2 June 2009; Accepted 14 September 2009

Academic Editor: Dragan Mihailovic

Copyright © 2010 Sven Larsson. This is an open access article distributed under the Creative Commons Attribution License, which permits unrestricted use, distribution, and reproduction in any medium, provided the original work is properly cited.

The critical temperature ( $T_C$ ) of superconductivity in  $A_3C_{60}$  compounds is generally lower smaller with alkali atoms (A). Furthermore  $T_C$  decreases with applied pressure. In the BCS model, these trends are explained by the lower density of states at the Fermi level for a decreased lattice constant ( $R$ ). There is more than one counterexample, however, suggesting that BCS does not give the whole truth. The most important one is that the compound with the largest lattice constant,  $Cs_3C_{60}$ , is not superconducting at all at ambient pressure. In this paper we derive a novel model where a negative lattice contribution to Hubbard  $U$ , proportional to  $1/R$ , is taken into account. It is possible to explain why  $A_3C_{60}$  compounds with  $A = Li$ , and  $Na$  have a low  $T_C$  or are not superconducting at all, and why  $Cs_3C_{60}$  is superconducting only at applied pressure and then with the highest  $T_C$  of all  $C_{60}$  alkali fullerenes. It is concluded that the density of states mechanism derived in the BCS model is in doubt. Nevertheless superconductivity in  $A_3C_{60}$  depends on electron-phonon coupling. The dominating phonon is the bond stretching  $A_g$  phonon, a breathing phonon for the whole fullerene molecular ion.

## 1. Introduction

The discoveries of conductivity and superconductivity (SC) in  $K_3C_{60}$  and  $Rb_3C_{60}$  were great events in science during the 1990s [1–5]. SC was later discovered in a number of other  $A_3C_{60}$  compounds, where A stand for alkali atoms: Li, Na, K, Rb, or Cs. Generally, increase of the lattice constant leads to a higher critical temperature  $T_C$ . Some of the  $A_3C_{60}$  compounds ( $A = Li, Na$ ) with the smallest lattice constants are not superconducting [6–8]. Only  $C_{60}$  fullerenes have proven to be superconducting (SC).

Remarkably, the compound with the highest lattice constant does not follow this trend [9–11]. Disorder-free  $Cs_3C_{60}$  is an antiferromagnetic insulator at ambient pressure. However, already at the quite modest pressure of 3 kbar ( $\approx 3000$  atm), it turns into a superconductor (SC) with the highest  $T_C$  known for any fullerene [9–11]. At temperatures above  $T_C$   $Cs_3C_{60}$  passes directly into a semiconducting and antiferromagnetic phase. This system thus needs an explanation model which is not depending on the existence of free electrons, as in the BCS model. Takabayashi et al. further point out [11] that transfer from SC to antiferromagnetic phase appears to be “purely electronic”, thus seemingly explicable without resorting to nuclear dynamics.

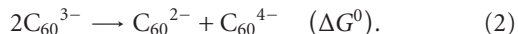
There are a number of peculiarities in experimental data in general, as summarized by Gunnarsson [12], Rosseinsky [13], Margadonna and Prassides [14], and Iwasa and Takenobu [15]. A widely accepted approach is to treat the metallic alkali  $C_{60}$  fullerenes as metals and apply the BCS model [12–15]. In the latter model,  $T_C$  increases if the density of states at the Fermi level increases. In the case of  $A_3C_{60}$  the Fermi level is in a narrow band, so the conclusion is that if the band width further decreases, the density of states will increase and hence also  $T_C$ . However, contrary to this deduction,  $Cs_3C_{60}$  is not superconducting at all.

Expansion of the lattice by intercalation of molecules leads to a higher density of states and to a higher  $T_C$ . Lattices of several  $A_3C_{60}$  compounds have been expanded by intercalating  $NH_3$  and this improved the SC properties [16–18] for some of them, but in  $K_3C_{60}$  and  $Rb_3C_{60}$ , SC was lost and antiferromagnetism appeared instead.

SC  $A_3C_{60}$  is a “molecular metal”. If so, one should be able to derive (Hubbard)  $U = 0$  for the solid, using molecular data. The molecular Hubbard  $U$  is defined by

$$U = I - A, \quad (1)$$

where  $I$  is the ionization energy and  $A$  is the electron affinity [12–15].  $\Delta G^0$  is the adiabatic energy [19] for charge disproportionation according to:



$U$  is thus the corresponding vertical energy. Usually  $U > 0$  for a molecule or insulator, but it is still possible to have  $\Delta G^0 = 0$ , that is, oxidation state degeneracy according to (2). The reason is that  $\Delta G^0$  corresponds to the optimum geometry of the products, in the present case for  $C_{60}^{2-}$  and  $C_{60}^{4-}$ , in (1).  $\Delta G^0 < 0$  means that the sites are differently occupied in a pair of electrons [charge alternant phase or charge density wave (CDW) phase].

In the CDW phase, equivalent sites may exchange electron pairs, but there may be an activation barrier. The activation barrier may be removed due to interaction with the  $C_{60}^{3-}$  state [19]. Interaction with  $C_{60}^{3-}$  is maximized when  $\Delta G^0 = 0$ . For  $K_3C_{60}$ , most estimations of  $U$  end up with values larger than 1 eV. This is too large to reach  $\Delta G^0 = 0$ . Below we will find that if the lattice contribution to  $U$  is taken into account, it is possible to achieve  $\Delta G^0 = 0$ .

As another or complimentary cause of SC, one has often referred to the Jahn-Teller effect. The Jahn-Teller effect does not include the degeneracy of (2), however. A possible rational for involving the Jahn-Teller effect at electron transport is that it is different for different site charges, but that effect must be of minor importance in comparison with the degeneracy between site oxidation states, directly related to the Mott-Hubbard problem and the structural dynamics generated by nonconserved oxidation states.

On the basis of the Jahn-Teller effect, one has concluded that a single  $H_g$  mode is important. In contradistinction, it will be argued here that the  $A_g$  breathing mode is the very cause of structural dynamics leading to SC.

In this paper we will use a mixed-valence model for three oxidation states (MV-3) [19–22]. “Valence” here meant the charge on the  $C_{60}$  molecule. The negative lattice contribution to Hubbard  $U$  is inversely proportional to the lattice constant  $R$ . Contraction of the lattice, for example by applied pressure [23–25] therefore leads to a lower  $U$ , a more negative  $\Delta G^0$  in (2), and reduced  $T_C$ .  $T_C$  in  $Rb_3C_{60}$  decreases almost linearly with applied pressure [25]. For  $Rb_3C_{60}$   $\Delta G^0$  is negative already ambient pressure but for  $Cs_3C_{60}$   $\Delta G^0$  is positive. This makes  $Cs_3C_{60}$  an antiferromagnet at ambient pressure, but applied pressure decreases the lattice constant enough to make  $\Delta G^0$  negative and therefore an almost perfect SC.

Finally we will discuss electron-phonon interactions, which are of fundamental importance for SC, in MV-3 as well as BCS theory. We will see, using MV-3, that the same electron-phonon coupling is applicable to all  $C_{60}$  fullerenes, including  $Cs_3C_{60}$ .

## 2. Molecular Electronic and Vibrational Structure

It was early established that the valence electrons of the alkali atoms are transferred to the threefold degenerate, lowest unoccupied (LU)  $t_{1u}$  molecular orbital (MO) of

$C_{60}$ , thereby forming  $A_N C_{60}^{N-}$  where  $N$  is the number of electrons in LUMO. We will only be interested in the case with incompletely filled LUMO ( $N < 6$ ). Due to the spherical symmetry, the electronic states for a single  $C_{60}$  may be compared to the multiplet states of a single atom in the second row with incompletely filled 2p shell. The  $2s^2 2p^2$  configuration of carbon produces the states:  $^3P$ ,  $^1D$ ,  $^1S$ . According to Hund’s rule, the ground state has the highest possible spin, therefore  $^3P$ . In the  $C_{60}$  anions the energy difference between high spin and low spin states is very small [26–28]. For  $C_{60}^{2-}$ , the reason is that the exchange integrals are numerically small, of about the same size as the relevant integrals for the  $t_{1u}^2 \rightarrow t_{2g}^2$  correlation effect [29–31].

The low spin ground state of  $C_{60}^{2-}$ ,  $C_{60}^{3-}$ , and  $C_{60}^{4-}$  is a prerequisite for superconductivity according to the MV-3 model. If in addition (2) also holds with a negative  $\Delta G^0$ , the diamagnetism of  $C_{60}^{3-}$  can be explained. Jahn-Teller effects and electron-phonon coupling are of minor importance in this case compared to electron correlation effects.

Another prerequisite for SC is that electron pair transfer (EPT) from a  $C_{60}^{4-}$  site to a  $C_{60}^{2-}$  site can take place without activation energy, or, in other words, that the electron pair is not trapped at the  $C_{60}^{4-}$  site. This has been discussed by Dušćes and the author, and it was found that the reorganization energy is only 0.24 eV for adding two electrons to  $C_{60}^{2-}$  [32]. The reason for this is that the bond length change is very small.

Typical for  $\pi$  systems is that occupation of the bonding  $\pi$ MOs up to and including HOMO tends to shorten some of the CC bonds. The shortened bonds are said to have “double bond character”. In  $C_{60}$  the shorter bonds are the thirty ( $3 \times 20/2$ ) bonds that are common to two hexagons (Figure 1). Occupation of LUMO lengthens these bonds, since LUMO tends to be antibonding in the double bonds. Full occupation of the  $t_{1u}$  LUMO to form  $C_{60}^{-6}$  leads to a lengthening of the double bonds of  $C_{60}$  to almost equal bond lengths over the whole molecular ion [32].

We are thus looking for a mode where the  $t_{1u}$  LUMO is stabilized on one molecule and at the same time destabilized on the other. The vibrational mode coupled to EPT between  $t_{1u}$  orbitals on different sites is the one that shortens the double bonds and lengthens the single bonds. This is the breathing mode of the strong bonds in Figure 1.

Experimentally, breathing modes have been found to be involved in superconducting systems [33]. The theory [19, 29, 30] is equivalent to the Holstein diatomic model for a single electron [34, 35]. In neutral  $C_{60}$  the relevant phonon should be the  $A_g$  phonon at  $1470 \text{ cm}^{-1}$  [12].

Gunnarsson pointed out that it is the size, not the mass of the alkali ion that determines  $T_C$  [12]. We therefore do not expect large contributions to the electron-phonon coupling due to the motion of the metal ions. The  $A_g$  breathing mode is very likely the phonon that couples to the electrons in SC. The  $H_g$  modes tend to increase some double bonds while decreasing the corresponding ones on the opposite side of the molecule, thus should be unimportant for EPT.

Next we will study EPT between two adjacent molecular ions A and B. The fundamental assumption in the chemical model for SC is that electrons and phonons are coupled

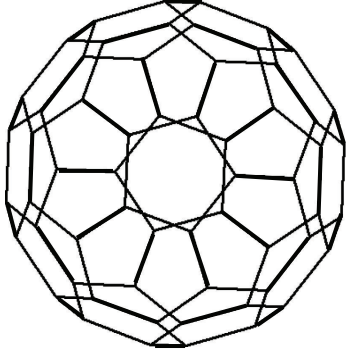


FIGURE 1:  $C_{60}$  molecule. The most relevant electron-phonon interaction mode for EPT is the in-phase bond stretch for the short and strong bonds, drawn with thick lines.

in a motion that makes the electron pair oscillate between adjacent sites (in a time-dependent treatment). For this to happen, the activation barrier has to be sufficiently low. The exact wave function for the electron pair transferring between A and B may be complicated to write down, in particular since the relevant states are correlated and cannot be represented by single Slater determinants. If the  $t_{1u}$  LUMO is called “a” on site A and “b” on the adjacent site B, there are three spin singlet states, where two electrons are localized on site A (aa), on site B (bb) or where the two electrons are localized on different sites (ab + ba). The symmetrized form of the former are  $aa + bb$  and  $aa - bb$ .  $ab + ba$  corresponds to the spin-coupled antiferromagnetic state [or spin density wave state (SDW)].  $aa + bb$  and  $aa - bb$  are the necessary states for EPT, thus for SC.

It is interesting that the three  $A_3C_{60}$  systems which are not superconducting at ambient pressure,  $NH_3K_3C_{60}$ ,  $NH_3Rb_3C_{60}$ , and  $Cs_3C_{60}$  with large lattice constant  $R$ , are all antiferromagnetic, thus with the  $ab + ba$  ground state [9, 36, 37]. The latter wave function cannot superconduct since the electrons are fixed one on each site.

### 3. Hubbard $U$ and Lattice Interactions

Estimation of  $U$  from molecules leads to a molecular  $U$  in the range 2.7–3.1 eV [12, 13, 38, 39]. For the solid there are experimental estimates of  $U$  in the range 0.8–1.27 eV [39–43]. This refers to a crystal where all site charges are the same, say  $Z$ . The charge disproportionated CDW phase, where the charges  $(Z - 1)$  and  $(Z + 1)$  alternate, is favored by an additional negative contribution according to the Born model. The Born radius  $R$  can be taken as the lattice constant. The decrease of the Born free energy is (atomic units)

$$\Delta G(\text{Born}) = -\frac{(Z-1)^2 + (Z+1)^2 - 2Z^2}{2R} = -\frac{1}{R}, \quad (3)$$

(neglecting the Born exponent).  $R$  is about 20 Bohr for fullerenes.  $\Delta G(\text{Born})$  is thus equal to  $-1/20$  Hartree or  $-1.3$  eV. This lowers the energy difference between the SDW and CDW state, thus Hubbard  $U$  decreases. After this correction we obtain roughly  $U \approx 0$  for the  $A_3C_{60}$

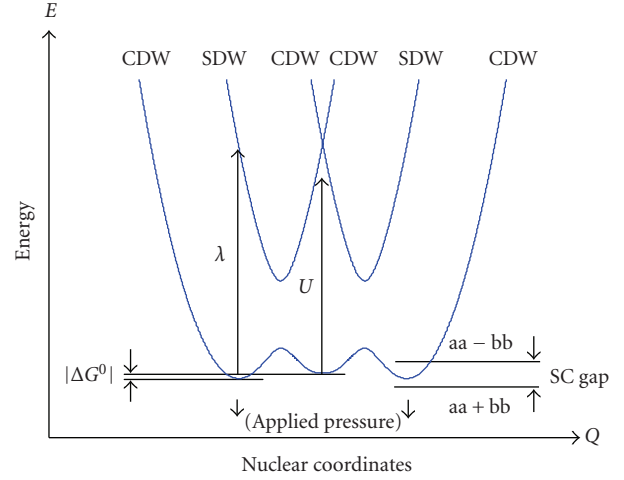


FIGURE 2: PESs of the MV-3 model. Curvatures are exaggerated.  $\lambda$  is reorganization energy. The fat horizontal bars are vibronic energy levels.  $aa + bb$  and  $aa - bb$  denote approximate wave functions for the given energy levels. For  $NH_3K_3C_{60}$ ,  $NH_3Rb_3C_{60}$ , and  $Cs_3C_{60}$ , the SDW-PES is lower than CDW-PES. Fat arrows show the behavior of CDW-PES at applied pressure.  $|\Delta G^0|$  is defined by (2).

fullerenes. In conclusion, Hubbard  $U$  is less smaller with lattice constant.

High pressure in  $A_3C_{60}$  systems leads to a smaller lattice constant. Thus the CDW phase with  $C_{60}^{2-}$  and  $C_{60}^{4-}$  is favored compared to the SDW phase with  $C_{60}^{3-}$  sites. If on the other hand the lattice is expanded, the SDW phase wins and becomes the ground state. SC cannot occur since the ground state is mainly  $ab + ba$ .

Figure 2 shows a total energy potential energy surfaces (PES) at the molecular level, as a function of a collective breathing mode for the carbon atoms. In the case given in Figure 2 the outer minima are lower, and this corresponds to the CDW case, the case that applies to all  $A_3C_{60}$  systems except  $Cs_3C_{60}$ .

The important thing is that the inner PES, corresponding to the SDW, is present slightly above the CDW-PES. In most cases there is an interaction between CDW and SDW that opens a gap. The lower state is  $aa + bb$  mixed with  $ab + ba$ . This energy level is denoted as  $aa + bb$  in Figure 2. The  $aa - bb$  is the upper state. Provided the lower state has a major component of  $aa + bb$ , the gap is a true SC gap. If, however, the SDW-PES is below the CDW-PES, the  $ab + ba$  component will be the major one in the lower state. Since  $ab + ba$  is the wave function which put an electron on A and one on B, EPT is not possible and hence there is no SC.

We arrive at the picture sketched in Figure 3. As the lattice constant ( $R$ ) increases the CDW states, denoted  $aa + bb$  and  $aa - bb$  in Figure 3 are increasing in energy due to the numerically smaller lattice energy contribution according to (3).  $aa + bb$  interacts with  $ab + ba$ , and this interaction is maximized at the crossing point (Figure 3). The ground state is mainly of  $aa + bb$  type except for  $Cs_3C_{60}$ . In  $Cs_3C_{60}$  the ground state has a very large component of  $ab + ba$ , which means that the antiferromagnetic phase wins

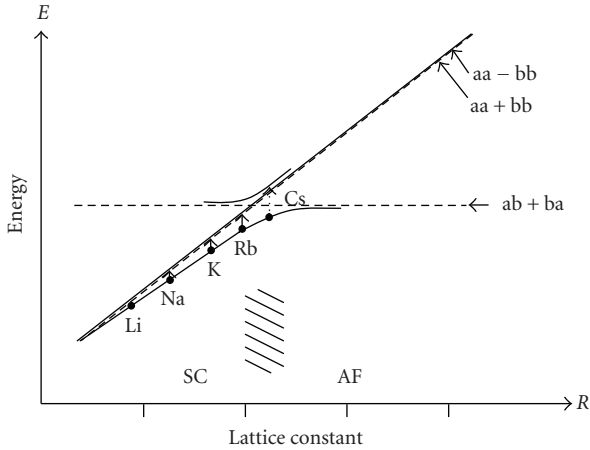


FIGURE 3: Free energies for the SDW and CDW states as a function of lattices constants in (3). Arrows at the symbol for the element show the superconducting gap.  $\text{Cs}_3\text{C}_{60}$  is in the antiferromagnetic region (AF) where the gap is a pseudogap.

over SC phase. High pressure decreases the lattice constant for  $\text{Cs}_3\text{C}_{60}$ , changing the composition of the ground state. Interestingly, when the pressure is sufficient to change the phase into a SC phase,  $T_C$  is the largest one, corresponding to  $\Delta G^0 = 0$  in Figure 2.

A number of experiments have been carried out on  $\text{NH}_3$ -doped fullerides [16–18].  $\text{NH}_3$  intercalates without causing any other change than increasing the lattice constant [13]. As a function of volume/ $\text{C}_{60}^{3-}$  the critical temperature  $T_C$  increases monotonically. If the increase in lattice constant is too large, the minimum of the SDW-PES appear below the minimum of the CDW-PES and the SC is lost. Instead the antiferromagnetic phase appears. This is very clear from Figure 3. As we move to the right in the diagram the ground state wave function gets increased character of  $ab + ba$ , equivalent to antiferromagnetic coupling.

The structural change at electron transfer is associated with a total energy lowering denoted as “reorganization energy” ( $\lambda$ ). Large  $\lambda$  is directly related to high effective mass in the Holstein model [34, 35]. For fullerenes  $\lambda$  has proven to be comparatively small in the cases examined, or about 0.05 eV for single electron transfer [32]. As a comparison,  $\lambda$  is about 0.22 eV in polyacetylene [44]. The Jahn-Teller effect or modifications due to chemical bonding between the fullerene molecules may modify some distances, but this is usually of little importance for  $\lambda$ .

The coupling in the case of electron pair transfer is well defined and different from the coupling in single electron transfer and, of course, different from magnetic couplings. The most important difference is that the  $a^2$  and  $b^2$  states do not couple directly, but assume the presence of the SDW  $ab + ba$  state. In principle the coupling may be calculated in a quantum chemical calculation that includes two molecules.

An important problem is to understand why  $\text{A}_4\text{C}_{60}$  is an insulator.  $\text{A}_4\text{C}_{60}$  with an unfilled shell-like  $\text{A}_3\text{C}_{60}$  has

a different Hubbard  $U$ . Equation (3) corresponds to the following equation:



We now see that the right member consists of two odd-electron systems, while  $\text{A}_4\text{C}_{60}$  itself has an even number of electrons, of course. Referring to the fact that systems with an even number of electrons generally have lower energy than systems with an odd number of electrons, it is quite simple to understand why (3) has a  $\Delta G^0$  close to zero, while  $\Delta G^0$  for (4) is decidedly positive. In any case this may be verified in quantum chemical calculations which involve two adjacent molecules.

Knupfer and Fink have used electron energy loss spectroscopy (EELS) for  $\text{A}_4\text{C}_{60}$  systems and found that Mott-Hubbard behavior with  $\Delta G^0$  is larger than the one for the  $\text{A}_3\text{C}_{60}$  systems [45]. Iwasa applied reflection techniques to  $\text{A}_3\text{C}_{60}$ , verifying the metallic properties with  $\Delta G^0 \approx 0$  [46]. Other experiments show a similar trend [47].

The reason why  $\text{A}_4\text{C}_{60}$  systems are nonSC may be large Hubbard  $U$ , as discussed by Rosseinsky [13]. Another important possibility may be that Jahn-Teller effect splits the  $t_{1u}$  level as shown in STM experiments [48]. The lower level is fully occupied [49], making charge transfer impossible.

## 4. Discussion

In this paper we have shown that a molecular model provides a satisfactory explanation of the dependence of  $T_C$  on lattice constant in  $\text{A}_3\text{C}_{60}$  systems. The model is based on the structural dynamics that is connected to EPT and oxidation state degeneracy. Decrease of the lattice constant in  $\text{Cs}_3\text{C}_{60}$  due to increased pressure leads to appearance of SC. If the pressure is further increased,  $T_C$  increases at first, but eventually  $\text{Cs}_3\text{C}_{60}$  shares the fate of the other  $\text{C}_{60}$  fullerides, so that  $T_C$  decreases with increased pressure. The fact that  $T_C$  increases with increased pressure at first is a problem not only in the BCS model but also in the present model. Since this problem has to do with the properties of the ground state wave function [( $ab + ba$ ) versus ( $aa + bb$ ) character], it would be unwise to dig deeper into this problem without accurate calculations.

In the BCS model too, decrease of the lattice constant leads to a lower  $T_C$ , but in that case the reason is decrease of the density of states. The BCS mechanism is doubtful to say the least, as has been shown during the historical development of the SC phenomenon. In the  $\text{A}_3\text{C}_{60}$  fullerides it is a quite successful model but it does not predict the nonSC behavior for  $\text{Cs}_3\text{C}_{60}$ . It also does not explain why  $\text{NH}_3\text{K}_3\text{C}_{60}$  and  $\text{NH}_3\text{Rb}_3\text{C}_{60}$  are antiferromagnets. The phase change from SC to antiferromagnetic is driven by the composition of the ground state wave function, which in its turn depends on the lattice constant.

The Jahn-Teller effect is overrun by intermolecular bonding or at least strongly modified. In the molecular SC model the importance of the Jahn-Teller effect is superceded by the oxidation state degeneracy (disproportionation). However, the Jahn-Teller effect (combined with the chemical

bonding effect) may well explain why  $A_4C_{60}$  systems are not superconducting, as illustrated in the STM experiments by Wachowiak et al. [48] and further detailed by O'Shea [49]. The  $t_{1u}$  degeneracy is split and the lower MO is fully occupied, thereby making SC impossible. An interesting discussion of the Jahn-Teller effect in  $C_{60}$  fullerenes and the dependence of lattice constant on superconductivity have recently been given by Capone et al. [50]. Some conclusions are different from those of this paper, however.

Another, or contributing reason for the absence of SC in  $A_4C_{60}$  compounds may be the large Hubbard  $U$  for these compounds as compared to the  $A_3C_{60}$  compounds. An important task is to obtain an accurate value of  $U$ , as has in fact been the goal in previous review articles [12–15]. The description here introduces the nuclear coordinate into the Mott-Hubbard problem. Thereby it becomes possible to discuss the vibronic states of importance in superconductivity. The distinction between  $\Delta G^0$  and  $U$  is important.

Phonons lower the energy in the SC phase where they interact with the electrons. The motion of the electron pair is correlated with the nuclear coordinates in the breathing mode. The vibration motions of the nuclei “pump” the electron pairs between the sites without expense of energy. This happens in a quantum mechanical manner and leads to an energy lowering that stabilizes the SC phase with an energy gap to the first excited state. The antiferromagnetic phase cannot behave in the same way, since the charge distribution is inert and almost independent of the exact positions of the nuclei. The relevant breathing phonon in the case of  $A_3C_{60}$  is very likely a double-bond stretching phonon with symmetry  $A_g$ .

In this paper the difference in lattice energy between the CDW and SDW phases has been pointed out as a general explanation of SC in  $A_3C_{60}$ . The BCS model on the other hand states that  $T_C$  depends on the density of states, but this does not hold for  $Cs_3C_{60}$ . Takabayashi et al. therefore concluded that SC in  $Cs_3C_{60}$  is of a different type, more similar to SC in cuprates with  $CuO_2$  plane [10, 11, 51]. This is possible, not least considering the change of crystal structure from fcc in most  $A_3C_{60}$  fullerides to A15-bcc in  $Cs_3C_{60}$ . Of particular importance is that in  $Cs_3C_{60}$  the density of states at the Fermi level is higher than in the  $A_3C_{60}$  fcc fullerides and should have a higher  $T_C$  rather than not being SC at all.

In model used here change of structure leads to different Born model contributions to the CDW state in (3) shifting the onset pressure of SC. Since it is not known which onset pressure would apply to the fcc phase, a detailed discussion of this problem would not be successful at this stage. To complicate matters further, change of structure also leads to differences in coupling between the SDW and CDW states.

The author firmly believes that the BCS model is a kind of rough limit model for the transition between ordinary metals (e.g., alkali metals and coinage metals at normal pressure) and SC metals. The presence of free electrons is there guaranteed. The BCS model should not be used in cases where insulating phases play roles [52]. In any case the BCS model appears to be too crude a model to allow adequate parametrization. In the BCS model the binding energy of a pair of electrons determines whether SC

appears, whereas in reality the binding energy depends on the presence of positive nuclei and the mobility on the structural reorganization energy versus coupling [52].

## References

- [1] A. F. Hebard, M. J. Rosseinsky, R. C. Haddon, et al., “Superconductivity at 18 K in potassium-doped  $C_{60}$ ,” *Nature*, vol. 350, no. 6319, pp. 600–601, 1991.
- [2] M. J. Rosseinsky, A. P. Ramirez, S. H. Glarum, et al., “Superconductivity at 28 K in  $Rb_xC_{60}$ ,” *Physical Review Letters*, vol. 66, no. 21, pp. 2830–2832, 1991.
- [3] R. M. Fleming, A. P. Ramirez, M. J. Rosseinsky, et al., “Relation of structure and superconducting transition temperatures in  $A_3C_{60}$ ,” *Nature*, vol. 352, no. 6338, pp. 787–788, 1991.
- [4] L. S. Cox and R. A. Laskey, “DNA replication occurs at discrete sites in pseudonuclei assembled from purified DNA in vitro,” *Cell*, vol. 66, no. 2, pp. 271–275, 1991.
- [5] R. C. Haddon, A. F. Hebard, M. J. Rosseinsky, et al., “Conducting films of  $C_{60}$  and  $C_{70}$  by alkali-metal doping,” *Nature*, vol. 350, no. 6316, pp. 320–322, 1991.
- [6] T. Yildirim, O. Zhou, J. E. Fischer, et al., “Intercalation of sodium heteroclusters into the  $C_{60}$  lattice,” *Nature*, vol. 360, no. 6404, pp. 568–571, 1992.
- [7] K. Prassides, C. Christides, I. M. Thomas, et al., “Crystal structure, bonding, and phase transition of the superconducting  $Na_2CsC_{60}$  fulleride,” *Science*, vol. 263, no. 5149, pp. 950–954, 1994.
- [8] Y. Maniwa, T. Saito, A. Ohi, et al., “Electronic states and superconductivity in alkali-intercalated fullerides:  $^{13}C$ -NMR study in  $Na_2RbC_{60}$ ,  $Na_2CsC_{60}$ ,  $K_3C_{60}$ ,  $K_2RbC_{60}$ ,  $K_2CsC_{60}$ ,  $KRbCsC_{60}$ ,  $Rb_2CsC_{60}$  and  $RbCs_2C_{60}$ ,” *Journal of the Physical Society of Japan*, vol. 52, pp. 1139–1148, 1994.
- [9] T. T. M. Palstra, O. Zhou, Y. Iwasa, P. E. Sulewski, R. M. Fleming, and B. R. Zegarski, “Superconductivity at 40 K in cesium doped  $C_{60}$ ,” *Solid State Communications*, vol. 93, no. 4, pp. 327–330, 1995.
- [10] A. Y. Ganin, Y. Takabayashi, Y. Z. Khimyak, et al., “Bulk superconductivity at 38 K in a molecular system,” *Nature Materials*, vol. 7, no. 5, pp. 367–371, 2008.
- [11] Y. Takabayashi, A. Y. Ganin, P. Jeglič, et al., “The disorder-free non-BCS superconductor  $Cs_3C_{60}$  emerges from an antiferromagnetic insulator parent state,” *Science*, vol. 323, no. 5921, pp. 1585–1590, 2009.
- [12] O. Gunnarsson, “Superconductivity in fullerides,” *Reviews of Modern Physics*, vol. 69, no. 2, pp. 575–606, 1997.
- [13] M. J. Rosseinsky, “Recent developments in the chemistry and physics of metal fullerides,” *Chemistry of Materials*, vol. 10, no. 10, pp. 2665–2685, 1998.
- [14] S. Margadonna and K. Prassides, “Recent advances in fullerene superconductivity,” *Journal of Solid State Chemistry*, vol. 168, no. 2, pp. 639–652, 2002.
- [15] Y. Iwasa and T. Takenobu, “Superconductivity, Mott-Hubbard states, and molecular orbital order in intercalated fullerides,” *Journal of Physics: Condensed Matter*, vol. 15, no. 13, pp. R495–R519, 2003.
- [16] M. J. Rosseinsky, D. W. Murphy, R. M. Fleming, and O. Zhou, “Intercalation of ammonia into  $K_3C_{60}$ ,” *Nature*, vol. 364, no. 6436, pp. 425–427, 1993.
- [17] O. Zhou, R. M. Fleming, D. W. Murphy, et al., “Increased transition temperature in superconducting  $Na_2CsC_{60}$  by intercalation of ammonia,” *Nature*, vol. 362, no. 6419, pp. 433–435, 1993.

- [18] O. Zhou, T. T. M. Palstra, Y. Iwasa, et al., "Structural and electronic properties of  $(\text{NH}_3)_x\text{K}_3\text{C}_{60}$ ," *Physical Review B*, vol. 52, no. 1, pp. 483–489, 1995.
- [19] S. Larsson, "Localization of electrons and excitations," *Chemical Physics*, vol. 326, no. 1, pp. 115–122, 2006.
- [20] K. Prassides, P. N. Schatz, K. Y. Wong, and P. Day, "Vibronic coupling model for mixed-valence compounds. Extension to two-site two-electron systems," *Journal of Physical Chemistry*, vol. 90, no. 22, pp. 5588–5597, 1986.
- [21] K. Prassides and P. N. Schatz, "Vibronic coupling model for mixed-valence compounds. Extension to the multimode case," *Journal of Physical Chemistry*, vol. 93, no. 1, pp. 83–89, 1989.
- [22] S. Larsson, "Electronic structure of planar superconducting systems: from finite to extended model," *Chemical Physics*, vol. 236, no. 1–3, pp. 133–150, 1998.
- [23] G. Sparr, J. D. Thompson, S.-M. Huang, et al., "Pressure dependence of superconductivity in single-phase  $\text{K}_3\text{C}_{60}$ ," *Science*, vol. 252, no. 5014, pp. 1829–1831, 1991.
- [24] J. E. Schirber, L. Hansen, B. Morosin, J. E. Fischer, J. D. Jorgensen, and G. H. Kwei, "Effect of pressure on the superconducting primitive cubic and "polymeric" phases of  $\text{Na}_2\text{CsC}_{60}$ ," *Physica C*, vol. 260, no. 3–4, pp. 173–176, 1996.
- [25] J. Diederichs, J. S. Schilling, K. W. Herwig, and W. B. Yelon, "Dependence of the superconducting transition temperature and lattice parameter on hydrostatic pressure for  $\text{Rb}_3\text{C}_{60}$ ," *Journal of Physics and Chemistry of Solids*, vol. 58, no. 1, pp. 123–132, 1997.
- [26] P. Bhyrappa, P. Paul, J. Stinchcombe, P. D. W. Boyd, and C. A. Reed, "Synthesis and electronic characterization of discrete buckminsterfulleride salts:  $\text{C}_{60}^{2-}$  and  $\text{C}_{60}^{3-}$ ," *Journal of the American Chemical Society*, vol. 115, no. 23, pp. 11004–11005, 1993.
- [27] P. C. Trulove, R. T. Carlin, G. R. Eaton, and S. S. Eaton, "Determination of the singlet-triplet energy separation for  $\text{C}_{60}^{2-}$  in DMSO by electron paramagnetic resonance," *Journal of the American Chemical Society*, vol. 117, no. 23, pp. 6265–6272, 1995.
- [28] S. Nakazawa, K. Sato, D. Shiomi, et al., "Electronic and molecular structures of  $\text{C}_{60}$ -based polyanionic high-spin molecular clusters: direct spin identification and electron spin transient nutation spectroscopy for high-spin chemistry," *Inorganica Chimica Acta*, vol. 361, no. 14–15, pp. 4031–4037, 2008.
- [29] S. Larsson, "Electron pair transfer in  $\text{A}_3\text{C}_{60}$ ," in *Chemical Physics of Intercalation II*, P. Bernier, J. E. Fischer, S. Roth, and S. A. Solin, Eds., vol. 305 of *NATO Science Series*, pp. 227–231, Plenum Press, New York, NY, USA, 1993.
- [30] S. Larsson and L. Rodríguez Monge, "Correlation and pairing in  $\text{C}[\text{stack}_{60}^{2n-}]$  ions. Superconductivity of alkali and alkaline earth compounds of  $\text{C}_{60}$ ," *International Journal of Quantum Chemistry*, vol. 27, pp. 655–665, 1993.
- [31] F. Negri, G. Orlandi, and F. Zerbetto, "Low-lying electronic excited states of buckminsterfullerene anions," *Journal of the American Chemical Society*, vol. 114, no. 8, pp. 2909–2913, 1992.
- [32] G. Duškesas and S. Larsson, "Bond lengths and reorganization energies in fullerenes and their ions," *Theoretical Chemistry Accounts*, vol. 97, no. 1–4, pp. 110–118, 1997.
- [33] D. Reznik, L. Pintschovius, M. Ito, et al., "Electron-phonon coupling reflecting dynamic charge inhomogeneity in copper oxide superconductors," *Nature*, vol. 440, no. 7088, pp. 1170–1173, 2006.
- [34] T. Holstein, "Studies of polaron motion—part I: the molecular-crystal model," *Annals of Physics*, vol. 8, no. 3, pp. 325–342, 1959, reprinted: *Annals of Physics*, vol. 281, pp. 706–724, 2000.
- [35] T. Holstein, "Studies of polaron motion—part II: the "small" polaron," *Annals of Physics*, vol. 8, no. 3, pp. 343–389, 1959.
- [36] K. Prassides, S. Margadonna, D. Arcon, A. Lappas, H. Shimoda, and Y. Iwasa, "Magnetic ordering in the ammoniated fulleride  $(\text{ND}_3)\text{K}_3\text{C}_{60}$ ," *Journal of the American Chemical Society*, vol. 121, no. 48, pp. 11227–11228, 1999.
- [37] J. Arvanitidis, K. Papagelis, T. Takenobu, et al., "Antiferromagnetic ordering in the expanded  $(\text{NH}_3)\text{Rb}_3\text{C}_{60}$  fulleride," *Physica B*, vol. 326, no. 1–4, pp. 572–576, 2003.
- [38] R. L. Martin and J. P. Ritchie, "Coulomb and exchange interactions in  $\text{C}_{60}^{n-}$ ," *Physical Review B*, vol. 48, no. 7, pp. 4845–4849, 1993.
- [39] R. W. Lof, M. A. van Veenendaal, B. Koopmans, H. T. Jonkman, and G. A. Sawatzky, "Band gap, excitons, and Coulomb interaction in solid  $\text{C}_{60}$ ," *Physical Review Letters*, vol. 68, no. 26, pp. 3924–3927, 1992.
- [40] P. A. Brühweiler, A. J. Maxwell, A. Nilsson, N. Mårtensson, and O. Gunnarsson, "Auger and photoelectron study of the Hubbard  $U$  in  $\text{C}_{60}$ ,  $\text{K}_3\text{C}_{60}$ , and  $\text{K}_6\text{C}_{60}$ ," *Physical Review B*, vol. 48, no. 24, pp. 18296–18299, 1993.
- [41] O. Gunnarsson, E. Koch, and R. M. Martin, "Mott transition in degenerate Hubbard models: application to doped fullerenes," *Physical Review B*, vol. 54, no. 16, pp. R11026–R11029, 1996.
- [42] M. R. Pederson and A. A. Quong, "Polarizabilities, charge states, and vibrational modes of isolated fullerene molecules," *Physical Review B*, vol. 46, no. 20, pp. 13584–13591, 1992.
- [43] V. P. Antropov, O. Gunnarsson, and O. Jepsen, "Coulomb integrals and model Hamiltonians for  $\text{C}_{60}$ ," *Physical Review B*, vol. 46, no. 20, pp. 13647–13650, 1992.
- [44] S. Larsson, A. Klimkšans, L. Rodríguez-Monge, and G. Duškesas, "Reorganization energies in organic  $\pi$  systems," *Journal of Molecular Structure: Theochem*, vol. 425, no. 1–2, pp. 155–159, 1998.
- [45] M. Knupfer and J. Fink, "Mott-Hubbard-like behavior of the energy gap of  $\text{A}_4\text{C}_{60}$  ( $\text{A} = \text{Na}, \text{K}, \text{Rb}, \text{Cs}$ ) and  $\text{Na}_{10}\text{C}_{60}$ ," *Physical Review Letters*, vol. 79, no. 14, pp. 2714–2717, 1997.
- [46] Y. Iwasa, K. Tanaka, T. Yasuda, T. Koda, and S. Koda, "Metallic reflection spectra of  $\text{K}_3\text{C}_{60}$ ," *Physical Review Letters*, vol. 69, no. 15, pp. 2284–2287, 1992.
- [47] E. Sohmen, J. Fink, and W. Krätschmer, "Electronic structure studies of undoped and  $n$ -type doped fullerene  $\text{C}_{60}$ ," *Europhysics Letters*, vol. 17, pp. 51–55, 1992.
- [48] A. Wachowiak, R. Yamachika, K. H. Khoo, et al., "Applied physics: visualization of the molecular Jahn-Teller effect in an insulating  $\text{K}_4\text{C}_{60}$  monolayer," *Science*, vol. 310, no. 5747, pp. 468–470, 2005.
- [49] J. N. O'Shea, "Molecular orbitals tell the story," *Science*, vol. 310, no. 5747, pp. 453–454, 2005.
- [50] M. Capone, M. Fabrizio, C. Castellani, and E. Tosatti, "Colloquium: modeling the unconventional superconducting properties of expanded  $\text{A}_3\text{C}_{60}$  fullerenes," *Reviews of Modern Physics*, vol. 81, no. 2, pp. 943–958, 2009.
- [51] G. R. Darling, A. Y. Ganin, M. J. Rosseinsky, Y. Takabayashi, and K. Prassides, "Intermolecular overlap geometry gives two classes of fulleride superconductor: electronic structure of 38 K  $\text{T}_c\text{CS}_3\text{C}_{60}$ ," *Physical Review Letters*, vol. 101, no. 13, Article ID 136404, 2008.
- [52] S. Larsson, accepted for publication, *International Journal of Quantum Chemistry*.

## Review Article

# Antiadiabatic Theory of Superconducting State Transition: Phonons and Strong Electron Correlations—The Old Physics and New Aspects

**Pavol Baňacký**

*Chemical Physics Division, Institute of Chemistry, Faculty of Natural Science, Comenius University, Mlynská dolina CH2, 84215 Bratislava, Slovakia*

Correspondence should be addressed to Pavol Baňacký, banacky@fns.uniba.sk

Received 31 May 2009; Accepted 3 September 2009

Academic Editor: Sasha Alexandrov

Copyright © 2010 Pavol Baňacký. This is an open access article distributed under the Creative Commons Attribution License, which permits unrestricted use, distribution, and reproduction in any medium, provided the original work is properly cited.

Complex electronic ground state of molecular and solid state system is analyzed on the ab initio level beyond the adiabatic Born-Oppenheimer approximation (BOA). The attention is focused on the band structure fluctuation (BSF) at Fermi level, which is induced by electron-phonon coupling in superconductors, and which is absent in the non-superconducting analogues. The BSF in superconductors results in breakdown of the adiabatic BOA. At these circumstances, chemical potential is substantially reduced and system is stabilized (effect of nuclear dynamics) in the antiadiabatic state at broken symmetry with a gap(s) in one-particle spectrum. Distorted nuclear structure has fluxional character and geometric degeneracy of the antiadiabatic ground state enables formation of mobile bipolarons in real space. It has been shown that an effective attractive e-e interaction (Cooper-pair formation) is in fact correction to electron correlation energy at transition from adiabatic into antiadiabatic ground electronic state. In this respect, Cooper-pair formation is not the primary reason for transition into superconducting state, but it is a consequence of antiadiabatic state formation. It has been shown that thermodynamic properties of system in antiadiabatic state correspond to thermodynamics of superconducting state. Illustrative application of the theory for different types of superconductors is presented.

## 1. Introduction

Superconductivity, an amazing physical phenomenon discovered nearly 100 years ago by Kamerlingh Onnes [1] and his assistant Gilles Holst whose name has been basically forgotten by history (see, e.g., [2]), has been one of the most important research fields of solid-state physics of last century and it remains until the present days. What is extremely irritating is the fact that microscopic mechanism of superconducting state transition, in spite of enormous attention which has been paid to this effect, remains still unclear and represents an open challenge for theory.

Until the discovery of high-temperature superconductivity of cuprates by Bednorz and Muller in 1986 [3] and synthesis of first 90 K superconductor [4] in 1987, understanding of microscopic mechanism of superconducting (SC) state transition formulated within the BCS theory in 1957 [5]

was generally accepted as a firm theoretical basis behind the physics of this phenomenon. Here, the basic physics is the idea of Cooper-pairs formation, that is, formation of boson-like particles in momentum space, which are stable in thin layer above the Fermi level and drive system into more stable-superconducting state. Sufficient condition of pair formation is whatever weak, but attractive, interaction between electrons. Real possibility of effective attractive electron-electron interactions was well known. Some years ago it was derived by Fröhlich [6, 7] as a consequence of electron-phonon (e-p) interactions.

The range of validity of the BCS theory with respect to e-p interactions has been specified by Migdal [8] and Eliashberg [9, 10]. It can be interpreted as Migdal's theorem and Eliashberg's restriction (ME approximation). The first is related to validity of the condition  $\omega\lambda/E_F \ll 1$  and the second one restricts the validity only for  $\lambda \leq 1$ , where  $\lambda$  is e-p

coupling strength and  $\omega$  and  $E_F$  are characteristic phonon and electron energy scales, respectively. Expressed explicitly, BCS-like theories are valid only for adiabatic systems that obey the adiabatic Born-Oppenheimer approximation (BOA):  $\omega/E_F \ll 1$ .

While for conventional (low-temperature) superconductors, the BCS theory within the ME approximation (i.e., weak coupling regime) is an excellent extension of standard theory of metals, for high-temperature cuprates in order to interpret high critical temperature and ensure the pairs condensation, beside (or instead of) the e-p interactions the important role of other interaction mechanisms has been advocated (see e.g., [11–13]). Since the copper, a transition metal with incompletely filled d-shell when chemically bounded, is a central atom of high- $T_c$  cuprates, it is quite natural that the attention has been focused on strong electron correlations (in a sense of standard Coulomb-repulsive e-e interactions), magnetic interactions, and/or spin fluctuation effects. At the present, the effect of Coulomb repulsion is usually incorporated via Coulomb pseudopotential  $\mu^*$  and critical temperature is calculated according to McMillan formula [14].

The e-p interactions, which have been accepted to be responsible for electron pairing that drive transition into superconducting state for classical low- $T_c$  superconductors, have become nearly abandoned and considered to be rather harmful for superconductivity in high- $T_c$  cuprates (see, e.g., [12]). Some aspects of d-wave superconductivity can be described within the models of strongly correlated electrons, for example, Hubbard-like or t-J models (e.g., [11, 15–19]), even without explicit account for e-p interactions. The underlying leitmotiv behind the electron correlation treatments has been to understand the phase diagram of high- $T_c$  cuprates, that is, the doping process. Introduction of charge carriers (holes or electrons) into the parent antiferromagnetic insulator that causes transition to superconductor (or metal) has been generally accepted to be a universal feature of high- $T_c$  cuprates and believed to be a matter intimately related to microscopic mechanism of superconductivity.

Bell-like-shaped dependence of  $T_c$  on hole doping in the doping range  $0.05 \leq x < 0.27$  for family of high- $T_c$  cuprates is well known (see, e.g., [20] and references therein). With the exception of YBCO ( $x = 0.05$ ), the optimal hole doping with maximal  $T_c$  is  $x \approx 0.16$ . The electron doping is usually less favorable, but basically either hole or electron doping can induce superconductivity. It is, for instance, the case of infinite-layer compound  $\text{CaCuO}_2$  (itself is an insulator) where by hole or electron doping in field-induced transistor configuration superconductivity can be induced with  $T_c$  up to 89 K (or 34 K for electron doping) at about 0.15 charge carriers per  $\text{CuO}_2$ .

Without any doubts, charge doping has no-negligible impact on e-e interactions and influences, to some extent, also more subtle spin interactions. Question remains if these are the key effects behind the physics which causes superconducting state transition upon doping?

In this respect, one has to realize that like  $T_c$ , the lattice parameters and, what is very important, the lattice dynamics is strongly influenced by doping. For instance, dependence of

$T_c$  on lattice parameter  $a$  in case of Hg-based cuprates follows similar dependence as it does  $T_c$  on hole doping [21]. In spite that isotope effect coefficient  $\alpha$  for optimally doped cuprates is very small ( $\alpha \approx 0.05$ , exception is YBCO— $\alpha \approx 0.8$ ), doping in underdoped as well in overdoped region for O-isotope effect (all-over the cuprates family), results in a huge changes of isotope effect coefficient  $\alpha$  (see, e.g., [22, 23]). It is important experimental evidence that doping induces very strong changes in lattice dynamics, in particular in dynamics of  $\text{CuO}_2$  layers. From theoretical stand point, it means that mechanism of superconducting state transition is a complex matter of electron and nuclear degrees of freedom.

The results of high-resolution ARPES study [24, 25] of wide family of different high- $T_c$  cuprates have brought the other experimental evidence indicating that beside doping, an abrupt change (decrease) of electron velocity near Fermi level, at about 50–80 meV in nodal direction, is the other feature common to high- $T_c$  cuprates. The kink in nodal direction is temperature independent. More important, from the stand point of microscopic theory of superconductivity, seems to be formation of temperature-dependent kink on momentum distribution curve (dispersion renormalization) close to Fermi level ( $\sim 60$  meV) in off-nodal direction at transition to superconducting state. It has been reported for  $\text{Bi2212}$  [26–29]. Recently, presence of the kink in off-nodal direction has been observed at VUV ARPES study with sub-meV resolution of optimally doped untwinned YBCO in superconducting state [30].

Formation of the off-nodal kink (dispersion renormalization) has been attributed by the authors [26] to the coupling of electrons to a bosonic excitations, preferably they consider a magnetic resonance mode such as observed in some inelastic neutron scattering experiments. The inconsistency in this interpretation has been pointed out by the authors of [27, 29]. The main points are described in [29] as follows: (a) magnetic resonance has not yet been observed by neutron scattering in such a heavily doped cuprates, and (b) magnetic resonance has little spectral weight and may be too weak to cause the effect seen by ARPES. They agree, however, with the opinion of the authors [26] that the renormalization effect seen by ARPES in cuprates may indeed be related directly to the microscopic mechanism of superconductivity. The authors of [27, 29] instead of magnetic resonance mode, attribute the dispersion renormalization to coupling with phonon mode, in particular, with  $B_{1g}$ -buckling mode of  $\text{CuO}_2$  plane. The temperature dependence of dispersion renormalization they attribute to the DOS enhancement due to SC-gap opening and to the thermal broadening of the phonon self-energy in normal state.

These results along with the results of neutron scattering [31, 32] indicate that also for high- $T_c$  cuprates the e-p coupling has to be considered as a crucial element of microscopic mechanism of SC state transition. Expressed explicitly, also in case of cuprates the role of phonons at superconducting state transition must not be overlooked. As soon as low-Fermi energy situation occurs ( $\omega \leq E_F$ ), one can expect important contribution of nonadiabatic vertex corrections at SC state transition. It is beyond the standard ME approximation and this problem has been

studied within the nonadiabatic theory of superconductivity [33–35]. On the other hand, as the ARPES results indicate, electron kinetic energy is decreased and importance of proper treatment of electron-electron Coulomb interactions is increased. The competition between Coulomb and e-p interactions has been intensively studied within the Holstein-Hubbard models [36–40] with both interactions of short-range character. The obtained results are not satisfactory since heavy-mass polarons are formed that yield low values of  $T_c$ . It has been improved within the Frohlich-Coulomb model [41] that introduces long-range repulsion between charge-carriers and also long-range e-p interactions. The results show that there is a narrow window of parameters of Coulomb repulsion  $V_c$  and e-p interactions  $E_p$  ( $V_c / E_p$ ) resulting in the light-mass bipolarons formation. In this case, according to bipolaron theory of superconductivity [42–44], coherent motion of bipolarons represents the supercarrier motion and high  $T_c$  can be reached.

The McMillan formula, which is very good approximation for  $T_c$  of elementary metals and their alloys [45], is often used also for calculation of critical temperature of high- $T_c$  superconductors within the BCS-generic framework. It has been shown [46] that in strong-coupling regime  $\lambda \gg 1$ ,  $T_c$  can be as large as  $k_B T_c = \hbar \omega \lambda^{1/2} / 2\pi$ . However, in reality there is problem with correct estimation of Coulomb pseudopotential  $\mu^*$  and with unrealistically large values of  $\lambda$  that would match high experimental  $T_c$  of novel superconductors. It has to be stressed, however, that strong coupling regime  $\lambda > 1$  violates adiabatic condition  $\omega/E_F \ll 1$  of the ME approximation, which is behind the derivation of the McMillan formula.

More over, new class of superconductors, for example, cuprates, fullerides, and  $\text{MgB}_2$  are systems that are rather pseudoadiabatic with sizeable adiabatic ratio  $\omega/E_F < 1$  [47], in contrast to elementary metals, where adiabatic condition  $\omega/E_F \ll 1$  is perfectly fulfilled. This situation indicates the importance of nonadiabatic contributions at calculation of e-p interactions within the BOA, an effect which is beyond the standard ME approach. As mentioned above, formulation of the nonadiabatic theory of superconductivity by Pietronero et al. [33–35, 48, 49], which accounts for vertex corrections and cross phonon scattering (beyond ME approximation), has solved this nontrivial problem by generalization of Eliashberg equations. The theory, which is nonperturbative in  $\lambda$  and perturbative in  $\lambda \omega_D/E_F$ , has been applied at simulation and interpretation of different aspects of high- $T_c$  superconductivity [50–54]. Basically, it can be concluded that accounts for nonadiabatic effects in quasiadiabatic state  $\omega/E_F \leq 1$  is able to simulate different properties of high- $T_c$  superconductors, including high-value of  $T_c$ , already at relatively moderate value of e-p coupling,  $\lambda \approx 1$ . Moreover, it has also been shown that increased electron correlation is important factor that makes corrections to vertex function positive, which is in this context crucial for increasing  $T_c$ .

Nonetheless, sophisticated treatment of high- $T_c$  superconductivity within the nonadiabatic theory faces serious problem related to possibility of polaron collapse of the band and bipolaron formation. According to bipolaron theory of Alexandrov [42–44, 47, 55–58], polaron collapse occurs

already at  $\lambda \approx 0.5$  for uncorrelated polarons and even at smaller value for a bare e-p coupling in strongly correlated systems. For  $\omega/E_F \leq 1$ , or  $\lambda \geq 1$ , and for  $\omega/E_F \geq 1$  at whatever small value  $\lambda \ll 1$ , the nonadiabatic polaron theory has been shown to be basically exact [58]. Bipolarons can be simultaneously small and light in suitable range of Coulomb repulsion and e-p interaction [59]. These results have important physical consequences. There are serious arguments that effect of polaron collapse cannot be covered through calculation of vertex corrections due to translation symmetry breaking and mainly, polaron collapse changes possible mechanism of pair formation, that is, instead of BCS scenario with Cooper pair formation in momentum space, the BEC with mobile bipolarons (charged bosons) in real space becomes operative.

Discovery of superconductivity in a simple compound  $\text{MgB}_2$  at 40 K [60] has been very surprising and has started a new revitalization of superconductivity research. Beside the many interesting aspects, discovery of the  $\text{MgB}_2$  superconductivity is, in my opinion, crucial for general theoretical understanding of SC state transition on microscopic level. It is related to band structure (BS) fluctuation and dramatic changes of BS topology at e-p coupling.

The  $\sigma$  bands splitting at coupling to  $E_{2g}$  mode in  $\text{MgB}_2$  has been reported [61] already in 2001 but, with exception of possible impact of anharmonicity [62], no special attention has been paid to this effect. Superconductivity in  $\text{MgB}_2$  has been straightforwardly interpreted [63] shortly after the discovery as a standard BCS-like, even of intermediate-strong coupling character. For clumped nuclear equilibrium geometry, the BS is of adiabatic metal-like character. The  $E_F^\sigma$  of  $\sigma$  band electrons (chemical potential  $\mu$ ) is relatively small,  $\approx 0.4$  eV, but still great enough comparing to vibration energy of  $E_{2g}$  phonon mode,  $\omega_{2g} \approx 0.07$  eV. Though the adiabatic ratio  $\omega/E_F \approx 0.15$  is sizable, it is small enough in order to interpret superconductivity within the BCS-generic framework. It is supposed that nonadiabatic effects, anharmonic contributions and/or Coulomb interactions within generalized Eliashberg approach should be important in this case. On the other hand, the value of e-p coupling,  $\lambda \approx 0.7$  indicates that polaron collapse can be expected and superconductivity should be of nonadiabatic bipolaron character rather than the BCS-like.

Nevertheless, the matter is even more complicated. It has been shown [64, 65] that analytic critical point (ACP—maximum, minimum, or saddle point of dispersion, in case of  $\text{MgB}_2$  it is maximum) of  $\sigma$  band at  $\Gamma$  point crosses Fermi level (FL) at vibration displacement  $\approx 0.016$  Å/B-atom, that is, with amplitude  $\approx 0.032$  Å, which is smaller than root-mean square (rms) displacement ( $\approx 0.036$  Å) for zero-point vibration energy in  $E_{2g}$  mode. It means, however, that in vibration when ACP approaches FL on the distance less than  $\pm \omega$ , the adiabatic Born-Oppenheimer approximation (BOA) is not valid. In this case, Fermi energy  $E_F^\sigma$  of  $\sigma$  band electrons (chemical potential  $\mu$ ) close to  $\Gamma$  point is smaller than  $E_{2g}$  mode vibration energy  $E_F^\sigma < \omega_{2g}$  and at the moment when the ACP of the band touches Fermi level, the Fermi energy is reduced to zero,  $E_F \rightarrow 0$ . Moreover, shift of the ACP substantially increases density of states (DOS) at FL,

$n_\sigma(E_F) = (\partial \varepsilon_\sigma^0 / \partial k)_{E_F}^{-1}$ , and induces corresponding decrease of effective electron velocity  $(\partial \varepsilon_\sigma^0 / \partial k)_{E_F}$  of fluctuating band in this region of  $k$ -space. From the physical stand point, it represents transition of the system from adiabatic  $\omega \leq E_F$  into true nonadiabatic  $\omega > E_F$ , or even into strong antiadiabatic state with  $\omega \gg E_F$ . This effect has crucial theoretical impact. At these circumstances, not only ME approximation is not valid (including impossibility to calculate nonadiabatic vertex corrections which represent off-diagonal corrections to adiabatic ground state) but adiabatic BOA itself does not hold as well.

The BOA is crucial approximation of theoretical molecular as well as of solid-state physics. It enables to solve many-body problem via separation of electronic and nuclear motion and to study electronic problem in a field which is created by fixed nuclei.

On the level of the BOA, the motion of the electrons is a function of the instantaneous nuclear coordinates  $Q$ , but is not dependent on the instantaneous nuclear momenta  $P$ . Usually, and in solid state physics basically always, only parametric dependence is considered, that is, nuclear coordinates are only parameters in solution of electronic problem within the clamped nuclei Hamiltonian treatment. Nuclear coordinate-dependence, when explicitly treated, modifies nuclear potential energy by so called diagonal BO correction (DBOC) that reflects an influence of small nuclear displacements out of the equilibrium positions and corrects the electronic energy of clamped nuclear structure. The DBOC enters directly into the potential energy term of nuclear motion (but leaves unchanged the nuclear kinetic energy) and in this way modifies vibration frequencies. The off-diagonal terms of the nuclear part of system Hamiltonian that mix electronic and nuclear motion through the nuclear kinetic energy operator term are neglected and it enables independent diagonalization of electronic and nuclear motion (adiabatic approximation). Neglecting the off-diagonal terms is justified only if these are very small, that is, if the energy scales of electron and nuclear motion are very different and when adiabatic condition holds, that is,  $\omega/E \ll 1$ . If necessary, small contribution of the off-diagonal terms can be calculated by perturbation methods as so called nonadiabatic correction to the adiabatic ground state.

Situation for superconductors seems to be substantially different, at least in case of the  $\text{MgB}_2$ . There is considerable reduction of electron kinetic energy, which for antiadiabatic state results even in dominance of nuclear dynamics ( $\omega \gg E_F$ ) in some region of  $k$ -space. In this case, it is necessary to study electronic motion as explicitly dependent on the operators of instantaneous nuclear coordinates  $Q$  as well as on the operators of instantaneous nuclear momenta  $P$ . It is a new aspect for many-body theory.

The electronic theory of solids has been developed with the assumption of validity of the adiabatic BOA. In this respect, it is natural that different theoretical-microscopic treatments of superconductivity based on model Hamiltonians which stress importance of one or the other type of interaction mechanism, implicitly assume validity of the BOA, and it is very seldom that possibility of the BOA breakdown at transition to SC state is risen. The notion

“nonadiabatic” effects in relation to electronic structure is commonly used for contributions of the off-diagonal matrix elements of interaction Hamiltonian (e.g., e-p coupling, e-e correlations, etc.) to the adiabatic ground state electronic energy calculated in second and higher orders of perturbation theory and does not account for true nonadiabatic-antiadiabatic situation,  $\omega > E_F$ .

In this connection, a lot of important questions arise, as the following examples.

- (i) How to treat antiadiabatic state?
- (ii) Can be system stable in antiadiabatic state?
- (iii) Are the physical properties of the system in antiadiabatic state different from the corresponding properties in adiabatic state?
- (iv) What is the driving force for adiabatic  $\leftrightarrow$  antiadiabatic state transition, that is, which type of interaction mechanism and at which circumstances trigger this type of transition?
- (v) How relevant is adiabatic  $\leftrightarrow$  antiadiabatic state transition for SC state transition in  $\text{MgB}_2$ ?
- (vi) Is the adiabatic  $\leftrightarrow$  antiadiabatic state transition an accidental effect at SC state transition which is present only in  $\text{MgB}_2$ , or this state transition is an inherent physical mechanism which is proper also for other superconductors?
- (vii) Can be adiabatic  $\leftrightarrow$  antiadiabatic state transition relevant for high, as well as for low-temperature superconductors?
- (viii) Phonons or strong electron correlations?
- (ix) What is the character of condensate-Cooper pairs or bipolarons?
- (x) Is there any relation of the adiabatic  $\leftrightarrow$  antiadiabatic state transition to Cooper pairs formation?
- (xi) Cooper pairs or correction to electron correlation energy?

Theoretical aspects related to the above problems have been elaborated and discussed in details within “Ab initio theory of complex electronic ground state of superconductors”, which has been published in the papers, [66–68]. The main theoretical point is generalization of the BOA by sequence of canonical-base functions transformations. The final electronic wave function is explicitly dependent on nuclear coordinates  $Q$  and nuclear momenta  $P$ , or alternatively, emerging new quasiparticles-nonadiabatic fermions are explicitly dependent on nuclear dynamics. As a result, the effect of nuclear dynamics can be calculated in a form of corrections to the clamped nuclei ground state electronic energy, to the one-particle spectrum and to the two-particle term, that is, to the electron correlation energy.

*Note.* To avoid confusion, it should be stressed that the notion electron correlation energy as used in this paper stands for improvement of e-e interaction term contribution beyond the Hartree-Fock (HF) level,  $E_{\text{corr}} = E_{\text{exact}} - E_{\text{HF}}$

( $E_{\text{exact}} < E_{\text{HF}}$ ), as it can be calculated, for example, by  $(1/r)$ -perturbation theory in the second and the higher orders, or by configurations interaction method. In condensed matter physics, electron correlation usually stands for an account for Coulomb e-e interaction at least on Hartree or HF level. On the HF level not only repulsive e-e term is present, like on Hartree level where spin is not considered at all, but also exchange term, fermion Coulomb-hole only for electrons with parallel spins. Correlation energy improves an account for unbalanced treatment of e-e interaction for electrons with parallel and antiparalel spins on HF level.

It has been shown that due to e-p interactions, which drive system from adiabatic into antiadiabatic state, adiabatic symmetry is broken and system is stabilized in the antiadiabatic state at distorted geometry with respect to the adiabatic equilibrium high symmetry structure. Stabilization effect is due to participation of nuclear kinetic energy term, that is, it is the effect of nuclear dynamics (dependence on  $P$ ) which is absent in the adiabatic state on the level of the BOA. The antiadiabatic ground state at distorted geometry is geometrically degenerate with fluxional nuclear configuration in the phonon modes that drive system into this state. It has been shown that while system remains in antiadiabatic state, nonadiabatic polaron-renormalized phonon interactions are zero in well defined  $k$ -region of reciprocal lattice. Along with geometric degeneracy of the antiadiabatic state, it enables formation of mobile bipolarons (in a form of polarized intersite charge density distribution) that can move over lattice in external electric potential as supercarriers without dissipation. Moreover, it has been shown that due to e-p interactions at transition into antiadiabatic state,  $k$ -dependent gap in one-electron spectrum has been opened. Gap opening is related to the shift of the original adiabatic Hartree-Fock orbital energies and to the  $k$ -dependent change of density of states of particular band(s) at the Fermi level. The shift of orbital energies determines in a unique way one-particle spectrum and thermodynamic properties of system. It has been shown that resulting one-particle spectrum yields all thermodynamic properties that are characteristic for system in superconducting state, that is, temperature dependence of the gap, specific heat, entropy, free energy, and critical magnetic field. The  $k$ -dependent change of the density of states at the Fermi level in transition from adiabatic (nonsuperconducting) into antiadiabatic state (superconducting) can be experimentally verified by ARPES or tunneling spectroscopy as spectral weight transfer at cooling superconductor from temperatures above  $T_c$  down to temperatures below  $T_c$ .

Results of the ab initio theory of antiadiabatic state have shown that Fröhlich's effective attractive electron-electron interaction term represents correction to electron correlation energy in transition from adiabatic into antiadiabatic state due to e-p interactions. Analysis of this term has shown that increased electron correlation is a consequence of stabilization of the system in superconducting electronic ground state, but not the reason of its formation.

In the present article, the key points of the theory are recapitulated and the adiabatic  $\leftrightarrow$  antiadiabatic state

transition is shown to be operative for different types of superconductors.

## 2. Electronic Ground State Beyond the Born-Oppenheimer Approximation

*2.1. Preliminary Remarks.* Development of the theory of molecules and solids has been enabled due to fundamental approximation, the Born-Oppenheimer approximation (BOA). With respect to electronic structure of superconductors and transition to superconducting state, some aspects of this approximation should be outlined at the beginning.

Solution of the Schrödinger equation of many-body system composed of  $N_e$  electrons and  $N_n$  nuclei (total system)

$$\hat{H}\Psi(r, R) = E^{TS}\Psi(r, R) \quad (1)$$

with the Hamiltonian

$$\hat{H} = \hat{T}_N + \hat{T}_e + \hat{V}_{ee}(r) + \hat{V}_{eN}(r, R) + E_{NN}(R), \quad (2)$$

and wave function  $\Psi(r, R)$ , which is a general function of the sets of electron  $\{r\}$  and nuclear  $\{R\}$  Cartesian coordinates, is possible at the assumption of validity of the Born-Oppenheimer approximation (BOA). The BOA, originally formulated in the work in [69] by power expansion of potential surface for nuclear motion at equilibrium geometry with respect to displacement and electron/nuclear mass ratio  $(m_e/M_n)^{1/4}$ , has been reformulated later by Born [70, 71] in a more practical form. According to it, the wave function of the total system (1) can be expressed in the factorized form

$$\Psi(r, R) = \sum_m \chi_m(R) \Phi_m(r, R), \quad (3)$$

as a linear combination of known adiabatic electronic wave functions  $\{\Phi_m(r, R)\}$  that are the eigenfunctions of clumped nuclei electronic Schrödinger equation

$$\hat{H}_e \Phi_m(r, R) = E_m^e \Phi_m(r, R), \quad (4)$$

with the electronic Hamiltonian:

$$\hat{H}_e = \hat{T}_e + \hat{V}_{ee}(r) + \hat{V}_{eN}(r, [R]), \quad (5)$$

at fixed nuclear configuration  $[R]$ . Expansion coefficients  $\{\chi_m(R)\}$  in (3), regarded as unknown, are nuclear wave functions for nuclear configuration  $R$  with the electronic subsystem in particular adiabatic electronic state  $\Phi_m(r, R)$ .

The  $R$ -dependence in (5) is only parametric and in general it should be calculated over the full configuration space  $\{R\}$  in order to calculate the adiabatic potential hypersurface  $\{E_m^e(R)\}$  of nuclear motion.

With respect to (3) and (4), the Schrödinger equation of the total system (1) for electronic state  $\Phi_n(r, R)$  can be written in the form

$$\{\hat{T}_N + E_n^{te}(R) - E^{TS}(R)\} \chi_n(R) = \sum_m \hat{\Lambda}_{nm}(R) \chi_m(R) \quad (6)$$

with the term  $\hat{\Lambda}_{nm}(R)$ , which couples electronic and nuclear motions, on the right-hand side (rhs):

$$\begin{aligned}\hat{\Lambda}_{nm}(R) &= \hat{A}_{nm}(R) - B_{nm}(R) \\ &= \sum_j \frac{\hbar^2}{M_j} \int \Phi_n^*(r, R_j) \frac{\partial}{\partial R_j} \Phi_m(r, R_j) dr \cdot \frac{\partial}{\partial R_j} \\ &\quad - \int \Phi_n^*(r, R) \hat{T}_N(R) \Phi_m(r, R) dr.\end{aligned}\quad (7)$$

The term  $E_n^{te}$  in (6):

$$E_n^{te}(R) = (E_n^e(R) + E_{NN}(R)) \quad (8)$$

is total adiabatic electronic energy, that is, adiabatic electronic energy plus nuclear Coulomb repulsion at nuclear configuration  $R$ .

Until the Born approach (3) is valid, (6) is exact and it still describes coupled motion of electrons and nuclei over the term (7),  $\hat{\Lambda}_{nm}(R)$ , which represents possibility of transitions between different adiabatic electronic states,  $\Phi_n(r, R) \leftrightarrow \Phi_m(r, R)$ , due to nuclear motion ( $R$ -dependence). If such transitions are forbidden from the symmetry reasons, or if there is physically reasonably justified assumption that contributions of such transitions are negligibly small, then one can omit the rhs term, and (6) can be written in the diagonal form:

$$\left\{ \hat{T}_N + (E_n^{te}(R) + B_{nn}(R)) - E_{n,\nu}^{TS}(R) \right\} \chi_{n,\nu}(R) = 0, \quad (9)$$

where  $B_{nn}$  is the only a nonzero diagonal contribution of the  $\Lambda$  term

$$\begin{aligned}B_{nn}(R) &= \int \Phi_n^*(r, R) \hat{T}_N(R) \Phi_n(r, R) dr \\ &= \sum_n \frac{\hbar^2}{2M_n} \int \Phi_n^*(r, R) \nabla_n^2 \Phi_n(r, R) dr \\ &= \sum_{n\alpha} \frac{\hbar^2}{2M_n} \int \left( \frac{\partial \Phi_n(r, \vec{R})}{\partial R_{n\alpha}} \right)^* \left( \frac{\partial \Phi_n(r, \vec{R})}{\partial R_{n\alpha}} \right) dr|_{[R]}.\end{aligned}\quad (10)$$

The term (10) is the mean-value of the nuclear kinetic energy for adiabatic electronic state  $\Phi_n(r, R)$  at nuclear configuration  $\{R\}$  and represents so called adiabatic diagonal Born-Oppenheimer (DBOC) correction to the total adiabatic electronic energy  $E_n^{te}(R)$ . However, (9) is then the equation of motion of nuclei and it has the form of Schrödinger equation with Hamiltonian:

$$\hat{H}_N(R) = \hat{T}_N + V_{NN}^{\text{eff}}(R). \quad (11)$$

The effective-adiabatic potential for nuclear motion  $V_{NN}^{\text{eff}}(R)$ :

$$V_{NN}^{\text{eff}}(R) = E_n^{te}(R) + B_{nn}(R) \quad (12)$$

is represented by the total electronic energy (8), that is, Coulomb potential energy of the bare nuclei repulsion

$E_{NN}(R)$  and adiabatic electronic energy  $E_n^e(R)$ , which is corrected by mean-value of the nuclear kinetic energy (DBOC) for the particular adiabatic electronic state  $\Phi_n(r, R)$  (10). Contribution of the adiabatic DBOC is usually neglected as very small quantity, mean value of kinetic energy of slowly moving heavy nuclei in contrast to fast motion of light adiabatic electrons.

At these circumstances, the motion of electrons and nuclei is effectively decoupled, that is, it is possible to realize an independent diagonalization of the electronic Schrödinger equation (4) and nuclear Schrödinger equation (9), electrons and nuclei of the system behave like two statistically independent sets. Assumed small contribution of the rhs term of (6) can be calculated by some approximate way, usually by perturbation theory. Then, problem with the Hamiltonian:

$$\hat{H}(R) = \hat{H}^0(R) + H'(R) \quad (13)$$

is studied, where

$$\hat{H}^0(R) = \hat{H}_{te}(R) + H_N(R) = \{(5) + E_{NN}(R)\} + (11) \quad (14)$$

is unperturbed part, and

$$H'(R) = \hat{\Lambda}_{mn}(R); \quad \left( H'_{mn}(R) = \int \chi_{m\mu}^*(R) \hat{\Lambda}_{mn}(R) \chi_{n\nu}(R) dR \right); \quad m \neq n \quad (15)$$

is a small perturbation.

In practice, physical and/or chemical properties of a many-body system in its ground electronic state  $\Phi_0(r, R)$  are of the prime interest. In this case, the Born approach (3) is usually restricted to the single term and the total wave function of system is a simple product of the adiabatic electronic wave function  $\Phi_0(r, R)$  and corresponding nuclear wave function:

$$\Psi_0(r, R) = \chi_{0,\nu}(R) \Phi_0(r, R). \quad (16)$$

The Born approach in the form (16) is the adiabatic approximation. In a common sense, what is usually called the Born-Oppenheimer approximation (BOA, or clamped nuclei-crude adiabatic BOA) is the adiabatic approximation where the contribution of the DBOC (i.e.,  $B_{00}(R)$  term in (12)) is also neglected and wave function (16) has the form

$$\Psi_0(r, R) = \chi_{0,\nu}(R) \Phi_0(r, R_{\text{eq}}). \quad (17)$$

Contributions of the off-diagonal terms  $\hat{\Lambda}_{0m}(R)$  in (15) which are calculated as a small perturbation to the Hamiltonian (14) represent a nonadiabatic correction to the unperturbed adiabatic ground state. The conditions at which the nonadiabatic correction can be expected to be small, and the BOA (16, and in general 3) is valid, can be estimated by analysis of the second-order contributions to the energy of the total system,  $E_0^{TS}(R)$ , which are small providing that

$$\left| \int \chi_{0,\nu}^*(R) \hat{\Lambda}_{0m}(R) \chi_{m,\mu}(R) dR \right| \ll \left| E_{0,\nu}^{TS}(R) - E_{n,\mu}^{TS}(R) \right|. \quad (18)$$

It can be derived (see, e.g., [72]), based on the expansion of the effective nuclear potential ( $V_{NN}^{\text{eff}}(R) = E_0^{te}(R)$ ) at equilibrium nuclear geometry  $R_{\text{eq}}$  (where the total electronic ground-state energy reaches its absolute minimum) at least up to the quadratic term in a displacement  $\Delta R$ :

$$\begin{aligned} E_0^{te}(R) &= E_0^{te}(R_{\text{eq}}) + \frac{1}{2} \frac{\partial^2 E_0^{te}(\Delta R)}{\partial \Delta R^2} \cdot \Delta R^2 + \dots \\ &= E_0^{te}(R_{\text{eq}}) + \frac{\hbar}{2} \sum_s \omega_s \xi_s^2 + \dots \end{aligned} \quad (19)$$

The result is that (18) holds and the BOA (16), (3) is valid, if inequality

$$\left| E_0^{te}(R_{\text{eq}}) - E_n^{te}(R_{\text{eq}}) \right| \gg \hbar \omega_s \quad (20)$$

is fulfilled for electronic and vibration (phonon) energy spectrum of a system. The meaning of (20) is clear, the electronic spectrum, that is, the differences between the total electronic energies of the excited electronic states and the ground-state energy has to be much greater than vibration (phonon) energy spectrum of system.

The long-time experience of theoretical molecular and solid-state physics has shown that for a ground electronic state of vast majority of molecular systems and solids at equilibrium geometry  $R_{\text{eq}}$ , the BOA is absolutely good approximation. In case of solids, it has enabled to derive (Bloch's assumption of small perturbation of the periodic lattice potential for small nuclear displacement out of equilibrium) the field theory Hamiltonian of total system (13) in a well-known form,  $\hat{H} = \hat{H}^0 + \hat{H}_{ep}$ , with

$$\hat{H}^0 = \sum_{k\sigma} \varepsilon_k^0 a_{k\sigma}^+ a_{k\sigma} + \sum_q \hbar \omega_q \left( b_{-q}^+ b_q + \frac{1}{2} \right). \quad (21)$$

The perturbation Hamiltonian  $\hat{H}_{ep}$  represents now, instead of nuclear kinetic energy  $\Lambda$ -perturbation term (15), an electron-phonon (e-p) interaction term:

$$\hat{H}_{ep} = \sum_{k,q,\sigma} u^q (b_q + b_{-q}^+) a_{k+q,\sigma}^+ a_{k,\sigma}. \quad (22)$$

In this case, no special attention has been paid to the diagonal correction (10) to the total electronic ground-state energy, and at derivation of (21) and (22), this correction has been omitted as negligibly small quantity. Moreover, since perturbation  $H'$  is now introduced as an e-p interaction  $H_{ep}$ , it is immediately seen from the form of (16) and (22) that the first-order correction, that is, diagonal perturbation term, equals zero:  $\langle \Phi_0 | \hat{H}_{ep} | \Phi_0 \rangle = 0$ . All interesting physics is then related to higher-order contributions with participation of excited electronic states, that is, the first possible nonzero contributions are in the second order of perturbation theory, that is, terms of the form  $\langle \Phi_0 | \hat{H}_{ep} | \Phi_n \rangle \langle \Phi_n | \hat{H}_{ep} | \Phi_0 \rangle / (E_0^{te} - E_n^{te})$ .

Hamiltonian (21), (22) has been the starting point for theoretical study of the effects connected to e-p interactions in solids. By means of the famous unitary transformation

of this Hamiltonian, Fröhlich has derived [6, 7] an effective electron-electron interaction term which is a crucial element at formulation of the BCS [5] or Migdal-Eliashberg (ME) theory of superconductivity [8–10]. The extension of the ME theory, that is, inclusion of higher-order contributions of e-p interactions by means of Feynman-Dyson perturbation expansion of  $H_{ep}$  (vertex corrections) is the basis for so called “nonadiabatic” theory of superconductivity, as it has been developed by Pietronero et al. [33–35, 48, 49]. It should be pointed-out that not only the above-mentioned standard and “nonadiabatic” theories of superconductivity but also other theoretical models of superconductivity which do not consider explicitly e-p interactions assume tacitly validity of the BOA as soon as the model Hamiltonian is written in the form

$$\hat{H}(R) = \hat{H}^e(R) + H'(R) \quad (23)$$

no matter what perturbation  $H'$  represents.

The reason for short sketch of the BOA in the introductory part is to attract an attention toward some aspects, which at study of solids, in particular of superconductors, are tacitly assumed to hold implicitly and seemingly there are no indications raising doubts that this class of solids should be an exception.

The main aspect is the  $R$ -dependence of the BOA. Whatever trivial it seems to be, it has to be stressed that the study of many-body system by means of the clumped nuclei Hamiltonian (21)–(23) requires validity of the Born ansatz (16), (3), that is, fulfillment of (20) to hold not only for equilibrium nuclear geometry  $R_{\text{eq}}$  but also for displaced geometry ( $R_{\text{eq}} + \Delta R$ ). Displacement  $\Delta R$  has to be as large as to cover full configuration space  $\{R\}$  experienced by nuclei in the vibration (phonon) modes of system. At 0 K temperature,  $\Delta R$  has to be greater than (or at least equal to) root-mean square displacement  $\bar{x}_{0(\nu)}$  of vibration (phonon) mode ( $\nu$ ) at zero-point energy:

$$|\Delta R| \geq \bar{x}_{0(\nu)}, \quad \bar{x}_{0(\nu)} = \left| \left\langle x_{0(\nu)}^2 \right\rangle \right|^{1/2}. \quad (24)$$

It means that for validity of the BOA, the inequality for the energy spectrum which, along with (20), has to be also fulfilled is

$$\left| E_0^{te}(R_{\text{eq}} + \bar{x}_{0(\nu)}) - E_n^{te}(R_{\text{eq}} + \bar{x}_{0(\nu)}) \right| \gg \hbar \omega_\nu. \quad (25)$$

In this context, the adiabatic electronic energies of the ground and excited electronic states  $\{E_0^{te}, (E_n^{te})\}$ , at fixed nuclear geometry  $[R]$ , need also some comment. Without the loss of generality, the Hartree-Fock (HF) calculation scheme in direct-real space orbital representation can be assumed. The adiabatic wave function of the electronic ground state is represented by the Slater determinant that satisfies requirement of antisymmetry:

$$\begin{aligned} \Phi_0(r, [R]) &= \left| \varphi_1(1) \bar{\varphi}_1(2) \varphi_2(3) \bar{\varphi}_2(4) \dots \varphi_{n_e}(2n_e - 1) \bar{\varphi}_{n_e}(2n_e) \right|, \\ &\quad (26) \end{aligned}$$

where for simplicity a closed-shell,  $N_e = 2n_e$  electron system, is considered. In (26), lowest lying  $n_e$  spatial orbitals are occupied, each being occupied twice, once by an electron with  $\alpha$  spin,  $\varphi_n$ , and once with  $\beta$  spin,  $\bar{\varphi}_n$ . Adiabatic total electronic energy of the ground state is then the sum of adiabatic electronic energy and Coulomb repulsion  $E_{NN}(R_0)$  of bare nuclei at fixed geometry  $[R] = R_0$ :

$$\begin{aligned} E_0^e(R_0) &= E_{NN}^0(R_0) + E_{SCF}^0(R_0) \\ &= E_{NN}^0(R_0) + \left( 2 \sum_I^{occ} h_{II}^0 + \sum_{IJ}^{occ} (2\nu_{IJI}^0 - \nu_{IJI}^0) \right) \\ &= E_{NN}^0(R_0) + \left( 2 \sum_I^{occ} h_{II}^0 + \sum_{IJ}^{occ} (2J_{IJ} - K_{IJ}) \right) \\ &= E_{NN}^0(R_0) + \sum_I^{occ} (\varepsilon_I^0 + h_{II}^0). \end{aligned} \quad (27)$$

Summation indices  $\{I, J\}$  in (27) run over the occupied states  $\{\varphi_I, \varphi_J\}$ .

Set of  $\{\varepsilon_I^0\}$  in (27), is one-electron spectrum of the adiabatic electronic ground state (26), that is, orbital energies  $\{\varepsilon_I^0\}$  are eigenvalues:

$$\varepsilon_P^0 = h_{PP}^0 + \sum_Q (2\nu_{PQP}^0 - \nu_{PQP}^0) \quad (28)$$

of the Fock operator  $F(R_0) = h^0(R_0) + \sum_Q (2J_Q - K_Q)$ :

$$F(R)\varphi_P(r, R_0) = \sum_Q \varepsilon_{PQ}^0 \varphi_Q(r, R_0) \quad (29)$$

and  $\{\varphi_Q\}$  is the set of corresponding eigenfunctions (orthonormal set of optimized orbitals). In (28),  $h_{PP}$  is diagonal element of one-electron core Hamiltonian  $h_{core}$  (integrals of electronic kinetic energy term plus electron-nuclear Coulomb attraction term), and  $J_Q, K_Q$  are 2-electron (1,2,3, or 4 nuclear center) Coulomb repulsion and exchange integrals.

In the next step, instead of independent calculation of electronic excited states energies  $\{E_{n(\neq 0)}^e(R)\}$ , which would require new optimization of excited state wave functions  $\Phi_m(r, R)$  (it should be extremely complicated since excited state wave functions have to be orthogonal to the ground state wave function), in practice a fairly good approach is used which is based on the orbitals  $\{\varphi_Q\}$  already optimized for the ground-state wave function  $\Phi_0(r, R_0)$ . Optimization is always performed within a basis set with some finite number  $n$  of basis set functions  $\{\mu_n\}$ , while  $n > N_e$ . Diagonalization of (29) then yields  $\{n\}$  eigenfunctions  $\{\varphi_n(R)\}$  and corresponding eigenenergies  $\{\varepsilon_n^0(R)\}$ , but only  $n_e$  lowest-lying spatial orbitals  $\{\varphi_I(R)\}_{(n_e)}$  are occupied and remaining  $(n - n_e)$  are virtual—unoccupied orbitals  $\{\varphi_A(R)\}_{(n-n_e)}$ . By promotion of electron(s) from occupied orbital(s)  $\{I, J, \dots\}$  to virtual—unoccupied orbital(s)  $\{A, B, \dots\}$ , excited state(s) configuration(s)  $\{\Phi_A\}$  as a linear combination of corresponding Slater determinants  $\{\Phi_{I-A}\}$  can be constructed. It can be shown that, for example,

single-electron excitations yield two excited state electronic configurations—lowest lying excited state, that is, singly excited triplet state  ${}^3\Phi_{A(I-A)}$ , and singly excited singlet state  ${}^1\Phi_{A(I-A)}$ . Differences in the electronic energies of these excited state configurations with respect to the electronic energy of the ground state are as follows:

(i) for singly excited triplet state,

$${}^3E_{A(I-A)}^e(R) - E_0^e(R) = \varepsilon_A^0(R) - \varepsilon_I^0(R) - J_{IA}; \quad (30)$$

(i) for singly excited singlet state,

$${}^1E_{A(I-A)}^e(R) - E_0^e(R) = \varepsilon_A^0(R) - \varepsilon_I^0(R) - J_{IA} + 2K_{IA}. \quad (31)$$

From (30), (31), it is clear that for approximations which do not consider explicitly for two-electron terms, the differences in energies of singly excited triplet and singlet states with respect to the ground-state energy are the same:

$$E_{A(I-A)}^e(R) - E_0^e(R) = \varepsilon_A^0(R) - \varepsilon_I^0(R). \quad (32)$$

Multiple electronic excitations can be calculated in a similar way, by generation of Slater determinants of  $p$ -particle,  $h(\equiv p)$ -hole states in the language of particle-hole formalism.

The important point is that clumped nuclei electronic ground-state energy calculation provides approximate information about electronic excited states over the one-electron spectrum which corresponds to the electronic ground state. In particular, over the optimized set of occupied ( $\varphi_I$ ) and unoccupied-virtual ( $\varphi_A$ ) spinorbitals.

In the simplest form, with respect to (32), the inequalities (20), (25) which have to be valid for save application of the BOA, are in the terms of the optimized ground state orbital energies expressed as follows:

(i) for system at equilibrium geometry  $R_{eq}$ ,

$$\left| \varepsilon_I^0(R_{eq}) - \varepsilon_A^0(R_{eq}) \right| \gg \hbar\omega_\nu \quad (33)$$

has to hold for the couple of frontier orbitals, that is, for highest occupied  $\varphi_I \equiv \varphi_{HOMO}$  and lowest unoccupied  $\varphi_A \equiv \varphi_{LUMO}$  orbitals;

(i) more over,

$$\left| \varepsilon_I^0(R_{eq} + \bar{x}_{0(\nu)}) - \varepsilon_A^0(R_{eq} + \bar{x}_{0(\nu)}) \right| \gg \hbar\omega_\nu \quad (34)$$

has to hold for the same system at displaced nuclear configuration with respect to particular vibration(phonon) mode  $\nu$ .

In case of solids with quasicontinuum of states, in momentum  $k$ -space representation, these inequalities can be rewritten in the form

$$\left| \varepsilon_S^0(k_c) - \varepsilon_F^0 \right|_{R_{eq}} \gg \hbar\omega_\nu \quad (35)$$

for equilibrium nuclear geometry, and

$$\left| \varepsilon_S^0(k_c) - \varepsilon_F^0 \right|_{R_{\text{eq}} + \bar{x}_{0(r)}} \gg \hbar\omega_r \quad (36)$$

for the same system at displaced nuclear configuration in particular phonon mode  $r$ .

These inequalities have to be valid in a multiband system for each band  $S$  and energies  $\{\varepsilon_S^0(k_c)\}$  of analytic critical points (ACP—i.e., absolute and local minima and maxima or inflex points) located on the particular band-dispersion curve of the first BZ with respect to the energy of the Fermi level  $\varepsilon_F^0$ .

An important aspect should be reminded at this place. Inequalities (33)–(36) have been derived on the basis of the expansion (19) of the effective nuclear potential (i.e., total electronic energy  $E_0^{te}(R)$ ) at  $R_{\text{eq}}$ . With respect to the inner structure of the total electronic energy (27), it is clear that in principle, the expansion (19) can be performed (i.e., smallness in energy change  $\Delta E_0^{te}(R_{\text{eq}} + \Delta R)$  as to ensure at least harmonic approximation) even if displacement  $\Delta R$  yields significant changes in the one-electron spectrum (orbital energies) of the ground state

$$\left\{ \varepsilon_Q^0 \right\}_{R_{\text{eq}}} \neq \left\{ \varepsilon_Q^0 \right\}_{R_{\text{eq}} + \bar{x}_0}, \quad (37)$$

provided that these changes are well balanced by changes  $\Delta h_{IJ}$  and  $\Delta E_{NN}$ , eventually also by changes  $\Delta\{J_{IJ}, K_{IJ}\}$  if two-electron terms are explicitly included. The main point is that for the electronic ground state, the one-electron spectrum at  $R_{\text{eq}}$ ,  $\{\varepsilon_Q^0\}_{R_{\text{eq}}}$ , can be significantly different from the one-electron spectrum  $\{\varepsilon_Q^0\}_{R_{\text{eq}} + \bar{x}_0}$  at displaced nuclear configuration ( $R_{\text{eq}} + \bar{x}_{0,\nu}$ ) for some phonon mode  $\nu$ .

In respect of it, possibility that displacement  $\bar{x}_{0,\nu}$  yields for some band situation when

$$\left| \varepsilon_S^0(k_c) - \varepsilon_F^0 \right|_{R_{\text{eq}} + \bar{x}_{0,\nu}} \leq \hbar\omega_\nu \quad (38)$$

even if for the equilibrium geometry  $R_{\text{eq}}$  (35) holds, is not excluded at all.

The reason of possibility for such substantial changes of the electronic (band) structure is hidden in the chemical composition and structure of particular system. With respect to (27)–(31), it is connected to the changes of one-electron core part ( $\Delta h_{IJ}$ ) and/or two-electron Coulomb repulsion and exchange integrals ( $\Delta J_{IJ}$ ,  $\Delta K_{IJ}$ ). Which of these are dominant (hopping terms, onsite/intersite repulsion, electron correlations, dynamic screening, etc.) can hardly be determined on the basis of model Hamiltonians without invoking for complete chemical composition and structure of the particular system.

Occurrence of such a situation means that nuclear motion (nuclear vibration, in particular, phonon mode) has induced sudden decrease of effective electron velocity  $(\partial|\varepsilon_{0,a}(k)|/\partial k)_{k_c}$ , in particular band close to analytic critical point  $k_c$  at the Fermi level  $\varepsilon_{0,F}$ . Or, what is equivalent, the effective mass of electrons have been increased in this region. In any case, however, it means that at displaced nuclear geometry ( $R_{\text{eq}} + \bar{x}_{0,\nu}$ ), electrons, and nuclei of the

system do not move as independent particles, that is, in this region, electrons are not able to follow nuclear motion adiabatically. The motion of electrons and nuclei is now strongly correlated. The new situation occurs, the adiabatic BOA is not valid for nuclear geometry ( $R_{\text{eq}} + \bar{x}_{0,\nu}$ ), and wave function cannot be factorized in the form (16) and (3), that is,

$$\Psi_0(r, R_{\text{eq}} + \bar{x}_{0,\nu}) \neq \chi_{0,\nu}(R_{\text{eq}} + \bar{x}_{0,\nu}) \Phi_0(r, R_{\text{eq}} + \bar{x}_{0,\nu}), \quad (39)$$

and standard adiabatic form of the Hamiltonian (21)–(23) cannot be applied to study an electron-phonon problem. What is crucial, however, is the fact that the nonadiabatic effect cannot be calculated as a perturbation, that is, as a nonadiabatic correction to the adiabatic ground state at  $R_{\text{eq}}$ . In this case, system is in true nonadiabatic or antiadiabatic state.

*2.2. Generalization of the BOA Beyond Adiabatic Regime.* In order to solve the problems which are sketched above, one needs to study electronic motion as explicitly dependent on nuclear dynamics, that is, dependent on instantaneous nuclear coordinates  $Q$  and nuclear momenta  $P$ . It means that electronic state has to be explicitly dependent on nuclear operators  $Q$  and  $P$ . Approximate solution of this problem can be found in [66]. It is based on the sequence of basis functions transformations, starting with fixed basis set ( $Q$ ,  $P$ -independent) over  $Q$ -dependent base up to  $QP$ -dependent basis set. A base function transformation is canonical transformation and it ensures that each transformation step preserves corresponding statistics. Moreover, since we start from fixed basis set (clamped nuclei situation) which enables factorization of total system wave function, this property is required to be preserved at each transformation step up to quadratic terms in  $Q$  and  $P$ . Consequently, it makes the solution of  $Q$ ,  $P$ -dependence tractable. It should be stressed that base functions transformation is equivalent to the quasiparticle transformation which we have formulated in 1992 [67].

Main aspects and the results of this treatment are presented below.

General nonrelativistic form of system Hamiltonian (2) can be written in second quantization formalism as

$$H = T_N(P) + E_{NN}(Q) + \sum_{PQ} h_{PQ}(Q) a_P^\dagger a_Q + \frac{1}{2} \sum_{PQRS} v_{PQRS}^0 a_P^\dagger a_Q^\dagger a_S a_R. \quad (40)$$

Nuclear potential energy  $E_{NN}$  and one-electron core term  $h_{PQ}$  (electron kinetic energy plus electron-nuclear coulomb attraction term) are functions of the nuclear coordinate  $Q_r$  operators (normal modes  $\{r\}$  nuclear displacements out of fixed nuclear geometry  $R_0$ ) and nuclear kinetic energy  $T_N$  is a quadratic function of the corresponding

nuclear momenta operators  $P_r$ . For nuclear coordinate and momentum operators hold:

$$\begin{aligned} Q_r &= (b_r + b_r^\dagger), & Q_{\bar{r}} &= (b_{\bar{r}} + b_{\bar{r}}^\dagger), & Q_r^+ &= (b_r^\dagger + b_r) = Q_{\bar{r}}, \\ P_r &= (b_r - b_r^\dagger), & P_{\bar{r}} &= (b_{\bar{r}} - b_{\bar{r}}^\dagger), & P_r^+ &= (b_r^\dagger - b_r) = -P_{\bar{r}}. \end{aligned} \quad (41)$$

The  $(a, a^\dagger)$ ,  $(b, b^\dagger)$  are standard fermion and boson annihilation and creation operators, respectively.

The  $Q$ -dependence of terms  $E_{NN}(Q)$  and  $h_{PQ}(Q)$  in (40) can be expressed through the Taylor's expansion at fixed nuclear configuration  $R_0$ :

$$\begin{aligned} E_{NN}(Q) &= E_{NN}^0(R_0) + \sum_{j=1}^{\infty} E_{NN}^{(j)}(Q), \\ h_{PQ}(Q) &= h_{PQ}^0(R_0) + \sum_{i=1}^{\infty} u_{PQ}^{(i)}(Q). \end{aligned} \quad (42)$$

The term  $E_{NN}^0(R_0)$  represents potential energy of bare nuclei at fixed nuclear configuration  $R_0$ ,  $h_{PQ}^0(R_0)$  is one-electron core term (electron kinetic energy plus electron-nuclear coulomb attraction term) at fixed nuclear configuration  $R_0$  and terms  $\{u_{PQ}^{(i)}(Q)\}$  are related to matrix elements of electron-vibration (phonon) coupling ( $u_{PQ}^{(i)}$ ), that is,

$$\begin{aligned} u_{PQ}^r(Q) &= \frac{\partial h_{PQ}(Q)}{\partial Q_r} Q_r = u_{PQ}^r Q_r; \\ u_{PQ}^{r \cdots s}(Q) &= \frac{\partial h_{PQ}(Q)}{\partial Q_r \cdots \partial Q_s} Q_r \cdots Q_s = u_{PQ}^{r \cdots s} Q_r \cdots Q_s. \end{aligned} \quad (43)$$

Two-electron terms  $v_{PQRS}^0$  (electron-electron coulomb repulsion and exchange integrals) do not depend explicitly on the nuclear operators.

**2.2.1. Crude-Adiabatic Approximation: Clamped Nuclei Solution.** Since the crude-adiabatic approximation is the reference level for study the effect of nuclear dynamics on electronic structure, some details should be introduced.

With respect to sequence of transformations, which will be presented in the following parts, let as distinguish particular representation; that is, dependence of electronic states on nuclear operator  $Q$  only by double-bar over particular operator symbol (e.g.,  $\bar{\bar{a}}, \bar{\bar{b}}$ ), dependence on both  $Q$  and  $P$  will be without bar  $(a, b)$  and for fixed basis (independent on  $Q$  and  $QP$ , resp.) the operators will be with a single-bar  $(\bar{a}, \bar{b})$  over the particular symbol. In this sense, the operators in crude-adiabatic approximation are written as single-bar operators, that is,  $(\bar{a}, \bar{b}, \bar{Q}, \bar{P})$ .

Provided that phonon and electronic energy spectrum are well separated and (20) holds for relevant configuration space  $R$  near to  $R_{eq}$ , crude-adiabatic (clamped nuclei) treatment is justified. Electronic Hamiltonian is now only

parametrically dependent on nuclear configuration, that is, nuclear geometry is fixed at nuclear configuration  $R_0$ :

$$\begin{aligned} H_e(R_0) &= E_{NN}^0(R_0) + \sum_{PQ} h_{PQ}^0(R_0) \bar{a}_P^\dagger \bar{a}_Q \\ &+ \frac{1}{2} \sum_{PQRS} v_{PQRS}^0 \bar{a}_P^\dagger \bar{a}_Q^\dagger \bar{a}_S \bar{a}_R. \end{aligned} \quad (44)$$

Application of Wick's theorem to the product of creation and annihilation operators yields for particular terms the normal product form (N-product) with corresponding contractions:

$$\begin{aligned} \sum_{PQ} h_{PQ}^0 \bar{a}_P^\dagger \bar{a}_Q &= \sum_{PQ} h_{PQ}^0 N[\bar{a}_P^\dagger \bar{a}_Q] + \sum_I^{occ} h_{II}^0, \\ \sum_{PQRS} v_{PQRS}^0 \bar{a}_P^\dagger \bar{a}_Q^\dagger \bar{a}_S \bar{a}_R &= \sum_{PQRS} v_{PQRS}^0 N[\bar{a}_P^\dagger \bar{a}_Q^\dagger \bar{a}_S \bar{a}_R] \\ &+ \sum \left( \sum_{PQ}^{occ} (v_{PIQI}^0 + v_{IPIQ}^0 - v_{PIIQ}^0 - v_{IPIQ}^0) \right) N[\bar{a}_P^\dagger \bar{a}_Q] \\ &+ \sum_{IJ}^{occ} (v_{IJIJ}^0 - v_{IJIJ}^0). \end{aligned} \quad (45)$$

Application of Wick's theorem introduces renormalized Fermi vacuum, that is, the total set of orthonormal base orbitals  $(\varphi_P, \varphi_Q, \dots)$  is divided on two distinct groups; the set of occupied  $(\varphi_I, \varphi_J, \dots)$  spinorbitals which form a Fermi sea (FS) and set of unoccupied-virtual  $(\varphi_A, \varphi_B, \dots)$  spinorbitals which are above the FS.

The electronic Hamiltonian (44) can now be written in a quasiparticle form as a sum of zero, one- and two-particle terms:

$$H_e(R_0) = H_{(0)}(R_0) + H_{(1)}(R_0) + H_{(2)}(R_0). \quad (47)$$

(I) *Electronic ground state energy.*

The scalar quantity in this Hamiltonian, that is, zero-particle term  $H_{(0)}(R_0)$ , is the result of the operators contractions and has the form

$$\begin{aligned} H_{(0)}(R_0) &= \langle \Phi_0 | H_e | \Phi_0 \rangle \\ &= \sum_I^{occ} h_{II}^0 + \frac{1}{2} \sum_{IJ}^{occ} (v_{IJIJ}^0 - v_{IJIJ}^0) \\ &= E_{SCF}^0(R_0). \end{aligned} \quad (48)$$

This term represents ground-state electronic energy calculated by unrestricted Hartree-Fock SCF (HF-SCF) procedure at fixed nuclear configuration  $R_0$ . It is obvious that addition of nuclear repulsion  $E_{NN}(R_0)$  to this term yields total electronic energy  $E_0^{te}(R_0)$ . Electronic ground state is represented by renormalized Fermi vacuum  $\Phi_0$ . It is an antisymmetric electronic wave function, that is, expressed in

the form of single Slater determinant constituted by lowest laying occupied spinorbitals  $\{\varphi_I\}$  of complete orthonormal base  $\{\varphi_P\}$ :

$$\Phi_0(r, R_0) = |\varphi_1 \cdots \varphi_I| \quad (49)$$

(II) *Electronic energy spectrum.*

The one-particle term  $H_{(1)}(R_0) = H'_{(cad)}(R_0)$  of the electronic Hamiltonian (47) has the form,

$$H_{(1)}(R_0) = \sum_{PQ} F_{PQ} N[\bar{a}_P^\dagger \bar{a}_Q]. \quad (50)$$

The elements  $F_{PQ}$  are calculated as matrix elements of Hartree-Fock one-particle operator:

$$F(R_0) = h^0(R_0) + \sum_Q (J_Q - K_Q). \quad (51a)$$

Diagonalization of (50),  $F_{PQ} = \varepsilon_P^0 \delta_{PQ}$ , that is, solution of electronic Hartree-Fock equations by HF-SCF procedure:

$$F(R_0)\varphi_P(r, R_0) = \sum_Q \varepsilon_{PQ} \varphi_Q(r, R_0) \quad (51b)$$

yields set of eigenvalues, that is, HF-orbital energies:

$$\varepsilon_P^0 = h_{PP}^0 + \sum_Q (\nu_{PQPQ}^0 - \nu_{PQPQ}^0), \quad (51c)$$

and corresponding set of eigenfunctions  $\{\varphi_P\}$ , the orthonormal set of optimized spinorbitals.

It means that one-particle term (50) can always be written in diagonal form and represents a set of unperturbed eigenenergies of system at fixed nuclear geometry  $R_0$ , that is,

$$H_{(1)}(R_0) = \sum_P \varepsilon_P^0 N[\bar{a}_P^\dagger \bar{a}_P], \quad (51d)$$

$$H_{(1)}(R_0)|\Phi_0\rangle = 0 \quad (51e)$$

for excited states hold:

$$H_{(1)}(R_0)|\Phi_{I-A}\rangle = (\varepsilon_A^0 - \varepsilon_I^0)|\Phi_{I-A}\rangle \quad \text{for } I \in FS, A \notin FS. \quad (51f)$$

In an approximate way, the one-particle Hamiltonian  $H_{(1)}(R_0)$  represents complete electronic spectrum expressed over occupied and unoccupied-virtual spinorbitals calculated for electronic ground state  $\Phi_0(r, R_0)$  by HF-SCF procedure. In particular,  $n$ -electron excited state wave function  $\Phi_{h_n p_n}$  can be constructed, as it has already been mentioned, by promotion of  $n$  electrons from  $n$  occupied spinorbitals to  $n$  unoccupied spinorbitals (i.e., the same number  $n$  of holes ( $h_n$ ) and particles ( $p_n$ ) are created). Electronic energy of such excited state can be calculated through HF-eigenenergies that correspond to optimized spinorbitals of the ground state. It should be pointed that it is only an approximate way for description of true electronic excited states.

In terms of orbital energies (51c), for total electronic ground state energy,  $E_0^{te}(R_0)$  holds:

$$\begin{aligned} E_0^{te}(R_0) &= E_{NN}^0(R_0) + E_{SCF}^0(R_0) \\ &= E_{NN}^0(R_0) + \left( \sum_I^{occ} h_{II}^0 + \frac{1}{2} \sum_{IJ}^{occ} (\nu_{IJIJ}^0 - \nu_{IJIJ}^0) \right) \\ &= E_{NN}^0(R_0) + \frac{1}{2} \sum_I^{occ} (\varepsilon_I^0 + h_{II}^0). \end{aligned} \quad (52)$$

For closed-shell electronic systems, within restricted HF approximation (doubly occupied spatial orbitals with  $\alpha$  and  $\beta$  spins, (27) holds. Total electronic ground-state energy of the system reaches the minimum at some equilibrium nuclear configuration  $R_0 = R_{eq}$ . Corresponding Slater determinant (49) represents wave function of the electronic ground state at equilibrium nuclear configuration.

(III) *Electron correlation energy.* (see Note in Section 1).

The third term of the electronic Hamiltonian (47), that is, the two-particle term has the form

$$H_{(2)}(R_0) = H''_{(cad)}(R_0) = \frac{1}{2} \sum_{PQRS} \nu_{PQRS}^0 N[\bar{a}_P^\dagger \bar{a}_Q^\dagger \bar{a}_S \bar{a}_R]. \quad (53)$$

Formally it looks like standard coulomb electron-electron interaction term in (44). With respect to the fact that after application of Wick's theorem (45) the renormalized Fermi vacuum has been introduced and zero-particle (scalar) quantity (48) represents electronic energy of the ground state that accounts also for coulomb electron-electron interactions (48) and one-particle term is diagonal (51d) and represents unperturbed HF-orbital energies  $\{\varepsilon_P^0\}$  of the system (one-electron energy spectrum), then two-particle term (53) represents perturbation part of the electronic Hamiltonian (47). Since perturbation (53) contains only electron-electron interaction term, contributions of this term represent electron correlation energy of the system in its ground electronic state. In this respect, electron correlation energy is treated as a perturbation. Calculation of the electron correlation energy up to higher order of perturbation theory is usually done by diagrammatic many-body perturbation theory. For correlation energy in second order of perturbation theory, analytic expression for closed-shell system can be derived in a simple form

$$E_{corr}(R_0) = H_{(h_1 h_2 p_1 p_2)}(R_0) = \sum_{IJ}^{occ} \sum_{AB}^{unocc} \frac{(2\nu_{IJAB}^0 - \nu_{IJBA}^0)}{(\varepsilon_I^0 + \varepsilon_J^0 - \varepsilon_A^0 - \varepsilon_B^0)}. \quad (54)$$

Related to energy of the Fermi level, energies of unoccupied states are  $\{\varepsilon_A^0\} > 0$  and energies of occupied states are  $\{\varepsilon_I^0\} < 0$ . It means that  $E_{corr}$  is negative, that is, it decreases electronic energy of the ground state (this contribution corrects and stabilizes total electronic energy of the system (27), (52)). This holds for arbitrary nuclear geometry  $R_0$  until system remains in a bound state.

Solution of nuclear problem (9) on crude-adiabatic level is now straightforward.

Nuclear part of Hamiltonian is

$$H_N = T_N + V_{NN}^{\text{eff}}(R) = \sum_r \hbar\omega_r \left( \bar{b}_r^+ \bar{b}_r + \frac{1}{2} \right). \quad (55)$$

For different, but fixed nuclear configurations  $[R]$  at  $R_0 = R_{\text{eq}}$ ,  $E_0^{te}(R)$  is calculated and effective potential for nuclear motion is derived  $V_{NN}^{\text{eff}}(R)$ . It has to be stressed that contributions of DBOC— $B_{00}(R)$ , that is, (10), to  $V_{NN}^{\text{eff}}(R)$  are in this case neglected.

Energy and wave function of the total system in the ground electronic state are

$$E_0^{TS}(R_0) = E_0^{te}(R_{\text{eq}}) + \sum_r \hbar\omega_r (n_r + 1/2), \quad (56)$$

$$\Psi_0(r, R) = \chi_0(R) \Phi_0(r, R_{\text{eq}}), \quad (57)$$

$$\text{or in terms of } Q: \Psi_0(r, Q) = \chi_0(Q) \Phi_0(r, 0).$$

Nuclear wave function is

$$\chi_0(R) = \prod_r \chi_{0r,n}(R) = \prod_r \frac{1}{\sqrt{n_r!}} (\bar{b}_r^+)^{n_r} |0\rangle. \quad (58a)$$

**2.2.2. Base Transformation-Introduction of New Dynamical Variables.** Each eigenfunction  $\varphi_j$  in Slater determinant (49) can be expressed as a linear combination of atomic orbital (AO) basis functions  $\{\mu\}$ ,  $\varphi_P = \sum_\mu c_{\mu P} |\mu\rangle$ , which are fixed at the positions of the particular nuclei in clamped nuclei configuration  $R_0$ . It represents fixed basis set  $\{\mu(x, 0) \equiv \mu(x, \bar{Q})\}$ .

In second quantization, with single-bar  $\bar{a}^+$  being creation operator of the crude-adiabatic electron (clamped nuclei approximation, independent on  $Q$  and  $QP$ ), base function  $\mu(x, 0)$  can be written with respect to “absolute” Fermi vacuum  $|0\rangle$  as

$$\mu(x, 0) = \bar{a}_\mu^+(x, 0) |0\rangle \quad (59)$$

and

$$\begin{aligned} \varphi_P(x, 0) &= \sum_\mu c_{\mu P} |\mu(x, 0)\rangle \\ &= \sum_\mu c_{\mu P} \bar{a}_\mu^+(x, 0) |0\rangle \\ &= \bar{a}_P^+(x, 0) |0\rangle. \end{aligned} \quad (60a)$$

For solids, in electronic quasimomentum  $k$ -space, the basis functions are Bloch-periodic orbitals  $\{\mu(k, x, 0)\}$ :

$$\mu(k, x, 0) = \frac{1}{\sqrt{N}} \sum_{tR} e^{ik \cdot tR} \mu(x - tR). \quad (60b)$$

In (60b),  $tR$  is translation vector and  $\mu(x - tR) = \mu(x)$ . The set of  $\{\mu(x)\}$  is fixed basis set  $\{\mu(x, 0)\}$  at frozen nuclear

configuration  $R_0(Q = 0)$ . An eigenfunction  $\varphi_P$  is then crystal orbital  $\text{CO}-\varphi_P$  (band  $\varphi_P$ ), which is a linear combination of the Bloch-periodic basis functions  $\{\mu(k, x, 0)\}$ .

In a second quantization, it has the form

$$\mu(k, x, 0) = \frac{1}{\sqrt{N}} \sum_{tR} e^{ik \cdot tR} \bar{a}_\mu^+(x, 0) |0\rangle, \quad (60c)$$

$$\begin{aligned} \varphi_P(k, x, 0) &= \sum_\mu c_{\mu P}^{(k)} |\mu(k, x, 0)\rangle \\ &= \sum_\mu c_{\mu P}^{(k)} \frac{1}{\sqrt{N}} \sum_{tR} e^{ik \cdot tR} \bar{a}_\mu^+(x, 0) |0\rangle \\ &= \frac{1}{\sqrt{N}} \sum_{tR} e^{ik \cdot tR} \bar{a}_{Pk}^+(k, x, 0) |0\rangle. \end{aligned} \quad (60d)$$

In this case, occupancy of the band is not distinguished by the index (subscript) of the band, but it is determined by the value of  $k$ -vector of particular band dispersion  $\varepsilon_P^0(k)$  with respect to the energy of Fermi level  $\varepsilon_F^0$ . It is obvious that Hamiltonian of system (40), (44) is now Hamiltonian which corresponds to the composition of unit cell and total electronic energy calculation results in corresponding band structure.

For fermion and boson creation and annihilation operators, the standard anticommutation, and commutation relations hold:

$$\{\bar{a}_P, \bar{a}_Q\} = 0, \quad \{\bar{a}_P, \bar{a}_Q^+\} = \delta_{PQ}, \quad (61a)$$

$$[\bar{b}_r, \bar{b}_s] = 0, \quad [\bar{b}_r, \bar{b}_s^+] = \delta_{rs}. \quad (61b)$$

Simultaneous diagonalization of electronic and nuclear part of system Hamiltonian, that is, factorized form of system wave function (57) within adiabatic BOA implies also validity of the following commutation relations:

$$[\bar{a}_P, \bar{b}_r] = 0, \quad [\bar{a}_P, \bar{b}_r^+] = 0. \quad (61c)$$

#### (1) $Q$ -Dependent Adiabatic Transformation.

In case of crude-adiabatic approximation, the electrons “see” the nuclei at their instantaneous positions at rest and nuclei do not “feel” internal dynamics of electrons. Within the spirit of the BOA, it would be correct if the electrons follow nuclear motion instantaneously, that is, electronic state has to dependent explicitly on instantaneous nuclear positions. In this case, the wave function of the system, instead of the form (57) with  $Q$ -independent electronic part should be replaced by  $Q$ -dependent form, that is,

$$\Psi_0(r, R) = \chi_{0,r}(R) \Phi_0(r, R), \quad (62)$$

$$\text{or } \Psi_0(r, \bar{Q}) = \chi_{0,r}(R) \Phi_0(r, \bar{Q}).$$

Adiabatic, nuclear displacement  $Q$ -dependent electronic wave function  $\Phi_0(r, \bar{Q})$  in (62) assumes existence of complete orthonormal basis set  $\{\varphi_R(x, \bar{Q})\}$ , that is, validity of the following relations:

$$\begin{aligned} \langle \varphi_R(x, \bar{Q}) | \varphi_S(x, \bar{Q}) \rangle &= \delta_{RS}, \\ \sum_R | \varphi_R(x, \bar{Q}) \rangle \langle \varphi_R(x, \bar{Q}) | &= 1. \end{aligned} \quad (63)$$

Now, electron creation and annihilation operators which correspond to the  $Q$ -dependent moving base are denoted as double-bar operators ( $\bar{a}^+, \bar{a}$ ). Also, the boson operators related to the  $Q$ -dependent moving base are written as double-bar operators:

$$\bar{Q}_r = (\bar{b}_r^+ + \bar{b}_r^-), \quad \bar{P}_r = (\bar{b}_r - \bar{b}_r^+). \quad (64)$$

Then,

$$\begin{aligned} \bar{a}_R^+(x, \bar{Q}) |0\rangle &= | \varphi_R(x, \bar{Q}) \rangle, \\ \bar{a}_R(x, \bar{Q}) | \varphi_R(x, \bar{Q}) \rangle &= 0. \end{aligned} \quad (65)$$

Since adiabatic electrons remain fermions, the operators have to obey standard fermion anticommutation relations:

$$\{\bar{a}_R, \bar{a}_S^+\} = \delta_{RS}, \quad \{\bar{a}_R, \bar{a}_S\} = 0. \quad (66)$$

Shorthand notation,  $\bar{a}_R \equiv \bar{a}_R(x, \bar{Q})$ ,  $\bar{a}_R^+ \equiv \bar{a}_R^+(x, \bar{Q})$  has been used in (66).

Crude-adiabatic electronic wave function  $\Phi_0(r, 0)$  which does not depend on the nuclear displacements  $Q$  is expanded over fixed basis set with spinorbitals  $\{\varphi_R(x, 0)\}$  that are eigenfunctions of clamped nuclear electronic Hartree-Fock equations (30). This is complete and orthonormal basis set

$$\begin{aligned} \langle \varphi_R(x, 0) | \varphi_S(x, 0) \rangle &= \delta_{RS}, \\ \sum_R | \varphi_R(x, 0) \rangle \langle \varphi_R(x, 0) | &= 1. \end{aligned} \quad (67)$$

Crude-adiabatic fermion creation and annihilation operators that correspond to the fixed basis set are written as single-bar operators ( $\bar{a}^+, \bar{a}$ ), that is,

$$\bar{a}_R^+(x, 0) |0\rangle = | \varphi_R(x, 0) \rangle, \quad \bar{a}_R(x, 0) | \varphi_R(x, 0) \rangle = |0\rangle,$$

or in short-hand notation

$$\bar{a}_R^+ |0\rangle = | \varphi_R(x, 0) \rangle, \quad \bar{a}_R | \varphi_R(x, 0) \rangle = |0\rangle.$$

These operators pertain to ordinary (crude-adiabatic) electrons and the standard anticommutation relations (61a) hold.

Due to properties (63), (67), the two bases are interconnected by the base transformation of the following form:

$$\begin{aligned} | \varphi_R(x, 0) \rangle &= \sum_S | \varphi_S(x, \bar{Q}) \rangle \langle \varphi_S(x, \bar{Q}) | \varphi_R(x, 0) \rangle \\ &= \sum_S (c_{RS}(\bar{Q}))^+ | \varphi_S(x, \bar{Q}) \rangle. \end{aligned} \quad (69)$$

Now, for fermion operators in  $Q$ -dependent moving base one can write

$$\bar{a}_R = \sum_S c_{RS}(\bar{Q}) \bar{a}_S, \quad \bar{a}_R^+ = \sum_S (c_{RS}(\bar{Q}))^+ \bar{a}_S^+. \quad (70)$$

Elements  $c(Q)$  of the  $Q$ -dependent transformation matrix  $C(Q)$  in (69), (70) are

$$c_{RS}(\bar{Q}) = \langle \varphi_R(x, 0) | \varphi_S(x, \bar{Q}) \rangle. \quad (71)$$

Since

$$c_{RS}^*(\bar{Q}) = \langle \varphi_S(x, \bar{Q}) | \varphi_R(x, 0) \rangle, \quad (72)$$

then due to closure property and orthonormality (63), (67) of the bases, it can be derived that base transformation matrix  $C(Q)$  is an unitary matrix:

$$\begin{aligned} \sum_T c_{RT} c_{ST}^* &= \delta_{RS} = \sum_T c_{TR}^* c_{TS}, \\ C^+ &= (C^T)^* = C^{-1}. \end{aligned} \quad (73)$$

It can be shown [66] that the base transformation is identical with canonical transformation of operators (see (70) and (74))

$$\begin{aligned} \bar{a}_R &= U^+ \bar{a}_R U, \quad \bar{a}_R^+ = U^+ \bar{a}_R^+ U, \\ \rightarrow \bar{a}_R &= \sum_S (e^{y_{RS}(\bar{Q})}) \bar{a}_S, \quad \bar{a}_R^+ = \sum_S (e^{y_{RS}(\bar{Q})})^+ \bar{a}_S^+. \end{aligned} \quad (74)$$

It ensures preservation of statistics, that is, validity of the anticommutation relations (66) for new,  $Q$ -dependent, adiabatic electrons. The exponential form of canonical transformation (74) legitimates Taylor's expansion of the matrix elements (71) and (72) of base transformation matrix, that is,

$$c_{PQ}(\bar{Q}) = \sum_{k=0}^{\infty} \frac{1}{k!} \sum_{r_1 \dots r_k} c_{PQ}^{r_1 \dots r_k} \bar{Q}_{r_1} \dots \bar{Q}_{r_k}. \quad (75)$$

The form of transformation relations for boson operators of system Hamiltonian has to respect the factorized form of the total system wave function (62). It implies possibility of simultaneous, independent diagonalization of electron and boson subsystems. It means that transformed fermion and transformed boson operators obey not only standard anticommutation and commutation relations within the individual subsystems:

$$\begin{aligned} \{\bar{a}_P, \bar{a}_Q\} &= 0, \quad \{\bar{a}_P, \bar{a}_Q^+\} = \delta_{PQ}, \\ [\bar{b}_r, \bar{b}_s] &= 0, \quad [\bar{b}_r, \bar{b}_s^+] = \delta_{rs}, \end{aligned} \quad (76)$$

but also transformed operators of both subsystems have to commute mutually like the original operators, that is, also the following commutation relations are required to hold:

$$[\bar{a}_P, \bar{b}_r] = 0, \quad [\bar{a}_P, \bar{b}_r^+] = 0. \quad (77)$$

With respect to the fermion transformation relations (70), the form of transformation relations for boson operators is expressed as

$$\begin{aligned}\bar{b}_r &= \bar{\bar{b}}_r + \sum_{PQ} d_{rPQ}(\bar{Q}) \bar{\bar{a}}_P^+ \bar{\bar{a}}_Q, \\ \bar{b}_r^+ &= \bar{\bar{b}}_r^+ + \sum_{PQ} (d_{rPQ}(\bar{Q}))^+ \bar{\bar{a}}_P^+ \bar{\bar{a}}_Q.\end{aligned}\quad (78)$$

Also for matrix elements  $d(\bar{Q})$  of transformation matrix  $D(\bar{Q})$ , the Taylor' expansion is defined as

$$d_{rPQ}(\bar{Q}) = \sum_{k=0}^{\infty} \frac{1}{k!} \sum_{s_1 \dots s_k} d_{rPQ}^{s_1 \dots s_k} \bar{Q}_{s_1} \dots \bar{Q}_{s_k}. \quad (79)$$

In order to ensure possibility of practical solution, in what follows, important restriction is imposed. The commutation relation (77) is required to hold up to quadratic terms in Taylor's expansions. It enables to express transformation coefficients  $d(\bar{Q})_{RS}$  through coefficients  $c(\bar{Q})_{RS}$  (see [66]—Appendix A). It will be shown that  $c_{PR}^r$  covers the strength of electron-vibration (phonon) coupling up to the first order of Taylor's expansion and determine also adiabatic correction to the electronic energy of the ground state  $\Delta E_{(ad)}^0$ .

The adiabatic transformation preserves total number of electrons, and nuclear coordinate operator is invariant under the transformation, that is,

$$\begin{aligned}\bar{\bar{N}}_e &= \sum_P \bar{\bar{a}}_P^+ \bar{\bar{a}}_P = \sum_P \bar{a}_P^+ \bar{a}_P = \bar{N}_e, \\ \bar{Q}_r &= (\bar{b}_r^+ + \bar{b}_r) = (\bar{\bar{b}}_r^+ + \bar{\bar{b}}_r) = \bar{Q}_r.\end{aligned}\quad (80)$$

Up to the first order of Taylor's expansion, the crude-adiabatic momentum operator  $\bar{P}_r = (\bar{b}_r - \bar{b}_r^+)$  is transformed as

$$\bar{P}_r = (\bar{b}_r - \bar{b}_r^+) + 2 \sum_{PQ} c_{PQ}^r \bar{\bar{a}}_P^+ \bar{\bar{a}}_Q = \bar{P}_r + 2 \sum_{PQ} c_{PQ}^r \bar{\bar{a}}_P^+ \bar{\bar{a}}_Q. \quad (81)$$

The term  $\bar{P}_r = (\bar{b}_r - \bar{b}_r^+)$  in (81) is nuclear momentum operator on adiabatic level.

For adiabatic Q-dependent spinorbitals  $|\varphi_P(x, \bar{Q})\rangle$ , which are the basis functions of the adiabatic Q-dependent electronic wave function of the ground state  $\Phi_0(r, Q)$ , expressed over crude-adiabatic orbitals can be derived:

$$\begin{aligned}|\varphi_P(x, \bar{Q})\rangle &= \bar{\bar{a}}_P^+(x, \bar{Q})|0\rangle \\ &= \left( \bar{a}_P^+ - \sum_{rR} c_{PR}^r \bar{Q}_r \bar{a}_R^+ + O(\bar{Q}^2) \right) |0\rangle \\ &= |\varphi_P(x, 0)\rangle - \sum_{rR} c_{PR}^r \bar{Q}_r |\varphi_R(x, 0)\rangle + \dots \\ &= |\varphi_P(x, 0)\rangle - \sum_{rR} c_{PR}^r \bar{Q}_r |\varphi_R(x, 0)\rangle + \dots.\end{aligned}\quad (82)$$

As it is seen from (82), adiabatic wave function is modulated by the instantaneous nuclear coordinates  $\{\bar{Q}_r = \bar{Q}\}$  of particular vibration (phonon) modes  $\{r\}$  with the weight proportional to transformation coefficients  $c_{PR}^r$  (coefficients of transformation matrix in the first order of Taylor's expansion— $c_{PR}^r = \partial c_{PR}(\bar{Q})/\partial \bar{Q}_r$ ).

At solution of the problem on adiabatic (Q-dependent) level, we have restricted ourselves to study total system in its electronic ground state with (62) representing wave function  $\Psi_0(r, R) = \chi_{0,v}(R)\Phi_0(r, R)$ . The Schrödinger equation of the total system (6) for electronic ground state  $\Phi_0(r, R)$  is then of the diagonal form (9). Seemingly we have lost the effect of electron-nuclear coupling through nuclear kinetic energy operator which is covered by  $\Lambda$  terms on the rhs of equation (6). The off-diagonal  $\Lambda$  terms are absent and from the diagonal  $\Lambda$  terms, the only non-zero element is  $B_{00}$ . It is the DBOC,  $\Lambda_{00}(\bar{Q}) \equiv B_{00}(\bar{Q}) = \langle \Phi_0(r, \bar{Q}) | T_N | \Phi_0(r, \bar{Q}) \rangle$ , the mean value of nuclear kinetic energy in the electronic ground state which is expected to be negligibly small for systems in adiabatic state. Nonetheless, it will be shown that this term ( $B_{00}$ ) covers the same effect of e-p coupling as it is routinely calculated in solid-state physics by perturbation theory with e-p coupling Hamiltonian (22) when electronic excited states are approximated by promotion of electrons to virtual orbitals of the electronic ground state.

#### (2) QP-Dependent Nonadiabatic Transformation.

As it has been mentioned in Section 1, study of band structure of superconductors indicates that e-p coupling induces fluctuation of some band through Fermi level. At the moment when ACP of such a band approaches Fermi level, there is considerable reduction of electron kinetic energy, which for antiadiabatic state results even for dominance of nuclear dynamics ( $\omega \gg E_F$ ) in some region of  $k$ -space. Electrons at these circumstances are not able to follow nuclear motion adiabatically. It means that electronic wave function, in order to respect this fact, should be dependent not only on instantaneous nuclear coordinates  $Q$  but it should also be an explicit function of the instantaneous nuclear momenta  $P$ , that is,  $\Phi_0 \equiv \Phi_0(r, Q, P)$ .

Let us assume that wave function of total system can be found in the following factorized form:

$$\Psi(r, Q, P) = \sum_m \chi_m(Q, P) \Phi_m(r, Q, P). \quad (83)$$

The form of the wave function (83) is basically  $P$ -dependent modification of the original  $Q$ -dependent BOA (3).

Like in adiabatic case, solution of the problem will be restricted to electronic ground state, that is, for total system, we have

$$\Psi_0(r, Q, P) = \chi_0(Q, P) \Phi_0(r, Q, P). \quad (84)$$

It means that effect of nuclear momenta will be covered only in the form of  $QP$ -dependent diagonal correction  $\Lambda_{00}(Q, P) = \langle \Phi_0(r, Q, P) | \tilde{T}_N | \Phi_0(r, Q, P) \rangle$ , that is, in a similar way as it has been covered the effect of instantaneous nuclear coordinates  $Q$  on the adiabatic level, that is,  $Q$ -dependent adiabatic DBOC,  $\Lambda_{00}(\bar{Q}) = \langle \Phi_0(r, \bar{Q}) | T_N | \Phi_0(r, \bar{Q}) \rangle$ .

Solution of this problem is similar to the transition from crude-adiabatic to adiabatic level as presented above. Now, however, the transition from adiabatic to antiadiabatic level is established.

Nonadiabatic, nuclear displacements, and momenta ( $QP$ )-dependent electronic wave function  $\Phi_0(r, Q, P)$  in (84) assume existence of complete orthonormal basis set  $\{\varphi_R(x, Q, P)\}$ , that is, validity of the following relations:

$$\begin{aligned} \langle \varphi_R(x, Q, P) | \varphi_S(x, Q, P) \rangle &= \delta_{RS}, \\ \sum_R | \varphi_R(x, Q, P) \rangle \langle \varphi_R(x, Q, P) | &= 1. \end{aligned} \quad (85)$$

Electron creation and annihilation operators that correspond to the ( $QP$ )-dependent moving base are written as bar-less operators ( $a^+, a$ ). Boson operators related to the ( $QP$ )-dependent moving base are denoted also as bar-less operators,  $Q_r = (b_r^+ + b_r^-)$  and  $P_r = (b_r - b_r^+)$ . Then,

$$\begin{aligned} a_R^+(x, Q, P) | 0 \rangle &= | \varphi_R(x, Q, P) \rangle, \\ a_R(x, Q, P) | \varphi_R(x, Q, P) \rangle &= | 0 \rangle. \end{aligned} \quad (86)$$

Since nonadiabatic electrons remain fermions, the operators obey standard fermion anticommutation relations (it follows from canonical transformation, see (91)):

$$\{a_R, a_S^+\} = \delta_{RS}, \quad \{a_R, a_S\} = 0. \quad (87)$$

In (87), shorthand notation is used, that is,  $a_R \equiv a_R(x, Q, P)$  and  $a_R^+ \equiv a_R^+(x, Q, P)$ .

Since adiabatic  $Q$ -dependent moving base derived by adiabatic transformation is complete and orthonormal (63), then due to (85), the base transformation to nonadiabatic ( $QP$ )-dependent moving base can be established over the base transformation relation:

$$\begin{aligned} | \varphi_R(x, \bar{Q}) \rangle &= \sum_S | \varphi_S(x, Q, P) \rangle \langle \varphi_S(x, Q, P) | \varphi_R(x, \bar{Q}) \rangle \\ &= \sum_S (\hat{c}_{RS}(P))^+ | \varphi_S(x, Q, P) \rangle. \end{aligned} \quad (88)$$

For fermion operators of second quantization, it follows that

$$\bar{a}_R = \sum_S \hat{c}_{RS}(P) a_S, \quad \bar{a}_R^+ = \sum_S (\hat{c}_{RS}(P))^+ a_S^+ \quad (89)$$

Elements of the  $P$ -dependent transformation matrix  $\hat{C}(P)$  are

$$\begin{aligned} \hat{c}_{RS}(P) &= \langle \varphi_R(x, \bar{Q}) | \varphi_S(x, Q, P) \rangle, \\ \hat{c}_{RS}^*(P) &= \langle \varphi_S(x, Q, P) | \varphi_R(x, \bar{Q}) \rangle. \end{aligned} \quad (90)$$

The  $P$ -dependent transformation matrix  $\hat{C}(P)$  is also unitary matrix, that is, the relations hold:

$$\begin{aligned} \sum_T \hat{c}_{RT} \hat{c}_{ST}^* &= \delta_{RS} = \sum_T \hat{c}_{TR}^* \hat{c}_{TS}, \\ \hat{C}^+ &= (\hat{C}^T)^* = \hat{C}^{-1}. \end{aligned} \quad (91)$$

The form of transformation relations for boson operators of system Hamiltonian has to respect again the factorized form of the total system wave function (84). Also in this case, it expresses possibility of simultaneous, independent diagonalization of electron and boson subsystems. It means that transformed-nonadiabatic fermion and transformed nonadiabatic boson operators obey not only standard anticommutation and commutation relations within the individual subsystems,

$$\begin{aligned} \{a_P, a_Q\} &= 0, \quad \{a_P, a_Q^+\} = \delta_{PQ}, \\ [b_r, b_s] &= 0, \quad [b_r, b_s^+] = \delta_{rs}, \end{aligned} \quad (92)$$

but also, like the original and adiabatic operators, transformed nonadiabatic operators of both subsystems have to commute mutually, that is, also commutation relations have to hold:

$$[a_P, b_r] = 0, \quad [a_P, b_r^+] = 0. \quad (93)$$

With respect to the fermion transformation relations (89), the form of transformation relations for boson operators that fully respects conditions (92) is

$$\begin{aligned} \bar{b}_r &= b_r + \sum_{PQ} \hat{d}_{rPQ}(P) a_P^+ a_Q, \\ \bar{b}_r^+ &= b_r^+ + \sum_{PQ} (\hat{d}_{rPQ}(P))^+ a_P^+ a_Q. \end{aligned} \quad (94)$$

Again, in order to enable practical solution, the commutation relation (93) is required to hold up to quadratic terms in Taylor's expansions. This restriction enables to express transformation coefficients  $\hat{d}_{RS}$  through coefficients  $\hat{c}_{RS}$ , see [66]—Appendix B.

It can be shown that also this transformation preserves the total number of particles, that is,

$$N_e = \sum_P a_P^+ a_P = \bar{N}_e = \sum_P \bar{a}_P^+ \bar{a}_P = \sum_P \bar{a}_P^+ a_P = \bar{N}_e. \quad (95)$$

Invariant of transformation is now momentum operator:

$$\begin{aligned} P_r &= (b_r - b_r^+) = \bar{P}_r = (\bar{b}_r - \bar{b}_r^+) \\ &\neq \bar{P} = (\bar{b}_r - \bar{b}_r^+), \quad P_r = \bar{P}_r \neq \bar{P}_r. \end{aligned} \quad (96)$$

However, coordinate operator is transformed up to first order of Taylor's expansion, as

$$\begin{aligned} Q_r &= (b_r + b_r^+) \\ &= (\bar{b}_r + \bar{b}_r^+) - 2 \sum_{PQ} \hat{c}_{PQ}^r(P) a_P^+ a_Q \\ &= \bar{Q}_r - 2 \sum_{PQ} \hat{c}_{PQ}^r(P) a_P^+ a_Q \\ &= \bar{Q}_r - 2 \sum_{PQ} \hat{c}_{PQ}^r(P) a_P^+ a_Q, \end{aligned} \quad (97)$$

that is,

$$\bar{Q}_r = \overline{\bar{Q}}_r \neq Q_r. \quad (98)$$

For nonadiabatic (QP)-dependent spinorbitals  $|\varphi_P(x, Q, P)\rangle$  which are the basis functions of the nonadiabatic (QP)-dependent electronic wave function of the ground state  $\Phi_0(r, Q, P)$ , expressed over crude-adiabatic orbitals can be derived:

$$\begin{aligned} |\varphi_P(x, Q, P)\rangle &= a_P^+(x, Q, P)|0\rangle \\ &= \left( \bar{a}_P^+ - \sum_{rR} c_{PR}^r \bar{Q}_r \bar{a}_R^+ \right. \\ &\quad \left. - \sum_{\bar{r}R} \tilde{c}_{PR}^{\bar{r}} P_{\bar{r}} \bar{a}_R^+ + O(\bar{Q}^2, \bar{Q}P, P^2) \right) |0\rangle \\ &= |\varphi_P(x, 0, 0)\rangle - \sum_{rR} c_{PR}^r \bar{Q}_r |\varphi_R(x, 0, 0)\rangle \\ &\quad - \sum_{\bar{r}R} \tilde{c}_{PR}^{\bar{r}} \bar{P}_{\bar{r}} |\varphi_R(x, 0, 0)\rangle + \dots \end{aligned} \quad (99)$$

Nonadiabatic wave function (99) in contrast to adiabatic wave function (82) is modulated not only by the instantaneous nuclear coordinates  $\{\bar{Q}_r\}$  of particular vibration (phonon) modes  $\{r\}$  but modulation is also over corresponding instantaneous nuclear momenta  $\{P_{\bar{r}}\}$ . The weight of momentum modulation is proportional to the  $P$ -dependent transformation coefficients  $\tilde{c}_{PR}^{\bar{r}}$ . It represents first derivative of  $\hat{c}_{PR}$  matrix element with respect to nuclear momentum  $P_r$ ,  $\tilde{c}_{PR}^{\bar{r}} = \partial \hat{c}_{PR}(P) / \partial P_r$ , that is, coefficient of transformation matrix in the first order of Taylor's expansion. It will be shown that these coefficients reflect not only the strength of e-p coupling but mainly the magnitude of nonadiabaticity. For true nonadiabatic situation, that is, for antiadiabatic state  $|\varepsilon_r^0(R) - \varepsilon_A^0(R)\rangle < \hbar\omega_r$ , the weight of such  $P$ -modulated state can be significant.

### 2.2.3. Solution of Nonadiabatic Problem:

#### Corrections to Energy Terms

##### (1) Transformations of System Hamiltonian

Base functions transformations have incorporated dependence of electronic states on operators of nuclear motion and vice versa. It implies, before the system Hamiltonian transformations, necessity to rearrange starting crude-adiabatic Hamiltonian:

$$\begin{aligned} H &= T_N(\bar{P}) + E_{NN}(\bar{Q}) \\ &\quad + \sum_{PQ} h_{PQ}(\bar{Q}) \bar{a}_P^+ \bar{a}_Q + \frac{1}{2} \sum_{PQRS} v_{PQRS}^0 \bar{a}_P^+ \bar{a}_Q^+ \bar{a}_S \bar{a}_R \end{aligned} \quad (100)$$

into more convenient form.

Let us formally divide this Hamiltonian on two parts,  $H_A$  and  $H_B$ .

(A) The nuclear part  $H_N$ , as we already know, is quantized on crude-adiabatic level as

$$H_N \rightarrow H_B = \sum_r^{\text{mod}} \hbar\omega_r (\bar{b}_r^+ \bar{b}_r + 1/2). \quad (101)$$

In general, this part can be written as the sum of nuclear kinetic and nuclear potential energy:

$$H_B = E_{kin}(\bar{P}) + E_{pot}(\bar{Q}), \quad (102)$$

whereas

$$E_{pot}(\bar{Q}) = E_{NN}^{(2)}(\bar{Q}) + V_N^{(2)}(\bar{Q}). \quad (103a)$$

The standard, usually harmonic-quadratic part of the nuclear potential energy,  $E_{NN}^{(2)}(\bar{Q})$  is corrected now by some, yet unknown, potential energy term  $V_N^{(2)}(\bar{Q})$ , that is, supposed to be also quadratic function of nuclear coordinate operators. Evidently, the  $V_N^{(2)}(\bar{Q})$  term is absent on crude-adiabatic level. This correction originates from the interaction of vibrating nuclei with electrons on adiabatic  $\bar{Q}$ -dependent level. In general, kinetic energy of vibration motion can also be corrected by some, yet unknown quadratic function of nuclear momenta operators- $W_N^{(2)}(\bar{P})$ , that is,

$$E_{kin}(\bar{P}) = T_N(\bar{P}) + W_N^{(2)}(\bar{P}). \quad (103b)$$

On the adiabatic  $Q$ -dependent level kinetic energy correction is negligibly small and it is neglected. It becomes important only when the BOA is broken,  $|E_n^{te}(R) - E_n^{te}(R_{eq})| \leq \hbar\omega_n$ , that is, in the case when electrons due to increased effective mass are not able to follow nuclear motion adiabatically and electronic states are QP-dependent. It should be stressed that both corrections are absent on crude-adiabatic level, they have been introduced just with respect to subsequent adiabatic and nonadiabatic transformation of system Hamiltonian.

(B) The second part of divided Hamiltonian is

$$\begin{aligned} H_A &= E_{NN}(\bar{Q}) - E_{NN}^{(2)}(\bar{Q}) - V_N^{(2)}(\bar{Q}) \\ &\quad - W_N^{(2)}(\bar{P}) + \sum_{PQ} h_{PQ}(\bar{Q}) \bar{a}_P^+ \bar{a}_Q \\ &\quad + \frac{1}{2} \sum_{PQRS} v_{PQRS}^0 \bar{a}_P^+ \bar{a}_Q^+ \bar{a}_S \bar{a}_R. \end{aligned} \quad (104)$$

It is evident that the division on the two parts is only formal

$$H = H_A + H_B = (100). \quad (105)$$

The reason of it is mainly pragmatic with respect to transformations and final solution. In this way the total system Hamiltonian is divided on quasi-bosonic (nuclear part  $H_B$ ) and quasifermionic (electronic  $H_A$ ) Hamiltonians.

The system Hamiltonian (in the form (105)) is now prepared for canonical transformations. The frequently used form of canonical transformation,

$$\begin{aligned} T : H(A_\mu) &\equiv \tilde{H}(A_\mu) = H(\tilde{A}_\mu) \\ &= H(U^+(A_\nu)A_\mu U(A_\nu)), \end{aligned} \quad (106)$$

$$\tilde{A}_\mu = U^+(A_\nu)A_\mu U(A_\nu) = f(A_\nu), \quad (107a)$$

is applied in order to get diagonal, or “more diagonal”, final form at least up to first order of commutation expansion,  $[H_0, S] + H_{\text{int}} = 0$ . This kind of transformation changes the form of the Hamiltonian, but leaves unchanged the system variables.

Base functions transformations, as presented in preceding parts, introduce new dynamical variables; starting from crude-adiabatic ( $\bar{a}, \bar{a}^+, \bar{b}, \bar{b}^+$ ), new adiabatic ( $\bar{\bar{a}}, \bar{\bar{a}}^+, \bar{\bar{b}}, \bar{\bar{b}}^+$ ), and nonadiabatic ( $a, a^+, b, b^+$ ) quasiparticles are introduced. At these circumstances, canonical transformation of Hamiltonian means introduction of new dynamical variables

$$A_\mu \equiv A_\mu(A'_\nu) = U^+(A'_\nu)A'_\nu U(A'_\nu). \quad (108)$$

Unlike to (106), now the Hamiltonian is not transformed itself, it remains of the original form, but its variables ( $A_\nu$ ) are replaced by new variables ( $A'_\nu$ ):

$$H(A_\mu) \equiv H(U^+(A'_\nu)A'_\nu U(A'_\nu)). \quad (109a)$$

The Hamiltonian written in new variables is

$$H(A_\mu(A'_\nu)) \equiv \tilde{H}(A'_\nu). \quad (109b)$$

Since at this transformation, there is no any requirement for fulfillment of condition like at (106), the transformation does not make Hamiltonian “more” diagonal. Usually it is more complex, but very often it discloses physical aspects of the problem that are not obvious from nontransformed form with the original variables of system Hamiltonian.

The system Hamiltonian (105) is now subjected to this type of transformation.

In the first step, transformation from crude-adiabatic to adiabatic quasiparticles is realized.

The adiabatic quasi-particle transformations, up to the second order of Taylor’s expansion, generate terms  $H_{A\bar{i}(j,k)}$  and  $H_{B\bar{i}(j,k)}$  whereas  $i, j, k$  in subscript  $\bar{i}(j,k)$  stand now for the  $i$ th order of Taylor’ series expansion in adiabatic representation, the  $j$ th order of the coordinate operator  $\bar{Q}$ , and the  $k$ th order of momentum operator  $\bar{P}$  within the given order  $i$  of Taylor’s expansion; that is,  $i = (j + k)$ .

Up to the second-order expansion in  $\bar{Q}, \bar{P}$  and in second-order expansion of the operators of quasiparticle transformation ( $\bar{c}_{PQ}, \bar{d}_{rPQ}$ ), the  $H_A$  and  $H_B$  parts are transformed in the following way:

$$H_{A\bar{0}(0,0)} \longrightarrow H_{A\bar{0}(0,0)} + H_{A\bar{1}(1,0)} + H_{A\bar{2}(2,0)}, \quad (110a)$$

$$H_{A\bar{1}(1,0)} \longrightarrow H_{A\bar{1}(1,0)} + H_{A\bar{2}(2,0)}, \quad (110b)$$

$$H_{A\bar{2}(2,0)} \longrightarrow H_{A\bar{2}(2,0)}, \quad (110c)$$

$$H_{A\bar{2}(0,2)} \longrightarrow H_{A\bar{2}(0,2)}, \quad (110d)$$

$$H_B = H_{B\bar{0}(0,0)} \longrightarrow H_{B\bar{0}(0,0)} + H_{B\bar{1}(0,1)} + H_{B\bar{2}(1,1)} + H_{B\bar{2}(0,0)}. \quad (110e)$$

The particular form of the terms (110a)–(110e) and details of adiabatic transformation are in [66, Appendix A], [67].

In the next step, the adiabatic form (terms (110a)–(110e)) is transformed to nonadiabatic form, nonadiabatic quasiparticles are introduced (up to the 2nd order of Taylor’ series expansion):

$$H_{A\bar{0}(0,0)} \longrightarrow H_{A0(0,0)} + H_{A1(0,1)} + H_{A2(0,2)}, \quad (111a)$$

$$H_{A\bar{1}(1,0)} \longrightarrow H_{A1(1,0)} + H_{A2(1,1)} + H_{A2(0,0)}, \quad (111b)$$

$$H_{A\bar{2}(2,0)} \longrightarrow H_{A2(2,0)}, \quad (111c)$$

$$H_{A\bar{2}(0,2)} \longrightarrow H_{A2(0,2)}, \quad (111d)$$

$$H_{B\bar{0}(0,0)} \longrightarrow H_{B0(0,0)} + H_{B1(1,0)} + H_{B2(1,1)} + H_{B2(0,0)}, \quad (111e)$$

$$H_{B\bar{1}(0,1)} \longrightarrow H_{B1(0,1)} + H_{B2(0,2)}, \quad (111f)$$

$$H_{B\bar{2}(1,1)} \longrightarrow H_{B2(1,1)}, \quad (111g)$$

$$H_{B\bar{2}(0,0)} \longrightarrow H_{B2(0,0)}. \quad (111h)$$

The particular form of the terms (111a)–(111h) and details of nonadiabatic transformation are in [66, Appendix B], [67].

(2) *Nonadiabatic Solution-Corrections to the Crude-Adiabatic Energy Terms*

Like in case of the Hamiltonian transformations, also details of nonadiabatic solution are published in [66, 67].

The main results of the solution can be written in the form of corrections to particular crude-adiabatic terms:

(A) Correction to the ground state electronic energy: correction to  $H_{(0)}(R)$  of (47) it is correction to zero-particle term of system Hamiltonian, that is, correction to the ground state electronic energy (48) calculated in clamped-nuclei approximation at fixed nuclear configuration  $[R]$  due to the effect of nuclear dynamics ( $QP$ -dependence). For total electronic energy then holds:

$$E^{0,te}(R) = [\langle \Phi_0(R) | H_e(r, R) | \Phi_0(R) \rangle + E_{NN}(R)] + \Delta E^0(R). \quad (112)$$

The correction  $\Delta E^0(R)$  is

$$\Delta E^0(R) = \sum_{rAI} \hbar\omega_r (|c_{AI}^r|^2 - |\tilde{c}_{AI}^r|^2), \quad (113)$$

$\{I\}$ -occupied orbitals,  $\{A\}$ -unoccupied orbitals

In (113),

$$c_{PR}^r = \frac{\partial c_{PR}(Q)}{\partial Q_r}, \quad \tilde{c}_{PR}^r = \frac{\partial \hat{c}_{PR}(P)}{\partial P_r} \quad (114)$$

are coefficients of adiabatic transformation (70) and nonadiabatic transformation (89) in first order of Taylor's expansion in  $Q$  or  $P$ , respectively.

Approximate solution (see [66, Appendix C],[67]) yields for these terms:

$$c_{PQ}^r = u_{PQ}^r \frac{(\varepsilon_P^0 - \varepsilon_Q^0)}{(\hbar\omega_r)^2 - (\varepsilon_P^0 - \varepsilon_Q^0)^2}; \quad P \neq Q, \quad \varepsilon_S^0 \equiv \varepsilon_S^0(R), \quad (115)$$

$$\tilde{c}_{PQ}^r = u_{PQ}^r \frac{\hbar\omega_r}{(\hbar\omega_r)^2 - (\varepsilon_P^0 - \varepsilon_Q^0)^2}; \quad P \neq Q, \quad \varepsilon_S^0 \equiv \varepsilon_S^0(R). \quad (116)$$

The final form of the correction is

$$\begin{aligned} \Delta E^0(R) &= \sum_{rAI} \hbar\omega_r (|c_{AI}^r|^2 - |\tilde{c}_{AI}^r|^2) \\ &= \sum_A \sum_I^{unocc} \sum_r^{occ} |u_{AI}^r|^2 \frac{\hbar\omega_r}{(\varepsilon_A^0 - \varepsilon_I^0)^2 - (\hbar\omega_r)^2} \\ &= \sum_A \sum_I^{unocc} \sum_r^{occ} \Omega_{AI}. \end{aligned} \quad (117)$$

The  $\Omega$  matrix is a symmetric matrix of the form

$$\begin{aligned} \Omega_{PQ} &= \sum_r \hbar\omega_r (|c_{PQ}^r|^2 - |\tilde{c}_{PQ}^r|^2) \\ &= \sum_r |u_{PQ}^r|^2 \frac{\hbar\omega_r}{(\varepsilon_P^0 - \varepsilon_Q^0)^2 - (\hbar\omega_r)^2}. \end{aligned} \quad (118)$$

From the final form of the correction (117), the two limiting situations can be extracted.

(i) True nonadiabatic or antiadiabatic state,  $(\varepsilon_A^0 - \varepsilon_I^0) < \hbar\omega_r$ .

In this case the correction is negative,  $\Delta E_{(nad)}^0 < 0$ , and represents stabilization contribution to the electronic ground state energy. It is evident from (117) that the ground-state energy stabilization is exclusively the effect of nuclear dynamics, which is expressed through the coefficients  $\tilde{c}_{AI}^r$  of  $P$ -dependent transformation. This contribution can be considerably large and reach the extreme negative value for left-hand side limit toward singular point in (117). Singular point itself is excluded [66, Appendix C]. The correction is always negative for the extreme case of strong nonadiabatic limit,  $\hbar\omega_r/|\varepsilon_P^0 - \varepsilon_Q^0| \rightarrow \infty$ . However, the contribution in this case does not represent the largest possible negative value and it is equal to  $\Delta E_{(sna)}^0 = -\sum_{rAI} \hbar\omega_r (|\tilde{c}_{AI}^r|^2) = -\sum_{rAI} |u_{AI}^r|^2/\hbar\omega_r$ .

(ii) The second limit corresponds to adiabatic level, when electronic state is only  $\bar{Q}$ -dependent. In this case the coefficients  $\tilde{c}_{AI}^r$  of  $P$ -dependent transformation are absent in (118) and for the correction holds:

$$\Delta E_{(ad)}^0 = \sum_{rAI} \hbar\omega_r (|c_{AI}^r|^2). \quad (119)$$

In case of strong adiabaticity,  $(\varepsilon_A^0 - \varepsilon_I^0) \gg \hbar\omega_r$ , which is standard condition for the BOA we have

$$\Delta E_{(sad)}^0 = \sum_{rAI} \hbar\omega_r (|c_{AI}^r|^2) = \sum_{rAI} |u_{AI}^r|^2 \frac{\hbar\omega_r}{(\varepsilon_A^0 - \varepsilon_I^0)^2} \rightarrow \approx 0. \quad (120)$$

In contrast to nonadiabatic level when the correction is negative,  $\Delta E_{(nad)}^0 < 0$ , on the adiabatic level the correction is whatever small, but always positive (119).

An important aspect has to be mentioned in relation to adiabatic level. Introduction of adiabatic quasiparticles, that is,  $\bar{Q}$ -dependent transformation, in solution of total system problem has to reproduce the basic results of standard treatment of solid state physics (or molecular physics) at solution of electron-phonon interactions by means of perturbation theory (see, e.g., (21), (22)). It can be shown that the base transformation is in this respect equivalent to standard treatment.

The exact adiabatic correction to the electronic ground state is, according to (9), the term  $B_{00}$ , that is, DBOC—the mean-value of nuclear kinetic energy in adiabatic electronic ground state:

$$\begin{aligned} B_{00}(R) &= \int \Phi_0^*(r, R) \hat{T}_N(R) \Phi_0(r, R) dr \\ &= \sum_n^{N_n} -\frac{\hbar^2}{2M_n} \int \Phi_0^*(r, R) \nabla_n^2 \Phi_0(r, R) dr \\ &= \sum_{n\alpha} \frac{\hbar^2}{2M_n} \int \left( \frac{\partial \Phi_0(r, \vec{R})}{\partial R_{n\alpha}} \right)^* \left( \frac{\partial \Phi_0(r, \vec{R})}{\partial R_{n\alpha}} \right) dr|_{[R]}. \end{aligned} \quad (121)$$

We have shown [73] that (121) is the same as the adiabatic correction (119) to the electronic energy of the ground state

$\Phi_0$ , calculated through the expansion coefficients  $c_{PQ}(\bar{Q})$  of  $\bar{Q}$ -dependent transformation, that is,

$$\begin{aligned}\Delta E_{(ad)}^0(R) &= B_{00}(R) \\ &= \langle \Phi_0(r, \bar{R}) | T_N | \Phi_0(r, \bar{R}) \rangle_{\bar{R}} \\ &= \sum_{rAI} \hbar\omega_r |c_{AI}^r|^2.\end{aligned}\quad (122)$$

Within the single Slater determinant representation of the ground electronic state, this relation is exact since the eigenfunctions—spinorbitals  $\{\varphi_Q(R)\}$  of the Hartree-Fock equations (29) are orthonormal and form complete basis set, that is, closure property holds

$$\sum_Q |\varphi_Q(r, R)\rangle \langle \varphi_Q(r, R)| = 1. \quad (123)$$

It means that both subsets, that is, occupied  $\{\varphi_I(r, R)\}$  and unoccupied  $\{\varphi_A(r, R)\}$  orbitals are included at calculation of (119), (121). As it is seen from (119), (122), electronic ground state energy correction is due to virtual transitions between occupied  $\{\varphi_I(r, R)\}$  and unoccupied orbitals  $\{\varphi_A(r, R)\}$  at nuclear vibration motion. It should be stressed that at these virtual transitions the system remains in its electronic ground state  $\Phi_0(r, R_{eq})$ . In this respect, even  $\Delta E_{(ad)}^0$  represents exactly the DBOC, it covers basically “nonadiabatic” (off-diagonal) corrections in the sense as these are calculated in a second order of perturbation theory when excited electronic states are approximated through virtual orbitals optimized for electronic ground-state  $\Phi_0(r, R_{eq})$  and perturbation is an electron-vibration coupling  $H_{ep}$ , as it has been discussed at the beginning. It can be seen very clearly from the derived expression for correction to frequency of normal modes:

$$\begin{aligned}\Delta\omega_r &= -2(\hbar\omega_r)^2 \sum_{AI} \frac{1}{(\varepsilon_A^0 - \varepsilon_I^0)} (c_{AI}^r)^2 \\ &= -2(\hbar\omega_r)^2 \sum_{AI} |u_{AI}^r|^2 \frac{(\varepsilon_A^0 - \varepsilon_I^0)}{\left[ (\varepsilon_A^0 - \varepsilon_I^0)^2 - (\hbar\omega_r)^2 \right]^2}.\end{aligned}\quad (124)$$

The final effect is softening of normal mode vibration frequency:

$$\hbar\omega_{r(ad)} = \hbar\omega_r - 2(\hbar\omega_r)^2 \sum_{AI} \frac{1}{(\varepsilon_A^0 - \varepsilon_I^0)} (c_{AI}^r)^2. \quad (125)$$

The normal mode energy correction (124) is identical to the normal mode energy correction which can be derived as nonadiabatic correction in second order of perturbation theory assuming single boson excitation processes, that is,

$$\Delta\omega_r = -2(\hbar\omega_r)^2 \sum_{AI} |u_{AI}^r|^2 \frac{(\varepsilon_A^0 - \varepsilon_I^0)}{\left[ (\varepsilon_A^0 - \varepsilon_I^0)^2 - (\hbar\omega_r)^2 \right]^2}. \quad (126)$$

The term nonadiabatic is related to the fact that within the perturbation treatment contributions to the correction arise due to virtual transitions between occupied  $\{I\}$  and unoccupied  $\{A\}$  states, that is, correction is calculated through off-diagonal elements of the form  $\langle \varphi_I | \hat{H}_{ep} | \varphi_A \rangle \langle \varphi_A | \hat{H}_{ep} | \varphi_I \rangle / (\varepsilon_I^0 - \varepsilon_A^0)$ .

For quasimomentum  $k$ ,  $q$ -space representation of multiband solids, with respect to  $(k; -k)$  symmetry, the temperature-dependent form of the equation for correction to electronic ground-state energy (117) can be expressed in the following form:

$$\begin{aligned}\Delta E_{(na)}^0 &= 2 \left( \sum_{R(k), S(k')} \left( \sum_{k < k_F, k' > k_F} |u^{k'-k}|^2 f_k (1 - f_{k'}) \right. \right. \\ &\quad \left. \left. \times \frac{\hbar\omega_{k'-k}}{(\varepsilon_{k'}^0 - \varepsilon_k^0)^2 - (\hbar\omega_{k'-k})^2} \right) \right), \\ \varphi_{Rk} &\neq \varphi_{Sk'}.\end{aligned}\quad (127)$$

Summations in (127) are over all bands  $\{\varphi_R, \varphi_S\}$  and  $k$  points of the first BZ of multiband system, while  $\varepsilon_k^0 < \varepsilon_F$ ;  $\varepsilon_{k'}^0 > \varepsilon_F$ .

For  $T = 0$  K, relation (127) is reduced to

$$\Delta E_{(na)}^0 = 2 \left( \sum_{R(k), S(k')} \left( \sum_{kk'} |u^{k'-k}|^2 \frac{\hbar\omega_{k'-k}}{(\varepsilon_{k'}^0 - \varepsilon_k^0)^2 - (\hbar\omega_{k'-k})^2} \right) \right). \quad (128)$$

In (128), the wave vector  $k$  corresponds to states fully occupied below Fermi level ( $f_k = 1$ ), and wave vector  $k'$  corresponds to empty-virtual states above the Fermi-level ( $f_{k'} = 0$ ). It should be noticed that  $u^{k'-k}$  is matrix element of e-p coupling (43).

(B) Correction to one-particle term: correction to  $H_{(1)}(R)$  of (47).

The one-particle correction has been derived in the form

$$\begin{aligned}\Delta H'_{ep} &= \sum_{rPQ} \hbar\omega_r \left( \sum_A (c_{PA}^r c_{QA}^{r*} - \tilde{c}_{PA}^r \tilde{c}_{QA}^{r*}) \right. \\ &\quad \left. - \sum_I (c_{PI}^r c_{QI}^{r*} - \tilde{c}_{PI}^r \tilde{c}_{QI}^{r*}) \right) N[a_P^+ a_Q] \\ &\quad + \sum_{rPR} \left( (\varepsilon_P^0 - \varepsilon_R^0) (|c_{PR}^r|^2 + |\tilde{c}_{PR}^r|^2) \right. \\ &\quad \left. - 2\hbar\omega_r \operatorname{Re}(\tilde{c}_{PR}^r c_{PR}^{r*}) \right) N[a_P^+ a_P].\end{aligned}\quad (129)$$

It should be noticed that the second contribution in (129) originates from boson excitation dependent terms of nonadiabatic Hamiltonian and expression in the second line of (129) is for boson vacuum. The first term in (129) originates from those terms of nonadiabatic Hamiltonian which are not dependent on boson operators (pure fermionic terms). At derivation of (129), restriction has been to the first order

of e-p coupling and the terms that are the products of e-p coupling and coulomb two-electron interactions (e.g.,  $(\nu_{PRPA}^0 - \nu_{PRAP}^0)(c_{IR}^r c_{IA}^{r*} + \hat{c}_{IR}^r \hat{c}_{IA}^{r*})$ ) have been expected to be negligibly small comparing to pure e-p coupling terms and were neglected. Details of derivation can be found in [66, 67].

(i) Nonadiabatic polarons

The diagonal form of the one-particle correction (129) is

$$\begin{aligned} \Delta H'_{ep}(dg) = & \sum_{rP} \hbar\omega_r \left( \sum_A (|c_{PA}^r|^2 - |\hat{c}_{PA}^r|^2) \right. \\ & \left. - \sum_I (|c_{PI}^r|^2 - |\hat{c}_{PI}^r|^2) \right) N[a_p^+ a_P] \\ & + \sum_{rPR} \left( (\varepsilon_P^0 - \varepsilon_R^0) (|c_{PR}^r|^2 + |\hat{c}_{PR}^r|^2) \right. \\ & \left. - 2\hbar\omega_r \text{Re}(\hat{c}_{PR}^r c_{PR}^{r*}) \right) N[a_p^+ a_P]. \end{aligned} \quad (130a)$$

Substitution for transformation coefficients (115), (116) and rearrangement of the expression yields for e-p interaction part of the Hamiltonian:

$$\begin{aligned} \Delta H'_{ep}(dg) &= \sum_{rPR(P \neq R)} |u_{PR}^r|^2 \frac{1}{(\varepsilon_P^0 - \varepsilon_R^0) - \hbar\omega_r} N[a_p^+ a_P] \\ & - 2 \sum_{rPI(P \neq I)} |u_{PI}^r|^2 \frac{\hbar\omega_r}{(\varepsilon_P^0 - \varepsilon_I^0)^2 - (\hbar\omega_r)^2} N[a_p^+ a_P]. \end{aligned} \quad (130b)$$

Transcription of (130b) to quasimomentum  $k, q$ -space of multiband solids has the form

$$\begin{aligned} \Delta H'_{ep}(dg) &= \sum_{Pk, Rk-q} \left( \sum_{qk\sigma} |u^q|^2 \frac{1}{(\varepsilon_k^0 - \varepsilon_{k-q}^0) - \hbar\omega_q} N[a_{k,\sigma}^+ a_{k,\sigma}] \right) \\ & - 2 \sum_{Pk, Sk-q} \left( \sum_{qk\sigma} |u^q|^2 f_{k-q} \frac{\hbar\omega_q}{(\varepsilon_k^0 - \varepsilon_{k-q}^0)^2 - (\hbar\omega_q)^2} \right. \\ & \left. \times N[a_{k,\sigma}^+ a_{k,\sigma}] \right). \end{aligned} \quad (130c)$$

Expression (130c) represents total one-electron energy correction on the general  $Q, P$ -dependent level due to e-p interactions. The first term of (130c) is standard adiabatic ( $Q$ -dependent) polaron as it can be derived from Fröhlich Hamiltonian by the Lee-Low-Pines transformation [74]. The second term of (130c) is the correction to polaron energy that arises due to dependence of electronic motion not only on nuclear coordinates but also on the nuclear momenta

$P$  (nonadiabatic modification of the BOA). This term can be interpreted as a correction to the energy of individual polaron by an effective field created by all other polarons of the system.

(ii) Correction to orbital energies: gap opening in one-particle spectrum of quasidegenerate states at Fermi level.

For quasicontinuum of states at Fermi level, which is characteristic for metal-like band structures, contribution of second term in (130a) can be expected to be negligibly small. Summation in this term runs over all states, occupied and unoccupied. Since the term is odd function of  $(\varepsilon_P^0 - \varepsilon_R^0)$ , contributions from occupied and unoccupied states will tend to cancel mutually. On the other hand, character of one-particle spectrum can be changed at the e-p coupling through contribution of the first term in (130a) since summations in this term run separately over occupied and unoccupied states. Moreover, magnitude of the change in orbital positions is temperature dependent through the temperature dependence of the population of states.

At these circumstances, for investigation of possible changes in the character of one-electron spectrum of system due to e-p interactions on  $Q, P$ -dependent level, the first term of (130a) is crucial. For correction to orbital energy  $\Delta\varepsilon_P$  of general state  $\varepsilon_P^0$ , from the first term in (130a), it follows that

$$\begin{aligned} \Delta\varepsilon_P &= \sum_r \hbar\omega_r \left( \sum_A (|c_{PA}^r|^2 - |\hat{c}_{PA}^r|^2) \right. \\ & \left. - \sum_I (|c_{PI}^r|^2 - |\hat{c}_{PI}^r|^2) \right) \quad (131) \\ &= \left( \sum_A^{unocc} \Omega_{PA} - \sum_I^{occ} \Omega_{PI} \right). \end{aligned}$$

Finally, corrected orbital energy is

$$\varepsilon_P = \varepsilon_P^0 + \Delta\varepsilon_P. \quad (132a)$$

Let us consider only the couple of quasidegenerate states at Fermi level, occupied state  $\varepsilon_I^0$ , and unoccupied state  $\varepsilon_A^0$ , a situation that can characterize couple of states in antiadiabatic state,  $|\varepsilon_A^0(R) - \varepsilon_I^0(R)| \ll \hbar\omega_r$ . From (131) and from the structure of  $\Omega$  matrix, (118) follows directly:

$$\begin{aligned} \Delta\varepsilon_A &= (\varepsilon_A - \varepsilon_A^0) = -\Omega_{AI} > 0, \\ \Delta\varepsilon_I &= \Omega_{IA} = \Omega_{IA} < 0, \quad (132b) \\ \Delta\varepsilon_I &= -\Delta\varepsilon_A. \end{aligned}$$

It means that orbital energy of unoccupied state has been increased,  $\varepsilon_A > \varepsilon_A^0$ , and orbital energy of the occupied state has been decreased,  $\varepsilon_I < \varepsilon_I^0$ . It can be generalized for a set of quasidegenerate occupied  $\{J\}$  and unoccupied  $\{B\}$  states (quasicontinuum of states) at Fermi level. Then, with respect to the fact that for antiadiabatic state correction to

the ground electronic state (117) is negative  $\sum_{AI} \Omega_{AI} < 0$ , the following relations can be derived:

$$\begin{aligned}\Delta\varepsilon_B &= \sum_A^{unocc} \Omega_{BA} - \sum_I^{occ} \Omega_{BI} \geq 0, \\ \Delta\varepsilon_J &= \sum_A^{unocc} \Omega_{JA} - \sum_I^{occ} \Omega_{JI} \leq 0.\end{aligned}\quad (133)$$

In particular,

$$\begin{aligned}\Delta\varepsilon_B &= \sum_r \sum_A^{unocc} |u_{BA}^r|^2 \frac{\hbar\omega_r}{(\varepsilon_B^0 - \varepsilon_A^0)^2 - (\hbar\omega_r)^2} \\ &\quad - \sum_r \sum_I^{occ} |u_{BI}^r|^2 \frac{\hbar\omega_r}{(\varepsilon_B^0 - \varepsilon_I^0)^2 - (\hbar\omega_r)^2},\end{aligned}\quad (134a)$$

$$\begin{aligned}\Delta\varepsilon_J &= \sum_r \sum_A^{unocc} |u_{JA}^r|^2 \frac{\hbar\omega_r}{(\varepsilon_J^0 - \varepsilon_A^0)^2 - (\hbar\omega_r)^2} \\ &\quad - \sum_r \sum_I^{occ} |u_{JI}^r|^2 \frac{\hbar\omega_r}{(\varepsilon_J^0 - \varepsilon_I^0)^2 - (\hbar\omega_r)^2}.\end{aligned}\quad (134b)$$

At finite temperature  $T$ , for a correction  $\Delta\varepsilon_P$  to an arbitrary state  $\varepsilon_P^0$ , from the set of quasidegenerate occupied and unoccupied states at Fermi level can be written:

$$\Delta\varepsilon_P(T) = \sum_Q \Omega_{PQ} (1 - 2f_Q), \quad (135)$$

$\{Q\}$ -set of quasidegenerate states at Fermi level.

The occupation factor  $f_Q$  obeys the Fermi-Dirac statistics:

$$f_Q = \left( \exp\left(\frac{\varepsilon_Q - \mu}{k_B T}\right) + 1 \right)^{-1}, \quad \varepsilon_Q = \varepsilon_Q^0 + \Delta\varepsilon_Q. \quad (136)$$

It is evident that for temperature 0 K, (135) is reduced to (131).

From (135), temperature dependence of energy gap which is open in one-particle spectrum at Fermi level can be derived in the form

$$\Delta(T) = \Delta(0) \operatorname{tgh}\left(\frac{\Delta(T)}{4k_B T}\right). \quad (137)$$

The gap is defined as the energy difference of lowest lying corrected unoccupied state  $\varepsilon_{B(LUMO)}$  and highest lying corrected occupied state  $\varepsilon_{J(HOMO)}$ , that is, as an energy gap in one-particle spectrum. At temperature 0 K holds:

$$\Delta(0) = (\varepsilon_{B(LUMO)} + |\varepsilon_{J(HOMO)}|). \quad (138)$$

Factor 4 in the denominator of the argument of  $\operatorname{tgh}$  in (137) follows from the assumption that at Fermi level density of quasidegenerate occupied  $\{\varepsilon_J^0\}$  and unoccupied  $\{\varepsilon_B^0\}$  states of the band with gap opening is the same and consequently  $\varepsilon_{B(LUMO)} = |\varepsilon_{J(HOMO)}|$ . This factor can be larger or smaller

than 4, depending on the actual difference in the density of states of occupied and unoccupied states of band at FL.

It is trivial to show that the corrections to orbital energies are negligibly small (basically zero) for a system in adiabatic state when  $(\varepsilon_A^0 - \varepsilon_I^0) \gg \omega$ .

(C) Correction to two-particle term - correction to  $H_{(2)}(R)$  of (47).

Correction to  $H_{(2)}(R)$  represents correction to electron correlation energy (see Note in Section 1) due to e-p interactions, in particular, it is dependence of electronic motion on nuclear vibration displacements  $Q$  and momenta  $P$ . It has been derived in the form [66, 67]

$$\Delta H''_{ep} = \sum_{rPQRS} \hbar\omega_r (c_{PR}^r c_{SQ}^{r*} - \tilde{c}_{PR}^r \tilde{c}_{SQ}^{r*}) N [a_P^+ a_Q^+ a_S a_R]. \quad (139)$$

Substituting for transformation coefficients (115), (116) yields

$$\begin{aligned}\Delta H''_{ep} &= \sum_{rPQRS(P \neq R, Q \neq S)} u_{PR}^r u_{SQ}^{r*} \\ &\quad \times \frac{\hbar\omega_r \left( (\varepsilon_P^0 - \varepsilon_R^0) (\varepsilon_S^0 - \varepsilon_Q^0) - (\hbar\omega_r)^2 \right)}{\left( (\varepsilon_P^0 - \varepsilon_R^0)^2 - (\hbar\omega_r)^2 \right) \left( (\varepsilon_S^0 - \varepsilon_Q^0)^2 - (\hbar\omega_r)^2 \right)} \\ &\quad \times N [a_P^+ a_Q^+ a_S a_R].\end{aligned}\quad (140)$$

Transcription of (140) to quasimomentum  $k, q$ -space representation of multiband solids has the form

$$\begin{aligned}\Delta H''_{ep} &= \sum_{R(k)S(k')} \sum_{kk'q\sigma\sigma'} |u^q|^2 \\ &\quad \times \frac{\hbar\omega_q \left( (\varepsilon_{k+q}^0 - \varepsilon_k^0) (\varepsilon_{k'+q}^0 - \varepsilon_{k'}^0) - (\hbar\omega_q)^2 \right)}{\left( (\varepsilon_{k+q}^0 - \varepsilon_k^0)^2 - (\hbar\omega_q)^2 \right) \left( (\varepsilon_{k'+q}^0 - \varepsilon_{k'}^0)^2 - (\hbar\omega_q)^2 \right)} \\ &\quad \times N [a_{k+q, \sigma}^+ a_{k', \sigma'}^+ a_{k'+q, \sigma'} a_{k, \sigma}].\end{aligned}\quad (141)$$

### 3. Adiabatic ↔ Antiadiabatic State Transition: Relevance for SC State Transition

**3.1. The Effect of e-p Coupling on Band Structure of Superconductors and Nonsuperconducting Analogues.** In Figures 1(a), 1(c), 1(e), 1(g), (the pictures on the left), there are band structures (BS) of four superconducting compounds of different types and crystal structures at optimized equilibrium geometries. The details of calculation are published elsewhere [64, 75, 76].

As it can be seen from Figure 1, all the band structures are of adiabatic metal-like character with a relatively low density of states at the FL (indicated by a dashed line). Coupling to the respective phonon mode(s) in particular compounds seemingly does not change the metal-like character of BS. In all cases, however, e-p coupling induces BS fluctuation (see the pictures on the right), which is characteristic by fluctuation of the analytic critical point (ACP) of some band across the FL (cf. a-b, c-d, e-f, g-h).

In particular, for  $\text{MgB}_2$  (hP3,  $P6mmm$ , #191;  $\text{AlB}_2\omega$ -type) coupling to the  $E_{2g}$  phonon mode (in-plane stretching vibration of B-B) results in splitting of  $\sigma$  bands ( $p_x, p_y$  electrons of B atoms in a-b plane) in  $\Gamma$  point of the first Brillouin zone (BZ)—Figure 1(b). Related to band topology, the analytic critical point (ACP, maximum) of  $\sigma$  bands is located at  $\Gamma$  point and, for the displacement  $\approx 0.016 \text{ \AA}^\circ/\text{B-atom}$  out of equilibrium position, the ACP crosses FL. This means periodic fluctuation of the BS between topologies 1a  $\leftrightarrow$  1b in coupling to vibration in the  $E_{2g}$  mode.

The situation is similar for  $\text{YB}_6$  (cP7,  $Pm3m$ , #221;  $\text{CaB}_6$  type). In this case, BS fluctuation is related to the  $T_{2g}$  mode (valence vibration of B atoms in basal **a-b** plane of B-octahedron). At the displacement  $\approx 0.017 \text{ \AA}^\circ/\text{B-atom}$  out of equilibrium position, the ACP (saddle point) of the band with dominance of B-p and Y-d electrons crosses FL in the M point and the BS fluctuates between topologies 1c  $\leftrightarrow$  1d.

In the case of  $\text{YBa}_2\text{Cu}_3\text{O}_7$  (oP14,  $Pm3m$ , #47, with chain oxygen in **b**-direction and vacancy in **a**-direction), the BS fluctuation is associated with coupling to three modes,  $A_g, B_{2g}, B_{3g}$ , with the apical O(4) and CuO-plane O(2), O(3) atom displacements. At displacements  $\approx 0.031 \text{ \AA}^\circ$  of apical O(4) in the  $A_g$  mode and  $\approx 0.022 \text{ \AA}^\circ$  of O(2) and O(3) in the  $B_{2g}, B_{3g}$  modes, the ACP (saddle point) of one of the Cu-O plane (d-p $\sigma$ ) band in Y point crosses FL and undergoes periodic fluctuation between topologies 1e  $\leftrightarrow$  1f.

An optical phonon mode is simulated by displacements of Zn atoms in the opposite directions  $\pm\Delta f_b$ , that is, by change of the fractional coordinates;  $(1/3, 2/3 - \Delta f_b, 1/4)$ ,  $(2/3, 1/3 + \Delta f_b, 3/4)$  in hexagonal lattice (hP2,  $P6_3/mmc$ , #194; Mg type). At relatively small displacements,  $\pm (0.0105 - 0.0157) \text{ \AA}^\circ/\text{Zn atom}$ , top of the  $\sigma$  band in  $\Gamma$  point approaches the Fermi level (Figure 2(h)), and continues to a position above it.

As it can be seen from Figure 1 in all cases a particular ACP of the band crosses FL at a displacement which is smaller than root-mean square (rms) displacement for zero-point vibration energy in respective phonon mode. This means, however, that in vibration where ACP approaches FL at the distance less than  $\pm\omega$ , the Fermi energy  $E_F$  (chemical potential  $\mu$ ) of the particular band-electrons close to the point where ACP crosses FL is smaller than the vibration energy of corresponding phonon mode,  $E_F < \omega_{2g}$ . At these circumstances the adiabatic BOA is not valid and standard adiabatic theories cannot be applied. Moreover, shift of the ACP increases substantially the density of states (DOS) at FL,  $n_\sigma(E_F) = (\partial\varepsilon_\sigma^0/\partial k)_{E_F}^{-1}$ , and induces the corresponding decrease in the effective electron velocity  $(\partial\varepsilon_\sigma^0/\partial k)_{E_F}$  of fluctuating band in this region of **k**-space. Under these

circumstances, the system is in the intrinsic nonadiabatic state, or even in the antiadiabatic state,  $E_F \ll \omega_{2g}$ , and electronic motion depends not only on nuclear coordinates  $Q$  but is strongly influenced by nuclear dynamics-momenta  $P$ . The main part of the effect of nuclear kinetic energy on electronic motion can be derived as diagonal correction by sequential  $Q, P$ -dependent base transformations as it has been presented in preceding parts.

Instability of the electronic structure at e-p coupling is absent in respective non-superconducting analogues, such as  $\text{XB}_2$  ( $X \equiv \text{Al, Sc, Y, Ti, Zr, Hf, V, Nb, Ta, Cr, Mo, W, Mn, etc.}$ ),  $\text{CaB}_6$ ,  $\text{YBa}_2\text{Cu}_3\text{O}_6$ , and Mg. Even in the case of the  $\text{XB}_2$ , coupling to the  $E_{2g}$  mode induces splitting of  $\sigma$  bands in the  $\Gamma$  point, the systems remain stable in the adiabatic state. For these systems, the ACP of  $\sigma$  band does not fluctuate across FL. As an illustration, in Figure 2 are band structures of corresponding nonsuperconducting analogues at equilibrium high-symmetry structure (Figures 2(a), 2(c), 2(e), and 2(g)) and at distorted geometry (Figures 2(b), 2(d), 2(f), and 2(h)) with the same displacements in respective phonon modes as those in the case of corresponding superconductors at the transition to the antiadiabatic state.

In the case of  $\text{AlB}_2$ , in spite of  $\sigma$  bands splitting and nearly the same value of the e-p interaction strength (the calculated mean value is  $\bar{u} \approx 1.01 \text{ eV/u.cell}$ ) as that of  $\text{MgB}_2$  ( $\bar{u} \approx 0.98 \text{ eV/u.cell}$ ),  $\text{AlB}_2$  remains in e-p coupling in the adiabatic state as a nonsuperconducting compound. In this case, BS fluctuation (bands splitting in EP coupling) does not decrease chemical potential, it remains in e-p coupling still larger than the vibration energy ( $\mu_{ad} > \hbar\omega$ ) and, consequently, there is no driving force for transition to the antiadiabatic state.

The  $\text{CaB}_6$  is an insulator, and coupling to the  $T_{2g}$  mode (valence vibration of B atoms in basal **a-b** plane of B-octahedron) does change the character of the BS (Figures 2(c) and 2(d)).

In the case of deoxygenated YBCO,  $\text{YBa}_2\text{Cu}_3\text{O}_6$ , in contrast to the superconducting  $\text{YBa}_2\text{Cu}_3\text{O}_7$ , a combination of electron coupling to  $A_g, B_{2g}$ , and  $B_{3g}$  phonon modes leaves band structure without substantial change (Figures 2(e) and 2(f)). In the case of  $\text{YBa}_2\text{Cu}_3\text{O}_7$ , the ACP (saddle point) at Y point fluctuates across FL (see Figures 1(e) and 1(f)), which yields substantial reduction of chemical potential  $-\mu_{antiad} < \hbar\omega$ . For  $\text{YBa}_2\text{Cu}_3\text{O}_6$  the ACP does not fluctuate across FL and chemical potential remains larger than the phonon energy spectrum,  $\mu_{ad} > \hbar\omega$ , and the system remains in the adiabatic state.

Also the band structure of Mg remains without changes at e-p coupling (Figures 2(g) and 2(h)).

### 3.2. Nonadiabatic e-p Coupling Effects in the Antiadiabatic State

#### 3.2.1. Formation of Antiadiabatic Ground State and Gap Opening.

On crude-adiabatic level, total ground state electronic energy  $E_0^{te}(R_{eq})$  has minimum at  $R_{eq}$ ,  $(dE_0^{te}/dR)_{R_{eq}} = 0$ , and within the HF-SCF approximation it is equal to (27).

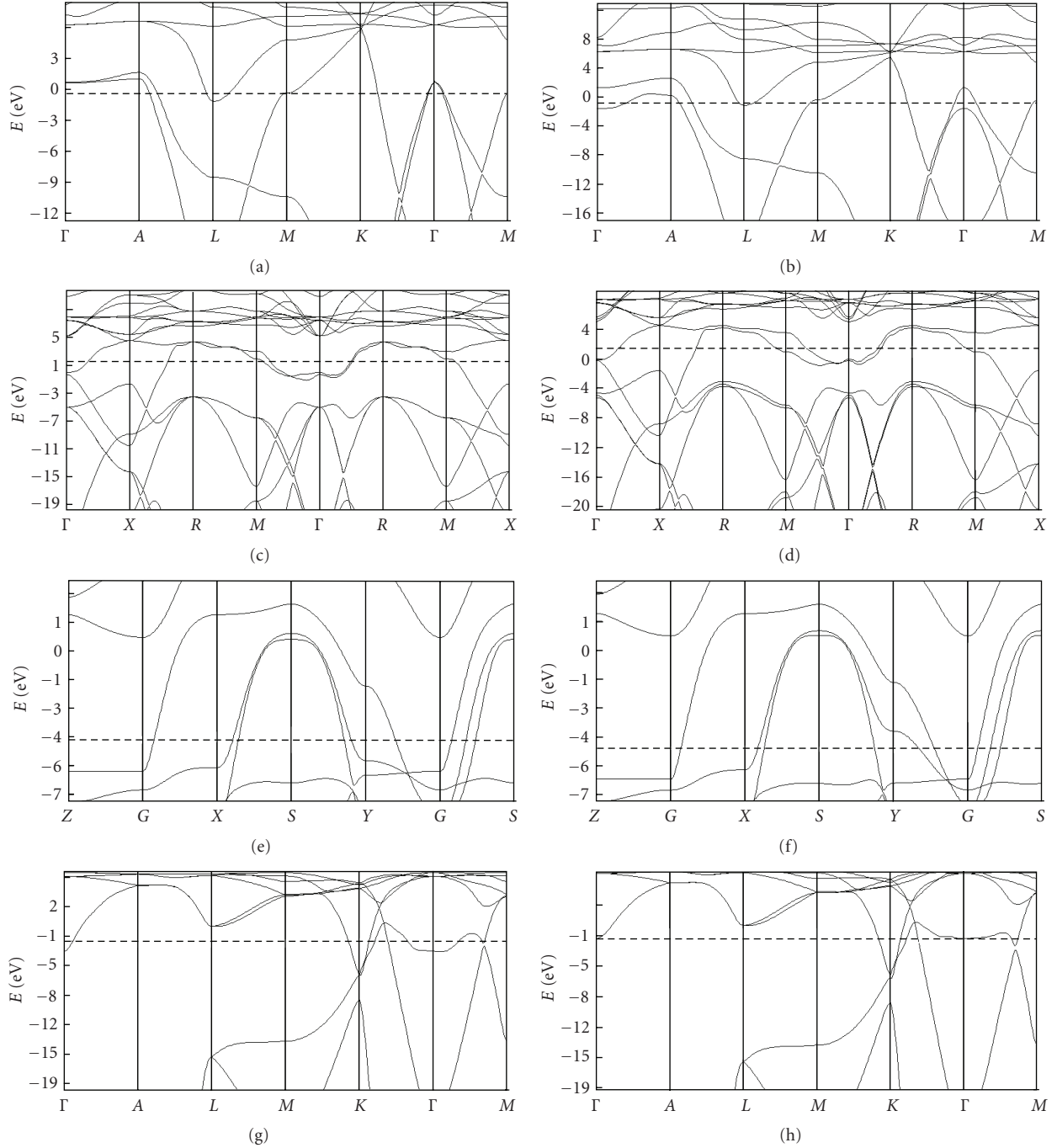


FIGURE 1: Band structures of  $\text{MgB}_2$  (a, b),  $\text{YB}_6$  (c, d),  $\text{YBa}_2\text{Cu}_3\text{O}_7$  (e, f) and  $\text{Zn}$  (g, h). Pictures on the left (a, c, e, g) correspond to equilibrium high-symmetry structures. On the right are the band structures (b, d, f, h) of distorted geometry with atom displacements in the respective phonon modes.

The only correction to this energy is electron correlation energy (53), or (54) in second order of PT, which is negative and contributes to stabilization of the ground state at equilibrium geometry  $R_{\text{eq}}$ :

$$E_{0\text{corr}}^{te}(R_{\text{eq}}) = E_0^{te}(R_{\text{eq}}) - |E_{\text{corr}}|_{R_{\text{eq}}}, \quad (142)$$

$$(dE_{0\text{corr}}^{te}/dR)_{R_{\text{eq}}} = 0.$$

Related to any phonon mode, nuclear displacements at vibration motion increase total electronic energy (potential energy of nuclear motion in particular phonon mode). For displaced geometry  $R_d$  on crude-adiabatic level holds:

$$E_{0\text{corr}}^{te}(R_d) = E_0^{te}(R_d) - |E_{\text{corr}}|_{R_d}. \quad (143)$$

Since two-electron coulomb interactions  $\{\nu_{PQRS}^0\}$  do not depend explicitly on nuclear variables it can be expected

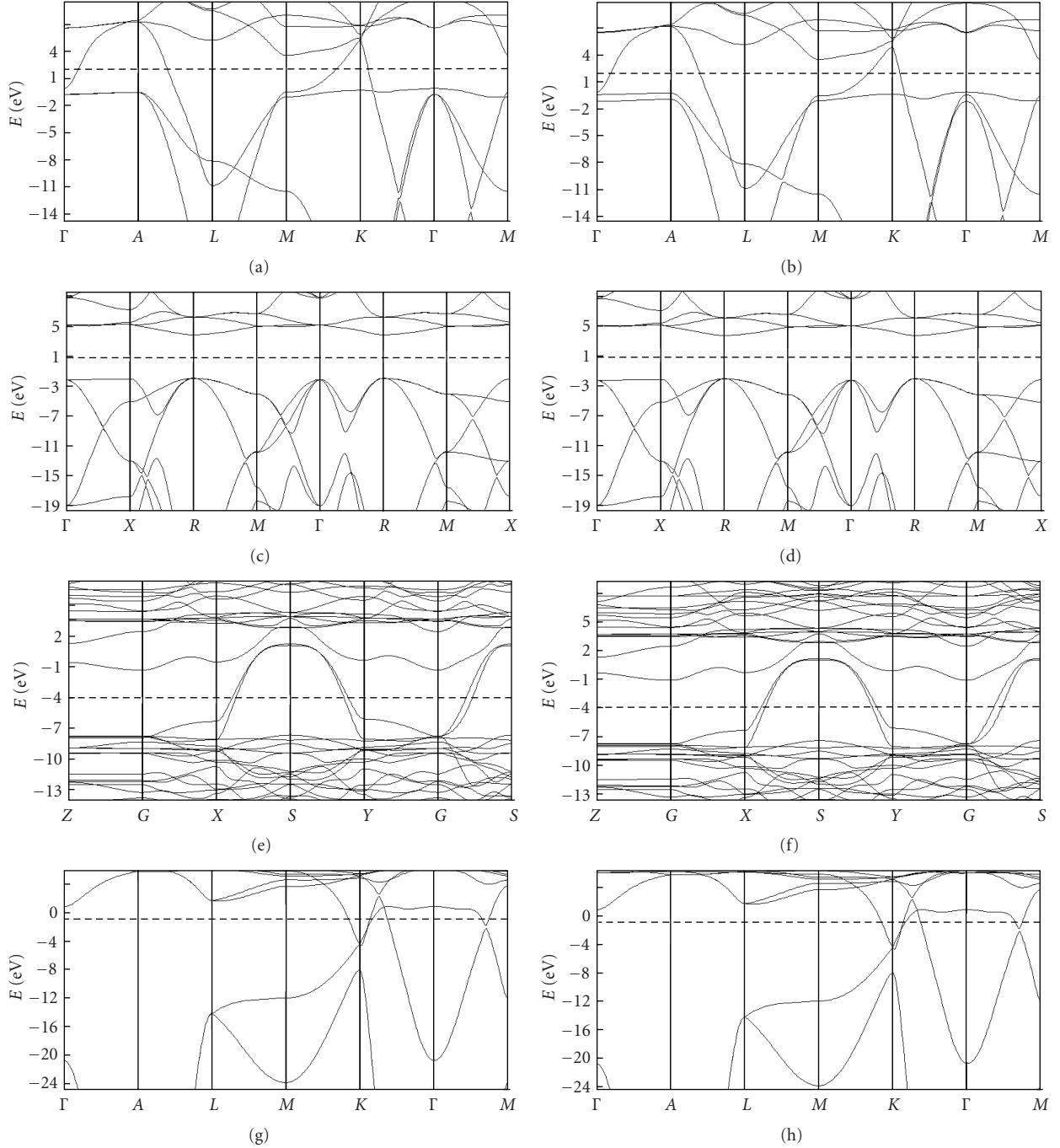


FIGURE 2: Band structure of  $\text{AlB}_2$ ,  $\text{CaB}_6$ ,  $\text{YBa}_2\text{Cu}_3\text{O}_6$ , and  $\text{Mg}$  at equilibrium geometry (a, c, e, g) and at distorted geometry (b, d, f, h).

that electron correlation energy at vibration displacement  $R_d$  has not been changed significantly, that is,  $(E_{\text{corr}})_{R_{\text{eq}}} \approx (E_{\text{corr}})_{R_d}$ . On crude-adiabatic level, for an increase of the total electronic energy  $\Delta E_d$  due to nuclear displacement  $R_d$  then holds:

$$\Delta E_d(R_d) = E_0^{te}(R_d) - E_0^{te}(R_{\text{eq}}) > 0. \quad (144)$$

In principle, two situations can occur; nuclear displacements related to some phonon mode(s) induce forma-

tion of antiadiabatic state, or system remains in adiabatic state with respect to vibration motion in all phonon modes.

The band structures in Figure 1 indicate possibility of antiadiabatic state formation for superconductors. The question if antiadiabatic state can be a stable state, that is, to be a ground electronic state of system at distorted nuclear configuration  $R_d$ , depends on the value of the ground state energy correction  $\Delta E^0(R_d)$  (117).

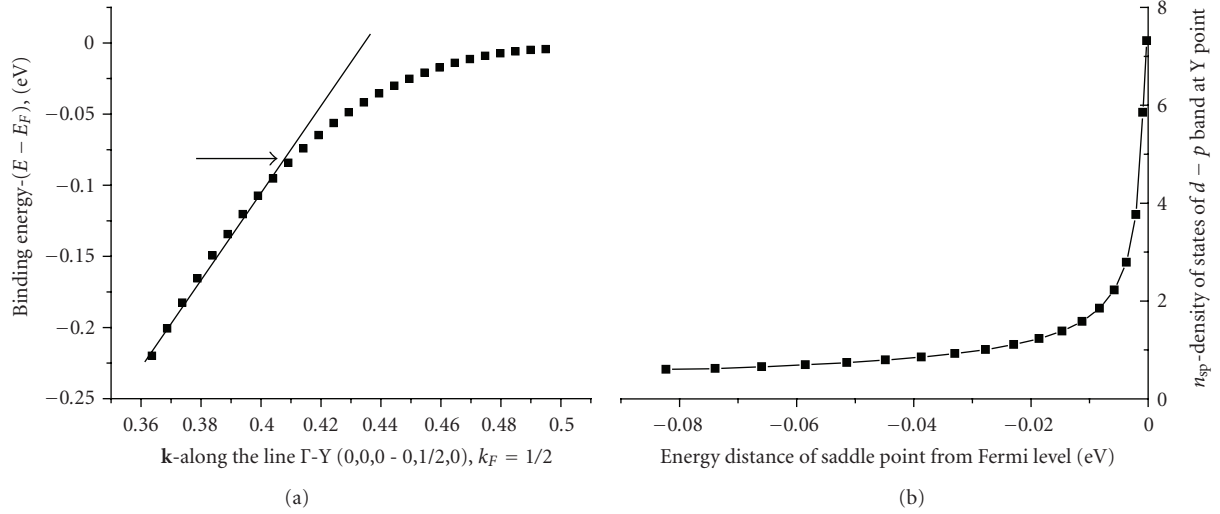


FIGURE 3: Calculated dispersion of  $\text{CuO}_2$  layer  $(d_{x^2-y^2} - p\sigma)$  band in the  $\Gamma$ -Y direction with the kink formation indicated by the arrow (a) and increase in the  $(d_{x^2-y^2} - p\sigma)$  band DOS when ACP approaches the FL (b) for  $\text{YBa}_2\text{Cu}_3\text{O}_7$  at e-p coupling (see text). In both figures, the energy of Fermi level is rescaled to 0 eV.

Since for antiadiabatic state this correction is negative,  $\Delta E_{(na)}^0(R_d) < 0$ , then if the inequality

$$\left| \Delta E_{(na)}^0(R_d) \right| > \Delta E_d(R_d) \quad (145)$$

holds, the electronic state of the system is stabilized at distorted geometry  $R_d$ . The reason of it is significant participation of the nuclear kinetic energy term expressed through contribution of the coefficients  $\hat{c}_{AI}^r$  of  $P$ -dependent transformation (see structure of (113)), which stabilizes fermionic ground state energy in antiadiabatic state at distorted nuclear configuration  $R_d$ .

Stabilization (condensation) energy at transition from adiabatic into antiadiabatic state is

$$E_{cond}^0 = \Delta E_d(R_d) - \left| \Delta E_{(na)}^0(R_d) \right|. \quad (146)$$

Correction (127) to the electronic ground-state energy in the  $k$ -space representation due to interaction of pair of states mediated by the phonon mode  $r$  can be rewritten as

$$\begin{aligned} \Delta E_{(na)}^0 &= 2 \sum_{\varphi_{Rk}} \sum_{\varphi_{Sk'}} \int_0^{\varepsilon_{k'}^{\max}} n_{\varepsilon_{k'}} (1 - f_{\varepsilon_{k'}}^0) d\varepsilon_{k'}^0 \\ &\times \int_{\varepsilon_{k'}^{\min}}^{\varepsilon_{k'}^{\max}} f_{\varepsilon_{k'}}^0 \left| u_{k-k'}^r \right|^2 n_{\varepsilon_k} \frac{\hbar\omega_r}{(\varepsilon_k^0 - \varepsilon_{k'}^0)^2 - (\hbar\omega_r)^2} d\varepsilon_k^0, \\ \varphi_{Rk} &\neq \varphi_{Sk'}. \end{aligned} \quad (147)$$

In general, all bands of 1st BZ of a multiband system are covered, including intraband terms, that is,  $\varphi_{Rk}, \varphi_{Rk'}, k \neq k'$ , while  $\varepsilon_k^0 < \varepsilon_F; \varepsilon_{k'}^0 > \varepsilon_F$ . Fermi-Dirac populations  $f_{\varepsilon_k^0}, f_{\varepsilon_{k'}^0}$  make correction (147) temperature-dependent. Term  $u_{k-k'}^r$  stands for matrix element of e-p coupling and  $n_{\varepsilon_k}, n_{\varepsilon_{k'}}$  are DOS of interacting bands at  $\varepsilon_k^0$  and  $\varepsilon_{k'}^0$ . For adiabatic systems,

such as metals, this correction is positive and negligibly small (DBOC). As it has been mentioned, only for systems in the antiadiabatic state the correction is negative and its absolute value depends on the magnitudes of  $u_{k-k'}^r$  and  $n_{\varepsilon_k}, n_{\varepsilon_{k'}}$  at displacement for FL crossing. At the moment when ACP approach FL, the system not only undergoes transition to the antiadiabatic state but also DOS,  $n_{\sigma}(E_F) = (\partial\varepsilon_{\sigma}^0/\partial k)_{E_F}^{-1}$ , of the fluctuating band is considerably increased at FL. It is a situation invoking possibility of van Hove singularity formation. Important role of van Hove singularity formation for high- $T_c$  superconductors has been proposed by Bok and his collaborators [77, 78].

For all the presented systems at 0 K,  $\Delta E_{(na)}^0$  which covers the effect of nuclear momenta prevails in absolute value the electronic energy increase  $\Delta E_d(R_{dcr})$ , that is, (145) is fulfilled at nuclear displacements  $d_{cr}$  when ACP crosses FL as calculated for clumped nuclear adiabatic structures.

The highest value of the ‘‘condensation energy’’ (146),  $E_{cond}^0 \approx -34$  meV/unit cell, has been calculated [76] for  $\text{YBa}_2\text{Cu}_3\text{O}_7$ . In the case of  $\text{MgB}_2$ ,  $E_{cond}^0 \approx -13$  meV/unit cell has been obtained. For  $\text{YB}_6$ , and  $\text{Zn}$  the values of  $E_{cond}^0$  are smaller but in both cases are also negative.

Under these circumstances, each of the studied systems is stabilized in the antiadiabatic electronic ground state at broken symmetry with respect to the adiabatic equilibrium high-symmetry structure. In my opinion, it can be identified experimentally by ARPES as a kink on momentum distribution curve at FL in form of the band curvature at the ACP when it approaches FL (see Figure 3(a), which presents calculated results for  $\text{YBa}_2\text{Cu}_3\text{O}_7$ ). The crucial influence on the final value of the correction  $\Delta E_{(na)}^0(R_d)$  is related to an increase of the DOS ( $n_{\varepsilon_k}, n_{\varepsilon_{k'}}$  in (147)) connected to the ACP when it approaches  $(\pm\omega)$  FL at transition into antiadiabatic state. Situation for  $\text{YBa}_2\text{Cu}_3\text{O}_7$  is presented in Figure 3(b). In the ARPES spectra of  $\text{YBa}_2\text{Cu}_3\text{O}_7$  a kink on momentum distribution curve in off-nodal direction ( $\Gamma$ -Y line, near

to Y point) should appear in low-energy region at FL for temperatures below  $T_c$  and it will be shifted away from FL, or will disappear above  $T_c$ . It is related to fluctuation of the ACP (inflex point) of one of CuO<sub>2</sub> layer ( $d_{x^2-y^2} - p\sigma$ ) band when it approaches FL at coupling to mentioned phonon modes. In my opinion, it is an effect of dispersion renormalization as it has been discussed in Section 1.

Nontrivial and very important property of system which is stabilized in the antiadiabatic state should be stressed. Due to translation symmetry of the lattice, the created antiadiabatic electronic ground state is geometrically degenerate in distorted geometry ( $R_{d,cr}$ ) with fluxional nuclear configuration in particular phonon mode(s) (see, e.g., [68, Figure 5] for case of MgB<sub>2</sub>). It means that the ground-state energy is the same for different positions of the involved atoms (in phonon modes which drive the system into this state). Expressed in the other way, the involved atoms can circulate over perimeters of the circles with the radii equal to displacements  $d_{cr}$  at FL crossing, without the energy dissipation.

In transition to the antiadiabatic state,  $\mathbf{k}$ -dependent gap  $\Delta_k(T)$  in quasicontinuum of adiabatic one-electron spectrum is opened. The gap opening is related to shift  $\Delta\varepsilon_{Pk}$  of the original adiabatic orbital energies  $\varepsilon_{Pk}^0$ ,  $\varepsilon_{Pk} = \varepsilon_{Pk}^0 + \Delta\varepsilon_{Pk}$ , and to the  $\mathbf{k}$ -dependent change of DOS of particular band(s) at Fermi level. Shift of orbital energies in band  $\varphi_P(k)$  has the form (134a), (134b). In quasimomentum  $k$ -space of multiband solids, these equations are

$$\begin{aligned} \Delta\varepsilon(Pk') &= \sum_{Rk_1 > k_F} \left| u^{k'-k_1'} \right|^2 \left( 1 - f_{\varepsilon_{k_1'}^0} \right) \\ &\quad \times \frac{\hbar\omega_{k'-k_1'}}{\left( \varepsilon_{k'}^0 - \varepsilon_{k_1'}^0 \right)^2 - \left( \hbar\omega_{k'-k_1'} \right)^2} \\ &- \sum_{Sk < k_F} \left| u^{k-k'} \right|^2 f_{\varepsilon_{k'}^0} \\ &\quad \times \frac{\hbar\omega_{k-k'}}{\left( \varepsilon_{k'}^0 - \varepsilon_k^0 \right)^2 - \left( \hbar\omega_{k-k'} \right)^2} \end{aligned} \quad (148a)$$

for  $k' > k_F$ , and

$$\begin{aligned} \Delta\varepsilon(Pk) &= \sum_{Rk_1 > k_F} \left| u^{k-k_1'} \right|^2 \\ &\quad \times \left( 1 - f_{\varepsilon_{k_1'}^0} \right) \frac{\hbar\omega_{k-k_1'}}{\left( \varepsilon_k^0 - \varepsilon_{k_1'}^0 \right)^2 - \left( \hbar\omega_{k-k_1'} \right)^2} \\ &- \sum_{Sk_1 < k_F} \left| u^{k-k_1} \right|^2 f_{\varepsilon_{k_1}^0} \\ &\quad \times \frac{\hbar\omega_{k-k_1}}{\left( \varepsilon_k^0 - \varepsilon_{k_1}^0 \right)^2 - \left( \hbar\omega_{k-k_1} \right)^2} \end{aligned} \quad (148b)$$

for  $k \leq k_F$ .

Replacement of discrete summation by integration,  $\sum_k \dots \rightarrow \int n(\varepsilon_k)$ , introduces DOS  $n(\varepsilon_k)$  into (148a),

(148b). It is of crucial importance in relation to fluctuating band (see Figure 3(b)). For corrected DOS  $n(\varepsilon_k)$ , which is the consequence of shift  $\Delta\varepsilon_k$  of orbital energies, the following relation can be derived:

$$n(\varepsilon_k) = \left| 1 + \left( \partial(\Delta\varepsilon_k)/\partial\varepsilon_k^0 \right) \right|^{-1} n^0(\varepsilon_k^0). \quad (149)$$

The term  $n^0(\varepsilon_k^0)$  stands for uncorrected DOS of the original adiabatic states of particular band:

$$n^0(\varepsilon_k^0) = \left| \left( \partial\varepsilon_k^0/\partial k \right) \right|^{-1}. \quad (150)$$

Close to the  $\mathbf{k}$ -point where the original band which interacts with fluctuating band intersects FL, the occupied states near FL are shifted downward below FL and unoccupied states are shifted upward, above FL. The gap is identified as the energy distance between created peaks in corrected DOS above FL (half-gap) and below FL. The formation of peaks is related to the spectral weight transfer, that is, observed by ARPES or tunneling spectroscopy in cooling below  $T_c$ .

For some of the studied compounds, the calculated corrected DOS (149) of particular band(s) with gap opening are in Figure 4.

In particular, YBa<sub>2</sub>Cu<sub>3</sub>O<sub>7</sub> exhibits an asymmetric gap in two directions: for Cu-O1 chain-derived ( $d-p\sigma$ ) band the gap in one-particle spectrum is  $\Delta_b(0) \approx 35.7$  meV in the  $\Gamma$ -Y direction (4a) and  $\Delta_a(0) \approx 24.2$  meV in the  $\Gamma$ -X direction (4b), respectively. The calculated asymmetry, that is, the ratio  $(\Delta_a(0)/\Delta_b(0))_{\text{theor}} \approx 0.68$ , or  $(\Delta_b(0)/\Delta_a(0))_{\text{theor}} \approx 1.47$  is very close to the experimental values,  $(\Delta_a/\Delta_b) \approx 0.66$  and  $\Delta_b/\Delta_a \approx 1.5$  which have been recorded [79, 80] for untwined YBa<sub>2</sub>Cu<sub>3</sub>O<sub>7</sub>. Inspection of the topology (Figures 1(e)-1(f)) of the Cu-O<sub>1</sub> chain-derived ( $d-p\sigma$ ) band suggests that one can expect gap opening in one-particle spectrum of this band not only in  $\Gamma$ -Y(b) and  $\Gamma$ -X (a) direction, but it can be expected to be opened also in nodal, that is,  $\Gamma$ -S direction. Based on  $k$ -dependence of DOS of this band in particular directions at FS, it can be expected that  $\Delta_{\Gamma-S} \leq \Delta_{\Gamma-X}$ , that is, top of the dispersion should appear  $\leq 15$  meV below FS. One can expect opening of very small gap for this band also in  $\Gamma$ -T(U) direction [76]. However, due to relatively large distance of CuO<sub>2</sub> layers ( $\approx 8.3$  Å), e-p coupling which mediates interactions between electrons of these layers is small, which suggests that gap in one-particle spectrum of CuO<sub>2</sub> layer-based ( $d_{x^2-y^2} - p\sigma$ ) bands is not expected to be opened.

Two gaps, in  $\sigma$  and  $\pi$  band, are opened in  $\Gamma$ -K(M) directions of MgB<sub>2</sub> (4c):  $\Delta_\sigma(0)/2 \approx 7.6$  meV and  $\Delta_\pi(0)/2 \approx 2.2$  meV. The result simulates tunneling spectra at positive bias voltage and calculated half-gaps are in a very good agreement with experimental high-precision measurements [81, 82].

A small gap opens on pd-band in the  $\Gamma$ -X direction of YB<sub>6</sub> (4d):  $\Delta_{pd}(0)/2 \approx 2.2$  meV.

The corrections to orbital energies (148a), (148b) and to the ground state energy (147) are temperature-dependent and decrease with increasing T. At a critical value  $T_c$ , the gap in one-particle spectrum (137) which is formed at 0 K disappears,  $\Delta(T_c) = 0$  (continuum of states is established at

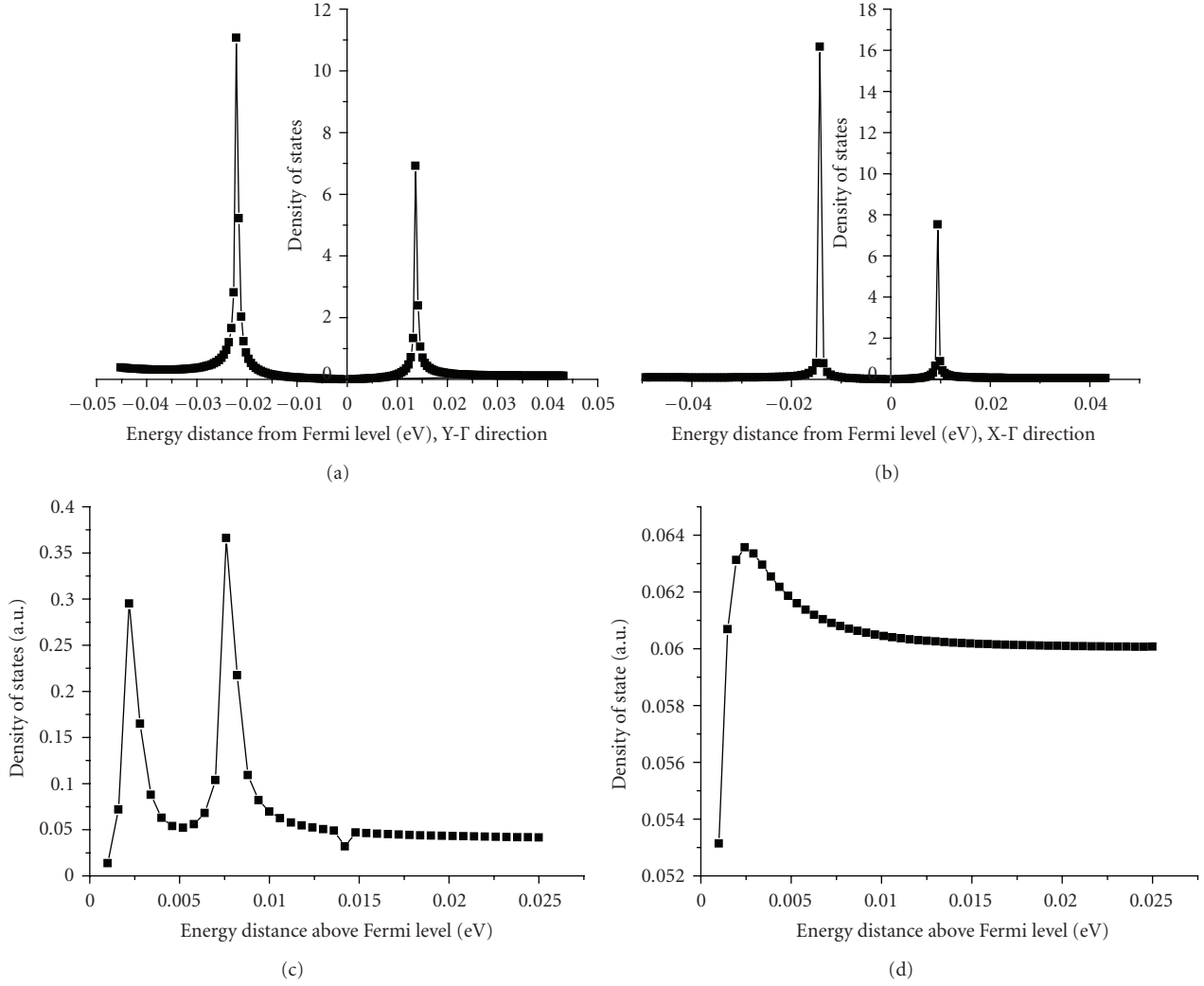


FIGURE 4: Corrected DOS and gap formation near  $k$  point where particular bands intersect FL, 0 K. Gap of  $\text{YBa}_2\text{Cu}_3\text{O}_7$  in  $\Gamma$ -Y(4a) and  $\Gamma$ -X(4b) direction. Half-gap in  $\text{MgB}_2$  (Figure 4(c)) and half-gap in  $\text{YB}_6$  (Figure 4(d)).

FL), while  $|\Delta E_{(na)}^0(T_c)| \leq \Delta E_{d,cr}$  and the system undergoes transition from the antiadiabatic into adiabatic state, which is stable for equilibrium high-symmetry structure above  $T_c$ . With respect to  $\Delta(0)$ , from (137) a simple approximate relation follows for critical temperature  $T_c$  of the adiabatic  $\leftrightarrow$  antiadiabatic state transition:

$$T_c = \Delta(0)/4k_B. \quad (151)$$

The calculated values of  $T_c$  for presented compounds are  $\text{YBa}_2\text{Cu}_3\text{O}_7, T_c \approx 92.8$  K,  $\text{MgB}_2, T_c \approx 39.5$  K, and  $\text{YB}_6, T_c \approx 11$  K. It is in a good agreement with the experimental values of  $T_c$  for superconducting state transition of these compounds [4, 60, 83].

**3.3. Thermodynamic Properties of System in the Antiadiabatic State.** Presented results naturally provoke the question if the antiadiabatic state is related in some way to superconducting state. Crucial in this respect are thermodynamic properties of antiadiabatic state, that is, at temperatures  $T < T_c$ .

#### (I) Character of condensation in antiadiabatic state

As it has already been mentioned, in the antiadiabatic state, ground-state total electronic energy of system is geometrically degenerate. Distorted nuclear structure, related to couple of nuclei in the phonon mode  $r$  that induces transition into antiadiabatic state, has fluxional character. There exist an infinite number of different, distorted configurations of this couple of nuclei in the phonon mode  $r$  and all these configurations, due to translation symmetry of the lattice, have the same ground state energy. Position of the involved displaced couple of nuclei is on the perimeter of circles with the centers at  $R_{eq}$  (equilibrium on crude-adiabatic level) and with radii equal to  $\Delta R = |R_{eq} - R_{d,cr}|$ . The  $R_{d,cr}$  is distorted geometry at which ACP approaches FL and system undergoes transition from adiabatic into antiadiabatic state.

Due to the geometric degeneracy of the ground state energy, the involved atoms can circulate over perimeters of the circles without the energy dissipation.

The dissipation-less motion of the couple of nuclei implies, however, that e-p coupling of involved phonon mode and electrons of corresponding band has to be zero.

Let as shown that in the antiadiabatic state this aspect is fulfilled.

The effective e-p interactions which cover the  $Q$ ,  $P$ -dependence has the form that is for boson vacuum represented by the second term in (130a) is

$$\begin{aligned} \Delta H'_{\langle e-p0 \rangle}(dg) = & \sum_{rPR} \left( (\varepsilon_P^0 - \varepsilon_R^0) (|c_{PR}^r|^2 + |\hat{c}_{PR}^r|^2) \right. \\ & \left. - 2\hbar\omega_r \operatorname{Re}(\hat{c}_{PR}^r c_{PR}^{r*}) \right) N[a_P^+ a_P]. \end{aligned} \quad (152)$$

After substitution for transformation coefficients  $c_{PR}^r, \hat{c}_{PR}^r$  (115), (116) and algebraic manipulation, the quasimomentum form of this term is

$$\begin{aligned} \Delta H'_{\langle e-p0 \rangle}(dg) = & \sum_{k,q} |u^q|^2 \left\{ \frac{(\varepsilon_k^0 - \varepsilon_{k-q}^0)}{\left[ (\varepsilon_k^0 - \varepsilon_{k-q}^0)^2 - (\hbar\omega_q)^2 \right]} \right\} \\ & \times N[a_k^+ a_k]. \end{aligned} \quad (153a)$$

For extreme nonadiabatic limit  $\hbar\omega_q/|\varepsilon_k^0 - \varepsilon_{k-q}^0| \rightarrow \infty$ , from (153a), it follows that

$$\Delta H'_{\langle e-p0 \rangle}(dg)_{na} \rightarrow 0. \quad (153b)$$

It means that for electrons that satisfy condition of extreme nonadiabaticity with respect to interacting phonon mode  $r$  in particular direction of reciprocal lattice where the gap in one-electron spectrum has been opened, the electron (nonadiabatic polaron)-renormalized phonon interaction energy equals zero. Expressed explicitly, in the presence of external electric potential, dissipation-less motion of relevant valence band electrons (holes) on the lattice scale can be induced at the Fermi level (electric resistance  $\rho = 0$ ), while motion of nuclei remains bound to fluxional revolution over distorted, energetically equivalent, configurations. The electrons move in a form of itinerant bipolarons, that is, as a polarized cloud of intersite charge density distribution (see Figure 5). Due to temperature increase, thermal excitations of valence band electrons to conduction band induce sudden transition from the antiadiabatic state into adiabatic state at  $T = T_c$ , that is, (145) does hold. For temperatures  $T \geq T_c$ , instead of (145),  $|\Delta E_{(na)}^0(R_d)| \leq \Delta E_d(R_d)$  holds and the system becomes stable at equilibrium  $R_{eq}$  as it is characteristic for adiabatic structure.

In the adiabatic state, properties of the electrons are in sharp contrast with the properties of electrons in antiadiabatic state. The electrons in this case are in a valence band more or less, tightly bound to respective nuclei at adiabatic equilibrium positions and their motion in conducting band is restricted by scattering with interacting phonon modes. It corresponds to situation at  $T > T_c$ .

For extreme adiabatic limit  $\hbar\omega_q/|\varepsilon_k^0 - \varepsilon_{k-q}^0| \rightarrow 0$ , from (153a) for electron-phonon interaction energy in this case it follows that

$$\Delta H'_{\langle e-p0 \rangle}(dg)_{ad} \rightarrow \sum_{qk} |u^q|^2 \frac{1}{(\varepsilon_k^0 - \varepsilon_{k-q}^0)}. \quad (153c)$$

Expression (153c) represents basically energy of standard adiabatic polarons (small, self-trapped) that contributes to the total energy of system.

II. *Electronic specific heat and entropy in antiadiabatic state.*

It has been shown that at formation of the antiadiabatic ground-state, electronic energy is decreased and for involved band(s) the gap in one-particle spectrum has been opened (shift of orbital energies). This fact has to be reflected by change of related thermodynamic properties. In particular, for electronic specific heat,

$$C_{V,el}(T) = \frac{d\Delta E_{(na)}^0}{dT} = T \frac{dS}{dT} \quad (154)$$

can be derived:

$$C_{V,el}(T) = -\frac{\bar{n}(\varepsilon_{k_F})}{2} \frac{\Delta(T)}{\Delta(0)} \left( \frac{\Delta(T)}{dT} \right). \quad (155)$$

At derivation of (155), it has been assumed that for the band with gap opening, uncorrected density of quasicontinuum of occupied and unoccupied states at Fermi level is the same. Expression (155) can be derived either from the ground-state energy correction (127), (147), or from the basic statistical relation for entropy:

$$S = -k_B \sum_k [f_k \ln f_k + (1 - f_k) \ln(1 - f_k)]. \quad (156)$$

In (156),  $f_k$  is the Fermi-Dirac occupation factor of state  $\varepsilon_k = \varepsilon_k^0 + \Delta\varepsilon_k$ . Then for entropy related to formation of antiadiabatic state can be derived:

$$S = k_B \ln 2 - \bar{n}(\varepsilon_{k_F}) \frac{(\Delta(T))^2}{2T\Delta(0)} + 2k_B \bar{n}(\varepsilon_{k_F}) \ln \left( \cosh \frac{\Delta(T)}{4k_B T} \right). \quad (157a)$$

For temperature derivative of entropy (157a), it follows that

$$\frac{dS}{dT} = -\frac{\bar{n}(\varepsilon_{k_F})}{2T} \frac{\Delta(T)}{\Delta(0)} \frac{d\Delta(T)}{dT}. \quad (157b)$$

It yields directly to final expression (155) for  $C_{V,el}(T)$ .

From the (155), in the limit  $T \rightarrow 0$  K, the exponential behavior characteristic for superconductors can be derived:

$$\lim (C_{V,el}(T))_{T \rightarrow 0} \approx \exp \left( -\frac{\Delta(0)}{2k_B T} \right). \quad (158)$$

The density of states at Fermi level  $\bar{n}(\varepsilon_{k_F})$  in the above equations represents mean value of corrected density of states close to the  $k$ -point where the peak in density of states has been formed. From practical reasons, it can be approximated

by the mean value of density of states of the fluctuating band in ACP at the moment when it approaches ( $\pm\omega/2$ ) Fermi level (antiadiabatic state). In the antiadiabatic state, density of states at Fermi level is considerably increased since density of states of fluctuating band at ACP is usually high (possibility of van Hove singularity formation at Fermi level).

### III. Magnetic properties of system in the antiadiabatic state-critical magnetic field

System in superconducting state can exhibit absolute diamagnetism and Meissner effect only if inside the system  $B = 0$ . In this case, there has to exist some critical value of external magnetic field  $H_c$  which destroys superconducting state and induces transition of the system into normal state (characteristic by finite-nonzero value of electric resistance  $\rho \neq 0$  at finite-nonzero density of electric current  $j$ ), like it occurs in case of temperature increase above  $T_c$ . It also means that at critical temperature and above it,  $T \geq T_c$ , critical magnetic field has to be zero,  $H_c(T \geq T_c) = 0$ .

It can be shown that antiadiabatic state exhibits this property.

From thermodynamics for critical magnetic field in this case, it follows that

$$\frac{H_c^2}{8\pi} = F_{(ad)} - F_{(na)}. \quad (159)$$

In (159),  $F_{(ad)}$  and  $F_{(na)}$  stand for free energies of the system in adiabatic and nonadiabatic (antiadiabatic) state. Then,

$$F_{(ad)} - F_{(na)} = \Delta E_{(na)}^0 - TS. \quad (160a)$$

From (154), (155), it follows that

$$\begin{aligned} \Delta E_{(na)}^0(T) &= \Delta E_{(na)}^0(0) + \int_0^T C_{V(el)}(T) dT \\ &= \Delta E_{(na)}^0(0) - \frac{\bar{n}(\varepsilon_{k_F})}{4\Delta(0)} \left( (\Delta(T))^2 - (\Delta(0))^2 \right) \\ &= -\frac{\bar{n}(\varepsilon_{k_F})}{4} \Delta(0) - \frac{\bar{n}(\varepsilon_{k_F})}{4\Delta(0)} \left( (\Delta(T))^2 - (\Delta(0))^2 \right). \end{aligned} \quad (160b)$$

After substitution of (160b), (157a) into (160a) and algebraic rearrangements, for critical magnetic field at finite temperature  $T$ , it follows that

$$\begin{aligned} \frac{(H_c(T))^2}{8\pi} &= -\frac{\bar{n}(\varepsilon_{k_F})}{4} \Delta(0) - \frac{\bar{n}(\varepsilon_{k_F})}{4\Delta(0)} \left( (\Delta(T))^2 - (\Delta(0))^2 \right) \\ &\quad + \frac{\bar{n}(\varepsilon_{k_F})}{2} \frac{(\Delta(T))^2}{\Delta(0)} \\ &\quad - 2k_B \bar{n}(\varepsilon_{k_F}) T \ln \left( \frac{\Delta(0)}{((\Delta(0))^2 - (\Delta(T))^2)^{1/2}} \right). \end{aligned} \quad (160c)$$

At temperature 0 K, for critical magnetic field results,

$$(H_c(0))^2 = 2\pi\Delta(0)\bar{n}(\varepsilon_{k_F}). \quad (160d)$$

The relation between critical magnetic fields at finite and zero temperature follows from (160c), (160d):

$$\begin{aligned} \left( \frac{H_c(T)}{H_c(0)} \right)^2 &= \left[ \left( \frac{\Delta(T)}{\Delta(0)} \right)^2 - \frac{8k_B T}{\Delta(0)} \ln \left( \frac{\Delta(0)}{((\Delta(0))^2 - (\Delta(T))^2)^{1/2}} \right) \right]. \end{aligned} \quad (161)$$

At critical temperature  $T_c$ , when due to thermal excitations the antiadiabatic state is suddenly changed into adiabatic state and above this temperature, critical magnetic field has to be zero,  $H_c(T \geq T_c) = 0$ . Since there is no gap in one-electron spectrum in metal-like adiabatic state,  $\Delta(T \geq T_c) = 0$ , then zero value of critical magnetic field follows directly from (160c), (161). Derived equations show that system in the antiadiabatic state, beside zero value of electric resistance  $\rho = 0$  (dissipation-less motion of bipolarons), has also specific property that is, necessary for occurrence of the Meissner effect.

## 4. Electron Correlation, Cooper's Pairs and Bipolarons

Correction  $\Delta H_{ep}''$  to the two-particle term  $H_{(2)}(R)$  represents correction to the electron correlation (see Note in Section 1) energy due to e-p coupling on QP-dependent nonadiabatic level and has the form (141). The electron correlation energy on crude-adiabatic level  $H_{(2)}(R)$  is a perturbation contribution to the electronic ground-state energy  $H_{(0)}(R_0) = E_{SCF}^0(R_0)$ , (48). It is an improvement of e-e interaction contribution beyond the level of HF method which treats electrons with  $\alpha$  and  $\beta$  spins in an unbalanced way. The electron correlation energy is negative (see Note in Section 1) and contributes to stabilization of ground state electronic energy as a perturbation contribution, which in the second order of perturbation theory has the form (54),  $E_{corr}(R_0)$ .

Let us see if the correction to correlation energy due to e-p coupling  $\Delta H_{ep}''$  represents stabilization or destabilization contribution [66, 67]. For antiadiabatic system  $|\varepsilon_{k'}^0 - \varepsilon_k^0| < \hbar\omega_{k'-k}$ , denominators in (141) are positive and negative value of the matrix elements of this two-particle correction is reached for a reduced form if nominators are negative, that is, if  $(\varepsilon_{k+q}^0 - \varepsilon_k^0) = -(\varepsilon_{k'+q}^0 - \varepsilon_{k'}^0)$ . Since  $q \neq 0$ , it can be reached if  $q = -k - k'$ . At these circumstances for reduced form which maximizes e-e attraction, it can be derived that

$$\begin{aligned} \Delta H_{ep}''(\text{red})_{na} &= -2 \sum_{k > k_F, k' < k_F} |u^{k'-k}|^2 \\ &\quad \times \frac{\hbar\omega_{k'-k} \left( (\varepsilon_{k'}^0 - \varepsilon_k^0)^2 + (\hbar\omega_{k'-k})^2 \right)}{\left( (\varepsilon_{k'}^0 - \varepsilon_k^0)^2 - (\hbar\omega_{k'-k})^2 \right)^2} \\ &\quad \times N \left[ a_{k'}^+, a_{-k'}^+, a_{-k}^-, a_{k'}^- \right]. \end{aligned} \quad (162)$$

In this expression, summation over bands is not explicitly indicated, but it should be understood implicitly. This correction is due to pairs of electrons with opposite quasi-momentum and antiparallel spins ( $k \uparrow, -k \downarrow$ ). It should be noticed that it is the contribution of biexcited configurations  $\{\Phi_{(k',-k') \rightarrow (k,-k)}\}$  (i.e., two-particle ( $k \uparrow, -k \downarrow$ ), two-hole ( $k' \uparrow, -k' \downarrow$ ) excited singlet states) to the electronic ground state, that is, represented by renormalized Fermi vacuum  $\Phi_0$ . Expressed explicitly, first nonzero contributions are from the matrix elements of the type  $\langle \Phi_0 | \Delta H''_{ep} | \Phi_{(k',-k') \rightarrow (k,-k)} \rangle^2$ , that is, contributions in the second order of perturbation theory. Now,  $\{\varepsilon_k\}$  represent particle states that are occupied above Fermi level and  $\{\varepsilon_{k'}\}$  are, due to excitations, empty-hole states below Fermi level.

From (162), it follows that due to e-p interactions on the  $Q, P$ -dependent nonadiabatic level, the electron correlation energy (54) of the electronic ground state is increased by contribution of this correction. Inspection of (162) indicates that the largest contribution to the correlation energy correction is for pair of electrons at Fermi level which satisfy the condition  $|\varepsilon_{k'}^0 - \varepsilon_k^0| < \hbar\omega_{k'-k}$ , that is, for system which is in antiadiabatic state.

In case of strong antiadiabatic regime  $|\varepsilon_{k'}^0 - \varepsilon_k^0|/\hbar\omega_{k'-k} \rightarrow 0$ , for correction to electron correlation energy, it follows that

$$\Delta H''_{ep}(\text{red})_{\text{sna}} = -2 \sum_{kk'} \frac{|u^{k'-k}|^2}{\hbar\omega_{k'-k}} N \left[ a_{k'\uparrow}^+ a_{-k'\downarrow}^+ a_{-k\downarrow} a_{k\uparrow} \right]. \quad (163a)$$

The second extreme case is for strong adiabatic regime  $\hbar\omega_{k'-k}/|\varepsilon_{k'}^0 - \varepsilon_k^0| \rightarrow 0$ . At these circumstances, correction to electron correlation energy approaches zero value:

$$\Delta H''_{ep}(\text{red})_{\text{sad}} = -2 \sum_{kk'} |u^{k'-k}|^2 \frac{\hbar\omega_{k'-k}}{(\varepsilon_{k'} - \varepsilon_k)^2} \times N \left[ a_{k'\uparrow}^+ a_{-k'\downarrow}^+ a_{-k\downarrow} a_{k\uparrow} \right] \rightarrow 0. \quad (163b)$$

General adiabatic expression on  $Q$ -dependent adiabatic level  $|\varepsilon_{k'}^0 - \varepsilon_k^0| > \hbar\omega_{k'-k}$ , that is, the adiabatic form of this correction can be derived directly from (139) in the limit  $\hat{c} = 0$ ,

$$\Delta H''_{ep}(\text{ad}) = \sum_{kk'q\sigma\sigma'} |u^q|^2 \frac{\hbar\omega_q}{(\varepsilon_{k+q}^0 - \varepsilon_k^0)(\varepsilon_{k'+q}^0 - \varepsilon_{k'}^0)} \times N \left[ a_{k+q,\sigma}^+ a_{k',\sigma'}^+ a_{k'+q,\sigma'} a_{k,\sigma} \right]. \quad (164)$$

The reduced form is

$$\Delta H''_{ep}(\text{red})_{\text{ad}} = -2 \sum_{kk'} |u^{k'-k}|^2 \frac{\hbar\omega_{k'-k}}{(\varepsilon_{k'}^0 - \varepsilon_k^0)^2} \times N \left[ a_{k'\uparrow}^+ a_{-k'\downarrow}^+ a_{-k\downarrow} a_{k\uparrow} \right]. \quad (165)$$

Like for nonadiabatic  $Q, P$ -dependent case also for adiabatic  $Q$ -dependent level, the correction to electron

correlation energy is negative. By comparing (162) with (163a) it can be seen that nonadiabatic correction to electron correlation energy is in absolute value larger than corresponding adiabatic correction. Moreover, for antiadiabatic state, when the system is close to singular point in (162), the nonadiabatic correction can be significant.

Along with crude-adiabatic correlation energy (54), also the correction to electron correlation energy (162) contributes to stabilization of system in antiadiabatic state, which is the ground state of the system at distorted nuclear geometry  $R_{d,cr}$ . It should be reminded, however, that regardless of the correction to electron correlation energy (which represents contributions of biexcited configurations in second and higher orders of perturbation theory), the system has already been stabilized in antiadiabatic state at distorted geometry due to correction to the ground state electronic energy (128) which represents zero-order correction in terms of perturbation theory. In this respect, increased electron correlation is the consequence of e-p interactions which have induced transition of the system from adiabatic into antiadiabatic state and stabilized it in this state no matter if correction to electron correlation energy is accounted for or not.

At finite temperature, the product of Fermi-Dirac occupation factors has to be introduced into derived equations:  $\sum_{kk'} \dots \rightarrow \sum_{kk'} f_k(1 - f_{k'}), \dots$ . With increasing temperature from 0K, the value of the correction (162) which is characteristic for antiadiabatic state decreases and at  $T = T_c$  when system undergoes sudden transition from antiadiabatic state at distorted geometry  $R_{d,cr}$  into adiabatic state at undistorted geometry  $R_0 = R_{eq}$  and above this temperature, for correction to electron correlation energy holds corresponding temperature-dependent adiabatic form (165). Above  $T_c$ , this correction along with crude-adiabatic correlation energy (54) stabilizes adiabatic ground state of system at undistorted-adiabatic equilibrium geometry  $R_0 = R_{eq}$ .

Let us turn attention to the Fröhlich effective Hamiltonian of e-e interactions [7]:

$$H''_{\text{eff}}(\text{Fr}) = \sum_{kk'q\sigma\sigma'} |u^q|^2 \frac{\hbar\omega_q}{(\varepsilon_{k+q}^0 - \varepsilon_k^0)^2 - (\hbar\omega_q)^2} \times a_{k+q,\sigma}^+ a_{k',\sigma'}^+ a_{k'+q,\sigma'} a_{k,\sigma}. \quad (166)$$

The reduced form of this Hamiltonian is

$$H''_{\text{red}}(\text{Fr}) = 2 \sum_{kk'} |u^{k'-k}|^2 \frac{\hbar\omega_{k'-k}}{(\varepsilon_k^0 - \varepsilon_{k'}^0)^2 - (\hbar\omega_{k'-k})^2} \times a_{k'\uparrow}^+ a_{-k'\downarrow}^+ a_{-k\downarrow} a_{k\uparrow}. \quad (167)$$

This interaction term is either attractive or repulsive depending on the sign of denominator. For antiadiabatic conditions  $|\varepsilon_{k'}^0 - \varepsilon_k^0| < \hbar\omega_{k'-k}$ , it represents effective attractive electron-electron interactions. It should be reminded that effective attractive e-e interactions are the crucial condition of Cooper's pair formation and the basis of the BCS theory.

In the limit of extreme antiadiabaticity  $|\varepsilon_p^0 - \varepsilon_q^0|/\hbar\omega_r \rightarrow 0$ , the form of the Fröhlich two-particle effective Hamiltonian

(166) and the correction to electron correlation energy (141) are identical and equal to

$$\begin{aligned} \lim_{\Delta\varepsilon/\hbar\omega \rightarrow 0} (\Delta H''_{ep})_{\Delta\varepsilon/\hbar\omega \rightarrow 0} &= \lim_{\Delta\varepsilon/\hbar\omega \rightarrow 0} (H''_{\text{eff}}(\text{Fr}))_{\Delta\varepsilon/\hbar\omega \rightarrow 0} \\ &= - \sum_{kk'q\sigma\sigma'} \frac{|u^q|^2}{\hbar\omega_q} a_{k+q,\sigma}^+ a_{k',\sigma'}^+ a_{k'+q,\sigma'} a_{k,\sigma}. \end{aligned} \quad (168)$$

On the adiabatic level  $|\varepsilon_{k'}^0 - \varepsilon_k^0| \gg \hbar\omega_{k'-k}$ , the results are substantially different. Adiabatic correction to correlation energy has the form (164), (165), which is always attractive. On the other hand, adiabatic limit  $|\varepsilon_{k'}^0 - \varepsilon_k^0| \gg \hbar\omega_{k'-k}$  of the Fröhlich form results in

$$\begin{aligned} H''_{\text{eff}}(\text{Fr})_{\text{ad}} &= \sum_{kk'q\sigma\sigma'} |u^q|^2 \frac{\hbar\omega_q}{(\varepsilon_{k+q}^0 - \varepsilon_k^0)^2} \\ &\times a_{k+q,\sigma}^+ a_{k',\sigma'}^+ a_{k'+q,\sigma'} a_{k,\sigma}. \end{aligned} \quad (169)$$

It is immediately seen that this interaction, in contrast to (165), is always repulsive and  $(k, k')$  symmetry is disturbed.

With respect to the fact that effective attractive e-e interaction is a pure correction to electron correlation energy, the Cooper's pair idea within the BCS treatment is without any doubts formally correct, nevertheless, it is rather a model treatment how to solve the instability problem with severe restriction to fixed nuclear framework, that is, within the crude-adiabatic BOA which requires for total system validity of the adiabatic condition  $|\varepsilon_{k'}^0 - \varepsilon_k^0| \gg \hbar\omega_{k'-k}$ . Discussion of these and related aspects, the BCS treatment of superconducting state transition and theory of antiadiabatic state formation have been analyzed in [68].

From the theory of the antiadiabatic ground state, instead of Cooper's pairs, formation of mobile bipolarons results in a natural way as a consequence of translation symmetry breakdown on antiadiabatic level. The bipolarons arise as polarized intersite charge density distribution that can move over lattice without dissipation due to geometric degeneracy (fluxional structure) of the antiadiabatic ground state at distorted nuclear configurations. Formation of polarized intersite charge density distribution at transition from adiabatic into antiadiabatic state is reflected by corresponding change of the wave function. For spinorbital (band)  $\varphi_{R(k)}$  relation (99) holds, that is,

$$\begin{aligned} &|\varphi_P(x, Q, P)\rangle \\ &= a_P^+(x, Q, P)|0\rangle \\ &= \left( \bar{a}_P^+ - \sum_{rR} c_{PR}^r \bar{Q}_r \bar{a}_R^+ - \sum_{\bar{r}R} \tilde{c}_{PR} \bar{P}_{\bar{r}} \bar{a}_R^+ + O(\bar{Q}^2, \bar{Q}P, P^2) \right) |0\rangle \\ &= |\varphi_P(x, 0, 0)\rangle - \sum_{rR} c_{PR}^r \bar{Q}_r |\varphi_R(x, 0, 0)\rangle \\ &\quad - \sum_{\bar{r}R} \tilde{c}_{PR} \bar{P}_{\bar{r}} |\varphi_R(x, 0, 0)\rangle + \dots \end{aligned} \quad (170)$$

At transition into antiadiabatic state  $|\varepsilon_S^0(k_c) - \varepsilon_F^0|_{R_{\text{eq}} \pm Q} \ll \hbar\omega_r$ , coefficients  $c_{RS}^r$  of  $Q$ -dependent transformation matrix become negligibly small and absolutely dominant for modulation of crude-adiabatic wave function are in this case coefficients  $\tilde{c}_{RS}^r$  of  $P$ -dependent transformation matrix. For simplicity, consider that transition into antiadiabatic state is driven by coupling to a phonon mode  $r$  with stretching vibration of two atoms (e.g., B-B in  $E_{2g}$  mode of  $\text{MgB}_2$ , valence  $T_{2g}$  mode vibration of B-B atoms in basal **a-b** plane of B-octahedron in  $\text{YB}_6$ , or vibration motion of O2, O3 in Cu-O planes,  $B_{2g}$ ,  $B_{3g}$  modes of YBCO). Let  $m_1$  and  $m_2$  are equilibrium site positions of involved nuclei on crude-adiabatic level and  $d_1$  and  $d_2$  are nuclear displacements at which crossing into antiadiabatic state occurs. At these circumstances, the original crude-adiabatic wave function  $\varphi_k^0(x, 0, 0)$  is changed in the following way:

$$\begin{aligned} \varphi_k(x, Q, P) &\propto \left( 1 + \sum_q u^{|q|} \frac{\hbar\omega_q}{(\hbar\omega_q)^2 - (\varepsilon_k^0 - \varepsilon_{k+q}^0)^2} \right. \\ &\quad \left. \times (P_1 e^{iq \cdot [x - (m_1 - d_1)]} + P_2 e^{iq \cdot [x - (m_2 + d_2)]}) \right) \\ &\quad \times \varphi_k^0(x, 0, 0). \end{aligned} \quad (171)$$

In (171), site approximation for momentum has been used, that is,  $P_q \propto (\text{sign} \cdot q) \sum_m P_m e^{iq \cdot m}$ .

In antiadiabatic state, for particular  $k$  and proper  $q$  values, nonadiabatic prefactors under summation symbol in (171) can be large. The prefactors, that is, coefficients of  $P$ -dependent transformation matrix, reflect influence of nuclear kinetic energy on electronic structure. At the dominance of these contributions (antiadiabatic state), strong increase in localization of charge density appears at distorted site-positions for  $x$  equal to  $(m_1 - d_1)$  and  $(m_2 + d_2)$ . It induces (or increases) intersite polarization of charge density distribution. As an example, calculated iso-density line for highest electron density in  $\text{MgB}_2$  is presented in Figure 5. For equilibrium high-symmetry structure ( $R_{\text{eq}}$ ), the highest electron density is localized at equilibrium position of B atoms (Figure 5(a)). For distorted nuclear geometry ( $R_{d,cr}$ ) in the  $E_{2g}$  mode, electron density is polarized and the highest value is shifted into the intersite positions, bipolarons are formed (Figure 5(b)). This kind of intersites polarization persists, and on a lattice scale, it has itinerant character at nuclear revolution over perimeters of the fluxional circles with the radius  $R_{d,cr}$ , until the system remains in the antiadiabatic state.

## 5. Discussion and Conclusion

Experimental results are always crucial for any theory which aims to formulate basic physics behind observed phenomenon or property. However, an experiment always cover much wider variety of different influences which have impact on results of experimental observation than any

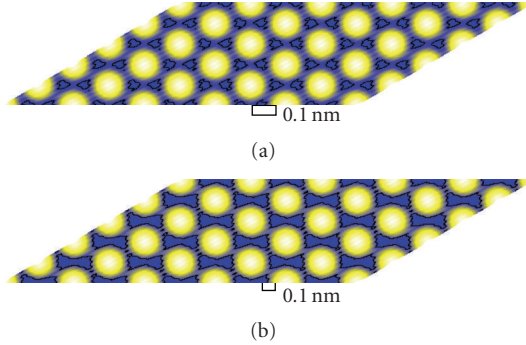


FIGURE 5: Iso-density line of highest electron density at equilibrium nuclear geometry  $R_{eq}$  of  $MgB_2$  (a) and at the distorted geometry of B atoms in  $E_{2g}$  phonon mode  $R_{d,cr}$  when nonadiabatic e-p interactions trigger transition into antiadiabatic state and intersites polarization is induced (b).

theory can account for, mainly if theory is formulated on microscopic level and some unnecessary approximations and assumptions are usually incorporated. On the other hand, interpretation of many experimental results is based on particular theoretical model. This is also the case of ARPES experiments at reconstruction of Fermi surface for electronic structure determination of high- $T_c$  cuprates. Interpretation of experimental results is based on band structure calculated for particular compound. Methods of band structure calculations are always approximate, with different level of sophistication. Calculated band structure, mainly its topology at FL, is a kind of reference frame for assignment of particular dispersion of energy distribution curve (EDC) or momentum distribution curve (MDC) to particular band of studied compound at interpretation of ARPES. This is in direct relation with theoretical understanding of crucial aspects of SC-state transition and with mechanism of superconductivity in general.

In case of high- $T_c$  cuprates, the crucial is considered to be the order parameter, that is, symmetry of superconducting gap which should be of  $(d_{x^2-y^2})$  symmetry. Within a simple orbital model consideration of  $CuO_2$  plane in square lattice configuration, this type of symmetry is generally accepted to simulate a-b plane superconductivity of cuprates in a best way.

In this sense, unexpected results have been published recently [30]. The high-resolved (sub-meV) ARPES with VUV laser as a light source for optimally doped untwined YBCO reveals that in superconducting state, gap is opened in one-particle spectrum. The momentum dependence is very interesting, however. Like for other cuprates, strong band renormalization (kink formation at  $\approx 60$  meV) in off-nodal direction has been observed. The gap is opened in off-nodal ( $\Gamma$ -X and  $\Gamma$ -Y) directions with top of the dispersion at  $\approx 20$  meV below FL. In contrast to [79, 80], the results of [30] do not indicate presence of a/b asymmetry. What is surprising, however, is the finding that gap remains finite also in nodal  $\Gamma$ -S direction, with top of dispersion at  $\approx 12$  meV below FL. Presence of finite “nodeless” gap (i.e., in nodal direction) sharply contradicts to commonly accepted idea of

cuprates as superconductors of  $(d_{x^2-y^2})$  symmetry. In normal state (100 K), the gap is closed in both, off-nodal and nodal directions.

The order parameter of  $(d_{x^2-y^2})$  symmetry assumes gap opening in a band with dominant contribution of Cu-based  $(d_{x^2-y^2})$  orbital. In layered cuprates, it corresponds to  $(d_{x^2-y^2} - p\sigma)$  bands of  $CuO_2$  planes. Respected band structure calculation for YBCO is the DFT-based LDA published by Andersen et al. [84] to which the authors [30] refer. Inspection of BS in [84] reveals, however, that  $Cu2-O2O3$  planes bands do not intersect FL in off-nodal  $\Gamma$ -X nor in  $\Gamma$ -Y direction, but the bands intersect FL in nodal  $\Gamma$ -S direction and in S-Y and S-X directions. It is an indication that experimentally detected gap [30], which is opened in off-nodal ( $\Gamma$ -X and  $\Gamma$ -Y) directions and also in nodal  $\Gamma$ -S direction, does not correspond probably to bands of  $CuO_2$  planes.

In spite that there is a general agreement among different DFT-based band structure calculations in overall character of band structure for particular cuprate, there are small, but important differences in details concerning topology of some bands at FL. In particular, for YBCO, DFT-based all-electron band structure calculation [85] using the FLAPW method yields important differences in topology of Cu-O chain-derived  $(d - p\sigma)$  band. In contrast to band structure [84], where the band intersects FL in S-X,  $\Gamma$ -Y and  $\Gamma$ -S directions, the BS [85] yields for Cu-O chain band intersections with FL in  $\Gamma$ -X,  $\Gamma$ -Y and  $\Gamma$ -S directions, respectively. Calculated Cu-O chain band topology [85] is in an excellent agreement with experimental electron-positron momentum density in optimally doped untwined YBCO detected [86] by 2D-angular correlation of electron-positron annihilation radiation (ACAR) technique. It should be stressed that ACAR is particularly sensitive for study of Cu-O chain Fermi sheets in YBCO. The character of ACAR, as experimentally detected, was predicted theoretically [87], and beside intersection of FL in  $\Gamma$ -X,  $\Gamma$ -Y directions, prediction has also been for FL intersection in  $\Gamma$ -T,  $\Gamma$ -U directions by Cu-O chain band.

With respect to topology of Cu-O chain band, as discussed above, this band should be the best candidate to be considered for gap opening in both, off-nodal ( $\Gamma$ -X,  $\Gamma$ -Y) and nodal ( $\Gamma$ -S) directions as seen in the ARPES results for YBCO [30]. One should stress, however, that also in case of gap opening in Cu-O chain band, expected  $(d_{x^2-y^2})$  symmetry is lost. Moreover, the authors in [30] attribute the effects seen in the ARPES to bands of  $Cu-O_2$  planes and declare that in the spectra dispersion of Cu-O chain band is not present. There are a lot of experimental peculiarities of ARPES experiments with YBCO (twinning/untwining, surface states, CuO-chain problems, spectral dependence on high-source energy, etc.), so it is difficult for me to make any comment about assignment of particular EDC/MDC to  $CuO_2$  plane or Cu-O chain bands as it has been done by the authors [30].

Nonetheless, an interpretation of the effects seen in the discussed ARPES from the stand-point of antiadiabatic theory should be of interest. The basic aspects concerning YBCO have been predicted [76] and shortly mentioned also in the Section 3.2.1. One should start with topology of the band

structure (Figures 1(e)-1(f)), in particular with dispersion of Cu-O chain band at FL. (It should be stressed that HF-SCF method with semiempirical INDO Hamiltonian used at band structure calculation (see reference 12 in [76]), overestimates bonding character and consequently bandwidth, which means that high-energy effects can hardly be studied, but for low-energy physics (like gap opening, kink formation, etc.) the method is reliable enough at least in a qualitative way.) It can be seen that dispersion of this band at FL corresponds qualitatively to Cu-O chain band dispersion as it has been calculated by FLAPW method [85] and to its experimental character as seen at FL by ACAR method [86].

Coupling to  $A_g$ ,  $B_{2g}$ ,  $B_{3g}$  phonon modes induces fluctuation (Figures 1(e)-1(f)) of the ACP (inflex) of Cu-O<sub>2</sub> plane ( $d_{x^2-y^2} - p\sigma$ ) band at Y point across the FL. In the moment when the ACP approaches FL from the bonding side, strong renormalization of dispersion of this band (kink formation) could be seen by ARPES in off-nodal Y- $\Gamma$  direction (Figure 3(a), this paper) at about  $k \approx 0.41/3.82 \approx 0.1 \text{ \AA}^{-1}$  (cf. [28, Figure 2a(c)]). At this situation, there is dramatic decrease of effective electron velocity and chemical potential ( $\mu_{ad} \gg \mu_{antiad} < \hbar\omega$ ), while DOS is increased (Figure 3(b), this paper) at FL and system undergoes transition into antiadiabatic state. Influence of nuclear dynamics on electronic structure is now significant, antiadiabatic theory of e-p coupling as presented in this paper. System is stabilized in antiadiabatic state at distorted nuclear configuration  $R_{d,cr}$  and gap is opened in one-particle spectrum. The gap (Section 3.2.1, Figures 4(a) and 4(b)) is opened only in the Cu-O chain ( $d - p\sigma$ ) band, in off-nodal directions  $\Gamma$ -X and  $\Gamma$ -Y ( $k_{\Gamma Y} \approx 0.053 \text{ \AA}^{-1}$ ,  $k_{\Gamma X} \approx 0.016 \text{ \AA}^{-1}$ ) and also in nodal  $\Gamma$ -S direction. The half-gaps in the off-nodal directions are  $\Delta_{\Gamma Y}/2, \approx 22 \text{ meV}$ ,  $\Delta_{\Gamma X}/2, \approx 15 \text{ meV}$  and gap in the nodal direction is expected to be  $\Delta_{\Gamma S}/2 \leq 15 \text{ meV}$  (cf. [28, Figures 1, 7, 8]). In contrast to [30], antiadiabatic theory yields a/b- gap asymmetry, which is in good agreement with other experimental results [79, 80]. At temperatures  $> T_c$ , the gap extinct. It should be manifested by disappearing of peaks on EDC (MDC) at FL in the ARPES spectra (see [30, Figure 8(e)]). In this situation, the adiabatic DOS, which is of constant value at FL, is established and system is in adiabatic-nonsuperconducting state.

It should be mentioned that considerably smaller gap ( $\Delta_{\Gamma T/U} \approx 5 \text{ meV}$ ) has been predicted [76] to be opened also in  $\Gamma$ -T/U directions. The prediction is related to the topology of the Cu-O chain ( $d - p\sigma$ ) band in these directions ([76, Figures 10, 11]). Theoretical calculation of the electron-positron momentum density [87] confirms this character of Cu-O chain topology. It is obvious that symmetry of the Cu-O chain band gap is not of ( $d_{x^2-y^2}$ ) character. Symmetry of the gap is, in my opinion, the matter of band structure topology at FL, which is far more complicated than the one emerging from simple model of CuO<sub>2</sub> plane confined in a square lattice. It is a complex matter of crystal structure and chemical composition of particular cuprate. It should be reminded that YBCO is the only high- $T_c$  cuprate with Cu-O chain in its structure. The gap opening in Cu-O chain band does not mean, however, that superconductivity in YBCO is realized in Cu-O chains. Superconductivity is realized by

bipolaron mechanism in Cu-O<sub>2</sub> planes, no matter if gap symmetry is ( $d_{x^2-y^2}$ ) or any other (antiadiabatic theory, see also [76]).

In conclusion, it can be summarized that based on the ab initio theory of complex electronic ground state of superconductors, it can be concluded that e-p coupling in superconductors induces the temperature-dependent electronic structure instability related to fluctuation of analytic critical point (ACP—maximum, minimum, or saddle point of dispersion) of some band across FL, which results in breakdown of the adiabatic BOA. When ACP approaches FL, chemical potential  $\mu_{ad}$  is substantially reduced to  $\mu_{antiad}$  ( $\mu_{ad} \gg \mu_{antiad} < \hbar\omega$ ). Under these circumstances, the system is stabilized due to the effect of nuclear dynamics, in the antiadiabatic state at broken symmetry with a gap in one-particle spectrum. Distorted nuclear structure, which is related to couple of nuclei in the phonon mode  $r$  that induces transition into antiadiabatic state, has fluxional character. It has been shown that while system remains in antiadiabatic state, nonadiabatic polaron-renormalized phonon interactions are zero in well-defined  $k$ -region of reciprocal lattice. Along with geometric degeneracy of the antiadiabatic ground state it enables formation of mobile bipolarons (in a form of polarized intersite charge density distribution in real space) that can move over lattice in external electric potential as supercarriers without dissipation. With increasing  $T$ , the stabilization effect of nuclear kinetic energy to the electronic ground-state energy decreases and at critical temperature  $T_c$  the gap(s) extinct and system is stabilized in the adiabatic metal-like state with a continuum of states at FL, which is characteristic by high-symmetry structure.

An analysis of e-p interaction Hamiltonian has shown that an effective attractive e-e interaction, which is, the basis of Cooper's pair formation, is in fact the correction to electron correlation energy at transition from adiabatic into antiadiabatic ground electronic state. In this respect, increased electron correlation is not the primary reason for transition into superconducting state, but it is a consequence of antiadiabatic state formation which is stabilized by nonadiabatic e-p interactions at broken translation symmetry. It has been shown that thermodynamic properties of system in the antiadiabatic state correspond to thermodynamics of superconducting state.

## Acknowledgment

The author acknowledges the support of the grant VEGA1/0013/08.

## References

- [1] K. Onnes, *Communications from the Physical Laboratory of the University of Leiden*, vol. 124c, 1911.
- [2] R. Simon and A. Smith, *Superconductors*, Plenum Press, New York, NY, USA, 1988.
- [3] J. G. Bednorz and K. A. Muller, "Possible high  $T_c$  superconductivity in the Ba-La-Cu-O system," *Zeitschrift für Physik B*, vol. 64, no. 2, pp. 189–193, 1986.

- [4] P. H. Hor, R. L. Meng, Y. Q. Wang, et al., "Superconductivity above 90 K in the square-planar compound system  $\text{ABa}_2\text{Cu}_3\text{O}_{6+x}$  with  $A = \text{Y, La, Nd, Sm, Eu, Gd, Ho, Er}$  and  $\text{Lu}$ ," *Physical Review Letters*, vol. 58, no. 18, pp. 1891–1894, 1987.
- [5] J. Bardeen, L. N. Cooper, and J. R. Schrieffer, "Theory of superconductivity," *Physical Review*, vol. 108, no. 5, pp. 1175–1204, 1957.
- [6] H. Fröhlich, "Theory of the superconducting state. I. The ground state at the absolute zero of temperature," *Physical Review*, vol. 79, no. 5, pp. 845–856, 1950.
- [7] H. Fröhlich, "Interaction of electrons with lattice vibrations," *Proceedings of the Royal Society A*, vol. 215, no. 1122, pp. 291–298, 1952.
- [8] A. B. Migdal, "Interaction between electrons and lattice vibrations in a normal metal," *Zh. Eksp. Teor. Fiz.*, vol. 34, pp. 1438–1446, 1958, English translation in *Journal of Experimental and Theoretical Physics*, vol. 7, p. 996, 1958.
- [9] G. M. Eliashberg, *Zh. Eksp. Teor. Fiz.*, vol. 38, p. 996, 1960, English translation in *Journal of Experimental and Theoretical Physics*, vol. 11, p. 696, 1960.
- [10] G. M. Eliashberg, *Zh. Eksp. Teor. Fiz.*, vol. 39, p. 1437, 1960, English translation in *Journal of Experimental and Theoretical Physics*, vol. 12, p. 1000, 1960.
- [11] E. Dagotto, "Correlated electrons in high-temperature superconductors," *Reviews of Modern Physics*, vol. 66, no. 3, pp. 763–840, 1994.
- [12] P. W. Anderson, *The Theory of Superconductivity in High- $T_c$  Cuprates*, Princeton University Press, Princeton, NJ, USA, 1997.
- [13] M. L. Kucic, "Interplay of electron phonon interaction and strong correlations: the possible way to high-temperature superconductivity," *Physics Reports*, vol. 338, no. 1-2, pp. 1–264, 2000.
- [14] W. J. McMillan, "Transition temperature of strong-coupled superconductors," *Physical Review B*, vol. 167, no. 2, pp. 331–344, 1968.
- [15] Th. Maier, M. Jarrell, T. Pruschke, and J. Keller, " $d$ -wave superconductivity in the Hubbard model," *Physical Review Letters*, vol. 85, no. 7, pp. 1524–1527, 2000.
- [16] S. Sorella, G. B. Martins, F. Becca, et al., "Superconductivity in the two-dimensional  $t$ - $J$  model," *Physical Review Letters*, vol. 88, no. 11, Article ID 117002, 4 pages, 2001.
- [17] S. R. White and D. Scalapino, "Density matrix renormalization group study of the striped phase in the 2D  $t$ - $J$  model," *Physical Review Letters*, vol. 80, no. 6, pp. 1272–1275, 1998.
- [18] S. R. White and D. Scalapino, "Competition between stripes and pairing in  $t$ - $t'$ - $J$  model," *Physical Review B*, vol. 60, no. 2, pp. R753–R756, 1999.
- [19] A. Paramekanti, M. Randeria, and N. Trivedi, "High- $T_c$  superconductors: a variational theory of the superconducting state," *Physical Review B*, vol. 70, no. 5, Article ID 054504, 21 pages, 2004.
- [20] A. Mourachkin, *High-Temperature Superconductivity in Cuprates*, Kluwer Academic Publishers, Dordrecht, The Netherlands, 2002.
- [21] A. Fukuoka, A. Tokima-Yamamoto, M. Itoh, R. Usami, S. Adachi, and S. Tamato, "Dependence of  $T_c$  and transport properties on the Cu valence in  $\text{HgBa}_2\text{Ca}_{n-1}\text{Cu}_n\text{O}_{2(n+1)+\delta}$  ( $n = 2, 3$ ) superconductors," *Physical Review B*, vol. 55, no. 10, pp. 6612–6620, 1997.
- [22] J. Frank, "Experimental studies of the isotope effect in high  $T_c$  superconductors," *Physica C*, vol. 282–287, pp. 198–201, 1997.
- [23] D. J. Pringle, G. V. M. Williams, and J. L. Tallon, "Effect of doping and impurities on the oxygen isotope effect in high-temperature superconducting cuprates," *Physical Review B*, vol. 62, no. 18, pp. 12527–12533, 2000.
- [24] A. Lanzara, P. V. Bogdanov, X. J. Zhou, et al., "Evidence for ubiquitous strong electron phonon coupling in high-temperature superconductors," *Nature*, vol. 412, pp. 510–514, 2001.
- [25] X. J. Zhou, T. Yoshida, A. Lanzara, et al., "High-temperature superconductors: universal nodal Fermi velocity," *Nature*, vol. 423, p. 398, 2003.
- [26] A. D. Gromko, A. V. Ferdorov, Y. D. Chuang, et al., "Mass-renormalized electronic excitations at  $(\pi, 0)$  in the superconducting state of  $\text{Bi}_2\text{Sr}_2\text{CaCu}_2\text{O}_{8+\delta}$ ," *Physical Review B*, vol. 68, no. 17, Article ID 174520, 7 pages, 2003.
- [27] T. Cuk, F. Baumberger, D. H. Lu, et al., "Coupling of the  $B_{1g}$  phonon to the antinodal electronic states of  $\text{Bi}_2\text{Sr}_2\text{Ca}_{0.92}\text{Y}_{0.08}\text{Cu}_2\text{O}_{8+\delta}$ ," *Physical Review Letters*, vol. 93, no. 11, Article ID 117003, 4 pages, 2004.
- [28] T. Takahashi, T. Sato, H. Matsui, and K. Terashima, "High-resolution ARPES study of quasi-particles in high- $T_c$  superconductors," *New Journal of Physics*, vol. 7, p. 105, 2005.
- [29] X. J. Zhou, T. Cuk, T. P. Devereaux, N. Nagaosa, and Z.-X. Shen, "Angle-resolved photoemission spectroscopy on electronic structure and electron—phonon coupling in cuprate superconductors," in *Handbook of High-Temperature Superconductivity*, J. R. Schrieffer and J. S. Brooks, Eds., pp. 87–138, Springer Science and Business Media LLS, New York, NY, USA, 2007.
- [30] M. Okawa, K. Ishizaka, M. Uchiyama, et al., "Superconducting electronic state in optimally doped  $\text{YBa}_2\text{Cu}_3\text{O}_{7-\delta}$  observed with laser-excited angle-resolved photoemission spectroscopy," *Physical Review B*, vol. 79, no. 14, Article ID 144528, 9 pages, 2009.
- [31] J. H. Chung, T. Egami, R. J. McQuinney, et al., "In-plane anisotropy and temperature dependence of oxygen phonon modes in  $\text{YBa}_2\text{Cu}_3\text{O}_{6.95}$ ," *Physical Review B*, vol. 67, no. 1, Article ID 014517, 9 pages, 2003.
- [32] L. Pintschovius, D. Reznik, W. Reichardt, et al., "Oxygen phonon branches in  $\text{YBa}_2\text{Cu}_3\text{O}_7$ ," *Physical Review B*, vol. 69, no. 21, Article ID 214506, 11 pages, 2004.
- [33] L. Pietronero, "Superconductivity mechanisms in doped  $\text{C}_{60}$ ," *Europhysics Letters*, vol. 17, pp. 365–371, 1992.
- [34] L. Pietronero and S. Strassler, "Theory of nonadiabatic superconductivity," *Europhysics Letters*, vol. 18, pp. 627–633, 1992.
- [35] L. Pietronero, S. Strassler, and C. Grimaldi, "Nonadiabatic superconductivity. I. Vertex corrections for the electron-phonon interactions," *Physical Review B*, vol. 52, no. 14, pp. 10516–10529, 1995.
- [36] L. Proville and S. Aubry, "Small bipolarons in the 2-dimensional Holstein-Hubbard model. I. The adiabatic limit," *The European Physical Journal B*, vol. 11, no. 1, pp. 41–58, 1999.
- [37] J. Bonca, S. A. Trugman, and I. Batistic, "Holstein polaron," *Physical Review B*, vol. 60, no. 3, pp. 1633–1642, 1999.
- [38] P. Benedetti and R. Zeyher, "Holstein model in infinite dimensions at half-filling," *Physical Review B*, vol. 58, no. 21, pp. 14320–14334, 1998.
- [39] H. Fehske, J. Loos, and G. Wellein, "Spectral properties of the 2D Holstein polaron," *Zeitschrift für Physik B*, vol. 104, no. 4, pp. 619–627, 1997.

- [40] A. R. Bishop and M. Salkola, in *Polarons and Bipolarons in High- $T_c$  Superconductors and Related Materials*, E. K. H. Salje, Ed., Cambridge University Press, Cambridge, UK, 1995.
- [41] A. S. Alexandrov and P. E. Kornilovitch, "Incorporating novel magnetism," *The Journal of Superconductivity*, vol. 15, no. 5, pp. 403–408, 2002.
- [42] A. S. Alexandrov and J. Runniger, "Theory of bipolarons and bipolaronic bands," *Physical Review B*, vol. 23, no. 4, pp. 1796–1801, 1981.
- [43] A. S. Alexandrov and J. Runniger, "Bipolaronic superconductivity," *Physical Review B*, vol. 24, no. 3, pp. 1164–1169, 1981.
- [44] A. S. Alexandrov, *Zh.Fiz.Chim*, vol. 57, p. 273, 1983, English translation in *Russian Journal of Physical Chemistry*, vol. 57, p. 167, 1983.
- [45] D. J. Scalapino, "Random magnetism, high temperature superconductivity," in *Superconductivity*, R. D. Parks, Ed., vol. 1, p. 449, Marcel Dekker, New York, NY, USA, 1969.
- [46] P. B. Allen and R. C. Dynes, "Transition temperature of strongly-coupled superconductors reanalyzed," *Physical Review B*, vol. 12, no. 3, pp. 905–922, 1975.
- [47] A. S. Alexandrov, "Nonadiabatic polaronic superconductivity in  $MgB_2$  and cuprates," *Physica C*, vol. 363, no. 4, pp. 231–236, 2001.
- [48] G. Grimaldi, L. Pietronero, and S. Strassler, "Nonadiabatic superconductivity. II. Generalized Eliashberg equations beyond Migdal's theorem," *Physical Review B*, vol. 52, no. 14, pp. 10530–10546, 1995.
- [49] G. Grimaldi, L. Pietronero, and S. Strassler, "Nonadiabatic superconductivity: electron-phonon interaction beyond Migdal's theorem," *Physical Review Letters*, vol. 75, no. 6, pp. 1158–1161, 1995.
- [50] G. Grimaldi, E. Cappelluti, and L. Pietronero, "Isotope effect on  $m^*$  in high- $T_c$  materials due to the breakdown of Migdal's theorem," *Europhysics Letters*, vol. 42, pp. 667–672, 1998.
- [51] G. Grimaldi, L. Pietronero, and M. Scottani, "The physical origin of the electron-phonon vertex correction," *The European Physical Journal B*, vol. 10, no. 2, pp. 247–255, 1999.
- [52] E. Cappelluti, G. Grimaldi, and L. Pietronero, "Nonadiabatic Pauli susceptibility in fullerene compounds," *Physical Review B*, vol. 64, no. 12, Article ID 125104, 8 pages, 2001.
- [53] M. Botti, E. Cappelluti, G. Grimaldi, and L. Pietronero, "Nonadiabatic theory of the superconducting state," *Physical Review B*, vol. 66, no. 5, Article ID 054532, 10 pages, 2002.
- [54] E. Cappelluti, S. Ciuchi, G. Grimaldi, and L. Pietronero, "Band-filling effects on electron-phonon properties of normal and superconducting states," *Physical Review B*, vol. 68, no. 17, Article ID 174509, 10 pages, 2003.
- [55] A. S. Alexandrov, *Theory of Superconductivity: From Weak to Strong Coupling*, IoP, Bristol, Pa, USA, 2003.
- [56] A. S. Alexandrov, "Strong coupling theory of high temperature superconductivity," in *Studies of High Temperature Superconductors, Golden Jubilee Volume*, A. Narlikar, Ed., pp. 1–69, Nova Science, New York, NY, USA, 2006.
- [57] A. S. Alexandrov and P. P. Edwards, "High- $T_c$  cuprates: a new electronic state of matter?" *Physica C*, vol. 331, no. 2, pp. 97–112, 2000.
- [58] A. S. Alexandrov, "Many-body effects in the normal-state polaron system," *Physical Review B*, vol. 23, no. 5, pp. 2838–2844, 1992.
- [59] J. P. Hauge, P. E. Kornilovitch, J. H. Samson, and A. S. Alexandrov, "Superlight small bipolarons," *Journal of Physics: Condensed Matter*, vol. 19, Article ID 255214, 26 pages, 2007.
- [60] J. Nagamatsu, N. Nakagawa, T. Muranaka, Y. Zenitani, and J. A. Kijima, "Superconductivity at 39 K in magnesium diboride," *Nature*, vol. 410, pp. 63–64, 2001.
- [61] J. M. An and W. E. Pickett, "Superconductivity of  $MgB_2$ : covalent bonds driven metallic," *Physical Review Letters*, vol. 86, no. 19, pp. 4366–4369, 2001.
- [62] T. Yildirim, O. Gulseren, J. W. Lynn, et al., "Giant anharmonicity and nonlinear electron-phonon coupling in  $MgB_2$ : a combined first-principles calculation and neutron scattering study," *Physical Review Letters*, vol. 87, Article ID 037001, 4 pages, 2001.
- [63] J. Kortus, I. I. Mazin, K. D. Belashchenko, V. P. Antropov, and L. L. Boyer, "Superconductivity of metallic Boron in  $MgB_2$ ," *Physical Review Letters*, vol. 86, no. 20, pp. 4656–4659, 2001.
- [64] P. Baňacký, "Nonadiabatic sudden increase of the cooperative kinetic effect at lattice energy stabilization—microscopic mechanism of superconducting state transition: model study of  $MgB_2$ ," *International Journal of Quantum Chemistry*, vol. 101, no. 2, pp. 131–152, 2005.
- [65] L. Boeri, E. Cappelluti, and L. Pietronero, "Small Fermi energy, zero-point fluctuations, and nonadiabaticity in  $MgB_2$ ," *Physical Review B*, vol. 71, no. 1, Article ID 012501, 4 pages, 2005.
- [66] P. Baňacký, "Ab initio theory of complex electronic ground state of superconductors: I. Nonadiabatic modification of the Born–Oppenheimer approximation," *Journal of Physics and Chemistry of Solids*, vol. 69, no. 11, pp. 2728–2747, 2008.
- [67] M. Svrček, P. Baňacký, and A. Zajac, "Nonadiabatic theory of electron-vibrational coupling: new basis for microscopic interpretation of superconductivity," *International Journal of Quantum Chemistry*, vol. 43, no. 3, pp. 393–414, 1992.
- [68] P. Baňacký, "Ab initio theory of complex electronic ground state of superconductors: II. Antiadiabatic state-ground state of superconductors," *Journal of Physics and Chemistry of Solids*, vol. 69, no. 11, pp. 2696–2712, 2008.
- [69] M. Born and J. R. Oppenheimer, *Annals of Physics*, vol. 84, p. 457, 1927.
- [70] M. Born and M. Göttinger, *Nachrichten der Akademie der Wissenschaften Mathematisch Physikalische Klasse*, p. 1, 1951.
- [71] M. Born and K. Huang, *Dynamical Theory of Crystal Lattices*, Oxford University Press, London, UK, 1956.
- [72] A. S. Davydov, *Quantum Mechanics*, Addison-Wesley, New York, NY, USA, 1965.
- [73] M. Svrček, P. Baňacký, S. Biskupič, J. Noga, P. Pelikán, and A. Zajac, "Adiabatic correction to the energy of molecular systems: the CPHF equivalent of the Born–Oppenheimer formula," *Chemical Physics Letters*, vol. 299, no. 2, pp. 151–157, 1999.
- [74] T. D. Lee, F. Low, and D. Pines, "The motion of slow electrons in a polar crystal," *Physical Review*, vol. 90, no. 2, pp. 297–302, 1953.
- [75] P. Baňacký, "Aspects of electronic structure instability in search for new superconductors: superconducting boride at liquid nitrogen temperature?" *Collection of Czechoslovak Chemical Communications*, vol. 73, pp. 795–810, 2008.
- [76] P. Baňacký, "Theoretical study of  $YBa_2Cu_3O_7$  beyond the Born–Oppenheimer approximation and Migdal theorem: Antiadiabatic ground state induced by phonon modes coupling," in *Superconducting Cuprates*, K. N. Courtland, Ed., chapter 6, pp. 187–212, Nova Science, New York, NY, USA, 2009.
- [77] J. Labbe and J. Bok, "Superconductivity in alkaline-earth-substituted  $La_2CuO_4$ : a theoretical model," *Europhysics Letters*, vol. 3, pp. 1225–1230, 1987.

- [78] J. Bok and J. Bouvier, “Van Hove scenario for high  $T_c$  superconductors,” *Physica C*, vol. 460, pp. 1010–1012, 2007.
- [79] D. H. Lu, D. L. Feng, N. P. Armitage, et al., “Superconducting gap and strong in-plane anisotropy in untwinned  $YBa_2Cu_3O_{7-\delta}$ ,” *Physical Review Letters*, vol. 86, no. 19, pp. 4370–4373, 2001.
- [80] H. J. M. Smilde, A. A. Golubov, A. G. Rijnders, et al., “Admixtures to  $d$ -wave gap symmetry in untwinned  $YBa_2Cu_3O_7$  superconducting films measured by angle-resolved electron tunneling,” *Physical Review Letters*, vol. 95, no. 25, Article ID 257001, 4 pages, 2005.
- [81] P. Martinez-Samper, J. G. Rodrigo, G. Rubio-Bollinger, et al., “Scanning tunneling spectroscopy in  $MgB_2$ ,” *Physica C*, vol. 385, no. 1-2, pp. 233–243, 2003.
- [82] P. Szabo, P. Samuely, J. Kacmarek, et al., “Evidence for two superconducting energy gaps in  $MgB_2$  by point-contact spectroscopy,” *Physical Review Letters*, vol. 87, no. 13, Article ID 137005, 4 pages, 2001.
- [83] B. T. Matthias, T. M. Gebale, and K. Andres, “Superconductivity and antiferromagnetism in boron-rich lattices,” *Science*, vol. 159, no. 3814, p. 530, 1968.
- [84] O. K. Andersen, A. I. Lichtenstein, O. Jepsen, and F. Paulsen, “LDA energy bands, low-energy hamiltonians,  $t'$ ,  $t''$ ,  $t_{\perp}(k)$ , and  $J_{\perp}$ ,” *Journal of Physics and Chemistry of Solids*, vol. 56, no. 12, pp. 1573–1591, 1995.
- [85] R. Kouba, C. Ambrosch-Draxl, and B. Zangger, “Structure optimization of  $YBa_2Cu_3O_7$  and its influence on phonons and Fermi surface,” *Physical Review B*, vol. 60, no. 13, pp. 9321–9324, 1999.
- [86] H. Haghighi, J. H. Kaiser, S. Raynar, et al., “Direct observation of Fermi surface in  $YBa_2Cu_3O_{7-\delta}$ ,” *Physical Review Letters*, vol. 67, no. 3, pp. 382–385, 1991.
- [87] D. Singh, W. E. Pickett, E. C. van Stetten, and S. Berko, “Theoretical electron-positron zone-reduced momentum density for  $YBa_2Cu_3O_7$ : Fermi surface and wave-function effects,” *Physical Review B*, vol. 42, no. 4, pp. 2696–2699, 1990.

## Research Article

# Lattice Instability in High Temperature Superconducting Cuprates and FeAs Systems: Polarons Probed by EXAFS

H. Oyanagi<sup>1</sup> and C. J. Zhang<sup>1,2</sup>

<sup>1</sup> Photonics Research Institute, National Institute of Advanced Industrial Science and Technology, 1-1-1 Umezono, Tsukuba, Ibaraki 305-8568, Japan

<sup>2</sup> High Magnetic Field Laboratory, Hefei Institute of Physical Sciences, Chinese Academy of Sciences, P.O. Box 1110, 350# Shushan Road, Hefei 230031, China

Correspondence should be addressed to H. Oyanagi, h.oyanagi@aist.go.jp and C. J. Zhang, zhangcj@hmfl.ac.cn

Received 11 June 2009; Accepted 7 October 2009

Academic Editor: Dragan Mihailovic

Copyright © 2010 H. Oyanagi and C. J. Zhang. This is an open access article distributed under the Creative Commons Attribution License, which permits unrestricted use, distribution, and reproduction in any medium, provided the original work is properly cited.

Carrier-induced lattice distortion (signature of polaron) in oxypnictide superconductors is found by an instantaneous local probe, extended X-ray absorption fine structure (EXAFS). Polaron formation is detected as two distinct nearest neighbor distances (Fe-As), *implying an incoherent local mode that develops coherence at the critical temperature*. Comparing the results with the unusual lattice response in cuprate superconductors, intimate correlation between evolution of local lattice mode and superconductivity is revealed. The results suggest that strong electron-lattice interaction is present as a common ingredient in the microscopic mechanism of superconducting transition. The effect of magnetic impurity atoms in cuprates further indicates that magnetic scattering becomes diluted as long as polaron formation is conserved. We argue that polaron coherence dominates electrical conduction and magnetic interaction in oxypnictide and cuprate superconductors.

## 1. Introduction

While the microscopic mechanism of high temperature superconductivity (HTSC) is still in mystery more than 23 years after the discovery [1], recently reported superconductivity in fluorine-doped LaFeAsO (LFAO) [2] has revived interests in the research of HTSC. Replacing oxygen by fluorine or oxygen vacancy control introduces charge (electrons) carriers which are transferred from the La-O(F) “charge reservoir” layer to the Fe-As conducting layer as illustrated in Figure 1. Superconductivity emerges as the F-doping concentration exceeds about 5%, away from nondoped antiferromagnetic (AFM) parent phase. In spite of similarity in the phase diagram with that of cuprates, that is, superconducting phase near the AFM phase, the mechanism of superconductivity is still unclear, allowing diversity and contradictions in theoretical models. A conventional phonon mechanism is unlikely as the DFT calculations indicated a weak electron-phonon coupling; yet, the purely electronic mechanism [3] is also less likely than the case of cuprates [4] as the Hubbard  $U$  is not large ( $U \sim 5$  eV) [5]. Recent muon

spin rotation experiments suggest possibility of multigap BCS-type superconductivity in  $\text{Ba}_{0.6}\text{K}_{0.4}\text{Fe}_2\text{As}_2$  [6].

A polaron is formed when an electron is strongly coupled to the atoms in a crystal. Reviewing article on a polaronic mechanism of superconductivity is elsewhere [7]. In manganites, coherent polaron condensation is believed to be the driving mechanism of colossal magnetoresistance (CMR) phenomena [8]. Strong coupling between electrons and lattice in HTSC cuprates is demonstrated by angle-resolved photoemission spectroscopy (ARPES) [9]. Reflecting these backgrounds, renewed interests on the role of polaron in HTSC mechanism are accumulating. Here we describe lattice effects in oxypnictide [10] studied by means of a local probe, extended X-ray absorption fine structure (EXAFS) and compared with the results for a typical cuprate  $\text{La}_{2-x}\text{Sr}_x\text{CuO}_4$  (LSCO) [11]. Previously, unusual carrier-induced local displacement found for LSCO was interpreted as a nanometer-scale self-organization (stripe) [12, 13]. In contrast, we take lattice instability as polarons as predicted by theoretical models [14–17]. As the magnitude of EXAFS oscillations is in the order of  $10^{-2}$ , a highly efficient

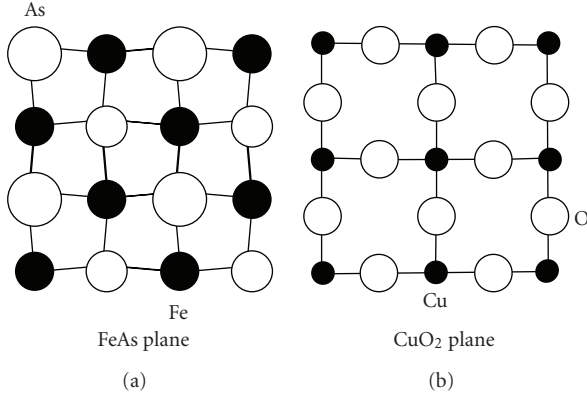


FIGURE 1: *In-plane* structure of the conducting layer in  $\text{LaFeAsO}_{1-x}\text{F}_x$  (a) and  $\text{La}_{1-x}\text{Sr}_x\text{CuO}_4$  (b). Use of polarization dependence ( $E//ab$ ) XAS measurement can probe the planar local lattice projected onto the  $ab$ -plane.

segmented detection is needed [18]. We have developed a state-of-the-art pixel X-ray detector to obtain high-quality EXAFS data for single crystals [19]. As chemical doping (substitution with heterovalent atom) modifies lattice itself, and ambiguity is always present, we took special approaches to control the critical temperature without influencing lattice, that is, (i) uniaxial strain dependence [20–22] and (ii) magnetic impurity effect [23].

## 2. Experimental

EXAFS experiments applied to bulk single crystals where the two polarization geometries ( $E//ab$ ,  $E//c$ ) in principle provide *in-plane* and *out-of-plane* information on the radial distribution function (RDF) of the  $\text{CuO}_2$  plane, respectively. Principle of EXAFS is simple but extreme care should be taken when applied to single crystalline samples. Difficulty in polarized experiments on *as-grown* single crystals is overcome by a fluorescence detection method that measures an emitted photon flux rather than a transmitted beam intensity. In monitoring fluorescence yield spectra for single crystals, strong diffractions often prevent reliable data taking. Experimental difficulty becomes intensified for thin film single crystals because of strong interference of substrate. Here we use segmented fluorescence monitoring to discriminate signal from noise. A novel germanium 100-pixel array detector (PAD) developed for this purpose is used, collecting signals over a segmented solid angle [24]. All EXAFS data were recorded for bulk, 100-nm-thick film LSCO, and polycrystalline LFAO(F) samples at the Photon Factory. The energy and maximum electron current of storage ring were 2.5 GeV and 400–500 mA, respectively. A directly water-cooled silicon (111) double-crystal monochromator was used, covering the energy range 4–25 keV. The energy resolution was better than 2 eV at 9 keV, calibrated from the near-edge features of copper metal at the Fermi energy,  $E_f$  (8.9803 keV). Single crystal sample was attached to an aluminum holder with a strain-free glue and cooled down using a closed-cycle He refrigerator

(cooling power 2 W at 20 K, stability  $\pm 0.1$  K) on a high-precision goniometer (Huber 420). As a typical magnitude of normalized EXAFS oscillations is several %, each data set must have photon statistics better than 0.1% or  $10^6$  photons. In a typical experiment, each data point collects average  $3.6 \times 10^7$  photons making statistical (nonsystematic) noise negligibly small. On the other hand, the most serious noise is systematic origin arising diffractions which distort a fluorescence detector, in particular highly directional Laue diffractions for a single crystalline sample. The advantage of segmented fluorescence detection is that fluorescence signal purity can be monitored over a wide solid angle. Use of segmented detector minimizes both systematic and unsystematic noise leading to a dramatically reduced magnitude of error bar. Repeated scans (about six runs) also reduce systematic error arising from incident beam instability intrinsic to insertion devices. For reliable data taking, non-statistic (systematic) error should be minimized for which segmented X-ray detection and repeated scans are useful. Fluorescence yield spectra for all channels of PAD were monitored in real time and the effect of scattering was inspected. By choosing a proper incidence angle (1 deg) corresponding to a film thickness and further adjustment of orientation, the substrate scattering effect is completely removed. A typical LSCO bulk single crystal grown by TSFZ method was  $2 \text{ mm} \times 2 \text{ mm} \times 1 \text{ mm}$  in dimension [11]. Thin film single crystals ( $10 \text{ mm} \times 10 \text{ mm} \times 100 \text{ nm}$ ) were grown on single crystal substrates by molecular beam epitaxy (MBE) [19]. Using a closed cycle He refrigerator, sample temperature is controlled to a temperature error within 1 K. Polycrystalline samples  $\text{LaFeAsO}_{1-x}\text{F}_x$  ( $x = 0, 0.07$ ) were prepared by solid-state synthesis as described elsewhere [2] and unpolarized EXAFS data were recorded at various temperatures [10].

## 3. Results and Discussion

**3.1. *LaFeAsO* System.** Parent LFAO has a double layer structure where the conducting FeAs layer is adjacent to the reservoir LaO layer in close similarity with LSCO where more two-dimensional  $\text{CuO}_2$  and LaO planes play their roles [1, 2]. Figure 1 illustrates the  $ab$ -plane view of the crystal structures for the FeAs layer in LFAO and the  $\text{CuO}_2$  plane in LSCO. In the FeAs layer, Fe and As atoms have tetrahedrally coordinated each other resulting in a more three-dimensional network while in LSCO copper atoms are fourfold coordinated by oxygen atoms within the plane and two apical oxygen atoms along the  $c$ -axis. EXAFS is an “incoherent” In HTSC research; local probes are often categorized into (i) static incoherent (NMR), (ii) dynamical coherent (X-ray and neutron scattering), and (iii) dynamical incoherent (XAS, Raman scattering) techniques. Here “incoherent” is local probe means it observes spatially-incoherent displacement which is not detected by a conventional diffraction techniques. In contrast, the disadvantage of XAS is that both static and dynamical displacements are observed and cannot be distinguished. local probe that arises from interference of incoming (scattered) and outgoing photoelectrons at the excited atom; local distortions of near

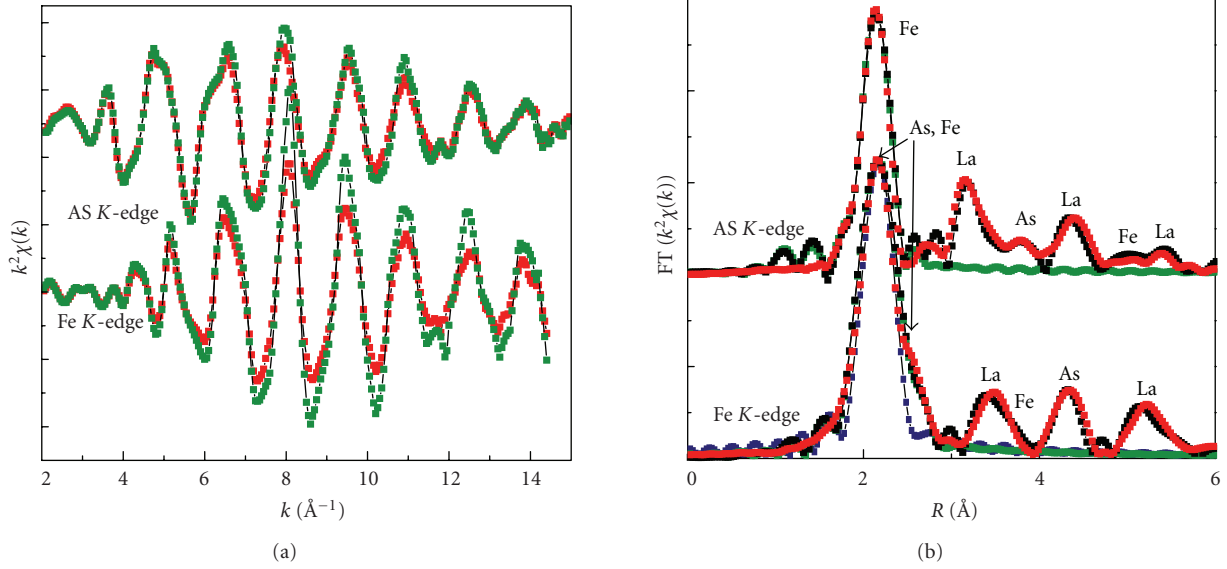


FIGURE 2: (a) The Fe K- and As K-edge EXAFS oscillations for  $\text{LaFeAsO}_{1-x}\text{F}_x$  ( $x = 0.07$ ) plotted as a function of photoelectron wave number  $k$ . Red and green marks indicate the data measured at 300 K and 10 K, respectively, with a fluorescence detection mode. (b) Fourier transform magnitude functions for the same data. Red marks indicate the simulated (fitted) curve and black marks represent the experimental data. Green marks denote the experimental nearest neighbour contribution while blue marks represent theoretical calculation for the nearest neighbour Fe-As correlations, taken from [10].

neighbor atoms with *static* and *dynamic* nature are sensitively detected as an interference (beat) of  $k$ -dependent oscillations ( $k < 15\text{\AA}^{-1}$ ), where  $k$  is a wave vector of photoelectron. Complex Fourier transform (FT) of EXAFS oscillations relates to the radial distribution function (RDF) if phase-shift of photoelectron scattering is corrected. Experimental EXAFS oscillations around Fe and As atoms are compared to those simulated by FEFF7 [25] based on the structural parameters determined by Rietveld analysis and all possible scattering paths including single-scattering and multiple-scattering paths [10].

Figures 2(a) and 2(b) illustrate the Fe K- and As K-EXAFS oscillations and FT magnitude functions for superconducting  $\text{LaFeAsO}_{1-x}\text{F}_x$  ( $x = 0.07$ ), respectively. Curve fitted theoretical curve (red) agreed well with those of experimental data (black). Contributions of the first nearest neighbor shell (green) are back Fourier transformed into  $k$ -space and analyzed, providing the Fe-As distance and mean square relative displacement (MSRD)  $\sigma_{\text{Fe-As}}^2$ , denoted here simply as a displacement parameter (DP). The As K-edge FT main peak consists of only the nearest neighbour Fe-As correlation but the Fe K-edge FT has a weak Fe-Fe correlation as a shoulder. We note that the As K-edge data is thus more straightforward in data analysis that directly yields the Fe-As bond distance. In this work, we derived  $\sigma_{\text{Fe-As}}^2$  independently from the Fe K- and As K-edge data and confirmed that they agree and show the same temperature anomalies. DP values for the Fe-As and Fe-Fe correlations are plotted in Figure 3 as a function of temperature where red and green marks represent the Fe-As (Fe K-edge data) and As-Fe (As K-edge data) correlations, respectively. One can notice that undoped sample data (red and green circles) show an indication of

magnetic phase transition but lower temperature data are smooth and have no lattice anomalies, in sharp contrast with doped specimen (red and green circles) that shows a complex temperature dependence at low temperatures. In the inset, the Fe-As DP ( $\sigma_{\text{Fe-As}}^2$ ) in doped LFAO is compared with that of *in-plane*  $\sigma_{\text{Cu-O}}^2$  in LSCO as a function of normalized temperature. Carrier doping creates a remarkable effect on the Fe-As DP, that is, the Fe-As DP in undoped sample shows no anomaly below the spin-density-wave (SDW) transition temperature [26, 27], whereas lattice instability (unusual DP variation with temperature) newly arises as magnetic instability is suppressed in the F-doped sample. Upturn trend beginning at  $1.5 T_c$  Pseudogap opening and local lattice distortion (polaron formation) are correlated. For optimally doped LSCO, pseudogap opening temperature ( $T_{\text{po}} \sim 1.5 T_c$ ) which explains why the onset of DP anomaly starts at  $1.5 T_c$ . More recently, in [28], Lee et al. demonstrated that tunneling spectroscopic signature of *d*-wave superconductivity (particle-hole symmetric ‘‘octet’’ of dispersive Bogoliubov QPI modulations) survives up to at least  $T \sim 1.5 T_c$ . and a sharp drop of DP at  $T_c$  is found in superconducting samples, suggesting strong coupling between the local displacement and superconductivity.

Here lattice instability is defined as unusual behavior of DP, a deviation from a smooth noncorrelated Debye-like function which is observed as carriers are doped. The increase of DP is usually taken as an increase of disorder but here it describes the interference (beat) of bonds having different (short and long) bond lengths. Elongation of bonds is an outcome of local distortion (polaron formation). The inset of Figure 3 shows that a sharp drop of DP occurs at  $T_c^{\text{onset}}$  in LFAO(F) and LSCO systems, indicating that local

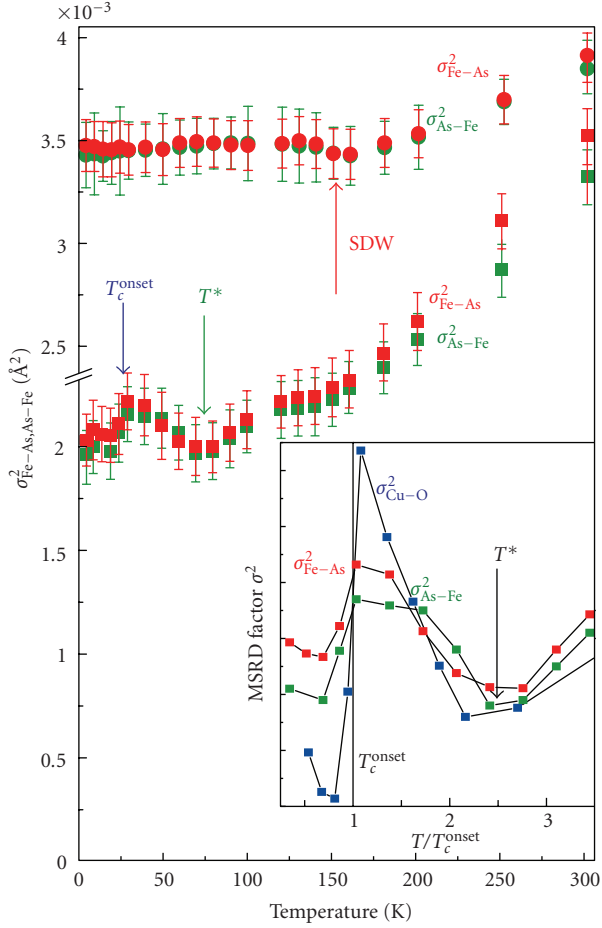


FIGURE 3: Temperature dependence of the Fe–As bond mean-square relative displacements for  $\text{LaFeAsO}_{0.93}\text{F}_{0.07}$  (squares) and  $\text{LaFeAsO}$  (circles). The red and green symbols denote the results for the Fe  $K$  edge and the As  $K$  edge EXAFS data respectively, taken from [10]. The inset shows an enlarged view of low temperature ( $T < 100$  K) mean-square relative displacements (MSRD) for the  $\text{LaFeAsO}_{0.93}\text{F}_{0.07}$  sample plotted as the function of normalized temperature ( $T/T_c^{\text{onset}}$ ) compared to the result for  $\text{La}_{1.85}\text{Sr}_{0.15}\text{CuO}_4$ .

lattice response directly relates to the microscopic mechanism of superconductivity (development of coherence) while the onset of polaron formation coincides with  $T^* = 70\text{--}80$  K.

**3.2. LaSrCuO System.** LSCO is a typical HTSC cuprate with a  $\text{K}_2\text{NiF}_4$ -type structure, where copper atoms are coordinated by four in-plane oxygen atoms ( $\text{O}_p$ ) and two apical oxygen atoms ( $\text{O}_{ap}$ ). The  $\text{CuO}_6$  octahedron is elongated along the  $c$ -axis with two long ( $2.40 \text{ \AA}$ ) and four short ( $1.89 \text{ \AA}$ ) bonds as a result of Jahn-Teller (JT) distortion [29]. Figure 4 illustrates temperature dependence of the *in-plane* and *out-of-plane* Cu–O DP ( $\sigma_{\text{Cu-O}}^2$ ) for LSCO ( $x = 0.15$ ) single crystals grown by TSFZ technique. In order to avoid the effect of disorder arising from doping, nonsuperconducting specimen was prepared by substituting copper atom with 5% Ni [11]. Complex FT and curve fitting were performed for all EXAFS data taken over a wide range in temperature down to 5 K. As temperature is decreased, the superconducting sample

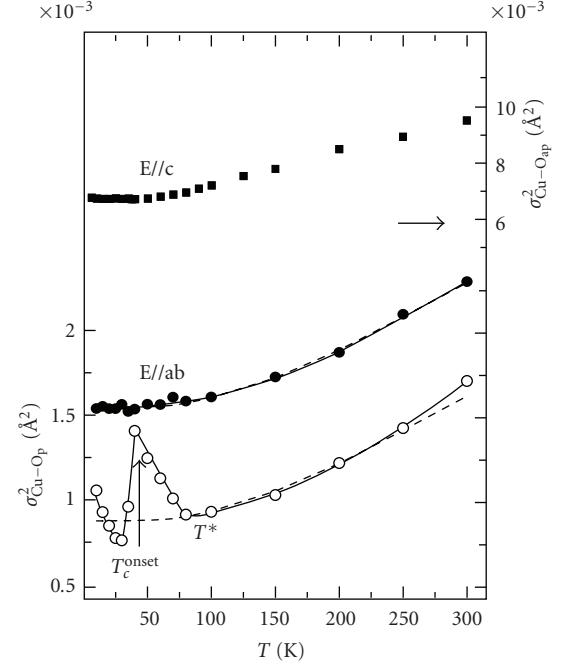


FIGURE 4: Mean-square relative displacement of the Cu–O bond in superconducting  $\text{La}_{1-x}\text{Sr}_x\text{CuO}_4$  ( $x = 0.15$ ) with the *in-plane* ( $E//ab$ ) and *out-of-plane* ( $E//c$ ) geometries as a function of temperature. Closed and open circles denote the results for  $\text{Cu-O}_p$  (*in-plane* oxygen) measured for superconducting and non-superconducting samples (prepared by doping 3% Ni), respectively. Closed squares represent the mean-square oxygen displacement for the  $\text{Cu-O}_{ap}$  (*out-of-plane* oxygen) in superconducting LSCO. Data were taken from [11].

shows lattice instability, that is, an upturn DP beginning at  $T^*$  (80 K), which sharply drops at the onset of superconductivity. These features are observed only after carrier doping and are not present in nonsuperconducting sample prepared by magnetic impurity doping [30]. This strict carrier-dependence shows the nature of lattice distortion caused by carrier doping.

Secondly, one may concern whether the apical oxygen atoms behave similarly or not, that is, lattice modes involve apical oxygen atoms or not. Anisotropic nature of lattice instability is studied by comparing the results for the *in-plane* and *out-of-plane* results obtained by independent polarized experiments. Here we show that the observed polaronic distortion gives rise to two different bond distances distinguished from broadening (disorder). In Figures 5(a) and 5(b), theoretically calculated EXAFS oscillations and FT magnitude functions for undistorted  $\text{CuO}_4$  and distorted model structures (linked two  $\text{CuO}_4$  units with  $\text{Q}_2$  JT or pseudo JT distortions) are illustrated. The appearance of beat feature at  $k \sim 12 \text{ \AA}^{-1}$  corresponds to the bond length difference of  $\sim 0.1 \text{ \AA}^{-1}$  which is observed in the experimental  $E//ab$  Cu–O EXAFS oscillations for LSCO shown in Figure 5(c). These results indicate that the *in-plane* distortion observed as an anomaly in superconducting LSCO is due to the elongated and short bond distances separated by  $\sim 0.1 \text{ \AA}^{-1}$ . The *out-of-plane* Cu–O bond has no anomaly although the curve

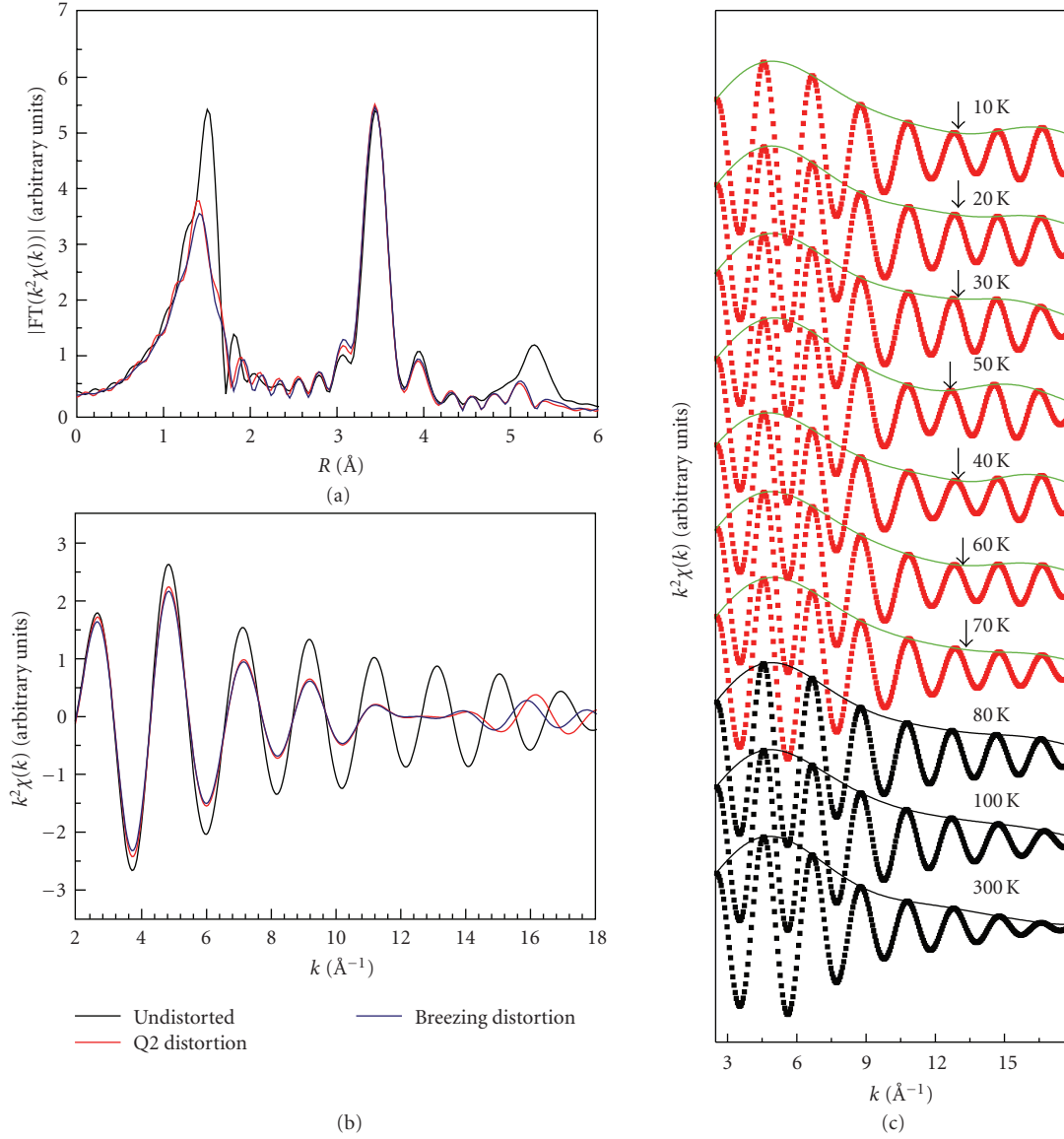


FIGURE 5: (a) Fourier transform magnitude curves of simulated E//ab EXAFS oscillations for undistorted (solid line) and distorted  $\text{CuO}_4$ - $\text{CuO}_4$  units (red curve: JT  $Q_2$  mode, purple curve: pseudo-JT (brezging) mode distortions). (b) Nearest neighbour contribution of simulated EXAFS oscillations for undistorted and distorted models. Interference of long and short Cu–O bonds give rise to beat features at  $k \sim 12 \text{ \AA}^{-1}$ . (c) Experimental nearest neighbor Cu–O EXFS curves measured at various temperatures. Beat feature similar to (b) is observed at  $k = 14 \text{ \AA}^{-1}$  near  $T_c$  (40 K).

fitting analysis for the  $c$ -axis geometry contains larger error (due to the statistics and multishell fitting procedure) [11], in contrast to the early works which related the anomaly to a low temperature tetragonal (LTT) deformation with correlative displacement of apical oxygen atoms leading to charged stripes.

**3.3. Strain Effects in  $\text{LaSrCuO}$  System.** Whether polaron formation probed by the nearest neighbor pair directly relates to superconductivity or not is of particular interest. Hydrostatic high pressure and uniaxial strain experiments are widely used to study the lattice effects on superconductivity. Here we use the mismatch in lattice constants between epitaxial thin

film single crystal and substrate that causes compressive or tensile strains. Chemical strain affects the superconducting critical temperature, that is,  $T_c$  of strained thin film single crystal is modified; LSCO on  $\text{LaSrAlO}_4$  (LSAO) and  $\text{SrTiO}_3$  (STO) is 43.4 K ( $\Delta T_c < 1.0$  K) and 19.0 K ( $\Delta T_c < 9.0$  K), respectively, in contrast to the bulk single crystal value (35 K) [29]. Figure 6(a) shows the  $\text{Cu-O}_p$  DP for LSCO under compressive and tensile strains as a function of temperature. The DP drop clearly shifts with the  $T_c^{\text{onset}}$  (chemical strain effect) and the magnitude of a sharp DP drop at  $T_c^{\text{onset}}$  is roughly proportional to the transition temperature, possibly reflecting superfluid density. The correlation of DP drop and the  $T_c^{\text{onset}}$  is demonstrated in Figure 6(b) plotted against a normalized temperature ( $T/T_c$ ).

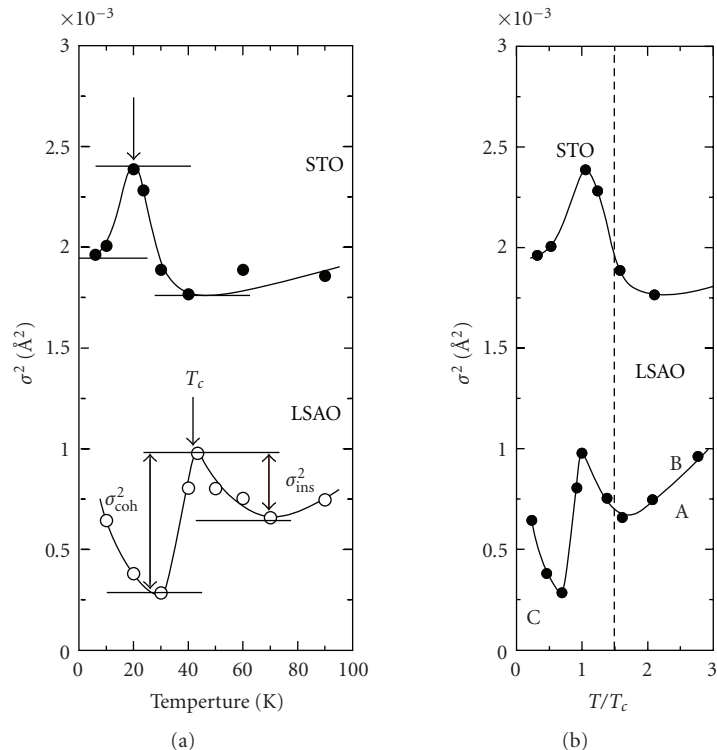


FIGURE 6: Mean-square relative displacement of the *in-plane* Cu–O bond in thin film single crystal  $\text{La}_{1-x}\text{Sr}_x\text{CuO}_4$  ( $x = 0.15$ ) plotted against temperature (a) and normalized temperature  $T/T_c$  (b), taken from [19].

As illustrated in Figures 6(a) and 6(b), the correspondence between the DP maximum and  $T_c$  is quite good, suggesting that the DP drop is related to superconducting coherence. We take this lattice instability starting at about  $1.5 T_c$  ( $T^* \sim 1.5 T_c$ ) as a signature of polaron formation, rather than charged magnetic domains with incommensurate spacings (stripes), although nanoscale polarons have strong similarity with stripes in cuprates as the underlying nature has a similar origin (large Hubbard  $U$ ). Note that the magnitude of DP due to polaron formation becomes enhanced and suppressed under tensile and compressive strain, respectively. This may suggest that the former stabilizes a relevant distortion mode with elongated bonds such as anti JT distortion.

Let us examine possible distortion modes that are consistent with the observed bond splitting. In Figure 7 upper column, possible distortion models with stretched bonds are illustrated. All those models have correlated displacement of apical oxygen atoms and are omitted because of irrelevance of apical oxygens (Figure 4). In contrast, in the lower column, two different types of *in-plane* distorted pairs, pseudo-JT mode [17] and  $Q_2$ -type JT mode [16, 31], are illustrated. These correlated distortions allow long-range propagation with minimized elastic energy increase. A puzzling question whether the nature of distortion is *static* or *dynamic*, that is, leading to *localized* [17] or *extended* [16] electron states of polaron, respectively, is unclear as the time scale of EXAFS experiments ( $10^{-15}$  seconds) is orders of magnitude faster than lattice motions ( $10^{-12}$  seconds).

Here we discuss implications of lattice fluctuation. It may arise from softening of LO phonons [32–34]. Bond-stretching-type LO phonon mode strongly couples with doped holes as a result of *d-p* mixing or Cu–O charge transfer and spin correlation. Femtosecond quasi-particle (QP) lifetime experiments indicated phonon-assisted charge transfer and charge inhomogeneity [35]. Nanometer-scale charge inhomogeneity is one of the fundamental properties of cuprates. Although polarons are expected localized in nature but tunneling [14, 35] or percolation [36] may result in extended states with a longer QP lifetime. Here we only note that the two polaron models with different types of in-plane modes (pseudo JT versus  $Q_2$ -type JT) are consistent with the experimental observation. The former model (pseudo JT distortions with the two  $\text{CuO}_6$  units) gives  $R = 1.82 \text{\AA}$  and  $1.96 \text{\AA}$  in good agreement with the EXAFS results [37].

**3.4. Magnetic Impurity Effects in LaSrCuO System.** Magnetic impurities in cuprate superconductors strongly affect the superconducting properties. We have studied how the Cu site substitution with magnetic impurities influences polaron formation. Polarized Cu *K*-edge EXAFS data were collected for the magnetic impurity-doped  $\text{La}_{1.85}\text{Sr}_{0.15}\text{Cu}_{1-x}\text{M}_x\text{O}_4$  ( $M = \text{Mn, Ni, Co}$ ) single-crystal samples. Temperature dependence of the in-plane Cu–O DP is shown in Figures 8(a) ( $M = \text{Ni, Co}$ ) and 8(b) ( $M = \text{Mn}$ ). Doping of impurities leads to different perturbations of the local lattice distortion (DP). Introducing a small amount of Ni and Co impurities

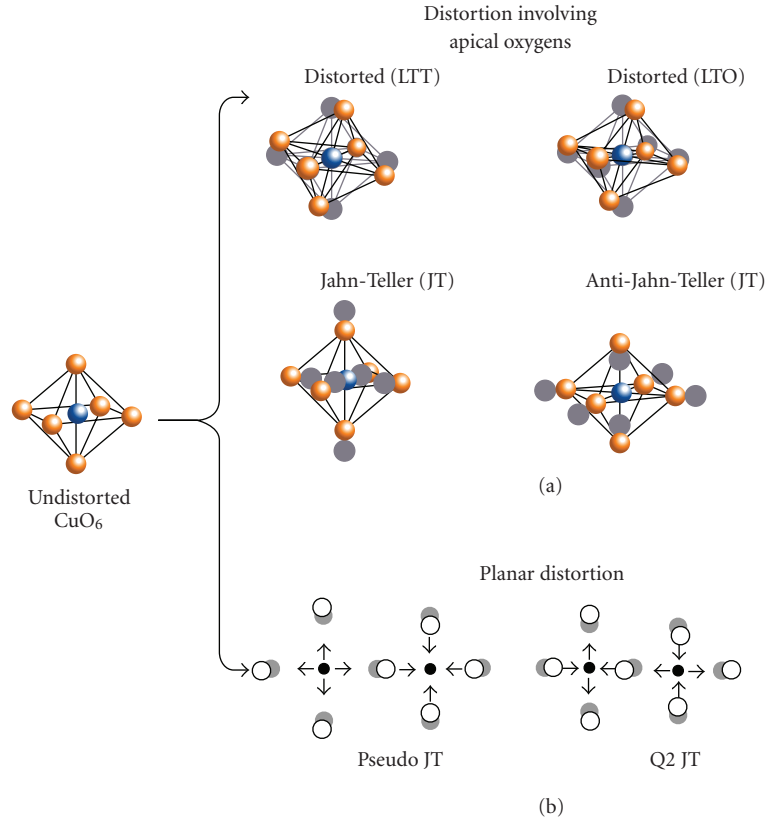


FIGURE 7: Schematic local lattice distortions. (a) Various single site deformation schemes involving apical oxygen displacement. (b) correlated deformation schemes with *in-plane* atomic displacements are schematically illustrated. In case of pseudo JT distortion model (left), oxygen atoms are distorted in a similar fashion with a breathing mode where all Cu–O bonds for each Cu are either elongated or shortened. In the case of Q<sub>2</sub> type JT distortion, half of Cu–O bonds are either elongated or shortened.

at the Cu site sensitively depresses the unusual upturn of the Cu–O DP. With 5% of Ni or Co substitution, the anomaly completely disappears with collapse of superconductivity. In contrast, substitution of Mn has less perturbation on lattice distortion for which superconductivity persists or the onset superconducting temperature is conserved. Magnetic impurities are thus detrimental to superconductivity in accordance with pair breaking theory. Such a magnetic scattering (pair breaking) has no indication of polaron formation but magnetic effect is weakened with the presence of polaron (Mn doping). The onset temperature of *in-plane* Cu–O DP was constant ( $T = 80$  K) for all Mn-doped LSCO samples. With increasing Mn doping, the magnitude of DP slightly decreases but the contribution of superconducting coherence persists in all samples up to  $x = 0.05$ , indicating that Mn doping does not suppress polaron formation. In Ni- and Co-doped LSCO samples, in contrast, the magnitude of DP and superconducting phase coherence (superfluid density) decrease with increasing doping concentration. The preference of elongated *in-plane* M–O bonds (anti JT-like local environments) around an impurity atom may contribute to unperturbed antiferromagnetic correlation length [38].

**3.5. Possible Models.** The effect of superconducting coherence probed by DP (proportional to polaron density)

precisely coincides with the inflection point of resistivity derivative  $\partial\rho/\partial T$ . This suggests that the onset of HTSC is induced as the density of metallic domains exceeds the critical value or the polaron density has a critical value for coherence. Let us consider a simple model (Figure 9) where the distance between polaronic domains  $L$  and the superconducting coherence length  $\zeta_0$  are key parameters. As doping proceeds, reduced Coulomb repulsion ( $U$ ) would promote integration into extended domains with a larger size. The average distance between extended domains  $L$  decreases allowing tunnelling over insulating domains [15, 35]. When  $L$  becomes greater than a critical value ( $\zeta$ ), quantum tunnelling is prohibited. Suppressed tunnelling under tensile strain decreases superfluid density, and hence the critical temperature. In contrast, polaron may also create perturbations in spin configuration so that spin vortices are formed that grows into a macroscopic supercurrent [17].

The Mn ions at Cu sites clearly favor polaron formation while the Ni or Co doping is strongly harmful to both polaron and superconductivity. This suggests that the dynamic nature of polaron is needed to conserve the superconducting transition. We found that the Mn impurities have elongated M–O bond which could be favorable for distortions that cost elongation of bond length such as anti JT distortion [39]. Near the Mn dopants, more and more nonsuperconducting regions are formed and

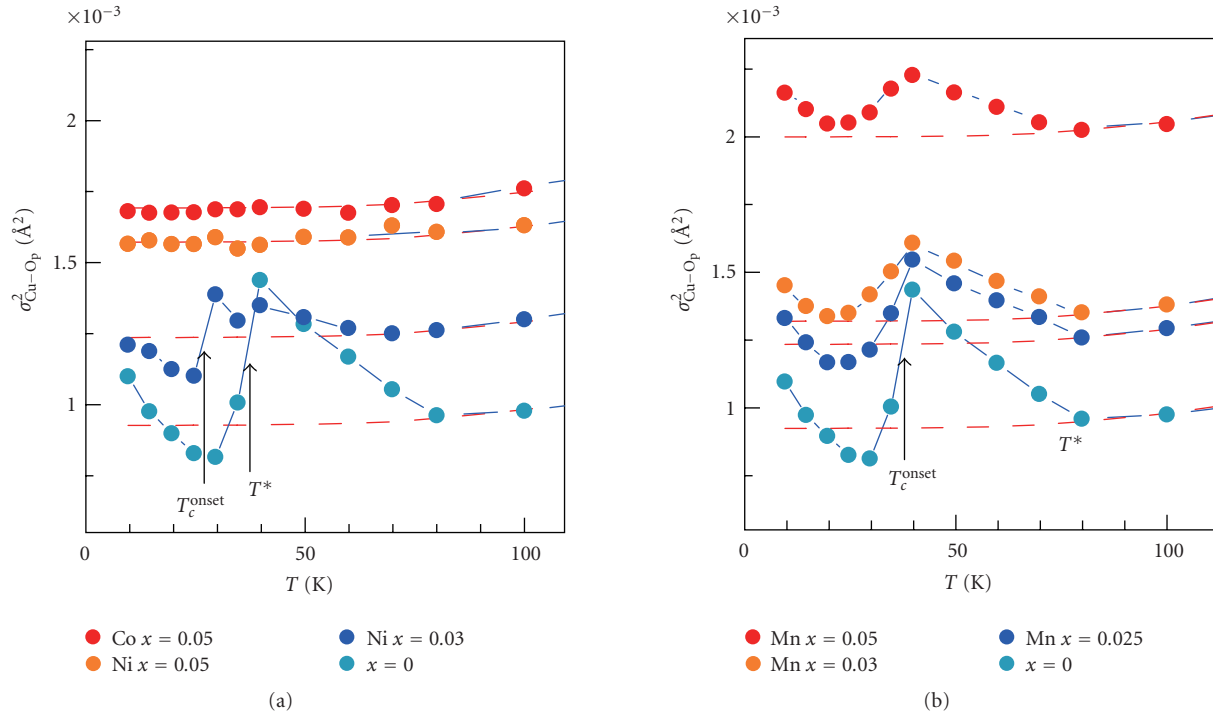


FIGURE 8: Mean-square relative displacement of the *in-plane* Cu-O bond in magnetic impurity doped  $M: \text{La}_{1-x}\text{Sr}_x\text{CuO}_4$  ( $x = 0.15$ ) as a function of temperature. (a)  $M = \text{Co}$ ,  $\text{Ni}$  and (b)  $M = \text{Mn}$ , taken from [11].

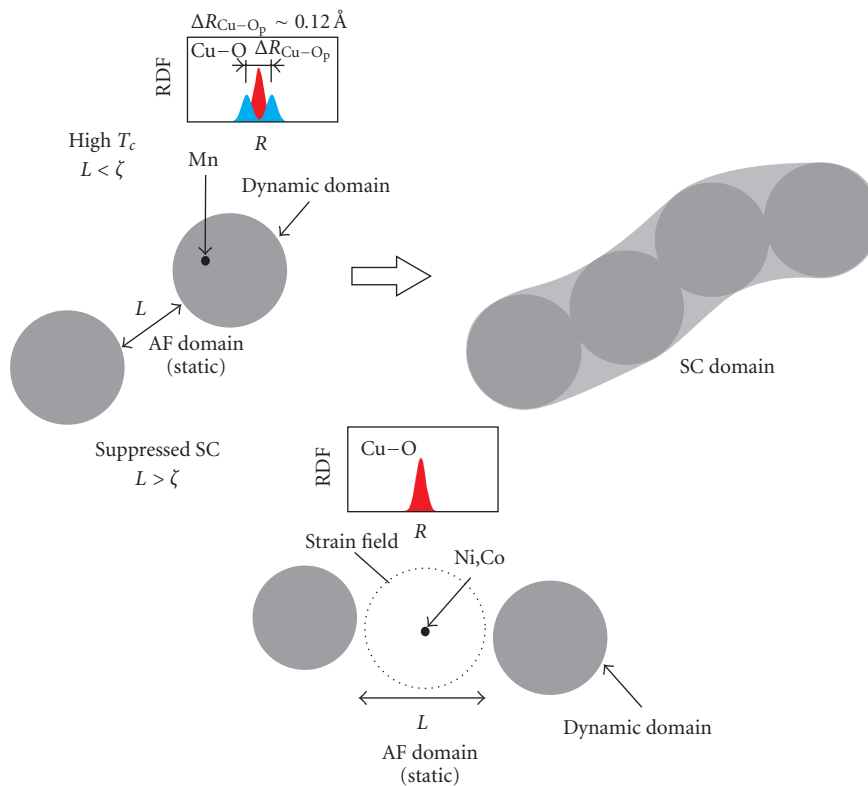


FIGURE 9: Schematic representation of quantum tunnelling in magnetic impurity doped  $\text{La}_{1-x}\text{Sr}_x\text{CuO}_4$  ( $x = 0.15$ ).

superconducting domains are divided into small superconducting domains but within these domains polarons are conserved. As the distance between the superconducting domains becomes large, quantum tunneling or percolation is prohibited and the superconductivity eventually disappears.

Deeper knowledge on the location of doped hole and details of polaron, that is, formation, development and its role in electrical conduction is urgently needed.

#### 4. Conclusion

The local lattice of  $\text{LaFeAsO}_{1-x}\text{F}_x$  superconductors was studied by X-ray absorption spectroscopy, EXAFS. We find an anomalous upturn of the mean-square relative displacement of the nearest neighbor (Fe–As) bond below  $T^*$  as electron carriers are introduced. The Fe–As local lattice fluctuation reveals the formation of two distinct bond lengths  $R_1$  and  $R_2$  where  $\Delta R = R_1 - R_2 \sim 0.1 \text{ \AA}$ . The onset of lattice effects coincides with the opening of pseudogap. The results indicate that oxypnictide superconductors have lattice instability as a signature of polaron formation similar to that of HTSC cuprates. Refined EXAFS data for high-quality (thin films and bulk)  $\text{La}_{1-x}\text{Sr}_x\text{CuO}_4$  single crystals show that the relative oxygen displacement has characteristic features that is, in-plane Cu–O bond splitting indicating dynamical lattice distortion and a sharp drop due to coherence associated with the superconducting state. The observed magnitude of oxygen displacement is in good agreement with the charged cluster calculation on the  $\text{CuO}_6$  deformed pair [37]. Relevant lattice distortions for LSCO likely involve in-plane oxygen atoms as the apical oxygen atoms do not show anomalous displacements. We further find that substitution of Mn atom into a Cu site causes little perturbation of local lattice instability in contrast to Ni and Co substitutions which strongly suppress polaron formation and superconductivity. Suppression of superconductivity is related to the perturbation of local lattice, indicating that polaron formation drives the microscopic mechanism of superconductivity. Whether polaron works to perturb spin configurations leading to spin vortices growing into spin loop current [17] or it enhances strong coupling of spin, charge, and lattice [16] is an open question.

#### Acknowledgments

This work is collaborated with Y. Kamimura, H. Hosono, A. Tsukada, and M. Naito to whom the authors express their thanks for sample preparations. The authors also express their thanks to A. Bussmann-Holder, H. Koizumi, T. Kakeshita, H. Kamimura, J. Mustre de Leon, N. L. Saini, A. Bianconi, and A. Bishop for their continuous encouragement and fruitful discussions.

#### References

- [1] J. G. Bednorz and K. A. Müller, “Possible high  $T_c$  superconductivity in the Ba–La–Cu–O system,” *Zeitschrift für Physik B*, vol. 64, no. 2, pp. 189–193, 1986.
- [2] Y. Kamihara, T. Watanabe, M. Hirano, and H. Hosono, “Iron-based layered superconductor  $\text{La}[\text{O}_{1-x}\text{F}_x]\text{FeAs}$  ( $x = 0.05 - 0.12$ ) with  $T_c = 26 \text{ K}$ ,” *Journal of the American Chemical Society*, vol. 130, no. 11, pp. 3296–3297, 2008.
- [3] C. Fang, H. Yao, W.-F. Tsai, J. Hu, and S. A. Kivelson, “Theory of electron nematic order in  $\text{LaFeAsO}$ ,” *Physical Review B*, vol. 77, no. 22, Article ID 224509, 2008.
- [4] P. W. Anderson, *The Theory of Superconductivity in the Cuprates*, Princeton University Press, Princeton, NJ, USA, 1997.
- [5] W. Malaeb, T. Yoshida, T. Kataoka, et al., “Electronic structure and electron correlation in  $\text{LaFeAsO}_{1-x}\text{F}_x$  and  $\text{LaFePO}_{1-x}\text{F}_x$ ,” *Journal of the Physical Society of Japan*, vol. 77, no. 9, Article ID 093714, 2008.
- [6] M. Hiraishi, R. Kadono, S. Takeshita, et al., “Full gap superconductivity in  $\text{Ba}_{0.6}\text{K}_{0.4}\text{Fe}_2\text{As}_2$  probed by muon spin rotation,” *Journal of the Physical Society of Japan*, vol. 78, no. 2, Article ID 023710, 2009.
- [7] A. S. Alexandrov, “Phase separation of electrons strongly coupled with phonons in cuprates and manganites,” *Journal of Superconductivity and Novel Magnetism*, vol. 22, no. 2, pp. 95–101, 2009.
- [8] N. Mannella, W. L. Yang, K. Tanaka, et al., “Polaron coherence condensation as the mechanism for colossal magnetoresistance in layered manganites,” *Physical Review B*, vol. 76, no. 23, Article ID 233102, 2007.
- [9] A. Lanzara, P. V. Bogdanov, X. J. Zhou, et al., “Evidence for ubiquitous strong electron-phonon coupling in high-temperature superconductors,” *Nature*, vol. 412, no. 6846, pp. 510–514, 2001.
- [10] C. J. Zhang, H. Oyanagi, Z. H. Sun, Y. Kamihara, and H. Hosono, “Low-temperature lattice structure anomaly in the  $\text{LaFeAsO}_{0.93}\text{F}_{0.07}$  superconductor by X-ray absorption spectroscopy: evidence for a strong electron-phonon interaction,” *Physical Review B*, vol. 78, no. 21, Article ID 214513, 2008.
- [11] C. J. Zhang and H. Oyanagi, “Local lattice instability and superconductivity in  $\text{La}_{1.85}\text{Sr}_{0.15}\text{Cu}_{1-x}\text{M}_x\text{O}_4$  ( $M = \text{Mn, Ni, and Co}$ ),” *Physical Review B*, vol. 79, no. 6, Article ID 064521, 2009.
- [12] A. Bianconi, N. L. Saini, A. Lanzara, et al., “Determination of the local lattice distortions in the  $\text{CuO}_2$  Plane of  $\text{La}_{1.85}\text{Sr}_{0.15}\text{CuO}_4$ ,” *Physical Review Letters*, vol. 76, no. 18, pp. 3412–3415, 1996.
- [13] N. L. Saini, A. Lanzara, H. Oyanagi, et al., “Local lattice instability and stripes in the  $\text{CuO}_2$  plane of the  $\text{La}_{1.85}\text{Sr}_{0.15}\text{CuO}_4$  system by polarized XANES and EXAFS,” *Physical Review B*, vol. 55, no. 18, pp. 12759–12769, 1997.
- [14] J. Mustre de Leon, S. D. Conradson, I. Batistić, and A. R. Bishop, “Evidence for an axial oxygen-centered lattice fluctuation associated with the superconducting transition in  $\text{YBa}_2\text{Cu}_3\text{O}_7$ ,” *Physical Review Letters*, vol. 65, no. 13, pp. 1675–1678, 1990.
- [15] D. Mihailovic, “Optical experimental evidence for a universal length scale for the dynamic charge inhomogeneity of cuprate superconductors,” *Physical Review Letters*, vol. 94, no. 20, Article ID 207001, 4 pages, 2005.
- [16] A. Bussmann-Holder and H. Keller, “Polaron formation as origin of unconventional isotope effects in cuprate superconductors,” *European Physical Journal B*, vol. 44, no. 4, pp. 487–490, 2005.
- [17] H. Koizumi, “Loop current excitations in effectively half-filled mott insulators,” *Journal of the Physical Society of Japan*, vol. 77, no. 3, Article ID 034712, 2008.

- [18] H. Oyanagi, C. Fonne, D. Gutknecht, et al., “Ge pixel array detector for high throughput X-ray spectroscopy,” *Nuclear Instruments and Methods in Physics Research A*, vol. 513, no. 1-2, pp. 340–344, 2003.
- [19] H. Oyanagi, A. Tsukada, M. Naito, and N. L. Saini, “Local structure of superconducting  $(\text{La}, \text{Sr})_2\text{CuO}_4$  under strain: Microscopic mechanism of strain-induced  $T_c$  variation,” *Physical Review B*, vol. 75, no. 2, Article ID 024511, 6 pages, 2007.
- [20] H. Sato, M. Naito, and H. Yamamoto, “Superconducting thin films of  $\text{La}_2\text{CuO}_{4+\delta}$  by oxygen doping using ozone,” *Physica C*, vol. 280, no. 3, pp. 178–186, 1997.
- [21] J.-P. Locquet, J. Perret, J. Fompeyrine, E. Mächler, J. W. Seo, and G. Van Tendeloo, “Doubling the critical temperature of  $\text{La}_{1.9}\text{Sr}_{0.1}\text{CuO}_4$  using epitaxial strain,” *Nature*, vol. 394, no. 6692, pp. 453–456, 1998.
- [22] I. Bozovic, G. Logvenov, I. Belca, B. Narimbetov, and I. Sveklo, “Epitaxial strain and superconductivity in  $\text{La}_{2-x}\text{Sr}_x\text{CuO}_4$  thin films,” *Physical Review Letters*, vol. 89, no. 10, Article ID 107001, 2002.
- [23] J. M. Tarascon, L. H. Greene, P. Barboux, et al., “3d-metal doping of the high-temperature superconducting perovskites  $\text{La-Sr-Cu-O}$  and  $\text{Y-Ba-Cu-O}$ ,” *Physical Review B*, vol. 36, no. 16, pp. 8393–8400, 1987.
- [24] H. Oyanagi, A. Tsukada, M. Naito, et al., “Fluorescence X-ray absorption spectroscopy using a Ge pixel array detector: application to high-temperature superconducting thin-film single crystals,” *Journal of Synchrotron Radiation*, vol. 13, no. 4, pp. 314–320, 2006.
- [25] J. J. Rehr, R. C. Albers, and S. I. Zabinsky, “High-order multiple-scattering calculations of X-ray-absorption fine structure,” *Physical Review Letters*, vol. 69, no. 23, pp. 3397–3400, 1992.
- [26] C. de la Cruz, Q. Huang, J. W. Lynn, et al., “Magnetic order close to superconductivity in the iron-based layered  $\text{LaO}_{1-x}\text{F}_x\text{FeAs}$  systems,” *Nature*, vol. 453, no. 7197, pp. 899–902, 2008.
- [27] T. Nomura, S. W. Kim, Y. Kamihara, et al., “Crystallographic phase transition and high- $T_c$  superconductivity in  $\text{LaFeAsO:F}$ ,” *Superconductor Science and Technology*, vol. 21, no. 12, Article ID 125028, 2008.
- [28] J. Lee, K. Fujita, A. R. Schmidt, et al., “Spectroscopic fingerprint of phase-incoherent superconductivity in the underdoped  $\text{Bi}_2\text{Sr}_2\text{CaCu}_2\text{O}_{8+\delta}$ ,” *Science*, vol. 325, no. 5944, pp. 1099–1103, 2009.
- [29] P. G. Radaelli, D. G. Hinks, A. W. Mitchell, et al., “Structural and superconducting properties of  $\text{La}_{2-x}\text{Sr}_x\text{CuO}_4$  as a function of Sr content,” *Physical Review B*, vol. 49, no. 6, pp. 4163–4175, 1994.
- [30] C. J. Zhang, H. Oyanagi, and C. H. Lee, “Single crystal growth and characterization of  $\text{La}_{2-x}\text{Sr}_x\text{CuO}_4$  with Mn doping,” *Physica C*, vol. 468, no. 11-12, pp. 898–902, 2008.
- [31] R. Khasanov, D. G. Eshchenko, H. Luetkens, et al., “Direct observation of the oxygen isotope effect on the in-plane magnetic field penetration depth in optimally doped  $\text{YBa}_2\text{Cu}_3\text{O}_{7-\delta}$ ,” *Physical Review Letters*, vol. 92, no. 5, Article ID 057602, 2004.
- [32] R. J. McQueeney, Y. Petrov, T. Egami, M. Yethiraj, G. Shirane, and Y. Endoh, “Anomalous dispersion of LO phonons in  $\text{La}_{1.85}\text{Sr}_{0.15}\text{CuO}_4$  at low temperatures,” *Physical Review Letters*, vol. 82, no. 3, pp. 628–631, 1999.
- [33] L. Pintschovius and M. Braden, “Anomalous dispersion of LO phonons in  $\text{La}_{1.85}\text{Sr}_{0.15}\text{CuO}_4$ ,” *Physical Review B*, vol. 60, no. 22, pp. R15039–R15042, 1999.
- [34] T. Fukuda, J. Mizuki, K. Ikeuchi, K. Yamada, A. Q. R. Baron, and S. Tsutsui, “Doping dependence of softening in the bond-stretching phonon mode of  $\text{La}_{2-x}\text{Sr}_x\text{CuO}_4$  ( $0 \leq x \leq 0.29$ ),” *Physical Review B*, vol. 71, no. 6, Article ID 060501, 2005.
- [35] D. Mihailovic, V. V. Kabanov, and K. A. Müller, “The attainable superconducting  $T_c$  in a model of phase coherence by percolating,” *Europhysics Letters*, vol. 57, no. 2, pp. 254–259, 2002.
- [36] J. C. Phillips, “Self-organized networks and lattice effects in high-temperature superconductors,” *Physical Review B*, vol. 75, no. 21, Article ID 214503, 2007.
- [37] S. Miyaki, K. Makoshi, and H. Koizumi, “Two-copper-atom units induce a pseudo Jahn-Teller polaron in hole-doped cuprate superconductors,” *Journal of the Physical Society of Japan*, vol. 77, no. 3, Article ID 034702, 2008.
- [38] H. Kamimura, H. Ushio, S. Matsuno, and T. Hamada, *Theory of Copper Oxide Superconductors*, Springer, Berlin, Germany, 2005.
- [39] C. J. Zhang and H. Oyanagi, in preparation.

## Review Article

# Misfit Strain in Superlattices Controlling the Electron-Lattice Interaction via Microstrain in Active Layers

**Nicola Poccia, Alessandro Ricci, and Antonio Bianconi**

*Department of Physics, University of Rome "La Sapienza", P. le A. Moro 2, 00185 Roma, Italy*

Correspondence should be addressed to Antonio Bianconi, antonio.bianconi@roma1.infn.it

Received 15 October 2009; Revised 27 November 2009; Accepted 3 December 2009

Academic Editor: Dragan Mihailovic

Copyright © 2010 Nicola Poccia et al. This is an open access article distributed under the Creative Commons Attribution License, which permits unrestricted use, distribution, and reproduction in any medium, provided the original work is properly cited.

High-temperature superconductivity (HTS) emerges in quite different electronic materials: cuprates, diborides, and iron-pnictide superconductors. Looking for unity in the diversity we find in all these materials a common lattice architecture: they are practical realizations of heterostructures at atomic limit made of superlattices of metallic active layers intercalated by spacers as predicted in 1993 by one of us. The multilayer architecture is the key feature for the presence of electronic topological transitions where the Fermi surface of one of the subbands changes dimensionality. The superlattice misfit strain  $\eta$  between the active and spacer layers is shown to be a key variable to drive the system to the highest critical temperature  $T_c$  that occurs at a particular point of the 3D phase diagram  $T_c(\delta, \eta)$  where  $\delta$  is the charge transfer or doping. The plots of  $T_c$  as a function of misfit strain at constant charge transfer in cuprates show a first-order quantum critical phase transition where an itinerant striped magnetic phase competes with superconductivity in the proximity of a structural phase transition, that is, associated with an electronic topological transition. The shape resonances in these multigap superconductors is associated with the maximum  $T_c$ .

## 1. Introduction

Enormous efforts have been spent since the discovery of high temperature superconductors (HTSs) in 1986 [1] to grab the physics that drives the macroscopic quantum effects from low to high-temperature. After twenty-three years of investigations the community is now looking for a single mechanism of high  $T_c$  superconductivity emerging in quite different layered systems made of copper oxides ( $\text{CuO}_2$ ) diborides ( $\text{B}_2$ ) and iron pnictides (FeAs) layers, discovered in 1986, 2001, and 2008, respectively. Understanding the lattice effects that control the critical temperature at constant doping is now considered a key point in the search for unity in the diversity among different HTSs [2–5]. The lattice control of the functional electronic properties has been found in colossal magneto-resistance (CMR) manganites and in the field of ultracold Fermi gases where it has been shown that the Bose or BCS condensation can be controlled by making optical lattices. A first common feature in the field of HTS is understanding the material dependent properties that are now considered a key physical term for understanding HTS. A second universal feature is the multicomponent scenario in the verge of phase separation. In

fact in cuprates the polarons [1, 6, 7] and free carriers coexist where the polarons (in the intermediate regime between small and large polarons) span about 8 Cu sites [8] forming a Wigner crystal at 1/8 doping [9, 10] and polaronic 1D charge density waves [11] that coexist with a free correlated Fermi liquid. The coexistence of polarons [12–16] and free carriers in cuprates is now well established. In fact many experiments show the coexistence of the pseudogap and superconductivity. In fact the pseudo gap is related with polaron ordering both in cuprates and in manganites where they are more close to the small polaron limit [17].

A lot of time has been lost looking for HTS in the proximity to a Mott insulating state, but this feature of cuprate superconductors is not shared with both borides and pnictides. On the contrary a common feature is the proximity to a first-order quantum phase transition where two metals [18–20] with comparable energy compete [21]. For example, in the case of cuprates at optimum doping the attention is addressed now toward the competition of a striped magnetic phase (a polaron Wigner crystal at 1/8 doping) with the superconducting phase as it is observed in oxygen doped  $\text{La}_2\text{CuO}_4$  [22].

It is possible that the common first-order quantum phase transition, triggering the HTS phase in cuprates, diborides, and pnictides, occurs where the chemical potential of a multiband system is tuned near a electronic topological transition (ETT) from a 2D (or 1D) metal to a 3D (or 2D) metal in only one of its subbands [23–27]. In fact in these conditions the exchange-like pairing between the different electronic components (polarons, in a narrow band near the electronic critical point, and free carriers) shows a shape resonance or Feshbach resonance [25, 26] that drives up the  $T_c$ .

In this scenario by tuning the chemical potential near a ETT the electronic, magnetic and elastic interactions drive the system near a lattice instability with a large electron-phonon interaction for one electronic portion of the system. In presence of disorder these complex materials systems are expected to show phase separation [28–31] with intrinsic, functional, and connected spatial multiple scales, associated with multiple temporal scales. The source of multiscale phenomena could be the local bonding constraints leading to a framework of coexisting short- and long-range fields and competing orders. In this scenario different experimental techniques probing different spatial and temporal scale provide different landscapes. The orchestrated interplay of several order parameters in these complex materials is believed to be in action with quantum critical fluctuations favouring the entanglement giving a quantum coherence that resists to the decoherence attacks of the high temperature. Several quantum criticalities have been proposed in pnictides [27] and cuprates [28] in a multivariable 3D space where the charge density, a variable determined by lattice effects, and disorder are the main variables driving the system to maximum  $T_c$ .

Billinge and Duxbury [32] have considered the “structural compliance”  $\delta_s$ , the ability of the structure to accommodate two different types of carriers with a different local bond shortening associated with the doped electronic hole. The structural compliance has been defined as  $\delta_s = (r_b - r_f)/r_b$  where  $r_b$  and  $r_f$  are the lengths of the Cu–O bond in the “buckled” and “flat” configurations. The effect of structural compliance on charge ordering in the copper oxygen planes can result in stripe nanostructures. The nonuniform nanoworld of sign varying textures in strain, charge, and magnetization has been investigated also in ferroelastic FE and colossal magnetoresistance CMR materials besides HTS [30, 31]. The central insight is that under doping a nonlinear lattice perturbation can produce intrinsic inhomogeneities that induce multiscale effects for local lattice integrity constraints. The intercell large strain texturing must be supported by intracell deformations, reflected in bond/angle distribution. It has been proposed that in high  $T_c$  cuprates the local bonding constraints and the long-range consequences of strongly anisotropic elasticity lead to coexisting short- and long-range forces which results in specific networks of multiple, connected scales. The elasticity self-consistently orders the polarons (producing strong local lattice distortions) into patterns of filaments and clumps. The strength of the local distortion versus the bulk modulus elasticity determines the scales of structural patterns from nano to micron and could explain

many experimental results in HTS, CMR and FE materials [31]. Several authors agree on the importance to introduce competitive interaction in order to describe the charge, spin, orbital, and energy configurations in different points of the phase diagram in complex functional materials such as HTS [32]. The JT pairing in the lattice gas model proposed by Miranda et al. [33] shows that the effect of Coulomb interactions between layers can stabilize the size of the charge clusters and make the bipolarons mobile. The calculated DOSs show the existence of up to four gaps, whose origin is due to the energy to break each of the four bonds created during the cluster formations. This multigap model suggests a connection between the scenario of several energy gaps and the local inhomogeneities observed in all HTSs systems. There is agreement that the inhomogeneities arise because all HTS are near a first-order transition tuned by the doping and superlattice misfit strain. It has been proved that without the long-range Coulomb repulsion, the system is unstable with respect to the first order phase transition by direct Monte Carlo simulations [34]. We have to remark that all these scenarios agree that HTS is a particular case of multigap superconductivity [35] both for diborides and for iron pnictides [26, 27].

## 2. The Superlattice Misfit Strain in HTS

There is the consensus that the cuprates showing high-temperature superconductivity, are not three-dimensional (3D) cubic perovskites, like  $ABO_3$ , but all HTS cuprates belong to the subclass of layered defective perovskites made of a stack of infinite layers of bcc  $CuO_2$  layers intercalated by different layers playing the role of spacers [36–39]. This is now a well-established common feature of all known HTSs (cuprates, diborides, and iron pnictides): their lattice architecture is made of stacks of active superconducting planes intercalated by spacers or block layers as shown in Figure 1. For example, the hole-doped oxygen-doped layered perovskite family  $La_2CuO_{4+y}$  is made of  $[CuO_2]_{\infty}^{-2+\delta}$  active bcc layers intercalated by rocksalt  $[La_2O_{2+y}]_{\infty}^{+2-\delta}$  spacer fcc layers.

The studies of the variation of the superconducting critical temperature  $T_c$  among cuprates by substitution of cations in the spacers, that have the same valence but different radii, show that their primary effect is a lattice effect which results in dramatic change on  $T_c$ . Therefore there is growing interest on the out-of-plane structural influence (i.e., going on in the spacer layers) that controls the basic intrinsic feature of the electronic structure of  $CuO_2$  plane. In fact the maximum  $T_c$  has been shown to vary widely (by up to a factor of 10) between crystals sharing the same hole density in  $CuO_2$  plane but different structures or ordering of dopants in the spacer layers. Therefore the identification of such an out-of-plane influence may be pivotal to finding a roadmap to higher- $T_c$  superconductors or manipulation of the superconducting state for novel electronic devices. The chemical pressure is a second variable, beyond doping, that has to be considered to drive the system toward the ETT of

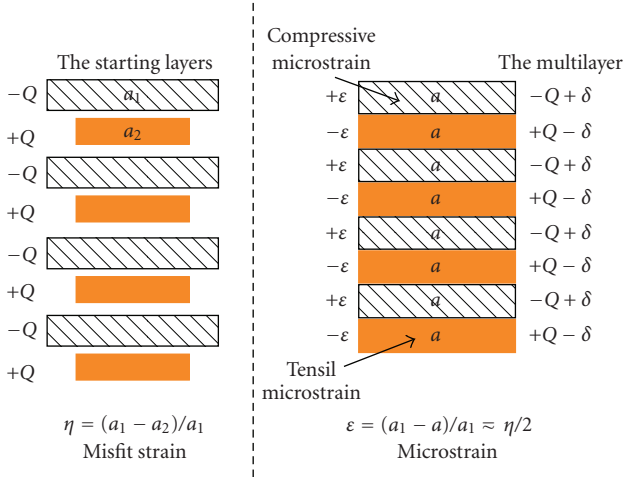


FIGURE 1: Pictorial view of the superlattice with a first layer with a first material characterized by lattice parameter  $a_1$  and a second layer with a second material characterized by a lattice parameter  $a_2$ . The superlattice misfit strain is  $\eta = (a_1 - a_2)/a$  where  $a$  is the mean averaged lattice parameter  $a = (a_1 + a_2)/2$ . The compensated superlattice, showed on the right, has an overall microstrain zero, with  $a$  first layer under compressive microstrain  $\epsilon(a - a_1)/a$  and a second intercalated layer under a tensile microstrain  $(a_2 - a)/a$ . It is therefore easy to show, because of the balance in the compensated superlattice of the microstrain, that the misfit strain is related to microstrain by the following relationship  $\eta = 2\epsilon$ .

one of its components that will trigger the shape resonance for the high  $T_c$  in HTS [25, 26].

In all 3D perovskites  $ABO_3$  and in manganites, it is well established that the phase diagram of the electronic phases depends on the two variables, charge density and chemical pressure. The chemical pressure is described by the tolerance factor [40]. In perovskites the tolerance factor  $t$  has been used to explain the variation of the ratio  $c/a$  in the  $K_2NiF_4$  structure at very large dopings; in fact for a  $t > 1$  the atomic displacements parallel to the  $c$  axis induce an increase of the  $c$  lattice parameter to relieve the compressive stress [41]. For La124 cuprate perovskites with  $K_2NiF_4$  structure it has been proposed that the tolerance factor drives the system in a regime of quantum critical magnetic fluctuations [42].

Since HTS superconductors are superlattices of metallic layers, the appropriate physical variable describing elastic effects is not the tolerance factor for 3D  $ABO_3$  systems but the superlattice misfit strain between the different layers [43, 44]. Therefore for the layered superconducting perovskites made of a superlattice of  $CuO_2$  layers separated by multiple complex spacer layers the relevant physical quantity is the misfit strain between the  $CuO_2$  active and the spacer layers. For layered high- $T_c$  superconductors, the superlattice misfit strain should be considered as important as the doping as it was first pointed out first for cuprates [45–48], after for the diborides [49], and finally for pnictides [50].

In cuprates it has not been trivial to introduce the measure of the superlattice misfit strain for because the spacer layers are made of complex different materials with

multiple cations having largely different coordination numbers. The measure of the superlattice misfit strain [45] and its introduction in the cuprate phase diagram besides doping and temperature has allowed to quantify the lattice effects in HTS. Increasing the value of the misfit strain above a critical value the systems are driven to a structural phase transition. High  $T_c$  occurs at low misfit strain but large disorder, dislocations, lattice stripes, and incommensurate lattice modulations appear approaching the structural phase transitions. As we show in Figure 1 the superlattice misfit strain is defined as  $\eta = (a_1 - a_2)/a$ , where  $a_1$  and  $a_2$  are the unit cell parameters of the ideal first and second layers, respectively, when they are well separated, and  $a = (a_1 + a_2)/2$ . In the compensated multilayer the first layers of the superlattice exhibit a compressive microstrain  $\epsilon_{1c} = (a_1 - a)/a$  and the second layers a tensile microstrain  $\epsilon_{2t} = (a - a_2)/a$ . The average strain is zero in the compensated superlattice, approximating the elastic constants in the active and the intercalated layers as equal,  $\epsilon = \epsilon_{1c} = \epsilon_{2t}$ , and the lattice parameter of the superlattice is close to  $(a_1 + a_2)/2$ . The microstrain can be obtained by measuring the lattice parameter of the superlattice,  $a$ , by knowing the unrelaxed ideal lattice parameter of only one of the two layers. The superlattice misfit strain will be given by  $\eta = \epsilon_{1c} + \epsilon_{2t} = 2\epsilon$  as it was proposed in [45].

Therefore the problem has been solved for cuprates by obtaining the misfit strain from the measure of the compressive microstrain  $\epsilon = (R_0 - r)/r$  in the  $CuO_2$  plane (that has the same absolute value as the tensile microstrain in the intercalated layers). The determination of the value of the equilibrium  $Cu-O$  distance for a  $Cu^{2+}$  ion with square planar coordination has been solved using the value  $R_0 = 197$  pm of the  $Cu^{2+}$  ion in water solution measured by EXAFS. The superlattice misfit strain measuring the elastic field acting on the active and intercalated layers of a superlattice can be therefore obtained by measuring the microstrain in the active layer [45–50].

The microstrain is changed in cuprates and in diborides by chemical substitution of ions with different ionic radii in the spacer layers. The internal chemical pressure acts as a complex anisotropic stress tensor that produces a compressive microstrain of the bcc  $CuO_2$  layer in cuprates and a tensile microstrain of the graphene-like B layer in magnesium diborides and of the Fe layers in pnictides.

A strong support for the misfit strain scenario is the behaviour of the spin-gap energy for several different cuprates at constant doping such as  $La_{2-x}Sr_xCuO_4$  ( $x = 0.16$ ) (LSCO)  $YBa_2Cu_3O_{6.85}$  (YBCO),  $Bi_2Sr_2CaCu_2O_{8+y}$  (BSCO), and for  $La_{2-x}Sr_xCuO_4$  (LBCO) as shown in Figure 2 [47]. The experimental results show a correlation between magnetic excitations and misfit strain at constant doping  $1/8$ . The cuprates at constant  $1/8$  doping show a bicritical point at a critical misfit strain  $\eta_c$  between the superconducting and a static magnetic order. Increasing further the misfit strain the system goes to the structural phase transition from the  $T$  to  $T'$  phase. This trend makes clear that the dynamical magnetic excitations show the typical behaviour in the proximity of a critical point of a quantum phase transition. The high  $T_c$  superconductivity occurs in the region of a quantum

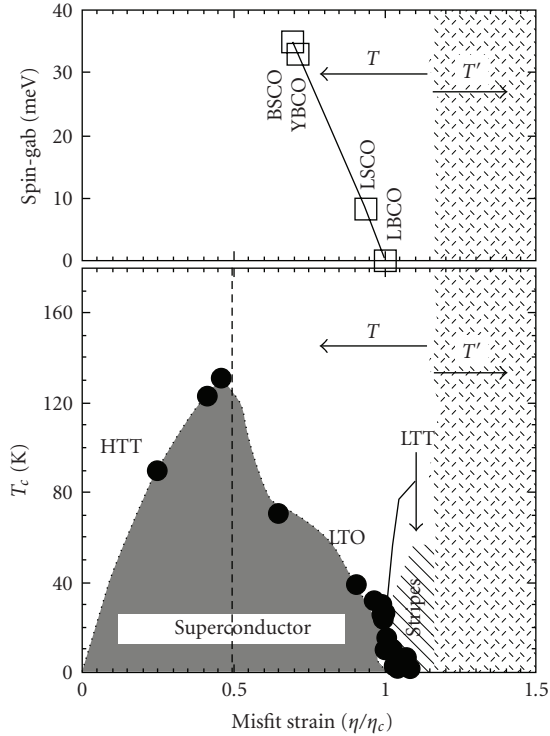


FIGURE 2: Lower panel: spin-gap energy as a function of misfit strain  $\eta/\eta_c$ , normalized to the critical values of the 1/8 phase, in different superconducting cuprates at optimum doping. Upper panel: the superconducting critical temperature as a function of the misfit strain at constant doping (1/8) and the Wigner polaron crystal in Nd doped La214 cuprate perovskites. The structural transition from  $T \rightarrow T'$  at high misfit strain is indicated.

paramagnetism near the onset of quantum fluctuation as shown in Figure 3.

The proposed 3D phase diagram  $T_c(\eta, \delta)$  of cuprates [45–48] in Figure 4 shows different regions of phase separation. The phase separation in the range of optimum doping has been reproduced in a recent work by a theoretical two band model [51, 52]. The phase with “more itinerant” electrons appears at small misfit strain, and the “more localized” and more ordered phase arises at high misfit strain. At doping 1/8 and at a critical misfit strain  $\eta_c$  a polaron Wigner crystal has been identified where the spin gap goes to zero and a static magnetic order appears [9, 10]. The stripe fluctuations in space and time and the phase-separated state appears in the proximity of the Wigner crystal and it is possible to move away from it changing the doping or the misfit strain or both.

A strong support to the key role of the misfit-strain variable besides doping and disorder for the phase diagram of HTS comes recently from many experimental results in superconducting pnictides [53]. Recently Cruz et al. [54] have provided support for the key role of misfit strain changing the crystal lattice structure without changing charge carrier density by isoelectronic substitution in undoped  $\text{CeFeAs}_{1-x}\text{P}_x\text{O}$ . The results show that decreasing the iron-iron distance the system shows a magnetic quantum

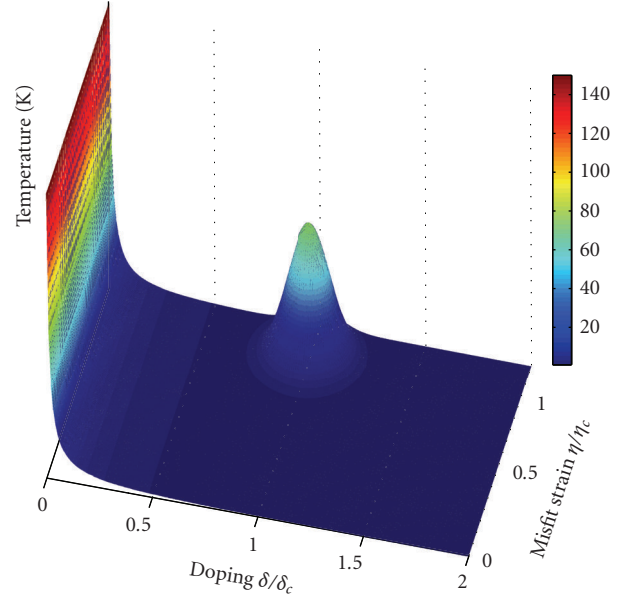


FIGURE 3: The magnetic phase diagram of cuprates:  $T_c$ , doping  $\delta$  and misfit strain  $\eta$ . The misfit strain  $\eta$  (i.e., microstrain or internal chemical pressure) and the doping  $\delta$  are normalized to the critical values of the 1/8 phase ( $\delta_c, \eta_c$ ), where the commensurate magnetic stripe phase occurs at  $\delta$  doping of 1/8 hole for Cu site and misfit strain 7%. Therefore the Aeppli-Bianconi critical point is near the point (1, 1) in the 2D space.

critical point where the striped antiferromagnetic order and orthorhombic distortions are suppressed. The work offers additional support for the role of the second axis besides electronic doping in the description of HTS phase diagram. The authors suggest that the pnictogen height in iron arsenide is the important controlling parameter for the electronic and magnetic properties; however it is worth to notice that increasing compressive (tensile) microstrain the As ions are pushed up (down) along the  $c$ -axis, and therefore the measure of the displacement of the As ion is an indirect measure of the misfit-strain in pnictides.

The misfit-strain can be used to cross a quantum critical point going near the striped phase without the influence of charge carrier doping. It is worth to note that is the same quantum critical state pointed out in cuprates at doping 1/8 and misfit strain 7% that is shown in Figure 3 [55–57]. Here a first-order quantum critical point occurs where an itinerant striped magnetic phase and superconductivity, in the proximity of a structural phase transition, compete.

In pnictides we have shown that electron-doped FeAs layers have a tensile microstrain due to the misfit strain between the active layers and the spacers. We have identified the critical range of doping and microstrain where the critical temperature gets amplified to its maximum value in Figure 5. The equilibrium Fe–Fe distance in the FeAs layers has been found by investigating a set of materials where the intercalated ions in spacer layer have the same charge and plotting the microstrain as a function of ionic radius in the spacer layers. The Fe–Fe distance decreases with the ionic

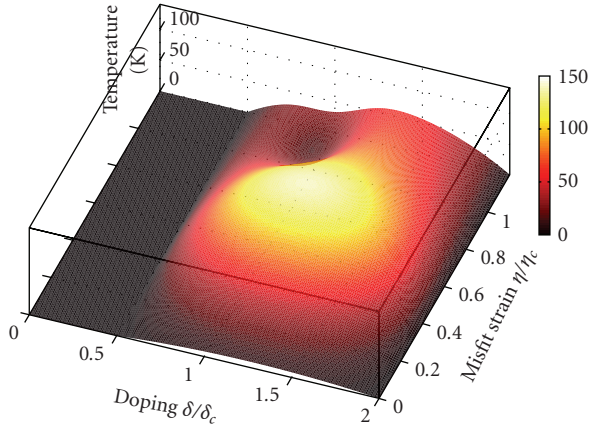


FIGURE 4: 3D universal phase diagram of the superconducting critical temperature of cuprates. The values of color plot of the superconducting transition temperature  $T_c$  go from 0 (black) to 135 K (white). The misfit strain  $\eta$  (i.e., microstrain or internal chemical pressure) and the doping  $\delta$  are normalized to the critical values of the 1/8 phase ( $\delta_c, \eta_c$ ); therefore the critical point is at (1, 1) where the superconducting critical temperature goes to zero (black). The maximum of the critical temperature occurs at (1.4, 0.5), that is, at doping 0.16 and misfit strain 0.35.

radius in the spacers but below a critical radius of the ions in the spacers they do not introduce any variation of the Fe–Fe distance in the FeAs layer. We have therefore taken the value of the Fe–Fe distance in this regime as the unstrained distances for the Fe ions  $R_0^{-1} = 276.35$  pm in the  $[\text{FeAs}]_{\infty}^{-1}$  layer. The microstrain of the  $[\text{FeAs}]_{\infty}^{-1}$  layers can therefore be easily measured. In fact these layers are made of edge sharing  $\text{FeAs}_4$  tetrahedral units; therefore the misfit strain induces mainly a rotation of the bonds pushing the As–Fe–As bond out of the ideal value of the tetrahedral angle  $109.28^\circ$ , where the ideal lattice parameter of the orthorhombic lattice is  $a_o = \sqrt{2}a_T = 552.7$  pm.

The phase diagrams for “122” and “1111” pnictides show that the maximum  $T_c$  occurs in the shaded area of doping and misfit strain shown in Figure 1.

The difference between the region of high  $T_c$  in “1111” and “122” systems in the misfit-strain doping space is determined by the fact that the two systems are superlattices of quantum wells with very different electronic potential barriers in the spacer layers for itinerant electrons in the active layers.

### 3. Conclusion

We have discussed the superlattice misfit strain as a key material dependent parameter besides doping and temperature for the phase diagram of HTS materials. We have proposed the superlattice misfit strain as the key parameter controlling the elastic field effects in the system that allow to describe the HTS phase diagram for cuprates, magnesium diborides, and iron arsenides. These systems are driven to the point of maximum  $T_c$  by all or one of the key variables doping, disorder and misfit strain.

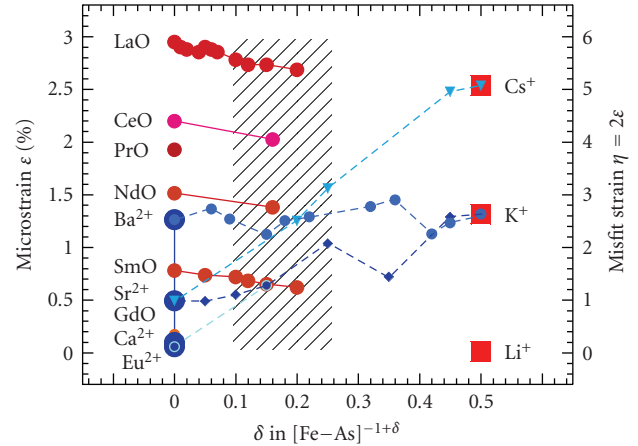


FIGURE 5: The microstrain  $\epsilon$  (proportional to the Fe–Fe distance) and the misfit strain  $\eta = 2\epsilon$  are plotted as a function of the doping for the “122” family and for the “1111” family of high-temperature superconducting FeAs compounds. The highlighted area is the region where the maximum  $T_c$  occurs.

In hole-doped superconductors the compressive strain in the  $\text{CuO}_2$  plane is related with the tensile RE–O microstrain on the rocksalt spacer layer. The different lattice misfit between the building blocks of the different perovskites induces a microstrain on the  $\text{CuO}_2$  lattice forming short range dynamic lattice stripes with a modulated Cu–O distance in the plane in the range of misfit strain  $0.5 < \eta_c < 1$ . Electron-doped cuprates and iron arsenides show a tensile microstrain exerted on the  $\text{CuO}_2$  or FeAs plane and a compressive microstrain on the fluorite spacer layers.

Finally the misfit strain provides a new insight in the complex physics of the HTS systems. A deep understanding of this point will help to material design of new high  $T_c$  superconductors [23, 37] with fascinating and exotic properties for novel technological applications.

### References

- [1] J. G. Bednorz and K. A. Müller, “Perovskite-type oxides—the new approach to high- $T_c$  superconductivity,” *Reviews of Modern Physics*, vol. 60, no. 3, pp. 585–600, 1988.
- [2] S. A. Kivelson and H. Yao, “Iron-based superconductors: unity or diversity?” *Nature Materials*, vol. 7, no. 12, pp. 927–928, 2008.
- [3] J. Zaanen, “Condensed-matter physics: the pnictide code,” *Nature*, vol. 457, no. 7229, pp. 546–547, 2009.
- [4] A. Bianconi, N. Poccia, and A. Ricci, “Unity in the diversity,” *Journal of Superconductivity and Novel Magnetism*, vol. 22, no. 6, pp. 527–528, 2009.
- [5] J. Annett, F. Kusmartsev, and A. Bianconi, “Anisotropic and multiband pairing: from borides to multicomponent superconductivity,” *Superconductor Science and Technology*, vol. 22, no. 1, Article ID 010301, 2009.
- [6] A. S. Alexandrov, J. Ranninger, and S. Robaszkiewicz, “Bipolaronic superconductivity: thermodynamics, magnetic properties, and possibility of existence in real substances,” *Physical Review B*, vol. 33, no. 7, pp. 4526–4542, 1986.

- [7] A. S. Alexandrov and A. B. Krebs, "Polarons in high-temperature superconductors," *Soviet Physics Uspekhi*, vol. 35, no. 5, pp. 345–383, 1992.
- [8] A. Bianconi, M. Missori, H. Oyanagi, et al., "The measurement of the polaron size in the metallic phase of cuprate superconductors," *Europhysics Letters*, vol. 31, no. 7, pp. 411–415, 1995.
- [9] A. Bianconi and M. Missori, "The instability of a 2D electron gas near the critical density for a Wigner polaron crystal giving the quantum state of cuprate superconductors," *Solid State Communications*, vol. 91, no. 4, pp. 287–293, 1994.
- [10] A. Bianconi, "On the Fermi liquid coupled with a generalized wigner polaronic CDW giving high  $T_c$  superconductivity," *Solid State Communications*, vol. 91, no. 1, pp. 1–5, 1994.
- [11] A. Bianconi, N. L. Saini, A. Lanzara, et al., "Determination of the local lattice distortions in the  $\text{CuO}_2$  plane of  $\text{La}_{1.85}\text{Sr}_{0.15}\text{CuO}_4$ ," *Physical Review Letters*, vol. 76, no. 18, pp. 3412–3415, 1996.
- [12] A. S. Alexandrov and N. F. Mott, *Polarons and Bipolarons*, World Scientific, Singapore, 1996.
- [13] A. Lanzara, G.-M. Zhao, N. L. Saini, et al., "Oxygen-isotope shift of the charge-stripe ordering temperature in  $\text{La}_{2-x}\text{Sr}_x\text{CuO}_4$  from X-ray absorption spectroscopy," *Journal of Physics: Condensed Matter*, vol. 11, no. 48, pp. L541–L546, 1999.
- [14] D. Mihailovic, T. Mertelj, and K. A. Müller, " $a$ - $b$  plane optical conductivity in  $\text{YBa}_2\text{Cu}_3\text{O}_{7-\delta}$  above and below  $T^*$ ," *Physical Review B*, vol. 57, no. 10, pp. 6116–6120, 1998.
- [15] A. S. Alexandrov, "Polaron dynamics and bipolaron condensation in cuprates," *Physical Review B*, vol. 61, no. 18, pp. 12315–12327, 2000.
- [16] A. Bussmann-Holder and H. Keller, "Polaron formation as origin of unconventional isotope effects in cuprate superconductors," *European Physical Journal B*, vol. 44, no. 4, pp. 487–490, 2005.
- [17] A. Lanzara, N. L. Saini, M. Brunelli, et al., "Crossover from large to small polarons across the metal-insulator transition in manganites," *Physical Review Letters*, vol. 81, no. 4, pp. 878–881, 1998.
- [18] R. B. Laughlin, G. G. Lonzarich, P. Monthoux, and D. Pines, "The quantum criticality conundrum," *Advances in Physics*, vol. 50, no. 4, pp. 361–365, 2001.
- [19] P. Coleman and A. J. Schofield, "Quantum criticality," *Nature*, vol. 433, no. 7023, pp. 226–229, 2005.
- [20] P. Goswami, D. Schwab, and S. Chakravarty, "Rounding by disorder of first-order quantum phase transitions: emergence of quantum critical points," *Physical Review Letters*, vol. 100, no. 1, Article ID 015703, 4 pages, 2008.
- [21] C. Castellani, C. Di Castro, and M. Grilli, "Stripe formation: a quantum critical point for cuprate superconductors," *Journal of Physics and Chemistry of Solids*, vol. 59, no. 10–12, pp. 1694–1698, 1998.
- [22] S. A. Kivelson, G. Aeppli, and V. J. Emery, "Thermodynamics of the interplay between magnetism and high-temperature superconductivity," *Proceedings of the National Academy of Sciences of the United States of America*, vol. 98, no. 21, pp. 11903–11907, 2001.
- [23] A. Bianconi, "Process of increasing the critical temperature  $T_c$  of a bulk superconductor by making metal heterostructures at the atomic limit," United State Patent no. :US6, 265, 019 B1, July 2001.
- [24] A. Bianconi, N. L. Saini, T. Rossetti, et al., "Stripe structure in the  $\text{CuO}_2$  plane of perovskite superconductors," *Physical Review B*, vol. 54, no. 17, pp. 12018–12021, 1996.
- [25] A. Bianconi, A. Valletta, A. Perali, and N. L. Saini, "Superconductivity of a striped phase at the atomic limit," *Physica C*, vol. 296, no. 3–4, pp. 269–280, 1998.
- [26] A. Bianconi, "Feshbach shape resonance in multiband superconductivity in heterostructures," *Journal of Superconductivity*, vol. 18, no. 5–6, pp. 25–36, 2005.
- [27] R. Caivano, M. Fratini, N. Poccia, et al., "Feshbach resonance and mesoscopic phase separation near a quantum critical point in multiband FeAs-based superconductors," *Superconductor Science and Technology*, vol. 22, no. 1, Article ID 014004, 12 pages, 2009.
- [28] A. R. Bishop, "HTC oxides: a collusion of spin, charge and lattice," *Journal of Physics: Conference Series*, vol. 108, no. 1, Article ID 012027, 8 pages, 2008.
- [29] A. R. Bishop, T. Lookman, A. Saxena, and S. R. Shenoy, "Elasticity-driven nanoscale texturing in complex electronic materials," *Europhysics Letters*, vol. 63, no. 2, pp. 289–295, 2003.
- [30] K. H. Ahn, T. Lookman, and A. R. Bishop, "Strain-induced metal-insulator phase coexistence in perovskite manganites," *Nature*, vol. 428, no. 6981, pp. 401–404, 2004.
- [31] T. Lookman, S. R. Shenoy, K. Ø. Rasmussen, A. Saxena, and A. R. Bishop, "Ferroelastic dynamics and strain compatibility," *Physical Review B*, vol. 67, no. 2, Article ID 0241142, 27 pages, 2003.
- [32] S. J. L. Billinge and P. M. Duxbury, "Structural compliance, misfit strain, and stripe nanostructures in cuprate superconductors," *Physical Review B*, vol. 66, no. 6, Article ID 064529, 4 pages, 2002.
- [33] J. Miranda, T. Mertelj, V. V. Kabanov, and D. Mihailovic, "Bipolaron Jahn-Teller pairing and charge transport in cuprates," *Journal of Superconductivity and Novel Magnetism*, vol. 22, no. 3, pp. 281–285, 2009.
- [34] T. Mertelj, V. V. Kabanov, J. M. Mena, and D. Mihailovic, "Self-organization of charged particles on a two-dimensional lattice subject to anisotropic Jahn-Teller-type interaction and three-dimensional Coulomb repulsion," *Physical Review B*, vol. 76, no. 5, Article ID 054523, 9 pages, 2007.
- [35] N. Kristoffel, P. Rubin, and T. Örd, "Multiband model of cuprate superconductivity," *International Journal of Modern Physics B*, vol. 22, no. 30, pp. 5299–5327, 2008.
- [36] Y. Tokura and T. Arima, "New classification method for layered copper oxide compounds and its application to design of new high  $T_c$  superconductors," *Japanese Journal of Applied Physics*, vol. 29, no. 11, pp. 2388–2402, 1990.
- [37] A. Bianconi, "On the possibility of new high  $T_c$  superconductors by producing metal heterostructures as in the cuprate perovskites," *Solid State Communications*, vol. 89, no. 11, pp. 933–936, 1994.
- [38] C. N. R. Rao and A. K. Ganguli, "Structure-property relationships in superconducting cuprates," *Chemical Society Reviews*, vol. 24, no. 1, pp. 1–7, 1995.
- [39] K. A. Müller, "On the superconductivity in hole doped cuprates," *Journal of Physics: Condensed Matter*, vol. 19, no. 25, Article ID 251002, 13 pages, 2007.
- [40] C. Li, K. C. K. Soh, and P. Wu, "Formability of  $\text{ABO}_3$  perovskites," *Journal of Alloys and Compounds*, vol. 372, no. 1–2, pp. 40–48, 2004.
- [41] K. K. Singh, P. P. Edwards, and J. B. Goodenough, "Effect of percolation in an intergrowth structure," *Journal of Physics: Condensed Matter*, vol. 3, no. 15, pp. 2479–2497, 1991.
- [42] G. Aeppli, T. E. Mason, S. M. Hayden, H. A. Mook, and J. Kulda, "Nearly similar magnetic fluctuations in the normal

- state of a high- $T_c$  cuprate superconductor,” *Science*, vol. 278, no. 5342, pp. 1432–1435, 1997.
- [43] G. Forgacs, R. Lipowsky, and T. M. Nieuwenhuizen, “The behaviour of the interfaces in ordered and disordered system,” in *Phase Transitions and Critical Phenomena*, C. Domb and J. L. Lebowitz, Eds., vol. 14, pp. 135–367, Academic Press, London, UK, 1991.
- [44] P. Bak, “Commensurate phases, incommensurate phases and the devil’s staircase,” *Reports on Progress in Physics*, vol. 45, no. 6, pp. 587–629, 1982.
- [45] A. Bianconi, G. Bianconi, S. Caprara, D. Di Castro, H. Oyanagi, and N. L. Saini, “The stripe critical point for cuprates,” *Journal of Physics: Condensed Matter*, vol. 12, no. 50, pp. 10655–10666, 2000.
- [46] S. Agrestini, N. L. Saini, G. Bianconi, and A. Bianconi, “The strain of  $\text{CuO}_2$  lattice: the second variable for the phase diagram of cuprate perovskites,” *Journal of Physics A*, vol. 36, no. 35, pp. 9133–9142, 2003.
- [47] M. Fratini, N. Poccia, and A. Bianconi, “The Feshbach resonance and nanoscale phase separation in a polaron liquid near the quantum critical point for a polaron Wigner crystal,” *Journal of Physics: Conference Series*, vol. 108, no. 1, Article ID 012036, 13 pages, 2008.
- [48] N. Poccia and M. Fratini, “The misfit strain critical point in the 3D phase diagrams of cuprates,” *Journal of Superconductivity and Novel Magnetism*, vol. 22, no. 3, pp. 299–303, 2009.
- [49] S. Agrestini, D. Di Castro, M. Sansone, et al., “High  $T_c$  superconductivity in a critical range of micro-strain and charge density in diborides,” *Journal of Physics: Condensed Matter*, vol. 13, no. 50, pp. 11689–11695, 2001.
- [50] A. Ricci, N. Poccia, G. Ciasca, M. Fratini, and A. Bianconi, “The microstrain-doping phase diagram of the iron pnictides: heterostructures at atomic limit,” *Journal of Superconductivity and Novel Magnetism*, vol. 22, no. 6, pp. 589–593, 2009.
- [51] K. I. Kugel, A. L. Rakhmanov, A. O. Sboychakov, F. V. Kusmartsev, N. Poccia, and A. Bianconi, “A two-band model for the phase separation induced by the chemical mismatch pressure in different cuprate superconductors,” *Superconductor Science and Technology*, vol. 22, no. 1, Article ID 014007, 7 pages, 2009.
- [52] K. I. Kugel, A. L. Rakhmanov, A. O. Sboychakov, N. Poccia, and A. Bianconi, “Model for phase separation controlled by doping and the internal chemical pressure in different cuprate superconductors,” *Physical Review B*, vol. 78, no. 16, Article ID 165124, 7 pages, 2008.
- [53] M. Fratini, R. Caivano, A. Puri, et al., “The effect of internal pressure on the tetragonal to monoclinic structural phase transition in  $\text{ReOFeAs}$ : the case of  $\text{NdOFeAs}$ ,” *Superconductor Science and Technology*, vol. 21, no. 9, Article ID 092002, 4 pages, 2008.
- [54] C. de la Cruz, W. Z. Hu, S. Li, et al., “Lattice distortion and magnetic quantum phase transition in  $\text{CeFeAs}_{1-x}\text{P}_x\text{O}$ ,” *Physical Review Letters*, vol. 104, Article ID 017204, 4 pages, 2010.
- [55] A. Bianconi, N. L. Saini, S. Agrestini, D. Di Castro, and G. Bianconi, “The strain quantum critical point for superstripes in the phase diagram of all cuprate perovskites,” *International Journal of Modern Physics B*, vol. 14, no. 29–31, pp. 3342–3355, 2000, <http://dx.doi.org/doi:10.1142/S0217979200003812>.
- [56] A. Bianconi, S. Agrestini, G. Bianconi, D. Di Castro, and N. L. Saini, “A quantum phase transition driven by the electron lattice interaction gives high  $t_c$  superconductivity,” *Journal of Alloys and Compounds*, vol. 317–318, no. 1–2, pp. 537–541, 2001, [http://dx.doi.org/10.1016/S0925-8388\(00\)01383-9](http://dx.doi.org/10.1016/S0925-8388(00)01383-9).
- [57] D. Di Castro, M. Colapietro, G. Bianconi, “Metallic stripes in oxygen doped  $\text{l2cuo4}$ ,” *Int. J. Mod. Phys.*, vol. 14, no. 29/31, pp. 3438–3443, 2000, <http://dx.doi.org/doi:10.1142/S0217979200003927>.

## Review Article

# Giant Electron-Phonon Anomaly in Doped $\text{La}_2\text{CuO}_4$ and Other Cuprates

**D. Reznik**<sup>1,2</sup>

<sup>1</sup>*Karlsruher Institut für Technologie (KIT), Institut für Festkörperphysik, Postfach 3640, D-76121 Karlsruhe, Germany*

<sup>2</sup>*Department of Physics, University of Colorado, Boulder, Colorado 80309, USA*

Correspondence should be addressed to D. Reznik, dmitry.reznik@colorado.edu

Received 1 July 2009; Accepted 24 September 2009

Academic Editor: Dragan Mihailovic

Copyright © 2010 D. Reznik. This is an open access article distributed under the Creative Commons Attribution License, which permits unrestricted use, distribution, and reproduction in any medium, provided the original work is properly cited.

Since conventional superconductivity is mediated by phonons, their role in the mechanism of high temperature superconductivity has been considered very early after the discovery of the cuprates. The initial consensus was that phonons could not produce transition temperatures near 100 K, and the main direction of research focused on nonphononic mechanisms. Subsequent work last reviewed by L. Pintschovius in 2005 showed that electron-phonon coupling in the cuprates is surprisingly strong for some phonons and its role is controversial. Experiments performed since then identified anomalous behavior of certain Cu–O bond-stretching phonons in cuprates as an important phenomenon that is somehow related to the mechanism of superconductivity. A particularly big advance was made in the study of doped  $\text{La}_2\text{CuO}_4$ . This work is reviewed here.

## 1. Introduction

In most cases superconductivity is mediated by phonons and the transition temperature  $T_c$  scales with the strength of electron-phonon coupling. In conventional superconductors with relatively high  $T_c$ s ( $>10$  K), it is often possible to identify specific modes exceptionally strongly coupled to electrons. Such phonons are softer and broader than expected from lattice-dynamical models. Knowing what these modes are makes it possible to influence  $T_c$  by variations in chemical compositions, pressure or other parameters. For a long time inelastic neutron scattering (INS) has been the only technique allowing their direct measurements throughout the Brillouin zone. In recent years high resolution inelastic X-ray scattering (IXS) emerged as an alternative technique with some advantages and disadvantages versus INS.

Shortly after the discovery of the high  $T_c$  cuprates, extensive effort focused on looking for effects of strong electron-phonon coupling. This task proved a lot more challenging than in conventional superconductors, because due to the large unit cell, the cuprates have many phonon branches. In addition, most soft phonons in conventional superconductors appear in acoustic branches at low energies (with a notable exception of  $\text{MgB}_2$ ), whereas we now know

that such phonons in the cuprates are at much higher energies and belong to optic branches. Furthermore, unlike in conventional superconductors, standard theory could not predict soft phonon behavior in the cuprates, so the identification of these modes had to be done by “blind search”. Another obstacle was that mapping phonon dispersions by neutron scattering requires large single crystals, which became available years after the initial discoveries of some cuprates and are still not available for others. The field received an important boost after the development of IXS [1]. It allows measurements of very small samples greatly increasing the range of materials that can be studied. Compared to neutron scattering it has a superior wavevector resolution and a superior energy resolution at large energy transfers. Some of its main drawbacks are scarcity of beam-time, lower resolution at low energies than INS, Lorentzian resolution function (versus Gaussian for INS), and weak intensities of high energy phonons in some materials. In the study of cuprates INS and IXS are used as complementary techniques. In recent years they provided important new insights reviewed here.

In order to establish proper context, I will begin by reviewing some old and new results on conventional systems. Most of the article will focus on the giant bond-stretching

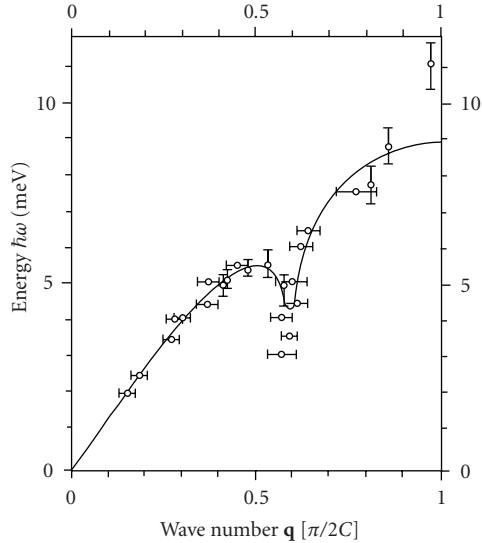


FIGURE 1: Longitudinal acoustic phonon branch of  $\text{K}_2\text{Pt}(\text{CN})_4\text{Br}_{0.30}\cdot 3\text{D}_2\text{O}$  in the [001] direction at room temperature. Solid line represents the result of a calculation based on the simple free-electron model as discussed in [3].

phonon anomaly in  $\text{La}_2\text{CuO}_4$ -based family of the high  $T_c$  cuprates where most progress has been made in the last few years. Finally, I will present recent results for other cuprates to demonstrate that this phonon effect is not limited to doped  $\text{La}_2\text{CuO}_4$ .

## 2. Electron-Phonon Coupling in Conventional Metals

**2.1. General Considerations.** Electron-phonon coupling typically enters theoretical frameworks as a cross section (matrix element) for scattering of a single valence electron by a single phonon. Unfortunately there is no experimental technique allowing direct measurements of this scattering cross section. The best one can do is to measure either spectral functions of specific phonons by INS and IXS or to measure electronic Green's functions by angle resolved photoemission (ARPES). The phonon spectral functions are influenced by scattering of a specific phonon by all electrons (electronic contribution to the phonon self-energy), whereas the electronic Green's function includes scattering of a specific electronic state by all phonons (phonon contribution to the electronic self-energy).

This review focuses on INS and IXS measurements of phonon spectral functions. Phonons couple to electronic polarizability, that is, the two-particle electronic response. Usually the electron-phonon coupling is weak and there are no singularities in the electronic response close to the phonon energy and wavevector. In this case the phonon spectral function is that of a damped harmonic oscillator. In the limit of weak damping it is close to a Lorentzian centered at the phonon frequency whose linewidth is proportional to the inverse phonon lifetime.

Electron-phonon scattering renormalizes the phonon frequency and reduces the lifetime (real/imaginary parts of

the phonon self-energy). The amount of this renormalization depends on the phase-space available for the scattering of electrons by the phonon as well as on the cross section (matrix element) for each of these electron-phonon scattering processes.

Isolating this electronic contribution requires knowledge of frequencies and linewidths in the absence of electron-phonon coupling, since anharmonicity, inhomogeneity, and impurities may have the same effect as electron-phonon coupling. Determining these accurately is typically a challenge. In fact even defining the real part of the phonon self-energy, is not at all straightforward (see Section 2.3). Thus very precise measurements of phonon frequencies and linewidths do not, in a general case, provide direct information on electron-phonon coupling. There are, however, special cases, where one can be fairly certain of the role of the electronic contribution to the phonon self-energy.

**2.2. Kohn Anomalies.** The simplest way to model phonons is by balls-and-springs models with the atomic nuclei serving as balls and the Coulomb forces screened by the electrons as springs. Shell models are more sophisticated modifications of this approach. Including only short-range interactions gives smooth phonon dispersions. Such models can be fit to the experimental dispersions that do not contain any sharp dips. In metals with Fermi surfaces, phonons may couple to singularities in the electronic density of states, which appear at specific wavevectors. These singularities can produce sharp features in phonon dispersions called Kohn anomalies [2]. These typically become stronger with reduced temperature, due to the sharpening of the Fermi surface. A classic example of this behavior is one-dimensional conductors such as  $\text{K}_2\text{Pt}(\text{CN})_4\text{Br}_{0.30}\cdot 3\text{D}_2\text{O}$  (KCP) (Figure 1) [3]. Due to the one-dimensionality of its electronic states, these systems are characterized by Fermi surface nesting at  $2\mathbf{k}_f$  ( $\mathbf{k}_f$  is Fermi momentum). This nesting greatly enhances the number of possible electronic transitions at  $2\mathbf{k}_f$  compared to other wavevectors, which results in softer and broader phonons. For this reason acoustic phonons in KCP show pronounced dips at  $\mathbf{q} = 2\mathbf{k}_f$  ( $\mathbf{Q}$  is the total wavevector,  $\mathbf{q}$  is reduced wavevector).

The amount of this phonon softening and broadening depends on the details of the interaction and varies greatly between different systems with Kohn anomalies. Often the broadening is much smaller than the experimental resolution, thus only the softening appears in the experiment.

**2.3. ab-Initio Calculations and the Role of the  $q$ -Dependence of the Electron-Phonon Matrix Element.** It was noticed early on that Fermi surface shape alone cannot adequately explain phonon softening resembling Kohn anomalies in many cases. For example dispersions of certain phonons in NbC and TaC dip relatively sharply and strongly at wavevectors where the FS nesting is relatively weak [4, 5] (Figure 2). These could be modeled by very long-range repulsive interactions or by adding an extra shell with attractive interactions [5]. Sinha and Harmon [6] introduced  $\mathbf{q}$ -dependent electron-phonon coupling to explain these effects. They included  $\mathbf{q}$ -dependent

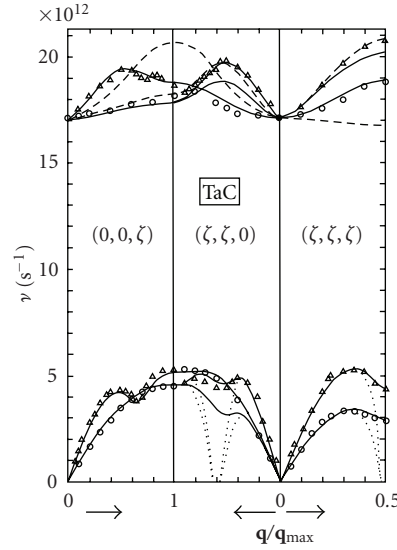


FIGURE 2: Phonon dispersions of TaC (data points) [4] and calculations based on the double-shell model of W. Weber [5].

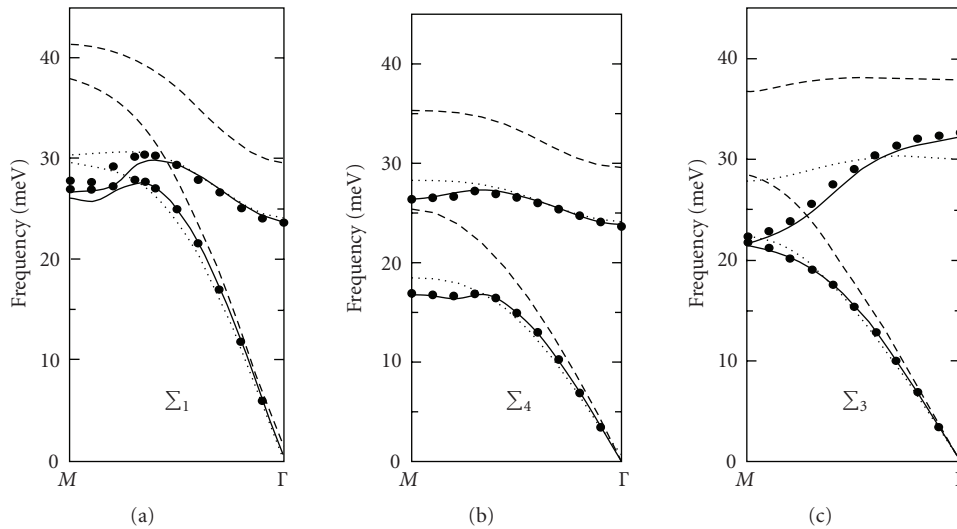


FIGURE 3: Phonon dispersions in Ru (from [8]). The data points correspond to experimental results. The solid lines represent results of the full DFT/LDA calculation. The Dotted lines were obtained by replacing  $\mathbf{q}$ -dependent electron-phonon matrix element with the average value (which was  $\mathbf{q}$ -independent). The dashed lines represent the DFT calculation without including the conduction electrons. Disappearance of the phonon softening near the M-point upon exclusion of conduction electrons demonstrates that the dip results from electron-phonon coupling.

dielectric screening into their model and obtained good agreement with experiment for certain values of adjustable parameters.

Further theoretical development led to ab-initio calculations based on the density functional theory (DFT). These can very accurately predict phonon dispersions and linewidths in many systems without adjustable parameters [7]. However, it is very difficult to isolate contributions of specific electronic states to the phonon self-energy using this approach.

Heid et al. made an attempt to overcome this problem in Ru [8]. First they performed both the ab-initio

DFT calculations and detailed measurements on a high quality single crystal. Phonons in Ru soften strongly near the M-point, which was well reproduced by theory. The calculated softening became much weaker when electron-phonon coupling was made  $\mathbf{q}$ -independent (Figure 3). This result indicated that both the Fermi surface nesting and the  $\mathbf{q}$ -dependence of electron-phonon matrix element were important (the latter more than the former). The phonon softening disappeared entirely upon exclusion of conduction electrons from the calculation. In addition, the entire dispersion hardened substantially, which may be an artifact of the procedure used to leave out the conduction electrons.

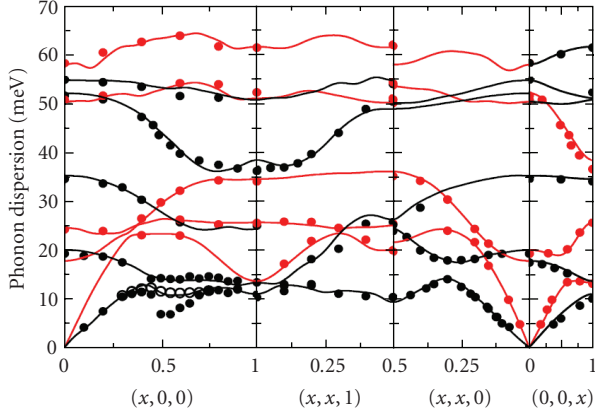


FIGURE 4: Calculated (lines) and observed (filled dots) phonon frequencies in  $\text{YNi}_2\text{B}_2\text{C}$  at 20 K. Open dots along [100] were measured at 300 K. Branches shown in red/black refer to phonons of predominantly longitudinal/transverse polarization respectively. The horizontal axes denote different crystallographic directions in reciprocal lattice units (r.l.u.). The theoretical results were scaled up by a factor of 1.03 (from [18]).

This method showed that the phonon dispersion dips in Ru originate from coupling to conduction electrons, but the bare dispersions obtained by excluding them were somewhat arbitrary. This study illustrates the difficulty in separating the bare dispersion from the real part of the phonon self-energy. It is not important for reproducing or predicting phonon anomalies, but is important for making connections with other experiments.

**2.4. Phonon Anomalies in Conventional Superconductors.** There are two interesting electron-phonon effects observed in measurements of phonon dispersions and linewidths in conventional superconductors. One is the normal state anomalies whose study can elucidate, which phonons contribute the most to the mechanism of superconductivity. The other is the effect of the superconducting gap  $2\Delta$  on the phonon spectra below  $T_c$ , which can be used as a probe of the superconducting gap.

In  $\text{MgB}_2$  the high superconducting transition temperature,  $T_c$ , is explained by strong electron-phonon coupling of  $E_g$  modes around 80 meV near the zone center. A strong dip in the dispersion of these phonons observed in experiments and reproduced by LDA calculations is a clear signature of this coupling [9, 10].

The ab-initio calculations based on DFT/LDA can predict all physical properties of materials that depend on electronic band structure, phonon dispersions and electron-phonon coupling without adjustable parameters. In particular, they can be used to calculate  $T_c$  based on Migdal-Eliashberg theory [11]. Several ab-initio calculations of phonon dispersions as well as  $T_c$ s were performed for the transition metal carbides and nitrides in order to explain relatively high transition temperatures in some and not in others [12–14]. They correctly reproduced phonon dispersions including the anomalies discussed in Section 2.3 [12, 14, 15], and

established a correlation between the phonon anomalies and  $T_c$ . They also suggested that the phonon anomalies are associated with the Fermi surface nesting [14], but more detailed calculations along the lines of [8] need to be performed to separate the role of nesting from the enhancement of the electron-phonon matrix element. One interesting possibility that may need to be explored, is that additional screening near the nesting wavevector may enhance the electron-phonon matrix elements, thus the Kohn anomalies at the nesting wavevectors may be stronger than expected from enhanced electronic response due to nesting alone.

In a conventional superconductor with  $T_c = 15$  K,  $\text{YNi}_2\text{B}_2\text{C}$ , the transverse acoustic phonons near  $\mathbf{q} = (0.5\ 0\ 0)$  soften and broaden on cooling [16] as expected from electron-phonon coupling. Reichardt et al. calculated phonon frequencies and linewidths using LDA [17]. These calculations reproduced this phonon anomaly and correctly predicted an additional wavevector ( $\mathbf{q} = 0.5\ 0.5\ 0$ ) where acoustic phonons couple strongly to conduction electrons [18] (Figure 4). The energies of both soft phonons are comparable to the superconducting gap energy. In this case the opening of the superconducting gap has a strong influence on the phonon spectral function.

These phonons were so broad, that their normal state spectra extended below the low temperature superconducting gap  $2\Delta$ . In this case, when the  $2\Delta$  opens in the electronic spectrum in the superconducting state, the damped harmonic oscillator approximation of the phonon breaks down. Allen et al. [19] developed a theory precisely for this case, which predicted that phonon lineshapes in the superconducting state should contain either a step or a sharp feature very close to  $2\Delta$  depending on the values of the phonon energy, electron-phonon coupling and  $2\Delta$ . Normal state lineshape fixes the first two parameters, which leaves only one adjustable parameter, that is, the superconducting gap. Detailed measurements of Weber et al. [20] confirmed this theory (Figure 5). They also suggested how to use phonon measurements to determine the magnitude of  $2\Delta$  and to probe gap anisotropy.

The effects of superconductivity on phonons in the cuprates were discussed in detail in [21] and will not be reviewed here.

Similar but much smaller effects of the superconducting gap on the phonon linewidths have been recently reported by P.Aynajian et al. in conventional elemental superconductors Pb and Nb using an extremely sensitive spin-echo technique [22].

**2.5. Phonon Anomalies with and without the Fermi Surface Nesting in Chromium.** A different situation appears in Chromium where the Fermi surface nesting is responsible for an incommensurate spin density wave (SDW) at a nesting wavevector  $\mathbf{q}_{\text{sdw}} = (0.94, 0, 0)$  and, as a secondary effect, of the charge density wave (CDW) at  $\mathbf{q}_{\text{cdw}} = (0.11, 0, 0)$  [23]. Shaw and Muhlestein measured phonon dispersions in chromium by INS [24]. They reported soft phonons around  $\mathbf{q} = (0.9, 0, 0)$ , which is near  $\mathbf{q}_{\text{sdw}}$ , as well as near  $\mathbf{q} = (0.45, 0.45, 0)$  where some nesting has also been calculated,

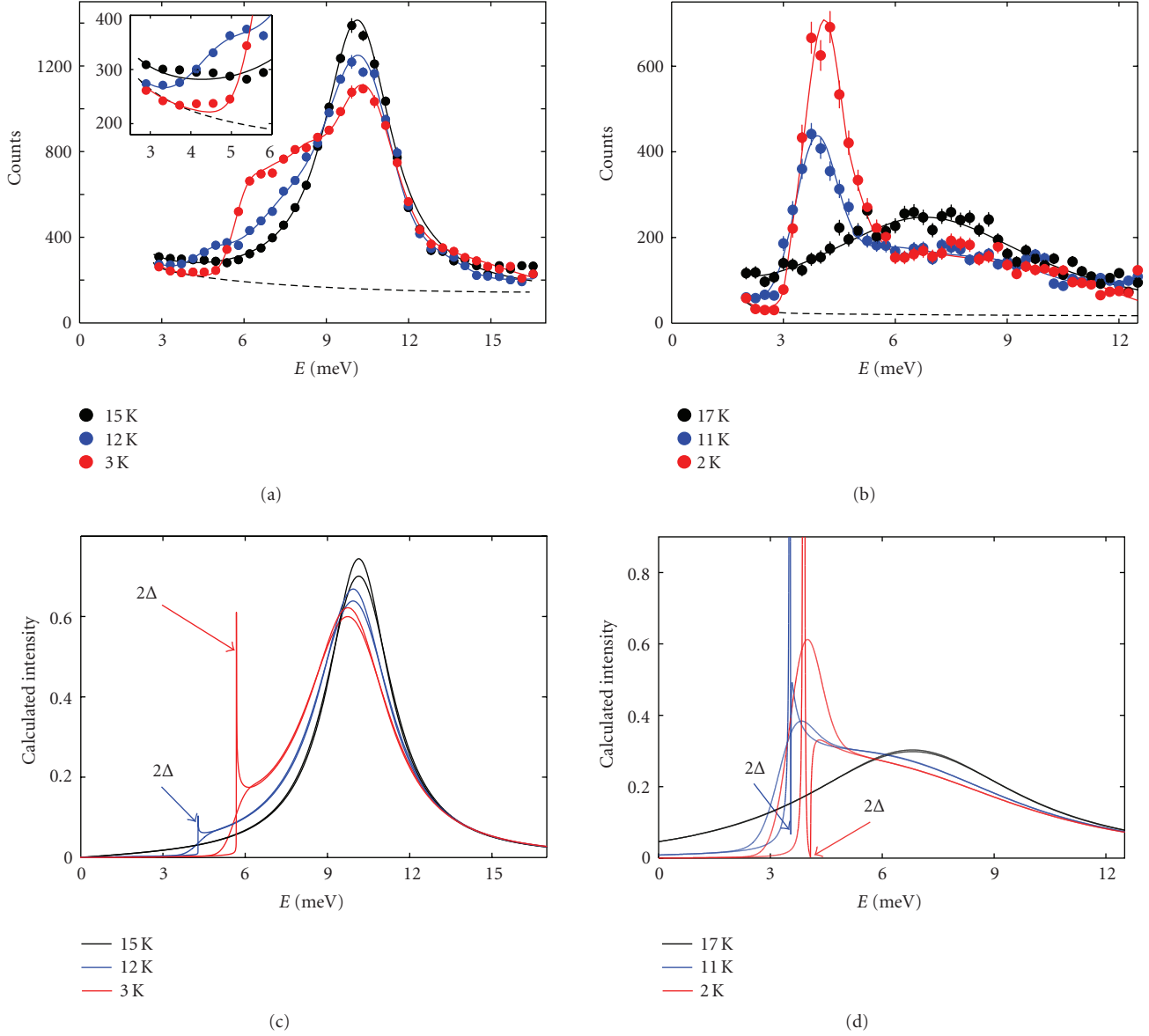


FIGURE 5: (a, b): Evolution of the neutron-scattering profile measured on  $\text{YNi}_2\text{B}_2\text{C}$  at  $\mathbf{Q} = (0.5, 0.5, 7)$  (left) and  $\mathbf{Q} = (0.5, 0, 8)$  (right) above and below  $T_c = 15$  K. (c, d): Thin lines represent calculated phonon lineshapes based on the theory of Allen et al. [19], using parameters extracted from the line-shape observed in the normal state. The thick lines are obtained after the convolution with the experimental resolution (from [20]).

although the data were not accurate enough to establish their exact wavevectors.

Recently Lamago et al. [25] performed a more precise and comprehensive set of measurements by IXS, which showed that the two anomalies actually appear at  $\mathbf{q}_{\text{sdw}}$  and  $\mathbf{q} = (0.5, 0.5, 0)$ , respectively. A surprising result was that a transverse phonon branch softened throughout the zone boundary between  $\mathbf{q} = (0.5, 0.5, 0)$  and  $(1, 0, 0)$ , that is, for  $\mathbf{q} = (0.5 + h, 0.5 - h, 0)$ , where  $0 < h < 0.5$ . LDA-based calculations performed as a part of this investigation, successfully reproduced the observed phonon softening (Figure 6). However, the electronic response function that couples to the phonons obtained from the same calculations showed no clear features corresponding to the phonon dips

along the zone boundary. Thus these phonon dips come exclusively from the  $\mathbf{q}$ -dependence of the electron-phonon matrix element. To the best of my knowledge, this is the first clear observation of a phonon softening in a narrow  $\mathbf{q}$ -range exclusively due to the  $\mathbf{q}$ -dependence of the electron-phonon matrix element.

This result was further corroborated by the effect of numerical smearing of the Fermi surface on the calculated phonon dispersions. The smearing suppressed only the calculated effect at  $\mathbf{q} = (0.94, 0, 0)$ , but not at  $\mathbf{q} = (0.5 + h, 0.5 - h, 0)$  for any  $h$  including  $h = 0$ . (Figures 6(a) and 6(b)). Such a smearing makes it possible to differentiate between the effects of the Fermi surface nesting and electron-phonon coupling enhancement because it reduces the former

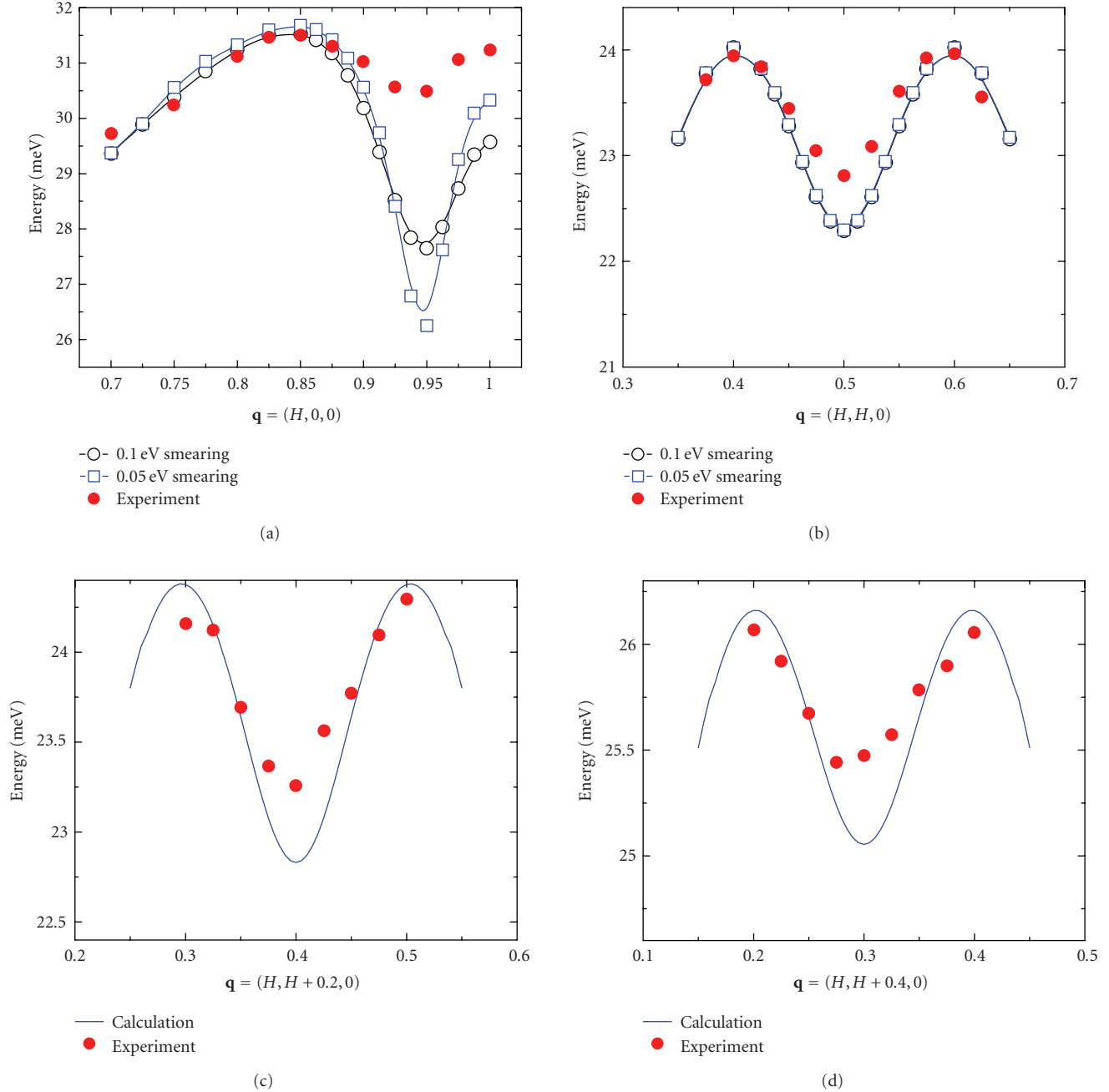


FIGURE 6: A comparison between measured (red) and calculated (blue, black) phonon dispersions and the LDA calculation in Cr. Only the data for the lowest energy transverse phonons near the zone boundary line connecting  $\mathbf{q} = (1, 0, 0)$  and  $\mathbf{q} = (0.5, 0.5, 0)$  are shown. The smearing has a strong effect in (a) but not in (b) (from [25]).

but not the latter. Lamago et al. concluded that only the softening at  $\mathbf{q}_{\text{sdw}}$  originates from Fermi surface nesting. The effect at  $\mathbf{q} = (0.5 + h, 0.5 - h, 0)$  comes exclusively from the  $\mathbf{q}$ -dependence of electron-phonon coupling. This is true even for  $h = 0$ , which is near a nesting feature previously thought [24] to be responsible for the phonon softening. In fact it makes a negligible contribution to the phonon self-energy, since the nesting feature disappears even at small  $h$ , but the phonon renormalization does not become smaller in either the calculation or the experiment [25].

**2.6. Lessons Learned from Conventional Metals.** It follows from the investigations reviewed above as well as from other similar work that conventional metals including phonon-mediated superconductors can be understood in terms of DFT in the approximations that ignore electron-electron interactions, except when mediated by phonons. These approximations work remarkably well in a variety of metals. They correctly reproduce electron-phonon effects, and account qualitatively for the variations in superconducting  $T_c$ s in compounds of similar structure and chemistry. The

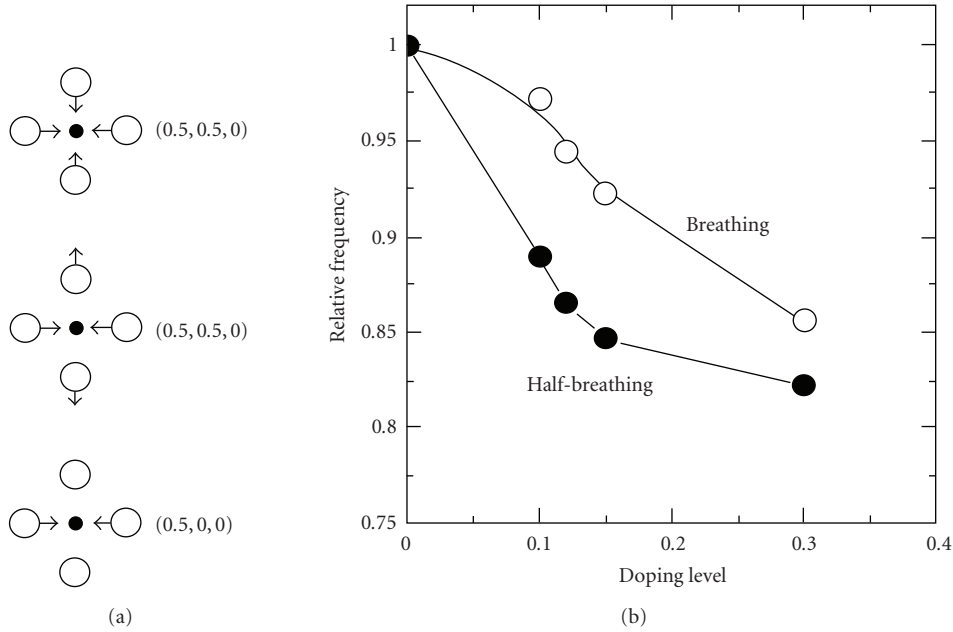


FIGURE 7: (a) Displacement patterns of zone-boundary bond-stretching modes in cuprates. Top: longitudinal mode in the [110] direction (breathing mode); middle: transverse mode in the [110]-direction (quadrupolar mode); bottom: longitudinal mode in the [100] direction (half-breathing mode). Circles and full points represent oxygen and copper atoms, respectively. Only the displacements in the Cu–O planes are shown. All other displacements are small for these modes. (b) Schematic of the doping dependence of the breathing  $\mathbf{q} = (0.5, 0.5, 0)$  and half-breathing  $\mathbf{q} = (0.5, 0, 0)$  zone boundary mode frequencies. This behavior is probably not directly related to the mechanism of superconductivity, since the softening continues into the overdoped nonsuperconducting part of the phase diagram from [30].

rest of this article will show that these approximations fail completely for phonons in the cuprates, most likely, because electronic correlations play a key role in bringing about experimentally observed strong electron-phonon coupling in the high  $T_c$  superconductors.

### 3. Phonon Anomalies in Doped $\text{La}_2\text{CuO}_4$

**3.1. Summary of Early Work.** Calculations performed soon after the discovery of high temperature superconductors suggested that electron-phonon coupling is too weak to account for high temperature superconductivity [26, 27]. However, measurements performed in conjunction with shell model calculations showed that the bond-stretching branch softened strongly towards the zone boundary as the doping increased from the insulating phase to the superconducting phase [28]. This behavior pointed towards strong electron-phonon coupling and a possible role of the zone boundary “half breathing” bond-stretching mode in the mechanism of high temperature superconductivity [29]. It later became apparent that this trend continues into the overdoped nonsuperconducting phase, which indicates that the zone boundary softening is related to the increase of the metallicity with doping rather than to the mechanism of superconductivity (Figure 7) [30].

These experiments and related calculations are extensively covered in the previous review by Pintschovius [21]. Here I will focus not on the zone boundary, but half-way to the zone boundary in the [100]-direction (along the Cu–O bond) where the most interesting physics has been observed.

This work began with the INS experiments of McQueeney et al. [31] who reported an anomalous lineshape and temperature dependence of the bond-stretching phonons in  $\text{La}_{1.85}\text{Sr}_{0.15}\text{CuO}_4$  near  $\mathbf{q} = (0.25, 0, 0)$  and interpreted these results in terms of line splitting due to unit cell doubling (Figure 8).

This interpretation evolved considerably in recent years as a result of further measurements and calculations. Pintschovius and Braden repeated the experiment using different experimental conditions, which had a higher energy resolution due to their use of the Cu220 monochromator [32]. They also measured the interesting wavevector range between  $q = 0.1$  and  $0.4$  in the so-called focusing condition with the tilt of the resolution ellipsoid matching the phonon dispersion, which further improved the resolution compared to [31] (see Section 3.2 for a more detailed discussion) Pintschovius and Braden reported enhanced linewidth near the same wavevector (with the strongest broadening at  $\mathbf{q} = (0.3, 0, 0)$ ), but did not see any splitting of the phonon line (Figure 9).

The origin of these effects was not clear at the time, but phonon anomalies near half way to the zone boundary suggested a possible connection to incipient stripe formation, that is, a nanoscale phase separation characterized by charge-rich lines separating charge poor antiferromagnetic domains [33–35].

Reznik et al. investigated the same bond stretching branch in  $\text{La}_{1.875}\text{Ba}_{0.125}\text{CuO}_4$  where static stripes appear at low temperatures [36]. They performed the first set of measurements in the same scattering geometry as

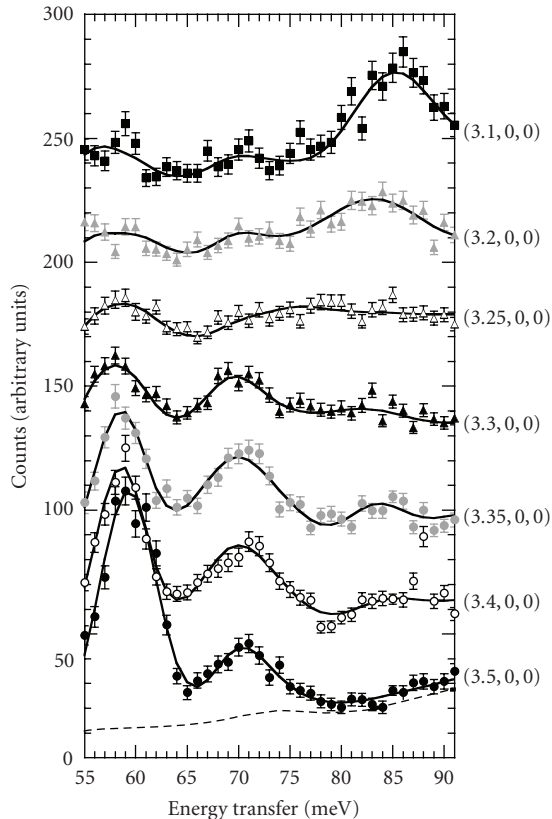


FIGURE 8: Bond-bending (around 60 meV) and bond-stretching (above 65 meV) branches in optimally-doped LSCO [31].

Pintschovius and Braden (at wavevectors  $(5-4.5, 0, 0)$  or  $(5-4.5, 0, 1)$ ) and found that the phonon dispersion could be described with two components: One had a “normal” dispersion following a cosine function (blue line), and the other softened and broadened abruptly at  $\mathbf{q} = (0.25, 0, 0)$  (black line) (Figure 10). The possible relationship between the phonon anomaly and stripe formation is further explored in Section 3.5.

Reznik et al. [36, 37] found that there was an overall hardening of the spectral weight on heating in both  $\text{La}_{1.875}\text{Ba}_{0.125}\text{CuO}_4$  and  $\text{La}_{1.85}\text{Sr}_{0.15}\text{CuO}_4$  at  $\mathbf{q} = (0.25, 0, 0)$  (see Figure 11). This indicates that the anomalous broadening does not originate from anharmonicity or structural inhomogeneity, since these have the opposite or no temperature dependence.

Pintschovius and Braden [32] observed no temperature dependence at  $q = (0.3, 0, 0)$  (it is equivalent to  $\mathbf{q} = (0.7, 0, 0)$  if interlayer interactions are neglected) although the zone center phonon of the same branch softened on heating. This softening is due to increased anharmonicity and should affect the entire branch. The absence of softening at  $\mathbf{q} = (0.3, 0, 0)$  that they report, indicates that there is a counterbalancing trend, which makes their results agree qualitatively with [36, 37]. I will explain the reason for the quantitative difference in the following section.

McQueeney et al. [31] reported a suppression of the anomalous behavior at room temperature. However, the room temperature data of [31] suffered from a much

stronger background than the low temperature data and a relatively large statistical error. Data presented in [37] had a much better resolution and signal-to-background ratio, but was limited to only three wavevectors. They also showed a suppression of the anomalous behavior at 330 K. In this regard the two studies are consistent, although [31] claims a much more radical change of the phonon dispersion than reported in [37]. To resolve this disagreement it is necessary to perform measurements covering the entire BZ at 300 K with the experimental configuration of [37].

**3.2. Recent IXS Results.** Neutron scattering experiments have a relatively poor  $\mathbf{Q}$  resolution. For the cuprates its full width half maximum (FWHM) is on the order of 15% of the in-plane Brillouin zone. The effects of finite  $\mathbf{Q}$  resolution in the longitudinal direction have been carefully considered in early studies, but the finite resolution in the transverse direction has not. In this section I will discuss recent IXS work and will show that some previous experiments need to be reinterpreted taking into account the finite transverse  $\mathbf{Q}$  resolution.

More recent measurements using both INS [37] and IXS [38] yielded a somewhat surprising result that the anomalous softening/broadening for  $\mathbf{q} = (0.25, k, 0)$  occurs only very close to  $k = 0$ . For example in  $\text{La}_{1.84}\text{Nd}_{0.04}\text{Sr}_{0.12}\text{CuO}_4$  the phonon anomaly significantly weakened at  $|k| \approx 0.08$  compared to  $k = 0$ , and disappeared entirely at  $|k| = 0.16$

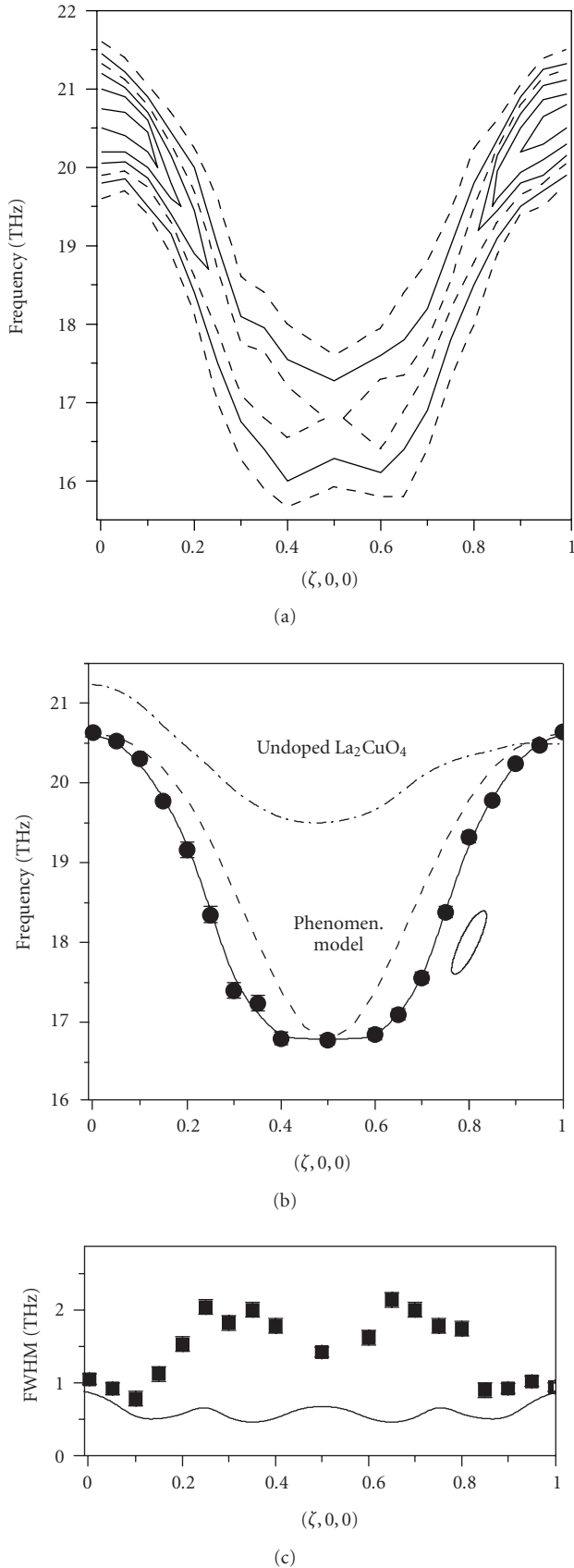


FIGURE 9: Results of measurements on  $\text{La}_{1.85}\text{Sr}_{0.15}\text{CuO}_4$  performed with a better energy resolution and similar in-plane wavevector resolution than in Figure 8 [32].

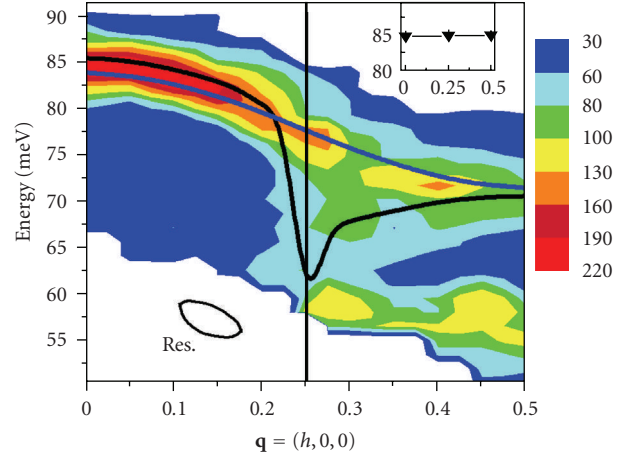


FIGURE 10: (a) Color-coded contour plot of the phonon spectra observed on  $\text{La}_{1.875}\text{Ba}_{0.125}\text{CuO}_4$  at 10 K. The intensities above and below 60 meV are associated with plane-polarized Cu–O bond-stretching vibrations and bond-bending vibrations, respectively. Lines are dispersion curves based on two-peak fits to the data. The white area at the lower left corner of the diagram was not accessible in this experiment. The ellipse illustrates the instrumental resolution. The inset shows the dispersion in the  $[110]$ -direction. The vertical line represents the charge stripe ordering wave vector. Blue/black line represents the “normal”/“anomalous” component respectively in the original interpretation of the authors. Subsequent work showed that a substantial part of the intensity in the “normal” component is an artifact of finite wavevector resolution in the transverse-direction (out of the page) [36].

(see Figure 12) [38]. The “normal” component for  $k \approx 0$  was significantly suppressed (Figure 12).

Neutron measurements have a much lower resolution in the  $k$ -direction, that is, INS experiments nominally performed with  $k = 0$  include a significant contribution from wavevectors with  $|k| > 0.08$  even in the most optimal configuration (a-b scattering plane). Thus most of the intensity in the “normal” component in the INS measurements probably comes from these phonons with  $|k| > 0.08$ .

With this information it now becomes possible to explain why the temperature effect in [32] was weaker than in [37]. The experiment of Pintschovius and Braden [32] was performed in the a-c scattering plane, which had poorer wavevector resolution in the  $k$ -direction, whereas the other study was performed in the a-b scattering plane, which had a better  $k$ -resolution (In order to maximize flux, triple axis neutron scattering instruments have a much larger beam divergence (factor 2-3) in the direction perpendicular to the scattering plane than in the scattering plane. Wavevector resolution scales with the beam divergence. The perpendicular direction for the a-c scattering plane is the  $b$ -direction, which corresponds to the  $k$ -direction in reciprocal space in my notation. In the a-b scattering plane the poor resolution is along  $l$ , and the good resolution along  $h$  and  $k$ ). Since the phonon anomaly is sharp in the  $k$ -direction, the anomalous behavior should be masked by the “normal” phonons with  $|k| > 0$  in the a-c scattering plane more than in the a-b scattering plane. This “masking” would also reduce the

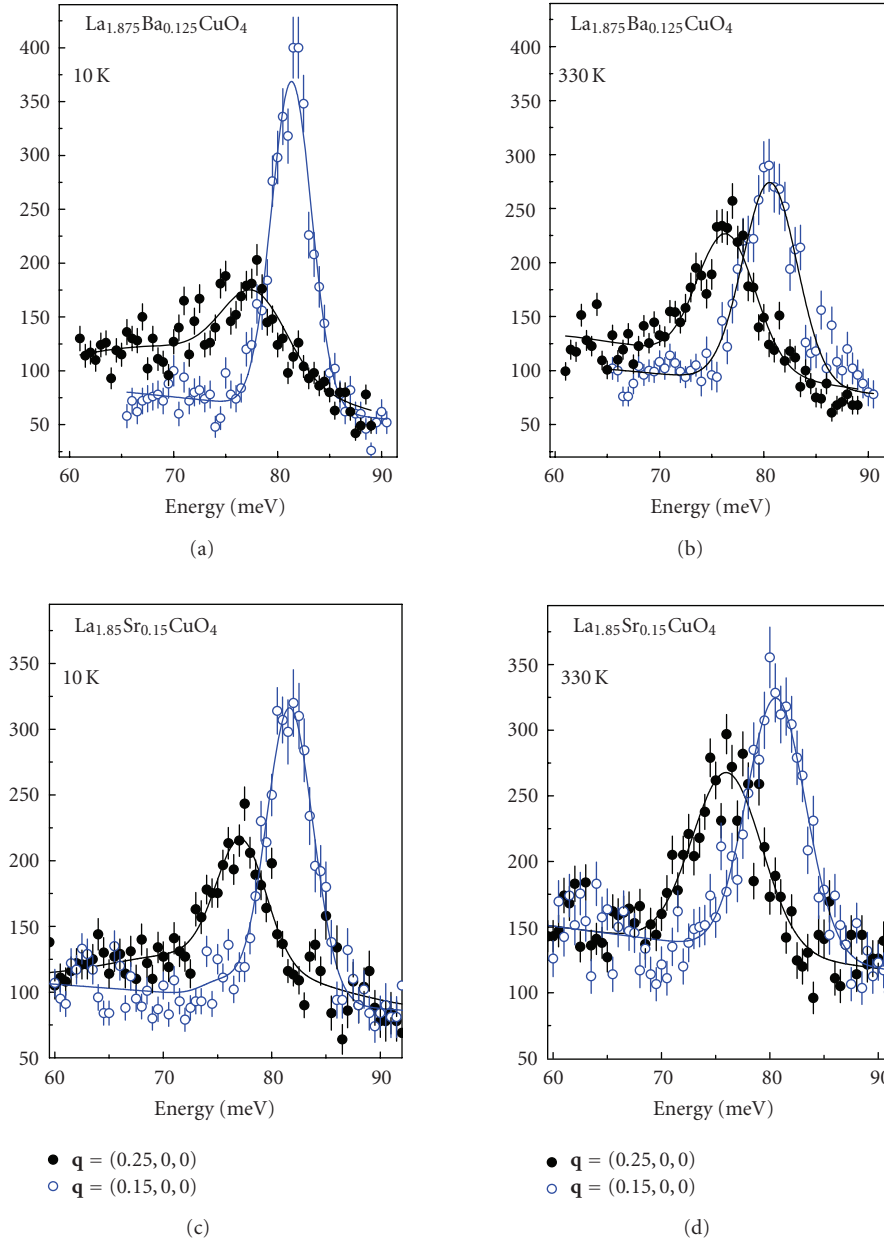


FIGURE 11: Temperature dependence of the bond-stretching phonons at select wavevectors. Energy scans taken on  $\text{La}_{1.875}\text{Ba}_{0.125}\text{CuO}_4$  (a, b) and on  $\text{La}_{1.85}\text{Sr}_{0.15}\text{CuO}_4$  (c, d, e) at 10 K (a, c) and 330 K (b, d) [37]. The phonon at  $\mathbf{q} = (0.15, 0, 0)$  is “normal” in that it has a Gaussian lineshape on top of a linear background. This background results from multiphonon and incoherent scattering and has no strong dependence on  $\mathbf{Q}$ . The intensity reduction of this phonon in  $\text{La}_{1.875}\text{Ba}_{0.125}\text{CuO}_4$  from 10 K (a) to 330 K (b) is consistent with the Debye-Waller factor. At  $\mathbf{q} = (0.25, 0, 0)$ , there is extra intensity on top of the background in the tail of the main peak. It originates from one-phonon scattering that extends to the lowest investigated energies, while the peak intensity is greatly suppressed as discussed in the text. The effect is reduced but does not disappear at 330 K. Note that 330 K in (b) is shown instead of 300 K in the same plot in [37] because of a typographical error in the latter. Integrated intensity of the phonon decreases from  $\mathbf{q} = (0.15, 0, 0)$  to  $\mathbf{q} = (0.25, 0, 0)$  due to the decrease of the structure factor.

phonon linewidth in [32] compared to the measurement in [37] performed with better  $k$ -resolution.

D’Astuto et al. [39] reported two-branch behavior in IXS spectra of  $\text{La}_{1.86}\text{Ba}_{0.14}\text{CuO}_4$  with clearly resolved “normal” and “anomalous” components (Figure 13). However, the  $\mathbf{Q} = (3.27, 0, 0)$  data of Figure 12 measured also by IXS with a much higher energy resolution as well as the results of J. Graf

et al. on  $\text{La}_{1.92}\text{Sr}_{0.08}\text{CuO}_4$  [40], are consistent with either a single broad peak or two strongly overlapping peaks. Since D’Astuto et al. measured a Ba-doped sample, and D. Reznik et al. and J. Graf et al. investigated the Sr-doped systems, it is possible that the difference may come from Ba versus Sr doping. It is necessary to perform further experiments to clarify this potentially important issue.

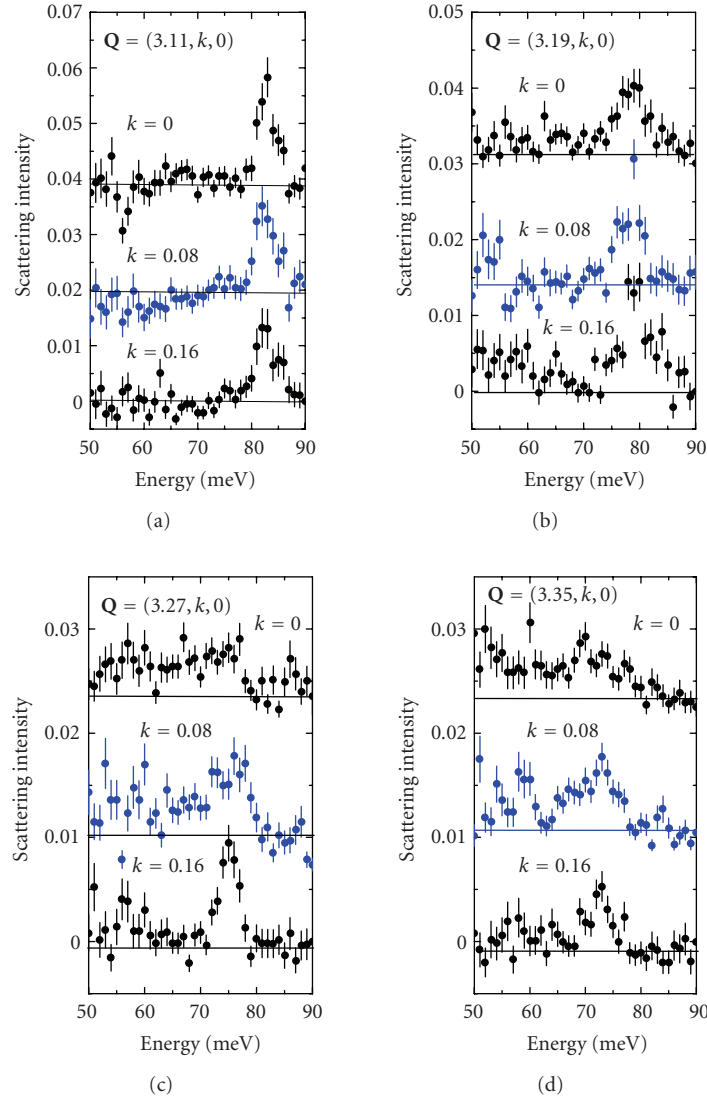


FIGURE 12: IXS energy scans after subtraction of the elastic tail and a constant term corresponding to the stray radiation. The scans were taken with  $\mathbf{q} = (h, k, 0)$  with  $h = 0.11, 0.19, 0.27, 0.35$  (from the left to the right column) and  $k$  as indicated in the figure. The most interesting features are the suppression of the two-component behavior seen by INS at 77 meV near  $\mathbf{Q} = (3.27, 0, 0)$  and the rapid narrowing and hardening of the phonon line from  $k = 0$  to  $k = 0.16$  for  $\mathbf{Q} = (3.27, k, 0)$ . From [38].

**3.3. Doping Dependence.** Figure 14 shows the bond-stretching phonon dispersion and linewidth for  $\text{La}_{2-x}\text{Sr}_x\text{CuO}_4$  with  $x = 0.07, 0.15$ , and  $0.3$ . The dispersion is compared with the cosine function that typically comes out of DFT calculations (see, e.g., [41–43]). Here the data presented in [36, Figure 4] are combined with some unpublished results and refitted using the model that includes all phonon branches picked up by the spectrometer resolution [44]. Such an analysis provides more accurate values of intrinsic phonon linewidths as opposed to gaussian peaks. The strongest dip below the cosine function and the biggest peak of the linewidth occur at optimal doping where the  $T_c$  is highest. These are smaller at  $x = 0.07$  and disappear in the overdoped nonsuperconducting sample with  $x = 0.3$ . The position of the phonon anomaly does not change with doping.

A Comparison with the overdoped sample, where the physics are conventional, allows to identify the effects of electron-phonon coupling that are intrinsic to optimal doping. Figure 15 shows the schematic of the anomalous phonon broadening that appears on top of the broadening observed in the  $x = 0.3$  sample. The anomalous broadening peaks at  $\mathbf{q} = (0.3, 0, 0)$  and weakens rapidly in the longitudinal and transverse directions.

This effect is phenomenologically very similar to the renormalization of the acoustic phonons at specific wavevectors discussed in Section 2. Next, I will show that profound differences exist between  $\text{La}_{2-x}\text{Sr}_x\text{CuO}_4$  and conventional metals.

**3.4. Comparison with Density Functional Theory.** As discussed in Section 2, density functional theory gives a

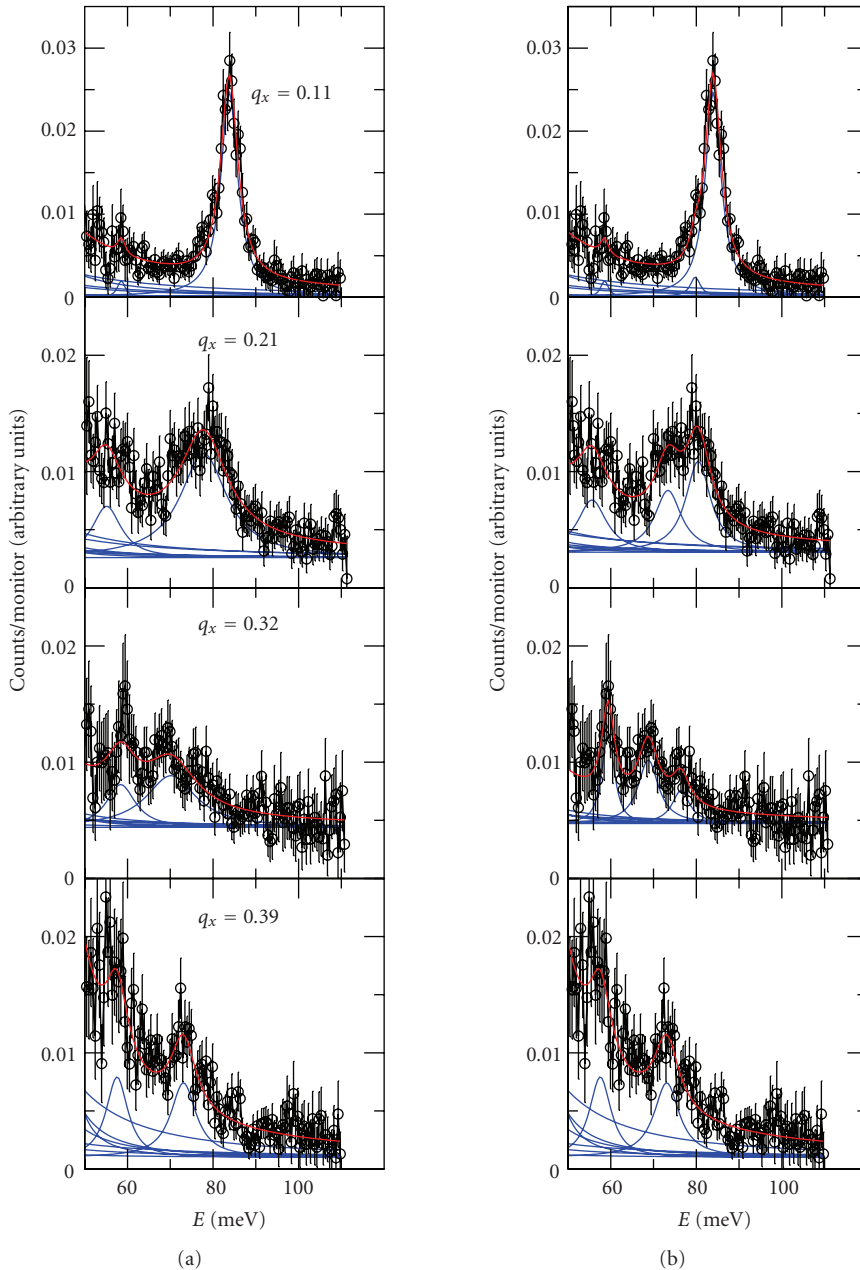


FIGURE 13: Inelastic X-ray scattering spectra of  $\text{La}_{1.86}\text{Ba}_{0.14}\text{CuO}_{4+\delta}$ , at  $\mathbf{Q} = (3 + q_x, q_y, 0)$  ( $q_y < 0.04$ ). In the left column a single peak is used to fit the data. In the right column the data are fitted with two Cu–O bond stretching modes (from [39]).

good description of phonon dispersions in metals where electron-electron interactions can be neglected. Giustino et al. [42] performed such a calculation in the generalized gradient approximation (GGA) for  $\text{La}_{1.85}\text{Sr}_{0.15}\text{CuO}_4$ , which approximately agreed with the experimental data of [31]. In particular, they reproduced the overall downward dispersion of the longitudinal bond-stretching branch. However, the strong effect in the bond-stretching phonon half way to the zone boundary was not apparent in [42, Figure 1], because the 300 K results and 10 K results were plotted together. In the brief communication arising from the article of Giustino

et al., Reznik et al. showed that DFT did not reproduce the phonon anomaly half way to the zone boundary that appears in [31, 32, 36–39] as well as in later experiments discussed above in detail (Figure 16, [45]).

Giustino et al. also calculated the phonon contribution to the kink in the electronic dispersion observed by photoemission spectroscopy (Figure 17). Such kinks may result from bosonic modes interacting with electrons. One of the proposed mechanisms of high temperature superconductivity is Cooper pairing via this boson, thus it is important to identify its origin. Figure 17 shows that in DFT phonon contribution

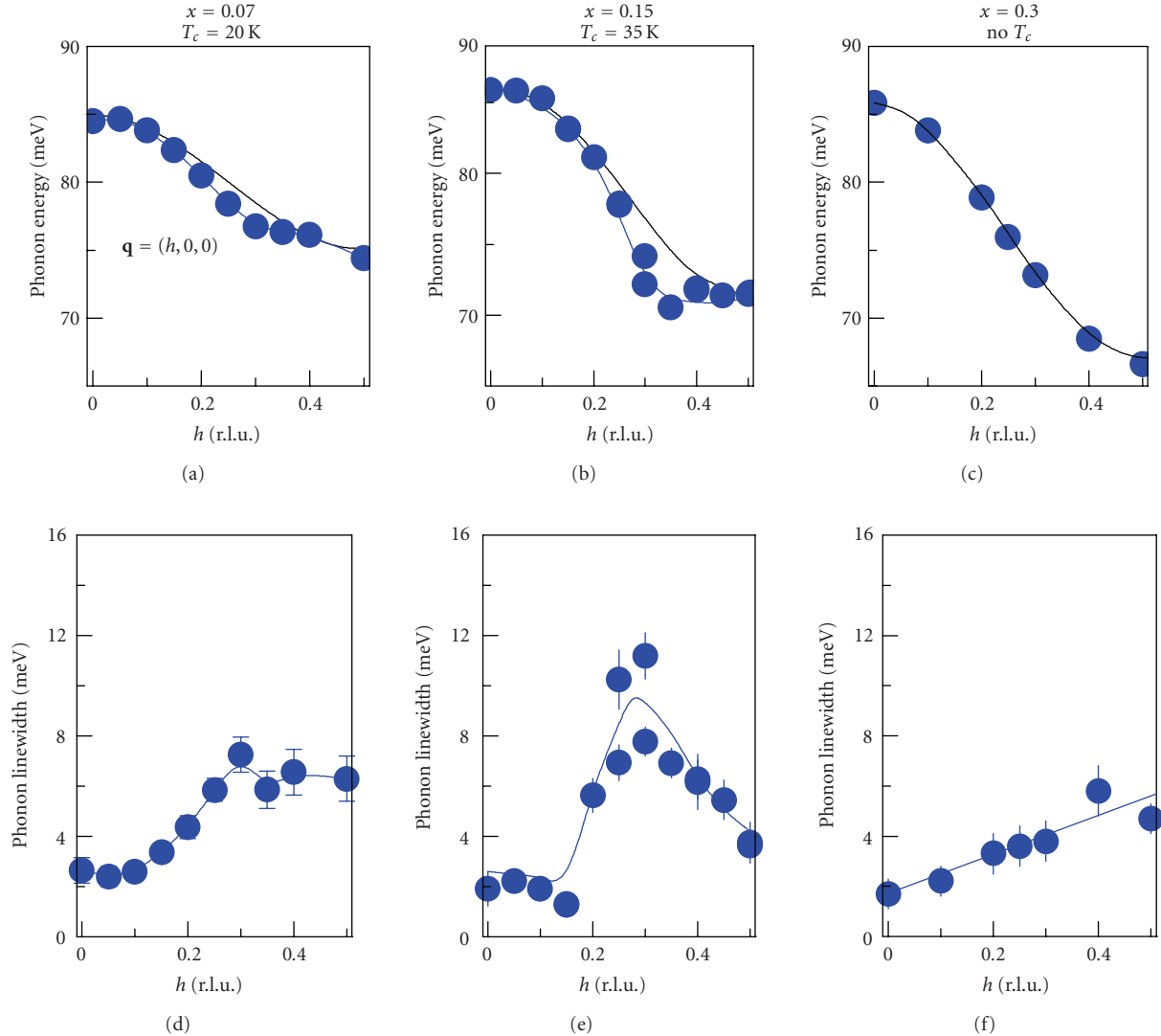


FIGURE 14: Bond-stretching phonon dispersion (top row) and linewidth (bottom row) at three doping levels. Black lines represent downward cosine dispersion. The overall increase in the linewidth of the bond-stretching mode towards the zone boundary appears to be doping-independent. Softening compared with the cosine dispersion as well as the linewidth enhancement half-way to the zone boundary do not shift with  $h$  between  $x = 0.07$  and  $0.15$  [44].

to the kink is five times smaller than observed. Analogous results for both the phonon dispersions [43] and the kink [46] were obtained earlier for  $\text{YBa}_2\text{Cu}_3\text{O}_7$ .

However, Reznik et al. argued that the failure of the DFT to reproduce the phonon anomaly indicates that it is possible that electronic correlations ignored by the DFT enhance electron-phonon coupling. This enhancement could result in a much stronger kink than calculated by the DFT. It is interesting that many-body calculations predict a substantial enhancement of the coupling to bond-stretching phonons compared to DFT (see, e.g., [29, 47]). t-J model-based calculations describe interesting doping dependence of the zone boundary phonons, suggesting that strong correlations might be relevant [48, 49]. Recent high resolution photoemission measurements found an isotope effect in the dispersion kink, hinting at an important role of phonons [50].

Agreement of both the electronic dispersion and of the phonon dispersion with DFT predictions in overdoped nonsuperconducting  $\text{La}_{2-x}\text{Sr}_x\text{CuO}_4$  as shown in Figure 18 reinforces the connection between the phonon anomalies near optimal doping and electronic correlations.

**3.5. Connection with Stripes and Other Charge-Inhomogeneous Models.** The bond-stretching phonon anomaly is strongest in  $\text{La}_{1.875}\text{Ba}_{0.125}\text{CuO}_4$  and  $\text{La}_{1.48}\text{Nd}_{0.4}\text{Sr}_{0.12}\text{CuO}_4$ , compounds that exhibit spatially modulated charge and magnetic order, often called stripe order. It appears when holes doped into copper-oxygen planes segregate into lines, which act as domain walls for an antiferromagnetically ordered background. Static long-range stripe order has been observed only in a few special compounds such as  $\text{La}_{1.48}\text{Nd}_{0.4}\text{Sr}_{0.12}\text{CuO}_4$  and  $\text{La}_{1.875}\text{Ba}_{0.125}\text{CuO}_4$  where anisotropy due to the transition to the low temperature

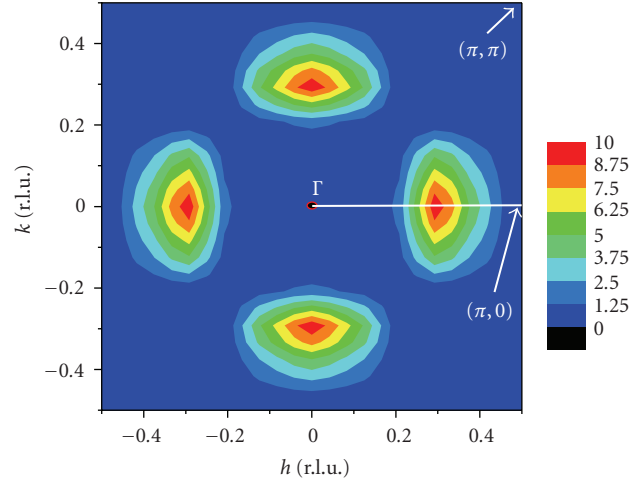


FIGURE 15: Qualitative picture of the difference in the linewidths of the bond-stretching phonon in optimally-doped ( $x = 0.15$ ) and overdoped ( $x = 0.3$ )  $\text{La}_{2-x}\text{Sr}_x\text{CuO}_4$  as a function of wavevector in the ab-basal plane based on [30, 37]. The units are meV. The solid line indicates the [100] direction along which most of measurements were performed.

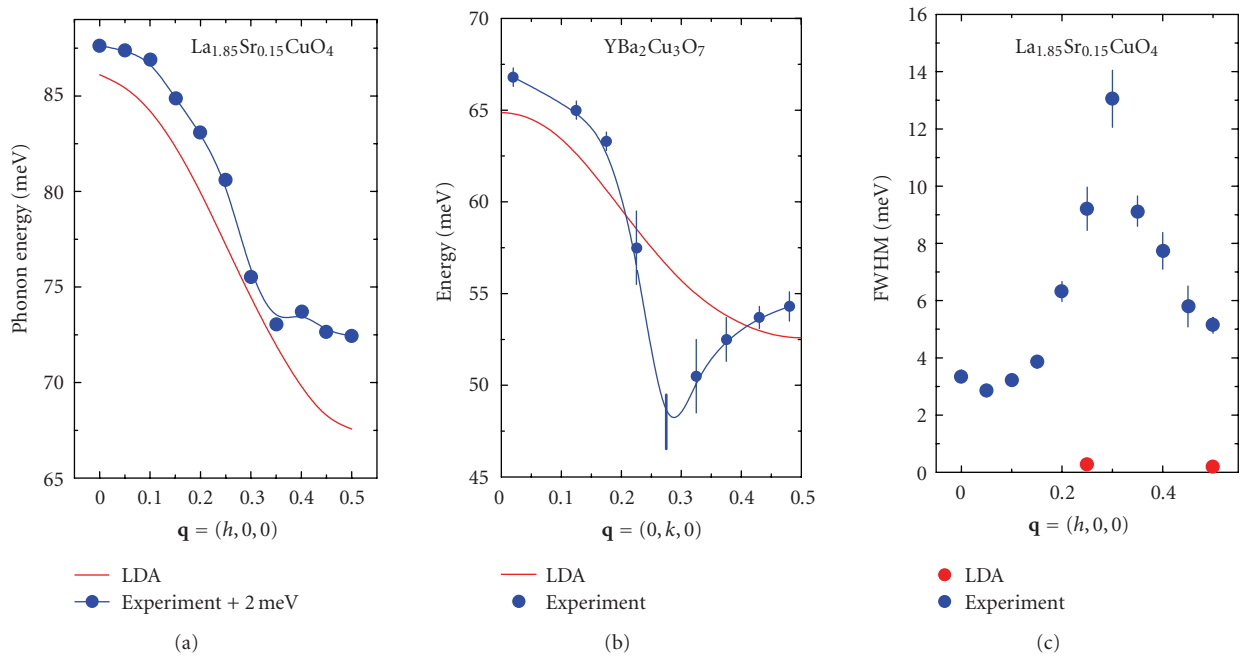


FIGURE 16: Comparison of some LDA predictions with experimental results for  $\text{La}_{1.85}\text{Sr}_{0.15}\text{CuO}_4$  [42] and  $\text{YBa}_2\text{Cu}_3\text{O}_7$  [72] at 10 K. (a,b) Experimental bond-stretching phonon dispersions compared to LDA results. The data in (a) are shifted by 2 meV. (c) Phonon linewidths in  $\text{La}_{1.85}\text{Sr}_{0.15}\text{CuO}_4$  compared with LDA results on  $\text{YBa}_2\text{Cu}_3\text{O}_7$  [42], contains no linewidth results for  $\text{La}_{1.85}\text{Sr}_{0.15}\text{CuO}_4$  but they should be similar.

tetragonal structure provides the pinning for the stripes while superconductivity is greatly suppressed [35]. In contrast, the more common low temperature orthorhombic (LTO) phase does not provide such a pinning and static stripes do not form. In the LTO phase the stripes are assumed to be purely dynamic, which makes their detection extremely difficult [51, 52]. Here I discuss the possible relation between the phonon anomaly and dynamic stripes.

A detailed comparison between the bond-stretching phonon dispersion in stripe-ordered compounds and

optimally-doped superconducting  $\text{La}_{1.85}\text{Sr}_{0.15}\text{CuO}_4$  was performed by Reznik et al. [37] They found the strongest phonon renormalization at  $h = 0.25$  in the presence of static stripes and  $h = 0.3$  at optimal doping (Figure 19). It appears that static stripes pin the phonon anomaly at the stripe ordering wavevector.

Two mechanisms of the impact of dynamic stripes on phonons have been proposed: One is that the phonon eigenvector resonates with the charge component of the stripes; The other is that one-dimensional nature of charge

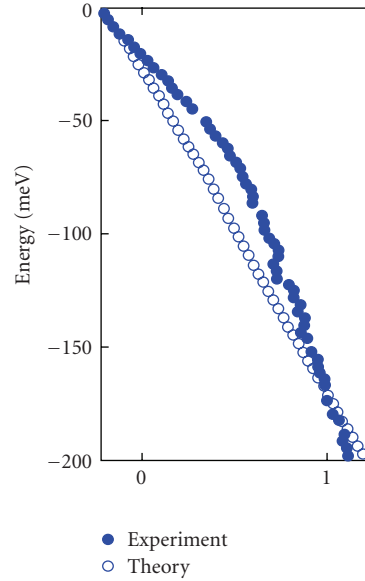


FIGURE 17: Comparison between the quasi particle dispersion relations obtained from the peaks of the photoemission spectra and calculations of [42], including the renormalization due to the electron-phonon interaction in  $\text{La}_{1.85}\text{Sr}_{0.15}\text{CuO}_4$ .

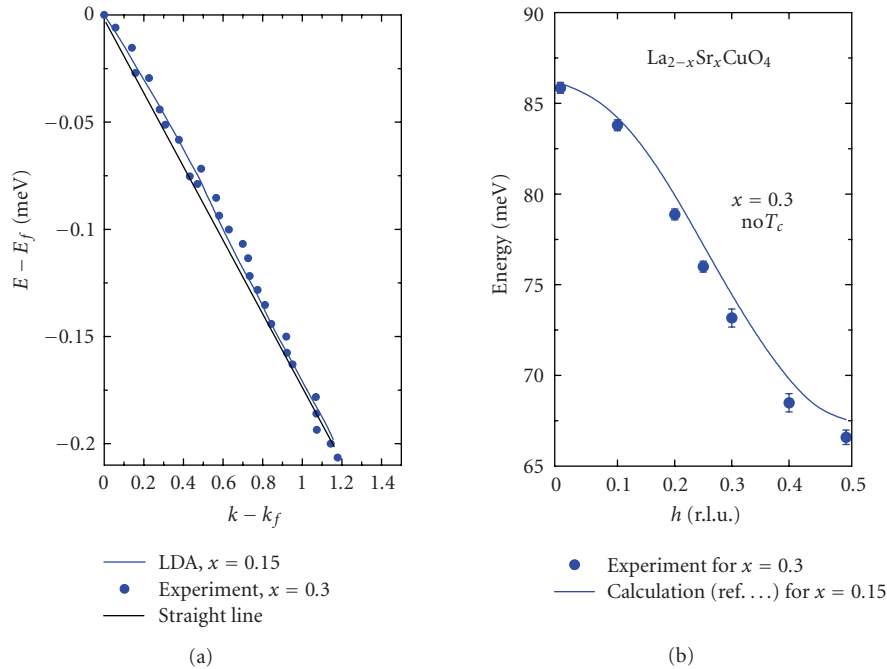


FIGURE 18: Comparison of the photoemission kink (a) and phonon dispersion (b) in  $\text{La}_{1.7}\text{Sr}_{0.3}\text{CuO}_4$  with the DFT calculations for  $\text{La}_{1.85}\text{Sr}_{0.15}\text{CuO}_4$ . (based on results of [30, 42, 82]). Black thin line in (a) is a straight line serving as a guide to the eye.

stripes makes them prone to a Kohn anomaly, which renormalizes the phonons. In the first scenario (2D picture) the propagation vector of the anomalous phonon must be parallel to the charge ordering wavevector, whereas in the second scenario (1D picture) it must be perpendicular to the charge ordering wavevector (Figure 20).

An important clue is that the phonon anomaly disappears quickly as one moves away from  $k = 0$  along

the line in reciprocal space:  $\mathbf{q} = (0.25, k, 0)$  as shown in [37, 38] and discussed in Section 2.2. Such behavior is expected from the matching of the phonon wavevector and the stripe propagation vector. In contrast, a simple picture of a Kohn anomaly due to 1-D physics inside the stripes predicts a phonon anomaly that only weakly depends on  $k$ . This observation favors the 2D picture, but an important caveat is that it may be possible to reconcile the 1D picture with

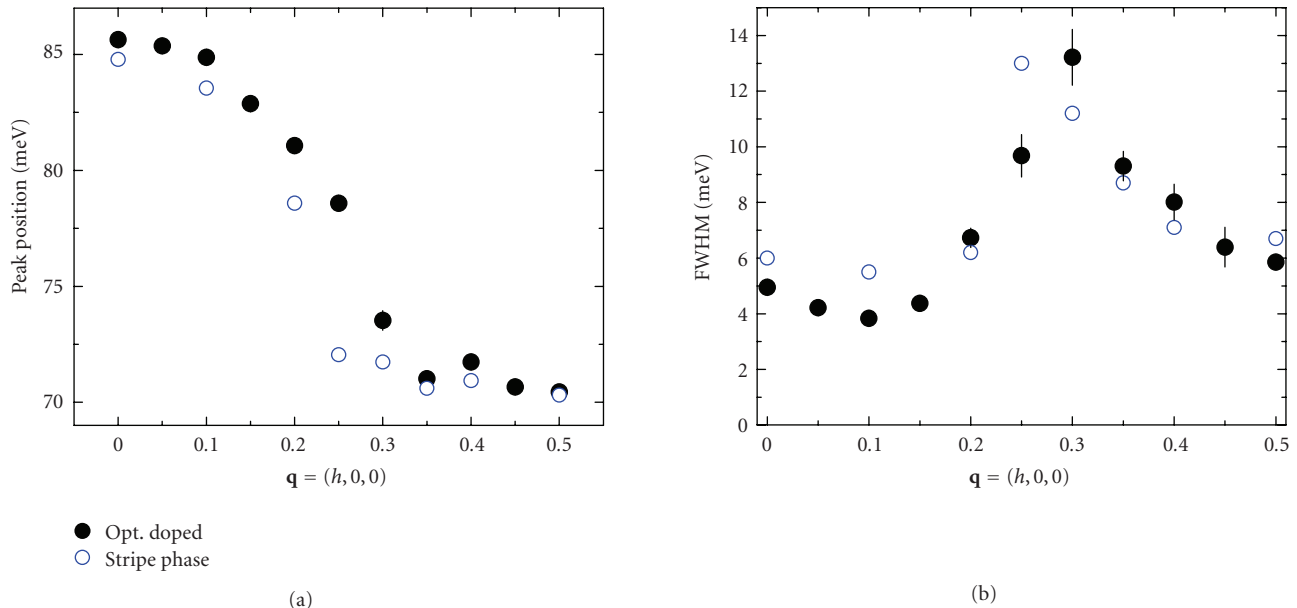


FIGURE 19: Comparison of the phonon dispersions (a) and linewidth (b) of the bond-stretching branch in  $\text{La}_{1.85}\text{Sr}_{0.15}\text{CuO}_4$  and  $\text{La}_{1.48}\text{Nd}_{0.4}\text{Sr}_{0.12}\text{CuO}_4$  (from [37]).

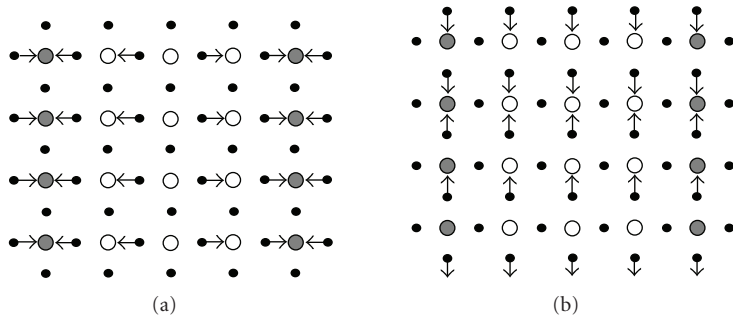


FIGURE 20: Schematic of the eigenvectors for the phonons with  $\mathbf{q} = (0.25\ 0\ 0)$  propagating perpendicular (a) and parallel (b) to the stripes. Open circles represent hole-poor antiferromagnetic regions, while the filled circles represent the hole-rich lines (from [37]).

experiment by including a decrease of the electron-phonon matrix element away from  $k = 0$  [53].

Another way to distinguish between the two scenarios is to consider the doping dependence of the wavevector of maximum phonon renormalization,  $\mathbf{q}_{\text{max}}$ . In the stripe picture,  $\mathbf{q}_{\text{max}} = 2\mathbf{q}_{\text{in}}$ , ( $\mathbf{q}_{\text{in}}$  is the wavevector of the incommensurability of low energy spin fluctuations) [51]. At doping levels of  $x = 0.12$  and higher,  $\mathbf{q}_{\text{in}} = 0.125$ , which gives the charge ordering wavevector of 0.25. This value is indeed close to  $\mathbf{q}_{\text{max}}$ . At  $x = 0.07$ ,  $\mathbf{q}_{\text{in}} = 0.07$ . This gives the charge stripe ordering wavevector of 0.14 whereas  $\mathbf{q}_{\text{max}} = 0.3$ . This discrepancy appears to contradict the 2D picture. But again there is a caveat: Anomalous phonons occur at a fairly high energy of about 75 meV, and a comparison to the dynamic stripe wavevector at low energies may not be appropriate.

Thus the question of which picture, 1D or 2D, agrees better with the data is not yet settled.

If the phonon renormalization is driven by static stripes, one may expect a different behavior for phonons propagating parallel or perpendicular to the stripe propagation vector

[54]. In this case the phonon should split into two peaks. The dynamic stripes, according to Vojta et al. [55], may not break tetragonal symmetry, because fluctuations can occur in both directions simultaneously. Thus a single-peak anomalous phonon lineshape is compatible with dynamic stripes.

**3.6. Phonon Anomalies and Superconductivity.** Origin of superconductivity in the cuprates is still hotly debated. A conventional phonon-mediated mechanism dropped out fairly early in this debate in large part because LDA calculations showed that electron-phonon coupling is too weak to explain superconductivity. However, recent measurements have shown (see Section 3.4) that electron phonon coupling of the bond-stretching mode is much stronger than calculated by LDA, which invalidates this claim. In fact the magnitude of the phonon renormalization in  $\text{La}_{1.85}\text{Sr}_{0.15}\text{CuO}_4$  is similar to that of the  $E_g$  phonon in  $\text{MgB}_2$  [56], which is held largely responsible for superconductivity with an even higher  $T_c$ . It is also interesting that these  $E_g$  phonons have roughly the same energy as the bond-stretching phonons in the

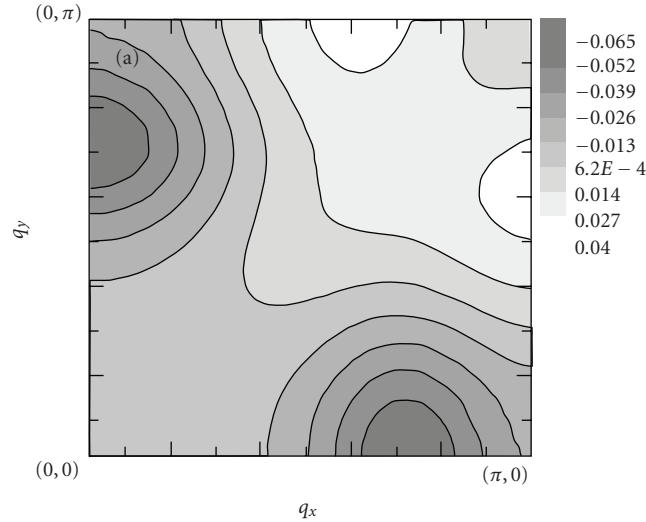


FIGURE 21: Contour map of the effective pairing interaction  $F(qW)$  calculated from the t-J model with the off-diagonal coupling case and the vertex correction (from [70]).

cuprates. In addition, the magnitude of the bond-stretching phonon renormalization in  $\text{La}_{1.85}\text{Sr}_{0.15}\text{CuO}_4$  is similar to that recently observed in a bilayer manganite where exceptionally strong electron-phonon coupling induces a structural phase transition accompanied by colossal magnetoresistance [57].

Can these results be interpreted in favor of a conventional mechanism of superconductivity at least in the  $\text{La}_{2-x}\text{Sr}_x\text{CuO}_4$  family where  $T_c$  is relatively low?

If the mechanism of superconductivity were conventional, DFT calculations based on Eliashberg formalism with noninteracting electrons (except for the exchange of phonons) should explain the experimental results at least qualitatively. Since this is not the case, in a strict sense the answer is “NO”. However, the appearance of the maximum  $T_c$  and the strongest bond-stretching phonon anomaly around the same doping points towards some other connection with the mechanism of superconductivity [37].

By now a general consensus emerged of a *d*-wave pairing state in the cuprates, with the superconducting gap changing sign around the nodal points along the [110]-direction on the Fermi surface. A simple inspection of the BCS gap equation shows that such a pairing state cannot be mediated by isotropic electron-phonon coupling. In fact, isotropic electron-phonon coupling would suppress a *d*-wave pairing state caused by another mechanism (e.g., spin fluctuations), because in such a case phonons would scatter quasiparticles between the parts of the Fermi surface with the opposite signs of the superconducting gap.

Alexandrov showed that a *d*-wave state can be mediated by acoustic phonons with highly anisotropic electron-phonon coupling [58]. No experimental evidence has appeared up to now of any electron-phonon coupling for acoustic phonons, but the self-energy of the bond-stretching modes is large and highly anisotropic (see Figure 20). In fact the bond-stretching phonons that couple most strongly to electrons connect the parts of the Fermi surface where the gap has the same sign, so these phonons will at least not

interfere with *d*-wave superconductivity and may actually enhance  $T_c$ .

Strong renormalization of the bond stretching phonons has been taken as evidence for a soft collective charge mode [59, 60] or an incipient instability [61] with respect to the formation of either polarons, bipolarons [62–65], charge density wave order [66], phase separation [61–64, 67], valence bond order [68], or other inhomogeneity [69]. These may or may not be related to the mechanism of stripe formation. A number of studies suggested that these instabilities may lead to superconductivity [64–66, 68].

Ishihara and Nagaosa examined the interplay of the interaction of the bond-stretching phonons with electrons in the t-J model and, after including vertex corrections, obtained the effective *d*-wave pairing interaction,  $F(qW)$ , mediated by the bond-stretching phonons [70] (see Figure 21). In the absence of strong nesting as in the case of  $\text{La}_{1.85}\text{Sr}_{0.15}\text{CuO}_4$ , such a pairing interaction scales with the phonon-self-energy. Interestingly, the functional form of  $F(qW)$  that they obtained is similar to Figure 15, which shows the color map of anomalous phonon broadening. This result was a prediction, since it was obtained before the full picture of the bond-stretching phonon renormalization was known. They also showed that this interaction can mediate *d*-wave pairing.

## 4. Other Cuprates

**4.1.  $\text{YBa}_2\text{Cu}_3\text{O}_{6+x}$ .** It is necessary to establish the universality of the phonon anomalies observed in the  $\text{La}_{2-x}\text{Sr}_x\text{CuO}_4$  family. Until now much less work has been performed on other cuprates, because they are more difficult to measure either due to a higher background, no availability of large samples for INS, or low IXS scattering cross section.

In the case of  $\text{YBa}_2\text{Cu}_3\text{O}_{6+x}$  the orthorhombic structure combined with twinning complicates interpretation of the results. Very little work has been done so far on detwinned samples [71] because they are smaller than the twinned ones.

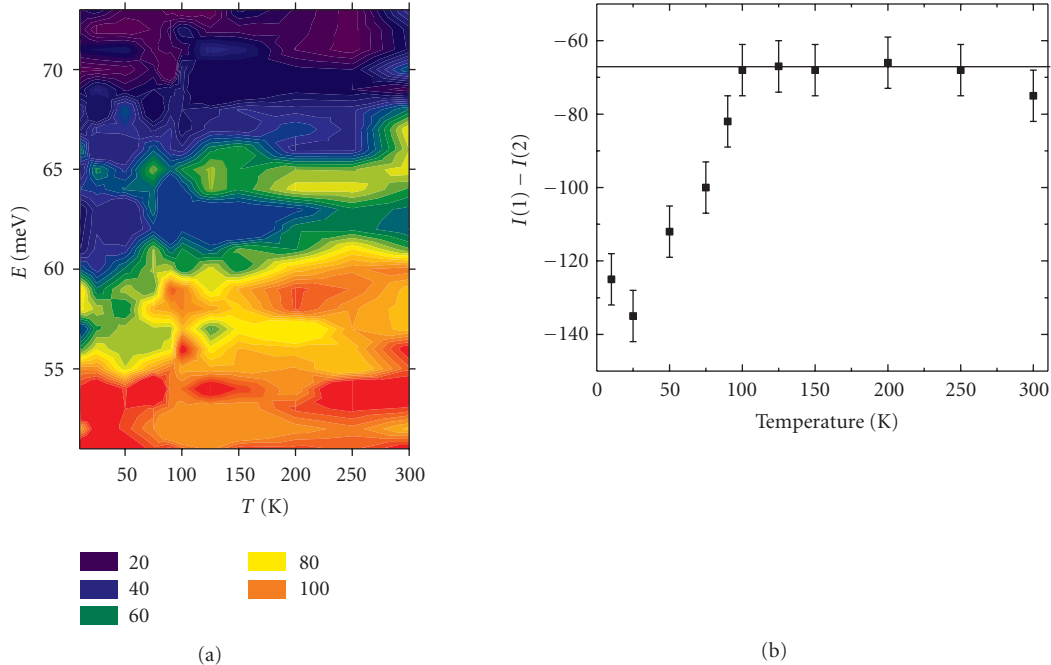


FIGURE 22: (b) Inelastic scattering intensity of  $\text{YBa}_2\text{Cu}_3\text{O}_{6.95}$  at  $\mathbf{Q} = (3.25, 0, 0)$  as a function of temperature, determined with the triple-axis spectrometer at the HFIR. Data were smoothed once to reduce noise. (a) Temperature dependence of the intensity difference  $I(1) - I(2)$ , where  $I(1)$  is the average intensity from 56 to 68 meV,  $I(2)$  from 51 to 55 eV, at  $\mathbf{Q} = (3.25, 0, 0)$ .  $T_c$  of the sample was 93 K (from [73]).

Furthermore, two  $\text{CuO}_2$  layers in the unit cell introduce two bond-stretching branches, of  $\Delta 1$  and  $\Delta 4$  symmetry.

At optimal doping bond-stretching phonons propagating along the chain direction show an anomaly that is in many respects similar to the one in  $\text{La}_{2-x}\text{Sr}_x\text{CuO}_4$  [72, 73]. It is absent at 300 K but appears at low temperatures. Chung et al. [73] reported that the spectral weight of the bond-stretching phonons in the  $\Delta 1$  symmetry redistributes to lower energies below the superconducting transition temperature,  $T_c = 93$  K (see Figure 22).

Pintschovius et al. [72] and Reznik et al. [74] found that a similar transfer of spectral weight occurs for the  $\Delta 4$  phonons but starting close to 200 K, not at  $T_c$ . They interpreted this transfer of spectral weight as arising from softening of the bond-stretching phonon polarized along  $b^*$ , which transfers its eigenvector to the branches that are lower in energy. This interpretation could explain the observed behavior with some important caveats, but more work is necessary to better understand this effect. Figure 23 shows that this transfer of spectral weight accelerated below  $T_c$  saturating near 50 K. While clearly related to the onset of superconductivity, this effect is not understood.

Reznik et al. also showed that the transfer of spectral weight in the  $\Delta 1$  symmetry also begins well above  $T_c$  with the most pronounced change below  $T_c$  (Figure 24). This result seems to contradict the observation of Chung et al. [73] who reported that the phonon intensity shift in  $\Delta 1$  symmetry occurs only below  $T_c$ . According to Reznik et al. the effect would also appear only below  $T_c$  if they excluded the intensity below 50 meV from their analysis [74] as was done in [73]. So in this respect the two studies are consistent.

The phonon anomaly in  $\text{YBa}_2\text{Cu}_3\text{O}_{6.95}$  seems to extend far in the transverse direction (Figure 25), that is, it may be consistent with the 1D picture [74] (also see Section 3.5). However, twinning of the sample made the data difficult to interpret. Otherwise, the phonon anomaly in optimally-doped  $\text{YBa}_2\text{Cu}_3\text{O}_{6.95}$  is similar to the effect in  $\text{La}_{2-x}\text{Sr}_x\text{CuO}_4$  [21].

Much less is known about  $\text{YBa}_2\text{Cu}_3\text{O}_{6+x}$  at lower doping levels. Stercel et al. [75] reported splitting of the bond-stretching branch arguing in favor of charge inhomogeneity, whereas Pintschovius et al. [76] explained similar results in terms of the difference between the dispersion of the stretching phonons propagating parallel and perpendicular to Cu–O chains. This disagreement needs to be settled by measurements on detwinned samples.

4.2.  $\text{HgBa}_2\text{CuO}_{4+x}$ . Bond-stretching phonons in  $\text{HgBa}_2\text{CuO}_{4+x}$  have been measured by Uchiyama et al. [77]. These measurements showed that the bond-stretching phonons soften similarly to  $\text{La}_{2-x}\text{Sr}_x\text{CuO}_4$  and  $\text{YBa}_2\text{Cu}_3\text{O}_{6+x}$  (Figure 26). It is important to extend this study to different dopings, temperatures and nonzero transverse wavevectors.

4.3.  $\text{Bi}_2\text{Sr}_{1.6}\text{La}_{0.4}\text{Cu}_2\text{O}_{6+x}$ . Graf et al. [78] measured phonon dispersions by IXS and electronic dispersions by ARPES in a single-layer Bi-based cuprate,  $\text{Bi}_2\text{Sr}_{1.6}\text{La}_{0.4}\text{Cu}_2\text{O}_{6+x}$  (Figure 27). They reported a similar phonon anomaly as in other cuprates and argued in favor of a correlation between this phonon anomaly, the kink observed in photoemission,

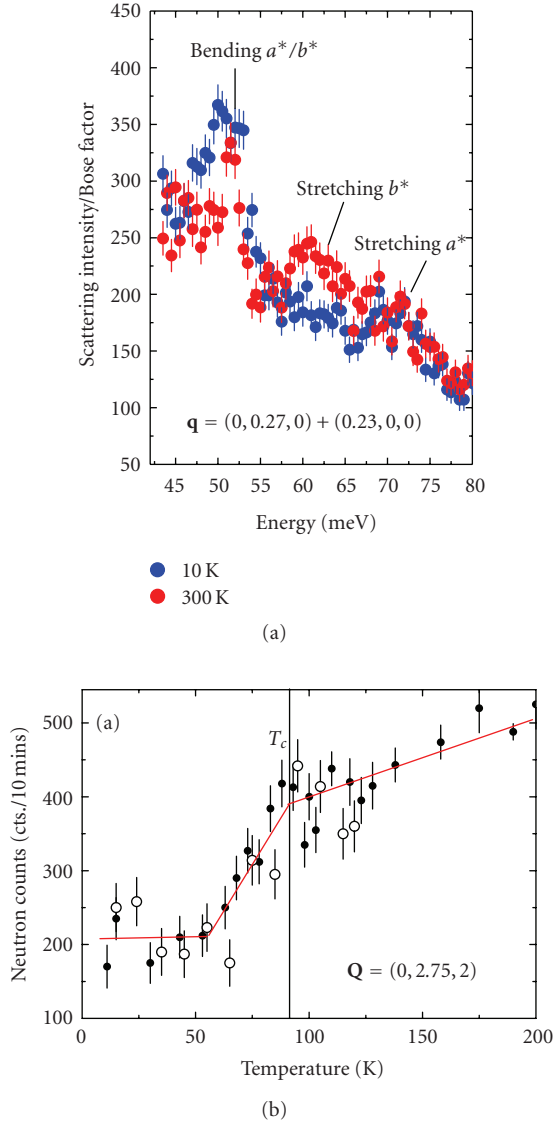


FIGURE 23: Data of [74] for the  $\Delta_4$  symmetry in  $\text{YBa}_2\text{Cu}_3\text{O}_{6.95}$ . (a) Comparison of the 300 K and 10 K spectra. (b) Background-subtracted intensity at  $\mathbf{Q} = (0, 2.75, 2)$  and  $E = 60$  meV (see text). Open and solid circles represent different datasets from [74].

and the Fermi arc that characterizes the pseudogap phase. They related the sudden onset of phonon broadening near  $\mathbf{q} = (0.2, 0, 0)$  to coupling of the phonon to the Fermi arc region of the Fermi surface, but not to the pseudogap region. The Fermi arc region is not nested, so exceptionally large electron-phonon coupling for the stretching branch is necessary for this interpretation to be valid (as in Cr as described in Section 3). In addition one needs to consider that in other families of cuprates, where the doping dependence has been investigated, the wavevector of the onset of the phonon effect is nearly doping independent, whereas the length of the Fermi arc strongly depends on doping. More detailed studies of this compound, especially as a function of doping, are necessary to clarify these issues.

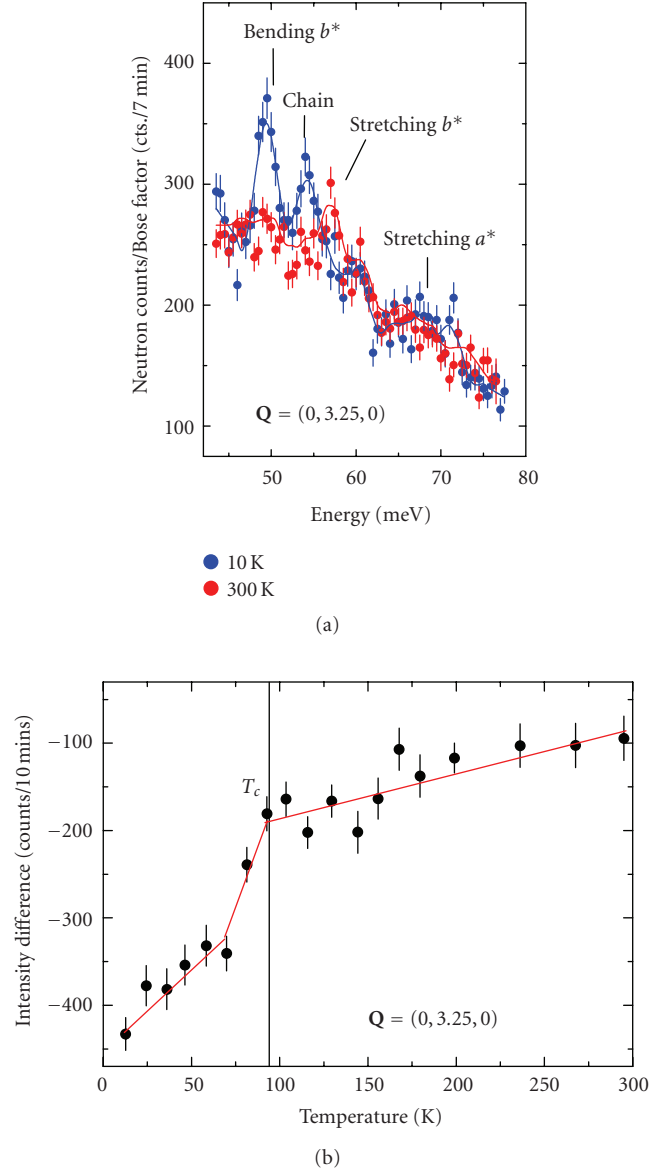


FIGURE 24: Data of [74] for the  $\Delta_1$  symmetry. (a) Phonon spectra at 300 K and 10 K. The main difference with [73] and Figure 22 is a bigger energy range here: 42–75 meV in [74] versus 51–72 meV in [73]. (b) The difference between the intensity at 57 meV and the average of intensities at 53 meV and 49 meV at  $\mathbf{Q} = (0, 3.25, 0)$ . Temperature dependence above  $T_c$  not seen in Figure 22 comes from including of the 49 meV phonon, which falls outside the energy range investigated in [73] and shown in Figure 22(a).

**4.4. Electron-Doped Cuprates.** Bond-stretching phonons have been investigated in electron-doped cuprates only in  $\text{Nd}_{2-x}\text{Ce}_x\text{CuO}_4$ . Phonon density of states measurements on powder samples showed that electron doping softens the highest energy oxygen phonons as occurs in the case of hole-doping [79]. The first single crystal experiment has been performed by d’Astuto et al. by IXS [80] who found that the bond-stretching phonon branch dispersed steeply downwards beyond  $h = 0.15$ . This work was, in fact, the

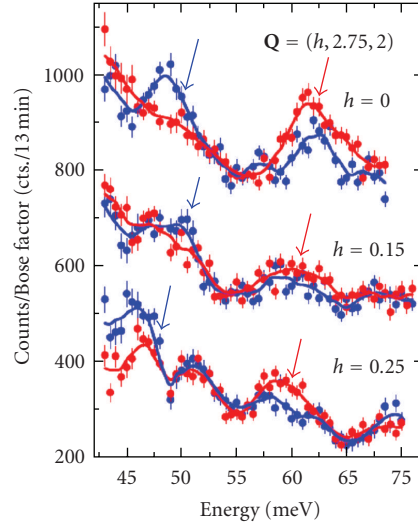


FIGURE 25: Energy scans taken at 200 K (red) and 10 K (blue). Data were taken with the final energy  $E_f = 13.4$  meV for  $E > 46$  meV and with  $E_f = 12.5$  meV for  $43 < E < 48$  meV. The 12.5-meV data were corrected for the different resolution volume by multiplying by  $(13.4/12.5)^2$ . The resulting intensities were averaged in the overlapping energy range (46.5–48 meV). The 200 K data were divided by the Bose factor and 23 counts were subtracted to correct for the temperature dependence of the background. Blue/red arrows indicate intensity gain/loss (from [74]).

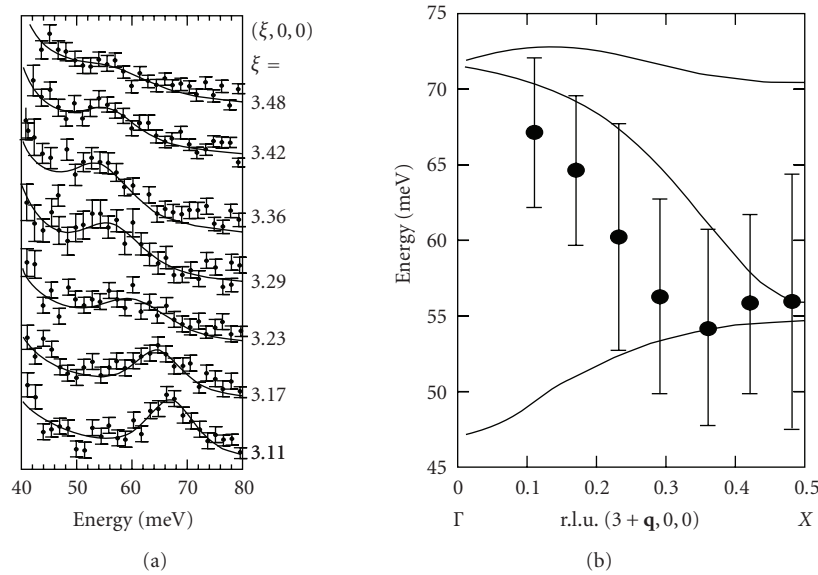


FIGURE 26: Bond stretching phonons in  $\text{HgBa}_2\text{CuO}_{4+x}$  (from [77]). (a) Enlarged spectra taken close to the bond stretching mode plotted on a linear scale. (b) Data points represent frequencies of the bond-stretching phonons. The lines show the shell model calculation in which the interaction between the next-nearest neighbor oxygens in the  $\text{CuO}_2$  plane is added. The lines indicate (top to bottom) the  $c$ -polarized apical oxygen mode, the  $a$ -polarized Cu–O bond stretching mode, and the  $a$ -polarized in-plane Cu–O bending mode, respectively. The vertical bars indicate the FWHM of the peaks determined in fitting data shown in (a).

first IXS experiment on the high  $T_c$  cuprates. These measurements, however, were complicated by the anticrossing of the bond-stretching branch with another branch due to Nd–O vibrations that dispersed sharply upwards. The anticrossing occurs near  $h = 0.2$  making the interpretation of the data near these wavevectors difficult. Another difficulty came from low IXS scattering cross sections for the oxygen vibrations.

A neutron scattering investigation has been performed by Braden et al. [81] once large single crystals became available. Oxygen phonons have a higher scattering cross section in the INS than in the IXS experiments, allowing a more accurate determination of the phonon dispersions.

The two studies showed that the bond-stretching phonon dispersion in  $\text{Nd}_{1.85}\text{Ce}_{0.15}\text{CuO}_4$  was similar to that in the hole-doped compounds (Figure 28). This similarity points

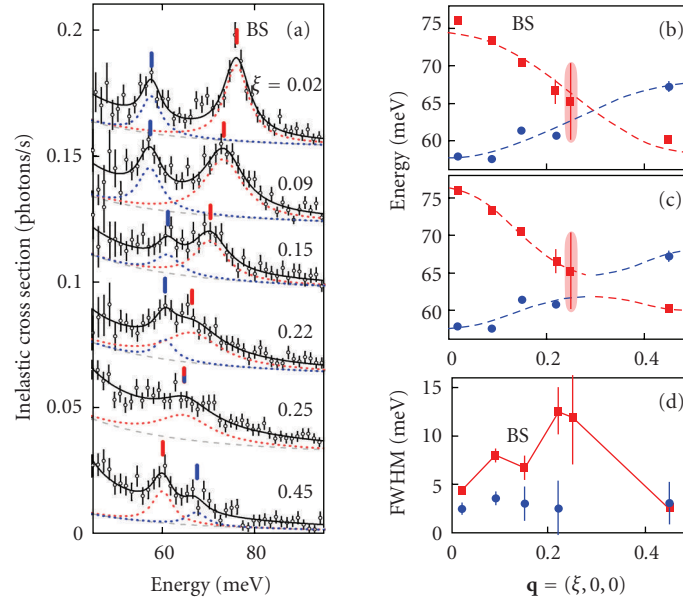


FIGURE 27: LO phonon dispersions in  $\text{Bi}_2\text{Sr}_{1.6}\text{La}_{0.4}\text{Cu}_2\text{O}_{6+x}$  [78]. (a) IXS spectra for  $\mathbf{Q} = (3+\xi, 0, 0)$  with  $\xi$  from the BZ center (top spectrum,  $\xi = 0.02$ ) to the BZ boundary (bottom spectrum,  $\xi = 0.45$ ). The spectra are vertically shifted. The solid lines show the harmonic oscillator fit, the dashed lines show the elastic tail and the dotted lines show the two modes used in the fit. (b,c) Phonon dispersions and linewidths. The cosine dashed lines are guides for the eye illustrating the crossing (b) and anticrossing (c) scenarios. (d) Full width at half maximum. The error bars are an estimate of the standard deviation of the fit coefficients.

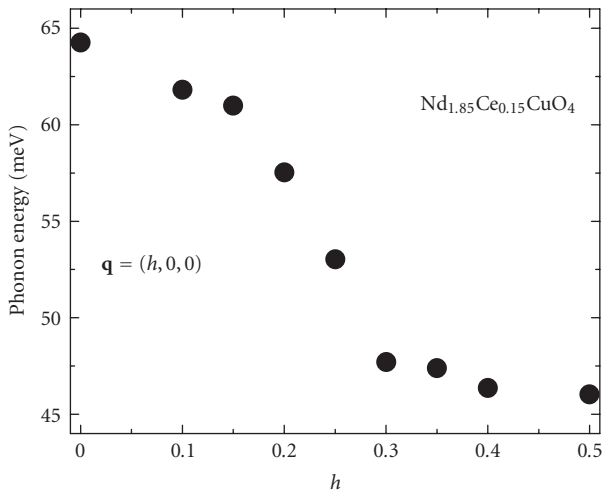


FIGURE 28: Dispersion of the Cu-O bond-stretching phonon in  $\text{Nd}_{1.85}\text{Ce}_{0.15}\text{CuO}_4$  adapted from [81].

at a commonality between the tendencies to charge inhomogeneity between the hole-doped and electron-doped compounds as discussed in [81].

## 5. Conclusions

I hope to have shown that a lot of progress has been made in recent years in understanding the phenomenology of the giant electron-phonon coupling of the bond-stretching phonons in  $\text{La}_{2-x}\text{Sr}_x\text{CuO}_4$ . The picture that emerged is that the bond-stretching phonons around  $\mathbf{q} = (0.3, 0, 0)$  are softer and broader than expected from conventional theory. This

effect may be related to incipient instability with respect to the formation of dynamic stripes or another charge-ordered or inhomogeneous state. Doping dependence of this phonon anomaly suggests that it is associated with the mechanism of superconductivity.

Much more experimental and theoretical work is necessary to understand the role of these phonons in superconductivity. The most important shortcoming of the present understanding is that  $\text{La}_{2-x}\text{Sr}_x\text{CuO}_4$  has a relatively low  $T_c$  and a number of its properties (e.g., the magnetic spectrum) differ in important ways from the cuprates with higher  $T_c$ s. Thus it is essential to put more emphasis on investigating cuprates with higher transition temperatures where similar phonon anomalies have been already found, but many open questions still remain.

## Acknowledgments

I greatly benefited from interactions with many people over the years without which this work would not have been possible. In particular, I would like to acknowledge discussions with L. Pintschovius, R. Heid, K.-P. Bohnen, W. Reichardt, H. v. Löhneysen, F. Weber, D. Lamago, A. Hamann, J. M. Tranquada, S. A. Kivelson, T. Egami, Y. Endoh, M. Arai, K. Yamada, P. B. Allen, I. I. Mazin, J. Zaanen, D. J. Singh, G. Khaliullin, B. Keimer, D. A. Neumann, J. W. Lynn, A. Mischenko, N. Nagaosa, F. Onufrieva, P. Pfeuty, P. Bourges, Y. Sidis, O. Gunnarson, S.I. Mukhin, P. Horsch, T. P. Devereaux, Z.-X. Shen, A.Q.R. Baron, D. S. Dessau, P. Böni, M. d'Astuto, A. Lanzara, M. Greven, F. Giustino, J. Noffsinger, and M. Hoesch.

## References

- [1] M. Krisch and F. Sette, "Inelastic X-ray scattering from phonons," in *Light Scattering in Solids IX*, vol. 108 of *Topics in Applied Physics*, pp. 317–370, Springer, Berlin, Germany, 2007.
- [2] W. Kohn, "Image of the fermi surface in the vibration spectrum of a metal," *Physical Review Letters*, vol. 2, no. 9, pp. 393–394, 1959.
- [3] B. Renker, L. Pintschovius, W. Gläser, et al., "Neutron-scattering study of the structural phase transition in the one-dimensional conductor  $K_2Pt(CN)_4Br_{0.3} \cdot 3D_2O$ ," *Physical Review Letters*, vol. 32, no. 15, pp. 836–839, 1974.
- [4] H. G. Smith and W. Gläser, "Phonon spectra in TaC and HfC," *Physical Review Letters*, vol. 25, no. 23, pp. 1611–1613, 1970.
- [5] W. Weber, "Lattice dynamics of transition-metal carbides," *Physical Review B*, vol. 8, no. 11, pp. 5082–5092, 1973.
- [6] S. K. Sinha and B. N. Harmon, "Electronically driven lattice instabilities," *Physical Review Letters*, vol. 35, no. 22, pp. 1515–1518, 1975.
- [7] S. Baroni, S. de Gironcoli, A. Dal Corso, and P. Gianozzi, "Phonons and related crystal properties from density-functional perturbation theory," *Reviews of Modern Physics*, vol. 73, no. 2, pp. 515–562, 2001.
- [8] R. Heid, L. Pintschovius, W. Reichardt, and K.-P. Bohnen, "Anomalous lattice dynamics of ruthenium," *Physical Review B*, vol. 61, no. 18, pp. 12059–12062, 2000.
- [9] A. Shukla, M. Calandra, M. d'Astuto, et al., "Phonon dispersion and lifetimes in  $MgB_2$ ," *Physical Review Letters*, vol. 90, no. 9, Article ID 095506, 4 pages, 2003.
- [10] A. Q. R. Baron, H. Uchiyama, Y. Tanaka, et al., "Kohn anomaly in  $MgB_2$  by inelastic X-ray scattering," *Physical Review Letters*, vol. 92, no. 19, Article ID 197004, 4 pages, 2004.
- [11] P. B. Allen and M. L. Cohen, "Superconductivity and phonon softening," *Physical Review Letters*, vol. 29, no. 24, pp. 1593–1596, 1972.
- [12] B. M. Klein and D. A. Papaconstantopoulos, "Electron-phonon interaction and superconductivity in transition metals and transition-metal carbides," *Physical Review Letters*, vol. 32, no. 21, pp. 1193–1195, 1974.
- [13] E. I. Isaev, R. Ahuja, S. I. Simak, et al., "Anomalous enhanced superconductivity and *ab initio* lattice dynamics in transition metal carbides and nitrides," *Physical Review B*, vol. 72, no. 6, Article ID 064515, 5 pages, 2005.
- [14] J. Noffsinger, F. Giustino, S. G. Louie, and M. L. Cohen, "First-principles study of superconductivity and Fermi-surface nesting in ultrahard transition metal carbides," *Physical Review B*, vol. 77, no. 18, Article ID 180507, 4 pages, 2008.
- [15] S. Y. Savrasov, "Linear-response theory and lattice dynamics: a muffin-tin-orbital approach," *Physical Review B*, vol. 54, no. 23, pp. 16470–16486, 1996.
- [16] H. Kawano, H. Yoshizawa, H. Takeya, and K. Kadowaki, "Anomalous phonon scattering below  $YNi_2^{11}B_2C$ ," *Physical Review Letters*, vol. 77, no. 22, pp. 4628–4631, 1996.
- [17] W. Reichardt, R. Heid, and K. P. Bohnen, "Phonons and electron-phonon coupling in nickel borocarbides," *Journal of Superconductivity*, vol. 18, no. 5-6, pp. 759–761, 2005.
- [18] L. Pintschovius, F. Weber, W. Reichardt, et al., "Phonon linewidths in  $YNi_2B_2C$ ," *Pramana—Journal of Physics*, vol. 71, no. 4, pp. 687–693, 2008.
- [19] P. B. Allen, V. N. Kostur, N. Takesue, and G. Shirane, "Neutron-scattering profile of  $Q \neq 0$  phonons in BCS superconductors," *Physical Review B*, vol. 56, no. 9, pp. 5552–5558, 1997.
- [20] F. Weber, A. Kreyssig, L. Pintschovius, et al., "Direct observation of the superconducting gap in phonon spectra," *Physical Review Letters*, vol. 101, no. 23, Article ID 237002, 2008.
- [21] L. Pintschovius, "Electron-phonon coupling effects explored by inelastic neutron scattering," *Physica Status Solidi B*, vol. 242, no. 1, pp. 30–50, 2005.
- [22] P. Aynajian, T. Keller, L. Boeri, S. M. Shapiro, K. Habicht, and B. Keimer, "Science 319," 2008, 1509.
- [23] E. Fawcett, "Spin-density-wave antiferromagnetism in chromium," *Reviews of Modern Physics*, vol. 60, no. 1, pp. 209–283, 1988.
- [24] W. M. Shaw and L. D. Muhlestein, "Investigation of the phonon dispersion relations of chromium by inelastic neutron scattering," *Physical Review B*, vol. 4, no. 3, pp. 969–973, 1971.
- [25] D. Lamago, M. Hoesch, M. Krisch, R. Heid, P. Böni, and D. Reznik, "Strong phonon softening without Fermi surface nesting," <http://arxiv.org/abs/0909.0594>.
- [26] W. Weber and L. F. Mattheiss, "Electron-phonon interaction in  $Ba_2YCu_3O_7$ ," *Physical Review B*, vol. 37, no. 1, pp. 599–602, 1988.
- [27] P. B. Allen, W. E. Pickett, and H. Krakauer, "Anisotropic normal-state transport properties predicted and analyzed for high- $T_c$  oxide superconductors," *Physical Review B*, vol. 37, no. 13, pp. 7482–7490, 1988.
- [28] L. Pintschovius and W. Reichardt, "Phonon dispersions and phonon density-of-states in copper-oxide superconductors," in *Neutron Scattering in Layered Copper-Oxide Superconductors*, A. Furrer, Ed., vol. 20 of *Physics and Chemistry of Materials with Low-Dimensional Structures*, pp. 165–223, Kluwer Academic Publishers, Dordrecht, The Netherlands, 1998.
- [29] S. Ishihara, T. Egami, and M. Tachiki, "Electron-lattice interaction in cuprates: effect of electron correlation," *Physical Review B*, vol. 55, no. 5, pp. 3163–3172, 1997.
- [30] L. Pintschovius, D. Reznik, and K. Yamada, "Oxygen phonon branches in overdoped  $La_{1.7}Sr_{0.3}Cu_3O_4$ ," *Physical Review B*, vol. 74, no. 17, Article ID 174514, 2006.
- [31] R. J. McQueeney, Y. Petrov, T. Egami, M. Yethiraj, G. Shirane, and Y. Endoh, "Anomalous dispersion of LO phonons in  $La_{1.85}Sr_{0.15}CuC_4$  at low temperatures," *Physical Review Letters*, vol. 82, no. 3, pp. 628–631, 1999.
- [32] L. Pintschovius and M. Braden, "Anomalous dispersion of LO phonons in  $La_{1.85}Sr_{0.15}CuO_4$ ," *Physical Review B*, vol. 60, no. 22, pp. R15039–R15042, 1999.
- [33] J. Zaanen and O. Gunnarsson, "Charged magnetic domain lines and the magnetism of high- $T_c$  oxides," *Physical Review B*, vol. 40, no. 10, pp. 7391–7394, 1989.
- [34] K. Machida, "Magnetism in  $La_2CuO_4$  based compounds," *Physica C*, vol. 158, no. 1-2, pp. 192–196, 1989.
- [35] J. M. Tranquada, B. J. Sternlieb, J. D. Axe, Y. Nakamura, and S. Uchida, "Evidence for stripe correlations of spins and holes in copper oxide superconductors," *Nature*, vol. 375, no. 6532, pp. 561–563, 1995.
- [36] D. Reznik, L. Pintschovius, M. Ito, et al., "Electron-phonon coupling reflecting dynamic charge inhomogeneity in copper oxide superconductors," *Nature*, vol. 440, no. 7088, pp. 1170–1173, 2006.
- [37] D. Reznik, L. Pintschovius, M. Fujita, K. Yamada, G. D. Gu, and J. M. Tranquada, "Electron-phonon anomaly related to charge stripes: static stripe phase versus optimally doped superconducting  $La_{1.85}Sr_{0.15}CuO_4$ ," *Journal of Low Temperature Physics*, vol. 147, no. 3-4, pp. 353–364, 2007.
- [38] D. Reznik, T. Fukuda, D. Lamago, et al., "q-dependence of the giant bond-stretching phonon anomaly in the stripe

- compound  $\text{La}_{1.48}\text{Nd}_{0.4}\text{Sr}_{0.12}\text{CuO}_4$  measured by IXS,” *Journal of Physics and Chemistry of Solids*, vol. 69, no. 12, pp. 3103–3107, 2008.
- [39] M. d’Astuto, G. Dhalenne, J. Graf, et al., “Sharp optical-phonon softening near optimal doping in  $\text{La}_{2-x}\text{Ba}_x\text{CuO}_{4+\delta}$  observed via inelastic X-ray scattering,” *Physical Review B*, vol. 78, no. 14, Article ID 140511, 2008.
- [40] J. Graf, M. d’Astuto, P. Giura, et al., “In-plane copper-oxygen bond-stretching mode anomaly in underdoped  $\text{La}_{2-x}\text{Sr}_x\text{CuO}_{4+\delta}$  measured with high-resolution inelastic X-ray scattering,” *Physical Review B*, vol. 76, no. 17, Article ID 172507, 4 pages, 2007.
- [41] C. Falter, T. Bauer, and F. Schnetgöke, “Modeling the electronic state of the high- $T_c$  superconductor  $\text{LaCuO}$ : phonon dynamics and charge response,” *Physical Review B*, vol. 73, no. 22, Article ID 224502, 2006.
- [42] F. Giustino, M. L. Cohen, and S. G. Louie, “Small phonon contribution to the photoemission kink in the copper oxide superconductors,” *Nature*, vol. 452, no. 7190, pp. 975–978, 2008.
- [43] K.-P. Bohnen, R. Heid, and M. Krauss, “Phonon dispersion and electron-phonon interaction for  $\text{YBa}_2\text{Cu}_3\text{O}_7$  from first-principles calculations,” *Europhysics Letters*, vol. 64, no. 1, pp. 104–110, 2003.
- [44] A. Hamann, et al., unpublished results.
- [45] D. Reznik, G. Sangiovanni, O. Gunnarsson, and T. P. Devereaux, “Photoemission kinks and phonons in cuprates,” *Nature*, vol. 455, no. 7213, pp. E6–E7, 2008.
- [46] R. Heid, K.-P. Bohnen, R. Zeyher, and D. Manske, “Momentum dependence of the electron-phonon coupling and self-energy effects in superconducting  $\text{YBa}_2\text{Cu}_3\text{O}_7$  within the local density approximation,” *Physical Review Letters*, vol. 100, no. 13, Article ID 137001, 2008.
- [47] P. Piekarczyk and T. Egami, “Dynamic charge transfer and spin-phonon interaction in high- $T_c$  superconductors,” *Physical Review B*, vol. 72, no. 5, Article ID 054530, 2005.
- [48] O. Rösch and O. Gunnarsson, “Electron-phonon interaction in the three-band model,” *Physical Review B*, vol. 70, no. 22, Article ID 224518, 7 pages, 2004.
- [49] P. Horsch and G. Khaliullin, “Doping dependence of density response and bond-stretching phonons in cuprates,” *Physica B*, vol. 359–361, pp. 620–622, 2005.
- [50] H. Iwasawa, J. F. Douglas, K. Sato, et al., “Isotopic fingerprint of electron-phonon coupling in high- $T_c$  cuprates,” *Physical Review Letters*, vol. 101, no. 15, Article ID 157005, 2008.
- [51] S. A. Kivelson, I. P. Bindloss, E. Fradkin, et al., “How to detect fluctuating stripes in the high-temperature superconductors,” *Reviews of Modern Physics*, vol. 75, no. 4, pp. 1201–1241, 2003.
- [52] M. Vojta, “Lattice symmetry breaking in cuprate superconductors: Stripes, nematics, and superconductivity,” *Advances in Physics*, vol. 58, p. 699, 2009.
- [53] S. I. Mukhin, A. Mesaros, J. Zaanen, and F. V. Kusmartsev, “Enhanced electronic polarizability of metallic stripes and the universality of the bond-stretching phonon anomaly in high-temperature cuprate superconductors,” *Physical Review B*, vol. 76, no. 17, Article ID 174521, 2007.
- [54] E. Kaneshita, M. Ichioka, and K. Machida, “Phonon anomalies due to collective stripe modes in high  $T_c$  cuprates,” *Physical Review Letters*, vol. 88, no. 11, Article ID 115501, 4 pages, 2002.
- [55] M. Vojta, T. Vojta, and R. K. Kaul, “Spin excitations in fluctuating stripe phases of doped cuprate superconductors,” *Physical Review Letters*, vol. 97, no. 9, Article ID 097001, 2006.
- [56] A. Y. Liu, I. I. Mazin, and J. Kortus, “Beyond Eliashberg superconductivity in  $\text{MgB}_2$ : anharmonicity, two-phonon scattering, and multiple gaps,” *Physical Review Letters*, vol. 87, no. 8, Article ID 087005, 4 pages, 2001.
- [57] F. Weber, N. Aliouane, H. Zheng, J. F. Mitchell, D. N. Argyriou, and D. Reznik, “Signature of checkerboard fluctuations in the phonon spectra of a possible polaronic metal  $\text{La}_{1.2}\text{Sr}_{1.8}\text{Mn}_2\text{O}_7$ ,” *Nature Materials*, vol. 8, no. 10, pp. 798–802, 2009.
- [58] A. S. Alexandrov, “Unconventional pairs glued by conventional phonons in cuprate superconductors,” *Journal of Superconductivity and Novel Magnetism*, vol. 22, no. 2, pp. 103–107, 2009.
- [59] S. Cojocaru, R. Citro, and M. Marinaro, “Bond-stretching phonon anomalies and charge fluctuations in copper oxide superconductors,” *Physical Review B*, vol. 75, no. 1, Article ID 014516, 8 pages, 2007.
- [60] S. Cojocaru, R. Citro, and M. Marinaro, “Isotope effect and bond-stretching phonon anomaly in high- $T_c$  cuprates,” submitted to *The European Physical Journal B*.
- [61] C. J. Zhang and H. Oyanagi, “Local lattice instability and superconductivity in  $\text{La}_{1.85}\text{Sr}_{0.15}\text{Cu}_{1-x}\text{M}_x\text{O}_4$  ( $M = \text{Mn}, \text{Ni}, \text{and Co}$ ),” *Physical Review B*, vol. 79, no. 6, Article ID 064521, 2009.
- [62] T. Mertelj, V. V. Kabanov, and D. Mihailovic, “Charged particles on a two-dimensional lattice subject to anisotropic Jahn-Teller interactions,” *Physical Review Letters*, vol. 94, no. 14, Article ID 147003, 2005.
- [63] J. Miranda, T. Mertelj, V. V. Kabanov, and D. Mihailovic, “Bipolaron Jahn-Teller pairing and charge transport in cuprates,” *Journal of Superconductivity and Novel Magnetism*, vol. 22, no. 3, pp. 281–285, 2009.
- [64] J. Ranninger and A. Romano, “Local dynamical lattice instabilities: prerequisites for resonant pairing superconductivity,” *Physical Review B*, vol. 78, no. 5, Article ID 054527, 2008.
- [65] H. Keller, A. Bussmann-Holder, and K. A. Müller, “Jahn-Teller physics and high- $T_c$  superconductivity,” *Materials Today*, vol. 11, no. 9, pp. 38–46, 2008.
- [66] S. Sykora, A. Hübsch, and K. W. Becker, “Coexistence of superconductivity and charge-density waves in a two-dimensional Holstein model at half-filling,” *Europhysics Letters*, vol. 85, no. 5, Article ID 57003, 2009.
- [67] A. S. Alexandrov, “Phase separation of electrons strongly coupled with phonons in cuprates and manganites,” *Journal of Superconductivity and Novel Magnetism*, vol. 22, no. 2, pp. 95–101, 2009.
- [68] M. Vojta and O. Rösch, “Superconducting  $d$ -wave stripes in cuprates: valence bond order coexisting with nodal quasiparticles,” *Physical Review B*, vol. 77, no. 9, Article ID 094504, 2008.
- [69] J. Röhler, “The bulge in the basal plane area of cuprate superconductors: evidence for  $3a$  singlet hole pairs,” *Physica C*, vol. 460–462, pp. 374–375, 2007.
- [70] S. Ishihara and N. Nagaosa, “Interplay of electron-phonon interaction and electron correlation in high-temperature superconductivity,” *Physical Review B*, vol. 69, no. 14, Article ID 144520, 13 pages, 2004.
- [71] D. Reznik, L. Pintschovius, W. Reichardt, et al., “Oxygen phonon branches in detwinned  $\text{YBa}_2\text{Cu}_3\text{O}_7$ ,” *Journal of Low Temperature Physics*, vol. 131, no. 3–4, pp. 417–422, 2003.
- [72] L. Pintschovius, D. Reznik, W. Reichardt, et al., “Oxygen phonon branches in  $\text{YBa}_2\text{Cu}_3\text{O}_7$ ,” *Physical Review B*, vol. 69, no. 21, Article ID 214506, 2004.
- [73] J.-H. Chung, T. Egami, R. J. McQueeney, et al., “In-plane anisotropy and temperature dependence of oxygen phonon modes in  $\text{YBa}_2\text{Cu}_3\text{O}_{6.95}$ ,” *Physical Review B*, vol. 67, no. 1, Article ID 014517, 9 pages, 2003.

- [74] D. Reznik, L. Pintschovius, J. M. Tranquada, et al., “Temperature dependence of the bond-stretching phonon anomaly in  $\text{YBa}_2\text{Cu}_3\text{O}_{6.95}$ ,” *Physical Review B*, vol. 78, no. 9, Article ID 094507, 2008.
- [75] F. Stercel, T. Egami, H. A. Mook, et al., “Composition dependence of the in-plane Cu-O bond-stretching LO phonon mode in  $\text{YBa}_2\text{Cu}_3\text{O}_{6+x}$ ,” *Physical Review B*, vol. 77, no. 1, Article ID 014502, 9 pages, 2008.
- [76] L. Pintschovius, W. Reichardt, M. Kläser, T. Wolf, and H. V. Löhneysen, “Pronounced in-plane anisotropy of phonon anomalies in  $\text{YBa}_2\text{Cu}_3\text{O}_{6.6}$ ,” *Physical Review Letters*, vol. 89, no. 3, Article ID 037001, 4 pages, 2002.
- [77] H. Uchiyama, A. Q. R. Baron, S. Tsutsui, et al., “Softening of Cu-O bond stretching phonons in tetragonal  $\text{HgBa}_2\text{CuO}_{4+\delta}$ ,” *Physical Review Letters*, vol. 92, no. 19, Article ID 197005, 2004.
- [78] J. Graf, M. d’Astuto, C. Jozwiak, et al., “Bond stretching phonon softening and kinks in the angle-resolved photoemission spectra of optimally doped  $\text{Bi}_2\text{Sr}_{1.6}\text{La}_{0.4}\text{Cu}_2\text{O}_{6+\delta}$  superconductors,” *Physical Review Letters*, vol. 100, no. 22, Article ID 227002, 2008.
- [79] H. J. Kang, P. Dai, D. Mandrus, et al., “Doping evolution of the phonon density of states and electron-lattice interaction in  $\text{Nd}_{2-x}\text{Ce}_x\text{CuO}_{4+\delta}$ ,” *Physical Review B*, vol. 66, no. 6, Article ID 064506, 5 pages, 2002.
- [80] M. d’Astuto, P. K. Mang, P. Giura, et al., “Anomalous dispersion of longitudinal optical phonons in  $\text{Nd}_{1.86}\text{Ce}_{0.14}\text{CuO}_{4+\delta}$  determined by inelastic X-ray scattering,” *Physical Review Letters*, vol. 88, no. 16, Article ID 167002, 4 pages, 2002.
- [81] M. Braden, L. Pintschovius, T. Uefuji, and K. Yamada, “Dispersion of the high-energy phonon modes in  $\text{Nd}_{1.85}\text{Ce}_{0.15}\text{CuO}_4$ ,” *Physical Review B*, vol. 72, no. 18, Article ID 184517, 10 pages, 2005.
- [82] X. J. Zhou, T. Yoshida, A. Lanzara, et al., “High-temperature superconductors: universal nodal Fermi velocity,” *Nature*, vol. 423, no. 6938, p. 398, 2003.

## Review Article

# Electron-Phonon Interaction in the High- $T_C$ Cuprates in the Framework of the Van Hove Scenario

Jacqueline Bouvier and Julien Bok

*Solid State Physics Laboratory, ESPCI ParisTech, 10 rue Vauquelin, 75231 Paris Cedex 05, France*

Correspondence should be addressed to Jacqueline Bouvier, jacqueline.bouvier@espci.fr

Received 17 June 2009; Revised 23 September 2009; Accepted 30 November 2009

Academic Editor: Sasha Alexandrov

Copyright © 2010 J. Bouvier and J. Bok. This is an open access article distributed under the Creative Commons Attribution License, which permits unrestricted use, distribution, and reproduction in any medium, provided the original work is properly cited.

Electron-lattice interaction was the original idea of Müller and Berdnorz who chose copper oxides, because of the strong Jahn-Teller effect of the Cu ion leading to the formation of bipolarons. Later several experimental features led to theoretical models based on strong electronic correlations. The high- $T_C$  superconductors cuprates are quasi-bidimensional (2D) and thus lead to the existence of Van Hove singularities (VHs) in the band structure, that is, a peak in the electronic density of states. The presence of VHs near the Fermi-level in the cuprates is now well established. In this context we show that many physical properties of these materials can be explained using electron-phonon interaction, in particular the high critical temperature  $T_C$ , the anomalous isotope effect, the superconducting gap and its anisotropy, and the marginal Fermi-liquid properties. These compounds present a topological transition for a critical hole doping  $p \approx 0.21$  hole per  $\text{CuO}_2$  plane.

## 1. Introduction

Twenty three years after the discovery of the high temperature superconductivity in cuprates compounds [1], the exact mechanism of superconductivity is still not yet understood. Müller and Berdnorz stressed that superconductivity occurs because of the Jahn-Teller effect of the Cu ion. But all these compounds are also strongly anisotropic and almost two dimensional, due to their  $\text{CuO}_2$  planes, where superconductivity mainly occurs. It is well known that electrons, in a periodic system in one or two dimensions, lead to divergences in the density of states (DOS), named Van Hove singularities (VHs) [2]. The Van Hove scenario is based on the assumption that in some superconductors the Fermi level lies close to such a singularity. Labbé and Friedel [3] applied this scenario for the first time to the  $\text{A15}$  compounds, where the Nb chains give an almost 1D behaviour. Hirsch and Scalapino [4] examined the 2D situation (logarithmic singularity) and applied it to excitonic superconductivity. Labbé and Bok [5] proposed the Van Hove scenario for the cuprates, using electron-phonon interaction and predicted an anomalous isotope effect. The presence of saddle points

(or VHs) near the Fermi level has been confirmed by many experiments, in particular by Angular Resolved Photoemission Spectroscopy (ARPES) [6, 7] in different compounds.

The origin of high- $T_C$  in the cuprates is still controversial, and the role of these singularities in the mechanism of high- $T_C$  superconductivity is not yet established, but we want to stress that the model of 2D itinerant electrons in presence of VHs in the band structure has already explained a certain number of experimental facts.

We know that several experimental features led to theoretical models based on electron-electron interaction [8, 9] (strong correlations between electrons). These features are the following:

- (i) the anomalous isotope effect,
- (ii) the observation of antiferromagnetic (AF) fluctuations,
- (iii) the marginal Fermi-liquid behaviour in the normal phase,
- (iv) the d-wave symmetry of the superconducting gap.

The strong correlations are surely very important in the underdoped regime but we shall show that electron-phonon interaction coupled with the Van Hove scenario may explain most of the properties in the region of optimum doping and the overdoped region.

In this paper, we give a rapid description of the band structure of the  $\text{CuO}_2$  planes. We give the results of our calculations for the critical temperature  $T_C$  [5, 10, 11], the anisotropic superconducting gap [10]. We show the importance of screening and Coulomb repulsion [10, 12]. We explain the anomalous isotope effect [5], the very small values of the coherence length [13, 14].

The variation with the doping is linked to the distance of the FL from the singularity level ( $E_F - E_S$ ), so does the variation with the temperature due to the Fermi-Dirac distribution [11]. We show that  $E_F - E_S$  is critical for these properties, leading to Fermi-liquid or marginal Fermi-liquid behaviour [15, 16].

We explain how the occurrence of a lattice deformation could place the Fermi level in an optimum situation of high DOS, leading to a high critical temperature for the superconducting phase.

In conclusion we show that taking into account both the electron-phonon interaction and the existence of the VHs, we obtain a model that fits with experiments in the optimum and overdoped regime of the cuprates. We hope that such an approach can help chemists to improve the HTSC.

## 2. Electronic Structure of the Cuprates and Van Hove Scenario

Van Hove singularities are general features of periodic system [2]. A one electron calculation is easy to perform [5]. A general feature of a 2D model is the presence of Van Hove singularity [5] (VHs) with logarithmic divergence of the DOS at an energy  $E = E_S$ . A simple calculation [17] gives the result shown in Figure 1 for the constant energy surfaces (CES) in  $k$ -space. This is very well confirmed by the results of Ino et al. [6] using angular resolved photoemission spectroscopy (ARPES) (see [6, Figure 7]).

A topological transition is well seen for a doping value  $p_c = 0.21$  hole per Cu atom. The CES are hole-like for  $p < p_c$  and electron-like for  $p > p_c$ . The resulting VHs gives a peak in the DOS, see Figure 2, and thus increases the transition temperature whatever the pairing mechanism. The main consequences of this Van Hove scenario are given in [17].

This approach is not valid for the underdoped region. The strong Coulomb repulsion  $U$  between two electrons on a same site is responsible for the fact that with  $p = 0$  the cuprates are Mott-insulators with antiferromagnetic (AF) order. The AF order disappears rather rapidly with doping, but AF fluctuations remain, and decrease, until the optimum doping. This region of strong correlations is present and the valid approach is that of a doped Mott-insulator [8]. This is also seen in ARPES; some points of the Fermi surface disappear for underdoped samples.

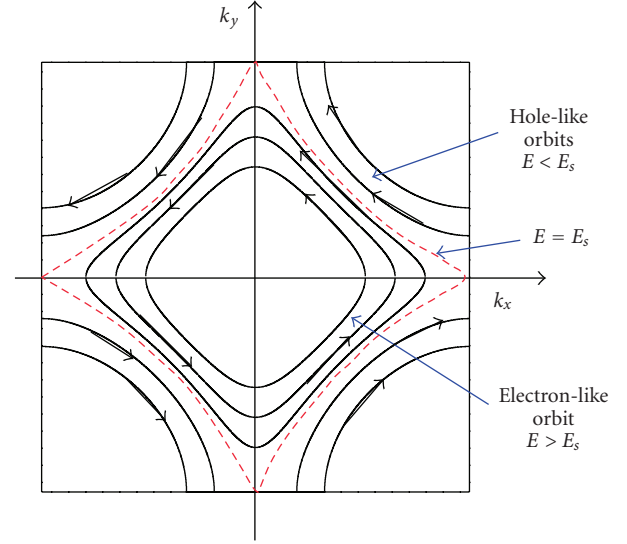


FIGURE 1: Constant energy surfaces.

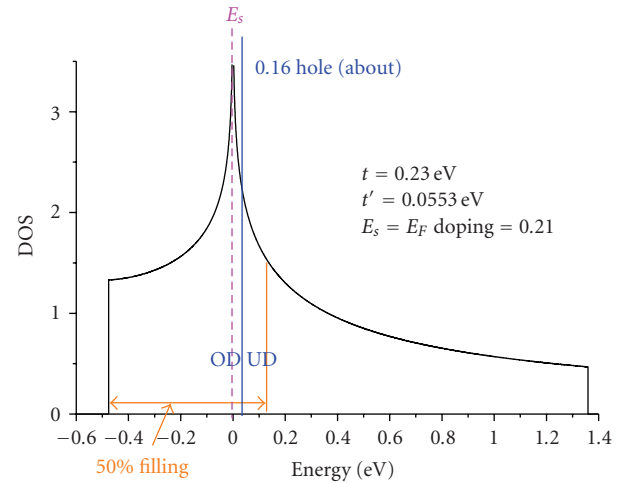


FIGURE 2: Density of States (DOS).

## 3. Calculation of $T_C$ with Electron-Phonon Interaction

**3.1. Calculation of  $T_C$  Using the BCS Approach.** Labbé and Bok [5] have computed the band structure for the bidimensional  $\text{CuO}_2$  planes of the cuprates, considered as a square lattice (quadratic phase). They obtained a formula for  $T_C$  using the following assumptions:

- (1) the Fermi level lies at the Van Hove singularity,
- (2) the BCS approach is valid,

(i) the electron-phonon interaction is isotropic and so is the superconducting gap  $\Delta$ ,

(ii) the attractive interaction  $V_p$  between electrons is nonzero only in an interval of energy  $\pm \hbar\omega_0$  around the Fermi level where it is constant. When this attraction is mediated by emission and absorption of phonons,  $\omega_0$  is a typical phonon frequency.

In that case, the critical temperature is given by

$$k_B T_c = 1.13D \exp \left[ - \left( \frac{1}{\lambda} + \ln^2 \left( \frac{\hbar\omega_0}{D} \right) - 1.3 \right)^{1/2} \right], \quad (1a)$$

where  $\lambda$  is an electron-phonon coupling constant [3].

A simplified version of Formula (1a), when  $\hbar\omega_0$  is not too small compared to  $D$ , is

$$k_B T_c = 1.13D \exp \left( - \frac{1}{\sqrt{\lambda}} \right). \quad (1b)$$

The two main effects enhancing  $T_C$  are the following.

- (1) The prefactor in Formula (1b) is an electronic energy that is much larger than a typical phonon energy  $\hbar\omega_0$ .
- (2)  $\lambda$  is replaced by  $\sqrt{\lambda}$  in Formula (1b) in comparison with the BCS formula, so that in the weak coupling limit when  $\lambda < 1$ , the critical temperature is increased.

As it is however, this approach already explains many of the properties of the high- $T_C$  cuprates near optimum doping.

**3.2. The Variation of  $T_C$  with Doping.** Then we did more accurate calculations (1995–1997) [10, 11]. By taking into account the repulsive interaction between second nearest neighbours (s.n.n.) and the variation of hole doping [11], the band structure becomes

$$E_k = -2t(\cos X + \cos Y) + 4t' \cos X \cos Y + D_e, \quad (2)$$

where  $t'$  is an integral representing the interaction with s.n.n., where  $D_e = E_F - E_S + (4t')$  represents the doping in hole  $p$ . The Fermi surface at the VHs is no longer a square but is rather diamond shaped, see Figure 1, and we obtain the DOS of Figure 2. For lower or higher doping the critical temperature decreases. We adjusted the experimental results of Koike et al. [18]; see Figure 3 [11]. In this case the authors varied the hole concentration in the  $\text{CuO}_2$  planes of  $\text{Bi}_2\text{Sr}_2\text{CaCu}_2\text{O}_{8+\delta}$  using different substitution of cations with different valences, obtaining different systems, that is

$$\begin{aligned} & \text{Bi}_2\text{Sr}_2\text{Ca}_{1-x}\text{Lu}_x\text{Cu}_2\text{O}_{8+\delta}, \text{Bi}_2\text{Sr}_2\text{Ca}_{1-x}\text{Na}_x\text{Cu}_2\text{O}_{8+\delta}, \\ & \text{Bi}_2\text{Sr}_{2-x}\text{Ca}_{1-x}\text{La}_x\text{CaCu}_2\text{O}_{8+\delta}, \text{Bi}_2\text{Sr}_{2-x}\text{K}_x\text{CaCu}_2\text{O}_{8+\delta}. \end{aligned} \quad (3)$$

In Figure 3 our model account for the variation of the holes in the  $\text{CuO}_2$  plane, from an optimum doping, here  $p \approx 0.20$ , of this group of compounds, and we calculate the corresponding  $T_C$  when  $E_F$  shift from  $E_S$ .

**3.3. Influence of the Coulomb Repulsion.** Although BCS theory [19] neglects Coulomb repulsion, Morel and Anderson [20] showed very early that it plays a central role in superconductivity. Assuming a constant repulsive potential  $V_C$  from 0 to  $E_F$ , they found that  $T_C$  is given by

$$T_C \cong T_0 \exp \left[ - \frac{1}{\lambda - \mu^*} \right] \quad (4)$$

with  $\mu = \text{No } V_C$  and  $\mu^* = \mu / (1 + \mu \ln E_F / \omega_0)$ .

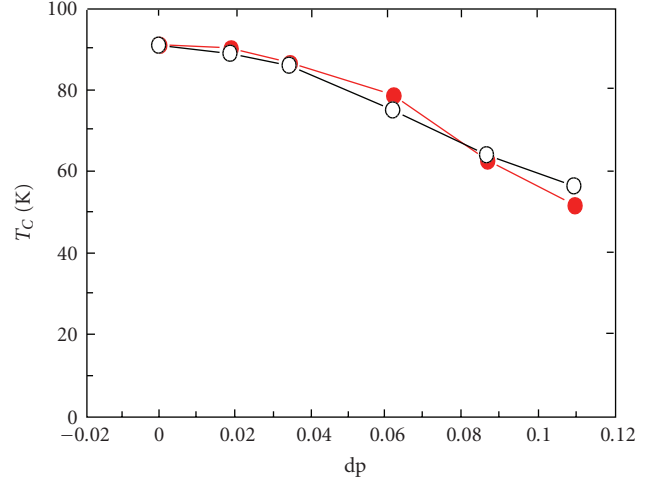


FIGURE 3: Comparison of the variation of  $T_C$  with the variation of the doping  $dp$  from the optimum doping at  $dp = 0$ , calculated in our model (red filled circles) and the experimental results of Koike et al. (black open circles) [18].

Cohen and Anderson [21] assumed that for stability reasons  $\mu$  is always greater than  $\lambda$ . Ginzburg [22] gave arguments that in some special circumstances  $\mu$  can be smaller than  $\lambda$ . Nevertheless if we take  $\mu \geq \lambda$ , superconductivity only exists because  $\mu^*$  is of the order of  $\mu/3$  to  $\mu/5$  for a Fermi energy  $E_F$  of the order of  $100 \hbar\omega_0$ . It is useless to reduce the width of the band  $W$ , because  $\lambda$  and  $\mu$  vary simultaneously and  $\mu^*$  becomes greater if  $E_F$  is reduced, thus giving a lower  $T_C$ . Superconductivity can even disappear in a very narrow band if  $\lambda - \mu^*$  becomes negative.

Force and Bok studied the renormalization of  $\mu$ , in the case of a peak in the DOS in the middle of a broad band [14]. They predict a high- $T_C$  in this case due to three main effects.

- (i)  $(\lambda - \mu^*)$  is replaced by the square root  $(\lambda - \mu^*)^{1/2}$ .
- (ii)  $\mu^*$  is reduced compared to  $\mu$  because the renormalization is controlled by the width  $W$  of the broad band and not the singularity.
- (iii) The prefactor before the exponential in the formula giving  $T_C$  is the width of the singularity  $D$  instead of the phonon energy  $\hbar\omega_0$ .

In Figure 4, we show the variation of  $T_C$  with the width of the singularity  $D$ , with all other parameters ( $W$ ,  $\omega_0$ ) remaining constant.

## 4. Anomalous Isotope Effect

The variation of  $T_C$  with the mass  $M$  of the atom of the metal is considered as an evidence for electron-phonon interaction as the origin of pairing. In this BCS model [19]  $T_C$  varies as  $M^{-1/2}$ . The almost absence of isotope effect when  $\text{O}^{18}$  was substituted to  $\text{O}^{16}$  in the cuprates [23] was considered as an evidence for non phonon origin of superconductivity. But Labbé and Bok [5], using Formula (1a), have shown

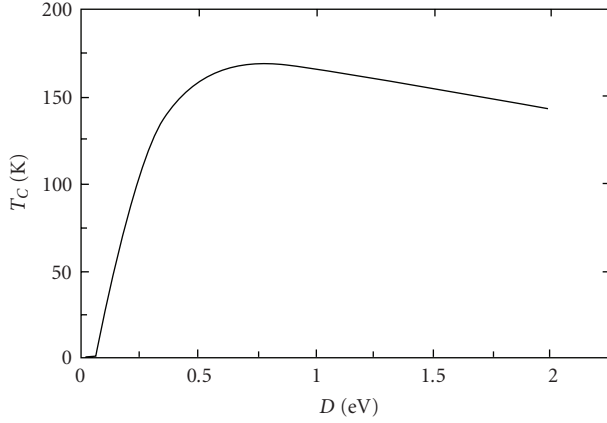


FIGURE 4: Effect of the band width  $D$  of the singularity on  $T_C$ .

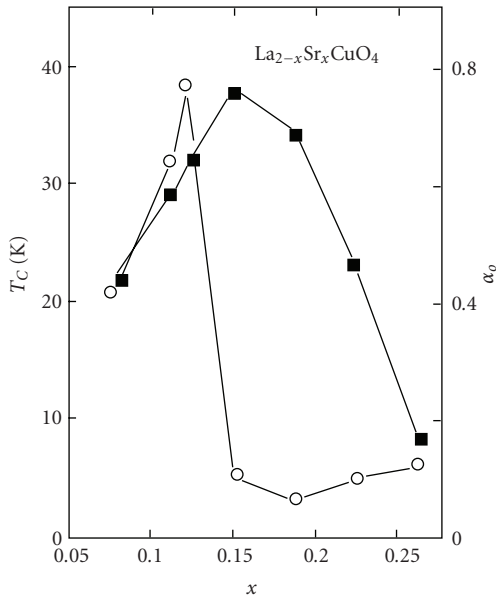


FIGURE 5: From [26], experimental results of  $T_C$  (■) and  $\alpha_o$  (○) as a function of doping concentration for  $\text{La}_{2-x}\text{Sr}_x\text{CuO}_4$  (the data where taken from [24]).

that the isotope effect is strongly reduced for HTCS cuprates at optimum doping. This is due to the fact that in this situation the Fermi level lies near the VHs and then the width of the singularity  $D$  is more important than the phonon frequency  $\omega_o$ . They also have predicted that the isotope effect should reappear for underdoped samples. This was later experimentally observed [24, 25]. The isotope effect may be measured by the coefficient  $\alpha$  defined as  $T_C$  proportional to  $M^{-\alpha}$  ( $\alpha = 0.5$  for usual superconductors). Tsuei et al. [26], using the VH scenario, have calculated the variation of  $\alpha$  with doping and shown in that it explains the experimental observations, see Figure 5.

## 5. Non-Fermi-liquid Properties

**5.1. Resistivity.** In a classical Fermi-liquid, the lifetime broadening  $1/\tau$  of an excited quasiparticle goes as  $\epsilon^2$  and

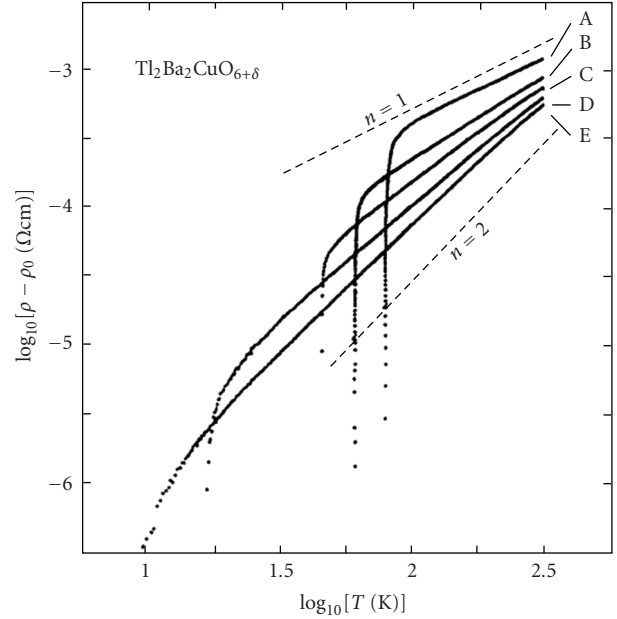


FIGURE 6: From [30], fit of the resistivity  $\rho$  of  $\text{Tl}_2\text{Ba}_2\text{CuO}_{6+\delta}$  to a power law temperature dependence  $\rho = \rho_o + AT^n$  shown on a log-log scan. The dashed lines indicate the slope for  $n = 1$  and  $n = 2$ .

the resistivity  $\rho$  varies as  $T^2$ . The marginal Fermi-liquid situation is the case where  $1/\tau$  goes as  $\epsilon$  (electronic energy) and  $\rho$  is linear in  $T$ . In the half-filled nearest-neighbour coupled Hubbard model on a square lattice, Newns et al. [15, 16] have shown that this can also occur when  $E_F$  is close to  $E_S$ . This calculation was however contradicted by Hlubina and Rice [27].

Experimental evidence of marginal Fermi-liquid behaviour has been seen in angle resolved photoemission [28], infrared data, and temperature dependence of electrical resistivity [29]. Marginal Fermi-liquid theory, in the framework of VHS, predicts a resistivity linear with temperature  $T$ . This was observed by Kubo et al. [30] and cited in [8]. They also observe that the dependence of resistivity goes from  $T$  for high- $T_C$  material to  $T^2$  as the system is doped away from the maximum  $T_C$ , see Figure 6, which is consistent with our picture; in lower  $T_C$  material the Fermi level is pushed away from the singularity.

**5.2. Hall Coefficient.** Many measurements of the Hall coefficient  $R_H$  in various high- $T_C$  cuprates have been published [31, 32]. The main results are the following

- (i) At low temperature  $T$ ,  $R_H \approx 1/p_{h0}e$ , where  $p_{h0}$  is the hole doping, when  $T$  increases  $R_H$  decreases, and for highly overdoped samples it becomes even negative.
- (ii) These authors are also able to define a temperature  $T_0$ , where  $R_H$  changes its temperature behaviour, and they found that  $R_H(T)/R_H(T_0)$  versus  $T/T_0$  is a universal curve for a large doping domain (from  $p_{h0} = 0.10$  to  $p_{h0} = 0.27$ ).

We can explain [33], following the approach given by Ong [34], these results by using the band structure for carriers in the  $\text{CuO}_2$  planes. In particular, the existence of hole-like and electron-like constant energy curves, see Figure 1, which give contributions of opposite sign to  $R_H$ . The transport properties explore a range of energy  $k_B T$  around the Fermi level, when  $T$  is increased more and more carriers are on the electron like orbits, resulting in a decrease of  $R_H$ . In [33] we present our calculations and the theoretical fits of many experimental results, and we show that it works and this supports our model.

## 6. Gap Anisotropy

**6.1. The Calculation.** Bouvier and Bok [10] have shown that using a weakly screening electron-phonon interaction, and the band structure of the  $\text{CuO}_2$  planes, an anisotropic superconducting gap is found.

We use the BCS equation for an anisotropic gap

$$\Delta_{\vec{k}} = \sum_{k'} \frac{V_{kk'} \Delta_{k'}}{\sqrt{\xi_{k'}^2 + \Delta_{k'}^2}}, \quad (5)$$

and instead of a constant potential as used in BCS, we choose a weakly screened attractive electron-phonon interaction potential:

$$V_{kk'} = \frac{-|g_q|^2}{q^2 + q_0^2} < 0, \quad (6)$$

where  $g(q)$  is the electron phonon interaction matrix element for  $\vec{q} = \vec{k}' - \vec{k}$  and  $q_0$  is the inverse of the screening length. We compute  $\Delta_{\vec{k}}$  for two values of  $\vec{k}$ :

$$\Delta_A \quad \text{for } k_x a = \pi, \quad k_y a = 0, \quad (7a)$$

$$\Delta_B \quad \text{for } k_x a = k_y a = \frac{\pi}{2}. \quad (7b)$$

We solve (5) by iteration for these two specific points of the Fermi surface, the saddle point  $A$  ( $\pi, 0$ ) or  $(1, 0)$  direction, and point  $B$  ( $\pi/2, \pi/2$ ) or  $(1, 1)$  direction. To obtain the entire dependence in the wave vector  $\vec{k}$ , we know from group theory considerations that  $V_{kk'}$  having a fourfold symmetry, the solution  $\Delta_k$  has the same symmetry, so we may use the angle  $\Phi$  between the 0 axis and the  $\vec{k}$  vector as a variable and expand  $\Delta(\Phi)$  in Fourier series:

$$\Delta(\Phi) = \Delta_0 + \Delta_1 \cos(4\Phi + \varphi_1) + \Delta_1 \cos(8\Phi + \varphi_2) + \dots \quad (8)$$

Further developments of the calculations and explanations about this model are done in [10]. We obtain, for the two computed values

$$\Delta_A = \Delta_{\max} = \Delta_0 + \Delta_1, \quad \Delta_B = \Delta_{\min} = \Delta_0 - \Delta_1 \quad (9)$$

The gap anisotropy is important because the scattering is essentially forward, this is due to the weak screening in

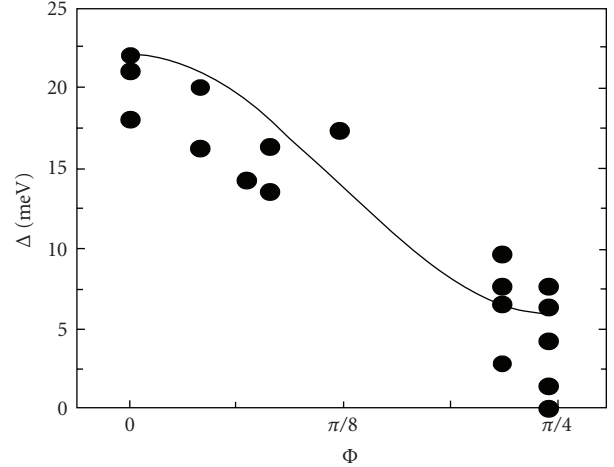


FIGURE 7: Anisotropic superconducting gap. Exact calculation for  $\Phi = 0$  and  $\pi/4$ . This represents an  $s$ -wave anisotropic superconducting gap with no nodes in  $\Phi = \pi/4$ .

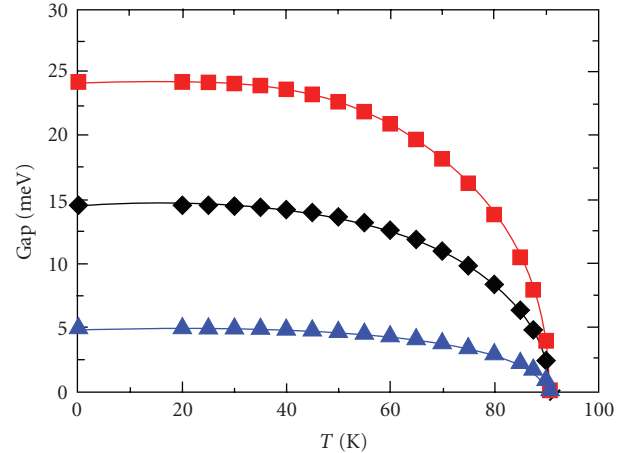


FIGURE 8: Variation of the various gaps  $\Delta_{\max}$ ,  $\Delta_{\min}$ , and  $\Delta_{\text{av}}$  versus temperature, at the optimum doping, with the following parameters,  $t = 0.2$  eV,  $\hbar\omega_o = 60$  meV,  $q_0 a = 0.12$ ,  $\lambda_{\text{eff}} = 0.665$ , red square symbol =  $\Delta_{\max}$ , black diamond symbol =  $\Delta_{\text{av}}$ , blue up triangle symbol =  $\Delta_{\min}$ .

two dimensions. The wave vector explores a small region in  $k$ -space. The gap is important in the direction of the saddle point, due to its high density of states, and its effect is reinforced by the weak screening. But for the point  $B$  ( $\pi/2, \pi/2$ ) the DOS is smaller and the effect is reduced.

From our theoretical results, we find an effective coupling constant  $\lambda_{\text{eff}}$  in agreement with the hypothesis of the BCS weak electron-phonon coupling.

**6.2. Results.** In Figure 7, we present the result of the iterative calculation.

We thus obtain an “extended  $s$ -wave” gap and not a  $d$ -wave pair function. The order parameter is never negative in our model. Abrikosov [35] has shown, however, that if a short-range repulsive interaction (which can represent either

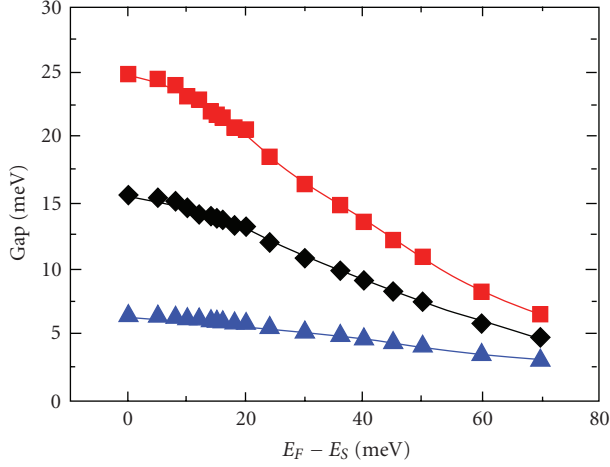


FIGURE 9: Variation of the various gaps  $\Delta_{\max}$ ,  $\Delta_{\min}$ ,  $\Delta_{\text{av}}$  versus the doping linked to  $E_F - E_S$  at  $T = 0$  K red square symbol =  $\Delta_{\max}$ , black diamond symbol =  $\Delta_{\text{av}}$ , blue up triangle symbol =  $\Delta_{\min}$ .

some part of the Hubbard repulsion at the copper sites or the interaction mediated by spin fluctuations) is added, then the order parameter can vary in sign and become negative at points of the Fermi surface distant from the singularity. Such an approach may reconcile all the observations leading sometimes to  $s$ -wave and other times to  $d$ -wave symmetry of the order parameter. The fact that the order parameter is negative in certain regions of the Fermi surface explains the results of experiments showing a  $\pi$  phase shift of the order parameter [36].

In Figure 8, we present the variation of the various gaps  $\Delta_{\max}$ ,  $\Delta_{\min}$ , and  $\Delta_{\text{av}}$  (or  $\Delta_0$ ) with temperature at optimum doping, that is, for a density of holes of the order of 0.20 per  $\text{CuO}_2$  plane. We find  $T_C = 91$  K and an anisotropy ratio  $\alpha = \Delta_{\max}/\Delta_{\min} = 4.2$  and for the ratios of  $2\Delta/k_B T_C$  the following values:

$$\frac{2\Delta_{\max}}{k_B T_C} = 6, \quad \frac{2\Delta_{\text{av}}}{k_B T_C} = 3.7, \quad \frac{2\Delta_{\min}}{k_B T_C} = 1.4. \quad (10)$$

This may explain the various values of  $2\Delta/k_B T_C$  observed in various experiments. The critical temperature found is  $T_C = 90.75$  K as for HTSC cuprates as  $\text{Bi}_2\text{Sr}_2\text{CaCu}_2\text{O}_8$  (Bi 2212),  $\text{YBa}_2\text{Cu}_3\text{O}_{7-\delta}$  (Y123).

In Figure 9, we present the same results,  $\Delta_{\max}$ ,  $\Delta_{\min}$ ,  $\Delta_{\text{av}}$  as a function of  $E_F - E_S$  linked to the variation of doping.

**6.3. Effect of the Screening on the Gap Anisotropy and  $T_C$ .** We stress the importance of  $q_0 a$ , the screening parameter, in the value of  $T_C$ , and the anisotropy ratio  $\alpha = \Delta_{\max}/\Delta_{\min}$ . We give the results of our study, in the approximation of weak screening ( $q_0 a < 0.2$ ). The results are presented in Figure 10. We see that increasing  $q_0 a$ , or, in other word, going towards more metallic system or 3D, the anisotropy of the gap decreases. For  $T_C$ , the results are presented in Figure 11. The effect of increasing the screening strength is to decrease  $T_C$ . An increase of the screening can be due to the proximity of  $E_F$  to  $E_S$ , where the DOS is high, and in the other side  $T_C$  is increased by the high DOS. There is a competition of the two

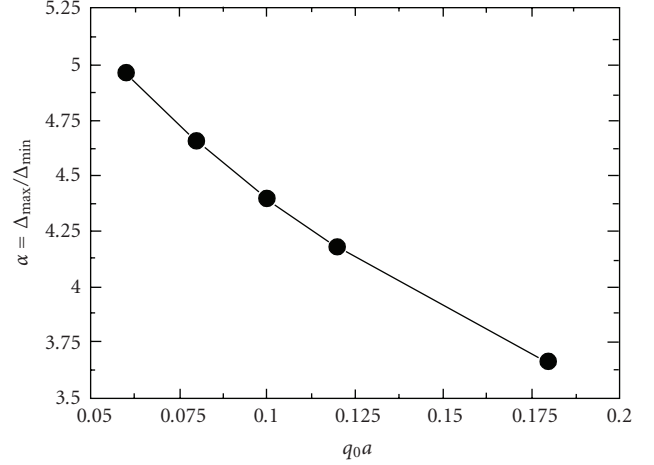


FIGURE 10: The anisotropy ratio  $\alpha = \Delta_{\max}/\Delta_{\min}$  versus the screening parameter  $q_0 a$ .

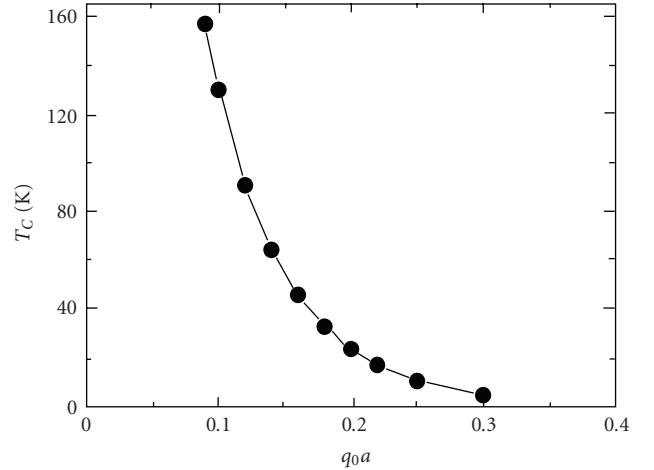


FIGURE 11:  $T_C$  versus the screening parameter  $q_0 a$ , Details calculations are done in [37].

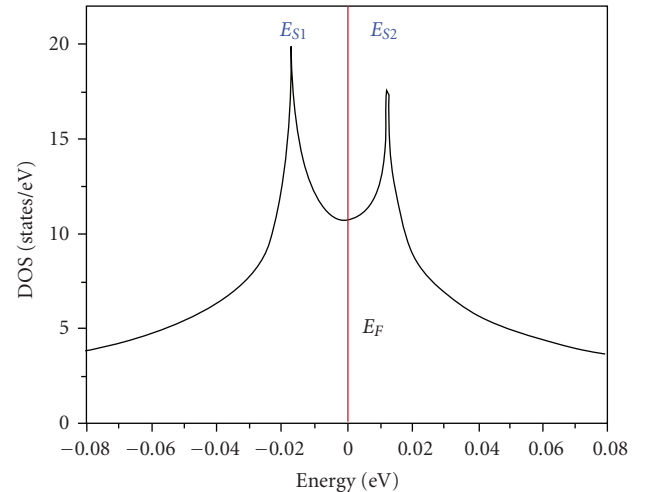


FIGURE 12: Density of States (DOS) in the orthorhombic phase.

effects to obtain the maximum  $T_C$ . It is why we have to take into account these two effects and why the experimental  $T_C$  is not maximum when  $E_F = E_S$  [37].

We show that the effect of increasing  $q_0a$  is to transform the system in a metallic and more isotropic one.

## 7. Evidence of Lattice Involvement

Labbé and Friedel [38–40] gave an explanation for the martensitic phase transformation from the cubic to the tetragonal structure observed at low temperature in the A15 compounds of formula  $V_3X$  ( $X = \text{Si, Ga, Ge, } \dots$ ) or  $\text{Nb}_3\text{Sn}$ . This change of structure occurs at a temperature  $T_m$  greater than  $T_C$ . The Vanadium (V) atoms form a linear chain and an almost one-dimensional approximation can be used for the  $d$  electrons. In these conditions a VHS appears at the bottom of the band and can explain high- $T_C$  [3, 41–43]. The electronic energy is reduced when the lattice is deformed and leads to a band type Jahn-Teller effect. This effect can explain the observed cubic to tetragonal transition at low temperature. This effect does not change very much  $T_C$  in these A15 compounds, because the role of the high DOS due to the VHS is important only for small doping (low concentration of  $d$  electrons).

The situation is more favorable in the cuprates, which are almost bidimensional and where the VHS lies near the middle of the band. Far or near  $T_C$ , lattice deformations tetragonal to orthorhombic phase transformations, deformation of the orthorhombic phase, even martensitic phase transformations, have been observed in the cuprates in function of temperature, doping, substitution, or under strained [11, 44–48]. This leads to a competition between electronic and elastic energies. Evidence of the role of phonon in the physics of cuprates has been seen experimentally; see, for example, the paper of Graf et al. [49].

When the Fermi level lies close to a VHS, of energy  $E_S$ , as it is the case for cuprates near optimum doping, the situation could be unstable and a small distortion increases the distance  $E_F - E_S$  and decreases strongly the electronic energy.

We propose a different scenario in most of these 2D compounds. When the lattice in the  $\text{CuO}_2$  plane is quadratic, the four saddle points correspond to the same electronic energy  $E_S$  and the VHS is fourfold degenerate. Due to the doping, and then to the effect of decreasing the temperature, the lattice becomes orthorhombic (rectangular unit cell). The degeneracy is lifted and we hope to obtain two VHS at different energy  $E_{S1}$  and  $E_{S2}$  corresponding to the saddle points along  $k_x$  and  $k_y$  in reciprocal space

$$E_k = -2t(1 + \beta) \cos X - 2t \cos Y + 4t' \cos X \cos Y + D_e. \quad (11)$$

Using the twofold degenerate electronic dispersion, see (11), where  $\beta t$  represents the difference in the interaction with the first neighbours in the  $x$  and  $y$  direction, we calculate the DOS versus energy, represented on Figure 12. In optimal conditions the Fermi level could lie between  $E_{S1}$  and  $E_{S2}$ .  $E_F$  is then between these energy levels of high DOS in a dip, itself

of a smaller but sufficiently high DOS, the lattice is stabilized. No more phase transformation could be possible, at lower temperature this situation favors the BCS condensation into a superconducting phase instead of a lattice transformation, leading to high- $T_C$  due to the high DOS.

The goal for experimentalists will be to find the optimal parameters (doping, strain, temperature, etc.) to lead the sample to such situation that it condensates when  $E_F$  is pinned in its dip in order to obtain a very high- $T_C$ .

We want to indicate in favour of the electron-lattice interaction that Deutscher and de Gennes [50] proposed a model valid in the underdoped regime based on the idea that if two holes occupy two adjacent copper sites, a contraction of the Cu–O–Cu band occurs. This increases significantly the transfer integral between the Cu and this can lead to the formation of bound hole pairs.

## 8. Conclusion

Strong correlations are probably the dominant factor in the underdoped region. But in the optimum and overdoped regions, we have shown that the experimental observations may be explained by electron-phonon or electron-lattice interaction coupled with the Van Hove scenario, both in the normal and superconducting states. The existence of VHS close to the Fermi level is now well established experimentally, and this fact must be taken into account in any physical description of the properties of high- $T_C$  superconducting cuprates.

## Acknowledgment

The authors would like to thank Professor Jacques Friedel for helpful and stimulating discussions.

## References

- [1] J. G. Bednorz and K. A. Müller, “Possible high  $T_C$  superconductivity in the Ba-La-Cu-O system,” *Zeitschrift für Physik B*, vol. 64, no. 2, pp. 189–193, 1986.
- [2] L. Van Hove, “The occurrence of singularities in the elastic frequency distribution of a crystal,” *Physical Review*, vol. 89, no. 6, pp. 1189–1193, 1953.
- [3] J. Labbé and J. Friedel, “Instabilité et changement de phase cristalline des composés du type  $V_3\text{Si}$  à basse température: Effet de la température,” *Journal de Physique et Le Radium*, vol. 27, p. 153, 303, 1966.
- [4] J. E. Hirsch and D. J. Scalapino, “Enhanced superconductivity in quasi two-dimensional systems,” *Physical Review Letters*, vol. 56, no. 25, pp. 2732–2735, 1986.
- [5] J. Labbé and J. Bok, “Superconductivity in alkaline-earth-substituted  $\text{La}_2\text{CuO}_4$ : a theoretical model,” *Europhysics Letters*, vol. 3, no. 11, pp. 1225–1230, 1987.
- [6] A. Ino, C. Kim, M. Nakamura, et al., “Doping-dependent evolution of the electronic structure of  $\text{La}_{2-x}\text{Sr}_x\text{CuO}_4$  in the superconducting and metallic phases,” *Physical Review B*, vol. 65, no. 9, Article ID 94504, 11 pages, 2002.
- [7] M. Abrecht, D. Ariosa, D. Cloetta, et al., “Strain and high temperature superconductivity: unexpected results from direct

- electronic structure measurements in thin films,” *Physical Review Letters*, vol. 91, no. 5, Article ID 057002, 4 pages, 2003.
- [8] P. A. Lee, N. Nagaosa, and X.-G. Wen, “Doping a Mott insulator: physics of high-temperature superconductivity,” *Reviews of Modern Physics*, vol. 78, no. 1, pp. 17–85, 2006.
- [9] J. Friedel and M. Kohmoto, “On the nature of antiferromagnetism in the  $\text{CuO}_2$  planes of oxide superconductors,” *European Physical Journal B*, vol. 30, no. 4, pp. 427–435, 2002.
- [10] J. Bouvier and J. Bok, “Gap anisotropy and Van Hove singularities in high- $T_c$  superconductors,” *Physica C*, vol. 249, no. 1-2, pp. 117–122, 1995.
- [11] J. Bouvier and J. Bok, “The Van Hove scenario of high  $T_c$  superconductors: the effect of doping,” *Physica C*, vol. 288, no. 3-4, pp. 217–225, 1997.
- [12] J. Bouvier and J. Bok, “Superconductivity in cuprates, the Van Hove scenario: a review,” in *The Gap Symmetry and Fluctuations in High- $T_c$  Superconductors*, J. Bok, et al., Ed., vol. 371 of *NATO Science Series: B*, pp. 37–54, Plenum Press, New York, NY, USA, 1998.
- [13] J. Bok and L. Force, “Origin of superconductivity in cuprates the Van Hove scenario,” *Physica C*, vol. 185–189, part 3, pp. 1449–1450, 1991.
- [14] L. Force and J. Bok, “Superconductivity in two dimensional systems: Van Hove singularity and Coulomb repulsion,” *Solid State Communications*, vol. 85, no. 11, pp. 975–978, 1993.
- [15] P. C. Pattnaik, C. L. Kane, D. M. Newns, and C. C. Tsuei, “Evidence for the Van Hove scenario in high-temperature superconductivity from quasiparticle-lifetime broadening,” *Physical Review B*, vol. 45, no. 10, pp. 5714–5717, 1992.
- [16] D. M. Newns, C. C. Tsuei, P. C. Pattnaik, and C. L. Lane, “Cuprate Superconductivity: The Van Hove Scenario,” *Comments on Condensed Matter Physics*, vol. 15, p. 273, 1992.
- [17] J. Bok and J. Bouvier, “Van Hove scenario for high  $T_c$  superconductors,” in *High  $T_c$  Superconductors and Related Transition Metal Oxides*, A. Bussmann-Holder and H. Keller, Eds., pp. 35–41, Springer, Berlin, Germany, 2007.
- [18] Y. Koike, Y. Iwabuchi, S. Hosoya, N. Kobayashi, and T. Fukase, “Correlation between  $T_c$  and hole concentration in the cation-substituted  $\text{Bi}_2\text{Sr}_2\text{CaCu}_2\text{O}_{8+\delta}$  system,” *Physica C*, vol. 159, no. 1-2, pp. 105–110, 1989.
- [19] J. Bardeen, L. N. Cooper, and J. R. Schrieffer, “Theory of superconductivity,” *Physical Review*, vol. 108, no. 5, pp. 1175–1204, 1957.
- [20] P. Morel and P. W. Anderson, “Calculation of the superconducting state parameters with retarded electron-phonon interaction,” *Physical Review*, vol. 125, no. 4, pp. 1263–1271, 1962.
- [21] M. L. Cohen and P. W. Anderson, “Comments on the Maximum Superconducting Transition Temperature,” in *Superconductivity in d and f Band Metals*, D. H. Douglass, Ed., A.I.P., New York, NY, USA, 1972.
- [22] V. L. Ginzburg, “Once again about high-temperature superconductivity,” *Contemporary Physics*, vol. 33, no. 1, pp. 15–23, 1992.
- [23] B. Batlogg, G. Kourouklis, W. Weber, et al., “Nonzero isotope effect in  $\text{La}_{1.85}\text{Sr}_{0.15}\text{CuO}_4$ ,” *Physical Review Letters*, vol. 59, no. 8, pp. 912–914, 1987.
- [24] M. K. Crawford, M. N. Kunchur, W. E. Farneth, E. M. McCarron III, and S. J. Poon, “Anomalous oxygen isotope effect in  $\text{La}_{2-x}\text{Sr}_x\text{CuO}_4$ ,” *Physical Review B*, vol. 41, no. 1, pp. 282–287, 1990.
- [25] H. Keller, “Unconventional isotope effects in cuprate superconductors,” in *Superconductivity in Complex Systems*, K. A. Müller and A. Bussmann-Holder, Eds., vol. 114 of *Structure and Bonding*, p. 143, Springer, Berlin, Germany, 2005.
- [26] C. C. Tsuei, D. M. Newns, C. C. Chi, and P. C. Pattnaik, “Anomalous isotope effect and Van Hove singularity in superconducting Cu oxides,” *Physical Review Letters*, vol. 65, no. 21, pp. 2724–2727, 1990.
- [27] R. Hlubina and T. M. Rice, “Resistivity as a function of temperature for models with hot spots on the Fermi surface,” *Physical Review B*, vol. 51, no. 14, pp. 9253–9260, 1995.
- [28] C. G. Olson, R. Liu, D. W. Lynch, et al., “High-resolution angle-resolved photoemission study of the Fermi surface and the normal-state electronic structure of  $\text{Bi}_2\text{Sr}_2\text{CaCu}_2\text{O}_8$ ,” *Physical Review B*, vol. 42, no. 1, pp. 381–386, 1990.
- [29] L. D. Rotter, Z. Schlesinger, R. T. Collins, et al., “Dependence of the infrared properties of single-domain  $\text{YBa}_2\text{Cu}_3\text{O}_{7-y}$  on oxygen content,” *Physical Review Letters*, vol. 67, no. 19, pp. 2741–2744, 1991.
- [30] Y. Kubo, Y. Shimakawa, T. Manako, and H. Igarashi, “Transport and magnetic properties of  $\text{Tl}_2\text{Ba}_2\text{CuO}_{6+\delta}$  showing a  $\delta$ -dependent gradual transition from an 85-K superconductor to a nonsuperconducting metal,” *Physical Review B*, vol. 43, no. 10, pp. 7875–7882, 1991.
- [31] D. Matthey, S. Gariglio, B. Giovannini, and J.-M. Triscone, “Hall effect in underdoped  $\text{GdBa}_2\text{Cu}_3\text{O}_{7-\delta}$  thin films: evidence for a crossover line in the pseudogap regime,” *Physical Review B*, vol. 64, no. 2, Article ID 024513, 5 pages, 2001.
- [32] F. F. Balakirev, J. B. Betts, A. Migiori, S. Ono, Y. Ando, and G. S. Boebinger, “Signature of optimal doping in Hall-effect measurements on a high-temperature superconductor,” *Nature*, vol. 424, no. 6951, pp. 912–915, 2003.
- [33] J. Bok and J. Bouvier, “Hall effect in the normal state of high- $T_c$  cuprates,” *Physica C*, vol. 403, no. 4, pp. 263–268, 2004.
- [34] N. P. Ong, “Geometric interpretation of the weak-field Hall conductivity in two-dimensional metals with arbitrary Fermi surface,” *Physical Review B*, vol. 43, no. 1, pp. 193–201, 1991.
- [35] A. A. Abrikosov, “On the nature of the order parameter in HTSC and influence of impurities,” *Physica C*, vol. 244, no. 3-4, pp. 243–255, 1995.
- [36] C. C. Tsuei, J. R. Kirtley, G. Hammerl, J. Mannhart, H. Raffy, and Z. Z. Li, “Robust  $d_{x^2-y^2}$  pairing symmetry in hole-doped cuprate superconductors,” *Physical Review Letters*, vol. 93, no. 18, Article ID 187004, 4 pages, 2004.
- [37] J. Bouvier and J. Bok, “Van Hove singularity and “pseudo-gap” in HTSC,” *Journal of Superconductivity*, vol. 10, no. 6, pp. 673–675, 1997.
- [38] J. Labbé and J. Friedel, “Instabilité électronique et changement de phase cristalline des composés du type  $\text{V}_3\text{Si}$  à basse température,” *Journal de Physique*, vol. 27, no. 3-4, pp. 153–165, 1966.
- [39] J. Labbé and J. Friedel, “Effet de la température sur l’instabilité électronique et le changement de phase cristalline des composés du type  $\text{V}_3\text{Si}$  à basse température,” *Journal de Physique*, vol. 27, no. 5-6, pp. 303–308, 1966.
- [40] J. Labbé and J. Friedel, “Stabilité des modes de distorsion périodiques d’une chaîne linéaire d’atomes de transition dans une structure cristalline du type  $\text{V}_3\text{Si}$ ,” *Journal de Physique*, vol. 27, no. 11-12, pp. 708–716, 1966.
- [41] J. Labbé, S. Barišić, and J. Friedel, “Strong-coupling superconductivity in  $\text{V}_3\text{X}$  type of compounds,” *Physical Review Letters*, vol. 19, no. 18, pp. 1039–1041, 1967.
- [42] S. Barišić and J. Labbé, “The elastic constants of  $\text{V}_3\text{Si}$  type compounds in the cubic phase,” *Journal of Physics and Chemistry of Solids*, vol. 28, no. 12, pp. 2477–2485, 1967.

- [43] J. Labbé, “Relation between superconductivity and lattice instability in the  $\beta$ -W compounds,” *Physical Review*, vol. 172, no. 2, pp. 451–455, 1968.
- [44] T. Kyömen, M. Oguni, M. Itoh, and J. D. Yu, “Calorimetric study of an electrochemically oxidized crystal of  $\text{La}_2\text{CuO}_{4.05}$ : stabilization phenomenon, phase transitions, and a glass transition due to freezing-in of the rearrangement of excess oxygen atoms,” *Physical Review B*, vol. 60, no. 9, pp. 6821–6826, 1999.
- [45] T. Egami, “Essential role of the lattice in the mechanism of high temperature superconductivity,” in *High- $T_C$  Superconductors and Related Transition Metal Oxides*, A. Bussmann-Holder and H. Keller, Eds., pp. 35–41, Springer, Berlin, Germany, 2007.
- [46] B. H. Toby, T. Egami, J. D. Jorgensen, and M. A. Subramanian, “Observation of a local structural change at  $T_C$  for  $\text{Tl}_2\text{Ba}_2\text{CaCu}_2\text{O}_8$  by pulsed neutron diffraction,” *Physical Review Letters*, vol. 64, no. 20, pp. 2414–2417, 1990.
- [47] H. Oyanagi, “Lattice effects in high temperature superconducting cuprates revealed by X-ray absorption spectroscopy,” in *High  $T_C$  Superconductors and Related Transition Metal Oxides*, A. Bussmann-Holder and H. Keller, Eds., pp. 35–41, Springer, Berlin, Germany, 2007.
- [48] J. Lee, K. Fujita, K. McElroy, et al., “Interplay of electron-lattice interactions and superconductivity in  $\text{Bi}_2\text{Sr}_2\text{CaCu}_2\text{O}_{8+\delta}$ ,” *Nature*, vol. 442, no. 7102, pp. 546–550, 2006.
- [49] J. Graf, M. D’Astuto, C. Jozwiak, et al., “Bond stretching phonon softening and kinks in the angle-resolved photoemission spectra of optimally doped  $\text{Bi}_2\text{Sr}_{1.6}\text{La}_{0.4}\text{Cu}_2\text{O}_{6+\delta}$  superconductors,” *Physical Review Letters*, vol. 100, no. 22, Article ID 227002, 4 pages, 2008.
- [50] G. Deutscher and P.-G. de Gennes, “A spatial interpretation of emerging superconductivity in lightly doped cuprates,” *Comptes Rendus Physique*, vol. 8, no. 7-8, pp. 937–941, 2007.

## Review Article

# Spin-Lattice Coupling and Superconductivity in Fe Pnictides

**T. Egami,<sup>1,2,3</sup> B. V. Fine,<sup>4</sup> D. Parshall,<sup>2</sup> A. Subedi,<sup>2</sup> and D. J. Singh<sup>3</sup>**

<sup>1</sup>Department of Materials Science and Engineering, Joint Institute for Neutron Sciences, University of Tennessee, Knoxville, TN 37996, USA

<sup>2</sup>Department of Physics and Astronomy, University of Tennessee, Knoxville, TN 37996, USA

<sup>3</sup>Oak Ridge National Laboratory, Oak Ridge, TN 37831, USA

<sup>4</sup>Institute for Theoretical Physics, University of Heidelberg, Heidelberg 69120, Germany

Correspondence should be addressed to T. Egami, [egami@utk.edu](mailto:egami@utk.edu)

Received 19 July 2009; Revised 25 October 2009; Accepted 22 December 2009

Academic Editor: Igor Mazin

Copyright © 2010 T. Egami et al. This is an open access article distributed under the Creative Commons Attribution License, which permits unrestricted use, distribution, and reproduction in any medium, provided the original work is properly cited.

We consider strong spin-lattice and spin-phonon coupling in iron pnictides and discuss its implications on superconductivity. Strong magneto-volume effect in iron compounds has long been known as the Invar effect. Fe pnictides also exhibit this effect, reflected in particular on the dependence of the magnetic moment on the atomic volume of Fe defined by the positions of the nearest neighbor atoms. Through the phenomenological Landau theory, developed on the basis of the calculations by the density functional theory (DFT) and the experimental results, we quantify the strength of the spin-lattice interaction as it relates to the Stoner criterion for the onset of magnetism. We suggest that the coupling between electrons and phonons through the spin channel may be sufficiently strong to be an important part of the superconductivity mechanism in Fe pnictides.

## 1. Introduction

Recent discovery of superconductivity in Fe pnictides [1] with the critical temperature  $T_C$  up to 55 K [2] caused enormous excitement in the field, for various reasons. First, this is the first noncuprate family of superconductors with  $T_C$  above 40 K. Second, superconductivity appears when the antiferromagnetic (AFM) order is suppressed by doping [3], just as in the cuprates. Third, unlike the cuprates, strong electron correlations are not observed by spectroscopy [4], suggesting that the Mott physics may not be a necessary ingredient for the mechanism of high-temperature superconductivity. Finally, there is a large family of similar compounds that show superconductivity, making experimental research less restricted by chemical or materials issues. The field is making surprisingly fast development, partly because of the accumulated experience of working on the cuprates. It is possible that the origin of the superconductivity in this family of compounds may be easier to identify than for the cuprates, and the success of solving this problem hopefully will facilitate understanding of the cuprate problem.

Even though the AFM order is suppressed by doping, spins are active in the doped Fe pnictide superconductors.

Again, just as in the cuprates strong magnetic excitations, including the so-called resonance peak, are observed by inelastic neutron scattering [5–8]. Core level spectroscopy is consistent with the local Fe moment of about  $1\mu_B$  [4]. Interestingly, the density functional theory (DFT) calculations always predict the magnetic ground state (AFM or incommensurate order) for the experimental lattice constants [9–12]. The phonon dispersions observed by inelastic X-ray scattering are consistent with the DFT calculations only when the magnetic ground state is assumed [13]. Only in the collapsed phase of  $\text{CaFe}_2\text{As}_2$ , in which the  $c$ -axis lattice constant is reduced by as much as 10% compared to the magnetic state, does the material become truly spin-degenerate [14]. All these observations strongly suggest that the superconducting samples are locally and dynamically spin-polarized, and show strong dynamic Fe spin fluctuations. Although we do not have precise knowledge of their spin dynamics, judged from the absence of strong quasielastic scattering in neutron scattering with energy resolution of 1 meV, the time-scale of fluctuation must not be slower than 1 ps. This result supports the view that spins are involved in the mechanism of superconductivity, for instance through the spin-fluctuation mechanism [15–17].

However, there are many puzzling, important questions that need to be answered before addressing the question of the mechanism: the first puzzle is the effect of doping. In the cuprates, doping is necessary for introducing mobile charge carriers, since the parent compounds are Mott-Hubbard insulators. In Fe pnictides, on the other hand, the parent compounds are already metallic, and doping does not appear to change the charge carrier density very much [9]. Rather, the main effect of doping is to suppress the AFM ground state. In the pnictide parent compounds strongly two-dimensional spin fluctuations are observed above  $T_N$  [18], just as in the superconducting Fe pnictides [6, 8]. However, whereas the LaFeAsO (1111) type compounds are strongly two-dimensional [10], BaFe<sub>2</sub>As<sub>2</sub> (122) type compounds are much more three-dimensional [19]. The second curious behavior is that the observed magnetic moment on the AFM phase varies from a compound to compound, but is always significantly smaller than predicted by the DFT calculations [10–12]. Third, there is an interesting interplay between both the lattice and magnetism [20], and the lattice and superconductivity [21, 22]. In this article, we focus on the third point, that of the lattice effect. For the purpose of highlighting the essence of the effect, we use simple approximations, namely the Landau theory and the Stoner theory, using the results of the LDA calculations as a guide. We argue that through the spin-lattice coupling effect the lattice may play a much larger role than generally acknowledged in determining the properties of Fe pnictides, possibly including even the superconductivity.

## 2. Magneto-Volume Effect in Fe Pnictides

**2.1. Dependence of Fe Moment on the Structure.** It has long been known that the magnetic moment of transition metals depends on volume [23]. Because of the Pauli exclusion principle, the electron kinetic energy of the spin-polarized state is higher for parallel spins if the volume is the same, and volume expansion relaxes the kinetic energy. In some iron alloys, thermal volume expansion due to lattice anharmonicity cancels the decrease in volume associated in the decrease in spin-splitting, resulting in zero thermal expansion, widely known as the Invar behavior. The negative or zero thermal expansion is indeed observed for PrFeAsO [24]. The collapsed phase of CaFe<sub>2</sub>As<sub>2</sub> is a dramatic case of such a magneto-volume effect. This compound shows AFM order below 140 K, but with the pressure of 0.4 GPa it undergoes the first-order phase transition into a nonmagnetic phase with the reduction in volume of 5% [14].

In Fe pnictides, layers of Fe atoms are sandwiched by layers of pnictide such as As or P [1]. Thus if the layer-layer distance of pnictide is changed, the magnetic moment of Fe is strongly affected. This coupling of the Fe moment to the pnictide position in the lattice was recognized early by the DFT calculations [9, 20]. Figure 1 shows the calculated dependence of the Fe moment in Ba(Fe<sub>0.92</sub>Co<sub>0.08</sub>)<sub>2</sub>As<sub>2</sub> on the separation between the As layer and the Fe layer ( $z$ ). The calculations were done within virtual crystal approximation (VCA) and local density approximation (LDA) with general

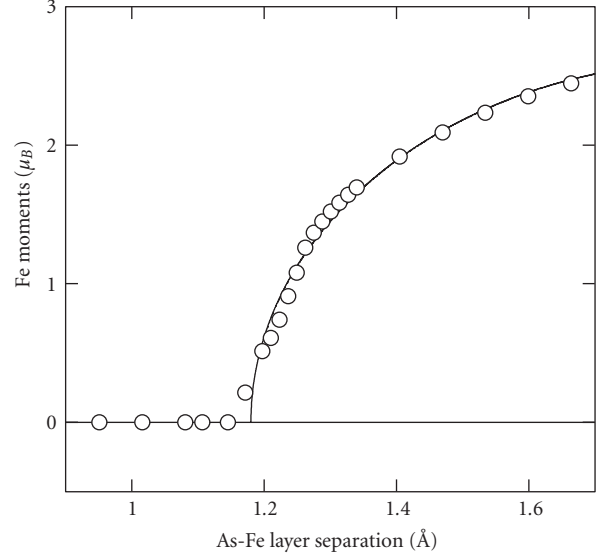


FIGURE 1: The magnetic moment,  $M$ , as a function of the Fe-As layer separation,  $z$ , calculated for Ba(Fe<sub>0.92</sub>Co<sub>0.08</sub>)<sub>2</sub>As<sub>2</sub>. The solid curve is a fit by (3).

potential linearized augmented plane-wave (LAPW) method [25], including local orbitals [26]. LAPW sphere radii of  $2.2 a_0$ ,  $2.0 a_0$ , and  $2.0 a_0$ , where  $a_0$  is Bohr radius, were used for Ba, Fe, and As, respectively. To account for Co doping, an electron number of 26.08 was used for Fe. We used the experimentally reported tetragonal lattice parameters ( $a = 3.9625 \text{ \AA}$ ,  $c = 13.0168 \text{ \AA}$ ) [27]. In the calculated result, clearly there is a quantum critical point (QCP) for magnetism near  $z_c = 1.20 \text{ \AA}$  as shown in Figure 1. The local exchange interaction is strong enough to spin-split the band by overcoming the kinetic energy cost only for  $z > z_c$ . We obtain similar results from the calculation on undoped BaFe<sub>2</sub>As<sub>2</sub>. Compared also with other data [12, 20], the relation between  $z$  and Fe moment  $M$  appears to be rather insensitive to compositions, and the relation shown in Figure 1 appears to be a nearly universal property of the FeAs triple layer. This must be because the in-plane lattice constant, thus the Fe-Fe distance, is very similar within  $\pm 1\%$  among many Fe pnictide compounds. Thus the parameter  $z$ , the As-Fe layer separation, is a good common measure of the magneto-volume effect. For instance, in the collapsed phase of CaFe<sub>2</sub>As<sub>2</sub> the value of  $z$  is  $1.23 \text{ \AA}$  [14], close to the value of  $z_c$  in Figure 1.

**2.2. Landau Theory.** Let us develop a Landau-type theory to describe the dependence of the local magnetic moment,  $M$ , on the As-Fe layer separation,  $z$ . We may write the magnetic free energy as

$$F_M = AM^2 + BM^4 + F_{s-l}, \quad (1)$$

where  $F_{s-l}$  is the spin-lattice interaction energy expanded by  $z - z_c$ ,

$$F_{s-l} = \left[ \alpha(z - z_c) + \beta(z - z_c)^2 \right] M^2, \quad (2)$$

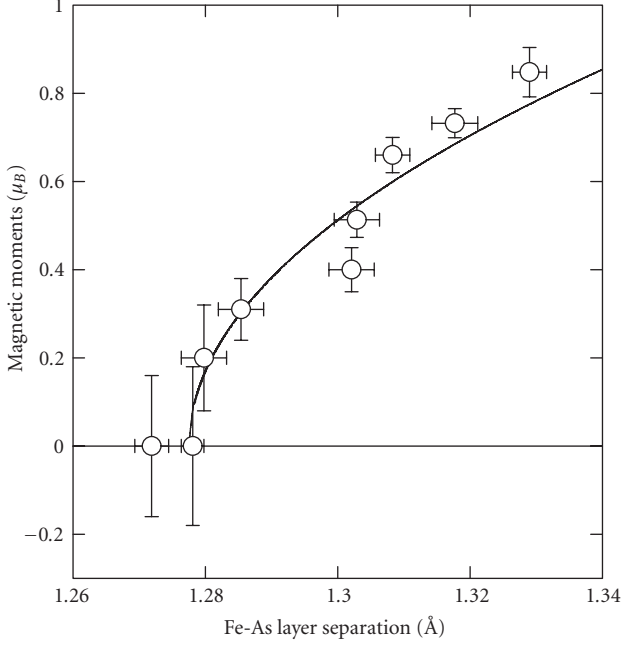


FIGURE 2: Dependence of the experimentally determined magnetic moment on the Fe-As layer separation for CeFe(As,P)O (open circles) [28], and the fit by (3) (solid curve).

where  $\alpha < 0$ .  $F_{s-1}$  is negative only for  $z > z_c$ . We retain only the terms with even powers of  $M$  because of the symmetry. We set  $A = 0$  so that  $z_c$  is the critical point. By minimizing  $F_M$  with respect to  $M$  we obtain,

$$M^2 = \frac{|\alpha|}{2B} \left[ (z - z_c) + \frac{\beta}{\alpha} (z - z_c)^2 \right]. \quad (3)$$

The dashed line in Figure 1 gives the fit of this equation to the calculated moment. From this fit we obtain  $z_c = 1.20 \text{ \AA}$ ,  $\alpha/2B = 19.16 \mu_B^2/\text{\AA}$ , and  $\alpha/\beta = -1.40 \text{ \AA}$ . In  $\text{CaFe}_2\text{As}_2$ , the QCP is hidden because the nature of the transition is strongly first order. In the vicinity of  $z_c$ , the moment is proportional to  $(z - z_c)^{1/2}$ .

Recently, the magnetic moment was experimentally determined for the series of compounds,  $\text{CeFe}(\text{As}_{1-x}\text{P}_x)\text{O}$  [28]. Because As and P are isovalent, the replacement of As by P does not dope carriers to the system, but merely change the Fe(As/P) layer separation. Indeed (3) fits the results nicely as shown in Figure 2 [29]. Since the range of  $z$  is relatively, small  $\beta$  was neglected. The fit to the data gave  $z_c = 1.278 \text{ \AA}$ ,  $\alpha/2B = 11.67 (\mu_B/\text{\AA})$ . Theoretical calculations for the CeFe(As,P)O system are in progress. Note that in the calculation presented in Figure 1, the lattice is assumed to be static. In reality, however, the zero-point phonons are present, with the amplitude of the order of  $0.1 \text{ \AA}$ . This should shift the critical point upward, in better agreement with the data in Figure 2.

**2.3. Phonon Softening.** We now add the lattice elastic energy in order to consider the phonon softening due to the magneto-volume effect. The phonon to be considered here is

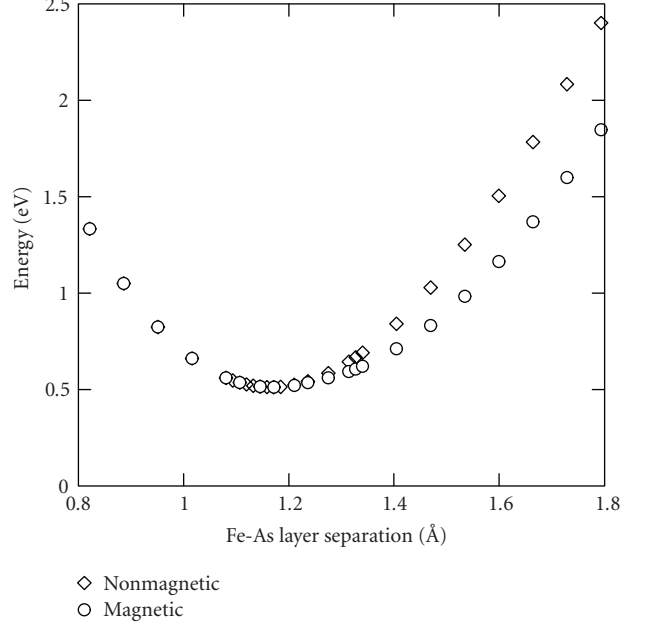


FIGURE 3: Electron energy as a function of the Fe-As layer separation is calculated by LDA for  $\text{Ba}(\text{Fe}_{0.92}\text{Co}_{0.08})_2\text{As}_2$ , with spin polarization; the elastic constant is reduced by 29% compared to the state without spin polarization, accounting for the phonon softening by 15% due to spin polarization.

the As Raman mode, in which As layers move against each other along the  $c$ -axis, either toward or away from the Fe layer. The magneto-elastic free energy is

$$\begin{aligned} F_S(z) &= \left[ \alpha(z - z_c) + \beta(z - z_c)^2 \right] M^2 + K(z - z_1)^2 \\ &= -\frac{\alpha^2(z - z_c)^2}{2B} \left[ 1 + \frac{\beta}{\alpha}(z - z_c) \right]^2 + K(z - z_1)^2. \end{aligned} \quad (4)$$

By minimizing  $F_S$  with respect to  $z$  we obtain the As position,  $z_M$ ,

$$\begin{aligned} \frac{\partial F_S}{\partial z} \Big|_{z=z_M} &= -\frac{\alpha^2(z_M - z_c)}{B} \left[ 1 + \frac{2\beta}{\alpha}(z_M - z_c) \right] \left( 1 + \frac{\beta}{\alpha}(z_M - z_c) \right) \\ &\quad + 2K(z_M - z_1) = 0. \end{aligned} \quad (5)$$

Then by taking the second derivative we obtain the elastic stiffness renormalized by the spin-lattice interaction,

$$K' = K \left\{ 1 - \frac{\alpha^2}{2KB} \left[ 1 + \frac{6\beta}{\alpha}(z_M - z_c) + 6 \left( \frac{\beta}{\alpha} \right)^2 (z_M - z_c)^2 \right] \right\}. \quad (6)$$

As shown in Figure 3, allowing spin polarization softens the As Raman phonon frequency by 15% at  $z_M = 1.36 \text{ \AA}$ . This effect was noted earlier [12], and agrees with the experimental observations [13]. Note that the energy minimum of the DFT calculation systematically underestimates the lattice constant. Thus we obtain,  $\alpha = -0.193 \text{ eV}/\text{\AA} \mu_B^2$ ,

$\beta = 0.137 \text{ eV}/\text{\AA}^2 \mu_B^2$ , and  $z_1 = 1.32 \text{ \AA}$ . The value of  $z_1$  is in good agreement with the LDA calculation ( $1.32 \text{ \AA}$  after correcting for the systematic underestimation), proving the internal consistency. Thus this theory elucidates how the magneto-volume interaction, (2) can induce magnetization as a function of the As-Fe layer separation, and softening of the As Raman phonon mode.

### 3. Generalized Stoner Condition

We now turn our attention to the Fe band splitting. We start with the classical Stoner theory of itinerant ferromagnetism [30], and generalize it to an antiferromagnet [31–33]. Even though more complex and accurate DFT calculations can be made, this is a useful exercise for simplicity and clarity of logic. In the Stoner theory the electron energy is given by

$$E = \int_0^{\epsilon_{F1}} \epsilon N_{\uparrow}(\epsilon_1) d\epsilon_1 + \int_0^{\epsilon_{F1}} \epsilon N_{\downarrow}(\epsilon_1) d\epsilon_1 + In_1 n_{\downarrow}, \quad (7)$$

where  $N_{\uparrow}(\epsilon)$  is the electron density of states for up spins,  $n_{\uparrow}$  is the density of electrons with up spin, and  $\epsilon_1$  is the energy of an electron with up spin. Magnetization is given by  $M = n_{\uparrow} - n_{\downarrow}$ . If we start with the nonmagnetic state and introduce a small spin splitting by shifting the up spin by  $d\epsilon_1$ , the energy changes

$$dE = 2N(\epsilon_F)[1 - IN(\epsilon_F)]d\epsilon_1^2, \quad (8)$$

which gives the Stoner criterion,

$$IN(\epsilon_F) \geq 1. \quad (9)$$

Near the Stoner QCP,

$$M = dn_{\uparrow} - dn_{\downarrow} = 2dn_{\uparrow} = 2N(\epsilon_F)d\epsilon_1, \quad (10)$$

thus

$$dE = \frac{1 - IN(\epsilon_F)}{2N(\epsilon_F)} M^2, \quad (11)$$

and in (1),

$$A = \frac{1 - IN(\epsilon_F)}{2N(\epsilon_F)}. \quad (12)$$

Thus  $A = 0$  at the QCP.

In the case of an antiferromagnet, the same argument can be constructed for the staggered spin-split bands, except that the exchange energy term  $I$  includes the kinetic energy cost for modulating the spin split band by  $K = \pi/a$  [32, 33]. Therefore, we can interpret  $z_c$  as the generalized Stoner QCP. In general for a spin density wave (SDW) ordering with  $Q$ , within the random phase approximation (RPA), the magnetic moment above the SDW ordering temperature is given by

$$M(Q) = \frac{\chi_0(Q)}{1 - I\chi_0(Q)} h_Q, \quad (13)$$

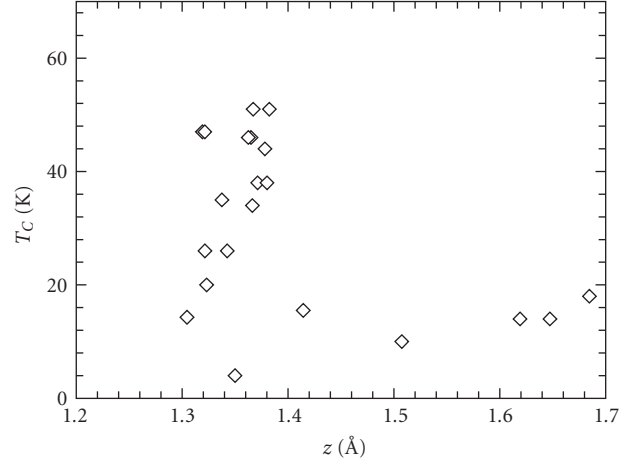


FIGURE 4: Superconducting critical temperature  $T_C$ , as a function of the As-Fe layer separation,  $z$ .

where  $M(Q)$  is the SDW amplitude,  $\chi_0(Q)$  is the generalized bare susceptibility, and  $h_Q$  is the SDW mean-field [31]. Thus the generalized Stoner condition is given by [31–33]

$$I\chi_0(Q) \geq 1. \quad (14)$$

Note that  $\chi_0(Q = 0) = N(\epsilon_F)$ , which recovers the Stoner condition for ferromagnetism. Now the effect of lattice strain is to modify the generalized Stoner condition. For instance, reducing the As-Fe separation increases the bandwidth, thus decreases the generalized susceptibility. This brings the system closer to the Stoner QCP, and reduces the magnetic moment. Because the Fe pnictides are close to the Stoner QCP, even a small lattice strain, including phonons, can have very significant effects. Similarly, the in-plane Fe phonon mode that is relevant to the tetragonal-orthorhombic structural phase transition could also be important to the magnetism of Fe pnictides. The strong anisotropy of the spin exchange in the Fe plane [34] is indicative of the strong spin-lattice coupling in the Fe plane.

### 4. Relation to Superconductivity

One of the most intriguing lattice effects on the superconductivity of Fe pnictides is the dependence of the critical temperature,  $T_C$ , on the geometry of the FeAs<sub>4</sub> tetrahedron [21, 22]. Data show that  $T_C$  is strongly related to the As-Fe-As angle. Because the As-Fe-As angle is directly related to the Fe-As layer separation,  $z$ , in Figure 4, we plotted  $T_C$  as a function of  $z$ , using the published results of crystallographic analysis. The results are shown also in Table 1, with references for the data. Clearly the behavior above  $z_a = 1.4 \text{ \AA}$  is different from that below  $z_a$ . Above  $z_a$   $T_C$  is not much dependent on  $z$ , whereas there is strong dependence below. It is possible that the systems with  $z > z_a$  are regular BCS superconductors, and the enhancement is present only for  $z < z_a$ . Below  $z_a$ , there is recognizable correlation between  $T_C$  and  $z$ , except for a few outliers. This correlation supports the idea that  $z$  is a universal parameter for the properties of FeAs

TABLE 1: The values of  $z$ ,  $T_C$  for various Fe pnictides. Na-111 means NaFeAs, K-Ba122 means  $K_{1-x}Ba_xFe_2As_2$ , and so forth.

Compound	$z$ (Å)	$T_C$ (K)	Ref.
Na111	1.41	15.5	[35]
K-Ba122	1.37	38	[36]
F-La1111	1.34	26	[37]
F-Nd1111	1.37	46	[38]
F-Ce1111	1.34	35	[39]
F-Pr1111	1.32	47	[40]
F-La1111	1.32	20	[41]
Pr1111	1.32	47	[40]
O-Sm1111	1.37	34	[42]
V-Nd1111	1.38	51	[43]
Co-La1111	1.34	14.3	[44]
Fe(Se <sub>0.416</sub> Te <sub>0.584</sub> )	1.65	14	[45]
Fe(Se <sub>0.493</sub> Te <sub>0.507</sub> )	1.62	14	[45]
Li111	1.51	10	[46]
Li111	1.68	18	[47]
F-Sm1111	1.36	46	[48]
F-Tb1111	1.38	44	[49]
V-Nd1111	1.37	51	[43]
Co-SrFeAsF	1.35	4	[50]
K-Ba122	1.38	38	[36]

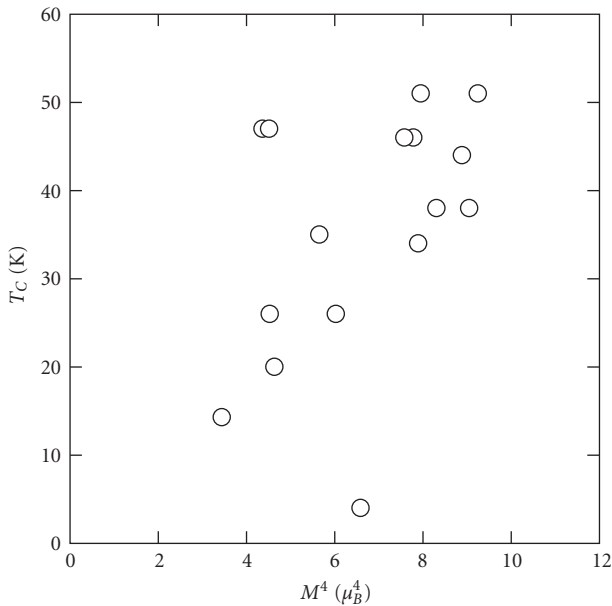


FIGURE 5: Superconducting critical temperature,  $T_C$ , against  $M^4$  calculated by the LDA.

compounds, including the superconductivity, regardless of the composition.

It is interesting to note that, from (2) and (3),  $F_{s-p} = -2BM^4$ . Thus we plotted  $T_C$  against  $M^4$  calculated by (3), not the experimental values of  $M$ , in Figure 5. Again a linear correlation appears to be present, although the correlation is far from perfect. On the other hand, the relation,  $T_C \propto M^2$ ,

is observed if we plot  $T_C$  against the moment experimentally determined for the CeFe(As, P)O system shown in Figure 2 [29]. An obvious implication of these correlations is that indeed magnetism is deeply involved in superconductivity, even though there is no static magnetic order in most of the superconducting samples. However, the involvement of spins in the mechanism may not be limited to the spin-fluctuation mechanism. The spin-lattice coupling could be involved in the superconductivity mechanism through the electron-phonon ( $e-p$ ) coupling in the spin-channel.

For instance, the phonon can modify the electron hopping integral  $t_{ij}$  [51]. In the presence of antiferromagnetic correlation, the phonon-induced charge transfer from one spin sublattice to the other can be given by

$$H = \sum_{q,k,s} \Delta t_{q,k} \left[ \left( a_q^+ f_{k,s}^+ g_{k+q,s} + a_q f_{k,s}^+ g_{k-q,s} \right) + H.c. \right], \quad (15)$$

where  $s$  refers to spin ( $\downarrow$  or  $\uparrow$ ),  $\Delta t_{q,k}$  is the derivative of  $t$  with respect to phonon displacement,  $a_q$  is a phonon annihilation operator, and  $f_k$  and  $g_k$  are electron annihilation operators for the spin  $\uparrow$  sublattice and the spin  $\downarrow$  sublattice. The  $\uparrow$  spin is a minority spin for the spin  $\downarrow$  sublattice, so (15) results in the spin transfer between the majority band and the minority band. Note that this coupling is different from the usual spin-phonon coupling through the modification of the exchange integral  $J$  by phonons, and ultimately we will have to consider both [52]. Even though the conventional charge-channel  $e-p$  coupling (Fröhlich coupling) is weak for the Fe pnictides [53], the  $e-p$  coupling through the spin-channel, such as the one in (15), may be strong enough to make a difference. Other possibility includes the mechanism proposed by Kulic and Haghhighrad [54] in which the on-site Hubbard repulsion,  $U$ , is modified by the dipolar moment of pnictide ions.

Possible importance of the spin-phonon coupling in the cuprates was discussed earlier [55–57]. Whereas many people speculate that the spin-fluctuation is the common mechanism for the cuprates as well as for Fe pnictides, it is possible that the spin-channel  $e-p$  coupling is the common thread for high-temperature superconductors, although much remain to be researched before we reach any definite conclusion.

## 5. Conclusions

The conventional electron-phonon ( $e-p$ ) coupling through the charge channel is quite small for the Fe pnictide compounds [53]. This led many to conclude that lattice and phonons are irrelevant to the superconductivity of the Fe pnictides. Consequently, the spin-fluctuation mechanism is regarded to be the leading mechanism to explain their high  $T_C$  [15]. However, the lattice is intimately involved in the magnetism of this compound through the magneto-volume effect, as shown in this paper. This coupling has been known for a long time as Invar effect. The lattice controls the Stoner condition, and thus the onset of spin-splitting. Because the lattice is so intimately involved in magnetism, it is furthermore possible that the  $e-p$  coupling through the spin-channel is relevant, for instance involving the As Raman

phonon mode or the in-plane Fe mode. The lattice effect may be much more important than generally assumed to the properties of Fe pnictides, including superconductivity.

## Acknowledgments

The authors are grateful to I. I. Mazin, T. Yildirim, A. Bussman-Holder, N. Mannella, M. Tachiki, P. Dai, and D. J. Scalapino for stimulating and useful discussions. This work was supported by the Department of Energy, Office of Basic Sciences, through the EPSCoR Grant, DE-FG02-08ER46528. The work at the Oak Ridge National Laboratory was supported by the Scientific User Facilities Division and by the Division of Materials Science and Engineering, Office of Basic Energy Sciences, Department of Energy.

## References

- [1] Y. Kamihara, T. Watanabe, M. Hirano, and H. Hosono, "Iron-based layered superconductor  $\text{La}[\text{O}_{1-x}\text{F}_x]\text{FeAs}$  ( $x = 0.05 - 0.12$ ) with  $T_c = 26\text{ K}$ ," *Journal of the American Chemical Society*, vol. 130, no. 11, pp. 3296–3297, 2008.
- [2] Z.-A. Ren, W. Lu, J. Yang, et al., "Superconductivity at 55 K in iron-based F-doped layered quaternary compound  $\text{Sm}[\text{O}_{1-x}\text{F}_x]\text{FeAs}$ ," *Chinese Physics Letters*, vol. 25, no. 6, pp. 2215–2216, 2008.
- [3] C. de la Cruz, Q. Huang, J. W. Lynn, et al., "Magnetic order close to superconductivity in the iron-based layered  $\text{LaO}_{1-x}\text{F}_x\text{FeAs}$  systems," *Nature*, vol. 453, no. 7197, pp. 899–902, 2008.
- [4] F. Bondino, E. Magnano, M. Malvestuto, et al., "Evidence for strong itinerant spin fluctuations in the normal state of  $\text{CeFeAsO}_{0.89}\text{F}_{0.11}$  iron-oxypnictide superconductors," *Physical Review Letters*, vol. 101, no. 26, Article ID 267001, 4 pages, 2008.
- [5] A. D. Christianson, E. A. Goremychkin, R. Osborn, et al., "Unconventional superconductivity in  $\text{Ba}_{0.6}\text{K}_{0.4}\text{Fe}_2\text{As}_2$  from inelastic neutron scattering," *Nature*, vol. 456, no. 7224, pp. 930–932, 2008.
- [6] M. D. Lumsden, A. D. Christianson, D. Parshall, et al., "Two-dimensional resonant magnetic excitation in  $\text{BaFe}_{1.84}\text{Co}_{0.16}\text{As}_2$ ," *Physical Review Letters*, vol. 102, no. 10, Article ID 107005, 4 pages, 2009.
- [7] S. Chi, A. Schneidewind, J. Zhao, et al., "Inelastic neutron-scattering measurements of a three-dimensional spin resonance in the FeAs-based  $\text{BaFe}_{1.9}\text{Ni}_{0.1}\text{As}_2$  superconductor," *Physical Review Letters*, vol. 102, no. 10, Article ID 107006, 4 pages, 2009.
- [8] D. Parshall, K. A. Lokshin, J. Niedziela, et al., "Spin excitations in  $\text{BaFe}_{1.84}\text{Co}_{0.16}\text{As}_2$  superconductor observed by inelastic neutron scattering," *Physical Review B*, vol. 80, no. 1, Article ID 012502, 4 pages, 2009.
- [9] D. J. Singh and M.-H. Du, "Density functional study of  $\text{LaFeAsO}_{1-x}\text{F}_x$ : a low carrier density superconductor near itinerant magnetism," *Physical Review Letters*, vol. 100, no. 23, Article ID 237003, 4 pages, 2008.
- [10] I. I. Mazin, M. D. Johannes, L. Boeri, K. Koepnik, and D. J. Singh, "Problems with reconciling density functional theory calculations with experiment in ferropnictides," *Physical Review B*, vol. 78, no. 8, Article ID 085104, 4 pages, 2008.
- [11] I. I. Mazin and M. D. Johannes, "A key role for unusual spin dynamics in ferropnictides," *Nature Physics*, vol. 5, no. 2, pp. 141–146, 2009.
- [12] T. Yildirim, "Strong coupling of the Fe-Spin state and the As-As hybridization in iron-pnictide superconductors from first-principle calculations," *Physical Review Letters*, vol. 102, no. 3, Article ID 037003, 4 pages, 2009.
- [13] D. Reznik, K. Lokshin, D. C. Mitchell, et al., "Phonons in doped and undoped  $\text{BaFe}_2\text{As}_2$  investigated by inelastic x-ray scattering," *Physical Review B*, vol. 80, no. 21, Article ID 214534, 5 pages, 2009.
- [14] A. Kreyssig, M. A. Green, Y. Lee, et al., "Pressure-induced volume-collapsed tetragonal phase of  $\text{CaFe}_2\text{As}_2$  as seen via neutron scattering," *Physical Review B*, vol. 78, no. 18, Article ID 184517, 6 pages, 2008.
- [15] I. I. Mazin, D. J. Singh, M. D. Johannes, and M. H. Du, "Unconventional superconductivity with a sign reversal in the order parameter of  $\text{LaFeAsO}_{1-x}\text{F}_x$ ," *Physical Review Letters*, vol. 101, no. 5, Article ID 057003, 4 pages, 2008.
- [16] T. A. Maier and D. J. Scalapino, "Theory of neutron scattering as a probe of the superconducting gap in the iron pnictides," *Physical Review B*, vol. 78, no. 2, Article ID 020514, 4 pages, 2008.
- [17] M. M. Korshunov and I. Eremin, "Theory of magnetic excitations in iron-based layered superconductors," *Physical Review B*, vol. 78, no. 14, Article ID 140509, 4 pages, 2008.
- [18] M. Ishtkado, R. Kajtmoto, S.-I. Shamoto, et al., "Two-dimensional spin density wave state in  $\text{LaFeAsO}$ ," *Journal of the Physical Society of Japan*, vol. 78, no. 4, Article ID 043705, 4 pages, 2009.
- [19] D. J. Singh, "Electronic structure of  $\text{BaCu}_2\text{As}_2$  and  $\text{SrCu}_2\text{As}_2$ : sp-band metals," *Physical Review B*, vol. 79, no. 15, Article ID 153102, 4 pages, 2009.
- [20] Z. P. Yin, S. Lebegue, M. J. Han, B. P. Neal, S. Y. Savrasov, and W. E. Pickett, "Electron-hole symmetry and magnetic coupling in antiferromagnetic  $\text{LaFeAsO}$ ," *Physical Review Letters*, vol. 101, no. 4, Article ID 047001, 4 pages, 2008.
- [21] C.-H. Lee, A. Iyo, H. Eisaki, et al., "Effect of structural parameters on superconductivity in fluorine-free  $\text{LnFeAsO}_{1-y}$  ( $\text{Ln} = \text{La}, \text{Nd}$ )," *Journal of the Physical Society of Japan*, vol. 77, no. 8, Article ID 083704, 4 pages, 2008.
- [22] J. Zhao, Q. Huang, C. de la Cruz, et al., "Structural and magnetic phase diagram of  $\text{CeFeAsO}_{1-x}\text{F}_x$  and its relation to high-temperature superconductivity," *Nature Materials*, vol. 7, no. 12, pp. 953–959, 2008.
- [23] S. Chikazumi, *Physics of Magnetism*, John Wiley & Sons, New York, NY, USA, 1964.
- [24] S. A. J. Kimber, D. N. Argyriou, F. Yokaichiya, et al., "Magnetic ordering and negative thermal expansion in  $\text{PrFeAsO}$ ," *Physical Review B*, vol. 78, no. 14, Article ID 140503, 4 pages, 2008.
- [25] D. J. Singh and L. Nordstrom, *Planewaves, Pseudopotentials and the LAPW Method*, Springer, Berlin, Germany, 2nd edition, 2006.
- [26] D. Singh, "Ground-state properties of lanthanum: treatment of extended-core states," *Physical Review B*, vol. 43, no. 8, pp. 6388–6392, 1991.
- [27] M. Rotter, M. Tegel, D. Johrendt, I. Schellenberg, W. Hermes, and R. Pöttgen, "Spin-density-wave anomaly at 140 K in the ternary iron arsenide  $\text{BaFe}_2\text{As}_2$ ," *Physical Review B*, vol. 78, no. 2, Article ID 020503, 4 pages, 2008.
- [28] C. de la Cruz, W. Z. Hu, S. Li, et al., "Lattice Distortion and Magnetic Quantum Phase Transition in  $\text{CeFeAs}_{1-x}\text{P}_x\text{O}$ ," *Physical Review Letters*, vol. 104, no. 1, Article ID 017204, 4 pages, 2010.
- [29] T. Egami, B. Fine, D. J. Singh, D. Parshall, C. de la Cruz, and P. Dai, "Spin-lattice coupling in iron-pnictide superconductors," *Physica C* in press, 2010.

- [30] E. C. Stoner, "Ferromagnetism," *Reports on Progress in Physics*, vol. 11, no. 1, pp. 43–112, 1947.
- [31] R. P. Gupta and S. K. Sinha, "Wave-number-dependent susceptibility function for paramagnetic chromium," *Physical Review B*, vol. 3, no. 8, pp. 2401–2411, 1971.
- [32] H. L. Skriver, "The electronic structure of antiferromagnetic chromium," *Journal of Physics F*, vol. 11, no. 1, pp. 97–111, 1981.
- [33] E. Fawcett, "Spin-density-wave antiferromagnetism in chromium," *Reviews of Modern Physics*, vol. 60, no. 1, pp. 209–283, 1988.
- [34] J. Zhao, D. T. Adroja, D.-X. Yao, et al., "Spin waves and magnetic exchange interactions in  $\text{CaFe}_2\text{As}_2$ ," *Nature Physics*, vol. 5, no. 8, pp. 555–560, 2009.
- [35] S. Li, C. de la Cruz, Q. Huang, et al., "Structural and magnetic phase transitions in  $\text{Na}_{1-\delta}\text{FeAs}$ ," *Physical Review B*, vol. 80, no. 2, Article ID 020504, 4 pages, 2009.
- [36] M. Rotter, M. Tegel, and D. Johrendt, "Superconductivity at 38 K in the iron arsenide  $(\text{Ba}_{1-x}\text{K}_x)\text{Fe}_2\text{As}_2$ ," *Physical Review Letters*, vol. 101, no. 10, Article ID 107006, 4 pages, 2008.
- [37] Y. Qiu, M. Kofu, W. Bao, et al., "Neutron-scattering study of the oxypnictide superconductor  $\text{LaFeAsO}_{0.87}\text{F}_{0.13}$ ," *Physical Review B*, vol. 78, no. 5, Article ID 052508, 4 pages, 2008.
- [38] Y. Qiu, W. Bao, Q. Huang, et al., "Crystal structure and antiferromagnetic order in  $\text{NdFeAsO}_{1-x}\text{F}_x$  ( $x = 0.0$  and  $0.2$ ) superconducting compounds from neutron diffraction measurements," *Physical Review Letters*, vol. 101, no. 25, Article ID 257002, 4 pages, 2008.
- [39] J. Zhao, Q. Huang, C. de la Cruz, et al., "Structural and magnetic phase diagram of  $\text{CeFeAsO}_{1-x}\text{F}_x$  and its relation to high-temperature superconductivity," *Nature Materials*, vol. 7, no. 12, pp. 953–959, 2008.
- [40] J. Zhao, Q. Huang, C. de la Cruz, et al., "Lattice and magnetic structures of  $\text{PrFeAsO}$ ,  $\text{PrFeAsO}_{0.85}\text{F}_{0.15}$ , and  $\text{PrFeAsO}_{0.85}$ ," *Physical Review B*, vol. 78, no. 13, Article ID 132504, 4 pages, 2008.
- [41] T. Nomura, S. W. Kim, Y. Kamihara, et al., "Crystallographic phase transition and high- $T_c$  superconductivity in  $\text{LaFeAsO:F}$ ," *Superconductor Science and Technology*, vol. 21, no. 12, Article ID 125028, 9 pages, 2008.
- [42] A. Martinelli, M. Ferretti, P. Manfrinetti, et al., "Synthesis, crystal structure, microstructure, transport and magnetic properties of  $\text{SmFeAsO}$  and  $\text{SmFeAs}(\text{O}_{0.93}\text{F}_{0.07})$ ," *Superconductor Science and Technology*, vol. 21, no. 9, Article ID 095017, 7 pages, 2008.
- [43] C.-H. Lee, A. Iyo, H. Eisaki, et al., "Effect of structural parameters on superconductivity in fluorine-free  $\text{LnFeAsO}_{1-y}$  ( $\text{Ln} = \text{La}, \text{Nd}$ )," *Journal of the Physical Society of Japan*, vol. 77, no. 8, Article ID 083704, 4 pages, 2008.
- [44] A. S. Sefat, A. Huq, M. A. McGuire, et al., "Superconductivity in  $\text{LaFe}_{1-x}\text{Co}_x\text{AsO}$ ," *Physical Review B*, vol. 78, no. 10, Article ID 104505, 9 pages, 2008.
- [45] S. Li, C. de la Cruz, Q. Huang, et al., "First-order magnetic and structural phase transitions in  $\text{Fe}_{1+y}\text{Se}_x\text{Te}_{1-x}$ ," *Physical Review B*, vol. 79, no. 5, Article ID 054503, 7 pages, 2009.
- [46] M. J. Pitcher, D. R. Parker, P. Adamson, et al., "Structure and superconductivity of  $\text{LiFeAs}$ ," *Chemical Communications*, no. 45, pp. 5918–5920, 2008.
- [47] X. C. Wang, Q. Q. Liu, Y. X. Lv, et al., "The superconductivity at 18 K in  $\text{LiFeAs}$  system," *Solid State Communications*, vol. 148, no. 11–12, pp. 538–540, 2008.
- [48] N. D. Zhigadlo, S. Katrych, Z. Bukowski, S. Weyeneth, R. Puzniak, and J. Karpinski, "Single crystals of superconducting  $\text{SmFeAsO}_{1-x}\text{F}_y$  grown at high pressure," *Journal of Physics: Condensed Matter*, vol. 20, no. 34, Article ID 342202, 5 pages, 2008.
- [49] J.-W. G. Bos, G. B. S. Penny, J. A. Rodgers, D. A. Sokolov, A. D. Huxley, and J. P. Attfield, "High pressure synthesis of late rare earth  $\text{RFeAs}(\text{O},\text{F})$  superconductors;  $\text{R} = \text{Tb}$  and  $\text{Dy}$ ," *Chemical Communications*, no. 31, pp. 3634–3635, 2008.
- [50] S. Matsuishi, Y. Inoue, T. Nomura, M. Hirano, and H. Hosono, "Cobalt-substitution-induced superconductivity in a new compound with  $\text{ZrCuSiAs}$ -type structure,  $\text{SrFeAsF}$ ," *Journal of the Physical Society of Japan*, vol. 77, no. 11, Article ID 113709, 3 pages, 2008.
- [51] W. P. Su, J. R. Schrieffer, and A. J. Heeger, "Solitons in polyacetylene," *Physical Review Letters*, vol. 42, no. 25, pp. 1698–1701, 1979.
- [52] B. Normand, H. Kohno, and H. Fukuyama, "Spin-phonon coupling in the single-layer extended t-J model," *Physical Review B*, vol. 53, no. 2, pp. 856–870, 1996.
- [53] L. Boeri, O. V. Dolgov, and A. A. Golubov, "Is  $\text{LaFeAsO}_{1-x}\text{F}_x$  an electron-phonon superconductor?" *Physical Review Letters*, vol. 101, no. 2, Article ID 026403, 4 pages, 2008.
- [54] M. L. Kulić and A. A. Haghighirad, "Possible strong electron-lattice interaction and giant magneto-elastic effects in Fe-pnictides," *Europhysics Letters*, vol. 87, no. 1, Article ID 17007, 6 pages, 2009.
- [55] S. Ishihara, T. Egami, and M. Tachiki, "Electron-lattice interaction in cuprates: effect of electron correlation," *Physical Review B*, vol. 55, no. 5, pp. 3163–3172, 1997.
- [56] M. L. Kulić, "Interplay of electron-phonon interaction and strong correlations: the possible way to high-temperature superconductivity," *Physics Report*, vol. 338, no. 1–2, pp. 1–264, 2000.
- [57] P. Piekarczyk and T. Egami, "Dynamic charge transfer and spin-phonon interaction in high- $T_c$  superconductors," *Physical Review B*, vol. 72, no. 5, Article ID 054530, 9 pages, 2005.

## Review Article

# Existence of an Intermediate Metallic Phase at the SDW-CDW Crossover Region in the One-Dimensional Holstein-Hubbard Model at Half-Filling

**Ashok Chatterjee**

*School of Physics, University of Hyderabad, Hyderabad 500 046, India*

Correspondence should be addressed to Ashok Chatterjee, [acsp@uohyd.ernet.in](mailto:acsp@uohyd.ernet.in)

Received 5 September 2009; Accepted 8 December 2009

Academic Editor: Alexandre Sasha Alexandrov

Copyright © 2010 Ashok Chatterjee. This is an open access article distributed under the Creative Commons Attribution License, which permits unrestricted use, distribution, and reproduction in any medium, provided the original work is properly cited.

The Holstein-Hubbard model serves as a useful framework to investigate this interplay between the phonon-induced electron-electron attractive interaction and the direct Coulomb repulsion and can afford interesting phase diagrams due to competition among charge-density wave (CDW), spin-density wave (SDW), and superconductivity. However the detailed nature of the CDW-SDW transition is still not very well known. It is generally believed that the system undergoes a direct insulator to insulator transition from CDW to SDW with the increase of the on-site Coulomb repulsion for a given strength of the electron-phonon coupling and this is the main bottleneck for the polaronic/bipolaronic mechanism of high-temperature superconductivity. We have recently made an investigation to study the nature of the transition from SDW phase to CDW phase within the framework of a one-dimensional Holstein-Hubbard model at half-filling using a variational method. We find that an intervening metallic phase may exist at the crossover region of the CDW-SDW transition. We have also observed that if the anharmonicity of the phonons is taken into account, this metallic phase widens and the polarons become more mobile, which is a more favorable situation from the point of view of superconductivity. We shall finally show that an improved variational calculation widens the metallic phase and makes the polarons more mobile, which reconfirms the existence of the intermediate metallic phase at the SDW-CDW crossover region.

## 1. Introduction

The discovery of high-temperature cuprate superconductors is more than twenty years old [1]; however, the basic mechanism involved for inducing superconductivity in these systems has remained hitherto elusive. Though several mechanisms [2] have been suggested over the last three decades, there has hardly been any consensus on any particular model. One of the potential mechanisms that have been advocated for inducing pairing in cuprates is again the electron-phonon interaction [3–16]. There have also been quite a few experiments which have supported this conjecture [17–27]. According to some of these models, electron-phonon interaction being large enough in the high  $T_c$  materials, polarons, or bipolarons should be the natural quasiparticles in the normal phase of these systems. However, these materials being strongly correlated systems

with narrow bands, it is more convincing to describe the corresponding polarons or bipolarons through the Holstein approach [15, 16, 28] instead of the usual Frohlich picture [29]. There are several temperature scales in these systems. One is  $T_{BCS}$ , which is the transition temperature for the polaronic superconductivity through BCS mechanism [30]. The second temperature scale is  $T_{BP}$ , which is the temperature at which two polarons can form a stable local bipolaron which is a static pair as opposed to the dynamic Cooper pair of the usual BCS theory. If  $T_{BP}$  is higher than  $T_{BCS}$ , then the normal phase would be a bosonic phase containing bipolarons as the quasiparticles. In this case, there should exist a temperature  $T_{BEC}$ , the third temperature scale, which is the Bose-Einstein condensation temperature for the bipolarons. The superconducting phase is then naturally the Bose-Einstein condensate of static bipolarons. The polaronic or bipolaronic mechanism for inducing pairing can explain

many of the properties of high-temperature cuprates, but there has also been a strong opposition to these theories by some researchers. The polaronic/bipolaronic theories require a strong electron-phonon interaction for the formation of polarons and bipolarons which in the opinion of these researchers is the greatest bottleneck of these theories because at large electron-phonon coupling a system would normally prefer to settle into a charge-density wave (CDW) ground state (GS) which is a Peierls insulating phase. On the other hand, if the electron-phonon coupling is not too strong to overcome the Coulomb correlation, the system would prefer to be in a spin-density wave (SDW) GS which is an antiferromagnetic Mott insulating phase. Thus, they argue, that the electron-phonon interaction cannot play any role in high- $T_c$  superconductivity. However, a deeper and more careful look suggests that there could be yet another effect arising due to the competition between the phonon-induced attractive interaction between electrons and the direct Coulomb repulsion which might lead to some kind of a compromise at the crossover region so much so that the transition from one insulating state to the other may not be direct as normally believed but may go through an intermediate phase and it is this phase which is the subject of our interest.

The most suitable model to study the interplay between the electron-phonon interaction and the Coulomb repulsion in narrow-band systems is the Holstein-Hubbard model. Last three decades have witnessed a flurry of investigations [15, 16, 31–43] on this model primarily for its potential role in the context of high- $T_c$  superconductivity, and also for its intrinsic appeal from the point of view of fundamental physics, for it provides a very useful framework for the investigation of polaronic effects on correlated electrons in narrow-band systems. So far, several studies on the Hubbard-Holstein model have revealed that it can afford interesting phase diagrams due to the competition among charge-density wave (CDW), spin-density wave (SDW), and superconductivity as we change the parameters involved in the system. Recently, Takada and Chatterjee [44] (hereafter referred to as TC) have shown for the first time within the framework of one-dimensional (1D) HH model at half-filling that there may exist an intervening phase at the CDW-SDW crossover region and, interestingly enough, this phase is metallic. This theoretical observation is of great importance because such a metallic state, if exists, would be just ideal for high- $T_c$  superconductivity. TC have shown in a subsequent paper [45] that the presence of phonon anharmonicity makes the polarons even more mobile and also widens the metallic phase favoring superconductivity even more. More recently, Krishna and Chatterjee (KC) [46] have made an improved calculation to test the veracity of the results of TC. The goal was to see whether using a more accurate phonon GS yields results which are more conducive or less conducive for the phenomenon of superconductivity. KC have shown that a better variational analysis in fact broadens the metallic region even further, thus lending more credence to the prediction about the existence of the intermediate metallic phase at the CDW-SDW crossover region made earlier by

TC. In this article we shall present a review of the above scenario.

## 2. The Model Hamiltonian

The Holstein-Hubbard Hamiltonian may be written as

$$H = - \sum_{\langle ij \rangle \sigma} t_{ij} c_{i\sigma}^{\dagger} c_{j\sigma} + U \sum_i n_{i\uparrow} n_{i\downarrow} + \omega_0 \sum_i b_i^{\dagger} b_i + \sum_{i\sigma} g n_{i\sigma} (b_i + b_i^{\dagger}), \quad (1)$$

where  $c_{i\sigma}^{\dagger}$  ( $c_{i\sigma}$ ) is the creation (annihilation) operator for an electron with spin  $\sigma$  at the  $i$ th lattice site,  $n_{i\sigma} = c_{i\sigma}^{\dagger} c_{i\sigma}$  is the electron number operator,  $t_{ij}$  is the bare hopping integral, and  $U$  is the on-site Coulomb interaction energy. The notation  $\langle ij \rangle$  in the hopping term denotes that the summation over  $i$  and  $j$  has to be carried over nearest neighbors only and we shall write  $t_{ij} = t$ .  $b_i^{\dagger}$  ( $b_i$ ) is the phonon creation (annihilation) operator at the  $i$ th site and  $\omega_0$  is the dispersionless optical phonon frequency.  $g$  is the dispersionless electron-phonon interaction strength which may be written as  $g = \sqrt{\alpha} \omega_0$ , where  $\alpha$  is the dimensionless electron-phonon coupling constant. In (1) we have chosen units in such a way that  $\hbar = 1$ . As has been alluded to above, the above Hamiltonian is able to provide the CDW and SDW phases; however, the details of the CDW-SDW transition are not at all clear. The usual belief is that the transition is direct. However, an exact-diagonalization study [41] on the two-site HH model has suggested the appearance of a superconducting phase. As related to this issue, a metal-insulator transition has been predicted in the Holstein model using either the density-matrix renormalization group [42] or a unitary transformation method [43]. Thus, our aim has been to carefully consider the transition region at half-filling by approaching the HH model from the antiadiabatic region in which  $t$  is much smaller than  $\omega_0$ . In order to avoid any error that might enter through the approximations involved in dealing with the Coulomb correlation term, we have investigated the one-dimensional (1D) system so that the exact solution of Lieb and Wu [47] can be taken advantage of.

## 3. Theory

We shall attempt to solve the above Hamiltonian using a variational approach. The first step is to apply a variable-displacement (VD) Lang-Firsov (LF) canonical transformation [48–50] with a generator  $R_1$ , defined as

$$R_1 = g' \sum_{i\sigma} n_{i\sigma} (b_i^{\dagger} - b_i), \quad (2)$$

where  $g'$  is a variational parameter. We assume that  $g'$  is of form  $g' = \omega_0 \sqrt{\alpha} \eta$ . In the conventional LF approach [48], one chooses  $\eta = 1$  so that  $g' = g$  and obtains the GS energy by averaging the transformed Hamiltonian with respect to the zero-phonon state which, however, would be a good

enough approximation for strong  $\alpha$  in the antiadiabatic limit. In the weak and intermediate coupling region, however, a lower GS energy can be obtained by optimizing  $\eta$ . Furthermore, our variable Lang-Firsov transformation (VDLFT) assumes that the phonon coherence coefficient depends linearly on the electron concentration,  $n_i$ . The parameter  $\eta$  essentially gives a measure of the lattice deformation; in the strong-coupling limit it approaches unity, but in the intermediate-coupling region, it becomes smaller than that, so as to provide a better total energy by balancing the tendency to localization of an electron by the electron-phonon coupling and its itinerant nature due to the hopping motion. Then the transformed Hamiltonian reads

$$\begin{aligned} H_1 &= e^R H e^{-R} \\ &= -\alpha\omega_0\eta(2-\eta)\sum_{i\sigma} n_{i\sigma} - t \sum_{\langle ij \rangle\sigma} e^{(x_i-x_j)} c_{i\sigma}^+ c_{j\sigma} \\ &\quad + [U - 2\alpha\omega_0\eta(2-\eta)]\sum_i n_{i\uparrow} n_{i\downarrow} + \omega_0 \sum_i b_i^+ b_i \\ &\quad + \sqrt{\alpha}\omega_0(1-\eta)\sum_{i\sigma} n_{i\sigma} (b_i^+ + b_i), \end{aligned} \quad (3)$$

where the operator  $x_i$  is defined as  $x_i = \sqrt{\alpha}\eta(b_i^+ - b_i)$ . In constructing a trial wave function  $\Psi$  for the ground state in the antiadiabatic region, we consider it as a product of the electronic part  $\Phi_{\text{el}}$  and the phonon part  $\Phi_{\text{ph}}$ , whereby  $\Phi_{\text{ph}}$  may include electronic variables, either explicitly or implicitly, but it depends on them only as  $c$ -number parameters, not quantum variables, in just the same way as the ion positions are regarded in the electronic wave function in the conventional adiabatic Born-Oppenheimer approximation. Then the energy expectation value  $E_0$  can be evaluated as

$$E_0 = \langle \Psi | H_1 | \Psi \rangle = \langle \Phi_{\text{el}} | H_{\text{eff}} | \Phi_{\text{el}} \rangle, \quad (4)$$

where

$$H_{\text{eff}} = \langle \Phi_{\text{ph}} | H_1 | \Phi_{\text{ph}} \rangle \quad (5)$$

is the effective electronic Hamiltonian. Normally for the phonon subsystem, one chooses the zero-phonon state,  $\prod_i |0_i\rangle$ , for the ground state of the electron-phonon composite system. In our treatment, however, we have improved on it by assuming that

$$|\Phi_{\text{ph}}\rangle = \prod_i e^{(-h_i^2/2) - h_i b_i^+} |0_i\rangle, \quad (6)$$

where  $h_i$  is another variational parameter and  $|0_i\rangle$  is the zero-phonon state at the  $i$ th site. Note that this state is normalized;  $\langle \Phi_{\text{ph}} | \Phi_{\text{ph}} \rangle = 1$ . If  $h_i$  is taken to be zero, then it is reduced to the zero-phonon state, but a solution with nonzero  $h_i$  gives a much lower  $E_0$ , especially for a large positive  $U$ , as we shall show later. In this paper, we shall be interested only in the half-filled case, that is, we shall consider only one electron per site. Therefore, we assume that all the sites are equivalent; consequently we can assume that  $h_i = h$ , for all  $i$ , which is

consistent with the choice of the  $i$  independent  $\eta$  in defining  $R$ . This assumption is also in tune with the form of the electron-phonon interaction taken in the initial Hamiltonian where the electron-phonon interaction coefficient  $g$  is same for all sites. Then we can derive  $H_{\text{eff}}$  in (5) for the  $N$ -site system using (6) for  $|\Phi_{\text{ph}}\rangle$ . One can immediately see that using the phonon state (6) implies first employing a coherent state transformation on  $H_1$  with a generator  $R_2$  given by

$$R_2 = \sum_i [h(b_i^+ - b_i)] \quad (7)$$

and then performing an averaging with respect to the unperturbed zero-phonon state. The two transformations performed so far look together as

$$R_{12} = \sum_{i\sigma} \left[ h + \eta\sqrt{\alpha} \left( n_{i\sigma} - \frac{h}{\sqrt{\alpha}} \right) \right] (b_i^+ - b_i). \quad (8)$$

The first transformation corresponds to the antiadiabatic limit ( $\eta = 1$ ) while the second transformation corresponds to the adiabatic limit ( $\eta = 0$ ). Thus both the adiabatic and antiadiabatic regions are considered by taking  $0 < \eta < 1$ . The effective electronic Hamiltonian (5) is obtained as

$$\begin{aligned} H_{\text{eff}} &= Nh^2\omega_0 - [\alpha\eta(2-\eta) + 2\sqrt{\alpha}h(1-\eta)]\omega_0 \sum_{i\sigma} n_{i\sigma} \\ &\quad - t_{\text{eff}} \sum_{\langle ij \rangle} c_{i\sigma}^+ c_{j\sigma} + U_{\text{eff}} \sum_i c_{i\sigma}^+ c_{i\sigma}, \end{aligned} \quad (9)$$

where  $t_{\text{eff}}$  is the renormalized hopping integral, given by

$$t_{\text{eff}} = t e^{-\alpha\eta^2}, \quad (10)$$

and  $U_{\text{eff}}$  is the effective on-site Coulomb interaction, expressed as

$$U_{\text{eff}} = U - 2\alpha\omega_0\eta(2-\eta) = \tilde{U} + 2\alpha\omega_0(1-\eta)^2, \quad (11)$$

where  $\tilde{U} = U - 2\alpha\omega_0$ . One can see that the effective hopping parameter  $t_{\text{eff}}$  is reduced by the factor  $e^{-\alpha\eta^2}$ , called the Holstein reduced factor which leads to the phenomenon of band narrowing due to polaron formation. The band reduction factor is maximum for  $\eta = 1$ . One may also note that both  $t_{\text{eff}}$  and  $U_{\text{eff}}$  are independent of  $h$ , reflecting the fact that the phonon background represented in  $|\Phi_{\text{ph}}\rangle$  is independent of the electron motion in contrast with the situation described by the operator  $R$  in (2). Furthermore if  $\eta$  is not equal to unity, then  $U_{\text{eff}}$  is larger than  $\tilde{U}$  due to the retardation effect of phonons on the phonon-mediated attraction.

In one dimension, the effective Hubbard Hamiltonian (7) can be solved exactly using the Bethe ansatz method as was shown by Lieb and Wu. The solution of Lieb and Wu [47] is, however, valid for  $U_{\text{eff}} > 0$ . We have performed the following transformations [44]:

$$c_{i1} \rightarrow c_{i1}, \quad c_{i2} \rightarrow (-1)^i c_{i1}^+, \quad (12)$$

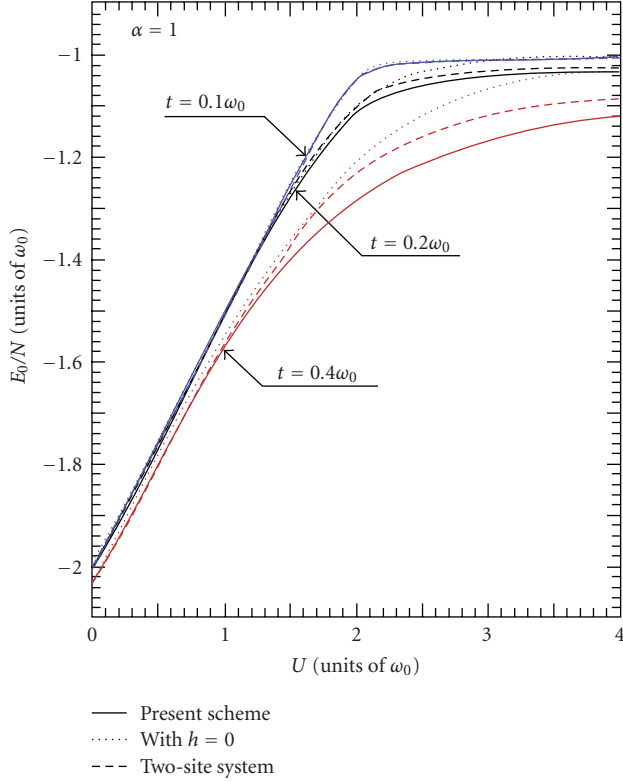


FIGURE 1: (Color online) Ground-state energy per site as a function of  $U$  for  $\alpha = 1$  and three cases of  $t/\omega_0 = 0.1, 0.2,$  and  $0.4$ .

to obtain results which will be valid for both  $U_{\text{eff}} > 0$  and  $U_{\text{eff}} < 0$ . The energy per site is obtained as

$$\epsilon_0 = \frac{E_0}{N} = -\alpha\omega_0 + [h - \sqrt{\alpha}(1 - \eta)]^2\omega_0 + \frac{U_{\text{eff}} - |U_{\text{eff}}|}{4} - 4t_{\text{eff}} \int_0^\infty \frac{dz}{z} \frac{J_0(z)J_1(z)}{[1 + \exp(z|U_{\text{eff}}|/2t_{\text{eff}})]}, \quad (13)$$

where  $J_0(z)$  and  $J_1(z)$  are the Bessel functions of zeroth order and first order, respectively. One can immediately see that the variational parameter “ $h$ ” can be analytically obtained. Namely,

$$\frac{d\epsilon_0}{dh} = 0 \quad (14)$$

yields  $h = \sqrt{\alpha}(1 - \eta)$ .

#### 4. Numerical Results and Discussion

Minimization with respect to  $\eta$  has to be done numerically. The energy per site as function of  $U$  for  $\alpha = 1$  is shown in Figure 1.

In the antiadiabatic limiting region, for example, in the case of  $t = 0.1\omega_0$ , the effect of the parameter  $h$  is not so significant, as can be seen by comparing the present result (the solid curve) with the one obtained by choosing  $h = 0$  (the dotted curve). This is because in this case the optimized

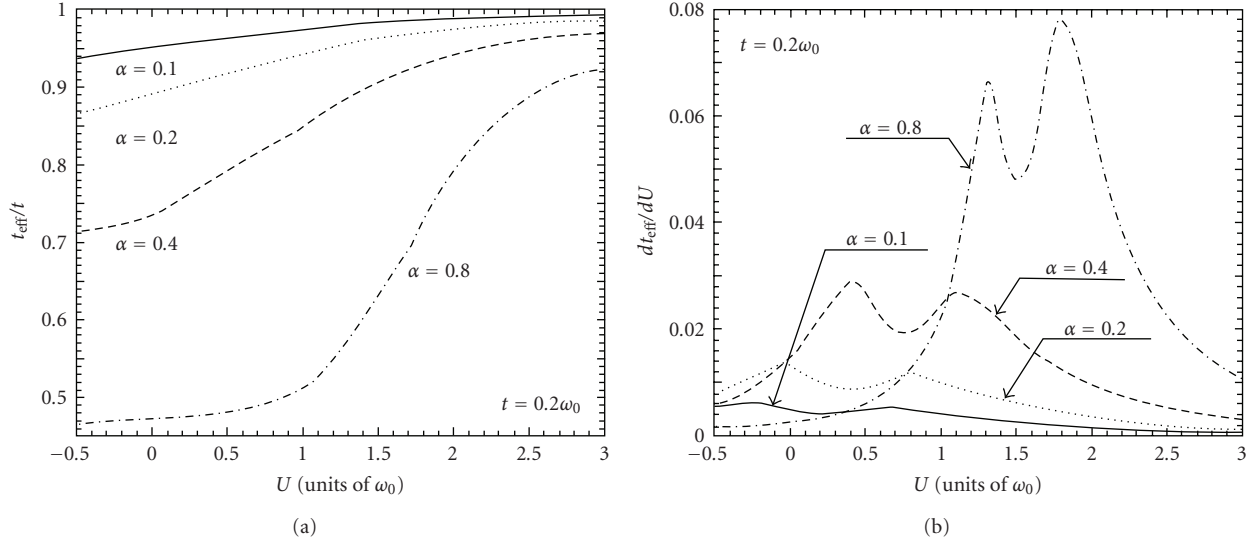
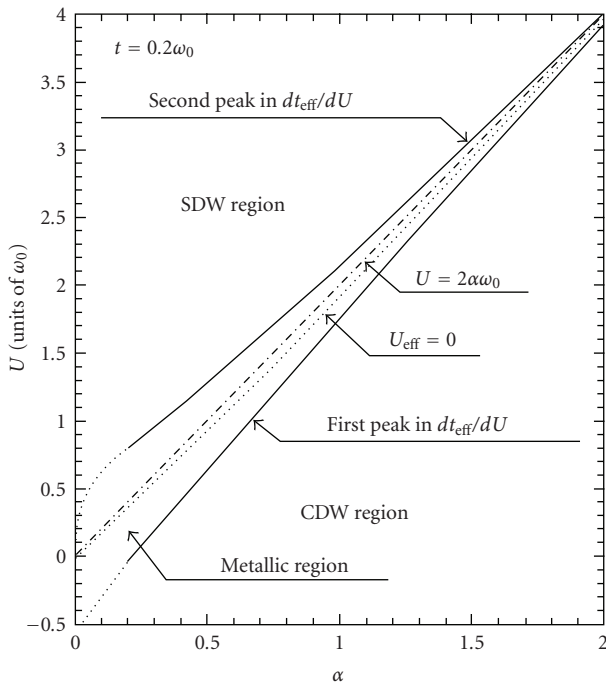
value of  $\eta$  is pretty close to 1. The present results for the energy  $\epsilon_0$  are also in good agreement with the energy of the corresponding two-site system obtained by Takada [41] by using exact diagonalization. This implies that physics of the present system in this region can be essentially captured by the two-site problem. It is evident that at the crossover region there is a rounding-off in the energy. It may also be pointed out that  $U_{\text{eff}}$  changes sign in the crossover region. Had the change in the energy been sharp at the crossover region, one would have expected a direct transition from the CDW to the SDW phase. But the rounding off in the energy suggests that there may be an intermediate state at the cross-over region. As  $t$  increases, the rounding-off region also increases. Thus adiabaticity seems to favor the intermediate state.

In Figure 2(a), we plot  $t_{\text{eff}}$  as a function of  $U$  for various values  $\alpha$  and for  $t = 0.2\omega_0$ . This is essentially equivalent to plotting the antiadiabaticity parameter  $\eta$ . A careful observation shows that the curves have some interesting structures. To decipher them, we plot in Figure 2(b) the derivative of  $t_{\text{eff}}$  with respect to  $U$ , that is,  $dt_{\text{eff}}/dU$  as a function of  $U$ . One can immediately see that there are peaks on both sides of the cross-over point defined by  $U_{\text{eff}} = 0$  which is roughly given by  $U = 2\alpha\omega_0$ . The peak structure becomes more prominent as the electron-phonon coupling constant is increased. As  $\alpha$  decreases, the peaks reduce in height and eventually it becomes rather difficult to clearly identify the transition points if  $\alpha\omega_0 \sim 1$ . For values of  $U$  less than those at the first peak,  $t_{\text{eff}}$  is very small which means that  $\eta$  is close to 1. In this case one would expect the formation of massive localized bipolarons or in other words a CDW phase. For values of  $U$  larger than the second transition,  $\eta$  approaches zero, and thus  $t_{\text{eff}}$  tends to the bare hopping integral  $t$ . This does not, however, mean that the electrons become free. Rather, the system essentially reduces to the original Hubbard model describing the antiferromagnetic insulating phase. Between the two transition points, we observe that  $t_{\text{eff}}$  and  $U_{\text{eff}}$  obey the condition  $t_{\text{eff}}/U_{\text{eff}} \gg 0.25$ , which seems to be a sign of a metallic behavior of a system of many free polarons.

In Figure 3, we have plotted the CDW-SDW phase diagram in  $(\alpha, U)$  plane. The boundaries of the phase diagram have been obtained from the maxima of the  $dt_{\text{eff}}/dU$  versus  $U$  curve. We find it difficult to draw the phase diagram for small  $\alpha$  or small  $U$ . However it seems that for  $\alpha = 0$  and  $U < 0$ , that is, attractive on-site interaction, the normal state is unstable against superconducting transition. We have already argued that the region along increasing  $U$  beyond the second peak of  $dt_{\text{eff}}/dU$  corresponds to the SDW phase while that along decreasing  $U$  from the first peak corresponds to the CDW phase. The region in between the CDW and SDW phases corresponds to  $t_{\text{eff}}/U_{\text{eff}} \gg 0.25$  and is, therefore, a metallic phase.

To obtain another evidence for the existence of the intermediate metallic state, we have calculated the average local spin moment per site which is given by

$$L_0 = \frac{\sum_i [\langle S_i^2 \rangle]}{N} = \sum_i [\langle S_i^2 \rangle] = \frac{N[3 - 6 \sum_i \langle n_i n_{i+1} \rangle]}{4} \quad (15)$$

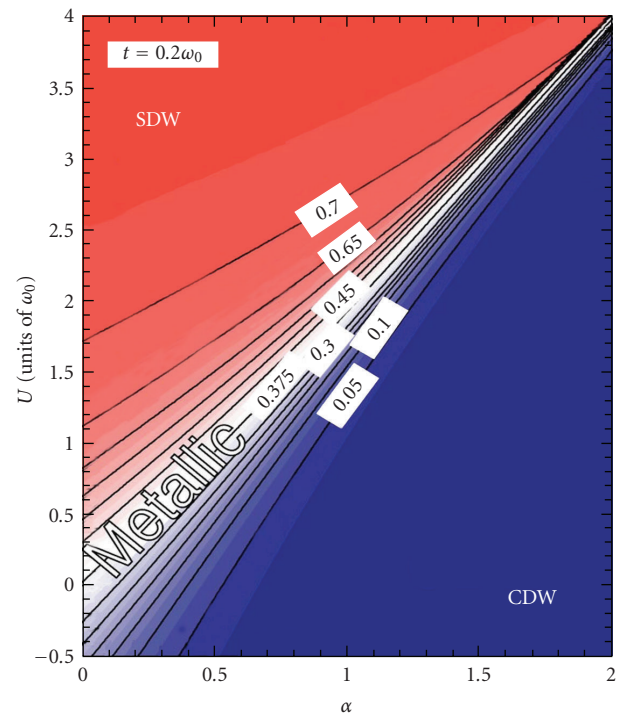

 FIGURE 2: Renormalized hopping integral  $t_{\text{eff}}$  and its derivative as a function of  $U$  for various values of  $\alpha$  at  $t = 0.2\omega_0$ .

 FIGURE 3: Phase diagram in  $(\alpha, U)$  plane determined by the peaks in  $dt_{\text{eff}}/dU$ . The curve corresponding to  $U_{\text{eff}} = 0$  is also given by the dotted curve.

which by using (13) can be written as

$$L_0 = \frac{[3 - (6d\epsilon_0/dU)]}{4}. \quad (16)$$

For totally uncorrelated motion of electrons as in the case of noninteracting electrons, one can easily obtain from (7) the value of  $d\epsilon_0/dU$  which then yields

$$L_0 = \frac{3}{8} = 0.375. \quad (17)$$


 FIGURE 4: Contour plots of the local moment  $L_0$  in  $(\alpha, U)$  plane.

Using (17) and (13), one can obtain contour plots for  $(\alpha, U)$  for different values of  $L_0$ . In Figure 4 we show these plots. It is evident that  $L_0 = 0.375$  lies in the same region where  $t_{\text{eff}}/U_{\text{eff}} \gg 0.25$ , thus confirming the existence of a metallic phase at the cross-over region of the CDW and SDW phases.

## 5. Effect of Anharmonic Phonons

For the sake of simplicity, we have considered the phonons to be harmonic in [44] and in Sections 2–4, while in reality

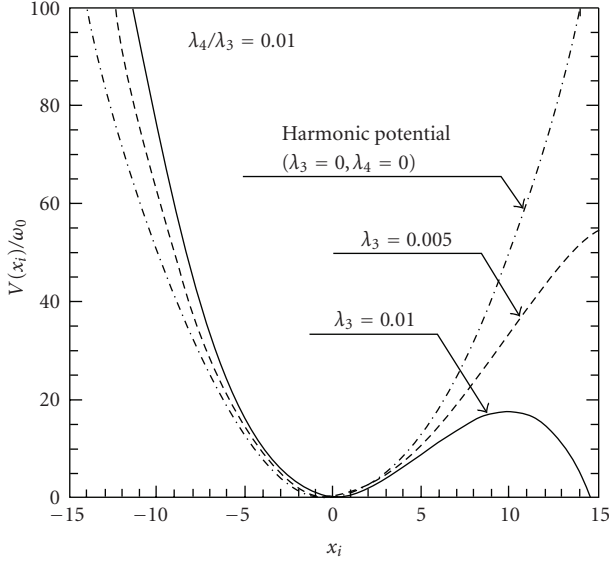


FIGURE 5: Anharmonic potential in units of  $\omega_0$  as a function of the one-dimensional lattice displacement  $x_i$  for  $\lambda_3 = 0.005$  and  $0.01$  with  $\lambda_4/\lambda_3 = 0.01$ .

the ion-ion potential in a solid should also contain anharmonic terms giving rise to phonon-phonon interactions, and hence a finite lifetime for phonons. Those phonon-phonon interaction terms are absolutely necessary to explain certain thermal properties like thermal expansion, but their effects on the electronic properties are normally very small, and therefore they are generally neglected. However, several investigations have shown that phonon anharmonicity can produce some profound effects on the electronic properties as well, particularly in the study of high- $T_c$  superconductivity [24–27, 51–53]. In this context, anharmonic vibration of the apex oxygen atoms in cuprates has attracted much attention and its effects have been studied in terms of various models for the anharmonic phonons such as the double-well potential model [54–56] and the Hubbard model coupled to a local two-level system [57]. Since it can mimic a double-well potential with a proper choice of the adjustable parameters, the local Gaussian potential model [58] has also been analyzed. Furthermore, the competition between superconductivity and CDW has been studied in the Holstein-Hubbard model with the quartic anharmonic contribution to the phonon potential energy [59]. One of the features that are common to all these investigations is that the anharmonic potential  $V(x_i)$  with the lattice displacement  $x_i$  is symmetric with respect to the inversion of  $x_i$  or  $x_i \rightarrow -x_i$ . Such a symmetric  $V(x_i)$ , however, would never give rise to thermal expansion of lattice. Chatterjee and collaborators [60, 61] have given an appropriate form for  $V(x_i)$ , which quantitatively explains the thermal expansion behavior of actual materials. It is found that the most dominant anharmonic effect of the lattice potential would come from the terms that are cubic and quartic in the lattice displacement. Indeed, it has recently been shown that the thermal expansion data for both YBaCuO and Bi-2223 superconductors can be explained quite satisfactorily

by using  $V(x_i)$  consisting of cubic and quartic terms [62, 63]. This model also predicts the values of the Debye temperature which for both materials compare quite impressively with the values quoted in the literature. This imparts a fair amount of confidence in this model. Since we have come to know a form of the anharmonic lattice potential which is physically motivated and also supported by experiment, it would be interesting to investigate quantitatively how those cubic and quartic anharmonic phonons will modify the polaronic properties in general and the nature of the CDW-SDW transition in particular. We adopt the same variational method as the one introduced in the above Holstein-Hubbard model so that we can make a direct comparison between harmonic and anharmonic models and at the same time restrict ourselves to the one-dimensional problem so that the exact solution of Lieb and Wu [47] can be used. The present calculation has led us to obtain an important observation that the main effect of the phonon anharmonicities is to effectively shift the on-site Coulomb repulsion  $U$  with the direction of the shift depending on the sign of the electron-phonon coupling constant  $g$ . With the use of the realistic magnitudes for the anharmonicities, we find that the overall features of the anharmonic system are basically similar to those in the harmonic one for positive  $g$ , while they may become radically different for negative  $g$ . In the latter case, in particular, a first-order phase transition can be seen, which constitutes an unexpected and very interesting theoretical observation.

The one-dimensional (1D) Hubbard-Holstein model with cubic and quartic anharmonic phonons may be described by the Hamiltonian  $H$ , given by

$$\begin{aligned}
 H &= H_e + H_{\text{ph}} + H_{e\text{-ph}}, \text{ with} \\
 H_e &= -t \sum_{\langle ij \rangle \sigma} c_{i\sigma}^\dagger c_{j\sigma} + U \sum_i n_{i\uparrow} n_{i\downarrow}, \\
 H_{\text{ph}} &= \omega_0 \sum_i b_i^\dagger b_i - \omega_0 \sum_{k=3}^4 \lambda_k \sum_i (b_i^\dagger + b_i)^k, \\
 H_{e\text{-ph}} &= g \sum_{i\sigma} n_{i\sigma} (b_i^\dagger + b_i),
 \end{aligned} \tag{18}$$

where  $H_{\text{ph}}$  contains the anharmonic phonon terms and rest of the terms are same as in (1).

In terms of the local displacement of an ion at the  $i$ th site,

$$x_i \left[ \equiv \frac{(b_i + b_i^\dagger)}{\sqrt{2}} \right]. \tag{19}$$

$H_{\text{ph}}$  in (18) can be derived from the local potential  $V(x_i)$  given by

$$V(x_i) = \omega_0 \left( \frac{1}{2} x_i^2 - 2\sqrt{2}\lambda_3 x_i^3 - 4\lambda_4 x_i^4 \right). \tag{20}$$

The parameters  $\lambda_3$  and  $\lambda_4$  should be positive as required by the consideration of thermal expansion [60, 61, 64]. Quantitatively, their magnitudes can be evaluated by analyzing experiment on thermal expansion of crystals to find that

$$\lambda_3 \approx 0.001 - 0.01, \quad \frac{\lambda_4}{\lambda_3} = 0.001 - 0.01. \quad (21)$$

In Figure 5,  $V(x_i)$  is plotted as a function of  $x_i$  (the dimensionless lattice displacement in some suitable unit) for  $\lambda_3 = 0$  (the harmonic case),  $0 : 005$ , and  $0 : 01$  with  $\lambda_4/\lambda_3 = 0.01$ . It should be noted that, even though it is very small, a positive value of  $\lambda_4$  eventually leads to a situation where  $V(x_i)$  becomes negative for sufficiently large  $|x_i|$ . However, we shall not be interested in such large variations in  $x_i$  here; we shall rather look for local minima of the total energy around  $x_i = 0$ . As long as both  $\lambda_3$  and  $\lambda_4$  are small enough, such local minima are always expected to exist. This restriction to small variations in  $x_i$  is consistent with the choice of a linear coupling between the lattice displacement and the electron charge in the Hamiltonian. We follow the same variational approach to solve (18) as the one presented in order to solve (1). The energy per site is obtained as

$$\epsilon_0 = \frac{E_{\text{ph}}}{N} + e_{\text{eff}} + \frac{U_{\text{eff}} - |U_{\text{eff}}|}{4} - 4t_{\text{eff}} \int_0^\infty \frac{dz}{z} \frac{J_0(z)J_1(z)}{[1 + \exp(z|U_{\text{eff}}|/2t_{\text{eff}})]}, \quad (22)$$

where, as before,  $J_0$  and  $J_1$  are, respectively, the zeroth-order and the first-order Bessel functions,  $E_{\text{ph}}/N$  is the virtually excited phonon energy given by

$$\frac{E_{\text{ph}}}{N} = [h^2 + 2\lambda_3 h(4h + 3) - \lambda_4(16h^2 + 24h^2 + 3)]\omega_0, \quad (23)$$

$e_{\text{eff}}$  is the effective polaron energy given by

$$e_{\text{eff}} = -\frac{g^2}{\omega_0} - h^2\omega_0 + \left[ (1 - \eta)\frac{g}{\omega_0} - h \right]^2 \omega_0 + \lambda_3 \tilde{\eta}[\tilde{\eta}^2 + 6h\tilde{\eta} + 3(4h^2 + 1)]\omega_0 - \lambda_4 \tilde{\eta}[\tilde{\eta}^3 + 8h\tilde{\eta}^2 + 6(4h^2 + 1)\tilde{\eta} + 8\beta(4h^2 + 3)]\omega_0 \quad (24)$$

with

$$\tilde{\eta} \equiv 2\eta \frac{g}{\omega_0}, \quad (25)$$

$t_{\text{eff}}$  is the effective hopping integral given by

$$t_{\text{eff}} = t \exp\left(-\frac{\tilde{\eta}^2}{4}\right), \quad (26)$$

and the effective on-site Coulomb energy  $U_{\text{eff}}$  is given by

$$U_{\text{eff}} = U - 2\frac{g^2}{\omega_0} + 2(1 - \eta)^2 \frac{g^2}{\omega_0} + 6\lambda_3 \tilde{\eta}^2 (\tilde{\eta} + 2h)\omega_0 - 2\lambda_4 \tilde{\eta}^2 (7\tilde{\eta}^2 + 24h\tilde{\eta} + 24h^2 + 6)\omega_0. \quad (27)$$

$L_0$  is again given by a similar expression as (16). Equation (22) is now minimized with respect to  $\eta$  and  $h$ . The average lattice displacement is obtained as

$$\langle x_i \rangle = -\sqrt{2} \left( h + \eta \frac{g}{\omega_0} \right). \quad (28)$$

The variations of  $\langle x_i \rangle$ ,  $t_{\text{eff}}$ ,  $U_{\text{eff}}$ , and  $L_0$  as function of  $g$  are shown in Figure 6. Though in the absence of the cubic anharmonic term the sign of  $g$  is of little physical relevance; in its presence, however, the sign of  $g$  becomes quite important. Usually  $g$  is taken as a positive quantity and is expressed as  $g = \sqrt{\alpha}\omega_0$ , with  $\alpha$  as the dimensionless electron-phonon coupling constant. With this  $g$ , we would expect that  $\langle x_i \rangle$  will not be so much different from its value in the harmonic model, namely,  $-\sqrt{2}\alpha$ , as long as both  $\lambda_3$  and  $\lambda_4$  are small. This can be easily seen by substituting the harmonic value of  $h$  in (28). This implies that  $\langle x_i \rangle$  must be negative. According to Figure 5, the potential  $V(x_i)$  increases from the corresponding value in the harmonic model for negative  $x_i$  due to the cubic term, indicating that the cubic anharmonicity increases the total energy. In fact, for positive  $g$ , the cubic anharmonicity increases the values of both  $E_{\text{ph}}$  and  $e_{\text{eff}}$ , as can be seen from (23) and (24), respectively. Even more importantly, it shifts  $U_{\text{eff}}$  in (27) to the positive side, showing that this anharmonicity gives rise to a repulsive contribution to the effective electron-electron interaction. On the other hand, the quartic anharmonicity has a totally opposite effect on those physical quantities. Thus we may conclude that the effect of anharmonicity on the polaron motion depends on the order of the anharmonicity; the cubic one enhances the effect of  $U$ , while the quartic one suppresses it. These competing effects of anharmonicity can be well captured in the Holstein-Hubbard model in which the (harmonic) phonon-mediated attractive interaction and the direct Coulomb repulsion are treated on the same footing. For this reason, the Hubbard-Holstein model is quite relevant in clarifying the physics of the cubic and quartic anharmonicities. For negative  $g$  given by  $-\sqrt{\alpha}\omega_0$ ,  $\langle x_i \rangle$  will be a positive quantity, because, while  $\eta$  remains to be positive, the value of  $h$  turns out to be negative in this case. Since the lattice displacement  $x_i$  in the positive side makes  $V(x_i)$  decrease from the corresponding value in the harmonic model due to the combined effects of the cubic and the quartic terms, we may expect that both anharmonicities shift  $U_{\text{eff}}$  to the negative side, leading to another conclusion that the effect of the cubic anharmonicity depends critically on the sign of  $g$ . As shown in Figures 6(a)–6(d) for  $\langle x_i \rangle$ ,  $t_{\text{eff}}$ ,  $U_{\text{eff}}$ , and  $L_0$ , we can clearly see the asymmetry with respect to  $g$ . For positive  $g$ ,  $\langle x_i \rangle$  deviates from the value in the harmonic case  $-\sqrt{2}\alpha$  (the dotted-dashed straight line) to a smaller magnitude of the lattice displacement. This change is associated with the increase in  $U_{\text{eff}}$ ,  $t_{\text{eff}}$ , and  $L_0$ . It may be noted that the increase in  $t_{\text{eff}}$  has a direct consequence on the reduction of the optimized value for  $\eta$  from the corresponding value in the harmonic system. Thus we may conclude that anharmonicity reduces the effective mass of a polaron in this case. On the other hand,  $\langle x_i \rangle$  becomes much larger from the corresponding value in the harmonic case for negative  $g$ . In particular,  $\langle x_i \rangle$  shows a very steep upturn

if both  $|g|$  and  $\lambda_3$  are sufficiently large. This abrupt upturn is connected with the sudden change of the polaron feature into immobile particles due to the strong electron-electron attractive interaction. Judging from the fact that  $L_0$  tends to vanish at the same time, we may further conclude that this change is nothing but the formation of immobile bipolarons.

In order to study the effect of anharmonicity on the phase transition, we have plotted  $t_{\text{eff}}/t$ ,  $dt_{\text{eff}}/dU$ , and  $L_0$  as a function of  $U$  in Figures 7(a)–7(c), together with the energy per site,  $\epsilon_0$  in Figure 8, respectively. For positive  $g$ , all the features obtained in these figures are qualitatively the same as those in the harmonic system (the dotted-dashed curves). Two peaks in  $dt_{\text{eff}}/dU$  in Figure 7(b) along with  $L_0 = 3/8$  for the state between the peaks clearly indicate the existence of an intervening metallic phase, leading to the observation that exactly the same phase transition is expected even in the anharmonic system. The quantitative difference can be accounted for by adjusting the values of both  $U$  and  $t$ . Thus we may conclude that anharmonicity does not change the situation radically in this case. Only quantitative changes such as the reduction in the effective mass associated with the polaron motion occur. For negative  $g$ , however, we can see a similar behaviour only in the case of weak anharmonicity. For sufficiently strong  $\lambda_3$  (but still within the realistic range), the feature of the transition changes radically. The intervening metallic state is suppressed and a direct first-order SDW-to-CDW transition is predicted. The CDW is characterized by the formation of immobile bipolarons. This insulator-to-insulator transition is clearly seen by both the cusp in  $\epsilon_0$  in Figure 8 and the jump in  $L_0$  in Figure 7(c) from the vanishingly small value to the nearly full electron spin moment.

In the first-principles approach,  $g$  is connected with  $-\xi\hat{e} \cdot \nabla V(\mathbf{r})$  in the rigid-ion approximation, where  $V$  is the electron-ion interaction potential,  $\xi$  is the time-dependent lattice displacement, and  $\hat{e}$  is a polarization vector of the relevant lattice displacement. Since there is no definite rule for the direction of  $\hat{e}$  and  $V(\mathbf{r})$  may be considered as a pseudopotential, no definite argument can be made on the sign of  $g$ . Thus both positive and negative  $g$ 's will appear in actual situations. From the viewpoint of superconductivity, we need at least a metallic phase. Thus the strong anharmonic case with negative  $g$  should be avoided. However, anharmonicity with positive  $g$  seems to provide a more favorable condition to support superconductivity, partly because the metallic region is widened and partly because the polarons become more mobile.

## 6. An Improved Variational Treatment

More recently, Clay and Hardikar [65] have studied the same model by a numerical method based on the density-matrix renormalization group technique and confirmed the findings of TC. By calculating the Luttinger liquid correlation exponent  $K_q$ , they have further suggested that this phase is indeed superconductive. We believe that this issue is of paramount importance in the current scenario of superconductivity and needs a more rigorous analytical

investigation. In a recent investigation we have chosen a more improved variational wave function for the phonon subsystem in order to obtain a lower GS energy and then analyzed the behaviour of the intermediate metallic phase. The idea has been that if the width of the metallic phase gets reduced in the improved calculation, then there can be an element of doubt about the veracity of the existence of the metallic phase. On the other hand, if an improved variational calculation leads to a widening of the metallic phase, then the prediction about the existence of the metallic phase becomes certainly much more justified.

In Section 3 we have described the method adopted by TC for the approximate solution of the phonon subsystem. TC have completely neglected in their analysis the phonon correlation effect which may play a rather important role as is well known from polaron physics. In the language of field theory, an electron is the source of phonons, and when an electron emits a phonon, it recoils back due to the finite phonon momentum, and while recoiling the electron can emit another phonon, particularly in the case of reasonable electron-phonon coupling, and in that case those two successively emitted virtual phonons will be correlated. This correlation leads to the squeezing of the coherent phonon state and it has been shown by Zheng [66] that it also reduces the Holstein reduction factor considerably and consequently makes the polaron bandwidth larger leading to a higher mobility of the polarons which is more favorable for high  $T_c$  superconductivity. Therefore it is desirable that one should include the phonon correlations in the calculation. We have included the on-site (OS) and nearest-neighbor (NN) phonon correlations in one of our recent investigations. We have, however, neglected the anharmonic phonons in our calculation for the sake of simplicity. In fact, the inclusion of phonon correlations is expected to take care of the phonon anharmonicity at least partially. So we consider the same Hamiltonian (1) again. As before we perform first the transformation  $e^{R_1}$  and  $e^{R_2}$  where  $R_1$  and  $R_2$  are given by (2) and (7). As already mentioned earlier, we next perform, following Zheng [66], a squeezing transformation with a generator

$$R_3 = \alpha_s \sum_i (b_i b_i - b_i^\dagger b_i^\dagger), \quad (29)$$

where  $\alpha_s$  is the squeezing parameter to be obtained variationally. This transformation takes care of the phonon correlation at a particular site, and thus partially includes the electron recoil effect, and secondly, it takes into account through the choice of the phonon state some effects of the anharmonic phonons, that is, the phonon-phonon interactions which indirectly introduce the finite lifetime effects of the phonon and thus incorporates the phonon dynamics in a more realistic way. However, it neglects all intersite phonon correlations. Following Lo and Sollie [67], we, therefore, perform a correlated squeezing transformation with a generator

$$R_4 = \frac{1}{2} \sum_{i \neq j} \beta_{ij} (b_i b_j - b_i^\dagger b_j^\dagger), \quad (30)$$

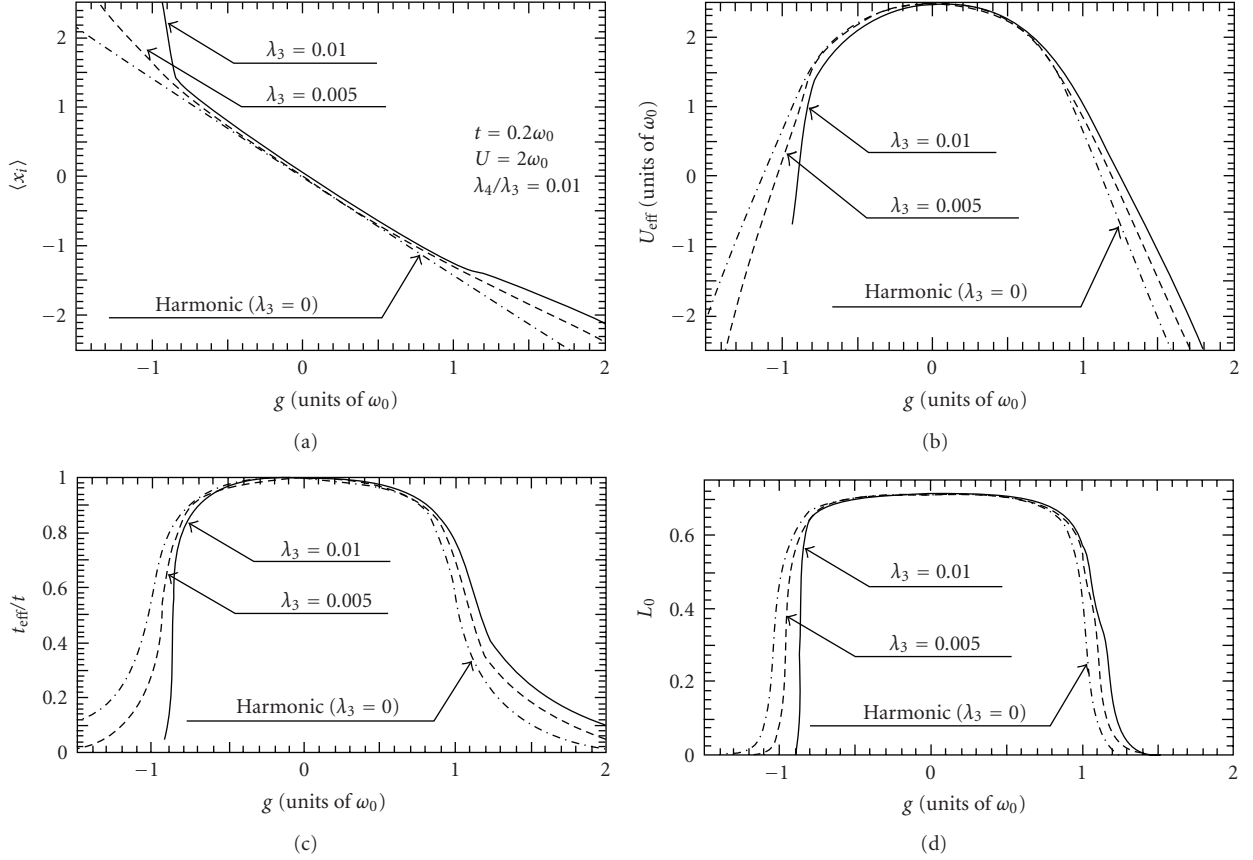


FIGURE 6: Plots of (a) the lattice displacement, (b) the effective electron-electron interaction, (c) the renormalized hopping integral, and (d) the local spin moment as a function of  $g$ .

where we choose, for simplicity,  $\beta_{ij} = \beta$ , when  $i$  and  $j$  are nearest neighbors and zero otherwise. Obviously the last two squeezing transformations (29) and (30) may spoil the coherence of phonons at the expense of including correlations and introduce some fluctuations. Therefore, in order to deal with these fluctuations, we perform another CST to bring back the complete phonon coherence with a generator

$$R_5 = \Delta \sum_i (b_i^\dagger - b_i), \quad (31)$$

where  $\Delta$  is another variational parameter. Averaging the transformed Hamiltonian with respect to the zero-phonon state  $|0\rangle = \prod_i |0_i\rangle$ , where the product over  $i$  runs over  $N$  sites, we then obtain an effective electronic Hamiltonian

$$\begin{aligned} H_{\text{eff}} = & -J \sum_{i\sigma} n_{i\sigma} - t_{\text{eff}} \sum_{\langle ij \rangle \sigma} c_{i\sigma}^\dagger c_{j\sigma} + U_{\text{eff}} \sum_i n_{i1} n_{i1} \\ & + \frac{N\omega_0 [e^{4\alpha} (e^{2\beta})_{00} + e^{-4\alpha} (e^{-2\beta})_{00} - 2]}{4} \\ & + N\omega_0 h^2 + N\omega_0 M \Delta e^{2\alpha_s} (2h + \Delta e^{2\alpha_s}), \end{aligned} \quad (32)$$

with

$$\begin{aligned} J &= \omega_0 [\alpha(2 - \eta) + 2\sqrt{\alpha}(1 - \eta)(h + M\Delta e^{2\alpha_s})], \\ U_{\text{eff}} &= [U - 2\alpha\omega_0\eta(2 - \eta)], \\ t_{\text{eff}} &= t \cdot \exp[\alpha\eta^2 e^{-4\alpha_s} ((e^{-2\beta})_{00} - (e^{-2\beta})_{01})], \\ M &= (e^\beta)_{00} + 2[(e^\beta)_{01} + (e^\beta)_{02} + (e^\beta)_{03} + \dots], \\ (e^{\pm 2\beta})_{0n} &= \sum_{m=0, 1, 2, \dots} (\pm 1)^n \frac{(2\beta)^{2m+n}}{m!(m+n)!}. \end{aligned} \quad (33)$$

The GS energy per site is, thus, obtained for all values of  $U$  (both positive and negative) as

$$\begin{aligned} \epsilon_0 = & -J + N\omega_0 \left[ h^2 + \frac{((e^{2\beta})_{00} \cosh 4\alpha - 1)}{2} \right] \\ & + \left[ \frac{(U_{\text{eff}} - |U_{\text{eff}}|)}{4} \right] + N\Delta\omega_0 M e^{2\alpha_s} (2h + \Delta e^{2\alpha_s}) \\ & - 4t_{\text{eff}} \int_0^\infty dy \frac{J_0(y)J_1(y)}{y[1 + \exp(y|U_{\text{eff}}|/2t_{\text{eff}})]}. \end{aligned} \quad (34)$$

The GS energy is now minimized with respect to five variational parameters. It is found that the energy results

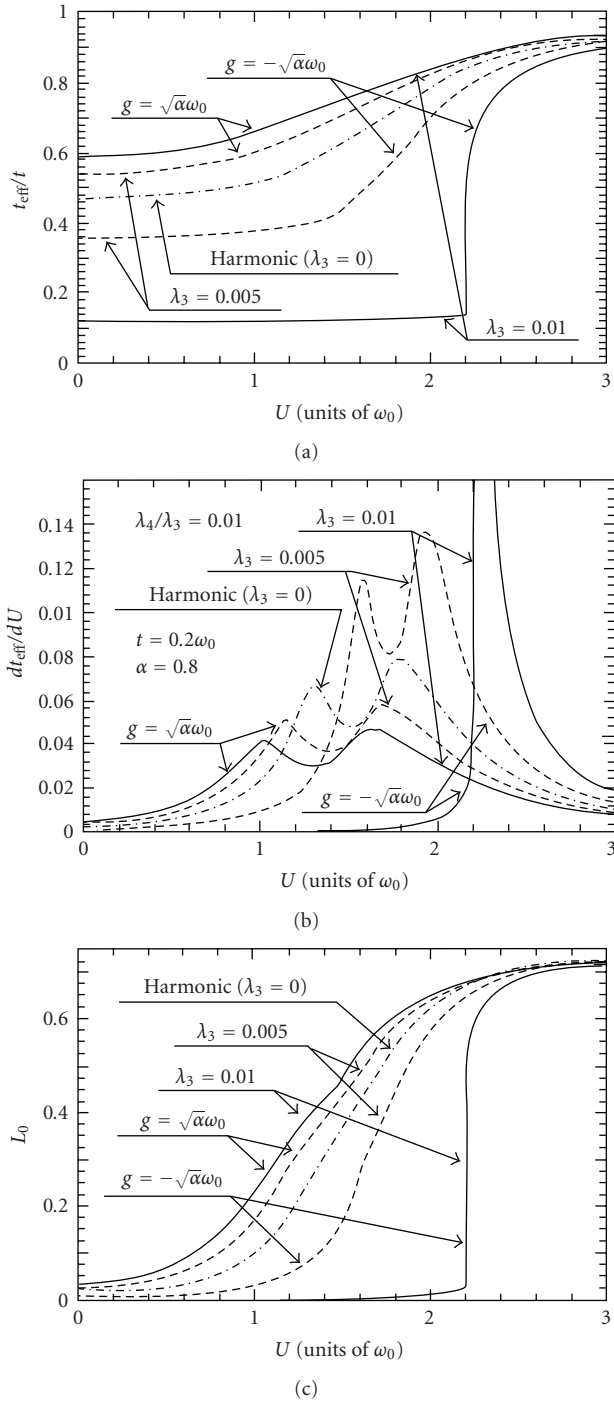


FIGURE 7: Plots of (a) the renormalized hopping integral, (b) the derivative of the renormalized hopping integral with respect to  $U$ , and (c) the local spin moment as a function of  $U$ .

are only marginally better. However, we find that even this marginal improvement in the energy can have substantial effect on the polaron mobility and the phase diagram.

One can see from Figure 9 that  $t_{\text{eff}}$  and its derivative show qualitatively the same behaviour as obtained by TC, but the present solutions show pronounced quantitative difference,

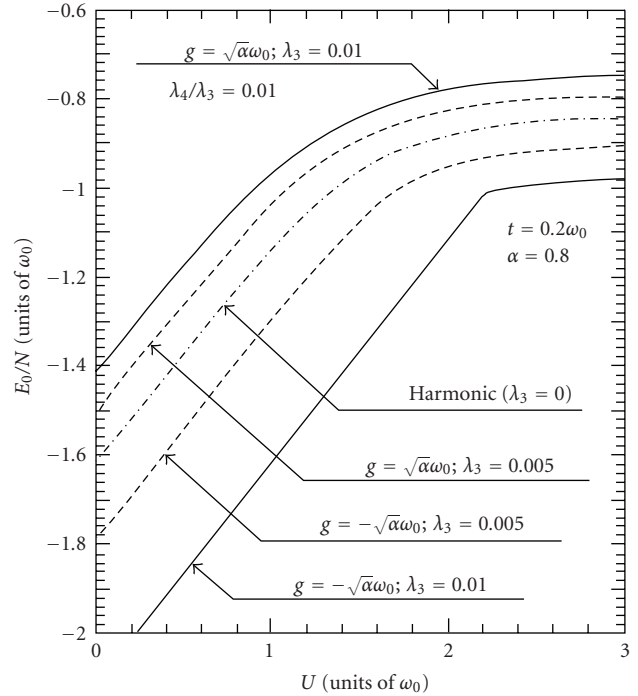


FIGURE 8: Ground-state energy per site as a function of  $U$ .

as clearly evident from the peak structures in the  $dt_{\text{eff}}/dU$  curves (Figure 9(b)). The important point to note here is that the present method leads to an enhancement in the polaron mobility as compared with the TC results save for a small region of  $U$  where the two methods almost agree. Again, the region in between the transition points satisfies the criterion  $t_{\text{eff}}/U_{\text{eff}} \gg 0.25$ , typical of a metallic state. Now the peaks are a little wider apart as compared to the TC results. Figure 10 shows the phase diagram in the parameter space ( $\alpha, U$ ) and comparison with the TC results again clearly shows that the present method predicts a wider metallic phase at the crossover region. Including the phonon anharmonicity at the Hamiltonian level will make the intermediate metallic phase even more wider, as shown in [45] and already discussed in Section 5, and the polarons more mobile, which is certainly a more favorable situation for high- $T_c$  superconductivity.

## 7. Conclusion

We have first considered the Holstein-Hubbard model at half-filling in one dimension and used a variable Lang-Firsov transformation and coherent state transformation with a generator which is independent of the electron variables. The transformed Hamiltonian is then averaged with respect to the unperturbed zero-phonon state to obtain an effective electronic Hamiltonian which could be solved exactly using the Bethe ansatz method of Lieb and Wu. Calculation of the polaron bandwidth and the local spin density have shown that there can exist an intermediate metallic state at the crossover region of SDW and CDW phases. It is not known for sure whether this kind of a metallic phase has already been observed in actual materials or not, but Takada has

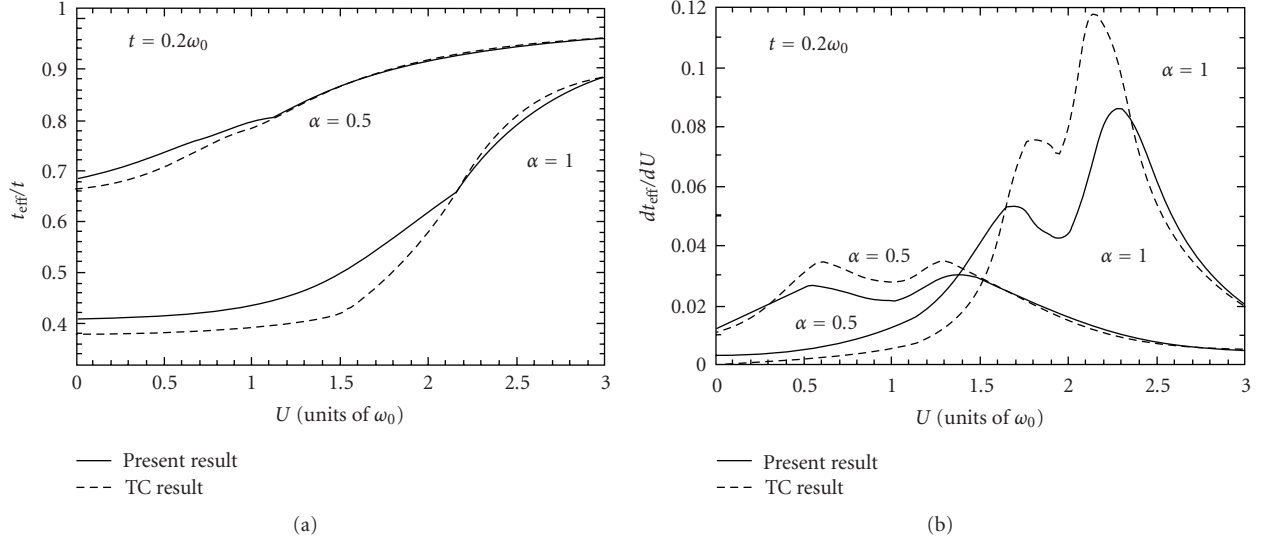


FIGURE 9:  $t_{\text{eff}}$  and its derivative as a function of  $U$  for two values of  $\alpha$  and for  $t = 0.2\omega_0$ . The TC results are shown for comparison.

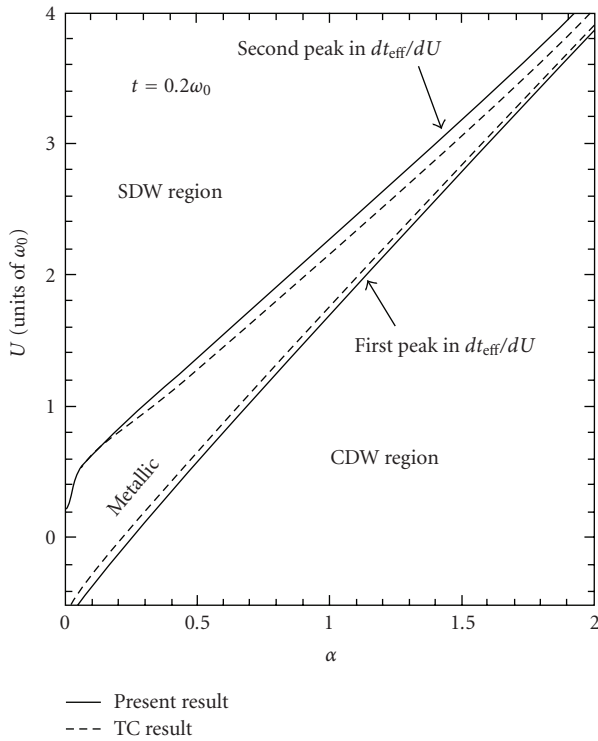


FIGURE 10: Phase diagram in  $(\alpha, U)$  determined by the peaks in  $dt_{\text{eff}}/dU$ . The corresponding phase diagram obtained by TC in [44] is shown in dashed lines for comparison.

already speculated that the physical properties including superconductivity in the alkali-doped fullerenes ( $A_3C_{60}$ ) [68, 69] can be explained in a unified way in terms of a picture that envisages the existence of such a kind of a metallic state in ( $A_3C_{60}$ ) [70, 71]. This metallic state is of importance from the point of view of superconductivity. We have next shown that the inclusion of phonon anharmonicity can make

polarens more mobile and widen the metallic regime and can, thus, provide a more favorable condition to support superconductivity. Our prediction has been supported by a recent exact DMRG analysis. We have finally attempted to make a further improvement on our variational calculation by including the effect of phonon correlations through on-site and correlated squeezing transformations. Interestingly, this widens the metallic phase even further and makes the polarens more mobile which is more conducive for superconductivity. That a better variational calculation does widen the metallic phase is itself a positive test for its existence. We do not believe that such a behaviour is unique in 1D and we expect a similar behaviour in higher dimensions too. We do not believe that the case in point is a usual phase transition of the thermodynamic kind; rather it could be a quantum phase transition or a crossover phenomenon. It is of course possible to explore the superconducting nature of this phase within the present scenario. In fact, it goes without saying that being a metallic phase, this phase will certainly be superconductive as one will cool the temperature. However to find the transition temperature itself, one does need to do a rigorous calculation. It is, however, worthwhile to make a few qualitative remarks about the nature of the superconducting phase. The normal phase here is a polaronic or a bipolaronic metal. Therefore as the temperature would decrease, the system can undergo a polaronic superconductivity induced by dynamical pairing of polarens like what happens in the case of Cooper pairs in the BCS mechanism. On the other hand, it is also possible that bipolarons which are essentially “static” Cooper pairs can undergo Bose-Einstein condensation and give rise to a superconductive phase. Which route will actually lead to the superconductive phase in an actual system will depend on the characteristic temperatures of the corresponding mechanisms which will certainly depend on the material parameters, and therefore requires a rigorous calculation. Another remark that we would like to make is about

the assumption of half-filling in the present analysis. This assumption has been used in order to obtain analytical results. Even for the case of “away from half-filling” exact result can be obtained for the effective Hubbard model, albeit numerically. For less than half-filling, the system will have more mobility in the charge carriers, and therefore it is expected that the metallic phase will be more favorable in this case than that for half-filling. For more than half-filling, the situation is not very clear and one needs to make a separate investigation.

## References

- [1] J. G. Bednorz and K. A. Müller, “Possible high  $T_c$  superconductivity in the Ba–La–Cu–O system,” *Zeitschrift für Physik B*, vol. 64, no. 2, pp. 189–193, 1986.
- [2] J. W. Halley, Ed., *Theories of High Temperature Superconductivity*, Addison Wesley, Harlow, UK, 1988.
- [3] T. Jarlborg, “Band structure and electron-phonon coupling in the  $La_{1-x}Sr_xCuO_4$  superconductors,” *Helvetica Physica Acta*, vol. 61, p. 421, 1988.
- [4] R. E. Cohen, W. E. Pickett, H. Krakauer, and D. A. Papaconstantopoulos, “High  $T_c$  superconductors as ionic metals and the role of phonons in high  $T_c$  superconductivity,” *Phase Transitions*, vol. 22, no. 1–4, pp. 167–183, 1990.
- [5] R. E. Cohen, W. E. Pickett, and H. Krakauer, “Theoretical determination of strong electron-phonon coupling in  $YBa_2Cu_3O_7$ ,” *Physical Review Letters*, vol. 64, no. 21, pp. 2575–2578, 1990.
- [6] C. O. Rodriguez, A. I. Liechtenstein, I. I. Mazin, O. Jepsen, O. K. Andersen, and M. Methfessel, “Optical near-zone-center phonons and their interaction with electrons in  $YBa_2Cu_3O_7$ : results of the local-density approximation,” *Physical Review B*, vol. 42, no. 4, pp. 2692–2695, 1990.
- [7] R. Zeyher, “Importance of long-range electron-phonon coupling in high- $T_c$  superconductors,” *Zeitschrift für Physik B*, vol. 80, no. 2, pp. 187–192, 1990.
- [8] B. K. Chakraverty, D. Feinberg, Z. Hang, and M. Avignon, “Squeezed bipolaronic states and high temperature superconductivity in  $BaLaCuO$  systems,” *Solid State Communications*, vol. 64, no. 8, pp. 1147–1151, 1987.
- [9] D. Emin, “Formation, motion, and high-temperature superconductivity of large bipolarons,” *Physical Review Letters*, vol. 62, no. 13, pp. 1544–1547, 1989.
- [10] D. Emin and M. S. Hillery, “Formation of a large singlet bipolaron: application to high-temperature bipolaronic superconductivity,” *Physical Review B*, vol. 39, no. 10, pp. 6575–6593, 1989.
- [11] J. Ranninger, in *Proceedings of the Conference on Lattice Effects in High  $T_c$  Superconductors*, Y. Bar-Yam, T. Egami, J. Mustre de Leon, and A. R. Bishop, Eds., p. 389, 1992.
- [12] S. Sil and A. Chatterjee, “Multi-dimensional Fröhlich bipolaron and dimensional scaling,” *International Journal of Modern Physics B*, vol. 4, no. 11–12, pp. 1879–1888, 1990.
- [13] S. Sil and A. Chatterjee, “Stability of large optical singlet bipolarons, many-particle effects and high temperature superconductivity,” *Modern Physics Letters B*, vol. 6, no. 15, pp. 959–966, 1992.
- [14] J. R. Hardy and J. W. Hocken, “Possible origins of high- $T_c$  superconductivity,” *Physical Review Letters*, vol. 60, no. 21, pp. 2191–2193, 1988.
- [15] A. S. Alexandrov and N. F. Mott, “Bipolarons,” *Reports on Progress in Physics*, vol. 57, no. 12, pp. 1197–1288, 1994.
- [16] R. Micnas, J. Ranninger, and S. Robaszkiewicz, “Superconductivity in narrow-band systems with local nonretarded attractive interactions,” *Reviews of Modern Physics*, vol. 62, no. 1, pp. 113–171, 1990.
- [17] A. J. Mills, P. B. Littlewood, and B. I. Shraiman, “Double exchange alone does not explain the resistivity of  $La_{1-x}Sr_xMnO_3$ ,” *Physical Review Letters*, vol. 74, no. 25, pp. 5144–5147, 1995.
- [18] K. H. Kim, J. Y. Gu, H. S. Choi, G. W. Park, and T. W. Noh, “Frequency shifts of the internal phonon modes in  $La_{0.7}Ca_{0.3}MnO_3$ ,” *Physical Review Letters*, vol. 77, no. 9, pp. 1877–1880, 1996.
- [19] R. P. Sharma, L. E. Rehn, P. M. Baldo, and J. Z. Liu, “Direct evidence of anomalous Cu-O vibrational modes near  $T_c$  in  $ErBa_2Cu_3O_{7-\delta}$ ,” *Physical Review Letters*, vol. 62, no. 24, pp. 2869–2872, 1989.
- [20] R. P. Sharma, L. E. Rehn, P. M. Baldo, and J. Z. Liu, “Shift of phonon anomaly with  $T_c$  observed in  $(Y,Er)Ba_2Cu_3O_{7-\delta}$  by ion channeling,” *Physical Review B*, vol. 40, no. 16, pp. 11396–11399, 1989.
- [21] M. Arai, K. Yamada, Y. Hidaka, et al., “Anomaly of phonon state of superconducting  $YBa_2Cu_3O_7$  studied by inelastic neutron scattering,” *Physical Review Letters*, vol. 69, no. 2, pp. 359–362, 1992.
- [22] C. M. Foster, A. J. Heeger, Y. H. Kim, G. Stucky, and N. Herron, “Photogenerated carriers in  $La_2CuO_4$ ,  $YBa_2Cu_3O_{7-\delta}$  and  $Tl_2Ba_2Ca_{(1-x)}Gd_xCu_2O_8$ : polarizability-induced pairing of polarons,” *Synthetic Metals*, vol. 33, no. 2, pp. 171–183, 1989.
- [23] D. Mihailović, C. M. Foster, K. Voss, and A. J. Heeger, “Application of the polaron-transport theory to  $\sigma(\omega)$  in  $Tl_2Ba_2Ca_{1-x}Gd_xCu_2O_8$ ,  $YBa_2Cu_3O_{7-\delta}$ , and  $La_{2-x}Sr_xCuO_4$ ,” *Physical Review B*, vol. 42, no. 13, pp. 7989–7993, 1990.
- [24] S. D. Conradson, I. D. Raistrick, and A. R. Bishop, “Axial oxygen-centered lattice instabilities and high-temperature superconductivity,” *Science*, vol. 248, no. 4961, pp. 1394–1398, 1990.
- [25] J. Mustre de Leon, S. D. Conradson, I. Batistic, and A. R. Bishop, “Evidence for an axial oxygen-centered lattice fluctuation associated with the superconducting transition in  $YBa_2Cu_3O_7$ ,” *Physical Review Letters*, vol. 65, no. 13, pp. 1675–1678, 1990.
- [26] H. A. Mook, M. Mostoller, J. A. Harvey, N. W. Hill, B. C. Chakoumakos, and B. C. Sales, “Observation of phonon softening at the superconducting transition in  $Bi_2Sr_2CaCu_2O_8$ ,” *Physical Review Letters*, vol. 65, no. 21, pp. 2712–2715, 1990.
- [27] H. A. Mook, B. C. Chakoumakos, M. Mostoller, A. T. Boothroyd, and D. M. Paul, “Phonons and superconductivity in  $Bi_2Sr_2CaCu_2O_8$ ,” *Physical Review Letters*, vol. 69, no. 15, pp. 2272–2275, 1992.
- [28] T. Holstein, “Studies of polaron motion—part I: the molecular-crystal model,” *Annals of Physics*, vol. 8, no. 3, pp. 325–342, 1959.
- [29] T. K. Mitra, A. Chatterjee, and S. Mukhopadhyay, “Polarons,” *Physics Reports*, vol. 153, no. 2–3, pp. 91–207, 1987.
- [30] J. Bardeen, L. N. Cooper, and J. R. Schrieffer, “Theory of superconductivity,” *Physical Review*, vol. 108, no. 5, pp. 1175–1204, 1957.
- [31] A. Alexandrov and J. Ranninger, “Theory of bipolarons and bipolaronic bands,” *Physical Review B*, vol. 23, no. 4, pp. 1796–1801, 1981.

- [32] A. N. Das and S. Sil, "Electron-phonon interaction in a strongly correlated Hubbard system," *Physica C*, vol. 161, no. 3, pp. 325–330, 1989.
- [33] E. Berger, P. Valašek, and W. von der Linden, "Two-dimensional Hubbard-Holstein model," *Physical Review B*, vol. 52, no. 7, pp. 4806–4814, 1995.
- [34] S. Sil and B. Bhattacharyya, "Effect of electron-phonon interaction on a one-dimensional correlated electron system," *Physical Review B*, vol. 54, no. 20, pp. 14349–14354, 1996.
- [35] C.-H. Pao and H.-B. Schüttler, "Superconducting instability in the Holstein-Hubbard model: a numerical renormalization-group study," *Physical Review B*, vol. 57, no. 9, pp. 5051–5054, 1998.
- [36] A. Weiße, H. Fehske, G. Wellein, and A. R. Bishop, "Optimized phonon approach for the diagonalization of electron-phonon problems," *Physical Review B*, vol. 62, no. 2, pp. R747–R750, 2000.
- [37] V. Cataudella, G. De Filippis, and G. Iadonisi, "Polaron features of the one-dimensional Holstein molecular crystal model," *Physical Review B*, vol. 62, no. 3, pp. 1496–1499, 2000.
- [38] W. Koller, A. C. Hewson, and D. M. Edwards, "Polaronic quasiparticles in a strongly correlated electron band," *Physical Review Letters*, vol. 95, no. 25, Article ID 256401, 4 pages, 2005.
- [39] G. Sangiovanni, M. Capone, C. Castellani, and M. Grilli, "Electron-phonon interaction close to a mott transition," *Physical Review Letters*, vol. 94, no. 2, Article ID 026401, 4 pages, 2005.
- [40] P. Barone, R. Raimondi, M. Capone, and C. Castellani, "Effective electron-phonon coupling and polaronic transition in the presence of strong correlation," *Physical Review B*, vol. 73, no. 8, Article ID 085120, 5 pages, 2006.
- [41] Y. Takada, "Superconductivity in the half-filled Hubbard-Holstein model in the antiadiabatic region," *Journal of the Physical Society of Japan*, vol. 65, no. 6, pp. 1544–1547, 1996.
- [42] E. Jeckelmann, C. Zhang, and S. R. White, "Metal-insulator transition in the one-dimensional Holstein model at half filling," *Physical Review B*, vol. 60, no. 11, pp. 7950–7955, 1999.
- [43] Q. Wang, H. Zheng, and M. Avignon, "Phase diagram and optical conductivity of the one-dimensional spinless Holstein model," *Physical Review B*, vol. 63, no. 1, Article ID 014305, 5 pages, 2001.
- [44] Y. Takada and A. Chatterjee, "Possibility of a metallic phase in the charge-density-wave–spin-density-wave crossover region in the one-dimensional Hubbard-Holstein model at half filling," *Physical Review B*, vol. 67, no. 8, Article ID 081102, 4 pages, 2003.
- [45] A. Chatterjee and Y. Takada, "The Hubbard-Holstein model with anharmonic phonons in one dimension," *Journal of the Physical Society of Japan*, vol. 73, no. 4, pp. 964–969, 2004.
- [46] P. M. Krishna and A. Chatterjee, "Existence of a metallic phase in a 1D Holstein-Hubbard model at half filling," *Physica C*, vol. 457, no. 1-2, pp. 55–59, 2007.
- [47] E. H. Lieb and F. Y. Wu, "Absence of mott transition in an exact solution of the short-range, one-band model in one dimension," *Physical Review Letters*, vol. 20, no. 25, pp. 1445–1448, 1968.
- [48] I. G. Lang and Yu. A. Firsov, *Zh. Éksp. Teor. Fiz.*, vol. 43, p. 1843, 1962, *Soviet Physics—JETP*, vol. 16, p. 1301, 1963.
- [49] A. N. Das and S. Sil, "A study of the polaronic band width and the small-to-large-polaron transition in a many-polaron system," *Journal of Physics: Condensed Matter*, vol. 5, no. 44, pp. 8265–8276, 1993.
- [50] M. Zoli and A. N. Das, "Polaron crossover in molecular solids," *Journal of Physics: Condensed Matter*, vol. 16, no. 21, pp. 3597–3607, 2004.
- [51] M. Frick, I. Morgenstern, and W. von der Linden, "High-temperature superconductivity in the apex-oxygen model: a quantum Monte Carlo study," *Zeitschrift für Physik B*, vol. 82, no. 3, pp. 339–345, 1991.
- [52] M. Frick, I. Morgenstern, and W. von der Linden, "Anharmonic phonons and strong electronic correlations in high- $T_c$  superconductors: a Quantum Monte Carlo study," *Physica C*, vol. 185–189, part 3, pp. 1523–1524, 1991.
- [53] A. Bussmann-Holder and A. R. Bishop, "Anharmonicity-induced multiphonon processes in high-temperature superconductors," *Physical Review B*, vol. 44, no. 6, pp. 2853–2856, 1991.
- [54] N. M. Plakida, V. L. Aksenov, and S. L. Drechsler, "Anharmonic model for high- $T_c$  superconductors," *Europhysics Letters*, vol. 4, no. 11, pp. 1309–1314, 1987.
- [55] N. M. Plakida, "Lattice instability and strong electron-phonon coupling for high- $T_c$  superconductivity," *Physica C*, vol. 162–164, part 2, pp. 1341–1342, 1989.
- [56] N. M. Plakida and S. E. Krasavin, "A microscopical model of anharmonic lattice dynamics of  $\text{La}_2\text{CuO}_4$ ," *Physica C*, vol. 185–189, part 3, pp. 1531–1532, 1991.
- [57] H. de Raedt, T. Schneider, and M. P. Sørensen, "Superconductivity in Hubbard models coupled to non-fermionic degrees of freedom," *Zeitschrift für Physik B*, vol. 79, no. 3, pp. 327–332, 1990.
- [58] J. Konior, "Anharmonic polaronic model and high- $T_c$  superconductivity," *Physical Review B*, vol. 47, no. 21, pp. 14425–14433, 1993.
- [59] J. K. Freericks and G. D. Mahan, "Strong-coupling expansions for the anharmonic Holstein model and for the Holstein-Hubbard model," *Physical Review B*, vol. 54, no. 13, pp. 9372–9384, 1996.
- [60] G. D. Mukherjee, C. Bansal, and A. Chatterjee, "Thermal expansion study of ordered and disordered  $\text{Fe}_3\text{Al}$ : an effective approach for the determination of vibrational entropy," *Physical Review Letters*, vol. 76, no. 11, pp. 1876–1879, 1996.
- [61] G. D. Mukherjee, C. Bansal, and A. Chatterjee, "Thermal expansion analysis of  $\text{Fe}_{3-x}\text{Mn}_x\text{Al}$  alloys," *Physical Review B*, vol. 58, no. 10, pp. 6172–6179, 1998.
- [62] G. D. Mukherjee, A. Chatterjee, and C. Bansal, "Anomalous thermal expansion behavior of the  $\text{YBaCuO}$  superconductor. Indirect evidence of polaron formation," *Physica C*, vol. 232, no. 3-4, pp. 241–245, 1994.
- [63] G. D. Mukherjee, C. Bansal, and A. Chatterjee, "Thermal expansion study of  $\text{Bi-2223}$  superconductor: an evidence of polaronic mechanism of high  $T_c$  superconductivity with strong two-dimensional fluctuations," *Physica C*, vol. 333, no. 3, pp. 229–234, 2000.
- [64] C. Kittel, *Introduction to Solid State Physics*, John Wiley & Sons, New York, NY, USA, 1996.
- [65] R. T. Clay and R. P. Hardikar, "Intermediate phase of the one dimensional half-filled Hubbard-Holstein model," *Physical Review Letters*, vol. 95, no. 9, Article ID 096401, 4 pages, 2005.
- [66] H. Zheng, "Squeezed polarons in one dimension," *Physics Letters A*, vol. 131, no. 2, pp. 115–118, 1988.
- [67] C. F. Lo and R. Sollie, "Correlated squeezed polaron states in one dimension," *Physical Review B*, vol. 48, no. 14, pp. 10183–10187, 1993.
- [68] A. F. Hebard, M. J. Rosseinsky, R. C. Haddon, et al., "Superconductivity at 18 K in potassium-doped  $\text{C}_{60}$ ," *Nature*, vol. 350, no. 6319, pp. 600–601, 1991.

- [69] O. Gunnarsson, "Superconductivity in fullerides," *Reviews of Modern Physics*, vol. 69, no. 2, pp. 575–606, 1997.
- [70] Y. Takada, "Explanation of the anomalous isotope effect in superconducting alkali-metal-doped fullerenes," *Journal of the Physical Society of Japan*, vol. 65, no. 10, pp. 3134–3137, 1996.
- [71] Y. Takada and T. Hotta, "Superconductivity in the alkali-doped fullerides: competition of phonon-mediated attractions with coulomb repulsions in polaron pairing," *International Journal of Modern Physics B*, vol. 12, no. 29–31, pp. 3042–3051, 1998.

## Review Article

# Real-Time Observation of Cuprates Structural Dynamics by Ultrafast Electron Crystallography

F. Carbone,<sup>1,2</sup> N. Gedik,<sup>1,3</sup> J. Lorenzana,<sup>4</sup> and A. H. Zewail<sup>1</sup>

<sup>1</sup>Physical Biology Center for Ultrafast Science and Technology, Arthur Amos Noyes Laboratory of Chemical Physics, California Institute of Technology, Pasadena, CA 91125, USA

<sup>2</sup>Laboratory of Ultrafast Spectroscopy, Ecole Polytechnique Fédérale de Lausanne (EPFL), 1015 Lausanne, Switzerland

<sup>3</sup>MIT Department of Physics, 77 Mass. Avenue, Bldg. 13-2114 Cambridge, MA 02139, USA

<sup>4</sup>SMC-ISC-CNR, Department of Physics, Università di Roma La Sapienza, Piazzale Aldo Moro 2, 00185 Roma, Italy

Correspondence should be addressed to F. Carbone, fabrizio.carbone@epfl.ch and A. H. Zewail, zewail@caltech.edu

Received 20 October 2009; Accepted 19 January 2010

Academic Editor: Dragan Mihailovic

Copyright © 2010 F. Carbone et al. This is an open access article distributed under the Creative Commons Attribution License, which permits unrestricted use, distribution, and reproduction in any medium, provided the original work is properly cited.

The phonon-mediated attractive interaction between carriers leads to the Cooper pair formation in conventional superconductors. Despite decades of research, the glue holding Cooper pairs in high-temperature superconducting cuprates is still controversial, and the same is true for the relative involvement of structural and electronic degrees of freedom. Ultrafast electron crystallography (UEC) offers, through observation of spatiotemporally resolved diffraction, the means for determining structural dynamics and the possible role of electron-lattice interaction. A polarized femtosecond (fs) laser pulse excites the charge carriers, which relax through electron-electron and electron-phonon couplings, and the consequential structural distortion is followed by diffracting fs electron pulses. In this paper, the recent findings obtained on cuprates are summarized. In particular, we discuss the strength and symmetry of the directional electron-phonon coupling in  $\text{Bi}_2\text{Sr}_2\text{CaCu}_2\text{O}_{8+\delta}$  (BSCCO), as well as the  $c$ -axis structural instability induced by near-infrared pulses in  $\text{La}_2\text{CuO}_4$  (LCO). The theoretical implications of these results are discussed with focus on the possibility of charge stripes being significant in accounting for the polarization anisotropy of BSCCO, and cohesion energy (Madelung) calculations being descriptive of the  $c$ -axis instability in LCO.

## 1. Introduction

Despite two decades of intense research, the mechanism of high temperature superconductivity in cuprates is still unclear [1]. Besides their high temperature superconductivity, cuprates display a rich, yet poorly understood phase diagram covering electronic and structural phase transitions as a function of temperature, chemical doping, and magnetic field strength [2]. The unique behavior seen in these materials is a result of the delicate interplay between charge, spin, and lattice excitations. As a result of these couplings between different degrees of freedom, there usually exist several competing states, which give rise to multiple phases [3]. Understanding the dynamics between different electronic and structural phases of these materials is significant for an eventual understanding of superconductivity.

Several experimental techniques have been applied to the study of these materials. Information on structural dynam-

ics has been obtained through Raman spectroscopy [4], X-ray absorption spectroscopy (XAS) [5], Angle resolved photoemission spectroscopy (ARPES) [6–8], and oxygen isotope substitution studies [9–12]. In parallel, the effect of strong electron-electron interactions has been revealed by optical spectroscopy [13, 14], inelastic neutron scattering [15], ARPES [16], transport [17], and scanning tunneling microscopy [18]. Theoretically, a plethora of exotic many-body entities can emerge, either from electron-electron correlations [19], or electron-lattice interactions [20, 21], but to date, a consensus has not been reached yet on the exact nature of the ground state of cuprates superconductors.

The time scale for electron-electron interactions is usually much faster than that of lattice dynamics. As a result, the crystal structure can be considered at equilibrium while electronic scattering phenomena are taking place. However, this scenario can be perturbed when strong electron-phonon coupling (larger than what is found in  $\text{MgB}_2$ , which has a  $T_c$

close to 40 K [22]), and strong electron-electron correlations are involved. When the electron-phonon coupling time reaches the tens of fs scale, it becomes comparable to the time scale for interelectronic scatterings and magnetic interactions [23]. In this situation, the conventional approximations need to be revised [24]. Such issue of time scales can be addressed by UEC by resolving the atomic motions in real time.

Optical time-resolved techniques have been extensively used to study cuprates [25–30]. The most commonly involved to date is the pump-probe spectroscopy method. This technique is sensitive to the dynamics of electrons, and it is based on measuring the photoinduced changes in the reflectivity or transmission of an optical probe pulse in response to an absorption by a strong pump pulse. In the superconducting state, fs pulses were used to break Cooper pairs and repairing dynamics of the resulting quasiparticles were studied across the phase diagram. By changing the wavelength of the probe pulse from terahertz [31] to mid-infrared [27], and to optical frequencies [25, 28], dynamics of the superconducting condensate or quasiparticle subsystem could be studied as a function of time. These experiments yielded both the elastic and inelastic quasiparticle scattering rate [32], the quasiparticle diffusion rate [33] as a function of temperature, and the excitation density (and doping) in cuprates [28].

All of the previous time-resolved studies in cuprates were based on the probing of dynamics, as reflected in electrons response in spectroscopic probing, but with no direct information about the structural dynamics of the underlying lattice. In the superconducting state, for example, the quasiparticles give their energy to a boson when they recombine to make Cooper pairs, and optical experiments cannot directly follow the evolution of the system after this point, since the resulting excitation does not cause a significant reflectivity change. Whether the electrons are directly coupled to phonons or to other collective excitations is still an open question. The energy is ultimately transferred to the lattice as heat, but to date no direct time-resolved measurement of this process was made, nor do we know the actual structural deformations especially in relation to symmetry and direction of electron-phonon interactions.

In this paper, we describe the recent results obtained by UEC. The temporal evolution of the crystal structure of BSCCO samples, following polarized carrier excitation by a fs pulse, for different temperatures (for the metallic and superconducting states) and doping levels (from underdoped to optimally doped), has been reported [23]. Specifically, different compositions were investigated, by varying the doping level and number of Cu–O planes per unit cell in the BSCCO family, and by probing optimally doped LCO (La, Cu, O) nanoislands. In these experiments, the initial fs excitation drives the system from the superconducting into the metallic phase [29], breaking Cooper pairs [28]. With the electron and lattice temperatures being vastly different (see below), energy of carriers is lowered through electron-phonon coupling, and structural distortions are observable in diffraction [23, 34].

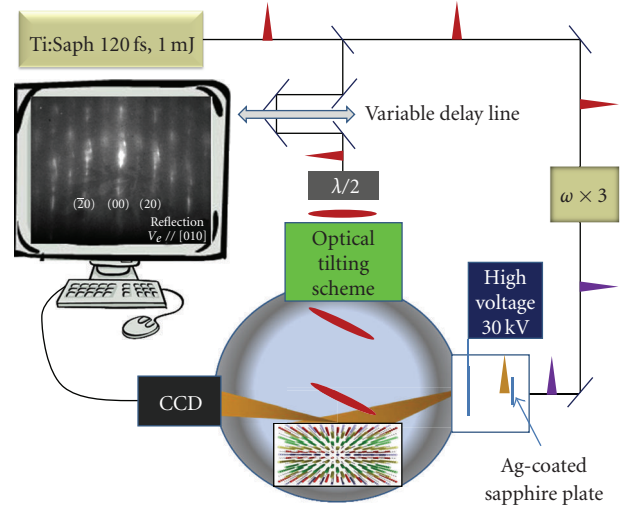


FIGURE 1: Experimental set-up. A train of pulses from an amplified Ti:Saph laser is used in order to excite a specimen with polarized light, and to generate electrons from a photocathode. The delay between pump photons and probe electrons is controlled by a motorized delay line. The scattered electrons are recorded by a CCD camera (see details in the text).

By varying the polarization of carrier excitation in BSCCO, major differences in the decay of Bragg diffraction were observed, for the  $c$ -axis structural dynamics. The striking polarization effect for this  $c$ -axis motion is consistent with a highly anisotropic electron-phonon coupling to the  $B_{1g}$  out-of-plane buckling mode (50 meV), with the maximum amplitude of atomic motions being  $\sim 0.15 \text{ \AA}$ . Out-of-plane motions give also rise to an out-of-equilibrium, structural phase transition in LCO nanoislands. For the latter, the  $c$ -axis lattice parameter value was, in fact, found to jump between two structures isobestically, in response to the optical excitation of the charge carriers [34].

In the following, we will describe these experimental findings in details and discuss the theoretical implications of the results. In particular, we will discuss the role of polarized light excitation in cuprates and the possibility that charge stripes may be behind the observed anisotropy in BSCCO. We will also show that simple cohesion energy calculations can account for the observed  $c$ -axis instability in LCO, based on the assumption that infrared pulses photo-dope the Cu–O planes through a charge transfer process.

## 2. Experimental

**2.1. The UEC Apparatus.** The experimental setup, displayed in Figure 1, consists of a fs laser system and three connected ultrahigh-vacuum chambers (for diffraction, load lock, and sample preparation/characterization). The laser system generates amplified pulses that are centered at 800 nm (1.55 eV), with a pulse width of 120 femtosecond and energy of 1.8 mJ per pulse at a repetition rate of 1 kHz. A beam splitter was placed to separate the beam into two arms: a pump beam used to excite the sample and a second beam for generating the probing electron packets. The second

beam was obtained by tripling (266 nm, 4.65 eV), via third harmonic generation in a nonlinear optical device, the fundamental frequency. The UV pulses impinged on a back-illuminated photocathode thus generating the fs electron bunches through the photoemission process. The time delay between the excitation and probing electron pulses was changed by adjusting the relative optical path length between the two arms using a motorized delay line.

The probing electrons were accelerated up to 30 keV, giving a de Broglie wavelength of  $\sim 0.07$  Å; they were focused by a magnetic lens and directed to the sample with an incidence angle typically between  $0^\circ$  and  $4^\circ$ . The light excitation pulse was focused onto the sample in a cylindrical spot, in order to overlap with the probe electrons footprint. The temporal mismatch, due to the difference in velocity between photons and electrons, was suppressed by tilting the optical wavefront of the laser pulses [35]. With this arrangement, the electrons and photons overlapped in time, with no delay, across the entire area probed (as pictorially displayed in Figure 1). The size of the laser spot was carefully measured to be about  $430 \mu\text{m}$  by  $3 \text{ mm}$  FWHM by using a separate CCD camera. The electron beam had a cross-section diameter of  $200 \mu\text{m}$  FWHM, as measured on the screen; in these studies, it contained  $\sim 1000$  electrons per pulse having a duration between 0.5 and 1 ps. The resulting average current density of electrons was relatively small, on the order of  $0.1 \text{ pA}/\text{mm}^2$ , which is not sufficient to induce damage.

The samples were mounted on a high precision five-axis goniometer capable of providing rotations with angular resolution of  $0.005^\circ$ . An external cryostat was coupled to the sample holder through a flexible copper braid, to vary the sample temperature between 10 and 400 K. The diffraction patterns were recorded using a low-noise image-intensified CCD camera assembly capable of single-electron detection. Typically, the averaging time for a single diffraction frame was around 10 seconds. Several diffraction frames were averaged over multiple time scans in order to obtain a good signal-to-noise ratio. The data were processed with home-built computer interface.

**2.2. BSCCO Samples and Static Diffraction.** The optimally doped samples of Bi2212 and Bi2223 were grown by the “travel solvent floating zone” technique, described in [36]. The superconducting transition temperature was found to be  $T_c = 91 \text{ K}$  in Bi2212 ( $\Delta T_c = 1 \text{ K}$ ), and  $T_c = 111 \text{ K}$  in Bi2223 ( $\Delta T_c = 4 \text{ K}$ ). The underdoped Bi2212 sample was grown by the self-flux method [37], annealed in an oxygen-deficient atmosphere, and its transition temperature was found to be  $T_c = 56 \text{ K}$  ( $\Delta T_c < 6 \text{ K}$ ). The magnetic susceptibility curves for two representative samples are given in [23]. All samples were cleaved in situ at low temperature (20 K) prior to diffraction experimental studies in order to ensure the presence of a high-quality, clean surface.

In Figure 2, we display the static diffraction pattern obtained from the optimally doped Bi2212 sample. The patterns were recorded in the reflection geometry with the electron beam directed along three different axes, namely, the [010], [110], and [100] directions, as displayed in Figures 2(a)–2(c). The penetration depth of 30 kV electrons in

BSCCO is expected to be less than 100 Å; the  $c$ -axis lattice parameter is 30 Å, therefore only few unit cells (3-4) are probed by electrons. As a result, the diffraction patterns present rods instead of spots. In Figure 2(a) the (20) rod shows a weak modulation consistent with the  $c$ -axis value of the material. The diffraction was indexed for the tetragonal structure, giving the in-plane lattice parameters of  $a = b = 5.40$  Å, and  $c = 30$  Å, consistent with X-ray values. The lattice modulation is resolved along the  $b$ -axis with a period of 27 Å, again in agreement with the X-ray data [38]. The in-plane lattice constants, as well as the modulation, were confirmed for the specimens studied using our electron microscope. One micrograph is shown in Figure 2(d).

In order to quantify the diffraction, different “cuts” along the momentum transfer vector were made; see Figure 3. The colored arrows in Figures 2 and 3 indicate the direction in which the cut is performed. From the 2D data we can extract with precision the in-plane and out-of-plane lattice parameters, and the presence of several higher-order diffraction features testifies for the good quality of the samples. In Figure 4, the diffraction image and the 2D cut parallel to the (11) direction for underdoped Bi2212 (Figures 4(c) and 4(d)) and optimally doped Bi2223 (Figures 4(a) and 4(b)) are also shown. The in-plane lattice parameter of Bi2223 is found to be  $a = b = 5.42$  Å, in agreement with earlier X-ray data [38].

In Figure 5, we present the unit cell of Bi2212 (Figure 5(a)); for clarity the different directions indexed in the diffraction patterns are indicated here. In the same graph, the red arrows departing from the oxygen ions represent the distortion induced by two particular phonon modes (the in-plane breathing and the out-of-plane buckling) which will be relevant for the following discussion. In Figure 5(b), one can see the effect of the  $c$ -axis modulation along the  $b$ -axis of a Bi2223 crystal. The modulation is present in all Pb-free BSCCO samples and is responsible for the satellites observed in the diffraction pattern recorded with electrons probing parallel to  $b$  (Figure 2(c)), and in transmission (Figure 2(d)).

**2.3. LCO Sample and Static Diffraction.** The  $\text{La}_2\text{CuO}_{4+\delta}$  (LCO) film used was 52 nm thick [34]; it has been grown on  $\text{LaSrAlO}_4$  (LSAO) using a unique atomic-layer molecular beam epitaxy (MBE) [39] system equipped with 16 metal sources (thermal effusion cells), a distilled ozone source, and a sophisticated, real-time, 16-channel rate monitoring system based on atomic absorption spectroscopy. It is also provided with a dual-deflection reflection high-energy electron diffraction (RHEED) system and a time-of-flight ion scattering and recoil spectroscopy (TOF-ISARS) system for real-time chemical analysis of the film surface. These advanced surface-science tools provide information about the film surface morphology, chemical composition, and crystal structure. The films under study were characterized by resistivity, X-ray diffraction (XRD), atomic force microscopy (AFM), and electrostatic force microscopy (EFM). The resistivity showed the onset of superconductivity around 32 K and the X-ray diffraction analysis confirmed the good crystallinity of the film with lattice parameters of  $a = b = 3.755$  Å and  $c = 13.2$  Å.

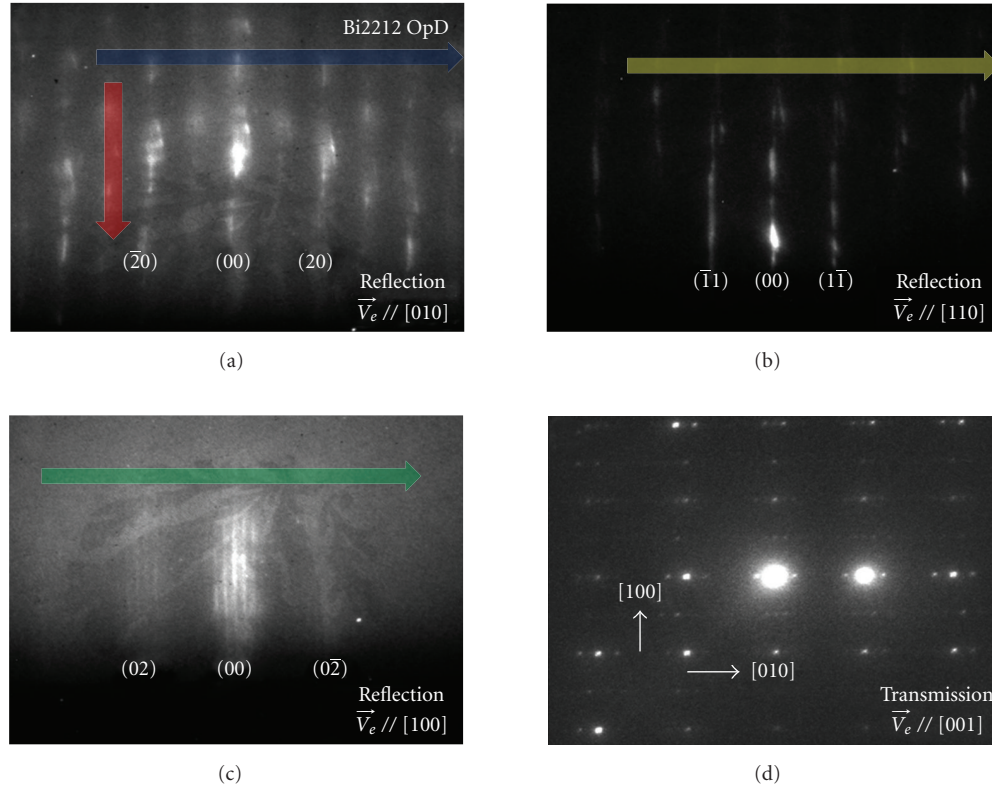


FIGURE 2: OpD Bi2212 static diffraction patterns. (a)–(c) Reflection patterns obtained at three different electron probing directions  $\vec{V}_e$  (by rotating the crystalline sample), as indicated in the lower right corner. The large lattice constant along  $c$  and the nm depth of electron probing give rise to the rod-like patterns; from (a), the intensity modulation along the diffraction rods gives the out-of-plane lattice parameter of  $c = 30 \text{ \AA}$ . The indices for different diffraction rods are given. Note that the satellites of the main diffraction rods in (c) manifest the 27- $\text{\AA}$  modulation along the  $b$ -axis of Bi2212. (d) Transmission diffraction pattern obtained by our electron microscope. The square in-plane structure is evident, with the presence of the  $b$ -axis modulation which is also seen in (c). The colored arrow indicates the direction of the cuts taken in the reciprocal space for the analysis of the data.

The growth of the samples was monitored with RHEED in the MBE chamber. During the growth, the pattern showed sharp streaks consistent with an atomically smooth surface. After the sample was taken out of the growth chamber and transported between laboratories, we could only observe transmission-like electron diffraction patterns on top of a broad background intensity, indicating the modification of the original surface and existence of three-dimensional structures on the film. Electron diffraction from these structures matches with the structure of the LCO film, as will be shown below. AFM measurements taken on the film after exposure to air showed atomically smooth surfaces (rms roughness in 0.3–0.6 nm range) except for some rare precipitates with the typical width of ca 50–200 nm. AFM topography images show that these precipitates typically have a cylindrical shape with diameters around 50 nm and typical height of 20 nm.

In Figure 6, static electron diffraction patterns obtained from two different orientations of the sample are shown. In Figure 6(a), the electron beam is incident at  $45^\circ$  with respect to the in-plane Cu–O bond direction (nodal direction); whereas in Figure 6(b) the beam is incident along the Cu–O bond direction (antinodal direction). The angle of incidence

was around  $1.5^\circ$  in both cases. The diffraction patterns observed in both cases are consistent with the LCO crystal structure. We have indexed these patterns based on the tetragonal structure. The obtained lattice constants ( $a = b = 3.76 \text{ \AA}$  and  $c = 13.1 \pm 0.1 \text{ \AA}$ ) are in agreement with the aforementioned X-ray diffraction measurements we made on the same film ( $a = b = 3.755 \text{ \AA}$  and  $c = 13.20 \text{ \AA}$ ). The uncertainty in the lattice constants obtained with electron diffraction comes mainly from the error in the determination of the sample to camera distance. The relative changes in the lattice constants can be measured with much better accuracy (below  $\pm 0.01 \text{ \AA}$ ).

The structure of LCO at high temperature is known to be tetragonal (HTT) with space group  $I4/mmm$ . Once the sample is cooled down, tilting of the  $\text{CuO}_6$  octahedra occurs and transition to a low temperature orthorhombic (LTO) phase takes place [40]. In the undoped compound, this transition occurs at  $\sim 530 \text{ K}$ . Depending on the oxygen concentration, these tilts can be ordered having a space group of  $B_{mab}$  or disordered with a space group of  $F_{mmm}$ . The tilting of the  $\text{CuO}_6$  octahedra results in the appearance of weak satellite peaks in the diffraction pattern at locations that are not allowed in the tetragonal symmetry; however these

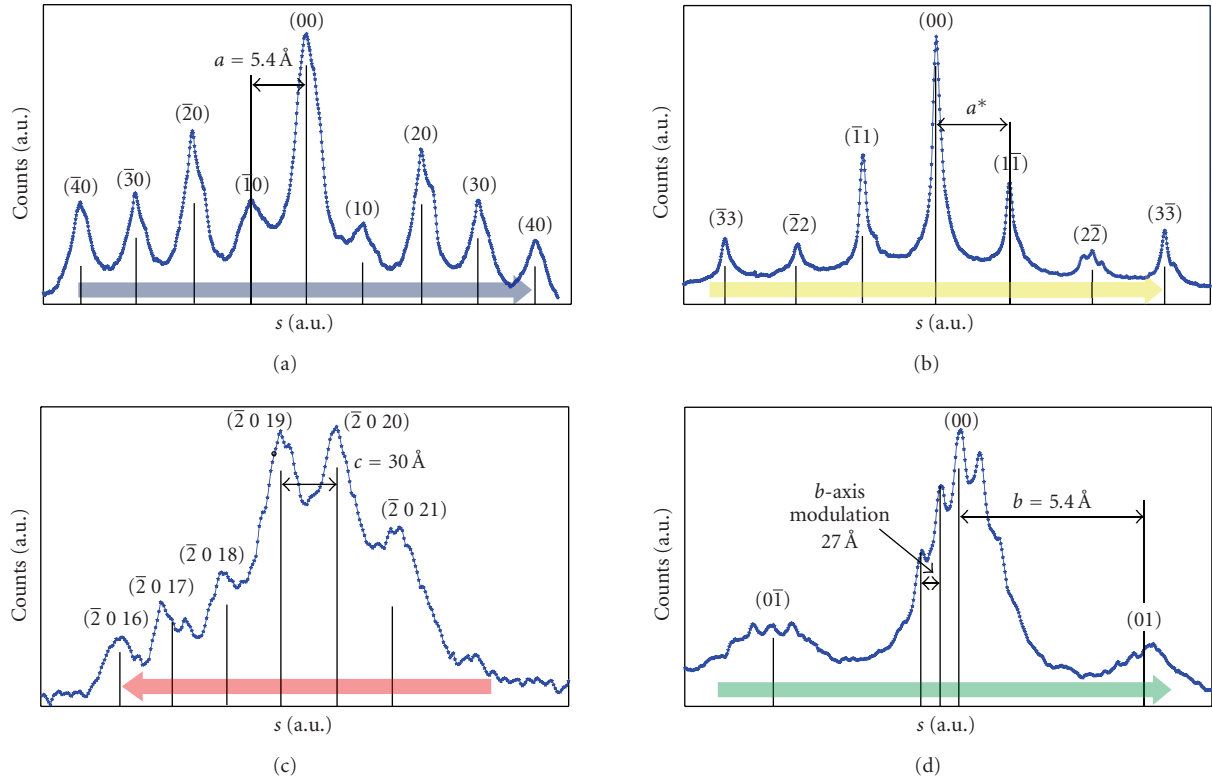


FIGURE 3: OpD Bi2223 Bragg peaks. Cuts along the directions indicated by the coloured arrows in Figure 2 are displayed. (a) Cut along the (n00) direction. (b) Cut along the (nn0) direction. (c) Cut along the (20n) direction. (d) Cut along the (0n0) direction. All Bragg peaks are indexed.

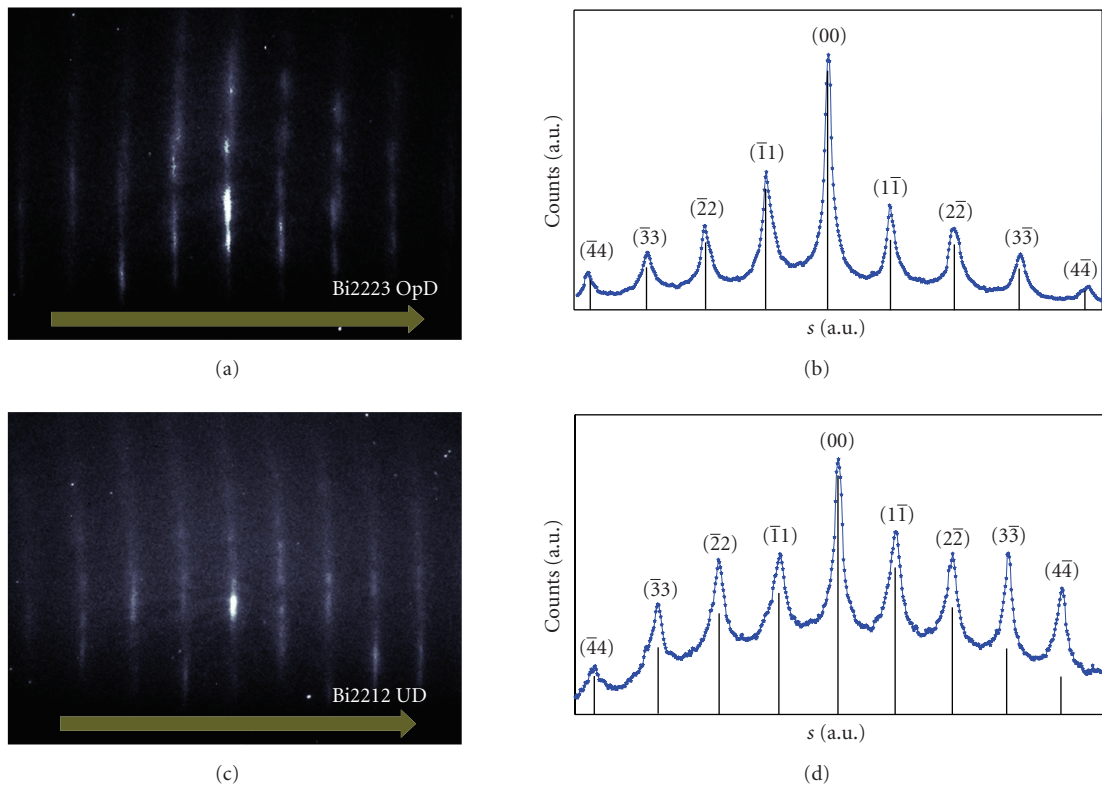


FIGURE 4: OpD Bi2223 and UD Bi2212 diffraction patterns and Bragg peaks. (a) Diffraction pattern of optimally doped Bi2223. The electron beam is parallel to the (110) direction. (b) Cut along the (nn0) direction of Bi2223. (c) Diffraction pattern of under-doped Bi2212. The electron beam is parallel to the (110) direction. (d) Cut along the (nn0) direction of under-doped Bi2212. All Bragg peaks are indexed.

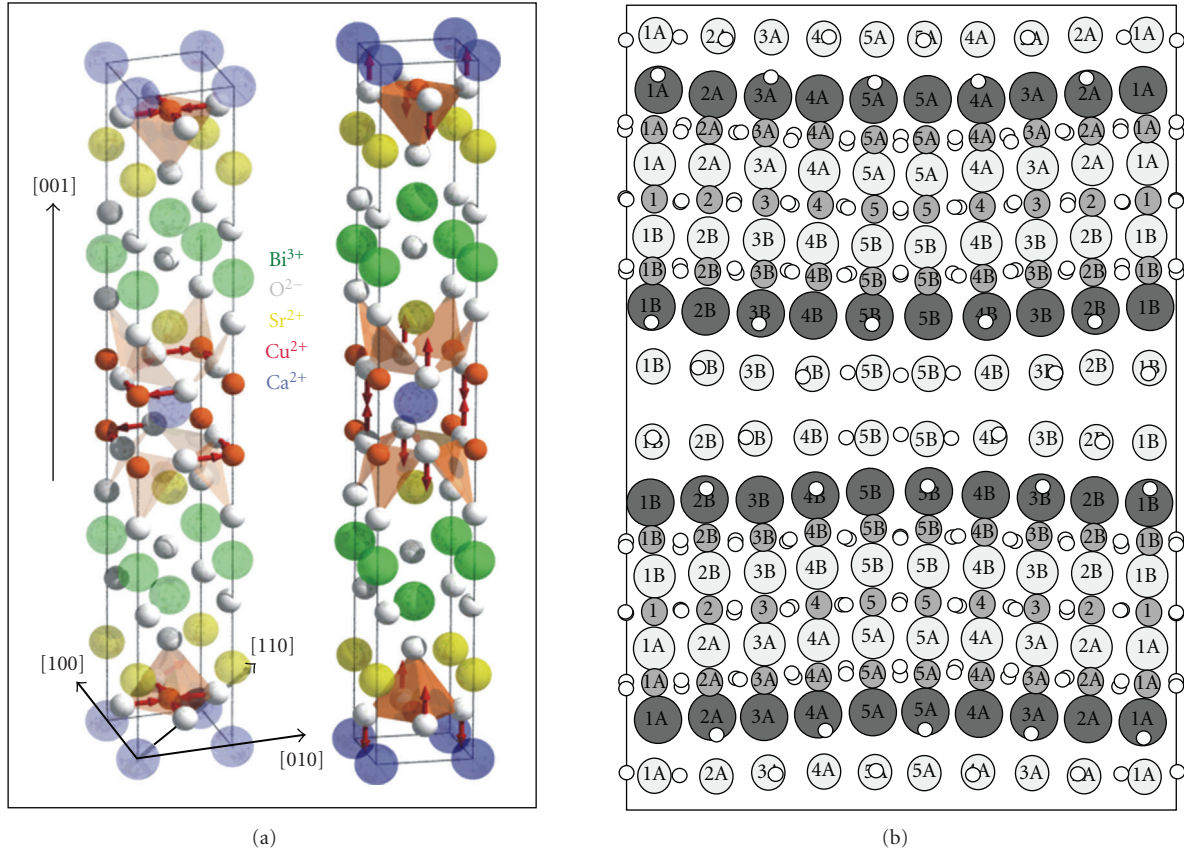


FIGURE 5: Bi2212 unit cell and Bi2223 modulated supercell. (a) Three-dimensional structure of Bi2212, indicating the main crystallographic directions. In panel (a), you can see that the crystal is depicted twice. In-plane breathing refers to the crystal on the left inside panel (a), while out-of-plane buckling mode refers to the crystal on the right always in panel (a). (b) Several unit cells of Bi2223 are shown, and the effect of the  $c$ -axis modulation is visible.

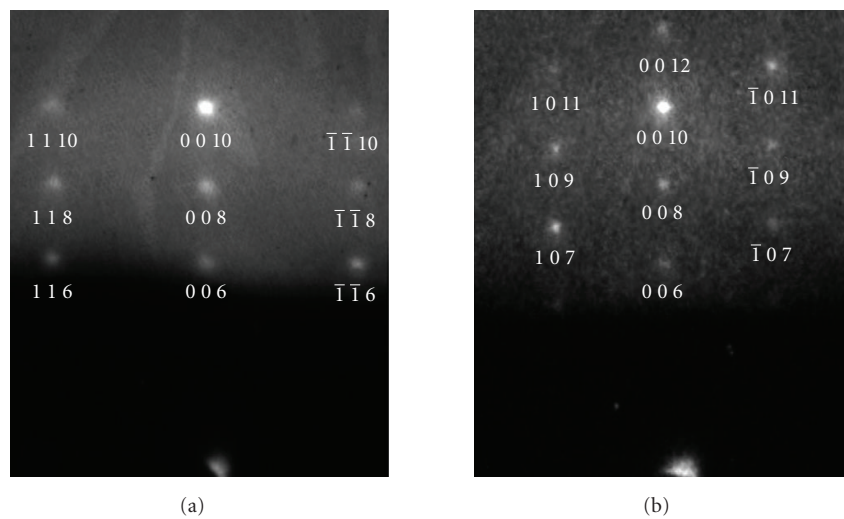


FIGURE 6: LCO thin film static electron diffraction. Multiple diffraction orders of sharp Bragg spots can be seen indicating a transmission-like pattern. These patterns come from transmission through the three-dimensional islands observed in AFM measurements. The patterns are indexed based on the tetragonal structure of LCO. (a) The electron beam is incident  $45^\circ$  to in-plane Cu-O bond direction (nodal direction); whereas in (b) the beam is incident along the Cu-O bond direction (antinode direction). The angle of incidence was around  $1.5^\circ$  in both cases.

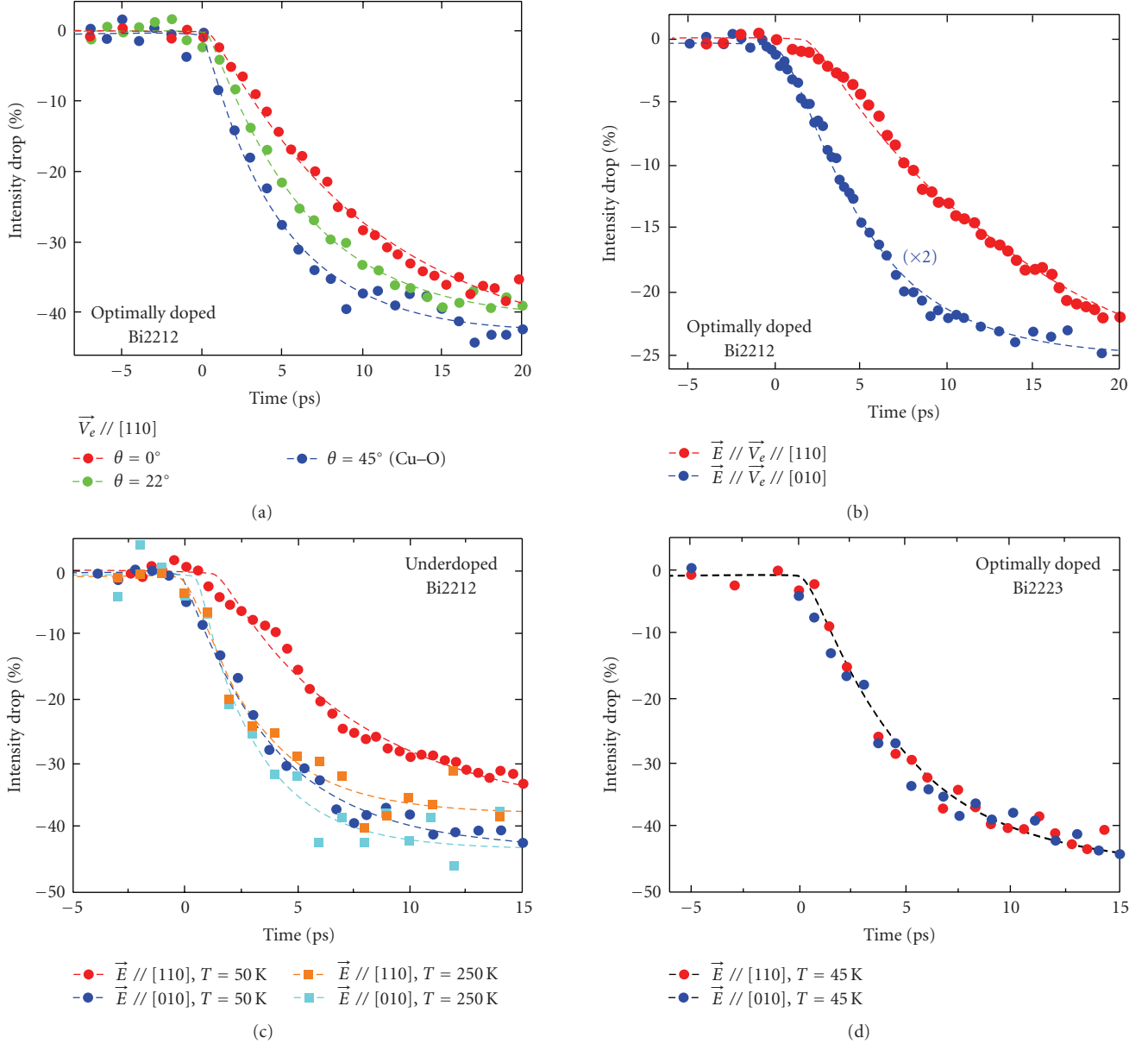


FIGURE 7: Time-resolved diffraction in BSCCO. (a) Diffraction intensity change of the (00) rod at different polarizations in optimally doped Bi2212. The laser fluence was 20 mJ/cm<sup>2</sup>, and the temperature was 50 K. The electron probing was kept along [110] (Figure 2(b)), and  $\theta$  is the angle of polarization away from the probing direction (controlled by rotation of a half-wave plate). The dotted lines (and also those in panels (b) to (d)) show the fits to an apparent exponential decay. (b) Diffraction intensity change of the (00) rod, from the same sample, obtained with the optical polarization being parallel to the electron probing. By rotating the crystal, the time-dependent change was measured for the two zone axes (Figures 2(a) and 2(b)). (c) Diffraction intensity change of the (00) rod for an underdoped Bi2212 sample ( $T_c = 56$  K), at two temperatures and two polarizations. (d) Diffraction intensity change obtained from a three-layered, optimally doped Bi2223 sample at 45 K for two polarizations.

satellite peaks were too weak to be seen in our diffraction patterns. Locations of the main lattice Bragg peaks are not affected. For simplicity, we used the tetragonal phase (I4/mmm) for indexing of patterns although the actual space group might not be strictly tetragonal.

### 3. Results and Discussion

**3.1. The Debye-Waller Effect in BSCCO.** We begin by discussing the results obtained for BSCCO samples. The

temporal evolution of diffraction frames (with polarized excitation) is sensitive to motions of atoms during the structural change. In Figure 7(a), the intensity decay due to motions of the ions (Debye-Waller effect) of the (00) rod is plotted for three different polarizations ( $\vec{E}$ ) of the excitation pulse:  $\vec{E} // [010]$ , the direction of Cu-O bonds;  $\vec{E} // [110]$ , the direction at 45°, and the one at 22°. The data were taken at  $T = 50$  K on an optimally doped Bi2212 sample. At longer times, up to 1 ns, these transients recover very

slowly; because of the poor  $c$ -axis conductivity and metallic  $ab$ -plane, heat transport is mainly lateral, but is complete on the time scale of our pulse repetition time (1 ms). In Figure 7(b), another set of data was obtained by rotating the same sample while keeping the polarization parallel to the electron beam direction. The temporal evolution of the (00) diffraction intensity obtained from the two different orientations (electron beam parallel to the Cu–O bond, see diffraction pattern in Figure 2(a) and the corresponding Bragg peak in Figure 3(a), and at  $45^\circ$ , pattern in Figure 2(b) and corresponding Bragg peak in Figure 3(b)) shows the same anisotropic behavior as that obtained by rotating the polarization, ruling out possible experimental artifacts.

The intensity decay for different polarizations was found to have distinct time constants (see below); the decay is faster when the polarization is along the Cu–O bond and slows down when polarization is along the [110] direction ( $45^\circ$  from the Cu–O bond). Such an effect was observed to be even stronger in an underdoped sample. In Figure 7(c), we display the results obtained for underdoped Bi2212 ( $T_c = 56$  K), also at two temperatures. The anisotropy is evident at low temperature, with the Debye-Waller decay being faster again for  $\vec{E} // [010]$ . However, at higher temperature, the decay of both polarizations is similar and reaches the fastest profile recorded. Surprisingly, in optimally doped Bi2223, we observed no significant anisotropy even in the low temperature regime (Figure 7(d)). In fact, the intensity decay of the (00) rod for light polarized along [110] becomes essentially that of the [010] direction.

**3.2. The Electron-Phonon Coupling Parameter.** When charge carriers are excited impulsively through light in a crystal, the electron and lattice temperatures are driven out of equilibrium, but they equilibrate through electron-phonon coupling. Excitation of phonons causes the diffraction intensity to change with time, and this decrease mirrors an increase of the mean atomic displacement in the corresponding direction, with a temperature assigned to the displacement through a time-dependent Debye-Waller factor

$$\ln \left[ \frac{I(t)}{I_0} \right] = -2W(t) = -\frac{s^2 \langle \delta u^2(t) \rangle}{3}, \quad (1)$$

where  $I(t)$  is the intensity of rod diffraction at a given time  $t$  after excitation,  $I_0$  is the intensity before excitation,  $s$  is the scattering vector, and  $\langle \delta u^2(t) \rangle$  is the mean-square atomic displacement. From the results reported here for  $[I(t)/I_0]_{\min}$ , the root-mean-square value for the amplitude of the motion is obtained to be  $\sim 0.15 \text{ \AA}$  for  $20 \text{ mJ/cm}^2$  fluence. Given the  $c$ -axis distance of  $30 \text{ \AA}$ , this represents a change of 0.5% of the  $c$ -axis; the Cu–O planes instead separate by  $3.2 \text{ \AA}$ .

We verified that different diffraction orders show changes which scale with the scattering vector, confirming that the observed changes in the diffraction intensity originate from phonon-induced structural dynamics. In a time-resolved diffraction experiment, different Bragg spots at a given time should exhibit intensity changes in accord with the value of the scattering vectors  $s$  (see (1)). Therefore, two distinct Bragg

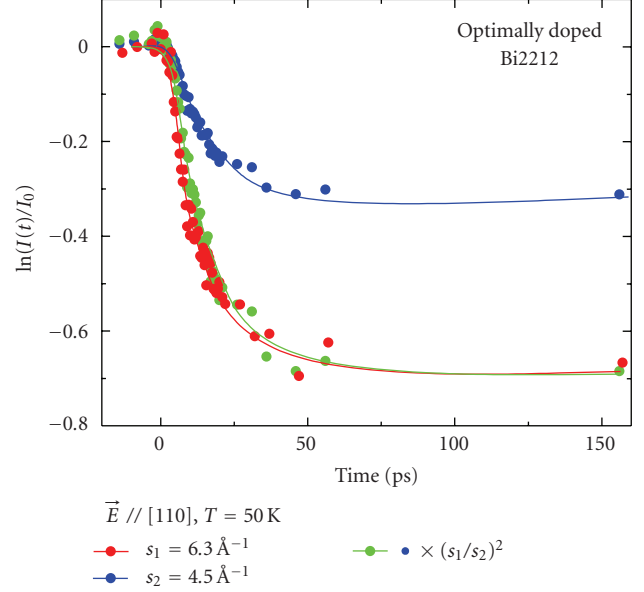


FIGURE 8: Scaling of Bragg intensities. Shown is the decay of two distinct Bragg peaks, observed at  $s_1 = 6.3 \text{ \AA}^{-1}$  (red) and  $s_2 = 4.5 \text{ \AA}^{-1}$  (blue). The green curve is obtained by multiplying the data at  $s = s_2$  by the factor of  $(s_1/s_2)^2$ , according to (2), and its match with the data at  $s = s_1$  confirms the structurally induced diffraction changes following the carrier excitation.

diffraction features appearing at  $s = s_1$  and  $s_2$  should obey the following scaling relation:

$$\frac{\ln(I_{s_1}/I_0)}{\ln(I_{s_2}/I_0)} = \left( \frac{s_1}{s_2} \right)^2. \quad (2)$$

In Figure 8, we plot the intensity changes for two different Bragg spots, recorded in the same pattern, but for different scattering vectors. The apparent scaling confirms that the observed intensity changes are indeed originating from structural motions.

The observed anisotropy of decays with polarization reflects the distinct  $c$ -axis distortion and the difference in electron-phonon coupling. In order to obtain the magnitude of the couplings we invoked the well-known model of electrons and lattice temperatures, dividing the lattice modes into those which are strongly coupled to the electrons and the rest which are not [23]. Thus, the decrease of the intensity at a given time tracks the change of  $\langle \delta u^2(t) \rangle$  with a corresponding effective temperature. For a Debye solid, the atomic displacement can be expressed as

$$\langle \delta u^2(t) \rangle = \frac{9\hbar^2 \Delta T(t)}{Mk_B \Theta_D^2}, \quad (3)$$

where  $M$  is the average mass in the unit cell,  $k_B$  is the Boltzmann constant,  $\hbar$  is the reduced Planck constant, and  $\Theta_D$  is the Debye temperature of the material [29]. Traditionally, the two-temperature model [41] is invoked to describe the laser-induced heating of electrons and phonons, as subsystems, in an elementary metal. Its success is the result of the isotropic electron-phonon coupling in a simple lattice structure, that

is, one atom per primitive unit cell. In complex, strongly correlated materials like high- $T_c$  superconductors, however, such model becomes inappropriate because photoexcited carriers may anisotropically and preferentially couple to certain optical phonon modes, making meaningless the assignment of a single temperature to the whole lattice structure [29, 42].

In the three-temperature model described in [29], in addition to the electron temperature  $T_e$ , two temperatures are defined for the lattice part: the hot-phonon temperature,  $T_p$ , for the subset of phonon modes to which the laser-excited conduction-band carriers transfer their excess energy, and the lattice temperature,  $T_l$ , for the rest of the phonon modes which are thermalized through anharmonic couplings. As an approximation, the spectrum of the hot phonons  $F(\Omega)$  is assumed to follow an Einstein model:  $F(\Omega) = \delta(\Omega - \Omega_0)$ , where  $\delta$  denotes the Dirac delta function, with  $\Omega$  being the energy and  $\Omega_0$  the energy of a hot phonon. Effectiveness of the energy transfer between the carriers and hot phonons is described by the dimensionless parameter  $\lambda$ :  $\lambda = 2 \int \Omega^{-1} \alpha^2 F d\Omega$ , where  $\alpha^2 F$  is the Eliashberg coupling function [41]. The rate equations describing the temporal evolution of the three temperatures are given by

$$\frac{dT_e}{dt} = -\frac{3\lambda\Omega_0^3}{\hbar\pi k_B^2} \frac{n_e - n_p}{T_e} + \frac{P}{C_e}, \quad (4)$$

$$\frac{dT_p}{dt} = \frac{C_e}{C_p} \frac{3\lambda\Omega_0^3}{\hbar\pi k_B^2} \frac{n_e - n_p}{T_e} - \frac{T_p - T_l}{\tau_a}, \quad (5)$$

$$\frac{dT_l}{dt} = \frac{C_p}{C_l} \frac{T_p - T_l}{\tau_a}, \quad (6)$$

where  $\tau_a$  is the characteristic time for the anharmonic coupling of the hot phonons to the lattice (in this case equals 2.8 ps),  $n_e$  and  $n_p$  are the electron and hot-phonon distributions given by  $n_{e,p} = (e^{\Omega_0/k_B T_{e,p}} - 1)^{-1}$ , and  $P$  is the laser fluence function; a ratio of  $10^3$  between the electronic specific heat  $C_e$  and the lattice specific heat ( $C_p$  and  $C_l$ ) is known [29].

In our calculations, the values of the parameters were chosen to be the same as in [29], except for the excitation source which in our case has a fluence of 20 mJ/cm<sup>2</sup> and duration of 120 fs. The fit of the simulated lattice temperature to our data (see Figures 9(a), 9(d), and 9(e)) gives the following results for the electron-phonon coupling constant in the different samples:  $\lambda_{[110]} = 0.12$ ,  $\lambda_{[010]} = 1.0$ , and their average  $\lambda_{\text{avg}} = 0.56$  in underdoped Bi2212, Figure 9(d);  $\lambda_{[110]} = 0.08$ ,  $\lambda_{[010]} = 0.55$ , and their average  $\lambda_{\text{avg}} = 0.31$  in optimally doped Bi2212, Figure 9(a);  $\lambda_{[110]} \approx \lambda_{[010]} = 0.40$  in optimally doped Bi2223, Figure 9(e).

In our procedure, the accuracy in determining  $\lambda$  depends on the precision in estimating the decay constant of the Debye-Waller factor, which can be very high given the signal to noise ratio achieved in our experiments. However, the absolute error in the determination of  $\lambda$  also depends on the approximations behind the three-temperature model. The best estimate of the likelihood of these numbers comes from the comparison with other techniques and calculations. The average value at optimal doping is in good agreement with

the results ( $\lambda = 0.26$ ) of [29], which angularly integrates the photoemission among different crystallographic directions. It is also in agreement with ‘‘frozen-phonon’’ calculations [43].

The rate of diffraction change provides the time scales of selective electron-phonon coupling and the decay of initial modes involved. The analysis of the first derivative of the Debye-Waller decay helps in distinguishing the different processes involved in the decay of the initial excitation, that is, electron-phonon coupling and anharmonic phonon-phonon interactions. In Figure 9(b), the derivatives of the diffraction intensity as a function of time,  $dI(t)/dt$ , are displayed for different polarizations. The presence of a clear inversion point reflects the two processes involved, the one associated with the coupling between excited carriers and optical phonons, and the second that corresponds to the decay of optical modes, by anharmonic coupling into all other modes. The minimum in the derivative, signaling the crossover between these two processes, shifts toward an earlier time when the polarization becomes along the Cu–O bond. In Figure 9(c), the derivative of the simulated lattice temperature within the three-temperature model,  $dT_l(t)/dt$ , shows a similar two-process behavior. The shift of the minimum to an earlier time can be reproduced by varying the electron-phonon coupling parameter  $\lambda$ ; in contrast, a change in the anharmonic coupling constant  $\tau_a$  does not affect the early process, and the corresponding time of the derivative minimum has little shift (Figure 9(c), *inset*). Thus, consistent with the results of Figure 9(a), this analysis suggests that the anisotropic behavior of the diffraction intensity is due to a directional electron-phonon coupling.

The derivative minima occur at times of  $\sim 1.0$ , 2.0, and 3.5 ps, respectively, for the polarization at  $0^\circ$ ,  $22^\circ$ , and  $45^\circ$  with respect to the Cu–O bond direction (Figure 9(b)). The initial rate of the electron-phonon scattering can be obtained through the equation [41]

$$\begin{aligned} \frac{1}{\tau_{\text{el-ph}}} &= \frac{3\hbar\lambda\langle\omega^2\rangle}{\pi k_B T_e} \left( 1 - \frac{\hbar^2\langle\omega^4\rangle}{12\langle\omega^2\rangle(k_B T_e)(k_B T_l)} + \dots \right) \\ &\approx \frac{3\hbar\lambda\langle\omega^2\rangle}{\pi k_B T_e}, \end{aligned} \quad (7)$$

where  $\tau_{\text{el-ph}}$  is the characteristic coupling time constant and  $\omega$  is the angular frequency of the coupled modes. Given the values of  $\lambda$  (0.55, 0.18, and 0.08 in Figure 9(c)), we obtained  $\tau_{\text{el-ph}}$  to be 290 fs, 900 fs, and 2.0 ps with an initial  $T_e = 6000$  K and  $T_l = 50$  K. In [29],  $\tau_{\text{el-ph}}$  was reported to be 110 fs for  $T_e \sim 600$  K. Given the difference in fluence, hence  $T_e$ , the values of  $\tau_{\text{el-ph}}$  obtained here (see (7)) are in reasonable agreement with the average value obtained in [29]. It should be emphasized that within such time scale for the electron-phonon coupling the lattice temperature  $T_l$  remains below  $T_c$ ; in Figure 9(a), the temperature crossover ( $T_l > T_c$ ) occurs at 2 to 3 ps. We also note that at our fluence the photon doping has similar charge distribution to that of chemical doping [34].

The influence of polarization on the (00) diffraction rod (which gives the structural dynamics along the  $c$ -axis) reveals the unique interplay between the in-plane electronic

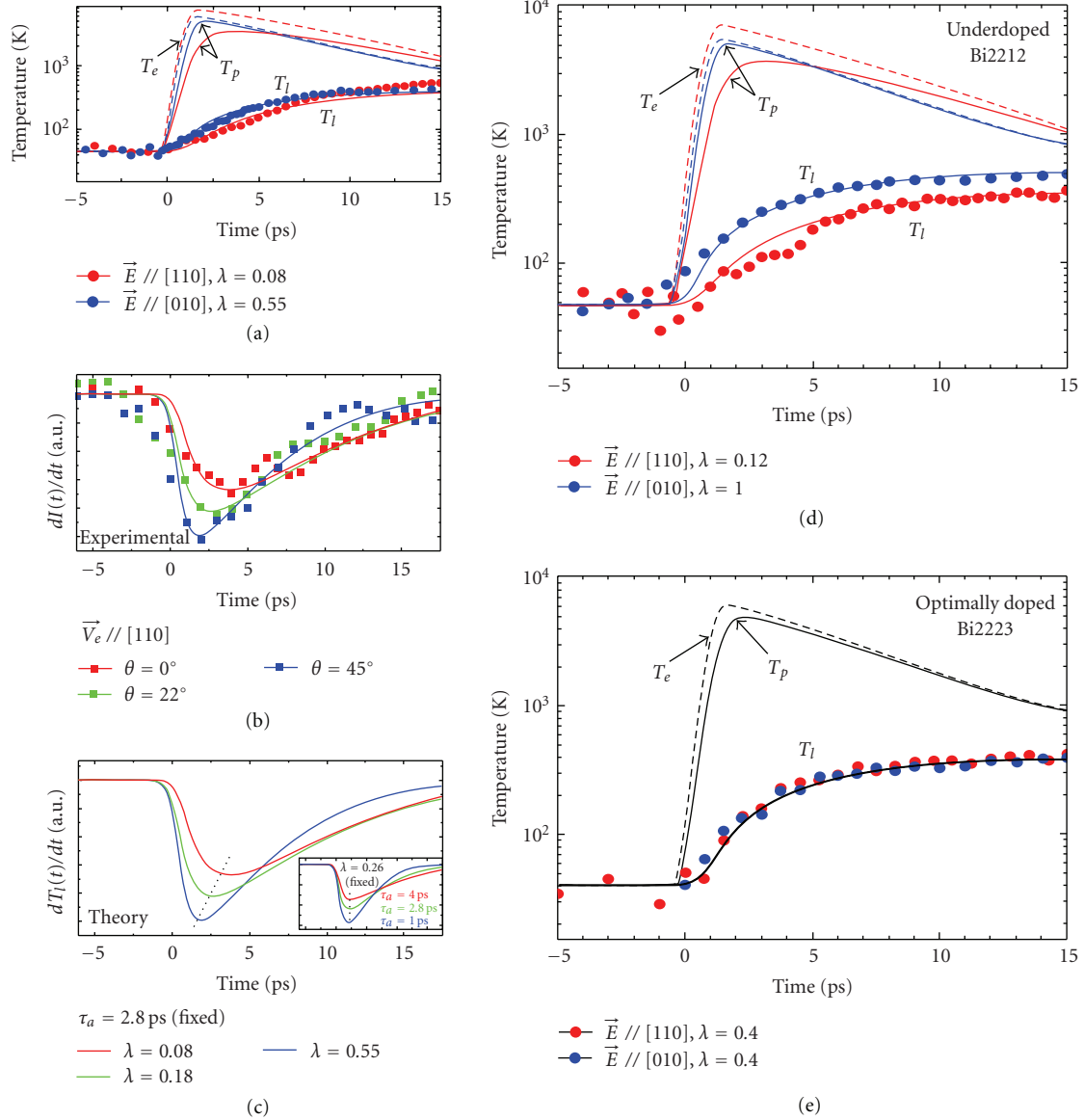


FIGURE 9: Experimental and theoretical intensity transients. (a) Lattice temperature derived from diffraction using (1) and (3), for different polarizations, along [010] (blue dots) and [110] (red dots), in optimally doped Bi2212. From the three-temperature model described in the text, we obtain that  $\lambda = 0.08$  for  $\vec{E} // [110]$  ( $T_l$ , red solid line) and  $\lambda = 0.55$  for  $\vec{E} // [010]$  ( $T_l$ , blue solid line). The electronic ( $T_e$ , dashed lines) and hot-phonon ( $T_p$ , solid lines) temperatures are also displayed. (b) Derivatives of the (00) diffraction intensity derived from Figure 2(a) for different polarizations. (c) Derivatives of the simulated lattice temperature within the three-temperature model, for different  $\lambda$  with a fixed anharmonic coupling time  $\tau_a = 2.8$  ps (also shown in (b)) and for different  $\tau_a$  with a fixed  $\lambda = 0.26$  (inset). The clear shift of the minimum position is only observed when  $\lambda$  is varied (black dotted lines). (d) Three-temperature model analysis for underdoped Bi2212. (e) Three-temperature model analysis for Bi2223.

properties and the out-of-plane distortion. Among the high-energy optical phonons that are efficiently coupled at early times, the in-plane breathing and out-of-plane buckling modes are favored (Figure 5(a)) [7, 8] because of their high energy and involvement with carrier excitation at 1.55 eV. Our observation of a faster  $c$ -axis dynamics when the polarization is along the Cu–O bond implies a selective coupling between the excitation of charge carriers and specific high-momentum phonons. A plausible scheme is the stronger coupling between the antinodal ([010]) charge carriers and

the out-of-plane buckling vibration of the oxygen ions in the Cu–O planes. More details will be discussed in the following sections.

**3.3. Implications Regarding the Material’s Phase Diagram.** Time-resolved electron diffraction provides the opportunity to examine the separate contributions of electronic and lattice heating to the temperature dependence of electron-phonon coupling. The effect of the equilibrium-temperature can be studied varying the initial sample temperature, and

at identical laser fluence, when the electronic temperature rise remains unchanged, and the lattice temperature can be tuned between 40 K and higher temperature, thus reaching different points of the phase transition region. If the laser fluence is varied instead, the temperature reached by the out-of-equilibrium electrons can be varied by about one order of magnitude (for fluences between 2 and 20 mJ/cm<sup>2</sup>), whereas the lattice-temperature change is much slower, and of lower value. The results from such different experiments are given in Figures 10(a) and 10(c).

In Figure 10(a), where the fluence varied, the overall intensity decay changes significantly, and a faster decay is observed at higher fluences. The overall characteristic time of an exponential fit to the data is displayed as black squares in the inset of Figure 10(a). As remarked before, these transients are the results of two processes: (i) the ultrafast electron-phonon coupling and (ii) the slower anharmonic decay of the hot phonon into thermal vibrations; see Figures 7(b) and 7(c). In order to separate these two contributions, we also plot in Figure 10(b) the derivative of the intensity decay for different fluences. The time-constant associated with the electron-phonon coupling is seen to vary modestly as a function of the fluence. The time scale corresponding to the minimum in the derivative is also plotted in the inset of Figure 10(a). From the comparison between this time scale and the longer one obtained from the single exponential fit we conclude that the electronic-temperature rise mainly affects the process caused by anharmonic coupling. We also notice that the fluence dependence of both time constants is not monotonic and shows an anomaly in the proximity of the fluence value inducing a lattice temperature rise similar to  $T_c$ .

In Figure 10(c), the dependence of the intensity decay rate as a function of the lattice temperature is displayed. In this case, the electronic temperature rise is constant, and so is the anharmonic coupling. In general, a faster decay is observed at higher temperatures, and the trend is understood in view of the two types of phonons present at high temperature: those created through carrier-phonon coupling (low temperature) and the ones resulting from thermal excitation. This behavior with temperature is consistent with the optical reflection studies made by Gedik et al. [32]. Also in this case we note that the temperature dependence of the decay rate is not monotonic when the light is polarized along [10]. The anisotropy observed in the Bi2212 samples is apparent at low temperature. Whether or not the anisotropy is related to  $T_c$  cannot be addressed with the current temperature resolution, although a correlation is suggested by the data.

The observed temperature dependences suggest that the electron-phonon coupling parameter, to large extent, is insensitive to the electronic temperature, while it could be influenced by the lattice temperature. The effect of heating on the electronic structure is expected to mainly broaden the electronic density of states, which is a determinant of the electron-phonon coupling. However, if there is no strong peak in the density of states at the Fermi level (as is the case for BSCCO cuprates), one may not expect a large effect for the electronic temperature on  $\lambda$ , consistent with our observation.

In Figure 10(d), the doping dependence of  $\lambda$  and the anisotropy observed for different polarizations,  $\Delta\lambda = \lambda_{[010]} - \lambda_{[110]}$  (obtained from repeated experiments on different samples and cleavages), are displayed, together with the qualitative trend of the upper critical field (Nernst effect) and coherence length [44]. The similarity in trend with the upper critical field behavior, which can be related to the pair correlation strength, is suggestive of lattice involvement especially in this distinct phase region where the spin binding is decreasing. In view of an alternative explanation for the doping dependence of the critical field [45], our observation of an anisotropic coupling for different light polarizations may also be consistent with the idea of a dichotomy between nodal and antinodal carriers, with the latter forming a charge-density wave competing with superconductivity [46]. Future experiments will be performed for completing the trends up to the overdoping regime for different superconductor transitions [47].

In the 3-layered sample, Bi2223, a much weaker, if not absent, anisotropy was observed at optimal doping (see Figure 7(d)). The electron-phonon coupling in Bi2223 is thus similar for both directions ( $\lambda = 0.40$ ) (see Figure 9(e)), signifying that the out-of-plane buckling motions are coupled more isotropically to the initial carrier excitation, likely due to the somewhat modified band structure (e.g., larger plasma frequency; see [48]) from that of Bi2212. This observation is consistent with the more isotropic superconducting properties of Bi2223 [38]. The screening effect for the inner Cu–O layer by the outer ones in Bi2223 [49, 50], and the less structural anisotropy between the in-plane and out-of-plane Cu–O distances [38], may also play a role in the disappearance of the anisotropic electron-phonon coupling. It is possible that the anisotropy of the excited carriers depends on the number of layers, as will be discussed in the next section.

*3.4. Anisotropy with Polarized Excitations.* In this section we discuss qualitatively different microscopic possibilities that could explain the observed anisotropy. We detail our speculations simulating the polarized optical excitation in a model system (the stripe ground state of LSCO). A rigorous discussion of this issue would require an unambiguous ab-initio description of the electronic properties of doped BSCCO, which to date is still lacking. It is now a well-established fact that doped holes in some cuprates self-organize in antiferromagnetic (AF) domain walls [51–55]. These quasi-one-dimensional (1D) structures called stripes were predicted by mean-field theories [56] inspired by the problem of solitons in conducting polymers [57]. In some compounds, stripes are clearly observed and are accompanied by a spontaneous breaking of translational and rotational symmetry in the Cu–O planes. For example, in 1995 Tranquada and collaborators observed a splitting of both spin and charge order peaks in La<sub>1.48</sub>Nd<sub>0.4</sub>Sr<sub>0.12</sub>CuO<sub>4</sub> by elastic neutron scattering [51]. The outcome of this experiment resembled the observation made in the nickelates, where both incommensurate antiferromagnetic (AF) order [58, 59] and the ordering of charges have been detected by neutron scattering and electron diffraction,

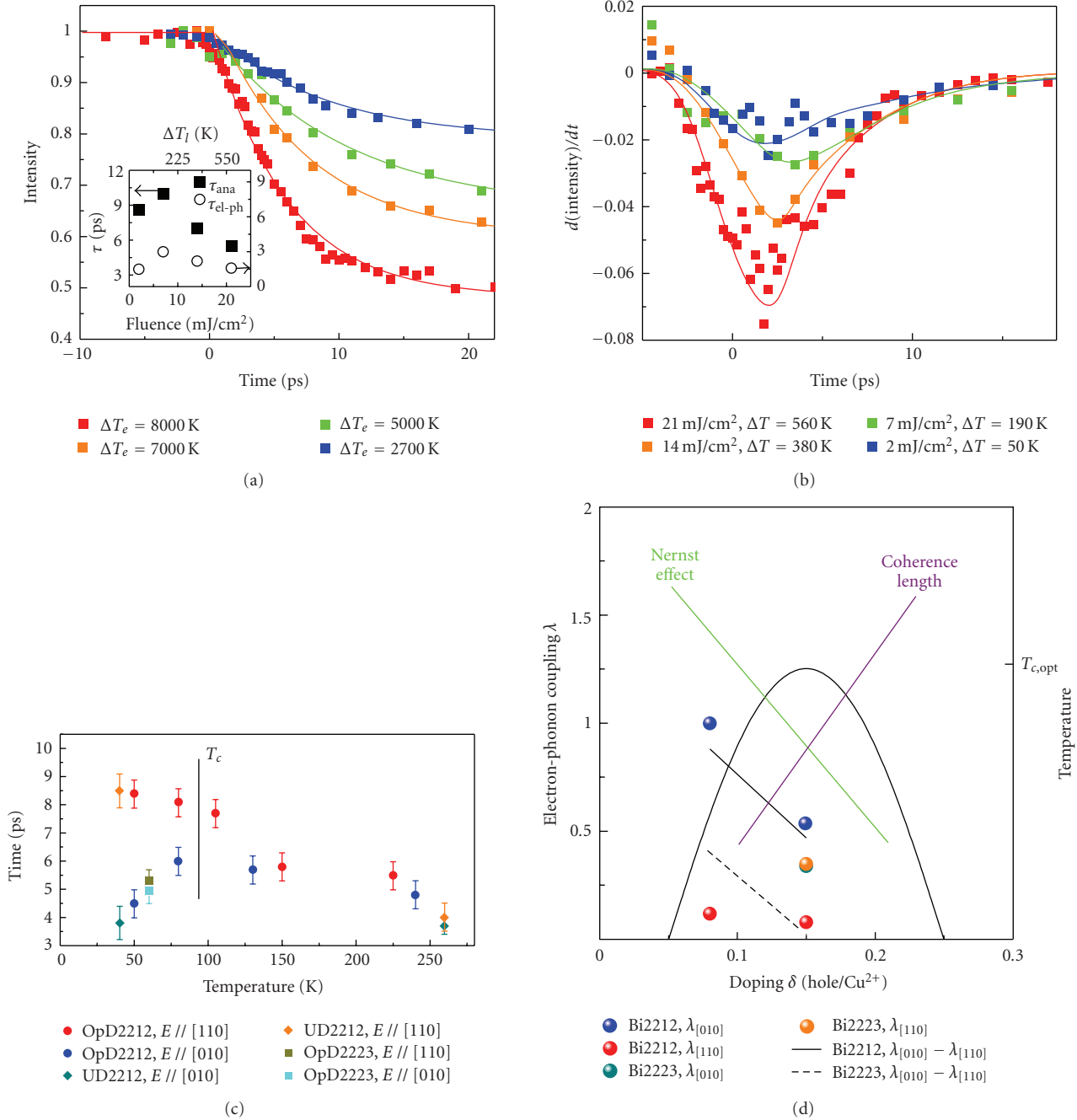


FIGURE 10: Temperature dependence and phase diagram. (a) Fluence dependence of the intensity decay along the (010) direction of optimally doped Bi2212. In the inset, the fluence dependence of the overall time constant of the decay, obtained from a simple exponential fit (filled black symbols), is shown together with the time constant associated to the electron-phonon coupling time (empty black symbols), obtained from Figure 10(b). (b) Fluence dependence of the derivative of the intensity decay along (010) in optimally doped Bi2212. The characteristic time related to the electron-phonon coupling process is estimated from the minimum in these curves (open black symbols in the inset of Figure 10(a)). (c) Lattice-equilibrium temperature dependence of the time constant for both polarizations in all samples. (d) The doping dependence of the coupling constant ( $\lambda$ ) along the [010] and [110] directions in Bi2212 (blue and red dots, resp.) and its anisotropy ( $\Delta\lambda$  between the two directions; black solid line), as well as  $\lambda$  along the [010] and [110] directions in Bi2223 (green and orange dots, resp.) and the extrapolated anisotropy (black dashed line). A qualitative sketch of the upper critical field and Cooper-pair coherence length (green and violet lines) is also shown.

respectively [59, 60]. In [59], it was shown that the magnetic ordering in  $\text{La}_2\text{NiO}_{4.125}$  manifests itself as occurring first and third harmonic Bragg peaks, whereas the charge ordering is associated with second harmonic peaks. From this, it

was concluded that the doped holes arrange themselves in quasi-one-dimensional structures, which simultaneously constitute antiphase domain walls for the AF order. There are several compounds, however, where static long-range order

has not been observed leading to the speculation that stripes survive as a dynamical fluctuation. An interesting possibility is that there exist precursor phases of the stripe phase where translational symmetry is preserved but rotational symmetry is spontaneously broken; this, in analogy with liquid crystals, has been called nematic order [61]. Stripe phases, breaking fundamental symmetries of the lattice, lead to the appearance of new collective modes that do not exist in a normal Fermi liquid. These collective modes may play an important role in the mechanism of superconductivity as pairing bosons. In our experiment we do not detect a spontaneous symmetry breaking; however, our results are compatible with the proximity to a nematic phase as explained below.

Although the three-temperature model gives a reasonable description of the relaxation times for each polarization, the basic assumptions of the model have to be reexamined when considering the anisotropy itself. In the standard formulation, one assumes that the electronic relaxation time ( $<100$  fs) is much shorter than the electron-phonon coupling time (few hundreds fs). The fact that one observes an anisotropy on the ps time scale suggests that this assumption breaks down, because electrons reaching thermal equilibrium in  $\sim 100$  fs would not have a memory of the excitation direction at later times. This means that some anisotropic electronic state is excited by the laser, which has a longer relaxation time in the nodal direction when compared with that of the antinodal direction. Anisotropic scattering rates are well documented in photoemission spectroscopy of cuprates [62]. The anomalous long electronic relaxation time suggested that the excited state is a low-lying collective electronic excitation, where the decay rate is limited by Fermi statistics and many-body effects, rather than by an interband or other high-energy excitation. Within the Fermi liquid theory, low-energy excitations can be characterized by the oscillatory modes of the Fermi surface.

The lowest-energy anisotropic excitations are the Pomeranchuk modes, which we illustrate schematically in Figures 11(c) and 11(d) for a cuprate Fermi surface. The thick red line is the undisturbed Fermi surface and the thin blue line is a snapshot of the oscillating Fermi surface. Thus, depending on the laser excitation direction, the Fermi surface can remain oscillating in the antinodal direction (Figure 11(c)) or the nodal direction (Figure 11(d)). If the system is close to a Pomeranchuk instability, the relaxation times of these two nonequilibrium configurations can be very different [63, 64]. A Pomeranchuk instability along the nodal direction would make that particular relaxation time very long and is one possible explanation for our results. After crossing the instability point, the deformation becomes static and the system acquires nematic order, that is, breaks the  $C_4$  symmetry of the lattice along the diagonals without breaking translational symmetry. This, however, is in contrast with the tendency of cuprates to break  $C_4$  symmetry along the Cu–O bond (except for slightly doped LSCO) through charge-ordered states, termed stripes. In Figure 13(b) we display static stripe order running along the  $y$  direction, according to a microscopic computation of stripes in the three-band Hubbard model [65]. Stripes are domain walls of

the antiferromagnetic order where holes tend to accumulate. In cuprates, static charge order as depicted is only seen under very special conditions which favor stripe pinning; more often stripes are believed to be dynamical objects. Indeed, the excitation spectrum of cuprates above some minimum energy  $\omega_0$  coincides with the excitation spectrum predicted by the stripe model even if static stripes are not detected [66]. The given  $\omega_0$  can be interpreted as the energy scale above which stripes look effectively static. Stripes are good candidates to disrupt the Fermi liquid ground state and be responsible for the peculiar properties of cuprates. Based on photoemission experiments [62, 67, 68], it has been proposed [69] that the Fermi surface has a dual nature: fluctuating stripes produce a blurred “holy cross” Fermi surface, see Figure 11(b), while low-energy quasiparticles average out the stripe fluctuations and hence propagate with long relaxation times along the nodes. In Figure 11(b), the two resulting structures are schematically shown; the Fermi surface is obtained from a calculation of static stripes on LSCO and has been artificially blurred to simulate the fluctuating character. This blurred FS coexists with the sharp FS due to nodal quasiparticles, indicated by the thin lines.

Another possible explanation of the anisotropy found for the scattering rates is that the Pomeranchuk Fermi surface modes have intrinsic long relaxation times, but the relaxation time along the antinodal direction becomes shorter because of scattering with stripe fluctuations which are known to be along the Cu–O bond. In this scenario, when the electric field is on the diagonals, the slowly relaxing nodal states are excited, but when the electric field is parallel to the Cu–O bond, internal excitations of the stripe are produced and relax fast due to electron-electron scattering and strong coupling to the lattice. This is consistent with the observation by photoemission that antinodal carriers (charges along the Cu–O bond) are strongly coupled to out-of-plane phonon modes of the oxygen ions. In fact, in diffraction, this would result in a faster decay of the Debye-Waller factor when more charges are involved along the Cu–O direction.

We now discuss the mechanism by which the Pomeranchuk modes are excited. This mechanism must necessarily involve more than one photon since single photon absorption is described by linear response theory where the response along the diagonals can be simply decomposed in the sum of the responses along the bonds. The possible path that would excite the Pomeranchuk modes is depicted in Figure 11(a), a sort of Raman or two-step process. First a photon is absorbed by a dipole-allowed transition. At a latter time another photon is emitted leaving the system in one of the two possible excited states with different lifetimes. This scenario would require the presence of resonant absorption states around the laser excitation energy (1.5 eV), as the triplet structure observed in the pair-breaking spectroscopy on YBCO sample, for example [70]; however, a thorough assignment of the absorption features in different cuprates optical spectra is difficult and still underway, as we discuss below. Dynamic stripes may be involved in this process too since their anisotropic character makes them couple well to the Pomeranchuk modes. For this to be possible there should be a stripe absorption mode at the energy of the incoming

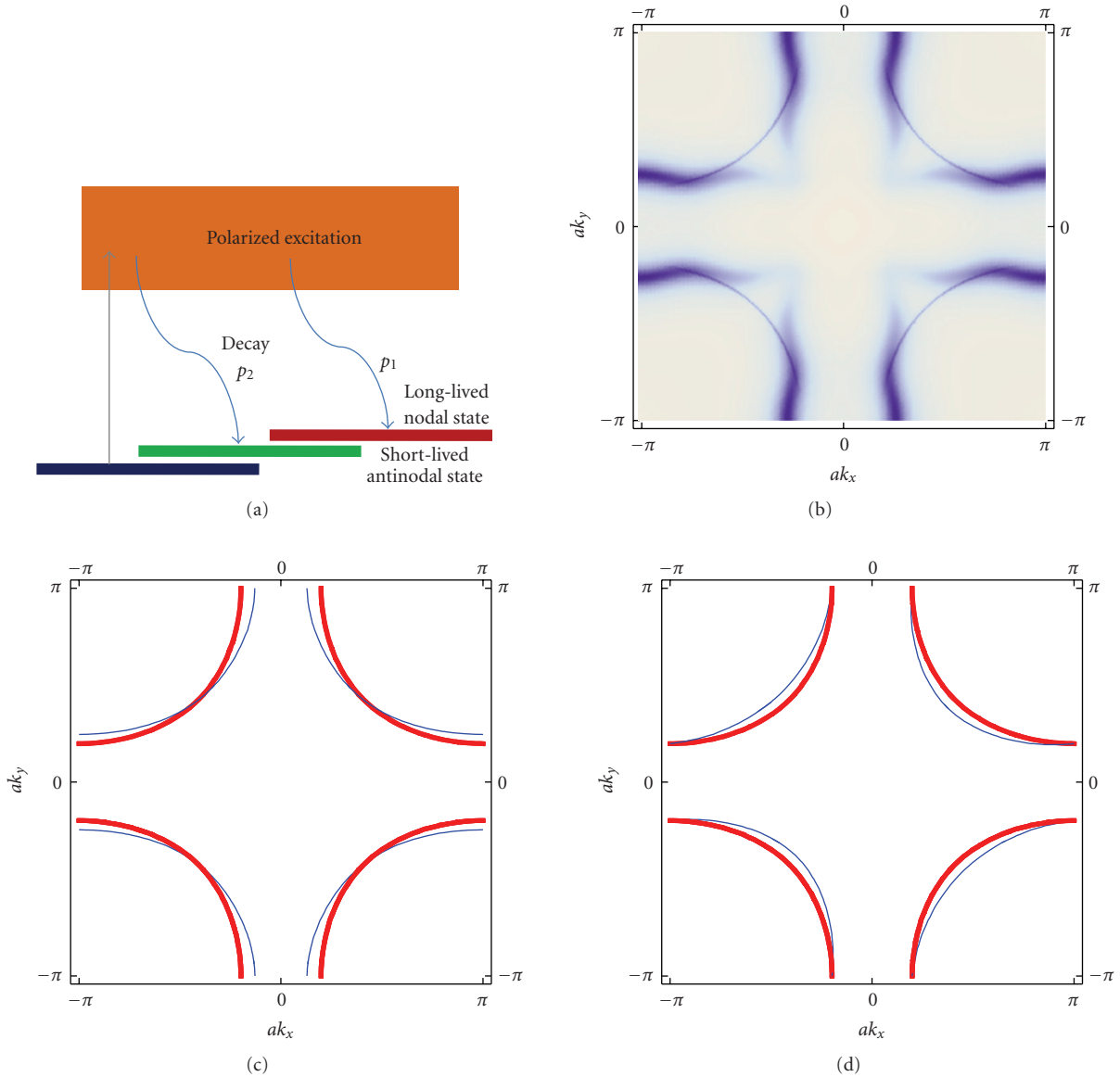


FIGURE 11: Excitation scheme and Fermi surface. (a) Possible excitation scheme of different Pomeranchuk modes. (b) Fermi surface predicted for cuprates. The cross-like blurred feature is the FS of the stripes, while the nodal arcs are the FS of nodal particles observed in ARPES. (c) Possible Pomeranchuk modes excited by the laser for the electric field in the antinodal direction and (d) The electric field in the nodal direction. The blue line is the equilibrium Fermi surface while the red lines show the out-of-equilibrium Fermi surface after the laser excitation.

photon. In order to substantiate this view, we present in what follows computations of the optical absorption of the stripes relevant for the first step of the process and compare with experimental results.

The in-plane optical absorption of different cuprates superconductors (Bi2212, Bi2223, and LSCO) is displayed in Figure 12. In Figure 12(b), the spectrum at different temperatures for Bi2223. A large metallic component is found at low frequency, often referred to as the Drude peak [14]. Most of the temperature dependence is observed in this part of the spectrum, and in the inset of Figure 12(b), one can see the effect of the opening of the superconducting gap below 100 meV in the optical spectrum. At higher energy, above

the plasma edge of the material ( $>1$  eV), several absorption features are observed. In Figure 12(b), the spectrum is decomposed into different components by a standard Drude-Lorentz fit, and one can see that a feature centered around 1.8–2 eV is obtained (evidenced by a blue trace). This absorption is often ascribed to a charge-transfer excitation between Cu and O ions in the  $ab$ -plane of the material, but in BSCCO, its assignment is complicated by the presence of other strong interband transition in that spectral region. However, since the electronic states close to the Fermi energy in all cuprates are Cu  $3d_{x^2-y^2}$  orbitals hybridized with O  $2p$  orbitals, most of the temperature dependence is expected to be found in spectroscopic features associated with these orbitals.

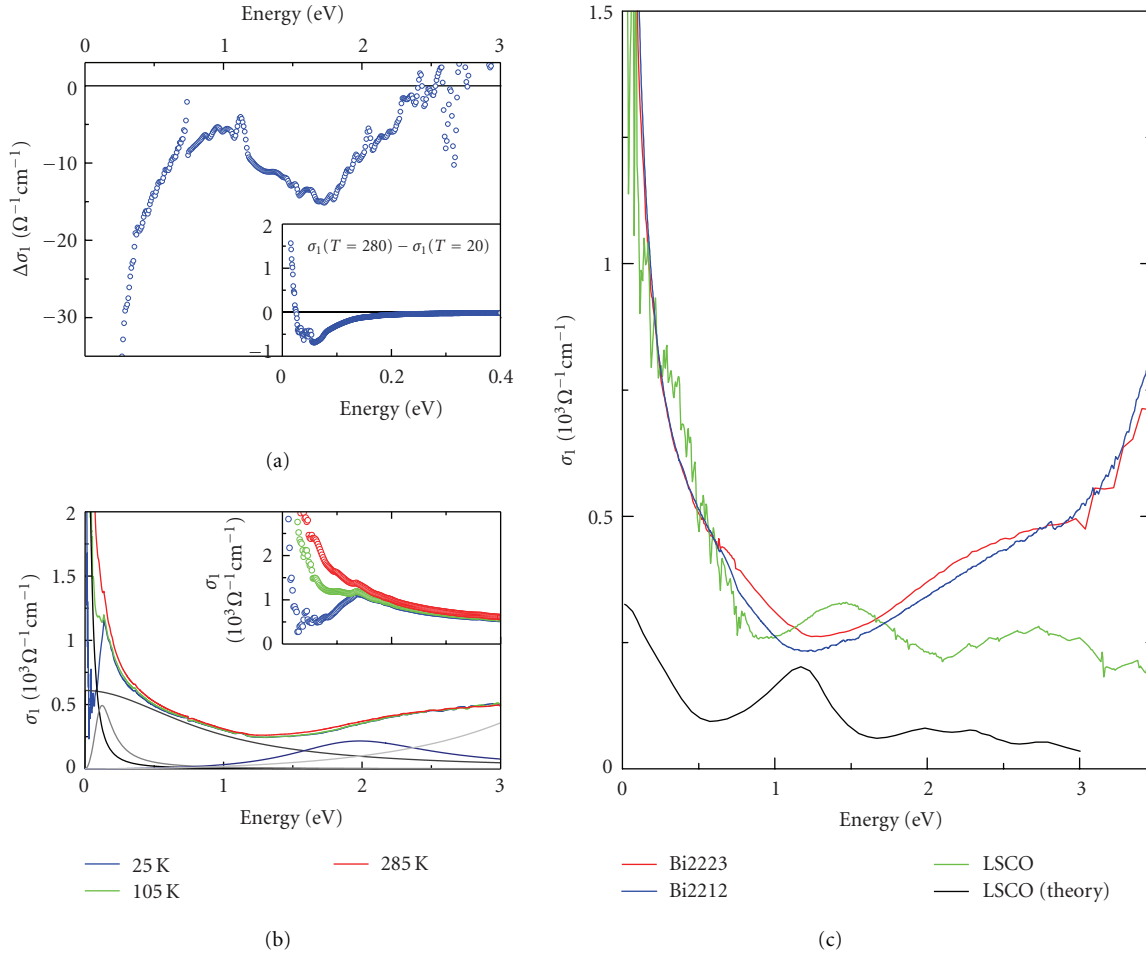


FIGURE 12: BSCCO and LCO optical spectra and temperature dependence. (a) The difference spectrum  $\sigma_1(T = 280) - \sigma_1(T = 20)$  for Bi2223 is displayed; the low-energy region is magnified in the inset. (b) The optical conductivity of Bi2223 at different temperatures is shown together with a Drude-Lorentz decomposition of the spectrum; the low-energy region is magnified in the inset. (c) The optical conductivity of different cuprates is shown for comparison, together with the theoretical spectrum obtained in LCO by the charge-stripes model.

In Figure 12(a), the difference between spectra at different temperatures ( $T = 280\text{ K} - T = 20\text{ K}$ ) is noted to be large in the Drude region of the metallic carriers (inset of Figure 12(a)), and peaks in correspondence to the charge-transfer peak around 2 eV. These features are quite common to cuprates. The reason is that the low-energy electronic structure of these materials is dominated by the physics of the Cu–O plaquettes, which are common features of high-temperature superconductors. To emphasize this point, we display, in Figure 12(c), the spectra of different chemical compositions, Bi2212, Bi2223, and LaSrCuO. The overall shape of the spectrum is similar in all cases, and the first absorption feature above the plasma edge is always attributed to Cu–O charge-transfer excitations.

LSCO is an ideal material for the theoretical investigation of the optical spectrum, because it has a single Cu–O layer per unit cell and its overall crystal structure is among the simplest of all cuprates. Also, experimental evidence of stripes has been reported in this material [17]. In Figure 12(c), we show the comparison between the theoretical optical absorption spectrum of LSCO based on the metallic stripes model

and the experimental one. The main features of the spectrum are reproduced by theory, and the 1.2–1.5 eV absorption feature is assigned to a charge-transfer mode inside the stripe, which again involves the motion of a charge along the Cu–O bond. This is expected to be the mode responsible for the first step of the Raman process. We investigated LSCO because of the good success of these calculations in reproducing the optical spectrum of the material, because of its inherently simpler structure. We expect the situation in BSCCO to be not very different, again because we focus on features mainly related to the Cu–O plane.

In BSCCO and LSCO cuprates, the in-plane linear optical absorption of light can be considered as nearly isotropic [14, 71]. Our observation of an anisotropic structural dynamics as a result of light excitation polarized in different directions within the plane suggests that the out-of-equilibrium electronic structure is capable, during its thermalization, to induce distinct structural changes which distort the lattice in a way that is observable at longer times. According to our computations [66], when the electric field is parallel to the Cu–O bond, the 1.5 eV polarized

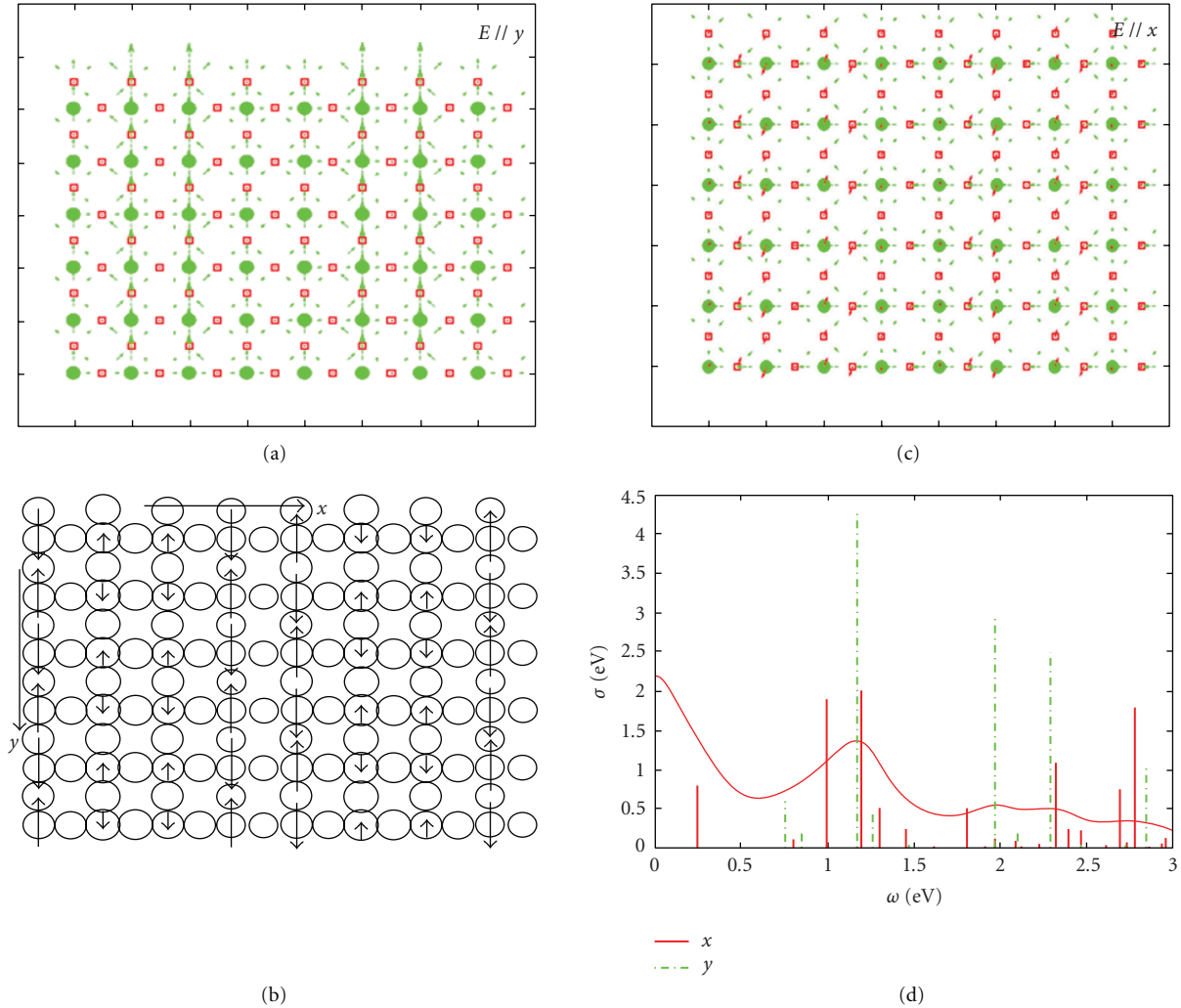


FIGURE 13: Theoretical description of the optical excitation. (a) Symmetry of charge excitation for 1.2 eV light polarized along the direction of the charge stripes ( $y$ , see Figure 13(b)). (b) The charge distribution inferred by the stripes model in LCO. (c) Symmetry of charge excitation for 1.2 eV light polarized perpendicular to the direction of the charge stripes ( $x$ , see Figure 13(b)). (d) Theoretically derived optical conductivity spectrum in LCO.

light couples strongly with the stripe excitation. In Figures 13(a) and 13(c), the charge variation induced by 1.2 eV light polarized parallel (Figure 13(a)) and perpendicular (Figure 13(c)) to the charge stripe is shown. The red arrows indicate charge increase (up arrow) or charge decrease (down arrow) in a certain area, whereas the green arrows indicate the current induced by light absorption. When light is polarized perpendicular to the stripes (which would correspond to one of the two directions of Cu–O bonds, (10), e.g.), a charge-transfer mode within the stripe is excited. This is visible as red arrows in Figure 13(c) indicating a charge increase on the oxygen site and a charge decrease on the neighboring copper site.

When light is polarized parallel to the charge stripe (along the other Cu–O direction, (01), e.g.), no such charge transfer is observed. For light polarized at 45 degrees, we expect that the nodal quasiparticles are excited through other intermediate states (note that they are not considered in the present calculations for technical reasons) and long

relaxations times are found. In Bi2223, where the anisotropy of the electron-phonon coupling was found to be much weaker, a weaker stripe charge ordering may be present due to the different doping of the layers and the increased three-dimensional properties of the system. It would be interesting to study in more detail the doping and temperature dependence of the anisotropy to verify if there is a precise point in the temperature-doping plane where a Pomeranchuk instability manifests as a divergence of the relaxation time or if the phenomenon is more related to stripe physics. Another important check would be to study the dependence of the result on the laser excitation energy to verify the importance of the 1.2–1.5 eV stripe absorption band.

**3.5. Nonequilibrium Phase Transitions in LCO: The Structural Isosbestic Point.** As discussed above, charge-transfer excitations can play a crucial role in the dynamics of cuprates. In  $\text{La}_2\text{CuO}_4$ , manifestations of structural dynamics can be observed when the electrostatic imbalance induced

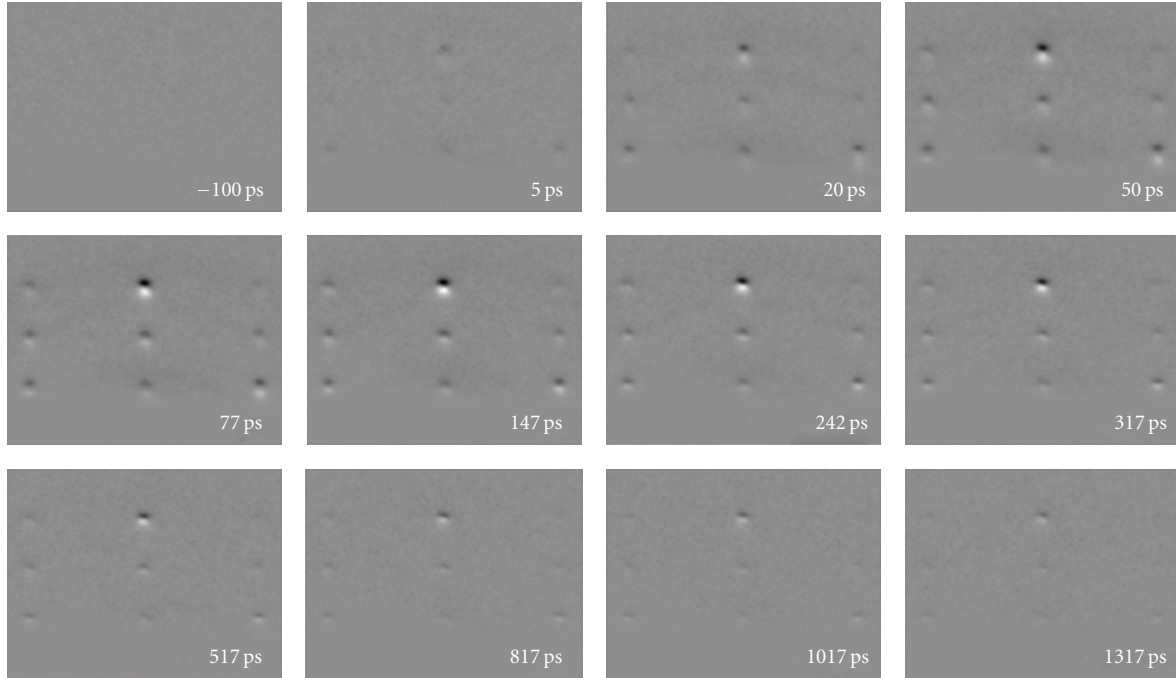


FIGURE 14: LCO dynamical diffraction pattern. The effect of laser excitation on the diffraction pattern is shown by displaying diffraction difference frames at different times after the arrival of the laser pulse. These frames were obtained by referencing diffraction patterns at each time delay to a negative-time frame by subtraction. Bright regions indicate positive intensity and dark regions show the negative intensity. Laser excitation results in a movement of the Bragg spot profiles along the  $c$ -axis direction to lower momentum transfer values. The laser-induced changes reach a maximum around  $\sim 120$  ps and relax back to equilibrium on longer time scale (1 ns). These patterns were obtained at room temperature for a laser fluence of  $20.6 \text{ mJ}/\text{cm}^2$ .

by charge-transfer excitations causes lattice changes in the direction perpendicular to the Cu–O planes.

The dynamical behavior of LCO structure is displayed in Figure 14. Here, shown are the time resolved diffraction difference images at room temperature, displaying the changes induced by the excitation pulse with a fluence of  $20.6 \text{ mJ}/\text{cm}^2$ . These frames were obtained at the specified times and referenced, by subtraction, to a frame at negative time. White regions indicate intensity increase, while dark regions relate to intensity decrease. After the excitation, Bragg spots move down vertically, as evidenced by the appearance of white spots below dark regions in the difference frames. No substantial movement is observed along the horizontal direction. The changes are maximized around  $\sim 120$  ps and relax on a longer time scale ( $\sim 1$  ns).

In Figure 15, the profiles of the 0010 and 008 Bragg spots along the  $c$ -axis direction are shown at different times after the laser excitation (in this probing geometry, 006 is not shown since it shifts below the shadow edge at 112 ps and partially disappears for geometrical reasons). Before the laser excitation, both Bragg spots are centered at the equilibrium values, but at 112 ps after the excitation, they are centered at smaller  $s$  values (upper curves in Figure 15(a) show  $\Delta s/s = -2.5\%$  for a fluence of  $20.6 \text{ mJ}/\text{cm}^2$ ). In between these two time frames, the evolution of the Bragg spot profiles is not a continuous shift of its center position.

Rather, all the curves obtained at different time delays cross at a certain  $s$  value. Furthermore, the total intensity

underneath each Bragg spot stays constant within 2%-3% during the entire time scale of the experiment. This behavior is very different from all other studied materials, and from that of BSCCO as well. In GaAs [72], for example, the center position of the Bragg peaks shifts continuously to a lower momentum transfer value, indicating a continuous expansion along the surface normal direction, and the total intensity underneath the profiles decreases because of the Debye-Waller effect. In BSCCO samples [23], the very large value of the  $c$ -axis, and the presence of a heavy element like bismuth, causes the diffraction to be of a rod-like shape, preventing careful analysis of the position changes. However, the main effect of light excitation was found to be the Debye-Waller decrease of the diffraction intensity. In LCO, electrons probe the specimen in transmission at a lower scattering vector with respect to the experiments on BSCCO, giving a smaller Debye-Waller effect, according to (1). Also, the temperature jump induced by pump pulses in LCO is significantly smaller than in BSCCO, again limiting the magnitude of the average atomic displacement. These facts, together with the nanometric size of the probed domains, could play a role in reducing the Debye-Waller effect below our observation capabilities.

The conservation of the total intensity and the existence of a crossing point (as clearly seen in Figures 15(a) and 16(a)) are not consistent with a continuous expansion; it rather indicates a direct population transfer between two phases of the lattice with different  $c$ -axis constants. Such a

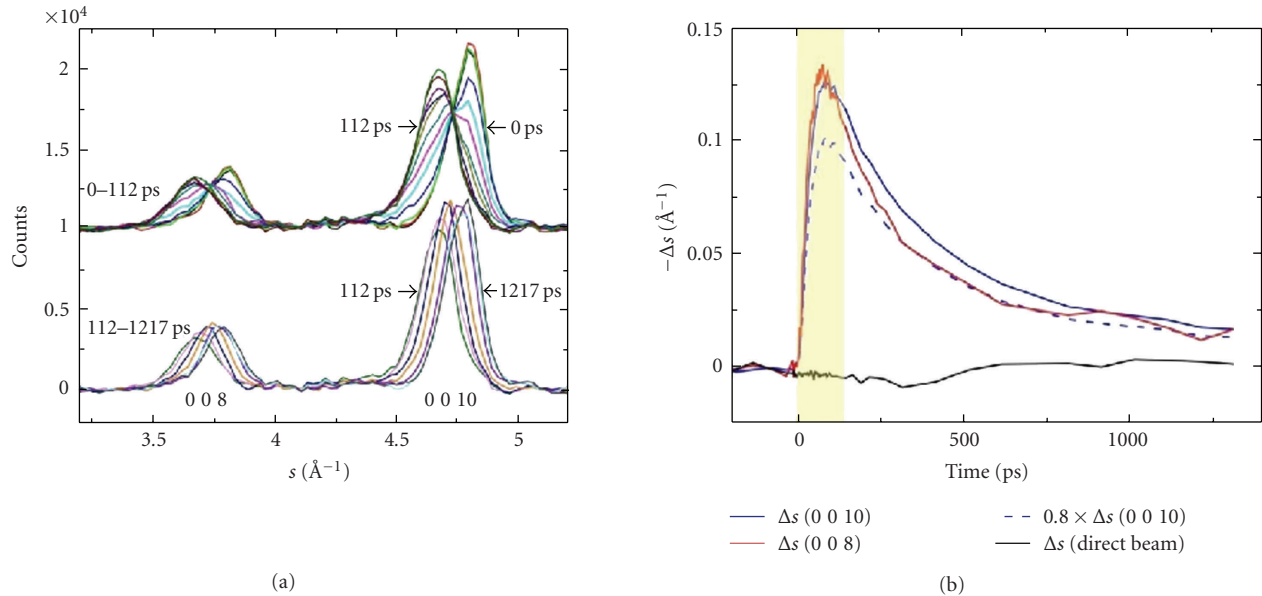


FIGURE 15: Bragg peak position shift and scaling of different orders. Detailed analysis of the photo-induced changes of the Bragg peaks for the pattern shown in Figure 6. (a) the profiles of the 008 and 0010 Bragg spots are shown at selected time delays. The profiles for time delays between 0 and 112 ps are displaced vertically for clarity. The time delays for the curves displayed in the top panel are  $t = -233, -33, -4, 8, 20, 32, 44, 56, 68, 80, 92,$  and 112 ps, for the curves in the bottom panel  $t = 112, 147, 217, 317, 617, 917,$  and 1217 ps. For the curves in the top panel, a structural isosbestic point can be seen for both Bragg spots (see text). The curves in the bottom do not cross; the center positions of the Bragg spots shift back to equilibrium continuously. (b) the relative changes of the center positions of 0010 (blue) and 008 (red) Bragg spots and direct electron beam (black) are plotted as a function of time. The center positions are obtained by fitting the curves in (a) to a single Gaussian form. The fit to such function is good except for the region shown by a transparent yellow strip during which a single Gaussian cannot describe the profiles since at least two structural phases coexist. We also plot the shift of the 0010 Bragg spot (blue curve) scaled by %80 as the dashed blue curve. The agreement between this and the red curve is consistent with a true structural change in which the shifts of the Bragg peaks scale proportionally to the order numbers since  $\Delta s/s = -\Delta c/c$ . Furthermore, no substantial movement of the direct beam is observed, indicating that the observed effects cannot be coming from shifting of the entire pattern.

crossing behavior in optical absorption spectroscopy would be termed “isosbestic point,” corresponding to the spectral position where the two interconverting species have equal absorbance; regardless of the populations of the two states, the total absorption at the isosbestic point does not change if the total concentration is fixed. In the present case, we term this point as “structural isosbestic point,” corresponding to the point in the momentum space where the two structures are contributing equally to the diffraction intensity.

The relaxation process back to the equilibrium value of this new phase follows a different dynamic. The lower trace of Figure 15(a) shows the evolution of the Bragg spot profiles between 112 ps and 1217 ps. In this period, no crossing point is observed and the center of the Bragg spot shifts continuously back to the equilibrium value. The time scale of the return to equilibrium is also slower by about an order of magnitude (about 300 ps as opposed to 30 ps).

Structural distortions give changes in diffraction obeying the scaling relation in (2). We test this scaling relation, as well as the presence of spurious motions of the electron beam, in order to verify that the observed dynamics originate from atomic motions.

In Figure 15(b), we compare the relative changes in the position of 008 and 0010 Bragg spots. We also plot the change in the position of the undiffracted direct beam. The center

position of each spot is obtained by fitting the vertical profile into a Gaussian form. Between 0–112 ps, the Bragg spots cannot be described by a single Gaussian curve since more than one phase with distinct structural parameters coexist. In this time period (shown by a transparent yellow strip), a fit to a single Gaussian cannot adequately describe the profiles. Outside this region, a single Gaussian can fit the data properly.

Since the direct beam position does not change with time, we excluded the possibility that the observed behavior comes from the shift of the entire pattern or that surface charging is contributing to the diffraction. Moreover, for the structure, the change in different orders should scale according to the order number, that is,  $\Delta s/s = -\Delta c/c$ , where  $\Delta s$  is the shift of the  $n$ th-order Bragg spot (as was verified for BSCCO as well). This means that the 008 Bragg spot should move only by 80% of the 0010 Bragg spot. The dashed blue curve in Figure 15(b) shows the shift of the 0010 Bragg spot scaled by 80%. Furthermore, the agreement between this and the shift of 008 spot (red curve) confirms that the observed dynamics are due to real structural changes.

The dependence on the excitation density of the observed phase transition reveals detail of the interplay between the lattice and the electronic structure. In Figure 16(a), the generation of the new phase between 0 and 112 ps is depicted,

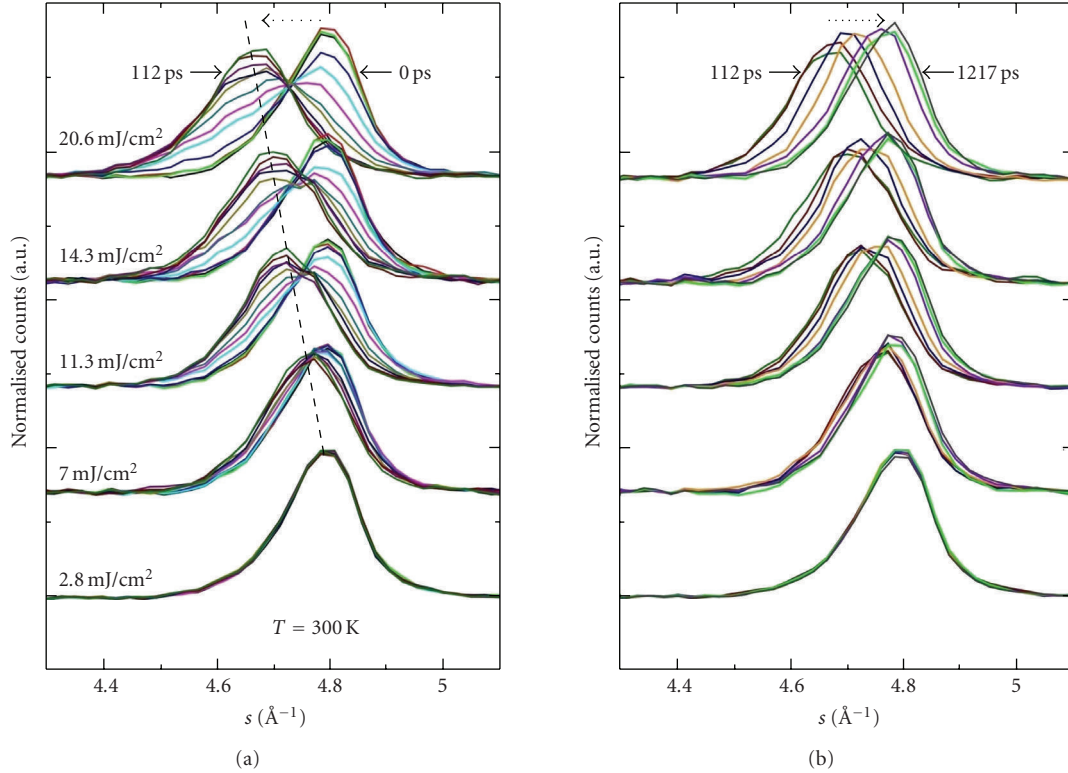


FIGURE 16: Structural isobestic point and fluence dependence. The Bragg spot profiles of the 0010 spot are shown at different delay times for five laser fluences (2.8, 7.0, 11.3, 14.3, and 20.6 mJ/cm<sup>2</sup>) at room temperature. The amplitude of the profiles is normalized by the height of the highest curve at each intensity, and curves at different fluences are displaced vertically for clarity. No laser-induced change can be observed at the lowest fluence (2.8 mJ/cm<sup>2</sup>). Above this fluence, transitions into a higher  $c$  axis constant state can be observed as evidenced by the existence of structural isobestic points. The change in the center position of the Bragg spot ( $\Delta s$ ) increases linearly with increasing intensity. (a) Phase transition region showing the times  $t = -233, -33, -4, 8, 20, 32, 44, 56, 68, 80, 92,$  and 112 ps. (b) Relaxation region showing the times  $t = 112, 147, 217, 317, 617, 917,$  and 1217 ps. Here, no crossing point is observed at any fluence; all the peaks relax back to equilibrium by continuously shifting their center positions.

whereas in Figure 16(b), we show the relaxation back to the ground state for different laser fluences at room temperature. First, we see that at 2.8 mJ/cm<sup>2</sup> there is no observable change. Above this intensity, there is a crossing point observed in Figure 16(a), whereas the peak position shifts continuously back to the equilibrium value in Figure 16(b). The maximum change in the position of the Bragg spot increases with increasing fluence (Figure 16(a)). The characteristic time of this process does not depend on the laser fluence and is  $\sim 30$  ps.

In Figure 17(b), the maximum  $c$ -axis expansion,  $\Delta c$ , obtained on the time scale indicated by the dotted line in Figure 17(a), is displayed as a function of laser fluence. These data are reported for two temperatures, 20 and 300 K, respectively. For these measurements, we have used a polarizer and a half-wave plate in order to be able to adjust the laser fluence in fine steps. This arrangement enabled us to change the laser fluence continuously without changing the spatial overlap or the relative arrival times of the laser and electron pulses. At each laser fluence, we obtain  $\Delta c$  by recording two profiles at times  $-85$  ps and 130 ps. Below a threshold intensity of  $\sim 5$  mJ/cm<sup>2</sup>, no change was

observed. Above this threshold intensity,  $\Delta c$  grows linearly with increasing fluence.

In order to better understand the microscopic meaning of this threshold fluence, we consider the number of photons absorbed per copper site for each fluence. The energy ( $u$ ) deposited into the cuprate film per unit volume for each pulse (in the surface region probed by the electron beam) is given by  $u = F_0(1-R)\alpha$ , where  $F_0$  is the incident laser fluence,  $R$  is the reflectivity of the cuprate film, and  $\alpha$  is the absorption coefficient of the film. The energy absorbed per unit cell ( $u_c$ ) is given by  $u_c = u \cdot v_c$ , where  $v_c$  is the volume of the unit cell. The number of photons absorbed per copper site ( $\delta_p$ ) can be calculated by dividing the energy absorbed per unit cell by the energy of each photon ( $\hbar\omega = 1.5$  eV), after taking into account that there are two copper atoms per unit cell, that is,  $\delta_p = F_0 v_c (1-R)\alpha / (2\hbar\omega)$ . Given the values of  $R = 0.1$ ,  $\alpha = 7 \times 10^4$  cm<sup>-1</sup> ( $R$  and  $\alpha$  were obtained from Figures 12 and 9 of [73], resp., measured for a similar sample), and  $v_c = a \times b \times c = 186.12$  Å<sup>3</sup>, we obtain  $\delta_p = F_0 \times (24.4$  cm<sup>2</sup>/J). Using this expression, the laser fluence can be converted into the number of photons absorbed per copper site, as shown in the top horizontal axis of Figure 17(b). It is intriguing that the

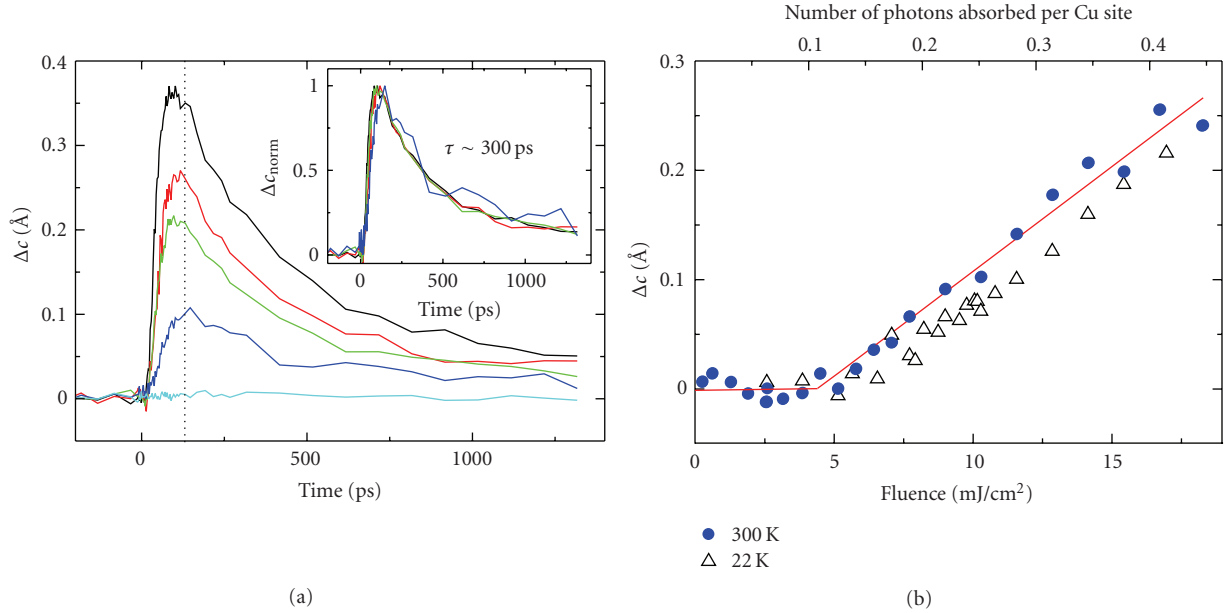


FIGURE 17: Fluence dependence of the expansion. (a) The change in the  $c$ -axis constant ( $\Delta c$ ) is plotted as a function of time for each laser fluence (2.8 (cyan), 7.0 (blue), 11.3 (green), 14.3 (red), and 20.6 mJ/cm<sup>2</sup> (black)). The  $c$ -axis lattice constant at each time delay was obtained by fitting the profiles in Figure 16 to a single Gaussian form. The inset shows the same curves normalized.  $\Delta c$  relaxes back to ground state with a time constant of about 300 ps independent of the laser fluence. Even after 1 ns, the system does not completely relax back to equilibrium; a small residual expansion is present and has a much longer time constant. (b)  $\Delta c$  (130 ps) around the dotted line shown in (a) was measured as a function of laser fluence at both 20 K and 300 K. Below a threshold intensity of about  $\sim 5$  mJ/cm<sup>2</sup>, no change can be observed. Above this threshold,  $\Delta c$  grows linearly with the laser fluence. The top horizontal scale shows the number of photons absorbed per copper site calculated using the absorption coefficient (see text). The threshold fluence corresponds to  $\sim 0.1$  photons absorbed per copper site. The red line is a linear fit to room temperature data above the threshold value.

threshold intensity corresponds to  $\sim 0.1$  photons absorbed per copper site. This is very close to the number of chemically doped carriers needed to induce superconductivity.

As far as the temperature dependance is concerned, only a slight increase in the rise time can be seen as the sample is cooled down, similar to what was observed also in BSCCO.

### 3.6. Theoretical Modeling of the Light-Doped Phase Transition.

The structural dynamics observed in the cuprate film show several distinct features which need to be addressed by a theoretical model. These are a large increase of the  $c$ -axis constant, the existence of a structural isosbestic point at intermediate times, a continuous shifting of the Bragg spot profiles in the relaxation regime, and the existence of a threshold fluence and a linear dependence of the expansion on the laser fluence above this threshold. Furthermore, the characteristic timescales involved (30 ps for the onset and 300 ps for the relaxation) do not strongly depend on temperature and fluence. Below, we will present a simple energy landscape model that can account for these findings.

**3.6.1. Thermal Expansion Model.** A simple thermal expansion mechanism cannot explain the experimental observations for three reasons. First, a 2.5% increase in the  $c$ -axis lattice constant would correspond to an unphysical 2500 K rise in the lattice temperature, since the linear thermal expansion is  $\alpha_l \leq 1.0 \times 10^{-5} \text{ K}^{-1}$  [74]. Second, in the thermal expansion

scenario, the total intensity underneath a Bragg spot is expected to decrease due to the Debye-Waller effect, caused by the phonon generation following the photoexcitation, whereas in our case the total integrated intensity underneath a Bragg spot is found to be nearly constant. Finally, the thermal expansion model would predict a monotonic shift of the Bragg spots into lower momentum transfer values, whereas we observe a crossing point that can not be explained by a continuous increase of the interplanar distance.

### 3.6.2. Structural Changes and the In-Plane Charge Transfer.

Some absorption characteristics are worth considering. The substrate (LaAlSrO<sub>4</sub>) does not absorb at our laser wavelength of 800 nm. The penetration depth of the laser beam in the cuprate film was estimated to be 143 nm, given the absorption coefficient of  $\alpha = 7 \times 10^4 \text{ cm}^{-1}$  [73]. The electron beam is at a grazing incidence angle of  $1.5^\circ$ , and due to the small mean-free path of the high-energy electrons, and the low incidence angle, only the top few nm of the 52 nm thick film can be probed. Therefore, only the cuprate film can contribute to the dynamics, and the substrate is not expected to have any direct role.

As shown in a previous section, a charge transfer excitation in cuprates is expected around 2 eV. This excitation involves a charge transfer from the  $2p$  orbital of oxygen into the  $3d$  orbital of copper [14]. Our excitation energy (1.55 eV) falls in the proximity of such charge transfer. It should be

noted, however, that this assumption is model-dependent since a consensus has not been reached yet on the assignment of the different absorption features in cuprates.

LCO is a highly ionic compound with a large cohesive energy. As a result of a charge transfer excitation, and subsequent changes in the valency of the in-plane copper and oxygen, a weakening of the coulomb attraction between the planes is induced, which leads to expansion. In the experiment, we observe that almost the entire Bragg spot, and not a fraction of it, undergoes the change, indicating that macroscopic scale domains (which define the coherence length of the Bragg diffraction) are involved in this phase transformation. Above a certain fluence, charge transfer excitations are shared among multiple unit cells, and macroscopically sized domains are created with distinct electronic and structural properties.

**3.6.3. Cohesion Energy Calculations.** In order to quantitatively describe the effect of the in-plane charge transfer on the lattice structure, we calculated the cohesion energy as a function of structural parameters both in the ground and in the charge transfer state; we will refer to the latter as the excited state. In order to model the excited state at each fluence, we calculated the number of photons absorbed per copper atom ( $\delta_p$ ) as displayed on the top scale of Figure 17(b) by using the absorption coefficient and the carefully measured laser fluence. When the charge transfer excitations are shared uniformly across the Cu–O planes, the valence of in-plane Cu atom changes from +2 to  $+2 - \delta_p$ , and the valence of oxygen changes from  $-2$  to  $-2 + \delta_p/2$ . We then calculate the cohesion energy as a function of the structural parameters for each value of  $\delta_p$ , and find the values of these parameters that minimize its energy (Figure 18). Below we will describe the results of two independent calculations.

In the first of these calculations, we used the model of Piveteau and Noguera [75] to compute the cohesion energy. It was originally used to reproduce the structural parameters of LCO at equilibrium. The cohesion energy is expressed as the sum of pair wise interaction between the atoms, taking into account three microscopic terms: the direct Coulomb interaction treated in the point charge approximation, a hard-core repulsion of the Born-Mayer type, accounting for the orthogonality of the atomic orbitals on different atoms at short distances, and the van der Waals term. The interaction energy ( $E_{ij}$ ), of two atoms  $i$  and  $j$ , having charges  $Q_i$  and  $Q_j$  at a distance  $R_{ij}$  is given by

$$E_{ij} = \frac{Q_i Q_j}{R_{ij}} + B_{ij} \exp\left(-\frac{R_{ij}}{\rho_{ij}}\right) - \frac{C_{ij}}{R_{ij}^6}. \quad (8)$$

This expression contains three sets of parameters ( $B_{ij}$ ,  $C_{ij}$ , and  $\rho_{ij}$ ) which are obtained from the atomic values ( $B_{ii}$ ,  $C_{ii}$ , and  $\rho_{ii}$ ), using the following empirical expressions:  $B_{ij} = (B_{ii} B_{jj})^{1/2}$ ,  $C_{ij} = (C_{ii} C_{jj})^{1/2}$ ,  $2/\rho_{ij} = 1/\rho_{ii} + 1/\rho_{jj}$ . These expressions are based on the fact that the van der Waals interactions are related to the product of the atomic polarizabilities, and the hard-core repulsion involves a product of exponentially decreasing atomic wave functions. In our calculation, we used the same parameters that were

invoked in order to reproduce the equilibrium structure [75]. In order to obtain these parameters, Piveteau and Noguera used the nine atomic values ( $B_{ii}$ ,  $C_{ii}$ ,  $\rho_{ii}$ ) for  $\text{Cu}^{2+}$ ,  $\text{O}^{2-}$ , and  $\text{La}^{3+}$  from the literature [76], and adjusted them in such a way that they reproduced the more simple structures of CuO and  $\text{La}_2\text{O}_3$ .

The total internal energy of the crystal ( $E_T$ ) was obtained by summing the internal energy ( $E_P$ ) of the units (defined below) of  $\text{La}_2\text{CuO}_4$ , and the interaction energy  $E_{PQ}$  between two units  $P$  and  $Q$  as

$$E_P = \frac{1}{2} \sum_{i,j} E_{ij} \quad (i \in P, j \in P, i \neq j), \quad (9)$$

$$E_{PQ} = \sum_{i,j} E_{ij} \quad (i \in P, j \in Q). \quad (10)$$

The total internal energy of  $N$  units is given by

$$E_T = \sum_P E_P + \frac{1}{2} \sum_{P,Q} E_{PQ} \quad (P \neq Q), \quad (11)$$

where the sums go over  $N$  units. The energy per unit ( $E$ ) is given by

$$E = \frac{E_T}{N} = E_{P_0} + \frac{1}{2} \sum_{Q(\neq P_0)} E_{P_0 Q}, \quad (12)$$

where  $P_0$  denotes any central unit.

For rapid convergence, we grouped the atoms into elementary units without dipolar moments [75], as shown in Figure 18(a). It includes a  $\text{CuO}_6$  octahedron and two La atoms. The oxygen atoms in the  $\text{CuO}_2$  planes are labeled as O(2) and out-of-plane oxygen atoms are labeled as O(1). The O(2) atoms are counted as 1/2 in the summations, since they are shared by two units.  $\text{La}_2\text{CuO}_4$  in the tetragonal structure can be described by four structural parameters: the distance between  $\text{CuO}_2$  planes ( $c/2$ ), Cu–O(1) distance ( $d_1$ ), the Cu–O(2) distance ( $d_2$ ), and the Cu–La distance ( $d_3$ ). We calculated the internal energy per elementary unit as a function of these four parameters  $E(c, d_1, d_2, d_3)$  by summing up  $\sim 40,000$  interactions. The minimum value was found to be  $E(c = 13.1315 \text{ \AA}, d_1 = 2.4004 \text{ \AA}, d_2 = 1.897 \text{ \AA}, d_3 = 4.7694 \text{ \AA}) = -173.8462 \text{ eV}$ . These values are in very good agreement with the results of Piveteau and Noguera  $E(c = 13.15 \text{ \AA}, d_1 = 2.399 \text{ \AA}, d_2 = 1.897 \text{ \AA}, d_3 = 4.7780 \text{ \AA}) = -173.83 \text{ eV}$ .

The effect of inplane charge transfer was accounted for in the following way. We assumed that the excitations are shared uniformly to create domains of modified valencies of Cu and O(2) atoms in the  $\text{CuO}_2$  planes. If the number of photons absorbed per Cu atom is  $\delta_p$ , then the valencies of Cu atoms are changed from +2 to  $+2 - \delta_p$ , and the valencies of O(2) atoms are changed from  $-2$  to  $-2 + \delta_p/2$ . The valencies of O(1) and La atoms remain unchanged. Because the cuprate film is epitaxially grown on the substrate, there cannot be any change of inplane structural parameters, since they are anchored by the underlying substrate (as confirmed experimentally). Therefore, we assume that the value of the in-plane Cu–O(1) distance  $d_2$  can not change during the

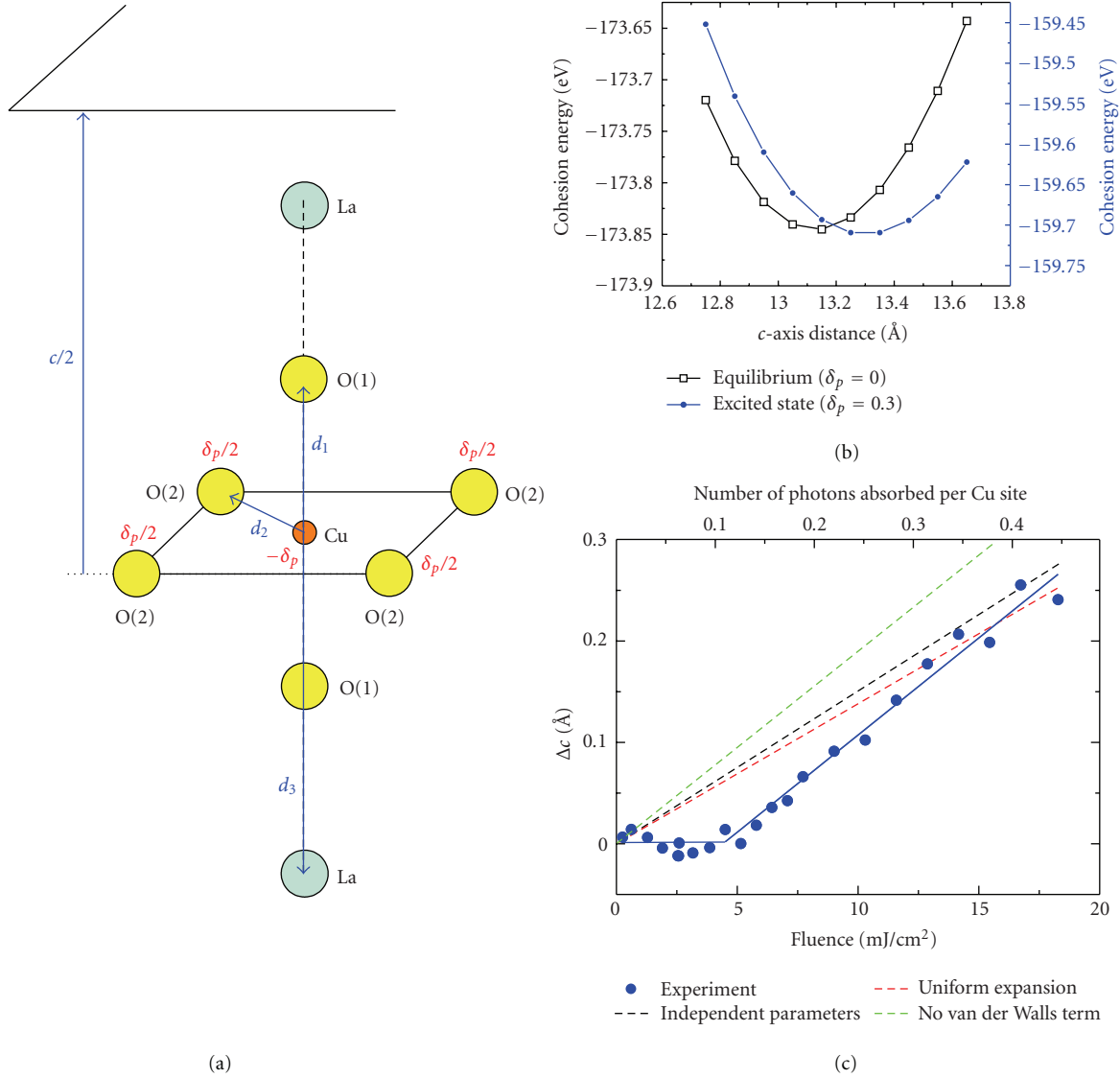


FIGURE 18: Cohesion energy calculations. (a) An elementary unit of  $\text{La}_2\text{CuO}_4$  in the tetragonal structure that includes a  $\text{CuO}_6$  octahedron and two La atoms is shown. The oxygen atoms in the  $\text{CuO}_2$  planes are labeled as O(2), and out-of plane oxygen atoms are labeled as O(1). O(2) atoms are counted as 1/2 in the summations, since they are shared by two units.  $\text{La}_2\text{CuO}_4$  in the tetragonal structure can be described by four structural parameters; distance between  $\text{CuO}_2$  planes ( $c/2$ ), Cu–O(1) distance ( $d_1$ ), Cu–O(2) distance ( $d_2$ ), and Cu–La distance ( $d_3$ ). In the excited state, the valence of a Cu atom is decreased by  $\delta_p$ , and the valence of an O(2) atom is increased by  $\delta_p/2$ , where  $\delta_p$  is the number of photons absorbed per copper atom. (b) Calculated cohesion energy as a function of the  $c$ -axis constant in the ground ( $\delta_p = 0$ ) and excited states with  $\delta_p = 0.3$  assuming a uniform expansion along the  $c$ -axis direction. Calculated cohesion energy in the excited state is accurate up to an overall constant. (c) Comparison of the calculated  $\Delta c$  using different methods with the experiment (blue points). The dashed green line is the result of the calculation without considering the van der Waals interactions; dashed red and black lines are the calculated  $\Delta c$  after taking van der Waals interaction into account and assuming uniform expansion or independently variable parameters, respectively (see text). All of the calculations reproduce the magnitude of the observed expansion remarkably well.

time-resolved measurements and is fixed at its equilibrium value of  $1.897$  Å.

For a given  $\delta_p$ , we search for the parameters ( $c, d_1, d_3$ ) that minimize the energy per elementary unit  $E(c, d_1, d_2 = 1.897 \text{ Å}, d_3, \delta_p)$  using two different methods. In the first method, we assume that only a uniform stretching of the unit cell can take place in the  $c$ -axis direction. We search for the minimum energy configuration by varying  $c$ ,  $d_1$ , and

$d_3$  proportionally. In Figure 18(b), we present the calculated cohesion energy as a function of the  $c$  axis constant for the ground state ( $\delta_p = 0$ ), and excited state with  $\delta_p = 0.3$ . The absolute value of the cohesion energy in the excited state is correct up to an overall constant because of the uncertainties in the electronegativity and ionization energy of copper and oxygen, respectively. The dashed red curve in Figure 18(c) shows the calculated  $\Delta c$  as a function of  $\delta_p$ . In the second

method, we calculate  $\Delta c$  (dashed black curve in Figure 18(c)) by allowing the structural parameters ( $c, d_1, d_3$ ) to change independently.

Besides the calculation mentioned above, independent calculations were performed by our collaborators [77], which ignore the relatively small van der Waals contribution and uses a somewhat different parameters ( $B_{ij}, C_{ij}$ ). (We thank Z. Radovic and N. Bozovic at BNL for performing the cohesive energy calculations that ignore the relatively small van der Waals contribution.) The cohesion energy was written as the sum of the Madelung energy and the core repulsion energy. The standard Born-Meier form of  $B_{ij} \cdot \exp(-R_{ij}/\rho_{ij})$  was used in order to model the core repulsion energy, where the indexes  $i$  and  $j$  enumerate the relevant nearest neighbour pairs (O–O, Cu–O, and La–O). The constants ( $B_{ij}, \rho_{ij}$ ) in the ground state ( $\delta_p = 0$ ) were first optimized by matching the experimentally determined equilibrium distances and the known lattice elastic constants with the minimum of the cohesion energy and the values of its derivatives. It was further assumed that, since the film is epitaxially constrained to the substrate in the horizontal direction, the in-plane lattice constants are fixed by the substrate and could not change, as observed in the experiment. Since there was no stress on the film surface, it can freely expand along the vertical direction (along the  $c$ -axis). For a given fluence (equivalent to  $\delta_p$ ), the cohesive energy  $E(\mathbf{r}_1, \dots, \mathbf{r}_N, \delta_p)$  was calculated as a function of the structural parameters, and the new crystal configuration is determined by minimizing the potential energy. We find that the new minimum of  $E(\mathbf{r}_1, \dots, \mathbf{r}_N, \delta_p)$  occurs at a higher  $c$ -axis constant, and  $\Delta c$  depends linearly on  $\delta_p$  as shown by the green line in Figure 18(c). The agreement between the slope of the green theoretical curve and the slope of experimental data (blue curve) is excellent.

Considering that all the parameters required for these calculations were obtained from equilibrium constants, and there were no adjustable parameters to model the time-resolved changes; cohesion energy calculations reproduce the experimentally observed trend remarkably well (Figure 18(c)). The inclusion of van der Waals term in the cohesion energy calculation and/or the usage of slightly different atomic constants ( $B_{ij}, C_{ij}, \rho_{ij}$ ) do not change the results significantly (about 20% change in the slope of  $\Delta c$  versus  $\delta_p$ ).

**3.6.4. The Energy Landscape.** Based on the above discussion, we can construct a descriptive energy landscape (see Figure 19). If we consider that multiple coordinates are involved, the observed time-resolved dynamic is the result of the trajectory of motion on this multidimensional energy landscape. In the simplest form, there are two main coordinates that we need to consider: the charge redistribution process in the  $\text{CuO}_2$  planes and the macroscopic structural change, mainly expansion along the  $c$ -axis.

After photoexcitation, the microscopic excitations are formed with no apparent delay. This represents the first step occurring on the ultrafast time scale and is shown in Figure 19 as the movement from the initial Franck-Condon region to the modified charge transfer state on the

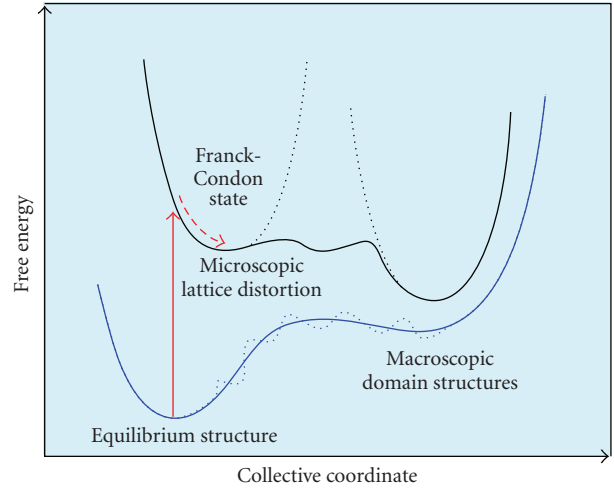


FIGURE 19: Energy landscape. A depiction of the excited state energy landscape is shown.

energy surface. This time scale is consistent with the direct movement along a potential energy surface. It is very likely that the initial fast relaxation observed in the time-resolved optical experiments in cuprates is in fact probing this initial step. The time scale for the generation of the macroscopic phase with a longer  $c$ -axis constant is  $\sim 30$  ps. This time is too long to be a direct motion along a repulsive potential energy surface. Instead, it involves a transition of a barrier-type crossing from the initial local minimum to the macroscopic minimum stabilized by the lattice relaxation. A well-defined crossing point also supports this argument. The existence of a structural isosbestic point shows that there is a direct population transfer between the two states which have two well-defined values of the  $c$ -axis constant. The values of the  $c$ -axis constants in between these two are not observed. This situation can happen if the system is crossing a hill in the potential energy surface during the motion between two local minima. The actual barrier crossing should be very fast, and most of the times it should be found in one of the valleys. The time scale is related to the height of the barrier. A sketch of the excited energy surface showing these initial motions is displayed in Figure 19.

In the relaxation regime, the  $c$ -axis constant decreases continuously with a very slow time constant of about 300 ps. This is too slow to be just a movement along an energy surface. It also cannot be explained by a single barrier crossing since we observe transition through all the  $c$ -axis constant values continuously. We should consider the fact that more than one local minimum state may exist as a result of a nonadiabatic “covalent-ionic” interactions between the excited states and ground state energy surfaces. As a result, this might produce a rough energy landscape consisting of small hills and valleys. The observed dynamics might reflect the motion of the system on this kind of an energy landscape.

Another way to understand the slow time scale is to consider the fact that electronic and structural relaxations are coupled. In order for the charges to fully recombine, the lattice has to relax as well, which naturally takes a long

time especially if the acoustic phonons are involved. The agreement between the observed 300 ps decay constant in our experiment and the decay time of long lived acoustic phonons seen by the time-resolved reflectivity experiments [78] also supports the involvement of acoustic degrees of freedom in the relaxation regime. We do not observe strong temperature dependence in this rate between room temperature and 20 K which is also consistent with a scenario dominated by acoustic phonons, as the Debye temperature for this material is 163 K [79]. The fact that the total intensity of the [0 0 10] Bragg spots does not change appreciably suggests that the modes involved are mostly in-plane phonons with vibrations orthogonal to the  $c$  axis direction.

#### 4. Conclusions

The observation of strong charge-lattice interaction in cuprates superconductors, in particular the interplay between the electronic excitations and the  $c$ -axis motion of the ions, suggests considerations beyond the standard 2D models [20, 80]. Recent theoretical work has incorporated lattice phonons in the  $t$ - $J$  model to account for the observed optical conductivity [81], and new analysis of the optical conductivity on a variety of samples confirmed the scenario of a strong coupling between a bosonic spectrum, consistent with a combination of phonon modes and magnetic excitations [82]. Moreover, new band structure calculations suggested that large and directional electron-phonon coupling can favor spin ordering [21]. The anisotropic coupling observed in BSCCO and the intermediate-to-high values of  $\lambda$  obtained imply that the time scale for the scattering of electrons by certain phonon modes can be very fast, comparable to that of spin exchange (40 fs in the undoped phase). As a result, both the magnetic interactions and lattice structural changes should be taken into account in the microscopic description of the pair formation.

In order to explain the microscopic origin of the anisotropy itself, we invoked the charge stripes model. In this model, the material has a non-Fermi liquid ground state consisting of ordered charges and spins along particular directions. It is shown that excitations of this ground state can be anisotropic with respect to light polarization, and that a particular charge transfer can be excited within the stripe domain when light is polarized along the Cu–O bond. The interplay between stripes and more conventional quasiparticles could be responsible for the observed anisotropy, as already suggested by photoemission data and theoretical considerations.

The nature of the observed anisotropy and the symmetry of the carriers involved also stress the importance of the interplay between the in-plane charge redistributions and the out-of-plane distortion of the unit cell. Another striking manifestation of this is the structural isosbestic point observed in LCO thin films. In this case, the charge-transfer nature of the optical excitation is used in order to explain, with success, a structural instability along the  $c$ -axis. Above a certain threshold, a direct conversion between two distinct structural phases of the lattice having different  $c$ -axis values was formed. The observed structural changes

can be explained by a model based on changes in the valencies of the in-plane oxygen and the copper which are caused by the charge transfer excitation. The amount of expansion in the  $c$ -axis constant can be correctly calculated by minimizing the cohesion energy as a function of structural parameters. The value of the threshold fluence corresponds to  $\sim 0.1$  photons per copper site, which is very close to the number of chemically doped holes required to induce superconductivity. Using the observed time constants and the sequence of distinct structural changes, we presented a picture of the energy landscape and the trajectory that is taken by the system.

#### Acknowledgments

This work was supported by the National Science Foundation and the Air Force Office of Scientific Research in the Gordon and Betty Moore Center for Physical Biology at Caltech. The authors acknowledge stimulating discussions with Professor Z. X. Shen, Professor A. Georges, Dr. Th. Jarlborg, Dr. A. Kuzmenko, Dr. E. Giannini, and Professor D. van der Marel. Dr. F. Carbone acknowledges the support from the Suisse National Science Foundation through an Ambizione grant.

#### References

- [1] A. Cho, “High  $T_c$ : the mystery that defies solution,” *Science*, vol. 314, no. 5802, pp. 1072–1075, 2006.
- [2] M. Cyrot and D. Pavuna, *Introduction to Superconductivity and High- $T_c$  Materials*, World Scientific, River Edge, NJ, USA, 1992.
- [3] W. E. Pickett, “Electronic structure of the high-temperature oxide superconductors,” *Reviews of Modern Physics*, vol. 61, no. 2, pp. 433–512, 1989.
- [4] T. P. Devereaux, A. Virosztek, and A. Zawadowski, “Charge-transfer fluctuation,  $d$ -wave superconductivity, and the  $B_{1g}$  Raman phonon in cuprates,” *Physical Review B*, vol. 51, no. 1, pp. 505–514, 1995.
- [5] A. Bianconi, N. L. Saini, A. Lanzara, et al., “Determination of the local lattice distortions in the  $\text{CuO}_2$  plane of  $\text{La}_{1.85}\text{Sr}_{0.15}\text{CuO}_4$ ,” *Physical Review Letters*, vol. 76, pp. 3412–3415, 1996.
- [6] T. Cuk, F. Baumberger, D. H. Lu, et al., “Coupling of the  $B_{1g}$  Phonon to the antinodal electronic states of  $\text{Bi}_2\text{Sr}_2\text{Ca}_{0.92}\text{Y}_{0.08}\text{Cu}_2\text{O}_{8+\delta}$ ,” *Physical Review Letters*, vol. 93, no. 11, Article ID 117003, 2004.
- [7] T. P. Devereaux, T. Cuk, Z.-X. Shen, and N. Nagaosa, “Anisotropic electron-phonon interaction in the cuprates,” *Physical Review Letters*, vol. 93, no. 11, Article ID 117004, 2004.
- [8] X. J. Zhou, T. Cuk, T. P. Devereaux, N. Nagaosa, and Z. X. Shen, “Angle-resolved photoemission spectroscopy on electronic structure and electron-phonon coupling in cuprate superconductors,” in *Handbook of High-Temperature Superconductivity: Theory and Experiment*, pp. 87–144, Springer, New York, NY, USA, 2007.
- [9] G.-H. Gweon, T. Sasagawa, S. Y. Zhou, et al., “An unusual isotope effect in a high-transition-temperature superconductor,” *Nature*, vol. 430, no. 6996, pp. 187–190, 2004.
- [10] D. Zech, H. Keller, K. Conder, et al., “Site-selective oxygen isotope effect in optimally doped  $\text{YBa}_2\text{Cu}_3\text{O}_{6+x}$ ,” *Nature*, vol. 371, no. 6499, pp. 681–683, 1994.

- [11] R. Khasanov, A. Shengelaya, E. Morenzoni, et al., “Site-selective oxygen isotope effect on the magnetic-field penetration depth in underdoped  $Y_{0.6}Pr_{0.4}Ba_2Cu_3O_{7-\delta}$ ,” *Physical Review B*, vol. 68, no. 22, Article ID 220506, 4 pages, 2003.
- [12] J. Hofer, K. Conder, T. Sasagawa, et al., “Oxygen-isotope effect on the in-plane penetration depth in underdoped  $La_{2-x}Sr_xCuO_4$  single crystals,” *Physical Review Letters*, vol. 84, no. 18, pp. 4192–4195, 2000.
- [13] F. Carbone, A. B. Kuzmenko, H. J. A. Molegraaf, et al., “Doping dependence of the redistribution of optical spectral weight in  $Bi_2Sr_2CaCu_2O_{8+\delta}$ ,” *Physical Review B*, vol. 74, no. 6, Article ID 064510, 2006.
- [14] N. D. Basov and T. Timusk, “Electrodynamics of high-temperature superconductors,” *Reviews of Modern Physics*, vol. 77, no. 2, pp. 721–729, 2005.
- [15] S. M. Hayden, H. A. Mook, P. Dal, T. G. Perring, and F. Dohan, “The structure of the high-energy spin excitations in a high-transition-temperature superconductor,” *Nature*, vol. 429, no. 6991, pp. 531–534, 2004.
- [16] A. Damascelli, Z. Hussain, and Z.-X. Shen, “Angle-resolved photoemission studies of the cuprate superconductors,” *Reviews of Modern Physics*, vol. 75, no. 2, pp. 473–541, 2003.
- [17] J. M. Tranquada, G. D. Gu, M. Hucker, et al., “Evidence for unusual superconducting correlations coexisting with stripe order in  $La_{1.875}Ba_{0.125}CuO_4$ ,” *Physical Review B*, vol. 78, no. 17, Article ID 174529, 2008.
- [18] O. Fischer, M. Kugler, I. Maggio-Aprile, C. Berthod, and C. Renner, “Scanning tunneling spectroscopy of high-temperature superconductors,” *Reviews of Modern Physics*, vol. 79, no. 1, pp. 353–419, 2007.
- [19] P. A. Lee, N. Nagaosa, and X.-G. Wen, “Doping a Mott insulator: physics of high-temperature superconductivity,” *Reviews of Modern Physics*, vol. 78, no. 1, article 17, 2006.
- [20] J. Tahir-Kheli and W. A. Goddard III, “Chiral plaquette polaron theory of cuprate superconductivity,” *Physical Review B*, vol. 76, no. 1, Article ID 014514, 2007.
- [21] T. Jarlborg, “Spin-phonon interaction and band effects in the high- $T_c$  superconductor  $HgBa_2CuO_4$ ,” *Physical Review B*, vol. 68, no. 17, Article ID 172501, 4 pages, 2003.
- [22] K. McElroy, J. Lee, J. A. Slezak, et al., “Atomic-scale sources and mechanism of nanoscale electronic disorder in  $Bi_2Sr_2CaCu_2O_{8+\delta}$ ,” *Science*, vol. 309, no. 5737, pp. 1048–1052, 2005.
- [23] F. Carbone, D.-S. Yang, E. Giannini, and A. H. Zewail, “Direct role of structural dynamics in electron-lattice coupling of superconducting cuprates,” *Proceedings of the National Academy of Sciences of the United States of America*, vol. 105, no. 51, pp. 20161–20166, 2008.
- [24] P. Benedetti, C. Grimaldi, L. Pietronero, and G. Varelogiannis, “Superconductivity beyond Migdal’s theorem and high- $T_c$  phenomenology,” *Europhysics Letters*, vol. 28, pp. 351–356, 1994.
- [25] V. V. Kabanov, J. Demsar, B. Podobnik, and D. Mihailovic, “Quasiparticle relaxation dynamics in superconductors with different gap structures: theory and experiments on  $YBa_2Cu_3O_{7-\delta}$ ,” *Physical Review B*, vol. 59, no. 2, pp. 1497–1506, 1999.
- [26] G. P. Segre, N. Gedik, J. Orenstein, D. A. Bonn, R. Liang, and W. N. Hardy, “Photoinduced changes of reflectivity in single crystals of  $YBa_2Cu_3O_{6.5}$  (ortho II),” *Physical Review Letters*, vol. 88, no. 13, Article ID 137001, 4 pages, 2002.
- [27] R. A. Kaindl, M. Woerner, T. Elsaesser, et al., “Ultrafast mid-infrared response of  $YBa_2Cu_3O_{7-\delta}$ ,” *Science*, vol. 287, no. 5452, pp. 470–473, 2000.
- [28] N. Gedik, M. Langner, J. Orenstein, S. Ono, Y. Abe, and Y. Ando, “Abrupt transition in quasiparticle dynamics at optimal doping in a cuprate superconductor system,” *Physical Review Letters*, vol. 95, no. 11, Article ID 117005, 4 pages, 2005.
- [29] L. Perfetti, P. A. Loukakos, M. Lisowski, U. Bovensiepen, H. Eisaki, and M. Wolf, “Ultrafast electron relaxation in superconducting  $Bi_2Sr_2CaCu_2O_{8+\delta}$  by time-resolved photoelectron spectroscopy,” *Physical Review Letters*, vol. 99, no. 19, Article ID 197001, 2007.
- [30] R. P. Saichu, I. Mahns, A. Goos, et al., “Two-component dynamics of the order parameter of high temperature  $Bi_2Sr_2CaCu_2O_{8+\delta}$  superconductors revealed by time-resolved Raman scattering,” *Physical Review Letters*, vol. 102, no. 17, Article ID 177004, 2009.
- [31] R. A. Kaindl, M. A. Carnahan, D. S. Chemla, S. Oh, and J. N. Eckstein, “Dynamics of Cooper pair formation in  $Bi_2Sr_2CaCu_2O_{8+\delta}$ ,” *Physical Review B*, vol. 72, no. 6, Article ID 060510, 2005.
- [32] N. Gedik, P. Blake, R. C. Spitzer, et al., “Single-quasiparticle stability and quasiparticle-pair decay in  $YBa_2Cu_3O_{6.5}$ ,” *Physical Review B*, vol. 70, no. 1, Article ID 014504, 2004.
- [33] N. Gedik, J. Orenstein, R. Liang, D. A. Bonn, and W. N. Hardy, “Diffusion of nonequilibrium quasi-particles in a cuprate superconductor,” *Science*, vol. 300, no. 5624, pp. 1410–1412, 2003.
- [34] N. Gedik, D.-S. Yang, G. Logvenov, I. Bozovic, and A. H. Zewail, “Nonequilibrium phase transitions in cuprates observed by ultrafast electron crystallography,” *Science*, vol. 316, no. 5823, pp. 425–429, 2007.
- [35] P. Baum and A. H. Zewail, “Breaking resolution limits in ultrafast electron diffraction and microscopy,” *Proceedings of the National Academy of Sciences of the United States of America*, vol. 103, no. 44, pp. 16105–16110, 2006.
- [36] E. Giannini, V. Garnier, R. Gladyshevskii, and R. Flukiger, “Growth and characterization of  $Bi_2Sr_2Ca_2Cu_3O_{10}$  and  $(Bi,Pb)_2Sr_2Ca_2Cu_3O_{10-\delta}$  single crystals,” *Superconductor Science and Technology*, vol. 17, no. 1, pp. 220–226, 2004.
- [37] N. Nakamura and M. Shimotomai, “Growth of  $YBa_2Cu_3O_x$  single crystals by a self-flux method with alkali chlorides as additives,” *Physica C*, vol. 185–189, pp. 439–440, 1991.
- [38] E. Giannini, R. Gladyshevskii, N. Clayton, et al., “Growth, structure and physical properties of single crystals of pure and Pb-doped Bi-based high  $T_c$  superconductors,” *Current Applied Physics*, vol. 8, no. 2, pp. 115–119, 2008.
- [39] I. Bozovic, “Atomic-layer engineering of superconducting oxides: yesterday, today, tomorrow,” *IEEE Transactions on Applied Superconductivity*, vol. 11, no. 1, pp. 2686–2695, 2001.
- [40] Y. S. Lee, R. J. Birgeneau, M. A. Kastner, et al., “Neutron-scattering study of spin-density wave order in the superconducting state of excess-oxygen-doped  $La_2CuO_{4+y}$ ,” *Physical Review B*, vol. 60, no. 5, pp. 3643–3654, 1999.
- [41] P. B. Allen, “Theory of thermal relaxation of electrons in metals,” *Physical Review Letters*, vol. 59, no. 13, pp. 1460–1463, 1987.
- [42] T. Mertelj, J. Demsar, B. Podobnik, I. Poberaj, and D. Mihailovic, “Photoexcited carrier relaxation in  $YBa_2Cu_3O_{7-\delta}$  by picosecond resonant Raman spectroscopy,” *Physical Review B*, vol. 55, no. 9, pp. 6061–6069, 1997.
- [43] S. Y. Savrasov and O. K. Andersen, “Linear-response calculation of the electron-phonon coupling in doped  $CaCuO_2$ ,” *Physical Review Letters*, vol. 77, no. 21, pp. 4430–4433, 1996.
- [44] Y. Wang, S. Ono, Y. Onose, et al., “Dependence of upper critical field and pairing strength on doping in cuprates,” *Science*, vol. 299, no. 5603, pp. 86–89, 2003.

- [45] A. D. Beyer, C.-T. Chen, M. S. Grinolds, M. L. Teague, and N.-C. Yeh, "Competing orders and the doping and momentum dependent quasiparticle excitations in cuprate superconductors," *Physica C*, vol. 468, no. 6, pp. 471–479, 2008.
- [46] C.-T. Chen, A. D. Beyer, and N.-C. Yeh, "Effects of competing orders and quantum phase fluctuations on the low-energy excitations and pseudogap phenomena of cuprate superconductors," *Solid State Communications*, vol. 143, no. 10, pp. 447–452, 2007.
- [47] P. P. Edwards, N. F. Mott, and A. S. Alexandrov, "The insulator-superconductor transformation in cuprates," *Journal of Superconductivity*, vol. 11, no. 1, pp. 151–154, 1998.
- [48] F. Carbone, A. B. Kuzmenko, H. J. A. Molegraaf, E. van Heumen, E. Giannini, and D. van der Marel, "In-plane optical spectral weight transfer in optimally doped  $\text{Bi}_2\text{Sr}_2\text{Ca}_2\text{Cu}_3\text{O}_{10}$ ," *Physical Review B*, vol. 74, no. 2, Article ID 024502, 2006.
- [49] H. Kotegawa, Y. Tokunaga, K. Ishida, et al., "Unusual magnetic and superconducting characteristics in multilayered high- $T_c$  cuprates:  $^{63}\text{Cu}$  NMR study," *Physical Review B*, vol. 64, no. 6, Article ID 064515, 5 pages, 2001.
- [50] M. Di Stasio, K. A. Muller, and L. Pietronero, "Nonhomogeneous charge distribution in layered high- $T_c$  superconductors," *Physical Review Letters*, vol. 64, no. 23, pp. 2827–2830, 1990.
- [51] J. M. Tranquada, B. J. Sternlieb, J. D. Axe, Y. Nakamura, and S. Uchida, "Evidence for stripe correlations of spins and holes in copper oxide superconductors," *Nature*, vol. 375, no. 6532, pp. 561–563, 1995.
- [52] J. M. Tranquada, J. D. Axe, N. Ichikawa, A. R. Moodenbaugh, Y. Nakamura, and S. Uchida, "Coexistence of, and competition between, superconductivity and charge-stripe order in  $\text{La}_{1.6-x}\text{Nd}_{0.4}\text{Sr}_x\text{CuO}_4$ ," *Physical Review Letters*, vol. 78, no. 2, pp. 338–341, 1997.
- [53] K. Yamada, C. H. Lee, K. Kurahashi, et al., "Doping dependence of the spatially modulated dynamical spin correlations and the superconducting-transition temperature in  $\text{La}_{2-x}\text{Sr}_x\text{CuO}_4$ ," *Physical Review B*, vol. 57, no. 10, pp. 6165–6172, 1998.
- [54] M. Arai, T. Nishijima, Y. Endoh, et al., "Incommensurate spin dynamics of underdoped superconductor  $\text{YBa}_2\text{Cu}_3\text{O}_{6.7}$ ," *Physical Review Letters*, vol. 83, no. 3, pp. 608–611, 1999.
- [55] M. Arai, Y. Endoh, S. Tajima, and S. M. Bennington, "Spin-Charge stripe structure of superconducting  $\text{YBa}_2\text{Cu}_3\text{O}_{6+x}$ ," *International Journal of Modern Physics B*, vol. 14, no. 29–31, pp. 3312–3321, 2000.
- [56] J. Zaanen and O. Gunnarsson, "Charged magnetic domain lines and the magnetism of high- $T_c$  oxides," *Physical Review B*, vol. 40, no. 10, pp. 7391–7394, 1989.
- [57] W. P. Su, J. R. Schrieffer, and A. J. Heeger, "Solitons in polyacetylene," *Physical Review Letters*, vol. 42, no. 25, pp. 1698–1701, 1979.
- [58] S. M. Hayden, G. H. Lander, J. Zarestky, et al., "Incommensurate magnetic correlations in  $\text{La}_{1.8}\text{Sr}_{0.2}\text{NiO}_4$ ," *Physical Review Letters*, vol. 68, no. 7, pp. 1061–1064, 1992.
- [59] J. M. Tranquada, D. J. Buttrey, V. Sachan, and J. E. Lorenzo, "Simultaneous ordering of holes and spins in  $\text{La}_2\text{NiO}_{4.125}$ ," *Physical Review Letters*, vol. 73, no. 7, pp. 1003–1006, 1994.
- [60] C. H. Chen, S.-W. Cheong, and A. S. Cooper, "Charge modulations in  $\text{La}_{2-x}\text{Sr}_x\text{NiO}_{4+y}$ : ordering of polarons," *Physical Review Letters*, vol. 71, no. 15, pp. 2461–2464, 1993.
- [61] S. A. Kivelson, E. Fradkin, and V. J. Emery, "Electronic liquid-crystal phases of a doped mott insulator," *Nature*, vol. 393, no. 6685, pp. 550–553, 1998.
- [62] J. Chang, M. Shi, S. Pailh s, et al., "Anisotropic quasiparticle scattering rates in slightly underdoped to optimally doped high-temperature  $\text{La}_{2-x}\text{Sr}_x\text{CuO}_4$  superconductors," *Physical Review B*, vol. 78, no. 20, Article ID 205103, 2008.
- [63] V. Oganesyan, S. A. Kivelson, and E. Fradkin, "Quantum theory of a nematic Fermi fluid," *Physical Review B*, vol. 64, no. 19, Article ID 195109, 6 pages, 2001.
- [64] C. J. Halboth and W. Metzner, " $d$ -wave superconductivity and Pomeranchuk instability in the two-dimensional Hubbard model," *Physical Review Letters*, vol. 85, no. 24, pp. 5162–5165, 2000.
- [65] J. Lorenzana and G. Seibold, "Metallic mean-field stripes, incommensurability, and chemical potential in cuprates," *Physical Review Letters*, vol. 89, no. 13, Article ID 136401, 4 pages, 2002.
- [66] J. Lorenzana and G. Seibold, "Dynamics of metallic stripes in cuprates," *Physical Review Letters*, vol. 90, no. 6, Article ID 066404, 4 pages, 2003.
- [67] X. J. Zhou, T. Yoshida, S. A. Kellar, et al., "Dual nature of the electronic structure of  $(\text{La}_{2-x-y}\text{Nd}_y\text{Sr}_x)\text{CuO}_4$  and  $\text{La}_{1.85}\text{Sr}_{0.15}\text{CuO}_4$ ," *Physical Review Letters*, vol. 86, no. 24, pp. 5578–5581, 2001.
- [68] X. J. Zhou, P. Bogdanov, S. A. Kellar, et al., "One-dimensional electronic structure and suppression of  $d$ -wave node state in  $(\text{La}_{1.28}\text{Nd}_{0.6}\text{Sr}_{0.12})\text{CuO}_4$ ," *Science*, vol. 286, no. 5438, pp. 268–272, 1999.
- [69] M. Grilli, G. Seibold, A. Di Ciolo, and J. Lorenzana, "Fermi surface dichotomy in systems with fluctuating order," *Physical Review B*, vol. 79, no. 12, Article ID 125111, 2009.
- [70] E. Li, R. P. Sharma, S. B. Ogale, et al., "Sharp resonant multiplet in femtosecond optical pair-breaking spectroscopy of optimally doped, underdoped, and Zn-doped  $\text{YBa}_2\text{Cu}_3\text{O}_{7-\delta}$ : transient insulating regions in the superconducting state," *Physical Review B*, vol. 65, no. 18, Article ID 184519, 7 pages, 2002.
- [71] M. A. Quijada, D. B. Tanner, R. J. Kelley, M. Onellion, H. Berger, and G. Margaritondo, "Anisotropy in the ab-plane optical properties of  $\text{Bi}_2\text{Sr}_2\text{CaCu}_2\text{O}_8$  single-domain crystals," *Physical Review B*, vol. 60, no. 21, pp. 14917–14934, 1999.
- [72] D.-S. Yang, N. Gedik, and A. H. Zewail, "Ultrafast electron crystallography. 1. Nonequilibrium dynamics of nanometer-scale structures," *Journal of Physical Chemistry C*, vol. 111, no. 13, pp. 4889–4919, 2007.
- [73] M. Suzuki, "Hall coefficients and optical properties of  $\text{La}_{2-x}\text{Sr}_x\text{CuO}_4$  single-crystal thin films," *Physical Review B*, vol. 39, no. 4, pp. 2312–2321, 1989.
- [74] J. D. Yu, Y. Inaguma, M. Itoh, M. Oguni, and T. Kyomen, "Effect of oxygen content on the anomalies at successive phase transitions of  $\text{La}_2\text{CuO}_{4+\delta}$  single crystal below 320 K," *Physical Review B*, vol. 54, no. 10, pp. 7455–7461, 1996.
- [75] B. Piveteau and C. Noguera, "Cohesion energy and structural phase stability in  $\text{La}_2\text{CuO}_4$ : the orthorhombic state," *Physical Review B*, vol. 43, no. 1, pp. 493–504, 1991.
- [76] M. Evain, M.-H. Whangbo, M. A. Beno, U. Geiser, and J. M. Williams, "Simulation of crystal structures by empirical atom-atom potentials. 1. The tetragonal-to-orthorhombic distortion in  $\text{La}_2\text{CuO}_4$  and in the high-temperature superconductors  $\text{La}_{2-x}\text{M}_x\text{CuO}_4$  ( $M = \text{Ba}, \text{Sr}$ )," *Journal of the American Chemical Society*, vol. 109, no. 25, pp. 7917–7918, 1987.
- [77] Z. Radović, N. Božović, and I. Božović, "Photoinduced expansion of cuprate superconductors: evidence of strong electron-lattice coupling," *Physical Review B*, vol. 77, no. 9, Article ID 092508, 2008.

- [78] I. Bozovic, M. Schneider, Y. Xu, et al., “Long-lived coherent acoustic waves generated by femtosecond light pulses,” *Physical Review B*, vol. 69, no. 13, Article ID 132503, 2004.
- [79] K. Kumagai, Y. Nakamichi, I. Watanabe, et al., “Linear temperature term of heat capacity in insulating and superconducting La-Ba-Cu-O systems,” *Physical Review Letters*, vol. 60, no. 8, pp. 724–727, 1988.
- [80] J. C. Phillips, “Quantum percolation in cuprate high-temperature superconductors,” *Proceedings of the National Academy of Sciences of the United States of America*, vol. 105, no. 29, pp. 9917–9919, 2008.
- [81] A. S. Mishchenko, N. Nagaosa, Z.-X. Shen, et al., “Charge dynamics of doped holes in high  $T_c$  cuprate superconductors: a clue from optical conductivity,” *Physical Review Letters*, vol. 100, no. 16, Article ID 166401, 2008.
- [82] E. van Heumen, E. Muhlethaler, A. B. Kuzmenko, et al., “Optical determination of the relation between the electron-boson coupling function and the critical temperature in high- $T_c$  cuprates,” *Physical Review B*, vol. 79, no. 18, Article ID 184512, 7 pages, 2009.

## Review Article

# Material and Doping Dependence of the Nodal and Antinodal Dispersion Renormalizations in Single- and Multilayer Cuprates

S. Johnston,<sup>1,2</sup> W. S. Lee,<sup>2,3</sup> Y. Chen,<sup>2,4</sup> E. A. Nowadnick,<sup>2,5</sup> B. Moritz,<sup>2,6</sup>  
Z.-X. Shen,<sup>2,3,5,7</sup> and T. P. Devereaux<sup>2,3</sup>

<sup>1</sup> Department of Physics and Astronomy, University of Waterloo, Waterloo, ON, Canada N2L 3G1

<sup>2</sup> Stanford Institute for Materials and Energy Science, SLAC National Accelerator Laboratory, Stanford University, Stanford, CA 94305, USA

<sup>3</sup> Geballe Laboratory for Advanced Materials, Stanford University, Stanford, CA 94305, USA

<sup>4</sup> Advanced Light Source, Lawrence Berkeley National Laboratory, Berkeley, CA 94720, USA

<sup>5</sup> Department of Physics, Stanford University, Stanford, CA 94305, USA

<sup>6</sup> Department of Physics and Astrophysics, University of North Dakota, Grand Forks, ND 58202, USA

<sup>7</sup> Department of Applied Physics, Stanford University, Stanford, CA 94305, USA

Correspondence should be addressed to T. P. Devereaux, [tpd@stanford.edu](mailto:tpd@stanford.edu)

Received 30 September 2009; Accepted 4 January 2010

Academic Editor: Igor Mazin

Copyright © 2010 S. Johnston et al. This is an open access article distributed under the Creative Commons Attribution License, which permits unrestricted use, distribution, and reproduction in any medium, provided the original work is properly cited.

We present a review of bosonic renormalization effects on electronic carriers observed from angle-resolved photoemission spectra in the cuprates. Specifically, we discuss the viewpoint that these renormalizations represent coupling of the electrons to the lattice and review how materials dependence, such as the number of CuO<sub>2</sub> layers, and doping dependence can be understood straightforwardly in terms of several aspects of electron-phonon coupling in layered correlated materials.

## 1. Introduction

The discovery of a “kink” in the nodal  $((0,0)-(\pi, \pi))$  dispersion of the high- $T_c$  cuprates, and band renormalizations, in the form of a peak-dip-hump structure in the antinodal  $(0, \pi)-(\pi, \pi)$  dispersion [1–18], has attracted considerable attention in recent years. (We note that while a kink in the electronic band dispersion can be seen in the earlier data of Valla et al., this paper focused on quantum critical behavior of the frequency-dependent imaginary part of the self-energy and does not make any mention of a kink. Further, the authors stressed a quantum critical self energy form that does not contain any energy scale.) These band renormalizations have been interpreted as due to electron-boson coupling, and it is believed that understanding origin of these renormalizations will provide crucial information about the underlying pairing mechanism in these materials. There is still considerable debate as to number and to the identity of the responsible bosonic mode(s) and whether these modes might be relevant to superconductivity [19].

In terms of coupling to a bosonic mode, the candidate modes have been associated with either coupling to electron spins or to the lattice. Both viewpoints have their merits and at present the debate is unsettled. Initially the kinks had been associated with coupling to a collective mode found in neutron scattering near antiferromagnetic (AF) momentum transfers  $(\pi, \pi)$ , the so-called magnetic resonance mode [4, 9, 11, 12]. The basis for the association was mainly due to the observation that the mode, as well as the kinks, was largely found only below the superconducting transition temperature. However, since then, it has been realized that the kink features exist both above and below  $T_c$ . Furthermore, the relatively narrow momentum range of the mode itself implies that the renormalizations should be relatively localized to impact electrons in a narrow region of the Fermi surface (FS) near the AF zone boundary. Given that kinks have been observed throughout the Brillouin zone (BZ), some of the original advocates of coupling to the neutron resonance mode indicate that this mode cannot be the mode responsible for the observed kink in the nodal direction [20].

The renormalizations could also be due to coupling of electrons to a damped magnon continuum, which has a less well-defined momentum structure. This has the appeal that as the magnons become better defined nearing the AF phase, the strength of the kinks would be expected to increase, in agreement with experiments. However, the strength of the coupling of magnons to electrons is still under debate [21, 22]. For example, quantitative comparisons of angle-resolved photoemission spectroscopy (ARPES) and neutron measurements on  $\text{YBa}_2\text{Cu}_3\text{O}_{6.6}$  (YBCO) have been made, and the overall strength of the coupling inferred from the data was indicated to be of sufficient strength to give rise to superconductivity [17]. We remark that a quantitative comparison between the neutron scattering and ARPES measurements reported in [17] can be complicated by the polar surface of cleaved YBCO (as opposed to Bi- and Tl-compounds which have no polar surface) resulting in a surface reconstruction with the potential to produce significant differences between the bulk and surface layers of this material. This leads to an inconsistency where the FS revealed from ARPES matches that of an overdoped material, while the neutron scattering spectra used in the phenomenology were obtained on an underdoped material exhibiting a pseudogap. Since this comparison has only been performed on one cuprate, which has the abovementioned issues, we believe that at present the issue remains open.

A nonbosonic origin of the kink has been proposed whereby the kink is produced by many-body correlations [23]. The energy scale of the renormalization is set by the strength of the quasiparticle residue  $Z$  and is generic to any strongly correlated material with a sizable Hubbard interaction. Since the correlation strength is set by the combination of the charge transfer energy to move a hole from copper to oxygen in the cuprates, the kink strength and position would be then fairly universal across the cuprate family.

A systematic examination of the effects of doping, material class, and temperature have not been thoroughly explored. In fact, given that both the electronic correlations and the spin continuum arise from the  $\text{CuO}_2$  plane, one might expect the coupling to electrons which might give rise to a putative kink to be relatively material-class independent. On the other hand, it is wellknown that a neutron resonance displays a material dependence, appearing at larger energies for larger  $T_c$  materials including both the single- and multi-layer cuprates. This opens the possibility of linking the neutron resonance with ARPES renormalizations via a material-dependent study.

An alternative proposal is coupling to a spectrum of oxygen vibrational phonon modes [3, 7, 24, 25], specifically the  $c$ -axis out-of-phase bond-buckling oxygen vibration or  $B_{1g}$  mode ( $\Omega \sim 35\text{--}45$  meV) and the in-plane bond-stretching oxygen mode ( $\Omega \sim 70\text{--}80$  meV). This multi-phonon proposal has been able to account for many experimental observations including the anisotropy of the observed renormalizations [24], fine structure in the form of subkinks observed in the temperature dependence of the self-energy in  $\text{Bi}_2\text{Sr}_2\text{CaCu}_2\text{O}_{8+\delta}$  (Bi-2212) [25], which track the opening of the superconducting gap, and doping-dependent

changes in the self-energy [15, 26]. This interpretation is further supported by recent ARPES experiments that have measured an  $^{16}\text{O} \rightarrow ^{18}\text{O}$  isotope shift in the nodal kink position [27].

In general, the energy scale of the kink for a  $d$ -wave superconductor coupled to an Einstein mode occurs at  $\Omega + \Delta_0$  where  $\Omega$  is the energy of the mode and  $\Delta_0$  is the maximum value of the superconducting gap. This is independent of the identity of the mode, such as phonons or for a spin resonance mode for example, and arises from the large density of states pile-up at the gap edge  $\Delta_0$  below  $T_c$  [24, 25, 28, 29]. An exception arises in the limit of extreme forward scattering by the mode, where the coupling constant becomes sharply peaked at  $\mathbf{q} = 0$  [30]. Theoretical work has shown that correlations can enhance the electron-phonon coupling vertex for small momentum transfer leading to a coupling which favors forward scattering [31–34]. In the nodal region, where the gap is zero, such a coupling will produce a peak in the self-energy at the mode energy  $\Omega$ . However, such a peak would gap shift as a function of momentum following the momentum dependence of the gap away from the node. Since the energy scale of the kink does not exhibit a dispersion in the vicinity of the node one can conclude that the enhancement of the  $\mathbf{q} = 0$  el-ph vertex is not sharp enough to produce the strong forward scattering assumed in [30].

The phonon scenario has been criticized using evidence based on density functional theory (DFT) approaches, which have traditionally not provided evidence of strong electron-phonon coupling in YBCO and  $\text{La}_{2-x}\text{Sr}_x\text{CuO}_4$  (see [35–37] for recent works). LDA predicts the total coupling to all of the modes to be less than one, and when a self-energy calculated within the Migdal limit is compared to nodal ARPES cuts in the cuprates, it was found that the coupling was too small by a factor of 3–5 to account for the observed kinks. However, while DFT has done a remarkably good job of predicting phonon dispersions, the width of the phonon lineshapes is underestimated in most cases in comparison with experiment, sometimes by an order of magnitude [38]. This is not unexpected given that DFT predicts metallic behavior for undoped cuprates and does not account for the factor of five reduced bandwidth over DFT values observed in optimally doped Bi-2212 [39]. A simple reduction of the bandwidth might account for the discrepancy. It is not clear if these findings indicate that lattice effects are small or that DFT-based approaches alone are inadequate to represent the physics of the cuprates.

Analogous features to those observed in ARPES have been observed in scanning tunneling microscopy (STM). These features have also been interpreted in terms of coupling to a bosonic mode [40–43], and possibly the same mode responsible for the ARPES observed kink. As with the kink observed in the single-particle dispersion by ARPES, the origin of this feature remains a source of debate [44, 45]. Pilgram et al. [44] invoke a cotunneling mechanism between the tip and sample via an apical oxygen pathway. Taking this view, the modulations in the STM derived density of states (DOS) are unrelated to the physics of the  $\text{CuO}_2$  plane. In contrast, the observed STM spectra look similar in Bi-2212

(which has an apical oxygen) and  $\text{Ca}_{2-x}\text{Na}_x\text{CuO}_2\text{Cl}_2$  [46] (which does not) indicating that the tunneling pathway from the STM tip to the conduction electrons does seem to be that critical, and that the renormalizations observed in both STM and ARPES could have a common origin. Reference [40] also reported an  $^{18}\text{O}$  isotope shift of the feature in a Bi-2212 sample. While at face value this would indicate a lattice origin to the renormalizations in the tunneling spectra, this too remains controversial [20]. Therefore, even though there exists a wide array of experimental data from ARPES and other probes, it is clear that the identity of the bosonic mode is still hotly debated.

It would take much too much space to review each and every interpretation of each and every experimental observation relating to kinks, and it is not clear whether such a review would be useful. Rather than attempting to outline all possible scenarios, we instead present a review of ways in which different scenarios may be differentiated by studying the material, doping, and temperature dependence of the band renormalizations. We admit at the outset our bias that the electronic renormalizations are best interpreted in terms of coupling to the lattice. As there are many articles advocating other points of view, and this volume is organized according to the effects of electron-phonon coupling in the cuprates, our choice of presentation is thusly defined.

This work will focus on how  $c$ -axis phonons provide a material dependence to the ARPES kinks due to the phonon's sensitivity to local symmetry and the environment surrounding the  $\text{CuO}_2$  plane. We consider doping-dependent changes to the renormalization in Bi-2212 as well as the dependence of these renormalizations within the Bi- and Tl- families as the number of  $\text{CuO}_2$  layers is varied. We will also discuss some recent ARPES results on the  $n = 4$  layer system  $\text{Ba}_2\text{Ca}_3\text{Cu}_4\text{O}_8\text{F}_2$  (F0234) [47]. In this system, the inner and outer layers occupy different crystal environments resulting in differing Madelung energies associated with each plane in the undoped compound. This difference drives inequivalent dopings between the two sets of layers, with one set  $n$ -type and the other  $p$ -type. The inequivalent doping in each plane generates further symmetry breaking in the layers, and the el-ph coupling in each layer is expected to differ. Indeed, [47] observes stronger kink features in the plane associated with the outer ( $n$ -type) layer of the material. Here, we will discuss these observations in the context of the el-ph coupling scenario.

The organization of this paper is as follows. In Section 2 we discuss the role of symmetry breaking in producing el-ph coupling to  $c$ -axis phonons and how such coupling is expected to vary with the crystal structure of the high- $T_c$  cuprates. In Section 3 we present ARPES data for various multilayer cuprates in order to examine how band renormalizations vary with the number of  $\text{CuO}_2$  layers. Of particular interest are the results for the single-layer Tl cuprate Tl-2201. Here, we show that Tl-2201 does not resolve the typical peak-dip-hump structures in the antinodal region despite the fact that the spin resonance mode exists in this system [48]. In Section 4 the doping dependence of the nodal and antinodal dispersions for Bi-2122 is presented. The renormalizations in each region behave differently as

the samples are overdoped, pointing to presence of multiple bosonic modes. In Section 5 we present aspects of the nodal kink for the multi-layer F-family of cuprates. Electronic dispersions for the  $p$ -bands of the F-family are presented together with a theoretical basis for understanding the self-doping phenomena in  $\text{Ba}_2\text{Ca}_3\text{Cu}_4\text{O}_8\text{F}_2$  (F0234). We also discuss what implications this process has on coupling to  $c$ -axis phonons. Finally, in Section 6, we conclude with a brief summary and some additional remarks.

## 2. Electron-Phonon Coupling in Multilayer Cuprates

In this section we discuss how  $c$ -axis phonons can be sensitive to the material environment off the  $\text{CuO}_2$  planes. There are many different sorts of phonons in the layered cuprates; however not all of these modes are expected to be sensitive to carrier concentration (such as those involving atoms in the charge reservoirs), and of those involving Cu and O, only a subset may be expected to vary across cuprate materials and family classes. Deformation electron-phonon (el-ph) coupling, involving in-plane bond-stretching modes, for example [49], depends on the Cu–O bond distance which is relatively constant in all cuprates. Therefore coupling to these modes is expected to be relatively material independent. They can be doping dependent, however, due to either correlation effects or due to the changeover from 2D to 3D transport with increased hole concentration which changes the character of charge screening. However, a clear material dependence may arise for modes which electrostatically couple to the Madelung environment coming from all ions in the unit cell. This sort of coupling is believed to be most relevant for  $c$ -axis bond-buckling modes such as the out-of-phase planar oxygen vibration (which is  $B_{1g,1u}$  Raman, infrared active in multi-layer cuprates), or the in-phase ( $A_{1g,1u}$  vibration of the planar oxygen atoms. These modes have been studied extensively in the context Raman, infrared and neutron spectroscopy [50–55]. Although the nomenclature only holds for Raman  $\mathbf{q} = 0$  momentum transfers, we denote the out-of-phase mode as the “ $B_{1g}$ ” mode, and the in-phase mode as “ $A_{1g}$ ” [50, 51]. Since our goal is to explore the materials dependence of the band renormalizations, we will focus our attention to the  $c$ -axis modes.

El-ph coupling to  $c$ -axis phonons can arise due to the modulated Madelung environment the ion feels. If the ion sits in a mirror plane, such as the oxygens in the  $\text{CuO}_2$  plane in an ideal single-layer cuprate, the Madelung energy is at local minima and the modulation of the energy and the coupling must be of second order in the ion displacements [24, 50, 51, 56, 57]. However, steric forces may force the  $\text{CuO}_2$  to buckling along the  $c$ -axis which then creates a coupling to linear order in the displacements [58]. In terms of material dependence, such steric forces are present in all  $\text{CuO}_2$  systems and, therefore, do not contribute to differences between materials. Another second pathway for mirror symmetry breaking can occur locally by introducing substitutional or interstitial dopant atoms in the charge

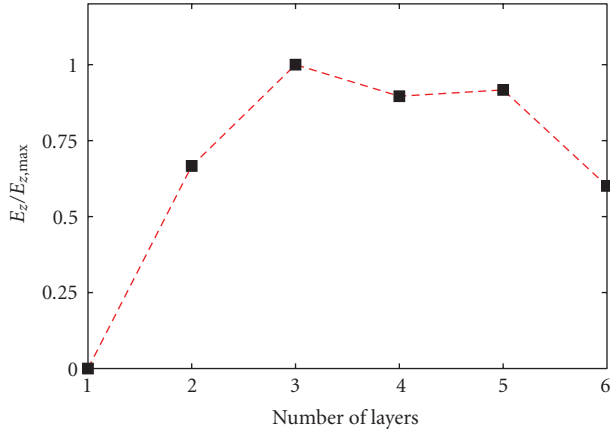


FIGURE 1: The local crystal field strength at the planar oxygen site of the outermost  $\text{CuO}_2$  plane of the Hg-family of cuprates. All results have been normalized by the maximum field which occurs for the  $n = 3$  layer system.

reservoir area off the  $\text{CuO}_2$  planes. These dopants donate charge to the  $\text{CuO}_2$  plane(s), and cast  $c$ -axis electric fields  $E_z$  that are poorly screened by the in-plane carriers [59, 60]. Through this mechanism, coupling to  $c$ -axis phonons can occur in single-layer systems where they are normally forbidden by symmetry. This would then lead to a doping-dependence electron-phonon coupling.

This is to be contrasted with multi-layer cuprates, where even in an ideal material the  $\text{CuO}_2$  plane does not necessarily lie in a mirror plane (for odd number of  $\text{CuO}_2$  layers, there will always be one  $\text{CuO}_2$  plane which lies in the mirror plane), and a coupling which is first order in the  $c$ -axis displacement is expected, whereby the strength of the coupling is determined by the spatial variation of the Madelung energy along the  $c$ -axis. This is characterized by the local crystal field  $E_z$  which varies from material to material with the chemical environment (number of layers and doping from the ideal stoichiometric compound). The strength of the coupling to these modes scales as  $\lambda \propto E_z^2$ . Due to the oxygen charge-transfer form factors, it has been shown that the  $B_{1g}$  mode couples most strongly to antinodal electrons [24]. This is the case for the spin resonance mode due to its strong tendency to scatter electrons near the AF zone boundary. Therefore, the material dependence of the antinodal electrons offers a straightforward way to distinguish between these two scenarios.

To quantify the effect of the crystal environment in the parent systems, in Figure 1., the local crystal field at the outermost  $\text{CuO}_2$  layer for the  $\text{HgBa}_2\text{Ca}_n\text{Cu}_n\text{O}_{2(n+1)+\delta}$  ( $n = 1-6$ ) family of cuprates is presented. Using experimental structural data [61–65] and assuming an ionic point-charge model with formal valences assigned to each atom, the Ewald summation method [66] is used to perform the electrostatic sums for the Madelung energy and its variation along the  $c$ -axis, determining the electric field strength. As mentioned, the local field is zero in the single-layer compound, and rises for  $n > 1$ . A maximum is reached for  $n = 3$  and decreasing field values are found for  $n > 3$  (We note here that the reports

for the structural data for the  $n = 4$  and  $n = 5$  compounds have a large degree of scatter, presumably from the difficulty in sample growth.)

This effect can be understood in terms of the spatial variation of the Madelung potential. The gradient of the Madelung potential, which determines the  $E$ -field in an electrostatic model, is identically zero at the mirror planes, which generically lie at the middle and edges of the unit cell. The electrostatic periodicity requires that a point of steepest decent of the Madelung energy exist at a location between these mirror planes [67]. Empirically, our Madelung potential calculations indicate that for  $n = 1-3$  the outermost plane approaches this point of steepest decent and experiences a larger field due to the increased gradient. For  $n > 3$  the outermost layer has passed this point and, therefore, experiences a reduced field for increasing  $n$ . Finally, as the number of layers continues to increase, there is an overall reduction in the range of the amplitude of the Madelung potential variation such that a uniform profile in the limit of the infinite layer compound (such as  $\text{CaCuO}_2$ ).

While it is noteworthy that this dependence of the local  $c$ -axis  $E$ -field mimics the variation of  $T_c$  in these compounds and that these  $c$ -axis phonons are the dominant phonons which provide pairing in the  $d_{x^2-y^2}$  channel, the strength of the coupling determined from LDA, even with a factor of five enhancement, in no way can account for  $T_c$  itself. However it is an intriguing possibility that this electron-phonon coupling may provide a bootstrap to an underlying pairing mechanism dependent only upon the properties of the  $\text{CuO}_2$  plane itself, and may directly impart a material dependence to  $T_c$ . Multiple pairing channels may then be required to explain superconductivity in the cuprates [68]. However, the relation between those channels, the role of correlations, and a formalism valid to describe superconductivity in the cuprates are all open problems central to the field for which definitive answers and methods are missing.

### 3. Layer Dependence

In the previous section we discussed how the material dependence of the renormalizations is expected to arise in the various families of cuprates and how this coupling is expected to differ in the phonon and spin resonance proposals. We now wish to review the available ARPES data in light of the theoretical considerations of the previous section. Here, our focus is on the observed changes in the renormalizations as the number of layers within the Bi- and Tl-families.

Single crystals of nearly optimally doped  $\text{Tl}_2\text{Ba}_2\text{CaCu}_2\text{O}_8$  (Tl-2212),  $\text{TlBa}_2\text{Ca}_2\text{Cu}_3\text{O}_9$  (Tl-1223), and slightly overdoped  $\text{Tl}_2\text{Ba}_2\text{CuO}_6$  (Tl-2201) were grown using the flux method. As-grown Tl2212 ( $T_c = 107$  K) and Tl-1223 ( $T_c = 123$  K) crystals were chosen for the ARPES measurements. Tl-2201 crystals used in our measurement were prepared by annealing the as-grown crystal ( $T_c \sim 30$  K) under a nitrogen flow at a temperature of  $500^\circ\text{C}$ , yielding a  $T_c$  of 80 K. The data were collected using a Scienta R4000 photoelectron spectrometer. Measurements were performed at the Stanford

Synchrotron Radiation Lightsource (SSRL) beam line 5-4 using 28 eV photons and at the Advanced Light Source beam line 10.0.1 using 50 eV photons. The energy resolution was set at 15–20 meV for the TI data presented in this work. Samples were cleaved and measured in ultrahigh vacuum ( $< 4 \times 10^{-11}$  Torr) to maintain a clean surface. Detailed ARPES results on these compounds have been reported in [48].

Although the dispersion kink along the nodal direction has been found universally in high- $T_c$  cuprates [3], the momentum dependence of this renormalization feature, when moving away from the nodal direction, exhibits a material dependence [48, 69]. It has been confirmed recently that there is a dependence on the number of  $\text{CuO}_2$  planes in the unit cell in the Bi-family and, most recently, in the TI-family of cuprates [48]. In the multi-layer compounds, the kink becomes more dramatic and eventually breaks the band dispersion into two branches: one branch with a sharp peak and another branch with a broader hump structure [4, 7, 10, 48, 69]. The two branches asymptotically approach one another at a characteristic energy scale of 70 meV and coincide with the dominant energy scale of the kink along the nodal dispersion for nearly optimallydoped cuprates. This separation of the band dispersion becomes most prominent near the antinodal region and results in the famous peak-dip-hump structure [11] in the energy distribution curves (EDCs), as shown in Figure 2.

The momentum dependence of the kink is quite different in the single-layer compound, where the dispersion kink becomes less prominent moving away from the node. In addition, the band dispersion retains a single branch with no separation observed, unlike the case of the multi-layer compounds [70, 71]. As a result, no apparent peak-dip-hump structure can be seen in the EDCs near the antinodal region for the single-layer compounds Figure 2. (The peak-dip-hump structure in the single-layer Bi-2201 is rather weak and appears abruptly in a narrow range of momentum space with a different energy scale than that along the nodal direction [70]. In addition, the issue of a peak-dip hump structure in the single-layer compound seems more uncertain, as the reported peak-dip-hump lineshape appears to be inconsistent among the literature [70, 72].) Similar results have been reported for optimal and underdoped LSCO [73–75] as well as overdoped TI-2201 [76].

In summary, the layer dependent renormalization near the antinodal region is due most likely to electrons coupled to a sharp bosonic mode, whose origin is strictly constrained by the number of layers in the material. This mode is either absent or has a negligible coupling to the electrons, in single-layer compounds, but exhibits prominent coupling in the multi-layer compounds. The spin resonance mode does exist in some single-layer cuprates [77] (notably TI-2201 but not  $\text{La}_2\text{CuO}_{4+\delta}$ ). Therefore, one can conclude that the spin resonance mode is an unlikely candidate for the mode responsible for the renormalizations in the antinodal region. On the other hand, coupling to  $c$ -axis phonons can exhibit a very different coupling in single- and multi-layer compounds. As we have discussed, the  $B_{1g}$  phonon couples strongly to the electrons in multi-layer compounds and weakly to electrons in single-layer compounds. This mode

can also reproduce the observed anisotropic momentum dependence of the renormalization in bi-layer Bi2212 [24]. We also note that the form for the  $B_{1g}$  coupling is attractive in the  $d$ -wave pairing channel [50, 51], which could be one factor enhancing  $T_c$  in the multi-layer systems.

#### 4. Energy Scales and Doping Dependence

In the el-ph coupling picture the carriers couple to a spectrum of bosonic modes and we have already seen how the  $c$ -axis modes can produce a materials dependence of the renormalizations. It is important to note that the coupling to the out-of-plane bond-buckling ( $B_{1g}$ ) mode is highly anisotropic and may dominate the antinodal region in the normal state, and through the pile-up of the density of states at the gap edge strengthens around the antinode and becomes visible in the nodal region, obscuring the in-plane bond-stretching (breathing) modes. Since these modes have different frequencies, one would naturally expect the multiple energy scales to manifest in the experimental data. Indeed, evidence for multiple energy scales has been found in both the temperature dependence [7, 24, 25] as well as the doping dependence of Bi-2212 [8, 15, 26]. In this section we revisit the doping dependence of the nodal and antinodal renormalizations, highlighting the different behavior in each region of the Brillouin zone, and discuss how this dichotomy further supports the el-ph scenario.

High-quality single crystals of optimally doped  $\text{Bi}_2\text{Sr}_2\text{Ca}_{0.92}\text{Y}_{0.08}\text{Cu}_2\text{O}_{8+\delta}$  (Bi-2212 OP,  $T_c = 96$  K) were grown by the floating-zone method. The overdoped crystals with  $T_c = 88$  K were prepared by postannealing the optimally doped Bi-2212 crystal under oxygen flow at a temperature of 400°C. The overdoped sample with  $T_c = 65$  K is a derivative of the Bi-2212 family with lead doped into the crystal to achieve such an overdoped configuration. The data were collected by using He I light (21.2 eV) from a monochromated and modified Gammadata HE Lamp with a Scienta-2002 analyzer and in SSRL beamline 5-4 using 19 eV photons with a Scienta-200 analyzer. The energy resolution is  $\sim 10$  meV and angular resolution  $\sim 0.35^\circ$ . The samples were cleaved and measured in ultrahigh vacuum ( $< 4 \times 10^{-11}$  Torr) to maintain a clean surface.

In Figure 3 ARPES data taken along a cut in the antinodal region illustrate this effect. The upper panels show the measured spectral function along the cut while the lower panels show the ARPES spectral function  $A(k, \omega)$  at a fixed  $k$ -point as indicated by the dashed lines.

Near  $(0, \pi)$ , the energy of the dip feature is the best measure of the energy scale of the mode responsible for the renormalization [24, 28]. For the optimally doped sample (OP96K), shown in the first column of Figure 3, the dip position is clearly located at  $\omega \sim 70$  meV. This can be seen in both the false color plot and the EDC cut. For moderate overdoping (OD88K), the energy of the dip is lowered to  $\sim 58$  meV while for heavily overdoped (OD65K) the energy is lowered further to  $\sim 32$  meV. In both overdoped cases, contributions from the bonding- (BB) and antibonding (AB) bands contribute to the quasiparticle peak at the Fermi level.

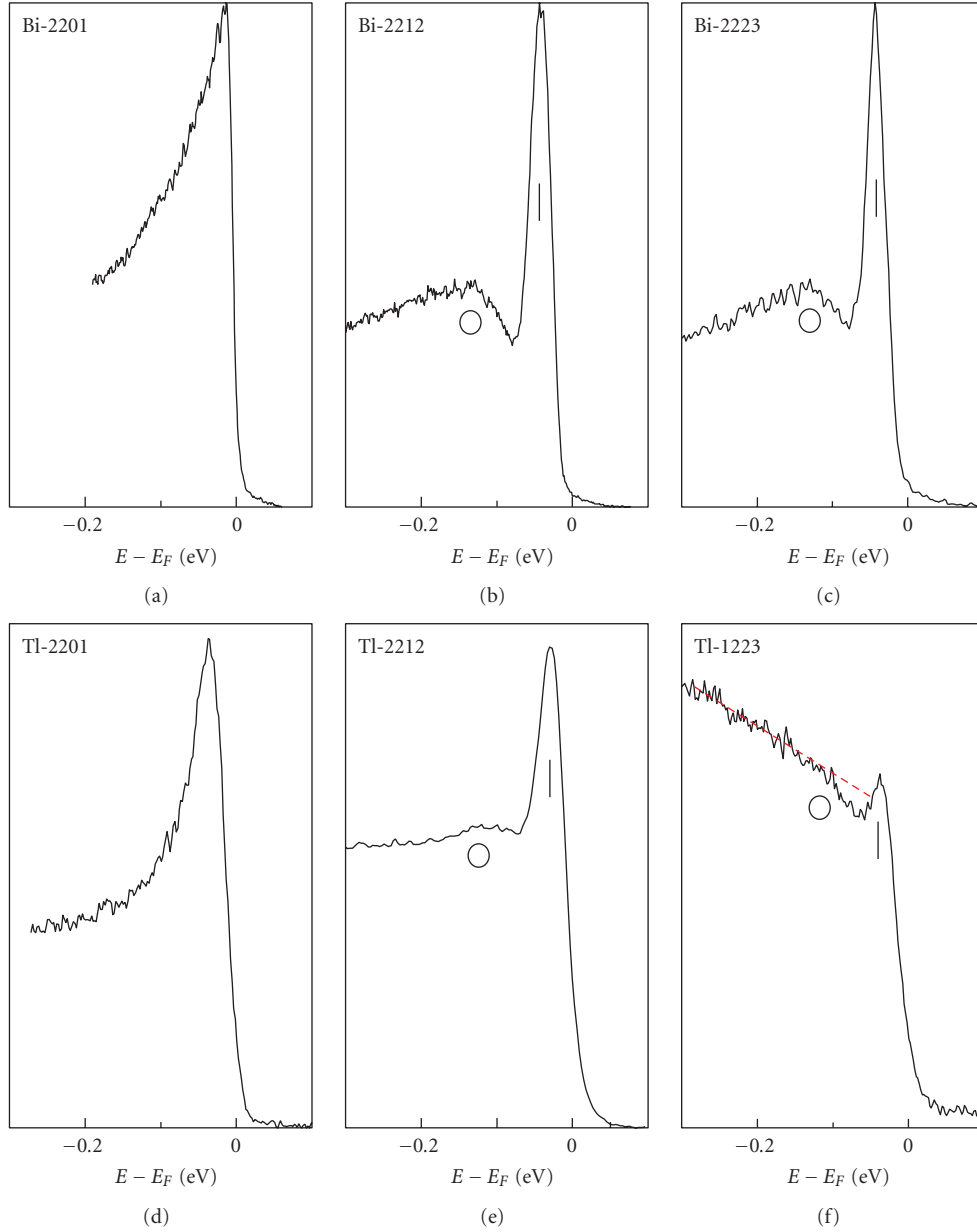


FIGURE 2: Representative EDCs near the antinodal region of the Bi- and Tl-families of cuprates, including single-layer (Bi-2201 and Tl-2201), bilayer (Bi-2212 and Tl-2212), and trilayer (Bi-2223 and Tl-1223) compounds. The high background in the data of Tl-1223 is probably due to the absence of a natural cleaving plane in the crystal structure. Nevertheless, a peak-dip-hump structure in the spectrum can still be discerned. The red dashed line is a guide-to-the-eye to make the “hump” more discernible.

In the OD65K case, the contribution from the AB makes an exact determination of the dip position difficult and the estimate of  $\sim 32$  meV should be considered a lower bound.

Turning now to the nodal region, we find qualitatively different behavior. Figure 4 presents  $A(k, \omega)$  along the nodal cut  $((0,0)-(\pi, \pi))$  for the same three samples. The highlighted region indicates the approximate position of the kink. In the nodal region the overall bandwidth is much larger than the energy of the bosonic modes so the dramatic band breakup does not occur [24] and the renormalization manifests as a kink in the dispersion. In this case, the energy scale of the

kink is most easily determined from the structure of the real part of the self-energy  $\text{Re}\Sigma$ . The MDC-derived estimate for  $\text{Re}\Sigma$ , obtained from subtracting the MDC-derived dispersion from an assumed linear band, is also in the lower panels of Figure 4.

The nominal doping dependence (The nominal doping level is estimated from  $T_c$  using the empirical law  $T_c = T_c^{\text{max}}[1 - 82.6(x - 0.16)^2]$ .) of the energy scales in the nodal and antinodal region of Bi-2212 is summarized in Figure 5(a). For reference, the superconducting gap  $\Delta_0$  is shown also, which is determined from the peak positions

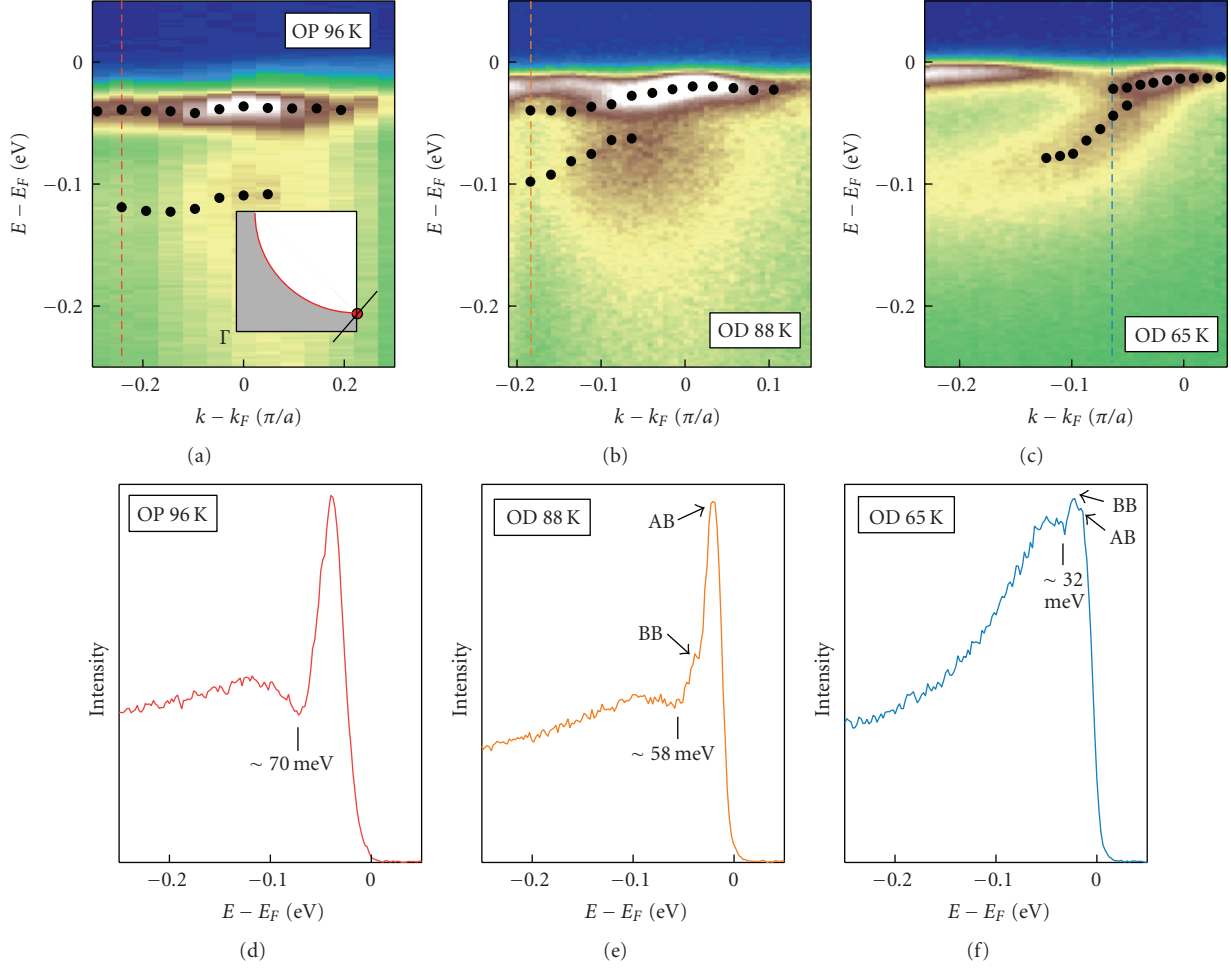


FIGURE 3: The doping dependence of the antinodal spectrum of Bi-2212 taken in the superconducting state (10 K). Shown in the upper row are the false color plots of the spectra taken along the indicated cut direction (inset). The black dots are the peak and hump positions of the bonding band seen in the EDCs. Shown in the lower row are the EDCs along the dashed line indicated in the false color plots. The symbols “AB” and “BB” represent the antibonding and binding bands while the numbers are the energy position of the dip of the EDC.

of the Fermi function divided spectrum at the Fermi level. While the characteristic energy in the antinodal region (dip energy) follows the decrease in the superconducting gap, the characteristic energy in the nodal region remains more or less constant ( $\sim 70$  meV). The difference in the doping dependence of the two energy scales lends further support to the existence of coupling to multiple modes. If a single mode were responsible for the renormalization throughout the zone, one would expect the doping dependence to follow the same trend in the nodal and antinodal regions.

The energy of the dominant mode  $\Omega$  can be obtained by subtracting the magnitude of the superconducting gap from the observed energy scale, expected to be  $\Omega + \Delta_0$  [24]. The results of this procedure are shown in Figure 5(b). The energy of the dominant mode in the antinodal region, within the error bars of the data, is independent of doping. The behavior in the nodal region is different; the energy of the dominant mode changes with doping. At optimal doping the energy of the dominant mode is  $\sim 35$  meV but in the overdoped samples the energy is larger  $\sim 60$  meV. This result

is consistent with the picture of coupling to multiple modes outlined in [24]. We also note that in OD88K a secondary feature can be observed in  $\text{Re}\Sigma$  at precisely the same energy as the dip energy of the antinodal region. Similar fine structure was reported earlier in [25]. The presence of this subfeature in the UD88K data as the sample is progressively overdoped, along with the 35 meV scale in the nodal data at optimal doping, is evidence of a tradeoff between a coupling dominated by the  $B_{1g}$  mode and one dominated by the bond stretching mode. We further note that [8] reached similar conclusions but assigned the antinodal renormalizations to the spin resonance mode. We believe that the multi-layer data of the previous section, especially the single-layer Tl data which show no renormalization in the antinodal region, directly refute this conclusion and favor the el-ph scenario.

## 5. The F-Family of Multilayer Cuprates

In this final section we turn attention to aspects of the kink in the multi-layer F-family of cuprates with  $n = 3-5$   $\text{CuO}_2$

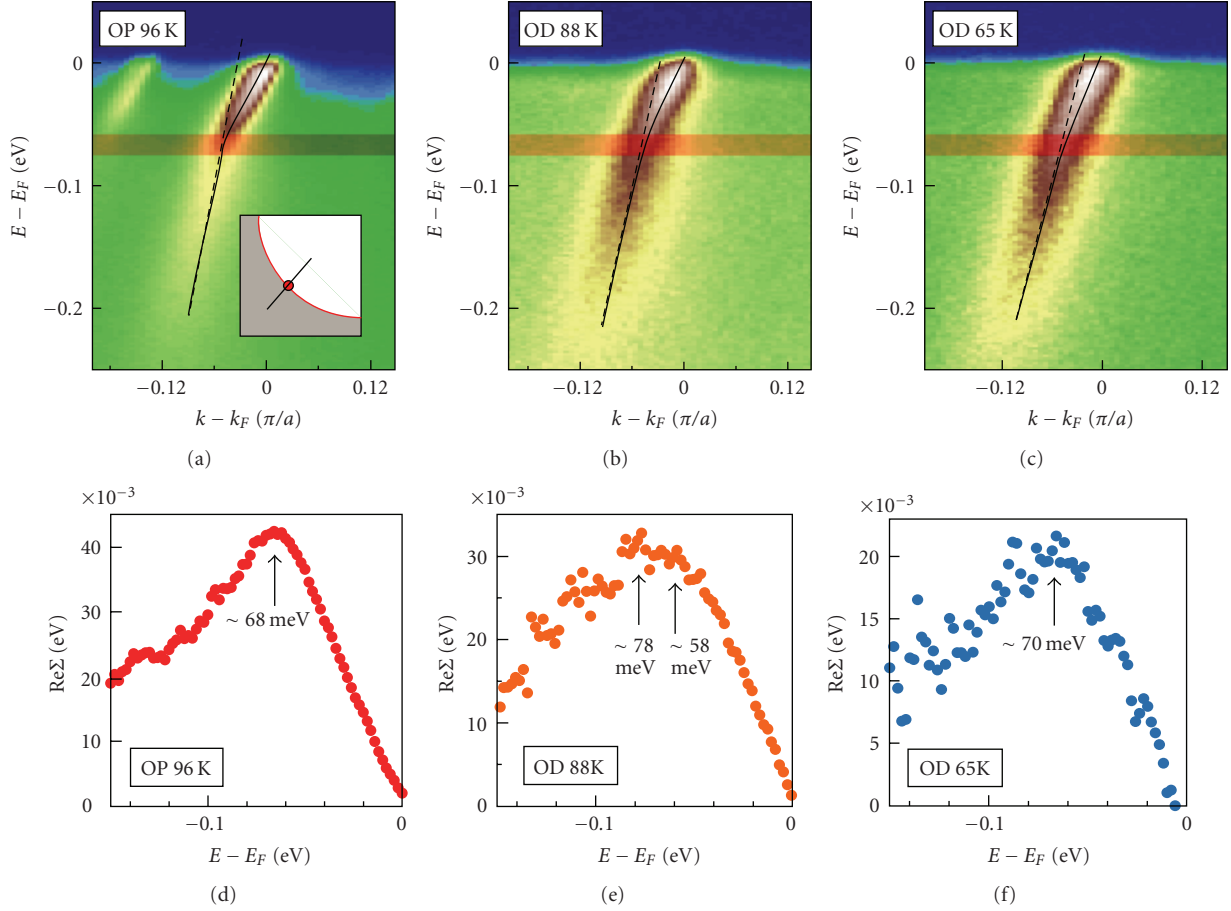


FIGURE 4: The doping dependence of the nodal spectrum at a temperature well below  $T_c$  (10 K). Shown in the upper row are the false color plots of the spectra taken along the cut as indicated in the inset. The black curves are band dispersion obtained by fitting momentum dispersion curves (MDCs) to Lorentzian functions. The apparent kink positions in the dispersion are marked by the yellow-shaded area, which appears to be approximately the same for all three dopings. The dashed lines serve as a guide-to-the-eye for visualizing the apparent kink in the dispersion. Shown in the lower row are the real parts of the self-energy extracted from subtracting the band dispersion from a linear bare band. The arrows indicate the positions of fine structure in the extracted  $\text{Re}\Sigma$ .

layers. The single-crystalline samples were grown by the flux method under high pressure [78]. ARPES measurements on the F-family were performed at beamline 10.0.1 of the Advance Light Source (ALS) at Lawrence Berkeley National Laboratory. The measurement pressure was kept  $< 4 \times 10^{11}$  Torr at all time and data were recorded by Scienta R4000 Analyzers at 15 K sample temperature. The total convolved energy and angle resolution were 16 meV and  $0.2^\circ$ , respectively, for photoelectrons generated by 55 eV photons.

In Figure 6 MDC-derived dispersions for  $p$ -type bands of the three ( $\text{Ba}_2\text{Ca}_1\text{Cu}_2\text{O}_6(\text{O},\text{F})_2$ , F0223), four ( $\text{Ba}_2\text{Ca}_3\text{Cu}_4\text{O}_8(\text{O},\text{F})_2$ , F0234), and five- ( $\text{Ba}_2\text{Ca}_4\text{Cu}_5\text{O}_{10}(\text{O},\text{F})_2$ , F0245) layer F-based cuprates are presented. In all three cases the dispersions show clear kinks, but at increased energy scales in the four- and five-layer materials. As noted earlier, for a  $d$ -wave superconductor coupled to an Einstein mode, the energy scale of the kink occurs at  $\Omega + \Delta_0$  where  $\Omega$  is the energy of the mode and  $\Delta_0$  is the maximum value of the superconducting gap. Therefore the shift in energy is due to the change in the

superconducting gap size as  $n$  varies from 3 to 5. In order to quantify the strength of the kink, slopes are extracted from the dispersion above and below the kink position,  $d\epsilon/dk|_>$  and  $d\epsilon/dk|_<$ . An estimate for the relative coupling strength  $\lambda'$  is then given by

$$\left. \frac{d\epsilon}{dk} \right|_> = (1 + \lambda') \left. \frac{d\epsilon}{dk} \right|_<. \quad (1)$$

This procedure produces  $\lambda' = 0.89, 0.75,$  and  $0.49$  for  $n = 3, 4,$  and  $5$ , respectively. This trend is easily understood in the phonon scenario where the dominant mode in the superconducting state is the  $B_{1g}$  mode for which the coupling strength is proportional to the local crystal field. The observed decrease in coupling strength can be understood if one recalls the expected local field strength in the outermost layers (recall Figure 1), which decreases for  $n > 3$ .

We now turn our attention to the identification of the carrier types in the inner and outer planes of F0234. Experimentally, the parent compound of F0234 is known

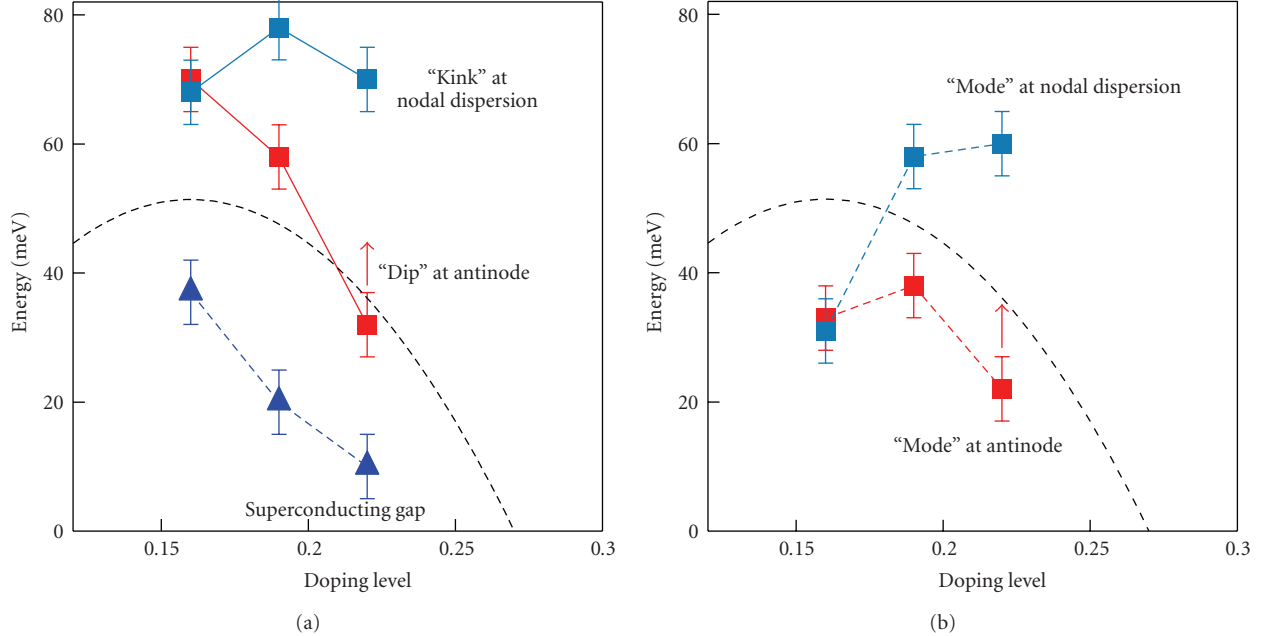


FIGURE 5: A summary of some energy scales relevant to the renormalized band dispersions. (a) The apparent kink position in the nodal dispersion, dip energy at the antinodal region, and the superconducting gap are summarized for the three doping levels shown in Figure 3. (b) The mode energy obtained by subtracting the superconducting gap from the characteristic energies of the renormalization effects is given. The red arrow is to remind the reader that the shown quantity at the antinodal region of the OD65K sample is a lower bound for the actual value.

to self-dope with the inner and outer planes having Fermi surfaces of different carrier type. A recent ARPES study [47] found that the  $p$ -type bands are bilayer split along the nodal direction. Since the inner planes are expected to have a stronger interplanar coupling than the outer planes, the observation of bilayer splitting provides strong evidence that the inner layers are  $p$ -type while the outer layers are  $n$ -type. Furthermore, kinks in the nodal dispersion of both sets of planes were observed but the strength of the coupling in the  $n$ -type layer by a factor of two.

The doping of individual layers may be driven electrostatically from Madelung (site) energy differences between the inner and outer planes. In order to determine the Madelung potential  $\Phi$  of each site, we again employ the Ewald summation technique using the structural data from [78] and assigning formal valence charges to each atom. The Madelung potentials we obtain for a hole located on the inner planes are  $\Phi_{\text{Cu}}^{\text{ip}} = -26.97$ ,  $\Phi_{\text{O}}^{\text{ip}} = 19.61$  eV/Å while for a hole located on the outer planes we obtain  $\Phi_{\text{Cu}}^{\text{op}} = -26.06$ ,  $\Phi_{\text{O}}^{\text{op}} = 19.61$  eV/Å. The corresponding values of the local crystal field at the inner and outer planar oxygen sites are  $E_z^{\text{ip}} = 5.79 \times 10^{-2}$  and  $E_z^{\text{op}} = 5.66 \times 10^{-1}$  eV/Å. The differences in Madelung energies between the layers are  $\Delta\Phi = \Phi^{\text{op}} - \Phi^{\text{ip}}$ ,  $\Delta\Phi_{\text{Cu}} = 0.91$ , and  $\Delta\Phi_{\text{O}} = 1.09$  eV. A positive value for  $\Delta\Phi$  indicates that holes will flow from the outer layer to the inner plane in order to minimize their electrostatic energy. Therefore, our results indicate that the outer layer is  $n$ -type while the inner layer is  $p$ -type. Furthermore, the strength of the E-field in the outer layer is substantially larger than that

of the inner layer and, therefore, the el-ph coupling of the  $n$ -type layer will be stronger, in agreement with experiment.

In order to determine the relative doping of the two sets of layers, the Madelung energies are now used as input to a model tight-binding calculation. Our electrostatic calculations show that even though the separate Madelung energies of Cu and O are found to vary across the unit cell, these variations tend to cancel within each layer individually and there are no substantial differences in the charge-transfer energy between Cu and O within each plane. Therefore, in the absence of coherent  $c$ -axis hopping, the bands may be treated in terms of the usual single-band downfolded tight-binding methods apart, from a layer-dependent shift of the site energies. The bands crossing the Fermi level are then determined by the four  $\text{CuO}_2$  antibonding bands, with the outer planes shifted in energy and with all four coupled by an interplanar hopping term.

Rather than addressing the full multiorbital problem, we take a 5-parameter tight-binding model for the low-energy dispersion [79] and uniformly shift the site energy of the bands associated with the outer planes by the amount indicated by our Ewald calculation. The usual interplanar coupling term [80] is introduced at this level with  $t_{\perp}(\mathbf{k}) = t_{\perp}(\cos(k_x a) - \cos(k_y a))^2/4$  and  $t_{\perp} = 50$  meV. The resulting model Hamiltonian is

$$H = \sum_{\alpha=1}^4 \sum_{\mathbf{k}, \sigma} (\epsilon_{\alpha}(\mathbf{k}) - \mu) d_{\alpha, \sigma, \mathbf{k}}^{\dagger} d_{\alpha, \sigma, \mathbf{k}} + \sum_{\langle \alpha \neq \alpha' \rangle} t_{\perp}(\mathbf{k}) d_{\alpha, \sigma, \mathbf{k}}^{\dagger} d_{\alpha', \sigma, \mathbf{k}}, \quad (2)$$

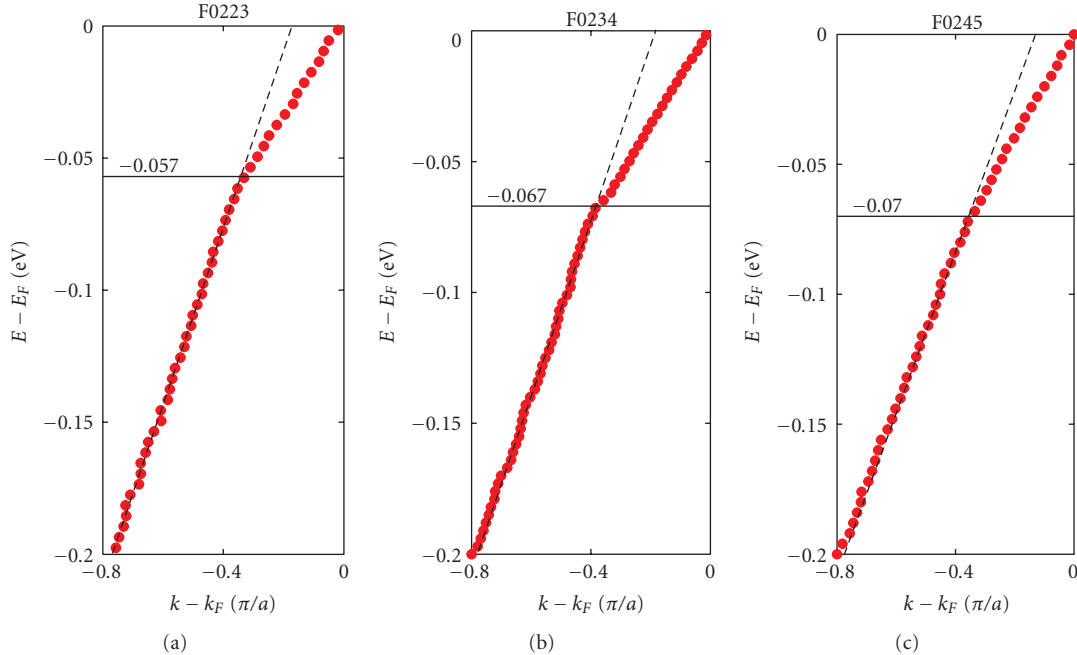


FIGURE 6: MDC-derived dispersions along the nodal direction  $(0,0)$ - $(\pi,\pi)$  of the  $p$ -type band in the 3-layer (F0223), 4-layer (F0234), and 5-layer (F0245) F-family of cuprates.

where  $\alpha = 1 - 4$  is the plane index,  $\epsilon_\alpha(\mathbf{k}) = \epsilon(\mathbf{k}) + \delta\epsilon$  for the outer planes and  $\epsilon_\alpha(\mathbf{k}) = \epsilon(\mathbf{k})$  for the inner planes,  $\delta\epsilon = \Delta\Phi/\epsilon(\infty)$  with  $\epsilon(\infty) = 3.5$  is the dielectric constant [59, 60], and  $\langle \cdot \cdot \cdot \rangle$  is a sum over neighboring planes. Here,  $\mu$  is the chemical potential which is adjusted to maintain the total filling of the parent compound. The resulting model is then diagonalized for  $\delta\epsilon = 0.29$  in order to obtain the relative filling of the four planes. We obtain fillings of 0.68 and 1.32 for the inner and outer layers, respectively. Experimentally, the carrier concentrations of the two sets of planes, determined from the Luttinger fraction, were reported in [81] with dopings of  $0.60 \pm 0.04$  and  $0.4 \pm 0.03$ , relative to half-filling, in the  $p$ - and  $n$ -type bands, which is in agreement with our results.

To summarize, our straightforward electrostatic model predicts an inequivalent filling for the inner and outer layers of F0234 which is driven by differences in the crystal environment of the two types planes. Using structural data, we find that the outer layers are expected to be of  $n$ -type while the inner layers are of  $p$ -type. The environmental asymmetry of the two sets of planes also results in differing electric field strengths with the  $n$ -type (outer) layer experiencing a larger el-ph coupling. Both of these trends are in line with the findings of [47]. However, this calculation does predict a larger ratio of the coupling strengths in the two layers. This discrepancy is probably due to the fact that the redistribution of charge between the layers has not been feed back into the electrostatic calculation. Doing so will likely reduce the ratio of E-fields predicted by in the electrostatic calculation. However, such a feedback scheme will require further guidance as to the distribution of doped carriers in the plane and, at the moment, we are not aware of any reliable indication of such.

## 6. Conclusions

In this work we have presented aspects of the material and doping dependence of the dispersion renormalizations in the nodal and antinodal regions of various single- and multi-layer cuprates. We have found that the strength of the nodal kink has a strong material dependence and varies with the number of layers present in the material. In general, the kink strength mirrors  $T_c$ , taking on a maximal value in the  $n = 3$  compounds. The issue can be complicated further in the multi-layer cuprates, where Madelung potential differences can lead to inequivalent dopings in the various layers. This can lead to further symmetry breaking across the  $\text{CuO}_2$  planes, and results in different kink strength in the different layers within the same material. Using a simple tight-binding model and electrostatic calculations, we have developed a picture of this phenomenon in self-doped F0234, which is consistent with recent ARPES studies.

The renormalization in the antinodal region also shows a marked dependence on the number of layers present in the material and is unresolved in the single-layer cuprates. This result is difficult to reconcile for coupling to the spin resonance mode, which is expected not to vary with the number of layers, but is naturally explained by coupling to the  $B_{1g}$  phonon when one considers the crystal structure of these materials.

Further evidence for multiple phonon modes was found in the doping dependence of Bi-2212. Here, the features in the nodal and antinodal regions exhibit different behavior. Once gap referenced, the energy scale in the nodal region changes from  $\sim 35$ – $40$  meV to  $\sim 70$ – $80$  meV as the sample is overdoped. This change of energy scales cannot be explained

by coupling to a single mode and, therefore, rules out the spin resonance mode, at least as the sole player. In the phonon scenario this signifies a tradeoff between dominant coupling to the  $B_{1g}$  mode near optimal doping and a dominant coupling to the bond-stretching mode in the overdoped samples. The change of relative coupling is due to increased screening of the  $B_{1g}$  mode as the carrier concentration is increased.

Both the doping and materials dependence presented here provide compelling evidence that a spectrum of phonon modes is responsible for both the nodal and antinodal low-energy renormalizations observed in the cuprates.

## Acknowledgments

This work was supported by the US Department of Energy, Office of Basic Energy Science under contract no. DE-AC02-76SF00515. Portions of this research were carried out at the Stanford Synchrotron Radiation Lightsources (SSRL), a national user facility operated by Stanford University on behalf of the US Department of Energy, Office of Basic Energy Sciences. This research used resources of the National Energy Research Scientific Computing Center, which is supported by the Office of Science of the U S Department of Energy under contract no. DE-AC02-05CH11231. S. Johnston and T P Devereaux would like to acknowledge support from NSERC and SHARCNET.

## References

- [1] P. V. Bogdanov, A. Lanzara, S. A. Kellar, et al., “Evidence for an energy scale for quasiparticle dispersion in  $Bi_2Sr_2CaCu_2O_8$ ,” *Physical Review Letters*, vol. 85, no. 12, pp. 2581–2584, 2000.
- [2] P. D. Johnson, T. Valla, A. V. Fedorov, et al., “Doping and temperature dependence of the mass enhancement observed in the cuprate  $Bi_2Sr_2CaCu_2O_{8+\delta}$ ,” *Physical Review Letters*, vol. 87, no. 17, Article ID 177007, 4 pages, 2001.
- [3] A. Lanzara, P. V. Bogdanov, X. J. Zhou, et al., “Evidence for ubiquitous strong electron-phonon coupling in high-temperature superconductors,” *Nature*, vol. 412, no. 6846, pp. 510–514, 2001.
- [4] A. Kaminski, M. Randeria, J. C. Campuzano, et al., “Renormalization of spectral line shape and dispersion below  $T_c$  in  $Bi_2Sr_2CaCu_2O_{8+\delta}$ ,” *Physical Review Letters*, vol. 86, no. 6, pp. 1070–1073, 2001.
- [5] T. Cuk, D. H. Lu, X. J. Zhou, Z.-X. Shen, T. P. Devereaux, and N. Nagaosa, “A review of electron-phonon coupling seen in the high- $T_c$  Superconductors by angle-resolved photoemission studies (ARPES),” *Physica Status Solidi B*, vol. 242, no. 1, pp. 11–29, 2005.
- [6] D. S. Dessau, B. O. Wells, Z.-X. Shen, et al., “Anomalous spectral weight transfer at the superconducting transition of  $Bi_2Sr_2CaCu_2O_{8+\delta}$ ,” *Physical Review Letters*, vol. 66, no. 16, pp. 2160–2163, 1991.
- [7] T. Cuk, F. Baumberger, D. H. Lu, et al., “Coupling of the  $B_{1g}$  Phonon to the antinodal electronic states of  $Bi_2Sr_2Ca_{0.92}Y_{0.08}Cu_2O_{8+\delta}$ ,” *Physical Review Letters*, vol. 93, no. 11, Article ID 117003, 4 pages, 2004.
- [8] A. D. Gromko, A. V. Fedorov, Y.-D. Chuang, et al., “Mass-renormalized electronic excitations at  $(\pi,0)$  in the superconducting state of  $Bi_2Sr_2CaCu_2O_{8+\delta}$ ,” *Physical Review B*, vol. 68, no. 17, Article ID 174520, 7 pages, 2003.
- [9] T. K. Kim, A. A. Kordyuk, S. V. Borisenko, et al., “Doping dependence of the mass enhancement in  $(Pb,Bi)_2Sr_2CaCu_2O_8$  at the antinodal point in the superconducting and normal states,” *Physical Review Letters*, vol. 91, no. 16, Article ID 167002, 4 pages, 2003.
- [10] T. Sato, H. Matsui, T. Takahashi, et al., “Observation of band renormalization effects in hole-doped high- $T_c$  superconductors,” *Physical Review Letters*, vol. 91, no. 15, Article ID 157003, 4 pages, 2003.
- [11] M. R. Norman, H. Ding, J. C. Campuzano, et al., “Unusual dispersion and line shape of the superconducting state spectra of  $Bi_2Sr_2CaCu_2O_{8+\delta}$ ,” *Physical Review Letters*, vol. 79, no. 18, pp. 3506–3509, 1997.
- [12] S. V. Borisenko, A. A. Kordyuk, V. Zabolotnyy, et al., “Kinks, nodal bilayer splitting, and interband scattering in  $YBa_2Cu_3O_{6+x}$ ,” *Physical Review Letters*, vol. 96, no. 11, Article ID 117004, 4 pages, 2006.
- [13] S. V. Borisenko, A. A. Kordyuk, A. Koitzsch, et al., “Parity of the pairing bosons in a high-temperature  $Pb-Bi_2Sr_2CaCu_2O_8$  bilayer superconductor by angle-resolved photoemission spectroscopy,” *Physical Review Letters*, vol. 96, no. 6, Article ID 067001, 4 pages, 2006.
- [14] A. A. Kordyuk, S. V. Borisenko, V. B. Zabolotnyy, et al., “Constituents of the quasiparticle spectrum along the nodal direction of high- $T_c$  cuprates,” *Physical Review Letters*, vol. 97, no. 1, Article ID 017002, 4 pages, 2006.
- [15] W. Meevasana, N. J. C. Ingle, D. H. Lu, et al., “Doping dependence of the coupling of electrons to bosonic modes in the single-layer high-temperature  $Bi_2Sr_2CuO_6$  superconductor,” *Physical Review Letters*, vol. 96, no. 15, Article ID 157003, 4 pages, 2006.
- [16] X. J. Zhou, J. Shi, T. Yoshida, et al., “Multiple bosonic mode coupling in the electron self-energy of  $(La_{2-x}Sr_x)CuO_4$ ,” *Physical Review Letters*, vol. 95, no. 11, Article ID 117001, 4 pages, 2005.
- [17] T. Dahm, V. Hinkov, S. V. Borisenko, et al., “Strength of the spin-fluctuation-mediated pairing interaction in a high-temperature superconductor,” *Nature Physics*, vol. 5, no. 3, pp. 217–221, 2009.
- [18] T. Valla, A. V. Fedorov, P. D. Johnson, et al., “Evidence for quantum critical behavior in the optimally doped cuprate  $Bi_2Sr_2CaCu_2O_{8+\delta}$ ,” *Science*, vol. 285, no. 5436, pp. 2110–2113, 1999.
- [19] P. W. Anderson, “Is there glue in cuprate superconductors?” *Science*, vol. 316, no. 5832, pp. 1705–1707, 2007.
- [20] E. Schachinger, J. P. Carbotte, and T. Timusk, “Characteristics of oxygen isotope substitutions in the quasiparticle spectrum of  $Bi_2Sr_2CaCu_2O_{8+\delta}$ ,” *Europhysics Letters*, vol. 86, no. 6, Article ID 67003, 2009.
- [21] Ar. Abanov, A. V. Chubukov, M. Eschrig, M. R. Norman, and J. Schmalian, “Neutron resonance in the cuprates and its effect on fermionic excitations,” *Physical Review Letters*, vol. 89, no. 17, Article ID 177002, 4 pages, 2002.
- [22] H.-Y. Kee, S. A. Kivelson, and G. Aeppli, “Spin-1 neutron resonance peak cannot account for electronic anomalies in the cuprate superconductors,” *Physical Review Letters*, vol. 88, no. 25, Article ID 257002, 4 pages, 2002.
- [23] K. Byczuk, M. Kollar, K. Held, et al., “Kinks in the dispersion of strongly correlated electrons,” *Nature Physics*, vol. 3, no. 3, pp. 168–171, 2007.

- [24] T. P. Devereaux, T. Cuk, Z.-X. Shen, and N. Nagaosa, "Anisotropic electron-phonon interaction in the cuprates," *Physical Review Letters*, vol. 93, no. 11, Article ID 117004, 4 pages, 2004.
- [25] W. S. Lee, W. Meevasana, S. Johnston, et al., "Superconductivity-induced self-energy evolution of the nodal electron of optimally doped  $\text{Bi}_2\text{Sr}_2\text{Ca}_{0.92}\text{Y}_{0.08}\text{Cu}_2\text{O}_{8+\delta}$ ," *Physical Review B*, vol. 77, no. 14, Article ID 140504, 4 pages, 2008.
- [26] W. Meevasana, T. P. Devereaux, N. Nagaosa, Z.-X. Shen, and J. Zaanen, "Calculation of overdamped  $c$ -axis charge dynamics and the coupling to polar phonons in cuprate superconductors," *Physical Review B*, vol. 74, no. 17, Article ID 174524, 6 pages, 2006.
- [27] H. Iwasawa, J. F. Douglas, K. Sato, et al., "Isotopic fingerprint of electron-phonon coupling in high- $T_c$  cuprates," *Physical Review Letters*, vol. 101, no. 15, Article ID 157005, 4 pages, 2008.
- [28] A. W. Sandvik, D. J. Scalapino, and N. E. Bickers, "Effect of an electron-phonon interaction on the one-electron spectral weight of a  $d$ -wave superconductor," *Physical Review B*, vol. 69, no. 9, Article ID 94523, 11 pages, 2004.
- [29] W. S. Lee, S. Johnston, T. P. Devereaux, and Z.-X. Shen, "Aspects of electron-phonon self-energy revealed from angle-resolved photoemission spectroscopy," *Physical Review B*, vol. 75, no. 19, Article ID 195116, 7 pages, 2007.
- [30] M. L. Kulić and O. V. Dolgov, "Dominance of the electron-phonon interaction with forward scattering peak in high- $T_c$  superconductors: theoretical explanation of the ARPES kink," *Physical Review B*, vol. 71, no. 9, Article ID 092505, 4 pages, 2005.
- [31] M. L. Kulić, "Interplay of electron-phonon interaction and strong correlations: the possible way to high-temperature superconductivity," *Physics Report*, vol. 338, no. 1-2, pp. 1–264, 2000.
- [32] M. L. Kulić and R. Zeyher, "Influence of strong electron correlations on the electron-phonon coupling in high- $T_c$  oxides," *Physical Review B*, vol. 49, no. 6, pp. 4395–4398, 1994.
- [33] R. Zeyher and M. L. Kulić, "Renormalization of the electron-phonon interaction by strong electronic correlations in high- $T_c$  superconductors," *Physical Review B*, vol. 53, no. 5, pp. 2850–2862, 1996.
- [34] Z. B. Huang, W. Hanke, E. Arrigoni, and D. J. Scalapino, "Electron-phonon vertex in the two-dimensional one-band Hubbard model," *Physical Review B*, vol. 68, no. 22, Article ID 220507, 4 pages, 2003.
- [35] R. Heid, K.-P. Bohnen, R. Zeyher, and D. Manske, "Momentum dependence of the electron-phonon coupling and self-energy effects in superconducting  $\text{YBa}_2\text{Cu}_3\text{O}_7$  within the local density approximation," *Physical Review Letters*, vol. 100, no. 13, Article ID 137001, 4 pages, 2008.
- [36] R. Heid, R. Zeyher, D. Manske, and K.-P. Bohnen, "Phonon-induced pairing interaction in  $\text{YBa}_2\text{Cu}_3\text{O}_7$  within the local-density approximation," *Physical Review B*, vol. 80, no. 2, Article ID 024507, 6 pages, 2009.
- [37] F. Giustino, M. L. Cohen, and S. G. Louie, "Small phonon contribution to the photoemission kink in the copper oxide superconductors," *Nature*, vol. 452, no. 7190, pp. 975–978, 2008.
- [38] D. Reznik, G. Sangiovanni, O. Gunnarsson, and T. P. Devereaux, "Photoemission kinks and phonons in cuprates," *Nature*, vol. 455, no. 7213, pp. E6–E7, 2008.
- [39] R. S. Markiewicz, S. Sahrakorpi, M. Lindroos, H. Lin, and A. Bansil, "One-band tight-binding model parametrization of the high- $T_c$  cuprates including the effect of  $k_z$  dispersion," *Physical Review B*, vol. 72, no. 5, Article ID 054519, 13 pages, 2005.
- [40] J. Lee, K. Fujita, K. McElroy, et al., "Interplay of electron-lattice interactions and superconductivity in  $\text{Bi}_2\text{Sr}_2\text{CaCu}_2\text{O}_{8+\delta}$ ," *Nature*, vol. 442, no. 7102, pp. 546–550, 2006.
- [41] N. Jenkins, Y. Fasano, C. Berthod, et al., "Imaging the essential role of spin fluctuations in high- $T_c$  superconductivity," *Physical Review Letters*, vol. 103, no. 22, Article ID 227001, 4 pages, 2009.
- [42] J.-X. Zhu, K. McElroy, J. Lee, et al., "Effects of pairing potential scattering on Fourier-transformed inelastic tunneling spectra of high- $T_c$  cuprate superconductors with bosonic modes," *Physical Review Letters*, vol. 97, no. 17, Article ID 177001, 4 pages, 2006.
- [43] J.-X. Zhu, A. V. Balatsky, T. P. Devereaux, et al., "Fourier-transformed local density of states and tunneling into a  $d$ -wave superconductor with bosonic modes," *Physical Review B*, vol. 73, no. 1, Article ID 014511, 9 pages, 2006.
- [44] S. Pilgram, T. M. Rice, and M. Sgrist, "Role of inelastic tunneling through the insulating barrier in scanning-tunneling-microscope experiments on cuprate superconductors," *Physical Review Letters*, vol. 97, no. 11, Article ID 117003, 4 pages, 2006.
- [45] J. Hwang, T. Timusk, and J. P. Carbotte, "Scanning-tunnelling spectra of cuprates: commentary," *Nature*, vol. 446, no. 7132, pp. E3–E4, 2007.
- [46] T. Hanaguri, Y. Kohsaka, J. C. Davis, et al., "Quasiparticle interference and superconducting gap in  $\text{Ca}_{2-x}\text{Na}_x\text{CuO}_2\text{Cl}_2$ ," *Nature Physics*, vol. 3, no. 12, pp. 865–871, 2007.
- [47] Y. Chen, A. Iyo, W. Yang, et al., "Unusual layer-dependent charge distribution, collective mode coupling, and superconductivity in multilayer cuprate  $\text{Ba}_2\text{Ca}_3\text{Cu}_4\text{O}_8\text{F}_2$ ," *Physical Review Letters*, vol. 103, no. 3, Article ID 036403, 4 pages, 2009.
- [48] W. S. Lee, K. Tanaka, I. M. Vishik, et al., "Dependence of band-renormalization effects on the number of copper oxide layers in  $\text{tl}$ -based copper oxide superconductors revealed by angle-resolved photoemission spectroscopy," *Physical Review Letters*, vol. 103, no. 6, Article ID 067003, 4 pages, 2009.
- [49] L. Pintschovius, "Electron-phonon coupling effects explored by inelastic neutron scattering," *Physica Status Solidi B*, vol. 242, no. 1, pp. 30–50, 2005.
- [50] T. P. Devereaux, A. Virosztek, and A. Zawadowski, "Charge-transfer fluctuation,  $d$ -wave superconductivity, and the  $B_{1g}$  Raman phonon in cuprates," *Physical Review B*, vol. 51, no. 1, pp. 505–514, 1995.
- [51] T. P. Devereaux, A. Virosztek, and A. Zawadowski, "Neutron scattering and the  $B_{1g}$  phonon in the cuprates," *Physical Review B*, vol. 59, no. 22, pp. 14618–14623, 1999.
- [52] B. Friedl, C. Thomsen, and M. Cardona, "Determination of the superconducting gap in  $\text{RBa}_2\text{Cu}_3\text{O}_{7-\delta}$ ," *Physical Review Letters*, vol. 65, no. 7, pp. 915–918, 1990.
- [53] E. Altendorf, X. K. Chen, J. C. Irwin, R. Liang, and W. N. Hardy, "Temperature dependences of the 340-, 440-, and 500- $\text{cm}^{-1}$  Raman modes of  $\text{YBa}_2\text{Cu}_3\text{O}_y$  for  $6.7 \lesssim y \lesssim 7.0$ ," *Physical Review B*, vol. 47, no. 13, pp. 8140–8150, 1993.
- [54] H. A. Mook, M. Mostoller, J. A. Harvey, N. W. Hill, B. C. Chakoumakos, and B. C. Sales, "Observation of phonon softening at the superconducting transition in  $\text{Bi}_2\text{Sr}_2\text{CaCu}_2\text{O}_8$ ," *Physical Review Letters*, vol. 65, no. 21, pp. 2712–2715, 1990.
- [55] N. Pyka, W. Reichardt, L. Pintschovius, G. Engel, J. Rossat-Mignod, and J. Y. Henry, "Superconductivity-induced phonon

- softening in  $\text{YBa}_2\text{Cu}_3\text{O}_7$  observed by inelastic neutron scattering,” *Physical Review Letters*, vol. 70, no. 10, pp. 1457–1460, 1993.
- [56] T. P. Devereaux, A. Virosztek, A. Zawadowski, et al., “Enhanced electron phonon coupling and its irrelevance to high  $T_c$  superconductivity,” *Solid State Communications*, vol. 108, no. 7, pp. 407–411, 1998.
- [57] M. Opel, R. Hackl, T. P. Devereaux, et al., “Physical origin of the buckling in  $\text{CuO}_2$ : electron-phonon coupling and Raman spectra,” *Physical Review B*, vol. 60, no. 13, pp. 9836–9844, 1999.
- [58] O. K. Andersen, S. Y. Savrasov, O. Jepsen, and A. I. Liechtenstein, “Out-of-plane instability and electron-phonon contribution to s- and d-wave pairing in high-temperature superconductors; LDA linear-response calculation for doped  $\text{CaCuO}_2$  and a generic tight-binding model,” *Journal of Low Temperature Physics*, vol. 105, no. 3-4, pp. 285–304, 1996.
- [59] S. Johnston, F. Vernay, and T. P. Devereaux, “Impact of an oxygen dopant in  $\text{Bi}_2\text{Sr}_2\text{CaCu}_2\text{O}_{8+\delta}$ ,” *Europhysics Letters*, vol. 86, no. 3, Article ID 37007, 5 pages, 2009.
- [60] Y. Ohta, T. Tohyama, and S. Maekawa, “Apex oxygen and critical temperature in copper oxide superconductors: universal correlation with the stability of local singlets,” *Physical Review B*, vol. 43, no. 4, pp. 2968–2982, 1991.
- [61] Q. Huang, J. W. Lynn, Q. Xiong, and C. W. Chu, “Oxygen dependence of the crystal structure of  $\text{HgBa}_2\text{CuO}_{4+\delta}$  and its relation to superconductivity,” *Physical Review B*, vol. 52, no. 1, pp. 462–470, 1995.
- [62] P. G. Radaelli, J. L. Wagner, B. A. Hunter, et al., “Structure, doping and superconductivity in  $\text{HgBa}_2\text{CaCu}_2\text{O}_{6+\delta}$  ( $T_c \leq 128$  K),” *Physica C*, vol. 216, no. 1-2, pp. 29–35, 1993.
- [63] A. R. Armstrong, W. I. F. David, I. Gameson, et al., “Crystal structure of  $\text{HgBa}_2\text{Ca}_2\text{Cu}_3\text{O}_{8+\delta}$  at high pressure (to 8.5 GPa) determined by powder neutron diffraction,” *Physical Review B*, vol. 52, no. 21, pp. 15551–15557, 1995.
- [64] M. Paranthaman and B. C. Chakoumakos, “Crystal chemistry of  $\text{HgBa}_2\text{Ca}_{n-1}\text{Cu}_n\text{O}_{2n+2+\delta}$  ( $n = 1, 2, 3, 4$ ) superconductors 1,” *Journal of Solid State Chemistry*, vol. 122, no. 1, pp. 221–230, 1996.
- [65] Q. Huang, O. Chmaissem, J. J. Capponi, et al., “Neutron powder diffraction study of the crystal structure of  $\text{HgBa}_2\text{Ca}_4\text{Cu}_5\text{O}_{12+\delta}$  at room temperature and at 10 K,” *Physica C*, vol. 227, no. 1-2, pp. 1–9, 1994.
- [66] P. Ewald, “Die Berechnung optischer und elektrostatischer Gitterpotentiale,” *Annalen der Physik*, vol. 369, no. 3, pp. 253–287, 1921.
- [67] S. Johnston, F. Vernay, B. Moritz, et al., to be published.
- [68] Y. Bang, “Effects of phonon interaction on pairing in high- $T_c$  superconductors,” *Physical Review B*, vol. 78, no. 7, Article ID 075116, 10 pages, 2008.
- [69] W. S. Lee, et al., “Band renormalization effect of  $\text{Bi}_2\text{Sr}_2\text{Ca}_2\text{Cu}_3\text{O}_{10+\delta}$ ,” in *High  $T_c$  Superconductors and Related Transition Metal Oxides*, A. Bussmann-Holder and H. Keller, Eds., Springer, Berlin, Germany, 2007.
- [70] J. Wei, Y. Zhang, H. W. Ou, et al., “Superconducting coherence peak in the electronic excitations of a single-layer  $\text{Bi}_2\text{Sr}_{1.6}\text{La}_{0.4}\text{CuO}_{6+\delta}$  cuprate superconductor,” *Physical Review Letters*, vol. 101, no. 9, Article ID 097005, 4 pages, 2008.
- [71] J. Graf, M. D’Astuto, C. Jozwiak, et al., “Bond stretching phonon softening and kinks in the angle-resolved photoemission spectra of optimally doped  $\text{Bi}_2\text{Sr}_{1.6}\text{La}_{0.4}\text{Cu}_2\text{O}_{6+\delta}$  superconductors,” *Physical Review Letters*, vol. 100, no. 22, Article ID 227002, 4 pages, 2008.
- [72] J. Meng, W. Zhang, G. Liu, et al., “Monotonic d-wave superconducting gap of the optimally doped  $\text{Bi}_2\text{Sr}_{1.6}\text{La}_{0.4}\text{CuO}_6$  superconductor by laser-based angle-resolved photoemission spectroscopy,” *Physical Review B*, vol. 79, no. 2, Article ID 024514, 4 pages, 2009.
- [73] Y. X. Xiao, T. Sato, K. Terashima, et al., “Single-particle excitation gap in  $\text{La}_{2-x}\text{Sr}_x\text{CuO}_4$  studied by high-resolution angle-resolved photoemission,” *Physica C*, vol. 463–465, pp. 44–47, 2007.
- [74] M. Shi, J. Chang, S. Pailhès, et al., “Coherent d-Wave superconducting gap in underdoped  $\text{La}_{2-x}\text{Sr}_x\text{CuO}_4$  by angle-resolved photoemission spectroscopy,” *Physical Review Letters*, vol. 101, no. 4, Article ID 047002, 4 pages, 2008.
- [75] T. Sato, K. Terashima, K. Nakayama, et al., “Bogoliubov quasiparticle and low-energy dispersion kink in the superconducting state of  $\text{La}_{1.85}\text{Sr}_{0.15}\text{CuO}_4$ ,” *Physica C*, vol. 460–462, pp. 864–865, 2007.
- [76] D. C. Peets, J. D. F. Mottershead, B. Wu, et al., “ $\text{Ti}_2\text{Ba}_2\text{CuO}_{6+\delta}$  brings spectroscopic probes deep into the overdoped regime of the high- $T_c$  cuprates,” *New Journal of Physics*, vol. 9, article 28, 2007.
- [77] H. He, P. Bourges, Y. Sidis, et al., “Magnetic resonant mode in the single-layer high-temperature superconductor  $\text{Ti}_2\text{Ba}_2\text{CuO}_{6+\delta}$ ,” *Science*, vol. 295, no. 5557, pp. 1045–1047, 2002.
- [78] A. Iyo, M. Hirai, K. Tokiwa, T. Watanabe, and Y. Tanaka, “Crystal growth of  $\text{Ba}_2\text{Ca}_{n-1}\text{Cu}_n\text{O}_{2n}(\text{O},\text{F})_2$  ( $n = 3$  and  $4$ ) multi-layered superconductors under high pressure,” *Superconductor Science and Technology*, vol. 17, no. 1, pp. 143–147, 2004.
- [79] M. R. Norman, M. Randeria, H. Ding, and J. C. Campuzano, “Phenomenological models for the gap anisotropy of  $\text{Bi}_2\text{Sr}_2\text{CaCu}_2\text{O}_8$  as measured by angle-resolved photoemission spectroscopy,” *Physical Review B*, vol. 52, no. 1, pp. 615–622, 1995.
- [80] T. Xiang and J. M. Wheatley, “ $c$  axis superfluid response of copper oxide superconductors,” *Physical Review Letters*, vol. 77, no. 22, pp. 4632–4635, 1996.
- [81] Y. Chen, A. Iyo, W. Yang, et al., “Anomalous Fermi-surface dependent pairing in a self-doped high- $T_c$  superconductor,” *Physical Review Letters*, vol. 97, no. 23, Article ID 236401, 4 pages, 2006.

## Review Article

# Through a Lattice Darkly: Shedding Light on Electron-Phonon Coupling in the High $T_c$ Cuprates

D. R. Garcia<sup>1</sup> and A. Lanzara<sup>1,2</sup>

<sup>1</sup>Department of Physics, University of California, Berkeley, CA 94720, USA

<sup>2</sup>Material Science Division, Lawrence Berkeley National Laboratory, Berkeley, CA 94720, USA

Correspondence should be addressed to A. Lanzara, [alanzara@lbl.gov](mailto:alanzara@lbl.gov)

Received 6 December 2009; Accepted 22 January 2010

Academic Editor: Carlo Di Castro

Copyright © 2010 D. R. Garcia and A. Lanzara. This is an open access article distributed under the Creative Commons Attribution License, which permits unrestricted use, distribution, and reproduction in any medium, provided the original work is properly cited.

With its central role in conventional BCS superconductivity, electron-phonon coupling appears to play a more subtle role in the phase diagram of the high-temperature superconducting cuprates. Their added complexity due to potentially numerous competing phases, including charge, spin, orbital, and lattice ordering, makes teasing out any unique phenomena challenging. In this review, we present our work using angle-resolved photoemission spectroscopy (ARPES) exploring the role of the lattice on the valence band electronic structure of the cuprates. We introduce the ARPES technique and its unique ability to probe the effect of bosonic renormalization (or “kink”) on near- $E_F$  band structure. Our survey begins with the establishment of the ubiquitous nodal cuprate kink leading to how isotope substitution has shed a critical new perspective on the role and strength of electron-phonon coupling. We continue with recently published work connecting the phonon dispersion seen with inelastic X-ray scattering (IXS) to the location of the kink observed by ARPES near the nodal point. Finally, we present very recent and ongoing ARPES work examining how induced strain through chemical pressure provides a potentially promising avenue for understanding the broader role of the lattice to the superconducting phase and larger cuprate phase diagram.

## 1. Foreword

The challenge of understanding the origin of high-temperature superconductivity in the cuprates stems from the complicated interplay of differing orders and phenomena believed to exist. The goal of this article is to focus on one such phenomenon, the role of the lattice coupling to electronic states. Though historically significant in conventional superconductivity, it has only lately been receiving attention as a potentially important player in the physics of the cuprate phase diagram. Over the course of this article, we will be addressing the following areas: (1) how Angle Resolved Photoemission Spectroscopy (ARPES) can be used to probe and better understand electron self-energy effects; (2) a brief history of the ARPES “kink” seen in the cuprates and how both the energy scale it defines and its ubiquity in these systems open the door to continued debate over low-energy excitations; (3) how the cuprate isotope effect illuminates issues such as the role of phonons, the nature of the coherent and incoherent parts of the electronic dispersion, the limitations

of current theory, and the subtle way differing competing orders that may be interrelated within these systems; (4) recent work mapping phonon dispersion and relating it to ARPES data to underscore how phonon mode nesting may relate to the observed kink; and (5) a survey of recent and ongoing work examining the role lattice strain may play in understanding electron-phonon coupling and potentially the larger phase diagram. Thus, our goal in this review is not to argue how much significance the lattice has to the development of high-temperature superconductivity, but rather the ways in which we find it manifesting within these systems.

## 2. Signature of Electron-Phonon Coupling in ARPES

The use of ARPES to study electron-phonon coupling could be seen as the union of two different approaches to the study of phonons. First, and perhaps most obvious, is the mapping of phonon dispersions using inelastic scattering

techniques such as inelastic neutron or X-ray scattering. This momentum space perspective is generally the most intuitive manner for understanding phonon modes within the lattice. Still, if we are seeking information about how electronic states interact with phonons, it is, at best, an indirect technique. Historically, tunneling measurements such as those done on conventional superconductors, such as Pb [1], have provided insight into how electron-phonon coupling directly affects electronic states near the Fermi energy  $E_F$ . The previously unexpected features seen in the spectra were then able to be explained within a strong coupling form of Migdal-Eliashberg theory [2]. Still, to be able to have the direct information of how phonon modes affect electronic states yet seen within a momentum space perspective requires a different approach, an approach that ARPES is well-suited to offer.

**2.1. ARPES and  $A(\mathbf{k}, \omega)$  Analysis.** Over the last decade, ARPES has become a truly unique experimental probe with an ever growing number of publications in the field of correlated electronic systems. Its central ability to directly probe the single particle spectral function,  $A(\mathbf{k}, \omega)$ , makes its experimental insights highly sought after by condensed matter theorists. With angular resolution approaching  $0.1^\circ$ , a steadily improving energy resolution exceeding 1 meV, as well as numerous experimental advances involving highly localized beam spots (Nano-ARPES), spin resolution, and laser-based pump-probe experiments, ARPES continues to be and will likely remain on the cutting edge of experimental solid state physics. Because of the central role that it plays in the work described in this review, we will begin with a brief overview of the theory of ARPES, with an emphasis on the analytical techniques which are critical for studying systems such as the high  $T_c$  cuprates.

It is customary to write the ARPES photocurrent intensity,  $I(\mathbf{k}, \omega)$ , as

$$I(\mathbf{k}, \omega) = M(\mathbf{k}, \omega) f(\omega) A(\mathbf{k}, \omega), \quad (1)$$

where  $A(\mathbf{k}, \omega)$  is the crucial single particle spectral function, that is, the imaginary part of the single particle Green's function,  $G(\mathbf{k}, \omega)$  with  $\mathbf{k}$  referring to the crystal momentum, while  $\omega$  is energy relative to the chemical potential. Modifying the spectral function,  $M(\mathbf{k}, \omega)$  is the matrix element associated with the transition from the initial to final electronic state which can be affected by such things as incident photon energy and polarization as well as the Brillouin zone (BZ) of the photoemitted electrons. Finally,  $f(\omega)$  is the Fermi-Dirac function indicating that only filled electronic states can be accessed. Because of the temperature scales used for data in this review, we will not distinguish between the chemical potential and the Fermi energy,  $E_F$ , which should match at  $T = 0$  for conductors. Since ARPES measures the electron removal part of  $A(\mathbf{k}, \omega)$ , we use high and low energy to refer to large and small negative  $\omega$  value, respectively. (Additionally, "Binding energy" and "Energy" are often used for the same axis in figures, differing by a minus sign.) As a final point, one might find the contribution of the matrix element  $M(\mathbf{k}, \omega)$  in (1) a serious issue to an

accurate interpretation of  $A(\mathbf{k}, \omega)$  from  $I(\mathbf{k}, \omega)$ . In practice, the  $\omega$  dependence is small over an energy range of order 0.1 eV while the  $\mathbf{k}$  dependence of  $M(\mathbf{k}, \omega)$ , though important to consider, is reasonably understood by the ARPES cuprate community for the range of the data presented here.

Of particular importance to our exploration of bosonic mode coupling is how electron self-energy effects appear in our ARPES analysis. This is nicely done by introducing the electron proper self-energy  $\Sigma(\mathbf{k}, \omega) = \text{Re}\Sigma(\mathbf{k}, \omega) + i\text{Im}\Sigma(\mathbf{k}, \omega)$  which contains all the information on electron energy renormalization and lifetime. This leads to Green's and spectral functions given in terms of the electron self energy  $\Sigma(\mathbf{k}, \omega)$ :

$$G(\mathbf{k}, \omega) = \frac{1}{\omega - \epsilon(\mathbf{k}) - \Sigma(\mathbf{k}, \omega)}, \quad (2)$$

$$A(\mathbf{k}, \omega) = -\frac{1}{\pi} \frac{\text{Im}\Sigma(\mathbf{k}, \omega)}{(\omega - \epsilon(\mathbf{k}) - \text{Re}\Sigma(\mathbf{k}, \omega))^2 + \text{Im}\Sigma(\mathbf{k}, \omega)^2}, \quad (3)$$

where  $\epsilon(\mathbf{k})$  is the single electron band energy, often referred to as the bare band structure. Finally, causality requires that  $\text{Re}\Sigma(\mathbf{k}, \omega)$  and  $\text{Im}\Sigma(\mathbf{k}, \omega)$  are connected to each other by the Kramers-Kronig relation.

With advancements in the late 1990s, the unit information of an ARPES experiment consists of a two-dimensional intensity map of binding energy and momentum along a "cut" though momentum space. These two-dimensional maps offer us two natural and complementary methods for analysis. First, one can hold the energy value of the electronic states studied fixed and observe the photoemission intensity as a function of momentum, a momentum distribution curve (MDC). Similarly, one can fix the momentum space position and observe photoemission intensity as a function of energy at that momentum value, an energy distribution curve (EDC). These two methods constitute the core techniques for analysis of the spectral function  $A(\mathbf{k}, \omega)$  using ARPES.

Within our review, "MDC analysis" refers to the method of fitting Lorentzian distributions to features in the MDCs as is commonly done in the field. This method of analysis has been very successful and can be understood based on some basic conditions, specifically the condition of "local" linearity in both the self energy  $\Sigma(\mathbf{k}, \omega)$  and  $\epsilon(\mathbf{k})$ . In order for each MDC at a given energy  $\omega$  to be described with a Lorentzian function, both  $\Sigma(\mathbf{k}, \omega)$  and  $\epsilon(\mathbf{k})$  need to be linear within the narrow energy and momentum range corresponding to the width of the analyzed peak. This condition is expected to generally hold since both  $\Sigma(\mathbf{k}, \omega)$  and  $\epsilon(\mathbf{k})$  are able to be expanded using simple Taylor expansions in the following way:

$$\begin{aligned} \Sigma(\mathbf{k}, \omega) &\approx \Sigma(k_p(\omega), \omega) + \Sigma_k(k_p(\omega), \omega) (k - k_p(\omega)), \\ \epsilon(\mathbf{k}) &\approx \epsilon(k_p(\omega)) + v(k_p(\omega)) (k - k_p(\omega)), \end{aligned} \quad (4)$$

where  $k_p$  is the peak position of the MDC at  $\omega$  and  $\Sigma_k(k_p(\omega), \omega) = [\partial\Sigma/\partial k]_{k=k_p(\omega)}$ . Plugging in these expressions into (3), we obtain the following equations:

$$A(\mathbf{k}, \omega) = -\frac{1}{\pi} \frac{\Gamma(\omega)}{(k - k_p(\omega))^2 + \Gamma(\omega)^2}, \quad (5)$$

$$\text{Re}\Sigma(k_p(\omega), \omega) = \omega - \epsilon(k_p(\omega)), \quad (6)$$

$$\text{Im}\Sigma(k_p(\omega), \omega) = \Gamma(\omega) \left[ v(k_p(\omega)) + \Sigma_k(k_p(\omega), \omega) \right]. \quad (7)$$

It is worth noting that we need not make the standard assumption of momentum independence of  $\Sigma(\mathbf{k}, \omega)$  for these results to be valid. This is important since momentum dependence does exist for states away from the nodal cut (the diagonal direction to the Cu–O bonds.) It is the last two equations which provide us with a precise meaning for  $k_p(\omega)$  and  $\Gamma(\omega)$  as determined in the MDC analysis and, thus, our determination of  $\Sigma(\mathbf{k}, \omega)$  from ARPES. Equation (6) demonstrates that a reasonable assumption for  $\epsilon(\mathbf{k})$  is needed to determine  $\text{Re}\Sigma(k_p(\omega), \omega)$  while  $\text{Im}\Sigma(k_p(\omega), \omega)$  presents the additional challenge of requiring the derivative  $\Sigma_k(k_p(\omega), \omega)$ . This is further complicated since though  $\Sigma(\mathbf{k}, \omega)$  is a causal function for a *fixed*  $\mathbf{k}$  value,  $\Sigma(k_p(\omega), \omega)$  is not. Thus, one cannot invoke the Kramers-Kronig relation to relate real and imaginary parts. Nevertheless, so long as these considerations are kept in mind to prevent over-interpretation, qualitatively  $\Gamma(\omega)$  and  $k_p(\omega)$  do offer access to the causal  $\Sigma(\mathbf{k}, \omega)$  since important structures such as the ARPES kink appear in both self-energies.

Before the instrumental advances which pushed the unit information of ARPES towards a two-dimensional map, one-dimensional data was taken, making EDC analysis the more traditional method. Indeed, there are many advantages of this line of analysis. (1) Fixed momentum helps simplify the matrix element contribution to the photocurrent. (2) Momentum is a good quantum number in a single crystal approximation making the EDC a more physical quantity, opening up spectral weight sum rules, as well as providing a clear physical meaning to the dispersion of EDC peaks. (3) In principle, an EDC analysis should be able to provide us with the causal  $\Sigma(\mathbf{k}, \omega)$  throughout in the entire two-dimensional plane rather than a particular path determined by  $k_p$  in the plane as with MDC analysis. However, EDC analysis is uniquely complicated by contributions from the Fermi function cutoff,  $f(\omega)$ , as well as both elastic and inelastic photoelectron background. This leads to a challenging lineshape to analyze in practice. Still, employing a similar method of Taylor expansion analysis as used earlier, we can expand the self-energy locally near the EDC peak yielding

$$\Sigma(\mathbf{k}, \omega) \approx \Sigma(\mathbf{k}, \omega_p(\mathbf{k})) + \Sigma_\omega(\mathbf{k}, \omega_p(\mathbf{k})) (\omega - \omega_p(\mathbf{k})), \quad (8)$$

where  $\Sigma_\omega(\mathbf{k}, \omega)$  is the  $\omega$ -partial derivative of  $\Sigma(\mathbf{k}, \omega)$ . Like before, we can insert these expressions into (3) getting the following relations in the vicinity of the peak:

$$A(\mathbf{k}, \omega) = \frac{Z(\mathbf{k})}{\pi} \frac{\Gamma(\mathbf{k}, \omega)}{(\omega - \omega_p(\mathbf{k}))^2 + \Gamma(\mathbf{k}, \omega)^2}, \quad (9)$$

$$\text{Re}\Sigma(\mathbf{k}, \omega_p(\mathbf{k})) = \omega_p(\mathbf{k}) - \epsilon(\mathbf{k}), \quad (10)$$

$$\text{Im}\Sigma(\mathbf{k}, \omega_p(\mathbf{k})) = \frac{\Gamma(\mathbf{k}, \omega)}{Z(\mathbf{k})} - \text{Im}\Sigma_\omega(\mathbf{k}, \omega_p(\mathbf{k})) (\omega - \omega_p(\mathbf{k})), \quad (11)$$

$$Z(\mathbf{k}) = \frac{1}{1 - \text{Re}\Sigma_\omega(\mathbf{k}, \omega_p(\mathbf{k}))}. \quad (12)$$

When we compare these with our results for MDC analysis, the complementary nature of these two approaches begins to appear. Unlike the Lorentzian lineshape of the MDCs, the EDC lineshape is modified by an asymmetry, which makes EDC analysis less favorable for extracting self energy near  $E_F$  than MDC analysis. However, the spectra at large  $\omega$  is better analyzed with EDCs thanks to the spectral sum-rule requiring  $A(\mathbf{k}, \omega) \rightarrow 1/\omega$ , leading us to consequently expect  $Z(\mathbf{k}) \rightarrow 1$  and  $\Sigma_\omega(\mathbf{k}, \omega) \rightarrow 0$ . This means that the portion of the spectral function which we associate with incoherent excitations should begin approaching a Lorentzian lineshape and is better explored with EDCs, although inelastic background contributions at higher energy remain important. In contrast, MDCs at higher energies begin to be affected by momentum dependent matrix element contributions as well as potential deviations of  $\epsilon(\mathbf{k})$  from a locally linear behavior. Thus, with both tools in our ARPES arsenal, we can undertake a more complete understanding of self-energy effects as they appear in  $A(\mathbf{k}, \omega)$ .

*2.2. Visualizing the Kink with ARPES.* Turning our attention to the physics of electron-phonon coupling in the superconducting cuprates, our prior discussion on how self-energy manifests in the ARPES spectral function points us towards the now well-known ‘‘kink’’ feature. As (6) and (10) quickly indicate, a sudden increase in the real part of  $\Sigma(\mathbf{k}, \omega)$  at a particular energy  $\omega$  would lead to a deviation of the measured peak from the single electron band structure  $\epsilon(\mathbf{k})$  at this energy scale.

The result is seen in Figure 1 which shows superconducting phase data taken on the well-studied cuprate Bi2212 at its optimal doping ( $T_c = 92$  K). The two ARPES cuts are taken for states both at (panels (a–c)) and off (panels (d–f)) the nodal point. The different visualization methods used for each cut are designed to enhance some key characteristics of the ARPES kink phenomenon prior to a more detailed, quantitative approach involving fittings. As labeled in the figure caption, the ‘‘MDC map’’ allows us to track the MDC dispersion and width. This is similarly true for EDCs in the ‘‘EDC map’’. The color scaling is chosen to give the peak maximum and half maximum distinct colors, red and blue, respectively.

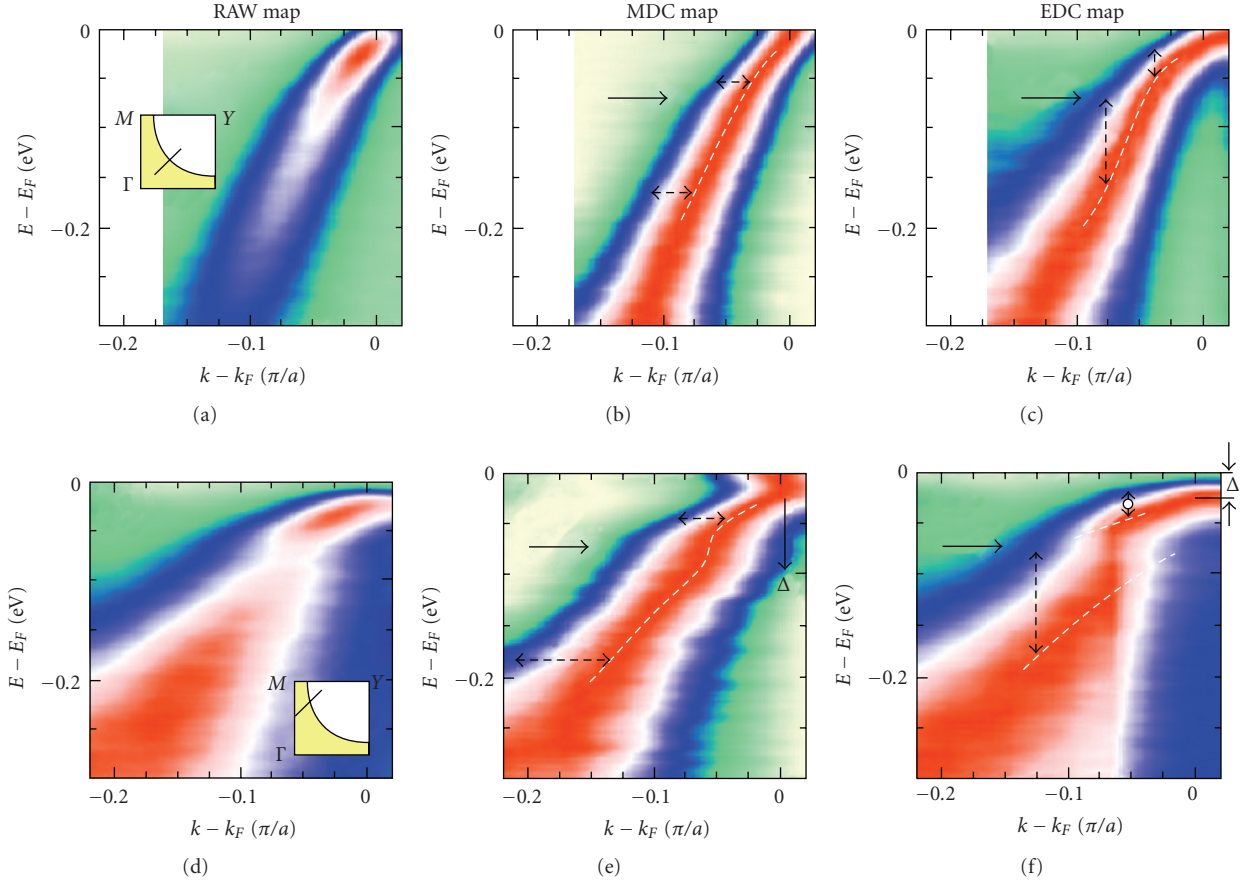


FIGURE 1: (a–c) ARPES data taken at 25 K on optimally doped Bi2212 superconductor ( $T_c = 92$  K), for a cut along the  $\Gamma Y$  direction through the nodal point in momentum space (indicated in panel (a) inset). (d–f) The same sample and orientation, but taken nearer the Brillouin zone (BZ) edge (or antinodal point) in momentum space (indicated in panel (d) inset). (a) and (d) Raw ARPES data taken with a color scale where intensity increases from pale yellow to green to blue to white to red. Here, blue (white) corresponds to 1/2 (3/4) of the maximum intensity. (b) and (e) Same data but as an “MDC map”, where each MDC has been normalized so that its maximum and minimum intensities are 1 and 0, respectively. (c) and (f) Same data but now each EDC has been appropriately normalized to create an “EDC map”. Thick black arrows indicate the energy of the bosonic mode while the  $\Delta$  is the superconducting gap. Energy resolution used here is  $\sim 15$  meV.

From these maps, we can observe the following features.

(1) The anisotropic d-wave nature of the superconducting gap is immediately apparent in the MDC “backbending” observed in panel (e) near  $E_F$  within the gap energy scale. Evidence of this gap disappears for the nodal cut (panels (a–c)) as expected. (2) There is an abrupt deviation in the electron dispersion around 70 meV below  $E_F$  (large black arrow) for both cuts. In both cuts, this corresponds to slower electron dispersion at lower energy while there is faster dispersion at higher energies above the 70 meV energy scale. (3) Focusing particularly on the off-nodal cut, one sees evidence, even in the raw map, of an intensity decrease forming a local minimum at the 70 meV energy scale. This lineshape, further enhanced by the EDC map (panel (f)), is known as a “peak-dip-hump” and is associated with the presence of self-energy effects due to the coupling of electrons with a bosonic mode leading to a redistribution of the spectral weight in the EDC spectra. (4) Although one would expect quasiparticles in a Landau Fermi liquid paradigm to become sharper (i.e., longer living) as one

approaches  $E_F$ , it is significant that the kink energy scale also marks a sudden change in coherence. One can make out from the panels, in particular the EDC maps, abrupt changes in the MDC and EDC linewidths as one passes from states above and below the kink energy scale. To bring it all together, we can define the ARPES kink as an energy crossover separating sharp, slowly dispersing, coherent states nearer  $E_F$  from broader, quickly dispersing incoherent states at higher energy.

**2.3. The Nodal Kink.** With the initial discovery of the ARPES “kink” in the superconducting cuprate Bi2212 [4], we have begun to develop a fuller picture of how low-energy many-body effects manifest in the cuprates. On the heels of this discovery and the resulting debate, a systematic study regarding the origin of this kink discovered the feature’s remarkable ubiquity across all cuprate families and dopings accessible by ARPES [3]. Figure 2 summarizes these results particularly in double-layered Bi2212 and single-layered

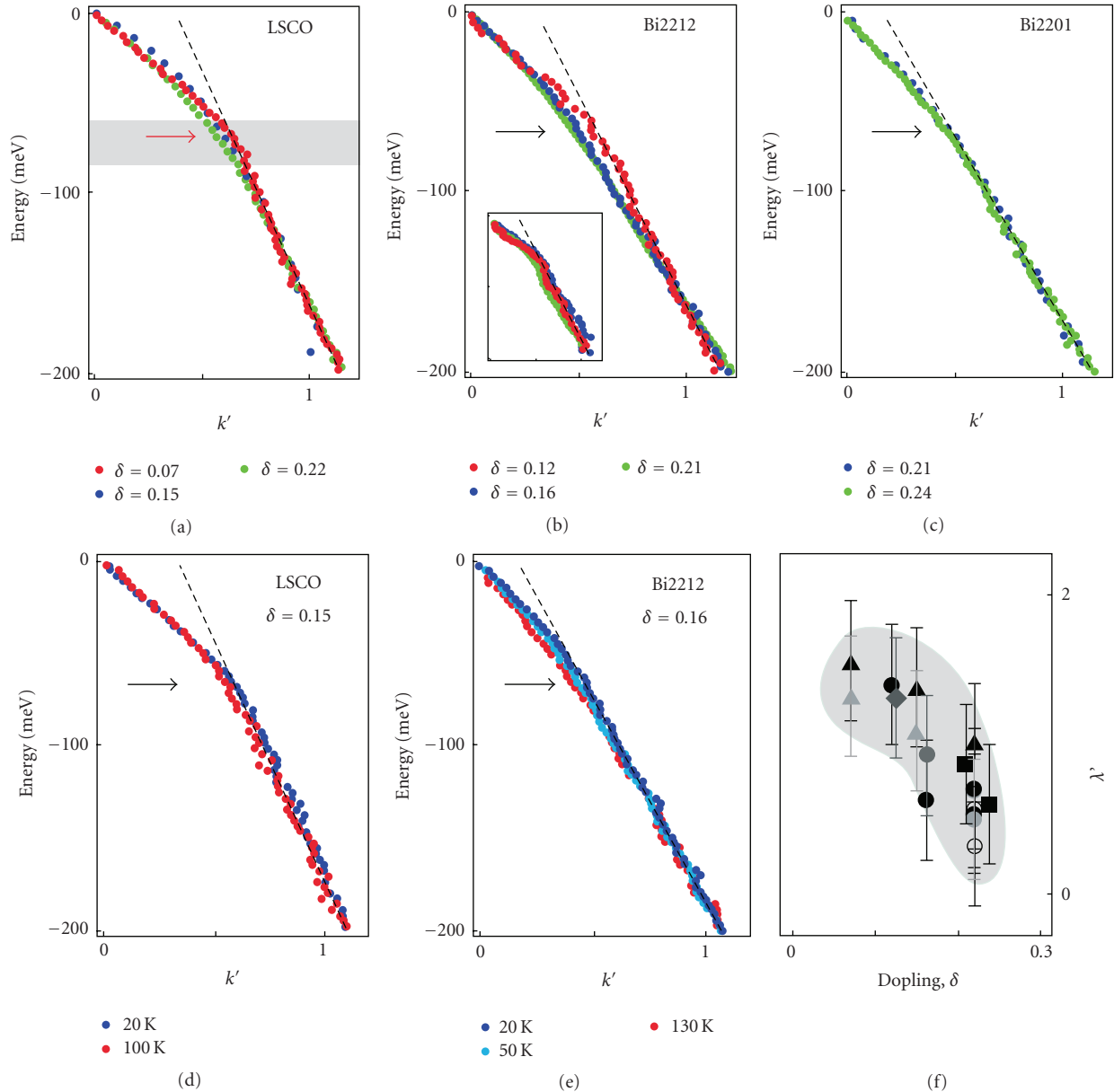


FIGURE 2: (a–e) ARPES data at the nodal point showing the ubiquity of the ARPES dispersion kink as determined from MDC fittings over a variety of cuprates systems, dopings, and temperatures above and below  $T_c$ . The kink energy is indicated by the thick arrow and the momentum is rescaled so that  $k'$  is 1 at 170 meV binding energy. (f) Estimating the electron coupling constant  $\lambda$  for the different samples as a function of their doping. Filled triangles, diamonds, squares, and circles are LSCO, Nd-LSCO, Bi2201, and Bi2212 in the first BZ, respectively. Open circles are Bi2212 in the second zone. Different shadings represent data from different experiments. The figures are from [3].

Bi2201 and LSCO showing that the kink in the nodal direction exists all across these systems at essentially the same energy,  $\sim 70$  meV. One can give an estimate of the coupling constant,  $\lambda$ , between the electrons and this bosonic mode by comparing the ratio of the group velocities above and below the kink energy,  $(1 + \lambda) = v_{\text{High}}/v_{\text{Low}}$  [5]. From this analysis, one finds evidence for a trend between doping and the strength of the mode with an enhancement of  $\Sigma(\mathbf{k}, \omega)$  as one tends to the underdoped side of the superconducting dome (panel (f)).

Additionally significant is the continued existence of the kink below *and* above the superconducting transition temperature (panel (d–e)), casting doubt on scenarios based on superconducting gap opening and particularly the magnetic mode scenario [6–11]. Comparing the photoemission data with the neutron phonon energy at  $q = (\pi, 0)$  (thick red arrow in panel (a)) and its dispersion (shaded area) [12, 13] it was proposed [3] that the nodal kink results from coupling between quasiparticles and this zone boundary in-plane oxygen-stretching longitudinal optical (LO) phonon.

Although this is the highest phonon mode contributing to the kink, quasi-particles are also coupled to other low-energy phonon modes [14].

In favor of the electron-phonon coupled system is the drop of the quasi-particle width (Figure 3) below the kink energy and the existence of a well-defined peak-dip-hump in the EDCs, a signature of an energy scale within the problem, persisting up to temperatures much higher than the superconducting critical temperature [15].

*2.4. The Near Antinodal Kink.* Many-body effects near the antinodal region of the BZ (Cu–O bond direction) had been suspected for some time from earlier ARPES studies of the cuprates where evidence of the aforementioned peak-dip-hump lineshape was reported [17, 18]. Although controversy has existed regarding the role of bilayer band splitting on the observed spectra in the double layered Bi2212 compounds, the presence of the peak-dip-hump lineshape was initially interpreted in terms of a magnetic phenomenon observed in YBCO and Bi2212 by inelastic neutron scattering [19–21]. With the resolution of the bilayer splitting [22–24], a low-energy kink of approximately 40 meV near the antinodal region was reported for Bi2212 [25–27]. The disappearance of the kink above  $T_c$  and the decrease of its strength moving away from the antinodal region has led people to interpret the onset of this kink as coupling to collective magnetic excitations [25–27], despite the absence of these excitations for more heavily doped samples [25].

More recent studies [16, 28] have reported that the near antinode kink also persists above  $T_c$ , as seen in Figure 4. However, the energy of this kink shifts towards higher energy, from 40 meV to 70 meV, upon entering the superconducting state. This shift is consistent with the opening of a 30 meV gap below  $T_c$ . The persistence of this energy scale above  $T_c$  can be clearly seen both in the dispersion (Figure 4(a)) and in the MDC width (Figures 4(b) and 4(c)). This observation has led to a new interpretation of the antinodal kink in terms of electron-phonon coupling. In this case, it was proposed that the responsible phonon, with the right energy and momentum, is the  $B_{1g}$  mode [28].

Still, it should be noted that spin fluctuations also exist in the normal phase. Indeed they have been used within marginal Fermi liquid (MFL) theory to provide the anomalous self energy [29] and have traditionally been called on to describe ARPES data in the normal phase just above  $T^*$ . What is interesting is that although MFL theory can explain the ARPES dispersion Figures 3(a) and 4(a), it cannot explain the drop in linewidth seen of Figures 3(c) and 4(c), presenting difficulties to the original theory [29]. Nevertheless, what we will find in the next section may suggest a profound connection between the physics of the lattice and spin.

The results presented so far clearly suggest that the electron-lattice coupling could not be so easily neglected in any microscopic theory of cuprate superconductivity. As discussed in Section 2.2, the kink and its energy consistently indicate a sudden transition from sharp coherent electronic excitations into broader more incoherent ones. This makes

understanding the origin of this phonon mode and its energy scale critical since it has such a substantial effect on low-energy electronic states.

### 3. ARPES Isotope Effect in Bi2212

The role of the isotope effect (IE) in establishing the electron-phonon nature of Cooper pairing for traditional BCS superconductors is well known. However, when we consider the IE in the superconducting cuprates, its effect on  $T_c$  is substantially less, leading researchers away from the electron-phonon paradigm of the BCS superconductors. But with the ubiquitous cuprate kink seen by ARPES, the importance of the lattice returns to the forefront. Additionally from our discussion in Section 2.2, the kink brings up questions about the relationship between the coherent peak (CP) seen at lower energies near  $E_F$  and the incoherent peak (IP) seen at higher energies. Indeed, hole doping affects the formation of these peaks differently [30] with the CP strongly affected while the IP appears minimally changed. Should we be thinking of the CP and IP as different objects or fundamentally connected to each other? In this light, the kink energy scale, and thus the phonon mode responsible for it, becomes increasingly significant as the key crossover between these two domains. It is in light of such questions that we undertook our ARPES study of the IE to better understand the role of the lattice in these issues.

*3.1. Prelude-Isotope Effect in ARPES Dispersion of H/W.* Using APRES to explore isotope substituted samples presents us with an entirely new and wide open field of study. As of our work, the only other study in the literature explores the surface state on W induced by H chemisorption [31]. Figure 5 shows data taken for H on W (indicated in blue) compared to D on W (indicated in red). In spite of the broad peaks due to the instrumental resolution when compared to data on the cuprates, extracting the EDC peak dispersion clearly shows two types of dispersions akin to that seen with the cuprate kink studies. Specifically, the slower low energy and faster high-energy dispersions were understood in terms of the CP and IP, respectively. These results could be compared to predictions from the strong coupling form of Migdal-Eliashberg (ME) theory which, as discussed earlier, already explained the existence of peak-dip-hump features in tunneling spectroscopy as coupling to phonon modes. There was fair agreement with ME since the high-energy linewidth (noted from panels (a-b)) and the kink energy position (dotted lines in panels (a-b)) were found to approximately scale as  $1/\sqrt{M}$  where  $M$  is the mass of H or D. Additionally as expected from ME theory, the electron-phonon coupling was  $\sim 0.5$ , and the linewidth at high-energy was  $\sim \hbar\omega_p$ . Finally, Figure 5(c) illustrates how the dispersions near the kink energy are affected by the isotope change, deviating most substantially near the kink energy while decreasing along both directions in energy, consistent with ME theory.

*3.2. Isotope Effect in ARPES Dispersion of Bi2212.* When we compare the ARPES IE seen in the H/W system to

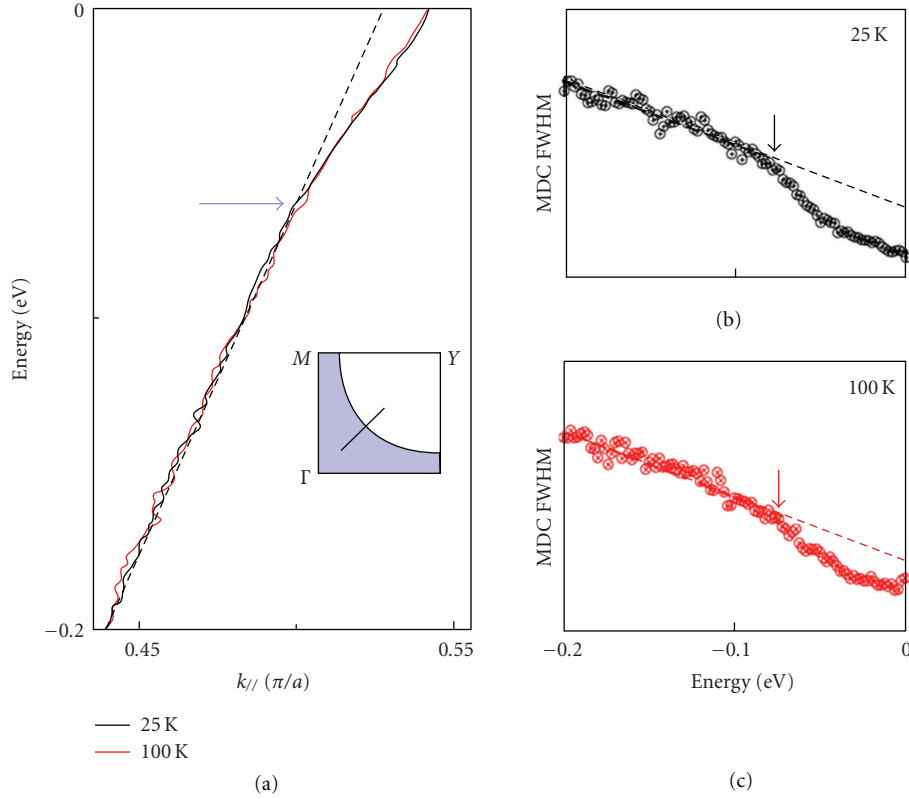


FIGURE 3: ARPES MDC dispersion data taken optimally doped  $\text{Bi}_2\text{Sr}_2\text{CaCu}_2\text{O}_{8+\delta}$  ( $T_c = 92$  K) as discussed in [16]. Nodal point data (see inset) comparing (a) dispersion and (b-c) MDC full width half max (FWHM) showing little change in the energy of the ARPES kink with  $T_c$ . The MDC FWHM is related to the  $\text{Im}\Sigma(\mathbf{k}, \omega)$ .

that measured on optimally doped  $\text{Bi}_2\text{Sr}_2\text{CaCu}_2\text{O}_{8+\delta}$ , we find surprisingly different behavior. First, let us consider the behavior of the ARPES kink energy as summarized in Figure 6. Panels (a-b) are MDC maps, as discussed in Figure 1, from data taken at the nodal point in the  $\Gamma$ -Y direction. The two samples examined contain  $^{16}\text{O}$  and  $^{18}\text{O}$  in their Cu-O planes which, as indicated by the horizontal arrow, already reveals a potential shift in the kink to lower energy with the substituted  $^{18}\text{O}$  sample.

Analyzing this more carefully, we turn to the MDC fitted dispersion for both isotopes plus a reexchanged sample,  $^{16}\text{O}_{\text{Re-exch}}$ , whereby we can take a studied  $^{18}\text{O}$  sample and re-exchange  $^{16}\text{O}$  back into the lattice. This provides us with a unique check on the IE. As indicated in panel (c), we can observe, from the dispersions, a subtle shift in the kink energy between the isotopes of approximately 5 meV. We can additionally quantify the kink by estimating the bare single electron dispersion (using a linear approximation) and extracting the real part of the electron self-energy,  $\text{Re}\Sigma(\mathbf{k}, \omega)$ , as described by (6). The location of the peak in  $\text{Re}\Sigma(\mathbf{k}, \omega)$  corresponds to the kink energy and we similarly observe a shift in this peak with isotope change. Thus, the IE does have measurable effect on the nodal ARPES kink energy, as later work would also confirm [32], further establishing its phonon origin.

A second aspect of panel (c) worth noting is the energy range where the IE is most pronounced. The maximum

change in the dispersion occurs at higher energies, particularly, beyond the kink energy, and is nearly nonexistent at energies closer to  $E_F$ . This is particularly significant when we compare this result to the H/W work where the greatest deviation occurs near the kink energy; Figure 5. We can explore this further by looking at the EDCs taken from this nodal cut, as presented in Figure 7. Panel (a) shows the dispersion of the EDC peak from where it crosses  $E_F$  at  $k_F$  as a sharp CP, to higher binding energy where it broadens and becomes the IP. Consistent with the MDC dispersions, we see very little change in the lineshape between the two isotopes for the CP near  $E_F$ . However, the IP at higher energy has a lineshape clearly affected by the IE.

In light of this change at higher energy as compared to localization around the kink, a crucial question to ask is at what energy the IE goes away? Figure 7(b) attempts to address this issue by following the MDC dispersion to even higher energies. Apparently, the IE seems to disappear around an energy scale of 2 to 3 times the antiferromagnetic coupling constant  $J$  (where  $J = 4t^2/U$  in the  $t$ - $J$  model). This could suggest a profound interconnection between the effects of the lattice and spin on the electronic states in the superconducting cuprates. Further work is needed to better understand the connections between these phenomena.

Up until now, we have focused entirely on the nodal point. Figure 8 provides MDC dispersions for  $\Gamma$ -Y slices moving outward from the nodal point towards the antinode,

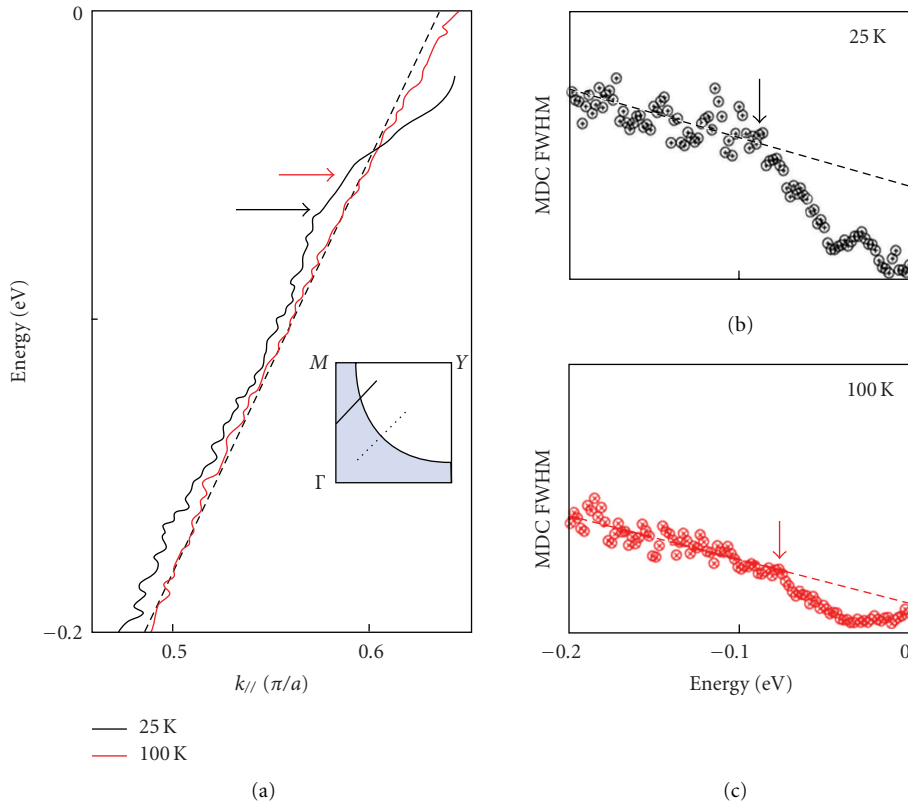


FIGURE 4: ARPES MDC dispersion data taken optimally doped  $\text{Bi}_2\text{Sr}_2\text{CaCu}_2\text{O}_{8+\delta}$  ( $T_c = 92$  K) as discussed in [16]. Near antinodal point data (see inset) comparing (a) dispersion and (b-c) FWHM showing that the ARPES kink energy is shifted to lower energy when passing above  $T_c$ . The MDC FWHM is related to the  $\text{Im}\Sigma(\mathbf{k}, \omega)$ .

both above and below  $T_c$ . There are a few important observations to make from this data. First, the kink energy shows a subtle shift of approximately 5 meV for all momentum cuts. Second, from comparing panel (a) with (b), it appears that the magnitude of the IE may be, for all curves, diminished above  $T_c$ . Third, the IE remains relatively weak near the node while comparatively more pronounced near the antinode leading to a general correspondence between the kink strength,  $\lambda$ , and the IE at high-energy. Plotting this IE shift with respect to the isotope averaged superconducting gap gives a linear relationship seen in the inset of panel (a). Finally, and potentially most surprising, there appears to be a sign change between the two dispersions as we transition from the node towards the antinode, which also appears both above and below  $T_c$ .

This sign change is significant since one can examine its location in momentum space. When we plot these crossover points, surprisingly we find that they fall along a line defined in momentum space as  $\mathbf{q}_{\text{CO}} = 0.21\pi/a$ , where  $a$  is the lattice constant of the  $\text{CuO}_2$  plane. This is illustrated in Figure 9. This particular wavevector (panel (a)) is in excellent agreement with the charge ordering wavevector seen in the far underdoped  $\text{Bi}2212$  cuprate at low temperatures as explored by STM [34] (panel (b)), implying that the high-energy part of the electronic structure is strongly coupled to the order parameter, which is in turn strongly coupled to the lattice.

To understand why at the  $\mathbf{q}_{\text{CO}}$  line the isotope effect changes sign, we used a simple charge density wave formation model, to show how an ordering mechanism can affect the quasiparticles dispersion at all energies. In panels (c-d) we present the opening of a gap in the dispersion at the  $\mathbf{q}_{\text{CO}}$  vector, due to a charge density wave formation. Based on the report that the pseudogap temperature is strongly isotope dependent and increases for the  $^{18}\text{O}$  sample [35–37], we assume that the magnitude of the gap is different between the two isotope samples, for example, larger for the  $^{18}\text{O}$  sample (panel (d)). This automatically leads to the appearance of the sign change at  $\mathbf{q}_{\text{CO}}$  that migrates to lower energy as we move away from the node, as observed in the data. Although further studies are needed, we believe that the main reason why the pseudogap opening due to an ordering phenomena has never been observed in any ARPES experiment so far, is likely due to the short range nature of such ordering [38, 39].

This result has led us to consider a possible correlation between the charge or spin instability, with  $4 \sim 5a$  periodicity, observed in the underdoped regime [34, 40] and the lattice effects relevant at optimal doping. In summary, these results suggest that the lattice degrees of freedom play a key role in the cuprates to “tip the balance” towards a particular ordered state. Simply put, the raw electron-phonon interaction may be small, but it can assist a certain kind of order through a cooperative enhancement of both the assisted order and the electron-lattice interaction

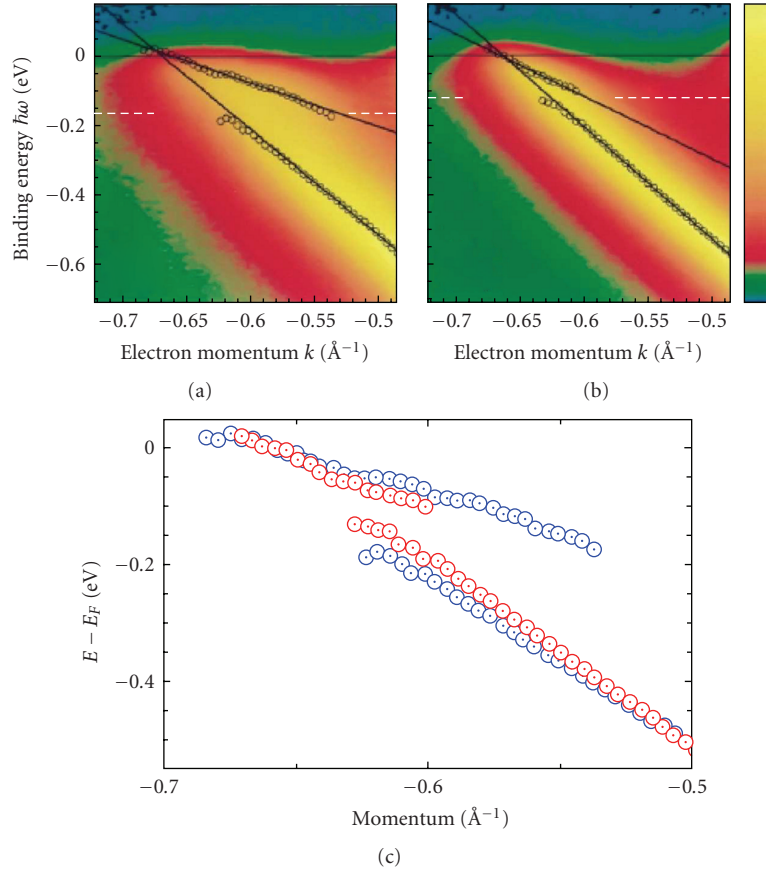


FIGURE 5: (a-b) ARPES dispersions of a surface state for (a) H monolayer on W and (b) D monolayer on W. The dispersions are determined by peak positions from EDC fits and appear as circles while the lines serve as guides to the eye. (c) These two dispersions are compared where H = blue and D = red. The figure is from [31].

[35, 36]. In particular, using a model which considers this electron-coupling boson as the critical source of charge order fluctuations [41], the sign change observed in our dispersion can be well reproduced [39].

**3.3. Isotope Effect in ARPES Width of Bi2212.** In addition to the shape of the electron dispersion, information about linewidth,  $\Gamma(\omega)$ , can be extracted and provide critical information on the electronic states. As previously discussed, MDC analysis is not ideally suited to determining the linewidth at high energies, leaving us to examine the linewidth as it is obtained from EDC analysis. Additionally, we have already observed a significant difference between states above and below the kink energy, even prior to our discussion of IE. Thus, Figure 10 divides up the electronic states into those roughly between  $E_F$  and the kink energy (0 to 70 meV) and those beyond the kink energy (70 meV to  $\sim 250$  meV). Taking the average change in width of the EDC peaks shown in Figure 7 between the isotopes for each of these two energy regions we find that IE on the linewidth is very similar to its effect on the dispersion. (1) It is very small for the low-energy coherent electronic states, while much more significant for the higher-energy incoherent states. (2) The magnitude of the IE is small at the node for these

higher energy states, but it grows more substantial as one moves towards the antinode. (3) The effect is roughly linear with respect to the isotope averaged superconducting gap,  $\Delta$ , as seen in Figure 8. Yet, it does differ from the IE in the dispersion since it lacks the sign change previously discussed. As will be addressed in depth later, the corresponding ME IE linewidth change is much smaller, about 2 meV, making the trend in the high energy linewidth a serious failing of the theory for explaining the cuprate IE.

**3.4. Doping Dependence.** So far, the data shown has been on optimally doped Bi2212 with a hole doping determined by our ARPES experiment to be  $x = 0.16$ . But the question naturally arises: how is the IE on the ARPES data affected by a change in doping? Figure 11(a) shows angle integrated photoemission data obtained on two samples at optimal doping ( $x = 0.16$ ) and one at slight over doping ( $x = 0.18$ ). The effect is dramatic that given such a small change of only 2%, the IE, which normally shifts the IP position by  $\sim 30$  meV, is substantially reduced. This work was initially inspired by a separate study claiming not to see the IE in optimally doped samples of Bi2212 [43]. However, from superstructure analysis and studying the MDC dispersions, the samples discussed in [43] were actually slightly over

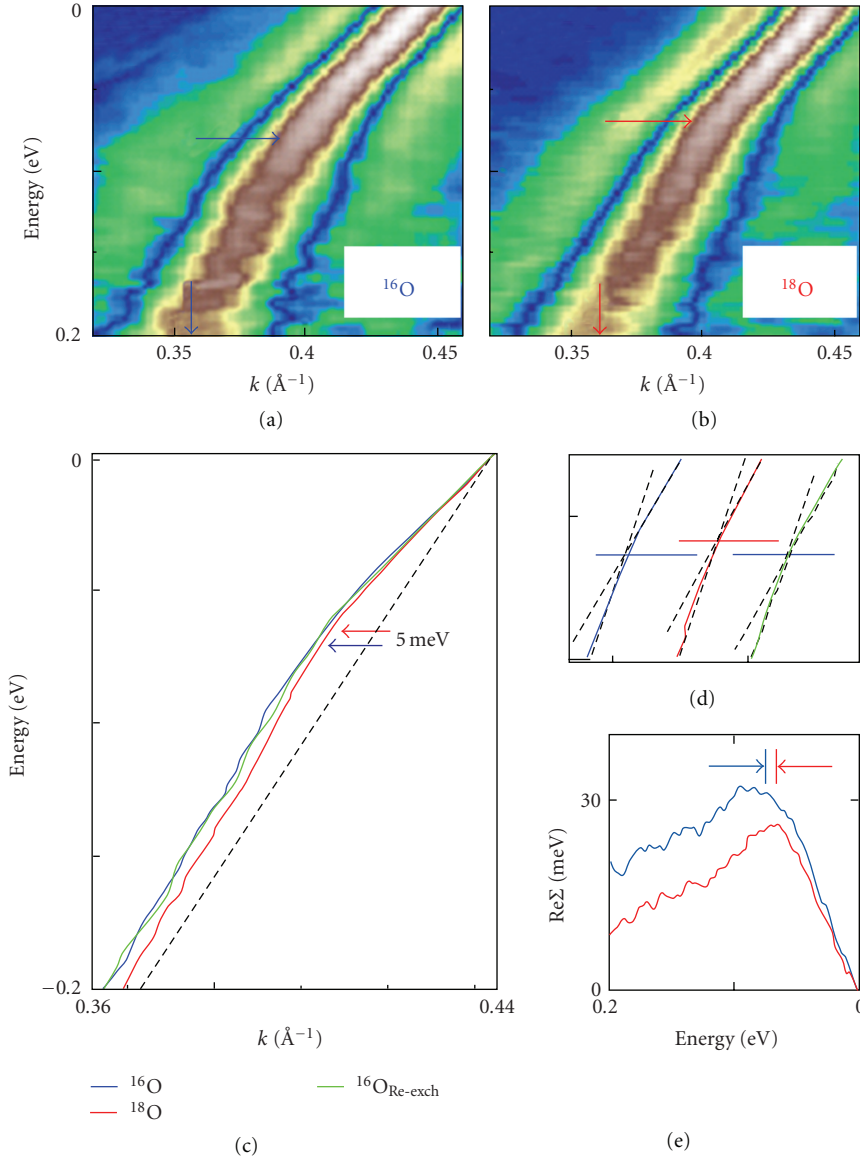


FIGURE 6: (a-b) MDC maps of the nodal point electronic states for cuts along the  $\Gamma$ -Y direction. (a) The  $^{16}\text{O}$  sample and (b) the  $^{18}\text{O}$  substituted sample with the horizontal arrows indicating the shift in ARPES kink energy with oxygen isotope. (c) The MDC dispersions determined from the  $^{16}\text{O}$ ,  $^{18}\text{O}$ , as well as a resubstituted  $^{16}\text{O}$  samples for the cuts in (a-b). (d) Cartoon illustration of the kink shift in (c). (e) Real part of the electron self-energy,  $\text{Re}\Sigma(\mathbf{k}, \omega)$ , determined from the MDC dispersion using a linear approximation for the single electron bare band. As before, the ARPES kink position, defined by the peak in  $\text{Re}\Sigma(\mathbf{k}, \omega)$ , is shifted to higher energy as indicated by the arrows.

doped. This doping dependence is intriguing but potentially puzzling given such sensitivity. Still, work in other correlated electronic systems, such as the manganites, demonstrates that such a small doping change does cause a qualitative change in the electronic structure [44]. Thus, the IE has a strong sensitivity to optimal doping and, therefore, there exists a rapid change in the electron-lattice interaction near optimal doping.

**3.5. Failure of Conventional Explanations.** Although the work of [43] had proposed that the IE was not apparent from ARPES on Bi2212, there are additional explanations that one could invoke to explain the presence of this subtle effect

which are important to address. As we will show, all of these conventional explanations turn out to be inadequate. Indeed, the strong temperature dependence by itself rules out all of the following explanations as possible candidates. Still, this position can be made stronger when we consider only the large low-temperature IE in light of the following scenarios.

**3.5.1. Doping Issue.** As the previous section discussed, establishing the doping of our samples, particularly that their optimal doping has remained unchanged after the isotope substitution, is critical to establishing the veracity of our claims. Doping level was preserved during the sample growth process by annealing the two samples ( $^{16}\text{O}$  and  $^{18}\text{O}$ )

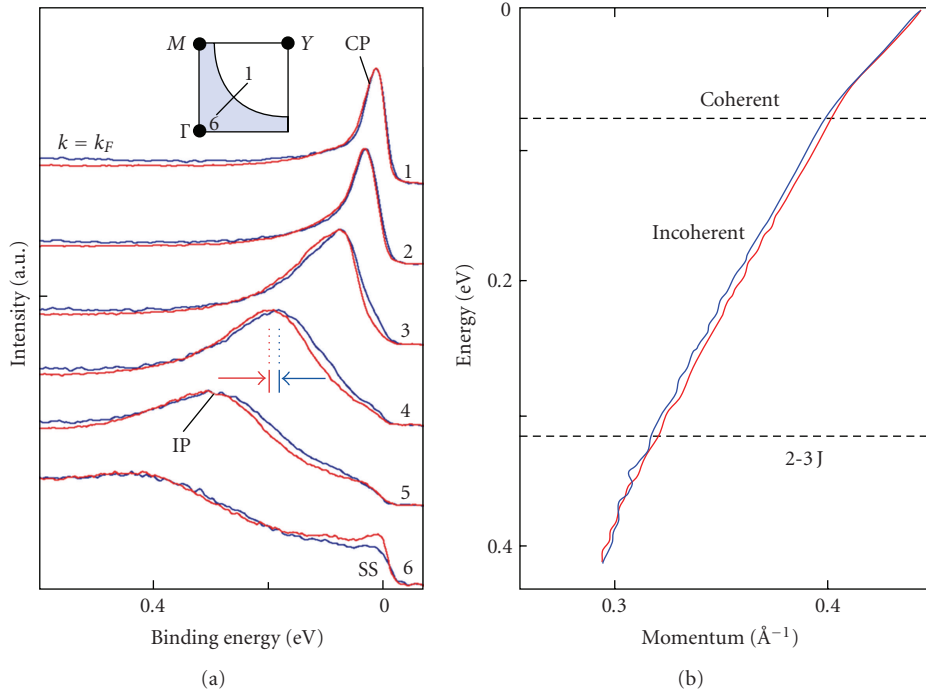


FIGURE 7: (a) EDCs taken on optimally doped  $\text{Bi}_2\text{Sr}_2\text{CaCu}_2\text{O}_{8+\delta}$  samples with different oxygen isotopes at  $T = 25$  K. The EDCs are from the same cut as in Figure 6 and indicated by the inset. The sharp coherent peak (CP) near  $E_F$  and broader incoherent peak (IP) at higher energy are identified. The CP has nearly no isotope dependence while the IP has a more substantial IE, most strongly seen in curve 4. The small peak at  $E_F$  in curve 6 is the well-known superstructure (SS) replica of the main band. This figure is from [33]. (b) MDC dispersion taken to higher binding energy indicating that the IE, more pronounced for the IP as in (a), disappears again above roughly 2-3 times the antiferromagnetic coupling energy,  $J$ .

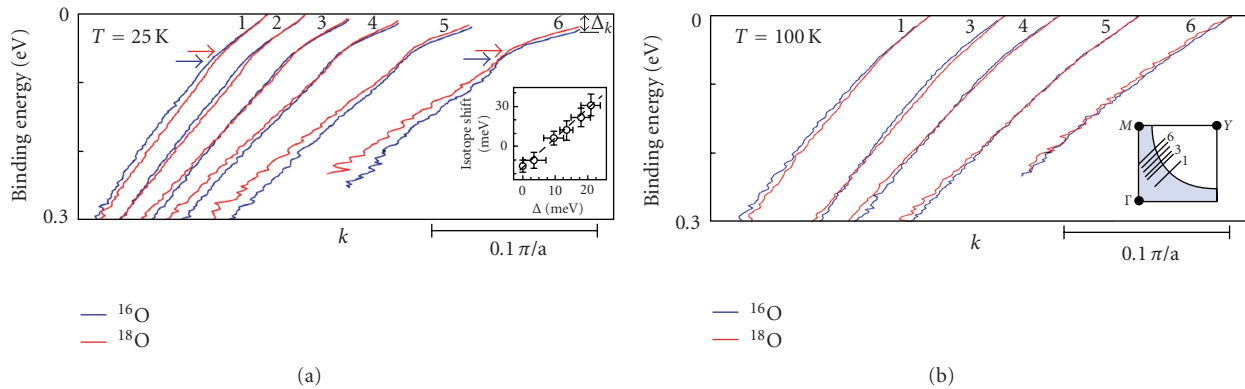


FIGURE 8: MDC dispersions from cuts parallel to  $\Gamma$ -Y taken off node towards the antinodal point. (a) Data taken in the superconducting phase ( $T = 25$  K). The inset shows the isotope energy shift versus the isotope-averaged superconducting gap,  $\Delta$ . The isotope shift is measured at the momentum value where the isotope-averaged binding energy is 220 meV. The apparent linear correlation indicated by the dashed line is independent of the binding energy used. (b) MDC dispersions from the same cuts measured above  $T_c$  ( $T = 100$  K). The inset illustrates the location of the cuts. The figures are from [33].

in the exactly same environment save the oxygen gas. Yet, ARPES on the cuprates provides us with in situ signatures of the doping level and its consistency. Most notably, one can use the Fermi surface size to quite precisely determine doping level, taking advantage of the well-known superstructure reflections of the main hole band structure.

Using the nodal cut and making use particularly of the  $2^{\text{nd}}$ -order reflection from the opposite side of the  $\Gamma$  point,

Figure 11(b) shows the associated MDCs near  $E_F$  for three samples, including the resubstituted sample. All three curves have good agreement with respect to peak positions. Of particular interest is the peak  $S'_r$  which is due to the  $2^{\text{nd}}$ -order superstructure Fermi surface replica from the opposite side of  $\Gamma$ . This means that any doping change in the sample will affect the distance between  $M$  and  $S'_r$  twice as fast as the distance between  $M$  and  $\Gamma$ , while the distance between  $S$

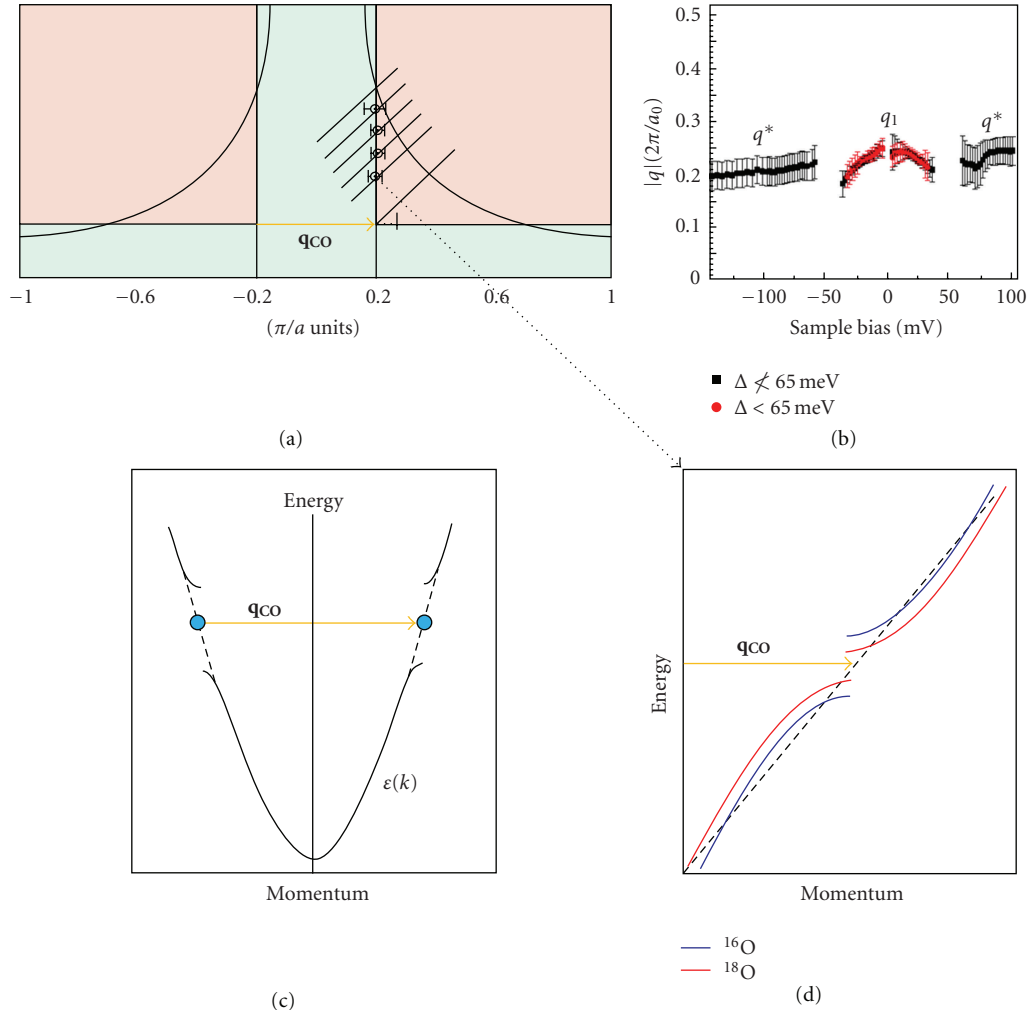


FIGURE 9: (a) Fermi surface of the upper half of the first BZ. Diagonal lines indicate cuts used in Figure 8 while circles indicate the location in momentum space of the sign change crossover point for each of those cuts. These lie on a line indicated by the wavevector,  $q_{CO}$  and illustrated by the colored regions. (b) STM data independently determining this wavevector taken from [34]. (c) Cartoon illustrating how the charge ordering wavevector,  $q_{CO}$ , can open a gap at a binding energy where the electronic states are nestable. (d) Additional cartoon illustrating how the splitting, if slightly different in magnitude between the isotopes, can explain the observed sign change in the bands and its evolution as the dispersions intersect with  $q_{CO}$ .

and  $M$  remains fixed by the superstructure wavevector. This makes the distance between  $M$  and  $S'_x$  a sensitive measure of doping change. In fact, plotted on top of the red  $^{18}\text{O}$  curve is a grey curve modeling a doping change of 0.01 based on a tight binding fit. From looking at how the  $^{18}\text{O}$  peak positions compare to this, it is clear that the uncertainty in doping value is well below 0.01.

However, one might be initially inclined to argue that the doping values between the two isotope samples are different based on the small difference in energy gap that has been previously reported [33] which would explain the observed IE. But this argument loses its plausibility for a few reasons. First, examining the two sets of data we report [33], the difference in energy gap  $\Delta_{16} - \Delta_{18}$  actually differed in sign, with an  $\sim -4$  meV change for [33, Figure 1] and an  $\sim 5$  meV change for [33, Figures 2 and 3]. Clearly, an empirically consistent change of gap is not obvious from our

data. Secondly, this becomes more evident over the many measurements ( $\sim 20$ ) we have done finding the  $\Delta_{16} - \Delta_{18}$  gap difference averaging to zero with a less than 1 meV difference, even while each individual value of  $\Delta_{16}$  or  $\Delta_{18}$  fluctuated by as much as 5 meV. This was consistent with a typical uncertainty in the gap value from other sources at the time [46]. Thirdly, even if there were a consistently measured gap difference of 5 meV and this were taken to mean that the doping values were different, it still does not explain the observed crossover behavior in Figure 8. More quantitatively, the doping change implied by a difference of 5 meV in gap ( $\Delta x = 0.017$ ) is not sufficient to explain the large IE we have seen. With the associated doping change converted into shift in peak position at high energy, it corresponds to 5 meV for the nodal cut, and only 10 meV for the near-antinodal cut. So, these numbers not only have the same sign but also are off in magnitude by a factor of 3 to 4. Thus, doping

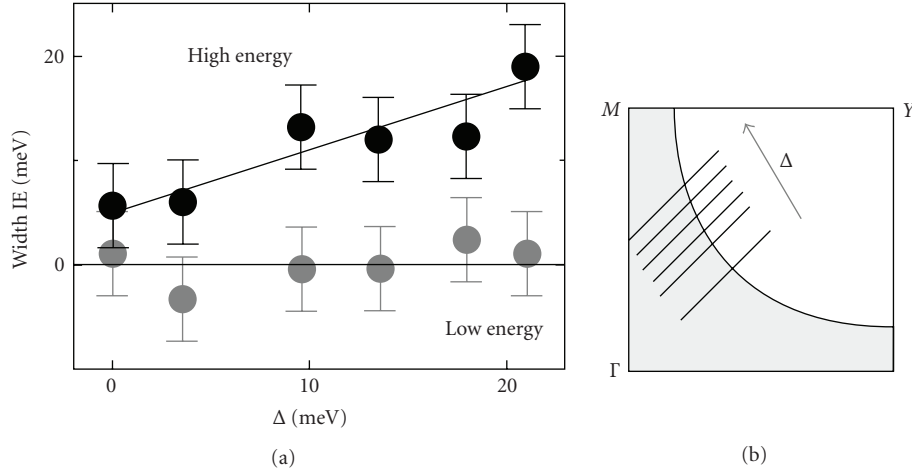


FIGURE 10: Isotope effect on EDC widths determined from ARPES data taken at the slices indicated in the smaller panel (same as Figure 8) within the superconducting phase. The width change for each cut comes from an average over binding energies below and above the kink energy: low (70 meV to 0) and high ( $\sim 250$  meV to 70 meV) energies. These widths are plotted with respect to the isotope averaged superconducting gap,  $\Delta$ , of each cut, showing little change at low energies but significant change above the kink energy. The figure is from [42].

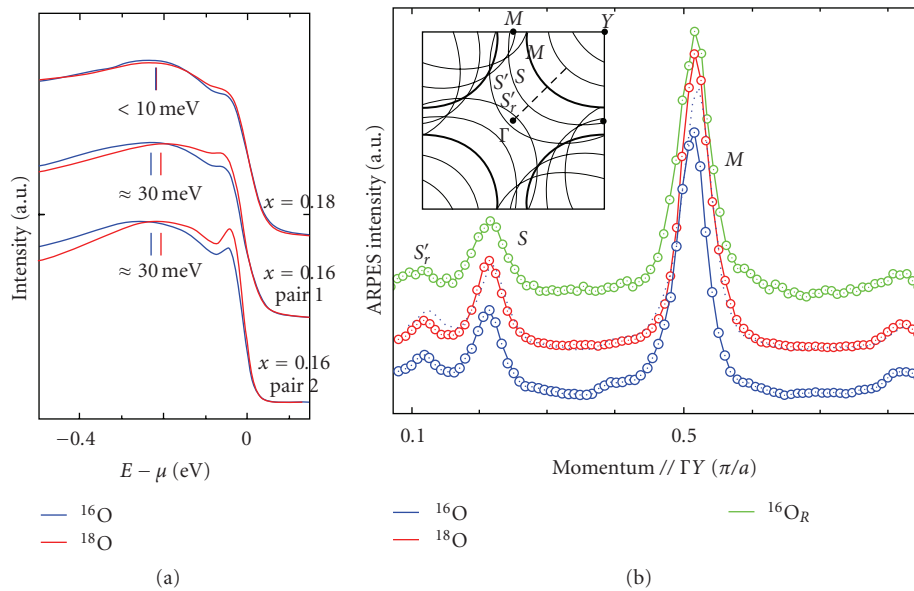


FIGURE 11: (a) Angle integrated photoemission data from two sets of data at optimal doping ( $x = 0.16$ ) and one set at a slight over-doping ( $x = 0.18$ ). Data has been normalized to the area under curves for energies 0.5 and above. (b) MDCs taken near  $E_F$  along the  $\Gamma$ -Y nodal direction as seen from the inset. The peaks correspond to the intersection of the cut with the main Fermi surface band ( $M$ ) as well as first-order superstructure reflections ( $S$ ) and a second-order reflection ( $S'_r$ ). Overlaid on top of the red curve is a thin grey line representing the  $^{16}\text{O}$  curve shifted to model a 0.01 change in doping for comparison. Panel (a) is from [45].

considerations do not offer a convincing explanation of the observed IE.

**3.5.2. Alignment Issue.** Another conventional explanation for our observed IE could be sample alignment since even a small misalignment could create an apparent difference in the observed dispersion. A careful examination led us to focus on two particular issues: the exact location of the  $\Gamma$

point and the relative azimuthal orientation of samples with respect to each other.

For the cuts 0–6 discussed here, we have found some evidence of deviations from our alignment based on the Fermi surfaces  $M$ ,  $S$ , and  $S'_r$  as described Figure 11(b). These slightly different momentum paths are indicated in Figure 12 to give a sense of magnitude. However, we have found that, as panels (b) and (c) demonstrate, the expected difference in the dispersion, based again on our tight binding fit, is none

for cut 0 and roughly about 4 times too small for our cut 6 when compared to our measured IE. It is also worth noting that the IE was reproduced for data taken with analyzer slits rotated  $45^\circ$  with respect to this geometry, parallel to the  $MY$  direction [33]. This geometry has the advantage of being less sensitive to azimuthal tilting. Thus, alignment issues are not a likely explanation for the observed data.

**3.5.3. Static Lattice Issue.** A final concern that should be considered is that a static lattice effect may be responsible for the large IE since there are no high-quality structural studies to rely on for insight. However, when we consider differences in crystal structure for isotope exchanged LSCO, they are only 0.1%. Given that a static structural effect is known to be more common in the LBCO and LSCO systems than the Bismuth based cuprates, one may reasonably assume that static lattice effects are significantly small in the Bi2212 cuprates and are an unlikely explanation for the observed IE. This is particularly strengthened since even if a static lattice effect were significant, it would need to be a particularly complicated static distortion which would make explaining the IE crossover difficult to accomplish.

**3.6. Beyond the Migdal-Eliashberg Picture.** With the IE results more soundly established in light of other potential explanations, we return our attention to the ME theory and ask whether its applicability is still appropriate for the results seen. One would initially expect ME theory to offer the best theoretical model of the observed ARPES kink in this doping region of the phase diagram. However, in view of the discussion at the start of this section, it is not entirely obvious that ME theory can be used to describe the broader incoherent spectral weight. This is a significant concern because of the prevalent use of ME theory in the context of the ARPES kink in the cuprates despite many experimental [48–56] and theoretical [57–59] works indicating an interaction strength beyond this theory. So, in light of our work, we will distinguish between those aspects which clearly go beyond ME theory as well as those more consistent with the theory.

To illustrate this former point, Figure 13, begins by showing EDCs for two cuts, a nodal (panel (a)) and a near antinodal (panel (b)). Although subtle near the nodal point, there is a significant deviation between the  $^{16}\text{O}$  (or the re-substituted  $^{16}\text{O}_R$ ) and the  $^{18}\text{O}$  which is not effectively modeled within the expected change from ME theory (panel (c)) and already mentioned previously in regards to the IE on ARPES width. This certainly comes as no surprise since we already knew that the behavior of the dispersion near the kink energy for the cuprate data was not well modeled by ME as compared to the H/W data which better follows its predictions. This is again emphasized in Figure 14, where the IE on the MDC dispersions near the node and antinode (panels (a-b)) is much bigger when compared to the substantially smaller expected change from the ME theory (panel (c)) as well as the aforementioned localization of the change to just near the kink energy. Additionally, as again illustrated in Figure 14, the presence of the momentum

dependent sign change in the dispersion (panels (a-b)) would defy explanation by any simple application of ME theory at least in the absence of an additional ordering phenomenon.

Fundamentally, the failure of the ME theory has its origin in the single phonon loop approximation for the electron self-energy, resulting in a small IE, particularly at higher energy. This suggests to us that we need to increase the electron-phonon coupling in our model. To accomplish this, we employ a Holstein model in the strong-coupling limit as described in [47]. The resulting comparison of this small polaron theory to the data can be found in Figure 15. These simulate the lineshape at  $k = k_F$  for the off-nodal cut (b). The multiple peaks seen in panel (a) occur due to the strong multiphonon “shake-up” peaks which appear at harmonics of  $\omega_P$ . With the expected broadening due to the phonon continuum and strong electron-electron interactions, the result, modeled in panel (b), successfully reproduces the weaker IE for the low-energy CP as well as the larger IE for the broader IP ( $\sim 30$ ). Additionally, it produces an ARPES linewidth which is more realistic.

These results clearly indicate that the ME theory is insufficient for describing the ARPES data. However, it should be noted that this strong coupling theory used is not quite the right solution either. Within the strong coupling theory, the IP is not expected to have any dispersion while the CP is expected to be nearly nondispersive as well. Furthermore, it predicts a very small quasiparticle weight ( $Z \ll 0.1$ ) for the CP (panels (c-d)) which is not observed. Both of these issues are better modeled by ME theory; so it is important to note that these shortcomings in the theory are overcome by weakening the interaction strength. This leads us to propose that the proper paradigm for understanding self-energy in the optimally doped cuprates is an intermediate regime. In this regime, there is a significant multiphonon contribution to electron self-energy and both the CP and IP show strong dispersions. Though one may have reasonably expected the IE to also weaken with diminished coupling, some studies [60, 61] show anomalous *enhancement* of the IE at intermediate couplings. Nevertheless, the key message here is that as far as modeling the electron-phonon physics seen in IE, the ME theory is not sufficient and that any subsequent theory must incorporate electron-phonon coupling with a strength beyond the ME paradigm.

## 4. Linking IXS and ARPES through Phonons

With this renewed interest regarding the role of the lattice in the superconducting cuprates as seen by ARPES, a natural direction to explore is to more carefully map the phonon dispersion in addition to that of the electron. A comparison of these dispersions can reveal particularly interesting physics such as when a phonon wavevector matches  $2k_F$ , where  $k_F$  is the Fermi momentum, leading to the well-known Kohn anomaly. Additional, nesting of the Fermi surface in systems with particularly strong electron-lattice coupling can drive the formation of charge density waves. Thus, it becomes important to compare data that directly probes

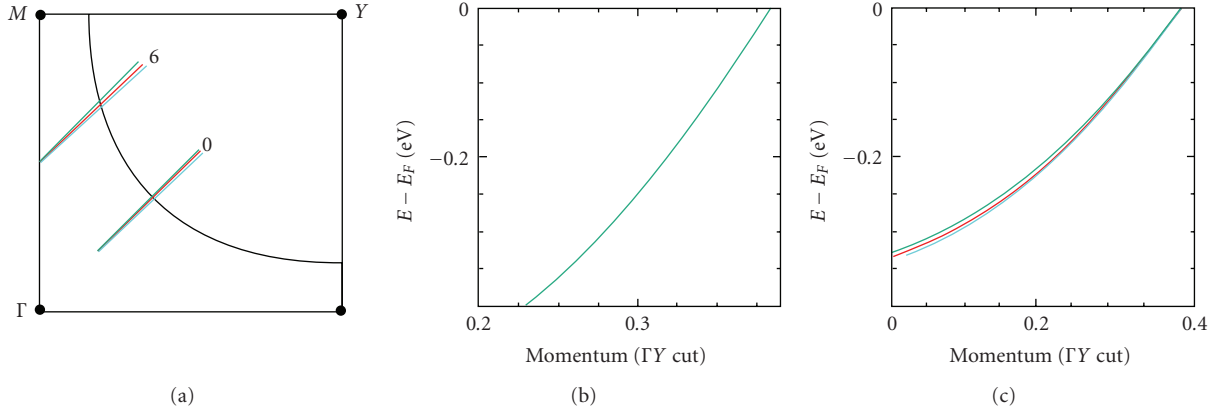


FIGURE 12: (a) Estimated azimuthal variation for cuts at and far off node indicated by the teal colored cuts relative to the red cut ( $\Gamma$ - $Y$ ). (b-c) Tight binding model for the nodal and off nodal cuts, respectively, representing the expected variation in dispersion due to the misalignment.

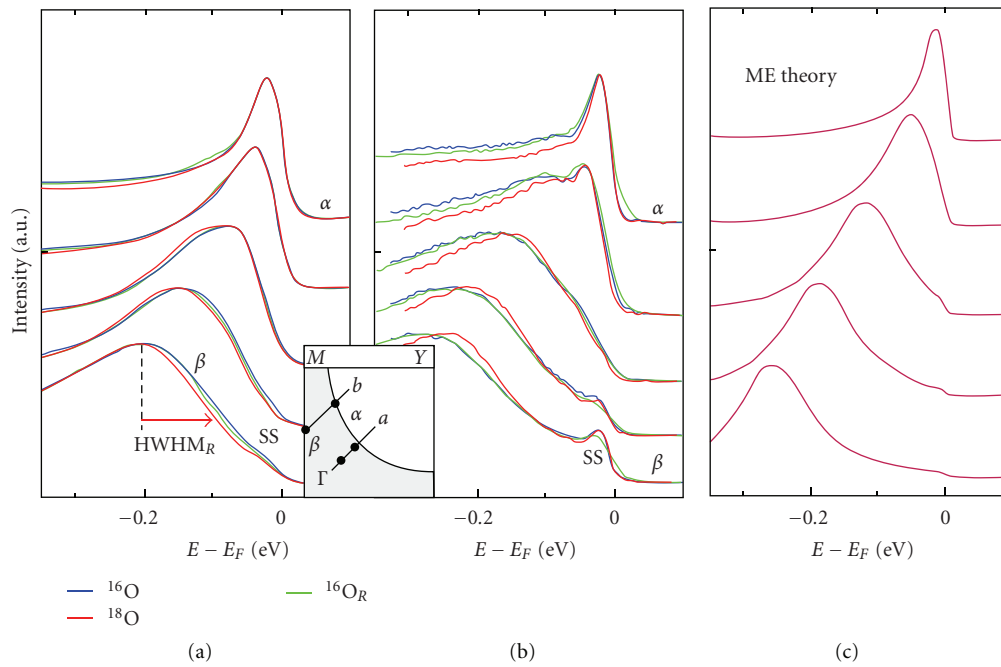


FIGURE 13: (a-b) Comparison of ARPES EDCs for the three samples from Figure 6(c), each normalized to same peak height. The cuts a and b for each panel, respectively, are indicated in the inset spanning the two panels along with the approximate location along the cut in  $k$ -space for the EDCs. (c) Migdal-Eliashberg (ME) simulations for the expected change to (a) and (b) from ME for  $^{16}\text{O}$  and  $^{18}\text{O}$ , under-predicting the observed IE as described in text. The figures are from [42].

the phonon mode dispersions within the Cu-O plane, such as the one we can get from inelastic neutron scattering (INS) and X-ray scattering (IXS) as discussed in Section 2. Then we can compare these results with the observations of the ARPES kink particularly in light of the potential change in the binding energy of the kink as one moves from the nodal point (60–70 meV) towards the antinodal point (30–40 meV). Further establishing the phonon nature of the nodal kink as well as shedding light on the lower energy antinodal kink is something that a combined ARPES and IXS study could achieve.

**4.1. IXS Measurements on La-Bi2201.** We turn our attention to the single-layered  $\text{Bi}_2\text{Sr}_{1.6}\text{La}_{0.4}\text{CuO}_{6+\delta}$  (La-Bi2201) cuprate which has several advantages for such a study. Like other Bismuth superconducting cuprates, the sample surfaces are high quality for ARPES experiments. These samples have never shown any evidence of magnetic resonance modes, simplifying the comparison between ARPES kink and scattering by removing a potentially additional bosonic mode to couple with the electrons. Moreover, no experimental reports of the optical phonon dispersion exist on these materials to date. The challenge for scattering is

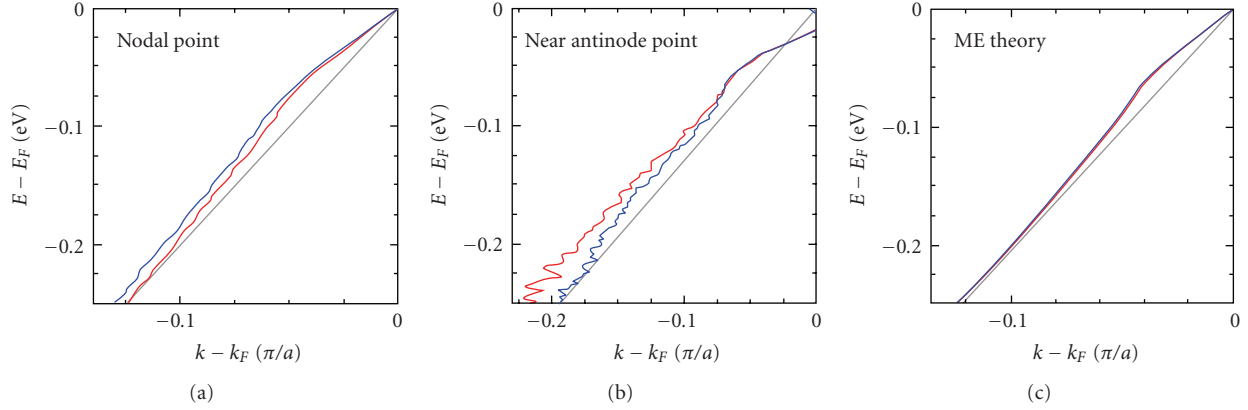


FIGURE 14: (a-b) Comparison of ARPES MDC dispersions for these two locations with the different isotopes. (c) Migdal-Eliashberg (ME) simulation for change in dispersion with isotope again under-predicting the magnitude and location of the expected band structure change.

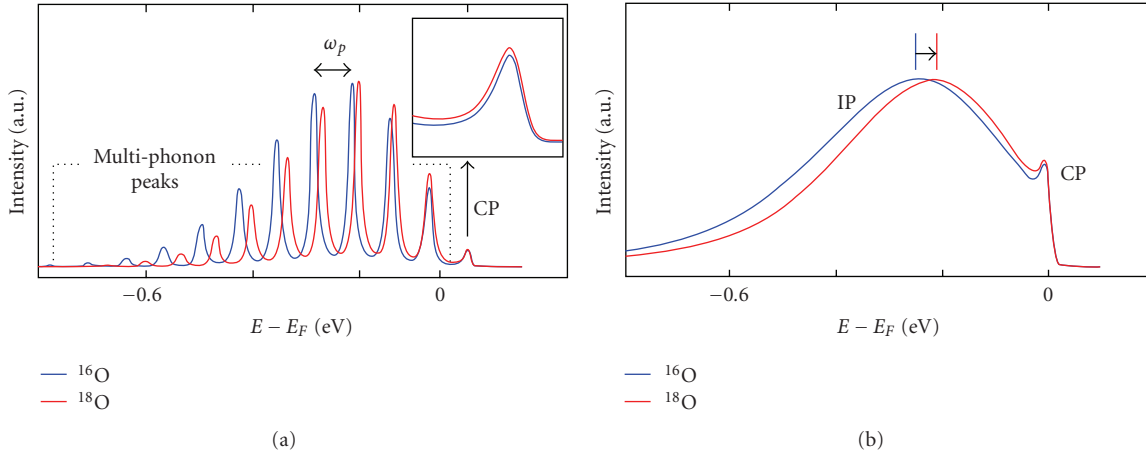


FIGURE 15: (a) Simulation of EDCs at  $k = k_F$  for the off-nodal cut seen in Figure 13(b) modeled with a small polaron theory [47]. (b) The expected broadening of this lineshape showing the small IE at low energy (see panel (a) inset) with a more substantial IE shift at higher energy. The figures are from [42].

the lack of large single crystals, effectively ruling out an INS experiment. Additionally, though IXS can probe the sub-millimeter single crystals available, there is a very low inelastic cross section associated with the bond stretching (BS) mode, a likely candidate for the nodal kink, making observing the mode challenging. Still, both IXS and INS have observed evidence in the past of the Cu–O bond stretching (BS) mode at the metal-insulator phase transition in the superconducting cuprates.

Figure 16 encapsulates the IXS experiment with panels (a) and (b) illustrating the relative weakness of the BS phonon peak relative to both the elastic line as well as other modes. Focusing on these higher-energy longitudinal optical modes, we map out their dispersion across the BZ from the center ( $\xi = 0$ ) towards the BZ face. Panel (a) shows this evolution where the red peak is identified as the BS mode and the results of which are plotted in panels (c) and (d). We see the two distinct peaks at the zone center but they disperse, becoming indistinguishable around  $\xi$  of 0.22–0.25. When  $\xi = 0.45$ , the two peaks clearly emerge again,

leading to two potential scenarios of panels (c) and (d) depending on the symmetry of the two branches. If they have the same symmetry, they anticross (panel (d)); otherwise they simply cross (panel (c)). Our attempts at distinguishing between these two scenarios using classical shell model calculations could not reproduce the low- and high-energy modes observed in a reliable way. Thus, we have been unable to distinguish between the potential scenarios. Finally, we compared our data with other IXS data in the literature, summarized in Figure 17. We find broad agreement for a softening of the BS mode (panel (a)) between  $\xi = 0.2$ –0.3 as well as a maxima in the full-width half-max (FWHM) of the BS mode peak.

**4.2. ARPES Measurements on La-Bi2201.** These results take on a deeper meaning when we compare them with our ARPES studies on La-Bi2201. Figure 18 displays the ARPES results in comparison to the IXS data. Panel (a) shows MDC analysis of the electronic dispersions taken at the nodal point (curve 1) and away from the node (curves 2 and 3) as

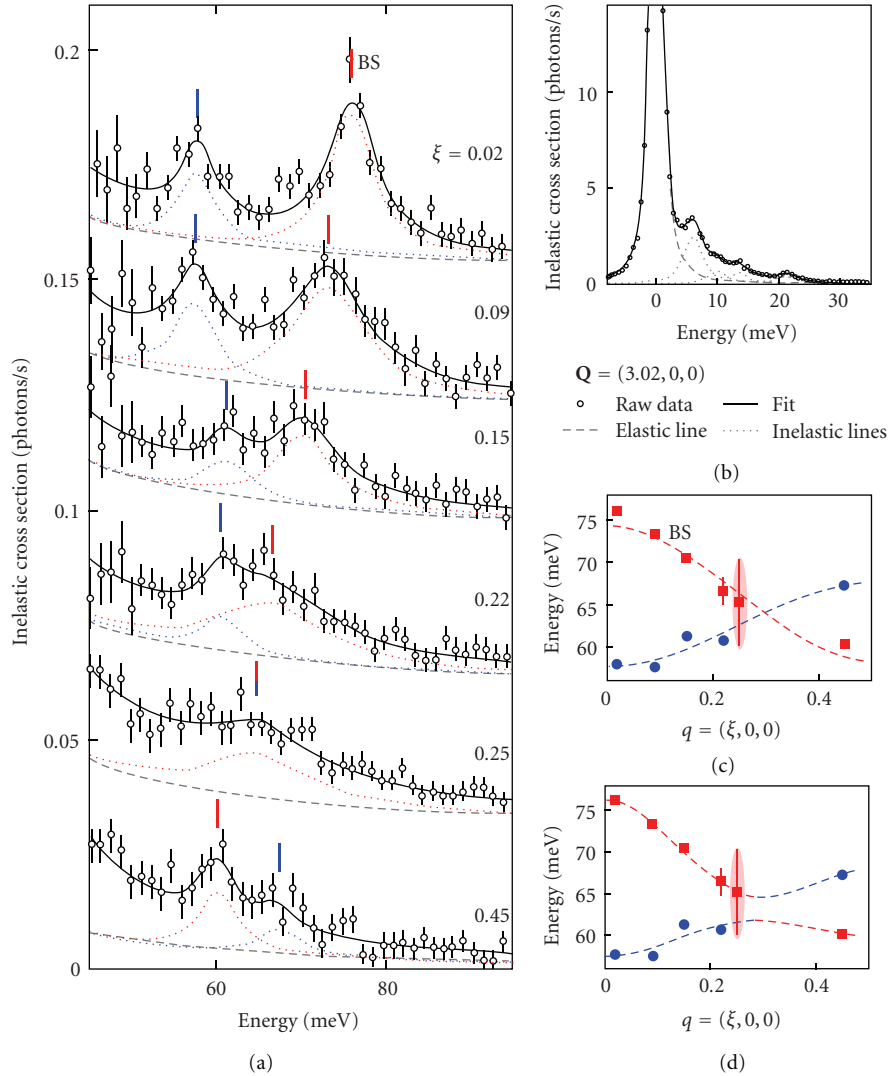


FIGURE 16: (a-b) Raw IXS phonon spectrum taken from optimally doped La-Bi2201 at 10 K. (a) Focusing on the high-energy part and the LO phonon dispersions for  $\mathbf{Q} = (3 + \xi, 0, 0)$  with  $\xi$  ranging from the BZ center to the BZ face. (b) Stronger low-energy part of the phonon spectrum. Solid lines indicate fits, dashed lines show the elastic tail, and dotted lines indicate the modes. (c-d) The peaks of these dispersions are plotted with cosine-dashed lines for the two potential dispersion scenarios: crossing (c) and anticrossing (d). The figures taken are from [62].

indicated by the slices along the Fermi surface in panel (b). We see the well-established higher-energy kink at  $63 \pm 5$  meV for the nodal cut. As we move away from the node, this kink abruptly disappears between curves 2 and 3, replaced with only a lower-energy kink of 35 meV. It is significant that this shift occurs at the tips of the so-called “Fermi Arc”, region of the Fermi surface which becomes ungapped at temperatures above the superconducting  $T_c$  but below the so-called pseudogap temperature,  $T^*$  [66]. Beyond the Fermi arc as one moves towards the BZ edge, the gap reopens again for reasons which remain mysterious. It is this transition point in momentum space between the arc and where the gap opens that curves 2 and 3 straddle, though our data was taken in the superconducting phase.

When we compare this with the IXS data as seen in the inset of panel (b), we discover that the 63 meV kink has an energy that corresponds well to the softened BS mode.

Even more interesting, as the grey-shaded region in panel (b) illustrates, the region where the 63 meV kink is observed corresponds to a section of the Fermi surface nestable by wavevectors within the softened part of the phonon mode dispersion from IXS. The sudden disappearance of this kink between curves 2 and 3 corresponds to the stiffening of the BS mode when  $\xi < 0.22$ . A final insight is that this BS mode is supposed to be nondispersive at about 80 meV along other momentum directions, in particular the [110]. We see no strong feature above 63 meV in our data, helping confirm that the nodal charge carriers are preferentially coupled to the softer Cu–O half-breathing BS mode which disperses along the [100] direction, a result suggested by local spin-density approximation +  $U$  results [67]. This work not only provides additional direct evidence for the lattice origin for the 60–70 meV kink seen near the node but also associates it with the softened Cu–O half-breathing BS mode along the

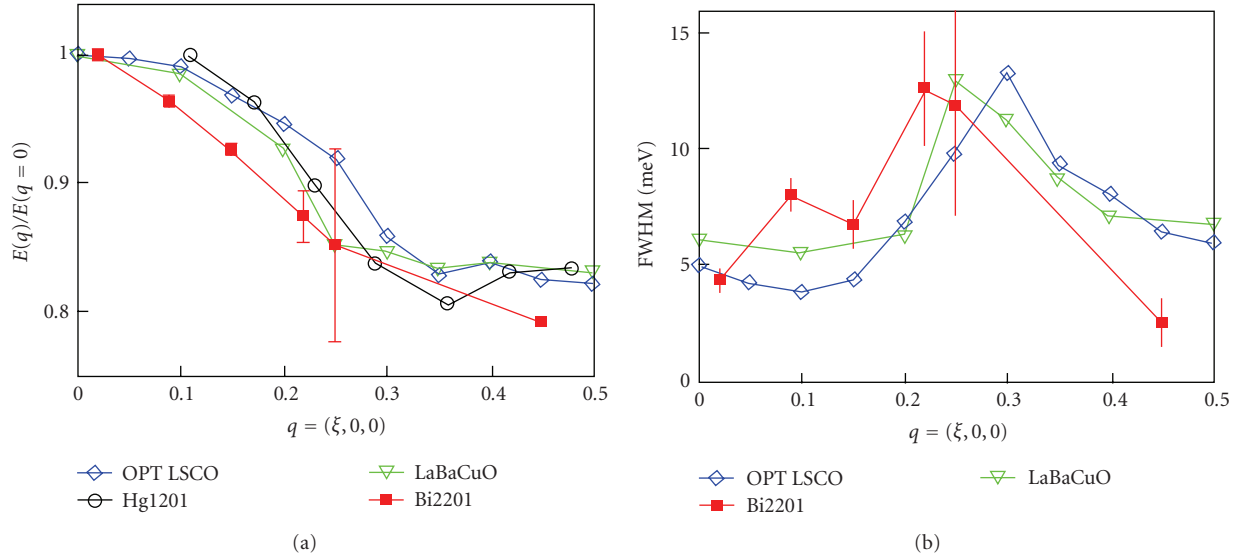


FIGURE 17: (a) Bond stretching mode softening in a variety of optimally hole-doped cuprates compared to the La-Bi2201 data. (b) Similar comparison of peak FWHM. The figures are from [62]. Data on LSCO and LaBaCuO come from [63] and the Hg1201 comes from [64].

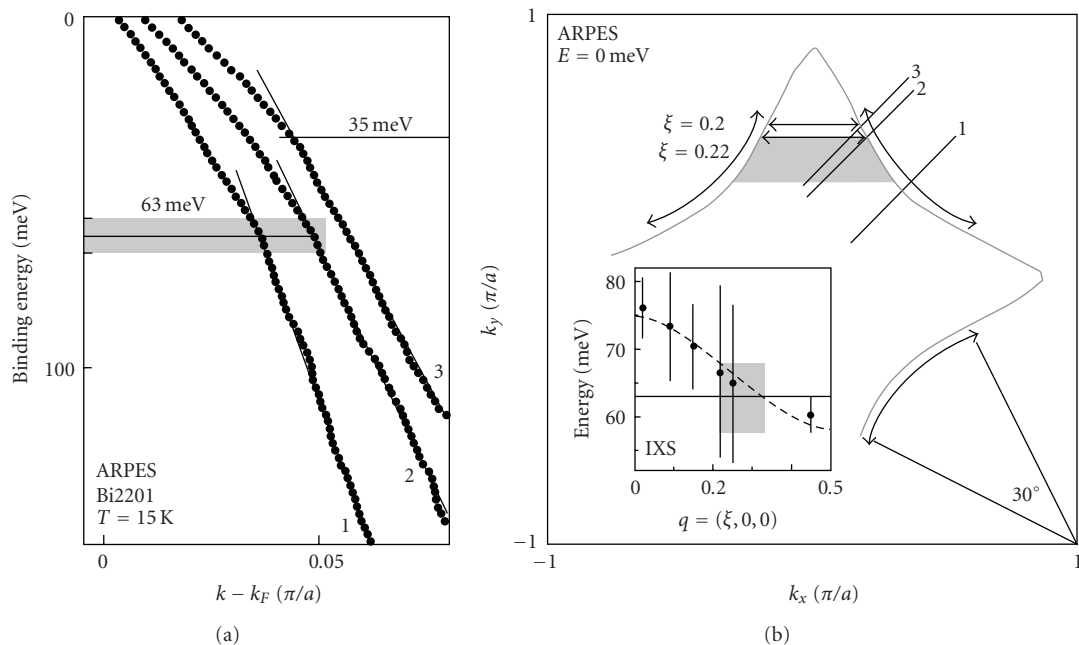


FIGURE 18: (a) MDC dispersions measured for three different momentum cuts along the  $G$ - $Y$  orientation with cut 1 at the nodal point while cuts 2 and 3 are further toward the BZ boundary, near to the edge of the pseudogap phase Fermi arcs [65]. (b) Fermi surface with the cuts from (a) indicated. The solid line indicates a constant energy contour at the kink energy, 63 meV, while the shadow area indicates the region where the nodal kink appears bounded by the indicated nesting wavevectors. The inset shows the IXS dispersion and peak FWHM (seen as error bars) of the BS mode. Note: The apparent Fermi arcs due to the experimental resolution are indicated by the curved arrows. The complete figures can be found in [62].

[100] direction. Its ability to nest the Fermi surface topology once again underscores the importance of electron-phonon interactions to the physics of the superconducting cuprates.

## 5. Lattice Strain in Bi2201

Our most recent work has continued this exploration into the role of the lattice from yet another perspective. There

has been growing independent work from a variety of experimental probes [69–71] positioning the role of the lattice not simply as a source of self-energy effects on the near- $E_F$  low-energy electronic states but potentially as an additional axis within the hole-doped phase diagram. Specifically, it is the effect of lattice strain, both external and internal via chemical pressure, which offers us this new axis to the cuprate phase diagram affecting the superconducting

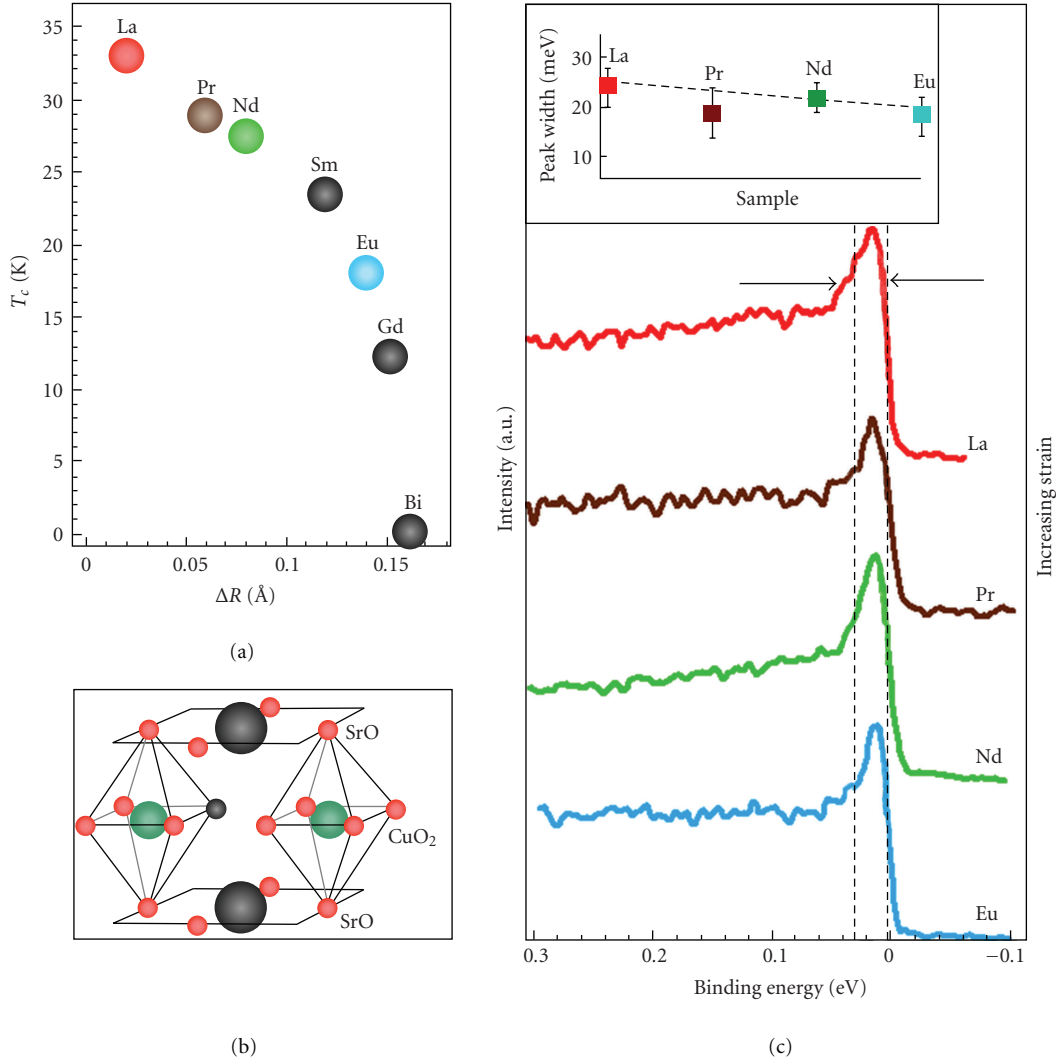


FIGURE 19: (a) Superconducting  $T_c$  for optimally doped  $\text{Bi}_2\text{Sr}_{1.6}\text{Ln}_{0.4}\text{Cu}_2\text{O}_6$  for a series of substituted Lanthanides (Ln) with increasing atomic radius mismatch,  $\Delta R = |R_{\text{Sr}} - R_{\text{Ln}}|$ . See [68]. (b) Cartoon illustrating the location of the substituted Lanthanide right above the Cu-O plane. (c) Nodal point EDCs illustrating the quasiparticle peak for samples with increasing strain, colored in (a), from La to Eu. Inset quantifies the half-width half-max of the peaks for these samples.

dome. Work using external pressure has indicated critical pressures where the  $T_c$  appears to saturate for a range of cuprate hole dopings [69] as well as being coupled to other physical quantities suggesting a significant new critical point along this axis [70]. With chemical pressure, work has suggested that combining doping with strain on the Cu-O layer also reveals that the true quantum critical point is shifted along the strain axis [71]. Additionally, effects related to lattice disorder, particularly in the Sr-O blocks nearest the Cu-O planes, may also have a dramatic effect on the formation of the superconducting phase within the cuprates [72]. Thus, better understanding of this aspect of the role of the lattice is important to our general understanding of electron-lattice physics in these systems.

**5.1. Lanthanide Substituted Bi2201.** Due to experimental considerations, the best method for introducing strain into

the lattice for an ARPES study is via chemical pressure. Specifically, we can use Lanthanide substituted single-layered  $\text{Bi}_2\text{Sr}_{1.6}\text{Ln}_{0.4}\text{CuO}_6$  to access this strain in a tunable way [68]. All the samples were grown at optimal doping to simplify the analysis, making the focus solely on the tuning parameter of strain. As Figure 19 illustrates, the substitution of the Lanthanide elements for the Strontium right above the critical Cu-O plane (panel (b)) leads to a monotonic decrease in the measured  $T_c$  of the samples. The essential variable to quantify this  $T_c$ -competing strain is the atomic radius mismatch,  $\Delta R$ , as seen on the abscissa of panel (a), which is determined by the difference between the Strontium and the substituted Lanthanide atomic radii,  $|R_{\text{Sr}} - R_{\text{Ln}}|$ .

We have been able to take data on samples throughout this spectrum of radius mismatch. Although these samples allow us a lattice-based, tunable parameter which competes with superconductivity, one can pose the question if this

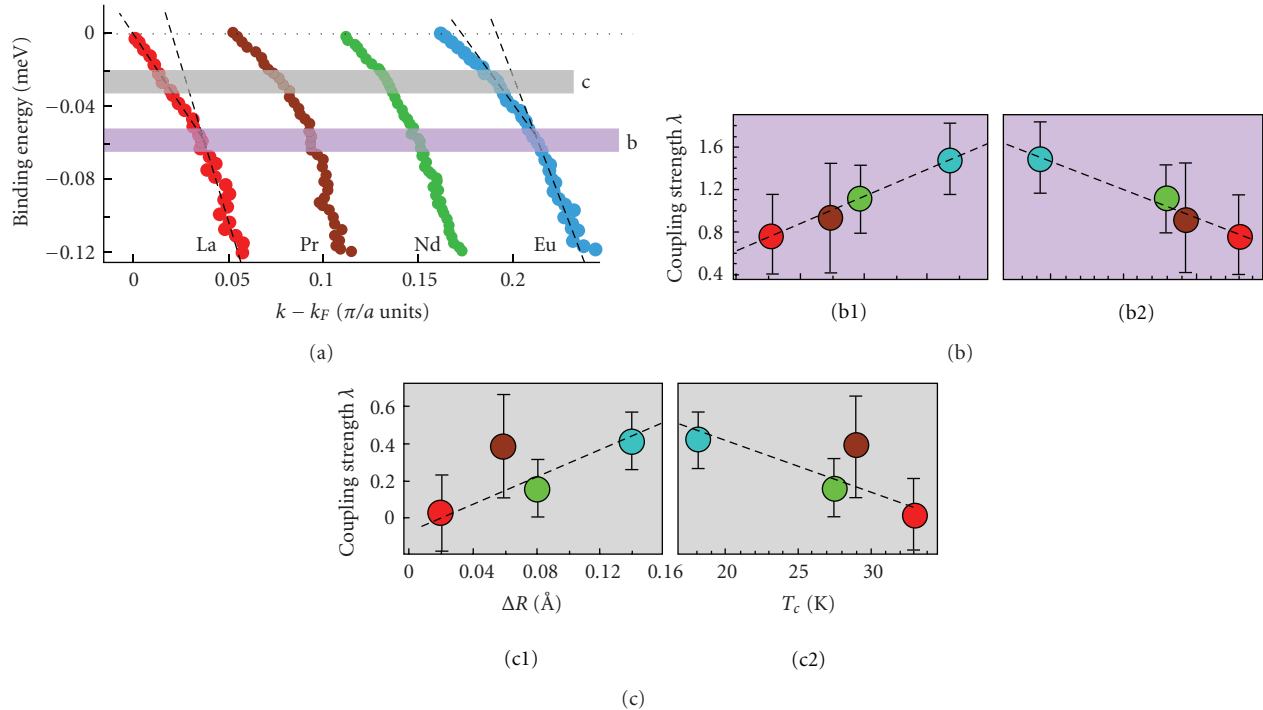


FIGURE 20: (a) Nodal point MDC dispersions taken from  $\Gamma$ -Y cuts on four different samples of increasing strain (La, Pr, Nd, and Eu). Lines serve as guides to determine deviation from the expected dispersion. Horizontal shaded regions correspond to the two potential ARPES kink energy scales. (b-c) Estimating the electron coupling  $\lambda$  on the electronic states from each of the two regions indicated in (a). (b1) and (b2) Higher energy kink  $\lambda$  for each strain as a function of (1) Lattice mismatch  $\Delta$ , and (2)  $T_c$ . (c1) and (c2) Lower energy kink  $\lambda$  analyzed like (b).

should be thought of within a lattice strain or lattice disorder paradigm. Figure 19(c) provides evidence that, at least for the nodal states, the strain paradigm appears valid. With increasing lattice mismatch, the width of the quasiparticle peak does not increase but, on close examination, may even be decreasing with increased strain. The introduction of lattice disorder should decrease the lifetime of the electronic states, seen as an increase in the width of the CP. It also has been broadly suggested within the ARPES cuprate community that observing a sharp quasiparticle peak at the nodal point is necessary for confirming that the cleaved surface can provide trustworthy ARPES results.

**5.2. ARPES Kink versus Strain.** Throughout this review, we have continually discussed the ARPES kink, particularly near the node, in terms of electron-phonon coupling. So considering the expected effect of the substituted lanthanides on lattice strain and the view that these states at least can be understood within a strain paradigm, we focus our attention again on the MDC dispersions at the nodal point. Figure 20 presents our findings for substituted Ln = La, Pr, Nd, Eu [73].

There are two aspects of these dispersions we wish to focus on in the context of this review. First, in agreement with the earlier work on La-Bi2201 discussed in Section 4.2, we can observe a kink around 55–60 meV which remains at that energy, for the most part, throughout the strain spectrum.

However, what appears to change with strain is the electron-coupling constant,  $\lambda$  associated with the renormalization of these states. In the same manner as was done for the cuprate systems described in Section 2.3, we can estimate  $\lambda$  for this mode, which is plotted in panel (b). We find that the strength of this mode appears enhanced by the increasing strain of the lattice mismatch with a generally linear behavior. Equivalently, one can plot  $\lambda$  as a function of sample  $T_c$  (panel (b) inset) and, as one would expect, there is a negative, linear relationship between the superconducting  $T_c$  and strength of this phonon mode. Secondly, we find that although it appears linear for the La-Bi2201 at energies less than the 60 meV kink, the more strained compounds appear to have additional rounding of the band structure nearer to  $E_F$ , most obvious in the highly strained Eu-Bi2201. This mode appears to be around 25–30 meV which could be important since this is closer to the mode energy observed near the antinodal point (as discussed in Section 2.4) from the peak-dip-hump EDC lineshape. We have also observed this from the kink in the MDC analysis beyond the nestable region of the IXS softened phonon mode in Section 4.2.

As with the higher-energy mode, we can attempt to extract the  $\lambda$  from this more elusive mode independent of the 60 meV kink, the result of which is seen in panel (c). Unlike the higher-energy mode which is apparent in all strain, this lower-energy feature appears to turn on at the node only as strain is introduced, leading to a broadly linear relationship similar to the higher-energy mode. The origin of this feature,

remains mysterious, potentially related to an apical oxygen mode particularly in light of the location of the substituted lanthanide above the Cu–O plane.

These results are significant for at least three reasons. First, it has been a prevailing thought that the electronic states at the nodal point are uniquely unaware of the entry into the superconducting phase. With the d-wave symmetry of the gap function, the nodal point states are the only electronic states which still cross through  $E_F$  with no gap opening. Additionally, one could argue that the continued appearance of a sharp quasiparticle at the node is merely because these states are protected from the superconducting physics. However, clearly the affect of lattice strain can be seen on these states and the weakening of the superconducting state is present in the electronic dispersion of the nodal quasiparticles. Secondly, one finds still additional evidence that the  $\sim 60$  meV kink has its origin in the physics of the lattice. Even more intriguing, the appearance and potential enhancement of the lowerenergy kink with lattice strain would tentatively suggest that its origin also is somehow connected to the lattice (such as the aforementioned apical oxygen mode) and not merely a magnetic mode at the nodal point. It could be pointed out that the lanthanides do carry with them magnetic moments whose effect on the Cu–O plane is far from understood. While La has no magnetic moment, Pr, Nd, and Eu all have experimentally determined magnetic moments of around  $3.5\mu_B$  [74]. Whether this may be related to the sudden appearance of this mode at the node for samples beyond La requires further study. Finally, at least for the 60 meV mode, one finds evidence that this phonon mode is somehow connected to the formation of the superconducting phase. From its behavior, it appears to be related to a competing order, associated with the lattice, which may be affecting the formation of the superfluid.

## 6. Summary

Throughout this work, the reoccurring theme has been the growing importance that the lattice and its coupling with electronic states has within the still mysterious phase diagram of the hole doped cuprates. Beginning with the ubiquitous nodal kink and its likely origin in the bond stretching phonon mode, we have explored the effect of the lattice on both the coherent and incoherent parts of the near  $E_F$  electronic band structure through the IE. This has confirmed that, near optimal doping, the traditional ME model must give way to a stronger electron-phonon coupling, yet still shy of a polaronic picture. We have traced out the dispersion of the BS phonon mode with IXS and have found its important connection to the ARPES kink near the nodal point. From this, we find that the electronic states within the BZ can be divided up accordingly, with those nearest to the node (often argued to be responsible for the superfluid) uniquely impacted by the mode wavevector's ability to nest them. Finally, the potential for understanding the role of the lattice via the additional axis of pressure/strain has already produced remarkable results for the evolution of the nodal electronic states and their self-energy along

this axis as well as pointing towards additional insights. In all, our work has and continues to explore how the cuprate electronic structure is affected by electron-phonon coupling as yet another pillar in our nearly 25 years quests to construct a full understanding of this unconventional superconducting phase.

## Acknowledgments

The authors first would like to acknowledge all the members of the group who have greatly contributed to this work: Gey Hong Gweon, Shuyun Zhou, Jeff Graf, and Chris Jozwiak. They also would like to acknowledge many useful scientific discussions with Dung-Hai Lee, Z. Hussain, K. A. Muller, A. Bianconi, T. Sasagawa, and H. Takagi. This work was supported by the Director, Office of Science, Office of Basic Energy Sciences, Materials Sciences and Engineering Division, of the U.S. Department of Energy under Contract no. DE-AC02-05CH11231.

## References

- [1] J. M. Rowell, P. W. Anderson, and D. E. Thomas, "Image of the phonon spectrum in the tunneling characteristic between superconductors," *Physical Review Letters*, vol. 10, no. 8, pp. 334–336, 1963.
- [2] J. R. Schrieffer, D. J. Scalapino, and J. W. Wilkins, "Effective tunneling density of states in superconductors," *Physical Review Letters*, vol. 10, no. 8, pp. 336–339, 1963.
- [3] A. Lanzara, P. V. Bogdanov, X. J. Zhou, et al., "Evidence for ubiquitous strong electron-phonon coupling in high-temperature superconductors," *Nature*, vol. 412, no. 6846, pp. 510–514, 2001.
- [4] P. V. Bogdanov, A. Lanzara, S. A. Kellar, et al., "Evidence for an energy scale for quasiparticle dispersion in  $Bi_2Sr_2CaCu_2O_8$ ," *Physical Review Letters*, vol. 85, no. 12, pp. 2581–2584, 2000.
- [5] N. W. Ashcroft and N. D. Mermin, *Solid State Physics*, Saunders College, Philadelphia, Pa, USA, 1976.
- [6] L. P. Regnault, P. Bourges, P. Burllet, et al., "Spin dynamics in the normal and superconducting states of  $YBa_2Cu_3O_{6+x}$ ," *Physica C*, vol. 235–240, part 1, pp. 59–62, 1994.
- [7] H. F. Fong, B. Keimer, D. L. Milius, and I. A. Aksay, "Superconductivity-induced anomalies in the spin excitation spectra of underdoped  $YBa_2Cu_3O_{6+x}$ ," *Physical Review Letters*, vol. 78, no. 4, pp. 713–716, 1997.
- [8] M. Arai, T. Nishijima, Y. Endoh, et al., "Incommensurate spin dynamics of underdoped superconductor  $YBa_2Cu_3O_{6.7}$ ," *Physical Review Letters*, vol. 83, no. 3, pp. 608–611, 1999.
- [9] P. Dai, H. A. Mook, S. M. Hayden, et al., "The magnetic excitation spectrum and thermodynamics of high- $T_c$  superconductors," *Science*, vol. 284, no. 5418, pp. 1344–1347, 1999.
- [10] E. Demler and S.-C. Zhang, "Theory of the resonant neutron scattering of high- $T_c$  superconductors," *Physical Review Letters*, vol. 75, no. 22, pp. 4126–4129, 1995.
- [11] P. Dai, M. Yethiraj, H. A. Mook, T. B. Lindemer, and F. Dogan, "Magnetic dynamics in underdoped  $YBa_2Cu_3O_{7-x}$ : direct observation of a superconducting gap," *Physical Review Letters*, vol. 77, no. 27, pp. 5425–5428, 1996.
- [12] R. J. McQueeney, Y. Petrov, T. Egami, M. Yethiraj, G. Shirane, and Y. Endoh, "Anomalous dispersion of LO phonons in  $La_{1.85}Sr_{0.15}CuO_4$  at low temperatures," *Physical Review Letters*, vol. 82, no. 3, pp. 628–631, 1999.

- [13] Y. Petrov, et al., “Phonon signature of charge inhomogeneity in high temperature superconductors,” <http://arxiv.org/abs/cond-mat/0003414>.
- [14] X. J. Zhou, et al., “Angle-resolved photoemission spectroscopy on electronic structure and electron-phonon coupling in cuprate superconductors,” in *Handbook of High-Temperature Superconductivity: Theory and Experiment*, J. R. Schrieffer, Ed., pp. 87–144, Springer, Berlin, Germany, 2007.
- [15] A. Lanzara, P. V. Bogdanov, X. J. Zhou, et al., “Normal state spectral lineshapes of nodal quasiparticles in single layer Bi2201 superconductor,” *Journal of Physics and Chemistry of Solids*, vol. 67, no. 1–3, pp. 239–243, 2006.
- [16] G.-H. Gweon, S. Y. Zhou, and A. Lanzara, “Strong influence of phonons on the electron dynamics of Bi<sub>2</sub>Sr<sub>2</sub>CaCu<sub>2</sub>O<sub>8+δ</sub>,” *Journal of Physics and Chemistry of Solids*, vol. 65, no. 8–9, pp. 1397–1401, 2004.
- [17] D. S. Dessau, B. O. Wells, Z.-X. Shen, et al., “Anomalous spectral weight transfer at the superconducting transition of Bi<sub>2</sub>Sr<sub>2</sub>CaCu<sub>2</sub>O<sub>8+δ</sub>,” *Physical Review Letters*, vol. 66, no. 16, pp. 2160–2163, 1991.
- [18] Y. Hwu, L. Lozzi, M. Marsi, et al., “Electronic spectrum of the high-temperature superconducting state,” *Physical Review Letters*, vol. 67, no. 18, pp. 2573–2576, 1991.
- [19] J. Rossat-Mignod, L. P. Regnault, C. Vettier, et al., “Neutron scattering study of the YBa<sub>2</sub>Cu<sub>3</sub>O<sub>6+x</sub> system,” *Physica C*, vol. 185–189, part 1, pp. 86–92, 1991.
- [20] H. A. Mook, M. Yethiraj, G. Aeppli, T. E. Mason, and T. Armstrong, “Polarized neutron determination of the magnetic excitations in YBa<sub>2</sub>Cu<sub>3</sub>O<sub>7</sub>,” *Physical Review Letters*, vol. 70, no. 22, pp. 3490–3493, 1993.
- [21] H. F. Fong, P. Bourges, Y. Sidis, et al., “Neutron scattering from magnetic excitations in Bi<sub>2</sub>Sr<sub>2</sub>CaCu<sub>2</sub>O<sub>8+δ</sub>,” *Nature*, vol. 398, no. 6728, pp. 588–591, 1999.
- [22] D. L. Feng, N. P. Armitage, D. H. Lu, et al., “Bilayer splitting in the electronic structure of heavily overdoped Bi<sub>2</sub>Sr<sub>2</sub>CaCu<sub>2</sub>O<sub>8+δ</sub>,” *Physical Review Letters*, vol. 86, no. 24, pp. 5550–5553, 2001.
- [23] Y.-D. Chuang, A. D. Gromko, A. Fedorov, et al., “Doubling of the bands in overdoped Bi<sub>2</sub>Sr<sub>2</sub>CaCu<sub>2</sub>O<sub>8+δ</sub>: evidence for c-axis bilayer coupling,” *Physical Review Letters*, vol. 87, no. 11, Article ID 117003, 4 pages, 2001.
- [24] P. V. Bogdanov, A. Lanzara, X. J. Zhou, et al., “Photoemission study of Pb doped Bi<sub>2</sub>Sr<sub>2</sub>CaCu<sub>2</sub>O<sub>8</sub>: a Fermi surface picture,” *Physical Review B*, vol. 64, no. 18, Article ID 180505, 4 pages, 2001.
- [25] A. D. Gromko, A. V. Fedorov, Y.-D. Chuang, et al., “Mass-renormalized electronic excitations at (π, 0) in the superconducting state of Bi<sub>2</sub>Sr<sub>2</sub>CaCu<sub>2</sub>O<sub>8+δ</sub>,” *Physical Review B*, vol. 68, no. 17, Article ID 174520, 7 pages, 2003.
- [26] A. Kaminski, M. Randeria, J. C. Campuzano, et al., “Renormalization of spectral line shape and dispersion below T<sub>c</sub> in Bi<sub>2</sub>Sr<sub>2</sub>CaCu<sub>2</sub>O<sub>8+δ</sub>,” *Physical Review Letters*, vol. 86, no. 6, pp. 1070–1073, 2001.
- [27] T. K. Kim, A. A. Kordyuk, S. V. Borisenko, et al., “Doping dependence of the mass enhancement in (Pb, Bi)<sub>2</sub>Sr<sub>2</sub>CaCu<sub>2</sub>O<sub>8</sub> at the antinodal point in the superconducting and normal states,” *Physical Review Letters*, vol. 91, no. 16, Article ID 167002, 4 pages, 2003.
- [28] T. Cuk, F. Baumberger, D. H. Lu, et al., “Coupling of the B<sub>1g</sub> phonon to the antinodal electronic states of Bi<sub>2</sub>Sr<sub>2</sub>Ca<sub>0.92</sub>Y<sub>0.08</sub>Cu<sub>2</sub>O<sub>8+δ</sub>,” *Physical Review Letters*, vol. 93, no. 11, Article ID 117003, 4 pages, 2004.
- [29] C. M. Varma, P. B. Littlewood, S. Schmitt-Rink, E. Abrahams, and A. E. Ruckenstein, “Phenomenology of the normal state of Cu-O high-temperature superconductors,” *Physical Review Letters*, vol. 63, no. 18, pp. 1996–1999, 1989.
- [30] K. M. Shen, F. Ronning, D. H. Lu, et al., “Nodal quasiparticles and antinodal charge ordering in Ca<sub>2-x</sub>Na<sub>x</sub>CuO<sub>2</sub>Cl<sub>2</sub>,” *Science*, vol. 307, no. 5711, pp. 901–904, 2005.
- [31] E. Rotenberg, J. Schaefer, and S. D. Kevan, “Coupling between adsorbate vibrations and an electronic surface state,” *Physical Review Letters*, vol. 84, no. 13, pp. 2925–2928, 2000.
- [32] H. Iwasawa, J. F. Douglas, K. Sato, et al., “Isotopic fingerprint of electron-phonon coupling in high-T<sub>c</sub> cuprates,” *Physical Review Letters*, vol. 101, no. 15, Article ID 157005, 4 pages, 2008.
- [33] G.-H. Gweon, T. Sasagawa, S. Y. Zhou, et al., “An unusual isotope effect in a high-transition-temperature superconductor,” *Nature*, vol. 430, no. 6996, pp. 187–190, 2004.
- [34] K. McElroy, D.-H. Lee, J. E. Hoffman, et al., “Coincidence of checkerboard charge order and antinodal state decoherence in strongly underdoped superconducting Bi<sub>2</sub>Sr<sub>2</sub>CaCu<sub>2</sub>O<sub>8+δ</sub>,” *Physical Review Letters*, vol. 94, no. 19, Article ID 197005, 4 pages, 2005.
- [35] S. Andergassen, S. Caprara, C. Di Castro, and M. Grilli, “Anomalous isotopic effect near the charge-ordering quantum criticality,” *Physical Review Letters*, vol. 87, no. 5, Article ID 056401, 4 pages, 2001.
- [36] A. Lanzara, G.-M. Zhao, N. L. Saini, et al., “Oxygen-isotope shift of the charge-stripe ordering temperature in La<sub>2-x</sub>Sr<sub>x</sub>CuO<sub>4</sub> from X-ray absorption spectroscopy,” *Journal of Physics Condensed Matter*, vol. 11, no. 48, pp. L541–L546, 1999.
- [37] D. Rubio Temprano, J. Mesot, S. Janssen, et al., “Large isotope effect on the pseudogap in the high-temperature superconductor HoBa<sub>2</sub>Cu<sub>4</sub>O<sub>8</sub>,” *Physical Review Letters*, vol. 84, no. 9, pp. 1990–1993, 2000.
- [38] A. Bianconi, N. L. Saini, A. Lanzara, et al., “Determination of the local lattice distortions in the CuO<sub>2</sub> plane of La<sub>1.85</sub>Sr<sub>0.15</sub>CuO<sub>4</sub>,” *Physical Review Letters*, vol. 76, no. 18, pp. 3412–3415, 1996.
- [39] G. Seibold and M. Grilli, “Influence of incommensurate dynamic charge-density-wave scattering on the photoemission line shape of superconducting high-T<sub>c</sub> cuprates,” *Physical Review B*, vol. 63, no. 22, Article ID 224505, 7 pages, 2001.
- [40] J. M. Tranquada, B. J. Sternlieb, J. D. Axe, Y. Nakamura, and S. Uchida, “Evidence for stripe correlations of spins and holes in copper oxide superconductors,” *Nature*, vol. 375, no. 6532, pp. 561–563, 1995.
- [41] C. Castellani, C. Di Castro, and M. Grilli, “Singular quasiparticle scattering in the proximity of charge instabilities,” *Physical Review Letters*, vol. 75, no. 25, pp. 4650–4653, 1995.
- [42] G.-H. Gweon, S. Y. Zhou, M. C. Watson, T. Sasagawa, H. Takagi, and A. Lanzara, “Strong and complex electron-lattice correlation in optimally doped Bi<sub>2</sub>Sr<sub>2</sub>CaCu<sub>2</sub>O<sub>8+δ</sub>,” *Physical Review Letters*, vol. 97, no. 22, Article ID 227001, 4 pages, 2006.
- [43] J. F. Douglas, H. Iwasawa, Z. Sun, et al., “Superconductors: unusual oxygen isotope effects in cuprates?” *Nature*, vol. 446, no. 7133, p. E5, 2007.
- [44] C. Jozwiak, J. Graf, and S. Y. Zhou, “Bilayer splitting and c-axis coupling in bilayer manganites showing colossal magnetoresistance,” *Physical Review B*, vol. 80, no. 23, Article ID 235111, 7 pages, 2009.
- [45] G.-H. Gweon, et al., “Unusual oxygen isotope effects in cuprates—importance of doping,” <http://arxiv.org/abs/0708.1027>.
- [46] S. V. Borisenko, A. A. Kordyuk, T. K. Kim, et al., “Superconducting gap in the presence of bilayer splitting in underdoped

- (Pb,Bi)<sub>2</sub>Sr<sub>2</sub>CaCu<sub>2</sub>O<sub>8+δ</sub>,” *Physical Review B*, vol. 66, no. 14, Article ID 140509, 4 pages, 2002.
- [47] A. S. Alexandrov and J. Ranninger, “Polaronic effects in the photoemission spectra of strongly coupled electron-phonon systems,” *Physical Review B*, vol. 45, no. 22, pp. 13109–13112, 1992.
- [48] P. Calvani, M. Capizzi, S. Lupi, P. Maselli, A. Paolone, and P. Roy, “Polaronic optical absorption in electron-doped and hole-doped cuprates,” *Physical Review B*, vol. 53, no. 5, pp. 2756–2766, 1996.
- [49] C. Taliani, R. Zamboni, G. Ruani, F. C. Matarotta, and K. I. Pokhodnya, “Infrared photoinduced absorption in the YBa<sub>2</sub>Cu<sub>3</sub>O<sub>7-γ</sub> high T<sub>c</sub> superconducting system,” *Solid State Communications*, vol. 66, no. 5, pp. 487–490, 1988.
- [50] Y. H. Kim, A. J. Heeger, L. Acedo, G. Stucky, and F. Wudl, “Direct evidence of the importance of electron-phonon coupling in La<sub>2</sub>CuO<sub>4</sub>: photoinduced ir-active vibrational modes,” *Physical Review B*, vol. 36, no. 13, pp. 7252–7255, 1987.
- [51] A. Bianconi and M. Missori, “The Coupling of a Wigner Charge Density Wave with Fermi Liquid from the Instability of a Wigner Polaron Crystal: A Possible Pairing Mechanism in High T<sub>c</sub> Superconductors,” in *Phase Separation in Cuprate Superconductors*, E. Sigmund and A. K. Müller, Eds., p. 272, Springer Verlag, Berlin-Heidelberg, Germany, 1994.
- [52] I. Bozovic, D. Kirillov, A. Kapitulnik, et al., “Optical measurements on oriented thin YBa<sub>2</sub>Cu<sub>3</sub>O<sub>7-δ</sub> films: lack of evidence for excitonic superconductivity,” *Physical Review Letters*, vol. 59, no. 19, pp. 2219–2221, 1987.
- [53] S. J. L. Billinge and T. Egami, “Short-range atomic structure of Nd<sub>2-x</sub>Ce<sub>x</sub>CuO<sub>4-y</sub> determined by real-space refinement of neutron-powder-diffraction data,” *Physical Review B*, vol. 47, no. 21, pp. 14386–14406, 1993.
- [54] D. Mihailovic and K. A. Muller, *High-T<sub>c</sub> Superconductivity 1996: Ten Years after the Discovery*, vol. 343 of *NATO Advanced Study Institutes, Series E*, Kluwer Academic Publishers, Dordrecht, The Netherlands, 1997.
- [55] T. Imai, C. P. Slichter, K. Yoshimura, and K. Kosuge, “Low frequency spin dynamics in undoped and Sr-doped La<sub>2</sub>CuO<sub>4</sub>,” *Physical Review Letters*, vol. 70, no. 7, pp. 1002–1005, 1993.
- [56] B. I. Kochelaev, J. Sichelschmidt, B. Elschner, W. Lemor, and A. Loidl, “Intrinsic EPR in La<sub>2-x</sub>Sr<sub>x</sub>CuO<sub>4</sub>: manifestation of three-spin polarons,” *Physical Review Letters*, vol. 79, no. 21, pp. 4274–4277, 1997.
- [57] A. S. Mishchenko and N. Nagaosa, “Numerical study of the isotope effect in underdoped high-temperature superconductors: calculation of the angle-resolved photoemission spectra,” *Physical Review B*, vol. 73, no. 9, Article ID 092502, 4 pages, 2006.
- [58] S. Fratini and S. Ciuchi, “Spectral properties and isotope effect in strongly interacting systems: Mott-Hubbard insulator versus polaronic semiconductor,” *Physical Review B*, vol. 72, no. 23, Article ID 235107, 9 pages, 2005.
- [59] A. S. Alexandrov and J. Ranninger, “Polaronic effects in the photoemission spectra of strongly coupled electron-phonon systems,” *Physical Review B*, vol. 45, no. 22, pp. 13109–13112, 1992.
- [60] A. S. Mishchenko and N. Nagaosa, “Numerical study of the isotope effect in underdoped high-temperature superconductors: calculation of the angle-resolved photoemission spectra,” *Physical Review B*, vol. 73, no. 9, Article ID 092502, 4 pages, 2006.
- [61] P. Paci, M. Capone, E. Cappelluti, S. Ciuchi, C. Grimaldi, and L. Pietronero, “Polaronic and nonadiabatic phase diagram from anomalous isotope effects,” *Physical Review Letters*, vol. 94, no. 3, Article ID 036406, 4 pages, 2005.
- [62] J. Graf, M. D’Astuto, C. Jozwiak, et al., “Bond stretching phonon softening and kinks in the angle-resolved photoemission spectra of optimally doped Bi<sub>2</sub>Sr<sub>1.6</sub>La<sub>0.4</sub>CuO<sub>6+δ</sub> superconductors,” *Physical Review Letters*, vol. 100, no. 22, Article ID 227002, 4 pages, 2008.
- [63] D. Reznik, L. Pintschovius, M. Fujita, K. Yamada, G. D. Gu, and J. M. Tranquada, “Electron-phonon anomaly related to charge stripes: static stripe phase versus optimally doped superconducting La<sub>1.85</sub>Sr<sub>0.15</sub>CuO<sub>4</sub>,” *Journal of Low Temperature Physics*, vol. 147, no. 3-4, pp. 353–364, 2007.
- [64] H. Uchiyama, A. Q. R. Baron, S. Tsutsui, et al., “Softening of Cu-O bond stretching phonons in tetragonal HgBa<sub>2</sub>CuO<sub>4+δ</sub>,” *Physical Review Letters*, vol. 92, no. 19, Article ID 197005, 4 pages, 2004.
- [65] T. Kondo, T. Takeuchi, A. Kaminski, S. Tsuda, and S. Shin, “Evidence for two energy scales in the superconducting state of optimally doped (Bi, Pb)<sub>2</sub>(Sr, La)<sub>2</sub>CuO<sub>6+δ</sub>,” *Physical Review Letters*, vol. 98, no. 26, Article ID 267004, 4 pages, 2007.
- [66] A. Kanigel, M. R. Norman, M. Randeria, et al., “Evolution of the pseudogap from Fermi arcs to the nodal liquid,” *Nature Physics*, vol. 2, no. 7, pp. 447–451, 2006.
- [67] P. Zhang, S. G. Louie, and M. L. Cohen, “Electron-phonon renormalization in cuprate superconductors,” *Physical Review Letters*, vol. 98, no. 6, Article ID 067005, 4 pages, 2007.
- [68] H. Eisaki, N. Kaneko, D. L. Feng, et al., “Effect of chemical inhomogeneity in bismuth-based copper oxide superconductors,” *Physical Review B*, vol. 69, no. 6, Article ID 064512, 2004.
- [69] X.-J. Chen, V. V. Struzhkin, R. J. Hemley, H.-K. Mao, and C. Kendziora, “High-pressure phase diagram of Bi<sub>2</sub>Sr<sub>2</sub>CaCu<sub>2</sub>O<sub>8+δ</sub> single crystals,” *Physical Review B*, vol. 70, no. 21, Article ID 214502, 7 pages, 2004.
- [70] T. Cuk, V. V. Struzhkin, T. P. Devereaux, et al., “Uncovering a pressure-tuned electronic transition in Bi<sub>1.98</sub>Sr<sub>2.06</sub>Y<sub>0.68</sub>Cu<sub>2</sub>O<sub>8+δ</sub> using raman scattering and X-ray diffraction,” *Physical Review Letters*, vol. 100, no. 21, Article ID 217003, 4 pages, 2008.
- [71] A. Bianconi, S. Agrestini, G. Bianconi, D. Di Castro, and N. L. Saini, “A quantum phase transition driven by the electron lattice interaction gives high T<sub>c</sub> superconductivity,” *Journal of Alloys and Compounds*, vol. 317-318, pp. 537–541, 2001.
- [72] H. Hobou, S. Ishida, K. Fujita, et al., “Enhancement of the superconducting critical temperature in Bi<sub>2</sub>Sr<sub>2</sub>CaCu<sub>2</sub>O<sub>8+δ</sub> by controlling disorder outside CuO<sub>2</sub> planes,” *Physical Review B*, vol. 79, no. 6, Article ID 064507, 6 pages, 2009.
- [73] D. R. Garcia, et al., to be submitted to *Physical Review B*.
- [74] R. L. Carlin, *Magnetochemistry*, Springer, New York, NY, USA, 1986.

## Review Article

# Bosonic Spectral Function and the Electron-Phonon Interaction in HTSC Cuprates

E. G. Maksimov,<sup>1</sup> M. L. Kulić,<sup>2,3</sup> and O. V. Dolgov<sup>4</sup>

<sup>1</sup>*I. E. Tamm Theoretical Department, Lebedev Physical Institute, 119991 Moscow, Russia*

<sup>2</sup>*Institute for Theoretical Physics, Goethe University, 60438 Frankfurt am Main, Germany*

<sup>3</sup>*Max-Born-Institut für Nichtlineare Optik und Kurzzeitspektroskopie, 12489 Berlin, Germany*

<sup>4</sup>*Theoretische Abteilung, Max-Planck-Institut für Festkörperphysik, 70569 Stuttgart, Germany*

Correspondence should be addressed to M. L. Kulić, kulic@th.physik.uni-frankfurt.de

Received 20 July 2009; Revised 1 November 2009; Accepted 24 February 2010

Academic Editor: Carlo Di Castro

Copyright © 2010 E. G. Maksimov et al. This is an open access article distributed under the Creative Commons Attribution License, which permits unrestricted use, distribution, and reproduction in any medium, provided the original work is properly cited.

In this paper we discuss experimental evidence related to the structure and origin of the bosonic spectral function  $\alpha^2F(\omega)$  in high-temperature superconducting (HTSC) cuprates at and near optimal doping. Global properties of  $\alpha^2F(\omega)$ , such as number and positions of peaks, are extracted by combining optics, neutron scattering, ARPES and tunnelling measurements. These methods give evidence for strong electron-phonon interaction (EPI) with  $1 < \lambda_{ep} \lesssim 3.5$  in cuprates near optimal doping. We clarify how these results are in favor of the modified Migdal-Eliashberg (ME) theory for HTSC cuprates near optimal doping. In Section 2 we discuss theoretical ingredients—such as strong EPI, strong correlations—which are necessary to explain the mechanism of d-wave pairing in optimally doped cuprates. These comprise the ME theory for EPI in strongly correlated systems which give rise to the forward scattering peak. The latter is supported by the long-range part of EPI due to the weakly screened Madelung interaction in the ionic-metallic structure of layered HTSC cuprates. In this approach EPI is responsible for the strength of pairing while the residual Coulomb interaction and spin fluctuations trigger the d-wave pairing.

## 1. Experimental Evidence for Strong EPI

**1.1. Introduction.** In spite of an unprecedented intensive experimental and theoretical study after the discovery of high-temperature superconductivity (HTSC) in cuprates, there is, even twenty-three years after, no consensus on the pairing mechanism in these materials. At present there are two important experimental facts which are not under dispute: (1) the critical temperature  $T_c$  in cuprates is high, with the maximum  $T_c^{\max} \sim 160$  K in the Hg-1223 compounds; (2) the pairing in cuprates is *d*-wave like, that is,  $\Delta(\mathbf{k}, \omega) \approx \Delta_d(\omega)(\cos k_x - \cos k_y)$ . On the contrary there is a dispute concerning the scattering mechanism which governs normal state properties and pairing in cuprates. To this end, we stress that in the HTSC cuprates, a number of properties can be satisfactorily explained by assuming that the quasiparticle dynamics is governed by some electron-boson scattering and in the superconducting state bosonic quasiparticles are responsible for Cooper pairing. Which

bosonic quasiparticles are dominating in the cuprates is the subject which will be discussed in this work. It is known that the electron-boson (phonon) scattering is well described by the Migdal-Eliashberg theory if the adiabatic parameter  $A \equiv \alpha \cdot \lambda(\omega_B/W_b)$  fulfills the condition  $A \ll 1$ , where  $\lambda$  is the electron-boson coupling constant,  $\omega_B$  is the characteristic bosonic energy,  $W_b$  is the electronic band width, and  $\alpha$  depends on numerical approximations [1, 2]. The important characteristic of the electron-boson scattering is the Eliashberg spectral function  $\alpha^2F(\mathbf{k}, \mathbf{k}', \omega)$  (or its average  $\alpha^2F(\omega)$ ) which characterizes scattering of quasiparticle from  $\mathbf{k}$  to  $\mathbf{k}'$  by exchanging bosonic energy  $\omega$ . Therefore, in systems with electron-boson scattering the knowledge of the spectral function is of crucial importance.

There are at least two approaches differing in assumed pairing bosons in the HTSC cuprates. The *first one* is based on the electron-phonon interaction (EPI), with the main proponents in [3–11], where mediating bosons are *phonons* and where the average spectral function  $\alpha^2F(\omega)$  is similar

to the phonon density of states  $F_{\text{ph}}(\omega)$ . Note that  $\alpha^2 F(\omega)$  is not the product of two functions although sometimes one defines the function  $\alpha^2(\omega) = \alpha^2 F(\omega)/F(\omega)$  which should approximate the energy dependence of the strength of the EPI coupling. There are numerous experimental evidences in cuprates for the importance of the EPI scattering mechanism with a rather large coupling constant in the normal scattering channel  $1 < \lambda_{ep} \lesssim 3$ , which will be discussed in detail below. In the EPI approach  $\alpha^2 F_{\text{ph}}(\omega)$  is extracted from tunnelling measurements in conjunction with IR optical measurements. The HTSC cuprates are on the borderline and it is a natural question—under which condition can high  $T_c$  be realized in the nonadiabatic limit  $A \approx 1$ ?

The *second approach* [12–17] assumes that EPI is too weak to be responsible for high  $T_c$  in cuprates and it is based on a phenomenological model for spin-fluctuation interaction (*SFI*) as the dominating scattering mechanism, that is, it is a nonphononic mechanism. In this (phenomenological) approach the spectral function is proportional to the imaginary part of the spin susceptibility  $\text{Im} \chi(\mathbf{k} - \mathbf{k}', \omega)$ , that is,  $\alpha^2 F(\mathbf{k}, \mathbf{k}', \omega) \sim g_{\text{sf}}^2 \text{Im} \chi(\mathbf{k} - \mathbf{k}', \omega)$  where  $g_{\text{sf}}$  is the SFI coupling constant. NMR spectroscopy and magnetic neutron scattering give evidence that in HTSC cuprates  $\chi(\mathbf{q}, \omega)$  is peaked at the antiferromagnetic wave vector  $\mathbf{Q} = (\pi/a, \pi/a)$  and this property is favorable for *d*-wave pairing. The *SFI* theory roots basically on the strong electronic repulsion on Cu atoms, which is usually studied by the Hubbard model or its (more popular) derivative the *t*-*J* model. Regarding the possibility to explain high  $T_c$  *solely by strong correlations*, as it is reviewed in [18], we stress two facts. First, at present there is no viable theory as well as experimental facts which can justify these (nonphononic) mechanisms of pairing with some exotic pairing mechanism such as RVB pairing [18], fractional statistics, anyon superconductivity, and so forth. Therefore we will not discuss these, in theoretical sense interesting approaches. Second, the central question in these nonphononic approaches is the following—do models based solely on the Hubbard Hamiltonian show up superconductivity at sufficiently high critical temperatures ( $T_c \sim 100$  K)? Although the answer on this important question is not definitely settled, there are a number of *numerical studies* of these models which offer negative answers. For instance, the sign-free variational Monte Carlo algorithm in the 2D repulsive ( $U > 0$ ) Hubbard model gives *no evidence for superconductivity with high  $T_c$* , neither the BCS-like nor the Berezinskii-Kosterlitz-Thouless- (BKT-) like [19]. At the same time, similar calculations show that there is a strong tendency to superconductivity in the attractive ( $U < 0$ ) Hubbard model for the same strength of  $U$ , that is, at finite temperature in the 2D model with  $U < 0$  the BKT superconducting transition is favored. Concerning the possibility of HTSC in the *t*-*J* model, various numerical calculations such as Monte Carlo calculations of the Drude spectral weight [20] and high-temperature expansion for the pairing susceptibility [21] give evidence that there is no superconductivity at temperatures characteristic for cuprates and if it exists  $T_c$  must be rather low—few Kelvins. These numerical results tell us that the lack of high  $T_c$  (even in 2D BKT phase) in the repulsive

( $U > 0$ ) single-band Hubbard model and in the *t*-*J* model is not only due to thermodynamical 2D-fluctuations (which at finite  $T$  suppress and destroy superconducting phase coherence in large systems) but it is also mostly due to an *inherent ineffectiveness of strong correlations to produce solely high  $T_c$  in cuprates*. These numerical results signal that the simple single-band Hubbard and its derivative the *t*-*J* model are insufficient to explain solely the pairing mechanism in cuprates and some additional ingredients must be included.

Since *EPI* is rather strong in cuprates, then it must be accounted for. As it will be argued in the following, the experimental support for the importance of EPI in cuprates comes from optics, tunnelling, and recent ARPES measurements [22, 23]. It is worth mentioning that recent ARPES activity was a strong impetus for renewed experimental and theoretical studies of EPI in cuprates. However, in spite of accumulating experimental evidence for importance of EPI with  $\lambda_{ep} > 1$ , there are occasionally reports which doubt its importance in cuprates. This is the case with recent interpretation of some optical measurements in terms of SFI only [24–27] and with the LDA-DFT (local density approximation-density functional theory) band-structure calculations [28, 29], where both claim that EPI is negligibly small, that is,  $\lambda_{ep} < 0.3$ . The inappropriateness of these statements will be discussed in the following sections.

The paper is organized as follows. In Section 1 we will mainly discuss experimental results in *cuprates at and near optimal doping* by giving also minimal theoretical explanations which are related to the *bosonic spectral function*  $\alpha^2 F(\omega)$  as well as to the transport spectral function  $\alpha_{\text{tr}}^2 F(\omega)$  and their relations to EPI. The reason that we study only cuprates at and near optimal doping is that in these systems there are rather well-defined quasiparticles—although strongly interacting—while in highly underdoped systems the superconductivity is perplexed and possibly masked by other phenomena, such as pseudogap effects, formation of small polarons, interaction with spin and (possibly charge) order parameters, pronounced inhomogeneities of the scattering centers, and so forth. As the ARPES experiments confirm, there are no polaronic effects in systems at and near the optimal doping, while there are pronounced polaronic effects due to EPI in undoped and very underdoped HTSC [8–11]. In this work we consider mainly those direct one-particle and two-particle probes of low-energy quasiparticle excitations and scattering rates which give information on the structure of the spectral functions  $\alpha^2 F(\mathbf{k}, \mathbf{k}', \omega)$  and  $\alpha_{\text{tr}}^2 F(\omega)$  in systems near optimal doping. These are angle-resolved photoemission (ARPES), various arts of tunnelling spectroscopy such as superconductor/insulator/normal metal (*SIN*) junctions, break junctions, scanning-tunnelling microscope spectroscopy (*STM*), infrared (*IR*) and Raman optics, inelastic neutron and X-ray scattering, and so forth. We will argue that these direct probes give evidence for a rather strong EPI in cuprates. Some other experiments on EPI are also discussed in order to complete the arguments for the importance of EPI in cuprates. The detailed contents of Section 1 are the following. In Section 1.2 we discuss some prejudices related to the strength of *EPI* as well as on the Fermi-liquid behavior of

HTSC cuprates. We argue that any nonphononic mechanism of pairing should have very large bare critical temperature  $T_{c0} \gg T_c$  in the presence of the large EPI coupling constant,  $\lambda_{ep} \geq 1$ , if the EPI spectral function is weakly momentum dependent, that is, if  $\alpha^2 F(\mathbf{k}, \mathbf{k}', \omega) \approx \alpha^2 F(\omega)$  like in low-temperature superconductors. The fact that EPI is large in the normal state of cuprates and the condition that it must conform with  $d$ -wave pairing imply that EPI in HTSC cuprates should be *strongly momentum dependent*. In Section 1.3 we discuss *direct and indirect experimental evidences for the importance of EPI* in cuprates and for the weakness of SFI in cuprates. These are the following.

(a) *Magnetic Neutron Scattering Measurements*. These measurements provide dynamic spin susceptibility  $\chi(\mathbf{q}, \omega)$  which is in the *SFI phenomenological approach* [12–17] related to the Eliashberg spectral function, that is,  $\alpha^2 F_{sf}(\mathbf{k}, \mathbf{k}', \omega) \sim g_{sf}^2 \text{Im} \chi(\mathbf{q} = \mathbf{k} - \mathbf{k}', \omega)$ . We stress that such an approach can be theoretically justified only in the weak coupling limit,  $g_{sf} \ll W_b$ , where  $W_b$  is the band width and  $g_{sf}$  is the phenomenological SFI coupling constant. Here we discuss experimental results on YBCO which give evidence for strong rearrangement (with respect to  $\omega$ ) of  $\text{Im} \chi(\mathbf{q}, \omega)$  (with  $\mathbf{q}$  at and near  $\mathbf{Q} = (\pi, \pi)$ ) by doping toward the optimal doped HTSC [30, 31]. It turns out that in the optimally doped cuprates with  $T_c = 92.5$  K  $\text{Im} \chi(\mathbf{Q}, \omega)$  is *drastically suppressed* compared to that in slightly underdoped ones with  $T_c = 91$  K. This fact implies that the SFI coupling constant  $g_{sf}$  must be small.

(b) *Optical Conductivity Measurements*. From these measurements one can extract the transport relaxation rate  $\gamma_{tr}(\omega)$  and indirectly an approximative shape of the transport spectral function  $\alpha_{tr}^2 F(\omega)$ . In the case of systems near optimal doping we discuss the following questions. (i) First is the physical and quantitative difference between the optical relaxation rate  $\gamma_{tr}(\omega)$  and the quasiparticle relaxation rate  $\gamma(\omega)$ . It was shown in the past that equating these two (unequal) quantities is dangerous and brings incorrect results concerning the quasiparticle dynamics in most metals by including HTSC cuprates too [3–6, 32–38]. (ii) Second are methods of extraction of the transport spectral function  $\alpha_{tr}^2 F(\omega)$ . Although these methods give at finite temperature  $T$  a blurred  $\alpha_{tr}^2 F(\omega)$  which is (due to the ill-defined methods) temperature dependent, it turns out that the width and the shape of the extracted  $\alpha_{tr}^2 F(\omega)$  are in favor of *EPI*. (iii) Third is the restricted sum rule for the optical weight as a function of  $T$  which can be explained by strong *EPI* [39, 40]. (iv) Fourth is the good agreement with experiments of the  $T$ -dependence of the resistivity  $\rho(T)$  in optimally doped YBCO, where  $\rho(T)$  is calculated by using the spectral function from tunnelling experiments. Recent femtosecond time-resolved optical spectroscopy in  $\text{La}_{2-x}\text{Sr}_x\text{CuO}_4$  which gives additional evidence for importance of EPI [41] will be shortly discussed.

(c) *ARPES Measurements and EPI*. From these measurements the self-energy  $\Sigma(\mathbf{k}, \omega)$  is extracted as well as some properties of  $\alpha^2 F(\mathbf{k}, \mathbf{k}', \omega)$ . Here we discuss the following items: (i) the existence of the nodal and antinodal kinks in optimally and slightly underdoped cuprates, as well as the structure of the ARPES self-energy ( $\Sigma(\mathbf{k}, \omega)$ ) and its isotope dependence, which are all due to EPI; (ii) the appearance

of different slopes of  $\Sigma(\mathbf{k}, \omega)$  at low ( $\omega \ll \omega_{ph}$ ) and high energies ( $\omega \gg \omega_{ph}$ ) which can be explained by the strong EPI; (iii) the formation of small polarons in the undoped HTSC which was interpreted to be due to strong EPI—this gives rise to phonon side bands which are clearly seen in ARPES of undoped HTSC [10, 11].

(d) *Tunnelling Spectroscopy*. It is well known that this method is of an immense importance in obtaining the spectral function  $\alpha^2 F(\omega)$  from tunnelling conductance. In this part we discuss the following items: (i) the extracted Eliashberg spectral function  $\alpha^2 F(\omega)$  with the coupling constant  $\lambda^{(tun)} = 2\text{--}3.5$  from the tunnelling conductance of break-junctions in optimally doped YBCO and Bi-2212 [42–55] which gives that the maxima of  $\alpha^2 F(\omega)$  coincide with the maxima in the phonon density of states  $F_{ph}(\omega)$ ; (ii) the existence of *eleven peaks* in  $-d^2 I/dV^2$  in superconducting  $\text{La}_{1.84}\text{Sr}_{0.16}\text{CuO}_4$  films [56], where these peaks match precisely with the peaks in the intensity of the existing phonon Raman scattering data [57]; (iii) the presence of the dip in  $dI/dV$  in STM which shows the pronounced oxygen isotope effect and important role of these phonons.

(e) *Inelastic Neutron and X-Ray Scattering Measurements*. From these experiments one can extract the phonon density of state  $F_{ph}(\omega)$  and in some cases the strengths of the quasiparticle coupling with various phonon modes. These experiments give sufficient evidence for quantitative inadequacy of LDA-DFT calculations in HTSC cuprates. Here we argue that the *large softening and broadening* of the half-breathing Cu–O bond-stretching phonon, of the apical oxygen phonons and of the oxygen  $B_{1g}$  buckling phonons (in LSCO, BSCO, YBCO), cannot be explained by LDA-DFT. It is curious that the magnitude of the softening can be partially obtained by LDA-DFT but the calculated widths of some important modes are an order of magnitude smaller than the neutron scattering data show. This remarkable fact confirms that additionally *the inadequacy of LDA-DFT in strongly correlated systems* and a more sophisticated many-body theory for EPI is needed. The problem of EPI will be discussed in more details in Section 2.

In Section 1.4 brief summary of Section 1 is given. Since *we are dealing with the electron-boson scattering in cuprates near the optimal doping*, then in Appendix A (and in Section 2) we introduce the reader briefly to the Migdal-Eliashberg theory for superconductors (and normal metals) where the quasiparticle spectral function  $\alpha^2 F(\mathbf{k}, \mathbf{k}', \omega)$  and the transport spectral function  $\alpha_{tr}^2 F(\omega)$  are defined.

Finally, one can pose a question—do the experimental results of the above enumerated spectroscopic methods allow a building of a satisfactory and physically reasonable microscopic theory for basic scattering and pairing mechanism in cuprates? The posed question is very modest compared to the much stringent request for the *theory of everything*—which would be able to explain all properties of HTSC materials. Such an ambitious project is not realized even in those low-temperature conventional superconductors where it is definitely proved that in most materials the pairing is due to EPI and many properties are well accounted for by the Migdal-Eliashberg theory. For an illustration, let us mention only two examples. First, the experimental value

for the coherence peak in the microwave response  $\sigma_s$  ( $T < T_c$ ,  $\omega = \text{const}$ ) at  $\omega = 17$  GHz in the superconducting Nb is much higher than the theoretical value obtained by the strong coupling Eliashberg theory [58]. So to say, the theory explains the coherence peak at 17 GHz in Nb qualitatively but not quantitatively. However, the measurements at higher frequency  $\omega \sim 60$  GHz are in agreement with the Eliashberg theory [59]. Then one can say that instead of the theory of everything we deal with a satisfactory theory, which allows us qualitative and in many aspects quantitative explanation of phenomena in superconducting state. Second example is the experimental boron (B) isotope effect in  $\text{MgB}_2$  ( $T_c \approx 40$  K) which is smaller than the theoretical value, that is,  $\alpha_B^{\text{exp}} \approx 0.3 < \alpha_B^{\text{th}} = 0.5$ , although the pairing is due to EPI for boron vibrations [60]. Since the theory of everything is impossible in the complex materials such as HTSC cuprates in Section 1, we will not discuss those phenomena which need much more microscopic details and/or more sophisticated many-body theory. These are selected by chance: (i) large ratio  $2\Delta/T_c$  which is on optimally doped YBCO and BSCO  $\approx 5$  and 7, respectively, while in underdoped BSCO one has even  $(2\Delta/T_c) \approx 20$ ; (ii) peculiarities of the coherence peak in the microwave response  $\sigma(T)$  in HTSC cuprates, which is peaked at  $T$  much smaller than  $T_c$ , contrary to the case of LTSC where it occurs near  $T_c$ ; (iii) the dependence of  $T_c$  on the number of  $\text{CuO}_2$  in the unit cell; (iv) the temperature dependence of the Hall coefficient; (v) distribution of states in the vortex core, and so forth.

The microscopic theory of the mechanism for superconducting pairing in HTSC cuprates will be discussed in Section 2. In Section 2.1 we introduce an *ab initio many-body theory* of superconductivity which is based on the fundamental (microscopic) Hamiltonian and the many-body technique. This theory can in principle calculate measurable properties of materials such as the critical temperature  $T_c$ , the critical fields, the dynamic and transport properties, and so forth. However, although this method is in principle exact, which needs only some fundamental constants  $e$ ,  $\hbar$ ,  $m_e$ ,  $M_{\text{ion}}$ ,  $k_B$  and the chemical composition of superconducting materials, it was practically never realized in practice due to the complexity of many-body interactions—electron-electron and electron-lattice—as well as of structural properties. Fortunately, the problem can be simplified by using the fact that superconductivity is a low-energy phenomenon characterized by the *very small energy parameters* ( $T_c/E_F, \Delta/E_F, \omega_{\text{ph}}/E_F$ )  $\ll 1$ . It turns out that one can integrate high-energy electronic processes (which are not changed by the appearance of superconductivity) and then solve the *low-energy problem* by the (so-called) strong-coupling Migdal-Eliashberg theory. It turns out that in such an approach the physics is separated into the following: (1) the solution of the *ideal band-structure Hamiltonian with the nonlocal exact crystal potential* (sometimes called the excitation potential)  $V_{\text{IBS}}(\mathbf{r}, \mathbf{r}')$  (IBS—the *ideal band structure*) which includes the static self-energy ( $\Sigma_{c0}^{(h)}(\mathbf{r}, \mathbf{r}', \omega = 0)$ ) due to high-energy electronic processes, that is,  $V_{\text{IBS}}(\mathbf{r}, \mathbf{r}') = [V_{e-i}(\mathbf{r}) + V_H(\mathbf{r})]\delta(\mathbf{r} - \mathbf{r}') + \Sigma_{c0}^{(h)}(\mathbf{r}, \mathbf{r}', \omega = 0)$ , with  $V_{e-i}$  and  $V_H$  being the electron-ion and Hartree potential, respectively;

(2) solving the low-energy Eliashberg equations. However, the calculation of the (excited) potential  $V_{\text{IBS}}(\mathbf{r}, \mathbf{r}')$  and the real EPI coupling  $g_{ep}(\mathbf{r}, \mathbf{r}') = \delta V_{\text{IBS}}(\mathbf{r}, \mathbf{r}')/\delta \mathbf{R}_n$ , which include high-energy many-body electronic processes—for instance, the large Hubbard  $U$  effects—is extremely difficult at present, especially in strongly correlated systems such as HTSC cuprates. Due to this difficulty the calculations of the EPI coupling in the past were usually based on the LDA-DFT method which will be discussed in Section 2.2 in the context of HTSC cuprates, where the nonlocal potential is replaced by the *local potential*  $V_{\text{LDA}}(\mathbf{r})$ —the ground-state potential—and the real EPI coupling by the “local” LDA one  $g_{ep}(\mathbf{r}) = \delta V_{\text{LDA}}(\mathbf{r})/\delta \mathbf{R}_n$ . Since the exchange-correlation effects enter  $V_{\text{LDA}}(\mathbf{r}) = V_{e-i}(\mathbf{r}) + V_H(\mathbf{r}) + V_{\text{XC}}(\mathbf{r})$  via the local exchange-correlation potential  $V_{\text{XC}}(\mathbf{r})$ , it is clear that the LDA-DFT method describes strong correlations scarcely and it is inadequate in HTSC cuprates (and other strongly correlated systems such as heavy fermions) where one needs an approach beyond the LDA-DFT method. In Section 2.3 we discuss a *minimal theoretical model* for HTSC cuprates which takes into account minimal number of electronic orbitals and strong correlations in a controllable manner [6]. This theory treats the *interplay of EPI and strong correlations* in systems with finite doping in a systematic and controllable way. The minimal model can be further reduced (in some range of parameters) to the single-band *t-J* model, which allows the approximative calculation of the excited potential  $V_{\text{IBS}}(\mathbf{r}, \mathbf{r}')$  and the nonlocal EPI coupling  $g_{ep}(\mathbf{r}, \mathbf{r}')$ . As a result one obtains the momentum-dependent EPI coupling  $g_{ep}(\mathbf{k}_F, \mathbf{q})$  which is for small hole-doping ( $\delta < 0.3$ ) strongly peaked at small transfer momenta—the *forward scattering peak*. In the framework of this minimal model it is possible to explain some important properties and resolve some puzzling experimental results, like the following, for instance. (a) Why is *d*-wave pairing realized in the presence of strong EPI? (b) Why is the transport coupling constant ( $\lambda_{\text{tr}}$ ) rather smaller than the pairing one  $\lambda$ , that is,  $\lambda_{\text{tr}} \lesssim \lambda/3$ ? (c) Why is the mean-field (one-body) LDA-DFT approach unable to give reliable values for the EPI coupling constant in cuprates and how many-body effects can help? (d) Why is *d*-wave pairing robust in the presence of nonmagnetic impurities and defects? (e) Why are the ARPES nodal and antinodal kinks differently renormalized in the superconducting states, and so forth? In spite of the encouraging successes of this minimal model, at least in a qualitative explanation of numerous important properties of HTSC cuprates, we are at present stage rather far from a fully microscopic theory of HTSC cuprates which is able to explain high  $T_c$ . In that respect at the end of Section 2.3 we discuss possible improvements of the present minimal model in order to obtain at least a semiquantitative theory for HTSC cuprates.

Finally, we would like to point out that in real HTSC materials there are numerous experimental evidences for nanoscale inhomogeneities. For instance, recent STM experiments show rather large gap dispersion, at least on the surface of BSCO crystals [61–63], giving rise to a pronounced inhomogeneity of the superconducting order parameter  $\Delta(\mathbf{k}, \mathbf{R})$ , where  $\mathbf{k}$  is the relative momentum of the Cooper

pair and  $\mathbf{R}$  is the center of mass of Cooper pairs. One possible reason for the inhomogeneity of  $\Delta(\mathbf{k}, \mathbf{R})$  and disorder on the atomic scale can be due to extremely high doping level of  $\sim(10\text{--}20)\%$  in HTSC cuprates which is many orders of magnitude larger than in standard semiconductors ( $10^{21}$  versus  $10^{15}$  carrier concentration). There are some claims that high  $T_c$  is exclusively due to these inhomogeneities (of an extrinsic or intrinsic origin) which may effectively increase pairing potential [64], while some others try to explain high  $T_c$  solely within the inhomogeneous Hubbard or  $t$ - $J$  model. Here we will not discuss this interesting problem but mention only that the concept of  $T_c$  increase by inhomogeneity is not well-defined, since the increase of  $T_c$  is defined with respect to the average value  $\bar{T}_c$ . However,  $\bar{T}_c$  is experimentally not well defined quantity and the hypothesis of an increase of  $T_c$  by material inhomogeneities cannot be tested at all. In studying and analyzing *HTSC cuprates near optimal doping* we assume that basic effects are realized in nearly homogeneous systems and inhomogeneities are of secondary role, which deserve to be studied and discussed separately.

*1.2. EPI versus Nonphononic Mechanisms.* Concerning the high  $T_c$  values in cuprates, two dilemmas have been dominating after its discovery: (i) which interaction is responsible for strong quasiparticle scattering in the normal state? This question is related also to the dilemma of Fermi versus non-Fermi liquid; (ii) What is the mediating (gluing) boson responsible for the superconducting pairing, that is, *phonons or nonphonons*? In the last twenty-three years, the scientific community was overwhelmed by numerous proposed pairing mechanisms, most of which are hardly verifiable in HTSC cuprates.

*(1) Fermi versus Non-Fermi Liquid in Cuprates.* After discovery of HTSC in cuprates there was a large amount of evidence on strong scattering of quasiparticles which contradicts the canonical (popular but narrow) definition of the Fermi liquid, thus giving rise to numerous proposals of the so called non-Fermi liquids, such as Luttinger liquid, RVB theory, marginal Fermi liquid, and so forth. In our opinion there is no need for these radical approaches in explaining basic physics in cuprates at least *in optimally, slightly underdoped and overdoped* metallic and superconducting HTSC cuprates. Here we give some clarifications related to the dilemma of Fermi versus non-Fermi liquid. The definition of the *canonical Fermi liquid* (based on the Landau work) in interacting Fermi systems comprises the following properties: (1) there are quasiparticles with charge  $q = \pm e$ , spin  $s = 1/2$ , and low-energy excitations  $\xi_{\mathbf{k}} (= \epsilon_{\mathbf{k}} - \mu)$  which are much larger than their inverse life-times, that is,  $\xi_{\mathbf{k}} \gg 1/\tau_{\mathbf{k}} \sim \xi_{\mathbf{k}}^2/W_b$ . Since the level width  $\Gamma = 2/\tau_{\mathbf{k}}$  of the quasiparticle is negligibly small, this means that the excited states of the Fermi liquid are placed in one-to-one correspondence with the excited states of the free Fermi gas; (2) at  $T = 0$  K there is an energy level  $\xi_{k_F} = 0$  which defines the Fermi surface on which the Fermi quasiparticle distribution function  $n_F(\xi_{\mathbf{k}})$  has finite jump at  $k_F$ ; (3) the

number of quasiparticles under the Fermi surface is equal to the total number of conduction particles (we omit here other valence and core electrons)—the Luttinger theorem; (4) the interactions between quasiparticles are characterized by the set of Landau parameters which describe the low-temperature thermodynamics and transport properties. Having this definition in mind one can say that if fermionic quasiparticles interact with some bosonic excitation, for instance, with phonons, and if the coupling is sufficiently strong, then the former are not described by the canonical Fermi liquid since at energies and temperatures of the order of the characteristic (Debye) temperature  $k_B\Theta_D (\equiv \hbar\omega_D)$  (for the Debye spectrum  $\sim \Theta_D/5$ ), that is, for  $\xi_{\mathbf{k}} \sim \Theta_D$ , one has  $\tau_{\mathbf{k}}^{-1} \gtrsim \xi_{\mathbf{k}}$  and the quasiparticle picture (in the sense of the Landau definition) is broken down. In that respect an electron-boson system can be classified as a *noncanonical Fermi liquid* for sufficiently strong electron-boson coupling. It is nowadays well known that, for instance, Al, Zn are weak coupling systems since for  $\xi_{\mathbf{k}} \sim \Theta_D$  one has  $\tau_{\mathbf{k}}^{-1} \ll \xi_{\mathbf{k}}$  and they are well described by the Landau theory. However, in (the noncanonical) cases where for higher energies  $\xi_{\mathbf{k}} \sim \Theta_D$  one has  $\tau_{\mathbf{k}}^{-1} \gtrsim \xi_{\mathbf{k}}$ , the electron-phonon system is satisfactorily described by the *Migdal-Eliashberg theory and the Boltzmann theory*, where thermodynamic and transport properties depend on the spectral function  $\alpha^2F_{sf}(\mathbf{k}, \mathbf{k}', \omega)$  and its higher momenta. Since in HTSC cuprates the electron-boson (phonon) coupling is strong and  $T_c$  is large, then it is natural that in the normal state (at  $T > T_c$ ) we deal with a strong interacting noncanonical Fermi liquid which is for modest nonadiabaticity parameter  $A < 1$  described by the Migdal-Eliashberg theory, at least qualitatively and semiquantitatively. In order to justify this statement we will in the following elucidate some properties in more details by studying optical, ARPES, tunnelling and other experiments in HTSC oxides.

*(2) Is There Limit of the EPI Strength?* In spite of the reached experimental evidence in favor of strong EPI in HTSC oxides, there was a disproportion in the research activity (especially theoretical) in the past, since the investigation of the SFI mechanism of pairing prevailed in the literature. This trend was partly due to an incorrect statement in [65, 66] on the possible upper limit of  $T_c$  in the phonon mechanism of pairing. Since in the past we have discussed this problem thoroughly in numerous papers—for the recent one see [67]—we will outline here the main issue and results only.

It is well known that in an electron-ion crystal, besides the attractive EPI, there is also repulsive Coulomb interaction. In case of an isotropic and homogeneous system with weak quasiparticle interaction, the effective potential  $V_{\text{eff}}(\mathbf{k}, \omega)$  in the leading approximation looks like as for two external charges ( $e$ ) embedded in the medium with the *total longitudinal dielectric function*  $\epsilon_{\text{tot}}(\mathbf{k}, \omega)$  ( $\mathbf{k}$  is the momentum and  $\omega$  is the frequency) [68, 69], that is,

$$V_{\text{eff}}(\mathbf{k}, \omega) = \frac{V_{\text{ext}}(\mathbf{k})}{\epsilon_{\text{tot}}(\mathbf{k}, \omega)} = \frac{4\pi e^2}{k^2 \epsilon_{\text{tot}}(\mathbf{k}, \omega)}. \quad (1)$$

In case of strong interaction between quasiparticles, the state of embedded quasiparticles changes significantly due

to interaction with other quasiparticles, giving rise to  $V_{\text{eff}}(\mathbf{k}, \omega) \neq 4\pi e^2/k^2 \varepsilon_{\text{tot}}(\mathbf{k}, \omega)$ . In that case  $V_{\text{eff}}$  depends on other (than  $\varepsilon_{\text{tot}}(\mathbf{k}, \omega)$ ) response functions. However, in the case when (1) holds, that is, when the weak-coupling limit is realized,  $T_c$  is given by  $T_c \approx \bar{\omega} \exp(-1/(\lambda_{ep} - \mu^*))$  [68–70]. Here,  $\lambda_{ep}$  is the EPI coupling constant,  $\bar{\omega}$  is an average phonon frequency, and  $\mu^*$  is the Coulomb pseudopotential,  $\mu^* = \mu/(1 + \mu \ln E_F/\bar{\omega})$  ( $E_F$  is the Fermi energy). The couplings  $\lambda_{ep}$  and  $\mu$  are expressed by  $\varepsilon_{\text{tot}}(\mathbf{k}, \omega = 0)$ :

$$\begin{aligned} \mu - \lambda_{ep} &= \langle N(0) V_{\text{eff}}(\mathbf{k}, \omega = 0) \rangle \\ &= N(0) \int_0^{2k_F} \frac{k dk}{2k_F^2} \frac{4\pi e^2}{k^2 \varepsilon_{\text{tot}}(\mathbf{k}, \omega = 0)}, \end{aligned} \quad (2)$$

where  $N(0)$  is the density of states at the Fermi surface and  $k_F$  is the Fermi momentum—see more in [3–5]. In [65, 66] it was claimed that the lattice stability of the system with respect to the charge density wave formation implies the condition  $\varepsilon_{\text{tot}}(\mathbf{k}, \omega = 0) > 1$  for all  $\mathbf{k}$ . If this were correct, then from (2) it would follow that  $\mu > \lambda_{ep}$ , which limits the maximal value of  $T_c$  to the value  $T_c^{\text{max}} \approx E_F \exp(-4 - 3/\lambda_{ep})$ . In typical metals  $E_F < (1-10)$  eV, and if one accepts the statement in [65, 66] that  $\lambda_{ep} \leq \mu (\leq 0.5)$ , one obtains  $T_c \sim (1-10)$  K. The latter result, if it would be correct, means that EPI is ineffective in producing not only high- $T_c$  superconductivity but also low-temperature superconductivity (LTS with  $T_c \lesssim 20$  K). However, this result is in conflict first of all with experimental results in LTSC, where in numerous systems one has  $\mu \leq \lambda_{ep}$  and  $\lambda_{ep} > 1$ . For instance,  $\lambda_{ep} \approx 2.6$  is realized in *PbBi* alloy which is definitely much higher than  $\mu (< 1)$ , and so forth.

Moreover, the basic theory tells us that  $\varepsilon_{\text{tot}}(\mathbf{k} \neq 0, \omega)$  is not the response function [68, 69] (contrary to the assumption in [65, 66]). Namely, if a small external potential  $\delta V_{\text{ext}}(\mathbf{k}, \omega)$  is applied to the system (of electrons and ions in solids), it induces screening by charges of the medium and the total potential is given by  $\delta V_{\text{tot}}(\mathbf{k}, \omega) = \delta V_{\text{ext}}(\mathbf{k}, \omega)/\varepsilon_{\text{tot}}(\mathbf{k}, \omega)$ , which means that  $1/\varepsilon_{\text{tot}}(\mathbf{k}, \omega)$  is the response function. The latter obeys the Kramers-Kronig dispersion relation which implies the following stability condition [68, 69]:

$$\frac{1}{\varepsilon_{\text{tot}}(\mathbf{k}, \omega = 0)} < 1, \quad \mathbf{k} \neq 0, \quad (3)$$

that is, either

$$\varepsilon_{\text{tot}}(\mathbf{k} \neq 0, \omega = 0) > 1, \quad (4)$$

or

$$\varepsilon_{\text{tot}}(\mathbf{k} \neq 0, \omega = 0) < 0. \quad (5)$$

This important theorem invalidates the restriction on the maximal value of  $T_c$  in the EPI mechanism given in [65, 66]. We stress that the condition  $\varepsilon_{\text{tot}}(\mathbf{k} \neq 0, \omega = 0) < 0$  is not in conflict with the lattice stability at all. For instance, in inhomogeneous systems such as crystal, the total longitudinal dielectric function is matrix in the space of reciprocal lattice vectors ( $\mathbf{Q}$ ), that is,  $\hat{\varepsilon}_{\text{tot}}(\mathbf{k} + \mathbf{Q}, \mathbf{k} +$

$\mathbf{Q}', \omega)$ , and  $\varepsilon_{\text{tot}}(\mathbf{k}, \omega)$  is defined by  $\varepsilon_{\text{tot}}^{-1}(\mathbf{k}, \omega) = \hat{\varepsilon}_{\text{tot}}^{-1}(\mathbf{k} + \mathbf{0}, \mathbf{k} + \mathbf{0}, \omega)$ . In dense metallic systems with one ion per cell (such as metallic hydrogen) and with the electronic dielectric function  $\varepsilon_{\text{el}}(\mathbf{k}, 0)$ , the macroscopic total dielectric function  $\varepsilon_{\text{tot}}(\mathbf{k}, 0)$  is given by [71–73]

$$\varepsilon_{\text{tot}}(\mathbf{k}, 0) = \frac{\varepsilon_{\text{el}}(\mathbf{k}, 0)}{1 - 1/\varepsilon_{\text{el}}(\mathbf{k}, 0)G_{ep}(\mathbf{k})}. \quad (6)$$

At the same time the energy of the longitudinal phonon  $\omega_l(\mathbf{k})$  is given by

$$\omega_l^2(\mathbf{k}) = \frac{\Omega_p^2}{\varepsilon_{\text{el}}(\mathbf{k}, 0)} \left[ 1 - \varepsilon_{\text{el}}(\mathbf{k}, 0)G_{ep}(\mathbf{k}) \right], \quad (7)$$

where  $\Omega_p^2$  is the ionic plasma frequency, and  $G_{ep}$  is the local (electric) field correction—see [71–73]. The right condition for lattice stability requires that  $\omega_l^2(\mathbf{k}) > 0$ , which implies that for  $\varepsilon_{\text{el}}(\mathbf{k}, 0) > 0$  one has  $\varepsilon_{\text{el}}(\mathbf{k}, 0)G_{ep}(\mathbf{k}) < 1$ . The latter condition gives automatically  $\varepsilon_{\text{tot}}(\mathbf{k}, 0) < 0$ . Furthermore, the calculations [71–73] show that in the *metallic hydrogen* (H) crystal  $\varepsilon_{\text{tot}}(\mathbf{k}, 0) < 0$  for all  $\mathbf{k} \neq \mathbf{0}$ . Note that in metallic H the EPI coupling constant is very large, that is,  $\lambda_{ep} \approx 7$  and  $T_c$  may reach very large value  $T_c \approx 600$  K [74]. Moreover, the analyses of crystals with more ions per unit cell [71–73] give that  $\varepsilon_{\text{tot}}(\mathbf{k} \neq 0, 0) < 0$  is *more a rule than an exception*—see Figure 1. The physical reason for  $\varepsilon_{\text{tot}}(\mathbf{k} \neq 0, 0) < 0$  is local field effects described by  $G_{ep}(\mathbf{k})$ . Whenever the local electric field  $\mathbf{E}_{\text{loc}}$  acting on electrons (and ions) is different from the average electric field  $\mathbf{E}$ , that is,  $\mathbf{E}_{\text{loc}} \neq \mathbf{E}$ , there are corrections to  $\varepsilon_{\text{tot}}(\mathbf{k}, 0)$  which may lead to  $\varepsilon_{\text{tot}}(\mathbf{k}, 0) < 0$ .

The above analysis tells us that in real crystals  $\varepsilon_{\text{tot}}(\mathbf{k}, 0)$  *can be negative* in the large portion of the Brillouin zone thus giving rise to  $\lambda_{ep} - \mu > 0$  in (2). This means that analytic properties of the dielectric function  $\varepsilon_{\text{tot}}(\mathbf{k}, \omega)$  *do not limit  $T_c$  in the phonon mechanism of pairing*. This result does not mean that there is no limit on  $T_c$  at all. We mention in advance that the local field effects play important role in HTSC cuprates, due to their layered structure with very unusual *ionic-metallic binding*, thus opening a possibility for large EPI.

In conclusion, we point out that there are no serious theoretical and experimental arguments for ignoring EPI in HTSC cuprates. To this end it is necessary to answer several important questions which are related to experimental findings in HTSC cuprates. (1) If EPI is important for pairing in HTSC cuprates and if superconductivity is of *d*-wave type, how are these two facts compatible? (2) Why is the transport EPI coupling constant  $\lambda_{\text{tr}}$  (entering resistivity) rather smaller than the pairing EPI coupling constant  $\lambda_{ep} (> 1)$  (entering  $T_c$ ), that is, why one has  $\lambda_{\text{tr}} (\approx 0.6-1.4) \ll \lambda_{ep} (\sim 2-3.5)$ ? (3) If EPI is ineffective for pairing in HTSC oxides, in spite of  $\lambda_{ep} > 1$ , why is it so?

(3) *Is a Nonphononic Pairing Realized in HTSC?* Regarding EPI one can pose a question about whether it contributes significantly to *d*-wave pairing in cuprates. Surprisingly, despite numerous experiments in favor of EPI, there is a belief that EPI is irrelevant for pairing [12–17]. This belief is mainly

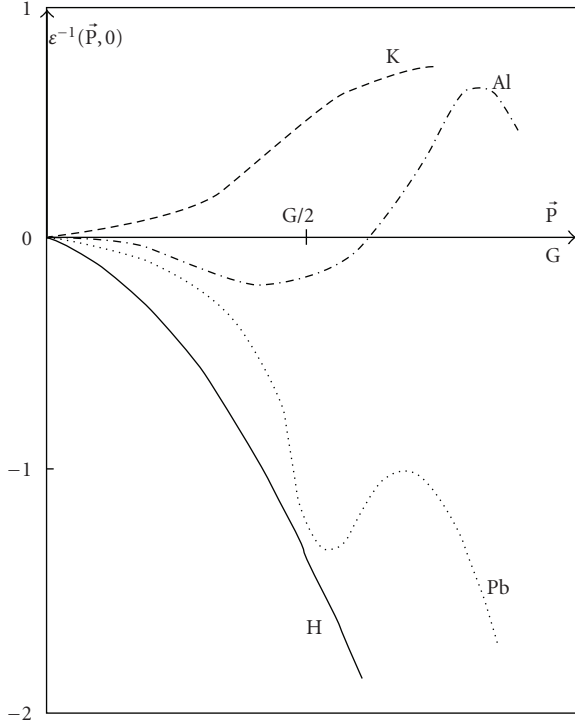


FIGURE 1: Inverse total static dielectric function  $\varepsilon^{-1}(\mathbf{p})$  for normal metals (K, Al, Pb) and metallic H in  $\mathbf{p} = (1, 0, 0)$  direction.  $\mathbf{G}$  is the reciprocal lattice vector.

based, first, on the above discussed incorrect lattice stability criterion related to the sign of  $\varepsilon_{\text{tot}}(\mathbf{k}, 0)$ , which implies small EPI and, second, on the well-established experimental fact that  $d$ -wave pairing is realized in cuprates [75], which is believed to be incompatible with EPI. Having in mind that EPI in HTSC and near optimal doping is strong with  $2 < \lambda_{ep} < 3.5$  (see below), we assume for the moment that the leading pairing mechanism in cuprates, which gives  $d$ -wave pairing, is due to some nonphononic mechanism. For instance, let us assume an *exitonic* mechanism due to the high-energy pairing boson ( $\Omega_{\text{nph}} \gg \omega_{\text{ph}}$ ) and with the bare critical temperature  $T_{c0}$  and look for the effect of EPI on  $T_c$ . If EPI is approximately *isotropic*, like in most LTSC materials, then it would be very detrimental for  $d$ -wave pairing. In the case of dominating *isotropic* EPI in the normal state and the exitonic-like pairing, then near  $T_c$  the linearized Eliashberg equations have an approximative form for a weak nonphonon interaction (with the large characteristic frequency  $\Omega_{\text{nph}}$ )

$$Z(\omega_n)\Delta_n(\mathbf{k}) \approx \pi T_c \sum_m \sum_{\mathbf{q}} V_{\text{nph}}(\mathbf{k}, \mathbf{q}, n, m) \frac{\Delta_m(\mathbf{q})}{|\omega_m|}, \quad (8)$$

$$Z(\omega_n) \approx 1 + \frac{\Gamma_{ep}}{\omega_n}.$$

For pure  $d$ -wave pairing with the pairing potential  $V_{\text{nph}} = V_{\text{nph}}(\theta_{\mathbf{k}}, \theta_{\mathbf{q}}) \cdot \Theta(\Omega_{\text{nph}} - |\omega_n|)\Theta(\Omega_{\text{nph}} - |\omega_{n'}|)$  with  $V_{\text{nph}}(\mathbf{k}, \mathbf{q}) = V_0 \cdot Y_d(\theta_{\mathbf{k}})Y_d(\theta_{\mathbf{q}})$  and  $Y_d(\theta_{\mathbf{k}}) = \pi^{-1/2} \cos 2\theta_{\mathbf{k}}$ ,

one obtains  $\Delta_n(\mathbf{k}) = \Delta_d \cdot \Theta(\Omega_{\text{nph}} - |\omega_n|)Y_d(\theta_{\mathbf{k}})$  and the equation for  $T_c$ —see [3–5]

$$\ln \frac{T_c}{T_{c0}} \approx \Psi\left(\frac{1}{2}\right) - \Psi\left(\frac{1}{2} + \frac{\Gamma_{ep}}{2\pi T_c}\right). \quad (9)$$

Here  $\Psi$  is the di-gamma function. At temperatures near  $T_c$  one has  $\Gamma_{ep} \approx 2\pi\lambda_{ep}T_c$  and the solution of (9) is approximately  $T_c \approx T_{c0} \exp\{-\lambda_{ep}\}$  with  $T_{c0} \approx \Omega_{\text{nph}} \exp\{-\lambda_{\text{nph}}\}$ ,  $\lambda_{\text{nph}} = N(0)V_0$ . This means that for  $T_c^{\text{max}} \sim 160$  K and  $\lambda_{ep} > 1$  the bare  $T_{c0}$  due to the nonphononic interaction must be very large, that is,  $T_{c0} > 500$  K.

Concerning other nonphononic mechanisms, such as the SFI one, the effect of EPI in the framework of Eliashberg equations was studied numerically in [76]. The latter is based on (A.1) in Appendix A with the kernels in the normal and superconducting channels  $\lambda_{\text{kp}}^Z(i\nu_n)$  and  $\lambda_{\text{kp}}^\Delta$ , respectively. Usually, the spin-fluctuation kernel  $\lambda_{\text{sf},\text{kp}}(i\nu_n)$  is taken in the FLEX approximation [77]. The calculations [76] confirm the very detrimental effect of the isotropic ( $\mathbf{k}$ -independent) EPI on  $d$ -wave pairing due to SFI. For the bare SFI critical temperature  $T_{c0} \sim 100$  K and for  $\lambda_{ep} > 1$  the calculations give very small (renormalized) critical temperature  $T_c \ll 100$  K. These results tell us that a more realistic pairing interaction must be operative in cuprates and that EPI must be *strongly momentum dependent* and peaked at small transfer momenta [78–80]. Only in that case does strong EPI conform with  $d$ -wave pairing, either as its main cause or as a supporter of a nonphononic mechanism. In Section 2 we will argue that the strongly momentum-dependent EPI is important scattering mechanism in cuprates providing the strength of the pairing mechanism, while the residual Coulomb interaction (by including weaker SFI) triggers it to  $d$ -wave pairing.

**1.3. Experimental Evidence for Strong EPI.** In the following we discuss some important experiments which give evidence for strong electron-phonon interaction (EPI) in cuprates. However, before doing it, we will discuss some indicative *inelastic magnetic neutron scattering* (IMNS) *measurements* in cuprates whose results in fact seriously doubt in the effectiveness of the phenomenological SFI mechanism of pairing which is advocated in [12–17, 81]. First, the experimental results related to the pronounced imaginary part of the susceptibility  $\text{Im}\chi(\mathbf{k}, k_z, \omega)$  in the normal state at and near the AF wave vector  $\mathbf{k} = \mathbf{Q} = (\pi, \pi)$  were interpreted in a number of papers as a support for the SFI mechanism for pairing [12–17, 81]. Second, the existence of the so called magnetic resonance peak of  $\text{Im}\chi(\mathbf{k}, k_z, \omega)$  (at some energies  $\omega < 2\Delta$ ) in the superconducting state was also interpreted in a number of papers either as the origin of superconductivity or as a mechanism strongly affecting superconducting gap at the antinodal point.

### 1.3.1. Magnetic Neutron Scattering and the Spin-Fluctuation Spectral Function

(a) *Huge Rearrangement of the SFI Spectral Function and Small Change of  $T_c$ .* Before discussing experimental results in cuprates on the imaginary part of the spin susceptibility

Im $\chi(\mathbf{k}, \omega)$  we point out that in the (phenomenological) theories based on the spin-fluctuation interaction (SFI) the quasiparticle self-energy  $\hat{\Sigma}_{\text{sf}}(\mathbf{k}, \omega_n)$  ( $\omega_n$  is the Matsubara frequency and  $\hat{\tau}_0$  is the Nambu matrix) in the normal and superconducting state and the effective (repulsive) pairing potential  $V_{\text{sf}}(\mathbf{k}, \omega)$  (where  $i\omega_n \rightarrow \omega + i\eta$ ) are assumed in the form [12–17]

$$\hat{\Sigma}_{\text{sf}}(\mathbf{k}, \omega_n) = \frac{T}{N} \sum_{\mathbf{k}', m} V_{\text{sf}}(\mathbf{k} - \mathbf{k}', \omega_{nm}^-) \hat{\tau}_0 \hat{G}(\mathbf{k}', \omega_m) \hat{\tau}_0, \quad (10)$$

$$V_{\text{sf}}(\mathbf{k}, \omega_{nm}^-) = g_{\text{sf}}^2 \int_{-\infty}^{\infty} \frac{d\nu}{\pi} \frac{\text{Im}\chi(\mathbf{q}, \nu + i0^+)}{\nu - i\omega_{nm}^-},$$

where  $\omega_{nm}^- \equiv \omega_n - \omega_m$ . Although the form of  $V_{\text{sf}}$  cannot be justified theoretically, except in the weak coupling limit ( $g_{\text{sf}} \ll W_b$ ) only, it is often used in the analysis of the quasiparticle properties in the normal and superconducting state of cuprates where the spin susceptibility (spectral function)  $\text{Im}\chi(\mathbf{q}, \omega)$  is strongly peaked at and near the AF wave vector  $\mathbf{Q} = (\pi/a, \pi/a)$ .

Can the pairing mechanism in HTSC cuprates be explained by such a phenomenology and what is the prize for it is? The best answer is to look at the experimental results related to the inelastic magnetic neutron scattering (IMNS) which gives  $\text{Im}\chi(\mathbf{q}, \omega)$ . In that respect very indicative and impressive IMNS measurements on  $\text{YBa}_2\text{Cu}_3\text{O}_{6+x}$ , which are done by Bourges group [30], demonstrate that the normal-state susceptibility  $\text{Im}\chi^{(\text{odd})}(\mathbf{q}, \omega)$  (the odd part of the spin susceptibility in the bilayer system) at  $\mathbf{q} = \mathbf{Q} = (\pi, \pi)$  is strongly dependent on the hole-doping as it is shown in Figure 2.

The most pronounced result for our discussion is that by varying doping *there is a huge rearrangement* of  $\text{Im}\chi^{(\text{odd})}(\mathbf{Q}, \omega)$  in the normal state, especially in the energy (frequency) region which might be important for superconducting pairing, let us say  $0 \text{ meV} < \omega < 60 \text{ meV}$ . This is clearly seen in the last two curves in Figure 2 where *this rearrangement is very pronounced*, while at the same time there is only *small variation of the critical temperature*  $T_c$ . It is seen in Figure 2 that in the underdoped  $\text{YBa}_2\text{Cu}_3\text{O}_{6.92}$  crystal  $\text{Im}\chi^{(\text{odd})}(\mathbf{Q}, \omega)$  and  $S(\mathbf{Q}) = N(0)g_{\text{sf}}^2 \int_0^{60} d\omega \text{Im}\chi^{(\text{odd})}(\mathbf{Q}, \omega)$  are much larger than that in the near optimally doped  $\text{YBa}_2\text{Cu}_3\text{O}_{6.97}$ , that is, one has  $S_{6.92}(\mathbf{Q}) \gg S_{6.97}(\mathbf{Q})$ , although the difference in the corresponding critical temperatures  $T_c$  is very small, that is,  $T_c^{(6.92)} = 91 \text{ K}$  (in  $\text{YBa}_2\text{Cu}_3\text{O}_{6.92}$ ) and  $T_c^{(6.97)} = 92.5 \text{ K}$  (in  $\text{YBa}_2\text{Cu}_3\text{O}_{6.97}$ ). This *pronounced rearrangement and suppression* of  $\text{Im}\chi^{(\text{odd})}(\mathbf{Q}, \omega)$  in the normal state of YBCO by doping (toward the optimal doping) but with the negligible change in  $T_c$  is *strong evidence* that the SFI pairing mechanism is not the dominating one in HTSC cuprates. This insensitivity of  $T_c$ , if interpreted in terms of the SFI coupling constant  $\lambda_{\text{sf}}(\sim g_{\text{sf}}^2)$ , means that the latter is small, that is,  $\lambda_{\text{sf}}^{(\text{exp})} \ll 1$ . We stress that the explanation of high  $T_c$  in cuprates by the SFI phenomenological theory [12–17] assumes very large SFI coupling energy with  $g_{\text{sf}}^{(\text{th})} \approx 0.7 \text{ eV}$  while the frequency (energy) dependence of  $\text{Im}\chi(\mathbf{Q}, \omega)$  is extracted from the fit

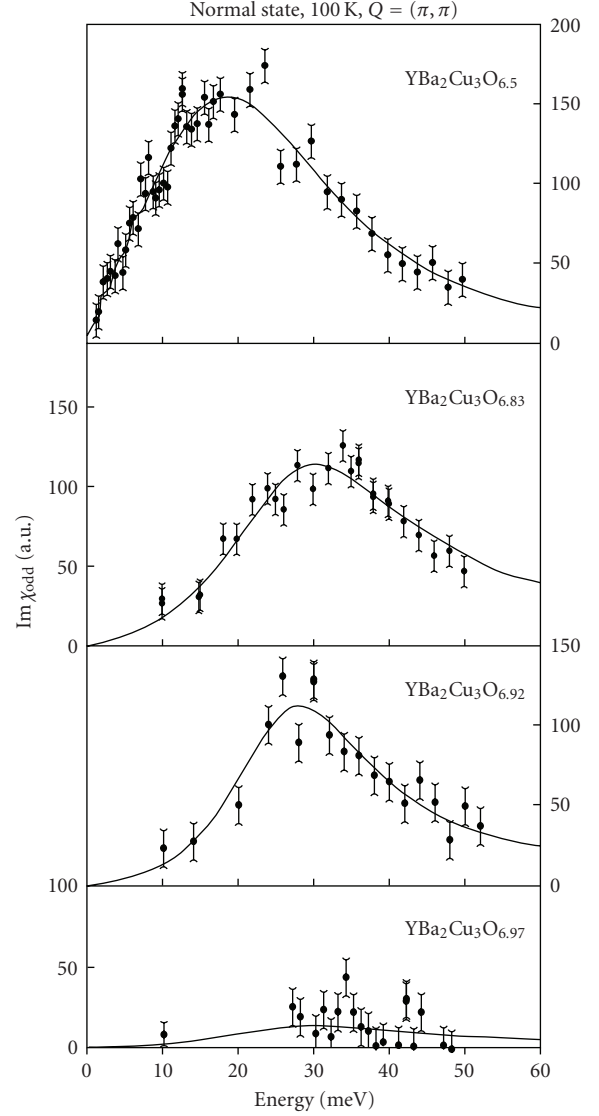


FIGURE 2: Magnetic spectral function  $\text{Im}\chi^{(-)}(\mathbf{k}, \omega)$  in the normal state of  $\text{YBa}_2\text{Cu}_3\text{O}_{6+x}$  at  $T = 100 \text{ K}$  and at  $\mathbf{Q} = (\pi, \pi)$ . 100 counts in the vertical scale correspond to  $\chi_{\text{max}}^{(-)} \approx 350 \mu_B^2/\text{eV}$ . The superconducting critical temperature  $T_c(x)$  by increasing doping ( $x$ ) from the underdoped system with  $x = 0.5$  (top) to the optimally doped one with  $x = 0.97$  (bottom):  $T_c(x) = 45 \text{ K}$  ( $x = 0.5$ ),  $85 \text{ K}$  ( $x = 0.83$ ),  $91 \text{ K}$  ( $x = 0.92$ ), and  $92.5 \text{ K}$  ( $x = 0.97$ ). From [30].

of the NMR relaxation rate  $T_1^{-1}$  which gives  $T_c^{(\text{NMR})} \approx 100 \text{ K}$  [12–17]. To this point, the NMR measurements (of  $T_1^{-1}$ ) give that there is an *anticorrelation* between the decrease of the NMR spectral function  $I_Q = \lim_{\omega \rightarrow 0} \text{Im}\chi^{(\text{NMR})}(\mathbf{Q}, \omega)/\omega$  and the increase of  $T_c$  by increasing doping toward the optimal one—see [6] and references therein. The latter result additionally disfavors the SFI model of pairing [12–17] since the strength of pairing interaction is little affected by SFI. Note that if instead of taking  $\text{Im}\chi(\mathbf{Q}, \omega)$  from NMR measurements one takes it from IMNS measurements, as it was done in [82], than for the same value  $g_{\text{sf}}^{(\text{th})}$  one obtains much smaller  $T_c$ . For instance, by taking the experimental

values for  $\text{Im}\chi^{(\text{IMNS})}(\mathbf{Q}, \omega)$  in underdoped  $\text{YBa}_2\text{Cu}_3\text{O}_{6.6}$  with  $T_c \approx 60$  K one obtains  $T_c^{(\text{IMNS})} < T_c^{(\text{NMR})}/3$  [82], while  $T_c^{(\text{IMNS})} \rightarrow 50$  K for  $g_{\text{sf}}^{(\text{th})} \gg 1$ . The situation is even worse if one tries to fit the resistivity with  $\text{Im}\chi^{(\text{IMNS})}(\mathbf{Q}, \omega)$  in  $\text{YBa}_2\text{Cu}_3\text{O}_{6.6}$  since this fit gives  $T_c^{(\text{IMNS})} < 7$  K. These results point to a deficiency of the SFI phenomenology (at least that based on (10)) to describe pairing in HTSC cuprates.

Having in mind the results in [82], the recent theoretical interpretation in [81] of IMNS experiments [83, 84] and ARPES measurements [85, 86] on the underdoped  $\text{YBa}_2\text{Cu}_3\text{O}_{6.6}$  in terms of the SFI phenomenology deserve to be commented. The IMNS experiments [83, 84] give evidence for the “hourglass” spin excitation spectrum (in the superconducting state) for the momenta  $\mathbf{q}$  at, near and far from  $\mathbf{Q}$ , which is richer than the common spectrum with magnetic resonance peaks measured at  $\mathbf{Q}$ . In [81] the self-energy of electrons due to their interaction with spin excitations is calculated by using (10) with  $g_{\text{sf}}^2 = (3/2)\tilde{U}^2$  and  $\text{Im}\chi(\mathbf{q}, \omega)$  taken from [83, 84]. However, in order to fit the ARPES self-energy and low-energy kinks (see discussion in Section 1.3.3) the authors of [81] use *very large value*  $\tilde{U} = 1.59$  eV, that is, much larger than the one used in [82]. Such a large value of  $\tilde{U}$  has been obtained earlier within the Monte Carlo simulation of the Hubbard model [87]. In our opinion this value for  $\tilde{U}$  is unrealistically large in the case of strongly correlated systems where spin fluctuations are governed by the effective electron-exchange interaction  $J_{\text{Cu-Cu}} \lesssim 0.15$  eV [88]. This implies that  $\tilde{U} \ll 1$  eV and  $T_c \ll 60$  K. Note that this value for  $J_{\text{Cu-Cu}} (\sim 0.15$  eV) comes out also from the theory of strongly correlated electrons in the three-band Emery model which gives  $J_{\text{Cu-Cu}} \approx [4t_{pd}^4/(\Delta_{dp} + U_{pd})^2, (1/U_d) + 2/(U_p + 2\Delta)]$ —for parameters see Section 2.3. We would like to emphasize here that an additional richness of the spin-fluctuations spectrum (the hourglass instead of the spin resonance) does not change the situation with the smallness of the exchange coupling constant  $\tilde{U}$  (and  $g_{\text{sf}}$ ).

Concerning the problem related to the rearrangement of the SFI spectral function  $\text{Im}\chi(\mathbf{Q}, \omega)$  in  $\text{YBa}_2\text{Cu}_3\text{O}_{6+x}$  [30] we would like to stress that despite the fact that the latter results were obtained ten years ago they are not disputed by the new IMNS measurements [31] on high quality samples of the same compound (where much longer counting times were used in order to reduce statistical errors). In fact the results in [30] are confirmed in [31] where the magnetic intensity  $I(\mathbf{q}, \omega) (\sim \text{Im}\chi(\mathbf{q}, \omega))$  (for  $\mathbf{q}$  at and in the broad range of  $\mathbf{Q}$ ) for the optimally doped  $\text{YBa}_2\text{Cu}_3\text{O}_{6.95}$  (with  $T_c = 93$  K) is *at least three times smaller* than in the underdoped  $\text{YBa}_2\text{Cu}_3\text{O}_{6.6}$  with  $T_c = 60$  K. This result is again very indicative sign of the weakness of SFI since such a huge reconstruction would decrease  $T_c$  in the optimally doped  $\text{YBa}_2\text{Cu}_3\text{O}_{6.95}$  if analyzed in the framework of the phenomenological SFI theory based on (10). It also implies that due to the suppression of  $\text{Im}\chi(\mathbf{q}, \omega)$  by increasing doping toward the optimal one a straightforward extrapolation of the theoretical approach in [81] to the explanation of  $T_c$  in the optimally doped  $\text{YBa}_2\text{Cu}_3\text{O}_{6.95}$  would require an increase of  $\tilde{U}$  to the value even larger than 4 eV, which is highly improbable.

(b) *Ineffectiveness of the Magnetic Resonance Peak.* A less direct argument for *smallness of the SFI coupling constant*, that is,  $g_{\text{sf}}^{\text{exp}} \leq 0.2$  eV and  $g_{\text{sf}}^{\text{exp}} \ll g_{\text{sf}}$ , comes from other experiments related to the magnetic resonance peak in the superconducting state, and this will be discussed next. In the superconducting state of optimally doped YBCO and BSCO,  $\text{Im}\chi(\mathbf{Q}, \omega)$  is significantly suppressed at low frequencies except near the resonance energy  $\omega_{\text{res}} \approx 41$  meV where a pronounced narrow peak appears—the *magnetic resonance peak*. We stress that there is no magnetic resonance peak in some families of HTSC cuprates, for instance, in LSCO, and consequently one can question the importance of the resonance peak in the scattering processes. The experiments tell us that the relative intensity of this peak (compared to the total one) is small, that is,  $I_0 \sim (1-5)\%$ —see Figure 3. In underdoped cuprates this peak is present also in the normal state as it is seen in Figure 2.

After the discovery of the resonance peak there were attempts to relate it, first, to the origin of the superconducting condensation energy and, second, to the kink in the energy dispersion or the peak-dimp structure in the ARPES spectral function. In order that the condensation energy is due to the magnetic resonance, it is necessary that the peak intensity  $I_0$  is small [89].  $I_0$  is obtained approximately by equating the condensation energy  $E_{\text{con}} \approx N(0)\Delta^2/2$  with the change of the magnetic energy  $E_{\text{mag}}$  in the superconducting state, that is,  $\delta E_{\text{mag}} \approx 4I_0 \cdot E_{\text{mag}}$ :

$$E_{\text{mag}} = J \iint \frac{d\omega d^2k}{(2\pi)^3} (1 - \cos k_x - \cos k_y) S(\mathbf{k}, \omega), \quad (11)$$

where  $S(\mathbf{k}, \omega) = (1/\pi)[1 + n(\omega)] \text{Im}\chi(\mathbf{k}, \omega)$  is the spin structure factor and  $n(\omega)$  is the Bose distribution function. By taking  $\Delta \approx 2T_c$  and the realistic value  $N(0) \sim 1/(10J) \sim 1$  states/eV · spin, one obtains  $I_0 \sim 10^{-1}(T_c/J)^2 \sim 10^{-3}$ . However, such a small intensity cannot be responsible for the anomalies in ARPES and optical spectra since it gives rise to small coupling constant  $\lambda_{\text{sf, res}}$  for the interaction of holes with the resonance peak, that is,  $\lambda_{\text{sf, res}} \approx (2I_0 N(0) g_{\text{sf}}^2 / \omega_{\text{res}}) \ll 1$ . Such a small coupling does not affect superconductivity at all. Moreover, by studying the width of the resonance peak one can extract an order of magnitude of the SFI coupling constant  $g_{\text{sf}}$ . Since the magnetic resonance disappears in the normal state of the optimally doped YBCO, it can be qualitatively understood by assuming that its broadening scales with the resonance energy  $\omega_{\text{res}}$ , that is,  $\gamma_{\text{res}} < \omega_{\text{res}}$ , where the line width is given by  $\gamma_{\text{res}} = 4\pi(N(0)g_{\text{sf}}^2)\omega_{\text{res}}$  [89]. This condition limits the SFI coupling to  $g_{\text{sf}} < 0.2$  eV. We stress that in such a way obtained  $g_{\text{sf}}$  is *much smaller* (at least by factor three) than that assumed in the phenomenological spin-fluctuation theory [12–17, 81] where  $g_{\text{sf}} \sim 0.6-0.7$  eV and  $\tilde{U} \approx 1.6$  eV, but much larger than estimated in [89] (where  $g_{\text{sf}} < 0.02$  eV). The smallness of  $g_{\text{sf}}$  comes out also from the analysis of the antiferromagnetic state in underdoped metals of LSCO and YBCO [90], where the small (ordered) magnetic moment  $\mu (< 0.1\mu_B)$  points to an itinerant antiferromagnetism with small coupling constant  $g_{\text{sf}} < 0.2$  eV. The conclusion from this analysis is that in the optimally doped YBCO the sharp magnetic resonance

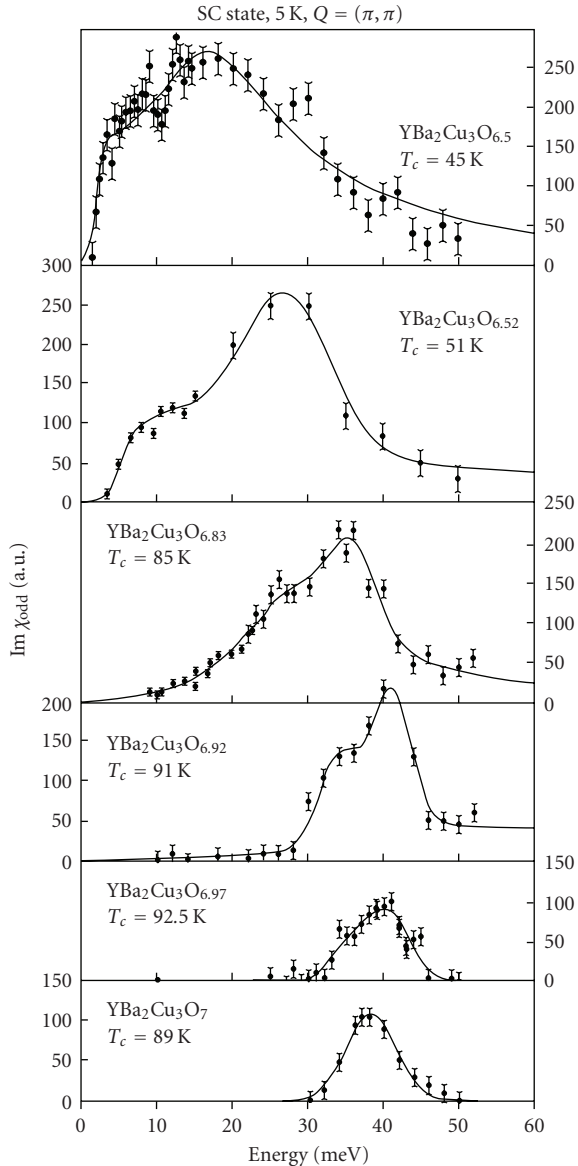


FIGURE 3: Magnetic spectral function  $\text{Im} \chi^{(-)}(\mathbf{k}, \omega)$  in the superconducting state of  $\text{YBa}_2\text{Cu}_3\text{O}_{6+x}$  at  $T = 5$  K and at  $Q = (\pi, \pi)$ . 100 counts in the vertical scale correspond to  $\chi_{\text{max}}^{(-)} \approx 350 \mu_B^2/\text{eV}$ . From [30].

is a consequence of the onset of superconductivity and not its cause. There is also one principal reason against the pairing due to the magnetic resonance peak at least in optimally doped cuprates. Since the intensity of the magnetic resonance near  $T_c$  is vanishingly small, though not affecting pairing at the second-order phase transition at  $T_c$ , then, if it would be solely the origin for superconductivity, the phase transition at  $T_c$  would be *first order*, contrary to experiments. Recent ARPES experiments give evidence that the magnetic resonance cannot be related to the kinks in ARPES spectra [91, 92]—see the discussion below.

Finally, we would like to point out that the recent magnetic neutron scattering measurements on optimally

doped large-volume crystals  $\text{Bi}_2\text{Sr}_2\text{CaCu}_2\text{O}_{8+\delta}$  [93], where the absolute value of  $\text{Im} \chi(\mathbf{q}, \omega)$  is measured, are questioning also the interpretation of the electronic magnetism in cuprates in terms of the itinerant magnetism. This experiment shows a lack of temperature dependence of the local spin susceptibility  $\text{Im} \chi(\omega) = \sum_{\mathbf{q}} \text{Im} \chi(\mathbf{q}, \omega)$  across the superconducting transition  $T_c = 91$  K, that is, there is only a minimal change in  $\text{Im} \chi(\omega)$  between 10 K and 100 K. Note that if the magnetic excitations were due to itinerant quasiparticles we should have seen dramatic changes of  $\text{Im} \chi(\omega)$  as a function of  $T$  over the whole energy range. This  $T$ -independence of  $\text{Im} \chi(\omega)$  strongly opposes the theoretical results in [24–27] which assume that the bosonic spectral function is proportional to  $\text{Im} \chi(\omega)$  and that the former can be extracted from optic measurements. Namely, the fitting procedure in [24–27] gives that  $\text{Im} \chi(\omega)$  is strongly  $T$ -dependent contrary to the experimental results in [93]—see more in Section 1.3.2 on optical conductivity.

**1.3.2. Optical Conductivity and EPI.** Optical spectroscopy gives information on *optical conductivity*  $\sigma(\omega)$  and on two-particle excitations, from which one can indirectly extract the transport spectral function  $\alpha_{\text{tr}}^2 F(\omega)$ . Since this method probes bulk sample (on the skin depth), contrary to ARPES and tunnelling methods which probe tiny regions (10–15 Å) near the sample surface, this method is indispensable. However, one should be careful not to overinterpret the experimental results since  $\sigma(\omega)$  is *not a directly measured quantity* but it is derived from the reflectivity  $R(\omega) = |(\sqrt{\epsilon_{ii}(\omega)} - 1)/(\sqrt{\epsilon_{ii}(\omega)} + 1)|^2$  with the transversal dielectric tensor  $\epsilon_{ii}(\omega) = \epsilon_{ii,\infty} + \epsilon_{ii,\text{latt}} + 4\pi i \sigma_{ii}(\omega)/\omega$ . Here,  $\epsilon_{ii,\infty}$  is the high-frequency dielectric function,  $\epsilon_{ii,\text{latt}}$  describes the contribution of the lattice vibrations, and  $\sigma_{ii}(\omega)$  describes the optical (dynamical) conductivity of conduction carriers. Since  $R(\omega)$  is usually measured in the limited-frequency interval  $\omega_{\text{min}} < \omega < \omega_{\text{max}}$ , some physical modelling for  $R(\omega)$  is needed in order to guess it outside this range—see more in reviews in [3–6]. This was the reason for numerous misinterpretations of optic measurements in cuprates, which will be uncovered below. An illustrative example for this claim is large dispersion in the reported value of  $\omega_{\text{pl}}$ —from 0.06 to 25 eV—that is, almost three orders of magnitude. However, it turns out that *IR* measurements of  $R(\omega)$  in conjunction with ellipsometric measurements of  $\epsilon_{ii}(\omega)$  at high frequencies allow more reliable determination of  $\sigma(\omega)$  [94].

(1) *Transport and Quasiparticle Relaxation Rates.* The widespread misconception in studying the quasiparticle scattering in cuprates was an ad hoc assumption that the *transport relaxation rate*  $\gamma_{\text{tr}}(\omega)$  is equal to the *quasiparticle relaxation rate*  $\gamma(\omega)$ , in spite of the well-known fact that the inequality  $\gamma_{\text{tr}}(\omega) \neq \gamma(\omega)$  holds in a broad-frequency (energy) region Allen. This (incorrect) assumption was one of the main arguments against the relevance of the EPI scattering mechanism in cuprates. Although we have discussed this problem several times before, we do it again due to the importance of this subject.

The dynamical conductivity  $\sigma(\omega)$  consists of two parts, that is,  $\sigma(\omega) = \sigma^{\text{inter}}(\omega) + \sigma^{\text{intra}}(\omega)$  where  $\sigma^{\text{inter}}(\omega)$  describes *interband transitions* which contribute at higher than intraband energies, while  $\sigma^{\text{intra}}(\omega)$  is due to *intra-band transitions* which are relevant at low energies  $\omega < (1-2)$  eV. (Note that in the *IR* measurements the frequency is usually given in  $\text{cm}^{-1}$ , where the following conversion holds:  $1 \text{ cm}^{-1} = 29.98 \text{ GHz} = 0.123985 \text{ meV} = 1.44 \text{ K}$ .) The experimental data for  $\sigma(\omega) = \sigma_1 + i\sigma_2$  in cuprates are usually processed by the generalized (extended) Drude formula [32–36, 95]:

$$\sigma(\omega) = \frac{\omega_p^2}{4\pi} \frac{1}{\gamma_{\text{tr}}(\omega) - i\omega m_{\text{tr}}(\omega)/m_\infty} \equiv \frac{i\omega_p^2}{4\pi\tilde{\omega}_{\text{tr}}(\omega)}, \quad (12)$$

where  $m$  is the mass of the band electrons while the quantity  $\tilde{\omega}_{\text{tr}}(\omega)$  is defined in (19). The expression (12) is a useful representation for systems with single-band electron-boson scattering which is justified in HTSC cuprates. However, this procedure is inadequate for interpreting optical data in multiband systems such as new high-temperature superconductors Fe-based pnictides since even in absence of the inelastic intra- and interband scattering the effective optic relaxation rate may be strongly frequency dependent [96]. (The usefulness of introducing the optic relaxation  $\tilde{\omega}_{\text{tr}}(\omega)$  will be discussed below.) Here,  $i = a, b$  enumerates the plane axis;  $\omega_p$ ,  $\gamma_{\text{tr}}(\omega, T)$ , and  $m_{\text{op}}(\omega)$  are the electronic plasma frequency, the transport (optical) scattering rate, and the optical mass, respectively. Very frequently it is analyzed the quantity  $\gamma_{\text{tr}}^*(\omega, T)$  given by [95]

$$\gamma_{\text{tr}}^*(\omega, T) = \frac{m_\infty}{m_{\text{tr}}(\omega)} \gamma_{\text{tr}}(\omega, T) = \frac{\omega \text{Im } \sigma(\omega)}{\text{Re } \sigma(\omega)}. \quad (13)$$

In the weak coupling limit  $\lambda_{ep} < 1$ , the formula for conductivity given in Appendix A, equations (A.20) and (A.21) can be written in the form of (12) where  $\gamma_{\text{tr}}$  reads [33–36]

$$\begin{aligned} \gamma_{\text{tr}}(\omega, T) &= \pi \sum_l \int_0^\infty d\nu \alpha_{\text{tr},l}^2 F_l(\nu) \\ &\times \left[ 2(1 + 2n_B(\nu)) - 2\frac{\nu}{\omega} - \frac{\omega + \nu}{\omega} n_B(\omega + \nu) \right. \\ &\quad \left. + \frac{\omega - \nu}{\omega} n_B(\omega - \nu) \right]. \end{aligned} \quad (14)$$

Here  $n_B(\omega)$  is the Bose distribution function. For completeness we give also the explicit form of the transport mass  $m_{\text{tr}}(\omega)$ , see [3–6, 32–36]:

$$\frac{m_{\text{tr}}(\omega)}{m_\infty} = 1 + \frac{2}{\omega} \sum_l \int_0^\infty d\nu \alpha_{\text{tr},l}^2 F_l(\nu) \text{Re } K\left(\frac{\omega}{2\pi T}, \frac{\nu}{2\pi T}\right), \quad (15)$$

with the Kernel  $K(x, y) = (i/y) + \{((y-x)/x)[\psi(1-ix+iy) - \psi(1+iy)]\} - \{y \rightarrow -y\}$  where  $\psi$  is the di-gamma function. In the presence of impurity scattering one should add  $\gamma_{\text{imp, tr}}$  to  $\gamma_{\text{tr}}$ . It turns out that (14) holds within a few percents also for large  $\lambda_{ep} (> 1)$ . Note that  $\alpha_{\text{tr},l}^2 F_l(\nu) \neq \alpha_l^2 F_l(\nu)$  and the index  $l$  enumerates all scattering bosons—phonons—spin

fluctuations, and so forth. For comparison, the quasiparticle scattering rate  $\gamma(\omega, T)$  is given by

$$\begin{aligned} \gamma(\omega, T) &= 2\pi \int_0^\infty d\nu \alpha^2 F(\nu) \\ &\times \{2n_B(\nu) + n_F(\nu + \omega) + n_F(\nu - \omega)\} + \gamma^{\text{imp}}, \end{aligned} \quad (16)$$

where  $n_F$  is the Fermi distribution function. For completeness we give also the expression for the quasiparticle effective mass  $m^*(\omega)$ :

$$\begin{aligned} \frac{m^*(\omega)}{m} &= 1 + \frac{1}{\omega} \sum_l \int_0^\infty d\nu \alpha_l^2 F_l(\nu) \\ &\times \text{Re} \left\{ \psi\left(\frac{1}{2} + i\frac{\omega + \nu}{2\pi T}\right) - \psi\left(\frac{1}{2} - i\frac{\omega - \nu}{2\pi T}\right) \right\}. \end{aligned} \quad (17)$$

The term  $\gamma^{\text{imp}}$  is due to the impurity scattering. By comparing (14) and (16), it is seen that  $\gamma_{\text{tr}}$  and  $\gamma$  are different quantities, that is,  $\gamma_{\text{tr}} \neq \gamma$ , where the former describes the *relaxation of Bose particles (excited electron-hole pairs)* while the latter one describes *the relaxation of Fermi particles*. This difference persists also at  $T = 0 \text{ K}$  where one has (due to simplicity we omit in the following summation over  $l$ ) [32]

$$\begin{aligned} \gamma_{\text{tr}}(\omega) &= \frac{2\pi}{\omega} \int_0^\omega d\nu (\omega - \nu) \alpha_{\text{tr}}^2(\nu) F(\nu), \\ \gamma(\omega) &= 2\pi \int_0^\omega d\nu \alpha^2(\nu) F(\nu). \end{aligned} \quad (18)$$

In the case of EPI with the constant electronic density of states, the above equations give that  $\gamma_{ep}(\omega) = \text{const}$  for  $\omega > \omega_{\text{ph}}^{\text{max}}$  while  $\gamma_{ep, \text{tr}}(\omega)$  (as well as  $\gamma_{ep, \text{tr}}^*$ ) is monotonic growing for  $\omega > \omega_{\text{ph}}^{\text{max}}$ , where  $\omega_{\text{ph}}^{\text{max}}$  is the maximal phonon frequency. So, the growing of  $\gamma_{ep, \text{tr}}(\omega)$  (and  $\gamma_{ep, \text{tr}}^*$ ) for  $\omega > \omega_{\text{ph}}^{\text{max}}$  is ubiquitous and natural for the EPI scattering and has nothing to do with some exotic scattering mechanism. This behavior is clearly seen by comparing  $\gamma(\omega, T)$ ,  $\gamma_{\text{tr}}(\omega, T)$ , and  $\gamma_{\text{tr}}^*$  which are calculated for the EPI spectral function  $\alpha_{ep}^2(\omega) F_{\text{ph}}(\omega)$  extracted from tunnelling experiments in YBCO (with  $\omega_{\text{ph}}^{\text{max}} \sim 80 \text{ meV}$ ) [42–45]—see Figure 4.

The results shown in Figure 4 clearly demonstrate the physical difference between two scattering rates  $\gamma_{ep}$  and  $\gamma_{ep, \text{tr}}$  (or  $\gamma_{\text{tr}}^*$ ). It is also seen that  $\gamma_{\text{tr}}^*(\omega, T)$  is even more linear function of  $\omega$  than  $\gamma_{\text{tr}}(\omega, T)$ . From these calculations one concludes that the quasilinearity of  $\gamma_{\text{tr}}(\omega, T)$  (and  $\gamma_{\text{tr}}^*$ ) is not in contradiction with the EPI scattering mechanism but it is in fact a natural consequence of EPI. We stress that such behavior of  $\gamma_{ep}$  and  $\gamma_{ep, \text{tr}}$  (and  $\gamma_{ep, \text{tr}}^*$ ), shown in Figure 4, is in fact not exceptional for HTSC cuprates but it is *generic for many metallic systems*, for instance, 3D metallic oxides, low-temperature superconductors such as Al, Pb, and so forth—see more in [3–6] and references therein.

Let us discuss briefly the experimental results for  $R(\omega)$  and  $\gamma_{\text{tr}}^*(\omega, T)$  and compare these with theoretical predictions obtained by using a single-band model with  $\alpha_{ep}^2(\omega) F_{\text{ph}}(\omega)$  extracted from the tunnelling data with the EPI coupling constant  $\lambda_{ep} \gtrsim 2$  [42–45]. In the case of YBCO the

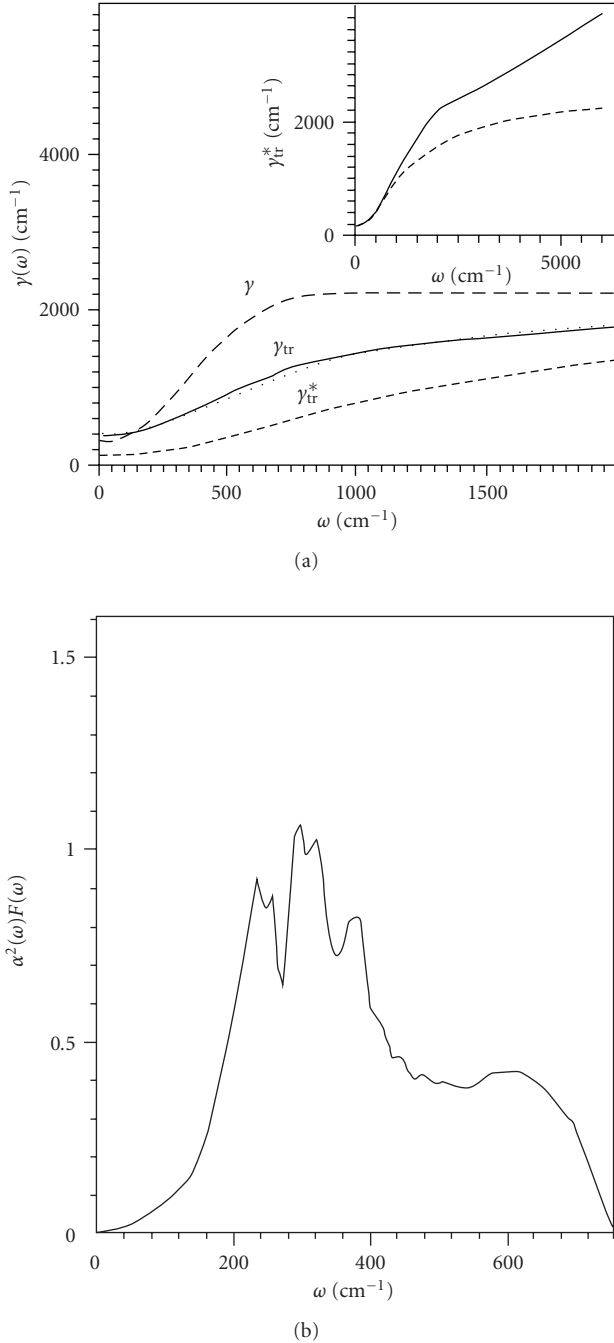


FIGURE 4: (a) Scattering rates  $\gamma(\omega, T)$ ,  $\gamma_{\text{tr}}(\omega, T)$ , and  $\gamma_{\text{tr}}^*$ —from top to bottom—for the Eliashberg function in (b). From [33–35]. (b) Eliashberg spectral function  $\alpha_{ep}^2(\omega)F_{\text{ph}}(\omega)$  obtained from tunnelling experiments on break junctions [42–45]. Inset shows  $\gamma_{\text{tr}}^*$  with (full line) and without (dashed line) interband transitions [3–5].

agreement between measured and calculated  $R(\omega)$  is very good up to energies  $\omega < 6000 \text{ cm}^{-1}$ , which confirms the importance of EPI in scattering processes. For higher energies, where a mead-infrared peak appears, it is necessary to account for interband transitions [3–5]. In optimally doped  $\text{Bi}_2\text{Sr}_2\text{CaCu}_2\text{O}_6$  (*Bi2212*) [97, 98] the experimental results for  $\gamma_{\text{tr}}^*(\omega, T)$  are explained theoretically by assuming

that the EPI spectral function  $\alpha_{ep}^2(\omega)F(\omega) \sim F_{\text{ph}}(\omega)$ , where  $F_{\text{ph}}(\omega)$  is the phononic density of states in BSCO, with  $\lambda_{ep} = 1.9$  and  $\gamma_{\text{imp}} \approx 320 \text{ cm}^{-1}$ —see Figure 5(a). At the same time the fit of  $\gamma_{\text{tr}}^*(\omega, T)$  by the marginal Fermi liquid phenomenology fails as it is evident in Figure 5(b).

Now we will comment the so called pronounced linear behavior of  $\gamma_{\text{tr}}(\omega, T)$  (and  $\gamma_{\text{tr}}^*(\omega, T)$ ) which was one of the main arguments for numerous inadequate conclusions regarding the scattering and pairing bosons and EPI. We stress again that the measured quantity is reflectivity  $R(\omega)$  and derived ones are  $\sigma(\omega)$ ,  $\gamma_{\text{tr}}(\omega, T)$ , and  $m_{\text{tr}}(\omega)$ , which are very sensitive to the value of the dielectric constant  $\epsilon_{\infty}$ . This sensitivity is clearly demonstrated in Figure 6 for Bi-2212 where it is seen that  $\gamma_{\text{tr}}(\omega, T)$  (and  $\gamma_{\text{tr}}^*(\omega, T)$ ) for  $\epsilon_{\infty} = 1$  is linear up to much higher  $\omega$  than in the case  $\epsilon_{\infty} > 1$ .

However, in some experiments [100–103] the extracted  $\gamma_{\text{tr}}(\omega, T)$  (and  $\gamma_{\text{tr}}^*(\omega, T)$ ) is linear up to very high  $\omega \approx 1500 \text{ cm}^{-1}$ . This means that the ion background and interband transitions (contained in  $\epsilon_{\infty}$ ) are not properly taken into account since too small  $\epsilon_{\infty} (\gtrsim 1)$  is assumed. The recent ellipsometric measurements on YBCO [104] give the value  $\epsilon_{\infty} \approx 4$ –6, which gives much less spectacular linearity in the relaxation rates  $\gamma_{\text{tr}}(\omega, T)$  (and  $\gamma_{\text{tr}}^*(\omega, T)$ ) than it was the case immediately after the discovery of HTSC cuprates, where much smaller  $\epsilon_{\infty}$  was assumed.

Furthermore, we would like to comment two points related to  $\sigma$ ,  $\gamma_{\text{tr}}$ , and  $\gamma$ . First, the parametrization of  $\sigma(\omega)$  with the generalized Drude formula in (12) and its relation to the transport scattering rate  $\gamma_{\text{tr}}(\omega, T)$  and the transport mass  $m_{\text{tr}}(\omega, T)$  is useful if we deal with electron-boson scattering in a single-band problem. In [36, 96] it is shown that  $\sigma(\omega)$  of a two-band model with only elastic impurity scattering can be represented by the generalized (extended) Drude formula with  $\omega$  and  $T$  dependence of effective parameters  $\gamma_{\text{tr}}^{\text{eff}}(\omega, T)$ ,  $m_{\text{tr}}^{\text{eff}}(\omega, T)$  despite the fact that the inelastic electron-boson scattering is absent. To this end we stress that the single-band approach is justified for a number of HTSC cuprates such as LSCO, BSCO, and so forth. Second, at the beginning we said that  $\gamma_{\text{tr}}(\omega, T)$  and  $\gamma(\omega, T)$  are physically different quantities and it holds that  $\gamma_{\text{tr}}(\omega, T) \neq \gamma(\omega, T)$ . In order to give the physical picture and qualitative explanation for this difference we assume that  $\alpha_{\text{tr}}^2 F(\nu) \approx \alpha^2 F(\nu)$ . In that case the renormalized quasiparticle frequency  $\tilde{\omega}(\omega) = Z(\omega)\omega = \omega - \Sigma(\omega)$  and the transport one  $\tilde{\omega}_{\text{tr}}(\omega)$ —defined in (12)—are related and at  $T = 0$  they are given by [32, 36]

$$\tilde{\omega}_{\text{tr}}(\omega) = \frac{1}{\omega} \int_0^{\omega} d\omega' 2\tilde{\omega}(\omega'). \quad (19)$$

(For the definition of  $Z(\omega)$  see Appendix A.) It gives the relation between  $\gamma_{\text{tr}}(\omega)$  and  $\gamma(\omega)$  as well as  $m_{\text{tr}}(\omega)$  and  $m^*(\omega)$ , respectively:

$$\begin{aligned} \gamma_{\text{tr}}(\omega) &= \frac{1}{\omega} \int_0^{\omega} d\omega' \gamma(\omega'), \\ \omega m_{\text{tr}}(\omega) &= \frac{1}{\omega} \int_0^{\omega} d\omega' 2\omega' m^*(\omega'). \end{aligned} \quad (20)$$

The physical meaning of (19) is the following: in optical measurements one photon with the energy  $\omega$  is absorbed

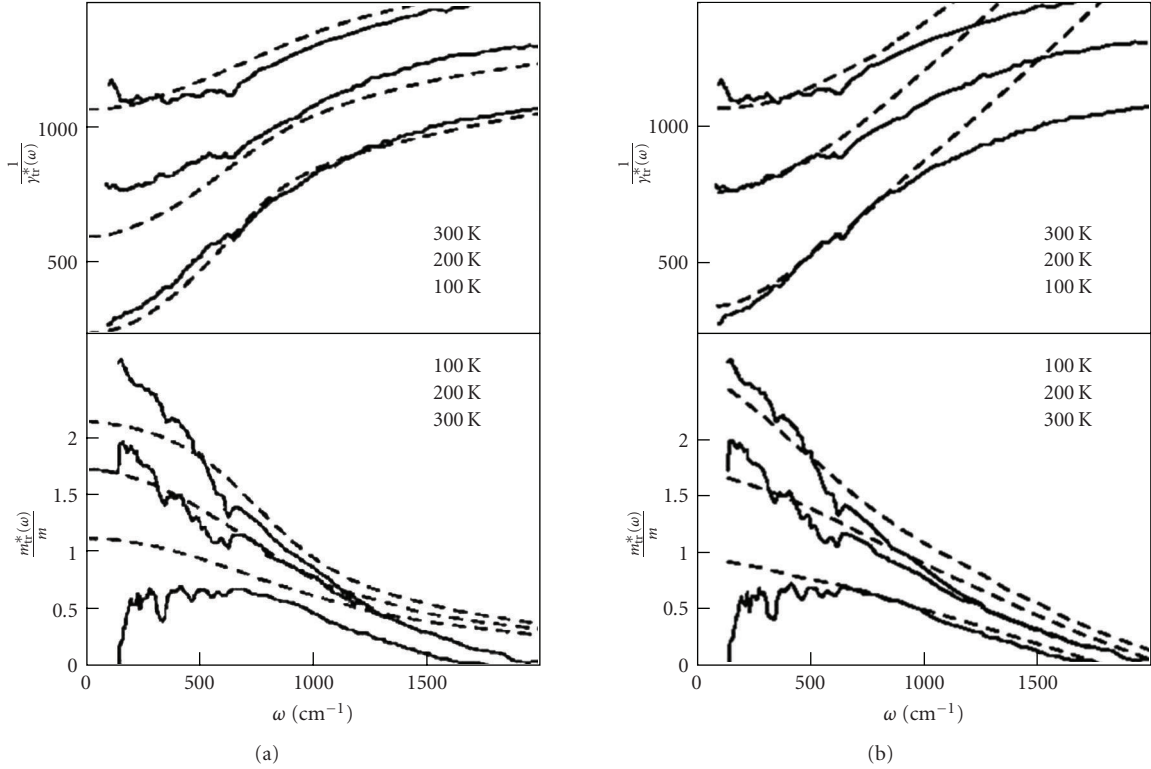


FIGURE 5: (a) Experimental transport scattering rate  $\gamma_{\text{tr}}^*$  (solid lines) for BSCO and the theoretical curve by using (A.20) and transport mass  $m_{\text{tr}}^*$  with  $\alpha^2 F(\omega)$  due to EPI which is described in text (dashed lines). (b) Comparison with the marginal Fermi liquid theory—dashed lines. From [3–5, 99].

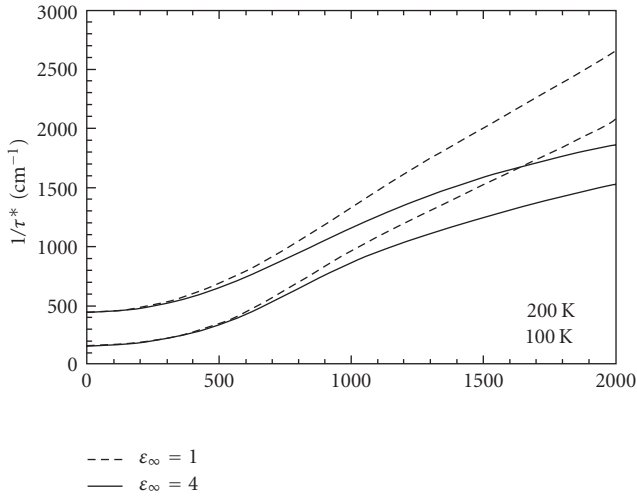


FIGURE 6: Dependence of  $\gamma_{\text{tr}}^*(\omega, T)$  on  $\epsilon_\infty$  in  $\text{Bi}_2\text{Sr}_2\text{CaCu}_2\text{O}_8$  for different temperatures:  $\epsilon_\infty = 4$  (solid lines) and  $\epsilon_\infty = 1$  (dashed lines). On the horizontal axis is  $\omega$  in units  $\text{cm}^{-1}$ . From [99].

and two excited particles (electron and hole) are created above and below the Fermi surface. If the electron has energy  $\omega'$  and the hole  $\omega - \omega'$ , then they relax as quasiparticles with the renormalized frequency  $\tilde{\omega}$ . Since  $\omega'$  takes values  $0 < \omega' < \omega$ , then the optical relaxation  $\tilde{\omega}_{\text{tr}}(\omega)$  is the energy-averaged  $\tilde{\omega}(\omega)$  according to (19). The factor 2 is due to

the two quasiparticles—electron and hole. At finite  $T$ , the generalization reads [32, 36]

$$\tilde{\omega}_{\text{tr}}(\omega) = \frac{1}{\omega} \int_0^\omega d\omega' [1 - n_F(\omega') - n_F(\omega - \omega')] 2\tilde{\omega}(\omega'). \quad (21)$$

(2) *Inversion of the Optical Data and  $\alpha_{\text{tr}}^2(\omega)F(\omega)$ .* In principle, the transport spectral function  $\alpha_{\text{tr}}^2(\omega)F(\omega)$  can be extracted from  $\sigma(\omega)$  (or  $\gamma_{\text{tr}}(\omega)$ ) only at  $T = 0\text{K}$ , which follows from (18) as

$$\alpha_{\text{tr}}^2(\omega)F(\omega) = \frac{\omega_p^2}{8\pi^2} \frac{\partial^2}{\partial \omega^2} \left[ \omega \text{Re} \frac{1}{\sigma(\omega)} \right], \quad (22)$$

or equivalently as  $\alpha_{\text{tr}}^2(\omega)F(\omega) = (1/2\pi)\partial^2(\omega\gamma_{\text{tr}}(\omega))/\partial\omega^2$ . However, real measurements are performed at finite  $T$  (at  $T > T_c$  which is rather high in HTSC cuprates) and the inversion procedure is an ill-posed problem since  $\alpha_{\text{tr}}^2(\omega)F(\omega)$  is the deconvolution of the inhomogeneous Fredholm integral equation of the first kind with the temperature-dependent Kernel  $K_2(\omega, \nu, T)$ —see (14). It is known that an ill-posed mathematical problem is very sensitive to input since experimental data contain less information than one needs. This procedure can cause, *first*, that the fine structure of  $\alpha_{\text{tr}}^2(\omega)F(\omega)$  get blurred (most peaks are washed out) in the extraction procedures and, *second*, the extracted  $\alpha_{\text{tr}}^2(\omega)F(\omega)$  be temperature dependent even when the true

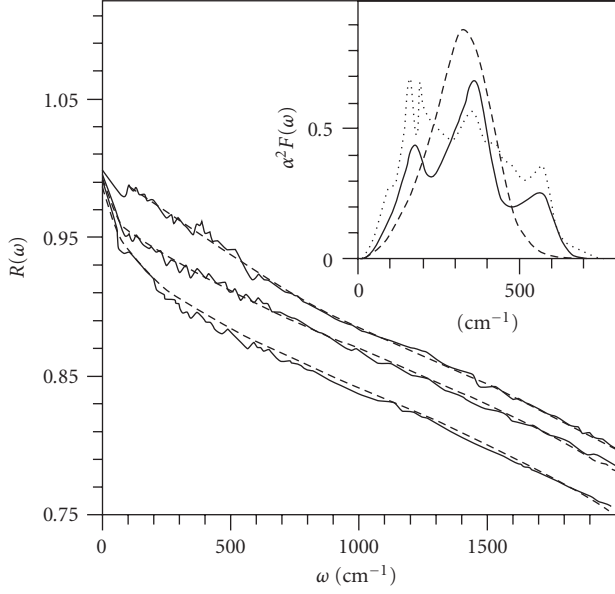


FIGURE 7: Experimental (solid lines) and calculated (dashed lines) data of  $R(\omega)$  in optimally doped YBCO [105] at  $T = 100, 200, 300$  K (from top to bottom). Inset: the two (solid and dashed lines) reconstructed  $\alpha_{\text{tr}}^2(\omega)F(\omega)$ 's at  $T = 100$  K. The phonon density of states  $F(\omega)$ —dotted line in the inset. From [33–35].

$\alpha_{\text{tr}}^2(\omega)F(\omega)$  is  $T$  independent. This artificial  $T$  dependence is especially pronounced in HTSC cuprates because  $T_c$  ( $\sim 100$  K) is very high. In the context of HTSC cuprates, this problem was first studied in [33–36] where this picture is confirmed by the following results: (1) *the extracted shape of  $\alpha_{\text{tr}}^2(\omega)F(\omega)$  in  $\text{YBa}_2\text{Cu}_3\text{O}_{7-x}$  as well as in other cuprates is not unique and it is temperature dependent*, that is, at higher  $T > T_c$  the peak structure is smeared and only a single peak (slightly shifted to higher  $\omega$ ) is present. For instance, the experimental data of  $R(\omega)$  in YBCO were reproduced by two different spectral functions  $\alpha_{\text{tr}}^2(\omega)F(\omega)$ , one with single peak and the other one with three-peak structure as it is shown in Figure 7, where all spectral functions give almost identical  $R(\omega)$ . The similar situation is *realized in optimally doped BSCO* as it is seen in Figure 8 where again different functions  $\alpha^2(\omega)F(\omega)$  reproduce very well curves for  $R(\omega)$  and  $\sigma(\omega)$ . However, it is important to stress that the obtained width of the extracted  $\alpha_{\text{tr}}^2(\omega)F(\omega)$  in both compounds coincide with the width of the phonon density of states  $F_{\text{ph}}(\omega)$  [33–36, 99]. (2) The upper energy bound for  $\alpha_{\text{tr}}^2(\omega)F(\omega)$  is extracted in [33–36] and it coincides approximately with the maximal phonon frequency in cuprates  $\omega_{\text{ph}}^{\text{max}} \lesssim 80$  meV as it is seen in Figures 7 and 8.

These results demonstrate the importance of EPI in cuprates [33–36]. We point out that the width of  $\alpha_{\text{tr}}^2(\omega)F(\omega)$  which is extracted from the optical measurements [33–36] coincides with the width of the quasiparticle spectral function  $\alpha^2(\omega)F(\omega)$  obtained in *tunnelling and ARPES spectra* (which we will discuss below), that is, both functions are spread over the energy interval  $0 < \omega < \omega_{\text{ph}}^{\text{max}}$  ( $\lesssim 80$  meV). Since in cuprates this interval coincides with the width in the phononic density of states  $F(\omega)$  and since the maxima of

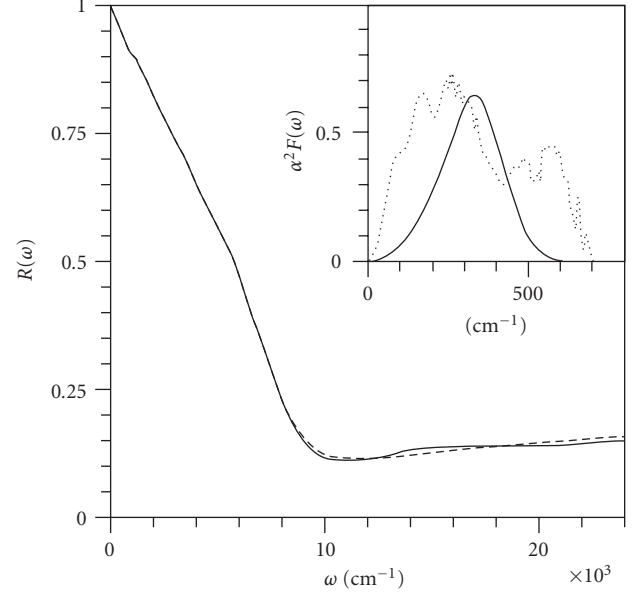


FIGURE 8: Experimental (solid line) and calculated (dashed line) data of  $R(\omega)$  in optimally doped BSCO [106] at  $T = 100$  K. Inset: the reconstructed  $\alpha_{\text{tr}}^2(\omega)F(\omega)$ —solid line. The phonon density of states  $F(\omega)$ —dotted line. From [33–35].

$\alpha^2(\omega)F(\omega)$  and  $F(\omega)$  almost coincide, this is further evidence for the importance of EPI.

To this end, we would like to comment two aspects which appear from time to time in the literature. *First*, in some reports [24–27] it is assumed that  $\alpha_{\text{tr}}^2(\omega)F(\omega)$  of cuprates can be extracted also in the superconducting state by using (22). However, (22) holds exclusively in the normal state (at  $T = 0$ ) since  $\sigma(\omega)$  can be described by the generalized (extended) Drude formula in (12) only in the normal state. Such an approach does not hold in the superconducting state since the dynamical conductivity depends not only on the electron-boson scattering but also on coherence factors and on the momentum and energy dependent order parameter  $\Delta(\mathbf{k}, \omega)$ . *Second*, if  $R(\omega)$ 's (and  $\sigma(\omega)$ 's) in cuprates are due to some other bosonic scattering which is pronounced up to much higher energies  $\omega_c \gg \omega_{\text{ph}}^{\text{max}}$ , this should be seen in the width of the extracted spectral function  $\alpha_{\text{tr}}^2(\omega)F(\omega)$ . In that respect in [25–27] it is assumed that SFI dominates in the quasiparticle scattering and that  $\alpha_{\text{tr}}^2(\omega)F(\omega) \sim g_{\text{sf}}^2 \text{Im}\chi(\omega)$  where  $\text{Im}\chi(\omega) = \int d^2k \chi(\mathbf{k}, \omega)$ . This claim is based on reanalyzing of some IR measurements [25–27] and the transport spectral function  $\alpha_{\text{tr}}^2(\omega)F(\omega)$  is extracted in [25] by using the maximum entropy method in solving the Fredholm equation. However, in order to exclude negative values in the extracted  $\alpha_{\text{tr}}^2(\omega)F(\omega)$ , which is an artefact and due to the chosen method, in [25] it is assumed that  $\alpha_{\text{tr}}^2(\omega)F(\omega)$  has a rather large tail at large energies—up to 400 meV. It turns out that even such an assumption in extracting  $\alpha_{\text{tr}}^2(\omega)F(\omega)$  does not reproduce the experimental curve  $\text{Im}\chi(\omega)$  [107] in some important aspects. First, the relative heights of the two peaks in the extracted spectral function  $\alpha_{\text{tr}}^2(\omega)F(\omega)$  at lower temperatures are opposite to

the experimental curve  $\text{Im}\chi(\omega)$  [107]—see [25, Figure 1]. Second, the strong temperature dependence of the extracted  $\alpha_{\text{tr}}^2(\omega)F(\omega)$  found in [25–27] is not an intrinsic property of the spectral function but it is an artefact due to the high sensitivity of the extraction procedure on temperature. As it is already explained before, this is due to the ill-posed problem of solving the Fredholm integral equation of the first kind with strong  $T$ -dependent kernel. *Third*, the extracted spectral weight  $I_B(\omega) = \alpha_{\text{tr}}^2(\omega)F(\omega)$  in [25] has much smaller values at larger frequencies ( $\omega > 100$  meV) than it is the case for the measured  $\text{Im}\chi(\omega)$ , that is,  $(I_B(\omega > 100 \text{ meV})/I_B(\omega_{\text{max}})) \ll \text{Im}\chi(\omega > 100 \text{ meV})/\text{Im}\chi(\omega_{\text{max}})$ —see [25, Figure 1]. *Fourth*, the recent magnetic neutron scattering measurements on optimally doped *large-volume* crystals  $\text{Bi}_2\text{Sr}_2\text{CaCu}_2\text{O}_{8+\delta}$  [93] (where the absolute value of  $\text{Im}\chi(\mathbf{q}, \omega)$  is measured) are not only questioning the theoretical interpretation of magnetism in HTSC cuprates in terms of itinerant magnetism but also opposing the finding in [25–27]. Namely, this experiment shows that the local spin susceptibility  $\text{Im}\chi(\omega) = \sum_{\mathbf{q}} \text{Im}\chi(\mathbf{q}, \omega)$  is temperature independent across the superconducting transition  $T_c = 91$  K, that is, there is only a minimal change in  $\text{Im}\chi(\omega)$  between 10 K and 100 K. This  $T$ -independence of  $\text{Im}\chi(\omega)$  strongly opposes the (above discussed) results in [24–27], where the fit of optic measurements gives strong  $T$  dependence of  $\text{Im}\chi(\omega)$ .

*Fifth*, the transport coupling constant  $\lambda_{\text{tr}}$  extracted in [25] is too large, that is,  $\lambda_{\text{tr}} > 3$  contrary to the previous findings that  $\lambda_{\text{tr}} \lesssim 1.5$  [33–36, 99]. Since in HTSC one has  $\lambda > \lambda_{\text{tr}}$ , this would probably give  $\lambda \approx 6$ , which is not confirmed by other experiments. *Sixth*, the interpretation of  $\alpha_{\text{tr}}^2(\omega)F(\omega)$  in LSCO and BSCO solely in terms of  $\text{Im}\chi(\omega)$  is in contradiction with the magnetic neutron scattering in the optimally doped and slightly underdoped YBCO [30]. The latter was discussed in Section 1.3.1, where it is shown that  $\text{Im}\chi(\mathbf{Q}, \omega)$  is small in the normal state and its magnitude is even below the experimental noise. This means that if the assumption that  $\alpha_{\text{tr}}^2(\omega)F(\omega) \approx g_{\text{sf}}^2 \text{Im}\chi(\omega)$  were correct then the contribution to  $\text{Im}\chi(\omega)$  from the momenta  $0 < k \ll Q$  would be dominant, which is detrimental for  $d$ -wave superconductivity.

Finally, we point out that very similar (to cuprates) properties, of  $\sigma(\omega)$ ,  $R(\omega)$  (and  $\rho(T)$  and electronic Raman spectra), were observed in 3D isotropic metallic oxides  $\text{La}_{0.5}\text{Sr}_{0.5}\text{CoO}_3$  and  $\text{Ca}_{0.5}\text{Sr}_{0.5}\text{RuO}_3$  which are nonsuperconducting [108] and in  $\text{Ba}_{1-x}\text{K}_x\text{BiO}_3$  which is superconducting below  $T_c \approx 30$  K at  $x = 0.4$ . This means that in all of these materials the scattering mechanism might be of similar origin. Since in these compounds there are no signs of antiferromagnetic fluctuations (which are present in cuprates), then the EPI scattering plays important role also in other oxides.

(3) *Restricted Optical Sum Rule.* The *restricted optical sum rule* was studied intensively in HTSC cuprates. It shows some peculiarities not present in low-temperature superconductors. It turns out that the restricted spectral weight  $W(\Omega_c, T)$  is strongly temperature dependent in the normal

and superconducting state, which was interpreted either to be due to EPI [39, 40] or to some nonphononic mechanisms [109]. In the following we demonstrate that the temperature dependence of  $W(\Omega_c, T) = W(0) - \beta T^2$  in the normal state can be explained in a natural way by the  $T$  dependence of the EPI transport relaxation rate  $\gamma_{\text{tr}}^{ep}(\omega, T)$  [39, 40]. Since the problem of the restricted sum rule has attracted much interest, it will be considered here in some details. In fact, there are two kinds of sum rules related to  $\sigma(\omega)$ . The first one is the *total sum rule* which in the normal state reads

$$\int_0^\infty d\omega \sigma_1^N(\omega) = \frac{\omega_{\text{pl}}^2}{8} = \frac{\pi n e^2}{2m}, \quad (23)$$

while in the *superconducting state* it is given by the Tinkham-Ferrell-Glover (TFG) sum rule

$$\int_0^\infty d\omega \sigma_1^S(\omega) = \frac{c^2}{8\lambda_L^2} + \int_{+0}^\infty d\omega \sigma_1^S(\omega) = \frac{\omega_{\text{pl}}^2}{8}. \quad (24)$$

Here,  $n$  is the total electron density,  $e$  is the electron charge,  $m$  is the bare electron mass, and  $\lambda_L$  is the London penetration depth. The first (singular) term  $c^2/8\lambda_L^2$  in (24) is due to the superconducting condensate which contributes  $\sigma_{1,\text{cond}}^S(\omega) = (c^2/4\lambda_L^2)\delta(\omega)$ . The total sum rule represents the fundamental property of matter—the conservation of the electron number. In order to calculate it one should use the total Hamiltonian  $\hat{H}_{\text{tot}} = \hat{T}_e + \hat{H}_{\text{int}}$  where all electrons, electronic bands, and their interactions  $\hat{H}_{\text{int}}$  (Coulomb, EPI, with impurities, etc.) are accounted for. Here,  $T_e$  is the *kinetic energy of bare electrons*:

$$\hat{T}_e = \sum_{\sigma} \int d^3x \hat{\psi}_{\sigma}^{\dagger}(x) \frac{\hat{\mathbf{p}}^2}{2m} \hat{\psi}_{\sigma}(x) = \sum_{\mathbf{p},\sigma} \frac{\mathbf{p}^2}{2m_e} \hat{c}_{\mathbf{p}\sigma}^{\dagger} \hat{c}_{\mathbf{p}\sigma}. \quad (25)$$

The *partial sum rule* is related to the energetics solely in the *conduction (valence) band* which is described by the Hamiltonian of the conduction (valence) band electrons:

$$\hat{H}_v = \sum_{\mathbf{p},\sigma} \xi_{\mathbf{p}} \hat{c}_{\mathbf{p}\sigma}^{\dagger} \hat{c}_{\mathbf{p}\sigma} + \hat{V}_{v,c}. \quad (26)$$

$\hat{H}_v$  contains the band energy with the dispersion  $\epsilon_{\mathbf{p}}$  ( $\xi_{\mathbf{p}} = \epsilon_{\mathbf{p}} - \mu$ ) and the effective Coulomb interaction of the valence electrons  $\hat{V}_{v,c}$ . In this case the *partial sum rule* in the normal state reads [110] (for a general form of  $\epsilon_{\mathbf{p}}$ )

$$\int_0^\infty d\omega \sigma_{1,v}^N(\omega) = \frac{\pi e^2}{2V} \sum_{\mathbf{p}} \frac{\langle \hat{n}_{v,\mathbf{p}} \rangle_{H_v}}{m_{\mathbf{p}}}, \quad (27)$$

where the number operator  $\hat{n}_{v,\mathbf{p}} = \sum_{\sigma} \hat{c}_{\mathbf{p}\sigma}^{\dagger} \hat{c}_{\mathbf{p}\sigma}$ ;  $1/m_{\mathbf{p}} = \partial^2 \epsilon_{\mathbf{p}} / \partial p_x^2$  is the momentum-dependent reciprocal mass and  $V$  is volume. In practice, the optic measurements are performed up to finite frequency and the integration over  $\omega$  goes up to some cutoff frequency  $\Omega_c$  (of the order of the band plasma frequency). In this case the restricted sum rule has the form

$$\begin{aligned} W(\Omega_c, T) &= \int_0^{\Omega_c} d\omega \sigma_{1,v}^N(\omega) \\ &= \frac{\pi}{2} [K^d + \Pi(0)] - \int_0^{\Omega_c} d\omega \frac{\text{Im} \Pi(\omega)}{\omega}, \end{aligned} \quad (28)$$

where  $K^d$  is the diamagnetic Kernel given by (30) below and  $\Pi(\omega)$  is the paramagnetic (current-current) response function. In the perturbation theory without vertex correction  $\Pi(i\omega_n)$  (at the Matsubara frequency  $\omega_n = \pi T(2n + 1)$ ) is given by [39, 40]

$$\Pi(i\omega) = 2 \sum_{\mathbf{p}} \left( \frac{\partial \epsilon_{\mathbf{p}}}{\partial \mathbf{p}} \right)^2 \sum_{\omega_m} G(\mathbf{p}, i\omega_{nm}^+) G(\mathbf{p}, i\omega_m), \quad (29)$$

where  $\omega_{nm}^+ = \omega_n + \omega_m$  and  $G(\mathbf{p}, i\omega_n) = (i\omega_n - \xi_{\mathbf{p}} - \Sigma(\mathbf{p}, i\omega_n))^{-1}$  is the electron Green's function. In the case when the interband gap  $E_g$  is the largest scale in the problem, that is, when  $W_b < \Omega_c < E_g$ , in this region one has approximately  $\text{Im} \Pi(\omega) \approx 0$  and the limit  $\Omega_c \rightarrow \infty$  in (28) is justified. In that case one has  $\Pi(0) \approx \int_0^{\Omega_c} (\text{Im} \Pi(\omega)/\omega) d\omega$  which gives the *approximate formula* for  $W(\Omega_c, T)$ :

$$\begin{aligned} W(\Omega_c, T) &= \int_0^{\Omega_c} d\omega \sigma_{1,v}^N(\omega) \approx \frac{\pi}{2} K^d \\ &= e^2 \pi \sum_{\mathbf{p}} \frac{\partial^2 \epsilon_{\mathbf{p}}}{\partial \mathbf{p}^2} n_{\mathbf{p}}, \end{aligned} \quad (30)$$

where  $n_{\mathbf{p}} = \langle \hat{n}_{v,\mathbf{p}} \rangle$  is the quasiparticle distribution function in the interacting system. Note that  $W(\Omega_c, T)$  is cutoff dependent while  $K^d$  in (30) does not depend on  $\Omega_c$ . So, one should be careful not to overinterpret the experimental results in cuprates by this formula. In that respect the best way is to calculate  $W(\Omega_c, T)$  by using the exact result in (28) which apparently depends on  $\Omega_c$ . However, (30) is useful for appropriately chosen  $\Omega_c$ , since it allows us to obtain semiquantitative results. In most papers related to the restricted sum rule in HTSC cuprates it was assumed, due to simplicity, the *tight-binding model with nearest neighbors* (n.n.) with the energy  $\epsilon_{\mathbf{p}} = -2t(\cos p_x a + \cos p_y a)$  which gives  $1/m_{\mathbf{p}} = -2ta^2 \cos p_x a$ . It is straightforward to show that in this case (30) is reduced to a simpler one:

$$\begin{aligned} W(\Omega_c, T) &= \int_0^{\Omega_c} d\omega \sigma_{1,v}^N(\omega) \\ &\approx \frac{\pi e^2 a^2}{2V} \langle -T_v \rangle, \end{aligned} \quad (31)$$

where  $\langle T_v \rangle_{H_v} = \sum_{\mathbf{p}} \epsilon_{\mathbf{p}} \langle n_{v,\mathbf{p}} \rangle_{H_v}$  is the average kinetic energy of the band electrons,  $a$  is the Cu-Cu lattice distance, and  $V$  is the volume of the system. In this approximation  $W(\Omega_c, T)$  is a direct measure of the average band (kinetic) energy. In the *superconducting state* the partial band sum rule reads

$$\begin{aligned} W_s(\Omega_c, T) &= \frac{c^2}{8\lambda_L^2} + \int_{+0}^{\Omega_c} d\omega \sigma_{1,v}^S(\omega) \\ &= \frac{\pi e^2 a^2}{2V} \langle -T_v \rangle_s. \end{aligned} \quad (32)$$

In order to introduce the reader to (the complexity of) the problem of the  $T$  dependence of  $W(\Omega_c, T)$ , let us consider the electronic system in the normal state and in absence of the quasiparticle interaction. In that case one has  $n_{\mathbf{p}} = f_{\mathbf{p}}$  ( $f_{\mathbf{p}}$

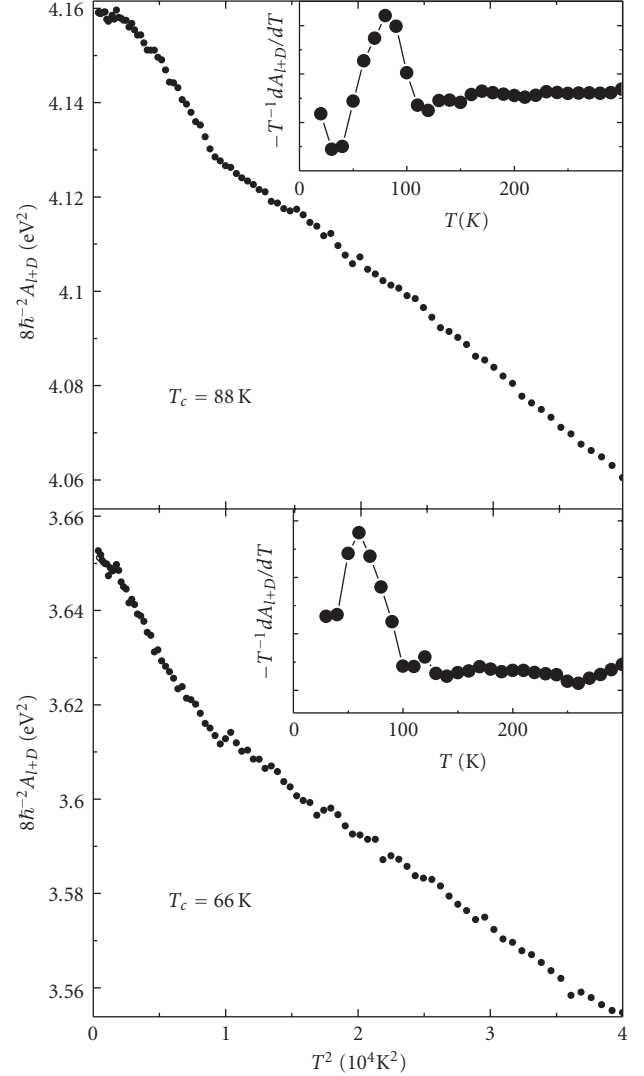


FIGURE 9: Measured spectral weight  $W_s(\Omega_c, T) (\sim A_{l+D}$  in figures) for  $\Omega_c \approx 1.25$  eV in two underdoped Bi2212 (with  $T_c = 88$  K and  $T_c = 66$  K). From [111].

is the Fermi distribution function) and  $W_n(\Omega_c, T)$  increases with the decrease of the temperature, that is,  $W_n(\Omega_c, T) = W_n(0) - \beta_b T^2$  where  $\beta_b \sim 1/W_b$ . To this end, let us mention in advance that the experimental value  $\beta_{\text{exp}}$  is much larger than  $\beta_b$ , that is,  $\beta_{\text{exp}} \gg \beta_b$ , thus telling us that the simple Sommerfeld-like smearing of  $f_{\mathbf{p}}$  by the temperature effects cannot explain quantitatively the  $T$  dependence of  $W(\Omega_c, T)$ . We stress that the smearing of  $f_{\mathbf{p}}$  by temperature lowers the spectral weight compared to that at  $T = 0$  K, that is,  $W_n(\Omega_c, T) < W_n(\Omega_c, 0)$ . In that respect it is not surprising that there is a lowering of  $W_s(\Omega_c, T)$  in the BCS superconducting state,  $W_s^{\text{BCS}}(\Omega_c, T \ll T_c) < W_n(\Omega_c, T \ll T_c)$  since at low temperatures  $f_{\mathbf{p}}$  is smeared mainly due to the superconducting gap, that is,  $f_{\mathbf{p}} = [1 - (\xi_{\mathbf{p}}/E_{\mathbf{p}})\text{th}(E_{\mathbf{p}}/2T)]/2$ ,  $E_{\mathbf{p}} = \sqrt{\xi_{\mathbf{p}}^2 + \Delta^2}$ ,  $\xi_{\mathbf{p}} = \epsilon_{\mathbf{p}} - \mu$ . The maximal decrease of  $W_s(\Omega_c, T)$  is at  $T = 0$ .

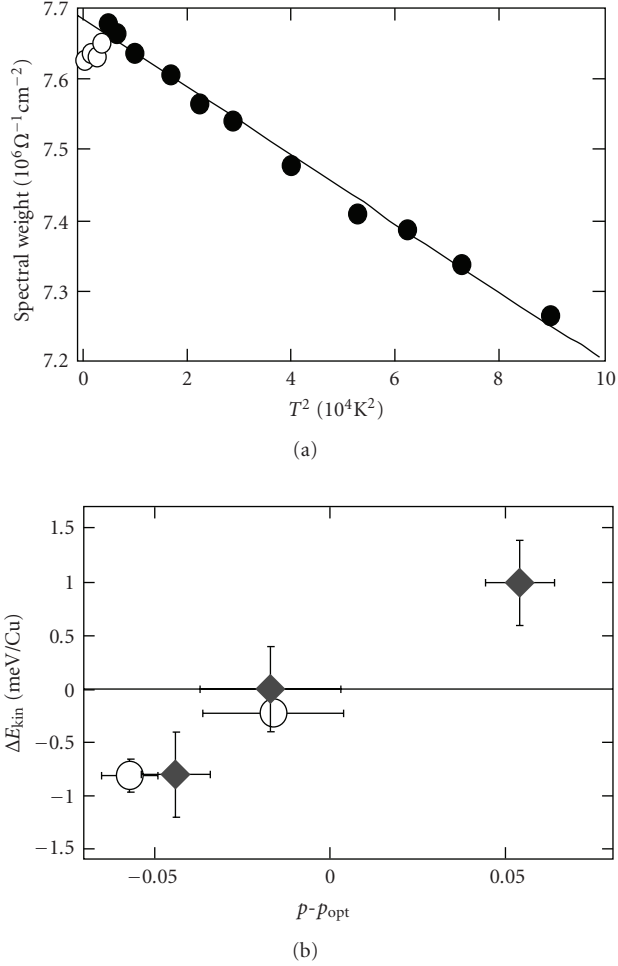


FIGURE 10: (a) Spectral weight  $W_n(\Omega_c, T)$  of the overdoped Bi2212 for  $\Omega_c = 1$  eV. Closed symbols—normal state. Open symbols—superconducting state. (b) Change of the kinetic energy  $\Delta E_{\text{kin}} = E_{\text{kin},S} - E_{\text{kin},N}$  in meV per Cu site versus the charge  $p$  per Cu with respect to the optimal value  $p_{\text{opt}}$ . From [112].

Let us enumerate and discuss the *main experimental results* for  $W(\Omega_c, T)$  in HTSC cuprates. (1) In the *normal state* ( $T > T_c$ ) of most cuprates, one has  $W_n(\Omega_c, T) = W_n(0) - \beta_{\text{ex}} T^2$  with  $\beta_{\text{ex}} \gg \beta_b$ , that is,  $W_n(\Omega_c, T)$  is increasing by decreasing  $T$ , even at  $T$  below  $T^*$ —the temperature for the opening of the pseudogap. The increase of  $W_n(\Omega_c, T)$  from the room temperature down to  $T_c$  is no more than 5%. (2) In the *superconducting state* ( $T < T_c$ ) of some underdoped and optimally doped Bi-2212 compounds [111, 113, 114] (and underdoped Bi-2212 films [115]) there is an *effective increase* of  $W_s(\Omega_c, T)$  with respect to that in the normal state, that is,  $W_s(\Omega_c, T) > W_n(\Omega_c, T)$  for  $T < T_c$ . This is a *non-BCS behavior* which is shown in Figure 9. Note that in the tight binding model the effective band (kinetic) energy  $\langle T_v \rangle$  is negative ( $\langle T_v \rangle < 0$ ) and in the standard BCS case (32) gives that  $W_s(T < T_c)$  *decreases* due to the increase of  $\langle T_v \rangle$ . Therefore the experimental increase of  $W_s(T < T_c)$  by decreasing  $T$  is called the non-BCS behavior. The latter means a lowering of the kinetic energy  $\langle T_v \rangle$  which is frequently interpreted to be due either to strong correlations

or to a Bose-Einstein condensation (BEC) of the preformed tightly bound Cooper pair-bosons, for instance, bipolarons [116]. It is known that in the latter case the kinetic energy of bosons is decreased below the BEC critical temperature  $T_c$ . In [117] it is speculated that the latter case might be realized in underdoped cuprates.

However, in some optimally doped and in most overdoped cuprates, there is a decrease of  $W_s(\Omega_c, T)$  at  $T < T_c$  ( $W_s(\Omega_c, T) < W_n(\Omega_c, T)$ ) which is the BCS-like behavior [112] as it is seen in Figure 10.

We stress that the non-BCS behavior of  $W_s(\Omega_c, T)$  for underdoped (and in some optimally doped) systems was obtained by assuming that  $\Omega_c \approx (1-1.2)$  eV. However, in [104] these results were questioned by claiming that the conventional BCS-like behavior was observed ( $W_s(\Omega_c, T) < W_n(\Omega_c, T)$ ) in the optimally doped YBCO and slightly underdoped Bi-2212 by using larger cutoff energy  $\Omega_c = 1.5$  eV. This discussion demonstrates how risky is to make definite conclusions on some fundamental physics based on the parameter- (such as the cutoff energy  $\Omega_c$ ) dependent analysis. Although the results obtained in [104] look very trustfully, it is fair to say that the issue of the reduced spectral weight in the superconducting state of the underdoped cuprates is still unsettled and under dispute. In overdoped Bi-2212 films, the BCS-like behavior  $W_s(\Omega_c, T) < W_n(\Omega_c, T)$  was observed, while in LSCO it was found that  $W_s(\Omega_c, T) \approx \text{const}$ , that is,  $W_s(\Omega_c, T < T_c) \approx W_n(\Omega_c, T_c)$ .

The first question is the following. How to explain the strong temperature dependence of  $W(\Omega_c, T)$  in the normal state? In [39, 40]  $W(T)$  is explained solely in the framework of the EPI physics where the EPI relaxation  $\gamma_{ep}(T)$  plays the main role in the  $T$  dependence of  $W(\Omega_c, T)$ . The main theoretical results of [39, 40] are the following: the calculations of  $W(T)$  based on the exact (30) give that for  $\Omega_c \gg \Omega_D$  (the Debye energy) the difference in spectral weights of the normal and superconducting states is small, that is,  $W_n(\Omega_c, T) \approx W_s(\Omega_c, T)$  since  $W_n(\Omega_c, T) - W_s(\Omega_c, T) \sim \Delta^2/\Omega_c^2$ . (2) In the case of large  $\Omega_c$  the calculations based on (30) give

$$W(\Omega_c, T) \approx \frac{\omega_{\text{pl}}^2}{8} \left[ 1 - \frac{\gamma(T)}{W_b} - \frac{\pi^2}{2} \frac{T^2}{W_b^2} \right]. \quad (33)$$

In the case when EPI dominates one has  $\gamma = \gamma_{ep}(T) + \gamma_{\text{imp}}$  where  $\gamma_{ep}(T) = \int_0^\infty dz \alpha^2(z) F(z) \coth(z/2T)$ . It turns out that for  $\alpha^2(\omega)F(\omega)$ , shown in Figure 4, one obtains (i)  $\gamma_{ep}(T) \sim T^2$  in the temperature interval  $100 \text{ K} < T < 200 \text{ K}$  as it is seen in Figure 11 for the  $T$  dependence of  $W(\Omega_c, T)$  [39, 40]; (ii) the second term in (33) is much larger than the last one (the Sommerfeld-like term). For the EPI coupling constant  $\lambda_{ep, \text{tr}} = 1.5$  one obtains rather good agreement between the theory in [39, 40] and experiments in [104, 111, 113, 114]. At lower temperatures,  $\gamma_{ep}(T)$  deviates from the  $T^2$  behavior and this deviation depends on the structure of the spectrum in  $\alpha^2(\omega)F(\omega)$ . It is seen in Figure 11 that, for a softer Einstein spectrum (with  $\Omega_E = 200 \text{ K}$ ),  $W(\Omega_c, T)$  lies above the curve with the  $T^2$  asymptotic behavior, while the curve with a harder phononic spectrum (with  $\Omega_E = 400 \text{ K}$ ) lies below it. This result means that different behavior of  $W(\Omega_c, T)$  in

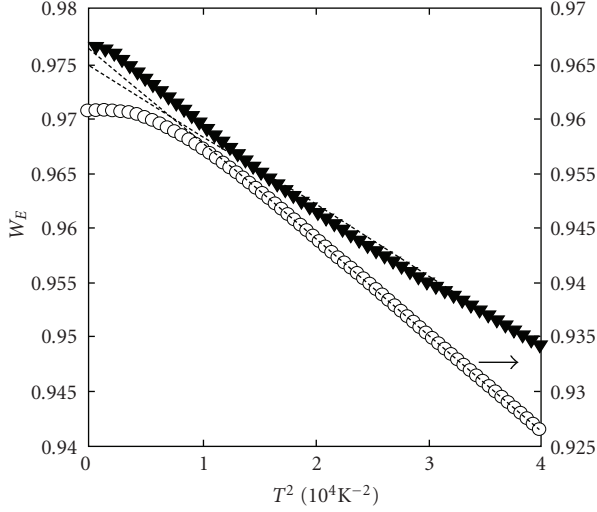


FIGURE 11: Spectral weight  $W(\Omega_c, T)$  in the normal state for Einstein phonons with  $\Omega_E = 200$  K (full triangles) and  $\Omega_E = 400$  K (open circles, left axis). Dashed lines show  $T^2$  asymptotic. From [40].

the superconducting state of cuprates for different doping might be simply related to different contributions of low- and high-frequency phonons. We stress that such a behavior of  $W(\Omega_c, T)$  was observed in experiments in [104, 111, 113, 114].

To summarize, the above analysis demonstrates that the theory based on EPI is able to explain in a satisfactory way the temperature behavior of  $W(\Omega_c, T)$  above and below  $T_c$  in systems at and near the optimal doping.

(4)  $\alpha^2(\omega)F(\omega)$  and the In-Plane Resistivity  $\rho_{ab}(T)$ . The temperature dependence of the in-plane resistivity  $\rho_{ab}(T)$  in cuprates is a direct consequence of the quasi-2D motion of quasiparticles and of the inelastic scattering which they experience. At present, there is no consensus on the origin of the linear temperature dependence of the in-plane resistivity  $\rho_{ab}(T)$  in the normal state. Our intention is not to discuss this problem, but only to demonstrate that the EPI spectral function  $\alpha^2(\omega)F(\omega)$ , which is obtained from tunnelling experiments in cuprates (see Section 1.3.4), is able to explain the temperature dependence of  $\rho_{ab}(T)$  in the optimally doped YBCO. In the Boltzmann theory  $\rho_{ab}(T)$  is given by

$$\rho_{ab}(T) = \rho_{\text{imp}} + \frac{4\pi}{\omega_p^2} \gamma_{\text{tr}}(T), \quad (34)$$

where

$$\gamma_{\text{tr}}(T) = \frac{\pi}{T} \int_0^\infty d\omega \frac{\omega}{\sinh^2(\omega/2T)} \alpha_{\text{tr}}^2(\omega) F(\omega). \quad (35)$$

The residual resistivity  $\rho_{\text{imp}}$  is due to the impurity scattering. Since  $\rho(T) = 1/\sigma(\omega = 0, T)$  and having in mind that the dynamical conductivity  $\sigma(\omega, T)$  in YBCO (at and near the optimal doping) is satisfactorily explained by the EPI scattering, then it is to expect that  $\rho_{ab}(T)$  is also dominated

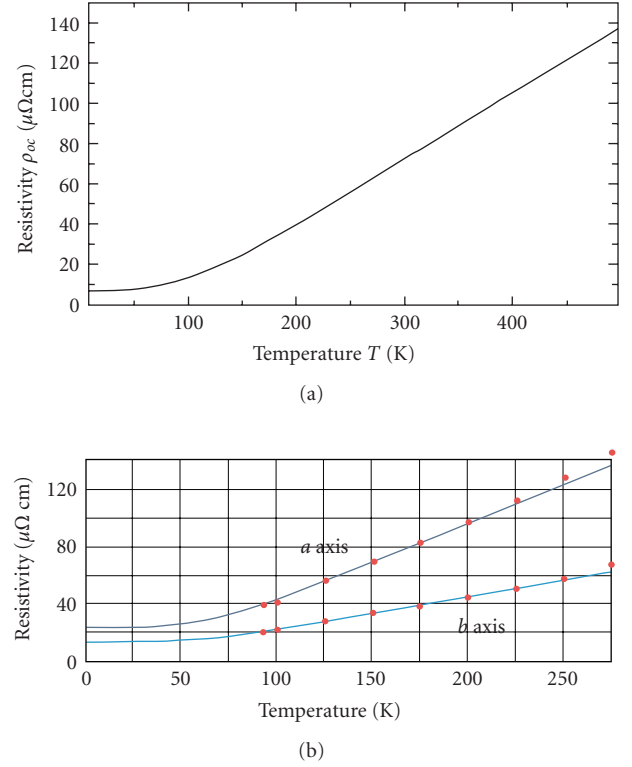


FIGURE 12: (a) Calculated resistivity  $\rho(T)$  for the EPI spectral function  $\alpha_{\text{tr}}^2(\omega)F(\omega)$  in [118]. (b) Measured resistivity in  $a(x)$ - and  $b(y)$ -crystal direction of YBCO [119] and calculated Bloch-Grüneisen curve (points) for  $\lambda^{ep} = 1$  [120].

by EPI in some temperature region  $T > T_c$ . This is indeed confirmed in the optimally doped YBCO, where  $\rho_{\text{imp}}$  is chosen appropriately and the spectral function  $\alpha_{\text{tr}}^2(\omega)F(\omega)$  is taken from the tunnelling experiments in [42–45]. The very good agreement with the experimental results [118] is shown in Figure 12. We stress that in the case of EPI there is always a temperature region where  $\gamma_{\text{tr}}(T) \sim T$  for  $T > \alpha\Theta_D$ ,  $\alpha < 1$  depending on the shape of  $\alpha_{\text{tr}}^2(\omega)F(\omega)$  (for the simple Debye spectrum  $\alpha \approx 0.2$ ). In the linear regime one has  $\rho(T) \approx \rho_{\text{imp}} + 8\pi^2 \lambda_{ep, \text{tr}} (k_B T / \hbar \omega_p^2) = \rho_{\text{imp}} + \rho' T$ .

There is experimental constraint on  $\lambda_{\text{tr}}$  since  $\lambda_{\text{tr}} \approx 0.25 \omega_{\text{pl}}^2 (\text{eV}) \rho' (\mu\Omega \text{ cm/K})$ . For instance, for  $\omega_{\text{pl}} \approx (2-3) \text{ eV}$  [108] and  $\rho' \approx 0.6$  in the oriented YBCO films and  $\rho' \approx 0.3-0.4$  in single crystals of BSCO, one obtains  $\lambda_{\text{tr}} \approx 0.6-1.4$ . In case of YBCO single crystals, there is a pronounced anisotropy in  $\rho_{ab}(T)$  [119] which gives  $\rho'_x(T) = 0.6 \mu\Omega \text{ cm/K}$  and  $\rho'_y(T) = 0.25 \mu\Omega \text{ cm/K}$ . The function  $\lambda_{\text{tr}}(\omega_{\text{pl}})$  is shown in Figure 13 where the plasma frequency  $\omega_{\text{pl}}$  can be calculated by LDA-DFT and also extracted from the width ( $\sim \omega_{\text{pl}}^*$ ) of the Drude peak at small frequencies, where  $\omega_{\text{pl}} = \sqrt{\epsilon_\infty} \omega_{\text{pl}}^*$ . We stress that the rather good agreement of theoretical and experimental results for  $\rho_{ab}(T)$ , in some optimally doped HTSC cuprates such as YBCO, *should not be overinterpreted* in the sense that the above rather simple electron-phonon approach can explain the resistivity in other HTSC cuprates and for various doping. For instance, in highly underdoped systems  $\rho_{ab}(T)$  is very different from the behavior in Figure 12 and the simple Migdal-Eliashberg theory based

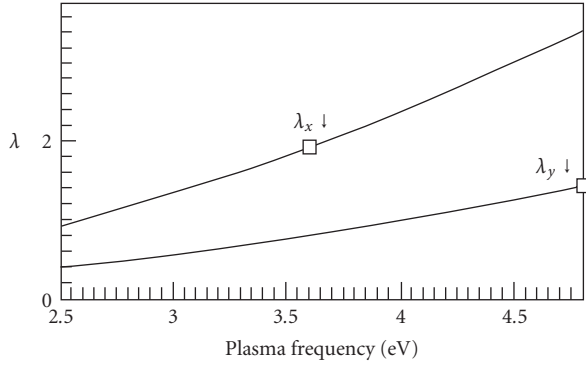


FIGURE 13: Transport EPI spectral function coupling constant in YBCO as a function of plasma frequency  $\omega_p$  as derived from the experimental slope of resistivity  $\rho'(T)$ .  $\lambda_x$  for  $\rho'_x(T) = 0.6 \mu\Omega\text{cm/K}$  and  $\lambda_y$  for  $\rho'_y(T) = 0.25 \mu\Omega\text{cm/K}$  [119]. Squares are LDA values [121].

on the EPI spectral function is inadequate. In this case one should certainly take into account polaronic effects [8–11], strong correlations, and so forth. The above analysis on the resistivity in the optimally doped YBCO demonstrates only that in this case if in (35) one uses the EPI spectral function  $\alpha^2(\omega)F(\omega)$  obtained from the tunnelling experiments (and optics) one obtains the correct  $T$  dependence of  $\rho_{a,b}(T)$ . This result is an additional evidence for the importance of EPI.

Concerning the temperature dependence of the resistivity in other (than YBCO) families of the optimally doped HTSC cuprates we would like to point out that there is some evidence that the linear (in  $T$ ) resistivity is observed in some of them even at temperatures  $T < 0.2\Theta_D$  [122, 123]. This possibility is argued also theoretically in [124] where it is shown that in two-dimensional systems with a broad interval of phonon spectra the quasilinear behavior of  $\rho_{ab}(T)$  is realized even at  $T < 0.2\Theta_D$ . The quasilinear behavior of the resistivity at  $T \ll 0.2\Theta_D$  has been observed in  $\text{Bi}_2(\text{Sr}_{0.97}\text{Pr}_{0.003})_2\text{CuO}_6$  [125], in LSCO, and in 1-layer Bi-2201 [122, 123, 126, 127], where in all these systems the critical temperature is rather small,  $T_c \approx 10\text{K}$ . In that respect all existing theories based on the electron-boson scattering are plagued and having difficulties to explain this low-temperature behavior of  $\rho_{ab}(T)$ . To this point, we would like to emphasize here that some of these (experimental) observations are contradictory. For example, the results obtained by the Vedenev group [127] show that some samples demonstrate the quasilinear behavior of the resistivity up to  $T = 10\text{K}$  but some others with approximately the same  $T_c$  have the usual Bloch-Grüneisen-type behavior characteristic for the EPI scattering. In that respect it is very unlikely that the linear resistivity up to  $T = 10\text{K}$  can be simply explained in the standard way by interactions of electrons with some known bosons *either by phonons or spin fluctuations* (magnons). The question why in some cuprates the linear resistivity is observed up to  $T = 10\text{K}$  is still a mystery and its explanation is a challenge for all kinds of the electron-boson scattering, not only for EPI. In that respect it is interesting to mention that the existence of the forward scattering peak in EPI (with the width  $q_c \ll k_F$ ),

which is due to strong correlations, may give rise to the linear behavior of  $\rho(T)$  down to very low temperatures  $T \sim \Theta_D/30$  [6, 128, 129]—see more in Section 2.3.4, item (6). We will argue in Section 1.3.4 that if one interprets the tunnelling experiments in systems near optimal doping [42–54] in the framework of the Eliashberg theory one obtains the large EPI coupling constant  $\lambda_{ep} \approx 2\text{--}3.5$  which implies that  $\lambda_{tr} \sim (\lambda/3)$ . This means that EPI is reduced much more in transport properties than in the self-energy. We stress that such a large reduction of  $\lambda_{tr}$  cannot be obtained within the LDA-DFT band-structure calculations, which means that  $\lambda_{ep}$  and  $\lambda_{tr}$  contain renormalization which do not enter in the LDA-DFT theory. In Section 2 we will argue that the strong suppression of  $\lambda_{tr}$  may have its origin in strong electronic correlations [78–80, 130] and in the long-range Madelung energy [3–6].

(5) *Femtosecond Time-Resolved Optical Spectroscopy*. The femtosecond time-resolved optical spectroscopy (FTROS) has been developed in the last couple of years and applied to HTSC cuprates. In this method a femtosecond ( $1\text{fs} = 10^{-15}\text{sec}$ ) laser pump excites in materials electron-hole pairs via interband transitions. These hot carriers release their energy via electron-electron (with the relaxation time  $\tau_{ee}$ ) and electron-phonon scattering reaching states near the Fermi energy within 10–100 fs—see [131]. The typical energy density of the laser pump pulses with the wavelength  $\lambda \approx 810\text{nm}$  ( $\hbar\omega = 1.5\text{eV}$ ) was around  $F \sim 1\mu\text{J}/\text{cm}^2$  (the *excitation fluence*  $F$ ) which produces approximately  $3 \times 10^{10}$  carriers per pulse (by assuming that each photon produces  $\hbar\omega/\Delta$  carriers,  $\Delta$  is the superconducting gap). By measuring photoinduced changes of the reflectivity in time, that is,  $\Delta R(t)/R_0$ , one can extract information on the relaxation dynamics of the low-lying electronic excitations. Since  $\Delta R(t)$  relax to equilibrium, the fit with exponential functions is used as

$$\frac{\Delta R(t)}{R_0} = f(t) \left[ A e^{-t/\tau_A} + B e^{-t/\tau_B} + \dots \right], \quad (36)$$

where  $f(t) = H(t)[1 - \exp\{-t/\tau_{ee}\}]$  ( $H(t)$  is the Heavyside function) describes the finite rise-time. The parameters  $A, B$  depend on the fluence  $F$ . This method was used in studying the superconducting phase of  $\text{La}_{2-x}\text{Sr}_x\text{CuO}_4$ , with  $x = 0.1$  and  $0.15$  and  $T_c = 30\text{K}$  and  $38\text{K}$ , respectively [41]. In that case one has  $A \neq 0$  for  $T < T_c$  and  $A = 0$  for  $T > T_c$ , while the signal  $B$  was present also at  $T > T_c$ . It turns out that the signal  $A$  is related to the quasiparticle recombination across the superconducting gap  $\Delta(T)$  and has a relaxation time of the order  $\tau_A > 10\text{ps}$  at  $T = 4.5\text{K}$ . At the so called threshold fluence ( $F_T = 4.2 \pm 1.7\mu\text{J}/\text{cm}^2$  for  $x = 0.1$  and  $F_T = 5.8 \pm 2.3\mu\text{J}/\text{cm}^2$  for  $x = 0.15$ ) the vaporization (destroying) of the superconducting phase occurs, where the parameter  $A$  saturates. This vaporization process takes place at the time scale  $\tau_r \approx 0.8\text{ps}$ . The external fluence is distributed in the sample over the *excitation volume* which is proportional to the optical penetration depth  $\lambda_{op}$  ( $\approx 150\text{nm}$  at  $\lambda \approx 810\text{nm}$ ) of the pump. The energy densities stored in the excitation volume at the vaporization threshold for  $x = 0.1$  and  $x = 0.15$  are  $U_p = F_T/\lambda_{op} = 2.0 \pm 0.8\text{K}/\text{Cu}$  and  $2.6 \pm 1.0\text{K}/\text{Cu}$ , respectively. The important fact is that  $U_p$  is

much larger than the superconducting condensation energy which is  $U_{\text{cond}} \approx 0.12 \text{ K/Cu}$  for  $x = 0.1$  and  $U_{\text{cond}} \approx 0.3 \text{ K/Cu}$  for  $x = 0.15$ , that is,  $U_p \gg U_{\text{cond}}$ . This means that the energy difference  $U_p - U_{\text{cond}}$  must be stored elsewhere on the time scale  $\tau_r$ . The only present reservoir which can absorb the difference in energy is the bosonic baths of phonons and spin fluctuations. The energy required to heat the spin reservoir from  $T = 4.5 \text{ K}$  to  $T_c$  is  $U_{\text{sf}} = \int_{T_c}^T C_{\text{sf}}(T) dT$ . The measured specific heat  $C_{\text{sf}}(T)$  in  $\text{La}_2\text{CuO}_4$  [41] gives very small value  $U_{\text{sf}} \approx 0.01 \text{ K}$ . In the case of the phonon reservoir one obtains  $U_{\text{ph}} = \int_{T_c}^T C_{\text{ph}}(T) dT = 9 \text{ K/Cu}$  for  $x = 0.1$  and  $28 \text{ K/Cu}$  for  $x = 0.15$ , where  $C_{\text{ph}}$  is the phonon specific heat. Since  $U_{\text{sf}} \ll U_p - U_{\text{cond}}$ , the spin reservoir cannot absorb the rest energy  $U_p - U_{\text{cond}}$ . The situation is opposite with phonons since  $U_{\text{ph}} \gg U_p - U_{\text{cond}}$  and phonon can absorb the rest energy in the excitation volume. The complete vaporization dynamics can be described in the framework of the Rothwarf-Taylor model which describes approaching of electrons and phonons to quasiequilibrium on the time scale of 1 ps [132]. We will not go into details but only summarize by quoting the conclusion in [132] that only phonon-mediated vaporization is consistent with the experiments, thus ruling out spin-mediated quasiparticle recombination and pairing in HTSC cuprates. The FTROS method tells us that at least for nonequilibrium processes EPI is more important than SFI. It gives also some opportunities for obtaining the strength of EPI but at present there is no reliable analysis.

*In conclusion*, optics and resistivity measurements in the normal state of cuprates give evidence that EPI is important while the spin-fluctuation scattering is weaker than it is believed. However, some important questions related to the transport properties remain to be answered. (i) What are the values of  $\lambda_{\text{tr}}$  and  $\omega_{\text{pl}}$ ? (ii) What is the reason that  $\lambda_{\text{tr}} \ll \lambda$  is realized in cuprates? (iii) What is the role of the Coulomb scattering in  $\sigma(\omega)$  and  $\rho(T)$ ? Later on we will argue that ARPES measurements in cuprates give evidence for an appreciable contribution of the Coulomb scattering at higher frequencies, where  $\gamma(\omega) \approx \gamma_0 + \lambda_c \omega$  for  $\omega > \omega_{\text{max}}^{\text{ph}}$  with  $\lambda_c \sim 1$ . One should stress that despite the fact that EPI is suppressed in transport properties it is sufficiently strong in the quasiparticle self-energy, as it comes out from tunnelling measurements discussed below.

**1.3.3. ARPES and the EPI Self-Energy.** The angle-resolved photoemission spectroscopy (ARPES) is nowadays one of leading spectroscopy methods in the solid-state physics [22, 23]. In some favorable conditions it provides direct information on the one-electron removal spectrum in a complex many-body system. The method involves shining light (photons) with energies between  $E_i = 5\text{--}1000 \text{ eV}$  on samples and by detecting momentum ( $\mathbf{k}$ )- and energy( $\omega$ )-distribution of the outgoing electrons. The resolution of ARPES has been significantly increased in the last decade with the energy resolution of  $\Delta E \approx 1\text{--}2 \text{ meV}$  (for photon energies  $\sim 20 \text{ eV}$ ) and angular resolution of  $\Delta\theta \lesssim 0.2^\circ$ . On the other side the ARPES method is surface-sensitive technique, since the average escape depth ( $l_{\text{esc}}$ )

of the outgoing electrons is of the order of  $l_{\text{esc}} \sim 10 \text{ \AA}$ , depending on the energy of incoming photons. Therefore, very good surfaces are needed in order that the results be representative for bulk samples. The most reliable studies were done on the bilayer  $\text{Bi}_2\text{Sr}_2\text{CaCu}_2\text{O}_8$  (*Bi2212*) and its single-layer counterpart  $\text{Bi}_2\text{Sr}_2\text{CuO}_6$  (*Bi2201*), since these materials contain weakly coupled BiO planes with the longest interplane separation in the cuprates. This results in a *natural cleavage* plane making these materials superior to others in ARPES experiments. After a drastic improvement of sample quality in other families of HTSC materials, the ARPES technique has become an important method in theoretical considerations. The ARPES can indirectly give information on the momentum and energy dependence of the pairing potential. Furthermore, the electronic spectrum of the (abovementioned) cuprates is highly *quasi-2D* which allows rather unambiguous determination of the initial state momentum from the measured final state momentum, since the component parallel to the surface is conserved in photoemission. In this case, the ARPES probes (under some favorable conditions) directly the single-particle spectral function  $A(\mathbf{k}, \omega)$ . In the following we discuss mainly those ARPES experiments which give evidence for the importance of the EPI in cuprates—see more in [22, 23].

ARPES measures a nonlinear response function of the electron system and it is usually analyzed in the so-called *three-step model*, where the total photoemission intensity  $I_{\text{tot}}(\mathbf{k}, \omega) \approx I_1 \cdot I_2 \cdot I_3$  is the product of three independent terms: (1)  $I_1$  that describes optical excitation of the electron in the bulk, (2)  $I_2$  that describes the scattering probability of the travelling electrons, and (3)  $I_3$  that describes the transmission probability through the surface potential barrier. The central quantity in the three-step model is  $I_1(\mathbf{k}, \omega)$  and it turns out that for  $\mathbf{k} = \mathbf{k}_{\parallel}$  it can be written in the form  $I_1(\mathbf{k}, \omega) \approx I_0(\mathbf{k}, \nu) f(\omega) A(\mathbf{k}, \omega)$  [22, 23] with  $I_0(\mathbf{k}, \nu) \sim |\langle \psi_f | \mathbf{p} \mathbf{A} | \psi_i \rangle|^2$  and the quasiparticle spectral function  $A(\mathbf{k}, \omega) = -\text{Im} G(\mathbf{k}, \omega)/\pi$ :

$$A(\mathbf{k}, \omega) = -\frac{1}{\pi} \frac{\text{Im} \Sigma(\mathbf{k}, \omega)}{[\omega - \xi(\mathbf{k}) - \text{Re} \Sigma(\mathbf{k}, \omega)]^2 + \text{Im} \Sigma^2(\mathbf{k}, \omega)}. \quad (37)$$

Here,  $\langle \psi_f | \mathbf{p} \cdot \mathbf{A} | \psi_i \rangle$  is the dipole matrix element which depends on  $\mathbf{k}$ , polarization, and energy  $E_i$  of the incoming photons. The knowledge of the matrix element is of a great importance and its calculation from first principles was done in [133].  $f(\omega)$  is the Fermi function;  $G$  and  $\Sigma = \text{Re} \Sigma + i \text{Im} \Sigma$  are the quasiparticle Green's function and the self-energy, respectively. We summarize and comment here some important ARPES results which were obtained in the last several years and which confirm the existence of the Fermi surface and importance of EPI in the quasiparticle scattering [22, 23].

**ARPES in the Normal State. (N1)** There is well-defined Fermi surface in the metallic state of *optimally and near optimally* doped cuprates with the topology predicted by the LDA-DFT. However, the bands are narrower than LDA-DFT predicts which points to a strong quasiparticle

renormalization. (N2) The spectral lines are broad with  $|\text{Im}\Sigma(\mathbf{k}, \omega)| \sim \omega$  (or  $\sim T$  for  $T > \omega$ ) which tells us that the quasiparticle liquid is a noncanonical Fermi liquid for larger values of  $T, \omega$ . (N3) There is a bilayer band splitting in *Bi2212* (at least in the overdoped state), which is also predicted by LDA-DFT. In the case when the coherent hopping  $t^\perp$  between two layers in the bilayer dominates, then the antibonding and bonding bands  $\xi_{\mathbf{k}}^{a,b} = \xi_{\mathbf{k}} \pm t_{\mathbf{k}}^\perp$  with  $t_{\mathbf{k}}^\perp = [t^\perp(\cos^2 k_x - \cos^2 k_y) + \dots]$  have been observed. It is worth to mention that the previous experiments did not show this splitting which was one of the reasons for various speculations on some exotic electronic scattering and non-Fermi liquid scenarios. (N4) In the underdoped cuprates and at temperatures  $T_c < T < T^*$  there is a *d*-wave-like pseudogap  $\Delta_{pg}(\mathbf{k}) \sim \Delta_{pg,0}(\cos k_x - \cos k_y)$  in the quasiparticle spectrum where  $\Delta_{pg,0}$  increases by lowering doping. We stress that the pseudogap phenomenon is not well understood at present and since we are interested in systems near optimal doping where the pseudogap phenomena are absent or much less pronounced we will not discuss this problem here. Its origin can be due to a precursor superconductivity or due to a competing order, such as spin- or charge-density wave, strong correlations, and so forth. (N5) The ARPES self-energy gives evidence that EPI interaction is rather strong. The arguments for the latter statement are the following: (i) at  $T > T_c$  there are *kinks* in the quasiparticle dispersion  $\omega(\xi_{\mathbf{k}})$  in the *nodal* direction (along the  $(0,0) - (\pi, \pi)$  line) at the characteristic phonon energy  $\omega_{\text{ph}}^{(70)} \sim (60\text{--}70)\text{ meV}$  [91], see Figure 14 (top), and near the *antinodal point*  $(\pi, 0)$  at 40 meV [134]—see Figure 14 (bottom).

(ii) The kink structure is observed in a variety of the hole-doped cuprates such as *LSCO*, *Bi2212*, *Bi2201*, *Tl2201* ( $\text{Ti}_2\text{Ba}_2\text{CuO}_6$ ), *Na-CCOC* ( $\text{Ca}_{2-x}\text{Na}_x\text{CuO}_2\text{Cl}_2$ ). These kinks exist also above  $T_c$ , which excludes the scenario with the magnetic resonance peak in  $\text{Im}\chi_s(\mathbf{Q}, \omega)$ . Moreover, since the tunnelling and magnetic neutron scattering measurements give small SFI coupling constant  $g_{\text{sf}} < 0.2\text{ eV}$ , then the kinks are not due to SFI. (iii) The position of the nodal kink is practically doping independent which points towards phonons as the scattering and pairing boson. (N6) The quasiparticles (holes) at and near the nodal-point  $\mathbf{k}_N$  couple practically to a rather broad spectrum of phonons since at least three groups of phonons were extracted in the bosonic spectral function  $\alpha^2 F(\mathbf{k}_N, \omega)$  from the ARPES effective self-energy in  $\text{La}_{2-x}\text{Sr}_x\text{CuO}_4$  [135]—Figure 15.

The latter result is in a qualitative agreement with numerous tunnelling measurements [42–54] which apparently demonstrate that the very broad spectrum of phonons couples with holes without preferring any particular phonons—see discussion below. (N7) Recent ARPES measurements in *Bi2212* [92] show very different slope  $d\omega/d\xi_{\mathbf{k}}$  of the quasiparticle energy  $\omega(\xi_{\mathbf{k}})$  at small  $|\xi_{\mathbf{k}}| \ll \omega_{\text{ph}}$  and at large energies  $|\xi_{\mathbf{k}}| \gg \omega_{\text{ph}}$ —see Figure 16. The theoretical analysis [137] of these results gives the total coupling constant  $\lambda^Z = \lambda_{ep}^Z + \lambda_c^Z \approx 3$ , and for the EPI coupling  $\lambda_{ep}^Z \approx 2$ , while the Coulomb coupling (SFI is a part of it) is  $\lambda_c^Z \approx 1$  [137]—see Figure 16. (Note that the upper index *Z* in the coupling constants means the quasiparticle renormalization in the

normal part of the self-energy.) To this end let us mention some confusion which is related to the value of the EPI coupling constant extracted from ARPES. Namely, [22, 23, 138, 139] the EPI self-energy was obtained by subtracting the high-energy slope of the quasiparticle spectrum  $\omega(\xi_{\mathbf{k}})$  at  $\omega \sim 0.3\text{ eV}$ . The latter is apparently due to the Coulomb interaction. Although the position of the low-energy kink is not affected by this procedure (if  $\omega_{\text{ph}}^{\text{max}} \ll \omega_c$ ), this subtraction procedure gives in fact an *effective EPI self-energy*  $\Sigma_{\text{eff}}^{ep}(\mathbf{k}, \omega)$  and *the effective coupling constant*  $\lambda_{ep,\text{eff}}^Z(\mathbf{k})$  only. We demonstrate below that the  $\lambda_{ep,\text{eff}}^Z(\mathbf{k})$  is smaller than the real EPI coupling constant  $\lambda_{ep}^Z(\mathbf{k})$ . The total self-energy is  $\Sigma(\mathbf{k}, \omega) = \Sigma^{ep}(\mathbf{k}, \omega) + \Sigma^c(\mathbf{k}, \omega)$  where  $\Sigma^c$  is the contribution due to the Coulomb interaction. At very low energies  $\omega \ll \omega_c$  one has usually  $\Sigma^c(\mathbf{k}, \omega) = -\lambda_c^Z(\mathbf{k})\omega$ , where  $\omega_c$  ( $\sim 1\text{ eV}$ ) is the characteristic Coulomb energies and  $\lambda_c^Z$  is the Coulomb coupling constant. The quasiparticle spectrum  $\omega(\mathbf{k})$  is determined from the condition  $\omega - \xi(\mathbf{k}) - \text{Re}[\Sigma^{ep}(\mathbf{k}, \omega) + \Sigma^c(\mathbf{k}, \omega)] = 0$  where  $\xi(\mathbf{k})$  is the bare band-structure energy. At low energies  $\omega < \omega_{\text{ph}}^{\text{max}} \ll \omega_c$  it can be rewritten in the form

$$\omega - \xi^{\text{ren}}(\mathbf{k}) - \text{Re}\Sigma_{\text{eff}}^{ep}(\mathbf{k}, \omega) = 0, \quad (38)$$

with  $\xi^{\text{ren}}(\mathbf{k}) = [1 + \lambda_c^Z(\mathbf{k})]^{-1}\xi(\mathbf{k})$ ,

$$\text{Re}\Sigma_{\text{eff}}^{ep}(\mathbf{k}, \omega) = \frac{\text{Re}\Sigma_{\text{eff}}^{ep}(\mathbf{k}, \omega)}{1 + \lambda_c^Z(\mathbf{k})}. \quad (39)$$

Since at very low energies  $\omega \ll \omega_{\text{ph}}^{\text{max}}$  one has  $\text{Re}\Sigma^{ep}(\mathbf{k}, \omega) = -\lambda_{ep}^Z(\mathbf{k})\omega$  and  $\text{Re}\Sigma_{\text{eff}}^{ep}(\mathbf{k}, \omega) = -\lambda_{ep,\text{eff}}^Z(\mathbf{k})\omega$ , then the real coupling constant is related to the effective one by

$$\lambda_{ep}^Z(\mathbf{k}) = [1 + \lambda_c^Z(\mathbf{k})]\lambda_{ep,\text{eff}}^Z(\mathbf{k}). \quad (40)$$

As a result one has  $\lambda_{ep}^Z(\mathbf{k}) > \lambda_{ep,\text{eff}}^Z(\mathbf{k})$ . At higher energies  $\omega_{\text{ph}}^{\text{max}} < \omega < \omega_c$ , where the EPI effects are suppressed and  $\Sigma^{ep}(\mathbf{k}, \omega)$  stops growing, one has  $\text{Re}\Sigma(\mathbf{k}, \omega) \approx \text{Re}\Sigma^{ep}(\mathbf{k}, \omega) - \lambda_c^Z(\mathbf{k})\omega$ . The measured  $\text{Re}\Sigma^{\text{exp}}(\mathbf{k}, \omega)$  at  $T = 10\text{ K}$  near and slightly away from the *nodal point* in the optimally doped *Bi2212* with  $T_c = 91\text{ K}$  [136] is shown in Figure 16.

It is seen that  $\text{Re}\Sigma^{\text{exp}}(\mathbf{k}, \omega)$  has *two kinks*—the first one at *low energy*  $\omega_1 \approx \omega_{\text{ph}}^{\text{high}} \approx 50\text{--}70\text{ meV}$  which is (as we already argued) most probably of the phononic origin [22, 23, 138, 139], while the second kink at *higher energy*  $\omega_2 \approx \omega_c \approx 350\text{ meV}$  which is due to the Coulomb interaction. However, the important results in [136] are that the slopes of  $\text{Re}\Sigma^{\text{exp}}(\mathbf{k}, \omega)$  at low ( $\omega < \omega_{\text{ph}}^{\text{high}}$ ) and high energies ( $\omega_{\text{ph}}^{\text{high}} < \omega < \omega_c$ ) are very *different*. The low-energy and high-energy slope *near the nodal point* are shown in Figure 16 schematically (thin lines). From Figure 16 it is obvious that EPI prevails at low energies  $\omega < \omega_{\text{ph}}^{\text{high}}$ . More precisely digitalization of  $\text{Re}\Sigma^{\text{exp}}(\mathbf{k}, \omega)$  in the interval  $\omega_{\text{ph}}^{\text{high}} < \omega < 0.4\text{ eV}$  gives the Coulomb coupling  $\lambda_c^Z \approx 1.1$  while the same procedure at  $20\text{ meV} \approx \omega_{\text{ph}}^{\text{low}} < \omega < \omega_{\text{ph}}^{\text{high}} \approx 50\text{--}70\text{ meV}$  gives the total coupling constant ( $\lambda_2 \equiv$ )  $\lambda^Z = \lambda_{ep}^Z + \lambda_c^Z \approx 3.2$  and the EPI coupling constant  $\lambda_{ep}^Z (\equiv \lambda_{ep,\text{high}}^Z) \approx$

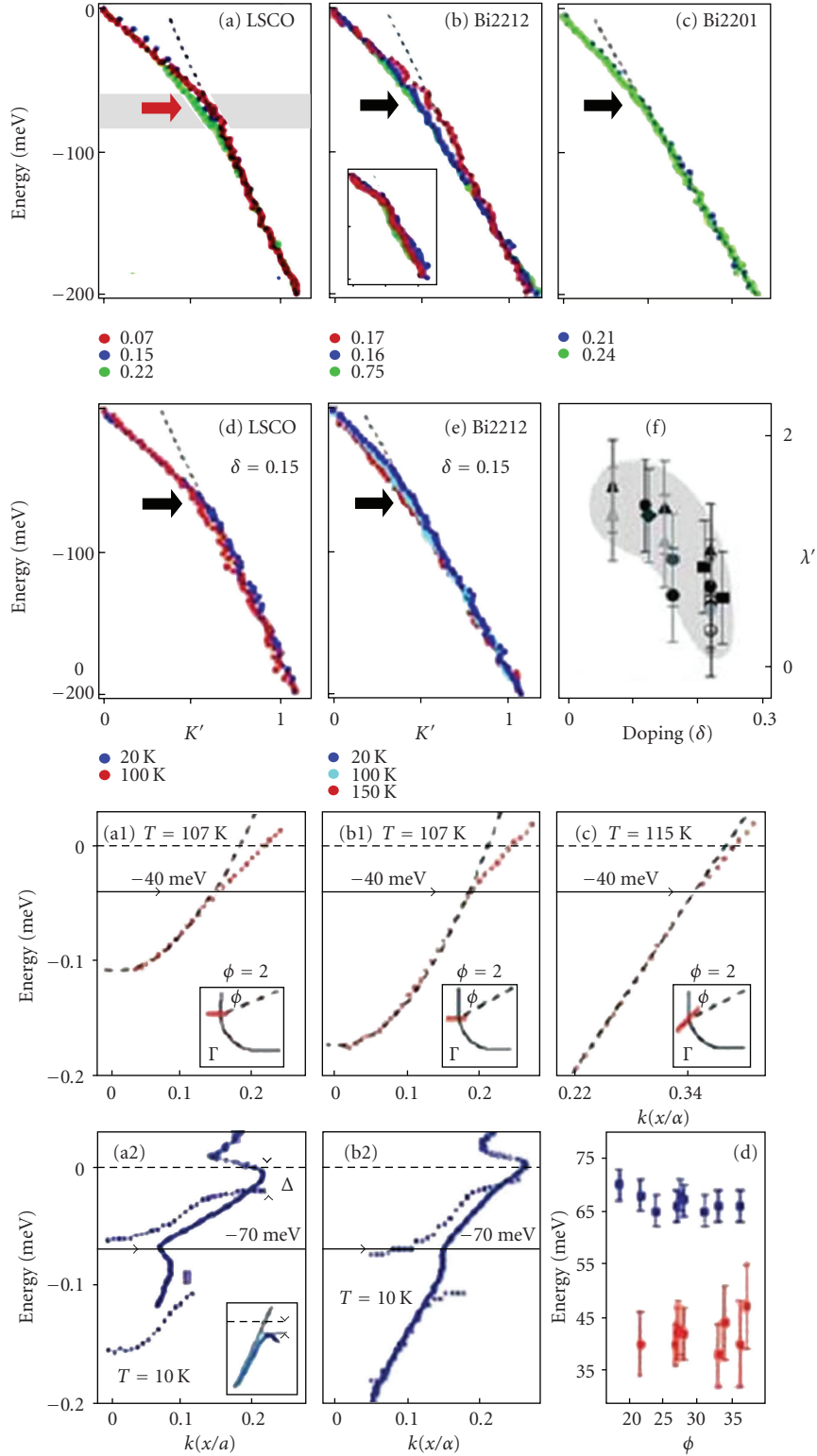


FIGURE 14: (top) Quasiparticle dispersion of *Bi2212*, *Bi2201*, and *LSCO* along the *nodal* direction, plotted versus the momentum  $k$  for (a)–(c) different doping, and (d)–(e) different  $T$ ; black arrows indicate the kink energy; the red arrow indicates the energy of the  $q = (\pi, 0)$  oxygen stretching phonon mode; inset of (e) shows  $T$ -dependent  $\Sigma'$  for optimally doped *Bi2212*; (f) shows doping dependence of the effective coupling constant  $\lambda'$  along  $(0, 0) - (\pi, \pi)$  for the different HTSC oxides. From [91]. (bottom) Quasiparticle dispersion  $E(k)$  in the normal state (a1, b1, c), at 107 K and 115 K, along various directions  $\phi$  around the *antinodal* point. The kink at  $E = 40$  meV is shown by the horizontal arrow. (a2 and b2) are  $E(k)$  in the superconducting state at 10 K with the shifted kink to 70 meV. (d) kink positions as a function of  $\phi$  in the antinodal region. From [134].

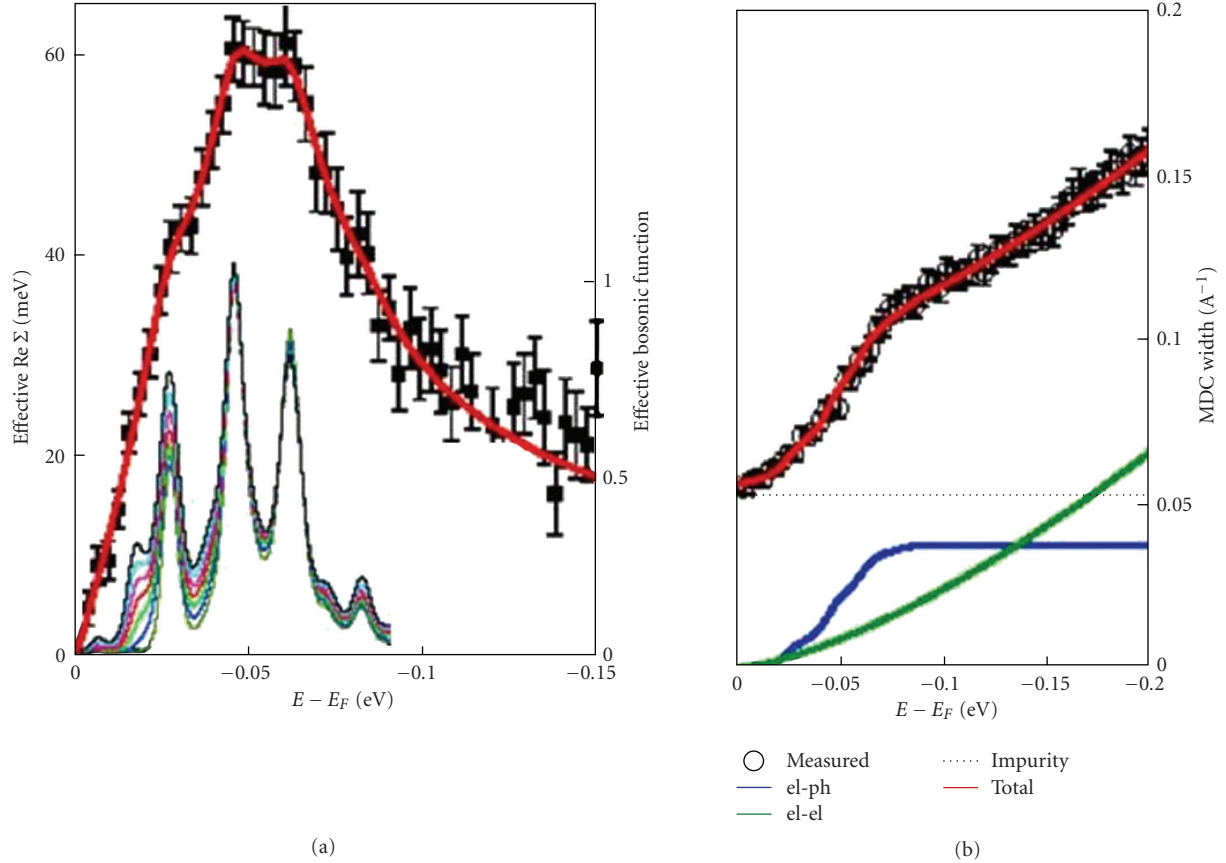


FIGURE 15: (a) Effective real self-energy for the nonsuperconducting  $\text{La}_{2-x}\text{Sr}_x\text{CuO}_4$ ,  $x = 0.03$ . Extracted  $\alpha_{\text{eff}}^2(\omega)F(\omega)$  is in the inset. (b) Top: the total MDC width—open circles. Bottom: the EPI contribution shows saturation, impurity contribution—dotted black line. The residual part is growing  $\sim \omega^{-1.3}$ . From [135].

$2.1 > 2\lambda_{ep,\text{eff}}^Z(\mathbf{k})$ , that is, the EPI coupling is at least twice larger than the effective EPI coupling constant obtained in the previous analysis of ARPES results [22, 23, 138, 139]. This estimation tells us that at (and near) the nodal point, *the EPI interaction dominates* in the quasiparticle scattering at low energies since  $\lambda_{ep}^Z(\approx 2.1) \approx 2\lambda_c^Z > 2\lambda_{sf}^Z$ , while at large energies (compared to  $\omega_{\text{ph}}$ ) the Coulomb interaction with  $\lambda_c^Z \approx 1.1$  dominates. We point out that EPI near the antinodal point can be even larger than in the nodal point, mostly due to the higher density of states near the antinodal point. (N8) Recent ARPES spectra in the optimally doped  $\text{Bi2212}$  near the nodal and antinodal point [139] show a low-energy isotope effect in  $\text{Re}\Sigma^{\text{exp}}(\mathbf{k}, \omega)$ , which can be well described in the framework of the Migdal-Eliashberg theory for EPI [140]. At higher energies  $\omega > \omega_{\text{ph}}$  obtained in [139] very pronounced isotope effect cannot be explained by the simple Migdal-Eliashberg theory [140]. However, there are controversies with the strength of the high-energy isotope effect since it was not confirmed in other measurements [141, 142]—see the discussion in Section 1.3.6(2) related to the isotope effects in HTSC cuprates. (N9) The ARPES experiments in  $\text{Ca}_2\text{CuO}_2\text{Cl}_2$  give strong evidence for the formation of *small polarons in undoped cuprates* which are due to phonons and strong EPI, while in the doped systems

quasiparticles are formed and there are no small polarons [143]. Namely, in [143] a broad peak around  $-0.8\text{eV}$  is observed at the top of the band ( $\mathbf{k} = (\pi/2, \pi/2)$ ) with the dispersion similar to that predicted by the  $t$ - $J$  model—see Figure 17.

However, the peak in Figure 17(a) is of Gaussian shape and can be described only by coupling to bosons, that is, this peak is a boson side band—see more in [10, 11] and references therein. The theory based on the  $t$ - $J$  model (in the antiferromagnetic state of the undoped compound) by including coupling to several (half-breathing, apical oxygen, low-lying) phonons, which is given in [144–146], explains successfully this broad peak of the boson side band by the formation of small polarons due to the EPI coupling ( $\lambda_{ep} \approx 1.2$ ). Note that this value of  $\lambda_{ep}$  is for the polaron at the bottom of the band while in the case where the Fermi surface exists (in doped systems) this coupling is even larger due to the larger density of states at the Fermi surface [144–146]. In [144–146] it was stressed that even when the electron-magnon interaction is stronger than EPI the polarons in the undoped systems are formed due to EPI. The latter mechanism involves excitation of many phonons at the lattice site (where the hole is seating), while it is possible to excite only one magnon at the given site. (N10) Recent

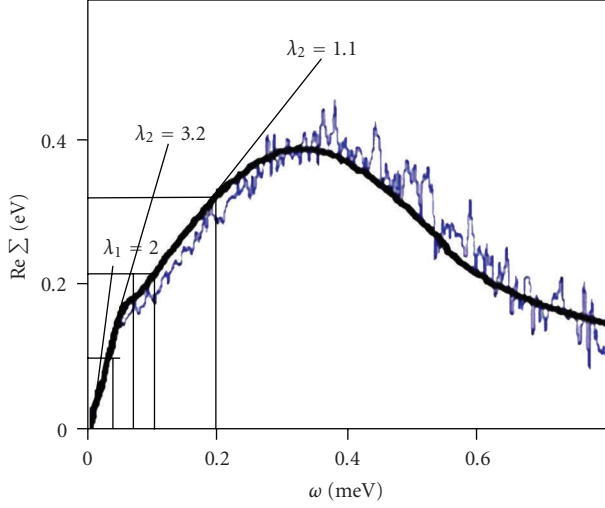


FIGURE 16: Figure 4b from [136]:  $\text{Re } \Sigma(\omega)$  measured in *Bi2212* (thin line) and model  $\text{Re } \Sigma(\omega)$  (bold line) obtained in [136]. The three thin lines ( $\lambda_1, \lambda_2, \lambda_3$ ) are the slopes of  $\text{Re } \Sigma(\omega)$  in different energy regions—see the text.

soft X-ray ARPES measurements on the *electron-doped* HTSC  $\text{Nd}_{1.85}\text{Ce}_{0.15}\text{CuO}_4$  [147], and  $\text{Sm}_{(2-x)}\text{Ce}_x\text{CuO}_4$  ( $x = 0.1, 0.15, 0.18$ ),  $\text{Nd}_{1.85}\text{Ce}_{0.15}\text{CuO}_4$ , and  $\text{Eu}_{1.85}\text{Ce}_{0.15}\text{CuO}_4$  [148] show kink at energies 50–70 meV in the quasiparticle dispersion relation along both the nodal and antinodal, directions as it is shown in Figure 18.

It is seen from this figure that the effective EPI coupling constant  $\lambda_{ep, \text{eff}} (< \lambda_{ep})$  is isotropic and  $\lambda_{ep, \text{eff}} \approx 0.8\text{--}1$ . It seems that the kink in the electron-doped cuprates is due solely to EPI and in that respect the situation is similar to the one in the hole-doped cuprates.

**ARPES Results in the Superconducting State.** (S1) There is an anisotropic superconducting gap in most HTSC compounds [22, 23], which is predominately *d*-wave like, that is,  $\Delta(\mathbf{k}) \approx \Delta_0(\cos k_x - \cos k_y)$  with  $2\Delta_0/T_c \approx 5\text{--}6$  in the optimally doped systems. (S2) The particle-hole coherence in the superconducting state which is expected for the BCS-like theory of superconductivity has been observed first in [149] and confirmed with better resolution in [150], where the particle-hole mixing is clearly seen in the electron and hole quasiparticle dispersion. To remind the reader, the excited Bogoliubov-Valatin quasiparticles ( $\hat{\alpha}_{\mathbf{k}, \pm}$ ) with energies  $E_{\mathbf{k}}^{\alpha_{\pm}} = \sqrt{\xi_{\mathbf{k}}^2 + |\Delta_{\mathbf{k}}|^2}$  are a mixture of electron ( $\hat{c}_{\mathbf{k}, \sigma}$ ) and hole ( $\hat{c}_{-\mathbf{k}, -\sigma}^\dagger$ ), that is,  $\hat{\alpha}_{\mathbf{k}, +} = u_{\mathbf{k}}\hat{c}_{\mathbf{k}, +} + v_{\mathbf{k}}\hat{c}_{-\mathbf{k}, -}^\dagger$ ,  $\hat{\alpha}_{\mathbf{k}, -} = u_{\mathbf{k}}\hat{c}_{-\mathbf{k}, -} + v_{\mathbf{k}}\hat{c}_{\mathbf{k}, +}^\dagger$  where the coherence factors  $u_{\mathbf{k}}, v_{\mathbf{k}}$  are given by  $|u_{\mathbf{k}}|^2 = 1 - |v_{\mathbf{k}}|^2 = (1 + \xi_{\mathbf{k}}/E_{\mathbf{k}})/2$ . Note that  $|u_{\mathbf{k}}|^2 + |v_{\mathbf{k}}|^2 = 1$ , which is exactly observed, together with *d*-wave pairing  $\Delta(\mathbf{k}) = \Delta_0(\cos k_x - \cos k_y)$ , in experiments in [150]. This is very important result since it proves that the *pairing in HTSC cuprates is of the BCS type* and not exotic one as it was speculated long time after the discovery of HTSC cuprates. (S3) The kink at (60–70) meV in the quasiparticle energy around the nodal point is *not shifted* (in energy) while the antinodal kink at  $\omega_{\text{ph}}^{(40)} \sim 40$  meV is *shifted* (in energy) in the superconducting

state by  $\Delta_0 (= (25\text{--}30) \text{ meV})$ , that is,  $\omega_{\text{ph}}^{(40)} \rightarrow \omega_{\text{ph}}^{(40)} + \Delta_0 = (65\text{--}70) \text{ meV}$  [22, 23]. To remind the reader, in the standard Eliashberg theory the kink in the normal state at  $\omega = \omega_{\text{ph}}$  should be shifted in the superconducting state to  $\omega_{\text{ph}} + \Delta_0$  at all  $\mathbf{k}$ -points at the Fermi surface. This puzzling result (that the quasiparticle energy around the nodal point is *not shifted* in the superconducting state) might be a smoking gun result since it makes an additional constraint on the quasiparticle interaction in cuprates. Until now there is only one plausible explanation [151] of this *nonshift puzzle* which is based on an assumption of the forward scattering peak (FSP) in EPI—see more in Section 2. The FSP in EPI means that electrons scatter into a narrow region ( $q < q_c \ll k_F$ ) around the initial point in the  $k$ -space, so that at the most part of the Fermi surface there is practically no mixing of states with different signs of the order parameter  $\Delta(\mathbf{k})$ . In that case the EPI bosonic spectral function (which is defined in Appendix A)  $\alpha^2 F(\mathbf{k}, \mathbf{k}', \Omega) \approx \alpha^2 F(\varphi, \varphi', \Omega)$  ( $\varphi$  is the angle on the Fermi surface) has a pronounced forward scattering peak (at  $\delta\varphi = \varphi - \varphi' = 0$ ) due to strong correlations—see Section 2. Its width  $\delta\varphi_c$  is narrow, that is,  $\delta\varphi_c \ll 2\pi$  and the angle integration goes over the region  $\delta\varphi_c$  around the point  $\varphi$ . In that case the kink is shifted (approximately) by the local gap  $\Delta(\varphi) = \Delta_{\text{max}} \cos 2\varphi$ —for more details see [151]. As a consequence, the antinodal kink is shifted by the maximal gap, that is,  $|\Delta(\varphi_{\text{AN}} \approx \pi/2)| = \Delta_{\text{max}}$  while the nodal gap is practically unshifted since  $|\Delta(\varphi_{\text{AN}} \approx \pi/4)| \approx 0$ . (S4) The recent ARPES spectra [152] in the undoped single crystalline 4-layered cuprate with the apical fluorine (F),  $\text{Ba}_2\text{Ca}_3\text{Cu}_4\text{O}_8\text{F}_2$  (F0234) give rather convincing evidence against the SFI mechanism of pairing—see Figure 19.

*First*, F0234 is not a Mott insulator—as expected from valence charge counting which puts Cu valence as  $2^+$ , but it is a superconductor with  $T_c = 60$  K. Moreover, the ARPES data [152] reveal at least two metallic Fermi-surface sheets with corresponding volumes equally below and above half-filling—see Figure 20.

*Second*, one of the Fermi surfaces is due to the electron-like (*N*) band (with  $20 \pm 6\%$  electron-doping) and the other one due to the hole-like (*P*) band (with  $20 \pm 8\%$  hole-doping) and their splitting along the nodal direction is significant and cannot be explained by the LDA-DFT calculations [153]. This electron and hole *self-doping of inner and outer layers* is in an appreciable contrast to other multilayered cuprates where there is only hole self-doping. For instance, in  $\text{HgBa}_2\text{Ca}_n\text{Cu}_{n+1}\text{O}_{2n+2}$  ( $n = 2, 3$ ) and  $(\text{Cu}, \text{C})\text{Ba}_2\text{Ca}_n\text{Cu}_{n+1}\text{O}_{3n+2}$  ( $n = 2, 3, 4$ ), the inner  $\text{CuO}_2$  layers are less hole-doped than outer layers. It turns out, unexpectedly, that the *superconducting gap on the N-band Fermi surface is significantly larger than on the P-one*, where in  $\text{Ba}_2\text{Ca}_3\text{Cu}_4\text{O}_8\text{F}_2$  the ratio is anomalous ( $\Delta_N/\Delta_P \approx 2$  and  $\Delta_N$  is an order of magnitude larger than in the electron-doped cuprate  $\text{Nd}_{2-x}\text{Ce}_x\text{CuO}_4$ ). *Third*, the *N-band Fermi surface is rather far from the antinodal point at  $(\pi, 0)$* . This is very important result which means that the antiferromagnetic spin fluctuations with the AF wave-vector  $\mathbf{Q} = (\pi, \pi)$ , as well as the van Hove singularity, are not dominant in the pairing in the *N*-band. To remind the reader, the SFI scenario assumes that the pairing is due to spin

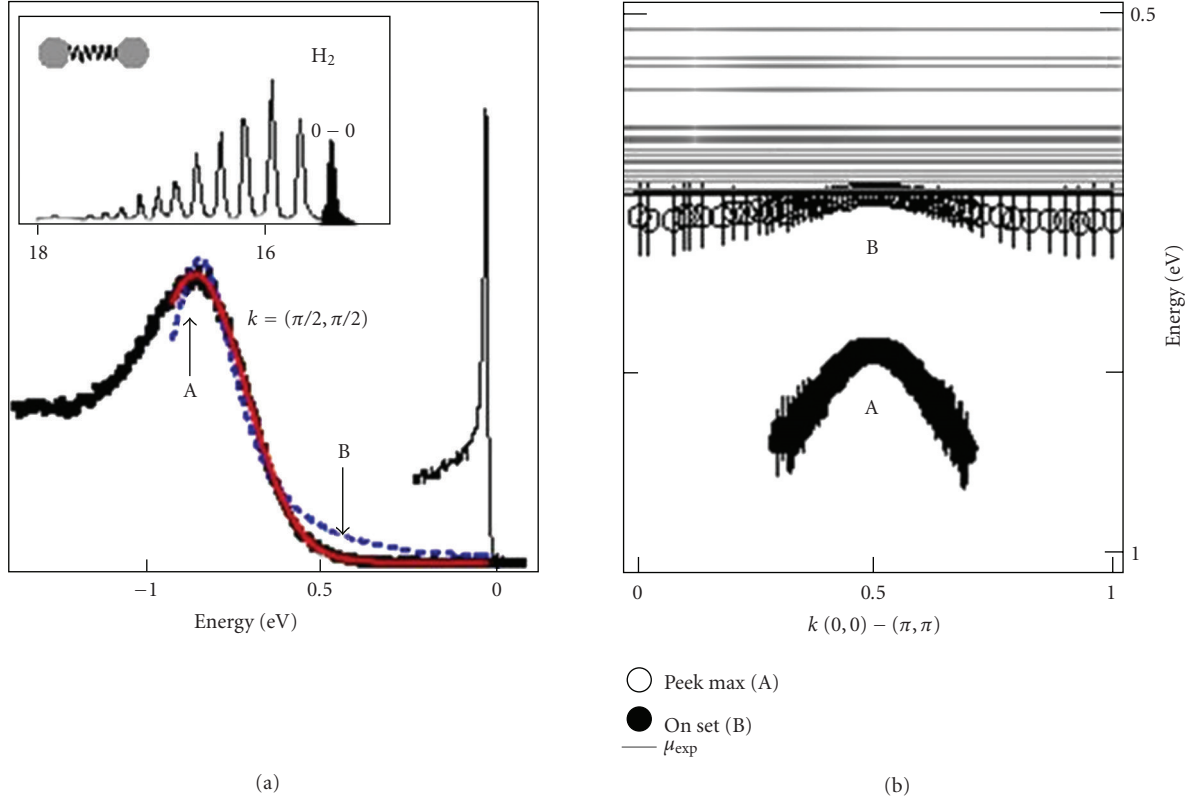


FIGURE 17: (a) The ARPES spectrum of undoped  $\text{Ca}_2\text{CuO}_2\text{Cl}_2$  at  $\mathbf{k} = (\pi/2, \pi/2)$ . Gaussian shape—solid line, Lorentzian shape—dashed line. (b) Dispersion of the polaronic band—A—and of the quasiparticle band—B—along the nodal direction. Horizontal lines are the chemical potentials for a large number of samples. From [143].

fluctuations with the wave-vector  $\mathbf{Q}$  (and near it) which connects two antinodal points which are near the van Hove singularity at the hole-surface (at  $(\pi, 0)$  and  $(0, \pi)$ ) giving rise to large density of states. This is apparently not the case for the  $N$ -band Fermi surface—see Figure 20. The ARPES data give further that there is a kink at  $\sim 85$  meV in the quasiparticle dispersion of both bands, while the kink in the  $N$ -band is stronger than that in the  $P$ -band. This result, together with the anomalous ratio  $(\Delta_N/\Delta_P) \approx 2$ , disfavors SFI as a pairing mechanism. (S5) Despite the presence of significant elastic quasiparticle scattering in a number of samples of optimally doped Bi-2212, there are dramatic sharpenings of the spectral function near the antinodal point  $(\pi, 0)$  at  $T < T_c$  (in the superconducting state) [154]. This effect can be explained by assuming that the small  $q$ -scattering (the forward scattering peak) dominates in the elastic impurity scattering as it is pointed in [78–80, 130, 155, 156]. As a result, one finds that the impurity scattering rate in the superconducting state is almost zero, that is,  $\gamma_{\text{imp}}(\mathbf{k}, \omega) = \gamma_n(\mathbf{k}, \omega) + \gamma_a(\mathbf{k}, \omega) \approx 0$  for  $|\omega| < \Delta_0$  for any kind of pairing ( $s$ -,  $p$ -,  $d$ -wave, etc.) since the normal ( $\gamma_n$ ) and the anomalous ( $\gamma_a$ ) scattering rates compensate each other. This *collapse of the elastic scattering rate* is elaborated in details in [154] and it is a consequence of the Anderson-like theorem for unconventional superconductors which is due to the dominance of the small  $q$ -scattering [78–80, 130, 155, 156]. In such a case  $d$ -wave pairing is weakly unaffected by nonmagnetic impurities and as a consequence there is

small reduction in  $T_c$  [156, 157]. The physics behind this result is rather simple. The small  $q$ -scattering (usually called forward scattering) means that electrons scatter into a small region in the  $k$ -space, so that at the most part of the Fermi surface there is no mixing of states with different signs of the order parameter  $\Delta(\mathbf{k})$ . In such a way the detrimental effect of nonmagnetic impurities on  $d$ -wave pairing is significantly reduced. This result points to the importance of strong correlations in the renormalization of the nonmagnetic impurity scattering too—see discussion in Section 2.

In conclusion, in order to explain the ARPES results in cuprates it is necessary to take into account (1) the electron-phonon interaction (EPI) since it dominates in the quasiparticle scattering in the energy region important for pairing, (2) the elastic nonmagnetic impurities with the forward scattering peak (FSP) due to strong correlations, and (3) the Coulomb interaction which dominates at higher energies  $\omega > \omega_{\text{ph}}$ . In this respect, the presence of ARPES kinks and the knee-like shape of the  $T$  dependence of the spectral width are important constraints on the scattering and pairing mechanism in HTSC cuprates.

**1.3.4. Tunnelling Spectroscopy and Spectral Function  $\alpha^2F(\omega)$ .** By measuring current-voltage  $I$ - $V$  characteristics in NIS (normal metal-insulator-superconductor) tunnelling junctions with large tunnelling barrier one obtains from tunnelling conductance  $G_{\text{NIS}}(V) = dI/dV$  the so called tunnelling density of states in superconductors  $N_T(\omega)$ .

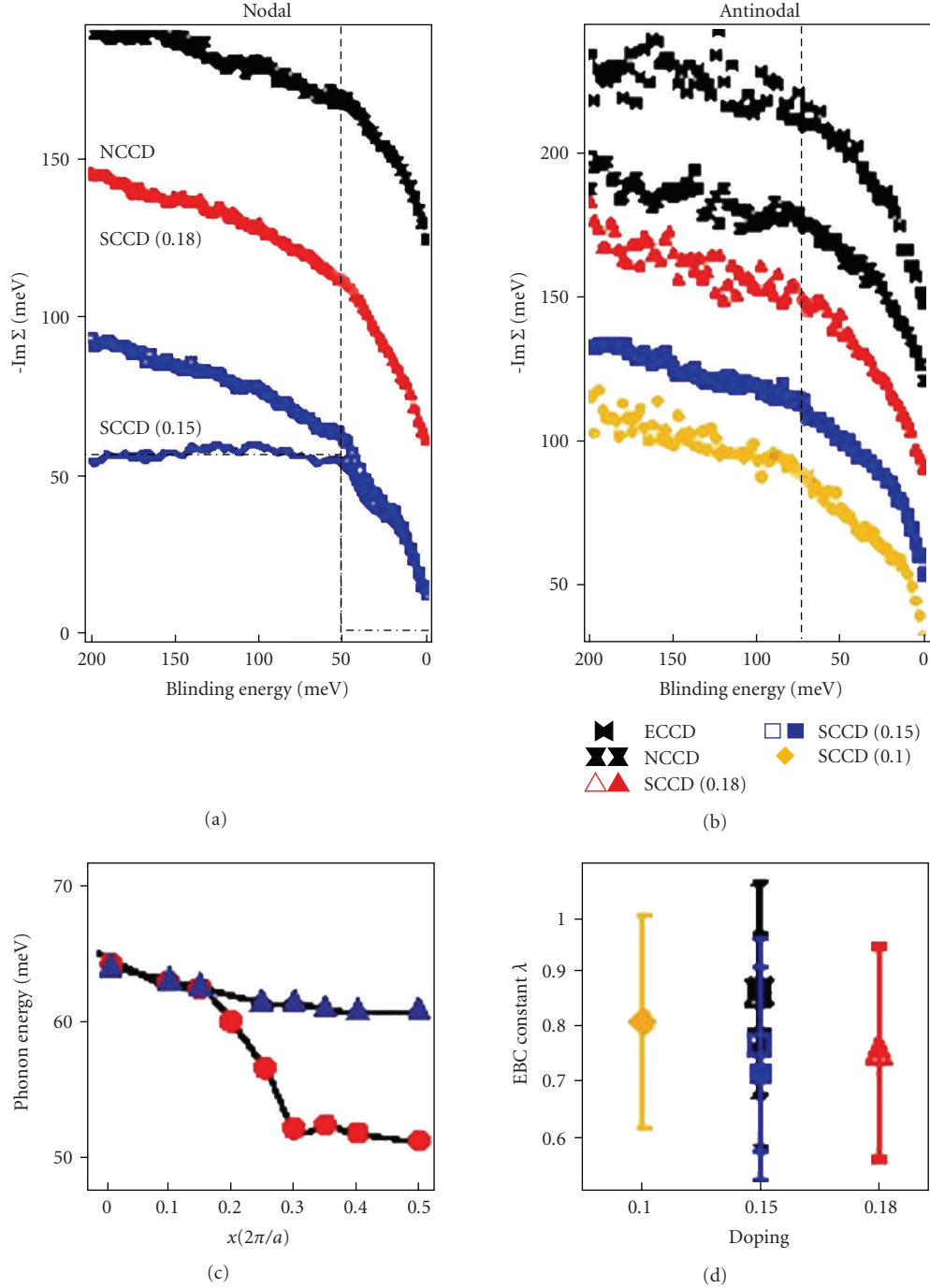


FIGURE 18: NCCO electron-doped: (a)  $\text{Im} \Sigma(\omega)$  measured in the nodal point. Curves are offsets by 50 meV for clarity. The change of the slope in the last bottom curve is at the phonon energy. (b)  $\text{Im} \Sigma(\omega)$  for the antinodal direction with 30 meV offset. (c) Experimental phonon dispersion of the bond stretching modes. (d) Estimated  $\lambda_{\text{eff}}^{\text{ep}}$  from  $\text{Im} \Sigma(\omega)$ . From [148].

Moreover, by measuring of  $G_{\text{NS}}(V)$  at voltages  $eV > \Delta$  it is possible to determine the Eliashberg spectral function  $\alpha^2 F(\omega)$  and finally to confirm the phonon mechanism of pairing in *LTSC* materials. Four tunnelling techniques were used in the study of *HTSC* cuprates: (1) vacuum tunnelling by using the *STM* technique—scanning tunnelling microscope; (2) point-contact tunnelling; (3) break-junction tunnelling; (4) planar-junction tunnelling. Each of these

techniques has some advantages although in principle the most potential one is the *STM* technique since it measures superconducting properties locally [158]. Since tunnelling measurements probe a surface region on the scale of the superconducting coherence length  $\xi_0$ , then this kind of measurements in *HTSC* materials with small coherence length  $\xi_0$  ( $\xi_{ab} \sim 20 \text{ \AA}$  in the  $a - b$  plane and  $\xi_c \sim 1-3 \text{ \AA}$  along the  $c$ -axis) depends strongly on the surface quality

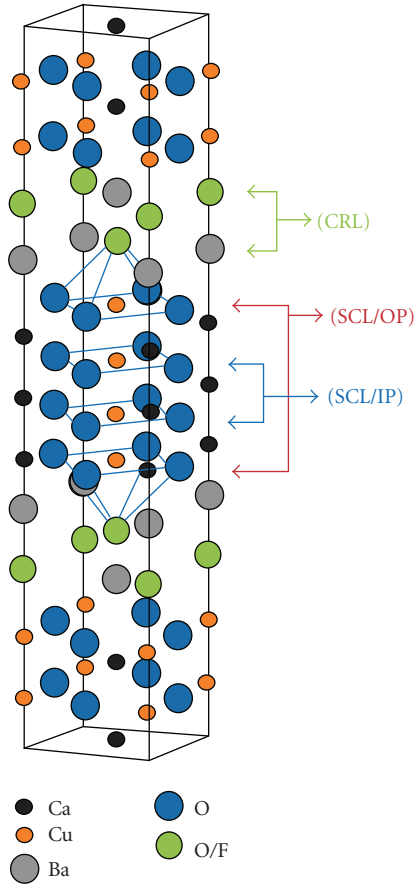


FIGURE 19: Crystal structure of  $\text{Ba}_2\text{Ca}_3\text{Cu}_4\text{O}_8(\text{O}_\delta\text{F}_{1-\delta})_2$ . There are four  $\text{CuO}_2$  layers in a unit cell with the outer having apical F atoms. CRL—charge reservoir layer; SCL/OP—superconducting layer/outer plane; SCL/IP—superconducting layer/inner plane. From [152].

and sample preparation. Nowadays, many of the material problems in *HTSC* cuprates are understood and as a result consistent picture of tunnelling features is starting to emerge.

From tunnelling experiments one obtains the (energy-dependent) gap function  $\Delta(\omega)$  in the superconducting state. Since we have already discussed this problem in [6], we will only briefly mention some important result. For instance, in most systems  $G_{\text{NS}}(V)$  has  $V$ -shape in all families of *HTSC* hole- and electron-doped cuprates. The  $V$ -shape is characteristic for  $d$ -wave pairing with gapless spectrum, which is also confirmed in the interference experiments on hole- and electron-doped cuprates [75]. Some experiments give a  $U$ -shape of  $G_{\text{NS}}(V)$  which resembles  $s$ -wave pairing. This controversy is explained to be the property of the tunnelling matrix element which filters out states with the maximal gap.

Here we are interested in the *bosonic spectral function*  $\alpha^2F(\omega)$  of *HTSC* cuprates *near optimal doping* which can be extracted by using tunnelling spectroscopy. We inform the reader in advance that the shape and the energy width of  $\alpha^2F(\omega)$ , which are extracted from the second derivative  $d^2I/dV^2$  at voltages above the superconducting gap, in most *HTSC* cuprates resemble the phonon density of states  $F_{\text{ph}}(\omega)$ .

This result is strong evidence for the importance of *EPI* in the pairing potential of *HTSC* cuprates. For instance, plenty of break junctions made from *Bi2212* single crystals [42–45] show that the peaks (and shoulders) in  $-d^2I/dV^2$  (or dips-negative peaks in  $d^2I/dV^2$ ) coincide with the peaks (and shoulders) in the phonon density of states  $F_{\text{ph}}(\omega)$  measured by neutron scattering—see Figure 21.

The tunnelling spectra in *Bi-2212* break junctions [42–45], which are shown in Figure 21 indicates that the spectral function  $\alpha^2F(\omega)$  is independent of magnetic field, which is in contradiction with the theoretical prediction based on the SFI pairing mechanism where this function should be sensitive to magnetic field. The reported broadening of the peaks in  $\alpha^2F(\omega)$  is partly due to the gapless spectrum of  $d$ -wave pairing in *HTSC* cuprates. Additionally, the tunnelling density of states  $N_T(\omega)$  at very low  $T$  and for  $\omega > \Delta$  shows a pronounced gap structure. It was found that  $2\bar{\Delta}/T_c = 6.2\text{--}6.5$ , where  $T_c = 74\text{--}85\text{ K}$  and  $\bar{\Delta}$  is some average value of the gap. In order to obtain  $\alpha^2F(\omega)$  the inverse procedure was used by assuming  $s$ -wave superconductivity and the effective Coulomb parameter  $\mu^* \approx 0.1$  [42–45]. The obtained  $\alpha^2F(\omega)$  gives large *EPI* coupling constant  $\lambda_{ep} \approx 2.3$ . Although this analysis [42–45] was done in terms of  $s$ -wave pairing, it mimics qualitatively the case of  $d$ -wave pairing, since one expects that  $d$ -wave pairing does not change significantly the global structure of  $d^2I/dV^2$  at  $eV > \Delta$  albeit introducing a broadening in it—see the physical meaning in Appendix A. We point out that the results obtained in [42–45] were *reproducible* on more than 30 junctions. In that respect very important results on slightly overdoped *Bi2212*–GaAs and on *Bi2212*–Au planar tunnelling junctions are obtained in [46, 47]—see Figure 22.

These results show very similar features to those obtained in [42–45] on break junctions. It is worth mentioning that several groups [48–52] have obtained similar results for the shape of the spectral function  $\alpha^2F(\omega)$  from the  $I$ - $V$  measurements on various *HTSC* cuprates—see the comparison in Figure 23. These facts leave no much doubts about the importance of the *EPI* in pairing mechanism of *HTSC* cuprates.

In that respect, the tunnelling measurements on *slightly overdoped*  $\text{Bi}_2\text{Sr}_2\text{CaCu}_2\text{O}_8$  [46, 47, 53, 54] give impressive results. The Eliashberg spectral function  $\alpha^2F(\omega)$  of this compound was extracted from the measurements of  $d^2I/dV^2$  and by solving the inverse problem—see Appendix A. The extracted  $\alpha^2F(\omega)$  has several peaks in broad energy region up to 80 meV as it is seen in Figures 22 and 23, which coincide rather well with the peaks in the phonon density of states  $F_{\text{ph}}(\omega)$ —more precisely the generalized phonon density of states  $GPDS(\omega)$  defined in Appendix A. In [53, 54] numerous peaks, from  $P1$ – $P13$ , in  $\alpha^2F(\omega)$  are discerned as shown in Figure 24, which correspond to various groups of phonon modes—laying in (and around) these peaks. Moreover, in [46, 47, 53, 54] the coupling constants for these modes are extracted as well as their contribution ( $\Delta T_c$ ) to  $T_c$  as it is seen in Table 1. Note that due to the nonlinearity of the problem the sum of  $(\Delta T_c)_i$ ,  $i = 1, 2, \dots, 13$ , due to various modes is not equal to  $T_c$ .

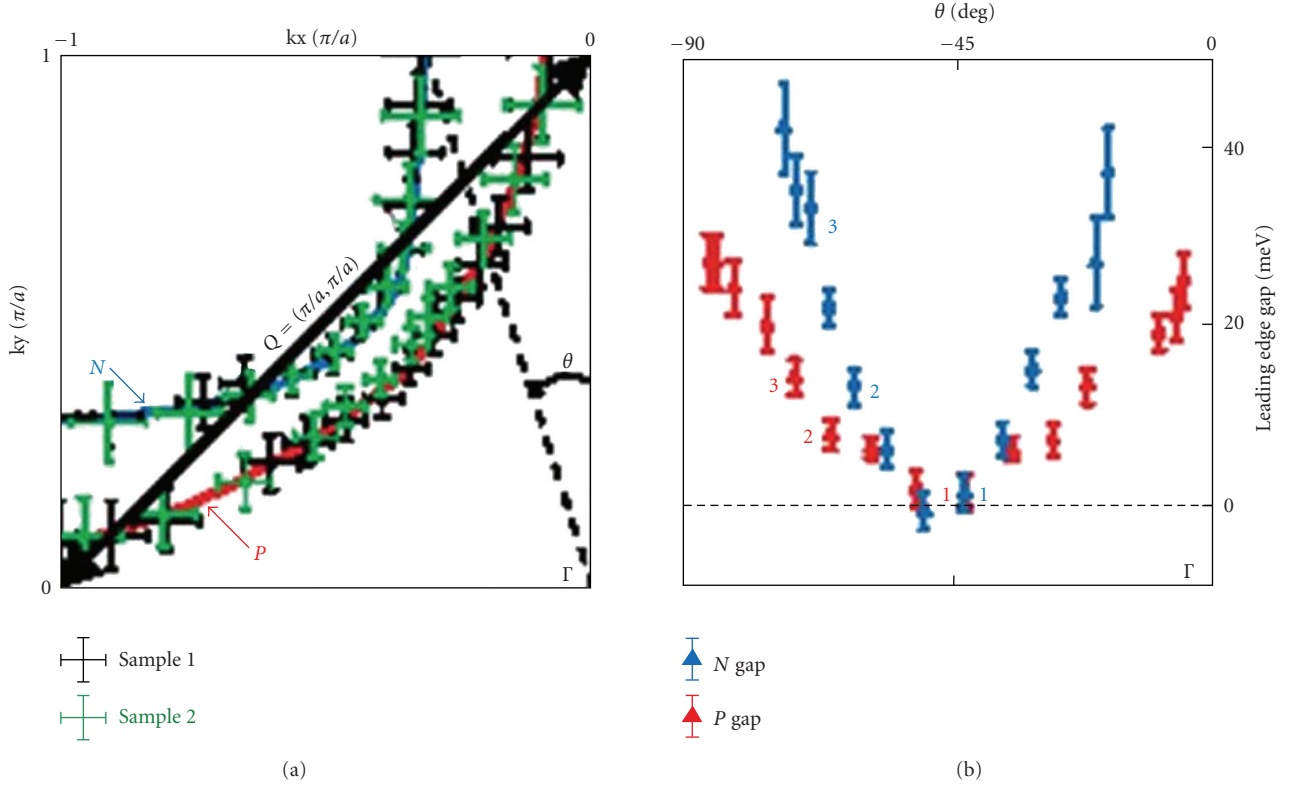


FIGURE 20: (a) Fermi surface (FS) contours from two samples of F0234.  $N$ —electron-like;  $P$ —hole-like. Bold arrow is  $(\pi, \pi)$  scattering vector. Angle  $\theta$  defines the horizontal axis in (b). (b) Leading gap edge along k-space angle from the two FS contours. From [152].

The next remarkable result is that the extracted EPI coupling constant is very large, that is,  $\lambda_{ep} (= 2 \int d\omega \alpha^2 F(\omega)/\omega) = \sum_i \lambda_i \approx 3.5$ —see Table 1. It is obvious from Figure 24 and Table 1 that almost all phonon modes contribute to  $\lambda_{ep}$  and  $T_c$ , which means that on the average each particular phonon mode is not too strongly coupled to electrons since  $\lambda_i < 1.3$ ,  $i = 1, 2, \dots, 13$ , thus *keeping the lattice stable*.

Let us discuss the content of Table 1 in more details where it is shown the strength of the EPI coupling and the relative contribution of different phononic modes to  $T_c$ . In Table 1 it is seen that lower-frequency modes from  $P1$ – $P3$ , corresponding to Cu, Sr, and Ca vibrations, are rather strongly coupled to electrons (with  $\lambda_i \sim 1$ ) which give appreciable contributions to  $T_c$ . It is also seen in Table 1 that the coupling constants  $\lambda_i$  of the high-energy phonons ( $P9$ – $P13$  with  $\omega \geq 70$  meV) have  $\lambda_i \ll 1$  and give moderate contribution to  $T_c$ —around 10%. These results give solid evidence for the *importance of the low-energy modes related to the change of the Madelung energy* in the ionic-metallic structure of HTSC cuprates—the idea advocated in [3–6] and discussed in Section 2. If confirmed in other HTSC families, these results are in favor of the *moderate oxygen isotope effect* in cuprates near the optimal doping since the oxygen modes are higher-energy modes and give smaller contribution to  $T_c$ . We stress that each peak  $P1$ – $P13$  in  $\alpha^2 F(\omega)$  corresponds to many modes. For a better understanding of the EPI coupling in these systems we show in Figure 25 the total and partial density of phononic states. It

TABLE 1: Phonon frequency  $\omega$ , EPI coupling constant  $\lambda_i$  of the peaks  $P1$ – $P13$ , and contribution  $\Delta T_c$  to  $T_c$  of each peak in  $\alpha^2 F(\omega)$ —as shown in Figure 24—obtained from the tunnelling conductance of  $\text{Bi}_2\text{Sr}_2\text{CaCu}_2\text{O}_8$ .  $\Delta T_c$  is the decrease in  $T_c$  when the peak in  $\alpha^2 F(\omega)$  is eliminated. From [53, 54].

No. of peak	$\omega$ [meV]	$\lambda_i$	$\Delta T_c$ [K]
$P1$	14.3	1.26	7.4
$P2$	20.8	0.95	11.0
$P3$	31.7	0.48	10.5
$P4$	35.1	0.28	6.7
$P5$	39.4	0.24	7.0
$P6$	45.3	0.30	10.0
$P7$	58.3	0.15	6.5
$P8$	63.9	0.01	0.6
$P9$	69.9	0.07	3.6
$P10$	73.7	0.06	3.3
$P11$	77.3	0.01	0.8
$P12$	82.1	0.01	0.7
$P13$	87.1	0.03	1.8

is seen that the low-energy phonons are due to the vibrations of the Ca, Sr, and Cu ions which correspond to the peaks  $P1$ – $P2$  in Figures 23 and 24. In order to obtain information on the structure of vibrations which are strongly involved in pairing, we show in Figures 26 and 27 the structure of

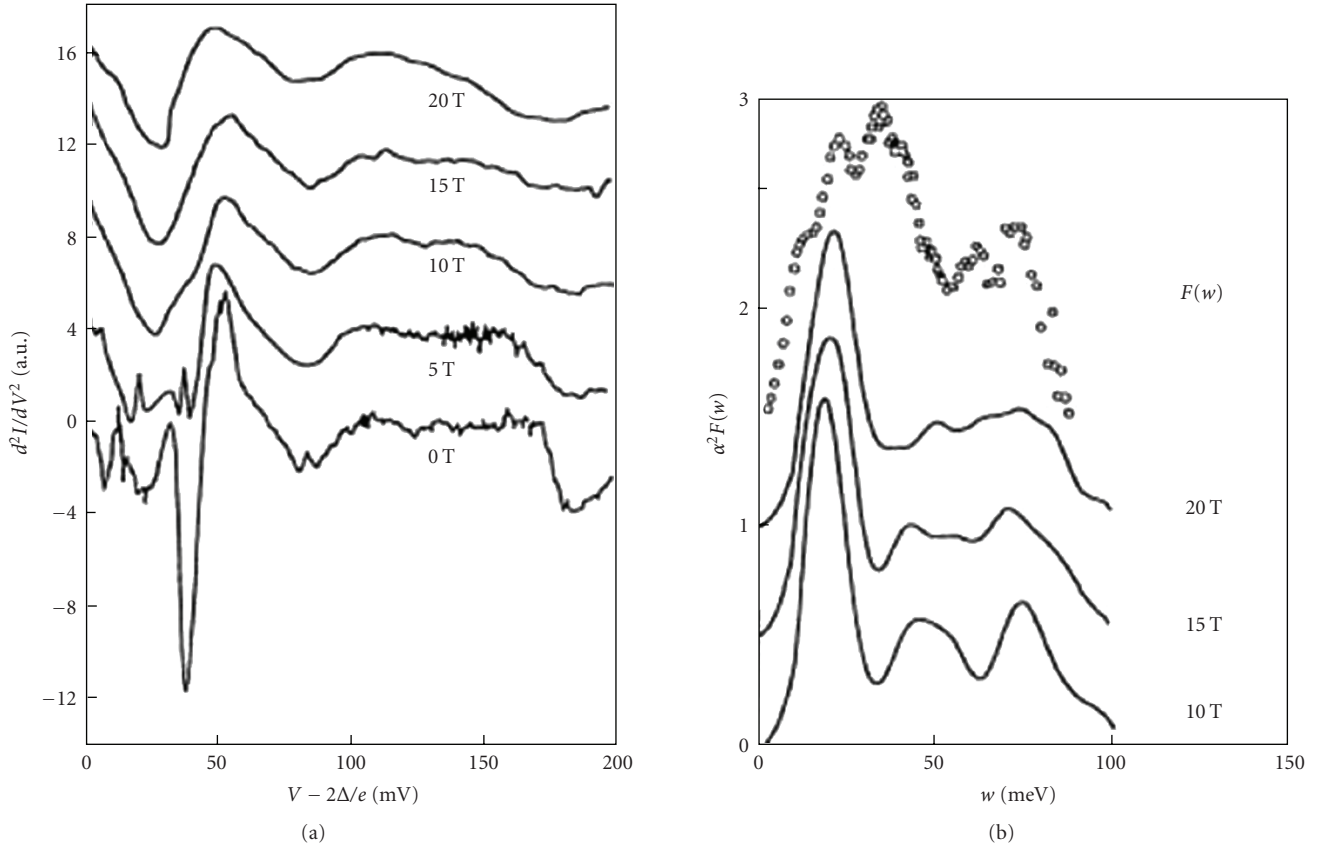


FIGURE 21: (a) Second derivative of  $I(V)$  for a Bi2212 break junction in various magnetic fields (from 0–20 T). The structure of dips (minima) in  $d^2I/dV^2$  can be compared with the phonon density of states  $F(\omega)$ ; (b) the spectral functions  $\alpha^2F(\omega)$  in various magnetic fields. From [42–45].

these vibrations at special points in the Brillouin zone. It is seen in Figure 26 that the low-frequency phonons P1–P2 are dominated by Cu, Sr, Ca vibrations.

Further, based on Table 1 one concludes that the P3 modes are strongerly coupled to electrons than the P4 ones, although the density of state for the P4 modes is larger. The reason for such an anomalous behavior might be due to symmetries of the corresponding phonons as it is seen in Figure 27. Namely, to the P3 peak contribute *axial vibrations* of O(1) in the CuO<sub>2</sub> plane which are odd under inversion, while in the P4 peak these modes are even. The in-plane modes of Ca and O(1) are present in P3 which are in-phase and out-of-phase modes, while in P4 they are all out-of-phase modes. For more information on other modes, P5–P13, see [53, 54]. We stress that the Eliashberg equations based on the extracted  $\alpha^2F(\omega)$  of the slightly overdoped Bi<sub>2</sub>Sr<sub>2</sub>CaCu<sub>2</sub>O<sub>8</sub> with the ratio  $(2\Delta/T_c) \approx 6.5$  describe rather well numerous optical, transport, and thermodynamic properties [53, 54]. However, in *underdoped systems* with  $(2\Delta/T_c) \approx 10$ , where the pseudogap phenomena are pronounced, there are *serious disagreements* between experiments and the Migdal-Eliashberg theory [53, 54]. We would like to stress that the contribution of the high-frequency modes (mostly the oxygen modes) to  $\alpha^2F(\omega)$  may be underestimated in tunnelling measurements due to their

sensitivity to the surface contamination and defects. Namely, the tunnelling current probes a superconductor to a depth of order of the quasiparticle mean-free path  $l(\omega) = v_F\gamma^{-1}(\omega)$ . Since the relaxation time  $\gamma^{-1}(\omega)$  decreases with increasing  $\omega$ , the mean-free path can be rather small and the effects of the high-energy phonons are sensitive to the surface contamination.

Similar conclusion regarding the structure of the *EPI* spectral function  $\alpha^2F(\omega)$  in *HTSC* cuprates comes out from tunnelling measurements on Andreev junctions (the BTK parameter  $Z \ll 1$ —low barrier) and Giaever junctions ( $Z \gg 1$ —high barrier) in La<sub>2-x</sub>Sr<sub>x</sub>CuO<sub>4</sub> and YBCO compounds [160], where the extracted  $\alpha^2F(\omega)$  is in good accordance with the phonon density of states  $F_{\text{ph}}(\omega)$ —see Figure 28.

Note that the BTK parameter  $Z$  is related to the transmission and reflection coefficients for the normal metal  $(1 + Z^2)^{-1}$  and  $Z^2(1 + Z^2)^{-1}$ , respectively.

Although most of the peaks in  $\alpha^2F(\omega)$  of *HTSC* cuprates coincide with the peaks in the phonon density of states, it is legitimate to put the following question. Can the magnetic resonance in the superconducting state give significant contribution to  $\alpha^2F(\omega)$ ? In that respect the inelastic magnetic neutron scattering measurements of the magnetic resonance as a function of doping [161] give that the resonance energy  $E_r$  scales with  $T_c$ , that is,  $E_r = (5-6)T_c$  as shown in Figure 29.

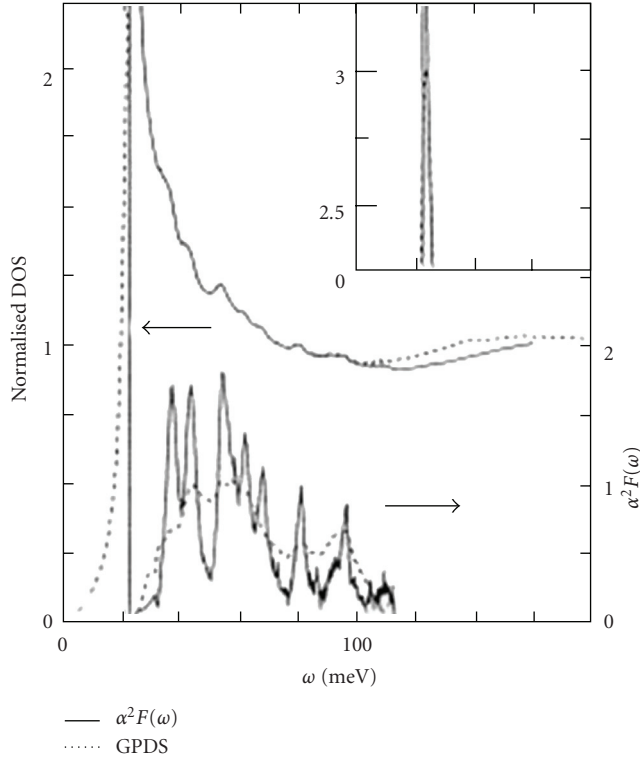


FIGURE 22: The spectral functions  $\alpha^2 F(\omega)$  and the calculated density of states at 0K (upper solid line) obtained from the conductance measurements, the Bi(2212)–Au planar junctions. GPDS—generalized phonon density of states. From [46, 47].

This means that if one of the peaks in  $\alpha^2 F(\omega)$  is due to the magnetic resonance at  $\omega = E_r$ , then it must shift strongly with doping as it is observed in [161]. This is contrary to phonon peaks (energies) whose positions are practically doping independent. To this end, recent tunnelling experiments on Bi-2212 [55] show clear *doping independence* of  $\alpha^2 F(\omega)$  as it is seen in Figure 30. This remarkable result is an additional evidence in favor of EPI and against the SFI mechanism of pairing in HTSC cuprates which is based on the magnetic resonance peak in the superconducting state. In that respect the analysis in [162] of the tunneling spectra of the electron-doped cuprate  $\text{Pr}_{0.88}\text{Ce}_{0.12}\text{CuO}_4$  with  $T_c = 24\text{K}$  shows the existence of the bosonic mode at  $\omega_B = 16\text{meV}$  which is significantly larger than the magnetic-resonance mode with  $\omega_r = (10\text{--}11)\text{meV}$ . This result excludes the magnetic-resonance mode as an important factor which modifies superconductivity.

The presence of pronounced phononic structures (and the importance of EPI) in the  $I(V)$  characteristics was quite recently demonstrated by the tunnelling measurements on the very good  $\text{La}_{1.85}\text{Sr}_{0.15}\text{CuO}_4$  films prepared by the molecular beam epitaxy on the [001]-symmetric  $\text{SrTiO}_3$  bicrystal substrates [56]. They give unique evidence for eleven peaks in the (negative) second derivative, that is,  $-d^2 I/dV^2$ . Furthermore, *these peaks coincide with the peaks in the intensities of the phonon Raman scattering data measured at 30 K in single crystals of LSCO with 20% of Sr* [57]. These results are shown in Figure 31. In spite of the

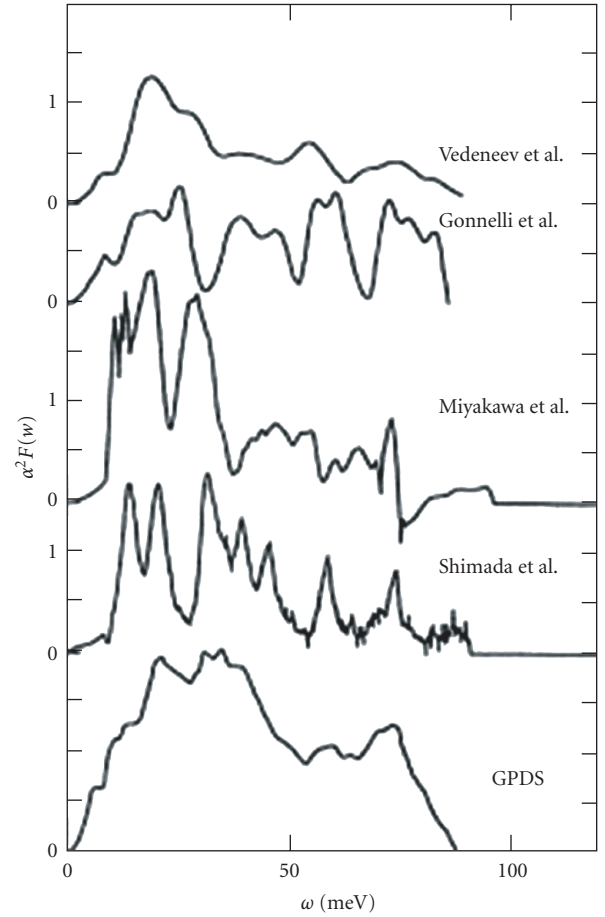


FIGURE 23: The spectral functions  $\alpha^2 F(\omega)$  from measurements of various groups: Vedeneev et al. [42–45], Gonnelli et al. [52], Miyakawa et al. [48, 49], and Shimada et al. [46, 47]. The generalized density of states GPDS for Bi2212 is at the bottom. From [46, 47].

lack of a quantitative analysis of the data in the framework of the Eliashberg equations, the results in [56] are important evidence that phonons are relevant pairing bosons in HTSC cuprates.

It is interesting that in the  $c$ -axis vacuum tunnelling  $STM$  measurements [163] the fine structure in  $d^2 I/dV^2$  at  $eV > \Delta$  was not seen below  $T_c$ , while the pseudogap structure is observed at temperatures near and above  $T_c$ . This result could mean that the  $STM$  tunnelling is likely dominated by the nontrivial structure of the tunnelling matrix element (along the  $c$ -axis), which is derived from the band-structure calculations [164]. However, recent  $STM$  experiments on Bi2212 [61–63] give information on the possible nature of the bosonic mode which couples with electrons. In [61–63] the local conductance  $dI/dV(\mathbf{r}, E)$  is measured where it is found that  $d^2 I/dV^2(\mathbf{r}, E)$  has peak at  $E(\mathbf{r}) = \Delta(\mathbf{r}) + \Omega(\mathbf{r})$  where  $dI/dV(\mathbf{r}, E)$  has the maximal slope—see Figure 32(a).

It turns out that the corresponding average phonon energy  $\bar{\Omega}$  depends on the oxygen mass, that is,  $\bar{\Omega} \sim M_O^{-1/2}$ , with  $\bar{\Omega}_{16} = 52\text{meV}$  and  $\bar{\Omega}_{18} \approx 48\text{meV}$ —as it is seen in Figure 32(b). This result is interpreted in [61–63] as an evidence that the oxygen phonons are strongly involved in

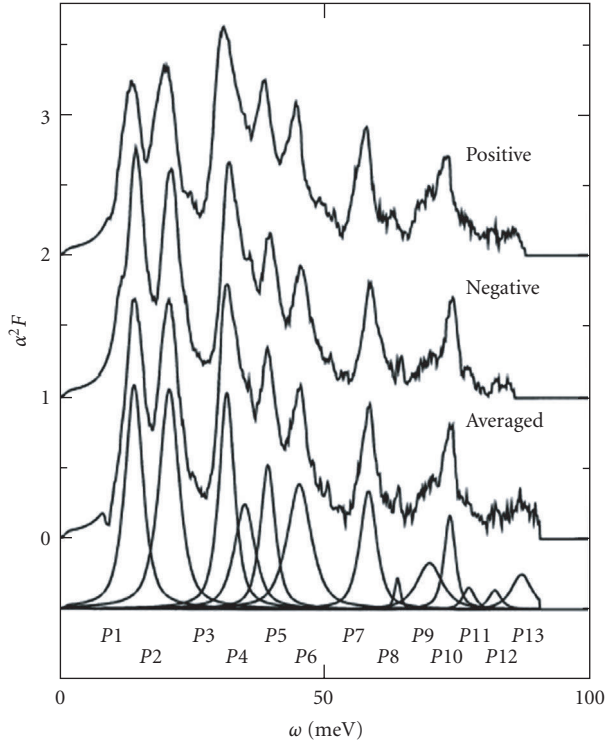


FIGURE 24: The spectral functions  $\alpha^2 F(\omega)$  from the tunnelling conductance of  $\text{Bi}_2\text{Sr}_2\text{CaCu}_2\text{O}_8$  for the positive and the negative bias voltages, and the averaged one [46, 47]. The averaged one is divided into 13 components. The origin of the ordinate is 2, 1, 0, and  $-0.5$  from the top down. From [46, 47, 53, 54].

the quasiparticle scattering. A possible explanation is put forward in [61–63] by assuming that this isotope effect is due to the  $B_{1g}$  phonon which interacts with the antinodal quasiparticles. However, this result requires a reanalysis since the energy of the bosonic mode in fact coincides with the dip and not with the peak of  $d^2I/dV^2(\mathbf{r}, E)$ —as reported in [61–63].

The important message of numerous tunnelling experiments in HTSC cuprates *near and at the optimal doping* is that there is strong evidence for the importance of EPI in the quasiparticle scattering and that no particular phonon mode can be singled out in the spectral function  $\alpha^2 F(\omega)$  as being the only one which dominates in pairing mechanism. This important result means that the high  $T_c$  is not attributable to a particular phonon mode in the EPI mechanism but all phonon modes contribute to  $\lambda_{ep}$ . Having in mind that the phonon spectrum in HTSC cuprates is very broad (up to 80 meV), then the large EPI constant ( $\lambda_{ep} \gtrsim 2$ ) obtained in the tunnelling experiments is not surprising at all. Note that similar conclusion holds for some other oxide superconductors such as  $\text{Ba}_{0.6}\text{K}_{0.4}\text{BiO}_3$  with  $T_c = 30$  K where the peaks in the bosonic spectral function/extracted from tunnelling measurements coincide with the peaks in the phononic density of states [165–167].

**1.3.5. Phonon Spectra and EPI.** Although experiments related to phonon spectra and their renormalization by EPI, such as inelastic neutron, inelastic X-ray, and Raman

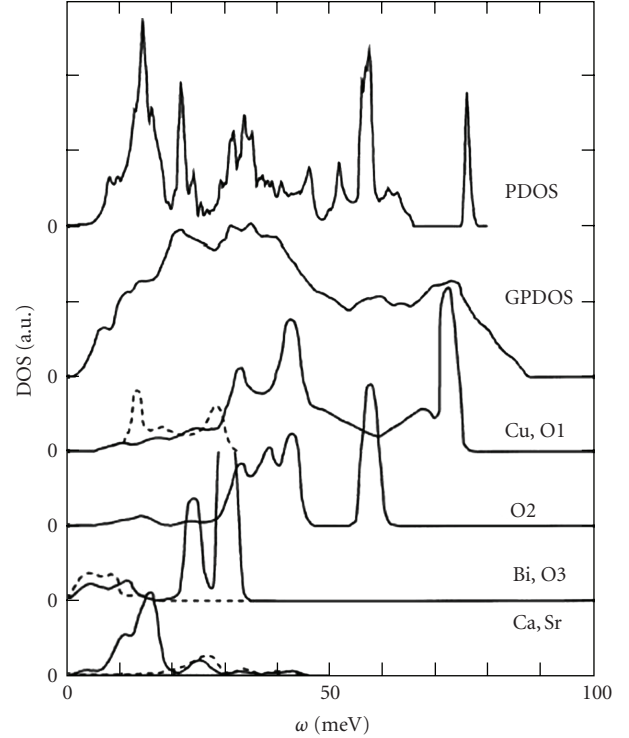


FIGURE 25: The phonon density of states  $F(\omega)$  (PDOS) of  $\text{Bi}_2\text{Sr}_2\text{CaCu}_2\text{O}_8$  compared with the generalized density of states (GPDOS) [159]. Atomic vibrations: O1—O in the  $\text{CuO}_2$  plane; O2—apical O; O3—O in the BiO plane. From [46, 47].

scattering, do not give the spectral function  $\alpha^2 F(\omega)$ , they nevertheless can give useful, but indirect, information on the strength of EPI for some particular phonons. We stress in advance that the interpretation of the experimental results in HTSC cuprates by the theory of EPI for weakly correlated electrons is inadequate since in strongly correlated systems, such as HTSC cuprates, the phonon renormalization due to EPI is different than in weakly correlated metals [168]. Since these questions are reviewed in [168], we will briefly enumerate the main points: (1) in strongly correlated systems the EPI coupling for a number of phononic modes can be significantly larger than the LDA-DFT and Hartree-Fock methods predict. This is due to many-body effects not contained in LDA-DFT [168, 169]. The lack of the LDA-DFT calculations in obtaining phonon line-widths is clearly demonstrated, for instance, in experiments on  $\text{L}_{2-x}\text{Sr}_x\text{CuO}_4$ —see review in [170] and references therein, where the bond-stretching phonons at  $\mathbf{q} = (0.3, 0, 0)$  are *softer and much broader* than the LDA-DFT calculations predict. (Note the wave vector  $\mathbf{q}$  is in units  $(2\pi/a, 2\pi/b, 2\pi/c)$ —for instance, in these units  $(\pi, \pi)$  corresponds to  $(0.5, 0.5)$ .) (2) The calculation of phonon spectra is in principle very difficult problem since besides the complexity of structural properties in a given material one should take into account appropriately the long-range Coulomb interaction of electrons as well as strong short-range repulsion. Our intention is not to discuss this complexity here—for that see, for instance, [69]—but

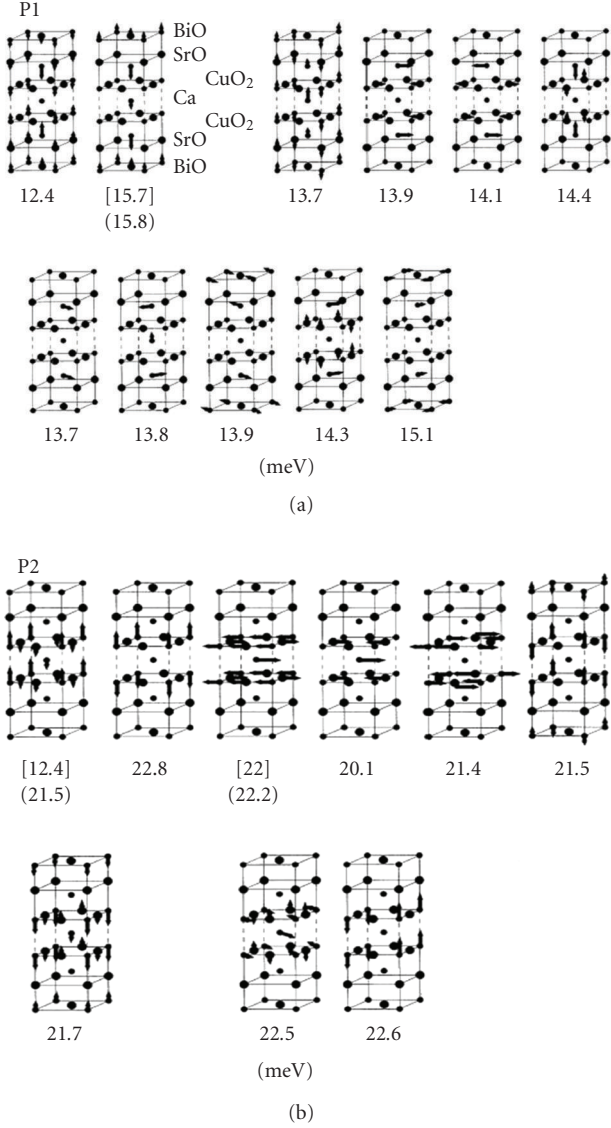


FIGURE 26: Atomic polarization vectors and their frequencies (in meV) at special points in the Brillouin zone. The larger closed circles in the lattice are O-ions.  $\Gamma - X$  is along the Cu-O-Cu direction. Arrows indicate displacements. The modes in square and round brackets are the transverse and longitudinal optical modes, respectively. (a) Modes of the P1 peak. (b) Modes of the P2 peak. From [46, 47, 53, 54].

we only stress some important points which will help to understand problems with which is confronted the theory of phonons in cuprates.

The phonon Green's function  $D(\mathbf{q}, \omega)$  depends on the phonon self-energy  $\Pi(\mathbf{q}, \omega)$  which takes into account all the enumerated properties (note that  $D^{-1}(\mathbf{q}, \omega) = D_0^{-1}(\mathbf{q}, \omega) - \Pi(\mathbf{q}, \omega)$ ). In cases when the EPI coupling constant  $g_{ep}(\mathbf{k}, \mathbf{k}')$  is a function of the transfer momentum  $\mathbf{q} = \mathbf{k} - \mathbf{k}'$  only, then  $\Pi(q)$  ( $q = (\mathbf{q}, i\omega_n)$ ) depends on the quasiparticle charge susceptibility  $\chi_c(q) = P(q)/\varepsilon_e(q)$ :

$$\Pi(q) = \left| g_{ep}(\mathbf{q}) \right|^2 \chi_c(q), \quad (41)$$

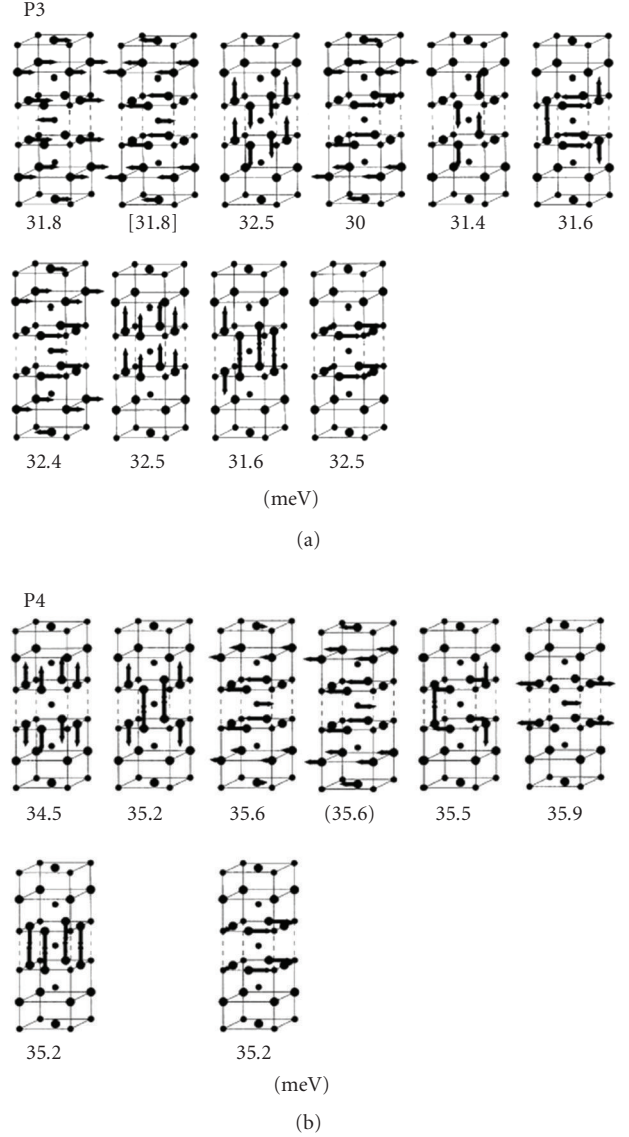


FIGURE 27: Atomic polarization vectors and their frequencies (in meV) at special points in the Brillouin zone. The larger closed circles in the lattice are O-ions.  $\Gamma - X$  is along the Cu-O-Cu direction. Arrows indicate displacements. The modes in square and round brackets are the transverse and longitudinal optical modes, respectively. (a) Modes of the P3 peak. (b) Modes of the P4 peak. From [46, 47, 53, 54].

and  $P(q)$  is the *irreducible electronic polarization* given by

$$P(q) = -\sum_p G(p+q)\Gamma_c(p,q)G(p). \quad (42)$$

The screening due to the long-range Coulomb interaction is contained in the electronic dielectric function  $\varepsilon_e(q)$  while the “screening” due to (strong) correlations is described by the charge vertex function  $\Gamma_c(p, q)$ . Due to complexity of the physics of strong correlations the phonon dynamics was studied in the  $t$ - $J$  model but without the long-range Coulomb interaction [168, 169, 171], in which case one has  $\varepsilon_e = 1$  and  $\chi_c(q) = P(q)$ . However, in studying the phonon

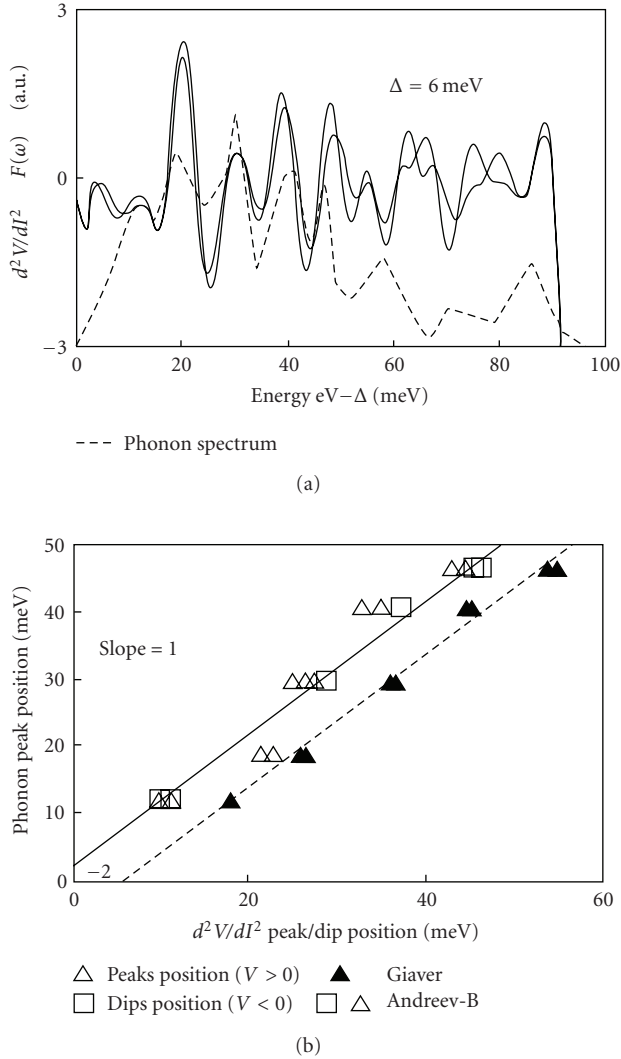


FIGURE 28: (a)  $d^2I/dV^2$  of a Giaever-like contact in  $\text{La}_{2-x}\text{Sr}_x\text{CuO}_4$ —note the large structure below 50 meV; (b)  $d^2I/dV^2$  of an Andreev- and Giaever-like contact compared to the peaks in the phonon density of states. From [160].

spectra in HTSC cuprates it is believed that this deficiency might be partly compensated by choosing the bare phonon frequency  $\omega_0(\mathbf{q})$  (contained in  $D_0^{-1}(\mathbf{q}, \omega)$ ) to correspond to the undoped compounds [168, 171]. It is a matter of future investigations to incorporate all relevant interactions in order to obtain a fully microscopic and reliable theory of phonons in cuprates. Additionally, the electron-phonon interaction (with the bare coupling constant  $g_{ep}(\mathbf{q})$ ) is dominated by the change of the energy of the Zhang-Rice singlet—see more in Section 2.3—and (41) for  $\Pi(q)$  is adequate one [6, 168, 169]. Since the charge fluctuations in HTSC cuprates are strongly suppressed (no doubly occupancy of the Cu  $3d^9$  state) due to strong correlations, and since the suppressed value of  $\chi_c(q)$  cannot be obtained by the band-structure calculations, this means that *LDA-DFT underestimates the EPI coupling constant significantly*. In the following we discuss this important result briefly.

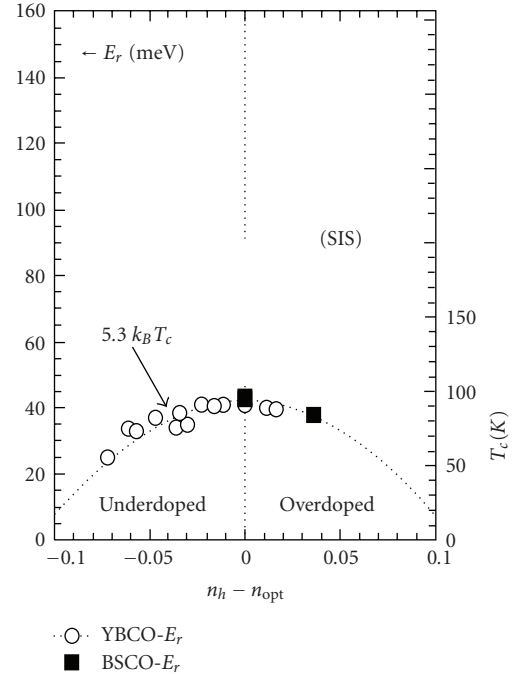


FIGURE 29: Doping dependence of the energy  $E_r$  of the magnetic resonance peak at  $\mathbf{Q} = (\pi, \pi)$  in YBCO and Bi2212 measured at low temperatures by inelastic neutron scattering. From [161].

(1) *Inelastic Neutron and X-Ray Scattering—The Phonon Softening and the Line-Width due to EPI*. The appreciable softening and broadening of numerous phonon modes has been observed in the normal state of HTSC cuprates, thus giving evidence for pronounced EPI effects and for inadequacy of the LDA-DFT calculations in treating strong correlations and suppression of the charge susceptibility [6, 10, 11, 168, 171]. There are several relevant reviews on this subject [10, 11, 168, 170, 172] and here we discuss briefly two important examples which demonstrate the inefficiency of the LDA-DFT-band structure calculations to treat quantitatively EPI in HTSC cuprates. For instance, the Cu–O bond-stretching phonon mode shows a *substantial softening* at  $\mathbf{q}_{hb} = (0.3, 0, 0)$  by doping of  $\text{La}_{1.85}\text{Sr}_{0.15}\text{CuO}_4$  and  $\text{YBa}_2\text{Cu}_3\text{O}_7$  [170, 172]—called the *half-breathing phonon*, and a *large broadening* by 5 meV at 15% doping [173–175] as it is seen in Figure 33. While the softening can be partly described by the LDA-DFT method [176], the latter theory *predicts an order of magnitude smaller broadening* than the experimental one. This failure of LDA-DFT is due to the incorrect treatment of the effects of strong correlations on the charge susceptibility  $\chi_c(q)$  and due to the absence of many-body effects which can increase the coupling constant  $g_{ep}(\mathbf{q})$ —see more in Section 2. The neutron scattering measurements in  $\text{La}_{1.85}\text{Sr}_{0.15}\text{CuO}_4$  give evidence for large (30%) softening of the  $O_Z^2$  with  $\Delta_1$  symmetry with the energy  $\omega \approx 60$  meV, which is theoretically predicted in [177], and for the large line-width about 17 meV which also suggests strong EPI. These apex modes are favorable for *d*-wave pairing since their coupling constants are peaked at small momentum  $q$  [10, 11]. Having in mind the above results, then it is not surprising that

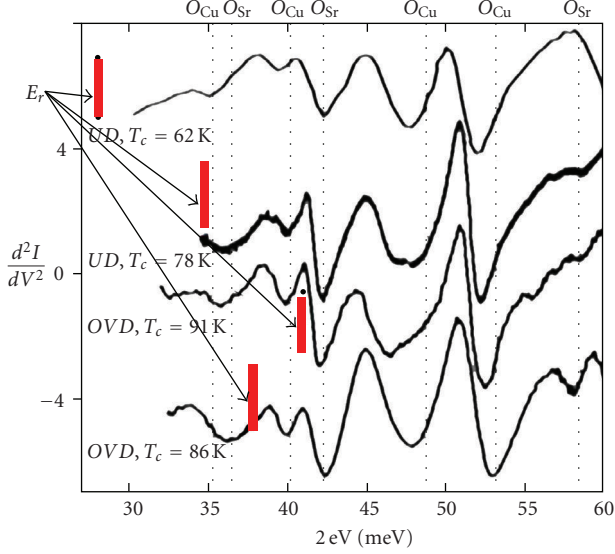


FIGURE 30: Second derivative of  $I(V)$  for  $Bi2212$  tunnelling junctions for various doping: UD—underdoped; OD—optimally doped; OVD—overdoped system. The structure of minima in  $d^2I/dV^2$  can be compared with the phonon density of states  $F(\omega)$ . The full and vertical lines mark the positions of the magnetic resonance energy  $E_r \approx 5.4T_c$  for various doping taken from Figure 29. Red tiny arrows mark positions of the magnetic resonance  $E_r$  in various doped systems. Dotted vertical lines mark various phonon modes. From [55].

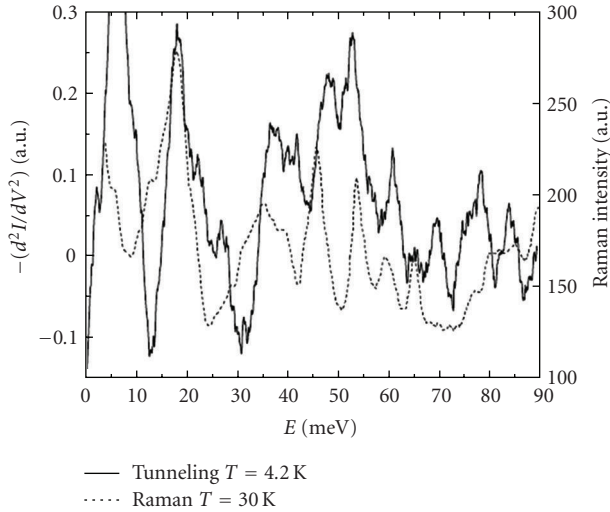


FIGURE 31: Second derivative data  $d^2I(V)/dV^2$  of the tunnelling spectra on thin films of  $La_{1.85}Sr_{0.15}CuO_4$  are shown along with phonon Raman scattering data on single crystals of LSCO with 20% Sr. The polarization of the incident and scattered light in the Raman spectra is parallel to the  $CuO_2$  planes. From [56].

the recent calculations of the EPI coupling constant  $\lambda_{ep}$  in the framework of LDA-DFT give very small EPI coupling constant  $\lambda_{ep} \approx 0.3$  [28, 29]. The critical analysis of the LDA-DFT results in HTSC cuprates is done in [6] and additionally argued in [10, 11, 178] by pointing their disagreement with

the inelastic neutron and X-ray scattering measurements—as it is shown in Figure 33.

In Section 2 we will discuss some theoretical approaches related to EPI in strongly correlated systems but without discussing the phonon renormalization. The latter problem was studied in more details in the review articles in [10, 11, 170]. Here, we point out only three (for our purposes) relevant results. *First*, there is an appreciable difference in the *phonon renormalization* in strongly and weakly correlated systems. Namely, the change of the phonon frequencies in the presence of the conduction electrons is proportional to the squared coupling constant  $|g_q|$  and charge susceptibility  $\chi_c$ , that is,  $\delta\omega(\mathbf{q}) \sim |g_{ep}(\mathbf{q})|^2 \text{Re}\chi_c$ , while the *line-width* is given by  $\Gamma_{\omega(\mathbf{q})} \sim |g_{ep}(\mathbf{q})|^2 |\text{Im}\chi_c|$ . All these quantities can be calculated in LDA-DFT and as we discussed above, where for some modes one obtains that  $\Gamma_{\omega(\mathbf{q})}^{(LDA)} \ll \Gamma_{\omega(\mathbf{q})}^{(exp)}$ . However, it turns out that in strongly correlated systems doped by holes (with the concentration  $\delta \ll 1$ ) the charge fluctuations are suppressed in which case the following sum rule holds [10, 11, 171]:

$$\frac{1}{\pi N} \sum_{\mathbf{q} \neq 0} \int_{-\infty}^{\infty} d\omega |\text{Im}\chi_c(\mathbf{q}, \omega)| = 2\delta(1 - \delta)N, \quad (43)$$

while in the LDA-DFT method one has

$$\frac{1}{\pi N} \sum_{\mathbf{q} \neq 0} \int_{-\infty}^{\infty} d\omega |\text{Im}\chi_c(\mathbf{q}, \omega)|^{(LDA)} = (1 - \delta)N. \quad (44)$$

The inequality  $\Gamma_{\omega(\mathbf{q})}^{(LDA)} \ll \Gamma_{\omega(\mathbf{q})}^{(exp)}$  (for some phonon modes) together with (43)-(44) means that for low doping  $\delta \ll 1$  the LDA calculations *strongly underestimate the EPI coupling constant* in the large portion of the Brillouin zone, that is, one has  $|g_{ep}^{(LDA)}(\mathbf{q})| \ll |g_{ep}^{(exp)}(\mathbf{q})|$ . The large softening and the large line-width of the half-breathing mode at  $q = (0.5, 0)$ , but very moderate effects for the breathing mode at  $q = (0.5, 0.5)$ , are explained in the framework of the one *slave-boson (SB) theory* (for  $U = \infty$ ) in [171], where  $\chi_c(\mathbf{q}, \omega)$  (i.e.,  $\Gamma_c(p, q) = \Gamma_c(\mathbf{p}, q)$ ) is calculated in leading  $O(1/N)$  order. We stress that there is another method for studying strong correlations—the *X-method*—where the controllable  $1/N$  expansion is performed in terms of the Hubbard operators and where the charge vertex  $\Gamma_c(\mathbf{p}, q)$  is calculated [6, 78–80, 130, 179, 180]. It turns out that in the adiabatic limit ( $\omega = 0$ ) the vertex functions  $\Gamma_c(\mathbf{p}_F, \mathbf{q})$  in these two methods have important differences. For instance,  $\Gamma_c^{(X)}(\mathbf{p}_F, q)$  (in the X-method) is peaked at  $\mathbf{q} = 0$ —the so called forward scattering peak (FSP)—while  $\Gamma_c^{(SB)}(\mathbf{p}_F, \mathbf{q})$  has maximum at finite  $|\mathbf{q}| \neq 0$  [181]—see Section 2.3.5. The enumerated properties of  $\Gamma_c^{(X)}(\mathbf{p}_F, q)$  are confirmed by the numerical Monte Carlo calculations in the finite- $U$  Hubbard model [182], where it is found that FSP exists for all  $U$ , but it is especially pronounced in the limit  $U \gg t$ . These results are also confirmed in [183] where the calculations are performed in the four-slave-boson technique—see more in Section 2.3.5. Having in mind this difference it would be useful to have calculations of  $\chi_c(\mathbf{q}, \omega)$  in the framework of the X-method which are unfortunately not done yet. *Second*,

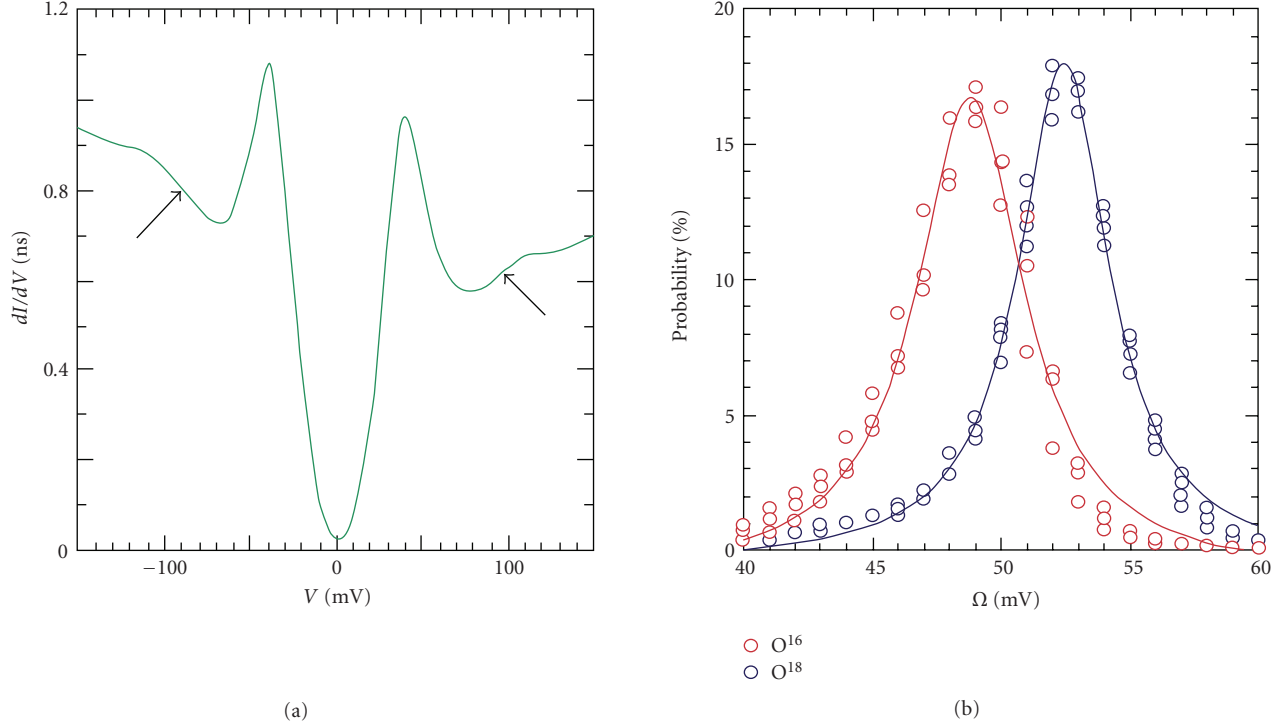


FIGURE 32: (a) Typical conductance  $dI/dV(\mathbf{r}, E)$ . The ubiquitous features at  $eV > \Delta(\text{gap})$  with maximal slopes, which give peaks in  $d^2I/dV^2(\mathbf{r}, E)$ , are indicated by arrows. (b) The histograms of all values of  $\Omega(\mathbf{r})$  for samples with  $\text{O}^{16}$ —right curve and with  $\text{O}^{18}$ —left curve. From [61–63].

the many-body theory gives that for coupling to some modes the coupling constant  $|g_{ep}(\mathbf{q})|$  in HTSC cuprates can be significantly larger than the LDA-DFT calculations predict [10, 11], which is due to some many-body effects not present in the latter [169]. In Section 2 it will be argued that for some phonon modes one has  $|g_{ep}(\mathbf{q})|^2 \gg |g_{ep}^{(\text{LDA})}(\mathbf{q})|^2$ . For instance, for the half-breathing mode, one has  $|g_{ep}(\mathbf{q})|^2 \approx 3|g_{ep}^{(\text{LDA})}(\mathbf{q})|^2$  [10, 11, 169]—see Section 2. These two results point to an inadequacy of LDA-DFT in calculations of EPI effects in HTSC cuprates. *Third*, the phonon self-energy  $\Pi(q)$  and quasiparticle self-energy  $\Sigma(k)$  are differently renormalized by strong correlations [6, 10, 11, 78–80, 130, 179, 180], which is the reason that  $\Pi(q)$  is much more suppressed than  $\Sigma(k)$ —see Section 2. The effects of the charge vertex on  $\Pi(q)$  and  $\Sigma(k)$  are differently manifested. Namely, the vertex function enters *quadratically* in  $\Sigma(k)$  and the presence of the forward scattering peak in the charge vertex *strongly affects* the EPI coupling constant  $g_{ep}(\mathbf{q})$  in  $\Sigma(k)$ :

$$\Sigma(k) = - \sum_{\mathbf{q}} \left| g_{ep}(\mathbf{q}) \gamma_c(\mathbf{k}, \mathbf{q}) \right|^2 D(q) g(k + \mathbf{q}), \quad (45)$$

where  $g(k) (\equiv G(k)/Q)$  is the *quasiparticle Green's function*,  $\gamma_c(\mathbf{k}, \mathbf{q}) = \Gamma_c(\mathbf{k}, \mathbf{q})/Q$  is the *quasiparticle vertex*, and  $Q(\sim \delta)$  is the Hubbard *quasiparticle spectral weight*—see Section 2.3. In the adiabatic limit  $|\mathbf{q}| > q_\omega = \omega_{\text{ph}}/v_F$  one has  $\gamma_c(\mathbf{k}, \mathbf{q}) \approx \gamma_c(\mathbf{k}, \mathbf{q})$  and for  $q \gg q_c (\approx \delta \cdot \pi/a)$  the charge vertex is strongly suppressed ( $\gamma_c(\mathbf{k}, \mathbf{q}) \ll 1$ ) making the effective EPI

coupling (which also enters the pairing potential) small at large (transfer) momenta  $\mathbf{q}$ . This has strong repercussion on the pairing due to EPI since for small doping it makes the *d-wave* pairing coupling constant to be of the order of the *s*-one ( $\lambda_d \approx \lambda_s$ ). Then in the presence of the residual Coulomb interaction EPI gives rise to *d-wave* pairing. On the other side the charge vertex  $\Gamma_c(\mathbf{k}, \mathbf{q})$  enters  $\Pi(q)$  *linearly* and it is *additionally integrated* over the quasiparticle momentum  $\mathbf{k}$ —see (42). Therefore, one expects that the effects of the forward scattering peak on  $\Pi(q)$  are less pronounced than on  $\Sigma(k)$ . Nevertheless, the peak of  $\Gamma_c(\mathbf{k}, \mathbf{q})$  at  $\mathbf{q} = 0$  may be (partly) responsible that the maximal experimental softening and broadening of the stretching (half-breathing) mode in  $\text{La}_{1.85}\text{Sr}_{0.15}\text{CuO}_4$  and  $\text{YBa}_2\text{Cu}_3\text{O}_7$  is at  $\mathbf{q}_{\text{hb}}^{(\text{exp})} = (0.3, 0, 0)$  [170] and not at  $\mathbf{q}_{\text{hb}} = (0.5, 0)$  for which  $g_{ep}(\mathbf{q}_{\text{hb}})$  reaches maximum. This means that the charge vertex function pushes the maximum of the renormalized EPI coupling constant to smaller momenta  $\mathbf{q}$ . It would be very interesting to have calculations for other phonons by including the vertex function obtained by the X-method—see Section 2.3.

(2) *The Phonon Raman Scattering.* The *phonon* Raman scattering gives an indirect evidence for importance of EPI in cuprates [184–188]. We enumerate some of them—see more in [6] and references therein. (i) There is a pronounced *asymmetric line-shape* (of the Fano resonance) in the metallic state. For instance, in  $\text{YBa}_2\text{Cu}_3\text{O}_7$  two Raman modes at  $115 \text{ cm}^{-1}$  (Ba dominated mode) and at  $340 \text{ cm}^{-1}$

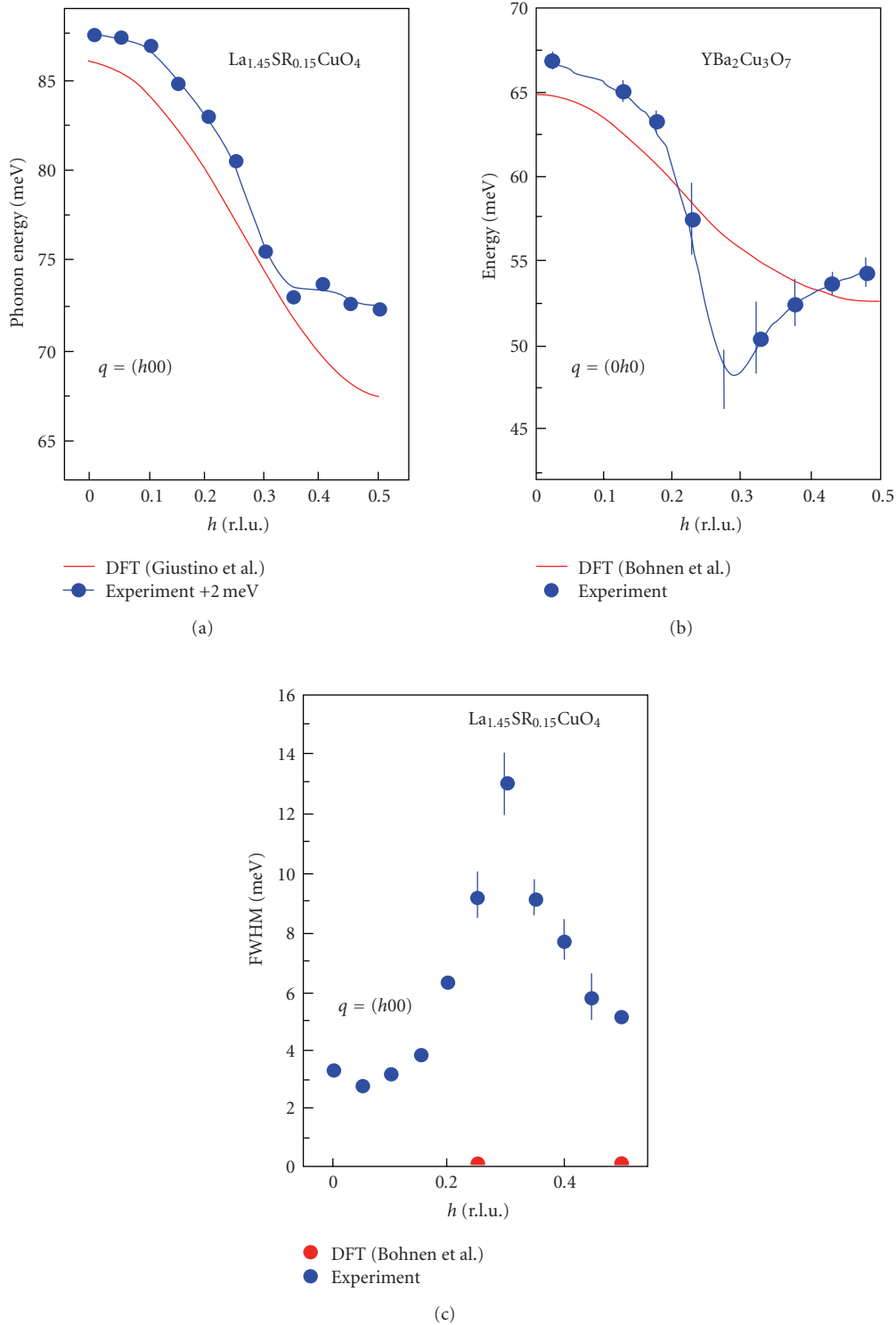


FIGURE 33: Comparison of DFT calculations with experimental results of inelastic X-ray scattering: (a) phonon energies in  $\text{La}_{1.85}\text{Sr}_{0.15}\text{CuO}_4$  and (b) in  $\text{YBa}_2\text{Cu}_3\text{O}_7$ ; (c) phonon line-widths in  $\text{La}_{1.85}\text{Sr}_{0.15}\text{CuO}_4$ . DFT calculations [28] give much smaller width than experiments [173–175]. From [178].

(O dominated mode in the  $\text{CuO}_2$  planes) show pronounced asymmetry which is absent in  $\text{YBa}_2\text{Cu}_3\text{O}_6$ . This asymmetry means that there is an appreciable interaction of Raman active phonons with continuum states (quasiparticles).

(ii) The phonon frequencies for some  $A_{1g}$  and  $B_{1g}$  are strongly renormalized in the superconducting state, between (6–10)%, pointing again to the importance of EPI [188]—see also [6, 37, 38]. To this point we mention that there is a

remarkable correlation between the electronic Raman cross-section  $\tilde{\Sigma}_{\text{exp}}(\omega)$  and the optical conductivity in the  $a - b$  plane  $\sigma_{ab}(\omega)$ , that is,  $\tilde{\Sigma}_{\text{exp}}(\omega) \sim \sigma_{ab}(\omega)$  [6]. In previous subsections it is argued that EPI with the very broad spectral function  $\alpha^2 F(\omega)$  ( $0 < \omega \lesssim 80$  meV) explains in a natural way the  $\omega$  and  $T$  dependence of  $\sigma_{ab}(\omega)$ . This means that the electronic Raman spectra in cuprates can be explained by EPI in conjunction with strong correlations. This conclusion is supported by the calculations of the Raman cross-section [189] which take into account EPI with  $\alpha^2 F(\omega)$  extracted from the tunnelling measurements in  $\text{YBa}_2\text{Cu}_3\text{O}_{6+x}$  and  $\text{Bi}_2\text{Sr}_2\text{CaCu}_2\text{O}_{8+x}$  [6, 42–54]. Quite similar properties (to cuprates) of the electronic Raman scattering, as well as of  $\sigma(\omega)$ ,  $R(\omega)$ , and  $\rho(T)$ , were observed in experiments [108] on isotropic 3D metallic oxides  $\text{La}_{0.5}\text{Sr}_{0.5}\text{CoO}_3$  and  $\text{Ca}_{0.5}\text{Sr}_{0.5}\text{RuO}_3$  where there are no signs of antiferromagnetic fluctuations. This means that low dimensionality and antiferromagnetic spin fluctuations cannot be a prerequisite for anomalous scattering of quasiparticles and EPI must be inevitably taken into account since it is present in all these compounds.

*1.3.6. Isotope Effect in  $T_c$  and  $\Sigma(\mathbf{k}, \omega)$ .* The isotope effect  $\alpha_{T_c}$  in the critical temperature  $T_c$  was one of the very important proofs for the EPI pairing mechanism in low-temperature superconductors (LTSCs). As a curiosity the isotope effect in LTSC systems was measured almost exclusively in monoatomic systems and in few polyatomic systems: the hydrogen isotope effect in PdH, the Mo and Se isotope shift of  $T_c$  in  $\text{Mo}_6\text{Se}_8$ , and the isotope effect in  $\text{Nb}_3\text{Sn}$  and  $\text{MgB}_2$ . We point out that very small ( $\alpha_{T_c} \approx 0$  in Zr and Ru) and even negative (in PdH) isotope effects in some polyatomic systems of LTSC materials are compatible with the EPI pairing mechanism but in the presence of substantial Coulomb interaction or lattice anharmonicity. The isotope effect  $\alpha_{T_c}$  cannot be considered as the smoking gun effect since it is sensitive to numerous influences. For instance, in  $\text{MgB}_2$  it is with certainty proved that the pairing is due to EPI and strongly dominated by the boron vibrations, but the boron isotope effect is significantly reduced, that is,  $\alpha_{T_c} \approx 0.3$  and the origin for this smaller value is still unexplained. The situation in HTSC cuprates is much more complicated because they are *strongly correlated systems and contain many atoms in unit cell*. Additionally, the situation is complicated with the presence of *intrinsic and extrinsic inhomogeneities, low dimensionality* which can mask the isotope effects. On the other hand new techniques such as ARPES, STM, and  $\mu\text{SR}$  allow studies of the isotope effects in quasiparticle self-energies, that is,  $\alpha_\Sigma$ , which will be discussed below.

(1) *Isotope Effect  $\alpha_{T_c}$  in  $T_c$ .* This problem will be discussed only briefly since more extensive discussion can be found in [6]. It is well known that in the pure EPI pairing mechanism the total isotope coefficient  $\alpha$  is given by  $\alpha_{T_c} = \sum_{i,p} \alpha_i^{(p)} = -\sum_{i,p} d \ln T_c / d \ln M_i^{(p)}$ , where  $M_i^{(p)}$  is the mass of the  $i$ th element in the  $p$ th crystallographic position. We stress that the total isotope effect is not measured in HTSC cuprates

but only some partial ones. Note that, in the case when the screened Coulomb interaction is negligible, that is,  $\mu_c^* = 0$ , the theory predicts  $\alpha_{T_c} = 1/2$ . From this formula one can deduce that the relative change of  $T_c$ ,  $\delta T_c / T_c$ , for heavier elements should be rather small—for instance, it is 0.02 for  $^{135}\text{Ba} \rightarrow ^{138}\text{Ba}$ , 0.03 for  $^{63}\text{Cu} \rightarrow ^{65}\text{Cu}$ , and 0.07 for  $^{138}\text{La} \rightarrow ^{139}\text{La}$ . This means that the measurements of  $\alpha_i$  for heavier elements are confronted with the ability of the present experimental techniques. Therefore most isotope effect measurements were done by substituting light atoms  $^{16}\text{O}$  by  $^{18}\text{O}$  only. It turns out that in most optimally doped HTSC cuprates  $\alpha_{\text{O}}$  is rather small. For instance,  $\alpha_{\text{O}} \approx 0.02$ – $0.05$  in  $\text{YBa}_2\text{Cu}_3\text{O}_7$  with  $T_{c,\text{max}} \approx 91$  K, but it is appreciable in  $\text{La}_{1.85}\text{Sr}_{0.15}\text{CuO}_4$  with  $T_{c,\text{max}} \approx 35$  K where  $\alpha_{\text{O}} \approx 0.1$ – $0.2$ . In  $\text{Bi}_2\text{Sr}_2\text{CaCu}_2\text{O}_8$  with  $T_{c,\text{max}} \approx 76$  K one has  $\alpha_{\text{O}} \approx 0.03$ – $0.05$  while  $\alpha_{\text{O}} \approx 0.03$  and even negative ( $-0.013$ ) in  $\text{Bi}_2\text{Sr}_2\text{Ca}_2\text{Cu}_2\text{O}_{10}$  with  $T_{c,\text{max}} \approx 110$  K. The experiments on  $\text{Tl}_2\text{Ca}_{n-1}\text{BaCu}_n\text{O}_{2n+4}$  ( $n = 2, 3$ ) with  $T_{c,\text{max}} \approx 121$  K are still unreliable and  $\alpha_{\text{O}}$  is unknown. In the electron-doped  $(\text{Nd}_{1-x}\text{Ce}_x)_2\text{CuO}_4$  with  $T_{c,\text{max}} \approx 24$  K one has  $\alpha_{\text{O}} < 0.05$  while in the underdoped materials  $\alpha_{\text{O}}$  increases. The largest  $\alpha_{\text{O}}$  is obtained even in the optimally doped compounds like in systems with substitution, such as  $\text{La}_{1.85}\text{Sr}_{0.15}\text{Cu}_{1-x}\text{M}_x\text{O}_4$ ,  $M = \text{Fe}, \text{Co}$ , where  $\alpha_{\text{O}} \approx 1.3$  for  $x \approx 0.4\%$ . In  $\text{La}_{2-x}\text{M}_x\text{CuO}_4$  there is a Cu-isotope effect which is of the order of the oxygen one, that is,  $\alpha_{\text{Cu}} \approx \alpha_{\text{O}}$  giving  $\alpha_{\text{Cu}} + \alpha_{\text{O}} \approx 0.25$ – $0.35$  for optimally doped systems ( $x = 0.15$ ). In case when  $x = 0.125$  with  $T_c \ll T_{c,\text{max}}$  one has  $\alpha_{\text{Cu}} \approx 0.8 - 1$  with  $\alpha_{\text{Cu}} + \alpha_{\text{O}} \approx 1.8$  [190, 191]. The appreciable copper isotope effect in  $\text{La}_{2-x}\text{M}_x\text{CuO}_4$  tells us that vibrations other than oxygen ions are important in giving high  $T_c$ . In that sense one should have in mind the tunnelling experiments discussed above, which tell us that all phonons contribute to the Eliashberg pairing function  $\alpha^2 F(\mathbf{k}, \omega)$  and according to these results the oxygen modes give moderate contribution to  $T_c$  [53, 54]. Hence the small oxygen isotope effect  $\alpha_{T_c}^{(\text{O})}$  in optimally doped cuprates, if it is an intrinsic property at all (due to pronounced local inhomogeneities of samples and quasi-two-dimensionality of the system), does not exclude the EPI mechanism of pairing.

(2) *Isotope Effect  $\alpha_\Sigma$  in the Self-Energy.* The fine structure of the quasiparticle self-energy  $\Sigma(\mathbf{k}, \omega)$ , such as kinks and slopes, can be resolved in ARPES measurements and in some respect in STM measurements. It turns out that there is isotope effect in the self-energy in the optimally doped  $\text{Bi}2212$  samples [139, 141, 142]. In the first paper on this subject [139] it is reported a *red shift*  $\delta\omega_{k,70} \sim -(10\text{--}15)$  meV of the nodal kink at  $\omega_{k,70} \approx 70$  meV for the  $^{16}\text{O} \rightarrow ^{18}\text{O}$  substitution. In [139] it is reported that the isotope shift of the self-energy  $\delta\Sigma = \Sigma_{16} - \Sigma_{18} \sim 10$  meV is very pronounced at large energies  $\omega = 100$ – $300$  meV. Concerning the latter result, there is a dispute since it is not confirmed in other experiments [141, 142]. However, the isotope effect in  $\text{Re}\Sigma(\mathbf{k}, \omega)$  at low energies [141, 142] is well described in the framework of the Migdal-Eliashberg theory for EPI [140] which is in accordance with the recent ARPES measurements with low-energy photons  $\sim 7$  eV [192]. The

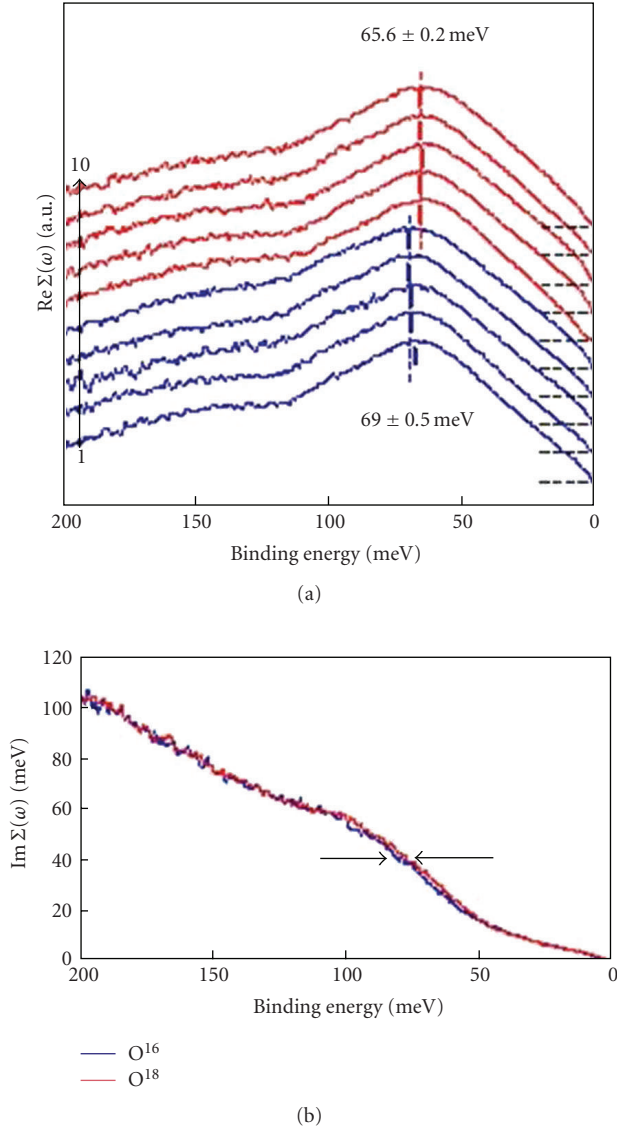


FIGURE 34: (a) Effective  $\text{Re}\Sigma$  for five samples for  $\text{O}^{16}$  (blue) and  $\text{O}^{18}$  (red) along the nodal direction. (b) Effective  $\text{Im}\Sigma$  determined from MDC full widths. An impurity term is subtracted at  $\omega = 0$ . From [192].

latter allowed very good precision in measuring the isotope effect in the nodal point of Bi-2212 with  $T_c^{16} = 92.1$  K and  $T_c^{18} = 91.1$  K [192]. They observed a shift in the maximum of  $\text{Re}\Sigma(\mathbf{k}_N, \omega)$ —at  $\omega_{k,70} \approx 70$  meV (it corresponds to the half-breathing or to the breathing phonon)—by  $\delta\omega_{k,70} \approx 3.4 \pm 0.5$  meV as shown in Figure 34.

By analyzing the shift in  $\text{Im}\Sigma(\mathbf{k}_N, \omega)$ —shown in Figure 34—one finds similar result for  $\delta\omega_{k,70} \approx 3.2 \pm 0.6$  meV. The similar shift was obtained in STM measurements [61–63] which is shown in Figure 32(b) and can have its origin in different phonons. We would like to stress two points: (i) in compounds with  $T_c \sim 100$  K the oxygen isotope effect in  $T_c$  is moderate, that is,  $\alpha_{T_c}^{(O)} < 0.1$  [192]. If we consider this value to be intrinsic, then even in this case it is not in conflict with the tunnelling experiments [53,

54] since the latter give evidence that vibrations of heavier ions contribute significantly to  $T_c$ —see the discussion in Subsection 1.3.4 on the tunnelling spectroscopy. (ii) In ARPES measurements of [192] the effective EPI coupling constant  $\lambda_{ep,eff} \gtrsim 0.6$  is extracted, while the theory in Subsection 1.3.3 gives that the real coupling constant is larger, that is,  $\lambda_{ep} > 1.2$ . This value is significantly larger than the LDA-DFT theory predicts  $\lambda_{ep,LDA} < 0.3$  [28, 29]. This again points that the *LDA-DFT method does not pick up the many-body effects* due to strong correlations—see Section 2.

**1.4. Summary of Section 1.** The analysis of experimental data in HTSC cuprates which are related to optics, tunnelling, and ARPES measurements *near and at the optimal doping* gives evidence for the large electron-phonon interaction (EPI) with the coupling constant  $1 < \lambda_{ep} < 3.5$ . We stress that this analysis is done in the framework of the Migdal-Eliashberg theory for EPI which is a reliable approach for systems near the optimal doping. The spectral function  $\alpha^2F(\omega)$ , averaged over the Fermi surface, is extracted from various tunnelling measurements on bulk materials and tin films. It contains peaks at the same energies as the phonon density of states  $F_{ph}(\omega)$ . So obtained spectral function when inserted in the Eliashberg equations provides sufficient strength for obtaining high critical temperature  $T_c \sim 100$  K. These facts are a solid proof for the important role of EPI in the normal-state scattering and pairing mechanism of cuprates. Such a large (experimental) value of the EPI coupling constant and the robustness of the *d*-wave superconductivity in the presence of impurities imply that the EPI potential and the impurity scattering amplitude must be strongly momentum dependent. The IR optical reflectivity data provide additional but indirect support for the importance of EPI since by using the spectral function (extracted from tunnelling measurements) one can quantitatively explain frequency dependence of the dynamical conductivity, optical relaxation rate, and optical mass. These findings related to EPI are additionally supported by ARPES measurements on BSCO compounds. The ARPES kinks, the phononic features and the isotope effect in the quasiparticle self-energy in the nodal and antinodal points at low energies ( $\omega \ll \omega_c$ ) persist in the normal and superconducting state. They are much more in favor of EPI than for the spin fluctuation (SFI) scattering mechanism. The transport EPI coupling constant in HTSC cuprates is much smaller than  $\lambda_{ep}$ , that is,  $\lambda_{tr} \sim \lambda_{ep}/3$ , which points to some peculiar scattering mechanism not met in low-temperature superconductors. The different renormalization of the quasiparticle and transport self-energies by the Coulomb interaction (strong correlations) hints to the importance of the small-momentum scattering in EPI. This will be discussed in Section 2.

The ineffectiveness of SFI to solely provide pairing mechanism in cuprates comes out also from the magnetic neutron scattering on YBCO and BSCO. As a result, the imaginary part of the susceptibility is drastically reduced in the low-energy region by going from slightly underdoped toward optimally doped systems, while  $T_c$  is practically unchanged. This implies that the real SFI coupling constant  $\lambda_{sf}(\sim g_{sf}^2)$  is small since the experimental value  $g_{sf}^{(exp)} < 0.2$  eV

is much smaller than the assumed theoretical value  $g_{sf}^{(th)} \approx (0.7-1.5) eV$ .

Inelastic neutron and X-ray scattering measurements in HTSC cuprates show that the broadening of some phonon lines is by an order of magnitude larger than the LDA-DFA methods predict. Since the phonon line-widths depend on the EPI coupling and the charge susceptibility, it is evident that calculations of both quantities are beyond the range of applicability of LDA-DFT. As a consequence, the LDA-DFT calculations overestimate the electronic screening and thus underestimate the EPI coupling, since many-body effects due to strong correlations are not contained in this mean-field theory. However, in spite of the promising and encouraging experimental results about the dominance of EPI in cuprates, the theory is still confronted with difficulties in explaining sufficiently large coupling constant in the  $d$ -channel. At present there is not such a satisfactory microscopic theory although some concepts, such as the dominant EPI scattering at small transfer momenta, are understood at least qualitatively. This set of problems and questions will be discussed in Section 2.

## 2. Theory of EPI in HTSC

The experimental results in Section 1 give evidence that the electron-phonon interaction (EPI) in HTSC cuprates is strong and in order to be conform with  $d$ -wave pairing *EPI must be peaked at small transfer momenta*. A number of other experiments in HTSC cuprates give evidence that these are *strongly correlated systems* with large on-site Coulomb repulsion of electrons on the Cu-ions. However, at present there is no satisfactory microscopic theory of pairing in HTSC cuprates which is able to calculate  $T_c$  and the order parameter. This is due to mathematical difficulties in obtaining a solution of the formally exact *ab initio many-body equations* which take into account two important ingredients—EPI and strong correlations [6]. In Section 2.1 we discuss first the *ab initio* many-body theory of superconductivity in order to point places which are most difficult to be solved. Since the superconductivity is low energy phenomenon (also in HTSC cuprates), one can simplify the structure of the *ab initio* equations in the low-energy sector (the Migdal-Eliashberg theory), where the high-energy processes are incorporated in the (so called) *ideal band-structure* (nonlocal) potential  $V_{IBS}(\mathbf{x}, \mathbf{y})$  and the *vertex function*  $\Gamma$ . This program of calculations of  $V_{IBS}(\mathbf{x}, \mathbf{y})$ ,  $\Gamma$ , and the EPI coupling (*matrix elements*)  $g_{ep}(\mathbf{x}, \mathbf{y})$  is not realized in HTSC superconductors due to its complexity. However, one pragmatical way out is to calculate  $g_{ep}$  in the framework of the LDA-DFT method which is at present stage unable to treat strong correlations in a satisfactory manner. Some achievements and results of the LDA-DFT methods which are related to HTSC cuprates are discussed in Section 2.2.

In the case of very complicated systems, such as the HTSC cuprates, the standard (pragmatical) procedure in physics is to formulate a minimal theoretical model—sometimes called *toy model*—which includes minimal set of important ingredients necessary for qualitative and semiquantitative study

of a phenomenon. As a consequence of the experimental results, the *minimal theoretical model* must comprise *two important ingredients*: (1) *EPI* and (2) *strong correlations*. In Section 2.3 we will formulate such a *minimal theoretical model*—called *the  $t$ - $J$  model which includes EPI* too. In the framework of this model we will discuss the renormalization of EPI by strong correlations. In recent years the interest in these problems is increased and numerous numerical calculations were done mostly on small clusters with  $n \times n$  atoms ( $n < 8$ ). We will not discuss this subject which is fortunately covered in the recent comprehensive review in [10, 11]. The analytical approaches in studying the renormalization of EPI by strong correlations, which are based on a controllable and systematic theory, are rather scarce. We will discuss such a systematic and controllable theory in the framework of the  $t$ - $J$  model with *EPI*, which is formulated and solved in terms of Hubbard operators. The theory of this (toy) model predicts some interesting effects which might be important for understanding the physics of HTSC cuprates. It predicts that the high-energy processes (due to the suppression of doubly occupancy for  $U \gg W_b$ ) give rise to a nonlocal contribution to the band-structure potential (self-energy  $\Sigma(\mathbf{x}, \mathbf{y}, \omega = 0)$ ) as well as to EPI. This nonlocality in EPI is responsible for the peak in the effective pairing potential ( $V_{ep,eff}(\mathbf{q}, \omega)$ ) at small transfer momenta ( $q (\leq q_c \ll k_F)$ ) [6, 78–80, 130]. The latter property allows that the (strong) EPI is conform with  $d$ -wave pairing in HTSC cuprates. Furthermore, the peculiar structural properties of HTSC cuprates and corresponding electronic quasi-two-dimensionality give an additional nonlocality in EPI. The latter is due to the change of the weakly screened Madelung energy which is involved in most of the lattice vibrations along the  $c$ -axis. Since at present there is no quantitative theory for the latter effect, we tackle this problem here only briefly. The next task for the future studies of the physics of HTSC cuprates is to incorporate these structural properties in the minimal theoretical  $t$ - $J$  model.

Finally, by writing this chapter our intention is not to overview the theoretical studies of EPI in HTSC cuprates—which is an impossible task—but first to elucidate the descending way from the (old) well-defined *ab initio* microscopic theory of superconductivity to the one of the minimal model which treats the interplay of EPI and strong correlations. Next, we would like to encourage the reader to further develop the theory of HTSC cuprates.

### 2.1. Microscopic Theory of Superconductivity

**2.1.1. *Ab Initio Many-Body Theory.*** The many-body theory of superconductivity is based on the fully microscopic electron-ion Hamiltonian for electrons and ions in the crystal—see, for instance, [193, 194]. It comprises mutually interacting electrons which interact also with the periodic lattice and with the lattice vibrations. In order to pass continually to the problem of the interplay of EPI and strong correlations and also to explain why the LDA-DFT method is inadequate for HTSC cuprates, we discuss this problem here with restricted details—more extended discussion can be

found in [6, 194]. In order to describe superconductivity the Nambu-spinor  $\hat{\psi}^\dagger(\mathbf{r}) = (\hat{\psi}_i^\dagger(\mathbf{r})\hat{\psi}_i(\mathbf{r}))$  is introduced which operates in the electron-hole space ( $\hat{\psi}(\mathbf{r}) = (\hat{\psi}^\dagger(\mathbf{r}))^\dagger$ ) where  $\hat{\psi}_i(\mathbf{r})$ ,  $\hat{\psi}_i^\dagger(\mathbf{r})$  are annihilation and creation operators for spin up, respectively, and so forth. The microscopic Hamiltonian of the system under consideration contains three parts:  $\hat{H} = \hat{H}_e + \hat{H}_i + \hat{H}_{e-i}$ . The *electronic Hamiltonian*  $\hat{H}_e$ , which describes the kinetic energy and the Coulomb interactions of electrons, is given by

$$\begin{aligned} \hat{H}_e = & \int d^3r \hat{\psi}^\dagger(\mathbf{r}) \hat{\tau}_3 \epsilon_0(\hat{p}) \hat{\psi}(\mathbf{r}) \\ & + \frac{1}{2} \int d^3r d^3r' \hat{\psi}^\dagger(\mathbf{r}) \hat{\tau}_3 \hat{\psi}(\mathbf{r}) V_c(\mathbf{r} - \mathbf{r}') \hat{\psi}^\dagger(\mathbf{r}') \hat{\tau}_3 \hat{\psi}(\mathbf{r}'), \end{aligned} \quad (46)$$

where  $\epsilon_0(\hat{p}) = \hat{p}^2/2m$  is the kinetic energy of electron and  $V_c(\mathbf{r} - \mathbf{r}') = e^2/|\mathbf{r} - \mathbf{r}'|$  is the electron-electron Coulomb interaction. Note that in the electron-hole space the pseudospin (Nambu) matrices  $\hat{\tau}_i$ ,  $i = 0, 1, 2, 3$  are Pauli matrices. Since we will discuss only the electronic properties, the explicit form of the *lattice Hamiltonian*  $\hat{H}_i$  [6, 194] is omitted here. The *electron-ion Hamiltonian* describes the interaction of electrons with the equilibrium lattice and with its vibrations, respectively:

$$\begin{aligned} \hat{H}_{e-i} = & \sum_n \int d^3r V_{e-i}(\mathbf{r} - \mathbf{R}_n^0) \hat{\psi}^\dagger(\mathbf{r}) \hat{\tau}_3 \hat{\psi}(\mathbf{r}) \\ & + \int d^3r \hat{\Phi}(\mathbf{r}) \hat{\psi}^\dagger(\mathbf{r}) \hat{\tau}_3 \hat{\psi}(\mathbf{r}). \end{aligned} \quad (47)$$

Here,  $V_{e-i}(\mathbf{r} - \mathbf{R}_n^0)$  is the electron-ion potential and its form depends on the level of description of the electronic subsystem. For instance, in the *all-electron calculations* one has  $V_{e-i}(\mathbf{r} - \mathbf{R}_n^0) = -Ze^2/|\mathbf{r} - \mathbf{R}_n^0|$  where  $Ze$  is the ionic charge. The second term which is proportional to the lattice distortion operator  $\hat{\Phi}(\mathbf{r}) = -\sum_{n,\alpha} \hat{u}_{an} \nabla_\alpha V_{e-i}(\mathbf{r} - \mathbf{R}_n^0) + \hat{\Phi}_{\text{anh}}(\mathbf{r})$  (because of convenience it includes also the *EPI* coupling  $\nabla_\alpha V_{e-i}$ ) describes the interaction of electrons with harmonic ( $\sim \hat{u}_{an}$ ) (or anharmonic  $\sim \hat{\Phi}_{\text{anh}}(\mathbf{r})$ ) lattice vibrations.

Dyson's equations for the electron and phonon Green's functions  $\hat{G}(1,2) = -\langle T \hat{\psi}(1) \hat{\psi}^\dagger(2) \rangle$ ,  $\tilde{D}(1-2) = -\langle T \hat{\Phi}(1) \hat{\Phi}(2) \rangle$  are  $\hat{G}^{-1}(1,2) = \hat{G}_0^{-1}(1,2) - \hat{\Sigma}(1,2)$  and  $\tilde{D}^{-1}(1,2) = \tilde{D}_0^{-1}(1,2) - \tilde{\Pi}(1,2)$ , where the  $\hat{G}_0^{-1}(1,2) = [(-\partial/\partial\tau_1 - \epsilon_0(\mathbf{p}_1) + \mu) \hat{\tau}_0 - u_{\text{eff}}(1) \hat{\tau}_3] \delta(1-2)$  is the bare inverse electronic Green's function. Here,  $1 = (\mathbf{r}_1, \tau_1)$ , where  $\tau_1$  is the imaginary time in the Matsubara technique, and the effective one-body potential  $u_{\text{eff}}(1) = V_{e-i}(1) + V_H + \langle \hat{\Phi}(1) \rangle$ , where  $V_H$  is the Hartree potential. The electron and phonon self-energies  $\hat{\Sigma}(1,2)$  and  $\tilde{\Pi}(1,2)$  take into account many-body dynamics of the interacting system. The *electronic self-energy*  $\hat{\Sigma}(1,2) = \hat{\Sigma}_c(1,2) + \hat{\Sigma}_{ep}(1,2)$  is obtained in the form

$$\hat{\Sigma}(1,2) = -V_{\text{eff}}(1,\bar{1}) \hat{\tau}_3 \hat{G}(1,\bar{2}) \hat{\Gamma}_{\text{eff}}(\bar{2},2;\bar{1}), \quad (48)$$

where integration (summation) over the bar indices is understood. The effective retarded potential  $V_{\text{eff}}(1,\bar{1})$  in (48)

contains the screened (by the electron dielectric function  $\epsilon_e(1,2)$ ) Coulomb and *EPI* interactions:

$$V_{\text{eff}}(1,2) = V_c(1-\bar{1}) \epsilon_e^{-1}(\bar{1},2) + \epsilon_e^{-1}(1,\bar{1}) \tilde{D}(\bar{1},\bar{2}) \epsilon_e^{-1}(\bar{2},2). \quad (49)$$

The inverse electronic dielectric permeability  $\epsilon_e^{-1}(1,2) = \delta(1-2) + V_c(1-\bar{1}) P(\bar{1},\bar{2}) \epsilon_e^{-1}(\bar{2},2)$  is defined via the irreducible electronic polarization operator  $P(1,2) = -S p \{ \hat{\tau}_3 \hat{G}(1,\bar{2}) \hat{\Gamma}_{\text{eff}}(\bar{2},\bar{3};2) \hat{G}(\bar{3},1^+) \}$ . The *vertex function*  $\hat{\Gamma}_{\text{eff}}(1,2;3) = -\delta \hat{G}(1,2) / \delta u_{\text{eff}}(3)$  in (48) is the solution of the complicated (and practically unsolvable) integro-differential functional equation

$$\begin{aligned} \hat{\Gamma}_{\text{eff}}(1,2;3) = & \hat{\tau}_3 \delta(1-2) \delta(1-3) \\ & + \frac{\delta \hat{\Sigma}(1,2)}{\delta \hat{G}(\bar{1},\bar{2})} \hat{G}(\bar{1},\bar{3}) \hat{G}(\bar{4},\bar{2}) \hat{\Gamma}_{\text{eff}}(\bar{3},\bar{4};3). \end{aligned} \quad (50)$$

Note that the effective vertex function  $\hat{\Gamma}_{\text{eff}}(1,2;3)$ , which takes into account all renormalizations going beyond the simple Coulomb (*RPA*) screening, is the functional of both the electronic and phononic Green's functions  $\hat{G}$  and  $\tilde{D}$ , thus making at present the ab initio microscopic equations practically unsolvable.

**2.1.2. Low-Energy Migdal-Eliashberg Theory.** If the vertex function  $\hat{\Gamma}_{\text{eff}}$  would be known, we would have a closed set of equations for Green's functions which describe dynamics of the interacting electrons and lattice vibrations (phonons) in the normal and superconducting state. However, this is a formidable task and at present far from any practical realization. Fortunately, we are mostly interested in *low-energy phenomena* (with energies  $|\omega_n|, \xi \ll \omega_c$  and for momenta  $k = k_F + \delta k$  in the shell  $\delta k \ll \delta k_c$  near the Fermi momentum  $k_F$ ;  $\omega_c$  and  $\delta k_c$  are some cutoffs), which allows us further simplification of equations [1, 2]. Therefore, the strategy is to *integrate high-energy processes*—see more in [194]. Here, we sketch this procedure briefly. Namely, Green's function  $\hat{G}(\mathbf{k}, \omega_n) = [i\omega_n - (\mathbf{k}^2/2m - \mu) \hat{\tau}_3 - \hat{\Sigma}(\mathbf{k}, \omega_n)]^{-1}$  can be formally written in the form

$$\hat{G}(\mathbf{k}, \omega_n) = \hat{G}^{\text{low}}(\mathbf{k}, \omega_n) + \hat{G}^{\text{high}}(\mathbf{k}, \omega_n), \quad (51)$$

where  $\hat{G}^{\text{low}}(\mathbf{k}, \omega_n) = \hat{G}(\mathbf{k}, \omega_n) \Theta(\omega_c - |\omega_n|) \Theta(\delta k_c - \delta k)$  is the low-energy Green's function and  $\hat{G}^{\text{high}}(\mathbf{k}, \omega_n) = \hat{G}(\mathbf{k}, \omega_n) \Theta(|\omega_n| - \omega_c) \Theta(\delta k - \delta k_c)$  is the high-energy one and analogously  $D = D^{\text{low}}(\mathbf{k}, \omega_n) + D^{\text{high}}(\mathbf{k}, \omega_n)$ . By introducing the *small parameter* of the theory  $s \sim (\omega/\omega_c) \sim (\delta k/\delta k_c) \ll 1$  one has in leading order  $\hat{G}^{\text{low}}(\mathbf{k}, \omega_n) \sim s^{-1}$ ,  $\hat{G}^{\text{high}}(\mathbf{k}, \omega_n) \lesssim 1$  and  $D^{\text{low}}(\mathbf{k}, \omega_n) \sim s^0$ ,  $D^{\text{high}}(\mathbf{k}, \omega_n) \sim s^2$ . Note that the coupling constants ( $V_{ei}$ ,  $\nabla V_{ei}$ ,  $V_{ii}$ , etc.) are of the order  $s^0 = 1$ .

The procedure of separating low-energy and high-energy processes lies also behind the *adiabatic approximation* since in most materials the characteristic phonon (Debye) energy  $\omega_D$  of lattice vibrations is much smaller than the characteristic electronic Fermi energy  $E_F$  ( $\omega_D \ll E_F$ ). In the

small  $s (\ll 1)$  limit the Migdal theory [1, 2] keeps in the total self-energy  $\Sigma$  linear terms in the phonon propagator  $\tilde{D}$  ( $D$ ) only. In that case the effective vertex function can be written in the form  $\hat{\Gamma}_{\text{eff}}(1, 2; 3) \cong \hat{\Gamma}_c(1, 2; 3) + \delta\hat{\Gamma}_{ep}(1, 2; 3)$  [1, 2], where the Coulomb charge vertex  $\hat{\Gamma}_c(1, 2; 3) = \hat{\tau}_3\delta(1-2)\delta(1-3) + \delta\hat{\Sigma}_c(1, 2)/\delta u_{\text{eff}}(3)$  contains correlations due to the Coulomb interaction only but does not contain *EPI* and phonon propagator  $\tilde{D}$  explicitly. The part  $\delta\hat{\Gamma}_{ep}(1, 2; 3) = \delta\hat{\Sigma}_{ep}(1, 2)/\delta u_{\text{eff}}(3)$  contains all linear terms with respect to *EPI*. Note that in these diagrams enters the dressed Green's function which contains implicitly *EPI* up to infinite order. By careful inspection of all (explicit) contributions to  $\delta\hat{\Gamma}_{ep}(1, 2; 3)$  which is linear in  $\tilde{D}$  one can express the self-energy in terms of the charge (Coulomb) vertex  $\hat{\Gamma}_c(1, 2; 3)$  only. As a result of this approximation, the part of the self-energy due to Coulomb interaction is given by

$$\hat{\Sigma}_c(1, 2) = -V_c^{\text{sc}}(1, \bar{1})\hat{\tau}_3\hat{G}(1, \bar{2})\hat{\Gamma}_c(\bar{2}, 2; \bar{1}), \quad (52)$$

where  $V_c^{\text{sc}}(1, 2) = V_c(1, \bar{2})\epsilon_e^{-1}(\bar{2}, 2)$  is the screened Coulomb interaction. The part which is due to *EPI* has the following form:

$$\hat{\Sigma}_{ep}(1, 2) = -V_{ep}(\bar{1}, \bar{2})\hat{\Gamma}_c(1, \bar{3}; \bar{1})\hat{G}(\bar{3}, \bar{4})\hat{\Gamma}_c(\bar{4}, 2; \bar{2}), \quad (53)$$

where  $V_{ep}(1, 2) = \epsilon_e^{-1}(1, \bar{1})\tilde{D}(\bar{1}, \bar{2})\epsilon_e^{-1}(\bar{2}, 2)$  is the screened *EPI* potential. Note that  $\hat{\Sigma}_{ep}(1, 2)$  depends now quadratically on the charge vertex  $\hat{\Gamma}_c$ , which is due to the adiabatic theorem.

It is well known that the Coulomb self-energy  $\hat{\Sigma}_c(1, 2)$  is the most complicating part of the electronic dynamics, but since we are interested in low-energy physics when  $s \ll 1$ , then the term  $\hat{\Sigma}_c(1, 2)$  can be further simplified by separating it in two parts:

$$\hat{\Sigma}_c(1, 2) = \hat{\Sigma}_c^{(h)}(1, 2) + \hat{\Sigma}_c^{(l)}(1, 2). \quad (54)$$

The term  $\hat{\Sigma}_c^{(h)}(1, 2)$  is due to high-energy processes contained in the product  $\hat{G}^{\text{high}}(1, \bar{2})\hat{\Gamma}_c^{\text{high}}(\bar{2}, 2; \bar{1})$  (e.g., due to the large Hubbard  $U$  in strongly correlated systems) and  $\hat{\Sigma}_c^{(l)}(1, 2)$  is due to low-energy processes. The leading part of  $\hat{\Sigma}_c^{(h)}(1, 2)$  is 1, that is,  $\hat{\Sigma}_c^{(h)}(1, 2) \sim s^0$ , while  $\hat{\Sigma}_c^{(l)}(1, 2)$  is small of order 1, that is,  $\hat{\Sigma}_c^{(l)}(1, 2) \sim s^1$ . For further purposes we define the quantity  $\hat{V}_0$  as

$$\hat{V}_0(1, 2) = \{V_{e-i}(1) + V_H(1)\}\hat{\tau}_3\delta(1-2) + \hat{\Sigma}_c^{(h)}(1, 2), \quad (55)$$

where  $V_{e-i}$ ,  $V_H$  are also of order  $s^0$ . After the Fourier transform with respect to time (and for small  $|\omega_n| \ll \omega_c$ )  $\hat{\Sigma}_c^{(h)}$  is given by

$$\hat{\Sigma}_c^{(h)}(\mathbf{x}_1, \mathbf{x}_2, \omega_n) \cong \Sigma_{c0}^{(h)}(\mathbf{x}_1, \mathbf{x}_2, 0)\hat{\tau}_3 + \left(\hat{\Sigma}_{c0}^{(h)}\right)'(\mathbf{x}_1, \mathbf{x}_2, 0) \cdot i\omega_n. \quad (56)$$

As we said,  $\Sigma_{c0}^{(h)} \sim s^0$  while  $\left(\hat{\Sigma}_{c0}^{(h)}\right)' \cdot \omega_n \sim s^1$  because  $\omega_n \sim s^1$ . From (52) it is seen that the part  $\hat{\Sigma}_c^{(l)}(1, 2)$  contains the low-energy Green's function  $\hat{G}^{\text{low}}(1, \bar{2})$  and this skeleton diagram

is of order  $s^1$ . The similar analysis based on (53) for  $\hat{\Sigma}_{ep}(1, 2)$  gives that the leading order is  $s^1$  which describes the low-energy part of *EPI*. After the separations of terms (of  $s^0$  and  $s^1$  orders) the Dyson equation in the low-energy region has the form

$$\begin{aligned} & \left[ i\omega_n Z_c(\mathbf{x}, \bar{\mathbf{x}}) - \hat{H}_0(\mathbf{x}, \bar{\mathbf{x}}) - \hat{\Sigma}_c^{(l)}(\mathbf{x}, \bar{\mathbf{x}}, \omega_n) - \hat{\Sigma}_{ep}(\mathbf{x}, \bar{\mathbf{x}}, \omega_n) \right] \\ & \times \hat{G}^{\text{low}}(\bar{\mathbf{x}}, \mathbf{y}, \omega_n) = \delta(\mathbf{x} - \mathbf{y})\hat{\tau}_0, \end{aligned} \quad (57)$$

where  $\bar{\mathbf{x}}$  means integration  $\int d^3\bar{x}$  over the crystal volume. The Coulomb renormalization function  $Z_c(\mathbf{x}, \mathbf{y}) = \delta(\mathbf{x} - \mathbf{y}) - (\Sigma_{0c}^{(h)})'(\mathbf{x}, \mathbf{y}, 0)$  and the single-particle Hamiltonian  $\hat{H}_0(\mathbf{x}, \mathbf{y})$  collect formally all high-energy processes which are unaffected by superconductivity (which is low-energy process) where

$$\hat{H}_0(\mathbf{x}, \mathbf{y}) = \left\{ \left( -\frac{1}{2m} \nabla_{\mathbf{x}}^2 - \mu \right) \delta(\mathbf{x} - \mathbf{y}) + V_0^{(h)}(\mathbf{x}, \mathbf{y}, 0) \right\} \hat{\tau}_3 \quad (58)$$

with

$$V_0^{(h)}(\mathbf{x}, \mathbf{y}, 0) = \{V_{e-i}(\mathbf{x}) + V_H(\mathbf{x})\}\delta(\mathbf{x} - \mathbf{y}) + \Sigma_{c0}^{(h)}(\mathbf{x}, \mathbf{y}, 0). \quad (59)$$

One can further absorb  $Z_c(\mathbf{x}, \mathbf{y})$  into the renormalized Green's function

$$\hat{G}_r(x, \mathbf{y}, \omega_n) = Z_c^{1/2}(\mathbf{x}, \bar{\mathbf{x}})\hat{G}^{\text{low}}(\bar{\mathbf{x}}, \bar{\mathbf{y}}, \omega_n)Z_c^{1/2}(\bar{\mathbf{y}}, \mathbf{y}), \quad (60)$$

the renormalized vertex function  $\hat{\Gamma}_{\text{ren}}(1, 2; 3) = Z_c^{-1/2}\hat{\Gamma}_c Z_c^{-1/2}$ , and the renormalized self-energies

$$\hat{\Sigma}_{r,c,ep}^{(l)}(\mathbf{x}, \mathbf{y}, \omega_n) = Z_c^{-1/2}(\mathbf{x}, \bar{\mathbf{x}})\hat{\Sigma}_{c,ep}^{(l)}(\bar{\mathbf{x}}, \bar{\mathbf{y}}, \omega_n)Z_c^{-1/2}(\bar{\mathbf{y}}, \mathbf{y}) \quad (61)$$

and introduce the ideal band-structure Hamiltonian  $\hat{h}_0(\mathbf{x}, \mathbf{y}) = Z_c^{-1/2}(\mathbf{x}, \bar{\mathbf{x}})\hat{H}_0(\bar{\mathbf{x}}, \bar{\mathbf{y}})Z_c^{-1/2}(\bar{\mathbf{y}}, \mathbf{y})$  given by

$$\hat{h}_0(\mathbf{x}, \mathbf{y}) = \left\{ \left( -\frac{1}{2m} \nabla_{\mathbf{x}}^2 - \mu \right) \delta(\mathbf{x} - \mathbf{y}) + V_{\text{IBS}}(\mathbf{x}, \mathbf{y}) \right\} \hat{\tau}_3. \quad (62)$$

Here,

$$V_{\text{IBS}}(\mathbf{x}, \mathbf{y}) = Z_c^{-1/2}(\mathbf{x}, \bar{\mathbf{x}})V_0^{(h)}(\bar{\mathbf{x}}, \bar{\mathbf{y}})Z_c^{-1/2}(\bar{\mathbf{y}}, \mathbf{y}) \quad (63)$$

is the ideal band-structure potential (sometimes called the excitation potential) and apparently nonlocal quantity, which is contrary to the standard local potential  $V_g(\mathbf{x})$  in the LDA-DFT theories—see Section 2.2. The static potential  $V_{\text{IBS}}(\mathbf{x}, \mathbf{y})$  is of order  $s^0$  and includes high-energy processes.

Finally, we obtain the matrix Dyson equation for the renormalized Green's function  $\hat{G}_r(x, \mathbf{y}, \omega_n)$  which is the basis for the (strong-coupling) Migdal-Eliashberg theory in the low-energy region

$$\begin{aligned} & \left[ i\omega_n \delta(\mathbf{x} - \bar{\mathbf{x}}) - \hat{h}_0(\mathbf{x}, \bar{\mathbf{x}}) - \hat{\Sigma}_{c,r}^{(l)}(\mathbf{x}, \bar{\mathbf{x}}, \omega_n) - \hat{\Sigma}_{ep,r}(\mathbf{x}, \bar{\mathbf{x}}, \omega_n) \right] \\ & \times \hat{G}_r(\bar{\mathbf{x}}, \mathbf{y}, \omega_n) = \delta(\mathbf{x} - \mathbf{y})\hat{\tau}_0, \end{aligned} \quad (64)$$

where  $\hat{\Sigma}_{c,r}^{(l)}$  and  $\hat{\Sigma}_{ep,r}$  have the same form as (52)-(53) but with the renormalized Green's and vertex functions  $\hat{G}_r, \hat{\Gamma}_r$  instead of  $\hat{G}, \hat{\Gamma}$ . We stress that (64) holds in the low-energy region only. In the superconducting state the set of Eliashberg equations in (64) are written explicitly in Appendix A, where it is seen that the superconducting properties depend on the Eliashberg spectral function  $\alpha_{\text{cp}}^2 F(\omega)$ . The latter function is defined also in Appendix A, (A.4), and it depends on material properties of the system.

The important ingredients of the low-energy Migdal-Eliashberg theory are the ideal band-structure Hamiltonian  $\hat{h}_0(\mathbf{x}, \mathbf{y})$ —given by (62) which contains many-body (excitation) ideal band-structure nonlocal periodic crystal potential  $V_{\text{IBS}}(\mathbf{x}, \mathbf{y})$ . The Hamiltonian  $\hat{h}_0(\mathbf{x}, \mathbf{y})$  determines the *ideal energy spectrum*  $\epsilon(\mathbf{k})$  of the conduction electrons and the wave function  $\psi_{i,\mathbf{p}}(\mathbf{x})$  through

$$\hat{h}_0(\mathbf{x}, \bar{\mathbf{y}}) \psi_{i,\mathbf{k}}(\bar{\mathbf{y}}) = [\epsilon_i(\mathbf{k}) - \mu] \psi_{i,\mathbf{k}}(\mathbf{x}), \quad (65)$$

where  $\mu$  is the chemical potential. We stress that the Hamiltonian  $\hat{h}_0(\mathbf{x}, \mathbf{y})$  also governs transport properties of metals in low-energy region.

After solving (65) the next step is to expand all renormalized Green's function, self-energies, vertices, and the renormalized *EPI* matrix element (written symbolically as  $g_{ep,r} = g_{ep,0} \Gamma_{\text{ren}} \epsilon_e^{-1}$ ) in the basis of  $\psi_{i,\mathbf{p}}(\mathbf{x})$  and to write down the Eliashberg equations in this basis. We will not elaborate further this program and refer the reader to the relevant literature in [193, 194]. We point out that even such simplified program of the low-energy Migdal-Eliashberg theory was never fully realized in low-temperature superconductors, because the nonlocal potential  $V_{\text{IBS}}(\mathbf{x}, \mathbf{y})$  (enters the ideal band-structure Hamiltonian  $h_0(\mathbf{x}, \mathbf{y})$ ) and the renormalized vertex function (entering the *EPI* coupling constant  $g_{ep,r}$ ) which include electronic correlations are difficult to calculate especially in strongly correlated metals. Therefore, it is not surprising at all that the situation is even more difficult in *HTS* materials which are strongly correlated systems with complex structural and material properties. Due to these difficulties the calculations of the electronic band structure and the *EPI* coupling are usually done in the framework of LDA-DFT where the many-body excitation potential  $V_{\text{IBS}}(\mathbf{x}, \mathbf{y})$  is replaced by some (usually local) potential  $V_{\text{LDA}}(\mathbf{x})$  which in fact determines the ground-state properties of the crystal. In the next section we briefly describe (i) the LDA-DFT procedure in calculating the *EPI* coupling constant and (ii) some results of the LDA-DFT calculations related to *HTSC* cuprates. We will also discuss why this approximation is inappropriate when applied to *HTS* materials.

**2.2. LDA-DFT Calculations of the *EPI* Matrix Elements.** We point out again two results which are important for the future microscopic theory of pairing in *HTSC* cuprates. *First*, numerous experiments (discussed in Part I) give evidence that the *EPI* coupling constant which enters the normal part of the quasiparticle self-energy  $\lambda_{ep}^Z = \lambda_s + \lambda_d + \dots$  is rather large, that is,  $1 < \lambda_{ep}^Z < 3.5$ . In order to be conform with

*d*-wave pairing the effective *EPI* potential must be nonlocal (and peaked at small transfer momenta  $q$ ), which implies that the *s*-wave and *d*-wave coupling constants are of the same order, that is,  $\lambda_d \approx \lambda_s$ . *Second*, the theory based on the minimal *t*-*J* model, which will be discussed in Section 2.3, gives that strong electronic correlations produce a peak at small transfer momenta in the effective *EPI* pairing potential thus giving rise to  $\lambda_d \approx \lambda_s$ . This is a striking property which allows that *EPI* is conform with *d*-wave pairing. However, the theory is seriously confronted with the problem of calculation of the coupling constants  $\lambda_{ep}^Z$ . It turns out that at present it is an illusory task to calculate  $\lambda_{ep}^Z$  and  $\lambda_d$  since it is extremely difficult (if possible at all) to incorporate the peculiar structural properties of *HTSC* cuprates (layered structure, ionic-metallic system, etc.) and strong correlations effects in a consistent and reliable microscopic theory which is described in Section 2.1. As it is stressed several times, the LDA-DFT methods miss some important many-body effects (especially in the band-structure potential) and therefore fail to describe correctly screening properties of *HTSC* cuprates and the strength of *EPI*. However, the LDA-DFT methods are able to incorporate diverse structural properties of *HTSC* cuprates much better than the simplified minimal *t*-*J* (toy) model. Here, we discuss briefly some achievements of the advanced LDA-DFT calculations which are able to take partially into account some nonlocal effects in the *EPI*. The latter are mainly due to the almost *ionic structure along the c-axis* which is reflected in the very small *c*-axis plasma frequency ( $\omega_c \ll \omega_{ab}$ ).

The main task of the LDA-DFT theory in obtaining the *EPI* matrix elements is to calculate the change of the ground-state (self-consistent) potential  $\delta V_g(\mathbf{r})/\delta R_\alpha$  and the *EPI* coupling constant (*matrix element*)  $g_\alpha^{\text{LDA}}(\mathbf{k}, \mathbf{k}')$  (see its definition below), which is the most difficult part of calculations. Since in the LDA-DFT method the *EPI* scattering cannot be formulated, then the recipe is that the calculated  $g_\alpha^{\text{LDA}}(\mathbf{k}, \mathbf{k}')$  is inserted into the many-body Eliashberg equations. By knowing  $g_\alpha^{\text{LDA}}(\mathbf{k}, \mathbf{k}')$  one can define the total ( $\lambda$ ) and partial ( $\lambda_{q,\nu}$ ) *EPI* coupling constants for the  $\nu$ th mode, respectively [195], as

$$\lambda = \frac{1}{Np} \sum_{\mathbf{q},\nu} \lambda_{q,\nu}, \quad \lambda_{q,\nu} = \frac{p\gamma_{q,\nu}}{\pi N(0)\omega_{q,\nu}}, \quad (66)$$

where  $p = 3\kappa$  is the number of phonon branches ( $\kappa$  is the number of atoms in the unit cell) and  $N(0)$  is the density of states at the Fermi energy (per spin and unit cell). The *phonon line-width*  $\gamma_{q,\nu}$  is defined in the Migdal-Eliashberg theory by

$$\begin{aligned} \gamma_{q,\nu} &= 2\pi\omega_{q,\nu} \frac{1}{N} \sum_{l'l'k} \frac{1}{2M\omega_{k-q,\nu}} |e_{\nu}^{\alpha}(\mathbf{q}) \cdot g_{\alpha,l'l'}(\mathbf{k}, \mathbf{k}-\mathbf{q})|^2 \\ &\times \left[ \frac{n_F(\xi_{l,k}) - n_F(\xi_{l,k} + \hbar\omega_{q,\nu})}{\hbar\omega_{q,\nu}} \right] \\ &\times \delta(\xi_{l',k-q} - \xi_{l,k} - \hbar\omega_{q,\nu}). \end{aligned} \quad (67)$$

Here,  $e_{\nu}^{\alpha}(\mathbf{q})$  is the phonon polarization vectors;  $n_F$  is the Fermi function. Since the ideal energy spectrum from (65)

$\xi_{l,\mathbf{k}} = E_{l,\mathbf{k}} - \mu$  and the corresponding eigenfunctions  $\psi_{kl}$  are unknown, then instead of these one sets in (67) the *LDA-DFT* eigenvalues for the  $l$ th band  $\xi_{l,\mathbf{k}}^{(\text{LDA})}$  and  $\psi_{kl}^{(\text{LDA})}$ . In the *LDA-DFT* method the *EPI matrix element*  $g_{\alpha,l'l'}^{(\text{LDA})}$  is defined by the change of the ground-state potential  $\delta V_g(\mathbf{r})/\delta R_\alpha$ :

$$g_{\alpha,l'l'}^{(\text{LDA})}(\mathbf{k}, \mathbf{k}') = \left\langle \psi_{kl}^{(\text{LDA})} \left| \sum_n \frac{\delta V_g(\mathbf{r})}{\delta R_{n\alpha}} \right| \psi_{k'l'}^{(\text{LDA})} \right\rangle. \quad (68)$$

The index  $n$  means summation over the lattice sites;  $\alpha = x, y, z$  and the wave function  $\psi_{kl}^{(\text{LDA})}$  are the solutions of the Kohn-Sham equation—see [6]. In the past various approximations within the *LDA-DFT* method have been used in calculating  $\delta V_g(\mathbf{r})/\delta R_\alpha$  and  $\lambda$  while here we comment some of them only. (i) In most calculations in *LTS* systems and in *HTSC* cuprates the *rigid-ion (RI)* approximation was used as well as its further simplifications which inevitably (due to its shortcomings and obtained small  $\lambda$ ) deserves to be commented. The *RI* approximation is based on the very specific assumption that the ground-state (crystal) potential  $V_g(\mathbf{r})$  can be considered as a sum of ionic potentials  $V_g(\mathbf{r}) = \sum_n V_g(\mathbf{r} - \mathbf{R}_n)$  where the ion potential  $V_g(\mathbf{r} - \mathbf{R}_n)$  and the electron density  $\rho_e(\mathbf{r})$  are carried rigidly with the ion at  $\mathbf{R}_n$  during the ion displacement ( $\mathbf{R}_n = \mathbf{R}_n^0 + \hat{u}_{an}$ ). In the *RI* approximation the change of  $V_g(\mathbf{r})$  is given by

$$\begin{aligned} \delta V_g(\mathbf{r}) &= \sum_n \nabla_\alpha V_g(\mathbf{r} - \mathbf{R}_n^0) u_{an}, \\ \frac{\delta V_g(\mathbf{r})}{\delta R_{n\alpha}} &= \nabla_\alpha V_g(\mathbf{r} - \mathbf{R}_n^0), \end{aligned} \quad (69)$$

which means that *RI* does not take into account changes of the electron density during the ion displacements. In numerous calculations applied to *HTSC* cuprates the *rigid-ion model* is even further simplified by using the *rigid muffin-tin approximation (RMTA)* (or similar version with the rigid-atomic sphere)—see discussions in [195–198]. The *RMTA* assumes that the ground-state potential and the electron density follow ion displacements rigidly inside the Wigner-Seitz cell while outside it  $V_g(\mathbf{r})$  is not changed because of the assumed very good metallic screening (e.g., in simple metals):

$$\nabla_\alpha V_g(\mathbf{r} - \mathbf{R}_n) = \begin{cases} \nabla_\alpha V_g(\mathbf{r} - \mathbf{R}_n), & \mathbf{r} \text{ in cell } n, \\ 0, & \text{outside.} \end{cases} \quad (70)$$

This means that the dominant *EPI* scattering is due to the nearby atoms only and that the scattering potential is isotropic. All nonlocal effects related to the interaction of electrons with ions far away are neglected in the *RMTA*. In this case  $g_{\alpha,n}^{\text{LDA}}(\mathbf{k}, \mathbf{k}')$  is calculated by the wave function centered at the given ion  $\mathbf{R}_n^0$  which can be expanded inside the muffin-tin sphere (outside it the potential is assumed to be constant) in the angular momentum basis  $\{l, m\}$ , that is,

$$\langle \mathbf{r} | \psi_{\mathbf{k}}^{(\text{RMTA})} \rangle = \sum_{lmn} C_{lm}(k, \mathbf{R}_n^0) \rho_l(|\mathbf{r} - \mathbf{R}_n^0|) Y_{lm}(\phi, \theta) \quad (71)$$

(the angles  $\phi, \theta$  are related to the vector  $\hat{\mathbf{r}} = (\mathbf{r} - \mathbf{R}_n^0)/|\mathbf{r} - \mathbf{R}_n^0|$ ). The radial function  $\rho_l(|\mathbf{r} - \mathbf{R}_n^0|)$  is zero outside the

muffin-tin sphere. In that case the *EPI* matrix element is given by  $g_{\alpha,n}^{\text{RMTA}}(\mathbf{k}, \mathbf{k}') \sim \langle Y_{lm} | \hat{\mathbf{r}} | Y_{l'm'} \rangle$  and because  $\hat{\mathbf{r}}$  is vector the selection rule implies that only terms with  $\Delta l \equiv l' - l = \pm 1$  contribute to the *EPI* coupling constant in the *RMTA*. This result is an immediate consequence of the assumed locality of the *EPI* potential in *RMTA*. However, since *nonlocal effects*, such as the long-range Madelung-like interaction, are important in *HTSC* cuprates, then additional terms contribute also to the coupling constant  $g_{\alpha,n}$ , that is,  $g_{\alpha,n}(\mathbf{k}, \mathbf{k}') = g_{\alpha,n}^{\text{RMTA}}(\mathbf{k}, \mathbf{k}') + g_{\alpha,n}^{\text{nonloc}}(\mathbf{k}, \mathbf{k}')$ , where a part ( $\delta g_{\alpha,n}^{\text{nonloc}}$ ) of the nonlocal contribution to  $g_{\alpha,n}^{\text{nonloc}}$  is represented schematically:

$$\delta g_{\alpha,n}^{\text{nonloc}}(\mathbf{k}, \mathbf{k}') \sim \langle Y_{lm} | (\mathbf{R}_n^0 - \mathbf{R}_m^0)_\alpha | Y_{l'm'} \rangle. \quad (72)$$

From (72) comes out the selection rule  $\Delta l = l' - l = 0$  for the nonlocal part of the  $E - P$  interaction. We stress that the  $\Delta l = 0$  (nonlocal) terms are omitted in the *RMTA* approach and therefore it is not surprising that this approximation works satisfactorily in elemental (isotropic) metals only. The latter are characterized by the large density of states at the Fermi surface which makes electronic screening very efficient. This gives rise to a local *EPI* where an electron feels potential changes of the nearby atom only. One can claim with certainty that the *RMTA* method is not suitable for *HTSC* cuprates which are highly anisotropic systems with pronounced ionic character of binding and pronounced strong electronic correlations. The *RMTA* method applied to *HTSC* cuprates misses just this important part—the long-range part *EPI* due to the change of the long-range Madelung energy in the almost ionic structure of *HTSC* cuprates. For instance, the first calculations done in [199] which are based on the *RMTA* give very small *EPI* coupling constant  $\lambda^{\text{RMTA}} \sim 0.1$  in *YBCO*, which is in apparent contradiction with the experimental finding that  $\lambda_{ep}$  is large—see Section 1.

However, these nonlocal effects are taken into account in [195] by using the *frozen-in phonon (FIP)* method in evaluating of  $\lambda_{ep}$  in  $\text{La}_{2-x}\text{M}_x\text{CuO}_4$ . In this method some symmetric phonons are considered and the band structure is calculated for the system with the super-cell which is determined by the periodicity of the phonon displacement. By comparing the unperturbed and perturbed energies the corresponding *EPI* coupling  $\lambda_\nu$  (for the considered phonon  $\nu$ th mode) is found. More precisely speaking, in this approach the matrix elements of  $\delta V_g(\mathbf{r})/\delta R_{0,\alpha}^\kappa$  are determined from the finite difference of the ground-state potential  $\Delta V_{g,q,\nu}(\mathbf{r}) = V_g(\mathbf{R}_{0,L}^\kappa + \Delta \tau_{q,\nu}^\kappa(L)) - V_g(\mathbf{R}_{0,L}^\kappa) = \sum_{L,\kappa} \Delta \tau_{q,\nu}^\kappa(L) \partial V_g(\mathbf{R}_{0,L}^\kappa) / \partial \mathbf{R}_{0,L}^\kappa$ , where  $L, \kappa$  enumerate elementary lattice cells and atoms in the unit cell, respectively. The frozen-in atomic displacements of the phonon  $\Delta \tau_{q,\nu}^\kappa(L)$  of the  $\nu$ th mode are given by  $\Delta \tau_{q,\nu}^\kappa(L) = \Delta u_{q,\nu}(\hbar/2M_\kappa \omega_{q,\nu})^{1/2} \text{Re}[\mathbf{e}_{\kappa,\nu}(\mathbf{q}) e^{i\mathbf{q} \cdot \mathbf{R}}]$  where  $\Delta u_{q,\nu}$  is the dimensionless phonon amplitude and the phonon polarization (eigen)vector  $\mathbf{e}_{\kappa,\nu}(\mathbf{q})$  fulfills the condition  $\sum_\kappa \mathbf{e}_{\kappa,\nu}^*(\mathbf{q}) \cdot \mathbf{e}_{\kappa,\nu}(\mathbf{q}) = \delta_{\nu,\nu'}$ . Based on this approach various symmetric  $A_g$  (and some  $B_{3g}$ ) modes of  $\text{La}_{2-x}\text{M}_x\text{CuO}_4$  were studied [195], where it was found that the large matrix elements are due to unusually long-range Madelung-like, especial for the  $c$ -axis phonon modes. The obtained large  $\lambda_{ep} \approx 1.37$  is the consequence of the following three main

facts. (i) The electronic spectrum in *HTSC* cuprates is highly anisotropic, that is, it is *quasi-two-dimensional*. This is an important fact for pairing because if the conduction electrons would be uniformly spread over the whole unit cell then due to the rather low electron density ( $n \sim 10^{21} \text{ cm}^{-3}$ ) the density of states on the Cu and O in-plane atoms would be an order of magnitude smaller than the real value. This would further give an order of magnitude smaller *EPI* coupling constant  $\lambda_{ep}$ . Note that the calculated density of states on the (heavy) Cu and (light) O in-plane atoms,  $N^{\text{Cu}}(0) \cong 0.54 \text{ states/eV}$  and  $N^{\text{O}_{xy}}(0) \cong 0.35 \text{ states/eV}$ , is of same order of magnitude as in some *LTS* materials. For instance, in NbC where  $T_c \approx 11 \text{ K}$  one has on (the heavy) Nb atom  $N^{\text{Nb}}(0) \cong 0.58 \text{ states/eV}$  and on (the light) C atom  $N^{\text{C}}(0) \cong 0.25 \text{ states/eV}$ . So, the quasi-two-dimensional character of the spectrum is crucial in obtaining appreciable density of states on the light O atoms in the  $\text{CuO}_2$  planes. (ii) In *HTSC* cuprates there is *strong Cu–O hybridization* leading to good in-plane metallic properties. This *large covalency in the plane* is due to the (fortunately) small energy separation of the electron levels on Cu and  $\text{O}_{xy}$  atoms which comes out from the band-structure calculations [200], that is,  $\Delta = |\epsilon_{\text{Cu}} - \epsilon_{\text{O}_{xy}}| \approx 3 \text{ eV}$ . The latter value gives rise to strong covalent mixing (the hybridization parameter  $t_{pd}$ ) of the  $\text{Cu}_{d_{x^2-y^2}}$  and  $\text{O}_{p_{xy}}$  states, that is,  $t_{pd} = -1.85 \text{ eV}$ . It is interesting that the small value of  $\Delta$  is not due to the ionic structure (crystal field effect) of the system but it is mainly due to the *natural falling* of the  $\text{Cu}_{d_{x^2-y^2}}$  states across the transition-metal series. So, the natural closeness of the atomic energy levels of the  $\text{Cu}_{d_{x^2-y^2}}$  and  $\text{O}_{p_{xy}}$  states is this distinctive feature of *HTSC* cuprates which basically allows achievement of high  $T_c$ . (iii) The *ionic structure of HTSC cuprates* which is very pronounced along the  $c$ -axis is responsible for the weak electronic screening along this axis and according to that for the significant contribution of the nonlocal (long-range) Madelung-like interaction to *EPI*. It turns out that because of the ionicity of the structure the  $\text{La}$  and  $\text{O}_z$  *axial modes are strongly coupled with charge carriers* in the  $\text{CuO}_2$  planes despite the fact that the local density of states on these atoms is very small [195], that is,  $N^{\text{La}}(0) = 0.13 \text{ states/eV}$  and  $N^{\text{O}_z}(0) = 0.016 \text{ states/eV}$ . (For comparison, on planar atoms Cu and  $\text{O}_{xy}$  one has  $N^{\text{Cu}}(0) = 0.54 \text{ states/eV}$  and  $N^{\text{O}_{xy}}(0) = 0.35 \text{ states/eV}$ .) These calculations show that the lanthanum mode (with  $\omega_{q,\nu} = 202 \text{ cm}^{-1}$ ) at the  $q = (0, 0.2\pi/c)$  zone boundary (fully symmetric  $Z$ -point) has ten times larger coupling constant  $\lambda_{q,\nu}^{\text{La}}(\text{FIP}) = 4.8$  than it is predicted in the *RMT* approximation  $\lambda_{q,\nu}^{\text{La}}(\text{RMT}) = 0.48$ . The similar increase holds for the average coupling constant, where  $\lambda_{\nu,\text{average}}^{\text{La}}(\text{FIP}) = 1.0$  but  $\lambda_{\nu,\text{average}}^{\text{La}}(\text{RMT}) = 0.1$ . Note that for the  $\mathbf{q} \approx 0$   $\text{La}$ -mode one obtains  $\lambda_{\nu}^{\text{La}}(\text{FIP}) = 4.54$  compared to  $\lambda_{\nu}^{\text{La}}(\text{RMT}) = 0.12$ . Similar results hold for the axial apex-oxygen  $q = (0, 0.2\pi/c)$  mode ( $\text{O}_z$ ) with  $\omega_{q,\nu} = 396 \text{ cm}^{-1}$  where the large (compared to the *RMT* method) coupling constant is obtained:  $\lambda_{q,\nu}^{\text{O}_z} = 14$  and  $\lambda_{\nu,\text{average}}^{\text{O}_z} = 4.7$ , while for  $q \approx 0$  axial apex-oxygen modes with  $\omega_{q,\nu} = 415 \text{ cm}^{-1}$  one has  $\lambda_{\nu,\text{average}}^{\text{O}_z} = 11.7$ . After averaging over all calculated modes it was estimated that  $\lambda = 1.37$  and  $\omega_{\log} \approx 400 \text{ K}$ . By assuming that  $\mu^* = 0.1$  one obtains  $T_c = 49 \text{ K}$  by using

Allen-Dynes formula for  $T_c \approx 0.83\omega_{\log} \exp\{-1.04(1+\lambda)/[\lambda - \mu^*(1+0.62\lambda)]\}$  with  $\omega_{\log} = 2 \int d\omega d\omega' \alpha^2(\omega)F(\omega) \ln \omega/\lambda\omega$ . For  $\mu^* = 0.15$  and  $0.2$  one obtains  $T_c = 41$  and  $32 \text{ K}$ , respectively. We stress that the rather large  $\lambda_{ep}$  (and  $T_c$ ) is due to the nonlocal (long range) effects of the metallic-ionic structure of *HTSC* cuprates and non-muffin-tin corrections in *EPI*, as was first proposed in [201, 202]. However, we would like to stress that the optimistic results for  $\lambda_{ep}$  obtained in [195] are in fact based on the calculation of the *EPI* coupling for some wave vectors  $\mathbf{q}$  with symmetric vibration patterns and in fact the obtained  $\lambda_{ep}$  is an extrapolated value. The all- $\mathbf{q}$  calculations of  $\lambda_{ep,\mathbf{q}}$  which take into account long-range effects are a real challenge for the *LDA-DFT* calculations and are still awaiting.

Finally, it is worth to mention important calculations of the *EPI* coupling constant in the framework of the *linear-response full-potential linear-muffin-tin-orbital method (LRFP-LMTO)* invented in [203, 204] and applied to the doped *HTSC* cuprate  $(\text{Ca}_{1-x}\text{Sr}_x)_{1-y}\text{CuO}_2$  for  $x \sim 0.7$  and  $y \sim 0.1$  with  $T_c = 110 \text{ K}$  [205]. Namely, these calculations give strong evidence that the structural properties of *HTSC* cuprates already alone make the dominance of small- $q$  scattering in *EPI*, whose effect is additionally increased by strong correlations. In order to analyze this compound in [205] the calculations are performed for  $\text{CaCuO}_2$  doped by holes in a uniform, neutralizing back-ground charge. The momentum ( $\mathbf{q} = (\mathbf{q}_{\parallel}, q_{\perp})$ ) dependent *EPI* coupling constant (summed over all phonon branches  $\nu$ ) in different  $L$  channels ( $s, p, d$ .) is calculated by using a standard expression

$$\lambda_L(\mathbf{q}) = M \sum_{\mathbf{k}, \nu} Y_L(\mathbf{k} + \mathbf{q}) \left| g_{\mathbf{k}, \mathbf{q}, \nu} \right|^2 Y_L(\mathbf{k}) \delta(\xi_{\mathbf{k}+\mathbf{q}}) \delta(\xi_{\mathbf{k}}). \quad (73)$$

Here,  $\xi_{\mathbf{k}}$  is the quasiparticle energy,  $g_{\mathbf{k}, \mathbf{q}, \nu}$  is the *EPI* coupling constant (matrix element) with the  $\nu$ th branch,  $Y_L(\mathbf{k})$  is the  $L$ -channel wave function, and the normalization factor  $M \propto N_L^{-1}(0)$  with the partial density of states is  $N_L(0) \propto \sum_{\mathbf{k}} Y_L^2(\mathbf{k}) \delta(\xi_{\mathbf{k}})$ . The total coupling constant in the  $L$ -channel is an average of  $\lambda_L(\mathbf{q})$  over the whole 2D Brillouin zone (over  $\mathbf{q}_{\parallel}$ ), that is,  $\lambda_L(q_{\perp}) = \langle \lambda_L(\mathbf{q}_{\parallel}) \rangle_{\text{BZ}}$ . We stress three important results of [205]. *First*, the  $s$ - and  $d$ -coupling constants,  $\lambda_s(\mathbf{q})$ ,  $\lambda_d(\mathbf{q})$ , are *peaked at small transfer momenta*  $\mathbf{q} \sim (\pi/3a, 0, 0)$  as it is shown in [205, Figure 3]. This result is mainly caused by the nesting properties of the Fermi surface shown in [205, Figure 1]. *Second*, the  $\mathbf{q}$ -dependence of the integrated *EPI* matrix elements  $|\bar{g}_{L,\mathbf{q}}|^2 = \lambda_L(\mathbf{q})/\chi_L''(\mathbf{q})$  (with  $\chi_L''(\mathbf{q}) \propto \sum_{\mathbf{k}} Y_L(\mathbf{k} + \mathbf{q}) Y_L(\mathbf{k}) \delta(\xi_{\mathbf{k}+\mathbf{q}}) \delta(\xi_{\mathbf{k}})$ ) for  $L = s, d$  is similar to that of  $\lambda_L(\mathbf{q})$ , that is, these are peaked at small transfer momenta  $q \ll 2k_F$ . Both of these results mean that the structural properties of *HTSC* cuprates imply the *dominance of small- $q$  EPI scattering*. *Third*, the calculations give similar values for  $\lambda_s(q_{\perp} = 0)$  and  $\lambda_d(q_{\perp} = 0)$ , that is,  $\lambda_s = 0.47$  for  $s$ -wave and  $\lambda_d = 0.36$  for  $d$ -wave pairing [205]. The result that  $\lambda_d \approx \lambda_s$  is due to the dominance of the small  $q$ -scattering in *EPI*, which means that the nonlocal effects (long-range forces) in *EPI* of *HTSC* cuprates are very important. This result together with the finding of the dominance of the small- $q$  scattering in *EPI* due to strong correlations [78–80, 130, 179, 180] mean that strong correlations and the

peculiar structural properties of HTSC cuprates make EPI conform with  $d$ -wave pairing, either as its main cause or as its supporter. We stress that the obtained coupling constant  $\lambda_d = 0.36$  is rather small to give  $d$ -wave pairing with large  $T_c$  and on the first glance this result is against the EPI mechanism of pairing in cuprates. However, it is argued throughout this paper that the LDA methods applied to strongly correlated systems overestimate the screening effects and underestimate the coupling constant and therefore their quantitative predictions are not reliable.

### 2.3. EPI and Strong Correlations in HTSC Cuprates

**2.3.1. Minimal Model Hamiltonian.** The *minimal microscopic model* for HTSC cuprates must include at least three orbitals: one  $d_{x^2-y^2}$ -orbital of the Cu-ion and two  $p$ -orbitals ( $p_{x,y}$ ) of the O-ion since they participate in transport properties of these materials—see more in [6] and references therein. The electronic part of the Hamiltonian (of the minimal model) is  $\hat{H}_0 = \hat{H}_d + \hat{H}_{\text{int}}$ —usually called the *Emery model* (or the  *$p$ - $d$  model*) [206], where the one-particle tight-binding Hamiltonian  $\hat{H}_0$  describes the lowering of the kinetic energy in the  $p$ - $d$  model (with three bands or orbitals):

$$\begin{aligned} \hat{H}_0 = & \sum_{i,\sigma} (\epsilon_d^0 - \mu) d_{i\sigma}^\dagger d_{i\sigma} + \sum_{j,\alpha,\sigma} (\epsilon_{p\alpha}^0 - \mu) p_{j\alpha\sigma}^\dagger p_{j\alpha\sigma} \\ & + \sum_{i,j,\alpha,\sigma} t_{ij\alpha}^{pd} d_{i\sigma}^\dagger p_{j\alpha\sigma} + \sum_{j,j',\alpha,\beta,\sigma} t_{jj',\alpha\beta}^{pp} p_{j\alpha\sigma}^\dagger p_{j'\beta\sigma}. \end{aligned} \quad (74)$$

Here  $t_{ij\alpha}^{pd}$  ( $i, j$  enumerate the Cu- and O-sites, resp.) is the hopping integral between the  $p_\alpha$  ( $\alpha = x, y$ )—and  $d$ -states and  $t_{jj',\alpha\beta}^{pp}$  between the  $p_\alpha$ - and  $p_\beta$ -states—while  $\epsilon_d^0$  and  $\epsilon_{p\alpha}^0$  are the bare  $d$ - and  $p$ -local energy levels and  $\mu$  is the chemical potential. This tight-binding Hamiltonian is written in the *electronic notation* where the charge-transfer energy  $\Delta_{dp,0} \equiv \epsilon_d^0 - \epsilon_p^0 > 0$  by assuming that there is one  $3d_{x^2-y^2}$  electron on the copper ( $\text{Cu}^{2+}$ ) while electrons in the  $p$ -levels of the  $\text{O}^{2-}$  ions occupy filled bands.  $\hat{H}_0$  contains the main ingredients coming from the comparison with the *LDA-DFT* band-structure calculations. The *LDA-DFT* results are reproduced by assuming that  $t^{pp} \ll t_{pd}$  (and  $\epsilon_{p\alpha}^0 = \epsilon_p^0$ ) where the good fit to the *LDA-DFT* band structure is found for  $\Delta_{dp,0} \equiv \epsilon_d^0 - \epsilon_p^0 \approx 3.2$  eV and  $t^{pd} (\equiv t_{pd}) = (\sqrt{3}/2)(pd\sigma)$ ,  $(pd\sigma) = -1.8$  eV. The total LDA bandwidth  $W_b = (4\sqrt{2})|t_{pd}| \approx 9$  eV [207].

The electron interaction is described by  $\hat{H}_{\text{int}}$ :

$$\hat{H}_{\text{int}} = U_d \sum_i n_i^d n_i^d + U_p \sum_{j,\alpha} n_{j\alpha}^p n_{j\alpha}^p + \hat{V}_c + \hat{V}_{ep}, \quad (75)$$

where  $U_d$  and  $U_p$  are the on-site Coulomb repulsion energies at Cu and O sites, respectively, while  $\hat{V}_c$  and  $\hat{V}_{ep}$  describe the long-range part of the Coulomb interaction of electrons (holes) and *EPI*, respectively. Note that the Hubbard repulsion  $U_d$  on the Cu-ion is different from its bare atomic value  $U_{d0}$  ( $\approx 16$  eV for Cu) due to various kinds of screening effects in solids [208–210]. It turns out that

in most transition metal oxides one has  $U_d \ll U_{d0}$ . This problem is thoroughly studied in [208–210] and applied to HTSC cuprates. The estimation from the numerical cluster calculations [211] gives  $U_d = 9$ –11 eV and  $U_p = 4$ –6 eV but because  $n_i^d U_d \gg n_j^p U_p$  the on-site repulsion on the oxygen ion is usually neglected at the first stage of the analysis.

Note that in the case of large  $U_d (\gg t_{pd}, \Delta_{dp,0})$  the *hole notation* is usually used where in the parent compound (and for  $|t_{pd}| \ll \Delta_{dp,0}$ ) one has  $\langle n_i^d \rangle = 1$ , that is, one hole in the 3D-shell (in the  $3d_{x^2-y^2}$  state) in the ground state. In the limit of large  $U_d \rightarrow \infty$  the *doubly occupancy on the Cu atoms is forbidden* and only two copper states are possible:  $\text{Cu}^{2+}$ —described by the quantum state  $d_{i\sigma}^\dagger |0\rangle$  with one hole in the 3D shell and  $\text{Cu}^{1+}$ —described by  $|0\rangle$  with zero holes in the filled 3D shell. In this (hole) notation the oxygen  $p$ -level is fully occupied by electrons, that is, there are no holes ( $\langle n_j^p \rangle = 0$ ) in the occupied oxygen  $2p$ -shell of  $\text{O}^{2-}$ . In this notation the vacuum state  $|0_v\rangle$  (not the ground state) of the Hamiltonian  $\hat{H}$  for large  $U_d$  corresponds to the closed-shell configuration  $\text{Cu}^{1+}\text{O}^{2-}$ . In the hole notation the hole  $p$ -level  $\epsilon_{ph}^0$  lies higher than the hole  $d$ -level  $\epsilon_{dh}^0$ , that is,  $\Delta_{pd,0} \equiv \epsilon_{ph}^0 - \epsilon_{dh}^0 > 0$  (note that in the electron notation it is opposite) and  $U_d$  means repulsion of two holes (in the  $3d_{x^2-y^2}$  orbital) with opposite spins— $3d^8$  configuration of the  $\text{Cu}^{3+}$  ion. Note that  $\epsilon_{ph}^0 = -\epsilon_p^0$ ,  $\epsilon_{dh}^0 = -\epsilon_d^0$ , and  $t_{pd,h} = -t_{pd}$ . In the following the index  $h$  in  $t_{pd,h}$  is omitted. The reason for  $\epsilon_{ph}^0 > \epsilon_{dh}^0$  is partly in different energies for the hole sitting on the oxygen and copper, respectively [207]. From this model one can derive in the limit  $U \rightarrow \infty$  the  $t$ - $J$  model for the 2D lattice in the  $\text{CuO}_2$  plane [212, 213], where now each lattice site corresponds to a Cu-atom. In the presence of one hole in the 3D-shell then in the *undoped* (no oxygen holes) HTSC cuprate each lattice site is occupied by one hole. By doping the system with holes the additional holes go onto O-sites. Furthermore, due to the strong Cu–O covalent binding the energetics of the system implies that an O-hole forms a Zhang-Rice singlet with a Cu-hole [212]. In the  $t$ - $J$  model the *Zhang-Rice singlet is described by an empty site*. Since in the  $t$ - $J$  model the doubly occupancy is forbidden, one introduces annihilation (Hubbard) operator of the composite fermion  $\hat{X}_i^{\sigma_1\sigma_2} = c_{i\sigma}^\dagger (1 - n_{i,-\sigma})$  which describes creation of a hole (in the 3D-shell of the Cu-atoms) on the  $i$ th site if this site is previously empty (thus excluding doubly occupancy), that is, the constraint  $n_{i,\sigma} + n_{i,-\sigma} \leq 1$  must be fulfilled on each lattice site. In this picture the doped-hole concentration  $\delta$  means at the same time the concentration of the oxygen holes, that is, of the Zhang-Rice singlets.

In order not to confuse the reader we stress the difference in the meaning of the hole in the ( $p$ - $d$ ) three-band Emery model and in the single-band (effective)  $t$ - $J$  model. In the Emery model the hole means the absence of the electron in the filled shell—the 3D shell for Cu atoms(ions) and  $2p$  shell for O atoms(ions). On the other side the hole on the  $i$ th lattice site in the  $t$ - $J$  model means the presence of the Zhang-Rice singlet on this site.

The *bosonic-like operators*  $\hat{X}_i^{\sigma_1\sigma_2} = \hat{X}_i^{\sigma_1 0} \hat{X}_i^{0\sigma_2}$  for  $\sigma_1 \neq \sigma_2$  create a *spin fluctuation* at the  $i$ th site and the spin operator is

given by  $\mathbf{S} = \hat{X}_i^{\bar{\sigma}_1 0} (\bar{\sigma})_{\bar{\sigma}_1 \bar{\sigma}_2} \hat{X}_i^{\bar{\sigma}_2 0}$  where summation over the bar indices is understood. The operator  $\sum_{\sigma} \hat{X}_i^{\sigma\sigma}$  has the meaning of the *hole number on the  $i$ th site*. It is useful to introduce the operator  $\hat{X}_i^{00} = \hat{X}_i^{0\sigma} \hat{X}_i^{\sigma 0}$  at the  $i$ th lattice site which is the *number of Zhang-Rice singlets on the  $i$ th site*. For  $\hat{X}_i^{00}|0\rangle = |1\rangle$  the  $i$ th site is occupied by the Zhang-Rice singlet, while for  $\hat{X}_i^{00}|1\rangle = |0\rangle$  there is no Zhang-Rice singlet on the  $i$ th site (i.e., this site is occupied only by one  $3d^9$  hole on the Cu site). This property of  $\hat{X}_i^{00}$  is due to the *local constraint*

$$\hat{X}_i^{00} + \sum_{\sigma=\uparrow\downarrow} \hat{X}_i^{\sigma\sigma} = 1, \quad (76)$$

which *forbids doubly occupancy* of the  $i$ th site by holes. By projecting out doubly occupied (high-energy) states the  $t$ - $J$  model reads

$$\begin{aligned} \hat{H}_{t-j} = & \sum_{i,\sigma} \epsilon_i^0 \hat{X}_i^{\sigma\sigma} - \sum_{i,j,\sigma} t_{ij} \hat{X}_i^{\sigma 0} \hat{X}_j^{0\sigma} \\ & + \sum_{i,j} J_{ij} \left( \mathbf{S}_i \cdot \mathbf{S}_j - \frac{1}{4} \hat{n}_i \hat{n}_j \right) + \hat{H}_3. \end{aligned} \quad (77)$$

The first term ( $\sim \epsilon_i^0$ ) describes an effective local energy of the hole (or the Zhang-Rice singlet), the second one ( $\sim t_{ij}$ ) describes hopping of the holes, and the third one ( $\sim J_{ij}$ ) is the Heisenberg-like exchange energy between two holes. The theory [212] predicts that  $|\epsilon_i^0| \gg |t_{ij}|$ . This property is very important in the study of EPI.  $\hat{H}_3$  contains three-site term which is usually omitted believing that it is not important. For charge fluctuation processes it is plausible to omit it, while for spin-fluctuation processes it is questionable approximation. If one introduces the enumeration  $\alpha, \beta, \gamma, \lambda = 0, \uparrow, \downarrow$ , then the Hubbard operators satisfy the following algebra:

$$\left[ \hat{X}_i^{\alpha\beta}, \hat{X}_j^{\gamma\lambda} \right]_{\pm} = \delta_{ij} \left[ \delta_{\gamma\beta} \hat{X}_i^{\alpha\lambda} \pm \delta_{\alpha\lambda} \hat{X}_i^{\gamma\beta} \right], \quad (78)$$

where  $\delta_{ij}$  is the Kronecker symbol. Note that the Hubbard operators possess the *projection properties* with  $\hat{X}_i^{\alpha\beta} \hat{X}_i^{\gamma\lambda} = \delta_{\beta\gamma} \hat{X}_i^{\alpha\lambda}$ . The (anti)commutation relations in (78) are more complicated than the canonical Fermi and Bose (anti)commutation relations, which complicates the mathematical structure of the theory. To escape these complications some novel techniques have been used, such as the one *slave boson-technique*. In this technique  $\hat{X}_i^{0\sigma} = f_{i\sigma} b_i^{\dagger}$ ,  $\hat{X}_i^{\sigma_1 \sigma_2} = f_{i\sigma_1}^{\dagger} f_{i\sigma_2}$  are represented in terms of the fermion (spinon) operator  $f_{i\sigma}$  which annihilates the spin on the  $i$ th and the boson (holon) operator  $b_i^{\dagger}$  which creates the Zhang-Rice singlet.

In the minimal theoretical model the electron-phonon interaction (EPI) contains in principle two leading terms:

$$\hat{H}_{ep} = \hat{H}_{ep}^{\text{ion}} + \hat{H}_{ep}^{\text{cov}}, \quad (79)$$

which are the “ionic” one ( $\hat{H}_{ep}^{\text{ion}}$ ) and the “covalent” one ( $\hat{H}_{ep}^{\text{cov}}$ ). The “ionic” term describes the change of the energy

of the hole (or the Zhang-Rice singlet) at the  $i$ th site due to lattice vibrations and it reads [6, 78–80, 130]

$$\hat{H}_{ep}^{\text{ion}} = \sum_{i,\sigma} \hat{\Phi}_i \hat{X}_i^{\sigma\sigma}, \quad (80)$$

where the “displacement” operator

$$\hat{\Phi}_i = \sum_{L\kappa} \left[ \epsilon (\mathbf{R}_i^0 - \mathbf{R}_{L\kappa}^0 + \hat{\mathbf{u}}_i - \hat{\mathbf{u}}_{L\kappa}) - \epsilon (\mathbf{R}_i^0 - \mathbf{R}_{L\kappa}^0) \right] \quad (81)$$

(which as in Section 2.1 includes the bare coupling constant) describes the change of the hole (or Zhang-Rice singlet) energy  $\epsilon_{a,i}^0$  by displacing atoms in the lattice by the vector  $\hat{\mathbf{u}}_{L\kappa}$ . In the harmonic approximation the EPI potential is given by  $\hat{\Phi}_i = \sum_{\mathbf{q},\lambda} g_i(\mathbf{q},\lambda) \exp\{i\mathbf{q}\mathbf{R}_i\} [b_{\mathbf{q},\lambda} + b_{-\mathbf{q},\lambda}^{\dagger}]$  where  $b_{\mathbf{q},\lambda}$  and  $b_{\mathbf{q},\lambda}^{\dagger}$  are the annihilation and creation operator of phonons with the polarization  $\lambda$ , respectively. This term describes in principle the following processes: (1) the change of the O-hole and Cu-hole bare energies  $\epsilon_{\text{ph}}^0, \epsilon_{\text{dh}}^0$  in the three-band model due to lattice vibrations, (2) the change of the long-range Madelung energy (which is due to the ionicity of the structure) by lattice vibrations along the  $c$ -axis, and (3) the change of the Cu–O hopping parameter  $t_{pd}$  in the presence of vibrations, and so forth. Here,  $L$  and  $\kappa$  enumerate unit lattice vectors and atoms in the unit cell, respectively. Usually, the EPI scattering is studied in the harmonic approximation where the phonon operator  $\hat{\Phi}_i$  is calculated in the harmonic approximation ( $\hat{\Phi} \sim \hat{\mathbf{u}}$ ) for the EPI interaction of holes with some specific phononic modes, such as the breathing and half-breathing ones [10, 11, 169]. The theory which includes also all other (than oxygen) vibrations in  $\hat{\Phi}_i$  is still awaiting.

It is interesting to make comparison of the EPI coupling constants in the  $t$ - $J$  model and in the Hartree-Fock (HF) approximation (which is the analogous of the LDA-DFT method) of the three-band Emery ( $p$ - $d$ ) model in (74)–(75) when the problem is projected on the single band. For instance, the coupling constant with the *half-breathing mode* at the zone boundary in the HF approximation (which mimics the LDA-DFT approach) is given by

$$g_{\text{hb}}^{\text{HF}} = \pm 4t_{pd} \frac{\partial t_{pd}}{\partial R_{\text{Cu-O}}} \frac{1}{\epsilon_d - \epsilon_p} u_0, \quad (82)$$

while the coupling constant in the  $t$ - $J$  model  $g_{\text{hb}}^{t-J} (= \partial \epsilon^0 / \partial R_{\text{Cu-O}})$  is given by

$$g_{\text{hb}}^{t-J} = \pm 4t_{pd} \frac{\partial t_{pd}}{\partial R_{\text{Cu-O}}} \left[ \frac{2p^2 - 1}{\epsilon_d - \epsilon_p} + \frac{2p^2}{U_d - |\epsilon_d - \epsilon_p|} \right] u_0, \quad (83)$$

where  $p = 0.96$ —see [10, 11, 169] and references therein. It is obvious that in the  $t$ - $J$  model the electron-phonon coupling is different from the HF one, since the former contains an *additional term* coming from the many-body effects, which are not comprised by the HF (LDA-DFT) calculations. The first term in (83) describes the hopping of a 3D hole into the O  $2p$ -states and this term exists also in the LDA-DFT coupling constant—see (82). However, the second term in (83), which is due to many-body effects, describes the

hopping of an O  $2p$ -hole into the (already) single occupied Cu 3D state and it does not exist in the LDA-DFT approach. Since the corresponding dimensionless coupling constant  $\lambda_{\text{hb}}$  is proportional to  $|g_{\text{hb}}|^2$ , one obtains that the bare  $t$ - $J$  coupling constant is almost three times larger than the LDA-DFT one:

$$\lambda_{\text{hb}}^{t-J} \approx 3\lambda_{\text{hb}}^{\text{HF}}. \quad (84)$$

This example demonstrates clearly that the LDA-DFT method is inadequate for calculating the EPI coupling constant in HTSC cuprates.

Note that there is also a covalent contribution to EPI which comes from the change of the effective hopping ( $t$ ) in of the  $t$ - $J$  model (77) and the exchange energy ( $J$ ) in the presence of atomic displacements:

$$\begin{aligned} \hat{H}_{ep}^{\text{cov}} = & - \sum_{i,j,\sigma} \frac{\partial t_{ij}}{\partial (\mathbf{R}_i^0 - \mathbf{R}_j^0)} (\hat{\mathbf{u}}_i - \hat{\mathbf{u}}_j) \hat{X}_i^{\sigma 0} \hat{X}_j^{0\sigma} \\ & + \sum_{i,j} \frac{\partial J_{ij}}{\partial (\mathbf{R}_i^0 - \mathbf{R}_j^0)} (\hat{\mathbf{u}}_i - \hat{\mathbf{u}}_j) \mathbf{S}_i \cdot \mathbf{S}_j. \end{aligned} \quad (85)$$

Here, we will not go into details but only stress that since  $|\epsilon_p^0| \gg |t_{ij}|$  then *the covalent term in the effective  $t$ - $J$  model is much smaller than the ionic term*—see more in [6, 10, 11, 169] and references therein—and in the following only the term  $\hat{H}_{ep}^{\text{ion}}$  will be considered [6, 78–80, 130].

### 2.3.2. Controllable $X$ -Method for the Quasiparticle Dynamics.

The minimal model Hamiltonian for strongly correlated holes with EPI (discussed above) is expressed via the Hubbard operators which obey “ugly” noncanonical commutation relations. The latter property is rather unpleasant for making a controllable theory in terms of Feynmann diagrams (for these “ugly” operators) and some other approaches are required. A possible way out is to express the Hubbard operators in terms of fermions and bosons (which must be confined) as, for instance, in the slave boson (SB) method. However, in real calculations which are based on some approximations the SB method is confronted with some subtle constraints whose fulfillments require very sophisticated mathematical treatment. Fortunately, there is a *mathematically controllable approach* for treating the problem directly with Hubbard operators and without using slave-boson (or fermion) techniques. This method—we call it the *X-method*—is based on the general Baym-Kadanoff technique which allows to treat the problem by the well-defined and controllable  $1/N$  expansion for the Green’s functions in terms of Hubbard operators. This approach is formulated in [214] while the important refinement of the method is done in [78–80, 130]. In the paramagnetic and homogeneous state (with finite doping) the Green’s function  $G_{\sigma_1\sigma_2}(1-2)$  is diagonal, that is,  $G_{\sigma_1\sigma_2}(1-2) = \delta_{\sigma_1\sigma_2} G(1-2)$  where

$$G(1-2) = -\langle T \hat{X}^{0\sigma}(1) \hat{X}^{\sigma 0}(2) \rangle = g(1-2)Q, \quad (86)$$

with the Hubbard spectral weight  $Q = \langle \hat{X}^{00} \rangle + \langle \hat{X}^{\sigma\sigma} \rangle$ . The function  $g(1-2)$  plays the role of the quasiparticle Green’s

function—see more in [6, 78–80, 130, 179, 180]. It turns out that in order to have a controllable theory ( $1/N$  expansion) one way is to increase the number of spin components from two to  $N$  by changing the constraint (76) into the new one

$$\hat{X}_i^{00} + \sum_{\sigma=1}^N \hat{X}_i^{\sigma\sigma} = \frac{N}{2}. \quad (87)$$

In order to reach the convergence of physical quantities in the limit  $N \rightarrow \infty$  the hopping and exchange energy are also rescaled, that is,  $t_{ij} = t_{0,ij}/N$  and  $J_{ij} = J_{0,ij}/N$ . In order to eliminate possible misunderstandings we stress that in the case  $N > 2$  the constraint in (87) spoils some projection properties of the Hubbard operators. Fortunately, these (lost) projection properties are not used at all in the refined theory. As a result one obtains the functional integral equation for  $G(1,2)$ , thus allowing *unambiguous mathematical and physical treatment* of the problem. In [78–80, 130, 179, 180] it is developed a systematic  $1/N$  expansion for the quasiparticle Green’s function  $g(1-2) (= g_0 + g_1/N + \dots)$ ,  $Q (= Nq_0 + q_1 + \dots)$  (also for  $G(1-2)$ ) and the self-energy. For large  $N (\rightarrow \infty)$  the leading term is  $G_0(1-2) = g_0(1-2)Q_0 = O(N)$  with  $g_0 = O(1)$  and  $Q_0 = \langle \hat{X}_i^{00} \rangle = N\delta/2$ . Here,  $\delta$  is the concentration of the oxygen holes (that is, of the Zhang-Rice singlets) which is related to the chemical potential by the equation  $1 - \delta = 2 \sum_{\mathbf{p}} n_F(\mathbf{p})$  with  $n_F(\mathbf{p}) = (e^{\epsilon_0(\mathbf{k}) - \mu} + 1)^{-1}$ . The quasiparticle Green’s function  $g_0(\mathbf{k}, \omega)$  and the quasiparticle spectrum  $\epsilon_0(\mathbf{k})$  in the leading order are given by

$$g_0(\mathbf{k}, \omega) \equiv \frac{G_0(\mathbf{k}, \omega)}{Q_0} = \frac{1}{\omega - [\epsilon_0(\mathbf{k}) - \mu]}, \quad (88)$$

$$\epsilon_0(\mathbf{k}) = \epsilon_c - \delta \cdot t(\mathbf{k}) - \sum_{\mathbf{p}} J_0(\mathbf{k} + \mathbf{p}) n_F(\mathbf{p}). \quad (89)$$

The level shift is  $\epsilon_c = \epsilon^0 + 2 \sum_{\mathbf{p}} t(\mathbf{p}) n_F(\mathbf{p})$  and  $t(\mathbf{p})$  is the Fourier transform of the hopping integral  $t_{ij}$ —see more in [6].

Let us summarize the *main results of the X-method* in leading  $O(1)$ -order for the quasiparticle properties in the  $t$ - $J$  model [6, 78–80, 130, 179, 180]. (i) The Green’s function  $g_0(\mathbf{k}, \omega)$  describes the *coherent motion of quasiparticles* whose contribution to the total spectral weight of the Green’s function  $G_0(\mathbf{k}, \omega)$  is  $Q_0 = N\delta/2$ . The coherent motion of quasiparticles is described in leading order by  $G_0(\mathbf{k}, \omega) = Q_0 g_0(\mathbf{k}, \omega)$  and *the quasiparticle residuum*  $Q_0$  disappears in the undoped Mott insulating state ( $\delta = 0$ ). This result is physically plausible since in the Mott insulating state the coherent motion of quasiparticles, which is responsible for finite conductivity, vanishes. (ii) The quasiparticle spectrum  $\epsilon_0(\mathbf{k})$  plays the same role as the eigenvalues of the ideal band-structure Hamiltonian  $\hat{h}_0(\mathbf{x}, \mathbf{y})$  (it contains the excitation potential  $V_{\text{IBS}}(\mathbf{x}, \mathbf{y})$  which is due to high-energy processes of the Coulomb interaction). So, if we would consider  $\epsilon_{tb}(\mathbf{k}) = -t(\mathbf{k})$  as the tight-binding parametrization of the LDA-DFT band-structure spectrum which takes into account only weak correlations (with the local potential  $V_{xc}(x)\delta(x - y)$ ), then

one can define a nonlocal *excitation potential*  $V_{\text{IBS}}^{tJ}(\mathbf{x}, \mathbf{y}) = \tilde{V}_{\text{IBS}}^{tJ}(\mathbf{x}, \mathbf{y}) + V_{xc}(\mathbf{x})\delta(\mathbf{x} - \mathbf{y})$  which mimics strong correlations in the  $t$ - $J$  model

$$\tilde{V}_{\text{IBS}}^{tJ}(\mathbf{x}, \mathbf{y}) \approx V_0\delta(\mathbf{x} - \mathbf{y}) + (1 - \delta)t(\mathbf{x} - \mathbf{y}) - \tilde{J}(\mathbf{x} - \mathbf{y}). \quad (90)$$

Here,  $V_0 = 2 \sum_{\mathbf{p}} t(\mathbf{p})n_F(\mathbf{p})$  and  $t(\mathbf{x} - \mathbf{y})$  is the Fourier transform of  $t(\mathbf{k})$  while  $\tilde{J}(\mathbf{x} - \mathbf{y})$  is the Fourier transform of the third term in (89). The relative excitation potential  $\tilde{V}_{\text{IBS}}^{tJ}(\mathbf{x}, \mathbf{y})$  is due to strong correlations (suppression of doubly occupancy on each lattice site) and as we will see below it is responsible for the short-range screening of EPI in such a way that the forward scattering peak appears in the effective EPI interaction—see discussion below. (iii) For the very low doping  $\epsilon_0(\mathbf{k})$  is dominated by the exchange parameter if  $J_0 > \delta \cdot t_0$ . However, in the case when  $J_0 \ll \delta \cdot t_0$  there is a *band narrowing* by lowering the hole-doping  $\delta$ , where the band width is proportional to the hole-concentration  $\delta$ , that is,  $W_b = z \cdot \delta \cdot t_0$ . (iv) The O(1)-order quasiparticle Green's function  $g_0(\mathbf{k}, \omega)$  and the quasiparticle spectrum  $\epsilon_0(\mathbf{k})$  in the X-method have similar form as the spinon Green's function  $g_{0,f}(\mathbf{k}, \omega) = -\langle T f_{\sigma} f_{\sigma}^{\dagger} \rangle_{\mathbf{k}, \omega}$  and the spinon energy  $\epsilon_s(\mathbf{k})$  in the SB method. However, in the SB method there is a broken gauge symmetry in the metallic state (with  $\delta \neq 0$ ) which is characterized by  $\langle \hat{b}_i \rangle \neq 0$ . This broken local gauge symmetry in the slave-boson method in O(1) order, which is due to the local decoupling of spinon and holon, is in fact forbidden by Elitzur's theorem. On the other side the local gauge invariance is not broken in the X-method where Green's function  $G_0(\mathbf{k}, \omega)$  describes motion of the *composite object*, that is, simultaneous creation of the hole and annihilation of the spin at a given lattice site, while in the SB theory there is a spin-charge separation because of the broken symmetry ( $\langle \hat{b}_i \rangle \neq 0$ ). The assumption of the broken symmetry ( $\langle \hat{b}_i \rangle \neq 0$ ) gives qualitative satisfactory results for the quasiparticle energy for the case  $N = \infty$  in  $D > 2$  dimensions. However, the analysis of response functions and of higher-order  $1/N$  corrections to the self-energies very delicate in the SB theory and special techniques must be implemented in order to restore the gauge invariance of the theory. On the other side *the X-method* is intrinsically gauge invariant and free of spurious effects in all orders of the  $1/N$  expansion. Therefore, one expects that these two methods may deliver different results in O(1) and higher order in response functions. This difference is already manifested in the calculation of EPI where the charge vertex in these two methods is peaked at different wave vectors  $\mathbf{q}$ , that is, at  $\mathbf{q} = 0$  in the X-method and  $|\mathbf{q}| \neq 0$  in the SB method—see Section 2.3.5. (v) In [215, 216] it is shown that in the superconducting state the anomalous self-energies (which are of O(1/N)-order in the  $1/N$  expansion) of the X- and SB-methods differ substantially. As a consequence, the SB method [217] predicts false superconductivity in the  $t$ - $J$  model (for  $J = 0$ ) with large  $T_c$  (due to the kinematical interaction), while the X-method gives extremely small  $T_c$  ( $\approx 0$ ) [215, 216]. So, although the two approaches yield some

similar results in leading O(1)-order they, are different at least in next to leading O(1/N)-order.

**2.3.3. EPI Effective Potential in the  $t$ - $J$  Model.** The theory of EPI in the minimal  $t$ - $J$  model based on the X-method predicts that the leading term in the EPI self-energy  $\Sigma_{ep}$  is given by the expression [6, 78–80, 130]

$$\Sigma_{ep}(1, 2) = -V_{ep}(\bar{1} - \bar{2})\gamma_c(1, \bar{3}; \bar{1})g_0(\bar{3} - \bar{4})\gamma_c(\bar{4}, 2; \bar{2}), \quad (91)$$

where the screened (by the dielectric constant) EPI potential

$$V_{ep}(1 - 2) = \epsilon_e^{-1}(1 - \bar{1})V_{ep}^0(\bar{1} - \bar{2})\epsilon_e^{-1}(\bar{2} - 2) \quad (92)$$

and  $V_{ep}^0(1 - 2) = -\langle T \hat{\Phi}(1) \hat{\Phi}(2) \rangle$  is the “phonon” propagator which may also describe an anharmonic EPI. It is obvious that (91) is equivalent to (53) in spite the fact that the theory is formulated in terms of the Hubbard operators. The *charge vertex*  $\gamma_c(1, 2; 3) = -\delta g_0^{-1}(1, 2)/\delta u_{\text{eff}}(3)$  corresponds to the renormalized vertex  $\Gamma_{c,r}$  in (53) and it describes the screening by strong correlations. It depends on the relative excitation potential  $\tilde{V}_{\text{IBS}}^{tJ}(\mathbf{x}, \mathbf{y})$ . The electronic dielectric function  $\epsilon_e(1 - 2)$  describes the screening of EPI by the long-range part of the Coulomb interaction. Note that in the harmonic approximation  $\hat{\Phi}(1)$  contains the bare EPI coupling constant  $g_{ep}^0$  and lattice displacement  $\hat{u}$ , that is,  $\hat{\Phi} \sim g_{ep}^0 \hat{u}$ —see more in [6]. (Note that in the above equations summation and integration over bar indices are understood.) The self-energy  $\Sigma_{ep}(\mathbf{k}, \omega)$  due to EPI reads

$$\Sigma_{ep}(\mathbf{k}, \omega) = \int_0^{\infty} d\nu \langle \alpha^2 F(\mathbf{k}, \mathbf{k}', \nu) \rangle_{\mathbf{k}'} R(\omega, \nu), \quad (93)$$

with  $R(\omega, \nu) = -2\pi i(n_B(\nu) + 1/2) + \psi(1/2 + i) - \psi(1/2 - i(\nu + \omega)/2\pi T)$  where  $n_B(\nu)$  is the Bose distribution function and  $\psi$  is di-gamma function. The Eliashberg spectral function is given by

$$\begin{aligned} \alpha^2 F(\mathbf{k}, \mathbf{k}', \omega) &= N(0) \sum_{\nu} |g_{\nu}(\mathbf{k}, \mathbf{k} - \mathbf{k}')|^2 \\ &\times \delta(\omega - \omega_{\nu}(\mathbf{k} - \mathbf{k}')) \gamma_c^2(\mathbf{k}, \mathbf{k} - \mathbf{k}'), \end{aligned} \quad (94)$$

where  $g_{\nu}(\mathbf{k}, \mathbf{p})$  is the EPI coupling constant for the  $\nu$ th mode, where the renormalization by long-range Coulomb interaction is included, that is,  $g_{\nu}(\mathbf{k}, \mathbf{p}) = g_{ep,\nu}^0(\mathbf{k}, \mathbf{p})/\epsilon_e(\mathbf{p})$ .  $\langle \dots \rangle_{\mathbf{k}}$  denotes Fermi-surface average with respect to the momentum  $\mathbf{k}$  and  $N(0)$  is the density of states renormalized by strong correlations. The effect of strong correlations in the adiabatic limit is stipulated in the *charge vertex function*  $\gamma_c(\mathbf{k}, \mathbf{k} - \mathbf{k}')$  which, as we will see in Section 2.3.4, changes the properties of  $V_{ep}(\mathbf{q}, \nu)$  drastically compared to weakly correlated systems. In fact the charge vertex depends on frequency  $\omega$  but in the adiabatic limit ( $\omega_{\text{ph}} \ll W$ ) and for  $q\nu_F > \omega_{\text{ph}}$  it is practically frequency independent, that is,  $\gamma_c^{(ad)}(\mathbf{k}, \mathbf{q}, \omega) \approx \gamma_c(\mathbf{k}, \mathbf{q}, \omega = 0)$  where the latter is *real quantity*. For  $J = 0$  in the  $t$ - $t'$  model the  $1/N$  expansion gives  $N(0) = N_0(0)/q_0$  where  $q_0 = \delta/2$ . For  $J \neq 0$  the density of states  $N(0)$  does not diverge for  $\delta \rightarrow 0$  where  $N(0) (\sim 1/J_0) > N_0(0)$ . The *bare density of states*  $N_0(0)$  is calculated in

absence of strong correlations, for instance, by the *LDA-DFT* method.

Depending on the symmetry of the superconducting order parameter  $\Delta(\mathbf{k}, \omega)$  (*s*- and *d*-wave pairing) various *projected averages* (over the Fermi surface) of  $\alpha^2 F(\mathbf{k}, \mathbf{k}', \omega)$  enter the Eliashberg equations. Assuming that the superconducting order parameter transforms according to the representation  $\Gamma_i$  of the point group  $C_{4v}$  of the square lattice (in the  $\text{CuO}_2$  planes) the appropriate *symmetry-projected spectral function* is given by

$$\begin{aligned} \alpha^2 F_i(\tilde{\mathbf{k}}, \tilde{\mathbf{k}}', \omega) &= \frac{N(0)}{8} \sum_{\nu, j} |g_\nu(\tilde{\mathbf{k}}, \tilde{\mathbf{k}} - T_j \tilde{\mathbf{k}}')|^2 \\ &\times \delta(\omega - \omega_\nu(\tilde{\mathbf{k}} - T_j \tilde{\mathbf{k}}')) \\ &\times \gamma_c^2(\tilde{\mathbf{k}}, \tilde{\mathbf{k}} - T_j \tilde{\mathbf{k}}') D_i(j) \end{aligned} \quad (95)$$

where  $\tilde{\mathbf{k}}$  and  $\tilde{\mathbf{k}}'$  are momenta on the Fermi line in the irreducible Brillouin zone (1/8 of the total Brillouin zone).  $T_j$ ,  $j = 1, \dots, 8$  denotes the eight point-group transformations forming the symmetry group of the square lattice. This group has five irreducible representations which we distinguish by the label  $i = 1, 2, \dots, 5$ . In the following we discuss the representations  $i = 1$  and  $i = 3$ , which correspond to the *s*- and *d*-wave symmetry of the full rotation group, respectively.  $D_i(j)$  is the representation matrix of the  $j$ th transformation for the representation  $i$ . Assuming that the superconducting order parameter  $\Delta(\mathbf{k}, \omega)$  does not vary much in the irreducible Brillouin zone, one can average over  $\tilde{\mathbf{k}}$  and  $\tilde{\mathbf{k}}'$  in the Brillouin zone. For each symmetry one obtains the corresponding *pairing spectral function*  $\alpha^2 F_i(\omega)$ :

$$\alpha^2 F_i(\omega) = \left\langle \left\langle \alpha^2 F_i(\tilde{\mathbf{k}}, \tilde{\mathbf{k}}', \omega) \right\rangle_{\tilde{\mathbf{k}}, \tilde{\mathbf{k}}'} \right\rangle, \quad (96)$$

which governs the transition temperature for the order parameter with the symmetry  $\Gamma_i$ . For instance,  $\alpha^2 F_3(\omega)$  is the pairing spectral function in the *d*-channel and it gives the coupling for *d*-wave superconductivity (the irreducible representation  $\Gamma_3$ —sometimes labelled as  $B_{1g}$ ). Performing similar calculations for the phonon-limited resistivity, one finds that the resistivity is related to the *transport spectral function*  $\alpha^2 F_{\text{tr}}(\omega)$ :

$$\alpha^2 F_{\text{tr}}(\omega) = \frac{\left\langle \left\langle \alpha^2 F(\mathbf{k}, \mathbf{k}', \omega) [\mathbf{v}(\mathbf{k}) - \mathbf{v}(\mathbf{k}')]^2 \right\rangle \right\rangle_{\mathbf{k}\mathbf{k}'}}{2 \langle \langle \mathbf{v}^2(\mathbf{k}) \rangle \rangle_{\mathbf{k}\mathbf{k}'}}. \quad (97)$$

The effect of strong correlations on EPI was discussed in [130] within the model where  $g_\nu(\mathbf{k}, \mathbf{p})$  and the phonon frequencies  $\omega_\nu(\tilde{\mathbf{k}} - \tilde{\mathbf{k}}')$  are weakly momentum dependent. In order to elucidate the main effect of strong correlations on EPI and  $\alpha^2 F_i(\omega)$  we consider the latter functions for a simple model with Einstein phonon, where these functions are proportional to the (so called) *relative coupling constant*  $\Lambda_i$ :

$$\Lambda_i = \frac{1}{8} \frac{N(0)}{N_0(0)} \sum_{j=1}^8 \left\langle \left\langle \left| \gamma_c(\tilde{\mathbf{k}}, \tilde{\mathbf{k}} - T_j \tilde{\mathbf{k}}') \right|^2 \right\rangle \right\rangle_{\tilde{\mathbf{k}}\tilde{\mathbf{k}}'} D_i(j). \quad (98)$$

Similarly, the resistivity  $\rho(T) (\sim \lambda_{\text{tr}} \sim \Lambda_{\text{tr}})$  is renormalized by the correlation effects where the transport coupling constant  $\Lambda_{\text{tr}}$  is given by

$$\Lambda_{\text{tr}} = \frac{N(0)}{N_0(0)} \frac{\left\langle \left\langle \left| \gamma_c(\tilde{\mathbf{k}}, \tilde{\mathbf{k}} - T_j \tilde{\mathbf{k}}') \right|^2 [\mathbf{v}(\mathbf{k}) - \mathbf{v}(\mathbf{k}')]^2 \right\rangle \right\rangle_{\mathbf{k}\mathbf{k}'}}{2 \langle \langle \mathbf{v}^2(\mathbf{k}) \rangle \rangle_{\mathbf{k}\mathbf{k}'}}. \quad (99)$$

As we see, all projected spectral functions  $\alpha_i^2 F(\omega)$  depend on the *charge vertex function*  $\gamma_c(\mathbf{k}, \mathbf{q})$  which describes the screening (renormalization) of EPI due to strong correlations (suppression of doubly occupancy) [78–80, 130]. This important ingredient (which respects also the Ward identities) is a decisive step beyond the MFA renormalization of EPI in strongly correlated systems which was previously studied in connection with heavy fermions—see review in [218].

**2.3.4. Charge Vertex and the EPI Coupling.** The charge vertex function  $\gamma_c(\mathbf{k}, \mathbf{q})$  (in the adiabatic approximation) has been calculated in [78–80, 130, 179, 180] in the framework of the  $1/N$  expansion in the X-method—see also [6]—and here we discuss only the main results. Note that  $\gamma_c(\mathbf{k}, \mathbf{q})$  renormalizes all charge fluctuation processes, such as the *EPI* interaction, the long-range Coulomb interaction, the nonmagnetic impurity scattering, and so forth. In fact  $\gamma_c(\mathbf{k}, \mathbf{q})$  describes specific *screening due to the vanishing of doubly occupancy in strongly correlated systems*. Note that the latter constraint is at present impossible to incorporate into the *LDA-DFT* band-structure calculations, thus making the latter method unreliable in highly correlated systems. In [78–80, 130, 179, 180]  $\gamma_c(\mathbf{k}, \mathbf{q}, \omega)$  was calculated as a function of the model parameters  $t, t', \delta, J$  in leading  $O(1)$  order of the *t*-*J* model:

$$\gamma_c(\mathbf{k}, \mathbf{q}) = 1 - \sum_{\alpha=1}^6 \sum_{\beta=1}^6 F_\alpha(\mathbf{k}) \left[ \hat{1} + \hat{\chi}(\mathbf{q}) \right]_{\alpha\beta}^{-1} \chi_{\beta 2}(q), \quad (100)$$

where  $\chi_{\alpha\beta}(q) = \sum_p G_\alpha(p, q) F_\beta(\mathbf{p})$ ,  $F_\alpha(\mathbf{k}) = [t(\mathbf{k}), 1, 2J_0 \cos k_x, 2J_0 \sin k_x, 2J_0 \cos k_y, 2J_0 \sin k_y]$ , and  $G_\alpha(p, q) = [1, t(\mathbf{p} + \mathbf{q}), \cos p_x, \sin p_x, \cos p_y, \sin p_y] \Pi(p, q)$ . Here,  $\Pi(k, q) = -g(k)g(k+q)$  and  $q = (\mathbf{q}, iq_n)$ ,  $q_n = 2\pi nT$ ,  $p = (\mathbf{p}, ip_m)$ ,  $p_m = \pi T(2m+1)$ . The physical meaning of the vertex function  $\gamma_c(\mathbf{k}, \mathbf{q})$  is following: in the presence of an external (or internal) charge perturbation there is screening due to the change of the excitation potential  $V_{\text{IBS}}^{ij}(\mathbf{x}, \mathbf{y})$ , that is, of the change of the bandwidth, as well as of the local chemical potential. The central result is that for momenta  $\mathbf{k}$  lying at (and near) the Fermi surface the vertex function  $\gamma_c(\mathbf{k}, \mathbf{q}, \omega = 0)$  has very *pronounced forward scattering peak* (at  $\mathbf{q} = 0$ ) especially at very low doping concentration  $\delta (\ll 1)$ , while the *backward scattering is substantially suppressed*, as it is seen in Figure 35 where  $\gamma_c(\mathbf{k}_F, \mathbf{q}, \omega = 0)$  is shown. The peak at  $q = 0$  is very narrow at very small doping since its width  $q_c$  is proportional to the doping  $\delta$ , that is,  $q_c \sim \delta(\pi/a)$  where  $a$  is the lattice constant. It is interesting that  $\gamma_c(\mathbf{k}, \mathbf{q})$ , as well as the dynamics of charge fluctuations, depend only weakly on the exchange energy  $J$  and are mainly

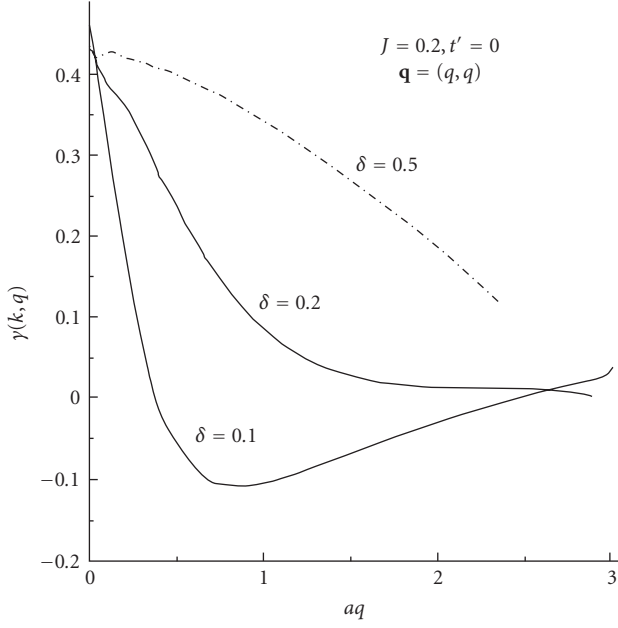


FIGURE 35: Adiabatic ( $\omega = 0$ ) vertex function  $\gamma(\mathbf{k}_F, \mathbf{q})$  of the  $t$ - $J$  model as a function of the momentum  $aq$  with  $\mathbf{q} = (q, q)$  for three different doping levels  $\delta$ . From [130].

dominated by the constraint of having no doubly occupancy of sites, as it is shown in [78–80, 130, 179, 180].

The existence of the forward scattering peak in  $\gamma_c(\mathbf{k}, \mathbf{q})$  at  $q = 0$  is confirmed by numerical calculations in the Hubbard model, which show that this peak is very pronounced at large  $U$  [182]. This is important result since it proves that the  $1/N$  expansion in the  $X$ -method is reliable method in studying charge fluctuation processes in strongly correlated systems. The strong suppression of  $\gamma_c(\mathbf{k}, \mathbf{q})$  at large  $q$  ( $\sim k_F$ ) means that at small distances the charge fluctuations are strongly suppressed (correlated). Such a behavior of the vertex function means that a quasiparticle moving in the strongly correlated medium digs up a *giant correlation hole* with the radius  $\xi_{ch}(\sim \pi/q_c) \approx a/\delta$ , where  $a$  is the lattice constant. As a consequence of this effect the renormalized EPI becomes long ranged which is contrary to the weakly correlated systems where it is short ranged.

By knowing  $\gamma_c(\mathbf{k}, \mathbf{q})$  one can calculate the relative coupling constants  $\Lambda_1 \equiv \Lambda_s$ ,  $\Lambda_3 \equiv \Lambda_d$ ,  $\Lambda_{tr}$ , and so forth. In the absence of correlations and for an isotropic band one has  $\Lambda_1 = \Lambda_{tr} = 1$ ,  $\Lambda_i = 0$  for  $i > 1$ . The averages in  $\Lambda_s$ ,  $\Lambda_d$ , and  $\Lambda_{tr}$  were performed numerically in [130] by using the realistic anisotropic band dispersion in the  $t$ - $t'$ - $J$  model and the results are shown in Figure 36. For convenience, the three curves are multiplied with a common factor so that  $\Lambda_s$  approaches 1 in the empty-band limit  $\delta \rightarrow 1$ , when strong correlations are absent. Note that the superconducting critical temperature  $T_c$  in the weak coupling limit and in the  $i$ th channel scales like  $T_c^{(i)} \sim \exp(-1/(\lambda_0 \Lambda_i - \mu_i^*))$  where  $\lambda_0$  is some effective coupling constant which depends on microscopic details. The parameter  $\mu_i^*$  is the effective residual Coulomb repulsion in the  $i$ th superconducting channel. We

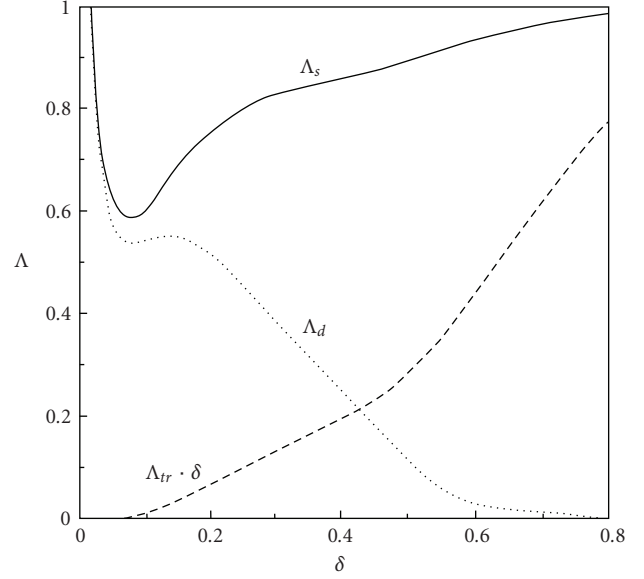


FIGURE 36: Normalized  $s$ -wave  $\Lambda_s$ ,  $d$ -wave  $\Lambda_d$ , and transport  $\Lambda_{tr} \cdot \delta$  coupling constants as a function of doping  $\delta$  for  $t' = 0$  and  $J = 0$ . From [179, 180].

stress here several interesting results which come out from the above theory and which are partially presented in Figures 35 and 36.

(1) In principle the bare EPI coupling constant  $g_\lambda^0(\mathbf{k}, \mathbf{q})$  depends on the quasiparticle momentum  $\mathbf{k}$  and the transfer momentum  $\mathbf{q}$ . In the  $t$ - $J$  model the EPI coupling is dominated by the ionic coupling  $\hat{H}_{ep}^{ion}$  (see (80)) and corresponding EPI depends only on the momentum transfer  $\mathbf{q}$ , that is,  $g_\lambda^0(\mathbf{k}, \mathbf{q}) \approx g_\lambda^0(\mathbf{q})$  while for the much smaller covalent coupling  $\hat{H}_{ep}^{cov}$  depends on both  $\mathbf{k}$  and  $\mathbf{q}$  [6, 10, 11]. However, the EPI couplings for most phonon modes are renormalized by the charge vertex and since the latter is peaked at small momentum transfer  $q = |\mathbf{k} - \mathbf{k}'|$  then the maxima of the corresponding effective potentials are pushed toward smaller values of  $q$ . The further consequence of the vertex renormalization is that in the absence of strong correlations the bare EPI coupling  $|g^0(\mathbf{k}, \mathbf{q})|^2$  for some phonon modes (which enters in the effective  $t$ - $J$  model) is detrimental for  $d$ -wave pairing; it can be less detrimental or even supports it in the presence of strong correlations (since the maximum is pushed toward smaller  $q$ ). To illustrate this let us consider the in-plane *oxygen breathing mode* with the frequency  $\omega_{br}$  which is supposed to be important in HTSC cuprates. The bare coupling constant (squared) for this mode is approximately given by  $|g_{br}^0(\mathbf{k}, \mathbf{q})|^2 = |g_{br}^0|^2 [\sin^2(q_x a/2) + \sin^2(q_y a/2)]$  which reaches maximum for large  $\mathbf{q} = (\pi/a, \pi/a)$ . By extracting the component in the  $d$ -channel one has

$$|g_{br}^0(\mathbf{k} - \mathbf{k}')|^2 = |g_{br}^0|^2 \left[ 1 - \left( \frac{1}{4} \right) \psi_d(\mathbf{k}) \psi_d(\mathbf{k}') + \dots \right] \quad (101)$$

with

$$\psi_d(\mathbf{k}) = \cos k_x a - \cos k_y a. \quad (102)$$

This gives the repulsive coupling constant  $\lambda_d^0$  in the  $d$ -channel, that is,

$$\lambda_d^0 = \frac{2}{\omega_{\text{br}}} \left\langle \psi_d(\mathbf{k}) \left| g_{\text{br}}^0(\mathbf{k} - \mathbf{k}') \right|^2 \psi_d(\mathbf{k}') \right\rangle < 0. \quad (103)$$

However, in the presence of strong correlations one expects that the effective coupling constant is given approximately by  $|g_{\text{br}}^{\text{eff}}(\mathbf{k}, \mathbf{k}')| \approx |g_{\text{br}}^0(\mathbf{k} - \mathbf{k}')|^2 \gamma_c^2(\mathbf{k}_F, \mathbf{k} - \mathbf{k}')$  which is at small doping  $\delta$  suppressed substantially at large  $q$  since  $\gamma_c^2$  starts to fall off drastically at  $q \sim q_c \sim \delta(\pi/a)$ . The latter property makes the effective coupling constant (in the  $d$ -channel)  $\lambda_d^{\text{eff}}$  for these modes less negative or even positive (depending on the ratio  $\xi_{\text{ch}}/a \sim 1/\delta$ ), that is, one has  $\lambda_d^{\text{eff}} > \lambda_d^0$ . We stress again that this analysis is only qualitative (and semiquantitative) since it is based on the  $t$ - $J$  model while the better quantitative results are expected in the strongly correlated three-band Emery model with  $U_d \gg t, \Delta_{pd}$ —see [6, Appendix D]. Unfortunately, these calculations are not finalized until now.

(2) In weakly correlated systems (or, e.g., in the empty-band limit  $\delta \rightarrow 1$ ) the relative  $d$ -wave coupling constant  $\Lambda_d$  is much smaller than the  $s$ -wave coupling constant  $\Lambda_s$ , that is,  $\Lambda_d \ll \Lambda_s$  as it is seen in Figure 36. Furthermore,  $\Lambda_s$  decreases with decreasing doping.

(3) It is indicative that independently on the value of  $t' \neq 0$  or  $t' = 0$  the coupling constant  $\Lambda_s$  and  $\Lambda_d$  meet each other (note that  $\Lambda_s > \Lambda_d$  for all  $\delta$ ) at some small doping  $\delta \approx 0.1$ – $0.2$  where  $\Lambda_s \approx \Lambda_d$ . We would like to stress that such a unique situation (with  $\Lambda_s \approx \Lambda_d$ ) was practically never realized in low-temperature and weakly correlated superconductors and in that respect the strong momentum-dependent EPI in HTSC cuprates is an exclusive but very important phenomenon.

(4) By taking into account the residual Coulomb repulsion of quasiparticles then the  $s$ -wave superconductivity (which is governed by  $\Lambda_s$ ) is suppressed, while the  $d$ -wave superconductivity (which is governed by  $\Lambda_d$ ) stays almost unaffected, since  $\mu_s^* \gg \mu_d^*$ . In that case the  $d$ -wave superconductivity which is mainly governed by EPI becomes more stable than the  $s$ -wave one at sufficiently low doping  $\delta$ . This transition between  $s$ - and  $d$ -wave superconductivity is triggered by electronic correlations because in the model calculations [78–80, 130] the bare EPI coupling is assumed to be momentum independent, that is, the bare coupling constant contains the  $s$ -wave symmetry only.

(5) The calculations of the charge vertex  $\gamma_c$  are performed in the *adiabatic limit*, that is, for  $\omega < \mathbf{q} \cdot \mathbf{v}_F(\mathbf{q})$  the frequency  $\omega$  in  $\gamma_c$  can be neglected. In the *nonadiabatic regime*, that is, for  $\omega > \mathbf{q} \cdot \mathbf{v}_F(\mathbf{q})$ , the function  $\gamma_c^2(\mathbf{k}_F, \mathbf{q}, \omega)$  may be substantially larger compared to the adiabatic case because  $\gamma_c(\mathbf{k}_F, \mathbf{q}, \omega)$  tends to the bare value 1 for  $q = 0$ . This means that EPI for different phonons (with different energies  $\omega$ ) is differently affected by strong correlations. For a given  $\omega$  the EPI coupling to those phonons with momenta  $q < q_\omega = \omega/v_F$  will be (relatively) enhanced since  $\gamma_c(\mathbf{k}_F, \mathbf{q}, \omega) \approx 1$ , while the

coupling to those with  $q > q_\omega = \omega/v_F$  will be substantially reduced due to the suppression of the backward scattering by strong correlations [37, 38]. These results are a consequence of the Ward identities and generally hold in the Landau-Fermi liquid theory [219].

(6) The transport EPI coupling constant  $\Lambda_{\text{tr}}$  is significantly reduced in the presence of strong correlations especially for low doping ( $\delta \ll 1$ ) where  $\Lambda_{\text{tr}} < \Lambda/3$ . This result is physically plausible since the resistivity is dominated by the backward scattering processes (large  $q \sim k_F$ ) which are suppressed by strong correlations—the suppression of  $\gamma_c(\mathbf{k}_F, \mathbf{q}, \omega)$  at large  $q$ .

The theory based on the forward scattering peak in EPI is a good candidate to explain the linear temperature behavior of the resistivity down to very small temperatures  $T(\sim \Theta_D/30) \approx 10$  K in some cuprates with low  $T_c(\approx 10$  K) [6, 128, 129]. One physically rather plausible model, which is based on the forward scattering peak in EPI, is elaborated in [128]. It takes into account (i) the quasiparticle *scattering on acoustic (a) and on optic (o) phonons*, (ii) the *extended van Hove singularity* in the quasiparticle density of states  $N(\xi)$  which in some cuprates is very near the Fermi surface, and (iii) the umklapp and “undulation” (due to the flat regions at the Fermi surface) processes with  $\mathbf{v}_{\mathbf{k}'} \cong -\mathbf{v}_{\mathbf{k}}$ —this condition can partly increase the EPI coupling. The transport Eliashberg function  $\alpha_{\text{tr}}^2 F(\omega)$  is calculated similarly to (97) by using the definition of  $\alpha^2 F(\mathbf{k}, \mathbf{k}', \omega)$  in (95) with the *renormalized coupling constant*  $g_\nu^{(r)}(\mathbf{k} - \mathbf{k}') = g_\nu(\mathbf{k} - \mathbf{k}') \gamma_c(\mathbf{k} - \mathbf{k}')$  of the  $\nu = a, o$  mode, respectively. In [128] it is assumed a phenomenological form for the forward scattering peak in  $\gamma_c(\mathbf{k} - \mathbf{k}')$  with the cutoff  $q_c \ll k_F$  (and which mimics the exact results from [78–80, 130, 179, 180]). Since the scattering of the quasiparticles on phonons (with the sound velocity  $v_s$ ) is limited to small- $q$  transfer processes (with  $q < q_c$ ), then the maximal energy of the acoustic branch is not the Debye energy  $\Theta_D(\approx k_F v_s)$  but the *effective Debye energy*  $\Theta_A(\approx q_c v_s) \ll \Theta_D$ . In the case of *Bi2201* in [128] it is taken (from the numerical results in [78–80, 130, 179, 180]) that  $q_c \approx k_F/10$  which gives  $\Theta_A \approx (30$ – $50)K$ . As a result the calculated  $\alpha_{\text{tr}}^2 F(\omega)$  gives that  $\rho_{ab}(T) \sim T$  down to very low  $T(\sim 0.2\Theta_A) \approx 10$  K. The slope ( $d\rho_{ab}/dT$ ) is governed by the effective EPI coupling constant for acoustic phonons. In systems with the extended van Hove singularity (in  $N(\xi)$ ) near the Fermi surface, which is the case in *Bi-2201*, the effective coupling constant for acoustic phonons can be sufficiently large to give experimental values for the slope ( $d\rho_{ab}/dT$ )  $\sim (0.5$ – $1)\mu\Omega\text{cm}/K$ —for details see [128]. This physical picture is applicable also to cuprates near and at the optimal doping but since in these systems  $T_c$  is large the linearity of  $\rho_{ab}(T)$  down to very low  $T$  is “screened” by the appearance of superconductivity.

(7) The width of the forward scattering peak in  $\gamma_c(\mathbf{k}_F, \mathbf{q})$  is very narrow in underdoped cuprates—with the width  $q_c \sim \delta(\pi/a)$ —which may have further interesting consequences. For instance, HTSC cuprates are characterized not only by strong correlations but also by the relatively small Fermi energy  $E_F$ , which is in *underdoped systems* not much larger than the characteristic (maximal) phonon frequency  $\omega_{\text{ph}}^{\text{max}}$ ,

that is,  $E_F \simeq 0.1\text{--}0.3$  eV,  $\omega_{\text{ph}}^{\text{max}} \simeq 80$  meV. Due to the appreciable magnitude of  $\omega_D/E_F$  it is necessary to correct the Migdal-Eliashberg theory by the non-Migdal vertex corrections due to the EPI. It is well known that these vertex corrections lower  $T_c$  in systems with the isotropic EPI. However, the non-Migdal vertex corrections in systems with the forward scattering peak in the EPI coupling with the cutoff  $q_c \ll k_F$  may increase  $T_c$  which can be appreciable. The corresponding calculations [220, 221] give two interesting results: (i) there is an appreciable increase of  $T_c$  by lowering  $Q_c = q_c/2k_F$ , for instance,  $T_c(Q_c = 0.1) \approx 4T_c(Q_c = 1)$ ; (ii) even small values of  $\lambda_{ep} < 1$  can give large  $T_c$ . The latter results open a new possibility in reaching high  $T_c$  in systems with appreciable ratio  $\omega_D/E_F$  and with the forward scattering peak in EPI. The difference between the Migdal-Eliashberg and the non-Migdal theory can be explained qualitatively in the framework of an approximative McMillan formula for  $T_c$  (for not too large  $\lambda$ ) which reads  $T_c \approx \langle \omega \rangle e^{-1/(\tilde{\lambda} - \mu^*)}$ . The Migdal-Eliashberg theory predicts

$$\tilde{\lambda}^{(\text{ME})} \approx \frac{\lambda}{1 + \lambda}, \quad (104)$$

while the *non-Migdal theory* [220, 221] gives

$$\tilde{\lambda}^{(\text{n-ME})} \approx \lambda(1 + \lambda). \quad (105)$$

For instance,  $T_c \sim 100$  K in HTSC oxides can be explained by the Migdal-Eliashberg theory for  $\lambda^{(\text{ME})} \sim 2$ , while in the non-Migdal theory much smaller coupling constant is needed, that is,  $\lambda^{(\text{n-ME})} \sim 0.5$ .

(8) The existence of the forward scattering peak in EPI can in a plausible way explain the ARPES puzzle that the antinodal kink is shifted by the maximal superconducting gap  $\Delta_{\text{max}}$  while the nodal kink is unshifted. The reason is (as explained in Section 1.3.3) that due to strong correlations the EPI spectral function  $\alpha^2 F(\mathbf{k}, \mathbf{k}', \Omega) \approx \alpha^2 F(\varphi - \varphi', \Omega)$  is strongly peaked at  $\varphi - \varphi' = 0$  [151].

(9) The scattering potential on nonmagnetic impurities is renormalized by strong correlations giving also the forward scattering peak in the impurity scattering potential (amplitude) [155]. The latter effect gives large  $d$ -wave channel in the renormalized impurity potential, which is the reason that  $d$ -wave pairing in HTSC cuprates is robust in the presence of nonmagnetic impurities (and defects) [6, 155].

**2.3.5. EPI and Strong Correlations—Other Methods.** The calculations of the static (adiabatic) charge-vertex  $\gamma_c(\mathbf{k}_F, \mathbf{q})$  in the X-method are done for the case  $U = \infty$  [78–80, 130, 179, 180] where it is found that it is peaked at  $q = 0$ —the forward scattering peak (FSP). This result is confirmed by the numerical Monte Carlo calculations for the finite- $U$  Hubbard model [182], where it is found that FSP exists for all  $U$ , but it is especially pronounced in the limit  $t \ll U$ . These results are additionally confirmed in the calculations [183] within the *four slave-boson method* of Kotliar-Rückenstein where  $\gamma_c(\mathbf{k}_F, \mathbf{q})$  is again peaked at  $\mathbf{q} = 0$  and the peak is also pronounced at  $t \ll U$ .

There are several calculations of the charge vertex in the *one slave-boson method* [219, 222–224] which is invented to

study the limit  $U \rightarrow \infty$ . It is interesting to compare the results for the charge vertex *in the X-method* [78–80, 130, 179, 180] and *in the one slave-boson theory* [222] which are calculated in  $O((1/N)^0)$  order. For instance, for  $J = 0$  one has

$$\begin{aligned} \gamma_c^{(X)}(\mathbf{k}, \mathbf{q}) &= \frac{1 + b(\mathbf{q}) - a(\mathbf{q})t(\mathbf{k})}{[1 + b(\mathbf{q})]^2 - a(\mathbf{q})c(\mathbf{q})}, \\ \gamma_c^{(\text{SB})}(\mathbf{k}, \mathbf{q}) &= \frac{1 + b(\mathbf{q}) - a(\mathbf{q})[t(\mathbf{k}) + t(\mathbf{k} + \mathbf{q})]/2}{[1 + b(\mathbf{q})]^2 - a(\mathbf{q})c(\mathbf{q})}. \end{aligned} \quad (106)$$

The explicit expressions for the “bare” susceptibilities  $a(\mathbf{q})$ ,  $b(\mathbf{q})$ , and  $c(\mathbf{q})$  can be found in [78–80, 130]. It is obvious from (106) that  $\gamma_c^{(X)}(\mathbf{k}, \mathbf{q} = 0) = \gamma_c^{(\text{SB})}(\mathbf{k}, \mathbf{q} = 0)$  but the calculations give that  $\max\{\gamma_c^{(X)}(\mathbf{k}, \mathbf{q})\}$  is for  $\mathbf{q} = 0$ , while  $\max\{\gamma_c^{(\text{SB})}(\mathbf{k}, \mathbf{q})\}$  is for  $|\mathbf{q}| \neq 0$  [181]. So, the SB vertex is peaked at finite  $q$  which is *in contradiction* with the numerical Monte Carlo results for the Hubbard model [182] and with the four slave-boson theory [183]. The reason for the discrepancy of the one slave-boson (SB) in studying EPI with the numerical results and the X-method is not quite clear and might be due to the symmetry breaking of the local gauge invariance in leading order of the SB theory.

**2.4. Summary of Section 2.** The experimental results in HTSC cuprates which are exposed in Section 1 imply that the EPI coupling constant is large and in order to be conform with  $d$ -wave pairing this interaction must be very nonlocal (long range), that is, weakly screened and peaked at small transfer momenta. In absence of quantitative calculations in the framework of the ab initio microscopic many-body theory the effects of strong correlations on EPI are studied within the minimal  $t$ - $J$  model where this *pronounced nonlocality* is due to two main reasons: (1) *strong electronic correlations* and (2) the combined *metallic-ionic layered structure* in these materials. In case (1) the pronounced nonlocality of EPI, which is found in the  $t$ - $J$  model system, is due to the suppression of doubly occupancy at the Cu lattice sites in the  $\text{CuO}_2$  planes, which drastically weakens the screening effect in these systems. The pronounced nonlocality and suppression of the screening are mathematically expressed by the charge vertex function  $\gamma_c(\mathbf{k}_F, \mathbf{q}, \omega)$  which multiplies the bare EPI matrix element. The vertex function is peaked at  $q = 0$  and strongly suppressed at large  $q$ , especially for low (oxygen) hole-doping  $\delta \ll 1$  near the Mott-Hubbard transition. Such a structure of  $\gamma_c$  gives that the  $d$ -wave and  $s$ -wave coupling constants are of the same order of magnitude around and below some optimal doping  $\delta_{\text{op}} \approx 0.1$ , that is,  $\lambda_d \approx \lambda_s$ . This is very peculiar situation never met before. Since the residual effective (low-energy) Coulomb interaction is much smaller in the  $d$ -channel than in the  $s$ -channel, that is,  $\mu_s^* \gg \mu_d^*$  (with the possibility that  $\mu_d^* < 0$ ), then the critical temperature for  $d$ -wave pairing is much larger than for the  $s$ -wave one, that is,  $T_c^{(d)} \gg T_c^{(s)}$ . Since all charge fluctuation processes are modified by strong correlations, then the quasiparticle scattering on nonmagnetic impurities is also drastically changed; the pair-breaking effect on  $d$ -wave

pairing is drastically reduced. This nonlocal effect, which is not discussed here—see more in [6] and references therein—is one of the main reasons for the robustness of  $d$ -wave pairing in HTSC oxides in the presence of nonmagnetic impurities and numerous local defects. The development of the forward scattering peak in  $\gamma_c(\mathbf{k}_F, \mathbf{q})$  and suppression at large  $q (\gg q_c = \delta(\pi/a))$  give rise to the suppression of the transport coupling constant  $\lambda_{tr}$  making it much smaller than the self-energy coupling constant  $\lambda$ , that is, one has  $\lambda_{tr} \approx \lambda/3$  near the optimal doping  $\delta = 0.1\text{--}0.2$ . Thus the behavior of the vertex function and the dominance of EPI in the quasiparticle scattering resolve the experimental puzzle that the transport and the self-energy coupling constant take very different values,  $\lambda_{tr,ep} \ll \lambda_{ep}$ . Note that this is not the case with the SFI mechanism which is dominant at large  $\mathbf{q} \approx \mathbf{Q} = (\pi, \pi)$  thus giving  $\lambda_{tr,sf} \approx \lambda_{sf}$ . This result means that if in the SFI mechanism one fits the temperature-dependent resistivity (governed by  $\lambda_{tr,sf}$ ) then one obtains very low  $T_c$ .

We stress that the strength of the EPI coupling constants  $\lambda_{ep}, \lambda_{ep,d}$  is at present impossible to calculate since it is difficult to incorporate strong correlations and numerous structural effects in a tractable microscopic theory.

**2.5. Discussions and Conclusions.** Numerous experimental results related to tunnelling, optics, ARPES, inelastic neutron, and X-ray scattering measurements in HTSC cuprates *at and near the optimal doping* give evidence for strong electron-phonon interaction (EPI) with the coupling constant  $1 < \lambda_{ep} < 3.5$ . The tunnelling measurements furnish evidence for strong EPI which give that the *peaks in the bosonic spectral function  $\alpha^2F(\omega)$  coincide well with the peaks in the phonon density of states  $F_{ph}(\omega)$* . The tunnelling spectra show that *almost all phonons contribute to  $T_c$*  and that no particular phonon mode can be singled out in the spectral function  $\alpha^2F(\omega)$  as being the only one which dominates in pairing mechanism. In light of these results the small oxygen isotope effect in optimally doped systems can be partly due to this effect, thus not disqualifying the important role of EPI in pairing mechanism. The compatibility of the strong EPI with  $d$ -wave pairing implies an important constraint on the EPI pairing potential—it must be nonlocal, that is, peaked at small transfer momenta. The latter is due to (a) strong electronic correlations and (b) the combined metallic-ionic structure of these materials. If the EPI scattering is the main player in pairing in HTSC cuprates, then this nonlocality implies that at and below some optimal doping ( $\delta_{op} \sim 0.1$ ) the magnitude of the EPI coupling constants in  $d$ -wave and  $s$ -wave channel must be of the same order, that is,  $\lambda_{ep,d} \approx \lambda_{ep,s}$ . This result in conjunction with the fact that the residual effective Coulomb coupling in  $d$ -wave channel is much smaller than in the  $s$ -wave one, that is,  $\mu_s^* \gg \mu_d^*$  (with the possibility that  $\mu_d^* < 0$ ) gives that the critical temperature for  $d$ -wave pairing is much larger than for  $s$ -wave pairing.

The numerous tunnelling, ARPES, optics, and magnetic neutron scattering measurements give sufficient evidence that the spin-fluctuation interaction (SFI) plays a secondary role in pairing in HTSC cuprates. Especially important evidence for the smallness of SFI (in pairing) comes from the magnetic neutron scattering measurements which show that

by varying doping slightly around the optimal one there is a huge reconstruction of the SFI spectral function  $\text{Im}\chi(\mathbf{q}, \omega)$  (imaginary part of the spin susceptibility) for  $\mathbf{q} \approx \mathbf{Q}$ , while there is very small change in the critical temperature  $T_c$ . These experimental results imply important constraints on the *pairing scenario for systems at and near optimal doping*: (1) the strength of the  $d$ -wave pairing potential is provided by EPI (i.e., one has  $\lambda_{ep,d} \approx \lambda_{ep,s}$ ) while the role of the residual Coulomb interaction and SFI, together, is to trigger  $d$ -wave pairing; (2) the Migdal-Eliashberg theory, but with the pronounced momentum dependent of EPI, is a rather good starting theory.

The ab initio microscopic theory of pairing in HTSC cuprates fails at present to calculate  $T_c$  and to predict the magnitude of the  $d$ -wave order parameter. From that point of view it is hard to expect a significant improvement of this situation at least in the near future. However, the studies of some minimal (toy) models, such as the single-band  $t$ - $J$  model, allow us to understand part of the physics in cuprates on a qualitative and in some cases even on a semiquantitative level. In that respect the encouraging results come from the theoretical studies of the EPI scattering in the  $t$ - $J$  model by using controllable mathematical methods in the X-method formulated in terms of the Hubbard operators [78–80, 130, 179, 180]. This theory predicts dressing of quasiparticles by strong correlations which dig up a large-scale correlation hole of the size  $\xi_{ch} \sim a/\delta$  for  $\delta \ll 1$ . These quasiparticles respond to lattice vibrations in such a way to produce an effective long-range electron interaction (due to EPI), that is, the effective pairing potential  $V_{\text{eff}}(\mathbf{q}, \omega)$  is peaked at small transfer momenta  $q$ —the forward scattering peak. This theory (of the toy model) is conform with the experimental scenario by predicting the following results: (i) the EPI coupling constants in  $d$ -wave and  $s$ -wave channels are of the same order, that is,  $\lambda_{ep,d} \approx \lambda_{ep,s}$ , at some optimal doping  $\delta_{op} \sim 0.1$ ; (ii) the transport coupling is much smaller than the pairing one, that is,  $\lambda_{tr} \approx \lambda/3$ ; (iii) due to strong correlations there is forward scattering peak in the potential for scattering on nonmagnetic impurities, thus making  $d$ -wave pairing robust in materials with a lot of defects and impurities. Applied to HTSC superconductors at and near the optimal doping, this theory is a realization of the Migdal-Eliashberg theory but with strongly momentum dependent EPI coupling, which is conform with the proposed experimental pairing scenario. This scenario which is also realized in the  $t$ - $J$  toy model may be useful in making a (phenomenological) theory of pairing in cuprates. However, all present theories are confronted with the unsolved and *challenging task*—the *calculation of  $T_c$* . From that point of view we do not have at present a proper microscopic theory of pairing in HTSC cuprates.

## Appendix

### A. Spectral Functions

**A.1. Spectral Functions  $\alpha^2F(k, k', \omega)$  and  $\alpha^2F(\omega)$ .** The quasiparticle bosonic (Eliashberg) spectral function  $\alpha^2F(\mathbf{k}, \mathbf{k}', \omega)$  and its Fermi surface average  $\alpha^2F(\omega) = \langle \langle \alpha^2F(\mathbf{k}, \mathbf{k}', \omega) \rangle \rangle_{\mathbf{k}, \mathbf{k}'}$

enter the quasiparticle self-energy  $\Sigma(\mathbf{k}, \omega)$ , while the transport spectral function  $\alpha^2 F_{\text{tr}}(\omega)$  enters the transport self-energy  $\Sigma_{\text{tr}}(\mathbf{k}, \omega)$  and dynamical conductivity  $\sigma(\omega)$ . Since the Migdal-Eliashberg theory for EPI is well defined, we define the spectral functions for this case and the generalization to other electron-boson interaction is straightforward. In the superconducting state Matsubara Green's functions  $\hat{G}(\mathbf{k}, \omega_n)$  and  $\hat{\Sigma}(\mathbf{k}, \omega_n)$  are  $2 \times 2$  matrices with the diagonal elements  $G_{11} \equiv G(\mathbf{k}, \omega_n)$ ,  $\Sigma_{11} \equiv \Sigma(\mathbf{k}, \omega_n)$  and the off-diagonal elements  $G_{12} \equiv F(\mathbf{k}, \omega_n)$ ,  $\Sigma_{12} \equiv \Phi(\mathbf{k}, \omega_n)$  which describe superconducting pairing. By defining  $i\omega_n[1 - Z(\mathbf{k}, \omega_n)] = [\Sigma(\mathbf{k}, \omega_n) - \Sigma(\mathbf{k}, -\omega_n)]/2$  and  $\chi(\mathbf{k}, \omega_n) = [\Sigma(\mathbf{k}, \omega_n) + \Sigma(\mathbf{k}, -\omega_n)]/2$ , the Eliashberg functions for EPI in the presence of the Coulomb interaction (in the singlet pairing channel) read [70, 225–227]

$$\begin{aligned} Z(\mathbf{k}, \omega_n) &= 1 + \frac{T}{N} \sum_{\mathbf{p}, m} \frac{\lambda_{\mathbf{k}\mathbf{p}}^Z(\omega_{nm}^-) \omega_m}{N(\mu) \omega_n} \frac{Z(\mathbf{p}, \omega_m)}{D(\mathbf{p}, \omega_m)}, \\ \chi(\mathbf{k}, \omega_n) &= -\frac{T}{N} \sum_{\mathbf{p}, m} \frac{\lambda_{\mathbf{k}\mathbf{p}}^Z(\omega_{nm}^-)}{N(\mu)} \frac{\epsilon(\mathbf{p}) - \mu + \chi(\mathbf{p}, \omega_m)}{D(\mathbf{p}, \omega_m)}, \quad (\text{A.1}) \\ \Phi(\mathbf{k}, \omega_n) &= \frac{T}{N} \sum_{\mathbf{p}, m} \left[ \frac{\lambda_{\mathbf{k}\mathbf{p}}^A(\omega_{nm}^-)}{N(\mu)} - V_{\mathbf{k}\mathbf{p}} \right] \frac{\Phi(\mathbf{p}, \omega_m)}{D(\mathbf{p}, \omega_m)}, \end{aligned}$$

where  $\omega_{nm}^- \equiv \omega_n - \omega_m$ ,  $\omega_n = \pi T(2n + 1)$ ,  $\Phi(\mathbf{k}, \omega_n) \equiv Z(\mathbf{k}, \omega_n) \Delta(\mathbf{k}, \omega_n)$ ,  $D = \omega_m^2 Z^2 + (\epsilon - \mu + \chi)^2 + \Phi^2$ , and  $N(\mu)$  is the density of states at the Fermi surface. (In studying some problems, such as optics, it is useful to define the renormalized frequency  $i\tilde{\omega}_n(i\omega_n) (\equiv i\omega_n Z(\omega_n)) = \omega_n - \Sigma(\omega_n)$  or its analytical continuation  $\tilde{\omega}(\omega) = Z(\omega)\omega = \omega - \Sigma(\omega)$ ). These equations are supplemented with the electron number equation  $n(\mu)$  ( $\mu$  is the chemical potential):

$$\begin{aligned} n(\mu) &= \frac{2T}{N} \sum_{\mathbf{p}, m} G(\mathbf{p}, \omega_m) e^{i\omega_m 0^+} \\ &= 1 - \frac{2T}{N} \sum_{\mathbf{p}, m} \frac{\epsilon(\mathbf{p}) - \mu + \chi(\mathbf{p}, \omega_m)}{D(\mathbf{p}, \omega_m)}. \quad (\text{A.2}) \end{aligned}$$

Note that in the case of EPI one has  $\lambda_{\mathbf{k}\mathbf{p}}^A(\nu_n) = \lambda_{\mathbf{k}\mathbf{p}}^Z(\nu_n) (\equiv \lambda_{\mathbf{k}\mathbf{p}}(\nu_n))$  (with  $\nu_n = \pi T n$ ) where  $\lambda_{\mathbf{k}\mathbf{p}}(\nu_n)$  is defined by

$$\lambda_{\mathbf{k}\mathbf{p}}(\nu_n) = 2 \int_0^\infty d\nu \frac{\nu}{\nu^2 + \nu_n^2} \alpha_{\mathbf{k}\mathbf{p}}^2 F(\nu), \quad (\text{A.3})$$

$$\alpha_{\mathbf{k}\mathbf{p}}^2 F(\nu) = N(\mu) \sum_{\kappa} \left| g_{\kappa, \mathbf{k}\mathbf{p}}^{\text{ren}} \right|^2 B_{\kappa}(\mathbf{k} - \mathbf{p}, \nu), \quad (\text{A.4})$$

where  $B_{\kappa}(\mathbf{k} - \mathbf{p}; \nu)$  is the phonon spectral function of the  $\kappa$ th phonon mode related to the phonon propagator

$$D_{\kappa}(\mathbf{q}, i\nu_n) = - \int_0^\infty d\nu \frac{\nu}{\nu^2 + \nu_n^2} B_{\kappa}(\mathbf{q}, \nu). \quad (\text{A.5})$$

However, very often it is measured the generalized phonon density of states  $GPDS(\omega) (\equiv G(\omega))$  (see Section 1.3.4) defined by  $G(\omega) = \sum_i (\sigma_i/M_i) F_i(\omega) / \sum_i (\sigma_i/M_i)$ . Here,  $\sigma_i$  and  $M_i$  are the cross-section and the mass of the  $i$ th nucleus and

$F_i(\omega) = (1/N) \sum_q |\epsilon_q^i|^2 \delta(\omega - \omega_q)$  is the amplitude-weighted density of states.

The renormalized coupling constant  $g_{\kappa, \mathbf{k}\mathbf{p}}^{\text{ren}} (\approx g_{\kappa, \mathbf{k}\mathbf{p}}^0 \gamma \epsilon_e^{-1})$  in (A.4) comprises the screening effect due to long-range Coulomb interaction ( $\sim \epsilon_e^{-1}$ —the inverse electronic dielectric function) and short-range strong correlations ( $\sim \gamma$ —the vertex function)—see more in Section 2. Usually in the case of low-temperature superconductors (LTS) with  $s$ -wave pairing the anisotropy is rather small (or in the presence of impurities it is averaged out) which allows an averaging of the Eliashberg equations [70, 225–227]:

$$\begin{aligned} Z(\omega_n) &= 1 + \frac{\pi T}{\omega_n} \sum_m \frac{\lambda(\omega_{nm}^-) \omega_m}{\sqrt{\omega_m^2 + \Delta^2(\omega_m)}}, \\ Z(\omega_n) \Delta(\omega_n) &= \pi T \sum_m [\lambda(\omega_{nm}^-) - \mu(\omega_c) \theta(\omega_c - |\omega_m|)] \\ &\quad \times \frac{\Delta(\omega_m)}{\sqrt{\omega_m^2 + \Delta^2(\omega_m)}}, \quad (\text{A.6}) \\ \lambda(\omega_{nm}^-) &= 2 \int_0^\infty d\nu \frac{\nu}{\nu^2 + (\omega_{nm}^-)^2} \alpha^2 F(\nu), \end{aligned}$$

where  $\omega_{nm}^- = \omega_n - \omega_m$ ,  $\alpha^2 F(\omega) = \langle \langle \alpha^2 F(\mathbf{k}, \mathbf{k}', \omega) \rangle \rangle_{\mathbf{k}, \mathbf{k}'}$ , and  $\langle \langle \dots \rangle \rangle_{\mathbf{k}, \mathbf{k}'}$  is the average over the Fermi surface. The above equations can be written on the real axis by the analytical continuation  $i\omega_m \rightarrow \omega + i\delta$  where the gap function is complex, that is,  $\Delta(\omega) = \Delta_R(\omega) + i\Delta_I(\omega)$ . The solution for  $\Delta(\omega)$  allows the calculation of the current-voltage characteristic  $I(V)$  and *tunnelling conductance*  $G_{\text{NS}}(V) = dI_{\text{NS}}/dV$  in the superconducting state of the NIS tunnelling junction where  $I_{\text{NS}}(V)$  is given by

$$I_{\text{NS}}(V) = 2e \sum_{\mathbf{k}, \mathbf{p}} |T_{\mathbf{k}, \mathbf{p}}|^2 \int_{-\infty}^{\infty} \frac{d\omega}{2\pi}, \quad (\text{A.7})$$

$$A_N(\mathbf{k}, \omega) A_S(\mathbf{p}, \omega + eV) [f(\omega) - f(\omega + eV)].$$

Here,  $A_{N,S}(\mathbf{k}, \omega) = -2 \text{Im} G_{N,S}(\mathbf{k}, \omega)$  are the spectral functions of the normal metal and superconductor, respectively, and  $f(\omega)$  is the Fermi distribution function. Since the angular and energy dependence of the tunnelling matrix elements  $|T_{\mathbf{k}, \mathbf{p}}|^2$  is practically unimportant for  $s$ -wave superconductors, then the relative conductance  $\sigma_{\text{NS}}(V) \equiv G_{\text{NS}}(V)/G_{\text{NN}}(V)$  is proportional to the tunnelling density of states  $N_T(\omega) = \int A_S(\mathbf{k}, \omega) d^3k / (2\pi)^3$ , that is,  $\sigma_{\text{NS}}(\omega) \approx N_T(\omega)$  where

$$N_T(\omega) = \text{Re} \left\{ \frac{\omega + i\tilde{\gamma}(\omega)}{\sqrt{(\omega + i\tilde{\gamma}(\omega))^2 - \tilde{Z}^2(\omega) \Delta(\omega)^2}} \right\}. \quad (\text{A.8})$$

Here,  $\tilde{Z}(\omega) = Z(\omega)/\text{Re} Z(\omega)$ ,  $\tilde{\gamma}(\omega) = \gamma(\omega)/\text{Re} Z(\omega)$ ,  $Z(\omega) = \text{Re} Z(\omega) + i\gamma(\omega)/\omega$ , and the *quasiparticle scattering rate* in the superconducting state  $\gamma_s(\omega, T) = -2 \text{Im} \Sigma(\omega, T)$  is given by

$$\begin{aligned} \gamma_s(\omega, T) &= 2\pi \int_0^\infty d\nu \alpha^2 F(\nu) N_s(\nu + \omega) \\ &\quad \times \{2n_B(\nu) + n_F(\nu + \omega) + n_F(\nu - \omega)\} + \gamma^{\text{imp}}, \quad (\text{A.9}) \end{aligned}$$

where  $N_s(\omega) = \text{Re}\{\omega/(\omega^2 - \Delta^2(\omega))^{1/2}\}$  is the quasiparticle density of states in the superconducting state;  $n_{B,F}(\nu)$  are Bose and Fermi distribution function, respectively. Since the structure of the phonon spectrum is contained in  $\alpha^2 F(\omega)$ , it is reflected on  $\Delta(\omega)$  for  $\omega > \Delta_0$  (the real gap obtained from  $\Delta_0 = \text{Re}\Delta(\omega = \Delta_0)$ ) which gives the structure in  $G_S(V)$  at  $V = \Delta_0 + \omega_{\text{ph}}$ . On the contrary one can extract the spectral function  $\alpha^2 F(\omega)$  from  $G_{\text{NS}}(V)$  by the inversion procedure proposed by Kulić [6] and McMillan and Rowell [228]. It turns out that in low-temperature superconductors the peaks of  $-d^2I/dV^2$  at  $eV_i = \Delta + \omega_{\text{ph},i}$  correspond to the peak positions of  $\alpha^2 F(\omega)$  and  $F(\omega)$ . However, we would like to point out that in HTSC cuprates the gap function is unconventional and very anisotropic, that is,  $\Delta(\mathbf{k}, i\omega_n) \sim \cos k_x a - \cos k_y a$ . Since in this case the extraction of  $\alpha^2 F(\mathbf{k}, \mathbf{k}', \omega)$  is difficult and at present rather unrealistic task, then an “average”  $\alpha^2 F(\omega)$  is extracted from the experimental curve  $G_S(V)$ . There is belief that it gives relevant information on the real spectral function such as the energy width of the bosonic spectrum ( $0 < \omega < \omega_{\text{max}}$ ) and positions and distributions of peaks due to bosons. It turns out that even such an approximate procedure gives valuable information in HTSC cuprates—see discussion in Section 1.3.4.

Note that in the case when both EPI and spin-fluctuation interaction (SFI) are present one should make difference between  $\lambda_{\mathbf{kp}}^Z(i\nu_n)$  and  $\lambda_{\mathbf{kp}}^\Delta(i\nu_n)$  defined by

$$\begin{aligned} \lambda_{\mathbf{kp}}^Z(i\nu_n) &= \lambda_{\text{sf},\mathbf{kp}}(i\nu_n) + \lambda_{ep,\mathbf{kp}}(i\nu_n), \\ \lambda_{\mathbf{kp}}^\Delta &= \lambda_{ep,\mathbf{kp}}(i\nu_n) - \lambda_{\text{sf},\mathbf{kp}}(i\nu_n). \end{aligned} \quad (\text{A.10})$$

In absence of EPI,  $\lambda_{\mathbf{kp}}^Z(i\nu_n)$  and  $\lambda_{\mathbf{kp}}^\Delta(i\nu_n)$  differ by sign, that is,  $\lambda_{\mathbf{kp}}^Z(i\nu_n) = -\lambda_{\mathbf{kp}}^\Delta(i\nu_n) > 0$  since the SFI potential is repulsive in the singlet pairing channel.

*a. Inversion of Tunnelling Data.* Phonon features in the conductance  $\sigma_{\text{NS}}(V)$  at  $eV = \Delta_0 + \omega_{\text{ph}}$  make the tunnelling spectroscopy a powerful method in obtaining the Eliashberg spectral function  $\alpha^2 F(\omega)$ . Two methods were used in the past for extracting  $\alpha^2 F(\omega)$ .

The *first method* is based on solving the *inverse problem* of the nonlinear Eliashberg equations. Namely, by measuring  $\sigma_{\text{NS}}(V)$ , one obtains the tunnelling density of states  $N_T(\omega)$  ( $\sim \sigma_{\text{NS}}(\omega)$ ) and by the inversion procedure one obtains  $\alpha^2 F(\omega)$  [228]. In reality the method is based on the iteration procedure—the McMillan-Rowell (MR) inversion, where in the first step an initial  $\alpha^2 F_{\text{ini}}(\omega)$ ,  $\mu_{\text{ini}}^*$ , and  $\Delta_{\text{ini}}(\omega)$  are inserted into Eliashberg equations (e.g.,  $\Delta_{\text{ini}}(\omega) = \Delta_0$  for  $\omega < \omega_0$  and  $\Delta_{\text{ini}}(\omega) = 0$  for  $\omega > \omega_0$ ) and then  $\sigma_{\text{ini}}(V)$  is calculated. In the second step the functional derivative  $\delta\sigma(\omega)/\delta\alpha^2 F(\omega)$  ( $\omega \equiv eV$ ) is found in the presence of a small change of  $\alpha^2 F_{\text{ini}}(\omega)$  and then the iterated solution  $\alpha^2 F_{(1)}(\omega) = \alpha^2 F_{\text{ini}}(\omega) + \delta\alpha^2 F(\omega)$  is obtained, where the correction  $\delta\alpha^2 F(\omega)$  is given by

$$\delta\alpha^2 F(\omega) = \int d\nu \left[ \frac{\delta\sigma_{\text{ini}}(V)}{\delta\alpha^2 F(\nu)} \right]^{-1} \left[ \sigma_{\text{exp}}(\nu) - \sigma_{\text{ini}}(\nu) \right]. \quad (\text{A.11})$$

The procedure is iterated until  $\alpha^2 F_{(n)}(\omega)$  and  $\mu_{(n)}^*$  converge to  $\alpha^2 F(\omega)$  and  $\mu^*$  which reproduce the experimentally obtained conductance  $\sigma_{\text{NS}}^{\text{exp}}(V)$ . In such a way the obtained  $\alpha^2 F(\omega)$  for *Pb* resembles the phonon density of states  $F_{\text{Pb}}(\omega)$ , which is obtained from neutron scattering measurements. Note that the method depends explicitly on  $\mu^*$  but on the contrary it requires only data on  $\sigma_{\text{NS}}(V)$  up to the voltage  $V_{\text{max}} = \omega_{\text{ph}}^{\text{max}} + \Delta_0$  where  $\omega_{\text{ph}}^{\text{max}}$  is the maximum phonon energy ( $\alpha^2 F(\omega) = 0$  for  $\omega > \omega_{\text{ph}}^{\text{max}}$ ) and  $\Delta_0$  is the zero-temperature superconducting gap. One pragmatical feature for the interpretation of tunnelling spectra (and for obtaining the spectral pairing function  $\alpha^2 F(\omega)$ ) in *LTS* and *HTSC* cuprates is that the negative peaks of  $d^2I/dV^2$  (or peaks in  $-d^2I/dV^2$ ) are at the peak positions of  $\alpha^2 F(\omega)$  and  $F(\omega)$ . This feature will be discussed later on in relation with experimental situation in cuprates.

The *second method* has been invented in [229, 230] and it is based on the combination of the Eliashberg equations and dispersion relations for Green’s functions—we call it GDS method. First, the tunnelling density of states is extracted from the tunnelling conductance in a more rigorous way [231]:

$$\begin{aligned} N_T(V) &= \frac{\sigma_{\text{NS}}(V)}{\sigma_{\text{NN}}(V)} - \frac{1}{\sigma^*(V)} \int_0^V du \\ &\times \frac{d\sigma^*(u)}{du} [N_T(V-u) - N_T(V)], \end{aligned} \quad (\text{A.12})$$

where  $\sigma^*(V) = \exp\{-\beta V\} \sigma_{\text{NN}}(V)$  and the constant  $\beta$  are obtained from  $\sigma_{\text{NN}}(V)$  at large biases—see [229, 230].  $N_T(V)$  under the integral can be replaced by the BCS density of states. Since the second method is used in extracting  $\alpha^2 F(\omega)$  in a number of LTSC as well as in HTSC cuprates—see below—we describe it briefly for the case of isotropic EPI at  $T = 0$  K. In that case the Eliashberg equations are given by [70, 225–227, 229, 230]:

$$\begin{aligned} Z(\omega)\Delta(\omega) &= \int_{\Delta_0}^{\infty} d\omega' \text{Re} \left[ \frac{\Delta(\omega')}{[\omega'^2 - \Delta^2(\omega')]^{1/2}} \right] \\ &\times [K_+(\omega, \omega') - \mu^* \theta(\omega_c - \omega)], \\ 1 - Z(\omega) &= \frac{1}{\omega} \int_{\Delta_0}^{\infty} d\omega' \text{Re} \left[ \frac{\omega'}{[\omega'^2 - \Delta^2(\omega')]^{1/2}} \right] K_-(\omega, \omega'), \end{aligned} \quad (\text{A.13})$$

where

$$\begin{aligned} K_{\pm}(\omega, \omega') &= \int_{\Delta_0}^{\omega_{\text{ph}}^{\text{max}}} d\nu \alpha^2 F(\nu) \\ &\times \left( \frac{1}{\omega' + \omega + \nu + i0^+} \pm \frac{1}{\omega' - \omega + \nu - i0^+} \right). \end{aligned} \quad (\text{A.14})$$

Here  $\mu^*$  is the Coulomb pseudopotential, the cutoff  $\omega_c$  is approximately  $(5-10)\omega_{\text{ph}}^{\text{max}}$ , and  $\Delta_0 = \Delta(\Delta_0)$  is the energy gap. Now by using the dispersion relation for the matrix Green’s functions  $\hat{G}(\mathbf{k}, \omega_n)$  one obtains [229, 230]

$$\text{Im} S(\omega) = \frac{2\omega}{\pi} \int_{\Delta_0}^{\infty} d\omega' \frac{N_T(\omega') - N_{\text{BCS}}(\omega')}{\omega^2 - \omega'^2}, \quad (\text{A.15})$$

where  $S(\omega) = \omega/[\omega^2 - \Delta^2(\omega)]^{1/2}$ . From (A.13) one obtains

$$\begin{aligned} & \int_0^{\omega-\Delta_0} d\nu \alpha^2 F(\omega - \nu) \operatorname{Re}\{\Delta(\nu)[\nu^2 - \Delta^2(\nu)]^{1/2}\} \\ &= \frac{\operatorname{Re} \Delta(\omega)}{\omega} \int_0^{\omega-\Delta_0} d\nu \alpha^2 F(\nu) N_T(\omega - \nu) + \frac{\operatorname{Im} \Delta(\omega)}{\pi} \\ &+ \frac{\operatorname{Im} \Delta(\omega)}{\pi} \int_0^\infty d\omega' N_T(\omega') \int_0^{\omega_{\text{ph}}^{\text{max}}} d\nu \frac{2\alpha^2 F(\nu)}{(\omega' + \nu)^2 - \omega^2}. \end{aligned} \quad (\text{A.16})$$

Based on (A.12)-(A.16) one obtains the scheme for extracting  $\alpha^2 F(\omega)$ :

$$\begin{aligned} & \sigma_{\text{NS}}(V), \sigma_{\text{NN}}(V) \longrightarrow N_T(V), \\ & \longrightarrow \operatorname{Im} S(\omega) \longrightarrow \Delta(\omega) \longrightarrow \alpha^2 F(\omega). \end{aligned} \quad (\text{A.17})$$

The advantage in this method is that the explicit knowledge of  $\mu^*$  is not required [229, 230]. However, the integral equation for  $\alpha^2 F(\omega)$  is linear Fredholm equation of the first kind which is ill defined—see the discussion in Section 1.3.2 item (2)

*b. Phonon Effects in  $N_T(\omega)$ .* We briefly discuss the physical origin for the phonon effects in  $N_T(\omega)$  by considering a model with only one peak, at  $\omega_0$ , in the phonon density of states  $F(\omega)$  by assuming for simplicity  $\mu^* = 0$  and neglecting the weak structure in  $N_T(\omega)$  at  $n\omega_0 + \Delta_0$ , which is due to the nonlinear structure of the Eliashberg equations [232]. In Figure 37 it is seen that the real part of the gap function  $\Delta_R(\omega)$  reaches a maximum at  $\omega_0 + \Delta_0$  then decreases and becomes negative and zero, while  $\Delta_I(\omega)$  is peaked slightly beyond  $\omega_0 + \Delta_0$  that is the consequence of the effective electron-electron interaction via phonons.

It follows that for  $\omega < \omega_0 + \Delta_0$  most phonons have higher energies than the energy  $\omega$  of electronic charge fluctuations and there is overscreening of this charge by the ions giving rise to attraction. For  $\omega \approx \omega_0 + \Delta_0$  the charge fluctuations are in resonance with ion vibrations giving rise to the peak in  $\Delta_R(\omega)$ . For  $\omega_0 + \Delta_0 < \omega$  the ions move out of phase with respect to the charge fluctuations giving rise to repulsion and negative  $\Delta_R(\omega)$ . This is shown in Figure 37(b). The structure in  $\Delta(\omega)$  is reflected on  $N_T(\omega)$  as shown in Figure 37(c) which can be reconstructed from the approximate formula for  $N_T(\omega)$  expanded in powers of  $\Delta/\omega$ :

$$\frac{N_T(\omega)}{N(0)} \approx 1 + \frac{1}{2} \left[ \left( \frac{\Delta_R(\omega)}{\omega} \right)^2 - \left( \frac{\Delta_I(\omega)}{\omega} \right)^2 \right]. \quad (\text{A.18})$$

As  $\Delta_R(\omega)$  increases above  $\Delta_0$ , this gives  $N_T(\omega) > N_{\text{BCS}}(\omega)$ , while for  $\omega \gtrsim \omega_0 + \Delta_0$  the real value  $\Delta_R(\omega)$  decreases while  $\Delta_I(\omega)$  rises and  $N_T(\omega)$  decreases giving rise for  $N_T(\omega) < N_{\text{BCS}}(\omega)$ .

*A.2. Transport Spectral Function  $\alpha_{tr}^2 F(\omega)$ .* The spectral function  $\alpha_{tr}^2 F(\omega)$  enters the dynamical conductivity  $\sigma_{ij}(\omega)$  ( $i, j =$

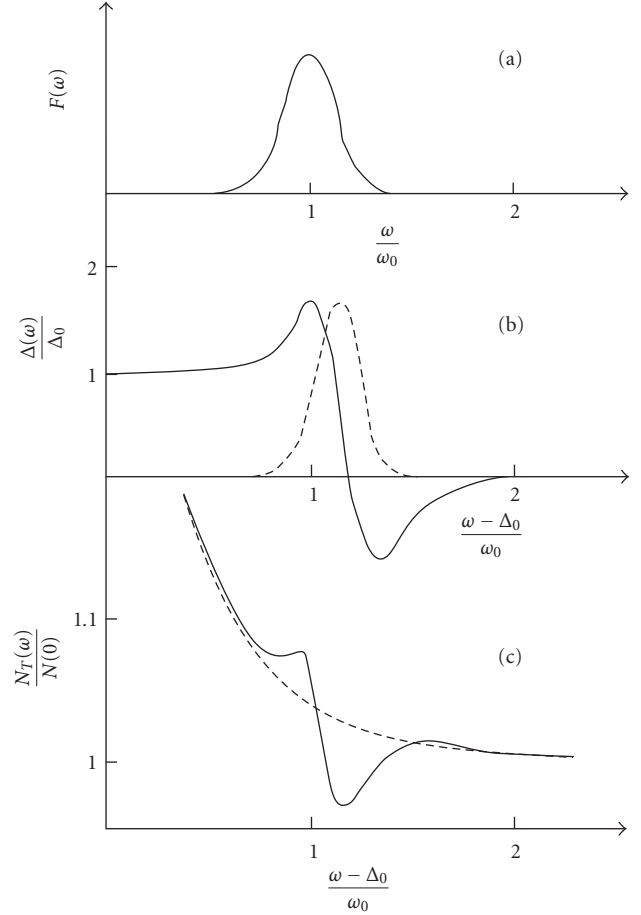


FIGURE 37: (a) Model phonon density of states  $F(\omega)$  with the peak at  $\omega_0$ . (b) The real (solid)  $\Delta_R$  and imaginary (dashed) part  $\Delta_I$  of the gap  $\Delta(\omega)$ . (c) The normalized tunnelling density of states  $N_T(\omega)/N(0)$  (solid) compared with the BCS density of states (dashed). From [232].

$a, b, c$  axis in HTS systems) which generally speaking is a tensor quantity given by the formula

$$\begin{aligned} \sigma_{ij}(\omega) = & -\frac{e^2}{\omega} \int \frac{d^4 q}{(2\pi)^4} \gamma_i(q, k+q) \\ & \times G(k+q) \Gamma_j(q, k+q) G(q), \end{aligned} \quad (\text{A.19})$$

where  $q = (\mathbf{q}, \nu)$  and  $k = (\mathbf{k} = 0, \omega)$  and the bare current vertex  $\gamma_i(q, k+q; \mathbf{k} = 0)$  is related to the Fermi velocity  $v_{F,i}$ , that is,  $\gamma_i(q, k+q; \mathbf{k} = 0) = v_{F,i}$ . The vertex function  $\Gamma_j(q, k+q)$  takes into account the renormalization due to all scattering processes responsible for finite conductivity [233]. In the following we study only the in-plane conductivity at  $\mathbf{k} = 0$ . The latter case is realized due to the fact that the long penetration depth in HTSC cuprates and the skin depth in the normal state are very large. In the EPI theory,  $\Gamma_j(q, k+q) \equiv \Gamma_j(\mathbf{q}, i\omega_n, i\omega_n + i\omega_m)$  is the solution of an approximative integral equation written in the symbolic form [118]  $\Gamma_j = \nu_j + V_{\text{eff}} G \Gamma_j$ . The effective potential  $V_{\text{eff}}$  (due to EPI) is given by  $V_{\text{eff}} = \sum_{\kappa} |g_{\kappa}^{\text{ren}}|^2 D_{\kappa}$ , where  $D_{\kappa}$  is the phonon Green's

function. In such a case the Kubo theory predicts  $\sigma_{ii}^{\text{intra}}(\omega)$  ( $i = x, y, z$ ):

$$\sigma_{ii}(\omega) = \frac{\omega_{p,ii}^2}{4i\pi\omega} \left\{ \int_{-\omega}^0 d\nu \operatorname{th}\left(\frac{\omega + \nu}{2T}\right) S^{-1}(\omega, \nu) + \int_0^{\infty} d\nu \left[ \operatorname{th}\left(\frac{\omega + \nu}{2T}\right) - \operatorname{th}\left(\frac{\nu}{2T}\right) \right] S^{-1}(\omega, \nu) \right\}, \quad (\text{A.20})$$

where  $S(\omega, \nu) = \omega + \Sigma_{\text{tr}}^*(\omega + \nu) - \Sigma_{\text{tr}}(\nu) + i\gamma_{\text{tr}}^{\text{imp}}$ , and  $\gamma_{\text{tr}}^{\text{imp}}$  is the impurity contribution. In the following we omit the tensor index  $ii$  in  $\sigma_{ii}(\omega)$ . In the presence of several bosonic scattering processes the transport self-energy  $\Sigma_{\text{tr}}(\omega) = \operatorname{Re} \Sigma_{\text{tr}}(\omega) + i \operatorname{Im} \Sigma_{\text{tr}}(\omega)$  is given by

$$\begin{aligned} \Sigma_{\text{tr}}(\omega) &= -\sum_l \int_0^{\infty} d\nu \alpha_{\text{tr},l}^2 F_l(\nu) [K_1(\omega, \nu) + iK_2(\omega, \nu)], \\ K_1(\omega, \nu) &= \operatorname{Re} \left[ \Psi\left(\frac{1}{2} + i\frac{\omega + \nu}{2\pi T}\right) - \Psi\left(\frac{1}{2} + i\frac{\omega - \nu}{2\pi T}\right) \right], \\ K_2(\omega, \nu) &= \frac{\pi}{2} \left[ 2\operatorname{cth}\left(\frac{\nu}{2T}\right) - \operatorname{th}\left(\frac{\omega + \nu}{2T}\right) + \operatorname{th}\left(\frac{\omega - \nu}{2T}\right) \right]. \end{aligned} \quad (\text{A.21})$$

Here  $\alpha_{\text{tr},l}^2 F_l(\nu)$  is the *transport spectral function* which measures the strength of the  $l$ th (bosonic) scattering process and  $\Psi$  is the di-gamma function. The index  $l$  enumerates EPI, charge, and spin-fluctuation scattering processes. Like in the case of EPI, the transport bosonic spectral function  $\alpha_{\text{tr},l}^2 F(\Omega)$  defined in (97) is given explicitly by

$$\begin{aligned} \alpha_{\text{tr},l}^2 F(\omega) &= \frac{1}{N^2(\mu)} \int \frac{dS_{\mathbf{k}}}{v_{F,\mathbf{k}}} \int \frac{dS_{\mathbf{k}'}}{v_{F,\mathbf{k}'}} \\ &\times \left[ 1 - \frac{v_{F,\mathbf{k}}^i v_{F,\mathbf{k}}^j}{(v_{F,\mathbf{k}}^i)^2} \right] \alpha_{\mathbf{k}\mathbf{k}',l}^2 F(\omega). \end{aligned} \quad (\text{A.22})$$

We stress that in the phenomenological SFI theory [12–17] one assumes that  $\alpha_{\mathbf{k}\mathbf{k}'}^2 F(\omega) \approx N(\mu) g_{\text{sf}}^2 \operatorname{Im} \chi(\mathbf{k} - \mathbf{p}, \omega)$ , which, as we have repeated several times, can be justified only for small  $g_{\text{sf}}$ , that is,  $g_{\text{sf}} \ll W_b$  (the bandwidth).

In case of weak coupling ( $\lambda < 1$ ),  $\sigma(\omega)$  can be written in the generalized (extended) Drude form as discussed in Section 1.3.2.

## Acknowledgments

The authors devote this paper to their great teacher and friend *Vitalii Lazarevich Ginzburg* who passed away recently. His permanent interest in their work and support in many respects over many years are unforgettable. M. L. Kulić is thankful to Karl Bennemann for inspiring discussions on many subjects related to physics of HTSC cuprates. They also thank Godfrey Akpojotor for careful reading of the manuscript. M. L. Kulić is thankful to the Max-Born-Institut für Nichtlineare Optik und Kurzzeitspektroskopie, Berlin, for the hospitality and financial support during his stay where part of this work has been done.

## References

- [1] A. B. Migdal, “Interaction between electrons and the lattice vibrations in a normal metal,” *Soviet Physics: Journal of Experimental and Theoretical Physics*, vol. 34, p. 996, 1958.
- [2] O. V. Danylenko and O. V. Dolgov, “Nonadiabatic contribution to the quasiparticle self-energy in systems with strong electron-phonon interaction,” *Physical Review B*, vol. 63, Article ID 094506, 9 pages, 2001.
- [3] V. L. Ginzburg and E. G. Maksimov, “Mechanisms and models of high temperature superconductors,” *Physica C*, vol. 235–240, pp. 193–196, 1994.
- [4] V. L. Ginzburg and E. G. Maksimov, “Superconductivity,” *Fizika Khimiiya Tekhnika*, vol. 5, p. 1505, 1992 (Russian).
- [5] E. G. Maksimov, “High-temperature superconductivity: the current state,” *Uspekhi Fizicheskikh Nauk*, vol. 170, p. 1033, 2000.
- [6] M. L. Kulić, “Interplay of electron-phonon interaction and strong correlations: the possible way to high-temperature superconductivity,” *Physics Report*, vol. 338, no. 1-2, pp. 1–264, 2000.
- [7] C. Falter, “Phonons, electronic charge response and electron-phonon interaction in the high-temperature superconductors,” *Physica Status Solidi (B)*, vol. 242, p. 118, 2005.
- [8] A. S. Alexandrov, “Unconventional pairs glued by conventional phonons in cuprate superconductors,” *Journal of Superconductivity and Novel Magnetism*, vol. 22, no. 2, pp. 103–107, 2009.
- [9] T. M. Hardy, J. P. Hague, J. H. Samson, and A. S. Alexandrov, “Superconductivity in a Hubbard-Froehlich model and in cuprates,” *Physical Review B*, vol. 79, Article ID 212501, 2009.
- [10] O. Gunnarsson and O. Rösch, “Interplay between electron-phonon and Coulomb interactions in cuprates,” *Journal of Physics*, vol. 20, no. 4, Article ID 043201, 2008.
- [11] O. Rösch, J. E. Hahn, O. Gunnarsson, and V. H. Crespi, “Phonons, electronic charge response and electron-phonon interaction in the high-temperature superconductors,” *Physica Status Solidi (B)*, vol. 242, p. 78, 2005.
- [12] A. J. Millis, H. Monien, and D. Pines, “Phenomenological model of nuclear relaxation in the normal state of  $\text{YBa}_2\text{Cu}_3\text{O}_7$ ,” *Physical Review B*, vol. 42, no. 1, pp. 167–178, 1990.
- [13] P. Monthoux and D. Pines, “Spin-fluctuation-induced superconductivity in the copper oxides: a strong coupling calculation,” *Physical Review Letters*, vol. 69, no. 6, pp. 961–964, 1992.
- [14] P. Monthoux and D. Pines, “ $\text{YBa}_2\text{Cu}_3\text{O}_7$ : a nearly antiferromagnetic Fermi liquid,” *Physical Review B*, vol. 47, no. 10, pp. 6069–6081, 1993.
- [15] B. P. Stojković and D. Pines, “Theory of the optical conductivity in the cuprate superconductors,” *Physical Review B*, vol. 56, no. 18, pp. 11931–11941, 1997.
- [16] D. Pines, preprint *CNSL Newsletter*, LALP-97-010, no. 138, June 1997.
- [17] D. Pines, “Spin excitations and superconductivity in cuprate oxide and heavy electron superconductors,” *Physica B*, vol. 163, no. 1–3, pp. 78–88, 1990.
- [18] P. A. Lee, N. Nagaosa, and C.-G. Wen, “Doping a Mott insulator: physics of high-temperature superconductivity,” *Reviews of Modern Physics*, vol. 78, p. 17, 2006.
- [19] T. Aimi and M. Imada, “Does simple two-dimensional Hubbard model account for high- $T_c$  superconductivity in copper oxides?” *Journal of the Physical Society of Japan*, vol. 76, no. 11, Article ID 113708, 4 pages, 2007.

- [20] D. J. Scalapino, S. R. White, and S. C. Zhang, "Superfluid density and the drude weight of the hubbard model," *Physical Review Letters*, vol. 68, no. 18, pp. 2830–2833, 1992.
- [21] L. P. Pryadko, S. A. Kivelson, and O. Zachar, "Incipient order in the t-J model at high temperatures," *Physical Review Letters*, vol. 92, no. 6, Article ID 067002, 4 pages, 2004.
- [22] A. Damascelli, Z. Hussain, and Z.-X. Shen, "Angle-resolved photoemission studies of the cuprate superconductors," *Reviews of Modern Physics*, vol. 75, no. 2, pp. 473–541, 2003.
- [23] J. C. Campuzano, M. R. Norman, and M. Randeria, "Photoemission in the high  $T_c$  superconductors," in *Physics of Conventional and Unconventional Superconductors Vol. II*, K. H. Bennemann and J. B. Ketterson, Eds., pp. 167–273, Springer, Berlin, Germany, 2004.
- [24] E. Schachinger and J. P. Carbotte, "Comparison of the in- and out-of-plane charge dynamics in  $\text{YBa}_2\text{Cu}_3\text{O}_{6.95}$ ," *Physical Review B*, vol. 64, no. 9, Article ID 094501, 10 pages, 2001.
- [25] J. Hwang, E. Schachinger, J. P. Carbotte, F. Gao, D. B. Tanner, and T. Timusk, "Bosonic spectral density of epitaxial thin-film  $\text{La}_{1.83}\text{Sr}_{0.17}\text{CuO}_4$  superconductors from infrared conductivity measurements," *Physical Review Letters*, vol. 100, no. 13, Article ID 137005, 2008.
- [26] J. Hwang, T. Timusk, E. Schachinger, and J. P. Carbotte, "Evolution of the bosonic spectral density of the high-temperature superconductor  $\text{Bi}_2\text{Sr}_2\text{CaCu}_2\text{O}_{8+\delta}$ ," *Physical Review B*, vol. 75, no. 14, Article ID 144508, 2007.
- [27] J. Hwang, T. Timusk, and G. D. Gu, "High-transition-temperature superconductivity in the absence of the magnetic-resonance mode," *Nature*, vol. 427, no. 6976, pp. 714–717, 2004.
- [28] R. Heid, K.-P. Bohnen, R. Zeyher, and D. Manske, "Momentum dependence of the electron-phonon coupling and self-energy effects in superconducting  $\text{YBa}_2\text{Cu}_3\text{O}_7$  within the local density approximation," *Physical Review Letters*, vol. 100, no. 13, Article ID 137001, 2008.
- [29] F. Giustino, M. L. Cohen, and S. G. Louie, "Small phonon contribution to the photoemission kink in the copper oxide superconductors," *Nature*, vol. 452, no. 7190, pp. 975–978, 2008.
- [30] Ph. Bourges, "From magnons to the resonance peak: spin dynamics in high- $T_c$  superconducting cuprates by inelastic neutron scattering," <http://arxiv.org/abs/cond-mat/9901333>.
- [31] D. Reznik, J.-P. Ismer, I. Eremin, et al., "Local-moment fluctuations in the optimally doped high- $T_c$  superconductor  $\text{YBa}_2\text{Cu}_3\text{O}_{6.95}$ ," *Physical Review B*, vol. 78, no. 13, Article ID 132503, 2008.
- [32] P. B. Allen, "Electron-phonon effects in the infrared properties of metals," *Physical Review B*, vol. 3, no. 2, pp. 305–320, 1971.
- [33] O. V. Dolgov and S. V. Shulga, "Analysis of intermediate boson spectra from FIR data for HTSC and heavy fermion systems," *Journal of Superconductivity*, vol. 8, no. 5, pp. 611–612, 1995.
- [34] S. V. Shulga, O. V. Dolgov, and E. G. Maksimov, "Electronic states and optical spectra of HTSC with electron-phonon coupling," *Physica C*, vol. 178, no. 4–6, pp. 266–274, 1991.
- [35] O. V. Dolgov, E. G. Maksimov, and S. V. Shulga, in *Electron-Phonon Interaction in Oxide Superconductors*, R. Baquero, Ed., p. 30, World Scientific, Singapore, 1991.
- [36] S. V. Shulga, "Electron-boson effects in the infrared properties of metals," in *High- $T_c$  Superconductors and Related Materials*, S.-L. Drechsler and T. Mishonov, Eds., p. 323, Kluwer Academic Publishers, 2001.
- [37] M. L. Kulić, *Lectures on the Physics of Highly Correlated Electron Systems*, vol. 715 of *AIP Conference Proceedings*, 2004.
- [38] M. L. Kulić and O. V. Dolgov, "Forward scattering peak in the electron-phonon interaction and impurity scattering of cuprate superconductors," *Physica Status Solidi (B)*, vol. 242, no. 1, pp. 151–178, 2005.
- [39] A. E. Karakozov, E. G. Maksimov, and O. V. Dolgov, "Electromagnetic response of superconductors and optical sum rule," *Solid State Communications*, vol. 124, no. 4, pp. 119–124, 2002.
- [40] A. E. Karakozov and E. G. Maksimov, "Optical sum rule in metals with a strong interaction," *Solid State Communications*, vol. 139, no. 2, pp. 80–85, 2006.
- [41] P. Kusar, V. V. Kabanov, S. Sugai, J. Demsar, T. Mertelj, and D. Mihailovic, "Controlled vaporization of the superconducting condensate in cuprate superconductors sheds light on the pairing boson," *Physical Review Letters*, vol. 101, Article ID 227001, 2008.
- [42] L. N. Bulaevskii, O. V. Dolgov, I. P. Kazakov, et al., "A tunnelling study of the oxide superconductors  $\text{La}_{2-x}\text{Sr}_x\text{CuO}_{4-y}$  and  $\text{EuBa}_2\text{Cu}_3\text{O}_7$ ," *Superconductor Science and Technology*, vol. 1, no. 4, pp. 205–209, 1988.
- [43] S. I. Vedenev, A. G. M. Jansen, P. Samuely, V. A. Stepanov, A. A. Tsvetkov, and P. Wyder, "Tunneling in the ab plane of the high- $T_c$  superconductor  $\text{Bi}_2\text{Sr}_2\text{CaCu}_2\text{O}_{8+\delta}$  in high magnetic fields," *Physical Review B*, vol. 49, no. 14, pp. 9823–9830, 1994.
- [44] S. I. Vedenev, A. G. M. Jansen, A. A. Tsvetkov, and P. Wyder, "Bloch-Grüneisen behavior for the in-plane resistivity of  $\text{Bi}_2\text{Sr}_2\text{CuO}_x$  single crystals," *Physical Review B*, vol. 51, no. 22, pp. 16380–16383, 1995.
- [45] S. I. Vedenev, A. G. M. Jansen, and P. Wyder, "Tunneling spectroscopy of  $\text{Bi}_2\text{Sr}_2\text{CaCu}_2\text{O}_8$  single crystals," *Physica B*, vol. 218, no. 1–4, pp. 213–216, 1996.
- [46] D. Shimada, Y. Shiina, A. Mottate, Y. Ohyagi, and N. Tsuda, "Phonon structure in the tunneling conductance of  $\text{Bi}_2\text{Sr}_2\text{CaCu}_2\text{O}_8$ ," *Physical Review B*, vol. 51, no. 22, pp. 16495–16498, 1995.
- [47] N. Miyakawa, A. Nakamura, Y. Fujino, et al., "Electron-phonon spectral function  $\alpha^2F(\omega)$  determined by quasiparticle tunneling spectroscopy for  $\text{Bi}_2\text{Sr}_2\text{CaCu}_2\text{O}_8/\text{Au}$  junctions," *Physica C*, vol. 282–287, pp. 1519–1520, 1997.
- [48] N. Miyakawa, Y. Shiina, T. Kaneko, and N. Tsuda, "Analysis of phonon structures in the tunneling conductance of Bi-cuprates," *Journal of the Physical Society of Japan*, vol. 62, pp. 2445–2455, 1993.
- [49] N. Miyakawa, Y. Shiina, T. Kido, and N. Tsuda, "Fine structure in the tunneling conductance of a  $\text{Bi}_2\text{Sr}_2\text{CaCu}_2\text{O}_8$ -GaAs junction," *Journal of the Physical Society of Japan*, vol. 58, pp. 383–386, 1989.
- [50] Y. Shiina, D. Shimada, A. Mottate, Y. Ohyagi, and N. Tsuda, "Temperature dependence of the tunneling conductance of  $\text{Bi}_2\text{Sr}_2\text{CaCu}_2\text{O}_8$ : phonon contribution to high- $T_c$  superconductivity," *Journal of the Physical Society of Japan*, vol. 64, pp. 2577–2584, 1995.
- [51] Y. Ohyagi, D. Shimada, N. Miyakawa, et al., "Reproducibility of phonon structures in the tunneling conductance of  $\text{Bi}_2\text{Sr}_2\text{CaCu}_2\text{O}_8$ ," *Journal of the Physical Society of Japan*, vol. 64, pp. 3376–3383, 1995.
- [52] R. S. Gonnelli, F. Asdente, and D. Andreone, "Reproducible inelastic tunneling in  $\text{Nb}/\text{Bi}_2\text{Sr}_2\text{CaCu}_2\text{O}_{8+x}$  point-contact junctions," *Physical Review B*, vol. 49, no. 2, pp. 1480–1483, 1994.

- [53] D. Shimada, N. Tsuda, U. Paltzer, and F. W. de Wette, "Tunneling phonon structures and the calculated phonon density of states for  $\text{Bi}_2\text{Sr}_2\text{CaCu}_2\text{O}_8$ ," *Physica C*, vol. 298, no. 3-4, pp. 195–202, 1998.
- [54] N. Tsuda, et al., "Contribution of the electron-phonon interaction to high- $T_c$  superconductivity: tunneling study of  $\text{Bi}_2\text{Sr}_2\text{CaCu}_2\text{O}_8$ ," in *New Research on Superconductivity*, B. P. Martinis, Ed., pp. 105–141, Nova Science Publishers, 2007.
- [55] Y. G. Ponomarev, et al., "Extended van Hove singularity, strong electron-phonon interaction and superconducting gap in doped Bi-2212 single crystal," *Physica Status Solidi (B)*, vol. 66, p. 2072, 2009.
- [56] H. Shim, P. Chaudhari, G. Logvenov, and I. Božović, "Electron-phonon interactions in superconducting  $\text{La}_{1.84}\text{Sr}_{0.16}\text{CuO}_4$  films," *Physical Review Letters*, vol. 101, no. 24, Article ID 247004, 2008.
- [57] S. Sugai, S. Shamoto, M. Sato, T. Ido, H. Takagi, and S. Uchida, "Symmetry breaking on the phonon Raman spectra only at the superconductor compositions in  $\text{La}_{2-x}\text{Sr}_x\text{CuO}_4$ ," *Solid State Communications*, vol. 76, no. 3, pp. 371–376, 1990.
- [58] F. Marsiglio, et al., "Eliashberg treatment of the microwave conductivity of niobium," *Physical Review B*, vol. 50, p. 7023, 1994.
- [59] O. Klein, E. J. Nicol, K. Holczer, and G. Grüner, "Conductivity coherence factors in the conventional superconductors Nb and Pb," *Physical Review B*, vol. 50, no. 9, pp. 6307–6316, 1994.
- [60] D. G. Hinks and J. D. Jorgensen, "The isotope effect and phonons in  $\text{MgB}_2$ ," *Physica C*, vol. 385, no. 1-2, pp. 98–104, 2003.
- [61] K. McElroy, R. W. Simmonds, J. E. Hoffman, et al., "Relating atomic-scale electronic phenomena to wave-like quasiparticle states in superconducting  $\text{Bi}_2\text{Sr}_2\text{CaCu}_2\text{O}_{8+\delta}$ ," *Nature*, vol. 422, no. 6932, pp. 592–596, 2003.
- [62] J. Lee, J. L. V. Lewandowski, and T. G. Jenkins, "Transport, noise, and conservation properties in gyrokinetic plasmas," *Bulletin of the American Physical Society*, vol. 50, p. 299, 2005.
- [63] J. C. Davis, et al., *Bulletin of the American Physical Society*, vol. 50, p. 1223, 2005.
- [64] J. C. Phillips, "Superconductive excitations and the infrared vibronic spectra of BSCCO," *Physica Status Solidi (B)*, vol. 242, no. 1, pp. 51–57, 2005.
- [65] M. L. Cohen and P. W. Anderson, "Comments on the maximum superconducting transition temperature," in *Superconductivity in d and f Band Metals*, D. H. Douglass, Ed., AIP Conference Proceedings, p. 17, AIP, New York, NY, USA, 1972.
- [66] P. W. Anderson, *A Career in Theoretical Physics*, World Scientific, Singapore, 1994.
- [67] O. V. Dolgov and E. G. Maksimov, "A note on the possible mechanisms of high-temperature superconductivity," *Uspekhi Fizicheskikh Nauk*, vol. 177, p. 983, 2007, translated in *Physics-Uspekhi*, vol. 50, p. 933, 2007.
- [68] D. A. Kirzhnits, "General properties of electromagnetic response functions," in *Dielectric Function of Condensed Systems*, L. V. Keldysh, D. A. Kirzhnits, and A. A. Maradudin, Eds., chapter 2, Elsevier, Amsterdam, The Netherlands, 1989.
- [69] V. L. Ginzburg and D. Kirzhnits, Eds., *High Temperature Superconductivity*, Consultant Bureau, New York, NY, USA, 1982.
- [70] P. B. Allen and B. Mitrović, *Solid State Physics*, vol. 37 of *H. Ehrenreich, F. Seitz and D. Turnbull Ed.*, Academic, New York, NY, USA, 1982.
- [71] O. V. Dolgov, D. A. Kirzhnits, and E. G. Maksimov, "On an admissible sign of the static dielectric function of matter," *Reviews of Modern Physics*, vol. 53, no. 1, pp. 81–93, 1981.
- [72] O. V. Dolgov, D. A. Kirzhnits, and E. G. Maksimov, "Dielectric function and superconductivity," in *Superconductivity, Superdiamagnetism and Superfluidity*, V. L. Ginzburg, Ed., chapter 2, MIR, Moscow, Russia, 1987.
- [73] O. V. Dolgov and E. G. Maksimov, "The dielectric function of crystalline systems," in *Dielectric Function of Condensed Systems*, L. V. Keldysh, D. A. Kirzhnits, and A. A. Maradudin, Eds., chapter 4, Elsevier, Amsterdam, The Netherlands, 1989.
- [74] E. G. Maksimov and D. Yu. Savrasov, "Lattice stability and superconductivity of the metallic hydrogen at high pressure," *Solid State Communications*, vol. 119, no. 10-11, pp. 569–572, 2001.
- [75] C. C. Tsuei and J. R. Kirtley, "Pairing symmetry in cuprate superconductors," *Reviews of Modern Physics*, vol. 72, no. 4, pp. 969–1016, 2000.
- [76] A. I. Lichtenstein and M. L. Kulić, "Electron-boson interaction can help d wave pairing self-consistent approach," *Physica C*, vol. 245, no. 1-2, pp. 186–192, 1995.
- [77] D. J. Scalapino, "The case for  $dx_2-y_2$  pairing in the cuprate superconductors," *Physics Report*, vol. 250, no. 6, pp. 329–365, 1995.
- [78] M. L. Kulić and R. Zeyher, "Influence of strong electron correlations on the electron-phonon coupling in high- $T_c$  oxides," *Physical Review B*, vol. 49, no. 6, pp. 4395–4398, 1994.
- [79] R. Zeyher and M. L. Kulić, "Electron-phonon coupling in the presence of strong correlations," *Physica B*, vol. 199-200, pp. 358–360, 1994.
- [80] R. Zeyher and M. L. Kulić, "Modifications of the transport and the pairing electron-phonon coupling in high- $T_c$  oxides due to strong electronic correlations," *Physica C*, vol. 235-240, pp. 2151–2152, 1994.
- [81] T. Dahm, V. Hinkov, S. V. Borisenko, et al., "Strength of the spin-fluctuation-mediated pairing interaction in a high-temperature superconductor," *Nature Physics*, vol. 5, no. 3, pp. 217–221, 2009.
- [82] H.-B. Schüttler and M. R. Norman, "Contrasting dynamic spin susceptibility models and their relation to high-temperature superconductivity," *Physical Review B*, vol. 54, no. 18, pp. 13295–13305, 1996.
- [83] S. M. Hayden, H. A. Mook, P. Dal, T. G. Perring, and F. Doan, "The structure of the high-energy spin excitations in a high-transition-temperature superconductor," *Nature*, vol. 429, no. 6991, pp. 531–534, 2004.
- [84] V. Hinkov, P. Bourges, S. Pailhès, et al., "Spin dynamics in the pseudogap state of a high-temperature superconductor," *Nature Physics*, vol. 3, no. 11, pp. 780–785, 2007.
- [85] S. V. Borisenko, A. A. Kordyuk, V. Zabolotnyy, et al., "Kinks, nodal bilayer splitting, and interband scattering in  $\text{YBa}_2\text{Cu}_3\text{O}_{6+x}$ ," *Physical Review Letters*, vol. 96, no. 11, Article ID 117004, 4 pages, 2006.
- [86] V. B. Zabolotnyy, S. V. Borisenko, A. A. Kordyuk, et al., "Momentum and temperature dependence of renormalization effects in the high-temperature superconductor  $\text{YBa}_2\text{Cu}_3\text{O}_{7-\delta}$ ," *Physical Review B*, vol. 76, no. 6, Article ID 064519, 2007.
- [87] T. A. Maier, A. Macridin, M. Jarrell, and D. J. Scalapino, "Systematic analysis of a spin-susceptibility representation of the pairing interaction in the two-dimensional Hubbard model," *Physical Review B*, vol. 76, no. 14, Article ID 144516, 2007.

- [88] P. W. Anderson, "Is there glue in cuprate superconductors?" *Science*, vol. 317, p. 1705, 2007.
- [89] H.-Y. Kee, S. A. Kivelson, and G. Aeppli, "Spin-1 neutron resonance peak cannot account for electronic anomalies in the cuprate superconductors," *Physical Review Letters*, vol. 88, no. 25, Article ID 257002, 4 pages, 2002.
- [90] M. L. Kulić and I. M. Kulić, "High- $T_c$  superconductors with antiferromagnetic order: limitations on spin-fluctuation pairing mechanism," *Physica C*, vol. 391, no. 1, pp. 42–48, 2003.
- [91] A. Lanzara, P. V. Bogdanov, X. J. Zhou, et al., "Evidence for ubiquitous strong electron-phonon coupling in high-temperature superconductors," *Nature*, vol. 412, no. 6846, pp. 510–514, 2001.
- [92] T. Valla, A. V. Fedorov, P. D. Johnson, et al., "Evidence for quantum critical behavior in the optimally doped cuprate  $\text{Bi}_2\text{Sr}_2\text{CaCu}_2\text{O}_{8+\delta}$ ," *Science*, vol. 285, no. 5436, pp. 2110–2113, 1999.
- [93] G. Xu, G. D. Gu, M. Hücker, et al., "Testing the itinerancy of spin dynamics in superconducting  $\text{Bi}_2\text{Sr}_2\text{CaCu}_2\text{O}_{8+\delta}$ ," *Nature Physics*, vol. 5, no. 9, pp. 642–646, 2009.
- [94] I. Božović, "Plasmons in cuprate superconductors," *Physical Review B*, vol. 42, no. 4, pp. 1969–1984, 1990.
- [95] Z. Schlesinger, R. T. Collins, F. Holtzberg, et al., "Superconducting energy gap and normal-state conductivity of a single-domain  $\text{YBa}_2\text{Cu}_3\text{O}_7$  crystal," *Physical Review Letters*, vol. 65, no. 6, pp. 801–804, 1990.
- [96] O. V. Dolgov and M. L. Kulić, "Optical properties of strongly correlated systems with spin-density-wave order," *Physical Review B*, vol. 66, no. 13, Article ID 134510, 7 pages, 2002.
- [97] D. B. Romero, C. D. Porter, D. B. Tanner, et al., "Quasiparticle damping in  $\text{Bi}_2\text{Sr}_2\text{CaCu}_2\text{O}_8$  and  $\text{Bi}_2\text{Sr}_2\text{CuO}_6$ ," *Physical Review Letters*, vol. 68, no. 10, pp. 1590–1593, 1992.
- [98] D. B. Romero, C. D. Porter, D. B. Tanner, et al., "On the phenomenology of the infrared properties of the copper-oxide superconductors," *Solid State Communications*, vol. 82, no. 3, pp. 183–187, 1992.
- [99] H. J. Kaufmann, Ph.D. thesis, University of Cambridge, Cambridge, UK, February 1999.
- [100] A. V. Puchkov, D. N. Basov, and T. Timusk, "The pseudogap state in high- $T_c$  superconductors: an infrared study," *Journal of Physics*, vol. 8, no. 48, pp. 10049–10082, 1996.
- [101] J. Hwang, T. Timusk, and G. D. Gu, "High-transition-temperature superconductivity in the absence of the magnetic-resonance mode," *Nature*, vol. 427, no. 6976, pp. 714–717, 2004.
- [102] M. Norman, "Shine a light," *Nature*, vol. 427, no. 6976, p. 692, 2004.
- [103] F. Gao, D. B. Romero, D. B. Tanner, J. Talvacchio, and M. G. Forrester, "Infrared properties of epitaxial  $\text{La}_{2-x}\text{Sr}_x\text{CuO}_4$  thin films in the normal and superconducting states," *Physical Review B*, vol. 47, no. 2, pp. 1036–1052, 1993.
- [104] A. V. Boris, N. N. Kovaleva, O. V. Dolgov, et al., "In-plane spectral weight shift of charge carriers in  $\text{YBa}_2\text{Cu}_3\text{O}_{6.9}$ ," *Science*, vol. 304, no. 5671, pp. 708–710, 2004.
- [105] J. Schutzmann, B. Gorshunov, K. F. Renk, et al., "Far-infrared hopping conductivity in the  $\text{CuO}$  chains of a single-domain  $\text{YBa}_2\text{Cu}_3\text{O}_7$ -crystal," *Physical Review B*, vol. 46, no. 1, pp. 512–515, 1992.
- [106] K. Kamaräs, S. L. Herr, C. D. Porter, et al., "Erratum: in a clean high- $T_c$  superconductor you do not see the gap (Physical Review Letters (1990) 64, 14 (1692))," *Physical Review Letters*, vol. 64, no. 14, p. 1692, 1990.
- [107] B. Vignolle, S. M. Hayden, D. F. McMorrow, et al., "Two energy scales in the spin excitations of the high-temperature superconductor  $\text{La}_{2-x}\text{Sr}_x\text{CuO}_4$ ," *Nature Physics*, vol. 3, no. 3, pp. 163–167, 2007.
- [108] I. Božović, J. H. Kim, J. S. Harris Jr., C. B. Eom, J. M. Phillips, and J. T. Cheung, "Reflectance and Raman spectra of metallic oxides,  $\text{LaSrCoO}$  and  $\text{CaSrRuO}$ : resemblance to superconducting cuprates," *Physical Review Letters*, vol. 73, no. 10, pp. 1436–1439, 1995.
- [109] J. E. Hirsch, "Superconductors that change color when they become superconducting," *Physica C*, vol. 201, no. 3-4, pp. 347–361, 1992.
- [110] P. F. Maldague, "Optical spectrum of a Hubbard chain," *Physical Review B*, vol. 16, no. 6, pp. 2437–2446, 1977.
- [111] H. J. A. Molegraaf, C. Presura, D. van der Marel, P. H. Kes, and M. Li, "Superconductivity-induced transfer of in-plane spectral weight in  $\text{Bi}_2\text{Sr}_2\text{CaCu}_2\text{O}_{8+\delta}$ ," *Science*, vol. 295, no. 5563, pp. 2239–2241, 2002.
- [112] R. Beck, Y. Dagan, A. Milner, et al., "Transition in the tunneling conductance of  $\text{YBa}_2\text{Cu}_3\text{O}_{7-\delta}$  films in magnetic fields up to 32.4T," *Physical Review B*, vol. 72, no. 10, Article ID 104505, 4 pages, 2005.
- [113] F. Carbone, A. B. Kuzmenko, H. J. A. Molegraaf, E. van Heumen, E. Giannini, and D. van der Marel, "In-plane optical spectral weight transfer in optimally doped  $\text{Bi}_2\text{Sr}_2\text{Ca}_2\text{Cu}_3\text{O}_{10}$ ," *Physical Review B*, vol. 74, no. 2, Article ID 024502, 2006.
- [114] F. Carbone, A. B. Kuzmenko, H. J. A. Molegraaf, et al., "Doping dependence of the redistribution of optical spectral weight in  $\text{Bi}_2\text{Sr}_2\text{CaCu}_2\text{O}_{8+\delta}$ ," *Physical Review B*, vol. 74, no. 6, Article ID 064510, 2006.
- [115] A. F. Santander-Syro, et al., *Europhysics Letters*, vol. 51, p. 16380, 1995.
- [116] L. Vidmar, J. Bonča, S. Maekawa, and T. Tohyama, "Bipolaron in the t-J model coupled to longitudinal and transverse quantum lattice vibrations," *Physical Review Letters*, vol. 103, no. 18, Article ID 186401, 2009.
- [117] G. Deutscher, A. F. Santander-Syro, and N. Bontemps, "Kinetic energy change with doping upon superfluid condensation in high-temperature superconductors," *Physical Review B*, vol. 72, no. 9, Article ID 092504, 3 pages, 2005.
- [118] H. J. Kaufmann, E. G. Maksimov, and E. K. H. Salje, "Electron-phonon interaction and optical spectra of metals," *Journal of Superconductivity and Novel Magnetism*, vol. 11, no. 6, pp. 755–768, 1998.
- [119] T. A. Friedman, et al., "Direct measurement of the anisotropy of the resistivity in the  $a$ - $b$  plane of twin-free, single-crystal, superconducting  $\text{YBa}_2\text{Cu}_3\text{O}_{7-\delta}$ ," *Physical Review B*, vol. 42, pp. 6217–6221, 1990.
- [120] P. B. Allen, "Is kinky conventional?" *Nature*, vol. 412, no. 6846, pp. 494–495, 2001.
- [121] I. I. Mazin and O. V. Dolgov, "Estimation of the electron-phonon coupling in  $\text{YBa}_2\text{Cu}_3\text{O}_7$  from the resistivity," *Physical Review B*, vol. 45, no. 5, pp. 2509–2511, 1992.
- [122] T. Kondo, T. Takeuchi, S. Tsuda, and S. Shin, "Electrical resistivity and scattering processes in  $(\text{Bi,Pb})_2(\text{Sr,Lu})_2\text{CuO}_{6+\delta}$  studied by angle-resolved photoemission spectroscopy," *Physical Review B*, vol. 74, no. 22, Article ID 224511, 2006.
- [123] J. Meng, G. Liu, W. Zhang, et al., "Growth, characterization and physical properties of high-quality large single crystals of  $\text{Bi}_2(\text{Sr}_{2-x}\text{La}_x)\text{CuO}_{6+\delta}$  high-temperature superconductors," *Superconductor Science and Technology*, vol. 22, no. 4, Article ID 045010, 2009.

- [124] W. E. Pickett, "Temperature-dependent resistivity from phonons in cuprate superconductors," *Journal of Superconductivity*, vol. 4, no. 6, pp. 397–407, 1991.
- [125] D. M. King, Z.-X. Shen, D. S. Dessau, et al., "Observation of a saddle-point singularity in  $\text{Bi}_2(\text{Sr}_{0.97}\text{Pr}_{0.03})_2\text{CuO}_{6+\delta}$  and its implications for normal and superconducting state properties," *Physical Review Letters*, vol. 73, no. 24, pp. 3298–3301, 1994.
- [126] S. Martin, A. T. Fiory, R. M. Fleming, L. F. Schneemeyer, and J. V. Waszczak, "Normal-state transport properties of  $\text{Bi}_{2+x}\text{Sr}_{2-y}\text{CuO}_{6+\delta}$  crystals," *Physical Review B*, vol. 41, no. 1, pp. 846–849, 1990.
- [127] S. I. Vedenev, A. G. M. Jansen, and P. Wyder, "Magnetotransport and magnetotunneling in single-layer, two-layer, and three-layer  $\text{Bi}_2\text{Sr}_2\text{Ca}_{n-1}\text{Cu}_n\text{O}_z$  ( $n = 1, 2, 3$ ) single crystals," *Physica B*, vol. 300, no. 1–4, pp. 38–51, 2001.
- [128] G. Varelogiannis and E. N. Economou, "Small-q electron-phonon scattering and linear dc resistivity in high- $T_c$  oxides," *Europhysics Letters*, vol. 42, no. 3, pp. 313–318, 1998.
- [129] M. L. Kulić and O. V. Dolgov, "Forward electron-phonon scattering and HTSC," in *High Temperature Superconductivity*, S. Barnes, J. Ashkenazi, J. Cohn, and F. Zuo, Eds., vol. 483 of *AIP Conference Proceedings*, p. 63, 1999.
- [130] R. Zeyher and M. L. Kulić, "Renormalization of the electron-phonon interaction by strong electronic correlations in high- $T_c$  superconductors," *Physical Review B*, vol. 53, no. 5, pp. 2850–2862, 1996.
- [131] D. Mihailovic and V. V. Kabanov, "Dynamic inhomogeneity, pairing and superconductivity in cuprates," *Structure and Bonding*, vol. 114, pp. 331–364, 2005.
- [132] V. V. Kabanov, J. Demsar, and D. Mihailovic, "Kinetics of a superconductor excited with a femtosecond optical pulse," *Physical Review Letters*, vol. 95, no. 14, Article ID 147002, 4 pages, 2005.
- [133] A. Bansil and M. Lindroos, "Importance of matrix elements in the ARPES spectra of BISCO," *Physical Review Letters*, vol. 83, no. 24, pp. 5154–5157, 1999.
- [134] T. Cuk, F. Baumberger, D. H. Lu, et al., "Coupling of the B1g Phonon to the antinodal electronic states of  $\text{Bi}_2\text{Sr}_2\text{Ca}_{0.92}\text{Y}_{0.08}\text{Cu}_2\text{O}_{8+\delta}$ ," *Physical Review Letters*, vol. 93, no. 11, Article ID 117003, 2004.
- [135] X. J. Zhou, J. Shi, T. Yoshida, et al., "Multiple bosonic mode coupling in the electron self-energy of  $(\text{La}_{2-x}\text{Sr}_x)\text{CuO}_4$ ," *Physical Review Letters*, vol. 95, no. 11, Article ID 117001, 4 pages, 2005.
- [136] T. Valla, T. E. Kidd, W.-G. Yin, et al., "High-energy kink observed in the electron dispersion of high-temperature cuprate superconductors," *Physical Review Letters*, vol. 98, no. 16, Article ID 167003, 2007.
- [137] M. L. Kulić and O. V. Dolgov, "Angle-resolved photoemission spectra of  $\text{Bi}_2\text{Sr}_2\text{CaCu}_2\text{O}_8$  show a Coulomb coupling  $\approx 1$  and an electron-phonon coupling of 2-3," *Physical Review B*, vol. 76, no. 13, Article ID 132511, 2007.
- [138] T. Cuk, D. H. Lu, X. J. Zhou, Z.-X. Shen, T. P. Devereaux, and N. Nagaosa, "A review of electron-phonon coupling seen in the high- $T_c$  Superconductors by angle-resolved photoemission studies (ARPES)," *Physica Status Solidi (B)*, vol. 242, no. 1, pp. 11–29, 2005.
- [139] G.-H. Gweon, T. Sasagawa, S. Y. Zhou, et al., "An unusual isotope effect in a high-transition-temperature superconductor," *Nature*, vol. 430, no. 6996, pp. 187–190, 2004.
- [140] E. G. Maksimov, O. V. Dolgov, and M. L. Kulić, "Electron-phonon interaction with the forward scattering peak and the angle-resolved photoemission spectra isotope shift in  $\text{Bi}_2\text{Sr}_2\text{CaCu}_2\text{O}_8$ ," *Physical Review B*, vol. 72, no. 21, Article ID 212505, 4 pages, 2005.
- [141] J. F. Douglas, H. Iwasawa, Z. Sun, et al., "Superconductors: unusual oxygen isotope effects in cuprates?" *Nature*, vol. 446, no. 7133, article E5, 2007.
- [142] H. Iwasawa, Y. Aiura, T. Saitoh, et al., "A re-examination of the oxygen isotope effect in ARPES spectra of  $\text{Bi}2212$ ," *Physica C*, vol. 463–465, pp. 52–55, 2007.
- [143] K. M. Shen, F. Ronning, D. E. Lu, et al., "Missing quasiparticles and the chemical potential puzzle in the doping evolution of the cuprate superconductors," *Physical Review Letters*, vol. 93, no. 26, Article ID 267002, 2004.
- [144] O. Rösch, O. Gunnarsson, X. J. Zhou, et al., "Polaronic behavior of undoped high- $T_c$  cuprate superconductors from angle-resolved photoemission spectra," *Physical Review Letters*, vol. 95, no. 22, Article ID 227002, 4 pages, 2005.
- [145] A. S. Mishchenko and N. Nagaosa, "Electron-phonon coupling and a polaron in the t-J model: from the weak to the strong coupling regime," *Physical Review Letters*, vol. 93, no. 3, Article ID 036402, 2004.
- [146] S. Ciuchi, F. De Pasquale, S. Fratini, and D. Feinberg, "Dynamical mean-field theory of the small polaron," *Physical Review B*, vol. 56, no. 8, pp. 4494–4512, 1997.
- [147] M. Tsunekawa, A. Sekiyama, S. Kasai, et al., "Bulk electronic structures and strong electron-phonon interactions in an electron-doped high-temperature superconductor," *New Journal of Physics*, vol. 10, Article ID 073005, 2008.
- [148] S. R. Park, D. J. Song, C. S. Leem, et al., "Angle-resolved photoemission spectroscopy of electron-doped cuprate superconductors: isotropic electron-phonon coupling," *Physical Review Letters*, vol. 101, no. 11, Article ID 117006, 2008.
- [149] J. C. Campuzano, H. Ding, M. R. Norman, et al., "Direct observation of particle-hole mixing in the superconducting state by angle-resolved photoemission," *Physical Review B*, vol. 53, no. 22, pp. R14737–R14740, 1996.
- [150] H. Matsui, T. Sato, T. Takahashi, et al., "BCS-like Bogoliubov quasiparticles in high- $T_c$  superconductors observed by angle-resolved photoemission spectroscopy," *Physical Review Letters*, vol. 90, no. 21, Article ID 217002, 4 pages, 2003.
- [151] M. L. Kulić and O. V. Dolgov, "Dominance of the electron-phonon interaction with forward scattering peak in high- $T_c$  superconductors: theoretical explanation of the ARPES kink," *Physical Review B*, vol. 71, no. 9, Article ID 092505, 4 pages, 2005.
- [152] Y. Chen, A. Iyo, W. Yang, et al., "Anomalous Fermi-surface dependent pairing in a self-doped high- $T_c$  superconductor," *Physical Review Letters*, vol. 97, no. 23, Article ID 236401, 2006.
- [153] W. Xie, O. Jepsen, O. K. Andersen, Y. Chen, and Z.-X. Shen, "Insights from angle-resolved photoemission spectroscopy of an undoped four-layered two-gap high- $T_c$  superconductor," *Physical Review Letters*, vol. 98, no. 4, Article ID 047001, 2007.
- [154] L. Zhu, P. J. Hirschfeld, and D. J. Scalapino, "Elastic forward scattering in the cuprate superconducting state," *Physical Review B*, vol. 70, no. 21, Article ID 214503, 13 pages, 2004.
- [155] M. L. Kulić and V. Oudovenko, "Why is d-wave pairing in HTS robust in the presence of impurities?" *Solid State Communications*, vol. 104, no. 7, pp. 375–379, 1997.
- [156] M. L. Kulić and O. V. Dolgov, "Anisotropic impurities in anisotropic superconductors," *Physical Review B*, vol. 60, no. 18, pp. 13062–13069, 1999.

- [157] H.-Y. Kee, "Effect of doping-induced disorder on the transition temperature in high- $T_c$  cuprates," *Physical Review B*, vol. 64, no. 1, Article ID 012506, 2001.
- [158] J. Kirtley, "Tunneling measurements of the cuprate superconductors," in *Handbook of High-Temperature Superconductivity: Theory and Experiment*, J. R. Schrieffer, Ed., p. 19, Springer, Berlin, Germany, 2007.
- [159] B. Renker, F. Gompf, D. Ewert, et al., "Changes in the phonon spectra of Bi 2212 superconductors connected with the metal-semiconductor transition in the series of  $\text{Bi}_2\text{Sr}_2(\text{Ca}_{1-x}\text{Y}_x)\text{Cu}_2\text{O}_8$  compounds," *Zeitschrift für Physik B*, vol. 77, no. 1, pp. 65–68, 1989.
- [160] G. Deutscher, N. Hass, Y. Yagil, A. Revcolevschi, and G. Dhalenne, "Evidence for strong electron-phonon interaction in point contact spectroscopy of superconducting oriented  $\text{La}_{1-x}\text{Sr}_x\text{CuO}_4$ ," *Journal of Superconductivity*, vol. 7, no. 2, pp. 371–374, 1994.
- [161] Y. Sidis, S. Pailhès, B. Keimer, P. Bourges, C. Ulrich, and L. P. Regnault, "Magnetic resonant excitations in high- $T_c$  superconductors," *Physica Status Solidi (B)*, vol. 241, no. 6, pp. 1204–1210, 2004.
- [162] G.-M. Zhao, "Fine structure in the tunneling spectra of electron-doped cuprates: no coupling to the magnetic resonance mode," *Physical Review Letters*, vol. 103, no. 23, Article ID 236403, 2009.
- [163] O. Fischer, M. Kugler, I. Maggio-Aprile, C. Berthod, and C. Renner, "Scanning tunneling spectroscopy of high-temperature superconductors," *Reviews of Modern Physics*, vol. 79, no. 1, pp. 353–419, 2007.
- [164] O. K. Andersen, O. Jepsen, A. I. Liechtenstein, and I. I. Mazin, "Plane dimpling and saddle-point bifurcation in the band structures of optimally doped high-temperature superconductors: a tight-binding model," *Physical Review B*, vol. 49, no. 6, pp. 4145–4157, 1994.
- [165] Q. Huang, J. F. Zasadzinski, N. Tralshawala, et al., "Tunnelling evidence for predominantly electron-phonon coupling in superconducting  $\text{Ba}_{1-x}\text{K}_x\text{BiO}_3$  and  $\text{Nd}_{2-x}\text{Ce}_x\text{CuO}_{4-y}$ ," *Nature*, vol. 347, no. 6291, pp. 369–372, 1990.
- [166] P. Samuely, N. L. Bobrov, A. G. M. Jansen, P. Wyder, S. N. Barilo, and S. V. Shiryaev, "Tunneling measurements of the electron-phonon interaction in  $\text{Ba}_{1-x}\text{K}_x\text{BiO}_3$ ," *Physical Review B*, vol. 48, no. 18, pp. 13904–13910, 1993.
- [167] P. Samuely, P. Szabó, A. G. M. Jansen, et al., "From superconducting to normal density of states of  $\text{Ba}_{1-x}\text{K}_x\text{BiO}_3$  by tunneling in high magnetic fields," *Physica B*, vol. 194–196, pp. 1747–1748, 1994.
- [168] O. Rösch and O. Gunnarsson, "Electron-phonon interaction in the t-J model," *Physical Review Letters*, vol. 92, no. 14, Article ID 146403, 2004.
- [169] K. J. von Szczepanski and K. W. Becker, "Coupling of electrons and phonons in a doped antiferromagnet," *Zeitschrift für Physik B*, vol. 89, no. 3, pp. 327–334, 1992.
- [170] D. Reznik, "Giant electron-phonon anomaly in doped  $\text{La}_2\text{CuO}_4$  and other cuprates," *Advances in Condensed Matter Physics*, vol. 2010, Article ID 523549, 2010.
- [171] G. Khaliullin and P. Horsch, "Theory of the density fluctuation spectrum of strongly correlated electrons," *Physical Review B*, vol. 54, no. 14, pp. R9600–R9603, 1996.
- [172] L. Pintschovius, "Electron-phonon coupling effects explored by inelastic neutron scattering," *Physica Status Solidi (B)*, vol. 242, no. 1, pp. 30–50, 2005.
- [173] D. Reznik, L. Pintschovius, M. Ito, et al., "Electron-phonon coupling reflecting dynamic charge inhomogeneity in copper oxide superconductors," *Nature*, vol. 440, no. 7088, pp. 1170–1173, 2006.
- [174] D. Reznik, L. Pintschovius, M. Fujita, K. Yamada, G. D. Gu, and J. M. Tranquada, "Electron-phonon anomaly related to charge stripes: static stripe phase versus optimally doped superconducting  $\text{La}_{1.85}\text{Sr}_{0.15}\text{CuO}_4$ ," *Journal of Low Temperature Physics*, vol. 147, no. 3–4, pp. 353–364, 2007.
- [175] L. Pintschovius, D. Reznik, W. Reichardt, et al., "Oxygen phonon branches in  $\text{YBa}_2\text{Cu}_3\text{O}_7$ ," *Physical Review B*, vol. 69, no. 21, Article ID 214506, 2004.
- [176] K.-P. Bohnen, R. Heid, and M. Krauss, "Phonon dispersion and electron-phonon interaction for  $\text{YBa}_2\text{Cu}_3\text{O}_7$  from first-principles calculations," *Europhysics Letters*, vol. 64, no. 1, pp. 104–110, 2003.
- [177] T. Bauer and C. Falter, "The impact of dynamical screening on the phonon dynamics of  $\text{LaCuO}$ ," *Physical Review B*, vol. 80, Article ID 094525, 2009.
- [178] D. Reznik, G. Sangiovanni, O. Gunnarsson, and T. P. Devereaux, "Photoemission kinks and phonons in cuprates," *Nature*, vol. 455, no. 7213, pp. E6–E7, 2008.
- [179] R. Zeyher and M. L. Kulić, "Statics and dynamics of charge fluctuations in the t-J model," *Physical Review B*, vol. 54, no. 13, pp. 8985–8988, 1996.
- [180] M. L. Kulić and R. Zeyher, "Novel 1/N expansion for self-energy and correlation functions of the Hubbard model," *Modern Physics Letters B*, vol. 11, no. 8, pp. 333–338, 1997.
- [181] M. L. Kulić and G. Akpojotor, in preparation.
- [182] Z. B. Huang, W. Hanke, E. Arrigoni, and D. J. Scalapino, "Electron-phonon vertex in the two-dimensional one-band Hubbard model," *Physical Review B*, vol. 68, no. 22, Article ID 220507, 4 pages, 2003.
- [183] E. Cappelluti, B. Cerruti, and L. Pietronero, "Charge fluctuations and electron-phonon interaction in the finite-U Hubbard model," *Physical Review B*, vol. 69, no. 16, Article ID 161101, 2004.
- [184] C. Thomsen, M. Cardona, B. Gegenheimer, R. Liu, and A. Simon, "Untwinned single crystals of  $\text{YBa}_2\text{Cu}_3\text{O}_7$ : an optical investigation of the  $a$ - $b$  anisotropy," *Physical Review B*, vol. 37, no. 16, pp. 9860–9863, 1988.
- [185] C. Thomsen and M. Cardona, in *Physical Properties of High Temperature Superconductors I*, D. M. Ginsberg, Ed., p. 409, World Scientific, Singapore, 1989.
- [186] R. Feile, "Lattice vibrations in high- $T_c$  superconductors: optical spectroscopy and lattice dynamics," *Physica C*, vol. 159, no. 1–2, pp. 1–32, 1989.
- [187] C. Thomsen, "Light scattering in high- $T_c$ -superconductors," in *Light Scattering in Solids VI*, M. Cardona and G. Guentherodt, Eds., p. 285, Springer, Berlin, Germany, 1991.
- [188] V. G. Hadjiev, X. Zhou, T. Strohm, M. Cardona, Q. M. Lin, and C. W. Chu, "Strong superconductivity-induced phonon self-energy effects in  $\text{HgBa}_2\text{Ca}_3\text{Cu}_4\text{O}_{10+\delta}$ ," *Physical Review B*, vol. 58, no. 2, pp. 1043–1050, 1998.
- [189] S. N. Rashkeev and G. Wendin, "Electronic Raman continuum for  $\text{YBa}_2\text{Cu}_3\text{O}_{7-\delta}$ : effects of inelastic scattering and interband transitions," *Physical Review B*, vol. 47, no. 17, pp. 11603–11606, 1993.
- [190] J. F. Franck, in *Physical Properties of High Temperature Superconductors V*, D. M. Ginsberg, Ed., World Scientific, Singapore, 1994.

- [191] J. P. Franck, "Experimental studies of the isotope effect in high  $T_c$  superconductors," *Physica C*, vol. 282–287, pp. 198–201, 1997.
- [192] H. Iwasawa, J. F. Douglas, K. Sato, et al., "An isotopic fingerprint of electron-phonon coupling in high- $T_c$  cuprates," *Physical Review Letters*, vol. 101, Article ID 157005, 2008.
- [193] D. J. Scalapino, "The Electron-phonon interaction and strong-coupling superconductors," in *Superconductivity*, R. D. Parks, Ed., vol. 1, chapter 11, Dekker, New York, NY, USA, 1969.
- [194] D. Rainer, "Principles of AB initio calculations of superconducting transition temperatures," in *Progress in Low-Temperature Physics*, D. F. Brewer, Ed., p. 371, Elsevier, Amsterdam, The Netherlands, 1986.
- [195] H. Krakauer, W. E. Pickett, and R. E. Cohen, "Large calculated electron-phonon interactions in  $\text{La}_{2-x}\text{M}_x\text{CuO}_4$ ," *Physical Review B*, vol. 47, no. 2, pp. 1002–1015, 1993.
- [196] C. Falter, M. Klenner, G. A. Hoffmann, and Q. Chen, "Origin of phonon anomalies in  $\text{La}_2\text{CuO}_4$ ," *Physical Review B*, vol. 55, no. 5, pp. 3308–3313, 1997.
- [197] C. Falter, M. Klenner, and G. A. Hoffmann, "Screening and phonon-plasmon scenario as calculated from a realistic electronic bandstructure based on LDA for  $\text{La}_2\text{CuO}_4$ ," *Physica Status Solidi (B)*, vol. 209, no. 2, pp. 235–266, 1998.
- [198] C. Falter, M. Klenner, and G. A. Hoffmann, "Anisotropy dependence of the c-axis phonon dispersion in the high-temperature superconductors," *Physical Review B*, vol. 57, no. 22, pp. 14444–14451, 1998.
- [199] I. I. Mazin, S. N. Rashkeev, and S. Y. Savrasov, "Nonspherical rigid-muffin-tin calculations of electron-phonon coupling in high- $T_c$  perovskites," *Physical Review B*, vol. 42, no. 1, pp. 366–370, 1990.
- [200] L. F. Mattheiss, "Electronic band properties and superconductivity in  $\text{La}_{2-y}\text{X}_y\text{CuO}_4$ ," *Physical Review Letters*, vol. 58, no. 10, pp. 1028–1030, 1987.
- [201] T. Jarlborg, "Electron-phonon coupling and charge transfer in  $\text{YBa}_2\text{Cu}_3\text{O}_7$  from band theory," *Solid State Communications*, vol. 67, no. 3, pp. 297–300, 1988.
- [202] T. Jarlborg, "Weak screening of high frequency phonons and superconductivity in  $\text{YBa}_2\text{Cu}_3\text{O}_7$ ," *Solid State Communications*, vol. 71, no. 8, pp. 669–671, 1989.
- [203] S. Yu. Savrasov, "Linear response calculations of lattice dynamics using muffin-tin basis sets," *Physical Review Letters*, vol. 69, no. 19, pp. 2819–2822, 1992.
- [204] S. Yu. Savrasov and D. Yu. Savrasov, "Full-potential linear-muffin-tin-orbital method for calculating total energies and forces," *Physical Review B*, vol. 46, no. 19, pp. 12181–12195, 1992.
- [205] S. Y. Savrasov and O. K. Andersen, "Linear-response calculation of the electron-phonon coupling in doped  $\text{CaCuO}_2$ ," *Physical Review Letters*, vol. 77, no. 21, pp. 4430–4433, 1996.
- [206] V. J. Emery, "Theory of high- $T_c$  superconductivity in oxides," *Physical Review Letters*, vol. 58, no. 26, pp. 2794–2797, 1987.
- [207] W. E. Pickett, "Electronic structure of the high-temperature oxide superconductors," *Reviews of Modern Physics*, vol. 61, p. 433, 1989.
- [208] J. van den Brink, M. B. J. Meinders, J. Lorenzana, R. Eder, and G. A. Sawatzky, "New phases in an extended hubbard model explicitly including atomic polarizabilities," *Physical Review Letters*, vol. 75, no. 25, pp. 4658–4661, 1995.
- [209] J. van den Brink, M. B. J. Meinders, J. Lorenzana, R. Eder, and G. A. Sawatzky, "New phases in an extended hubbard model explicitly including atomic probabilities," *Physical Review Letters*, vol. 76, p. 2826, 1996.
- [210] J. van den Brink, thesis, University Groningen, 1997.
- [211] H. Eskes and G. A. Sawatzky, "Doping dependence of high-energy spectral weights for the high- $T_c$  cuprates," *Physical Review B*, vol. 43, no. 1, pp. 119–129, 1991.
- [212] F. C. Zhang and T. M. Rice, "Effective Hamiltonian for the superconducting Cu oxides," *Physical Review B*, vol. 37, no. 7, pp. 3759–3761, 1988.
- [213] R. Hayn, V. Yushankhai, and S. Lovtsov, "Analysis of the singlet-triplet model for the copper oxide plane within the paramagnetic state," *Physical Review B*, vol. 47, no. 9, pp. 5253–5262, 1993.
- [214] A. E. Ruckenstein and S. Schmitt-Rink, "New approach to strongly correlated systems: 1N expansions without slave bosons," *Physical Review B*, vol. 38, no. 10, pp. 7188–7191, 1988.
- [215] A. Greco and R. Zeyher, "Superconducting instabilities in the  $t-t'$  hubbard model in the large-N limit," *Europhysics Letters*, vol. 35, no. 2, pp. 115–120, 1996.
- [216] R. Zeyher and A. Greco, "Superconductivity in the t-J model in the large-N limit," *Zeitschrift fur Physik B*, vol. 104, no. 4, pp. 737–740, 1997.
- [217] M. Grilli and G. Kotliar, "Fermi-liquid parameters and superconducting instabilities of a generalized t-J model," *Physical Review Letters*, vol. 64, no. 10, pp. 1170–1173, 1990.
- [218] P. Fulde, J. Keller, and G. Zwicknagel, "Theory of heavy fermion systems," in *Solid State Physics*, H. Ehrenreich and D. Turnbull, Eds., vol. 41, p. 2, Academic Press, 1988.
- [219] M. Grilli and C. Castellani, "Electron-phonon interactions in the presence of strong correlations," *Physical Review B*, vol. 50, no. 23, pp. 16880–16898, 1994.
- [220] C. Grimaldi, L. Pietronero, and S. Strässler, "Nonadiabatic superconductivity. I. Vertex corrections for the electron-phonon interactions," *Physical Review B*, vol. 52, no. 14, pp. 10516–10529, 1995.
- [221] C. Grimaldi, L. Pietronero, and S. Strässler, "Nonadiabatic superconductivity. II. Generalized Eliashberg equations beyond Migdal's theorem," *Physical Review B*, vol. 52, no. 14, pp. 10530–10546, 1995.
- [222] G. Kotliar and J. Liu, "Superconducting instabilities in the large-U limit of a generalized hubbard model," *Physical Review Letters*, vol. 61, no. 15, pp. 1784–1787, 1988.
- [223] J. H. Kim and Z. Teanović, "Effects of strong Coulomb correlations on the phonon-mediated superconductivity: a model inspired by copper oxides," *Physical Review Letters*, vol. 71, no. 25, pp. 4218–4221, 1993.
- [224] S. Ishihara and N. Nagaosa, "Interplay of electron-phonon interaction and electron correlation in high-temperature superconductivity," *Physical Review B*, vol. 69, no. 14, Article ID 144520, 2004.
- [225] O. V. Dolgov and E. G. Maksimov, "Critical temperature of superconductors with a strong coupling," *Uspekhi Fizicheskikh Nauk*, vol. 138, p. 95, 1982.
- [226] O. V. Dolgov and E. G. Maksimov, "Electron-phonon interaction and superconductivity," in *Thermodynamics and Electrodynamics of Superconductors*, V. L. Ginzburg, Ed., chapter 1, Nova Science, Hauppauge, NY, USA, 1987.
- [227] F. Marsiglio and J. P. Carbotte, "Electron-phonon superconductivity," in *Superconductivity I*, J. Ketterson and K. H. Bennemann, Eds., Springer, Berlin, Germany, 2008.
- [228] W. L. McMillan and J. M. Rowell, "Lead phonon spectrum calculated from superconducting density of states," *Physical Review Letters*, vol. 14, no. 4, pp. 108–112, 1965.
- [229] A. A. Galkin, A. I. Dyashenko, and V. M. Svistunov, "Determination of the energy gap parameter and the

- electron-phonon interaction function in superconductors on basis tunnel data," *Zhurnal Eksperimental'noi i Teoreticheskoi Fiziki*, vol. 66, p. 2262, 1974.
- [230] V. M. Svistunov, A. I. D'yachenko, and M. A. Belogolovskii, "Elastic tunneling spectroscopy of single-particle excitations in metals," *Journal of Low Temperature Physics*, vol. 31, no. 3-4, pp. 339–356, 1978.
- [231] Yu. M. Ivanshenko and Yu. V. Medvedev, "Many-body and inelastic tunnel spectroscopy of quasi-particle excitations in normal metals," *Fizika Nizkikh Temperatur*, vol. 2, p. 143, 1976.
- [232] D. J. Scalapino, J. R. Schrieffer, and J. W. Wilkins, "Strong-coupling superconductivity. I," *Physical Review*, vol. 148, no. 1, pp. 263–279, 1966.
- [233] J. R. Schrieffer, *Theory of Superconductivity*, W. A. Benjamin, New York, NY, USA, 1964.

## Review Article

# Electron-Phonon Interaction in Strongly Correlated Systems

**M. Capone, C. Castellani, and M. Grilli**

*ISC-CNR and Dipartimento di Fisica, Università di Roma “La Sapienza”, Piazzale Aldo Moro 5, 00185 Roma, Italy*

Correspondence should be addressed to M. Capone, massimo.capone@roma1.infn.it

Received 20 January 2010; Accepted 24 April 2010

Academic Editor: Alexandre Sasha Alexandrov

Copyright © 2010 M. Capone et al. This is an open access article distributed under the Creative Commons Attribution License, which permits unrestricted use, distribution, and reproduction in any medium, provided the original work is properly cited.

The Hubbard-Holstein model is a simple model including both electron-phonon interaction and electron-electron correlations. We review a body of theoretical work investigating, the effects of strong correlations on the electron-phonon interaction. We focus on the regime, relevant to high- $T_c$  superconductors, in which the electron correlations are dominant. We find that electron-phonon interaction can still have important signatures, even if many anomalies appear, and the overall effect is far from conventional. In particular in the paramagnetic phase the effects of phonons are much reduced in the low-energy properties, while the high-energy physics can still be affected by phonons. Moreover, the electron-phonon interaction can give rise to important effects, like phase separation and charge-ordering, and it assumes a predominance of forward scattering even if the bare interaction is assumed to be local (momentum independent). Antiferromagnetic correlations reduce the screening effects due to electron-electron interactions and revive the electron-phonon effects.

## 1. Introduction

A wealth of materials, including the most challenging systems (cuprates, manganites, fullerenes, etc), present clear signatures of both electron-electron (e-e) and electron-phonon (e-ph) interactions, leading to a competition-or- interplay which can give rise to different physics according to the value of relevant control parameters and of the chemical and electronic properties of the materials. The results presented in this paper are mainly motivated by high-temperature superconductors, with the copper-oxide compounds (cuprates) in a prominent role, and an attention to the alkali-doped fullerenes.

In the case of the cuprates, which are arguably the most accurately studied materials in the last twenty-five years, the signatures of electron-phonon interactions are nowadays clear, even though the overall scenario is far from ordinary [1–3]: Electron-phonon fingerprints are evident in some properties, while they are weak or absent in other observables. Specifically, clear polaronic features are observed in optical conductivity [4–6] as well as in angle-resolved photoemission experiments (ARPES) [7] in very lightly doped compounds. A substantial e-ph coupling can also be inferred by the Fano line shapes of phonons in Raman spectra and by the rather large frequency shift and

linewidth broadening of some phonons at  $T_c$ . Phonons are also good candidates to account for the famous “kink” in the electronic dispersions observed in ARPES experiments [8, 9]. Tunneling experiments are often advocated as providing the most important evidence of strong e-ph coupling [10]. Also Scanning Tunneling Spectroscopy measurements suggest a direct role of a phonon mode in superconductivity [11]. Isotope effects on different quantities can be sizable, even if they present highly unconventional features [12].

On the other hand, phonons, which typically affect resistivity in standard metals, hardly appear in transport experiments on cuprates. For instance, the resistivity around optimal doping is ubiquitously linear in temperature (even in systems with relatively low critical temperature) [13–16] and no high-temperature saturation seems to be present up to the highest achieved temperatures [17]. While in the overdoped materials the resistivity evolves towards a  $T^2$  Fermi-liquid behavior, it is the whole scenario at all dopings (and the material dependencies), which contrasts with the relevance of e-ph interaction in transport (at least in its standard formulation). If one were just considering cuprates with rather high critical temperatures around optimal doping (like, e.g.,  $\text{YBa}_2\text{Cu}_3\text{O}_7$ ) one would not find it difficult to get a reasonable agreement between transport experiments and the standard e-ph approach [10]. This dichotomous

behavior of cuprates, which display clear phononic features in some experiments and limited effects in others is one of the puzzling and challenging issues raised in these materials.

Although there is a wide range of suggestions for the superconducting mechanism, it is almost universally recognized that a key player in the cuprate game is the e-e correlation. Electron-electron correlation makes the parent compounds Mott insulators, and is expected to be important at least in the pseudogap region. Therefore, it is not surprising that the signatures of e-ph interaction in the cuprates can hardly be understood in terms of the standard theory of e-ph interactions in weakly correlated metals, and a new theoretical framework including e-e correlations is needed. We will argue here that this change of perspective can indeed reconcile the different relevance of phonons in the various observables in correlated systems.

On the other hand, the superconducting members of the fulleride family, of composition  $A_3C_{60}$  with A an alkali-metal atom, are often considered as standard phononic superconductors, in which the coupling between electrons and the local vibrations associated the distortion of the carbon buckyballs is the driving force of superconducting pairing [18]. The conventional nature of these compounds is indeed challenged by recent investigations in expanded fullerenes revealing several physical properties associated to e-e correlations [19]. Indeed, the  $Cs_3C_{60}$  solid with A15 structure is an antiferromagnetic Mott insulator at ambient pressure which becomes superconducting only under applied pressure, with  $T_c$  reaching 38 K [20, 21]. The phase diagram as a function of pressure closely resembles that of cuprates as a function of doping, suggesting a central role of correlations. Consequently, e-e interactions are expected to be important in other members of the fulleride family. Indeed, it has been shown that, thanks to the orbital degeneracy and the Jahn-Teller nature of the relevant phonons, there is no contradiction between a phononmediated superconductivity and the relevance of electronic correlations, and the two interactions turn out to cooperate in providing relatively high critical temperature [22].

In an extremely broad sense, these materials (cuprates and fullerenes), as well as many others that we did not talk about, raise the same conceptual problem, namely the investigation of systems in which both e-e interaction and e-ph coupling are nonnegligible and the physics can be explained only taking both into account. On the other hand the same phenomenology suggests that this competition may result in completely different physics according to specific aspects of the materials. In general, we can expect different behaviors because of: (i) Different parameters within the same model (e.g., which is the largest scale between electron-phonon interaction and electron-electron repulsion); (ii) Different form for the interaction term, or more generally, different models.

Here we focus on point (i), and we choose an extremely simplified model, the Hubbard-Holstein model, in which one band of correlated electrons with local Coulomb repulsion is coupled with a dispersionless phonon mode and the coupling only involves the local electronic charge [23]. Even for this simplified model we immediately realize that

several relevant physical parameters control the physics. As we will discuss in the following section, we have to deal at least with the electronic bandwidth, the Coulomb repulsion, the strength of electron-phonon interaction, the phononic frequency and the chemical potential that controls the band filling. This determines a multidimensional phase diagram, which can hardly be understood in its entirety within a single analysis and it is expected to present several different regimes. Therefore, even if we choose one given simple model, it may be useful to focus on a given physical regime, which essentially implies to select a hierarchy between the different energy scales, or to fix (or neglect) some of them.

Our choice is to focus on the “strongly correlated” metallic phases, that is, on system in which the Coulomb repulsion is the largest energy scale, and the system is either at half-filling (number of electrons equal to the number of sites) or close. The polar star of this work is the understanding of the fate of electron-phonon interaction in systems that are dominated by electron-electron interactions such as the cuprates. Nonetheless, our discussion will also follow some detours, which will help us to build a more comprehensive picture of the competition between the two interactions. One of these detours will touch point (ii) addressing the role of the phonon symmetry in its interplay with correlations. This point is crucial for the understanding of the synergy between e-ph interaction and e-e correlation in the fullerenes.

The paper is organized as follows: In Section 2 we introduce the Hubbard-Holstein model. Section 3 is devoted to a Fermi-liquid analysis of the effects of correlations on electron-phonon interactions and to a mean-field solution of the Hubbard-Holstein model within the slave-boson formalism. Section 4 presents a nonperturbative Dynamical Mean-Field Theory study of the Hubbard-Holstein model. Section 5 is dedicated to the charge instabilities of the model. Section 6 briefly compares the Hubbard-Holstein model with a three-band model with Jahn-Teller interactions introduced for the fullerenes. Section 7 presents our conclusions.

## 2. The Model

The simplest model of a strongly correlated electron system coupled to the lattice is given by the single-band Hubbard-Holstein (HH) model. In this work, the HH model is not used as a microscopic model for the cuprates, but rather as an idealized description of the competition between e-ph interaction and e-e interaction. In physical terms, the most crucial limitations is the local nature of the interactions. We refer to previous literature for analyses of nonlocal e-ph interactions [24–28]. Considering a single band is a reasonable assumption for the cuprates, while in many materials the multiband nature needs to be taken into account.

The single-band HH model reads

$$\begin{aligned}
 H = & -t \sum_{\langle i,j \rangle, \sigma} (c_{i\sigma}^\dagger c_{j\sigma} + H.c.) \\
 & - \mu_0 \sum_{i\sigma} n_{i\sigma} + U \sum_i n_{i\uparrow} n_{i\downarrow} \\
 & + \omega_0 \sum_i a_i^\dagger a_i + g \sum_{i,\sigma} (a_i^\dagger + a_i)(n_{i\sigma} - \langle n_{i\sigma} \rangle),
 \end{aligned} \tag{1}$$

where  $\langle i, j \rangle$  indicate nearest-neighbor sites.  $n_{i\sigma} = c_{i\sigma}^\dagger c_{i\sigma}$  is the local electron density, which is coupled via  $g$  to the field  $a_i$  of a dispersionless phonon [23]. The relevant physical parameters are the strength of the coulomb repulsion  $U$ , the bare bandwidth  $W$ , the bare phonon frequency  $\omega_0$ , the bare dimensionless electron-phonon coupling  $\lambda = 2g^2/(\omega_0 W)$ , the chemical potential and the details of the bandstructure (e.g., inclusion of next-neighbor hopping). The chosen expression for  $\lambda$  would coincide with the standard definition (see, e.g., [29]) in the case of a band with a flat density of states  $1/W$ . The dimensionality of the system also plays a major role. This multidimensional parameter space leads to an extremely rich physics, and the number of paper devoted to this simple model is countless. Various approaches have been considered to solve the HH model in the presence of strong correlations. Besides numerical techniques like quantum Monte Carlo [26, 30–33], exact diagonalization [34–39], and Dynamical Mean Field Theory (DMFT) [40–50], Density-Matrix Renormalization Group [51, 52], (semi) analytical approaches like slave bosons (SB) [53–57], large- $N$  expansions [58, 59], and variational approaches [24, 60–63] including a modified Gutzwiller scheme [64–66], have been useful to elucidate the renormalization of the e-ph coupling in the presence of (strong) correlations.

Even if our focus will be the strongly correlated HH model, we will discuss its results in comparison with some related models, like the Hubbard-tJ model, the three-band Hubbard model for the cuprates and a three-orbital Hubbard model with Jahn-Teller interactions for the doped fullerenes. Our investigation will be mainly dedicated to the effects of e-ph interaction on the self-energy and the quasiparticle renormalization factor  $z$  starting from a strongly correlated regime, in which the Coulomb interactions puts the system close to a Mott insulating phase. This is realized for large values of  $U/W$  and for an half-filled or weakly doped band. Since the study of superconductivity within DMFT (our main tool of investigation) is limited to s-wave symmetry, we will not discuss superconductivity in the HH model which is expected to be d-wave if (repulsive) correlation dominates (specifically when the model can be mapped into a t-J model plus phonons). On the other hand we will study s-wave superconductivity in a three-orbital model for fullerenes which emphasizes the role of the symmetry of e-ph interaction in presence of correlations.

### 3. Effect of Electron-Phonon Interaction in a Correlated Metal

*3.1. Fermi-Liquid Analysis.* In this section, we begin our analysis of the properties of e-ph interaction in a correlated metal within a Landau Fermi-liquid (FL) picture [29, 67]. Within this approach, the correlated metal is described as a collection of quasiparticles with an effective mass  $m^*$  instead of the physical electron mass  $m$ . In the presence of strong e-e correlations the motion of the carriers is naturally obstructed by the interactions, which is reflected in a large ratio between the effective mass and the bare mass  $m^*/m \gg 1$  and in a loss of low-energy spectral weight described by a small quasiparticle renormalization factor  $z_e$ . The former

reflects in an enhanced quasiparticle density of states  $N^* = m^*/mN_0$  ( $N_0$  being the bare density of states) and the latter renormalizes the quasiparticle interactions.

In order to characterize the fate of the e-ph interaction in a similar correlated metal, we need to consider also the vertex corrections introduced by e-e interactions, for which no Migdal theorem can be invoked.

We can gain a first insight on the way in which the e-ph interaction behaves in the presence of strong correlations by considering the effective dimensionless e-e interaction mediated by the exchange of a single-phonon

$$N^* \Gamma_{\text{eff}}^{\text{ph}}(\mathbf{q}, \omega) = N^* g^2 z_e^2 \Lambda_e^2(q, \omega) \frac{2\omega(q)}{\omega^2 - \omega^2(q)}. \quad (2)$$

By assuming that all the correlation effects are local, or equivalently that the self-energy is independent on momentum, the effective mass is related to  $z_e$  by  $z_e = m/m^*$ . In (2)  $\Lambda_e$  includes the vertex corrections which renormalizes the e-ph vertex, and the last factor is the free phonon propagator. In order to focus on the effect of correlations on the phononmediated interaction, in both  $z_e$  and  $\Lambda_e$  we include only processes due to e-e interactions, as reminded by the index “e” that we attached to them.

Within a Landau Fermi-liquid picture we can use the Ward identities that connect the vertex corrections  $\Lambda$  with the wavefunction renormalization  $z$ . In the small frequency ( $\omega$ ) and transferred momentum ( $q$ ) regimes, these identities have two distinct forms depending on the order of the  $\omega \rightarrow 0$  and  $q \rightarrow 0$  limits. In the case of the charge-density vertex, which is relevant for our Holstein coupling, we have

$$\begin{aligned} z_e \Lambda_e(\omega \rightarrow 0, q = 0) &= 1, \\ z_e \Lambda_e(\omega = 0, q \rightarrow 0) &= \frac{1}{1 + F_0^s}, \end{aligned} \quad (3)$$

where  $F_0^s$  is the symmetric Landau parameter. Equation (3) are exact Ward identities, which are satisfied irrespective of the details of the e-e interactions and show the drastic difference between the dynamic  $[(\omega \rightarrow 0, q = 0)]$  and static  $[(\omega = 0, q \rightarrow 0)]$  limits.

Plugging these results into (2) we obtain, in the two limits considered above

$$\begin{aligned} N^* \Gamma_{\text{eff}}^{\text{ph}}(\omega \rightarrow 0, q = 0) &= -\frac{2g^2 N^*}{\omega_0}, \\ N^* \Gamma_{\text{eff}}^{\text{ph}}(\omega = 0, q \rightarrow 0) &= -\frac{2g^2 N^*}{\omega_0} \frac{1}{[1 + (F_0^s)_e]^2} \\ &= -\frac{2g^2}{\omega_0} \frac{\kappa^e}{N^*}, \end{aligned} \quad (4)$$

where  $\kappa^e = N^*/[1 + (F_0^s)_e]$  is the charge compressibility in the absence of e-ph coupling. The difference between the dynamic and static case can be dramatic in the case of a Fermi liquid with a large mass enhancement  $m^*/m \gg 1$ , and small compressibility renormalization ( $\kappa^e \sim N_0$ ). This requires  $(F_0^s)_e$  to be much larger than one and proportional

to the quasiparticle density of states  $N^* = (m^*/m)N_0 \gg N_0$ . Equation (4) then lead to

$$\begin{aligned} N^* \Gamma_{\text{eff}}^{\text{ph}}(\omega \rightarrow 0, \mathbf{q} = 0) &= -\lambda \left( \frac{m^*}{m} \right), \\ N^* \Gamma_{\text{eff}}^{\text{ph}}(\omega = 0, \mathbf{q} \rightarrow 0) &= -\lambda \left( \frac{m}{m^*} \right), \end{aligned} \quad (5)$$

so that the effective one-phonon mediated e-e interaction is large ( $\sim m^*/m$ ) in the dynamic limit and small ( $\sim m/m^*$ ) in the static one. We emphasize that the key condition for the equalities (5) to hold is that  $\kappa^e \ll m^*/m$ . Therefore, they are verified also for a modest mass enhancement as long as the compressibility remains much smaller than it (cf. (4)).

The strong  $\omega - q$  dependence in (5) has been demonstrated on really general grounds only in the small- $q$  and small- $\omega$  limits, whereas the case of finite  $q$ 's and  $\omega$ 's needs (approximate) analyses of specific models. The cases of the single-band and of the three-band Hubbard models with infinite local repulsion have been extensively considered in the literature as prototypical models of strong correlations. In this framework the issue of e-ph coupling has been considered by means of the Holstein [45, 53, 54, 58, 66] or (less frequently) of the so-called Su-Schrieffer-Heeger coupling (where phonons couple to the electron hopping term) [68, 69].

Results for these models show that the product  $z\Lambda$  remains of order one in the dynamical regime as long as the momentum and frequency lie outside the particle-hole continuum, while it is strongly suppressed (as in the static limit) inside the particle-hole continuum, where important screening processes take place. Moreover, strong correlations provide further suppression of the e-ph coupling when, within the static limit  $\omega = 0$ , the transferred momentum is increased [58]. These additional screening channels depend on the details of the electronic band structure determining particle-hole screening processes.

The general Fermi liquid discussion and the specific analysis of models with strong correlations generically demonstrates the relevant role of dynamics in the screening effects that e-e correlations induce on the e-ph coupling. This strong dependence of the e-ph vertex on momentum and frequency (and on their ratio) makes the effects of the e-ph coupling rather subtle, since different physical quantities, involving different dynamical regimes, may display more or less suppressed e-ph effects. In particular the e-ph coupling (and the e-e interaction mediated by phonons) will be depressed by strong e-e interactions whenever small energy and large momentum transfer are involved (e.g., in transport). This suppression may be substantial, for instance, in the low-doping region of the superconducting cuprates, where e-e correlations are strong due to the relative proximity to a correlation-induced insulating phase. On the other hand different physical processes involving dynamical processes could experience a more pronounced e-ph coupling. Specific calculations carried out in a single-band Hubbard-Holstein model within a large- $N$  treatment of the e-e correlations [58, 59] find that the Eliashberg spectral function  $\alpha^2 F(\omega)$  determining superconductivity is

much less reduced than the analogous quantity  $\alpha^2 F_{\text{tr}}(\omega)$  determining transport properties. As we will discuss in the following section, this different renormalization will find a counterpart in nonperturbative dynamical mean-field theory calculations.

Even if our focus is on the Hubbard-Holstein model, it can be useful to recall that in the case of phonons coupled to the electron current, Ward identities similar to those of (3) can be derived [67]

$$\begin{aligned} z\Lambda_\alpha(\omega \rightarrow 0, q = 0) &= J_{q\alpha}, \\ z\Lambda_\alpha(\omega = 0, q \rightarrow 0) &= v_{q\alpha}, \end{aligned} \quad (6)$$

where  $\Lambda_\alpha$  is the  $\alpha$ th component of the electronic vector vertex part.  $v_{q\alpha}$  and  $J_{q\alpha}$  are instead the  $\alpha$ th components of the quasiparticle velocity and of the current, respectively. Similarly to the case of a coupling with the density, the correlations suppress much more strongly the e-ph coupling in the static limit, while they affect little the coupling in the dynamical case (remember that the current is weakly touched by interactions and it even remains constant in translationally invariant systems).

*3.2. The Hubbard-Holstein Model: Mean-Field Slave-Boson Approaches.* A natural tool to address the screening effects beyond the small- $q$  and small- $\omega$  regime are mean-field approaches based on a slave-boson representation of the Hilbert space. These methods, although approximate, capture the main physical ingredients of the problem with a description of a Fermi liquid of quasiparticles coupled by a residual interaction. This is why we briefly summarize here some results obtained [54] in the simplest formulation of the slave-boson large- $N$  approach to the infinite- $U$  Hubbard model. Here one can reach a semiquantitative understanding of the effects of correlations on the e-ph coupling, which are in substantial agreement with the results of more sophisticated approaches.

In this discussion we will consider the infinite-repulsion limit, which simplifies the formalism. In this limit we have a sharp constraint of no double occupancy on each lattice site  $\sum_\sigma n_{i\sigma} \leq 1$ . The standard slave-boson technique implements the constraint [70–76] by performing the usual substitution  $c_{i\sigma}^\dagger \rightarrow f_{i\sigma}^\dagger b_i$ ,  $c_{i\sigma} \rightarrow b_i^\dagger f_{i\sigma}$ , where the fermionic  $f_{i\sigma}$  operators represent quasiparticles, while the bosonic field  $b_i$  labels the state of a site with no fermions in it. This formulation of slave bosons is here used in connection with a large- $N$  expansion [71] in order to introduce a small parameter allowing for a systematic perturbative expansion without any assumption on the smallness of any physical quantity. Within the large- $N$  scheme, the spin index runs from 1 to  $N$  and the constraint assumes the form  $\sum_\sigma c_{i\sigma}^\dagger c_{i\sigma} + b_i^\dagger b_i = N/2$ . A suitable rescaling of the hopping amplitudes  $t_{ij} \rightarrow t_{ij}/N$  must, in this model, be joined by the similar rescaling of the e-ph coupling  $g \rightarrow g/\sqrt{N}$  in order to compensate for the presence of  $N$  fermionic degrees of freedom. It is beyond the scope of this paper to report the technical details of this technique, which have been extensively presented in previous works [54]. Here we simply remind that the leading order in the

large- $N$  expansion provides a mean-field description of the infinite- $U$  Hubbard model with uniform constant values of the bosonic field  $b_i \equiv b_0$  and of the Lagrange multiplier field implementing (on the average) the no-double-occupancy constraint. This gives rise to an insulating phase at half-filling ( $n = 1$ , doping  $\delta = 0$ ) and a Fermi liquid metallic phase at finite doping with small quasiparticle residue  $z = b_0^2 = \delta$  and large mass  $m^* = 1/zm$ . The treatment of the fluctuations at the next leading order beyond mean-field introduces residual interactions between the quasiparticles and allows to determine the scattering amplitudes in the particle-particle (Cooper) channel  $\Gamma^C(k, k'; q, \omega)$  and in the particle-hole channel  $\Gamma(k, k'; q, \omega)$ . Taking the small- $(\mathbf{q}, \omega)$  limits in this latter quantity also allows to determine the Landau parameter within the large- $N$  expansion. Setting  $N = 2$  we obtain

$$F_0^s = 2N^* \Gamma_\omega = N^* (-2\varepsilon_{k_F} - \lambda W). \quad (7)$$

Here  $\varepsilon_{k_F} \equiv -2t(\cos k_{F_x} + \cos k_{F_y}) + 4t' \cos(k_{F_x}) \cos(k_{F_y})$  is the bare electron dispersion calculated at the Fermi energy. As we already noted,  $F_0^s$  enters in the FL expression of the compressibility. When  $F_0^s < -1$  the thermodynamic stability condition  $\kappa > 0$  is violated and the system undergoes phase separation. We will discuss this issue in Section 6. We anticipate that, in the phase separated region, long-range Coulombic forces play a crucial role. It is indeed natural that a long-range interaction frustrates the formation of charge-rich regions. The outcome of this competition is, as we will see, a shift of the charge instability to finite momenta promoting the formation of a charge-density-wave phase. In this section we will consider parameters far from the phase separation instability. Nonetheless, in light of the central role played by long-range interactions in the phase separated case, we will also comment about their effect in these stable regions of parameters.

**3.2.1. Static Properties.** In the SB large- $N$  approach, the fluctuations of the bosonic fields mediate the residual interaction between the quasiparticles. If one only considers the fluctuations of the  $b$  and  $\lambda$  fields, then only the effects of the electronic Hubbard repulsion are described and one can accordingly discuss the effect of the pure electronic screening processes on the e-ph vertex. For the specific model that we here briefly discuss, Figure 1 reports the Feynman-diagram representation of the electronic processes (schematized by the dashed line of the bosonic propagators) dressing the bare (empty dot) e-ph vertex. The ratio between the resulting screened e-ph vertex and the bare e-ph coupling  $g$  is reported in Figure 2 both in the absence (dotted curve) and in the presence (solid curve) of a long-range Coulomb repulsion. In this latter case the strength is chosen to produce a repulsion of about 0.1 eV between electrons in nearest-neighbor cells. In both cases there is a strong reduction of the static e-ph coupling. In the short-range case the residual coupling is strongest at small momenta and it decreases as the momentum.

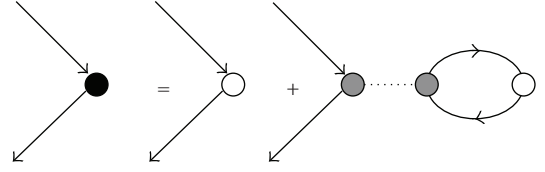


FIGURE 1: Leading-order in  $1/N$  diagrammatic structure of the effective e-ph vertex dressed by electronic processes only: the dashed line is the slave-boson propagator only involving  $b$  and  $\lambda$  bosons (pure e-e interaction), the solid dot is the dressed e-ph vertex, the open dots are the bare e-ph vertices and the grey dots are the quasiparticle-slave-boson vertices.

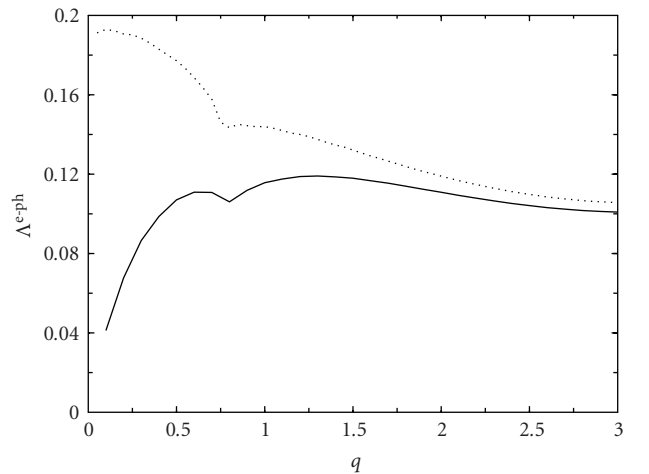


FIGURE 2: Static effective e-ph vertex in units of the bare e-ph coupling  $g$  as a function of the transferred momentum (in units of the inverse lattice spacing  $1/a$ ) in the  $(1, 0)$  direction. The vertex is calculated at leading order in  $1/N$  for a HH model with  $t = 0.5$  eV,  $t' = -(1/6)t$ ,  $\omega_0 = 0.04$  eV and doping  $x = 0.205$ . The dotted line is in the absence of long-range Coulomb forces ( $V_C = 0$ ); the solid line is in the presence of long-range Coulomb forces with  $V_C = 0.55$  eV (adapted from [54]).

On the other hand, as it is natural, the long-range potential screens out the long-range charge fluctuations thereby driving to zero the e-ph coupling at low momenta.

These findings can be obtained and confirmed with several different approaches. In particular, they reproduce exactly the results of large- $N$  calculations with Hubbard projectors instead of SB's [58, 59], and are in good agreement with calculations based on the flow-equation method [77] and recent Gutzwiller+RPA calculations at finite (but large)  $U$  [66]. They also agree qualitatively QMC analysis [33] (although some differences are present, which can be attributed to the fact that QMC calculations are performed at finite temperature and at finite Matsubara frequencies) (cf. [66, Figures 11 and 12]).

All these results show that e-ph scattering at large momenta is typically weaker than scattering at low momenta in the presence of short range forces only (which is the case of metallic phases far from phase separation charge instabilities, where, on the contrary, long-range interactions start to play a crucial role). This can be of obvious

relevance when the relative importance of e-ph couplings between the quasiparticles and specific phononic modes is considered [78]. Indeed it might well happen that in the presence of strong correlations modes that would be strongly coupled, but would exchange preferably large momenta, are more severely screened than other modes exchanging lower momenta. All this surely deserves a specific analysis.

**3.2.2. Dynamical Properties.** The previous subsection was focused on the screening of the static e-ph coupling by electronic processes. However the Fermi-liquid analysis carried out in Section 3.2 pointed out the great difference between screening processes in the static and in the dynamical regimes. While the Fermi liquid analysis was only able to provide definite statement in the small- $(q, \omega)$  regime, within the SB large- $N$  approach we can investigate the role of dynamics in the screening processes beyond this limit.

Figure 3 displays the behavior of the effective e-ph vertex (again normalized to the bare  $g$ ) as a function of Matsubara frequencies for two distinct momenta in the  $(1,0)$  direction for our HH model in the infinite- $U$  limit. In panel (a) a small momentum  $\mathbf{q} = (0.2, 0)$  (again unit lattice spacing is used here) is reported, while panel (b) shows the behavior at a larger momentum  $\mathbf{q} = (2.0, 0)$ . Clearly in the former case the e-ph coupling rapidly returns to its bare value, at Matsubara frequencies larger than  $\sim v_F |\mathbf{q}|$ . The  $v_F |\mathbf{q}|$  scale is instead much larger in panel (b), where the effective e-ph vertex stays small over a much broader frequency range. This fully parallels the low-frequency and low-momentum limits discussed in Section 3.1.

Again this result is not specific of this single-band model (or of its treatment) and it has been confirmed by the analysis of a three-band Hubbard model for the cuprate  $\text{CuO}_2$  planes with infinite repulsion on copper orbitals [53]. In this case, one can even notice in the small-momentum case an enhancement of the effective e-ph coupling above its bare value [79]. This is an overscreening effect due to interband processes. In any case, again one finds that low-momentum processes generically lead to larger e-ph couplings.

## 4. Strong-Coupling Regime and Polaron Formation in a Correlated Metal

**4.1. Proximity to a Paramagnetic Mott Insulator.** In this section we extend our analysis beyond the mean-field level and discuss the fate of the e-ph interaction in a correlated metal under the sole assumption that the physics is governed by the Hubbard repulsion close to a Mott-Hubbard transition, without assuming a weak e-ph coupling, and/or any approximation as far as the adiabatic ratio is concerned. This means that we need a theoretical approach able to treat several energy scales simultaneously, without assuming that any of them is negligible or perturbative. A natural candidate for this purpose is the Dynamical Mean-Field Theory (DMFT) [80], which treats all local interaction terms (such as both the Hubbard and the Holstein couplings) and the hopping term on the same footing and it is equally suitable to treat any parameter regime. Moreover, the

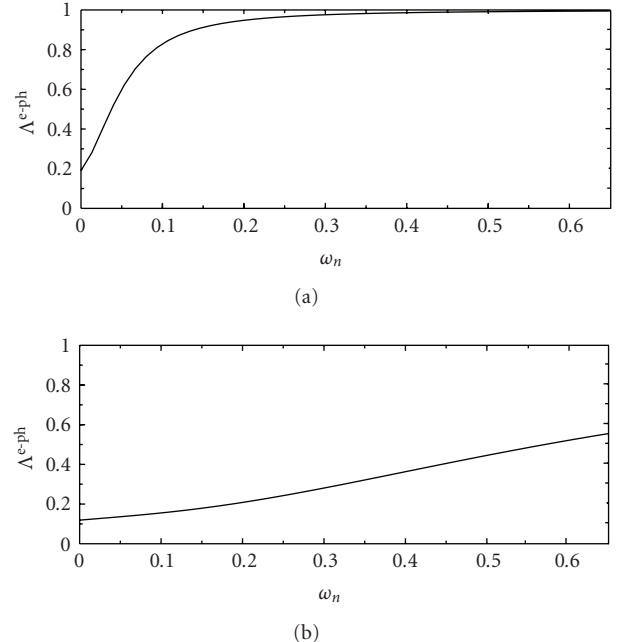


FIGURE 3: Effective e-ph vertex in units of the bare e-ph coupling as a function of the Matsubara frequency in the HH model at leading order in  $1/N$ . The parameters are the same as in Figure 2. Panel (a) is for a small transferred momentum  $\mathbf{q} = (0.2, 0)$  (in units of inverse lattice spacing  $1/a$ ); (b) is for a sizable transferred momentum  $\mathbf{q} = (2.0, 0)$  (after [54]).

method provides unbiased information about the dynamical properties.

The central approximation behind DMFT is the locality of the self-energy (both the electronic and the phononic contributions), a condition which becomes exact when the coordination number becomes large. The original lattice enters in the calculation only through the density of states, which we always choose to be a semicircular one of half-bandwidth  $D$  (Obviously  $W = 2D$ ). This approximation is appropriate for a model with local interactions such as our Hubbard-Holstein model, even if it does not allow to treat phases with nonlocal correlations such as intersite bipolarons [81] or d-wave superconductivity, which requires cluster extensions of DMFT. Even though these limitations imply that the approach can miss some important physics of the cuprates, our results provide valuable information about the interplay between e-e and e-ph interaction beyond any perturbative limit.

DMFT allowed to obtain a complete characterization of the Mott-Hubbard transition in the pure Hubbard model, and the emerging physical picture is able to explain several properties of correlated oxides. While we refer to original papers [80] for details, we recall here some aspects which are relevant to our discussion.

We first consider the half-filled system and, in order to focus on pure correlation effects, we consider a paramagnetic phase. In this regime, for large repulsion, the ground state of the HH model can become a “Mott” insulator, in which the electrons are localized because the electron motion is

energetically unfavorable. Starting from the uncorrelated systems and increasing the correlation strength  $U$ , the spectral weight is transferred from low to high frequency. In this process the spectral function evolves from a single band to a three-feature structure in which a renormalized band survives around the chemical potential, while precursors of the Hubbard bands develop around  $\omega \sim \pm U/2$ . As the correlation is further increased up to a value  $U \equiv U_{c2} \simeq 1.5W$  the quasiparticle band disappears, and the system becomes a Mott insulator with a preformed Hubbard gap. The key parameter that controls this Mott-Hubbard transition from a metal to an insulator is the quasiparticle weight  $z$ , which is directly computed from the self-energy (which is a natural outcome of a DMFT calculation).  $z$  measures the width and the total spectral weight of the low-energy quasiparticle peak, and its vanishing pinpoints the Mott transition. As soon as the system is doped away from half-filling the system is metallic regardless the value of  $U$ . The chemical potential remains within the quasiparticle peak which moves towards one of the bands, but it is still well defined for a sizable doping region (dependent on the value of  $U$  and on details of the bandstructure) [80]. Due to the momentum independence of the self-energy, also in DMFT we have that  $z = m/m^*$ , so that the Mott transition is associated with a divergent effective mass of the renormalized carriers.

In the following part, we discuss the effect of a nonperturbative electron-phonon coupling in the strongly correlated metallic solution, that is, a system in which a quasiparticle peak at the Fermi level is separated from the Hubbard bands realizing a separation of energy scale. Starting from this situation, in which the quasiparticle bandwidth is  $z$  times the bare width  $W$ , the effect of the e-ph coupling is far from trivial. Indeed, there are two main effects associated to e-ph interaction.

- (i) The e-ph interaction can introduce a further quasiparticle renormalization, associated to the increase of the quasiparticle effective mass, which may eventually lead to polaronic effects for very strong coupling. This effect leads to a decrease of  $z$ . In weak coupling we have  $1/z = 1 + (\pi/2)\lambda$  at half-filling and a semicircular density of states of half width  $D$ .
- (ii) The e-ph interaction mediates an attractive density-density interaction (the density-density form is specific for a Holstein coupling), which directly contrasts the Hubbard repulsion. If we integrate out the phonon degrees of freedom, the fermions interact through a dynamical (retarded) interaction [82]

$$U_{\text{eff}}(\omega) = U - \frac{2g^2\omega_0}{\omega_0^2 - \omega^2}. \quad (8)$$

In the antiadiabatic regime the frequency dependence of the second term can be neglected and overall interaction is a static term  $U_{\text{stat}} = U - \lambda W$ , in which the e-ph interaction reduces the strength of the Hubbard term. When the phonon frequency becomes finite the interaction is retarded, but we still expect a similar effect. If we assume that the repulsion is the

largest scale, the leading effect of e-ph interaction is to reduce the effective repulsion, making the system less correlated and *increasing*  $z$ .

The balance between this two effects is not generic and it depends on the adiabatic ratio and on the precise value of the interactions. Yet, important conclusions can be drawn in the correlated regime, in which, also in the presence of e-ph interaction, the separation of energy scales determined by correlations survives. In this regard, it is important to recall that, within DMFT, the quasiparticle weight is associated to a Kondo resonance of an Anderson-Holstein impurity model. Assuming that the Hubbard  $U$  is the largest scale of the problem, the Kondo coupling can be calculated in terms of virtual processes acting in the subspace in which the impurity is singly occupied obtaining an effective Hamiltonian for spin fluctuations [83]. The result is given by

$$J_K(\lambda) = J_K(0) \sum_{m=0}^{\infty} \frac{|\langle 0 | e^{g/\omega_0(a-a^\dagger)} | m \rangle|^2}{1 - 2g^2/\omega_0 U + 2m\omega_0/U}, \quad (9)$$

where the Kondo coupling in the absence of phonon is given by  $J_K(0) = 16V^2/U$ ,  $|m\rangle$  is the state with  $m$  phonons, and  $V$  is the hybridization between the impurity and the bath. After some algebra, and introducing

$$U_{\text{eff}} = U - \eta\lambda W, \quad (10)$$

we can write, for small  $\lambda W/U$

$$J_K(\lambda) \simeq J_K(0) \left(1 + \eta \frac{\lambda W}{U}\right) \simeq \frac{16V^2}{U_{\text{eff}}} = \frac{16V^2}{U - \eta\lambda W} \quad (11)$$

with

$$\eta = \frac{2\omega_0/U}{1 + 2\omega_0/U}. \quad (12)$$

This result would imply that the complicated interplay between the static Coulomb repulsion and the retarded e-ph coupling may be effectively described by an effective purely electronic Hubbard model with a reduced repulsion. We notice in passing that this calculation for the Anderson impurity model is analogous to the evaluation of the effect of phonons on the superexchange coupling of [84]. Interestingly the phonon dynamics only enters through the ratio  $\omega_0/U$ , which can be considered as typically small because  $U$  is by choice the largest scale of the problem, and  $\omega_0$  is smaller than the hopping scale. In the relevant regime of small  $\omega_0/U$ , we have  $U_{\text{eff}} = U - 4g^2/U$ .

These results can be tested through a DMFT solution of the Hubbard-Holstein model. We start our discussion from half-filling, where the separation of energy scales characteristic of correlated systems is clearer and more solid. We first computed the quasiparticle weight  $z(\lambda) = (1 - \partial\Sigma(\omega)/\partial\omega)^{-1}$  for finite fixed  $U$  as a function of  $\lambda$ .

In Figure 4, we show the ratio  $z(\lambda)/z(0)$ , in order to emphasize the phonon contribution to the quasiparticle weight. It is apparent that the value of  $U$  determines different regimes. For small  $U$ , the e-ph interaction reduces  $z$  (i.e.,

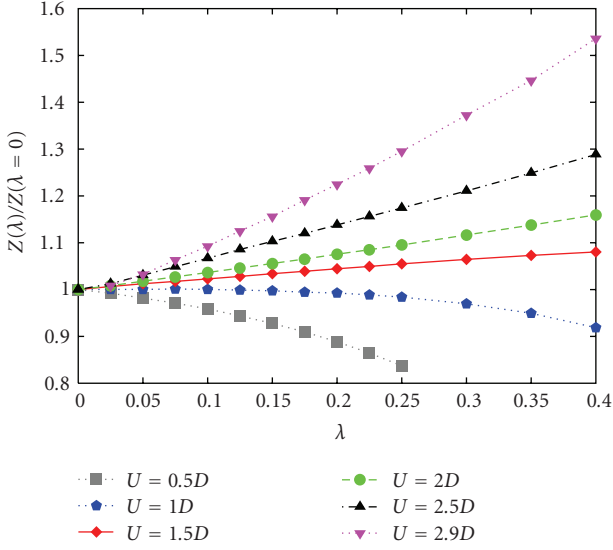


FIGURE 4: Effect of the electron-phonon interaction on the quasiparticle weight  $z$  in the presence of electron-electron interaction of different strengths. The quantity plotted as a function of  $\lambda$  is the ratio between the full  $z$  and the value of the Hubbard model without e-ph coupling ( $z(0)$ ) (after Sangiovanni et al. [45]).

increases the effective mass) as expected in weakly interacting systems. Increasing  $U$ , we approach an opposite behavior in which the e-ph interaction makes the quasiparticles *lighter* (even if they are obviously heavier than free particles because of the stronger renormalization determined by correlation, which is hidden in  $z(0)$ ). The effect becomes particularly strong at  $U = 1.45W$ , which is very close to the Mott transition. Here even small variations of the effective  $U$  can induce sizable variations in the effective mass. Obviously such sensitivity is enhanced in the present half-filling case, where an actual Mott transition can take place.

This behavior confirms that, when the e-e correlation dominates, the leading effect of the e-ph interaction is a reduction of the effective  $U$ , resulting in an increased quasiparticle mobility. We can now test the above prediction of an effective static repulsion including the effects of e-ph interaction as far as the low-energy physics is concerned.

Assuming a form  $U_{\text{eff}} = U - \eta\lambda W$  for such an effective interaction, we obtained  $\eta$  for several values of  $U$  and  $\omega_0$  simply determining the value of  $U$  which gives, for a pure Hubbard model, the same  $z$  we obtain for the Hubbard-Holstein model. The results are summarized in Figure 5, and confirm that  $\eta$  is essentially a function of  $\omega_0/U$  which starts off linear at small values of the argument before bending for larger values. The numerical value well reproduces (12) derived on the basis of the analogy with Kondo effect without fitting parameters. Obviously physically relevant frequencies are in the small  $\omega_0/U$  range.

On the basis of our knowledge about the DMFT results for the pure Hubbard model, the quasiparticle weight completely characterizes the low-energy quasiparticle peak. Therefore, our analysis should imply that the low-energy part of the spectral function of our Hubbard-Holstein model

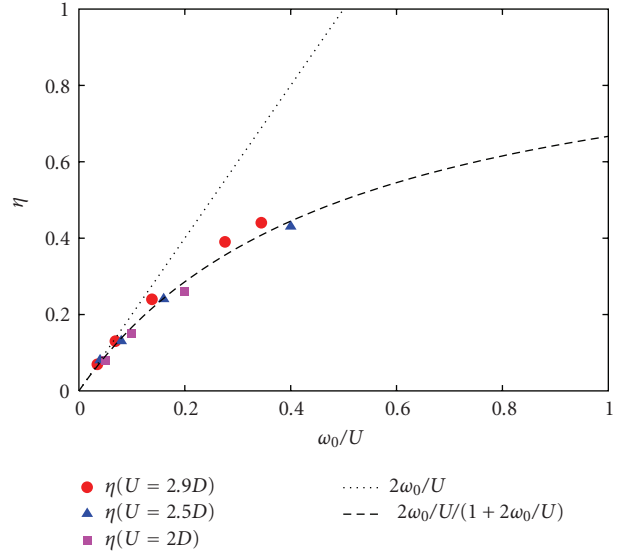


FIGURE 5: Effective static electron-electron interaction for the low-energy properties of the Hubbard-Holstein model. The picture shows the coefficient  $\eta$  in  $U_{\text{eff}} = U - \eta\lambda W$  as a function of  $\omega_0/U$  (after Sangiovanni et al. [45]).

can be described by means of the effective Hubbard model that we introduced. This is strikingly confirmed by a direct comparison, as shown in Figure 6. Here we show some examples of momentum integrated spectral functions  $\rho(\omega) = -1/\pi G(\omega)$  for the Hubbard-Holstein model compared with the associated effective Hubbard model with the proper  $\eta$ . Besides the spectacular confirmation of the validity of the effective model for the low-energy part of the spectrum (the quasiparticle peak), another important information emerges from the picture: The high-energy part of the spectrum is instead affected by phonons in a more “dynamical” way, meaning that the high-energy Hubbard bands acquire a modulation in frequency which can be related to phonon satellites, which are completely absent in the low-energy part, where nothing happens at the characteristic phonon frequency.

The picture that emerges for the half-filled model can be summarized as follows: Quasiparticle motion arises from virtual processes in which doubly occupied sites are created. Obviously, these processes are not so frequent, since the energy scale involved is large, but they are extremely rapid (the associated time scale is  $\propto 1/U$ ), and consequently are poorly affected by phonon excitations with a characteristic time scale  $1/\omega_0 \gg 1/U$ . When the phonon frequency is small with respect to  $U$ , the phonon degrees are frozen during the virtual excitation processes. Therefore, despite the overall electron motion is quite slow due to the small number of virtual processes (which is reflected by the large effective mass), the e-ph interaction has no major effect except for a slight reduction of the total static repulsion.

According to what we have just described, we can conclude that strong correlations reduce the effect of the e-ph interaction on the low-energy properties, associated to quasiparticle propagation, while the high-energy properties

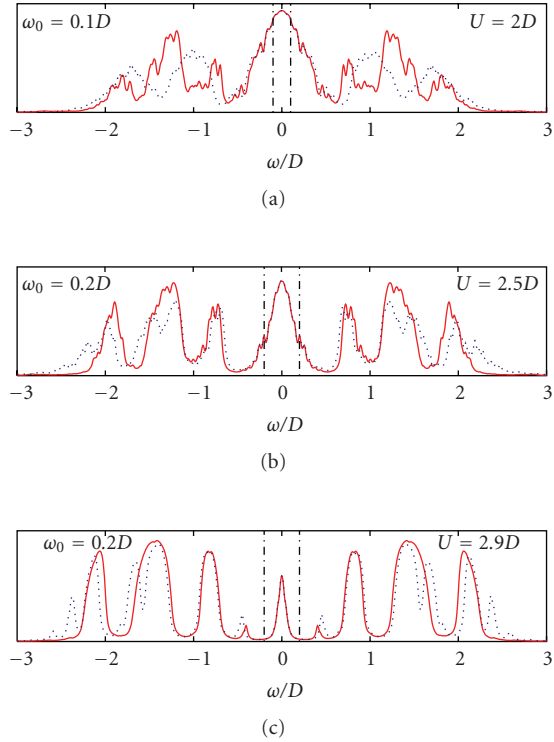


FIGURE 6: Comparison between the DMFT momentum-integrated spectral function  $\rho(\omega) = -1/\pi \text{Im} G(\omega)$  ( $G(\omega)$  being the local Green's function) for the Hubbard-Holstein model (dotted line) and the effective purely electronic Hubbard model with  $U = U_{\text{eff}}$  (solid line). The low-energy part of the spectra is perfectly reproduced by the effective model, while the high-energy features present phononic signatures that cannot be plugged in an effective static interaction (after Sangiovanni et al. [45]).

present more standard phonon signatures, such as the satellites at the phonon frequency scale.

It has to be underlined that DMFT is not able to introduce momentum-dependent corrections to the electronic properties. The above analysis therefore, shows indeed that the “standard” electron-phonon interaction is heavily screened (and it actually loses its dynamical nature) when the low-energy quasiparticle properties are considered. Only “nonstandard” effects, such as the prevalence of forward scattering that we discussed in Section 3.1 can survive at low energy.

The above scenario has been carried out at half-filling, where the presence of e-e correlations has its most striking effects, both in terms of the phase diagram, as it can give rise to a Mott transition, and in terms of the separation of energy scales, which is clearly sharper than for doped systems. Therefore, as soon as we dope the Hubbard-Holstein model, even for  $U > \lambda$  the dominance of repulsive correlations is weaker and the interplay with e-ph coupling will be more subtle [46]. As a result, it is not possible to describe the effect of phonons on the highly correlated metal in terms of an effective static potential unless the system is very close to the antiadiabatic limit. Therefore, for small and intermediate phonon frequencies, we do not find situations

in which increasing the electron-phonon coupling reduces the effective mass.

Nonetheless, if we consider reasonably large values of  $U$ , the dominance of correlations will determine a reduce effectiveness of the e-ph coupling, and, for example, polaron formation will be pushed to significantly larger values of  $\lambda$  than for uncorrelated systems, as shown by the DMFT results of Figure 7. Here we plot  $m^*/m = 1/z$  as a function of  $\lambda$  and we compare the uncorrelated system with the system with  $U/W = 2.5$  (Here, since the density is different from half-filling, the system is always metallic even if  $U$  is larger than the critical value for the Mott transition). While in the uncorrelated case  $m^*$  grows exponentially when  $\lambda$  approaches a critical value of order 1 for all densities, signaling polaron formation, the correlated system displays a significantly weaker growth of  $m^*$  up to  $\lambda \simeq 0.5 \div 0.75$ .

The role of the adiabatic ratio is illustrated by Figure 8, where we report the renormalization of the linear coefficient of the mass enhancement defined by the relation  $m^*(U)/m^*(U, \lambda) = 1 + r\lambda$ . Here  $m^*(U, \lambda)$  is the effective mass in the presence of both electron-electron and electron-phonon interactions and  $m^*(U)$  is the same quantity in the absence of coupling to the phonons. Here a negative  $r$  implies a standard increase of the effective mass due to phonons. The results (again for  $U/W = 2.5$ ) show that in all cases the coefficient is smaller than one, confirming that correlations reduce the effective e-ph coupling, and a strong (and nonmonotonic) dependence on the antiadiabatic ratio. Only for very large values of  $\omega_0/Wr$  becomes positive reflecting that the “screening” physics we described above is effective. The dependence on the density naturally reflects that fillings closer to  $n = 1$  display weaker phononic effects in the adiabatic regime of small frequencies and a more rapid evolution to an antiadiabatic regime in which  $r > 0$ .

The scenario which emerges from DMFT calculations at finite  $U/W$  can be confirmed by a semianalytical approach based on an extension of the Gutzwiller approach which treats phonon degrees of freedom on the same footing of the electrons. For more details see [64, 65]. The results of Figure 9 in the limit of infinite repulsion and for finite doping  $\delta = n - 1$  confirm the scenario arising from Figure 7: in the doped correlated system the electron-phonon interaction is considerably reduced with respect to the free system, but the qualitative effect of  $\lambda$  is an increase of the effective mass.

**4.2. Antiferromagnetic Correlations.** The above analysis suggests that, as expected, strong e-e correlation essentially opposes to e-ph coupling, even though “anomalous” signatures of e-ph coupling still survive even in regions of parameters for which correlations prevail. Yet, these results are limited to the metallic paramagnetic state, in which no broken symmetry is allowed. At half-filling and for some finite doping region, strong correlations lead to an antiferromagnetically ordered state, and it is expected that finite-range antiferromagnetic correlations survive in a wider doping region. The relation between antiferromagnetism and e-ph interaction is hinted by the experimental framework. Indications of phonon signatures in high- $T_c$  superconductors are indeed particularly strong in the extremely

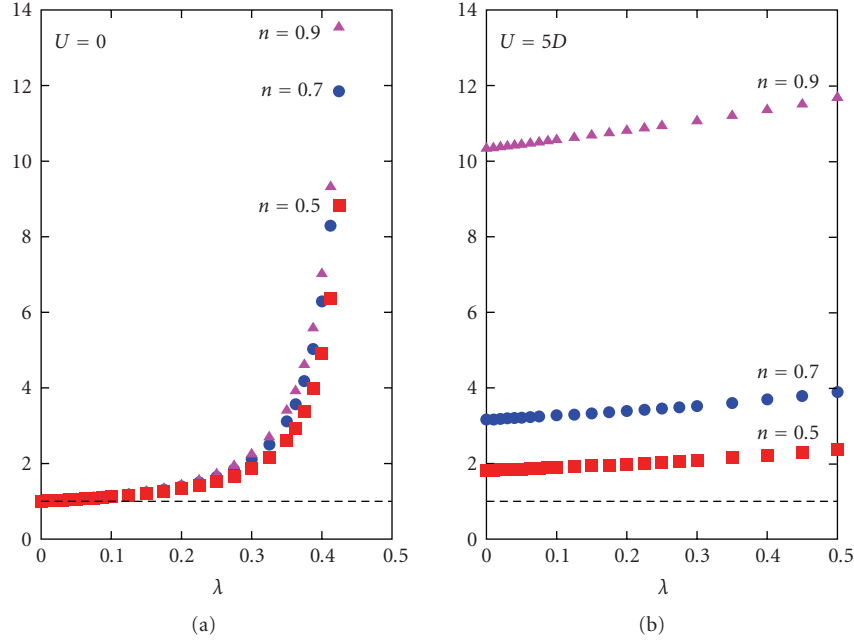


FIGURE 7: Effective mass  $m^* = 1/zm$  as a function of  $\lambda$  for three different densities different from half-filling ( $n = 0, 5, 0.7, 0.9$ ) in the uncorrelated (a) and strongly correlated ( $U = 2.5W$ , (b)) system (after Sangiovanni et al. [46]).

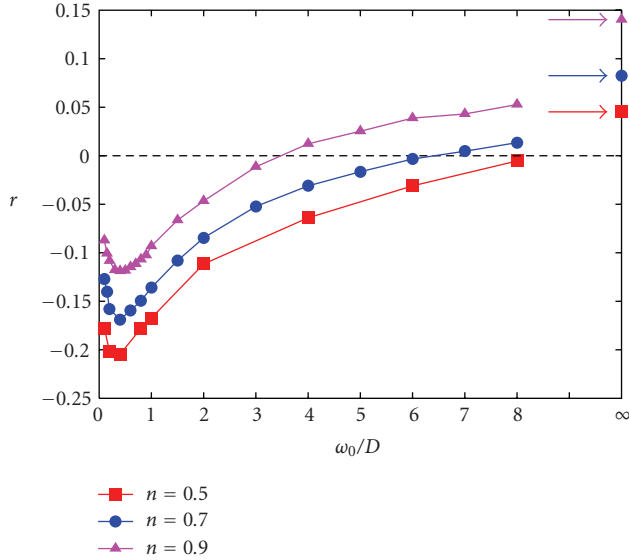


FIGURE 8: Renormalization of the quasiparticle electron-phonon coupling as a function of  $\omega_0/W$  for three different densities and  $U/W = 2.5$  (after Sangiovanni et al. [46]).

underdoped region, where some kind of antiferromagnetic correlation is certainly present. For example, clear polaronic features are observed in the optical spectroscopy [85] and ARPES [7] of underdoped materials.

From a theoretical point of view, several investigations indeed suggest that the e-ph interaction is particularly effective for a hole in an antiferromagnetic background [86–91], and for slightly doped t-J models. These results can

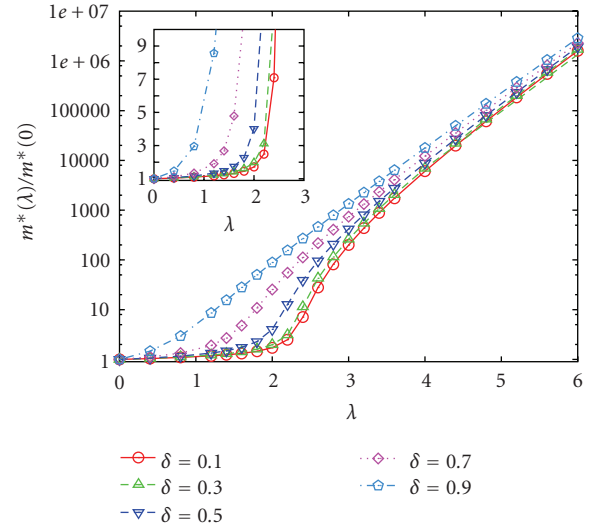


FIGURE 9: Renormalization of the effective mass due to electron-phonon coupling for infinite  $U$  and  $\omega_0/W = 0.1$  as a function of  $\lambda$  for different doping levels. The inset shows the same data in a smaller range. Here the doping  $\delta$  is given by  $\delta = n - 1$  and  $\lambda$  is twice as in the rest of the paper (after Barone et al. [64]).

be reconciled with the above findings for the nonmagnetic phase by simple arguments.

As we discussed in the previous sections, in the paramagnetic phase the effect of increasing correlations is a strong reduction of the quasiparticle weight  $z$  associated with a divergent self-energy, which in turn strongly renormalizes the e-ph vertex, leading to the strong reduction of low-energy phononic signatures that we described above. Once

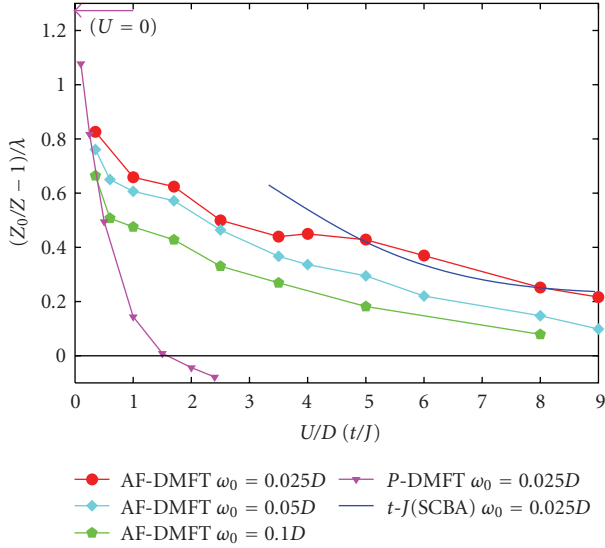


FIGURE 10: Effect of the Coulomb repulsion on the linear contribution in  $\lambda$  to the quasiparticle renormalization. DMFT results for the antiferromagnetic phase (AF-DMFT) are compared with DMFT in the paramagnetic state (P-DMFT) and to a self-consistent Born Approximation (SCBA) for the  $t$ -J model for parameters corresponding to the red dots AF-DMFT. Antiferromagnetism allows for a sizable e-ph coupling also in the present of very strong Coulomb repulsion, in contrast with paramagnetic results (after Sangiovanni et al. [92]).

antiferromagnetic correlations are allowed, the system can turn insulating even with a finite  $z$  and a nondivergent self-energy, hence the e-ph vertex is not severely screened [92]. From a more physical point of view, the antiferromagnetic insulator allows for more charge fluctuations with respect to the pure Mott state at the same value of  $U$ . Therefore, a Holstein coupling, which exploits precisely charge fluctuations to gain energy, is expected to be favored by antiferromagnetic correlations.

Direct DMFT calculations in the antiferromagnetic phase at half-filling confirm these expectations [92]. In Figure 10 we show the quantity  $[z/z(0) - 1]/\lambda$  for small  $\lambda$  ( $z(0)$  being  $z$  in the absence of e-ph interaction). This quantity measures the renormalization of the linear e-ph coupling induced by e-e correlations. The comparison between the paramagnetic solution and the antiferromagnetic state confirms the above expectations. While this coefficient rapidly drops as a function of  $U$  in the paramagnetic state, the inclusion of antiferromagnetism leads to a much more robust e-ph coupling. We underline that, however, the e-ph interaction is still substantially reduced with respect to the noninteracting systems [92].

The comparison with the uncorrelated system is shown in Figure 11, where the evolution of  $z$  as a function of  $\lambda$  is followed beyond the perturbative regime. In all cases  $z$  decreases monotonically, and a crossover from a metallic state to a polaronic one occurs. Yet, the decrease is more rapid for the uncorrelated system, and the characteristic coupling for polaron formation is significantly enhanced in the correlated antiferromagnetic state.

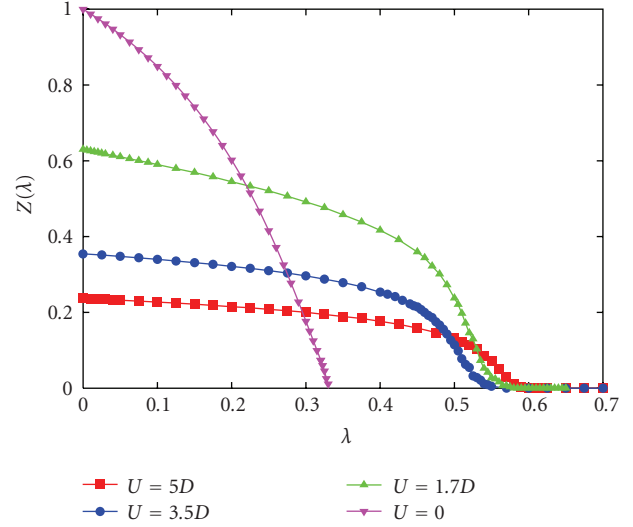


FIGURE 11: Quasiparticle renormalization as a function of  $\lambda$  for different values of  $U$  and  $\omega_0 = 0.0125W$ . The value of  $\lambda$  at which polaron formation occurs is only moderately increased by correlations with respect to the noninteracting case (after Sangiovanni et al. [92]).

The above discussion has been limited to half-filling. It is worth to briefly discuss the effect of doping in the antiferromagnetic state. In Figure 12 we present  $z$  as a function of  $\lambda$  for different densities, which imply different values of the staggered magnetization  $m = \langle \sum_i (-1)^i (n_{i\uparrow} - n_{i\downarrow}) \rangle$ . Notice that, within DMFT, the AFM state completely disappears only at  $n \approx 0.84$ . It is evident from the plots of Figure 12 that the reduction of the staggered magnetization reduces also the effect of the electron-phonon interaction. When the magnetization is small or vanishing,  $z$  becomes essentially independent on  $z$  for a wide range of values, signaling the screening of the e-ph interaction.

## 5. Phonon Mediated Charge Instabilities

In the previous sections we focused on the metallic phases, without discussing the possible instabilities, either directly driven by the interaction terms, or favored by the weakness of the correlated metallic state. One can indeed expect, on very general grounds, that the reduced kinetic energy characteristic of the strongly correlated metal can be easily overcome by different localizing effects thereby destabilizing the metal in favor of ordered phases.

As we did in Section 3.1 in the discussion of the e-e screening of the e-ph vertex, we can start our analysis in a general FL framework before discussing in some more details model-specific results. The charge compressibility  $\kappa = \partial n / \partial \mu$ , which in a FL theory reads [29, 67]

$$\kappa = \frac{N^*}{1 + F_0^s}, \quad (13)$$

is the key quantity that controls the stability of the charge degrees of freedom. A positive  $\kappa$  is the stability condition.

Therefore, if  $F_0^s < -1$  this condition is violated and the system undergoes a charge instability towards a phase-separated state.

It is important to stress that the results of Section 3.1 about the reduction of the static e-ph vertex do not necessarily imply that e-ph effects do not contribute to the charge compressibility in the presence of strong correlations. Indeed  $F_0^s \equiv 2N^* \Gamma_\omega$ , where  $\Gamma_\omega$  is the full *dynamic* effective scattering amplitude between the quasiparticles [67] including both e-e and e-ph interactions. As opposed to its static counterpart, the dynamic amplitude which enters  $F_0^s$  is not depressed by the e-e vertex corrections. For example, at lowest order in  $g^2$  and by performing an infinite-order RPA resummation of the e-ph screening processes,  $F_0^s$  reads

$$F_0^s = 2N^* \left( \Gamma_\omega^e - \frac{2g^2}{\omega_0} \right), \quad (14)$$

where  $\Gamma_\omega^e$  is the dynamic vertex function determined by e-e correlation processes only. This equation indicates that a sufficiently large bare  $g^2$  can overcome the effective residual repulsion between the quasiparticles  $\Gamma_\omega$  leading to a phase separation instability marked by the Pomeranchuk condition  $F_0^s < -1$ . It is worth pointing out that  $m^*/m \gg 1$  requires a large *bare* repulsion between the physical electrons (a large Hubbard  $U$  in our model) but this by no means requires a large residual interaction between the heavy quasiparticles. Therefore, even a small e-ph interaction can give rise to a phase separation instability.

Moreover, near the instability condition  $F_0^s = -1$ , the phonon contribution to the vertex becomes substantial and the e-ph interaction becomes relevant even in the static limit, at least at small  $q$ 's. At large  $q$  the analysis of specific models shows that the e-e interaction mediated by phonons is instead suppressed also near the instability region.

This is what indeed happens in the HH model treated within the SB-large- $N$  method described in Section 3.2. Within this approach it was first demonstrated that a metal with moderate e-ph coupling and strong e-e correlations could undergo a charge instability [54, 93] Specifically in the absence of long-range Coulombic forces the Pomeranchuk stability condition is violated. The doped HH model does not form a uniform phase and the system undergoes a phase separation between hole-rich regions and insulating half-filled regions (a phase separation instability was also found in the three-band HH model [53]).

In the presence of long-range Coulomb interactions the electrostatic cost of the charge-rich regions would become infinite, and the thermodynamic phase separation cannot take place. However, inhomogeneous charge-density wave ordering can establish as a compromise between the charge segregation tendency and the homogenizing effect of long-range interactions. This mechanism for charge ordering is the so-called “frustrated phase separation” [94–97]. For the specific HH model described here it was found that for realistic values of the e-ph coupling and of the long-range repulsion, frustrated phase separation gives rise to a second-order quantum phase transition (quantum critical point, QCP) around optimal doping (doping  $x = 0.19$ )

[93] with the ordering and the periodicity influenced but not directly related to the structure of the Fermi surface. This instability arises instead from the energetic balance between the tendency to phase separation and the frustrating electrostatic cost of the long-range Coulomb interaction. Near this instability the phonon spectrum becomes highly anomalous. First of all the phonon acquires a strong coupling to the electronic degrees of freedom near the instability wavevector  $\mathbf{q}_c$  (which usually tend to occur at  $\mathbf{q}_c \approx (\pm\pi/2, 0)$ ,  $(0, \pm\pi/2)$  for the relevant dopings and Fermi-surface shapes [54, 93]). Near the instability wavevector the phonon line-width becomes therefore, very broad and it even acquires a background of the order of the particle-hole continuum. At the same time the phonon dispersion softens and at the instability the frequency of this mixed phonon-electron mode vanishes. Remarkably, since the critical wavevector is not so large (typically of the order of  $\pi/2$ ) the region where the phonon dispersion becomes strongly anomalous is rather isotropic and substantial anomalies are present also in the (1,1) direction upon approaching the critical doping of the QCP. Figure 13 reports the anomalous phonon dispersion found in the HH model in [54].

Of course it is quite tempting to relate these anomalies, to the anomalies observed by inelastic neutron scattering [98–104]. An alternative possibility can also be proposed for the anomalies detected in underdoped cuprates: charge ordering can give rise to rather anisotropic nearly one-dimensional dynamical charge textures. In this case Kohn anomalies can be expected along the stripes at wavevectors of the order  $2k_F$  in the stripe direction [105, 106].

## 6. Jahn-Teller Coupling in the Fullerenes

All the above analysis has been carried out for the HH model. It has to be emphasized that some of the effects we discussed may be less general than what the simple form of the Hamiltonian may suggest. As we discussed in details, the HH model is indeed characterized by two interaction terms which are both related to the charge degrees of freedom, and they indeed directly compete, as clearly shown by (8). This direct competition makes the two effects more exclusive than in general situations in which the e-ph coupling does not directly compete with the Coulomb repulsion. We can have two different ways to avoid the direct competition: a different functional form for the e-ph coupling in a single-band model, or a Jahn-Teller coupling in a multiorbital model.

The first situation can obviously have relevance for the cuprates, in which different phonon modes with specific symmetries may play a role, or for system dominated by the so-called Su-Schrieffer-Heeger coupling in which the phonons modulate the nearest-neighbor hopping. The second situation occurs instead in the fullerenes, where the relevant conduction band is a three-fold degenerate manifold of  $t_{1u}$  ( $p$ -like) orbitals, which couple with Jahn-Teller active local distortions of the fullerene molecule. It is precisely this kind of coupling which is expected to be responsible for superconductivity in these compounds [18].

A three-band model which includes a strong Coulomb repulsion, a Hund's rule splitting and a moderate Jahn-Teller

e-ph coupling has been studied in several papers [22, 107–109], reaching an *a priori* surprising conclusion: The Jahn-Teller coupling is not harmed by large Coulomb repulsion, and the phonon-driven superconductivity can actually be strongly enhanced in the proximity of the Mott transition, that is, in the region in which the correlations are most effective.

Here we do not discuss the physics of this model in details, since we are mainly interested in contrasting its behavior with the HH model. The key point is that the Jahn-Teller interaction does not touch the total charge on each molecule, as it couples with a combination of local spin and orbital degrees of freedom [22]. As a consequence, even when correlations are sufficiently strong to suppress the electronic motion, the localized electrons can still interact within a single fullerene molecule via the e-ph interaction. For example, if we consider the experimentally relevant situation of three electrons per fullerene molecule, as we approach the Mott state three electrons will remain stuck on each fullerene. Yet, they can still be in a high-spin state or low-spin state, and the energetic gain associated to the multiplet splitting will be the same as for a noninteracting molecule. Therefore, the e-ph driven interaction will be not renormalized by correlations, as opposed to the Holstein model. From a Fermi-liquid point of view, the lack of renormalization is determined by very large vertex corrections (divergent like  $1/z$  as the Mott transition is approached) that compensate the  $z$  factors [22, 109].

As a matter of fact, the effective interaction between quasiparticles obtained in a nonperturbative DMFT study of the model corresponds to a severely screened Hubbard repulsion plus an essentially unscreened phonon-driven attraction that can be parameterized as

$$A_{\text{eff}} = zU - \frac{10}{3}J, \quad (15)$$

where  $J$  is the strength of the phonon-mediated attraction in the spin/orbital channel. This simple equation shows that, even if  $U$  is chosen to be significantly larger than  $J$ , when the Mott transition is approached (i.e.,  $z \rightarrow 0$ ) [107], the attraction will eventually prevail. Moreover, in this regime the quasiparticles are quite heavy, and their large effective density of states can lead to an enhancement of the effective dimensionless coupling, which is expected to reflect in an enhanced critical temperature.

This enhancement is explicitly found by solving the three-orbital model within DMFT in the *s*-wave superconducting phase. If we follow the evolution of the superconducting order parameter as a function of  $U$  for a fixed small  $J$  we first have a standard BCS-like region when  $U$  is so small that the bare attraction simply overcomes the bare repulsion. Then superconductivity disappears because  $U$  is large enough to kill the attraction, but  $z$  is still close to 1. Further increasing  $U$  we approach the Mott transition,  $z$  decreases and it strongly renormalizes down the effective repulsion. Eventually the effective interaction becomes attractive and superconductivity re-emerges, with an order parameter that follows a bell-shaped curve before vanishing at the Mott transition point [22, 107]. This

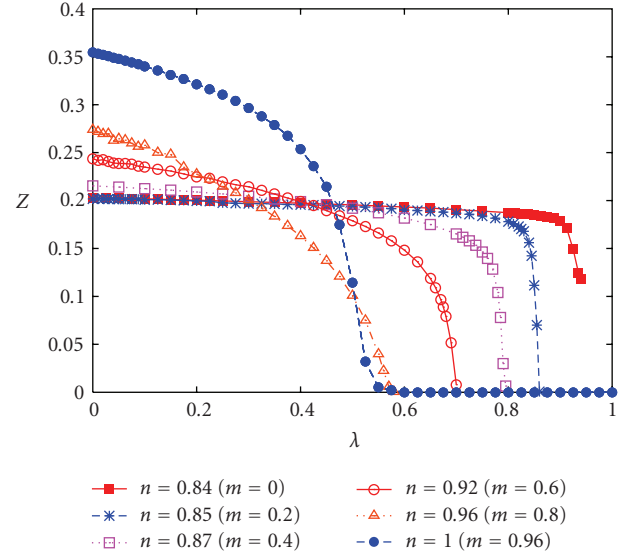


FIGURE 12: Quasiparticle renormalization as a function of  $\lambda$  for different values of the density  $n$  (and consequently different magnetization  $m$ ) at fixed  $U = 1.75W$  and  $\omega_0 = 0.0125W$  (after Sangiovanni et al. [92]).

strongly correlated superconducting pocket displays a maximum critical temperature which exceeds the weak-coupling BCS value. In other words, phonon-driven superconductivity is actually enhanced by strong correlations [22].

A full DMFT solution of the model has allowed both to predict the experimental observation only later provided in [20, 21], like the dome-behavior of the critical temperature as a function of doping, and the first-order transition to a spin-1/2 antiferromagnet when pressure is reduced to recover the ambient phase of  $A15 \text{ Cs}_3\text{C}_{60}$ , and to further characterize the properties of strongly correlated superconductors. For example, we predict a pseudogap in the photoemission spectra [110, 111], and a kinetic-energy driven superconductivity for the most expanded compounds [109].

In the context of this paper, our solution is a clear example of the crucial role of the phonon symmetry. In our multiband model it is possible to consider phonons which are by symmetry unharmed by correlations, as opposed to the Holstein model. The result is confirmed by investigations of simplified two-orbital models which share the same properties [110, 111]. When we go back to the cuprates, and to single-band models, our findings suggest that phonon modes which are coupled to operators which are not proportional to the charge can indeed survive much better in a strongly correlated environment, in analogy with the findings of mean-field methods.

## 7. Conclusions

The focus of the paper is on the effects of strong electron-electron correlations on the electron-phonon coupling. We mostly considered the Hubbard-Holstein model, where both e-e and e-ph interactions locally couple to electron density fluctuations. In this case the competition between these

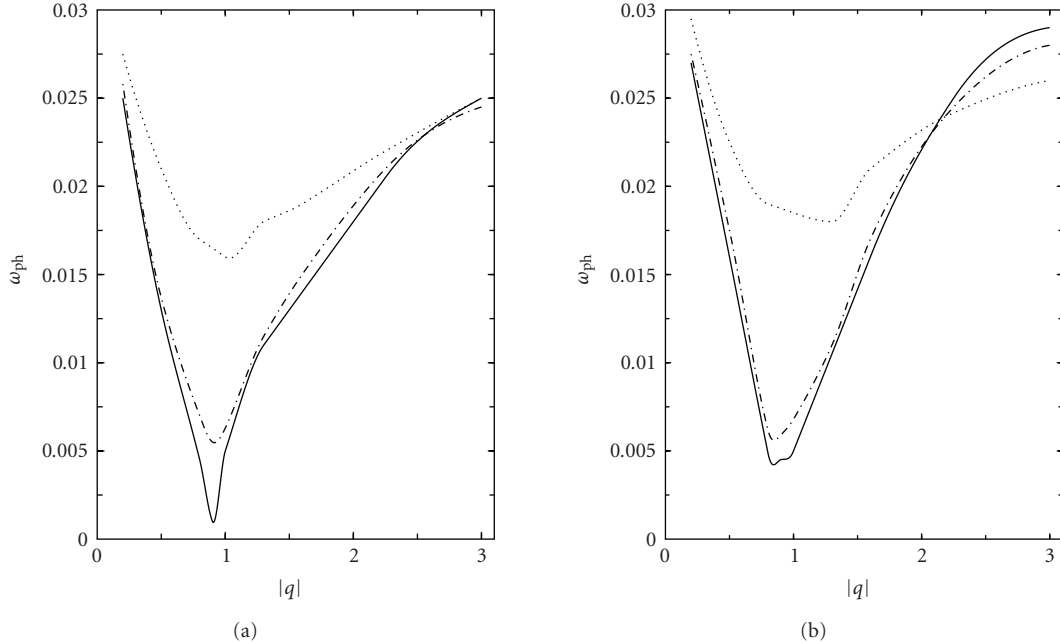


FIGURE 13: Phonon dispersion curves (a) in the instability (0.28,0.86) direction and (b) in the (1,1) direction, for  $t = 0.5$  eV,  $t' = -(1/6)t$ ,  $g = 0.240/\sqrt{2}$  eV,  $\omega_0 = 0.04$  eV, and  $V_C = 0.55$  eV. The solid curves correspond to the critical doping  $\delta_c = 0.195$ , the dot-dashed and the dotted curves correspond to  $\delta = 0.21$  and  $\delta = 0.3$ , respectively.

interactions is quite effective, particularly in the proximity of the Mott-Hubbard transition.

In particular, we study strongly correlated metallic phases, where the system is either at half-filling or at small doping, and the correlation strength is large enough to put the system close to a Mott-Hubbard transition. In these conditions, since the e-e Hubbard repulsion makes the density fluctuations stiffer, the Holstein e-ph coupling  $g$  is generically suppressed, even if the overall picture is far from trivial.

Along this paper we have discussed how this suppression depends on exchanged momentum and frequency, and on other physical parameters. A first observation is that the suppression is strong whenever the quasiparticle residuum  $z$  is small. On the contrary we observed that in the antiferromagnetic phase, where the suppression of double occupancy imposed by the large Hubbard repulsion  $U$  is due to the spin ordering and does not entail a small  $z$ , the e-ph coupling is only weakly suppressed. This easily explains why polaronic features are present and clearly visible in weakly doped antiferromagnetic cuprates. The weakness of this suppression is likely to persist even in the metallic paramagnetic regime, if substantial residual antiferromagnetic correlations persist on a local basis. The opposite case of a strong suppression of the e-ph coupling, occurring for small  $z$  (or more precisely when  $\kappa^e/N^* \ll 1$ ), needs further specification. In particular we find that  $g$  is more or less suppressed depending on the dynamical regime: for a small ratio between the transferred frequency  $\omega$  and the transferred momentum  $v_F q$  the e-ph coupling is strongly reduced, while in the opposite limit  $\omega/v_F q \gg 1$  no suppression is found and even an enhancement is possible. This latter finding

leaves the possibility open of substantial phononic residual attractions between the quasiparticles competing with the residual repulsions in driving the system unstable toward long-wavelength charge instabilities. These two dynamical regimes are also visible in the DMFT approach where the scale  $v_F q$  is reflected in the width of the quasiparticle resonance. For frequencies smaller than this latter scale phononic features are absent, while they are clearly present at high-energy in the Hubbard sidebands.

The nearly static case  $\omega/v_F q \ll 1$  again displays an intrinsic richness as far as momentum dependence is concerned: the strong suppression of  $g$  already occurring at small momenta becomes really very strong at large transferred momenta. This suppression found both on general grounds within a Fermi-liquid analysis and within specific fieldtheoretic treatments of the Hubbard-Holstein model [53, 54, 58, 59, 77] can account for the impressive elusiveness of phononic features in transport experiments in cuprates. Indeed the fact that the resistivity in the metallic phase does not display any clear phononrelated feature is naturally explained by the strong suppression of the e-ph coupling in transport processes, where very low-energy and large transferred momenta are involved. Thus the strongly correlated nature of the cuprates is the key ingredient to solve the puzzles related to the dichotomous behavior of these materials, which display clear phononic features in some cases and none in others.

All the above findings are only partly peculiar of the specific HH model, where the electron density locally involves both the e-e and e-ph coupling: The analysis of other models like the Su-Schrieffer-Heeger [112] essentially produce the same results [68, 69, 113]. A qualitative difference only

occurs for those phonons which couple to degrees of freedom which are not severely stiffened by the proximity to a Mott-Hubbard phase. In this regard we reported the important case of Jahn-Teller phonons in the Fullerenes. It would be interesting to search for similar phononic (or even nonphononic) degrees of freedom in the cuprates. In this regard, the buckling modes in some cuprates are interesting candidates, which are presently being investigated in this perspective [114].

## Acknowledgments

The work that we review has been carried out in collaboration with G. Sangiovanni, P. Barone, S. Ciuchi, C. Di Castro, J. Lorenzana, G. Seibold, A. Di Ciolo, F. Becca, M. Fabrizio, E. Koch, O. Gunnarsson, P. Paci, and R. Raimondi. We acknowledge financial support by MIUR PRIN 2007 Prot. 2007FW3MJX003. M. Capone's activity is funded by the European Research Council under FP7/ERC Starting Independent Research Grant "SUPERBAD" (Grant Agreement no. 240524). M. Grilli acknowledges financial support from the Vigoni Program of the Ateneo Italo-Tedesco.

## References

- [1] in *Proceedings of the Conference on Lattice Effects in High Temperature Superconductors*, Y. Bar-Yam, T. Egami, J. Mustre-de Leon, and A. R. Bishop, Eds., World Scientific, Singapore, 1992.
- [2] M. L. Kulić, "Interplay of electron-phonon interaction and strong correlations: the possible way to high-temperature superconductivity," *Physics Report*, vol. 338, no. 1-2, pp. 1–264, 2000.
- [3] O. Gunnarsson and O. Rösch, "Interplay between electron-phonon and Coulomb interactions in cuprates," *Journal of Physics Condensed Matter*, vol. 20, no. 4, Article ID 043201, 2008.
- [4] J. P. Falck, A. Levy, M. A. Kastner, and R. J. Birgeneau, "Charge-transfer spectrum and its temperature dependence in  $\text{La}_2\text{CuO}_4$ ," *Physical Review Letters*, vol. 69, no. 7, pp. 1109–1112, 1992.
- [5] P. Calvani, M. Capizzi, S. Lupi, and G. Belestrino, "Infrared active vibrational modes strongly coupled to carriers in high- $T_c$  superconductors," *Europhysics Letters*, vol. 31, p. 473, 1995.
- [6] P. Calvani, M. Capizzi, S. Lupi, P. Maselli, A. Paolone, and P. Roy, "Polaronic optical absorption in electron-doped and hole-doped cuprates," *Physical Review B*, vol. 53, no. 5, pp. 2756–2766, 1996.
- [7] K. M. Shen, F. Ronning, D. E. Lu et al., "Missing quasi-particles and the chemical potential puzzle in the doping evolution of the cuprate superconductors," *Physical Review Letters*, vol. 93, no. 26, Article ID 267002, 2004.
- [8] A. Lanzara, P. V. Bogdanov, X. J. Zhou et al., "Evidence for ubiquitous strong electron-phonon coupling in high-temperature superconductors," *Nature*, vol. 412, no. 6846, pp. 510–514, 2001.
- [9] D. Reznik, G. Sangiovanni, O. Gunnarsson, and T. P. Devereaux, "Photoemission kinks and phonons in cuprates," *Nature*, vol. 455, no. 7213, pp. E6–E7, 2008.
- [10] E. G. Maksimov, M. L. Kulić, and O. V. Dolgov, "Bosonic spectral function and the electron-phonon interaction in HTSC cuprates," to appear in *Advances in Condensed Matter Physics*, <http://arxiv.org/abs/1001.4859>.
- [11] J. Lee, K. Fujita, K. McElroy et al., "Interplay of electron-lattice interactions and superconductivity in  $\text{Bi}_2\text{Sr}_2\text{CaCu}_2\text{O}_{8+\delta}$ ," *Nature*, vol. 442, no. 7102, pp. 546–550, 2006.
- [12] G.-M. Zhao, H. Keller, and K. Conder, "Unconventional isotope effects in the high-temperature cuprate superconductors," *Journal of Physics Condensed Matter*, vol. 13, no. 29, pp. R569–R587, 2001.
- [13] M. Gurrutxaga and A. T. Fiory, "Resistivity of  $\text{La}_{1.825}\text{Sr}_{0.175}\text{CuO}_4$  and  $\text{YBa}_2\text{Cu}_3\text{O}_7$  to 1100 K: absence of saturation and its implications," *Physical Review Letters*, vol. 59, no. 12, pp. 1337–1340, 1987.
- [14] S. Martin, A. T. Fiory, R. M. Fleming, L. F. Schneemeyer, and J. V. Waszczak, "Normal-state transport properties of  $\text{Bi}_{2+x}\text{Sr}_{2-y}\text{CuO}_{6+\delta}$  crystals," *Physical Review B*, vol. 41, no. 1, pp. 846–849, 1990.
- [15] H. Takagi, B. Batlogg, H. L. Kao et al., "Systematic evolution of temperature-dependent resistivity in  $\text{La}_{2+x}\text{Sr}_x\text{CuO}_4$ ," *Physical Review Letters*, vol. 69, no. 20, pp. 2975–2978, 1992.
- [16] B. Batlogg, "A critical review of selected experiments in high- $T_c$  superconductivity," *Physica B*, vol. 169, no. 1–4, pp. 7–16, 1991.
- [17] M. Calandra and O. Gunnarsson, "Electrical resistivity at large temperatures: saturation and lack thereof," *Physical Review B*, vol. 66, no. 20, Article ID 205105, 20 pages, 2002.
- [18] O. Gunnarsson, "Superconductivity in fullerenes," *Reviews of Modern Physics*, vol. 69, no. 2, pp. 575–606, 1997.
- [19] E. Tosatti, "Physics: fullerenes in a squeeze," *Science*, vol. 323, no. 5921, pp. 1570–1571, 2009.
- [20] A. Y. Ganin, Y. Takabayashi, Y. Z. Khimyak et al., "Bulk superconductivity at 38 K in a molecular system," *Nature Materials*, vol. 7, no. 5, pp. 367–371, 2008.
- [21] Y. Takabayashi, A. Y. Ganin, P. Jeglic et al., "The disorder-free non-BCS superconductor  $\text{CS}_3\text{C}_{60}$  emerges from an antiferromagnetic insulator parent state," *Science*, vol. 323, no. 5921, pp. 1585–1590, 2009.
- [22] M. Capone, M. Fabrizio, C. Castellani, and E. Tosatti, "Strongly correlated superconductivity," *Science*, vol. 296, no. 5577, pp. 2364–2366, 2002.
- [23] T. Holstein, "Studies of polaron motion. Part I. The molecular-crystal model," *Annals of Physics*, vol. 8, no. 3, pp. 325–342, 1959.
- [24] J. Bonca and S. A. Trugman, "Bipolarons in the extended Holstein Hubbard model," *Physical Review B*, vol. 64, no. 9, Article ID 094507, 4 pages, 2001.
- [25] J. P. Hague and P. E. Kornilovitch, "Bipolarons from long-range interactions: singlet and triplet pairs in the screened Hubbard-Fröhlich model on the chain," *Physical Review B*, vol. 80, no. 5, Article ID 054301, 2009.
- [26] A. S. Alexandrov and P. E. Kornilovitch, "Mobile small polaron," *Physical Review Letters*, vol. 82, no. 4, pp. 807–810, 1999.
- [27] J. P. Hague, P. E. Kornilovitch, J. H. Samson, and A. S. Alexandrov, "Superlight small bipolarons," *Journal of Physics Condensed Matter*, vol. 19, no. 25, Article ID 255214, 2007.
- [28] T. M. Hardy, J. P. Hague, J. H. Samson, and A. S. Alexandrov, "Superconductivity in a Hubbard-Fröhlich model and in cuprates," *Physical Review B*, vol. 79, no. 21, Article ID 212501, 2009.
- [29] A. A. Abrikosov, L. P. Gorkov, and I. E. Dzyaloshinski, *Methods of Quantum Field Theory in Statistical Physics*, Dover, New York, NY, USA, 1975.

- [30] J. E. Hirsch, "Effect of coulomb interactions on the peierls instability," *Physical Review Letters*, vol. 51, no. 4, pp. 296–299, 1983.
- [31] J. E. Hirsch, "Phase diagram of the one-dimensional molecular-crystal model with Coulomb interactions: half-filled-band sector," *Physical Review B*, vol. 31, no. 9, pp. 6022–6031, 1985.
- [32] E. Berger, P. Valášek, and W. von der Linden, "Two-dimensional Hubbard-Holstein model," *Physical Review B*, vol. 52, no. 7, pp. 4806–4814, 1995.
- [33] Z. B. Huang, W. Hanke, E. Arrigoni, and D. J. Scalapino, "Electron-phonon vertex in the two-dimensional one-band Hubbard model," *Physical Review B*, vol. 68, no. 22, Article ID 220507, 4 pages, 2003.
- [34] M. Capone, M. Grilli, and W. Stephan, "Small polaron formation in many-particle states of the Hubbard-Holstein model: the one-dimensional case," *European Physical Journal B*, vol. 11, no. 4, pp. 551–557, 1999.
- [35] G. Wellein, H. Röder, and H. Fehske, "Polarons and bipolarons in strongly interacting electron-phonon systems," *Physical Review B*, vol. 53, no. 15, pp. 9666–9675, 1996.
- [36] B. Bäuml, G. Wellein, and H. Fehske, "Optical absorption and single-particle excitations in the two-dimensional Holstein t-J model," *Physical Review B*, vol. 58, no. 7, pp. 3663–3676, 1998.
- [37] A. Weiße, H. Fehske, G. Wellein, and A. R. Bishop, "Optimized phonon approach for the diagonalization of electron-phonon problems," *Physical Review B*, vol. 62, no. 2, pp. R747–R750, 2000.
- [38] H. Fehske, G. Wellein, G. Hager, A. Weiße, and A. R. Bishop, "Quantum lattice dynamical effects on single-particle excitations in one-dimensional Mott and Peierls insulators," *Physical Review B*, vol. 69, no. 16, Article ID 165115, 2004.
- [39] E. V. L. de Mello and J. Ranninger, "Dynamical properties of small polarons," *Physical Review B*, vol. 55, no. 22, pp. 14872–14885, 1997.
- [40] J. K. Freericks and M. Jarrell, "Competition between electron-phonon attraction and weak coulomb repulsion," *Physical Review Letters*, vol. 75, no. 13, pp. 2570–2573, 1995.
- [41] M. Capone, G. Sangiovanni, C. Castellani, C. Di Castro, and M. Grilli, "Phase separation close to the density-driven Mott transition in the Hubbard-Holstein model," *Physical Review Letters*, vol. 92, no. 10, Article ID 106401, 2004.
- [42] W. Koller, D. Meyer, Y. Ōno, and A. C. Hewson, "First- and second-order phase transitions in the Holstein-Hubbard model," *Europhysics Letters*, vol. 66, no. 4, pp. 559–564, 2004.
- [43] W. Koller, D. Meyer, and A. C. Hewson, "Dynamic response functions for the Holstein-Hubbard model," *Physical Review B*, vol. 70, no. 15, Article ID 155103, 2004.
- [44] G. S. Jeon, T.-H. Park, J. H. Han, H. C. Lee, and H.-Y. Choi, "Dynamical mean-field theory of the Hubbard-Holstein model at half filling: zero temperature metal-insulator and insulator-insulator transitions," *Physical Review B*, vol. 70, no. 12, Article ID 125114, 2004.
- [45] G. Sangiovanni, C. Castellani, and M. Grilli, "Electron-phonon interaction close to a mott transition," *Physical Review Letters*, vol. 94, no. 2, Article ID 026401, 2005.
- [46] G. Sangiovanni, M. Capone, and C. Castellani, "Relevance of phonon dynamics in strongly correlated systems coupled to phonons: dynamical mean-field theory analysis," *Physical Review B*, vol. 73, no. 16, Article ID 165123, 2006.
- [47] P. Werner and A. J. Millis, "Efficient dynamical mean field simulation of the holstein-hubbard model," *Physical Review Letters*, vol. 99, no. 14, Article ID 146404, 2007.
- [48] P. Paci, M. Capone, E. Cappelluti, S. Ciuchi, and C. Grimaldi, "Isotope effects in the Hubbard-Holstein model within dynamical mean-field theory," *Physical Review B*, vol. 74, no. 20, Article ID 205108, 2006.
- [49] A. MacRidini, B. Moritz, M. Jarrell, and T. Maier, "Synergistic polaron formation in the Hubbard-Holstein model at small doping," *Physical Review Letters*, vol. 97, no. 5, Article ID 056402, 2006.
- [50] A. Macridini, G. A. Sawatzky, and M. Jarrell, "Two-dimensional Hubbard-Holstein bipolaron," *Physical Review B*, vol. 69, no. 24, Article ID 245111, 2004.
- [51] E. Jeckelmann, "Mott-Peierls transition in the extended Peierls-Hubbard model," *Physical Review B*, vol. 57, no. 19, pp. 11838–11841, 1998.
- [52] M. Tezuka, R. Arita, and H. Aoki, "Phase diagram for the one-dimensional Hubbard-Holstein model: a density-matrix renormalization group study," *Physical Review B*, vol. 76, no. 15, Article ID 155114, 2007.
- [53] M. Grilli and C. Castellani, "Electron-phonon interactions in the presence of strong correlations," *Physical Review B*, vol. 50, no. 23, pp. 16880–16898, 1994.
- [54] F. Becca, M. Tarquini, M. Grilli, and C. di Castro, "Charge-density waves and superconductivity as an alternative to phase separation in the infinite-U Hubbard-Holstein model," *Physical Review B*, vol. 54, no. 17, pp. 12443–12457, 1996.
- [55] J. Keller, C. E. Leal, and F. Forsthofer, "Electron-phonon interaction in Hubbard systems," *Physica B*, vol. 206–207, pp. 739–741, 1995.
- [56] E. Koch and R. Zeyher, "Renormalization of the electron-phonon coupling in the one-band Hubbard model," *Physical Review B*, vol. 70, no. 9, Article ID 094510, 2004.
- [57] E. Cappelluti, B. Cerruti, and L. Pietronero, "Charge fluctuations and electron-phonon interaction in the finite-U Hubbard model," *Physical Review B*, vol. 69, no. 16, Article ID 161101, 2004.
- [58] M. L. Kulić and R. Zeyher, "Influence of strong electron correlations on the electron-phonon coupling in high- $T_c$  oxides," *Physical Review B*, vol. 49, no. 6, pp. 4395–4398, 1994.
- [59] R. Zeyher and M. L. Kulić, "Renormalization of the electron-phonon interaction by strong electronic correlations in high- $T_c$  superconductors," *Physical Review B*, vol. 53, no. 5, pp. 2850–2862, 1996.
- [60] J. Bonca, T. Katracnik, and S. A. Trugman, "Mobile bipolaron," *Physical Review Letters*, vol. 84, no. 14, pp. 3153–3156, 2000.
- [61] C. A. Perroni, V. Cataudella, G. De Filippis, and V. Marigliano Ramaglia, "Effects of electron-phonon coupling near and within the insulating Mott phase," *Physical Review B*, vol. 71, no. 11, Article ID 113107, 4 pages, 2005.
- [62] M. Hohenadler, M. Aichhorn, and W. von der Linden, "Single-particle spectral function of the Holstein-Hubbard bipolaron," *Physical Review B*, vol. 71, no. 1, Article ID 014302, 2005.
- [63] M. Hohenadler and W. von der Linden, "Temperature and quantum phonon effects on Holstein-Hubbard bipolarons," *Physical Review B*, vol. 71, no. 18, Article ID 184309, 2005.
- [64] P. Barone, R. Raimondi, M. Capone, C. Castellani, and M. Fabrizio, "Extended Gutzwiller wave function for the Hubbard-Holstein model," *Europhysics Letters*, vol. 79, no. 4, Article ID 47003, 2007.
- [65] P. Barone, R. Raimondi, M. Capone, C. Castellani, and M. Fabrizio, "Gutzwiller scheme for electrons and phonons: the

- half-filled Hubbard-Holstein model,” *Physical Review B*, vol. 77, no. 23, Article ID 235115, 2008.
- [66] A. Di Ciolo, J. Lorenzana, M. Grilli, and G. Seibold, “Charge instabilities and electron-phonon interaction in the Hubbard-Holstein model,” *Physical Review B*, vol. 79, no. 8, Article ID 085101, 2009.
- [67] P. Nozières, *Theory of Interacting Fermi Systems*, Benjamin, New York, NY, USA, 1964.
- [68] J. H. Kim and Z. Tesanovic, “Effects of strong Coulomb correlations on the phonon-mediated superconductivity: a model inspired by copper oxides,” *Physical Review Letters*, vol. 71, p. 4218, 1993.
- [69] C. Castellani and M. Grilli, “Comment on effects of strong coulomb correlations on the phonon-mediated superconductivity: a model inspired by copper oxides,” *Physical Review Letters*, vol. 74, no. 8, p. 1488, 1995.
- [70] S. E. Barnes, “New method for the Anderson model,” *Journal of Physics F*, vol. 6, no. 7, pp. 1375–1383, 1976.
- [71] P. Coleman, “New approach to the mixed-valence problem,” *Physical Review B*, vol. 29, no. 6, pp. 3035–3044, 1984.
- [72] N. Read and D. M. Newns, “On the solution of the Coqblin-Schrieffer Hamiltonian by the large- $N$  expansion technique,” *Journal of Physics C*, vol. 16, no. 17, pp. 3273–3295, 1983.
- [73] N. Read, “Role of infrared divergences in the  $1/N$  expansion of the  $U = \infty$  Anderson model,” *Journal of Physics C*, vol. 18, pp. 2651–2665, 1985.
- [74] G. Kotliar and J. Liu, “Superconducting instabilities in the large- $U$  limit of a generalized Hubbard model,” *Physical Review Letters*, vol. 61, no. 15, pp. 1784–1787, 1988.
- [75] A. J. Millis and P. A. Lee, “Large-orbital-degeneracy expansion for the lattice Anderson model,” *Physical Review B*, vol. 35, no. 7, pp. 3394–3414, 1987.
- [76] G. Kotliar and A. E. Ruckenstein, “New functional integral approach to strongly correlated fermi systems: the gutzwiller approximation as a saddle point,” *Physical Review Letters*, vol. 57, no. 11, pp. 1362–1365, 1986.
- [77] G. Aepia, C. Di Castro, M. Grilli, and J. Lorenzana, “Effective electron-electron and electron-phonon interactions in the Hubbard-Holstein model,” *Nuclear Physics B*, vol. 744, no. 3, pp. 277–294, 2006.
- [78] T. P. Devereaux, T. Cuk, Z.-X. Shen, and N. Nagaosa, “Anisotropic electron-phonon interaction in the cuprates,” *Physical Review Letters*, vol. 93, Article ID 117004, 2004.
- [79] C. Castellani and M. Grilli, “The electron-phonon interaction in strongly correlated systems,” in *Anharmonic Properties of High- $T_c$  Cuprates*, D. Mihailovic, G. Ruani, E. Kaldis, and K. A. Müller, Eds., World Scientific, Singapore, 1995.
- [80] A. Georges, G. Kotliar, W. Krauth, and M. J. Rozenberg, “Dynamical mean-field theory of strongly correlated fermion systems and the limit of infinite dimensions,” *Reviews of Modern Physics*, vol. 68, no. 1, pp. 13–125, 1996.
- [81] J. Bonca and S. A. Trugman, “Mobile bipolaron—strong coupling approach,” *Journal of Superconductivity and Novel Magnetism*, vol. 13, no. 6, pp. 999–1003, 2000.
- [82] A. C. Hewson and D. Meyer, “Numerical renormalization group study of the Anderson-Holstein impurity model,” *Journal of Physics Condensed Matter*, vol. 14, no. 3, pp. 427–445, 2002.
- [83] P. S. Cornaglia, H. Ness, and D. R. Grempel, “Many-body effects on the transport properties of single-molecule devices,” *Physical Review Letters*, vol. 93, no. 14, Article ID 147201, 2004.
- [84] W. Stephan, M. Capone, M. Grilli, and C. Castellani, “Influence of electron-phonon interaction on superexchange,” *Physics Letters A*, vol. 227, no. 1-2, pp. 120–126, 1997.
- [85] S. Lupi, P. Maselli, M. Capizzi, P. Calvani, P. Giura, and P. Roy, “Evolution of a polaron band through the phase diagram of  $\text{Nd}_{2-x}\text{Ce}_x\text{CuO}_{4-y}$ ,” *Physical Review Letters*, vol. 83, no. 23, pp. 4852–4855, 1999.
- [86] A. Ramak, P. Horsch, and P. Fulde, “Effective mass of quasiparticles in a t-J model with electron-phonon interactions,” *Physical Review B*, vol. 46, no. 21, pp. 14305–14308, 1992.
- [87] A. S. Mishchenko and N. Nagaosa, “Electron-phonon coupling and a polaron in the t-J model: from the weak to the strong coupling regime,” *Physical Review Letters*, vol. 93, no. 3, Article ID 036402, 2004.
- [88] O. Rösch and O. Gunnarsson, “Apparent electron-phonon interaction in strongly correlated systems,” *Physical Review Letters*, vol. 93, no. 23, Article ID 237001, 2004.
- [89] E. Cappelluti and S. Ciuchi, “Magnetic and lattice polaron in the Holstein t-J model,” *Physical Review B*, vol. 66, no. 16, Article ID 165102, 2002.
- [90] V. Cataudella, G. De Filippis, A. S. Mishchenko, and N. Nagaosa, “Temperature dependence of the angle resolved photoemission spectra in the undoped cuprates: self-consistent approach to the t-J holstein model,” *Physical Review Letters*, vol. 99, no. 22, Article ID 226402, 2007.
- [91] A. S. Mishchenko, N. Nagaosa, Z.-X. Shen et al., “Charge dynamics of doped holes in high  $T_c$  cuprate superconductors: a clue from optical conductivity,” *Physical Review Letters*, vol. 100, no. 16, Article ID 166401, 2008.
- [92] G. Sangiovanni, O. Gunnarsson, E. Koch, C. Castellani, and M. Capone, “Electron-phonon interaction and antiferromagnetic correlations,” *Physical Review Letters*, vol. 97, no. 4, Article ID 046404, 2006.
- [93] C. Castellani, C. Di Castro, and M. Grilli, “Singular quasiparticle scattering in the proximity of charge instabilities,” *Physical Review Letters*, vol. 75, no. 25, pp. 4650–4653, 1995.
- [94] V. J. Emery and S. A. Kivelson, “Frustrated electronic phase separation and high-temperature superconductors,” *Physica C*, vol. 209, no. 4, pp. 597–621, 1993.
- [95] R. Raimondi, C. Castellani, M. Grilli, Y. Bang, and G. Kotliar, “Charge collective modes and dynamic pairing in the three-band Hubbard model. II. Strong-coupling limit,” *Physical Review B*, vol. 47, no. 6, pp. 3331–3346, 1993.
- [96] U. Löw, V. J. Emery, K. Fabricius, and S. A. Kivelson, “Study of an Ising model with competing long- and short-range interactions,” *Physical Review Letters*, vol. 72, no. 12, pp. 1918–1921, 1994.
- [97] J. Lorenzana, C. Castellani, and C. Di Castro, “Phase separation frustrated by the long-range Coulomb interaction. I. Theory,” *Physical Review B*, vol. 64, no. 23, Article ID 235127, 15 pages, 2001.
- [98] R. J. McQueeney, Y. Petrov, T. Egami, M. Yethiraj, G. Shirane, and Y. Endoh, “Anomalous dispersion of LO phonons in  $\text{La}_{1.85}\text{Sr}_{0.15}\text{CuO}_4$  at low temperatures,” *Physical Review Letters*, vol. 82, no. 3, pp. 628–631, 1999.
- [99] R. J. McQueeney, J. L. Sarrao, P. G. Pagliuso, P. W. Stephens, and R. Osborn, “Mixed lattice and electronic states in high-temperature superconductors,” *Physical Review Letters*, vol. 87, no. 7, Article ID 077001, 2001.
- [100] L. Pintschovius, N. Pyka, W. Reichardt et al., “Lattice dynamical studies of HTSC materials,” *Physica C*, vol. 185–189, pp. 156–161, 1991.

- [101] L. Pintschovius and W. Reichardt, “Inelastic Neutron Scattering Studies of the Lattice Vibrations of High- $T_c$  compounds,” in *Physical Properties of High Temperature Superconductors IV*, P. Ginsberg, Ed., p. 295, World Scientific, Singapore, 1995.
- [102] L. Pintschovius and M. Braden, “Anomalous dispersion of LO phonons in  $\text{La}_{1.85}\text{Sr}_{0.15}\text{CuO}_4$ ,” *Physical Review B*, vol. 60, no. 22, pp. R15039–R15042, 1999.
- [103] D. Reznik, L. Pintschovius, M. Ito et al., “Electron-phonon coupling reflecting dynamic charge inhomogeneity in copper oxide superconductors,” *Nature*, vol. 440, no. 7088, pp. 1170–1173, 2006.
- [104] D. Reznik, L. Pintschovius, M. Fujita, K. Yamada, G. D. Gu, and J. M. Tranquada, “Electron-phonon anomaly related to charge stripes: static stripe phase versus optimally doped superconducting  $\text{La}_{1.85}\text{Sr}_{0.15}\text{CuO}_4$ ,” *Journal of Low Temperature Physics*, vol. 147, no. 3-4, pp. 353–364, 2007.
- [105] A. Di Ciolo and J. Lorenzana, unpublished .
- [106] A. Di Ciolo, J. Lorenzana, M. Grilli, and G. Seibold, unpublished.
- [107] M. Capone, M. Fabrizio, and E. Tosatti, “Direct transition between a singlet mott insulator and a superconductor,” *Physical Review Letters*, vol. 86, no. 23, pp. 5361–5364, 2001.
- [108] J. E. Han, O. Gunnarsson, and V. H. Crespi, “Strong superconductivity with local Jahn-Teller phonons in  $\text{C}_{60}$  solids,” *Physical Review Letters*, vol. 90, no. 16, Article ID 167006, 2003.
- [109] M. Capone, M. Fabrizio, C. Castellani, and E. Tosatti, “Colloquium: modeling the unconventional superconducting properties of expanded  $\text{A}_3\text{C}_{60}$  fullerides,” *Reviews of Modern Physics*, vol. 81, no. 2, pp. 943–958, 2009.
- [110] M. Capone, M. Fabrizio, C. Castellani, and E. Tosatti, “Strongly correlated superconductivity and pseudogap phase near a multiband mott insulator,” *Physical Review Letters*, vol. 93, no. 4, Article ID 047001, 2004.
- [111] M. Schiró, M. Capone, M. Fabrizio, and C. Castellani, “Strongly correlated superconductivity arising in a pseudogap metal,” *Physical Review B*, vol. 77, no. 10, Article ID 104522, 2008.
- [112] W. P. Su, J. R. Schrieffer, and A. J. Heeger, “Solitons in polyacetylene,” *Physical Review Letters*, vol. 42, no. 25, pp. 1698–1701, 1979.
- [113] E. von Oelsen, A. Di Ciolo, J. Lorenzana, G. Seibold, and M. Grilli, “Phonon renormalization from local and transitive electron-lattice couplings in strongly correlated systems,” *Physical Review B*, vol. 81, no. 155116, 2010.
- [114] G. Seibold, J. Lorenzana, and M. Grilli, unpublished.